

FEB - FRESENIUS ENVIRONMENTAL BULLETIN

Founded jointly by F. Korte and F. Coulston

Production by PSP - Vimy Str. 1e, 85354 Freising, Germany in
cooperation with PRT-Parlar Research & Technology

Vimy Str 1e, 85354 Freising

Copyright© by PSP and PRT, Vimy Str. 1e, 85354 Freising, Germany

All rights are reserved, especially the right to translate into foreign language or other processes - or convert to a machine language, especially for data processing equipment - without written permission of the publisher. The rights of reproduction by lecture, radio and television transmission, magnetic sound recording or similar means are also reserved.

Printed in Germany-ISSN 1018-4619

FEB-EDITORIAL BOARD**CHIEF EDITOR:****Prof. Dr. Dr. H. Parlar**Parlar Research & Technology-PRT
Vimy Str.1e
85354 Freising, Germany**MANAGING EDITOR:****Dr. P. Parlar**Parlar Research & Technology
PRT, Vimy Str.1e
85354 Freising, Germany**CO-EDITORS:****Environmental Spectroscopy****Prof. Dr. A. Piccolo**Universita di Napoli "Frederico II"
Dipto. Di Scienze Chimica Agrarie
Via Universita 100, 80055 Portici, Italy**Environmental Biology****Prof. Dr. G. Schuurmann**UFZ-Umweltzentrum
Sektion Chemische Ökotoxikologie
Leipzig-Halle GmbH,
Permoserstr.15, 04318
04318 Leipzig, Germany**Prof. Dr. I. Holoubek**Recetox-Tocoen
Kamenice126/3, 62500 Brno, Czech Republic**Prof. Dr. M. Hakki Alma**Kahramanmaras Sutcu Imam University
Avsar Kampusu, 46100 Kahramanmaras, Turkey**Environmental Analytical Chemistry****Prof. Dr. M. Bahadir**Lehrstuhl für Ökologische Chemie
und Umweltanalytik
TU Braunschweig
Lehrstuhl für Ökologische Chemie
Hagenring 30, 38106 Braunschweig, Germany**Dr. D. Kotzias**Via Germania29
21027 Barza(Va), Italy**Environmental Management****Dr. K. I. Nikolaou**Env.Protection of Thessaloniki
OMPEPT-54636 Thessaloniki
Greece**Environmental Toxicology****Prof. Dr. H. Greim**Senatkommision – DFG / TUM
85350 Freising, Germany**Environmental Proteomic****Dr. A. Fanous**Halal Control GmbH
Kobaltstr. 2-4
D-65428 Rüsselsheim, Germany**Environmental Education****Prof. Dr. C. Bayat**Esenyurt Üniversitesi
34510 Esenyurt, Istanbul, Turkey**Advisory Board****K. Bester, K. Fischer, R. Kallenborn****DCG. Muir, R. Niessner, W. Vetter,****A. Reichlmayr-Lais, D. Steinberg,****J. P. Lay, J. Burhenne, L. O. Ruzo****Marketing Manager****Cansu Ekici, B. of B.A.**PRT-Research and Technology
Vimy Str 1e
85354 Freising, Germany**E-Mail: parlar@wzw.tum.de
parlar@prt-parlar.de****Phone: +49/8161887988**



Fresenius Environmental Bulletin is abstracted/indexed in:

Biology & Environmental Sciences, BIOSIS, CAB International, Cambridge Scientific abstracts, Chemical Abstracts, Current Awareness, Current Contents/Agriculture, CSA Civil Engineering Abstracts, CSA Mechanical & Transportation Engineering, IBIDS database, Information Ventures, NISC, Research Alert, Science Citation Index (SCI), Scisearch, Selected Water Resources Abstracts

CONTENTS

ORIGINAL PAPERS

- INFLUENCE OF POLLUTED WATER ON SEDIMENT BACTERIAL COMMUNITY OF THE SHANMEI RESERVOIR, CHINA, ESTIMATED BY 454 PYROSEQUENCING 4325
Keqiang Shao, Chengrong Bai, Jian Cai, Yang Hu, Yi Gong, Jianying Chao, Jiangyu Dai, Yongping Wang, Xiangming Tang, Guang Gao
- HIGH METAL ACCUMULATION IN BITTER GOURD IRRIGATED WITH SEWAGE WATER CAN CAUSE HEALTH HAZARDS 4332
Zafar Iqbal Khan, Kafeel Ahmad, Rukhsana Parveen, Humayun Bashir, Naunain Mehmood
- FRACTIONATION OF Cd AND Pb IN AGRICULTURAL SOIL AND THEIR DETERMINATIONS USING INDUCTIVELY COUPLED PLASMA-OPTICAL EMISSION SPECTROMETRY 4338
Sukran Akkus Ozen, Mehmet Yaman
- ACCRETION AND DISPERSION OF HEAVY METALS IN A VEGETABLE GROWN IN CONTAMINATED SOIL WITH SEWAGE WATER: A MATTER OF GREAT CONCERN AND COMMUNITY HEALTH CONSEQUENCES 4345
Muhammad Saeed Ahmad, Zafar Iqbal Khan, Kafeel Ahmad, Aima Iram Batool, Sana Hamid, Muhammad Sher, Ijaz Rasool Noorka, Zafar Hayat, Humayun Bashir, Muhammad Sohail, Abid Ejaz, Zunaira Sheikh, Ahmed Muneeb, Naunain Mehmood, Hira Muqaddas, Faiza Zubair, Naila Amjad, Fauzia Naseem Taj, Sana Iqbal, Fauzia Batool
- SUBSTANTIAL WATER LOSS FROM FOREST SURFACE SOIL AFTER THE WENCHUAN EARTHQUAKE 4350
Gang Yang, Song Cheng, Li Zhang, Jiyue Li, Hui Yu
- HEAVY METAL CONTAMINATION AND ECOLOGICAL RISK ASSESSMENT IN THE SEDIMENTS OF MELEN RIVER, DUZCE, TURKEY 4357
Seref Keskin
- QUALITY ASSESSMENT OF MARITSA RIVER WATER AS A MAIN SOURCE FOR IRRIGATION IN THRACIAN VALLEY 4367
Gergana Kostadinova, Diayna Dermendzhieva, Georgi Beev, Georgi Petkov, Dimitar Pavlov, Elica Valkova
- THE EFFECTS OF NARINGIN AND OZONE IN HEPATIC ISCHEMIA REPERFUSION INJURY: AN EXPERIMENTAL STUDY 4375
Cebraail Gursul, Kemal Peker, Abdulkadir Coban, Hasan Kilicgun, Ilyas Sayar, Fazile Nur Ekinci Akdemir, Murat Cankaya, Mustafa Gul
- FREE RADICAL SCAVENGING ACTIVITY, PHENOLIC CONTENTS AND FLAVONOIDS OF FOUR CRUCIFEROUS VEGETABLES: EFFECTS OF EXTRACTION 4383
Okan Erken, Seckin Kaya
- COMPARISON OF CHLORAMPHENICOL ADSORPTION BEHAVIOR ON BIOCHARS DERIVED FROM REED STRAWS AND MUNICIPAL SEWAGE SLUDGE 4390
Hanyu Zhang, Zhaowei Wang, Xiaoyun Xie, Junhong Gao, Junmin Zhu, Chaoran Xie
- MOLECULAR APPROACHES TO EVALUATE ACTINOMYCETE DIVERSITY IN THE CRUDE OIL-CONTAMINATED SOIL 4400
Haijun Liu, Zhenzhen Wan, Chun Hu, Baohua Zhou, Kanaji Masakorala, Jun Yao
- PHTHALATE ESTERS MIGRATION FROM TWO KINDS OF PLASTIC FILMS AND THE ENRICHMENT IN PEANUT PLANT 4409
Kairong Wang, Ningning Song, Mingming Cui, Yanxi Shi
- ANALYSIS OF ADSORPTION AND KINETIC OF LIPASE ENZYME ON KAOLINITE 4416
Salih Alkan, Umit Turgut
- EVALUATION OF THE WOUND HEALING AND ANTI-INFLAMMATORY ACTIVITIES AND PHYTOCHEMICAL ANALYSIS OF MYRTUS COMMUNIS L. 4420
Ibrahim Tumen, Esra Kupeli Akkol, Ipek Suntar, Guler Erbey, Mehmet Kurtca, Hikmet Keles, Markku Reunanen, Andrey Pranovich
- FIXED-BED COLUMN SORPTION OF ANTIMONY(III) BY POROUS COMPOSITE OF IRON OXIDES AND CARBON WITH EUCALYPTUS WOOD MICROSTRUCTURE 4429
Yanhong Li, Xuehong Zhang, Yinian Zhu, Zongqiang Zhu, Liwei Xie

α -AMYLASE FROM BACILLUS SIMPLEX- PRODUCTION, CHARACTERIZATION AND PARTIAL PURIFICATION Veysi Ortakaya, Sema Aguloglu Fincan, Baris Enez	4446
RESPONSE TO HEAVY METALS ON POLLEN VIABILITY, GERMINATION AND TUBE GROWTH OF SOME APPLE CULTIVARS Ferhad Muradoglu, Omer Beyhan, Ferit Sonmez	4456
BIOLOGICAL PRE-TREATMENT OF SOFT-WOOD LARIX KAEMPFERI USING THREE WHITE-ROT FUNGI - CORTICIUM CAERULEUM, HETEROBASIDIUM INSULARE AND PSEUDOTRAMETES GIBBOSA Zhang Yue-Hua, Yu Jing-Ni, Zhao Cheng-Cheng, Li Jia-Lin	4462
EFFECTS OF LEAD APPLICATION ON GROWTH AND NUTRIENT ACCUMULATIONS IN MIRABILIS JALAPA L. Muhittin Dogan, Mustafa Pehlivan, Oguz Gumus Inan, Hasan Akgul	4470
YIELD AND FIBER TECHNOLOGICAL TRAITS OF ADVANCED COTTON LINES DEVELOPED BY LINE TESTER MATING DESIGN Cetin Karademir, Emine Karademir, Ugur Sevilmis	4477
KINETICS AND EQUILIBRIUM ADSORPTION STUDY OF LEAD(II) ONTO ACTIVATED CARBON PREPARED FROM PUMPKIN SEED SHELL Ilknur Demiral, Canan Aydin Samdan, Hakan Demiral	4484
OPTIMIZATION OF SLUDGE DEWATERING PERFORMANCE THROUGH RESPONSE SURFACE METHODOLOGY COMBINED WITH ULTRASONIC AND CALCIUM OXIDE Wen-Jun Liang, Xiu-Juan Shi, Yi-Li Li, Yan-Ling Li, Rui Shi	4495
GUIDELINES FOR EIA OF A FISHING PORT IN A SEMI-ENCLOSED WATER BODY Mohammed Rasheed, Saima Mian, Mohamad Almasri, David Aubrey	4504
ADVANCED TREATMENT OF COAL CHEMICAL INDUSTRY WASTEWATER BY EXPANSIVE FLOW BIOLOGICAL AERATED FILTER Baolin Hou, Zhi Li, Renjian Deng, Bozhi Ren	4517
ADSORPTION BEHAVIOR OF NEUTRAL RED FROM AQUEOUS SOLUTION ONTO NAOH-MODIFIED PEANUT SHELL Xia Du, Hong Yan, Yingjie Dai	4522
PHOTODEGRADATION OF ENROFLOXACIN UNDER DIFFERENT CONDITIONS IN AQUEOUS SYSTEMS: KINETICS, PRODUCTS AND QUANTUM YIELD Zheng Wenxiu, Deng Huanhuan, Wang Lan, Ge Liyun, Chen Libo	4528
REMOVAL OF HGO FROM SIMULATED FLUE GAS BY MAGNETIC SILVER-LOADED FIBER Ru Yang, Jinghong Wang, Yongfa Diao, Yan Zhao, Zhannan Lian	4536
LEACHING CHARACTERISTICS AND CHANGE OF BIOAVAILABILITY OF HEAVY METALS IN MSWI FLY ASH DURING VARIOUS WASHING PROCESSES Lei Wang, Li-ao Wang, Xue Zhao, Xiang Wang, Yifu Li, Chaochao Hu	4542
METAL CONCENTRATIONS IN TISSUES OF TWO FISH SPECIES (MYSTUS MACROPTERUS AND CYPRINUS CARPIO) FROM THE CHISHUI RIVER, A PROTECTED AREA IN CHINA Shenwen Cai, Jinhua Gan, Bin Liu, Jiazhen Wang	4549
THE COMPARATIVE ECONOMIC ANALYSIS OF ORGANIC AND CONVENTIONAL DRIED APRICOT PRODUCTION: A CASE STUDY FOR TURKEY Kubilay Ucar, Gamze Saner, Sait Engindeniz	4555
NANO-BIOLOGICAL MODIFICATION OF THE ELECTRODES IN MICROBIAL FUEL CELL Farzad Sadri, Alireza Khodavandi, Ali Shamsazar, Masoud Negahdary, Ghasem Rahimi	4561
TWO DIFFERENT MOLECULAR MARKERS (SSR AND IPBS) ASSESSMENT ON CORIANDRUM SATIVUM L. WITH CAPILLARY ELECTROPHORESIS Furan M Alp, Merve Dilek Gebologlu	4568
THE INFLUENCE OF SOIL CONFIGURATION OF RICE PADDY IN THE YELLOW RIVER BEACH ON THE RICE YIELD AND SOIL HYDRAULIC CHARACTERISTIC Daiwen Zhu, Jichang Han, Miao Cai, Yang Wei, Gang Li, Bo Yan, Nan Lu	4574

- ION-EXCHANGE PREPARATION OF NiFe₂O₄-CuFe₂O₄ COMPOSITE WITH ENHANCED VISIBLE-LIGHT PHOTOCATALYTIC PERFORMANCE FOR DEGRADATION 4582
Kuili Liu, Hongqiang Shen, Weidong Shi
- PREPARATION OF SULPHOALUMINATE CEMENT WITH RESIDUE OF MANGANESE DIOXIDE ORE LEACHED BY SO₂ 4588
Bo-zhi Wang, Shi-jun Su, Sang-lan Ding, Wei-yi Sun
- PRECURSOR-CONTROLLED SYNTHESIS OF GRAPHENE-LIKE CARBON NITRIDE FOR MC-LR DEGRADATION UNDER VISIBLE LIGHT 4595
Jiahui Ma, Liping Wang, Chengjie Song, Shaomang Wang, Fan Zhang
- YIELD REDUCTION ANALYSIS OF BREAD WHEAT UNDER HEAT STRESS AT TWO DIFFERENT ENVIRONMENTS IN PAKISTAN 4602
Muhammad Jamil, Aamir Ali, Abdul Ghafoor, Alvina Gul, Khalid Farooq Akbar, Humayun Bashir, Adeel Ijaz, Rameez Hussain, Ahmed Muneeb, Naima Huma Naveed, Nasim Ahmad Yasin, Abdul Aziz Napar, Abdul Mujeeb Kazi
- THE EFFECT OF MAGNETIC FIELD APPLICATIONS TO CHEMICAL CONTENT OF STRATIFIED SEEDS OF ORIENTAL BEECH (*Fagus orientalis* Lipsky.) 4606
Nezahat Turfan, Esra Nurten Yer, Sezgin Ayan
- EFFECTS OF VARIOUS MULCH MATERIALS ON FRUIT QUALITY CHARACTERISTICS ON ORGANICALLY GROWN STRAWBERRIES 4616
Sevinc Sener, Nurgul Fetiye Turemis
- COMPREHENSIVE REVIEWS ON ADVERSE HEALTH EFFECTS OF HUMAN EXPOSURE TO ENDOCRINE-DISRUPTING CHEMICALS 4623
Hussein Kehinde Okoro, Julius Oluwafunso Ige, Oluyinka Ajibola Iyiola, Sadanand Pandey, Isiaka Ayobamidele Lawal, Caliphs Zvinowanda, Catherine Jane Ngila
- OVERVIEW OF PEST MANAGEMENT PRACTICES IN TURKISH FOOD PROCESSING FACILITIES 4637
Eyyup Mennan Yildirim, Ayse Demet Karaman, Huseyin Yerlikaya
- PERFORMANCE OF GROWTH AND NUTRIENT CONTENT IN MELIA AZEDARACH L. UNDER WASTEWATER IRRIGATION 4645
Hayssam M Ali, Saud A Alamri, Manzer H Siddiqui, Mutahhar Y Y Al-Khaishany, Mohammed A Al-Qutami, Khaled A Alakeel
- NEXT GENERATION SEQUENCING TECHNOLOGIES AND USAGE IN FORENSIC GENETICS 4650
E Hulya Yukseloglu, Umut Kara, S Sibel Ramadanoglu, Faruk Ascioglu
- A COST-EFFECTIVENESS APPROACH FOR CONFIGURATION OF FEASIBLE SKYLINE YARDER FOR SPECIFIC FOREST REGIONS 4656
Selcuk Gumus, Taha Yasin Hatay
- EMISSION CHARACTERISTICS OF BIOMASS COMBUSTION IN A DOMESTIC HEATING BOILER FED WITH WOOD AND VIRGINIA MALLOW PELLETS 4663
Grzegorz Zajac, Joanna Szyszlak-Barglowicz, Tomasz Slowik, Jacek Wasilewski, Andrzej Kuranc
- IN VITRO SCREENING OF PRECONDITIONED PLUMULAR APICES EXPLANTS OF PEANUT (*ARACHIS HYPOGAEAE*) TO DIFFERENT SALTS CONCENTRATION 4671
Sibel Day, Muhammad Aasim
- IN VITRO EFFECTS OF SOME HEAVY METAL IONS ON CYTOSOLIC THIOREDOXIN REDUCTASE PURIFIED FROM RAINBOW TROUT GILL TISSUES 4677
Hatice Akyol, Muslum Kuzu
- DETERMINATION OF THE EFFECTS OF LIGHT INTENSITY AND LIGHT CYCLE PARAMETERS IN THE CULTIVATION OF CHLORELLA PROTOTHECOIDES MICROALGAE SPECIES 4684
Ahmet Konuralp Elicin
- IN VITRO SEED GERMINATION STUDY IN NARROW ENDEMIC PLANT *VERBASCUM ALYSSIFOLIUM* (SCROPHULARIACEAE) 4692
Muhip Hilooglu, Emel Sozen
- ACCUMULATION OF HEAVY METALS IN SURFACE SOILS OF BENGBU HIGHER EDUCATION MEGA CENTER, CHINA 4697
Li Ma, Herong Gui

TOXICOKINETIC OF CYPERMETHRIN IN BROILER CHICKENS Gokhan Eraslan, Muhammet Yasin Tekeli, Mursel Karabacak	4704
LEVELS OF ORGANOCHLORINE PESTICIDES RESIDUES IN HUMAN BREAST MILK FROM THE NORTHERN DISTRICTS IN JORDAN IN 2014/2015 Tawfiq M AlAntary, Mahmoud A Alawi, Mohammad Abu Othman, Nizar Haddad	4711
DETERMINATION OF ENERGY LOSS COEFFICIENT OF RAINWATER AND SEWER MANHOLES WITH CFD Ismail Hakki Ozolcer, Onur Dunder	4716
NEURITOGENIC ACTIVITY OF EPIGALLOCATECHIN GALLATE AND CURCUMIN COMBINATION ON RAT ADRENAL PHEOCHROMOCYTOMA CELLS Miris Dikmen, Elif Kaya-Tilki, Selin Engur, Yusuf Ozturk	4726
COMPARING THE VOLUME METHODS THROUGH USING DIGITAL ELEVATION MODELS CREATED BY DIFFERENT INTERPOLATION METHODS Nazan Yilmaz	4734
IMPACTS OF CARBON TARIFFS ON CHINA'S ECONOMIC STRUCTURE AND CARBON INTENSITY: SIMULATION ANALYSIS USING A DYNAMIC CGE MODEL Shi-Chun Xu, Wen-Wen Zhang, Chang Gao, Ru-Yin Long, Hong Chen	4742
DETERMINATION OF THERAPEUTIC POTENTIAL OF MENTHA LONGIFOLIA SSP. LONGIFOLIA Mustafa Sevindik, Hasan Akgul, Mustafa Pehlivan, Zeliha Selamoglu	4757
ALLEVIATION OF CARBOFURAN TOXICITY EFFECT BY PARSLEY ON LIPIDS PROFILE OF MALE ALBINO RATS Yasmin Emam Abdel-Mobdy, Hossam Saad El-Beltagi, Ahmed Emam Abdel-Mobdy	4764
OCCURRENCE OF EPILITHIC DIATOMS IN A STREAM WITH CLEAN WATER CONDITIONS: HARINGET STREAM, TURKEY Feray Sonmez	4774
EFFECT OF LIGHT PATH LENGTH OF TUBES ON GROWTH RATE OF NANNOCHLOROPSIS OCOLATA USING INDUSTRIAL SCALE TUBULAR PHOTOBIOREACTOR IN THE MARINE HATCHERY Yasar Durmaz, Gokhun Cagatay Erbil	4783
ELECTRO-FILTER RECYCLE POWDER OF CEMENT INDUSTRY AS A LOW-COST ADSORBENT FOR REMOVAL OF TEXTILE DYE ASTRAZON BLUE FGRL Ismail Nalbant, Halil Kumbur, Havva Duygu Bilgen, Gamze Koyuncu Turkey	4790
EFFECTS OF EMISSION CONTROL AND METEOROLOGICAL PARAMETERS ON URBAN AIR QUALITY SHOWED BY THE 2014 YOUTH OLYMPIC GAMES IN CHINA Xiao-San Luo, Zhen Zhao, Yan Chen, Xinlei Ge, Yu Huang, Chen Suo, Xue Sun, Dan Zhang	4798
AN IMPROVED EXPORT COEFFICIENT MODEL FOR PRIORITY AREA IDENTIFICATION AND LOAD ESTIMATION UNDER DIFFERENT HYDROLOGICAL YEAR IN MIYUN RESERVOIR WATERSHED, BEIJING, CHINA Runzhe Geng, Xiaoyan Wang	4808
DISSOLUTION OF Cu (OH) ₂ BY A NOVEL CHELATING SURFACTANT N-LAUROYL ETHYLENEDIAMINE TRIACETATE Jingru Diao, Baowei Zhao, Hongtao Qiao, Fengfeng Ma, Liping Huang	4817
REMOVAL OF NITRATE AND PHOSPHATE BY IMMOBILIZED BIOCHARS PREPARED FROM REEDS AND HEMATITE Bo Wang, Deng-Yue Yang, Fa-Yun Li	4825
FIRST ASSESSMENT OF MARINE LITTER IN SHALLOW SOUTH-EAST ADRIATIC SEA Vesna Macic, Milica Mandic, Branka Pestoric, Zoran Gacic, Momir Paunovic	4834
PREY SELECTION AND DIET COMPOSITION OF LARVAL PIKE, ESOX LUCIUS L., 1758, IN LAKE ISASZEG, HUNGARY Sevil Demirci, Kaya Gokcek, Ahmet Bozkurt, Tamas Szabo, Bela Urbanyi	4841
EVALUATION OF POLLUTION FROM RIVERS IN NORTHEASTERN MEDITERRANEAN REGION: HEAVY METALS Meltem Dural Eken, Besir Akman	4845

- EFFECTS OF BRASSINOLIDE ON PHYSIOLOGICAL PARAMETERS OF ROBINIA PSEUDOACACIA SEEDLINGS IN CRUDE OIL CONTAMINATED SOIL 4851
Gang Han, Yuanyuan Han, Kairong Li, Xiaoxi Zhang
- WHEAT STRIPE RUST DISEASE: QUANTITATIVE PROFILING OF YR10 GENE 4859
Tulin Tascioglu, Yildiz Aydin, Kadir Akan, Sandeep Kumar Verma, Ozge Karakas Metin, Ahu Altinkut Uncuoglu
- SELECTION OF OPTIMAL PARAMETERS FOR FUTURE RESEARCH MONITORING PROGRAMMES ON MSW LANDFILL IN NOVI SAD, SERBIA 4867
Maja Djogo, Jelena Radonic, Ivana Mihajlovic, Boris Obrovski, Dejan Ubavin, Maja Turk Sekulic, Mirjana Vojinovic Miloradov
- INFLUENCES OF PHYSALIS PERUVIANA L. AND LUPINUS ALBUS L. EXTRACTS ON THE LEVELS OF SOME BIOCHEMICAL PARAMETERS IN ERYTHROCYTES AND SERUM OF STREPTOZOTOCIN INDUCED DIABETIC RATS 4876
Fazilet Erman, Tubay Kaya, Okkes Yilmaz, Orhan Erman, Ayse Dilek Ozsahin
- BIOCHEMICAL AND HISTOPATHOLOGICAL CHANGES OF BABESIOSIS IN NATURALLY INFECTED SHEEP IN GAZIANTEP REGION 4883
Haci Ahmet Deveci, Gokhan Nur, Abdulsamed Kukurt
- ASSESSMENT THE NOISE LEVEL IN LIBRARIES AND DORMITORIES OF KERMANSHAH UNIVERSITY OF MEDICAL SCIENCES IN 2016 (KERMANSHAH, IRAN) 4890
Amir Hossein Nafez, Soheila Lotfi, Reza Rostami, Reza Saeedi, Shahla Lotfi

INFLUENCE OF POLLUTED WATER ON SEDIMENT BACTERIAL COMMUNITY OF THE SHANMEI RESERVOIR, CHINA, ESTIMATED BY 454 PYROSEQUENCING

Keqiang Shao¹, Chengrong Bai¹, Jian Cai¹, Yang Hu¹, Yi Gong¹, Jianying Chao², Jiangyu Dai³, Yongping Wang³, Xiangming Tang¹, Guang Gao^{1,*}

¹Taihu Laboratory for Lake Ecosystem Research, State Key Laboratory of Lake Science and Environment, Nanjing Institute of Geography and Limnology, Chinese Academy of Sciences, Nanjing 210008, China

²Nanjing Institute of Environmental Sciences, Ministry of Environmental Protection, Nanjing 210042, China

³State Key Laboratory of Hydrology-Water Resources and Hydraulic Engineering, Nanjing Hydraulic Research Institute, Nanjing 210029, China

ABSTRACT

A 20-day mesocosm experiments were carried out to examine the potential influence of polluted water on bacterial community composition of the sediment in Shanmei reservoir, China. Three treatment additions of different types of polluted water (agricultural drainage, fishpond water and domestic sewage) were performed in enclosures. The sediment bacterial communities were profiled by 16S rRNA multitag 454 pyrosequencing. The results showed that the bacterial diversity of the sediment increased significantly, and the composition of sediment bacterial community also significantly varied in all 3 treatments after 20 days of incubation. The relative abundance of bacteria affiliated with *Proteobacteria* and *Firmicutes* decreased, and the relative abundance of bacteria affiliated with *Bacteroidetes*, *Actinobacteria* and *Acidobacteria* increased after the import of polluted water. Our results strongly highlight the importance of allochthonous bacteria derived from polluted water on shaping the diversity and composition of sediment bacterial community in reservoir ecosystems.

KEYWORDS:

Shanmei reservoir, polluted water, sediment bacterial community, 454 pyrosequencing.

INTRODUCTION

Microbial communities play a key role in the transformation of complex organic matter and the biogeochemical cycling of the primary elements, in sediments of freshwater lakes [19]. The bacterial diversity determines the bacterial community structure, which in turn affects community function, and ultimately ecosystem function [18]. Within freshwater environments, investigation of the bacterial community in the sediment can provide important clues to understanding ecosystem process.

The water reservoir is an ecosystem, which could contribute significantly to regulate volume and flow of rivers, offer water resource for drinking, agricultural and industrial uses. However, it is always affected by human behavior, e.g. industrial and agricultural pollutions through the input of liquid wastes and rainwater [14]. These main pollutants are nutritive substances, including nitrogen, phosphorus and organic carbons [16]. The sediment of a reservoir is the compartment with the highest concentration of microbial biomass [28]. Some studies have focused on bacterial community composition (BCC) in sediments of reservoirs [14, 25, 31]. However, very little is known about whether the polluted water has an influence on the diversity and composition of bacterial community in reservoir sediment.

Shanmei Reservoir is characterized by a surface area of 1042 km² and is located in the northwest part of Quanzhou City (24°30'-25°56'-N and 117°25'-119°05'-E), Fujian province, China. In recent years, the catchment of Shanmei Reservoir was heavily polluted due to rapid industrialization and intensive application of chemical fertilizers and pesticides to arable fields in up-stream regions. In the present study, we collected three different source of polluted water with high concentration of nutrients from up-stream regions, and carried out the mesocosm experiments to investigate the response of the sediment bacterial community to polluted water.

MATERIAL AND METHODS

Experiment design. In the laboratory, a mesocosm experiment with 9 polyethylene barrels (100 L each) was carried out from 5 to 25 September 2012. The barrels were enclosed with the upside open to air. Sediment samples were collected using a sampler (HL-CN, Hengling Technology Ltd Corp., China) from this Reservoir. The vertical structure of all sediment samples was fully mixed, and mixed sediment (10 cm deep and 450 cm² in surface area) was transferred evenly into each barrel. Then each

barrel was filled carefully with 60 L of polluted water. The barrels of the experiments were placed for 7 days to form stable water-sediment layer before the beginning of sampling.

To explore the response of sediment bacterial community on three different source of polluted water, the 9 barrels were set up into three treatments: A enclosures were the agricultural sewage, B enclosures were the fishpond water, C enclosures were the domestic sewage. Each treatment was performed in triplicate

Sampling and physicochemical analysis. Water samples (1L) were collected on days 0, 20, and immediately stored at 4°C until further physicochemical analysis. Surface sediment samples were collected on days 0, 20, then transferred into sterile plastic containers and immediately stored frozen at -80°C. The pH of sediments was simultaneously measured on location. The sediment samples were dried with a freeze dryer (Alpha 1-2 LD, Martin Christ Instrument Co, Germany). The concentrations of total nitrogen (TN), total phosphorus (TP) of water, and the concentrations of TN, TP and organic matter (OM) of the sediment were analyzed in the laboratory according to the standard methods [7]. Dissolved organic carbon (DOC) of water was measured using a TOC analyzer (TOC-V CPN, Japan). All samples were analyzed at least three times, and the results were represented as “geometric mean ± geometric standard deviation”. All statistical analyses were with SPSS (Statistical Program for Social Sciences) 13.0 software, and significance levels regarded as significant at $p < 0.05$ (symbolized as *) and very significant at $p < 0.01$ (symbolized as **)

DNA extraction, bacterial 16S rRNA amplification and 454 pyrosequencing. Bacterial genomic DNA was extracted from 0.5-1.0 g samples of dried sediment [18]. DNA extraction was performed with an UltraClean soil DNA isolation kit according to the manufacturer’s instructions (MoBio Laboratory Inc., Solana Beach). A region ~526 bp in the 16S rRNA gene, covering the V1–V3 region was selected to construct 4 community library (S0 refer to library constructed from sediment samples at day 0; A20, B20 and C20 refer to libraries constructed from samples in 3 treatments at day 20, respectively.) through tag pyrosequencing. The bar-coded broadly conserved primers 27F and 533R containing the A and B sequencing adaptors (454 Life Sciences) were used to amplify this region. The forward primer B-27F was 5'-*CCTATCCCCTGTGTGCCTTGGCAGTCTCAGAGAGTTTGATCCTGGCTCAG*-3', where the sequence of the B adaptor is shown in italics and underlined. The reverse primer A-533R was 5'-*CCATCTCATCCCTGCGTGTCTCCGACTCAGNNNNNNNNNTTACCGCGGCTGCTGGCAC*-3',

where the sequence of the A adaptor is shown in italics and underlined and the number of sequences represent an eight-base sample specific barcode sequence. The PCR amplification was performed in triplicate with 50 µl reaction under the following conditions: 30 cycles of denaturation at 94°C for 30 s, annealing at 55 °C for 30 s, and extension at 72 °C for 30 s; with a final extension at 72 °C for 10 min. During amplification, negative controls were also performed. Triplicate PCR products of each sample were pooled together and purified by Agarose Gel DNA purification kit (DV805A, TaKaRa, Japan). Then, the PCR products from each sample were combined in equimolar ratio in a single tube. Amplicon pyrosequencing was performed from the A-end using a 454/Roche A sequencing primer kit on a Roche Genome Sequencer GS FLX Titanium platform at Majorbio Bio-Pharm Technology Co., Ltd., Shanghai, China. Each read file produced by a pyrosequencing run is associated with one quality file, which contains the quality score for each base.

Processing of pyrosequencing data. After sequencing was completed, all sequence reads were quality checked using Mothur software [17]. Any poor quality reads and primer dimers were removed. Raw sequence reads were filtered before subsequent analyses to minimize the effects of random sequencing errors. Briefly, we eliminated sequence reads that did not perfectly match the proximal PCR primer, were less than 200 bp or checked as chimeric artifact [12]. The rest of the sequences were trimmed and compared against the Bacterial Silva database (SILVA version 106; <http://www.arb-silva.de/documentation/background/release-106/>) as template, and a cutoff of 80% [17]. To normalize the sequencing depth of each sample, a randomly selected subset of 5553 sequences per sample were used for downstream analysis, based on the sample with the least number of sequences. Mothur was also used to construct the distance matrices, assign sequences to operational taxonomic units (OTUs, 97% similarity) with the furthest cluster method and calculate Chao1 richness estimators. β-Libshuff analysis was also performed by the Mothur program [17].

RESULTS AND DISCUSSION

Changes of 4 main physicochemical parameters in the sediment during the experiments are shown in Figure 1. The mean water temperature during the experiments ranged from 21 to 27 °C. The concentrations of TN, TP, OM and the value for pH in the sediment strongly increased in all 3 treatments during the 20 days of incubation except the TN concentration of the treatment A. In particular, the TN, TP concentrations in the treatment C, and OM concentration in the treatments A and C increased significantly. There were significant differences in increment of

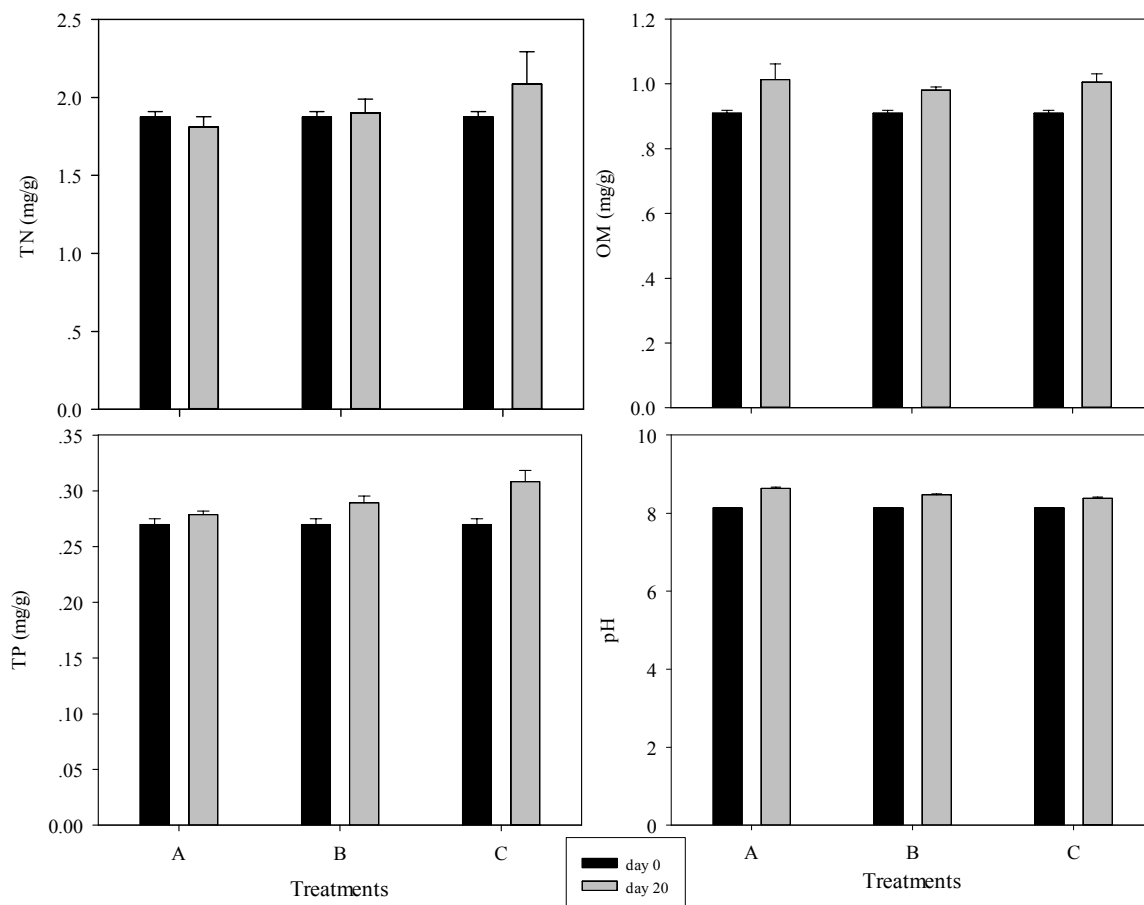


FIGURE 1

Changes in TN, TP, OM and pH of the sediment in the 3 treatments during the experiments: A treatments were the agricultural sewage, B treatments were the fishpond water, C treatments were the domestic sewage. Data are means and standard deviations from the triplicates.

TP and OM of sediment between 3 treatments except the TN concentration of the treatment A ($P < 0.05$); however, there were no significant differences in increment of TN and pH of sediment between 3 treatments (data not shown). In contrast, the TN, TP, OM concentrations and the value for pH in the water column decreased during the 20 days of incubation in all 3 treatments except the TN concentration of the treatments A and B (Figure 1). There were significant differences in decrement of TN, TP and OM of between 3 treatments ($P < 0.05$); however, there were no significant differences in decrement of pH between 3 treatments (data not shown). In consistent with our result, previous study also show that the change of sediment physicochemical parameters in our experiment may be caused by the particulate matter in the water body [13].

To identify the changes of BCC in sediments, a total of 24068 sequence reads with an average length of about 200 bp were generated in a single run of 454 pyrosequencing from each of the four sediment samples (Table 1). With phylotypes defined at the 97% sequences similarity level, we found that samples from treatments C, A and B on day 20 contained the

much higher OTUs numbers (860, 700 and 584, respectively), whereas the sample on day 0 contained the fewest (321). Rarefaction curves of OTUs showed that the sequencing depth is suitable for subsequent analysis (Figure 2). A comparison of the observed number of OTUs revealed that library A20 had lower coverage value (93.8%), whereas libraries S0 had the highest (97.3%). This comparison indicated that the C20 sample had higher diversity (Shannon indice = 5.18), whereas the B20 and S0 samples had the lower diversity (Shannon indices were 4.67 and 3.94, respectively; Table 1). These results showed that the distinct increase of the sediment bacterial diversity in all 3 treatments after the 20 days of incubation, suggesting import of different polluted water can increase the bacterial diversity of the sediment. Furthermore, the community from treatments C had the highest OTUs, Chao 1 estimator and Shannon indice (Table 2), indicating the highest bacterial phylotypes contained in the domestic sewage.

TABLE 1

Properties of the distributions of operational taxonomic units (OTUs, 97%) from four 16S rDNA clone libraries. S0 refer to library constructed from samples at day 0; A20, B20 and C20 refer to libraries constructed from samples in 3 treatments at day 20, respectively.

	S0	A20	B20	C20
Number of seqs	5934	5716	5553	6865
Coverage (%)	97.3	93.8	95.1	94.0
OTUs	321	700	584	860
Chao 1 estimator	601	1240	930	1401
non-parametric Shannon Index	3.94	4.99	4.67	5.18

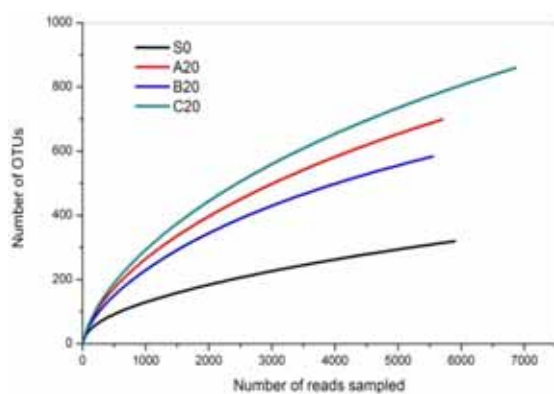


FIGURE 2

Rarefaction curves of OTUs sharing $\geq 97\%$ similarity for the sediment bacterial communities sampled from day 0 (S0) and 20 days incubation with agricultural sewage (A20), fishpond water (B20), and domestic sewage (C20).

TABLE 2

β -Libshuff comparisons of the heterogeneity of the four bacterial libraries. Libraries were considered significantly different when $p < 0.0042$ ($0.05/12 = 0.0042$, Singleton *et al.*, 2001). S0 refer to library constructed from samples at day 0; A20, B20 and C20 refer to libraries constructed from samples in 3 treatments at day 20, respectively.

Comparison	P-value	Significantly different
S0-A20	0.9965	Yes
A20-S0	<0.0001	Yes
S0-B20	0.0001	Yes
B20-S0	<0.0001	Yes
S0-C20	0.9797	Yes
C20-S0	<0.0001	Yes
A20-B20	0.7775	Yes
B20-A20	0.0034	Yes
A20-C20	0.2839	Yes
C20-A20	0.0020	Yes
B20-C20	0.2024	No
C20-B20	0.6932	No

β -Libshuff analysis showed that the bacterial community of S0 were significantly different from the other three communities which polluted water was imported and incubated for 20 days (Table 2). The sequencing results (Figure 3A) showed that the sediment bacterial community was dominated by *Proteobacteria* (46.12%), *Firmicutes* (41.69%), and *Bacteroidetes* (7.62%) on the first day (samples S0). However, after 20 days incubation, the sediment bacterial community in enclosure A (agricultural sewage) was dominated by *Firmicutes* (33.07%), *Proteobacteria* (26.49%), *Bacteroidetes* (17.70%) and *Actinobacteria* (6.23%); the sediment bacterial community in enclosure B (fishpond water) was dominated by *Firmicutes* (40.18%), *Proteobacteria* (21.39%), *Bacteroidetes* (18.71%) and *Actinobacteria* (6.88%) too; while the sediment bacterial community in enclosure C (domestic sewage) was also dominated by *Firmicutes* (27.59%), *Proteobacteria* (23.90%), *Bacteroidetes* (20.77%) and *Actinobacteria* (10.47%) (Figure 3A). From present work, we known that after 20 days of incubation, the relative abundance of *Proteobacteria* and *Firmicutes* decreased drastically, while the relative abundance of *Bacteroidetes*, *Actinobacteria* and *Acidobacteria* increased distinctively in all 3 treatments, suggesting the import of different polluted water can also strongly influence the composition of sediment bacterial community. This may be due to the import of bacteria from polluted water. Several studies have demonstrated significant influences by the import of allochthonous bacteria on bacterioplankton diversity in lakes [2, 9] and reservoirs [13]. The increased proportion of *Bacteroidetes* along with the increased nutrition in aquatic ecosystems was recorded in other studies as well [4, 26].

After 20 days of incubation, the relative abundances of *Alpha*- and *Gamma*-*proteobacteria* presented a slightly increase, while *Betaproteobacteria* decreased from 40.7% to 11.0% (Figure 3B). Most of the decreased *Betaproteobacteria* belong to *Oxalobacteraceae*, unclassified *Burkholderiales* and *Rhodocyclaceae*. In *Bacteroidetes*, the most abundant OTU (belong to *Chitinophagaceae*) increased 260% after 20 days incubation. In *Firmicutes*, however, while *Clostridiaceae* decreased from 34.4% of *Firmicutes* in S0 community to 3.5%-7.0% in other three communities, *Symbiobacterium* increased from 8.5% to 54.3%-65.9%. The variations of different bacterial groups were the response of sediment bacteria to the environmental change, i.e., the import of polluted water. There is a plausible explanation for this phenomenon. The surface sediment has a high level of organic matter particle exchange with the overlying water; sediment particles may be efficiently transported in to the overlying water, and particles of the water column may be mostly adsorbed on the surface sediment through exchange. These organic particles harbor numerous

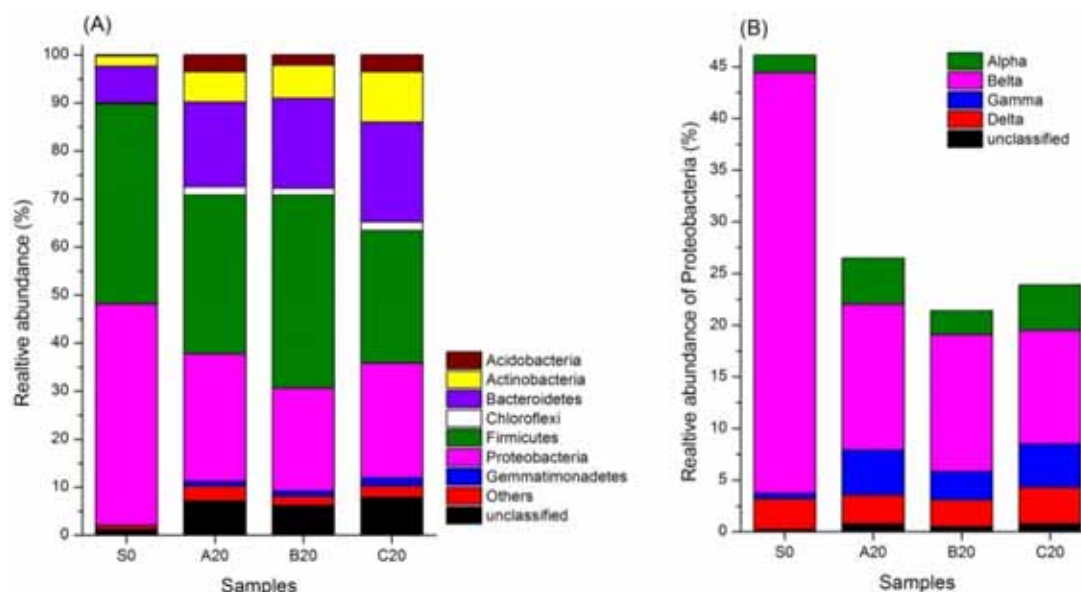


FIGURE 3
Relative abundance of bacterial phyla (A) and the relative abundance of *Proteobacteria* (B) of the sediment bacterial communities sampled from day 0 (S0) and 20 days incubation with agricultural sewage (A20), fishpond water (B20), and domestic sewage (C20).

bacteria [29], and dissolved nutrient and particulate organic matter fluxes between the sediment and the water column, which can be used by bacteria [1, 15, 27]. This is consistent with the increase of the OM concentration of the sediment in all enclosures. Previous study indicated that bacterioplankton community compositions in the lakes were to a high degree influenced by bacterial import [10]. It has been shown that the import of bacteria from the drainage area can be substantial [2] and, thus, can influence the composition of abundant bacterioplankton taxa in lakes and reservoirs [3, 8, 9, 13, 23].

Organic matter degradation by heterotrophic bacteria is known to be of key important for the carbon and energy flux in lakes and reservoirs [5]. *Acidobacteria* strains could be isolated under hypoxic atmosphere in a medium supplied with mixed carbon source, indicating that they could degrade some organic compounds under microaerophilic conditions [14]. *Chloroflexi* bacteria in the class, *Dehalococcoides*, could use chlorinated compounds as electron acceptors and degraded carbohydrates and amino acids [6]. In Lake Taihu, organic phosphorus degrading bacteria mainly include *Bacillus* spp., and inorganic phosphorus degrading bacteria mainly include *Pseudomonas* sp., often found around the colonial *Microcystis* [31].

The number of studies investigating the importance of cell import for bacterioplankton community structure in reservoirs is so far low. Still, it has been concluded that bacterioplankton communities can be influenced at times of high flow and in water bodies with short water retention time [3, 13]. Previous findings also indicate that the influence of import, in lakes of short turnover time, also remain after

the spring flood event [9]. Thus, although only three types of polluted water were studied here, the studies performed so far clearly show that bacterial cell import can be an important factor shaping aquatic bacterial communities of the sediment. To understand the sediment bacterial community dynamics, and in the long run the role of sediment bacterium in reservoir ecosystems, the importance of the up-stream regions for bacterioplankton community composition and function should therefore receive further attention.

CONCLUSIONS

After 20 days incubation with agricultural sewage, fishpond water, and domestic sewage, respectively, the diversity of surface sediment bacterial communities increased dramatically. Meanwhile, the relative abundance of *Beatproteobacteria* decreased from 40.7% to 11.0%, while the relative abundance of *Bacteroidetes*, *Actinobacteria* and *Acidobacteria* increased distinctively in all 3 mesocosms. Our study highlighted the important influence of importing of polluted water on the diversity and composition of surface sediment bacterial community in reservoir ecosystems.

ACKNOWLEDGEMENTS

This study was supported by the Youth Fund of Nanjing Institute of Geography and Limnology, Chinese Academy of Sciences, (No. NIGLAS2013QD10), the Natural Science Foundation of Jiangsu Province,

China (No. BK20151059), the National Natural Science Foundation of China (No. 41501101, 41471040, 41401617, 41301550, 41301544), the National Key Natural Science Foundation of China (No. 41471040, 41401617), and the National Key Basic Research Program, China (No. 2013FY112300). We are grateful to the editor and anonymous reviewers for their constructive comments and helpful suggestions.

REFERENCES

- [1] Arfi, R. and Bouvy, M. (1995) Size, composition and distribution of particles related to wind-induced resuspension in a shallow tropical lagoon. *J. Plankton. Res.* 17, 557–574.
- [2] Bergstrom, A.K. and Jasson, M. (2000) Bacterioplankton production in humic lake Ortrasket in relation to input of bacterial cells and input of allochthonous organic carbon. *Microb. Ecol.* 39, 101–115.
- [3] Crump, B.C. Kling, G.W. Bahr, M. and Hobbie, J.E. (2003) Bacterioplankton community shifts in an Arctic lake correlate with seasonal changes in organic matter source. *Appl. Environ. Microbiol.* 69, 2253–2268.
- [4] Dimitriu, P.A. Pinkart, H.C. Peyton, B.M. and Mormile, M. (2008) Spatial and temporal patterns in the microbial diversity of a meromictic soda lake in Washington State. *Appl. Environ. Microbiol.* 74, 4877–4888.
- [5] Hoch, B. Berger, B. Kavka, G. and Herndl, G. (1996) Influence of wastewater treatment on the microbial ecology of a large, temperate river system – the Danube River. *Hydrobiol.* 321, 205–218.
- [6] Inagaki, F. Nunoura, T. Nakagawa, S. Teske, A. Lever, M. Lauer, A. Suzuki, M. Takai, K. Delwiche, M. Colwell, F.S. Nealson, K.H. Horikoshi, K. D'Hondt, S. And Jørgensen, B.B. (2006) Biogeographical distribution and diversity of microbes in methane hydrate-bearing deep marine sediments on the Pacific Ocean-Margin. *PNAS.* 103, 2815–2820.
- [7] Jin, X.C. and Tu, Q.Y. (1990) Survey specification for lake eutrophication. China Beijing: Environmental Science Press, p. 208–230.
- [8] Lindström, E.S. (1998) Bacterioplankton community composition in a boreal forest lake. *FEMS. Microbiol. Ecol.* 27, 163–174.
- [9] Lindström, E.S. and Bergström, A.K. (2004) Influence of inlet bacteria on bacterioplankton assemblage composition in lakes of different hydraulic retention time. *Limnol. Oceanogr.* 49, 125–136.
- [10] Lindström, E.S. and Bergström, A.K. (2005) Community composition of bacterioplankton and cell transport in lakes in two different drainage areas. *Aquat. Sci.* 67, 210–219.
- [11] Lindström, E.S. Forslund, M. Algesten, G. and Bergström, A. (2006) External control of bacterial community structure in lakes. *Limnol. Oceanogr.* 51, 339–342.
- [12] Liu, R.Y. Yu, Z.S. Guo, H.G. Liu, M.M. Zhang, H.X. and Yang, M. (2012) Pyrosequencing analysis of eukaryotic and bacterial communities in faucet biofilms. *Sci. Total. Environ.* 435, 124–131.
- [13] Masin, M. Jezbera, J. Nedoma, J. Straskrabova, V. Hejzlar, J. and Simek, K. (2003) Changes in bacterial community composition and microbial activities along the longitudinal axis of two canyon-shaped reservoirs with different inflow loading. *Hydrobiol.* 504, 99–113.
- [14] Qu, J.H. Yuan, H.L. Wang, E.T. Li, C. Huang, H.Z. (2008) Bacterial diversity in sediments of the eutrophic Guanting Reservoir, China, estimated by analyses of 16S rDNA sequence. *Biodivers. Conserv.* 17, 1667–1683.
- [15] Pedersen, O.B. Christiansen, C. and Laursen, M.B. (1995) Windinduced long term increase and short term fluctuations of shallow water suspended matter and nutrient concentrations, Ringkøbing Fjord, Denmark. *Ophelia.* 41, 273–287.
- [16] Pu, P.M. Hu, W.P. Yan, J.S. Wang, G.X. and Hu, C.G. (1998) A physicoecological engineering experiment for water treatment in a hypertrophic lake in China. *Ecol. Eng.* 10, 79–90.
- [17] Schloss, P.D. Westcott, S.L. Ryabin, T. Hall, J.R. Hartmann, M. Hollister, E.B. Lesniewski, R.A. Oakley, B.B. Parks, D.H. Robinson, C.J. Sahl, J.W. Stres, B. Thallinger, G.G. Vanhorn, D.J. and Weber, C.F. (2009) Introducing mothur: open-source, platform-independent, community-supported software for describing and comparing microbial communities. *Appl. Environ. Microbiol.* 75, 7537–7541.
- [18] Shao, K.Q. Gao, G. Qin, B.Q. Tang, X.M. Wang, Y.P. Chi, K.X. and Dai, J.Y. (2011) Comparing sediment bacterial communities in the macrophyte-dominated and algae-dominated areas of eutrophic Lake Taihu, China. *Can. J. Microbiol.* 57(4), 263–272.
- [19] Shao, K.Q. Gao, G. Qin, B.Q. Tang, X.M. Chi, K.X. Yao, X. Dai, J.Y. (2012) Structural changes of the sediment bacterial community in Meiliang Bay of Lake Taihu, China, during typhoon Morakot, 2009. *J. Basic. Microb.* 52(1), 99–103.
- [20] Shao, K.Q. Gao, G. Chi, K.X. Qin, B.Q. Tang, X.M. Yao, X. and Dai, J.Y. (2013) Decomposition of *Microcystis* blooms: implications for the structure of the sediment bacterial community, as assessed by a mesocosm experiment in Lake Taihu, China. *J. Basic. Microb.* 53, 549–554.
- [21] Shao, K.Q. Gao, G. Wang, Y.P. Tang, X.M. and Qin, B.Q. (2013) Vertical diversity of sediment bacterial communities in two different trophic

- states of the eutrophic Lake Taihu, China. *J. Environ. Sci-China*. 25(6), 1186-1194.
- [22] Singleton, D.R. Furlong, M.A. Rathbun, S.L. and Whitman, W.B. (2001) Quantitative comparisons of 16S rRNA gene sequence libraries from environmental samples. *Appl. Environ. Microbiol.* 67, 4374–4376.
- [23] Stepanauskas, R. Moran, M.A. Bergamaschi, B.A. and Hollibaugh, J.T. (2003) Covariance of bacterioplankton composition and environmental variables in a temperate delta system. *Aquat. Microb. Ecol.* 31, 85–98.
- [24] Somerville, C.C. Knight, I.T. Straube, W.L. and Colwell, R.T. (1989) Simple, rapid method for direct isolation of nucleic acids from aquatic environments. *Appl. Environ. Microbiol.* 55, 548–554.
- [25] Tao, Q.H. and Tang, H.X. (2004) Effect of dye compounds on the adsorption of atrazine by natural sediment. *Chemosphere*. 56, 31–38.
- [26] Vieira, R.P. Gonzalez, A.M. Cardoso, A.M. Oliverira, D.N. Albano, R.M. Clementino, M.M. Martins, O.B. and Paranhos, R. (2008) Relationships between bacterial diversity and environmental variables in a tropical marine environment, Rio de Janeiro. *Environ. Microbiol.* 10, 189–199.
- [27] Wainright, S.C. (1990) Sediment-to-water fluxes of particulate material and microbes by resuspension and their contribution to the planktonic food web. *Mar. Ecol. Progr. Ser.* 62, 271–281.
- [28] Wobus, A. Bleul, C. Maassen, S. Scheerer, C. Schuppler, M. Jacobs, E. and Rske, I. (2003) Microbial diversity and functional characterization of sediments from reservoirs of different trophic state. *FEMS. Microbiol. Ecol.* 46, 331–347.
- [29] Wörner, U. Zimmermann-Timm, H. Kausch, H. (2002) Aggregate-associated bacteria and heterotrophic flagellates in the River Elbe-their relative significance along the longitudinal profile from km 46 to km 583. *Int. Rev. Hydrobiol.* 87, 255–266.
- [30] Yang, L.Y. (2004) Research on nutrient dynamics in the process of growth and metabolism of the dominated cyanobacteria in Lake Taihu. In: *Evolution Process and Mechanism of Water Environment in Lake Taihu* (Qin BQ, Hu WP, Chen WM., eds). Beijing: Science Press. 209–217
- [31] Zhang, S.Z. Wang, S.X. and Shan, X.Q. (2002) Distribution and speciation of heavy metals in surface sediments from Guanting Reservoir, Beijing. *J Environ Sci Health A* 37: 465–478.

Received: 19.10.2015

Accepted: 14.06.2017

CORRESPONDING AUTHOR

Guang Gao

Taihu Laboratory for Lake Ecosystem Research, State Key Laboratory of Lake Science and Environment, Nanjing Institute of Geography and Limnology, Chinese Academy of Sciences, Nanjing 210008, China

e-mail: guanggao@niglas.ac.cn

HIGH METAL ACCUMULATION IN BITTER GOURD IRRIGATED WITH SEWAGE WATER CAN CAUSE HEALTH HAZARDS

Zafar Iqbal Khan¹, Kafeel Ahmad¹, Rukhsana Parveen¹, Humayun Bashir¹, Naunain Mehmood²

¹Department of Botany, University of Sargodha, Sargodha, Pakistan

²Department of Zoology, University of Sargodha, Sargodha, Pakistan

ABSTRACT

The present study was conducted to determine the amount of heavy metalloids/metals in the vegetable and soil supplied with domestic wastewater. Advanced techniques to calculate the enrichment coefficient, health risk index, transfer coefficients and pollution load index were employed. All samples (vegetable and soil) were exposed to a process of wet digestion and metal analysis using an atomic absorption spectrophotometer. The concentrations of all heavy metals determined in the soil were considerably below the maximum permissible limits (MPL) in the study area. However, the concentrations of Mo, As, Mn, Ni and Zn were higher than the MPL in the bitter gourd. Highest enrichment coefficient and transfer coefficient were revealed for Cr and Cd, respectively. Higher level of pollution load index was found for Cd, Pb, Mo, Cu, Co, As and Se suggesting that the quality of the soil in the study area is inappropriate for vegetable growth and agricultural use. Only Co, Fe, Cr and Cu had health risk index below the limit which could be considered safe.

KEYWORDS:

Heavy metals, *Momordica charantia*, pollution load index, health risk index

INTRODUCTION

The sewage waste (domestic and industrial), is a major source of toxic metals accumulation in the soils used for agricultural purposes in different countries. Pakistani crops are under serious water stress due to the threat of changing climatic conditions [1-2]. In Pakistan, sewage waste water is also used for irrigation of crops or as supplemental irrigation, particularly when there is a shortage of water. Due to high accumulation of heavy metals, there is a possibility of contamination in the soil to plant continuum [3]. Use of contaminated fruits and vegetables adversely affects health of living organisms [4]. A rampant increase of heavy metal toxicity increases the awareness about risks linked with heavy metal accu-

mulation not only in soil but also in water and different plant [5]. Metals such as mercury, lead, copper, and cadmium are severely toxic as these are directly involved in health hazards [6].

Although various metalloids and metals like zinc, copper, manganese and iron are important for optimum functioning of biological system, but their intake in high concentration may cause deleterious effects on plants as well as animals [7]. Sewage wastes present in surface soil contains high concentration of heavy metals including Ni, Cu, Pb, Cd, Cr, Mn and Zn [8]. High levels of lead adversely affect bone joints, reproduction and cardiovascular system, kidney and hemoglobin synthesis [9]. Similarly, high levels of nickel cause giddiness, shortness of breath, vomiting, diarrhea, abdominal pain, nausea, headache and cough [10]. It is observed that after 3-12 h after ingestion of zinc, mass poisoning, nausea, stomach cramp, fever, vomiting, diarrhea and bleeding have been reported. High intake of zinc, more than 500 mg, may cause vomiting [11]. High concentration of chromium (Cr) is also toxic for the growth and development of number of plants. However, inter- or intra-specific responses have been observed in different plants to high accumulation of Cr [12]. The major sources of Cd and Zn are municipal and industrial waste waters. Higher arsenic (Ar) concentration in the soil interferes with plant growth [13].

Bitter gourd (*Momordica charantia*) is an important medicinal plant which is usually referred to the patients suffering in diabetes or microbial infections [14] hepatitis, parasitic diseases and fevers [15]. Fresh vegetables contain heavy metals contamination in their tissues due to Pb, Cu, Cr, Cd, Se, Ni and Co [16]. Of different metals, Pb mostly accumulates in the leaves and Ni, Cu, and Zn accumulate in the roots of vegetables grown in sewage water [17]. Accumulation of Al and Fe is very low in leaves while the reverse is true for Mn and Cu. Sharma et al. [18] reported that Pb, Ni, and Cd mainly accumulate in the edible parts of vegetables which are frequently irrigated with sewage water. Enrichment coefficients (EC) of Zn metal in leaf/root indicated that the intake capacity of this metal is more severe than any other metals within the vegetables.

The current study was designed to determine

the levels of different heavy metalloids and metals not only in the soil but also in the edible part of vegetable of two study sites in District Jhang, Punjab, Pakistan. In this study it was also determined the health risks, pollution load index, enrichment coefficient for vegetable-soil, and correlation between concentrations of different metals.

MATERIALS AND METHODS

The present study was conducted in District Jhang, Punjab, Pakistan. Two sites treated with sewage waste water were selected for the study. Distance between the two study sites was about one kilometer. District Jhang is comprised of diverse soil conditions from fertile to sandy deserts. The mean temperature during the month of June and January was 35°C and 12°C in 2013, respectively. Bitter gourd is grown commonly in this region, as this vegetable is utilized largely by the people of this region.

Collection and processing of soil samples.

From each study site, soil (silt-loam) samples (1kg) were collected from five different places 10 feet apart from each other. At the depth of 20 cm from the site of vegetable sampling, soil samples were collected. Before analyses all soil samples were sun dried followed by oven-drying at 75°C for three days. After pulverizing, these samples were kept in the plastic bags for the determination of different metals. The soil (1000 mg) was added to a glass flask containing H₂O₂ (8 mL) and H₂SO₄ (4 mL). All flasks were kept in the digestion chamber for one hour after adjusting its temperature at 250°C. After it, again H₂O₂ (2 ml) were poured to each flask by removing from chamber for a short while. All samples were kept in the digestion chamber at same temperature till discoloration. Then, after cooling at room temperature, volume upto 50 ml using distilled water was made.

Collection and processing of vegetable samples. Vegetable samples (edible part) were also collected randomly from five different places within each study site [19]. After washing carefully with water, the fresh vegetable samples were air dried. Then, all vegetable samples were kept in an oven for 6 days at 70°C. Dry vegetables were crushed and passed through a 1mm sieve prior o analysis. 1.0 g sample was taken in a glass flask and mixed with 2 ml of H₂SO₄ and 4 ml of H₂O₂ and placed in a digestion chamber for 30 minutes for wet acid digestion.

Metal analyses. The digested samples (soil and

vegetable) were run on an atomic absorption spectrophotometer (Perkin-Elmer Corp., 1980). The metals and metalloids under study were arsenic (As), cadmium (Cd), chromium (Cr), copper (Cu), iron (Fe), manganese (Mn), nickel (Ni), lead (Pb), selenium (Se), and zinc (Zn). An atomic absorption spectrophotometer equipped with a graphite furnace and D2 corrector (Perkin-Elmer Model 503) was used to determine soil and vegetable Co and Mo contents.

Se and As in soil and vegetable samples were determined by a fluorometric method. Precision and accuracy of analyses was ensured through repeated samples against National Institute of Standard Technology, Standard Reference Material (SRM 1570) for all the metals and metalloids

Statistical analyses. Normality of the data was checked before analyzing the data statistically. Parametric tests were applied on normally distributed data. Two sample t-test was employed to compare the levels of metals in the vegetable as well as soil of the two study sites. Pearson's correlation was employed to find out the relationship of metal concentration in the soil and vegetable. Statistical software SPSS (version 17) was used for analyzing the data. Difference was considered significant if P-values were less than 0.05.

Transfer coefficient for edible/root system (TC). To assess the concentrations of metals from root to edible portion, TC was calculated following [17].

Enrichment coefficient for vegetable/soil system (EC). By following the Antonidias and Alloway [20] procedure, a quantitative analysis of the interaction between corresponding soils and metal levels in the vegetable were determined by calculating EC for the vegetable/soil continuum.

Pollution load index (PLI). By following the procedure proposed by Liu et al. [21], PLI of metal concentrations were calculated as in Tabke 1.
 $PLI = \text{Metal present in soil} / \text{Reference value of the metal in soil}$

Health risk index (HRI). Health risk index (HRI) was obtained using the following formula:

$$HRI = DIM/RDf$$

Daily intake of metal (DIM) = C_{metal} × D_{food} intake / Baverage weight

Where Baverage weight= average body weight (kg); C_{metal}=Metal contents in vegetable (mg/kg) and D_{food} intake=Daily intake of vegetable (kg/day/person).

TABLE 1
Comparison of metals in soil collected from two different sites.

Metals and metalloids (mg/kg)	Sampling sites		Permissible maximum limit(PML)	t-value	P-value
	Site I (Means ±SE)	Site II (Means ±SE)			
Mn	14.51±0.39	15.96±0.26	80	-1.55	0.19
Zn	8.06±1.12	4.61±0.22	200	21.77	< 0.001
Se	1.79±0.21	1.80±0.23	3	-3.34	0.05
As	27.04±0.66	30.94±2.22	40	-10.98	< 0.001
Co	15.70±0.46	13.57±0.22	65	10.10	0.001
Fe	21.27±1.44	23.90±1.77	21000	-2.51	0.05
Cd	15.60±0.36	12.60±0.58	3	21.79	< 0.001
Cr	0.17±0.02	0.15±0.02	400	1.96	0.10
Ni	2.85±0.22	2.62±0.21	50	1.87	0.11
Cu	13.38±0.72	14.57±0.50	50	1.51	4.30
Mo	9.38±0.58	10.98±0.35	40	-0.96	0.40
Pb	13.84±0.81	16.65±0.79	300	9.01	< 0.001

Note: P-values less than 0.05 showed significant difference.

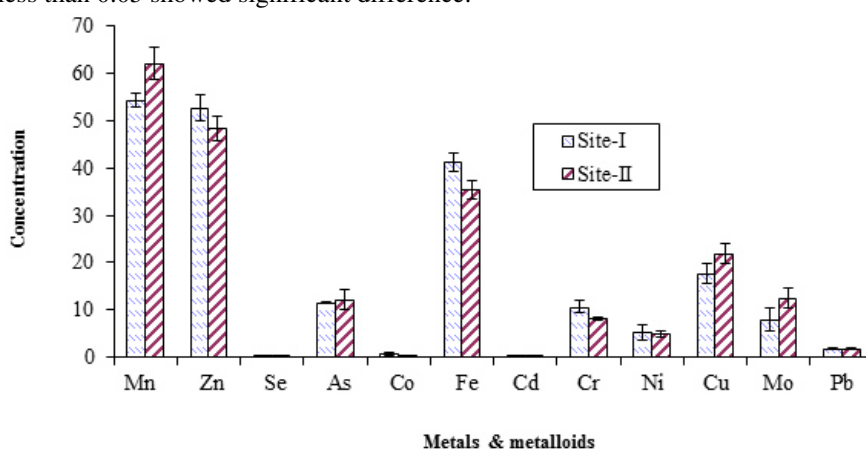


FIGURE 1

Concentration of metals and metalloids (mg / kg drywt.) in *Momordicacharantia* obtained from two different sites

RESULTS

During the present study, it was observed that soil of both study sites contained the concentration of metalloids or metals less than the maximum permissible limits (MPL; Table 1). Of both sites, lower concentrations of Zn, Co, and Cd were observed at site-II as compared to site-I. However, the levels of Pb, As and Fe were greater at site-II. Statistically, the levels of Se, Cr, Ni, Cu, Mo and Mn were almost same at both study sites (Table 1).

The concentrations of Zn, Co, Fe, Cr and Pb were considerably more in edible part of *M. charantia* available at site-I, while the concentrations of

Mn, Mo and Cu in that obtained from site-II (Figure 1). However, the levels of Se, As, Cd and Ni remained almost unchanged between both locations (Figure 1). The levels of Mo, Mn, Ni, As and Zn were greater than MPL.

High enrichment coefficient was obtained for Cr (Table 2), however, highest transfer coefficient was recorded for Cd (Table 3). There was a non-significant positive correlation between Pb, Se, Co, Mn, Zn, Ni, As and Mo of soil and those of vegetable (Table 4). However, a non-significant negative correlation was recorded in the levels of Cr, Fe, Cd and Cu of soil and vegetable (Table 4).

TABLE 2
Enrichment coefficient (EC) of metals from soil to vegetable root

Sam- pling area	Metal elements											
	Mn	Zn	Se	As	Co	Fe	Cd	Cr	Ni	Cu	Mo	Pb
Site I	4.23	5.67	0.54	0.51	0.039	1.96	0.016	73.44	1.24	1.45	3.45	0.127
Site II	4.20	13.45	0.243	0.332	0.056	1.64	0.017	80.9	1.54	1.37	4.76	0.133

TABLE 3
Transfer coefficient (TC) of each metal in *Momordica charantia* from roots to vegetables

Sampling area	Metal elements											
	Mn	Zn	Se	As	Co	Fe	Cd	Cr	Ni	Cu	Mo	Pb
Site I	1.062	0.989	0.587	1.134	1.155	1.055	1.2822	0.977	1.45	0.765	0.667	1.132
Site II	1.341	0.976	1.1891	1.412	0.755	0.976	1.755	0.765	1.187	1.087	1.178	0.87

TABLE 4
Relationship between soil and bittergourd elements levels

Metal elements	Mn	Zn	Se	As	Co	Fe	Cd	Cr	Ni	Cu	Mo	Pb
Soil-vegetable (r)	0.564	0.532	0.643	0.477	0.080	0.244	0.179	0.344	0.512	0.486	0.488	0.157

Note: Correlation is significant at 0.05.

TABLE 5
Pollution Load Index for elements (mg/kg) in soil with vegetable

Sampling area	Metal elements											
	Mn	Zn	Se	As	Co	Fe	Cd	Cr	Ni	Cu	Mo	Pb
Site I	0.310	0.182	2.557	0.932	1.725	0.379	10.469	0.016	0.314	1.6004	3.126	1.698
Site II	0.341	0.104	2.571	1.066	1.491	0.4261	8.456	0.014	0.289	1.742	3.666	2.042

TABLE 6
Healthiness hazard ingestion of metals via intake of vegetable from waste water irrigated sites

Sampling area	Metal elements											
	Mn	Zn	Se	As	Co	Fe	Cd	Cr	Ni	Cu	Mo	Pb
Site I	7.616	1.009	55.64	22.11	0.092	0.3382	2.1275	0.040	1.506	0.0076	5.130	2.957
Site II	8.714	0.927	0.552	23.21	0.053	0.2922	2.2425	0.031	1.414	0.0093	8.005	0.328

Variations in pollution load index of metal elements between the two study sites were observed, but these were statistically non-significant for all metals (Table 5). Variation in HRI of metal elements between the two study sites was observed and of all metals highest HRI at Site-I was observed for Se (55.64) and at Site-II for As (23.21; Table 6).

DISCUSSION

The levels of elements in the soil of both study places were under the secure limits. One possible explanation of lower levels of heavy metals is leaching of heavy metals deep in soil. The load of metalloids or metals at site-II was lower than that of site-I. This difference could be related to difference in ecological factors along with agricultural implementations at both study sites.

In the present study, we found that only the level of Cd was above the MPL (Table 1). We also found during the study that the study area is heavily loaded with Cu while it contained too low contents of Cr. The contents of Cd in the agricultural soils depend on a variety of factors [22] including the deposition of nutrients from the atmosphere, the concentration present in the parent rocks that change into

soil and/or the quantity of fertilizers. Hanaa et al. [23] also reported higher Cd level in industrial and sludge contaminated soil. We also observed that waste water treated soil under *M. charantia* possessed greater contents of Cd as compared to those determined in Faisalabad by Murtaza et al. [24].

The concentrations of As, Ni, Mn, Zn and Mo in the tissues of *M. charantia* were above the range of MPL. However, the concentration of Co was lower than the optimum level. So, high concentrations of metals in the vegetable tissues could be related to the contamination in the study sites due to presence of risky heavy metals in the frequently used sewage waste water. The level of Zn (111.02-123.07 mg/kg) in the current study was lower than the level observed by Uboh et al. [25] in pumpkin collected from the agricultural site of Jhang district. The level of Cd and Pb in the vegetable tissue was lower than the permissible level i.e., 0.5-2.0 mg/kg referred by Codex and Alimentarius [26]. Different environmental factors including soil reactions, redox potential, physiochemical properties, soil type and organic-matter affect the accumulation of metal elements in soil [27].

At both sites, the EC (enrichment coefficient) was higher for Cr (Table 2). It has been found that solubility of metals and nature of soil affects the EC.

Maximum value of EC for Cr shows that it is more mobile because of which its retention was less in soil. However, lower value of EC for Cd indicates that it is less mobile and binds to the soil. Previously, Brown et al. [28] proposed that the value of EC more than 1.0 in any plant indicates that the plant has the capacity to obtain metal from soil and transfer to the upper parts of the plants.

According to Zhao et al. [29], the transfer coefficient (TC) above 1.0 shows better ability of a plant to transfer metals from root to upper parts. The concentrations of all metals were less in shoots as compared to those in roots of the vegetable. Table 3 indicated that the range for all metals was observed to be 0.572-1.688 mg/kg TC in the present study. Highest TC was recorded for Cd in the present study. We found a positive relationship between the vegetable and soil for Se, As, Cu, Pb, Mo, Mn and Zn (Table 4). However, there was a negative relationship between the vegetable and the soil for Cu, Cd, Cr, and Fe in the present study. Current findings were similar in bitter melon collected from different sites of India. Cu showed a negative correlation, while Ni indicated a positive relationship in bitter melon [30]. A positive or negative correlation between the heavy metals in plants and soil has been observed due to differential uptake of different metals.

The pollution load index (PLI) is helpful to determine the level of metal in soil. Values of PLI suggest us whether or not the soil condition is favorable for agricultural purposes including for growth of crops and vegetables. In this study we recorded highest PLI for Cd at both study sites. The values of Pb, Mo, Cu, Co, As and Se also have PLI values higher than 1. High values of PLI at the study sites might be due to anthropogenic activities since both study sites have higher human population. Singh et al. [31] also recorded higher metal pollution index in *M. charantia* and recommended that this vegetable is a higher accumulator of heavy metals in the edible tissues, so its frequent use can cause health risk in humans. The results of present study also confirmed that the area under study is facing high Cd contents. This is happening due to increased rate of irrigation of the study area with non-treated industrial or sewage waste water.

In this study we found that health risk index (HRI) of heavy metals due to excessive intake of bitter melon varied from 0.0076-55.64. According to USEPA [32], HRI greater than 1 can cause health problems for humans. Normally heavy metal accumulation occurs in the body through food intake, however, its effect can take several years to appear in consumers. In the present study, we found that only Co, Fe, Cr and Cu have health risk index less than 1 and can be considered safe, while other elements are lethal.

ACKNOWLEDGEMENTS

The financial support by the Higher Education Commission through a research project # 2484/13 to the first and second authors is gratefully acknowledged. The authors also appreciate all the supporters of this project and the referees for their constructive comments.

Declaration of Interest. It is further declared that there is no conflict on the subject of this article's publication.

REFERENCES

- [1] Noorka, I.R. and M. Afzal. (2009). Global climatic and environmental change impact on agricultural research challenges and wheat productivity in Pakistan. *Earth Sci. Front.*, 16: 99-103.
- [2] Ali, A, M. Afzal, I. R.Noorka, E. Safdar and M.Ahmad. (2011). Sunflower (*Helianthus annuus* L.) hybrids performance at different plant spacing under agro-ecological conditions of Sargodha, Pakistan. *International Conference on Food Engineering and Biotechnology. IPCBEE* 9: 317- 322 .IACSIT Press, Singapore.
- [3] Fatoki, S.O., P. Gogwana, A.O. Ogunfowokan (2003). Pollution assessment in the Keiskamma River and in the impoundment downstream. *Water SA*. 29(3):183-187.
- [4] Sajjad, K., R. Farooq, S. Shahbaz, M.A. Khan and M. Sadique. (2009). Health risk assessment of heavy metals for population via consumption of vegetables. *World App. Sci. J.*, 6: 1602-1606.
- [5] Ahmed, G., M.K. Uddin, G.M. Khan, M.S. Rahman and D.A. Chowdhury. (2009). Distribution of trace metal pollutants in surface water system connected to effluent disposal points of Dhaka Export Processing Zone (DEPZ), Bangladesh: A statistical approach. *J. Nat. Sci. Sustain. Technol.*, 3: 293-304.
- [6] Sharma, R.K., M. Agrawal and F.M. Marshall. (2009). Heavy metals in vegetables collected from production and market sites of a tropical urban area of India. *Food Chem. Toxicol.*, 47: 583-591.
- [7] Wright, R.O. and A. Baccarelli,(2007). Metals and neurotoxicology. *J Nutr.*, 137: 2809-2813.
- [8] Luo, X., S. Yu, Y. Zhu and X. Li. (2012). Trace metal contamination in urban soils of China. *Sci. Total Environ.*, 442: 17-30.
- [9] Ogwuegbu, M.O.C. and W. Muhanga. (2005). Investigation of lead concentration in the blood of people in the copper belt province of Zambia. *J. Environ.*, 1: 66-75
- [10] Sunderman, F.W., B. Dingle, S.M. Hopfer and T. Swift.(1988). Acute nickel toxicity in electro-

- plating workers who accidentally ingested a solution of nickel sulphate and nickel chloride. *Am. J. Ind. Med.*, 14: 257-266.
- [11] Elinder C.G. (1986). Zinc. In L. Friberg, F.F. Nordberg and V. Vouk, editors. *Handbook on the toxicology of metals; Volume II*. Elsevier Science Publishers BV, 664-79.
- [12] Shanker, A.K., C. Cervantes, H. Loza-Tavera and S. (2005). Avudainayagam: Chromium toxicity in plants. *Environ. Int.*, 31, 739-753.
- [13] Abedin, M.J., J. Feldmann and A.A. Meharg. (2002). Uptake kinetics of arsenic species in rice plants. *Plant Physiol.*, 128: 1120-1128.
- [14] Beloin, N., M. Cbeassor, K. Akpagana, J. Hudson, K. Sousse, K. Koumaglo and J.T. Amason. (2005). Ethnomedicinal uses of *Momordica charontia* (Cucurbitaceae) in Togo and relation to its phytochemistry and biological activity. *J. Ethnopharmacol.*, 96:49-55.
- [15] Behera, T.K., J.E. Staub, S. Bohera and P.W. Simon. (2008c). Bitter melon and human health. *Med. Aram. Plant Sci. Biotechnol.*, 1:224-226.
- [16] Bigdeli, M. and M. Seilsepour. (2008). Investigation of metals accumulation in some vegetables irrigated with waste water in Shahre Rey-Iran and toxicological implications. *Am-Eur. J. Agric. Environ. Sci.*, 4 (1): 86-92.
- [17] Chao, W., L. Xiao-Chen, Z. Li-Min, W. Pei-Fang, and G. Zhi-Yong. (2007). Pb, Cu, Zn and Ni concentrations in vegetables in relation to their extractable fractions in soils in suburban areas of Nanjing, China. *Polish J. Environ. Stud.*, 16: 199-207.
- [18] Sharma, R.K., M. Agrawal and F. Marshall. (2006). Heavy metal contamination of soil and vegetables in suburban areas of Varanasi, India. *Ecotoxicol. Environ. Safety*, 66(2): 258-266.
- [19] Campbell, C.D. and C.O. Planks. (1992). An assessment of the hazards of lead in food. *Regul. Toxicol. Pharmacol.*, 16: 265-277.
- [20] Antoniadis, V., and B.J. Alloway. (2001). Availability of Cd, Ni and Zn to ryegrass in sewage sludge-treated soils at different temperatures. *Water Air Soil Pollut.*, 132(3-4): 201-214.
- [21] Liu, W., J.Z. Zhao, Z.Y. Ouyang, L. Soderlund and G. H. Liu. (2005). Impacts of sewage irrigation on heavy metal distribution and contamination in Beijing, China. *Environ. Int.*, 31: 805-812.
- [22] Sharma, R.K., M. Agrawal and F.M. Marshall. (2008a). Heavy metals (Cu, Cd, Zn and Pb) contamination of vegetables in urban India: A case study in Varanasi. *Environ. Pollut.*, 154: 254-263.
- [23] Hanaa, M., A. Eweida and A. Farag (2000). Heavy metals in drinking water and their environmental impact on human health. *International Conference on Environmental Hazards Mitigation*, Cairo University, Egypt, pp. 542-556.
- [24] Murtaza, G., A. Ghafoor, M. Qadir and M.K. Rashid. (2003). Accumulation and bioavailability of Cd, Co and Mn in soils and vegetables irrigated with city effluents. *Pak. J. Agric. Sci.*, 40 (1-2): 18-24.
- [25] Uboh, F.E., M.I. Akpanabiatu, E.E. Edet and I.E. Okon, (2011). Distribution of heavy metals in fluted pumpkin (*Telfeiria occidentalis*) leaves planted at different distances away from the traffic congested highways. *Int. J. Adv. Biotechnol. Res.*, 2: 250-256.
- [26] Codex Alimentarius Commission. (2001). *Joint FAO/WHO Food Standards Programme*, FAO, 00153 Rome, Italy.
- [27] Otitoju, O. and I.N.E. Onwurah. (2005). Super-oxide dismutase (SOD) activity and serum calcium level in rats exposed to a locally produced insect powder "Rambo". *Anim. Res. J.*, 2(1): 261-266.
- [28] Brown, S.L., R.L. Chaney, J.S. Angle and A.J.M. Baker. (1995). Zinc and cadmium uptake by hyperaccumulator *Thlaspi caerulescens* and metal-tolerant *Silene vulgaris* grown on sludge-amended soils. *Environ. Sci. Technol.*, 29: 1581-1585.
- [29] Zhao, F.J., R.E. Hamon, E. Lombi, M.J. Mclaughlin and S.P. McGrath. (2002). Characteristics of cadmium uptake in two constricting ecotypes of hyper-accumulator *Thlaspi caerulescens*. *J. Exp. Bot.*, 53: 535-543.
- [30] Sharma, R.K., M. Agrawal and F.M. Marshall. (2008b). Heavy metals (Cu, Cd, Zn and Pb) contamination of vegetables in Urban India: a case study in Varanasi. *Environ. Pollut.*, 154: 254-263.
- [31] Singh, A., R.K. Sharma, M. Agarwal and F.M. Marshall. (2010a). Health risk assessment of heavy metals via dietary intake of foodstuffs, from waste water irrigated site of dry tropical area of India. *Food Chem. Toxicol.*, 48: 611-619.
- [32] USEPA (US Environmental Protection Agency). (2006). *Integrated risk information system (2010)*. Voiculescu N., Hoza D., Spiță V., *Minerals elements in fruits*, Ed. Elisavaros, Bucharest (Published in Romanian), pp. 176.

Received: 24.11.2015

Accepted: 05.09.2016

CORRESPONDING AUTHOR

Zafar Iqbal Khan

Department of Botany, University of Sargodha, Sargodha, Pakistan

Email: zikhan11@gmail.com

FRACTIONATION OF Cd AND Pb IN AGRICULTURAL SOIL AND THEIR DETERMINATIONS USING INDUCTIVELY COUPLED PLASMA-OPTICAL EMISSION SPECTROMETRY

Sukran Akkus Ozen¹, Mehmet Yaman^{2,*}

¹ TUBITAK-UME, Chemistry Department, Kocaeli-Turkey

² Firat University, Sciences Faculty, Department of Chemistry, Elazig-Turkey

ABSTRACT

In this study, five-step sequential extraction procedures were employed to the soils that may be polluted by anthropogenic activities, to determine five species of Cd and Pb in agricultural soils. Soil samples were collected from twelve points on an agricultural area that was located near an airport and intercity roads in Elazig-Turkey. The species including exchangeable, organically bounded, carbonate bounded, adsorbed species on Fe and Mn oxides and residual species except silicates of Cd and Pb were extracted into solution by using CaCl₂, Na₄P₂O₇, Na₂EDTA, NH₂OH.HCl, HNO₃-H₂O₂, respectively. Mobile and total metal concentrations in soils fractions were determined by using inductively coupled plasma-optical emission spectrometry (ICP-OES). Total Cd and Pb concentrations were found in the range of 0.24-0.90 mg kg⁻¹ and 9.4-40.9 mg kg⁻¹, respectively. It was observed that total concentrations of the metals in all of the samples were lower than the permitted values. The sum of percentages of the mobile metals fractions in the first three steps was found to be lower than 50% except for Pb in one sample.

KEYWORDS:

Speciation; Toxic metals; Pollution; ICP-OES; Metal mobility

INTRODUCTION

The increased occurrence of metal pollution in the environment has been associated with anthropogenic activities as effluents and emissions from mines and smelters often contain elevated concentrations of toxic metals including cadmium (Cd) and lead (Pb). Heavy metals seem as a key marker because they are not degradable by natural processes unlike organic pollutants. Soil pollution is a result of many factors including atmospheric deposition and anthropogenic activities such as mining, unconscious use of fertilizers and chemicals, discharge of domestic and industrial wastes and municipal sewage sludge [1-2]. Heavy metals in-

cluding Pb and Cd have toxic effects on animals and human in case of long term exposure [3-6]. Toxicity, mobility, accumulation and bioavailability of metals depend strongly on their chemical forms in soil fractions as well as concentrations [7-9]. To predict metal uptake by plants, it is essential to know which metal species are taken up. Sequential extraction is a method which has commonly been used for recent three decades to determine the bio-accessible and immobile metal fractions particularly in contaminated soils in residential, industrial, and roadside area [10]. There is highly interested in determination of toxic heavy metals in soil and plant matrices to monitor the extent of environmental pollution [11-16]. National and international authorities setted maximum allowable concentrations (MAC) of Cd and Pb in agricultural soil as follow: 1 and 50 mg kg⁻¹ for pH=5-6 and 3 and 300 mg kg⁻¹ for pH>6 in Turkey, and in ranges of 2-5 and 100-500 mg kg⁻¹ in other countries, respectively [17-18].

Briefly, the knowledge of total metal concentrations in soil is not providing sufficient information to characterize the behavior of heavy metals in soils because these values do not represent mobile metal ions [19]. Importance of the fate and transport of heavy metals depends on their chemical form and speciation. It was highlighted in literature that heavy metals in immobile form in unpolluted soils are mainly bound to silicates, whereas polluted soils include metals at mobile forms bounded to different soil fractions [20]. The metal uptake of plants is affected by element mobility in soil and essentiality for plants. Plants can easily uptake the bioavailable metals at mobile forms in the soil phases such as exchangeable, organically bounded and bound to carbonate. It was shown that more than 40% of the total concentrations for Cd, Pb, Ni, Cu, and Zn can be counted as part of the mobile fractions [20]. To determine metal concentrations in mobile forms, the general approach has been to separate the soil into different fractions and, by analyzing each fraction, determining the amount of element combined or associated with each soil fraction or phase [7, 8, 20-21].

The use of fractionation procedures permits the determination of how much of the total analyte

is available for plants or is accessible to the environment [9, 22-26]. Thus, in all sequential extraction schemes, a series of reagents is applied to the same sample to sub-divide the total metal content. In Tessier procedure, soil was classified into five fractions: exchangeable, carbonate, adsorbed on Fe-Mn oxides, organically bounded, and residual fractions [22]. In 1987, a project by EC (European Community) Standards, Measurement and Testing Program, formerly Commission of the European Communities Bureau of Reference (BCR), harmonized method for soil and sediment was developed to consist of three-step procedure using: acetic acid (step 1); hydroxylamine (step 2); and, hydrogen peroxide (step 3) [23]. Due to irreproducibility in step 2, it was revised for selective extractions of the following phases: acid soluble (step 1), carbonates, reducible (step 2), oxides of ferric and manganese, and oxidizable metals as well as organic matter and sulfides (step 3) [26-27]. However, it was reported that BCR scheme did not fully reveal some regularities governing the state of Cd in soil [9]. In addition, there are many methods presented for sequential extraction modified or direct BCR [9, 21, 28-34]. The chemical reagents used in steps of sequential extraction processes were discussed and reviewed with their advantages and/or disadvantages [26, 35-36]. In the measurement step, different atomic spectroscopic methods such as flame atomic absorption spectrophotometry (FAAS), inductively coupled plasma-mass spectrometry (ICP-MS) and ICP-OES were used.

The primary objective of the present study is to determine the pollution extent from Cd and Pb concentrations in agricultural soil of Elazig-Turkey due to their high pollution potential by anthropogenic activities [37]. The study area is significant agricultural lowland that its area is about 325 km². In recent years, intensive industrial establishments as well as aircraft mobility in the airport located in the middle of this plain were considerably increased. Further, the results obtained from this study will contribute to evaluate the rate of pollution in the study area, in the future. Use of sequential extraction procedures may provide useful information for both short-term and long-term biological toxicity of trace metals because biological uptake is related more closely to the concentrations of a particular physico-chemical form. Five-step sequential extraction procedure modified from Tessier et al. (1979) [22] and Miller and McFee (1983) [43] was employed for fractionation of phases: exchangeable, organically bounded, bound to carbonate, adsorbed to Fe-Mn oxides, and residual soil except in silicates. The soil samples were also digested by the aqua regia procedure for their total metal concentrations except for silicates. The metal concentrations were determined by ICP-OES. Up to now, such a study for Cd and Pb hasn't been reported in this area.

MATERIALS AND METHODS

Apparatus. Perkin-Elmer Optima 2100 DV ICP-OES (Perkin-Elmer California, USA) was used to measurement of Cd and Pb concentrations. Instrumental conditions were applied as described elsewhere [38]. The Analytical wavelengths (nm) were selected as 228.802 nm for Cd and 220.356 nm for Pb. The pH of the solutions was adjusted with EDT GP 353 ATC pH meter. Some samples were analyzed by Perkin-Elmer Elan 9000 ICP-MS (Perkin Elmer SCIEX, Concord, Ontario, Canada) to assess the reliability of measurements. The operation conditions for this instrument were applied as recommended by the manufacturers.

Reagents and solutions. 1000 mg L⁻¹ of standard solutions (Merck, Darmstad Germany) of Cd and Pb were diluted to prepare working standards. All chemicals used were of analytical reagent grade. Doubly distilled water was used in experiments. All glass materials were kept permanently full of 1.0 M nitric acid when not in use. Concentrated nitric acid (65%), hydrogen peroxide (30%) and hydrochloric acid (37%) were used to digest the samples (Sigma St. Louis, MO, USA). In the sequential extraction procedure, 1.0 mol L⁻¹ of calcium chloride (CaCl₂) for exchangeable and weakly adsorbed fraction; 1.0 mol L⁻¹ of sodium pyrophosphate (Na₄P₂O₇) for organically bound fraction, 1.0 mol L⁻¹ of ethylenediamine tetra acetic acid disodium salt (Na₂EDTA) for carbonate bound fractions, 0.1 mol L⁻¹ of hydroxylamine hydrochloride (NH₂OH.HCl) for fractions bound to iron (Fe) and manganese (Mn) oxides, were used.

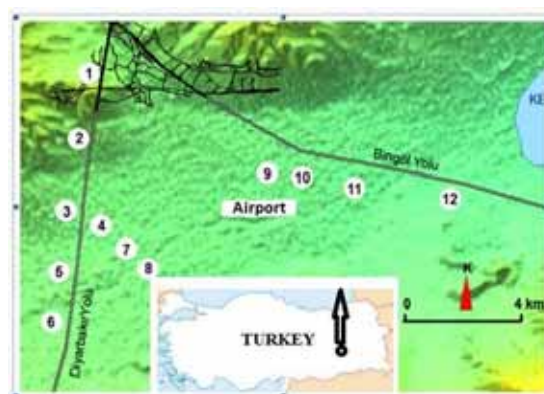


FIGURE 1
Map of the study area

Sampling. Soils were sampled from Altino-va/Uluova (named as gold-lowland) region where a large amount of vegetables consumed in Elazig-Turkey are growth. It is located among the intercity roads of Diyarbakir and Bingol cities given in Fig. 1. Samples were collected from twelve points that eight of them were on Diyarbakir road and four of them were on Bingol road. Probable stones and

TABLE 1
Variations in Cd concentrations of soil fractions (n=3)

Sample no	Cd mg/kg						Total by aqua regia*
	Step 1	Step 2	Step 3	Step 4	Step 5	Sum	
1	<d.l.	0.05±0.02	0.21±0.06	0.35±0.06	0.20±0.05	0.81±0.11	0.63±0.07(0.59±0.07)
2	<d.l.	0.05±0.01	0.23±0.02	0.37±0.05	0.22±0.03	0.87±0.13	0.65±0.07
3	<d.l.	0.09±0.02	0.26±0.14	0.30±0.06	0.23±0.04	0.88±0.12	0.58±0.06
4	<d.l.	0.08±0.02	0.27±0.03	0.34±0.06	0.19±0.03	0.88±0.10	0.36±0.04(0.33±0.04)
5	<d.l.	0.10±0.02	0.10±0.03	0.18±0.03	0.08±0.02	0.46±0.05	0.33±0.03
6	<d.l.	0.08±0.02	0.11±0.05	0.15±0.02	0.10±0.02	0.44±0.05	0.24±0.03
7	<d.l.	0.13±0.03	0.21±0.02	0.34±0.07	0.22±0.03	0.90±0.11	0.76±0.07
8	<d.l.	0.12±0.03	0.13±0.03	0.36±0.05	0.18±0.03	0.79±0.09	0.44±0.05
9	<d.l.	0.08±0.02	0.14±0.02	0.32±0.05	0.15±0.02	0.69±0.09	0.55±0.05
10	<d.l.	0.09±0.02	0.11±0.03	0.34±0.04	0.14±0.03	0.68±0.08	0.58±0.05
11	<d.l.	0.06±0.01	0.11±0.03	0.35±0.04	0.10±0.03	0.62±0.07	0.57±0.06(0.60±0.07)
12	<d.l.	0.12±0.02	0.13±0.03	0.40±0.07	0.21±0.03	0.86±0.11	0.45±0.06

d.l.: limit of detection

*The results in parenthesis were obtained by ICP-MS

TABLE 2
Variations in Pb concentrations of soil fractions (n=3)

Sample no	Pb mg/kg						Total by aqua regia*
	Step 1	Step 2	Step 3	Step 4	Step 5	Sum	
1	<d.l.	0.26±0.04	2.21±0.27	4.13±0.47	9.5±1.1	16.1±1.8	13.6±1.5(13.2±1.4)
2	<d.l.	0.47±0.06	2.76±0.24	4.06±0.47	10.8±1.3	17.4±1.9	25.7±3.3
3	<d.l.	0.15±0.03	2.41±0.25	3.14±0.35	8.1±1.2	13.8±1.4	22.4±2.7
4	<d.l.	0.17±0.03	2.36±0.27	2.96±0.33	3.9±0.5	9.4±1.5	9.4±1.2(9.0±1.1)
5	<d.l.	0.25±0.04	4.68±0.49	3.34±0.39	4.3±0.5	12.6±1.6	19.8±2.3
6	<d.l.	0.19±0.04	3.52±0.32	3.02±0.37	2.6±0.3	10.3±1.4	19.8±2.6
7	<d.l.	0.32±0.04	5.51±0.58	13.40±1.69	4.5±0.6	23.7±2.6	40.9±5.1
8	<d.l.	0.14±0.03	2.11±0.24	3.18±0.44	3.3±0.3	9.7±1.3	16.7±2.0
9	<d.l.	0.23±0.03	2.01±0.22	3.67±0.39	2.4±0.3	8.3±0.9	12.6±1.9
10	<d.l.	0.30±0.04	1.93±0.20	3.73±0.40	3.6±0.4	9.6±1.0	15.8±2.2
11	<d.l.	0.30±0.04	10.92±1.12	6.12±0.72	4.5±0.4	21.4±2.6	21.2±2.4(21.4±2.3)
12	<d.l.	0.34±0.04	2.07±0.21	6.27±0.72	4.5±0.6	13.2±1.6	22.0±2.7

d.l.: limit of detection

*The results in parenthesis were obtained by ICP-MS

plant fragments were removed from soil. For each point, a 250 g portion of soil from 10 – 20 cm depth of surface was taken using a plastic scoop. After dried at 60 °C, all of the samples were ground in a mortar and sieved on 2-mm pore.

Sequential extraction procedure. Sequential extraction was employed to monitor the mobility of metals in soil. For this purpose, each of soil samples was examined in five extraction steps as detailed elsewhere [38]. Briefly, a 2.0 g of soil was weighted and 8.0 mL of 1.0 M CaCl₂ (step 1) was added to extract exchangeable metal species. After shaking for 5 min and centrifugation, 3 mL of 1.0 M Na₄P₂O₇ (step 2) was added to residue from step 1, to extract organically bound species. Then, the mixture was shaken for 5 min and centrifuged. In step 3, carbonate species of Cd and Pb were released by adding 3 mL of 1.0 mol L⁻¹ Na₂EDTA to the residue obtained from step 2. Adsorbed species on Fe and Mn oxides were extracted by adding 3 mL of 0.1 M of NH₂OH.HCl (step 4) to the residue obtained from step 3. The remaining residue from step 4 was digested by addition 5 ml of HNO₃-H₂O₂ (2:1) mixture (step 5). After shaking and volatilization near to dryness, 2.0 mL of 0.5 M HNO₃ was

added and centrifuged. Concentrations of Cd and Pb in the clear solutions obtained from each of steps were determined by ICP-OES. The matrix interference correction was applied. The pH of soil samples were determined by treating 1.0 g of soil with 5.0 mL of distilled water.

Digestion of soil samples by aqua regia. Total concentrations (except in silicate minerals) of Cd and Pb in soil samples using aqua regia were determined by ICP-OES after digestion in microwave oven. For this purpose, 6.0 mL of the mixture of HNO₃:HCl (1:3) (aqua regia) was added to 0.5 g portion of soil in Teflon vessel. The applied microwave program was as the manual book. Then, it was heated with occasional shaking on a hot plate near to dryness. After cooling, 2.0 mL of 0.5 M HNO₃ was added to the remainder and centrifuged. The clear supernatant was analyzed by ICP-OES for the determination of Cd and Pb.

Related with statistically consideration, One-Way Analyses of Variance (ANOVA) were conducted to test the equality of mean values for each sample of interest. One of the pairwise comparison tests, Tukey HSD, was carried out to find which of the sample means is different from each other de-

pending on extraction step. SPSS (version 15) statistical program was used for all statistical computations. Statistical significance was considered when P was equal to or higher than 0.05.

RESULTS AND DISCUSSIONS

Limit of detection (LOD) values calculated from the ratio of three times of the standard deviation of blank to slope of the linear calibration plot were found to be 3 and 5 ng mL⁻¹ for Cd and Pb, respectively. From the practical point of view, ICP-OES used in this study has better sensitivity than FAAS, particularly for Pb. Blank digests were prepared and analyzed in the same way. All of the experiments were performed three times and standard deviations were given in related Tables (Tables 1-2). Some samples were also analyzed by ICP-MS to check the accuracy of results. It was found that the differences between the results obtained by ICP-OES and ICP-MS were not meaningful statistically (Tables 1-2). In other words, the differences were originated from unknown sources. Further, matrix matching method was applied to minimize matrix effects. For this purpose, the model metal solutions containing 30 mg Fe L⁻¹, 50 mg Ca L⁻¹ and 20 mg Mg L⁻¹ were used to obtain calibration graphs. So the major chemical compositions of the standards, blanks and samples are made identical taking into consider possible interferences from matrix.

Concentrations of total Cd and Pb after digesting by aqua regia of soil. The permitted Cd and Pb concentrations in soil samples depending on the soil pH are 1.0 and 50 for pH<6.0 and 3.0 and 300 for pH>6.0, respectively [17-18]. From Tables 1 and 2, the total Cd and Pb concentrations obtained by using aqua regia were found to be in the ranges of 0.24-0.65 mg kg⁻¹ and 9.4-40.9 mg kg⁻¹, respectively. It could be seen that Cd concentrations in all studied samples were lower than the permitted values (1-5 mg kg⁻¹) in Turkey and other countries. Lead concentrations in all samples were also lower than the limit values (50-300 mg kg⁻¹). It could be said that Cd concentrations in points of 5 and 6 were clearly lower than the other points ($p < 0.5$). Approximately two fold increasing was observed in point 7 compared to the other points. It was attributed to anthropogenic activities like plastic production (Cd is used as stabilizer in this factory) in this region. The pH values of the studied soils were found to be higher than 7.0 (maximum 7.8) except for soil number 5 that is 6.6.

Soil Fractionation by Sequential Extraction.

Cd and Pb concentrations in soil fractions such as exchangeable, organically bounded, carbonate bounded, adsorbed species on Fe and Mn oxides and residual species except for silicates using five-

step sequential extraction were given in Tables 1 and 2 with their standard deviations. From Table 1, Cd concentrations in the first step were found below the limit of quantitation (LOQ) due to its too low level in exchangeable species. Cd levels in organically and carbonate bounded (the steps 2 and 3) were found between 0.06-0.27 mg kg⁻¹. So, the percent Cd concentrations in potentially mobile forms (in the first three steps) were lower than 40% of total Cd in soils. Cd levels in adsorbed species on Fe and Mn oxides (the step 4) were found to be in range of 0.15-0.4 mg kg⁻¹. Cd concentrations in fifth step, digestion by HNO₃-H₂O₂, were unexpectedly found below the levels in step 4. This can be attributed to most of the Cd in the studied soil samples are the adsorbed species on Fe and Mn oxides. Similarly the obtained total Cd concentrations in soil using aqua regia were found lower than in the sum of sequential extraction procedures for all studied soils. From Table 2, Pb concentrations in the first step were found below the LOQ due to its too low level in exchangeable species, as similar to the Cd. Lead levels in organically and carbonate bounded (the steps 2 and 3) were found between 0.14-5.51 mg kg⁻¹, except one sample (sample 11 in step 3) of 10.92 mg kg⁻¹. So, the percent Pb levels in potentially mobile forms (in the first three steps) were lower than 40% of total Pb in soils except one sample mentioned above. Lead levels in adsorbed species on Fe and Mn oxides (the step 4) were found to be in the range of 2.96-13.40 mg kg⁻¹. Lead concentrations in fifth step, digestion by HNO₃-H₂O₂, were found around the levels in step 4 in most of samples. Similarly, the obtained total Pb concentrations in soil using aqua regia were found to be close in the sum of sequential extraction procedures for most of the studied soils. The obtained Cd and Pb concentrations for all soils were found lower than the maximum allowable concentrations (3.0 mg Cd kg⁻¹ and 300 mg Pb kg⁻¹) by national and international authorities [17-18].

In step 1, CaCl₂ was used to extract the 'exchangeable' metals from soil. It was more effective than Mg²⁺ and NH₄⁺ in view of ion exchange capability [26]. In Ca exchangeable fractions, metals bound to surface are released and replaced by calcium ions. The lowest amounts of Cd and Pb are in exchangeable fractions included metals with weak electrostatic interaction and they could be easily released by ion-exchange processes [17]. It was noted in literature that high levels of metals in the exchangeable fractions may indicate pollution from anthropogenic origin [35].

In step 2, organically bound metal species were determined by using Na₄P₂O₇ extracting. Although both Na₄P₂O₇ and EDTA can be used for this purpose, Na₄P₂O₇ is preferred to EDTA because EDTA will also dissolve the carbonate species [2]. Using of Na₄P₂O₇ is more selective for the easily soluble organic fraction such as metals associated

with humic and fulvic acids, and disperse colloidal organic material by complexing the flocculating Ca, Al and Fe cations [2]. From Table 2, concentrations of Pb in this fraction are in the ranges of 0.14-0.34 mg kg⁻¹. In this phase, the large amounts of metals are bounded to living organisms, detritus, or coatings on mineral particles [25].

In step 3, EDTA (ethylenediaminetetraacetic acid) was used for extraction of metals from carbonate species in soil. It was reported that EDTA was generally preferred instead of DTPA (diethylenetriaminepentaacetic acid) because of its extraction capability of both carbonate and organically bound fractions [2]. This was attributed to its low pH [39]. Organically bound metals were extracted in previous step 2. In this step 3, EDTA was used for the extraction of metals from its carbonate species in soil. Potentially available metal species in soils were also extracted in this fraction by using EDTA. Trace metals bound to sulfides might be extracted during this step [7]. From Table 2, concentrations of Pb in this fraction were followed as 1.93-10.92 mg kg⁻¹, respectively.

In step 4, acidified solution of NH₂OH-HCl (easily reducible mixture) was used to dissolve the manganese oxide and the amorphous iron oxide by releasing the trace metals coprecipitated in those phases. Sun et al. (2005) tested four different concentrations of NH₂OH-HCl, and they found the most of trace elements were released from soil by using 0.1 M of NH₂OH-HCl [40]. Reducing mechanism was effective for releasing of metals in this step [30]. The obtained Pb levels in this step were found to be close in the step 3 for the most of soils. A mixture of HNO₃-H₂O₂ (2:1) was used for the digestion of residue from fourth step. The majority of the metals present in the soils was generally found in the residual bulk fraction with less mobility and was not dissolved in the previous steps. However, Pb concentrations close to the levels in the step 4 were detected in this fraction, for the most of samples. The reported results in literature have more differences and contradictory values due to differences in soil structure, pollution sources such as kind/kinds of industrial organization and traffic intensity as well as applied extractions and digestion procedures and steps [1, 2, 20, 27-34, 41]. For example, Kaasalainen and Yli-Halla (2003) have reported that Cd, Cu and Ni appeared in mobile forms (up to 72% in exchangeable and reducible fractions) to a particularly large extent in the surface layer and also in the second horizon of the most polluted, sandy soil near the metal smelter in Finland [42]. Metal percentages in residual fraction determined in this study were agreed with the literature [28,42]. The study area is significant agricultural lowland that its area is about 325 km². In recent years, intensive industrial establishments as well as aircraft mobility in the airport located in the middle of this plain were considerably increased.

Finally, the results obtained in this study will contribute to evaluate the rate of pollution in the study area, in the future.

CONCLUSIONS

Sequential extraction method was employed to understand the mobility of metals through the simultaneous measurement by ICP-OES. The sequential extraction was modified from Tessier (1979) and Miller (1983) [22, 43], and applied for the fractionation of agricultural soils sampled from Elazığ-Turkey as similar to determine Ni, Cr and Cu in the same area [38, 44]. The results showed that the percentages of Cd and Pb in the residual fractions were founded to be close in other fractions. However, total concentrations of Cd and Pb were not exceeded the permitted limit values. Finally, it could be concluded that all the reagents used in the various schemes have advantages and disadvantages, and there is not an ideal reagent or an ideal procedure for general use. Therefore, the choice of procedure must be related to a definite objective, taking into account the nature of the sample including sediment, soil, sludge or industrially-polluted soil.

ACKNOWLEDGEMENTS

We thank to Dr. Ersin Kilinc from Mardin Artuklu University for his assistance.

REFERENCES

- [1] Bermond, A. (2001) Limits of sequential extraction procedures re-examined with emphasis on the role of H⁺ ion reactivity. *Anal. Chim. Acta*; 445:79-88.
- [2] Rao, C.R.M, Sahuquillo, A, Lopez, Sanchez, J.F. (2008) Review of the Different Methods Applied in Environmental Geochemistry For Single and Sequential Extraction of Trace Elements in Soils and Related Materials. *Water Air Soil Pollut.*;189:291-333.
- [3] Yaman, M. (2006) Comprehensive Comparison Of Trace Metal Concentrations In Cancerous And Non-Cancerous Human Tissues. *Curr. Med. Chem.*;13(21):2513-2525.
- [4] Yaman, M, Kaya, G, Yekeler, H. (2007) Distribution Of Trace Metal Concentrations In Cancerous And Non-Cancerous Human Stomach Tissues. *World J. Gastroenterol.*;13(4):612-618.
- [5] Er, C, Senkal, B.F, Yaman, M. (2013) Determination of lead in milk and yoghurt samples by solid phase extraction using a novel amino-thioazole-polymeric resin. *Food Chem.*;137(1-4):55-61.

- [6] Ozen, O.A, Songur, A, Sarsilmaz, M, Yaman, M, Kus, I. (2003) Zinc, Copper And Iron concentrations In cerebral cortex of Male Rats exposed To Formaldehyde inhalation. *J Trace Elem. Med. Biol.*;17(3):207-209.
- [7] Kaplan, O, Yaman, M. (2009) Selective and Sequential Extraction of Lead in Soil Samples and Plant Parts Taken from a Serpentine and Copper Mining Area. *At. Spectrosc.*;30:1-9.
- [8] Kaplan, O, Kay, a G, Yaman, M. (2011a) Sequential and Selective Extraction of Copper in Different Soil Phases and Plant Parts from Former Industrialized Area. *Commun. Soil Sci. Plant Anal.*;42:2391–2401.
- [9] Kaplan, O, Ince, M, Yaman, M. (2011b) Sequential extraction of cadmium in different soil phases and plant parts from a former industrialized area. *Environ. Chem. Lett.*;9:397-404.
- [10] Mukhtar, A, Limbeck, A. (2013) Recent developments in assessment of bio-accessible trace metal fractions in airborne particulate matter: A review. *Anal. Chim. Acta*;774:11–25.
- [11] Kaya, G, Yaman, M. (2008) Trace Metal Concentrations In Cupressacea Leaves As Biomonitors Of Environmental Pollution. *Trace Elem. Electrolyt.*;25(3):156-164.
- [12] Kaya, G, Ozcan, C, Yaman, M. (2010) Flame Atomic Absorption Spectrometric Determination of Pb, Cd, and Cu in *Pinus nigra* L. and *Eriobotrya japonica* Leaves Used as Biomonitors in Environmental Pollution. *Bull. Environ. Contam. Toxicol.*;84(2):191-196.
- [13] Karaaslan, NM, Yaman, M. (2011) Use of STAT-Flame AAS in the Determination of Lead and Cadmium Pollution in Urban Center. *At Spectrosc*;32(4):152-159.
- [14] Karaaslan, N.M, Yaman, M. (2013a) Seasonal Changes in Copper and Cobalt concentrations of *Pinus nigra* L., *Cedrus libani* and *Cupressus arizonica* leaves to monitor the effects of pollution in Elazig (Turkey). *Spectrosc. Spectral Anal.*;33(5):1331-1337.
- [15] Karaaslan, N.M, Yaman, M. (2013b) Determination of Nickel and Chromium in *Pinus nigra* L., *Cedrus libani* and *Cupressus arizonica* leaves to monitor the effects of pollution in Elazig (Turkey). *Inst. Sci. Tech.*;41(3):335-348.
- [16] Keskin, G, Bakirdere, S, Yaman, M. (2015) Sensitive determination of lead, cadmium and nickel in soil, water, vegetable and fruit samples by using STAT-FAAS after preconcentration with activated carbon. *Toxicol. Ind. Health*;31(10):881-889.
- [17] Pendias, A.K. (2001) *Trace Elements in Soils and Plants*, Third Edition, Taylor & Francis Group,; 413 pages.
- [18] TKKY, (2001). *Toprak Kirliligi Kontrol Yönetmeliği*, Resmi Gazete: 10.12.2001 tarih ve 24609 sayı.
- [19] Degryse, F, Smolders, E, Parker, D.R. (2009) Partitioning of metals (Cd, Co, Cu, Ni, Pb, Zn) in soils: concepts, methodologies, prediction and applications—a review. *Europ. J. Soil Sci.*;60:590–612.
- [20] Werkenthin, M, Kluge, B, Wessol, G. (2014) Metals in European roadside soils and soil pollution—A review. *Environ. Poll.*;189:98-110.
- [21] Yaman, M, Dilgin, Y, Gucer, S. (2000) Speciation of lead in soils and relation with its concentration in fruits. *Anal. Chim. Acta*;410:119–125.
- [22] Tessier, A, Campbell, PGC, Bisson, M. (1979) Sequential Extraction Procedure for the Speciation of Particulate Trace Metals. *Anal. Chem.*;51:844-851.
- [23] Gleyzes, C, Tellier, S, Astruc, M. (2002) Fractionation studies of trace elements in contaminated soils and sediments: a review of sequential extraction procedures. *Trends Anal. Chem.*;21:451-467.
- [24] Yaman, M, Bakirdere, S. (2003) Identification of Chemical Forms of Lead, Cadmium and Nickel in Sewage Sludge of Waste Water Treatment Facilities. *Microchim. Acta*;141:47–54.
- [25] Tokalioglu, S, Kartal, S, Gultekin, A. (2006) Investigation of heavy-metal uptake by vegetables growing in contaminated soils using the modified BCR sequential extraction method. *Inter. J. Environ. Anal. Chem.*;86(6):417-430.
- [26] Hass, A, Fine, P. (2010) Sequential Selective Extraction Procedures for the Study of Heavy Metals in Soils, Sediments, and Waste Materials—a Critical Review. *Crit. Rev. Environ. Sci. Technol.*;40:365-399.
- [27] Alonso Castillo, M.L, Vereda Alonso, E, Siles Cordero, M.T, Cano Pavón, J.M, García de Torres, A. (2011) Fractionation of heavy metals in sediment by using microwave assisted sequential extraction procedure and determination by inductively coupled plasma mass spectrometry. *Microchem. J.*;98:234–239.
- [28] Maiz, I, Esnaola, M.V, Millan, E. (1997) Evaluation of heavy metal availability in contaminated soils by a short sequential extraction procedure. *Sci. Total Environ.*;206:107-115.
- [29] Lead, J.R, Hamilton-Taylor, J, Davison, W. (1998) The effect of sequential extractions of suspended particulate matter on trace metal sorption and microbial cell stability. *Sci. Total Environ.*;209:193-199.
- [30] Davidson, C.M, Hursthouse, A.S, Tognarelli, D.M, Ure, A.M, Urquhart, G.J. (2004) Should acid ammonium oxalate replace hydroxylammonium chloride in step 2 of the revised BCR sequential extraction protocol for soil and sediment? *Anal. Chim. Acta*;508:193-199.
- [31] Alomary, A.A, Belhadj, S. (2007) Determination of heavy metals (Cd, Cr, Cu, Fe, Ni, Pb,

- Zn) by ICP-OES and their speciation in Algerian Mediterranean Sea sediments after a five-stage sequential extraction procedure. *Environ. Monit. Assess.*;135:265–280.
- [32] Bacon, J.R., Davidson, C.M. (2008) Is there a future for sequential chemical extraction? *Analyst*;133(1):25-46.
- [33] Altundag, H, Imamoglu, M, Doganci, S, Baysal, E, Albayrak, S, Tuzen, M. (2013) Determination of Heavy Metals and Their Speciation in Street Dusts by Inductively Coupled Plasma-Optical Emission Spectrometry after a Community Bureau of Reference Sequential Extraction Procedure. *J. AOAC Int.*;96(4):864-869.
- [34] Howard, J.L, Dubay, B.R, McElmurry, S.P, Clemence, J, Daniels, W.L. (2013) Comparison of Sequential Extraction and Bioaccessibility Analyses of Lead Using Urban Soils and Reference Materials. *Water Air Soil Pollut*;224(10):1678-1691.
- [35] Tack, F.M.G, Verloo, M.G. (1995) Chemical Speciation and Fractionation In Soil and Sediment Heavy Metal Analysis: A Review. *Inter. J. Environ. Anal. Chem.*;59:225-238.
- [36] Rauret, G. (1998) Extraction procedures for the determination of heavy metals in contaminated soil and sediment. *Talanta*,46:449–455.
- [37] Avci, H, Yaman, M.(2014) Concentrations, Accumulation, and Interactions of Redoximorphic Metals (Fe, Mn) Between Other Elements in Plants Grown on Wastewater-Irrigated and Control Soils. *Water Air Soil Pollut.*;225:1926-1942.
- [38] Akkus, S, Bal, T, Karaaslan, N.M, Yaman, E, Kilinc, E, Yaman, M. (2013) Fractionation of Ni, Cr and Cu in soil by sequential extraction procedure and determination by inductively coupled plasma optical emission spectrometry. *Clean-soil, air, water*; 41(12):1229-1234.
- [39] Bakircioglu, D, Bakircioglu Kurtulus, Y, Ibar, H. (2011) Comparison of Extraction Procedures for Assessing Soil Metal Bioavailability of Wheat Grains. *Clean-Soil, Air, Water*;39(8):728–734.
- [40] Sun, F, Xie, M, Wu, C. (2005) Quick sequential procedure for speciation analysis of heavy metals in soils by supersonic extraction. *Chem. Speci. Bioavail.*;17(4):137-146.
- [41] Sasmaz, A, Yaman, M. (2006) Distribution of Chromium, Nickel and Cobalt in Different Parts of Plant Species and Soil in Mining Area of Keban, Turkey. *Commun Soil Sci. Plant Anal.*;37(13-14):1845-1857.
- [42] Kaasalainen, M, Yli-Halla, M. (2003) Use of sequential extraction to assess metal partitioning in soils. *Environ. Poll.*;126:225–233.
- [43] Miller, WP, McFee, W.W. (1983) Distribution of cadmium, zinc, copper, and lead in soils of industrial northwestern Indiana. *J. Environ. Qual.*;12:29-33.
- [44] Yaman, M. (2014) Teucrium (*Teucrium polium* L.) as a novel discovered hyperaccumulator for phytoextraction of Ni-contaminated soils. *Ekoloji*;23(90):81-89.

Received: 10.01.2016

Accepted: 19.07.2016

CORRESPONDING AUTHOR

Mehmet Yaman

Firat University, Sciences Faculty, Department of Chemistry, Elazig-Turkey

e-mail: ijpacmy@gmail.com

ACCRETION AND DISPERSION OF HEAVY METALS IN A VEGETABLE GROWN IN CONTAMINATED SOIL WITH SEWAGE WATER: A MATTER OF GREAT CONCERN AND COMMUNITY HEALTH CONSEQUENCES

Muhammad Saeed Ahmad³, Zafar Iqbal Khan¹, Kafeel Ahmad¹, Aima Iram Batool⁵, Sana Hamid¹, Muhammad Sher³, Ijaz Rasool Noorka², Zafar Hayat², Humayun Bashir¹, Muhammad Sohail¹, Abid Ejaz¹, Zunaira Sheikh¹, Ahmed Muneeb¹, Naunain Mehmood⁵, Hira Muqaddas⁵, Faiza Zubair⁵, Naila Amjad⁵, Fauzia Naseem Taj¹, Sana Iqbal¹, Fauzia Batool¹

¹Department of Botany, University of Sargodha, Sargodha, Pakistan

²University College of Agriculture, University of Sargodha, Pakistan

³Department of Chemistry, University of Sargodha, Pakistan

⁴Department of Zoology, University of Sargodha, Pakistan

ABSTRACT

Coriander is an important leafy vegetable widely used in Pakistan for flavoring purpose. Due to scarcity of clean water, the coriander fields are irrigated with waste-water. The present study revealed the accumulation of different metals in coriander irrigated with wastewater in big cities such as Sargodha, Pakistan. The bioavailability of heavy metal from soil to plant was evaluated. Seven heavy metals were determined by using Atomic absorption spectrometer. The findings showed high level of arsenic as well as Pb, Cd, and Ni in coriander irrigated with waste-water. Regular monitoring of the contaminated area is recommended in order to reduce the health hazard.

KEYWORDS:

Heavy metals, coriander, health risk

INTRODUCTION

As compared with major commercial crops, vegetables are grown on a small scale, but vegetable yield entirely depends on the accessibility of canal or ground water. Under the existing conditions of water availability and global climatic changes, it is impossible to meet the irrigational requirements of Pakistan [1-2]. The area of vegetable cultivation in Pakistan is increasing continuously due to high domestic use. For example, during 2007-08 vegetables were cultivated at about 253,800 ha [3]. However, most of the commonly used vegetables are grown in peri-urban and adjacent areas. The total irrigational water availability is shrinking due to excessive use, increased cropping intensity and increased heat and

temperature situation [4]. Due to high shortage of irrigation water, farmers are helpless and sometimes greedy to use polluted water drained from sewage and factory outlets to irrigate the outskirts of cities. Thus, vegetables grown in peri-urban areas accumulate substantial aggregate of diverse heavy metals and cause public health problems [5].

It is presumed that wastewater is full of diverse type of metals like (Pb), cadmium (Cd), chromium (Cr), nickel (Ni), zinc (Zn), copper (Cu), and arsenic (As). Amount of heavy metals has increased to optimum level by the continuous irrigation with wastewater. Contaminated water or soil are the main cause of induction of heavy metals in our food system [6]. Keeping in view the great concern of this health issue, present study was initiated to get insight and out-reach the public awareness.

MATERIALS AND METHODS

Study Area. The present research was initiated in the diverse climatic zone of Sargodha- the 11th populated city of Punjab Province, Pakistan. Coriander, a leafy vegetable, is largely used in almost all cooking items by a big segment of the society. Fully grown lush green vegetable was used in sampling. Randomly collection of samples from four areas of Sargodha tehsil headquarter, Sillanwalli, were taken from the surface soil. To avoid external contamination the proper precautions were taken.

Pretreatment. Washing, Drying, Digestion and determination of the samples. Properly collected vegetable samples were thoroughly washed with tap water followed by distilled water to clean debris. The samples were air dried and then oven

dried at 72 °C for 24 hours. Along with leafy samples, the soil samples were also collected and dried at ambient temperature for 8 days to drain out the moisture. Wet acid digestion was followed as a pre-treatment procedure for estimation of heavy metals in the coriander.

Methodology Employed.

Leaf samples (1 gm) were digested using analytical grade H₂SO₄ (10 ml) and HClO₄ (4 ml). Continual heating on a hot plate at 180-220°C was done for 30 minutes. Samples were filtered using Whatman no. 42 filter paper after cooling and distilled water was added to make sample volume up to 50 ml. Similar method was used for digestion of soil samples; only the quantity of acids differed (HClO₄: 5 ml and H₂SO₄: 8 ml).

Instrumental analysis. Last step was the estimation of metals in the acid digested samples. Heavy metal contents were determined with the help of Atomic Absorption Spectrophotometer. To complete this task, standard solutions were prepared.

Standards. Standard solutions of the heavy metals like lead, cadmium, copper, chromium and zinc were made with their salts. The standards were prepared from the individual 1000mg/L standards. A series of working standards were prepared from these standard stock solutions. For trace metals, the digested samples were analyzed with the help of Atomic Absorption spectrophotometer (AAS) after proper calibration.

Statistical analysis. All tests were performed in triplicates to express the obtained results by means of ±SD.

Transfer factor. The transfer factor expresses the bioavailability of a metal at a particular position on a species of plant as delineated by the Cui et al. [7].

TF= concentration of metal in edible part/concentration of metal in soil. All the concentrations in this research are taken in ppm.

RESULTS AND DISCUSSION

The levels of Pb, Cd, Cr, Ni, Zn Cu and As were estimated in coriander to assess the extent of contamination. These metals present minimal risk to human health at normal concentrations; however, addition of metals in environment from sources other than natural like industrial and municipal waste make these a potential health hazard. The burgeoning population pressure and increased cropping intensity is the main cause for heavy metal intake. Some of the heavy metals like (copper, chromium and zinc) are

also essential for our health at low concentrations. Some heavy metals like (cadmium, lead, arsenic and nickel) not an essential part of our diet and becomes toxic when consumed in excess. There is an urgent need for research on this important issue to yield relevant information that could be used to initiate measures to eliminate heavy metals from soil and vegetables.

Soil Analysis. Concentration of heavy metals in soil. The soil samples at experimental site were collected and subjected to calculate the concentration of heavy metals (Table 2). The levels of Pb, Cd, Cr, Ni, Zn, Cu and As concentration were present with an average value of 35.66±3.91, 0.408±0.6, 65.29±6.4, 31.6±6.5, 55.31±10.3, 22.67±2.14 and 0.035±0.01 respectively (Table 2). Heavy metals in soil samples were within the USEPA and BIS-1991 limits, may be due the insolubility of metals as well as high soil pH. It was also noted that the factors like soil pH, the intensity of organic matter and soil redox potential affect metals adsorption and retention in soil [8]. Current study results were also supported by the earlier researches by Khan et al. [9] and Butt et al. [10] in Faisalabad, Punjab, Jawahar and Javed [11] in District Sheikhpura, Pakistan.

Plant Analysis. Concentration of heavy metals in coriander was investigated as follows:

Lead. Heavy metals have been in use since thousands of years. It is reported that lead has been used for at least 5000 years with early applications including building materials, pigments for glazing ceramics, and pipes for transporting water [12]. Lead is one of the major metals of concern in terms of contamination. Acute exposure to lead is the major reason to cause proximal renal tubular damage [13]. It is also noted that long-term lead exposure is damaging kidney, in a study conducted to check the Egyptian policemen health, the urinary excretion was found positively correlated with the duration of exposure to lead from automobile exhaust, blood lead and nail lead [14]. The maximum permissible limit of lead is 2.5ppm by Indian standard, however WHO the standard is 5ppm. The present study revealed that in coriander vegetable grown under waste water irrigation, the lead concentration was more than permitted level, so it is not suitable for consumption (Tab 1). It was also noted that the lead is a toxic heavy metal, usually the plants show high ability to accumulate the lead concentration [15].

Cadmium. Cadmium compounds are currently used in re-chargeable nickel-cadmium batteries mainly. Cadmium emissions have increased dramatically during the 20th century, one reason being that cadmium-containing products are rarely re-cycled, but often dumped together with house

TABLE 1
Concentrations of heavy metals in coriander

Metals	Pb	Cd	Cr	Ni	Zn	Cu	Ar
Values	16.36±4	0.547±0.03	10.06±0.7	10.86±1.9	24.31±1.8	17.18±1.9	0.073±0.01
Permissible Values	5	0.2	20	2	60	40	0.075

For each sample results are expressed in ppm. Permissible limit ^a = the maximum allowable limit set by WHO (World health organization).

TABLE 2
Concentrations of heavy metals in soil (mean±S.D)

	Pd	Cd	Cr	Ni	Zn	Cu	As
Soil	35.66±3.91	0.408±0.6	65.29±6.4	31.6±6.5	55.31±10.3	22.67±2.1	0.035±0.01
USEPA*	300	3	400	50	200	50	0.07
BIS**-1991	250	3-6	-	50	300	135-270	-

USEPA* stands for United States environmental protection agency

BIS** stands for Bureau of Indian Standards

TABLE 3
Transfer Factors (TF) of some of the Heavy metals from Soil to vegetable

TF of Vegetable	Heavy metals						
	Pb	Cd	Cr	Ni	Zn	Cu	As
Coriander	0.46s	1.34	0.154	0.343	0.44	0.757	2.07

hold waste [12]. Cigarette smoking is the major source of cadmium exposure. Adverse health effects of cadmium exposure may occur at lower exposure levels than previously anticipated, primarily in the form of kidney damage but possibly also bone effects and fractures [12-16]. Cadmium shows severe toxicity due to its bio-accumulation and it has a long shelf life of about 30 years [17]. Plants can readily absorb cadmium from soil and by plants, through ingestion, it enters the human food chain. Current study showed the higher concentrations of Cd similar to previous work [18-19-20].

Chromium. Chromium is one of the most important metals having serious concerns due to its exposure. It has specific transport mechanisms, by which only limited amounts of chromium (III) not only enter in the cells but also can lead to DNA damage of an organism [21]. It may occur through breathing air, contaminated food items and drinking water or even through skin contact. Chromium concentrations in blood, plasma, serum or urine may be used as yard stick to measure the safety in exposed workers [22].

In human beings and animals, chromium is under essential metal limits for the carbohydrate and lipid metabolism within a certain range of concentrations (up to 200µg/day). However, exceeding doses may lead to toxicity as well as hepatitis [23]. In our study the concentration of chromium was much lower than the permissible limit in all coriander samples (Tab-1).

Nickel. It is often said that the excess of everything is bad, the same is true for the prolonged exposure of heavy metals like nickel, zinc, copper and ar-

senic that can cause deleterious health effects in humans [24]. Nickel contents from soil as well as growing plant on contaminated water can easily be extracted [25]. In present study, the data revealed that the value of nickel was exceeding the maximum permissible limits (Table 1).

Zinc. Zinc an essential mineral for the proper functioning of our daily intake. It is also used as the food supplement and bio-fortification of the some cereals. Zinc is an important part of cellular metabolism as well as the catalytic activity of enzymes. Among all metals, Zinc (Zn) is least toxic and an essential element in the human diet because it enhances the immune function, protein synthesis and wound healing. Zinc deficiency in the diet may be more detrimental to human health than its abundance. The average daily intake of Zinc is 7.00-16.3 mg Zn/day, but the recommended dietary allowance for it is 15 mg Zn/day for men and 12 mg Zn/day for women [26]. On the other hand its high concentration in vegetables may cause some diseases and unrest like vomiting, renal damage, cramps in the body etc.

According to the Nair et al. [27] the best adopted limit for human consumption may be up to 150 ppm. In this study the Zn concentration in Coriander was under the limit (Table 1).

Copper. Like Zn, if copper exceeds its permissible range, it is considered as a hazardous metal. High concentrations of Cu cause hypertension, sporadic fever, uremias, coma, [27-28]. The recommended daily intake of Cu for human consumption is 900 µg g⁻¹. Present results revealed that the Cu concentration range in coriander is less than the safe limits prescribed for human health and hygiene (Table 1).

Arsenic. WHO [29] evaluation concluded that arsenic exposure via drinking water is causally related to cancer in the lungs, kidney, bladder and skin rashes. Arsenic has a short half-life of several weeks in the body, but its effects can be seen years after exposure has ceased and is considered to be a human carcinogen [30]. Fortunately, plants do not absorb arsenic as reported by researchers who have studied vegetable samples grown in agricultural soils high in As content [31-32]. The current levels in edible crop samples were below the analytical detection limit of 0.075µg/g (Table 1).

Transfer factors (TF) of the Heavy Metals from Soil to Vegetable. Transfer factor (TF) was calculated to check the risk and assessment of the outcome of hazard done by the waste water irrigation or supplemental irrigation and heavy metal consequences in the in edible portion of test vegetables as followed Cui et al. [7]. Health hazards due to heavy metal contamination in vegetable were assessed through TF (Table 3). Transfer of metals from soil to leafy portion of coriander was considered and it turned out to be highest for As (2.07).

REFERENCES

- [1] Noorka, I.R. and M. Afzal. (2009). Global Climatic and Environmental Change Impact on Agricultural Research Challenges and wheat productivity in Pakistan. *Earth Science Frontiers*, 16 (SI): 99-103
- [2] Ali, A., M. Afzal, I.R. Noorka, E. Safdar, M.Ahmad. (2011). Sunflower (*Helianthus annuus* L.) hybrids performance at different plant spacing under agro-ecological conditions of Sargodha, Pakistan. International Conference on Food Engineering and Biotechnology. IPCBEE 9: 317-322. IACSIT Press, Singapore
- [3] Perveen, S., Z. Malik and W. Nazif. (2010). Fertility status of vegetable growing area of Peshawar, Pakistan. *Pakistan Journal of Botany*, 42: 1871-1880.
- [4] Noorka, I.R. and S. Tabasum. (2015). Dose-response behavior of water scarcity towards genetical and morphological plant traits in spring wheat (*Triticum aestivum* L.). *Pakistan Journal of Botany*, 47(3):1225-1230.
- [5] Tahir, M., M. Ayub, H.M.R. Javeed, M. Naeem, H. Rehman, H. Waseem and M. Ali. (2011). Effect of different organic matter on growth and yield of wheat (*Triticum aestivum* L.). *Pakistan Journal of Life, Society and Science* 9: 63-66.
- [6] Wilson, B. and F.B. Pyatt. (2007). Heavy metal dispersion, persistence, and bioaccumulation around an ancient copper mine situated in Anglesey. UK. *Ecotoxicology and Environmental Safety* 66: 224-231.
- [7] Cui, Y.J., Y.G. Zhu, R.H. Zhai, D.Y. Chen, Y.Z. Huang, Y. Qui and J.Z. Liang. (2004). Transfer of metals from near a smelter in Nanning, China. *Environmental International* 30; 785-791.
- [8] McBride, M.B. (1994). *Environmental Chemistry in Soils*. Oxford Uni. Press, Oxford.
- [9] Khan, A., M. Ibrahim, N. Ahmad and S.A. Anwer. (1992). Studies on accumulation and distribution of heavy metals in agricultural soils receiving sewage effluents irrigation. In: *Proceedings of 4th National Congress of Soil Science*, 24-26 May, 1992. Islamabad. p 607-609.
- [10] Butt, M.S., K. Sharif, B.E. Bajwa and A. Aziz. (2005). Hazardous effect of sewage water on the environment; focus on heavy metals and chemical composition of soil and vegetables. *Management of Environmental Quality* 16(4): 338-346.
- [11] Jawahar, A. and M.A. Javed. (1997). Accumulation and distribution of Cd⁺⁺ and Pb⁺⁺ in sewage, effluent irrigated soils. *Journal of Engineering and Applied Sciences* 16 (1): 43-47.
- [12] Järup, L. (2003). Hazards of heavy metal contamination *British Medical Bulletin* 68: 167–182. DOI: 10.1093/bmb/ldg032.
- [13] Mortada W.I, M.A.Sobh, M.M.El-Defrawy, S.E.Farahat. (2001). Study of lead exposure from automobile exhaust as a risk for nephrotoxicity among traffic policemen. *Am. J.Nephrol* 21: 274-279.
- [14] WHO. (1995). *Lead. Environmental Health Criteria*, World Health Organization vol. 165. Geneva:
- [15] Wierzbicka, M. (1995). How lead loses its toxicity to plants. *Acta Societatis Botanicorum Poloniae*. 64: 81-90.
- [16] Hellström, L., C.G. Elinder, B. Dahlberg, M. Lundberg, L. Järup, B. Persson and O. Axelson. (2001). Cadmium exposure and end-stage renal disease. *Am. J. Kidney Dis*. 38: 1001-1008.
- [17] Lenntech. (2006). "Water Treatment and Air Purification", In: <http://www.lenntech.com/heavy-metals.htm>
- [18] Bernard, A., H. Roels, J.P. Buchet, A. Cardenas, and R. Lauwerys. 1992. Cadmium and health: the Belgian experience. *IARC Scientific Publications* 118:15–33.
- [19] Nordberg, G., T. Jin, A. Bernard, S. Fierens, J.P. Buchet, T. Ye, Q. Kong, and H. Wang. (2002). Low bone density and renal dysfunction following environmental cadmium exposure in China. *Ambio*. 6: 478-481.
- [20] Schuhmacher, M., M.A. Bosque, J.L. Domingo, and J. Corbella. (1991). Dietary intake of lead and cadmium from foods in Tarragons Province, Spain. *The Bulletin of Environmental Contamination and Toxicology* 46, 320-328.
- [21] Eastmond, D.A., J.T. MacGregor, and R.S. Slesinski. (2008). Trivalent Chromium: Assessing the Genotoxic Risk of an Essential Trace Element and Widely Used Human and Animal

Nutritional Supplement. Critical Reviews in Toxicology 38 (3): 173–190.

- [22] Baselt, R. (2008). Disposition of Toxic Drugs and Chemicals in Man, 8th edition, Biomedical Publications, Foster City, CA. pp. 305-307.
- [23] Lança, S., A. Alves, A.I. Vieira, J. Barata, J. de Freitas, and A. de Carvalho. (2002). Chromium-induced toxic hepatitis. *European Journal of Internal Medicine* 13(8), 518-520.
- [24] Lynch E, and Braithwaite R. (2005). A review of the clinical and toxicological aspects of 'traditional' (herbal) medicines adulterated with heavy metals. *Expert Opin Drug Saf.* 4:76–8. [PubMed]
- [25] Kabata-Pendias and Mukherjee. (2007). Trace element from soil to human. Berlin: Springer-verlag.
- [26] ATSDR (Agency for Toxic Substances and Disease Registry). (1994). Toxicological Profile for Zinc (Update). U.S. Department of Health and Human Services, Public Health Service, Agency for Toxic Substances and Disease Registry, Atlanta, GA. TP-93/15. 230pp.
- [27] Nair, M., K.K. Balachandran, V.N. Sankarnarayan, and T. Joseph. (1997). Heavy metals in fishes from coastal waters of Cochin, South West Coast of India. *Indian Journal of Marine Science*.26: 98-100
- [28] NRC, National Research Council. (1989). Recommended dietary allowances. Subcommittee on the Tenth Edition of the RDAs, Food and Nutrition Board, Commission on Life Sciences, National Research Council. Washington, DC: National Academy Press.
- [29] WHO.(2001). Arsenic and Arsenic Compounds. Environmental Health Criteria, World Health Organization vol. 224. Geneva.
- [30] Chilvers, D.C., and Peterson P.J.(1987). Global cycling of arsenic. In: Hutchinson TC, Meema KM (eds) Lead, Mercury, Cadmium and Arsenic in the Environment. Chichester: John Wiley & Sons, 279–303.
- [31] Nriagu, J.O. (1996). History of global metal pollution. *Science* 272: 223-224.
- [32] Kim, J.Y., K.W. Kim, J.U. Lee, J.S. Lee, and J. Cook. (2002). Assessment of As and heavy metal contamination in the vicinity of Duckum Au-Ag mine, Korea. *Environmental geochemistry and Health – Springer*, 24, 215-227.

Received: 07.03.2016

Accepted: 29.05.2017

CORRESPONDING AUTHOR

Zafar Iqbal Khan

Department of Botany, University of Sargodha,
Sargodha, Pakistan

Email: zikhan11@gmail.com

SUBSTANTIAL WATER LOSS FROM FOREST SURFACE SOIL AFTER THE WENCHUAN EARTHQUAKE

Gang Yang¹, Song Cheng^{2,3,*}, Li Zhang⁴, Jiyue Li⁵, Hui Yu⁶

¹School of Life Science and Engineering, Southwest University of Science and Technology, Mianyang 621010, China

²College of Life Science, Qufu Normal University, Qufu 273165 China 273165, China

³GeCheng Global Eco-Tech Inc., 988 Dodridge Road, Columbus, OH 43200, USA

⁴Everglades Wetland Research Park, Florida Gulf Coast University, Naples, FL 34112, USA

⁵College of Forestry, South China Agricultural University, Guangzhou 510642, China

⁶Institute of Mountain Hazards and Environment, Chinese Academy of Sciences, Chengdu 610041, China

ABSTRACT

This study aimed to determine the water loss quantity of surface soil from temperate forests after severe earthquake. We established three plots at each of the landslide and non-landslide *Cupressus funebris* stands at Shiyan site, two plots in the landslide and three in the non-landslide *Cryptomeria fortunei* forest stands at the Shuangdian site near the fault belt of the Wenchuan Earthquake. Each of the plots was 20 m × 20 m. In June and October, for analysis of soil water properties, soil samples were collected by aluminum cylinders (100 cm³) at each of three soil layers (0-10, 10-20, 20-40 cm), respectively, at the center and near the four corners of each plot. We found that saturated water content and capillary water capacity were lower in landslide plots than in non-landslide ones, with the landslide-induced soil water loss at the forest stands ranging from 74 to 357 t/hm², indicating that earthquake-induced landslide dried the surface soil of forest. Such earthquake-induced soil drying varied with different forest stands. Compared with that of *C. funebris*, the surface soil of *C. fortunei* lost less soil water, suggesting the greater water retention ability of the latter. The water stress created by earthquake-induced landslides may be the dominant contributor to the tree mortality in *C. funebris* and *C. fortunei* in the fault zone of the Wenchuan Earthquake.

KEYWORDS:

Wenchuan, Landslide, Soil water properties, Temperate forests, Tree mortality

INTRODUCTION

Natural disturbances are one of the most important factors driving ecosystem development [1]. Earthquakes, as a typical catastrophic disturbance, not only kill people and cause serious economic losses, but also lead to degradation of regional ecosystem function. The Wenchuan Earthquake, with a magnitude of 8.0, occurred on May 12, 2008 in

Southwest China, disturbing a mountainous area of about 20 000 km² along the fault zone in the Longmen Mountains, damaging 17.3 × 10⁴ hm² forests with the volume losses up to 1030.4 × 10⁴ m³ [2]. The damages to forests by the earthquake were mainly caused by collapses (66.2%) and landslides (33.2%). After the earthquake, bedrock and the soil/colluvium horizon simultaneously slid down [3], moving the forest as much as 60 m downhill from their original elevations along the slopes. Such great damage caused various hydrological responses, including changes in stream flow and ground water level [4-6]. It was reported that such damaged forests lost about 2,197 × 10⁶ m³ of water storage capacity, with more than half of the loss through the surface soil [2]. Substantial water losses from surface soil would influence tree growth in this region. According to our previous field survey, the two dominant trees (*Cupressus funebris*, *Cryptomeria fortunei*) have been dying after the earthquake, which would weaken ecosystem functions such as water regulation, soil erosion control, climate stability and may even transform this region from a net C sink to a net C source in a short term [7].

In our previous study, we explored the causes of tree death after the earthquake as well as the effects of the landslide on soil environment and root parameters. The landslides increase soil bulk density, decrease total porosity and capillary porosity, making the soil tightening and drying [8-9], with the effects different between the two dominant species due to their different genetic control. The main causes of tree deaths in our study sites include the great rocking of surface soil in the earthquake which changed soil physical properties, damaged soil surface water balance and decreased water use and absorption by tree root. As a follow-up of the previous research, the present study aimed (1) to evaluate soil water losses in the landslides and (2) to understand the patterns of soil water property variation in the dominant plant species in the earthquake area.



FIGURE 1
Sampling sites in the Wenchuan Earthquake region, China.



FIGURE 2
Photos of sampling sites. A is landslide site dominated by *Cryptomeria fortunei*; B is landslide site dominated by *Cupressus funebris*

MATERIALS AND METHODS

Study site and experimental design. The study site (E104°25.2' to 104°28.5' and N31°49.8' to 31°38.9', a.s.l. 690 m to 1400 m) was along the fault zone in the Longmen Mountains of Sichuan Province in southwest China (e.g. Fig. 1.). Its mean annual precipitation ranged from 800 mm to 1400 mm, and air temperature ranged from -6.2°C in January to 35.3°C in July. The soils of the study sites are generally limestone. *C. funebris* and *C. fortunei* (about 23-27 years old) are two of the dominant trees in the

area. After the earthquake, landslides and collapses induced widespread increases of tree mortality rates of the dominant trees. The tree mortality in *C. funebris* forest was 13.63% for landslide and 2.15% for non-slide stands; the mortality was 10.49% in *C. fortunei* forest stand with landslide. Besides the dominant trees, some bamboo (*Phyllostachys bambusoides* cv. *Tanakae* and *Cunninghamia lanceolata*) forests also grow in this area. The understory plants are mainly *Smilax china* L., *Cyrtococcum patens* L., and *Breynia fruticosa* L.

Eleven plots were established to study the surface soil water properties at two forest sites (Shiyan

dominated by *C. funebris* and Shuangdian by *C. fortunei* near the fault belt (Fig. 1, 2), including 3 plots for both slide and non-slide soils in the Shiyuan site, 3 for the non-slide soil and 2 for the slide soil of the Shuangdian site. Each sampling quadrat was 20 m × 20 m in size.

Soil samples collection. We collected soil samples in June and October of 2009 (13 and 17 months respectively after the earthquake). Within each plot, we chose five places to collect soil samples, one in the center and the other four in each corner of the quadrat. For each soil sampling, we took intact soil cores of about 100 cm³ (5 cm in diameter, and 5 cm in height) in every soil layers (0-10 cm, 10-20 cm and 20-40 cm in depth). Besides, we took approximately 20 g soils from all sampling sites to measure soil water content; these samples were packed and transported in aluminum boxes.

Measurements of soil water properties. We measured water content, saturated water content, capillary moisture capacity and field water capacity. For soil samples in the aluminum boxes, water content was determined by the difference between the fresh and dry soil weights of the boxes measured using a digital balance before and after drying in an oven at 105-110 °C for 72 h.

For the measurements of saturated water content, capillary moisture capacity and field water capacity, each of the soil cores was put on filter paper at the bottom then placed in a tray with water to be absorbed. When all the non-capillary and capillary were full of water (in about 12 h), m_1 was obtained by weighing the core immediately. Then the core with the paper was placed in a dry tray for 2 h to remove non-capillary water from the soil; m_2 was the weight of the core at that time. Thirdly, the core was placed in a dry tray again for another 24 h to continuously remove water, and was weighed for the value of m_3 . Fourthly, the core was dried in an oven at 105-110 °C for 72 h to gain m_4 . Finally, the net weight of the soil sample was measured and defined as m . The parameters of m , m_1 , m_2 , m_3 and m_4 were used to calculate soil saturated water content by Eq. (1), soil capillary moisture capacity by Eq. (2) and bulk density (D) by Eq. (3) respectively.

Total porosity (P_t), capillary porosity (P_c), non-capillary porosity (P_n), saturated water content (W_t : t/hm²), capillary water capacity (W_c : t/hm²), non-capillary water capacity (W_n : t/hm²), of the soil were calculated according to Eqs. (4)-(9). The equations are as follows:

$$S_w = \frac{m_1 - m_4}{m_4 - m} \times 100\% \quad (1)$$

$$C_w = \frac{m_2 - m_4}{m_4 - m} \times 100\% \quad (2)$$

$$D = \frac{m_3 - m_4}{V} \quad (3)$$

$$P_t(\%) = \left(1 - \frac{D}{D_s}\right) \times 100 \quad (4)$$

$$P_c(\%) = C_w \times \frac{D}{V} \times 100 \quad (5)$$

$$P_n(\%) = P_t(\%) - P_c(\%) \quad (6)$$

$$W_t = 10000P_t h \quad (7)$$

$$W_n = 10000P_n h \quad (8)$$

$$W_c = 10000P_c h \quad (9)$$

Where S_w is soil saturated water content (%); C_w is the capillary moisture capacity (%); V is the volume of the soil core (100 cm³); D_s is the soil particle density of 2.65 g/cm³ [8-9].

Data analyses. ANOVA was used to examine the effects of landslide, tree species, soil depth and their interaction on soil water properties. The effect of a variable was considered significant when $P < 0.05$. SPSS 10.0 statistical software (SPSS Inc., Chicago, USA) was used for all analyses.

RESULTS

Tree mortality and water losses. Tree mortality was found to vary with the tree species and occurrence of landslide. Mortality rate of *C. funebris* and *C. fortunei* in stands with and without landslides is shown in Table 1. In the *C. funebris* stand, tree mortality was 13.63% with landslide and 2.15% without landslide. In the *C. fortunei* stand, the data were 10.49% and 0% respectively (Table 1). The tree mortality rate was significantly higher in soils with landslide than in those without.

The surface soil was found to lose large amount of water after the earthquake. The *C. funebris* stand lost 245 t/hm² capillary moisture capacity and 117 t/hm² saturated water content in June, and 357 t/hm² capillary moisture capacity and 170 t/hm² saturated water content in October. Water lost from *C. fortunei* ranged from 73 to 165 t/hm² (Fig. 3).

TABLE 1
Mortality rate of *Cupressus funebris* and *Cryptomeria fortunei* growing in landslide and non-landslide stands

Forest type	Landslide	Tree mortality rate (%)
<i>Cu. funebris</i>	Landslide	13.63
	Non-landslide	2.15
<i>Cr. fortunei</i>	Landslide	10.49
	Non-landslide	0

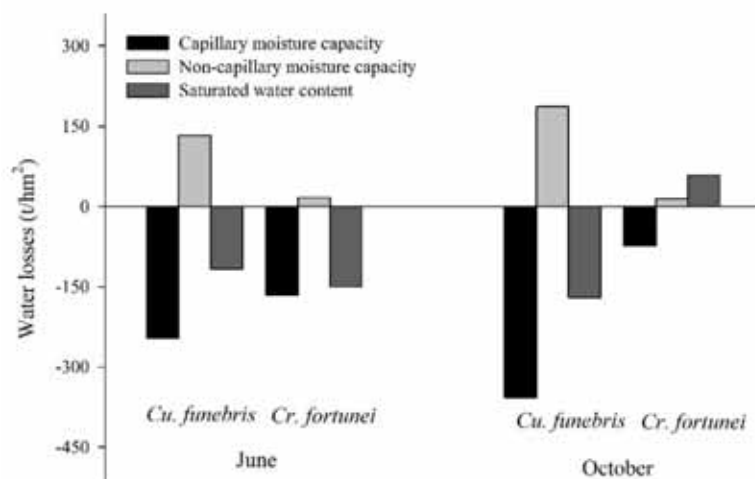


FIGURE 3
Water loss (0-40 cm) of two forest stands after earthquake.

TABLE 2
Analysis of variance (ANOVA) for the effects of month (June and October), landslide (non- and landslide), soil depth (0-10, 10-20, 20-40 cm) and their interaction on soil water properties.

	Month (M)	Landslide (L)	M*L
Water content (%)			
<i>Cu. funebris</i>	0.005	0.213	0.179
<i>Cr. fortunei</i>	0.001	0.236	0.023
Capillary water capacity (t/hm²)			
<i>Cu. funebris</i>	0.837	0.119	0.682
<i>Cr. fortunei</i>	0.029	0.007	0.258
Non-capillary water capacity (t/hm²)			
<i>Cu. funebris</i>	0.901	0.332	0.809
<i>Cr. fortunei</i>	0.414	0.864	0.995
Saturated water content (t/hm²)			
<i>Cu. funebris</i>	0.720	0.011	0.465
<i>Cr. fortunei</i>	0.846	0.260	0.617

Bold numbers are significant difference at $p < 0.05$.

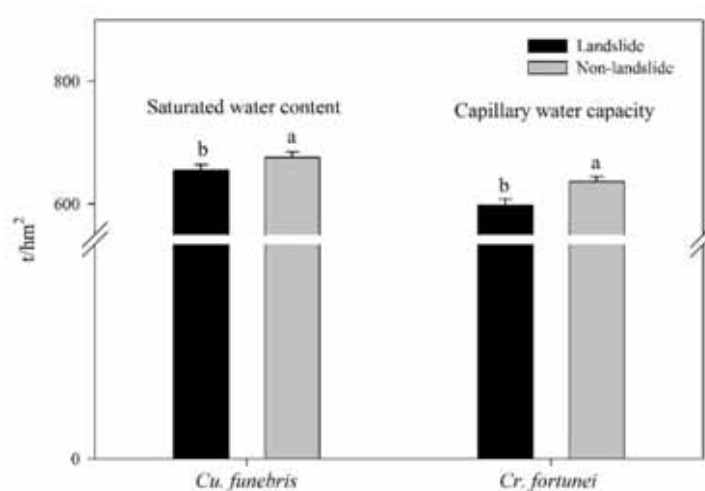


FIGURE 4
The effect of landslide on saturated water content and capillary water capacity of *C. funebris* and *C. fortunei* stands.
(Different letters indicate significant differences at $P < 0.05$.)

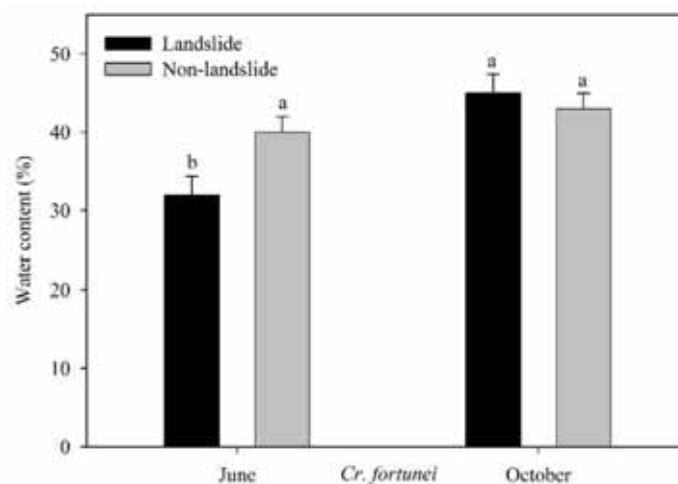


FIGURE 5
Interactive effects of landslide and sampling month (June and October) on water content of *C. fortunei* stand. (Different letters indicate significant differences at $P < 0.05$.)

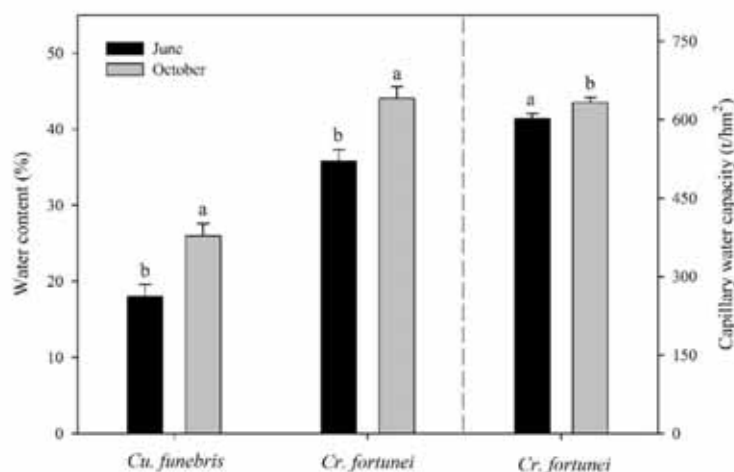


FIGURE 6
The water content and capillary water capacity at *C. funebris* and *C. fortunei* stands in different sampling months. (Different letters indicate significant differences at $P < 0.05$.)

Water properties in landslide soil and its seasonal variation. Statistical analyses indicated significant impact of landslides on the saturated water content and capillary water capacity (Table 2). Saturated water content was 655 t/hm² in *C. funebris* at landslide forest soil, lower than that in non-landslide forest soil (Fig. 4). Capillary water capacity in *C. fortunei* was also lower in landslide than that in non-landslide forest (Fig. 4). Water content and capillary water capacity also showed seasonal variations (Table 2). Saturated water content was significantly lower in June than in October in both types of forest, with that in *C. fortunei* forest with landslide significantly lower than that in the same forest stand without landslide in June, but no statistically significant

difference between stands with and without landslide in October (Fig. 5). Capillary water capacity in *C. fortunei* was also lower in June than in October (Fig. 6).

DISCUSSION

Different degrees of earthquake-induced soil drying between forest stands. Our study found significant impact of landslide on soil hydraulic properties. Both saturated water content and capillary water capacity were lower in landslide plots than in non-landslide ones (Fig. 4 and 6), indicating that the earthquake-induced landslide dried the surface soil.

The landslide-induced soil water loss ranged from 74 to 357 t/hm² in all forest stands (Fig. 3). Soil hydraulic properties varied with the forest stand. With much greater quantity of water loss (Fig. 3), the *C. funebris* stands were found to be more sensitive to the landslide than *C. fortunei* ones (Table 2). Such sensitivity was probably due to the significantly smaller root area and shorter root length of *C. funebris*, since lower root parameters usually indicated relatively lower water retention of the soil [9]. We also found seasonal variation of water content and capillary water capacity in *C. funebris* and *C. fortunei* stands. In addition to landslide, the sampling time also showed significant effect on soil hydraulic properties, with lower water content and capillary water capacity in June than in October (Fig. 5). Such result seemed contradictory to the higher value of precipitation in June (based on the mean of ten years precipitation in this region). We considered such unusual result as probably due to the raining weather of the date of sampling in October.

Drying after the earthquake and its implication for forest ecosystems. We found earthquake and its induced landslides significantly decreased soil water content and changed other soil hydraulic properties, probably resulting in drying of the surface soil of temperate forests in the disaster-stricken region. Changes in soil water content affect heat flux, which can alter micro climatic conditions, and reduce root growth and stand productivity [10-11]. This may be potentially dangerous to the forests involved, since drying has been reported to induce mortality in forests worldwide [12-14]. The mechanism of forest mortality induced by drying may lie in stressed water transport systems. Drying may lead to loss of hydraulic function in coarse roots, and the loss of conductivity in living coarse roots is a significant predictor of fine-root mortality [15].

In fact, we also found that many trees in both *C. funebris* and *C. fortunei* stands died after the Wenchuan Earthquake (Fig. 2). The death of trees was probably due to the decreasing water content of the surface soil. With the depletion of soil water in surface layers available to plants, small trees with roots established at the shallow surface layer die first. As the drying proceeds and deeper soil water exhausts, larger trees are also threatened [16]. As the earthquake-induced drought continues, damaged forests in this region will substantially die off, if no effective measure is taken to restore them.

CONCLUSION

Our data showed that Wenchuan Earthquake and subsequent landslides have significantly affected soil surface water properties. Large amount of water is lost in the landslide plots, though in different degrees between forest types and seasons. The

higher soil water loss in the *C. funebris* stand may be the main reason for its higher tree mortality.

ACKNOWLEDGEMENTS

This study was supported by the National Natural Science Foundation of China (No. 41671244) and the initiative Foundation of Guangdong Province. We would like to thank Zhongyong Zhang, Qian He, Yan Su, Bo Chen, Zhihua Li, Rongxi Li, Bo Peng and Gang Xiong for their assistance in the field and laboratory. Dr. Lujun Li was thanked for his valuable comment on the early manuscript. Ms. Wan Xiong was thanked for her great and patient help in our writing and editing.

REFERENCES

- [1] Attiwill, P.M. (1994) The disturbance of forest ecosystems: the ecological basis for conservative management. *Forest Ecol. Manag.* 63, 247-300.
- [2] Zhang, W., Zhou, L., Pan, F., Liu, B., Luo, J. and Wang, F. (2008) The Application of CBERS Data to Rapid Assessment of Forest Resources Loss in Wenchuan Earthquake Region. *J. Mount. Sci.* 26, 748-754.
- [3] Schuster, R.L. and Highland, L.M. (2007) Overview of the effects of mass wasting on the natural environment. *Environ. Eng. Geosci.* 13, 25-44.
- [4] Mohr, C.H., Montgomery, D.R., Huber, A., Bronstert, A. and Iroume, A. (2012) Streamflow response in small upland catchments in the Chilean coastal range to the MW 8.8 Maule earthquake on 27 February 2010. *J. Geophys. Res.: Earth Surface.* 117, F02032, doi:10.1029/2011JF002138.
- [5] Lai, G., Ge, H., Xue, L., Brodsky, E.E., Huang, F. and Wang, W. (2014) Tidal response variation and recovery following the Wenchuan earthquake from water level data of multiple wells in the nearfield. *Tectonophysics.* 619-620, 115-122.
- [6] Beyabanaki, S.A.R., Bagtzoglou, A.C. and Anagnostou, E.N. (2016) Effects of groundwater table position, soil strength properties and rainfall on instability of earthquake-triggered landslides. *Environ. Earth Sci.* 75, 1-13.
- [7] Chen, H., Wu, N., Yuan, X.Z., Gao, Y.H. and Zhu D., (2009). Aftermath of the Wenchuan Earthquake. *Fron. Ecol. Environ.* 7, 72-72.
- [8] Yang, G., Cheng, S., Yu, H., Zhang, L. and Gao, Y. (2011) Changes in Soil Physical Properties of Forest Floors in the Wenchuan Earthquake-Induced Landslides. *IEEE*, pp. 1-4.
- [9] Cheng, S., Yang, G., Yu, H., Li, J. and Zhang, L.

- (2012) Impacts of Wenchuan Earthquake-induced landslides on soil physical properties and tree growth. *Ecol. Indicators*. 15, 263-270.
- [10] Greacen, E.L. and Sands, R. (1980) Compaction of forest soils. A review. *Soil Res.* 18, 163-189.
- [11] Gerard, C., Sexton, P. and Shaw, G. (1982) Physical factors influencing soil strength and root growth. *Agron. J.* 74, 875-879.
- [12] McDowell, N., Pockman, W.T., Allen, C.D., Breshears, D.D., Cobb, N. and Kolb, T. (2008) Mechanisms of plant survival and mortality during drought: why do some plants survive while others succumb to drought? *New Phytologist*. 178, 719-739.
- [13] Allen, C.D., Macalady, A.K., Chenchouni, H., Bachelet, D., McDowell, N., Vennetier, M., Kitzberger, T., Rigling, A., Breshears, D.D., Hogg, E.H., Gonzalez, P., Fensham, R., Zhang, Z., Castro, Jorge., Demidova, Natalia., Lim, J.H., Allard, G., Running, S.W., Semerci, A. and Cobb, N. (2010) A global overview of drought and heat-induced tree mortality reveals emerging climate change risks for forests. *Forest Ecol. Manag.* 259, 660-684.
- [14] Peng, C., Ma, Z., Lei, X., Zhu, Q., Chen, H., Wang, W., Liu, S., Li, W., Fang, X. and Zhou, X. (2011) A drought-induced pervasive increase in tree mortality across Canada's boreal forests. *Nat. Clim. Change*. 1, 467-471.
- [15] Anderegg, W.R.L., Berry, J.A., Smith, D.D., Sperry, J.S., Anderegg, L.D.L. and Field, C.B. (2012) The roles of hydraulic and carbon stress in a widespread climate-induced forest die-off. *Proceedings of the National Academy of Sciences*. 109, 233-237.
- [16] Nepstad, D.C., Tohver, I.M., Ray, D., Moutinho, P. and Cardinot, G. (2007) Mortality of large trees and lianas following experimental drought in an Amazon forest. *Ecology*. 88, 2259-2269.

Received: 01.11.2016

Accepted: 06.04.2016

CORRESPONDING AUTHOR

Song Cheng

College of Life Science
Qufu Normal University
Qufu 273165 – CHINA

E-mail: chengs889@gmail.com

HEAVY METAL CONTAMINATION AND ECOLOGICAL RISK ASSESSMENT IN THE SEDIMENTS OF MELEN RIVER, DUZCE, TURKEY

Seref Keskin*

Department of Environmental Engineering, Duzce University, 81620, Duzce, Turkey

ABSTRACT

Sediment samples were collected from along the Melen River. Those sediments have been affected municipal and industrial discharges that generated in around Duzce City, Turkey. In this study, the Melen River sediment pollution parameters were investigated. All locations are moderately enriched for Cr, Zn, and Pb and significantly enriched for Cd, Ni, and As. Ecological risk for Cd above 80 (97.21) and As was 76.99, indicating that this heavy metals pose moderate, moderate/high risk to the local ecosystem. All of the samples fall in the polluted areas (PLI>) and the highest pollution load index (PLI) (11.36) value was observed at the DM14 site. According to PCA analysis, the pollution levels of heavy metals in DM1, DM2, and DM3 locations were relatively lower than other sample locations. Cu, Cr, As, and Ni contents falls between the TEL and PEL values, moreover Ni concentration exceed to both of the PEL and ERM values. Especially, according to high values of Eri, PCA, and SQG in between DM9 to DM15 locations, studied sediments have under the moderate toxicity risk for Ni, Cd, As, and Cu.

KEYWORDS:

Enrichment factor, Melen river, Contamination factor, Ecological risk index, Sediment quality

INTRODUCTION

Trace elements are produced from a variety of natural and anthropogenic sources. For example, in fluvial environments, metal pollution can be caused by direct atmospheric deposition, geologic weathering or through the discharge of agricultural, municipal, residential, and industrial waste products [1]. Sediments can be sensitive indicators for monitoring contaminants in aquatic environments [2, 3, 4, 5]. Heavy metals are one of the serious pollutants in environment because of their toxicity and bioaccumulation problems [6, 7, 8, 9]. At higher concentrations, they become dangerous and have toxic effects on liv-

ing organisms and humans. They may affect the ecosystem at several levels beginning with small organisms and ending with larger animals and humans [10]. The major problem encountered in the examination of heavy metal contaminations in sediments is that heavy metals accumulate in sediments as well as from both crustal and anthropogenic sources. Therefore, direct determination of heavy metals in sediments is an inappropriate way to assess the pollution [11].

More than 250 individual industrial units are located in Duzce city discharging of domestic and industrial wastewater directly into the Melen River. Therefore, the objectives of the present work were to (1) to distinguish natural background levels from human pollution in river sediments using geochemical approaches, (2) distribution of heavy metal contamination in sediments, and (3) to evaluate the relationship between heavy metals and estimate the associated ecological risk by considering different indexes.

MATERIALS AND METHODS

Study area. The study area is located in the western Black Sea region (40°54'-40°45'N; 30°57'-31°15'E) (Figure 1). The Melen River and its plain are approximately 160 m high from sea level. In the southern and eastern of the basin, the elevation reaches 1900 m. Due to rapid growth of industrial units in Duzce has dramatically increased urbanization and migration on last two decades. The Melen River is located in the province of Duzce and its water basin is approximately 2250 km² [12]. The Melen River is one of the largest rivers in the western Black Sea region of Turkey [13]. From northeast to south, three tributaries drain into the river that named Ugursuyu, Kucukmelen and Aksu River. All these tributaries, with the initial force provided by steep slopes, carry their erosion products into the Duzce plain. The Melen watershed should be regarded as a "sensitive area" in accordance with the European Union (EU) Urban Wastewater Treatment Directive [13, 14]. The Melen River has expected to be a water source that can supply the drinking water needs of Istanbul until 2040 [12].

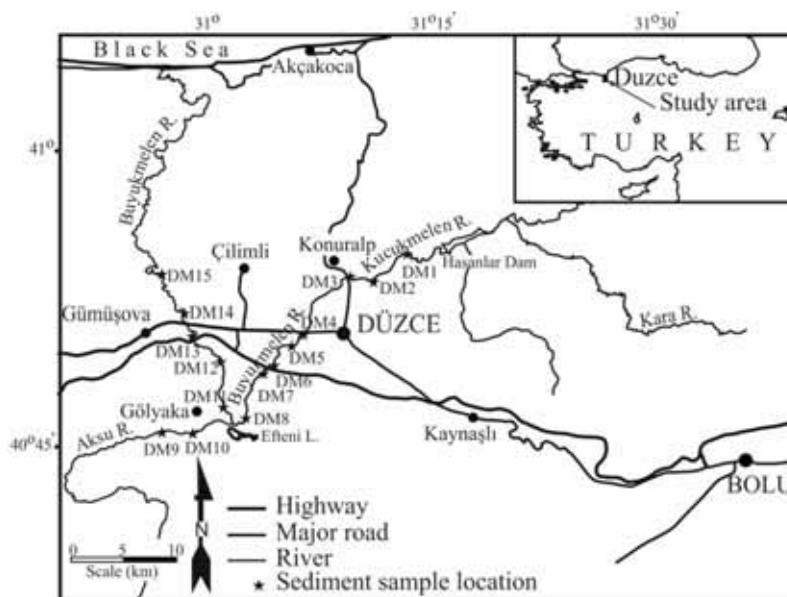


FIGURE 1
Locations of the sampling stations in Melen River, Duzce, Turkey

Sediment Sampling and Preparation. In the present study, total fifteen sites, located in different points along the Melen River and branches were selected (Figure 1). Sediment samples were acquired from the river territory whose water flow allowed for sample collection. A Global Positioning System (GPS) was used to locate sampling sites (Magellan eXplorist 500). Sediment samples collected between March to August 2015 were air-dried. Bulk samples were analyzed for trace element geochemistry. The dry (60°C) bulk sediment samples were finely powdered to 63 μ size using an agate mortar. Preparation organic carbon was determined using about 1 gr of dried and powdered sediment, decarbonated with 1 M solution of HCL, washed with deionized water and then analyzed using Shimadzu TOC-L analyzer at Duzce University Central Research Laboratory (DU-BIT). Trace elements were determined using high-resolution inductively coupled plasma mass spectrometer (ICP-MS) using aqua regia at the Bureau VERITAS Analytical Laboratories, Canada.

Assessment of sediment contamination. Enrichment factor was used to assess the level of pollution and the probable anthropogenic effect in sediments. We prefer to express the metal contamination with respect to the Upper Continental Crust (UCC) [15] to quantify the extent and degree of metal pollution [2,16,17,18]. The enrichment factor (EF) for any element is given by the following:

$$EF = (M_s * Al_s) / (M_x * Al_x)$$

Where M_s and Al_s are the sediment sample concentrations of the heavy metal and Al, while M_x and Al_x are their concentrations in UCC.

EF values between 0.5 and 1.5 propose that the heavy metals may be entirely from crustal materials or natural weathering processes while EF values greater than 1.5 suggests that considerable portion of trace metal is delivered from non-crustal materials [17, 19, 20]. EF \leq 1 No enrichment; EF < 2 Minimal enrichment; EF 2 – 5 Moderate enrichment; EF 5 – 20 Significant enrichment; EF > 20 Extremely high enrichment [8, 21].

Contamination factor (CF). Hakanson (1980) [22] proposed an overall indicator of pollution based on associate data for seven specific trace metals. CF itself is the quotient obtained by dividing the concentration of the elements [17]. The contamination factor for any element is given by the following equation;

$$CF = C_m / C_b$$

Where CF = contamination factor, C_m = mean content of metals in sediment, and C_b = background concentration of the metal. According to the equation: CF < 1 Low contamination, $1 \leq CF < 3$ Moderate contamination, $3 \geq CF < 6$ Considerable contamination, CF > 6 Very high contamination [22, 23].

The sum of contamination factors expresses the value of contamination degree (CD) which describes the contamination of the environment by all examined substances. The degree of contamination defines the quality of the environment in the following way: CD < 8 low degree of contamination, $8 < CD < 16$ moderate degree of contamination, $16 < CD < 32$ considerable degree of contamination, CD > 32 very high degree of contamination [23].

TABLE 1
Mean concentrations (mg/kg dry weight) of heavy metals in sediment samples

Sample No	Longitude	Latitude	Al	Cr	Cu	Zn	Cd	Pb	Ni	As	P	OC
DM 1	31°14'02''	40°54'48''	1.94	32.9	18.3	51.6	0.11	12.05	50.7	2.5	0.05	1.25
DM 2	31°11'51''	40°53'22''	1.19	17	17.	33.8	0.05	5.96	19.6	3.2	0.04	0.23
DM 3	31°10'11''	40°53'30''	1.52	31.5	22.3	41.9	0.14	10.42	44.7	4.2	0.04	1.55
DM 4	31°06'59''	40°50'44''	2.04	47.2	37.3	73.3	0.22	15.11	55.3	8.0	0.05	2.25
DM 5	31°06'04''	40°50'10''	1.35	34.5	19	49.3	0.05	6.36	36.4	2.7	0.04	1.15
DM 6	31°04'46''	40°49'02''	1.32	23.3	20.2	45.3	0.07	6.68	25.2	3.4	0.05	0.53
DM 7	31°04'22''	40°48'43''	1.74	40.4	32.3	61.4	0.11	11.82	41.1	5.5	0.08	1.00
DM 8	31°03'10''	40°46'21''	1.80	33.3	31.9	55.2	0.12	9.93	39	6.2	0.06	0.89
DM 9	30°57'42''	40°45'48''	2.13	95.1	34.7	65.2	0.10	10.59	113.6	4.4	0.06	1.97
DM 10	30°59'27''	40°45'44''	2.41	68.7	37.4	68	0.17	11.85	83.1	4.3	0.06	3.19
DM 11	31°01'43''	40°47'04''	1.98	72	38	71.4	0.14	11.22	88.1	5.2	0.07	1.16
DM 12	31°01'31''	40°49'18''	1.94	80.2	37.1	70.2	0.15	11.44	87.1	6.4	0.07	1.41
DM 13	30°59'44''	40°50'30''	2.54	80.2	54.3	104.7	0.21	15.06	96.7	7.9	0.09	2.17
DM 14	30°58'58''	40°51'39''	2.02	74.1	36.1	73.9	0.14	10.25	94.7	5.8	0.06	3.30
DM 15	30°57'19''	40°53'43''	1.72	58.3	26.1	57	0.08	7.72	79.2	4.6	0.06	2.55

OC; Organic Carbon

TABLE 2
Correlation matrix between heavy metal concentrations in the study area (n=15, p<0.05)

	Al	Cr	Cu	Zn	Cd	Pb	Ni	As	Org C
Al	1.00								
Cr	0.78	1.00							
Cu	0.86	0.77	1.00						
Zn	0.87	0.77	0.95	1.00					
Cd	0.79	0.48	0.80	0.77	1.00				
Pb	0.82	0.48	0.76	0.76	0.92	1.00			
Ni	0.80	0.98	0.72	0.74	0.48	0.48	1.00		
As	0.59	0.59	0.81	0.77	0.84	0.76	0.56	1.00	
Org C	0.69	0.64	0.52	0.57	0.54	0.43	0.71	0.36	1.00

Ecological risk index. Identification and evaluation of ecological risk have very important significances for strengthening regional ecological disaster preventing and protecting the regional ecological security [24]. Ecological risk index displays the potential risks of single heavy metal on the human and ecosystem and reflects the level of heavy metal toxicity and ecological sensitivity to the heavy metal pollution [22]. This method is able to reflect the effects of various contaminants and reveal the comprehensive influence of multiple contaminants in a particular environment [25].

$$Er^i = Tr^i \times CF$$

Where Er^i is the single heavy metal potential ecological risk factor, Tr^i is the response coefficient for the toxicity of the single heavy metal, and CF is contamination factor.

A toxic factor has been defined in the following way for the actual heavy metal: As = $10 \sqrt{5/\sqrt{BPI}}$; Cd = $30 \sqrt{5/\sqrt{BPI}}$; Co = $8 \sqrt{5/\sqrt{BPI}}$; Pb = Ni = Cu = $5 \sqrt{5/\sqrt{BPI}}$; Zn = $1 \sqrt{5/\sqrt{BPI}}$; Cr = $2 \sqrt{5/\sqrt{BPI}}$ [25,26]. BPI = (TP/TOC).100. Where BPI is bioproduction index, TP is phosphor, and TOC is Total Organic Carbon. According to the equation: $Er^i < 40$ Low risk, $40 \leq Er^i < 80$ Moderate risk, $80 \leq Er^i < 160$ Considerable risk, $160 \leq Er^i < 320$ High risk, $Er^i \geq 320$ Very high risk.

Risk index (RI) values were defined as the sum of all potential ecological risk factors (Er^i) for studied heavy metals for a given sediments [26]. $RI < 150$ Low ecological risk, $150 < RI < 300$ Moderate ecological risk, $300 < RI < 600$ Considerable ecological risk, and $RI > 600$ Very high ecological risk [27].

Pollution load index (PLI). That index is obtained as a product of the measured contamination factors of the different trace elements. Pollution load index for each location was determined following the method proposed by Tomlinson et al. (1980) [28].

$$PLI = \sqrt[n]{CF_1 \times CF_2 \times CF_3 \dots \times CF_n}$$

Where, CF is the contamination factor and n is the number of parameters. According to the equation, PLI value of > 1 is polluted whereas PLI value of < 1 indicates no pollution.

Principal component analysis (PCA). In multivariate statistical analysis, PCA has been widely used to deliver more information on links among sampling locations, pollutant concentrations, and correlation patterns [29, 30]. Principal Component (PCA) analysis has been used to find out the possible linear combination of the individual variables of heavy metals that could account for the largest part of the total variance [30, 31, 32, 33]. In this study,

the analysis was performed using the "XLSTAT" (software package).

PCAS₁, that was proposed to assess the pollution level of sediments by Zhiyuan et al., (2011) [32], was applied to assess the contamination levels of heavy metals in stream sediments. PCAS₁ is computed by the equation:

$$PCAS_1 = Z_1 S_1 * E_{i1} / (E_{i1} + E_{i2}) + Z_2 S_1 * E_{i2} / (E_{i1} + E_{i2})$$

$$Z_1 = 0.329 C_{Cr} + 0.388 C_{Cu} + 0.384 C_{Zn} + 0.350 C_{Cd} + 0.345 C_{Pb} + 0.323 C_{Ni} + 0.325 C_{As}$$

$$Z_2 = 0.524 C_{Cr} - 0.026 C_{Cu} + 0.016 C_{Zn} - 0.388 C_{Cd} - 0.354 C_{Pb} + 0.545 C_{Ni} - 0.377 C_{As}$$

Where, S₁ is the value of first sediment sample. Z₁ and Z₂ are the values of first two principal components respectively. E_{i1} and E_{i2} are eigenvalue of first and second. C_i (Cu, Pb, Zn, Ni, As, Cd, and Cr) is the contents of heavy metals in sediments [30, 32].

RESULT AND DISCUSSION

Heavy metal concentrations and distribution. The concentrations of heavy metals were determined in the bulk sediments. The results of trace element analysis in Melen River sediments are presented in Table 1. The amounts of metals ranged as follows; Cu: 54.32 -17.09 (average 30.38), Pb: 15.11- 5.96 (average 10.43), Zn: 104.7 - 33.8 (average 61.48), Ni: 131.9 - 19.6 (average 63.63), As: 8.4-2.5 (average 4.95), Cr: 105.5-17 (average 52.58), Cd: 0.22-0.05 (average 0.12), and Al: 2.59-1.19 (average 1.84) (all values in parts per million, except Al in %). The order of heavy metal concentrations in sediment samples measured in all station was Ni>Zn>Cr>Cu>Pb>As>Cd. In general, the highest values of all metals were found at DM13, except at DM4 for Cd and As, and DM9 for Cr and Ni.

Pearson correlation coefficient (r) values (significant at 0.05) results between heavy metal and other sediment characteristics are presented in Table 2. The Pearson correlation coefficient results show that Cr, Cu Zn, Cd, Pb, and Ni show strong positive correlation with Al (r= 0.78, 0.86, 0.87, 0.79, 0.82, and 0.80 respectively). Cu, Zn, and Ni also show significant correlation with Cr (r = 0.77, 0.77, and 0.98 respectively), probably indicating common influential factors on concentration of these heavy metals. There is a highly or moderately positive relation between Al, Cu, Ni, Cr, and Zn with Organic Carbon (Org C) (r=0.69, 0.52, 0.71, 0.64, and 0.57 respectively). As and Pb are moderately/low moderately correlated with Org C (r=0.36 and 0.43 respectively). This high/medium correlation relationship implies that the presence of Org C has an influence on accumulation of trace metals (except As and Pb) in sediments of the Melen River sediments. The significant correlation between Cr, Cu, Ni, As, Al, and Zn, could be exhausted to anthropogenic inputs of

these heavy metals. The correlation results show that heavy metals of the sampling sediments significantly and positively correlated with each other, demonstrating a collective trend of concentration variation.

Enrichment factor (EF). As can be seen in Figure 2, Melen River sediments showed a wide range of metal enrichment. In general, while the mean EF values shows that significant enrichment for Cu, Cd, Ni, and As, moderate enrichment for Cr, Pb, and Zn is observed. The highest average EF has seen for arsenic with value of 6.7-21.6 (average 14.4). The As EF increase value of 21 in the Duzce-Istanbul (D-100) road (location DM4). Nickel, cadmium, and copper have the other highest EF with average value of 6.07, 5.37, and 5.29 respectively. Overall, the average EF values of these metals followed the sequence As>Ni>Cd>Cu>Zn>Cr>Pb. From the pollution point of view, DM4 location is highly polluted and showed extremely high enrichment for As. DM4 has significant enrichment for Cu, Cd, and Ni, moderately enrichment for Cr, Zn, and Pb. None of the locations (except DM2 for Cr) along the river was free from anthropogenic enrichment. Comparison with Pearson correlation analysis and EF, all metals are moderate or strongly related. Moderate and significant EF values of heavy metals have indicated that an anthropogenic origin, mainly sources from activities such as industrial, household, and domestic wastes. On the other hand, EF for Cr less than 1.5 at the DM 2 location indicating that is mainly derived from different sources, such as the underlying geological rocks.

Contamination factor (CF). Results of heavy metals in Melen River sediments were summarized in Figure 3. All Pb and Cr values of the Melen River sediment samples (except DM9 for Cr) fall in the low/moderate contamination factor. In general, the mean values showed moderate contamination for Cu, Cd, and Ni, (average value 1.23, 1.27, and 1.45 respectively) and considerable contamination for As (average 3.3). The CF value of As increase to 5.33 on the Duzce-Istanbul (D100) road and near the industrial area. (location DM4). The average CF values of all metals followed the sequence As>Ni>Cd>Cu>Zn>Cr>Pb. From the contamination point of view, DM13 location (downstream part of the Melen River) is highly contaminated and showed considerable contamination for As, moderate contamination for Zn, Cd, Cu, and Ni and low contamination for Cr and Pb. Contamination degree same as contamination factor for study area. 73% sediment sampling location fall in moderate contamination degree area and only 27 % samples fall low contamination degree (Figure 3).

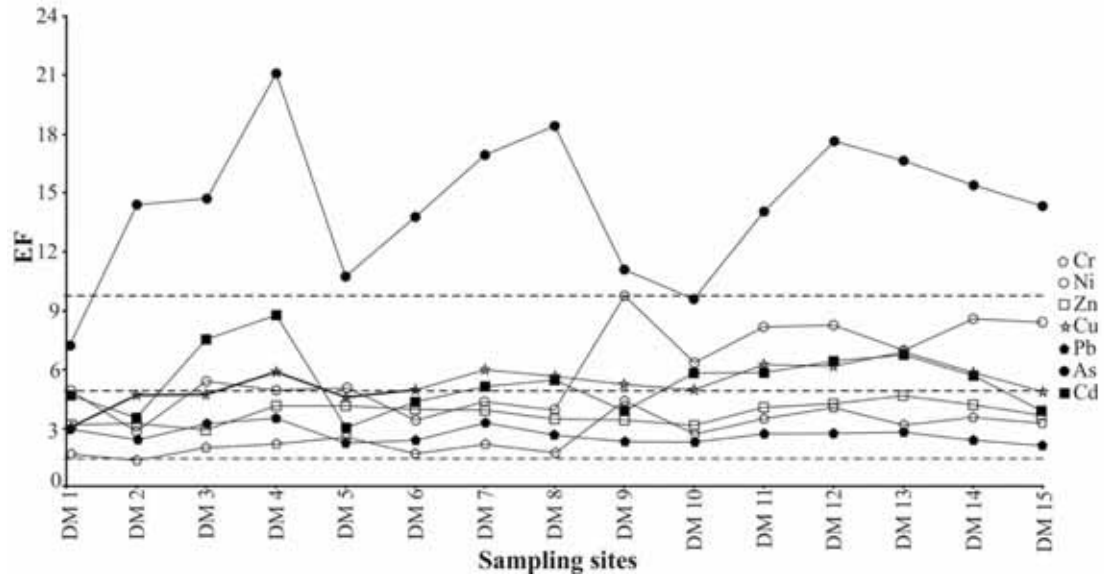


FIGURE 2
Enrichment factors (EF) in Melen River sediments normalized by element concentrations in average UCC [15]

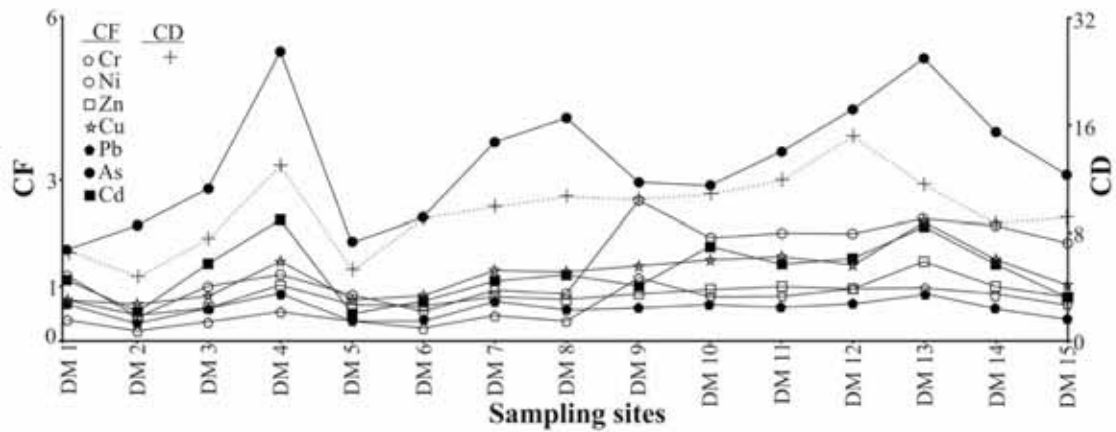


FIGURE 3
Contamination factor (CF) in Melen River sediments

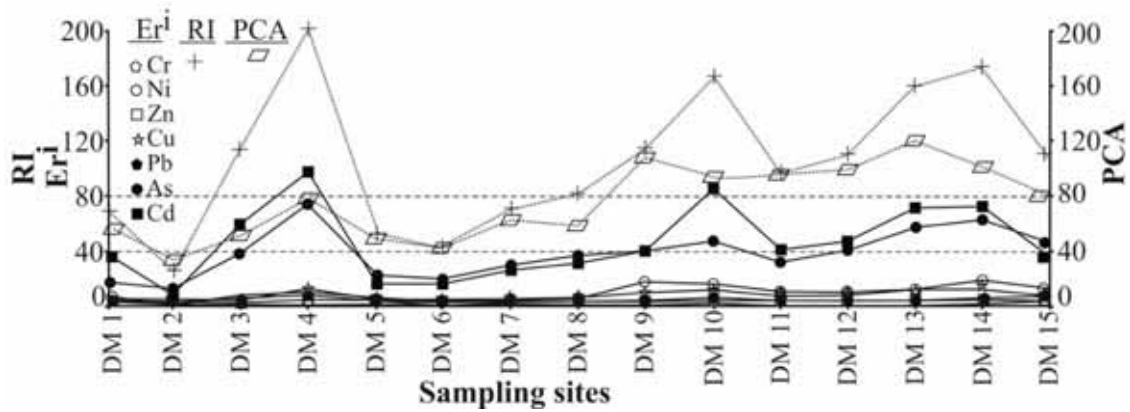


FIGURE 4
Ecological risk index (Er^i), Risk index (RI), and Principal component analysis (PCA_s) in Melen River sediments

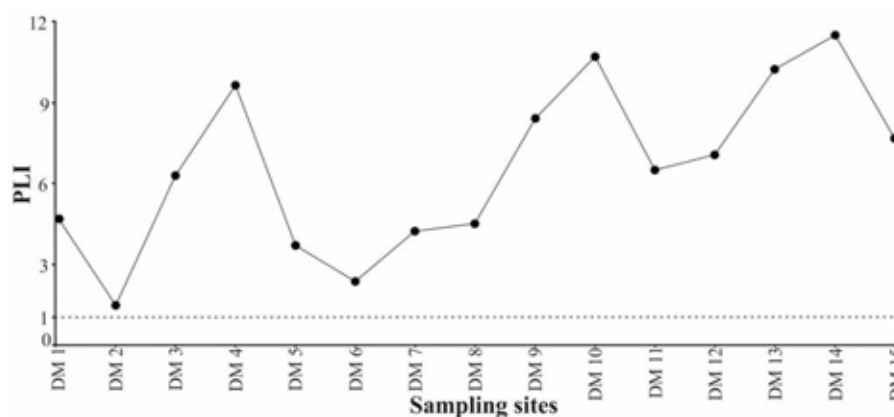


FIGURE 5
Pollution load index (PLI) in Melen River sediments

Ecological risk index (Er^i). The potential ecological risk index of the heavy metals in the Melen River sediments were calculated according to the Hakanson (1980) [22] index method (Figure 4). Cd is the main element give rise to ecological risks and its average Er^i value reaches 45.38. There are six locations with light ecological hazards and nine locations with moderate ecological hazards. Location DM1, DM2, and DM3 are so far from the municipal and industrial area (Figure 1) and the results show the low ecological risk index of heavy metals in those locations. In the different location samples, there is only minimum ecological risk above 80 (considerable risk) for some metals, that is Cd in DM4 (97.21) and DM10 (84.85), Cd in DM3 (58.22), DM9 (40.60), DM12 (45.13), DM13 (70.20), and DM14 (71.07) and As in DM4 (76.989), DM10 (46.74), DM12 (41.93), DM13 (57.51), DM14 (64.12), and DM15 (44.34) indicating moderate risk. Er^i values of all the other sediment samples show low risk. Judging from the total pollution level, the order of ecological risk associated with the seven heavy metals is $Cd > As > Ni > Cu > Pb > Cr > Zn$.

Ecological index (Er^i) only reflects the contamination of single heavy metals [22]. However, in the natural environment, heavy metal contamination is always complexes. Therefore, risk index provides the only concrete evaluation of the overall pollution. Ecological risk assessment analyses the possible process of negative ecological effects that may appear or are emerging when the ecosystem is exposed to one or more stress factors [24,33]. The maximum potential ecological risks are expressed by the Risk Index (RI). While the highest RI value of 15 sediment samples locations are 203.58 in DM 4, and the lowest RI value are 25.75 in the DM2 location (Figure 4). The average RI of 15 locations is 105.83. According to risk index, DM4 (203.58), DM10 (169.12), DM13 (160.12), and DM14 (174.69) have moderate ecological risk level ($150 \leq RI < 300$) and the other 11 locations have low potential ecological

risk levels with $RI < 150$. RI could characterize sensitivity of local ecosystem to the toxic metals and represent ecological risk resulted from the overall contamination [32]. As and Cd have a high ecological risk in the Duzce Plain because of very high CF, Er^i , and RI values. Especially, in the DM4, DM13, and DM14 locations have a moderate or high toxicity risk for all risk indexes. Location DM4 is near the industrial area (Duzce Small Industrial Area), DM13 is under the highway bridge in the Sultaniye village (east of Golyaka Town) and DM14 is located in the industrial zone of Golyaka Town. Probably Melen River sediments should have been affected by the pollution from those sites.

Pollution load index (PLI). As shown in Figure 5, the mean PLI value is 6.59, indicating pollutants. The highest PLI (11.36) value observes at the DM14 location (downstream part of the Melen River) and lowest PLI of 15 locations is 1.5 in location DM2 (upstream part of the Melen River). The order of locations in terms of pollution load index is $DM14 > DM10 > DM4 > DM13 > DM9 > DM15 > DM12 > DM11 > DM3 > DM1 > DM8 > DM7 > DM5 > DM6 > DM2$.

Principal component analysis (PCA). PCA is used to evaluate the principal components, compute the eigenvectors, identify the significant impact factors and further determine the common pollution sources [33]. Results of the studied sediment samples are reported Table 3. According to the results of the initial eigenvalues, two principal components are considered that accounted for 90.8% of the total variances. The first PCA accounts for 76.7% of the total variance and have strong positive loadings on Cu, Pb, Zn, Ni, As, Cd, and Cr and indicate that metals might have derived the same sources. The two main highways E5 and D-100 cross the study area (Figure 1).

TABLE 3
The results of Principal component analysis (PCA)

Eigenvalue	Proportion	Cumulative	Element	Component matrix	
				F1	F2
6.14	76.70	90.79	Al	0.38	0.10
1.13	14.09	96.03	Cr	0.33	0.52
0.42	5.24	98.01	Cu	0.39	-0.03
0.16	1.99	98.86	Zn	0.38	0.02
0.07	0.85	99.50	Cd	0.35	-0.39
0.05	0.64	99.89	Pb	0.35	-0.35
0.03	0.39	100.00	Ni	0.32	0.55
0.01	0.11	100.00	As	0.33	-0.38

TABLE 4
Results of Sediment Quality Guidelines (SQG) for single heavy metal from two methods for the Melen River sediments. TEL: Threshold Effects Level, PEL: Probable Effects Level, ERL: Effects Range Low 10th percentile values in effects, ERM: Effects Range Median 50th percentile value in effects [37, 39].

	Cr	Cu	Zn	Cd	Pb	Ni	As
TEL	52.3	18.7	124	0.68	30.24	15.9	7.24
PEL	160	108	271	4.21	112.18	42.8	41.6
ERL	81	34	150	1.2	46.70	20.9	8.2
ERM	370	270	410	9.6	218	51.6	70
Compared with TEL and PEL % of samples <TEL	53.3	13.3	100	100	100	0	86.7
% of sample between TEL and PEL	46.7	86.7	0	0	0	33.3	13.3
% of samples >PEL	0	0	0	0	0	66.7	0
Compared with ERL and ERM % of samples <ERL	93.3	53.3	100	100	100	6.7	100
% of sample between ERL and ERM	6.7	46.7	0	0	0	40	0
% of samples >ERM	0	0	0	0	0	53.3	0

High metal concentrations in the region, could have been related to heavy traffic, industrial and domestic wastewater, and large population density. The second PCA, which contributes 14.09% of the total variance highly, Cr and Ni and had significant correlations indicating that they may have similar sources. It is well known that ultramafic rocks consist of high level Cr and Ni. Unfortunately, these rocks are almost non-outcrop in background area of Duzce plain. Wastewater and sludge from metallurgy industries, metal refining, and smelting are the probably sources of chromium and nickel pollutions.

The method of PCAs determine the comprehensive pollution level; while the technique of Eri and RI are mainly show the ecological risk levels of elements, that have higher potential toxicity response value or higher concentrations in sediments. Although the PCAs cannot identify the ecological risk levels of heavy metals in soil, their results can give the comprehensive information of heavy metals contamination in sediments [32, 33, 35, 36]. The pollution levels of heavy metals in DM1, DM2, and DM3 locations are relatively lower than other sample locations. All these locations are located upstream part of the Melen River. Especially, in the upstream part of the region have almost no settlements and industry area. DM9 to DM15 locations have a relatively high-level heavy metal contents. Because of population density, industrialization, and the highway traffic are situated in the midstream and downstream parts of the region.

Sediment quality guidelines (SQG). Sediment quality guidelines are important tool for assessment of contamination in sediments [37, 38, 39, 40]. Heavy metal contamination refers to the excessive deposition of toxic heavy metals in the environment caused by human activities. The concentrations of some heavy metals are beneficial and essentially required for normal and healthy body growth and functions of living organisms such as metal nutritional requirements (Co, Cu, Fe, Mn, Mo, Ni, and Zn). On the other hand, some heavy metals can cause biological toxicity, such as Cd, As, Cr, and Pb etc. [41]. In the present study (Table 4), sets of SQG such as, threshold effects level (TEL), probable effects level (PEL), effect range low (ERL), and effect range median (ERM) parameters were investigated. In this way, it will be possible to estimate whether there is heavy metal contamination or environmental risks in Melen River basin sediments.

The present data for the Melen River sediments show considerable lower concentrations of Cd and Pb than those of TEL. In contrast, Ni concentration is at all locations higher than TEL value. Cr concentration at DM9, DM10, DM11, DM12, DM13, DM14, and DM15 locations is slightly higher than TEL value (Table 4). Cu concentration at DM2 location is less than TEL value. It has been suggested that the ERM and PEL parameters are better at predicting toxicity than are the ERL and TEL [38]. Cu is between TEL and PEL value in 86.7% of the locations. Cr, Ni, and As are fall between TEL and PEL param-

eters that its ratio in 46.7, 33.3, and 13.3 % (respectively) of the locations. 66.7 % of the locations have a higher Ni concentration than PEL. Among the studied heavy metals, nickel is the only metal that exceeds the ERM value (53.3 % locations). The highest Ni concentration shows more than two fold ERM value and found in DM9 location. Cu, Ni, and Cr are between ERL and ERM values and they have found in 46.7, 40.0, and 6.7 % (respectively) of the locations. Accordingly, it appears clearly that Melen River sediments have contaminated with Cr, Ni, and Cu, especially at the part of downstream locations (such as DM9 to DM15 locations).

CONCLUSIONS

The effect of anthropogenic heavy metal pollution in Melen River sediments were evaluated using enrichment factor, contamination factor, contamination degree, potential ecological risk index, and pollution load index for Cu, Cd, Cr, Zn, Pb, As, and Ni in bulk sediments in fifteen locations. Melen River sediments have mean concentrations of Cu, Cd, Cr, Zn, Pb, As, and Ni that exceed background metal values for the study area. EF results demonstrate almost all samples have Cu, Ni, and As significant enrichment. Contamination factor and contamination degree index indicated that the overall pollution in the reclaimed sediment sampling location fall in moderate contamination degree. Ecological risk for Cd above 80 (97.21) and As was near 80 (76.99), indicating that this heavy metals posed moderate, moderate/high risk to the local ecosystem. Especially, DM4, DM13 and DM14 locations have moderate toxicity risk. Concentrations of metals in sediment increased in Duzce (DM4) and Golyaka (DM13 and DM14) areas. These results show an anthropogenic source of heavy metals that mainly derived from activities such as industrialization, urbanization, industrial and domestic wastewater, and others. 66.7% samples for Ni exceed PEL value. Furthermore, nickel concentration is almost two times more than ERM value in the DM-9 location. In summary, all of the data indicate that the pollution parameters (especially for Cu, Ni, Cd, and As) have become an environmental problem in Melen River aquatic ecosystems.

ACKNOWLEDGEMENTS

The author thanks to Duzce University Scientific Research Project Funding (DUBAP) for financial support (Project No DUBAP-2015.06.02.278).

REFERENCES

- [1] Demirak, A., Yilmaz, F., Tuna, A.L. and Ozdemir, N. (2006) Heavy metals in water, sediment and tissues of *Leuciscus cephalus* from a stream in southwestern Turkey. *Chemosphere* 63, 1451-1458.
- [2] Ergin, M., Saydam, C., Basturk, O., Erdem, E. and Yoruk, R. (1991) Heavy metal concentrations in surface sediments from the two coastal inlets (Golden Horn Estuary and Izmit Bay) of the northeastern Sea of Marmara. *Chem Geol* 91(3), 269-285.
- [3] Ergin, M., Kazan, B., Yucesoy-Eryilmaz, F. and Eryilmaz, M. (1998) Metal contamination in the bottom sediments of the Gulf of Iskenderun. *International Environmental Studies* 55, 101-119.
- [4] Pekey, H., Karakas, D., Ayberk, S., Tolun, L. and Bakoglu, M. (2004) Ecological risk assessment using trace elements from surface sediments of Izmit Bay (Northeastern Marmara Sea) Turkey. *Mar Poll Bull* 48(9-10), 946-953.
- [5] Yalcin, M.G. (2009) Heavy mineral distribution as related to environmental conditions for modern beach sediments from the Susanoglu (Atakent, Mersin, Turkey). *Environ Geol* 58, 119-129.
- [6] Fang, T.H. and Hong, E. (1999) Mechanisms influencing the spatial distribution of trace metals in surficial sediments off the southwestern Taiwan. *Mar Poll Bull* 38(11), 1026-1037.
- [7] Tam, N.F.Y. and Wong, Y.S. (2000) Spatial variation of heavy metals in surface sediments of Hong Kong mangrove swamps. *Environ Poll* 110(2), 195-205.
- [8] Keskin, S. (2012) Distribution and accumulation of heavy metals in the sediments of Akkaya Dam, Nigde, Turkey. *Environ Monit Assess* 184(1), 449-460.
- [9] Polat, N. and Akkan, T. (2016) Assessment of heavy metal and detergent pollution in Giresun coastal zone, Turkey. *Fresen. Environ. Bull.* 25(8), 2884-2890.
- [10] Emam, A. and Saad-Eldin, M. (2013) Distribution and environmental geochemistry of some heavy metals in stream sediments of Wadi Allaqi, South Eastern Desert of Egypt. *Arabian J Geosci* 6, 1325-1332.
- [11] Idris, A. (2008) Combining multivariate analysis and geochemical approaches for assessing heavy metal level in sediments from Sudanese harbors along the Red Sea coast. *Microchemical Journal* 90, 159-163
- [12] Pehlivan, R. (2010) The effect of weathering in the Buyukmelen River basin on the geochemistry of suspended and bed sediments and the hydrogeochemical characteristics of river water, Duzce, Turkey. *J Asian Earth Sci* 39, 62-75.
- [13] Baykal, T., Acikgoz, I., Udoh, A. U. and Yildiz, K. (2011) Seasonal variations in phytoplankton

- composition and biomass in a small lowland river-lake system (Melen River, Turkey). *Turk J Biol* 35, 485-501.
- [14] Unsal, N. and Celik M. (2010) Hydrogeochemistry and water quality evaluation along the flow path in the unconfined aquifer of the Duzce plain, North-western Turkey. *Acta Geol Sinica* 84(1), 213-222.
- [15] Taylor, S.R. and McLennan, S.M. (1985) *The continental crust: Its composition and evolution*. Oxford: Blackwell, 312.
- [16] Pekey, H. (2006) Heavy metals pollution assessment in sediments of the Izmit Bay, Turkey. *Environ Monit Assess* 123, 219-231.
- [17] Abraham, G.M.S. and Parker, R.J. (2008) Assessment of heavy metal enrichment factors and the degree of contamination in marine sediments from Tamaki Estuary, Auckland, New Zealand. *Environ Monit Assess* 136, 227-238.
- [18] Harikumar, P.S. and Jisha, T.S. (2010) Distribution pattern of trace metal pollutants in the sediments of an urban wetland in the southwest coast of India. *Int J Eng Sci Tech* 2(5), 840-850.
- [19] Zhang, J. and Liu, C.L. (2002) Riverine composition and estuarine geochemistry of particulate metals in China-weathering features, anthropogenic impact and chemical fluxes. *Estuarine Coastal and Shelf Sci* 54, 1051-1070.
- [20] Zhang, W., Feng, H., Chang, J., Qu, J., Xie, H. and Yu, L. (2009) Heavy metal contamination in surface sediments of Yangtze River intertidal zone: An assessment from different indexes. *Environ Poll* 157, 1533-1543.
- [21] Chen, C.W., Kao, C.M., Chen, C.F. and Dong, C.D. (2007) Distribution and accumulation of heavy metals in the sediments of Kaohsiung Harbor, Taiwan. *Chemosphere*, 66(8), 1431-1440.
- [22] Hakanson, L. (1980) An ecological risk index for aquatic pollution control: A sedimentological approach. *Water Res* 14(8), 975-1001.
- [23] Loska, K., Cebula, J., Pelczar, I., Wiechula, D. and Kwapulinski, J. (1997) Use of enrichment and contamination factors together with geoaccumulation indexes to evaluate the content of Cd, Cu, and Ni in the Rybnik water reservoir in Poland. *Water, Air, Soil Poll* 93, 347-365.
- [24] Shao, J., Zhang, Q., Peng, X. and Liu, T. (2017) Risk assessment on ecosystem based on uncertain measurement theory. *Fresen. Environ. Bull.* 26(4), 2885-2894.
- [25] Wang, J., Liu, W., Yang, R., Zhang, L. and Ma, J. (2013) Assessment of the potential ecological risk of heavy metals in reclaimed soils at an opencast coal mine. *Disaster Advance* 6, 366-377.
- [26] Dauvalter, V. (1992) Concentrations of heavy metals in superficial lake sediments of Pechenga district Murmansk region, Russia. *Vatten* 48, 141-145.
- [27] Fiori, C.S., Rodriguez, A.P.C., Santelli, R.C., Cordeiro, R.C., Carnevali, R.G., Araujo, P.C., Castilhos, Z.C. and Bidone, E.D. (2013) Ecological risk index for aquatic pollution control: a case study of coastal water bodies from the Rio de Janeiro State, southeastern Brazil. *Geochim Brasil* 27(1), 24-36.
- [28] Tomlinson, D.L., Wilson, J.G., Harris, C.R. and Jeffrey D.W. (1980) Problems in the assessment of heavy metal levels in estuaries and the formation of a pollution index. *Helgolander Meeresuntersuchungen* 33, 566-575.
- [29] Skrbic, B., Szyrwinska, K., Durisic-Mladenovic, N., Nowicki, P. and Lulek, J. (2010) Principal component analysis of indicator PCB profiles in breast milk from Poland. *Environ Int* 36, 862-872.
- [30] Chabukdhara, M. and Nema, A. (2012) Assessment of heavy metal contamination in Hindon River sediments: A chemometric and geochemical approach. *Chemosphere* 87, 945-953.
- [31] Facchinelli, A., Sacchi, E. and Mallen, M. (2001) Multivariate statistical and GIS-based approach to identify heavy metal sources in soils. *Environ Poll* 111, 313-324.
- [32] Zhiyuan, W., Dengfeng, W., Huiping, Z. and Zhiping, Q. (2011) Assessment of soil heavy metal pollution with principal component analysis and geoaccumulation index. *Procedia Environmental Sciences (ESIAT2011)* 10, 1946-1952.
- [33] Wang, L., Li, Y., Yu, L., Lv, X., Wang, X. And Feng, M. (2016) Distribution, assessment and statistical analysis of sediment heavy metal pollution in the Shaying River Basin, China. *Fresen. Environ. Bull.* 25(8), 2909-2918.
- [34] Yisa, J., Jacob, J. O. and Onoyima, C.C. (2012) Assessment of toxic levels of some heavy metals in road deposited sediments in Suleja, Nigeria Jonathan. *Amer J Chem* 2(2), 34-37.
- [35] Brady, P.J., Ayoko, G.A., Martens, W.N. and Goonetilleke, A. (2015) Development of a hybrid pollution index for heavy metals in marine and estuarine sediments. *Environ Monit Assess* 187(5), 306.
- [36] Eroglu, E., Ak, N., Guney, I. and Sener, E. (2016) Component analysis of the different fish samples containing heavy metals in Istanbul Bosphorus. *Fresen. Environ. Bull.* 25(1), 292-299.
- [37] MacDonald, D.D., Ingersoll, C.G. and Berger, T.A. (2000) Development and evaluation of consensus-based sediment quality guidelines for freshwater ecosystems. *Archives of Environmental Contamination and Toxicology* 39, 20-31.
- [38] Zabetoglou, K., Voutsas, D. and Samara, C. (2002) Toxicity and heavy metal contamination

of surficial sediments from the Bay of Thessaloniki (Northwestern Aegean Sea) Greece. *Chemosphere* 49, 17-26.

- [39] Long, E.R, Ingersoll, C.G. and Macdonald, D.D. (2006) Calculation and uses of mean sediment quality guideline quotients: a critical review. *Environ Sci Tech* 40, 1726-1736.
- [40] Yalcin, M.G., Narin, I. and Soylak, M. (2007) Heavy metal contents of the Karasu Creek sediments, Nigde, Turkey. *Environ Monit Assess* 128(1-3), 351-357.
- [41] Mutlu E. and Kurnaz, A. (2017) Determination of seasonal variations of heavy metals and physicochemical parameters in Sakiz Pond (Kastamonu-Turkey). *Fresen. Environ. Bull.* 26(4), 2807-2816.

Received: 20.06.2016

Accepted: 15.05.2017

CORRESPONDING AUTHOR

Seref Keskin

Department of Environmental Engineering
Duzce University
81620, Duzce – TURKEY

E-Mail: serefkeskin@duzce.edu.tr

QUALITY ASSESSMENT OF MARITSA RIVER WATER AS A MAIN SOURCE FOR IRRIGATION IN THRACIAN VALLEY

Gergana Kostadinova¹, Diayna Dermendzhieva¹, Georgi Beev², Georgi Petkov^{1,*},
Dimitar Pavlov³, Elica Valkova²

¹Trakia University, Faculty of Agriculture, Department of Applied Ecology and Animal Hygiene, Stara Zagora, Bulgaria

²Trakia University, Faculty of Agriculture, Department of Biochemistry, Microbiology and Physics, Stara Zagora, Bulgaria

³Trakia University, Faculty of Agriculture, Department of Plant Science, Stara Zagora, Bulgaria

ABSTRACT

The water of many rivers all over the world is used for irrigation purposes. Maritsa River, located in the Thracian Valley, Balkan Peninsula, on the territory of Bulgaria, Turkey and Greece, is one of them. Apart the water quantity, the performance of irrigated agriculture depends also on its quality. In the present study, the quality of Maritsa River water as a source for irrigation was assessed at two monitoring points (MPs) in Bulgaria – MP-1 (upper river) and MP-2 (middle course of the river). The samples were taken in June and August 2014 and 31 physicochemical and microbiological parameters were screened. Water sampling and preparation were performed according to Bulgarian standard complied with ISO standards. Physicochemical parameters were determined spectrophotometrically, by Multi/340i SET and AAS. For the estimation of total and specific microbial load, selective chromogenic culture medium sheets were used. It was found that river water quality meets the requirements of Bulgarian standard for irrigation water with respect to: temperature, pH, electrical conductivity, total hardness, Ca, Mg, dissolved oxygen, BOD₅, COD, N-NH₄ (except for June), N-NO₃, Cl⁻, SO₄²⁻, P-PO₄ (except for August), suspended solids (except for June), Mn, Fe, Cu, Zn, Pb, Ni, Cd, Cr and As. Deviations from the standard were observed for all microbiological parameters at both MPs. The metal concentrations decrease in the order of Fe>Zn>Ni>Pb>Cr>Cu>As>Mn>Cd. Many significant correlations were revealed between controlled water parameters.

KEYWORDS:

Maritsa River, physicochemical parameters, heavy metals, microbiological parameters, assessment, water quality

INTRODUCTION

Traditionally, irrigation water is grouped into various quality classes in order to guide the user to the potential advantages as well as problems associated with its use and to achieve optimum crop production. The suitability of water for irrigation greatly depends on the water quality, climatic conditions, physical and chemical properties of the soil, the salt tolerance of the crop grown and agricultural practices [1, 2, 3, 4, 5]. The economic impact resulting from improving irrigation performance is not sufficiently investigated in Mediterranean region since a great number of factors influence them [6]. One of the main factors is the level of irrigation, which directly corresponds to the yield and mineral nutrient content of crops [7, 8, 9]. Another one is the quality of water for irrigation purposes.

The main water quality parameters that determine the suitability of water for irrigation are salinity, specific ion toxicity, trace elements, nutrients and pathogens [10, 11, 12]. These parameters are introduced in FAO [13], WHO [14] and USEPA [15] guidelines for water quality for irrigation [16], which were complied with Bulgarian standard, accepted in 2009 [17].

With a view of regional climate changes towards global warming and drought, the role of management and the quality of irrigation water will be of key importance for the Balkan countries [5, 18, 19]. Maritsa River, the biggest river in the Balkan Peninsula (521.6 km, with a catchment area of 53 000 km², of which 321 km and 21 084 km² in Bulgaria) is of great importance for the South East Balkan economy - agriculture, industry, energetics and other human activities. In recent years, of the total amount of river water - about 7786.2 million m³/y, for irrigation purposes are used about 15.4% (1201.8 million m³/y) [20]. The river is strongly impacted by anthropogenic activities as it passes through plenty of settlements, along industrial enterprises, farms and areas with intensive agriculture that discharge their wastewater into the river creating preconditions for deterioration of the water quality [21]. Some of the most fertile fields of Bulgaria, Turkey and Greece

are situated in Maritsa River valley. Their crop productivity strongly depends on irrigation from the water of the river, which provides increased yields of the crops (rice, tobacco, cotton, corn, vegetables, fruits, etc.) grown in the river basin from 20% to 100% [22].

The aim of the present study was to monitor the water quality of upper-middle course of Maritsa River using physicochemical and microbiological parameters and assess its suitability and applicability for irrigation, in accordance with Bulgarian standard [17].

MATERIAL AND METHODS

Study area and monitoring. The water quality of Maritsa River was monitored in June and August 2014, in two selected monitoring points (MPs): MP-1 (upper course of the river) at Belovo town (N 42.12830° E 24.01544°), type of water body R5 - semi-mountainous type, poor ecological condition of the water body and MP-2 (middle course of the river) at Mirovo village, Stara Zagora District (N 42.09548° E 25.07365°), type of water body R12 - big plane rivers type, poor ecological and chemical condition of the water body (Figure 1).



FIGURE 1
Maritsa River basin with monitoring points

Sampling and sample preparation. Water samples were collected once per month from both MPs. In compliance with the standard [17], the frequency of water quality monitoring should be at least once for every irrigation season (June-August). For water sampling and sample preparation for analysis, international references (ISO 5667-1, 2, 3, 6) were used. The samples for physicochemical analysis were collected in dark chemical clean glass containers (3 L) and for microbiological analysis in sterilized glass containers (0.25 L). The collected water samples were transported in a cool bag (at 4-6 °C) and processed for analysis within 2 h after the collection.

Parameters of water and methods for analysis. The following 31 parameters, characterizing irrigation water quality [17] were determined: physicochemical parameters – temperature (T °C), pH,

dissolved oxygen (DO) and electrical conductivity (EC) - *in situ*, with field Multi-340i/SET meter; total hardness (TH) by Bulgarian State Standard (BSS) 3775, calcium (Ca²⁺) and magnesium (Mg²⁺) content by ISO 6058, chlorides (Cl⁻) by ISO 9297, N-NH₄ by BSS 3587, N-NO₃ by BSS 3758, SO₄²⁻ by BSS 3588 and P-PO₄ by EN 6878-1, using UV-VIS Spectrophotometer JENWAY 6705; suspended solids (SS) by BSS 17.1.4.04; COD by ISO 6060 with a spectrophotometer; BOD₅ by EN 1899-1, 2; manganese (Mn), iron (Fe), copper (Cu), zinc (Zn), lead (Pb), nickel (Ni), cadmium (Cd), chromium (Cr) and arsenic (As) contents by ISO 15586 with an AAS (AAAnalyst/800 Perkin-Elmer); microbiological parameters – aerobic mesophilic microorganisms (AMO) [23], sanitary-indicator microorganisms (coliforms, *Escherichia coli*, *Enterobacteriaceae*) and pathogens (*Salmonella* spp.) were determined by plating of 1 ml of the sample solutions or appropriate dilutions on selective, chromogenic culture medium sheets (Rida[®]Count Total; Rida[®]Count *E. coli*/Coliform; Rida[®]Count *Salmonella*/Enterobacteriaceae, R-Biopharm AG, Germany). The sheets were inoculated in duplicates, incubated at 35°C for 24-48 h and the colonies were counted. Specific microorganisms form colonies of different colour on the specific test cards. The results are expressed in colony forming units (CFU/ml) and then are additionally transformed into total coli titer and *E. coli* titer, according to the requirements of the standard [17].

Water quality assessment. Assessment of Maritsa River water quality was carried out by comparing the results obtained for the investigated parameters with the standard limit values [17], separated in 5 groups: Group A – salinity (EC), Group B - water infiltration rate (Ca, Mg), Group C - toxicity (Mn, Fe, Cu, Zn, Pb, Ni, Cd, Cr, As), Group D – sanitary quality indices (total coli titer, *E. coli* titer, *Enterobacteriaceae* and *Salmonella* spp.), Group E – Miscellaneous (T °C, pH, TH, DO, SS, COD, BOD₅, N-NH₄, N-NO₃, SO₄²⁻, P-PO₄, Cl⁻).

Statistical analysis. All data were analyzed by STATISTICA 6.1 (Statsoft. Inc., Tulsa, OK, USA, 1984-2002).

RESULTS AND DISCUSSION

Parameters characterizing the water salinity. The basic parameter, characterizing the water salinity is EC. It is directly related to the sum of the cations (or anions), as determined chemically and is closely correlated, in general, with the total salt concentration. The EC values in both MPs were from 5.29 to 8.96 times lower than the permissible limit for irrigation water (Table 1). The established values are commonly found to river water - up to 300 μS/cm

[1]. It is argued that low salinity water decrease water infiltration rate [24].

Parameters characterizing the water infiltration rate. The two commonest water quality factors which influence the normal infiltration rate are salinity of the water and Na, Ca and Mg content. The measured Ca and Mg concentrations in water of both MPs were significantly lower than the limit values stipulated in standard [17] - for Ca content: from 13.8 to 18.5 times and for Mg content: from 16.2 to 61.7 times (Table 1).

Despite the fact that the water meets the requirements for irrigation with respect to Ca and Mg content, it should be noted that low-salt water, as in our case (determined indirectly by the EC values), can dissolve and leach more of the soluble minerals, including Ca, from the surface soil. So, the very low levels of Ca and Mg in irrigation water are not acceptable, because they reduce soil fertility [13].

Parameters characterizing the water toxicity. Concentrations of the investigated chemical compounds in Maritsa River water varied between < 0.001 mg/L for Cd, Cr and As to 0.294 mg/L for Fe (Table 1). In contrast with Cd levels that are without fluctuations we observed 4.32 times deviation for Fe content. The metal concentration in water followed

the order: Fe>Zn>Ni>Pb>Cr>Cu> As>Mn>Cd, which is similar with the results for Erzeni River water, Albania [25], but more different from that of the Tundzha River (Zn>Mn>Fe>Ni>Cu>Cr>VI>Pb>Cd), a large tributary of Maritsa River [26]. The observed diversity in the results together with the demonstrated dynamic variations suggests an impact of a number of various environmental factors on the pattern of metals distribution in the water. The metal ions concentrations strongly depend on the biological processes, redox potential, ionic strength, pH, the activity of organic and inorganic chelators and the purification processes in water [27].

Assessment of the quality of river water as a source for irrigation showed that all measured concentrations of the investigated elements were lower than the corresponding limit values [17] - from 7.1 times for Pb content to 50 times for Cd content (Table 1).

Although the content of trace elements in Maritsa River water is well below permissible thresholds, it should be mentioned that during the hot seasons the accumulation of minerals from the crops is more rapid than in cooler seasons [24]. Those findings are important for the countries in Maritsa River basin, because the irrigation of crops in them is carried out in the summer, i.e. during the hot part of the year.

TABLE 1
Maritsa River water quality in the investigated monitoring points by salinity, water infiltration rate and toxicity

Parameters	Unit	Month	MP-1*	MP-2	Standard Limit [17]
<i>Salinity</i>					
EC	μS/cm	June	229.0	296.0	2000
		August	223.0	378.0	
<i>Water Infiltration Rate</i>					
Ca	mg/L	June	21.6	28.9	400
		August	22.4	23.2	
Mg	mg/L	June	10.7	9.73	300
		August	4.86	18.5	
<i>Toxicity</i>					
Mn	mg/L	June	0.008	0.018	0.2
		August	0.005	0.009	
Fe	mg/L	June	0.087	0.294	5.0
		August	0.081	0.068	
Cu	mg/L	June	0.015	0.016	0.2
		August	0.015	0.019	
Zn	mg/L	June	0.066	0.044	2.0
		August	0.088	0.098	
Pb	mg/L	June	0.007	0.004	0.05
		August	0.002	0.002	
Ni	mg/L	June	0.005	0.004	0.2
		August	0.004	0.009	
Cd	mg/L	June	<0.001	<0.001	0.01
		August	<0.001	<0.001	
Cr	mg/L	June	0.003	0.004	0.1
		August	0.001	0.001	
As	mg/L	June	<0.001	<0.003	0.1
		August	<0.001	<0.003	

*MP-1 Belovo town; MP-2 Mirovo village, Stara Zagora District

TABLE 2
Maritsa River water quality in the investigated monitoring points by sanitary-indicator microorganisms

Parameters	Unit	Month	MP-1*	MP-2	Standard Limit [17]
Aerobic mesophilic microorganisms	CFU/mL	June	63	138	-
		August	18	74	-
Coliforms	CFU/mL	June	340	224	-
		August	155	157	-
<i>E.coli</i>	CFU/mL	June	122	71	-
		August	94	19	-
Total coli titer	mL	June	0.001	0.001	< 0.1
		August	0.001	0.001	< 0.1
<i>E.coli</i> titer	mL	June	0.001	0.01	< 1.0
		August	0.01	0.01	< 1.0
<i>Salmonella</i> spp.	CFU/mL	June	60	66	Not allowed
		August	21	35	Not allowed
<i>Enterobacteriaceae</i>	CFU/mL	June	445	430	Not allowed
		August	112	132	Not allowed

*MP-1 Belovo town; MP-2 Mirovo village, Stara Zagora District

Parameters characterizing the water quality by sanitary-indicator microorganisms. Regarding the investigated microbial groups two trends were observed. The first one is that microbial load in water from both MPs is time-dependent. Microbial counts in the water from both MPs were higher in June than in August (from 1.29 for *E.coli* to 3.97 times for *Enterobacteriaceae* counts) (Table 2). The second one is that for the same month, microbial counts were higher in MP-2 compared to MP-1. This trend is clearly outlined for AMO and *Salmonella* spp. counts which were higher in MP-2 than in MP-1 in both months from 1.10 to 4.11 times. For coliforms and *Enterobacteriaceae* counts, this relationship was present only in August, while the contrary one – in June, the higher values were established in MP-1 than in MP-2. The exception is also the number of *E.coli* that in both months was higher in MP-1 compared to MP-2.

The most convincing argument for the higher counts of the investigated microbial groups in river water from both MPs is the higher water temperature in June than in August - by 4.4 °C in MP-1 and by 0.5 °C in MP-2 (Table 3). It is well known that the higher water temperature favours the multiplication of microorganisms that explains the higher counts in June compared to August [14, 24]. At the same time the greater AMO and *Salmonella* spp. counts in river water at MP-2 than in MP-1 for both months and higher coliforms and *Enterobacteriaceae* counts in August, can be explained by the fact that the MP-2 is located in an area, which collects wastewater (treated or partially treated), rich in organic substances, from a large number of settlements (including the largest city – Plovdiv town with 338 000 residents), animal farms and enterprises of food industry, compared to MP-1, situated in an area with less pollution sources. For that reason microbial contamination of river water was stronger in PM-2 than in PM-1.

Quality assessment of river water as a source for irrigation showed that the values of all microbiological parameters did not meet the requirements of Bulgarian standard [17]. The established values exceeded 100 times the permissible limits for total coli titer and 100 to 1000 times for *E.coli* titer. *Salmonella* spp. and *Enterobacteriaceae*, which are intestinal pathogens and are not allowed in irrigation water, were also found. The reason for this restriction is that these organisms can infect soil and plants and retain their viability for long periods of time (for *E.coli* and *Salmonella* spp. up to 16-35 days in water, up to 150-200 days in soil and up to 180 days in plants [28]). The standard allows the use of such water for irrigation only after decontamination which is not always possible and economically justified.

Miscellaneous parameters characterizing the water quality. The maximum values of that group of parameters were below the permissible limits set by irrigation water quality standard [17], as followed: N-NH₄ < 1.09, N-NO₃ < 12.7, SO₄²⁻ < 131.0, P-PO₄ < 1.12, Cl⁻ < 17.2, COD < 2.5, BOD₅ < 1.67, T °C < 1.18, TH < 5,12 and SS < 1.16 times. DO content (> 6.21 mg/L) and pH values (7.04-7.96) also were within the norms. An exception was found for N-NH₄ and SS content in June, and for P-PO₄³⁻ content in August, as their values were 3.72, 2.8 and 1.15 times higher, respectively, than the permissible limits (Table 3). This deviation from the standard is very likely to be due to accidental contamination of the river.

Correlations. The correlation matrices, expressed by Pearson correlation coefficients values, revealed strong relationships (positive and negative) between the following pairs of parameters: minerals (Table 4): Fe – Ca (r = 0.964), Cu – EC (r = 0.975) and Cr – Zn (r = -0.979); physicochemical parameters (Table 5): BOD₅ – Cl⁻ (r = 0.991), T °C – N-NO₃

($r = 0.981$), SS – N-NH₄ ($r = 0.995$) and DO – P-PO₄ ($r = -0.967$); microbial parameters (Table 6): *Enterobacteriaceae* – *Salmonella* spp. ($r = 0.962$), *Enterobacteriaceae* – total coli titer ($r = -0.986$) and *Salmonella* spp. – total coli titer ($r = -0.969$); all parameters: As – SO₄²⁻ ($r = 0.977$), Cu – Cl⁻ ($r = 0.991$), Cu – *E.coli* counts ($r = 0.987$), EC – P-PO₄, BOD₅ and TH ($r = 0.951-0.987$), N-NH₄ – Ca, Mn and Fe ($r = 0.960-0.988$), BOD₅ – Cu and *E.coli* titer ($r = 0.987-0.996$), Ca – Cu, N-NH₄ and SS ($r = 0.964-0.988$), Mn – N-NH₄, SS and AMO ($r = 0.979-0.992$), Fe – N-NH₄ and SS ($r = 0.972-0.996$), Cr – *Salmonella* spp. and *Enterobacteriaceae* ($r = 0.951-0.952$), Cu –

E.coli titer ($r = -0.950$), *Salmonella* spp. – pH ($r = -0.952$), EC – *E.coli* counts ($r = -0.955$), BOD₅ – *E.coli* counts ($r = -0.950$), Cr – total coli titer ($r = -0.989$).

Some of these associations are logical and causally related, for example T °C – N-NO₃ (higher water temperatures, faster ammonification of nitrogen organic compounds), DO – P-PO₄ (higher content of phosphates, lower content of DO), etc. Other relationships, as SS – N-NH₄, BOD₅ – Cl⁻, SO₄²⁻ – As and etc., are difficult to be interpreted, so further research on the subject will confirm or deny them.

TABLE 3
Maritsa River water quality in the investigated monitoring points by physicochemical parameters (Miscellaneous)

Parameters	Unit	Month	MP-1*	MP-2	Standard Limit [17]
N-NH ₄	mg/L	June	1.25	18.6	5.0
		August	0.25	4.57	
N-NO ₃	mg/L	June	1.12	1.42	20
		August	0.43	1.58	
SO ₄ ²⁻	mg/L	June	1.25	2.29	300
		August	1.13	2.26	
P-PO ₄	mg/L	June	1.44	2.68	3.0
		August	1.40	3.45	
Cl ⁻	mg/L	June	9.91	11.2	300
		August	10.5	17.4	
pH	pH/units	June	7.28	7.04	6 – 9
		August	7.96	7.47	
COD	mg/L	June	14.0	20.0	100
		August	36.0	40.0	
BOD ₅	mg/L	June	7.00	9.00	25
		August	7.00	15.0	
T	°C	June	21.7	24.1	28
		August	17.3	23.6	
DO	mg/L	June	7.62	6.51	≥ 2
		August	7.29	6.21	
TH	mgeqv/L	June	1.96	2.24	14
		August	1.55	2.73	
SS	mg/L	June	34.0	140.0	50
		August	18.0	43.0	

*MP-1 Belovo town; MP-2 Mirovo village, Stara Zagora District

TABLE 4
Pearson's correlation matrix for the mineral concentrations

	EC	Ca	Mg	Mn	Fe	Cu	Zn	Pb	Ni	Cd	Cr	As
EC	1.000											
Ca	0.297	1.000										
Mg	0.882	-0.030	1.000									
Mn	0.343	0.948	0.144	1.000								
Fe	0.065	0.964*	-0.196	0.940	1.000							
Cu	0.975*	0.084	0.904	0.126	-0.157	1.000						
Zn	0.284	-0.708	0.330	-0.787	-0.866	0.483	1.000					
Pb	-0.455	-0.101	-0.092	0.151	0.125	-0.503	-0.586	1.000				
Ni	0.832	-0.277	0.930	-0.175	-0.477	0.925	0.652	-0.326	1.000			
Cd	0.539	0.327	0.719	0.595	0.318	0.440	-0.388	0.494	0.420	1.000		
Cr	-0.189	0.655	-0.163	0.794	0.810	-0.382	-0.979*	0.682	-0.513	0.556	1.000	
As	0.839	0.760	0.611	0.793	0.597	0.697	-0.252	-0.278	0.412	0.625	0.302	1.000

*Marked correlations are significant at $p < .05000$, $n=4$ (Casewise deletion of missing data)

TABLE 5
Pearson's correlation matrix for the physicochemical parameters

	N-NH ₄	N-NO ₃	SO ₄ ²⁻	P-PO ₄	Cl ⁻	pH	COD	BOD ₅	T °C	DO	TH	SS
N-NH ₄	1.000											
N-NO ₃	0.546	1.000										
SO ₄ ²⁻	0.751	0.861	1.000									
P-PO ₄	0.488	0.830	0.941	1.000								
Cl ⁻	0.007	0.615	0.659	0.874	1.000							
pH	-0.735	-0.780	-0.602	-0.383	0.010	1.000						
COD	-0.306	-0.124	0.162	0.413	0.685	0.682	1.000					
BOD ₅	0.125	0.710	0.747	0.927	0.991*	-0.121	0.600	1.000				
T °C	0.670	0.981*	0.856	0.759	0.464	-0.881	-0.273	0.576	1.000			
DO	-0.572	-0.701	-0.938	-0.967*	-0.804	0.289	-0.492	-0.853	-0.649	1.000		
TH	0.370	0.938	0.866	0.939	0.850	-0.518	0.218	0.909	0.860	-0.823	1.000	
SS	0.995*	0.538	0.707	0.427	-0.065	-0.778	-0.397	0.058	0.673	-0.501	0.333	1.000

*Marked correlations are significant at p < .05000, n=4 (Casewise deletion of missing data)

TABLE 6
Pearson's correlation matrix for the microbiological parameters

	Aerobic mesophilic microorganisms	Coliforms	<i>E.coli</i>	Total coli titer	<i>E.coli</i> titer	<i>Salmonella</i> spp.	<i>Enterobacte-ri-aceae</i>
Aerobic mesophilic microorganisms	1.000						
Coliforms	0.200	1.000					
<i>E.coli</i>	-0.283	0.697	1.000				
Total coli titer	-0.722	-0.760	-0.444	1.000			
<i>E.coli</i> titer	0.083	-0.538	-0.929	0.532	1.000		
<i>Salmonella</i> spp.	0.804	0.740	0.261	-0.969*	-0.315	1.000	
<i>Enterobacteriaceae</i>	0.635	0.855	0.513	-0.986*	-0.540	0.962*	1.000

*Marked correlations are significant at p < .05000, n=4 (Casewise deletion of missing data)

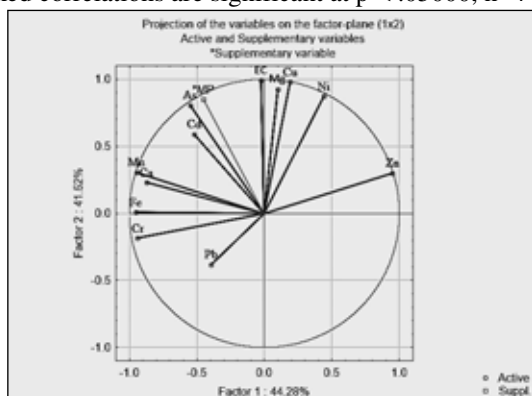


FIGURE 2
Scatter plot of minerals in Maritsa River water determined by PCA

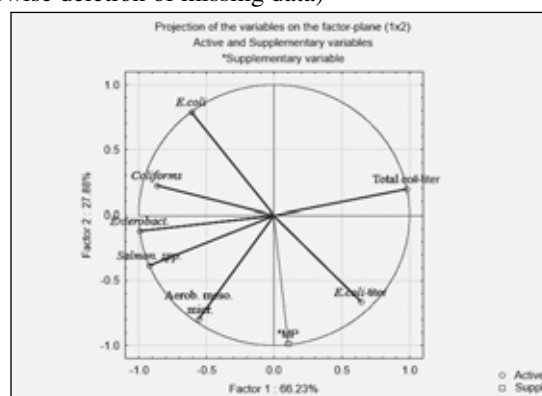


FIGURE 3
Scatter plot of sanitary-indicator microorganisms in Maritsa River water determined by PCA

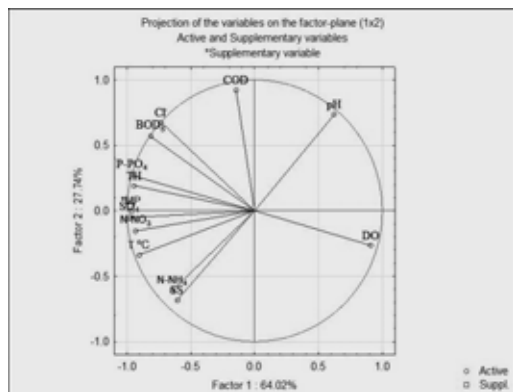


FIGURE 4
Scatter plot of physicochemical parameters in Maritsa River water determined by PCA

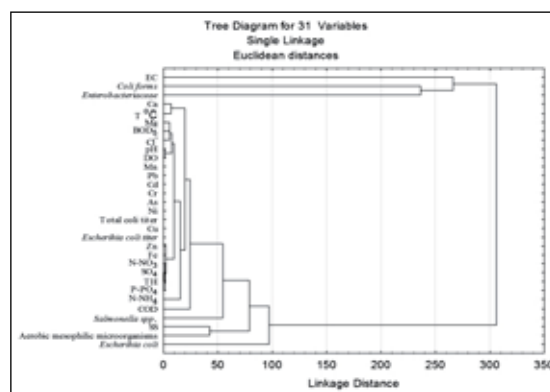


FIGURE 5
Dendrogram for Variables

TABLE 7
Factor analysis by groups

	SS	Degree of Freedom	MS	F	p	%
MP	30	1	30	0.00818	0.928115	0.0047
Month	22728.9	1	22728.9	6.20352	0.014272	3.59
Group compounds	179129.2	2	89564.6	24.44535	0.00000	28.28
MP*Month	96.7	1	96.7	0.02639	0.871243	0.02
MP*Group compounds	908.7	2	454.4	0.12401	0.883496	0.14
Month*Group compounds	34262.4	2	17131.2	4.67571	0.011285	5.41
MP*Month*Group compounds	607	2	303.5	0.08283	0.920566	0.10
Error	395697.9	108	3663.9			62.47

The scatter plots based on the case-wise F1 and F2 factor scores regarding investigated parameters of Maritsa River water are presented on Figures 2, 3, 4.

PCA demonstrated that Zn, Ni, Cu and Mg were positive parameters by the two factors, Pb and Cr were negative by both factors, while Fe, Ca, Mn, Cd and As were positive by F2, describing 41.52 % of variations and negative by F1 (Figure 2). With regard to the microbiological parameters PCA showed that the total coli titer was the only parameter influenced positively by the two factors (Figure 3). AMO, *Salmonella* spp. and *Enterobacteriaceae* were negatively affected by F1 and F2. Coliforms and *E. coli* were positive by F2 but negative by F1. *E. coli* titer was positive by F1, describing 66.23 % of the variations. PCA for physicochemical parameters revealed that only pH was a positive parameter for both factors (Figure 4). SO_4^{2-} , TH, PO_4 , BOD_5 , Cl⁻ and COD were positive by F2, describing 27.14 % of the variations. SS, N-NH₄, T °C, N-NO₃ were negative parameters by the two factors.

The dendrogram of hierarchical cluster analysis separated the investigated 31 parameters in 5 groups (Figure 5). First group: EC, coliforms and *Enterobacteriaceae* with the highest amount. Second group: *Escherichia coli*, AMO, SS and *Salmonella* spp. Third group: COD, Ca and T°C. Fourth group: Cl⁻, Mg, BOD_5 , pH, DO and N-NH₄. Fifth group: P- PO_4 , TH, SO_4 , N-NO₃, total coli titer, *E. coli* titer and all trace elements.

The analysis for the influence of the factors MP, Month and Compounds on the characteristics of the parameters and the water quality assessment demonstrated that in general, group compounds had the main effect – 28.28% in all variations (Table 7). This influence was statistically significant at $P < 0.001$. Second came the interaction between the Months and Group compounds with 5.41 %, significant at $P < 0.01$. Months as a factor were on the third place with 3.59 %, also significant at $P < 0.01$. The MP as a factor had a negligible influence on the parameters – 0.0047 %, which was not statistically significant.

CONCLUSION

In June and August 2014, Maritsa River water quality in upper (MP-1) and middle (MP-2) course of the river, assessed by 31 parameters, meets the requirements of Bulgarian standard with respect to 24 physicochemical parameters: T °C, pH, EC, TH, Ca, Mg, DO, N-NH₄ (except for June), N-NO₃, SO_4^{2-} , P- PO_4 (except for August), Cl⁻, COD, BOD_5 , SS (except for June), Mn, Fe, Cu, Zn, Pb, Ni, Cd, Cr and As. Deviations from the norms were established for all sanitary-indicator microorganisms (total coli titer, *E. coli* titer, *Salmonella* spp. and *Enterobacteriaceae*). The metal concentrations decrease in the order of Fe>Zn>Ni>Pb>Cr>Cu> As>Mn>Cd. Many positive ($r = 0.951 - 1.000$) and negative ($r = -0.950 - -0.986$) Pearson correlations existed between controlled water parameters. Generally, the Maritsa water quality did not meet the requirements for irrigation of crops, which was confirmed by the PCA.

ACKNOWLEDGEMENTS

This study was financially supported by the Faculty of Agriculture, Trakia University (Project No. 1E/2014).

REFERENCES

- [1] Pescod, M.B. (1992) Wastewater treatment and use in agriculture - FAO irrigation and drainage. FAO, Paper 47, Rome, 4-26.
- [2] Randall, G.W. and Mulla, D.J. (2001) Nitrate nitrogen in surface waters as influenced by climatic conditions and agricultural practices. *Journal of Environmental Quality*, 30, 337-344.
- [3] Agca, N., Odemiş, B. and Yalcin, M. (2009) Spatial and temporal variations of water quality parameters in Orontes river (Hatay, Turkey). *Fresen. Environ. Bull.*, 18, 456-460.
- [4] Yesilirmak, E. (2010) Seasonal and spatial variations of water quality for irrigation in Buyuk Menderes River, Turkey. *Fresen. Environ. Bull.*, 19, 3073-3080.

- [5] Gikas, D., Dimou, G.D. and Tsihrintzis, A.V. (2013) River water quantity and quality monitoring in an agricultural basin in North Greece. *Fresen. Environ. Bull.*, 22(7a), 2006-2016.
- [6] Pereira, L.S. (2004) Trends for irrigated agriculture in Mediterranean region: Coping with water scarcity. *European Water*, 7/8, 47-64.
- [7] Kirda, C.R. (2002) Deficit irrigation scheduling based on plant growth stages showing water stress tolerance. In: FAO (Ed), *Deficit Irrigation Practices*. FAO-UN, Water Reports 22, 32, 3-10.
- [8] Onder, D., Onder, S., Daghan, H. and Uygur, V. (2016) Influence of different irrigation level and different nickel (Ni) doses on phytoremediative capacity of *Tagetes erecta* L. *Fresen. Environ. Bull.*, 25(1), 190-199.
- [9] Kara, B., Ertek, A. and Atar, B. (2016) Mineral nutrient content of sweet corn under deficit irrigation. *Journal of Agricultural Sciences*, 22, 54-61.
- [10] Stambuk-Giljanovic, N. (2006) The pollution load by nitrogen and phosphorus in the Jadro River. *Environmental Monitoring and Assessment*, 123, 13-30.
- [11] Begum, A. and Harikrishna, R. (2008) Study on the quality of water in some streams of Cauvery River. *Journal of Chemistry*, 2, 377-384.
- [12] Nazari, R., Eslamian, S. and Khanbilvardi, R. (2012) Water reuse and sustainability. In: Kostas, V. and Voutsas, D. (Eds), *Ecological Water Quality – Water Treatment and Reuse*, Published by InTech, Rijeka, Croatia, 241-246.
- [13] Ayers, R.S. and Westcot, D.W. (1985) *Water quality for agriculture*. FAO, Rome, Italy, 29, Rev. 1, 28-116.
- [14] WHO (1989) *Health guideline for the use of wastewater in agriculture and aquaculture*. Technical Report Series, No. 778. Geneva, Switzerland.
- [15] USEPA (2004) *United States Environmental Protection Agency, 2004, Guidelines for Water Reuse*. USEPA, Washington, USA.
- [16] Akoto, O., Wi-Afedzi, T., Aidoo, G. and Apau, J. (2010) Evaluation of water from Bokro stream for irrigation and its effect on soil. *Journal of Science and Technology*, 30(2), 135-141.
- [17] Regulation No. 18 (2009) *Water quality for irrigation of agricultural crops*. State Gazette No. 43, 09.06.2009.
- [18] Stoyanova, A. (2009) Irrigation regime of grain maize. *Bulgarian Journal of Agricultural Science*, 15(6), 528-532.
- [19] Nazari, R., Eslamian, S. and Khanbilvardi, R. (2012) Water reuse and sustainability. In: Kostas, V. and Voutsas, D. (Eds), *Ecological Water Quality – Water Treatment and Reuse*, Published by InTech, Rijeka, Croatia, 241-246.
- [20] RSSW-EAB (2015) *Report on the status of surface water in the East Aegean Basin, Water Management Basin Directorate*. RSSW-EAB, Plovdiv, 1-6.
- [21] NRSPEB (2016) *National Report on the Status and Protection of the Environment in Bulgaria, 2016*. Executive Environment Agency, Sofia, 55-68.
- [22] Christov, I. (2012) *Ecotechnology for monitoring estimating and managing water and nutrient statuses of agroecosystems for economically effective crop production and environmental protection*. In: *Proceeding of International Conference, Ecology – Interdisciplinary Science and Practice*, 25-26 October, Sofia, Part II, PublishScieSet-Eco-Publisher, 377-381.
- [23] Morita, H. (2003) *Sensitivity and Specificity of Sanita-kun Aerobic Count: Internal validation and independent laboratory study*. *Journal of AOAC International*, 86(2), 355-366.
- [24] Westcot, D.W. (1997) *Quality control of wastewater for irrigated crop production*. *Water reports – 10*, FAO, Rome, 6-16.
- [25] Shehu, A., Vasjari, M., Baraj, E., Lilo, R. and Allabashi, R. (2016) *Contamination status of Erzeni River, Albania due to heavy metals spatial and temporal distribution*. *Fresen. Environ. Bull.*, 25(2), 525-533.
- [26] Kostadinova, G., Georgieva, N., Yaneva, Z., Petkov, G., Todorova, M. and Miteva, Ch. (2013) *Tundzha river water quality as a source for irrigation in agriculture*. *Bulgarian Journal of Agricultural Science*, 19(4), 635-643.
- [27] Ozmen, H., Kulahc, F., Cukuroval, A. and Dogru, M. (2004) *Concentrations of heavy metal and radioactivity in surface water and sediment of Hazar Lake (Elazig, Turkey)*. *Chemosphere*, 55, 401-408.
- [28] Rosen, B.H. (2000) *Waterborne pathogens in agricultural watersheds*. *Watershed Science Institute Publishers*, Ithaca, New York, 22-32.

Received: 03.05.2016
Accepted: 28.06.2017

CORRESPONDING AUTHOR

Georgi Petkov
 Trakia University,
 Faculty of Agriculture
 Stara Zagora 6000 – BULGARIA

E-mail: gpetkov@af.uni-sz.bg

THE EFFECTS OF NARINGIN AND OZONE IN HEPATIC ISCHEMIA REPERFUSION INJURY: AN EXPERIMENTAL STUDY

Cebraıl Gursul¹, Kemal Peker², Abdulkadir Coban³, Hasan Kilicgun⁴, İlyas Sayar⁵, Fazile Nur Ekinçi Akdemir⁶, Murat Cankaya⁷, Mustafa Gul⁸

¹Erzincan University, Faculty of Medicine, Department of Physiology, Erzincan, Turkey

²Erzincan University, Faculty of Medicine, Department of General Surgery, Erzincan, Turkey

³Erzincan University, Faculty of Medicine, Department of Biochemistry, Erzincan, Turkey

⁴Erzincan University, Health Academy, Department of Nutrition and Dietetics, Erzincan, Turkey

⁵Erzincan University, Faculty of Medicine, Department of Pathology, Erzincan, Turkey

⁶Agri Ibrahim Cecen University, Health Academy, Department of Nutrition and Dietetics, Agri, Turkey

⁷Erzincan University, Faculty of Art and Science, Department of Biology, Erzincan, Turkey

⁸Ataturk University, Faculty of Medicine, Department of Physiology, Erzincan, Turkey

ABSTRACT

Background and Aim. Hepatic ischemia reperfusion (I/R) injury is located between complications widely seen in clinical. Aim of this study was to investigate the protective roles of naringin and ozone effects and synergistic effects induced I/R injury on the liver in rats.

Methods. Thirty five Adult male Sprague–Dawley rats were divided into five groups (n=7 in each group): sham-operated, I/R, I/R with 80 mg/kg naringin, I/R with 0.5 mg/kg ozone, and I/R with 80 mg/kg naringin+0.5 mg/kg ozone. Before hepatic I/R was induced, ozone and naringin was injected intraperitoneally at doses of 80 mg/kg and 0.5 mg/kg. After 70-min ischemia and a 120-min reperfusion period, later at the end of experiment, liver tissues were excised. The levels of malondialdehyde (MDA) and activities of superoxide dismutase (SOD), glutathione reductase (GR), catalase (CAT) were measured in hepatic tissue.

Results. SOD, GR, and CAT activities decreased and MDA level, as a biomarker of the lipid peroxidation, increased in I/R group compared to Sham-operated group. In addition, SOD, GR, and CAT activities increased by the naringin, ozone, and naringin+ozone treatment.

Conclusions. The results of this study suggest that naringin, ozone, and naringin+ozone. may be strongly protective against hepatic I/R injury. This effect can be achieved by antioxidant and antiapoptotic activities.

KEYWORDS:

Hepatic ischemia–reperfusion injury; liver; naringin; ozone.

INTRODUCTION

Hepatic ischemia reperfusion (I/R) injury is one of the pathological process widely encountered in clinic, involving trauma, hypovolemic shock, liver transplantation, and hepatectomy [1] or hepatic pedicle clamping during liver surgery [2, 3]. The understanding as complete the damaging mechanisms of hepatic I/R is quite complex process but it has focused to explain this situation may lead to high post-operative morbidity and mortality rates, on production of oxygen radicals, intracellular calcium overload, an accumulation of inflammatory cells and mediators, activation of Kupffer cells and neutrophils or induce further cell death [4–6]. Reactive oxygen radicals are released by I/R injury and can directly damage cellular molecules such as protein, lipid and DNA. They initiates an inflammatory responses and tissue damage by activating chemical mediators [7]. A specific biomarker the malondialdehyde (MDA) levels demonstrating oxidative stress, the lipid peroxidation of the cellular and membrane lipids have increased by ROS [8]. Antioxidant enzymes such as superoxide dismutase (SOD), catalase (CAT), glutathione reductase (GR) protects from harmful effect of the ROS. But these enzymes are inadequate in pathologic conditions like ischemic reperfusion process [9]. For this reason it has been investigated various agents and drugs have anti-oxidative, anti-apoptotic, and anti-inflammatory effects for suppression or prevention against hepatic I/R injury in previous studies [10–12]. Also many studies have demonstrated that pretreatment of agents antioxidant effect is beneficial to attenuate tissue damage via I/R [13, 14]. Duration I/R treatment, pharmacologic agents such as drugs with antioxidant effect that lead to treatment of the liver damage were used by suppressing the formation of free oxygen radicals [12, 15].

Naringin (4',5,7-trihydroxyflavanone 7-rhamnoglucoside) is a bioflavonoid, polyphenolic compound in various fruits such as grapefruit and citrus

fruits. When naringin is administered orally and hydrolyzed by intestinal microflora, naringenin (4',5,7-trihydroxyflavone) is efficiency and absorbable great metabolite of the naringin [16] and possess several pharmacologic features anti-oxidant, anti-inflammatory, anti-ulcer, anti-diabetic and neuroprotective properties [17-19]. Lately, there are numerous the experiment studies point out the naringin has antioxidant features and has preventive effects on oxidative stress induced by ischemia reperfusion or H₂O₂ applied in various tissue [20, 21]. Beneficial effect of Ozone was first used in clinical situations like infection treatment in World War I period. It has been demonstrated that ozone because of its strongly oxidant properties showed a quite powerful effective on infection, inflammation, and ischemia, when it is used at low doses. Although ozone has strong oxidant character, it has been suggested that its property alike to effect in the ischemic preconditioning has preserved the tissue against I/R injury by several studies [22-25]. Ozone therapy against oxidative stress is used like therapeutic agent in several diseases by inducing antioxidant systems [25-27].

However, it remains unknown that the effects in case of usage separately and together of naringin and ozone on oxidative stress associated hepatic I/R injury of rat. Therefore, in this study, we have used hepatic I/R model experimentally in rats to expose the preventive effects of naringin and ozone. For this reason, we are assessed MDA level, SOD, CAT, and GR activities to exhibit effects of naringin and ozone therapy on hepatic I/R injury.

MATERIALS AND METHODS

Drugs and Chemicals. Naringin and ozone which have been used in our study were purchased from Sigma (St. Louis, MO, USA). Ketamine was bought from Eczacıbasi (Ketalar, Eczacıbasi, Luleburgaz-Turkey) and xylazine obtained from Bayer (Rompun, Bayer, İstanbul- Turkey).

Animals and Experimental Design. In this study has been used thirty five Sparague-Dawley type rats weighing between 200 and 250 g, also equally and randomly separated into five groups. The experimental protocols of the study were approved by the Local Ethics Committee of Experimental Animals of Ataturk University (2013-72). The rats used in the experiments were obtained Ataturk University Experimental Animals Research Center and kept held to a 12 h day/night cycle, %55 ±5 humidity, at a room temperature of 21±1 °C. Rats were kept in standardized cages (3/cage) under laboratory conditions and given ad libitum and free water. But it was fasted before experiment for 12 hours. Rats were anesthetized the mixture ketamine (50 mg/kg, intraperitoneal) and xylazine (10 mg/kg

i.p) and the dose of anesthesia was repeated as required. The abdominal region was cleaned and sterilized with povidone iodine solution. A midline incision was made and liver were isolated. All of the hepatic artery, portal vein and bile duct (all structures in the portal triad) to the left and median liver lobes were clamped by using a clip for create hepatic ischemia. The clip was opened after 70 min. Reperfusion was started, and later the region incision closed.

In our study, groups were prepared as follows; sham-operated group (Sham group): Only abdominal incision, without hepatic ischemia was performed, body temperature protected 36-37 °C throughout the asset of the operation with a heating pad and closed after 70 minutes. But any treatment was not implemented. Ischemia reperfusion group (I/R group): 0.9% NaCl, 1 ml was given intraperitoneally 30 minutes before the surgical procedures. Additional treatment was not given to this group. Ischemia reperfusion+naringin group (I/R+NAR): Naringin (80 mg/kg dose) was dissolved in serum physiologic and performed intraperitoneally before 30 minutes from the occlusion via clamping of the hepatic triad. Clamps were removed at the end of ischemia process and liver was reperfused for 120 minutes. Ischemia reperfusion+ozone group (I/R+Ozone): Ozone (0.5 mg/kg dose i.p) was prepared into serum physiologic and given before 30 minutes from the ischemia reperfusion period, later was performed in the hepatic artery occlusion as described in the I/R group. Ischemia reperfusion+combined with naringin and ozone group (I/R+NAR+Ozone): Naringin and ozone were given before 30 minutes from the ischemia reperfusion period as described in the I/R+NAR and I/R+Ozone groups, subsequently the hepatic ischemia reperfusion model has been created. At the end of the this processes, liver was removed for examined the hepatic tissue damage. Afterwards, rats were sacrificed by exsanguination through the abdominal aorta.

Biochemical Analysis. Liver tissues have been homogenized with homogenizer (IKA Ultra-Turrax T25 basic homogenizer, Germany) with pH 7.4 0.2 mM Tris-HCl buffer to make the antioxidant enzyme measurements. The tissue MDA level was measured in this homogenates. The homogenate have been centrifuged at 4000 rpm for 55 min. The clean portion of the upper remnant of the supernatant has been separated and stored as aliquots to measure CAT, SOD and GR activities. To measure the SOD levels, the supernatant has been extracted with an equal volume of ethanol-chloroform (5/3, v/v) mixture. A UV-Shimadzu 1600 (Shimadzu, Kyoto, Japan) has been used for the spectrophotometric measurements. We have measured the amount of thiobarbituric acid-reactive substances (TBARS) in the sample spectrophotometrically at 532 nm by assessing the reactivity of thiobarbituric acid in the

acidic medium at 90–95°C based on the method described by Esterbauer and Cheeseman [28]. The results have been calculated according to the standard and expressed as nmol/g wet tissue. We have analyzed the protein for supernatant and extracted samples using the method of Lowry et al [29]. We have examined catalase (CAT, EC 1.11.1.6) enzyme activity using as of Aebi method (1974) [30] in which the consumption of hydrogen peroxide (H₂O₂) by the catalase was measured spectrophotometrically at 240 nm. The buffer was adjusted to an optical density (OD) of 0.500 by adding H₂O₂ to a 50 mM phosphate buffer. The decrease in the absorbance with the addition of the sample have been recorded for every 15 s. The rate of consumed H₂O₂ in 1 min was expressed as k/g protein ($k = (2.3 \times \log(OD1/OD2))/30$ s). We have measured SOD (EC 1.15.1.1) enzyme activity spectrophotometrically at 560 nm based on the principle of reduction of O₂^{•-} with nitroblue tetrazolium (NBT). Enzyme activity has been assessed based on the activity of the enzyme inhibiting 50.0% NBT reduction and expressed as U/mg of protein (% enzyme inhibition = $(Abscontrol - Abssample)/Abscontrol \times 100$) [31]. Glutathione reductase (EC 1.8.1.7) catalyzes the reduction of glutathione disulfide to the sulfhydryl form glutathione. We have measured the enzyme activity of glutathione reductase using the reduction of NADPH at 340 nm. One enzyme unit is defined as the oxidation of 1 mmol NADPH per min under assay conditions (25 °C, pH 8.0) [32]. GR has been expressed as U/mg protein.

Statistical Analysis. Statistical comparisons among the groups of our data were performed using one-way analysis of variance (ANOVA) test based on their variance distribution type. To show the statistical significance with ANOVA test, post-hoc tests were used to identify the group difference, Tukey's post-hoc were used to identify differences between groups honestly. Later, Tukey test were applied for variables show normally distributed of variances and Tamhane's T2 test applied for variables not show homogeneous distributed of variances. $P < 0.05$ were considered as statistically significant difference for

comparisons of the binary group. Results were expressed as mean \pm standard error mean (SEM).

RESULTS

Hepatic tissue MDA levels were increased in sham-operated group rats compared to I/R group (Table 1), The naringin-treated, ozone-treated, and naringin+ozone group exhibited lower MDA levels compared to the I/R group. The MDA level of ozone treated was closer to sham-operated according to other treatment groups. SOD enzyme activity declined significantly in the I/R group in comparison with the sham-operated group ($p < 0.001$; Table 1). Naringin induced a statistically significant increase in SOD activity compared to the I/R group ($p < 0.05$). In the other treatment groups, SOD activity is higher than I/R and sham-operated groups. But, this result was not statistically significant. Also, CAT activity decreased in the I/R group compared to sham-operated group. There is statistically significant difference between the I/R and sham-operated groups ($P < 0.001$; Table 1). When we take a glance to the naringin, ozone, and naringin+ozone treated groups, CAT activities increased according to the I/R induced by hepatic damage and sham-operated groups. However, these increases were not statistically significant. A decrease has been viewed in the I/R group related to GR activity. But statistically significant increase viewed in GR activity with naringin treated group ($p < 0.05$; Table 1). Also the observed increase in ozone and combined naringin+ozone groups could not create a significant difference.

DISCUSSION

Ischemia reperfusion may originate by various events such as liver transplantation, sepsis trauma and cause metabolic and structural hepatic injury or hepatic pedicle clamping throughout liver surgery [3,5]. In many studies, an ideal solution has been examined for the prevention of hepatic I/R injury [33, 34].

TABLE 1
Effects of naringin (80 mg/kg, i.p.) and ozone (0.5 mg/kg, i.p.) treatment on MDA level, SOD, CAT, GR activities changes as assessed by biological examination of liver of the rats exposed to hepatic I/R. Values expressed as mean \pm S.E.M.

	MDA (nmol/g protein)	CAT (k/g protein)	GR (U/mg)	SOD (U/mg)
Sham-operated (n=7)	3,832 \pm 0,234	4,992 \pm 0,332 [#]	0,667 \pm 0,002	0,524 \pm 0,002 [*]
I/R (n=7)	4,973 \pm 0,602	3,187 \pm 0,295	0,743 \pm 0,004 ^{##}	0,355 \pm 0,003 ^{**}
I/R+NAR (n=7)	4,033 \pm 0,241	4,009 \pm 0,303	0,628 \pm 0,003	0,469 \pm 0,002
I/R+Ozone (n=7)	3,890 \pm 0,183	4,349 \pm 0,207	0,649 \pm 0,003	0,442 \pm 0,001
I/R+NAR+Ozone (n=7)	3,936 \pm 0,261	3,966 \pm 0,267	0,580 \pm 0,002	0,426 \pm 0,002

* $P < 0.05$ compared between Sham-operated and I/R groups

** $P < 0.05$ compared between I/R and I/R+NAR groups

$P < 0.05$ compared between Sham-operated and I/R groups

$P < 0.05$ compared between I/R and I/R+NAR groups

ROS normally is released as a product of the aerobic metabolism and scavenges via antioxidant defense mechanisms [35]. But, this condition changes and moves up to cytotoxicity from oxidative stress, when balance has been disrupted between the antioxidant defense system and ROS [36, 37]. Oxidative stress leads to peroxidation of the cellular lipids and generates MDA as a product. For this reason, MDA is a significant parameter to determine the oxidative stress level [38]. Endogenous antioxidant enzymes such as SOD, CAT, and GR -momentous defensive system against ROS- reduces the ROS which have harmful effects. Previous hepatic I/R studies demonstrated that antioxidant enzyme levels drop during the reperfusion followed ischemia and this situation due to an increment amount of ROS [15, 39]. Therefore many antioxidant drugs and agents were used to minimize hepatic I/R injury [15, 39].

Naringin exposes different pharmacological characteristics including anti-inflammatory, lipid-reducing, and anticarcinogenic [40, 41]. Also, antioxidant characteristic, metal chelating and free radical scavenging of naringin has been showed [42]. Newly, a significant act as an antioxidant have been indicated by up-regulating the gene expression of SOD and some antioxidant enzymes [43]. Until now, studies in clinical field have suggested that ozone therapy seems beneficial in various conditions such as infected wounds, burns, peritonitis, skin ulcers, initial gangrene, and advanced ischemic diseases [44]. As a result of extensive literature searches, we have seen that ozone therapy has a curable effect in reducing oxidative stress in necrotizing enterocolitis, methotrexate induced intestinal injury, acetaminophen-induced liver injury, and caustic esophageal burn in experimental studies [45-48]. It was also indicated that ozone increased antioxidant enzyme activities, such as GPx, SOD and CAT, under pathophysiological conditions mediated by ROS [49, 50]. For this purpose, the effects of naringin and ozone have been investigated against I/R injury in various organs [26, 51-54]. Also, the doses of naringin 80 mg/kg and ozone 0.5 mg/kg that applied in our study has been supplemented in the different previous studies [26, 52].

Reactive oxygen species, including superoxide radicals, hydroxyl, hydrogen peroxide are created further cellular injury and improved during reperfusion of the tissue exposed to ischemia [23, 24]. An important enhance in tissue MDA levels, as a marker of the lipid peroxidation, was defined in I/R group depend on I/R injury in numerous studies [15, 26, 52]. However, we have found increase in the levels of MDA in I/R group according to Sham-operated group. This case can be explained as an indicator of lipid peroxidation or tissue damage in liver depend on I/R. But tissue damage can be reduced by various antioxidant therapies. Protective effect of intraperitoneal ozone therapy has been shown by reducing

level of the MDA against ovarian ischemia reperfusion injury [26]. Koca et al. assessed effects of the treatment hyperbaric oxygen and ozone in the induced tourniquet ischemia reperfusion and showed that the levels of MDA increased by I/R but the levels of MDA reduced effectively by ozone [24]. Singh and Chopra have reported that naringin shows antioxidant effect by reducing the MDA level in renal ischemia reperfusion injury [19]. Also, in a study cerebral ischemia reperfusion injury it has been shown that naringin (50 and 100 mg/kg dose i.p.) drops the MDA level [51]. In our study, effectiveness of naringin and ozone is similar to results of previous studies. MDA level markedly reduced in the naringin and ozone groups. At the same time, combined ozone and naringin treatment had synergetic effects and had contribution by reducing the lipid peroxidation level.

Glutathione is one of the endogenous antioxidant defense system which protects cell from free radical damage. GSH metabolism is strongly arranged, including protection against environmental oxidants mediated injury and redox signaling. The normal glutathione cycle contains oxidation of the GSH to oxidized glutathione (GSSG). GSH is regulated back from GSSG within the cells in a reaction catalyzed by the glutathione reductase as a flavoenzyme [55]. The glutathione and its related enzymes attend in the continue of oxidant metabolism in aerobic cells [56]. In the experimental study, it has been demonstrated that GR activities elevate in the ozone, naringin and ozone+naringin groups on intestinal ischemia reperfusion injury [52]. Similar to the results of Isik et al.'s study, our study has been showed that level of GR increased depending on antioxidant treatment.

Alive tissues are preserved against hazardous effects of the free radical damage by SOD which catalyses from superoxide into hydrogen peroxide. But, throughout re-oxygenate of ischemic tissue the biological molecules protected against radical damage [57, 58]. Aslan et al have been reported that SOD activity increases via the ozone supplementation against ischemia reperfusion injury in ovarian [26]. In a previous study, the effect of hypothermia and ozone has been investigated against ischemia reperfusion injury in the skeletal muscle and increase of SOD activity via ozone has been demonstrated [54]. It has been shown antioxidant effect of naringin (400 mg kg⁻¹ dose, p.o), a bioflavonoid, increases SOD activity against renal ischemia reperfusion injury (45 min;24 h) [19]. Our results have been revealed separately or together of the naringin and ozone treatment have potent effects against hepatic injury induced by I/R. These treatments have a considerable achievement in naringin, ozone, and naringin+ozone groups compared to I/R group by increasing of the SOD activity. CAT is a strong scavenger of hydrogen peroxide and supplies a potent antioxidant defense. It intercepts the generation of the

more toxic hydroxyl radical. Thus, CAT provides the antioxidative prevention during I/R [59]. In the study that investigate the protective effects of naringin against post-stroke depression, increasing of the CAT activity has been showed [60]. Also, ozon and naringin increased CAT activity in the intestinal ischemia reperfusion study [52]. Our results are in the same direction with previous studies. CAT activity increased depending on naringin, ozone, and naringin+ozone.

The results of our research study have been revealed that liver damage depend on I/R originates by lipid peroxidation generating free radicals. Separately and/or together of the naringin and ozone application has protected the liver against I/R. In this situation, probably, naringin and ozone have achieved owing to their free radical scavenging and antioxidant properties. Ozone and naringin may be used for hepatic ischemia reperfusion safely, because of their protective effects.

ACKNOWLEDGEMENTS

This study was supported by Research Fund of Erzincan University (SAG-A-140613-0015). The authors are grateful to the Research Fund of Erzincan University for financial support.

Authors' contributions; C.G., K.P., A.C., H.K., I.S., F.N.E.A., M.C. and M.G declare that they have all participated in the design and perform of the experiments, biochemical analyzes and the data analyzes, and that they have approved the wrote the manuscript, presented the results and final version.

The authors declare no conflict of interest associated with this manuscript.

REFERENCES

- [1] Abu-Amara, M., Yang, S.Y., Tapuria, N., Fuller, B., Davidson, B. and Seifalian, A. (2010) Liver ischemia/reperfusion injury: processes in inflammatory networks--a review. *Liver transplantation : official publication of the American Association for the Study of Liver Diseases and the International Liver Transplantation Society.* 16(9), 1016-32.
- [2] Coban, S., Yildiz, F., Terzi, A., Al, B., Aksoy, N., Bitiren, M., Çelik, H. (2010) The effects of *Nigella sativa* on bile duct ligation induced-liver injury in rats. *Cell biochemistry and function.* 28(1), 83-8.
- [3] van Gulik, T.M., de Graaf, W., Dinant, S., Busch, O.R. and Gouma, D.J. (2007) Vascular occlusion techniques during liver resection. *Digestive surgery.* 24(4), 274-81.
- [4] Nastos, C., Kalimeris, K., Papoutsidakis, N., Tasoulis, M.K., Lykoudis, P.M., Theodoraki, K., Nastou, D., Smyrniotis, V., Arkadopoulos N. (2014) Global consequences of liver ischemia/reperfusion injury. *Oxidative medicine and cellular longevity.*
- [5] Shin, T., Kuboki, S., Huber, N., Eismann, T., Galloway, E., Schuster, R., Blanchard, J., Pritts, T.A., Lentsch, A.B. (2008) Activation of peroxisome proliferator-activated receptor-gamma during hepatic ischemia is age-dependent. *The Journal of surgical research.* 147(2), 200-5.
- [6] Yoshimura, Y., Kubo, S., Shirata, K., Hirohashi, K., Tanaka, H., Shuto, T. Takemura, S., Kinoshita, H. (2004) Risk factors for postoperative delirium after resection for hepatocellular carcinoma. *World journal of surgery.* 28(10), 982-6.
- [7] Montalvo-Jave, E.E., Escalante-Tattersfield, T., Ortega-Salgado, J.A., Pina, E. and Geller, D.A. (2008) Factors in the pathophysiology of the liver ischemia-reperfusion injury. *The Journal of surgical research.* 147(1), 153-9.
- [8] Scarfiotti, C., Fabris, F., Cestaro, B. and Giuliani, A. (1997) Free radicals, atherosclerosis, ageing, and related dysmetabolic pathologies: pathological and clinical aspects. *European journal of cancer prevention : the official journal of the European Cancer Prevention Organisation.* 6 Suppl 1, 31-6.
- [9] Tunc, T., Oter, S., Guven, A., Topal, T., Kul, M., Korkmaz, A., Öngürü, Ö., Sarıcı, Ü. (2009) Protective effect of sulfhydryl-containing antioxidants against ischemia/reperfusion injury of prepubertal rat intestine. *Journal of gastroenterology and hepatology.* 24(4), 681-7.
- [10] Oguz, A., Kapan, M., Kaplan, I., Alabalik, U., Ulger, B.V., Uslukaya, O., Türkoğlu, A., Polat, Y. (2015) The effects of sulforaphane on the liver and remote organ damage in hepatic ischemia-reperfusion model formed with pringle maneuver in rats. *International journal of surgery.* 18, 163-8.
- [11] Ozsoy, M., Gonul, Y., Bal, A., Ozkececi, Z.T., Celep, R.B., Adali, F., Hazman, O., Koçak, A., Tosun, M. (2015) Effect of IL-18 binding protein on hepatic ischemia-reperfusion injury induced by infrarenal aortic occlusion. *Annals of surgical treatment and research.* 88(2), 92-9.
- [12] Zhang, T., Shu, H.H., Chang, L., Ye, F., Xu, K.Q. and Huang, W.Q. (2015) Resolvin D1 protects against hepatic ischemia/reperfusion injury in rats. *International immunopharmacology.* 28(1), 322-7.
- [13] Boyuk, A., Onder, A., Kapan, M., Gumus, M., Fiotarat, U., Basaraliota, M.K., Alp, H. (2011) Ellagic acid ameliorates lung injury after intestinal ischemia-reperfusion. *Pharmacognosy magazine.* 7(27), 224-8.
- [14] Celebi, F., Yilmaz, I., Aksoy, H., Gumus, M., Taysi, S. and Oren, D. (2004) Dehydroepiandrosterone prevents oxidative injury in

- obstructive jaundice in rats. *The Journal of international medical research.* 32(4), 400-5.
- [15] Kocak, F.E., Kucuk, A., Ozyigit, F., Tosun, M., Kocak, C., Kocak, A. Ekici, M.F., Yaylak, F., Genç, O. (2015) Protective effects of simvastatin administered in the experimental hepatic ischemia-reperfusion injury rat model. *The Journal of surgical research.* 199(2), 393-401.
- [16] Ameer, B., Weintraub, R.A., Johnson, J.V., Yost, R.A. and Rouseff, R.L. (1996) Flavanone absorption after naringin, hesperidin, and citrus administration. *Clinical pharmacology and therapeutics.* 60(1), 34-40.
- [17] Dhalla, N.S., Elmoselhi, A.B., Hata, T. and Makino, N. (2000) Status of myocardial antioxidants in ischemia-reperfusion injury. *Cardiovasc Res.* 47(3), 446-56.
- [18] Sharma AK, Bharti S, Ojha S, Bhatia J, Kumar N, Ray R, Kumari, S., Arya, D.S. (2011) Up-regulation of PPARgamma, heat shock protein-27 and -72 by naringin attenuates insulin resistance, beta-cell dysfunction, hepatic steatosis and kidney damage in a rat model of type 2 diabetes. *The British journal of nutrition.* 106(11), 1713-23.
- [19] Singh, D. and Chopra, K. (2004) The effect of naringin, a bioflavonoid on ischemia-reperfusion induced renal injury in rats. *Pharmacological research.* 50(2), 187-93.
- [20] Akondi, B.R., Challa, S.R. and Akula, A. (2011) Protective effects of rutin and naringin in testicular ischemia-reperfusion induced oxidative stress in rats. *Journal of reproduction & infertility.* 12(3), 209-14.
- [21] Kanno, S., Shouji, A., Asou, K. and Ishikawa, M. (2003) Effects of naringin on hydrogen peroxide-induced cytotoxicity and apoptosis in P388 cells. *Journal of pharmacological sciences.* 92(2), 166-70.
- [22] Chen, H., Xing, B., Liu, X., Zhan, B., Zhou, J., Zhu, H., Chen, Z. (2008) Ozone oxidative preconditioning protects the rat kidney from reperfusion injury: the role of nitric oxide. *The Journal of surgical research.* 149(2), 287-95.
- [23] Koca, K., Yurttas, Y., Bilgic, S., Cayci, T., Topal, T., Durusu, M. Kaldirim, U., Akgul, E. O., Ozkan, H., Yanmis, I., Oguz, E., Tunay, S., Korkmaz, A., Basbozkurt, M. (2010) Effect of preconditioned hyperbaric oxygen and ozone on ischemia-reperfusion induced tourniquet in skeletal bone of rats. *The Journal of surgical research.* 164(1), 83-9.
- [24] Koca, K., Yurttas, Y., Yildiz, C., Cayci, T., Uysal, B. and Korkmaz, A. (2010) Effect of hyperbaric oxygen and ozone preconditioning on oxidative/nitrosative stress induced by tourniquet ischemia/reperfusion in rat skeletal muscle. *Acta orthopaedica et traumatologica turcica.* 44(6), 476-83.
- [25] Ozler, M., Oter, S. and Korkmaz, A. (2009) The use of ozone gas for medical purposes. *TAF Prev Med Bull.* 8, 59-64.
- [26] Aslan, M.K., Boybeyi, O., Senyucel, M.F., Ayva, S., Kisa, U., Aksoy, N., Soyer, T., Cesur, Ö., Çakmak, M. (2012) Protective effect of intraperitoneal ozone application in experimental ovarian ischemia/reperfusion injury. *Journal of pediatric surgery.* 47(9), 1730-4.
- [27] Inal, M., Dokumacioglu, A., Ozcelik, E. and Ucar, O. (2011) The effects of ozone therapy and coenzyme Q(10) combination on oxidative stress markers in healthy subjects. *Irish J Med Sci.* 180(3), 703-7.
- [28] Esterbauer, H. and Cheeseman, K.H. (1990) Determination of aldehydic lipid peroxidation products: malonaldehyde and 4-hydroxynonenal. *Methods in enzymology.* 186, 407-21.
- [29] Lowry, O.H., Rosebrough, N.J., Farr, A.L. and Randall, R.J. (1951) Protein measurement with the Folin phenol reagent. *The Journal of biological chemistry.* 193(1), 265-75.
- [30] Aebi, H. (1974) Catalase. *Methods Enzym Anal.* 10, 673-7.
- [31] Sun, Y., Oberley, L.W., Li, Y. (1988) A simple method for clinical assay of superoxide dismutase. *Clinical chemistry.* 34(3), 497-500.
- [32] Beutler, E. (1971) *Red Cell Metabolism. A Manual of Biochemical Methods.* 1st Grune Stratton, New York, USA.
- [33] Kapan, M., Gumus, M., Onder, A., Firat, U., Basarali, M.K., Boyuk, A. Aliosmanoğlu, I., Boyuk, A. (2012) The effects of ellagic acid on the liver and remote organs' oxidative stress and structure after hepatic ischemia reperfusion injury caused by pringle maneuver in rats. *Bratislavske lekarske listy.* 113(5), 274-81.
- [34] Oguz, A., Kapan, M., Onder, A., Kilic, E., Gumus, M., Basarali, M.K., Firat, U., Boyuk, A., Buyukbas, S. (2013) The effects of curcumin on the liver and remote organs after hepatic ischemia reperfusion injury formed with Pringle manoeuvre in rats. *European review for medical and pharmacological sciences.* 17(4), 457-66.
- [35] Toledo-Pereyra, L.H., Toledo, A.H., Walsh, J. and Lopez-Neblina, F. (2004) Molecular signaling pathways in ischemia/reperfusion. *Experimental and clinical transplantation : official journal of the Middle East Society for Organ Transplantation.* 2(1), 174-7.
- [36] Anaya-Prado, R., Toledo-Pereyra, L.H., Lentsch, A.B. and Ward, P.A. (2002) Ischemia/reperfusion injury. *The Journal of surgical research.* 105(2), 248-58.
- [37] Videla, L.A. and Fernandez, V. (1988) Biochemical aspects of cellular oxidative stress. *Archivos de biologia y medicina experimentales.* 21(1), 85-92.
- [38] Vali, L., Taba, G., Szentmihalyi, K., Febel, H., Kurucz, T., Pallai, Z., Kupcsulik, P., Blázovics,

- A. (2006) Reduced antioxidant level and increased oxidative damage in intact liver lobes during ischaemia-reperfusion. *World journal of gastroenterology*. 12(7), 1086-91.
- [39] Marubayashi, S., Dohi, K., Ochi, K. and Kawasaki, T. (1987) Protective effects of free radical scavenger and antioxidant administration on ischemic liver cell injury. *Transplantation proceedings*. 19(1 Pt 2), 1327-8.
- [40] Bok, S.H., Lee, S.H., Park, Y.B., Bae, K.H., Son, K.H., Jeong, T.S., Choi, M.S. (1999) Plasma and hepatic cholesterol and hepatic activities of 3-hydroxy-3-methyl-glutaryl-CoA reductase and acyl CoA: cholesterol transferase are lower in rats fed citrus peel extract or a mixture of citrus bioflavonoids. *The Journal of nutrition*. 129(6), 1182-5.
- [41] Choi, M.S., Do, K.M., Park, Y.S., Jeon, S.M., Jeong, T.S., Lee, Y.K., Lee, M.K., Bok, S.H. (2001) Effect of naringin supplementation on cholesterol metabolism and antioxidant status in rats fed high cholesterol with different levels of vitamin E. *Ann Nutr Metab*. 45(5), 193-201.
- [42] Jeon, S.M., Park, Y.B. and Choi, M.S. (2004) Antihypercholesterolemic property of naringin alters plasma and tissue lipids, cholesterol-regulating enzymes, fecal sterol and tissue morphology in rabbits. *Clinical nutrition*. 23(5), 1025-34.
- [43] Jeon, S.M., Bok, S.H., Jang, M.K., Lee, M.K., Nam, K.T., Park, Y.B., Rhee, S.J., Choi, M.S. (2001) Antioxidative activity of naringin and lovastatin in high cholesterol-fed rabbits. *Life sciences*. 69(24), 2855-66.
- [44] Re, L., Mawsouf, M.N., Menendez, S., Leon, O.S., Sanchez, G.M. and Hernandez, F. (2008) Ozone therapy: clinical and basic evidence of its therapeutic potential. *Archives of medical research*. 39(1), 17-26.
- [45] Gul, H., Uysal, B., Cakir, E., Yaman, H., Macit, E., Yildirim, A.O., Eyi, Y.E., Kaldirim, U., Oztase, E., Akgul, E.O., Cayci, T., Ozler, M., Topal, T., Oter, S., Korkmaz, A., Toygar, M., Demirbag, S. (2012) The protective effects of ozone therapy in a rat model of acetaminophen-induced liver injury. *Environmental toxicology and pharmacology*. 34(1), 81-6.
- [46] Guven, A., Gundogdu, G., Sadir, S., Topal, T., Erdogan, E., Korkmaz, A., Surer, I., Ozturk, H. (2008) The efficacy of ozone therapy in experimental caustic esophageal burn. *Journal of pediatric surgery*. 43(9), 1679-84.
- [47] Kesik, V., Uysal, B., Kurt, B., Kismet, E. and Koseoglu V. (2009) Ozone ameliorates methotrexate-induced intestinal injury in rats. *Cancer biology & therapy*. 8(17), 1623-8.
- [48] Uysal, B., Yasar, M., Ersoz, N., Coskun, O., Kilic A., Cayc, T., Kurt, B., Oter, S., Korkmaz, A., Guven, A. (2010) Efficacy of hyperbaric oxygen therapy and medical ozone therapy in experimental acute necrotizing pancreatitis. *Pancreas*. 39(1), 9-15.
- [49] Bocci, V. (1996) Ozone as a bioregulator. *Pharmacology and toxicology of ozonotherapy today. Journal of biological regulators and homeostatic agents*. 10(2-3), 31-53.
- [50] Bocci, V. (1996) Does ozone therapy normalize the cellular redox balance? Implications for therapy of human immunodeficiency virus infection and several other diseases. *Medical hypotheses*. 46(2), 150-4.
- [51] Gaur, V., Aggarwal, A. and Kumar, A. (2009) Protective effect of naringin against ischemic reperfusion cerebral injury: possible neurobehavioral, biochemical and cellular alterations in rat brain. *European journal of pharmacology*. 616(1-3), 147-54.
- [52] Isik, A., Peker, K., Gursul, C., Sayar, I., Firat, D., Yilmaz, I., Demiryilmaz, I. (2015) The effect of ozone and naringin on intestinal ischemia/reperfusion injury in an experimental model. *International journal of surgery*. 21, 38-44.
- [53] Isik, A., Peker, K., Soyuturk, M., Firat, D., Yoruker, U. and Yilmaz, I. (2015) Diagnostic evaluation and treatment of patients with rectus abdominis hematoma. *Cirugia espanola*. 93(9), 580-8.
- [54] Ozkan, H., Ekinci, S., Uysal, B., Akyildiz, F., Turkkan, S., Ersen, O., Koca, K., Seven, M.M. (2015) Evaluation and comparison of the effect of hypothermia and ozone on ischemia-reperfusion injury of skeletal muscle in rats. *The Journal of surgical research*. 196(2), 313-9.
- [55] Maher P. (2005) The effects of stress and aging on glutathione metabolism. *Ageing research reviews*. 4(2), 288-314.
- [56] Cruz, R., Almaguer Melian, W. and Bergado Rosado, J.A. (2003) [Glutathione in cognitive function and neurodegeneration]. *Revista de neurologia*. 36(9), 877-86.
- [57] Gulcin, I. (2006) Antioxidant and antiradical activities of L-carnitine. *Life sciences*. 78(8), 803-11.
- [58] Gulcin, I., Alici, H.A. and Cesur, M. (2005) Determination of in vitro antioxidant and radical scavenging activities of propofol. *Chemical & pharmaceutical bulletin*. 53(3), 281-5.
- [59] Chen, B.H., Caballero, S., Seo, S., Grant, M.B. and Lewin, A.S. (2009) Delivery of antioxidant enzyme genes protects against ischemia/reperfusion induced injury to retinal microvasculature. *Invest Ophthalmol Vis Sci*. 50, 5587-95.
- [60] Aggarwal, A., Gaur, V. and Kumar, A. (2010) Nitric oxide mechanism in the protective effect of naringin against post-stroke depression

(PSD) in mice. Life sciences. 86(25-26), 928-35.

Received: 11.08.2016

Accepted: 11.05.2017

CORRESPONDING AUTHOR

Fazile Nur Ekinçi Akdemir
Agri Ibrahim Cecen University
Health School
Department of Nutrition and Dietetics
TR-04100- Agri –TURKEY

E-mail: fazilenur85@gmail.com

FREE RADICAL SCAVENGING ACTIVITY, PHENOLIC CONTENTS AND FLAVONOIDS OF FOUR CRUCIFEROUS VEGETABLES: EFFECTS OF EXTRACTION

Okan Erken^{1,*}, Seckin Kaya²

¹Çanakkale Onsekiz Mart University, Faculty of Agriculture, Department of Agricultural Structures and Irrigation, Terzioğlu Kampüsü Çanakkale, Turkey.

²Çanakkale Onsekiz Mart University, Faculty of Agriculture, Department of Horticulture Terzioğlu Kampüsü Çanakkale, Turkey

ABSTRACT

Researchers developed many methods and extraction protocols to determine the antioxidant properties of plant-derived food. As well as targeting plants high in antioxidant activity it is also important to optimize appropriate extraction parameters. Three extracting solvents, aqueous, ethanolic and acetonetic, four Cruciferous species, cabbage, red cabbage, broccoli and cauliflower were evaluated to determine radical scavenging activity, total phenolics and flavonoids. Significant differences were found in the extracting abilities of the solvents to determine radical scavenging inhibition percentages of Cruciferous genus except cauliflower. Ethanolic extract worked well for cabbage, acetonetic extract and ethanolic extract work well respectively for red cabbages and acetonetic extract worked well for both cauliflower and broccoli in the determination of DPPH radical scavenging activity. Ethanolic extract of cabbage gave the highest total phenolic content (TPC). No significant differences were found in the extracting abilities of the solvents for red cabbage to determine TPC. Acetonetic extracts of broccoli and cauliflower found more effective than the other solvents to determine TPC. Ethanolic extracts of white and red cabbages and acetonetic extracts of broccoli and cauliflower found more effective to determine total flavonoids.

KEYWORDS:

Radical scavenging, Phenolics, Flavonoids, Extraction, Cruciferous

INTRODUCTION

Fruits and vegetables are rich sources of vitamins, mostly vitamins A and C. They are also excellent sources of fibre, contain some calories and are naturally low in fat [1]. Cruciferous vegetables include different types of cabbages, cauliflower, broccoli, kale, and Brussel sprouts and possess antioxidant and anticarcinogenic properties because of vitamins, carotenoids and polyphenols contents [2,3,4]. Antioxidant potential of Cruciferous vegetables is

high compared to others [5]. Phenolic substances can be categorized into simple phenols, phenolic acids, flavonoids, lignins and tannens [6]. Currently there is an increased interest for health promoting possibility of phytochemicals such as phenolics and flavonoids in vegetables [7]. Flavonoids are large compounds ubiquitously in plant derived foods. Many flavonoids are reported to be strong free radical scavengers and antioxidants and food-derived flavonoids have been reported to reduce risk of cancer [8]. Antioxidant contents of cruciferous vegetables are affected by various factors such as maturity at the harvest time, growing conditions, soil and storage conditions [9]. Several methods have been developed to measure the radical scavenging capacity (RSC) of food products [10, 11, 12]. On the other hand, extraction part of the methods was generally a mystery because of modifications on experiments and plant organ sample that used in the assays. Although methods were argumentative in some cases, many of them were widely used and accepted such as DPPH Radical Scavenging Capacity Assay described and reported by Brand-Williams et al. [13].

Antioxidative capacity and substances of the plant derived foods can be determined by different extraction protocols. Researchers investigate different extracting solvents such as water, acetone, methanol or ethanol. Bidchol et al. [14], investigated aqueous and ethanolic extracts of broccoli and reported that ethanolic extract was more effective than aqueous extract while determining the DPPH radical scavenging activity. Controversially they stated that phenolic content in the aqueous extract of broccoli was higher than ethanolic extract. Guo et al. [15], stated that methanolic extract work better than aqueous and acetonetic extracts respectively to determine the ferrous ion chelating power and DPPH radical scavenging activity for broccoli. On the other hand, Kaur & Kapoor [16], declared that antioxidant activities of cabbage and cauliflower were higher in ethanolic extract than aqueous extract. Llorach et al. [17] investigated the phenolics and antioxidative properties of aqueous and ethanolic extracts and reported that aqueous extract protocol gave higher phenolic content than ethanolic extract. They also reported that the highest antiradical activity against both

DPPH and ABTS have been found in ethanolic extract. Anwar et al. [18] also investigated volumetric ratios of ethanolic and methanolic extracts of cauliflower to determine antioxidant activity and phenolics. They reported that DPPH radical scavenging activity varied considerably in relation to both the extracting solvents and drying processes. They also stated that 80 % ethanolic extract worked well to determine total phenolic of cauliflowers.

This paper discusses the DPPH radical scavenging activity, flavonoid and phenolic contents of the aqueous, ethanolic and acetonic extracts of four different Cruciferous species.

MATERIALS AND METHODS

Plant material and preparation of samples.

A replicated pot trial was conducted in research fields of Faculty of Agriculture at Çanakkale Onsekiz Mart University, Dardanos, Çanakkale, Turkey. Çanakkale where the study was conducted is located in the south-western part of Anatolia and in the north-western part of the Thrace, at the southern end of the Sea of Marmara. The study area has a transition climate between Mediterranean and Black Sea. Plants were grown in 10 L pots filled with media which has clay loam soil structure, 7.02 pH, 0.65 mS/cm, 11.18% lime and 2.67% organic matter. The media used in the pots shows the most common characteristics of region's soil. Study was planned according to randomized block design with 4 repetitions and 4 plants in each repetition. Standard cultural practices were utilized and plants were grown until their standard edible maturity harvest time. Cabbage (*Brassica oleracea L. var. capitata*) cv. Yazgülü heads, red cabbage (*Brassica oleracea L. var. rubra*) cv. Integra heads, broccoli (*Brassica oleracea L. var. italica*) cv. Maraton florets and cauliflower (*Brassica oleracea L. var. botrytis*) cv. Twingo florets were harvested and immediately transferred to laboratory. Fresh heads and florets were washed and cut into small pieces then left to dry on a bench under ambient temperature for over an hour and then grounded in a blender for homogenization.

Chemicals and extraction methods. All chemicals were purchased from Sigma-Aldrich (USA), SPA (Milan, Italy), Merck (Germany), and Fluka Chemica (Switzerland) companies. Three different extraction solvent and four different Cruciferous species were used in the study. Five grams edible parts of plants homogenised before were sampled and then extracted for 4 hours on magnetic stirrer with 20 ml distilled water, 20 ml ethanol, 20 ml acetone separately. After 4 hours of extraction, samples were centrifuged for 10 minutes at 4000 rpm. Supernatant of each sample were collected and filtered through 0.45 µm pore sized filter.

Determination of DPPH free radical-scavenging activity. Extracts on 1,1-diphenyl-2-picrylhydrazyl (DPPH) was estimated as described by Brand-Williams et al. [13]. Samples were diluted with the solvent used in the extractions prior to the analysis (1 mg ml⁻¹). The DPPH solution was added to the diluted samples, mixed then left for 30 minutes. Absorbance of the samples was measured at 515 nm using a UV-Vis spectrophotometer (Thermo Aquamate). The percentage of DPPH radical scavenging activity was calculated by using the following equation;

$$\text{DPPH scavenging (\%)} = \frac{(A_{\text{control}} - A_{\text{sample}})}{A_{\text{control}}} \times 100$$

where A_{sample} is the absorbance of the sample after the time necessary to reach the plateau (30 min) and A_{control} is the absorbance of DPPH.

Extract concentrations providing IC₅₀ inhibition values (defined as the concentration of the compounds that was able to inhibit 50% of the total DPPH radicals) were calculated from graph plotting using nonlinear regression and expressed in microgram material equivalents per millilitre for sample extracts. Butylated hydroxytoluene (BHT) was used as a positive control. A lower value of IC₅₀ indicates a higher antioxidant activity and vice versa.

Analysis of total phenolic content. The amount of total phenolics was determined spectrophotometrically using Folin-Ciocalteu reagent method described by Singleton et al. [19] with modifications [20]. Half ml distilled water and 0.5 ml Folin-Ciocalteu reagent was added to the test tube containing extract and ethanol/acetone solution (0.2 ml, 500 mg ml⁻¹). The contents were shaken thoroughly and allowed to stand for a minute. Eight tenths ml of sodium carbonate solution (7.5%) was added and the mixture with stirring then allowed standing for 30 minutes with intermittent shaking. Absorbance was measured at 760 nm using a UV-Vis spectrophotometer (Thermo Aquamate). Total phenolic content of the extracts were expressed as gallic acid equivalents (GAE) in milligram per gram fresh weight. Each extract of samples were analysed in triplicate.

Analysis of total flavonoids content. The total flavonoid content was determined spectrophotometrically described by Oomah & Mazza [21] using rutin as a standard. The total flavonoid content was expressed as rutin equivalents in milligram per gram fresh fruit. Three replicates were used for the determination of the mean total flavonoid values of the fruit samples. General linear model (GLM) analyses of variance were evaluated using Minitab v.13 software with significant level for LSD means of $p=0.05$.

RESULTS AND DISCUSSION

Effects of extracts on DPPH radical scavenging activity. Bidchol et al. [14] stated that DPPH has been widely used to test the free radical scavenging ability of various samples. DPPH radical scavenging activity, inhibition (%) and IC₅₀ values according to the Cruciferous species were shown in Figure 1 and 2. Ethanolic extract was determined more active than the acetonic and aqueous extract with IC₅₀ values of 140, 210, 760 µg g⁻¹, in white cabbage, respectively. This result denoted that ethanolic extract has more free radical scavenging activity than acetonic and aqueous extracts. Bidchol et al. [14] also stated that free radical inhibition rate of ethanolic extract was higher than the aqueous extract of broccoli. Regarding to the solvent to be used DPPH method works well equally with methanol and ethanol compared to acetone and water [15,23]. Additionally Kaur & Kapoor [16] reported that antioxidant activity of ethanolic extracts gave better results than aqueous ones in white cabbages. Our data also well agree with other studies. On the other hand, some researchers stated that aqueous extracts of cabbages were more active compared to the ethanolic extracts [23]. However, DPPH assay method and the positive control organic compounds such as ascorbic acid or BHT should be considered when comparing the results of researches. Besides, radical scavenging activity and inhibition percentage might change according to the species, edible parts of vegetables such as broccoli florets, stems or leaves [15].

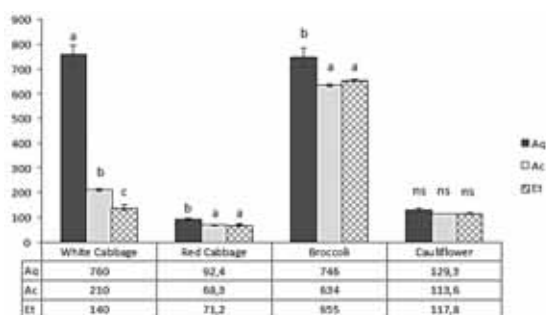


FIGURE 1

IC₅₀ values of aqueous, ethanolic and acetonic extracts of four different Cruciferous species (E_{Aq}: Aqueous extract; E_{Ac}: Acetonic extract; E_{Et}: Ethanolic extract)

Concerning with the results of extractions of red cabbages, while no significant differences were found from extraction with acetone and ethanol, extraction with water separated from the rest statistically with the lowest inhibition percentage (Figure 2). It seems that acetonic extract and ethanolic extract work well while determining DPPH radical scavenging activity of red cabbages compared to aqueous extract. Inhibition percentage was also affected by the extraction solvents. Pliszka et al. [24] reported that

DPPH radical scavenging activity of red head cabbages depended on cabbage cultivar. Also researchers stated that they had determined higher inhibition rates between 82.24% and 85.50% in red head cabbages with ethanolic extracts. We also determined the inhibition rates of 88.31%, 90.26% and 90.45% with the acetonic, ethanolic and aqueous extracts respectively (Figure 2). As stated before the use of aqueous extracts gave low values for the extent of reduction [15,22].

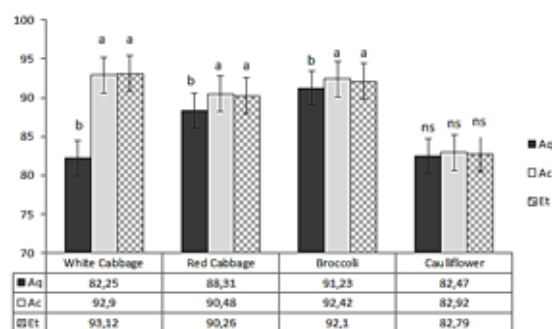


FIGURE 2

Inhibition (%) rates of aqueous, ethanolic and acetonic extracts of four different Cruciferous species (E_{Aq}: Aqueous extract; E_{Ac}: Acetonic extract; E_{Et}: Ethanolic extract)

According to the results obtained from broccoli florets extracted with different solvents, highest DPPH radical scavenging inhibition rates were determined from acetonic extract (92.42%) and this value was followed by ethanolic (92.10%) and aqueous (91.23%) extracts respectively. While there is no significant difference between acetonic and ethanolic extractions of broccoli florets, aqueous extraction involved in a different group statistically. According to the results obtained we found acetonic and ethanolic extract worked better than aqueous extract. This data confirms the observations of Bidchol et al. [14], who compared the FRSA of aqueous and ethanolic extracts of broccoli. Authors reported that ethanolic extract was more active than the aqueous extract. Controversially, Guo et al. [15] suggested that methanolic extract of broccoli had given the highest DPPH FRSA followed by aqueous and acetone extracts. Also they reported that acetonic extract showed the least FRSA lower than 20%. Our results with ethanolic and aqueous extract are consistent with the researcher's finding but are not with acetonic extract. Acetonic extract FRSA (92.42%) seems very high compared to the given literature but sampling and preparation of samples must be taken into consideration. The wide difference between the results of two researches may occur because of the freeze dried samples used by the researchers in the given literature.

Using different solvents showed no significant effect on inhibition percentage in the data obtained from the extraction of cauliflowers statistically. As shown in figure 2, highest inhibition percentage was

determined from acetic extract (82.92%) and this value was followed by ethanolic (82.79%) and aqueous (82.47%) extracts respectively. In this study we found that acetic extract works as well as ethanolic extract. Koksal & Gulcin [25] reported DPPH FRSA of 51 and 64% for aqueous and ethanol cauliflower extracts respectively. These researchers also stated that DPPH FRSA varied considerably in relation to both the extracting solvents and drying processes. Llorach et al. [17] stated that ethanolic extracts of cauliflower florets had given higher results compared to the aqueous extract. Anwar et al. [18] investigated the effects of aqueous-ethanol and aqueous-methanol mixtures for extraction and found that cauliflower extracted by 80% methanolic extract have the highest FRCA. These literatures given above prove that ethanolic extracts work better to determine DPPH FRSC of cauliflower. Results in the present study consistent with the results of given literature.

As seen on figure 1 and 2 extraction solvents effects on DPPH radical scavenging inhibition percentage of Cruciferous vegetables. White cabbage has the highest DPPH radical scavenging activity followed by broccoli, red cabbage and cauliflower according to the data obtained. Additionally we noticed that ethanolic extract works well for white cabbage and red cabbage. However, when the florets are concerned like broccoli or cauliflower we can state that acetic extraction works better both than ethanolic and aqueous extracts as a result.

Effects of extracts on total phenolic contents.

The highest amount of total phenolic contents in white cabbage was determined 314.43 mg GAE g⁻¹ with ethanolic extraction, 278.34 mg GAE 100 g⁻¹ with acetic extraction and 144.60 mg GAE 100 g⁻¹ with aqueous extraction, respectively (Figure 3). According to the results obtained ethanolic extracts work well to determine total phenolic content (TPC) of white cabbage in the present study. Researchers reported various results about TPC of white cabbages. For instance, Heimler et al. [26] reported that TPC of white cabbages were 5.31 mg GAE g⁻¹ with 70% ethanolic extraction protocol. Jacob et al. [27] investigated the effects of methanolic and aqueous extracts on green and red cabbages with various temperatures of water and reported that they had the highest results from methanolic extracts both for green and red cabbages. Besides, researchers suggested that total antioxidant content decreased because of deterioration of antioxidants at higher temperatures. Additionally, Chu et al. [3] determined 36.66 mg GAE 100 g⁻¹ TPC in cabbages by acetic extraction. This result seems so low comparing to our study. We concluded that this variation is influenced by the extraction solvent and long-time extraction (4 hours) of the samples in our study. Researchers determined various TPC of cabbages with different extraction methods. For instance, Ismail et al.

[29] determined 1107.57 mg ferulic acid 100 g⁻¹ by ethanolic extract and Kaur & Kapoor [16] determined 92.5 mg catechol 100 g⁻¹ with ethanolic extract.

Many researchers reported that red cabbage has higher TPC than cabbage [27, 29, 16]. The highest amount of total phenolic contents in red cabbage was determined 313.73 mg GAE g⁻¹ with ethanolic extraction, 313.71 mg GAE 100 g⁻¹ with aqueous extraction and 144.60 mg GAE 100 g⁻¹ with acetic extraction, respectively (Figure 3). No statistical significance was found among extraction solvent was determined. According to the results obtained ethanolic extracts work well to determine total phenolic content (TPC) of red cabbage in the present study. Karadeniz et al. [30] reported 216.6 mg GAE 100 g⁻¹ for red cabbages grown in Turkey with 70% aqueous methanol. Marinova et al. [31] determined 139.3 mg GAE g⁻¹ in Bulgarian red cabbages with aqueous extract. Leja et al. [29] investigated different red cabbage varieties and reported that TPC of red cabbages ranged between 43.3-248.8 mg 100 g⁻¹ with methanolic extraction method. Jacob et al. [27] reported that extraction method effects on TPC and flavonoid contents of cruciferous vegetables. Our results showed that ethanolic extracts work well to determine the TPC of red cabbages compared to aqueous and acetic extracts.

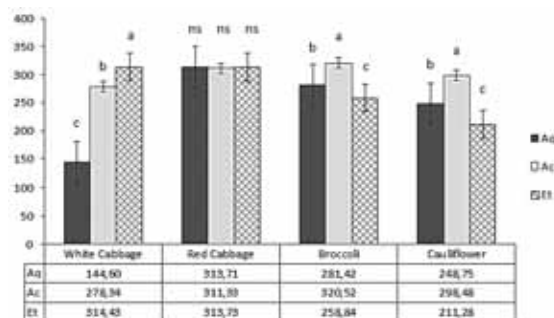


FIGURE 3
Total phenolic contents (TPC) of Cruciferous species by aqueous, ethanolic and acetic extracts (E_{Aq}: Aqueous extract; E_{Ac}: Acetic extract; E_{Et}: Ethanolic extract)

The highest amount of total phenolic contents in broccoli was determined to be 320.52 mg GAE g⁻¹ with acetic extraction, 281.42 mg GAE 100 g⁻¹ with aqueous extraction and 258.84 mg GAE 100 g⁻¹ with ethanolic extraction, respectively (Figure 3). Bidchol et al. [14] reported that phenolic contents in the aqueous extract of Broccoli were higher than that of the ethanolic extract. Our results also proved the literature given with the higher amounts of phenolics determined in the aqueous extract than ethanolic extract of broccoli florets. Researchers also declare that there were reports that antioxidant activity could also be from non-phenolic compounds [32]. Additionally, aqueous and ethanolic extracts of broccoli might contain non-phenolic compounds such as selenium,

glucosinolates etc. These compounds also behave like antioxidants and scavenge free radicals in vitro conditions. Controversially, we found that acetic extract more effective than ethanolic and aqueous extracts. Guo et al. [15] stated methanolic extract showed the highest ferrous ion chelating ability than aqueous and acetic extracts. However, acetic extract gave better results when the dry sample weight was increased. We thought that acetic extract gave better results than ethanolic extract because of the extracting period (4 hours) and the amount of sample weight (5 grams).

Cauliflower also has enabled us to achieve the highest total phenolic content with extraction of acetone as broccoli. The highest amount of total phenolic contents in cauliflower was determined to be 298.48 mg GAE 100 g⁻¹ with acetic extraction, 248.75 mg GAE 100 g⁻¹ with aqueous extraction and 211.28 mg GAE 100 g⁻¹ with ethanolic extraction, respectively (Figure 3). Significant differences were found from the results obtained by the different extraction protocols. Singh et al. [33] noticed that total phenolic contents of cabbages of 18 different cultivars ranged 34.41 mg g⁻¹ to 12.58 mg g⁻¹. Köksal & Gülçin [25] reported that aqueous extract is more effective for cauliflower than extraction with ethanol. Llorach et al. [17] reported that aqueous extract of cauliflower gave higher TPC than ethanolic extraction. This result is consistent with our findings. This might be due to the extraction of salts and other water soluble compounds that were not extracted with ethanol. In the present study it seems acetic extract works well to determine TPC of cauliflower than both ethanolic and aqueous extracts. This result may be due to extracting duration and amount of samples used in the extraction.

As seen on figure 3, extraction solvents effects on total phenolics of Cruciferous vegetables except red cabbage. It seems extract works better for white cabbage. On the other hand, it can be stated that acetic extraction works better both than ethanolic and aqueous extracts for broccoli and cauliflower.

Effects of extracts on flavonoid contents.

Highest total flavonoid content was determined from the extraction with ethanol as 1.11 mg g⁻¹ compared to the other extraction solvents. Significant differences were determined from the results obtained by the different extraction protocols of flavonoid contents of white cabbage (Figure 4). The lowest flavonoid content was obtained from aqueous extract and it seems that ethanolic extract work well while determining flavonoid content of white cabbages. Heimler et al. [26] reported that white cabbage has 1.98 mg CE g⁻¹ total flavonoid content in white cabbage with 70% ethanolic extract. Gorinstein et al. [34] investigated phenolic and antioxidant activities of different raw vegetables and stated that white cabbages have 1.67 catechin (CE) mg g⁻¹ flavonoid contents

extracted with 50% methanol/water. Additionally researchers reported that white cabbages have 3.22 catechin (CE) mg g⁻¹ flavonoid contents extracted with 1.2 M 50% methanol/water. These results proved that flavonoid contents were affected by the extraction method and extraction solvent.

Total flavonoids of red cabbages extracted with different solvents were ranged from 1.439 mg g⁻¹ to 0.713 mg g⁻¹. While the highest flavonoid content value is obtained from extraction with ethanol, the lowest flavonoid content was obtained from the extraction with pure water (Figure 4). Each extraction solvent was classified in different groups statistically. Results showed that ethanolic extract work well while determining total flavonoids of red cabbages. Karadeniz et al. [30] reported that red cabbages grown in Turkey have 0.842 mg g⁻¹ total flavonoid content with 70% aqueous methanol extract. They also used fresh vegetables for assay our results are consistent with results given by the author above. On the other hand, Marinova et al. [31] investigated total flavonoid contents various fruits and vegetables in their researches with 80 % aqueous methanol extraction and reported that red cabbage has 23.7 mg CE 100 g⁻¹. The results obtained from these authors may be quite different from our study because of freeze dried samples.

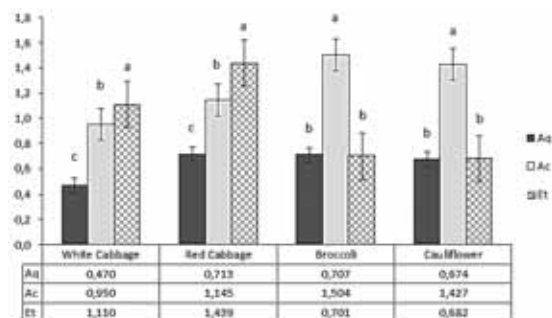


FIGURE 4
Flavonoid content of Cruciferous species by aqueous, ethanolic and acetic extracts
 (EAq: Aqueous extract; EAc: Acetic extract; EEt: Ethanolic extract)

The highest amount of total flavonoids in broccoli was determined to be 1.504 mg g⁻¹ with acetic extraction, 0.707 mg 100 g⁻¹ with aqueous extraction and 0.701 mg 100 g⁻¹ with ethanolic extraction, respectively (Figure 4). Results show that different extraction solvents effected flavonoid contents of broccoli florets statistically. It seems acetic extraction works better than both aqueous and ethanolic extracts for broccoli. Sun et al. [35] compared the effects of acetic, methanolic and aqueous extracts of broccoli and asparagus juice and reported that acetic extract found more effective for broccoli than methanolic and aqueous extracts respectively. This result is consistent with our data.

The highest amount of total flavonoids in cau-

liflower was determined to be 1.427 mg g⁻¹ with acetic extraction, 0.682 mg 100 g⁻¹ with aqueous extraction and 0.674 mg 100 g⁻¹ with ethanolic extraction, respectively (Figure 4). Based on our findings, acetic extract works better than ethanolic and aqueous extracts to determine the total flavonoids for cauliflower. Heimler et al. [26] determined 1.69 mg g⁻¹ catechin based flavonoids in cauliflower with 70% ethanolic extraction. We thought that acetic extraction works similar to broccoli or cauliflower.

Figure 4 shows the effects of aqueous, ethanolic and acetic extractions on total flavonoids of cruciferous vegetables. As seen on figure 4, extraction solvents effects on total flavonoids of Cruciferous vegetables. It can be stated that ethanolic extract works well both for white and cabbage. Additionally, acetic extraction works better both than ethanolic and aqueous extracts for broccoli and cauliflower.

CONCLUSIONS

In this study it was aimed to determine the amount of change of DPPH radical scavenging activity, antioxidant capacity and total flavonoid contents of 4 different cruciferous species extracted by 3 different solvents in the study. According to the results the highest DPPH radical scavenging activity was determined by ethanol extraction for cabbage and red cabbage and by acetone extraction for broccoli and cauliflower. Concerning with the total flavonoid contents the highest value was determined by ethanol extraction for cabbage and red cabbage and by acetone extraction for broccoli and cauliflower as in DPPH radical scavenging activity. The most interesting results are obtained from DPPH radical scavenging activity for red cabbage that no significant difference was determined between the solvents. On the other hand acetic extraction gave the highest flavonoid contents for cauliflower and broccoli.

REFERENCES

- [1] du Toit, R.; Volsteadt, Y.; Apostolides, Z. (2001) Comparison of the Antioxidant Content of Fruits, Vegetables and Teas Measured as Vitamin C Equivalents. *Toxicology*, 166, 63–69.
- [2] Cohen, J.; Kristal, R.; Stanford, J. (2000) Fruit and vegetable intakes and prostate cancer. *Journal of National Cancer Institute*, 9, 61-68.
- [3] Chu, Y-F.; Sun, J.; Wu, X. & Liu, R.H. (2002) Antioxidant and anti-proliferative activities of common vegetables. *Journal of Agricultural and Food Chemistry*, 50(23), 6910-6916.
- [4] Podsedek, A. (2007) Natural antioxidants and antioxidant capacity of brassica vegetables: A review. *Swiss Society of Food Science and Technology*, 40, 1-11.
- [5] Soengas, P.; Sotelo, T.; Velasco, P.; Cartea, M.E. (2011) Antioxidant properties of brassica vegetables. *Functional Plant Science and Biotechnology*, 5 (Special Issue 2), 43-55.
- [6] Kartika, H.; Li, Q.X.; Wall, M.M.; Nakamoto, S.T.; Iwaoka, W.T. (2007) Major phenolic acids and total antioxidant activity in Mamaki leaves, *Pipturus albidus*. *Journal of Food Science*, 72, 696-701.
- [7] Kim, D.O.; Padilla-Zakaour, O.I.; Griffiths, P.D. (2004) Flavonoids and antioxidant capacity of various cabbage genotypes at juvenile stage. *Food Chemistry and Toxicology*, 69(9), 685-689.
- [8] Chu, Y-H.; Chang, C-L.; Hsu, H-F. (2000) Flavonoid content of several vegetables and their antioxidant activity. *Journal of the Science of Food and Agriculture*, 80, 561-566.
- [9] Paolini, M. (1998) Brussel sprouts: An exceptionally rich source of ambiguity for anti-cancer strategies. *Toxicology and Applied Pharmacology*, 152, 293-294.
- [10] Cao, G.; Sofic, E.; Prior, R.L. (1996) Antioxidant capacity of tea and common vegetables. *Journal of Agricultural and Food Chemistry*, 44, 3426–3431.
- [11] Kantha, S.S.; Wada, S.; Takeuchi, M.; Watabe, S.; Ochi, H. (1996) A sensitive method to screen for hydroxyl radical scavenging activity in natural food extracts using competitive inhibition ELISA for 8-Hydroxydeoxyguanosine. *Biotechnology Techniques*, 10, 933–936.
- [12] Furuta, S.; Nishiba, Y.; Suda, I. (1997) Fluorometric assay for screening anti-oxidative activity of vegetables. *Journal of Food Science*, 62, 526–528.
- [13] Brand-Williams, W.; Cuvelier, M.E.; Berset, C. (1995) Use of a free radical method to evaluate antioxidant activity. *LWT-Food Science and Technology*, 28, 25-30.
- [14] Bidchol, A.E.; Wilfred, A.; Abhijna, P.A.; Harish, R. (2011) Free radical scavenging activity of aqueous and ethanolic extract of *Brassica oleracea* L. var. Italica. *Food Bioprocess Technology*, 4, 1137–1143.
- [15] Guo, J.; Hui-Lien, L.; Chiang, S.; Lin, F.; Chang, C. (2001) Antioxidant properties of the extracts from different parts of broccoli in Taiwan. *Journal of Food and Drug Analysis*, 9(2), 96-101.
- [16] Kaur, C.; Kapoor, H.C. (2002) Anti-oxidant activity and total phenolic content of some asian vegetables. *International Journal of Food Science and Technology*, 37, 153-161.
- [17] Llorach, R.; Espin, J.C.; Tomas-Barberan, F.A.; Ferreres, F. (2003) Volatilization of cauliflower (*Brassica Oleracea* L. Var. Botrytis) by-products as a source of antioxidant phenolics. *Journal of Agricultural and Food Chemistry*, 51, 2181-2187.
- [18] Anwar, F.; Kalsoom, U.; Sultana, B.; Mushtaq, M.; Mehmood, T.; Arshad, H.A. (2013) Effect

- of drying method and extraction solvent on the total phenolics and antioxidant activity of cauliflower (*Brassica oleracea* L.) extracts. *International Food Research Journal*, 20(2), 653-659.
- [19] Singleton V. L.; Orthofer, R.; Lamuela-Raventos, R. M. (1999) Analysis of total phenols and other oxidation substrates and antioxidants by means of Folin-Ciocalteu reagent. *Methods in Enzymology*, 299, 152-178.
- [20] Djeridane, A.; Yousfi, M.; Nadjemi, B.; Boutassouna, D.; Stocher Vidal, N. (2006) Antioxidant activity of some algerian medicinal plants extracts containing phenolic compounds. *Food Chemistry*, 97, 654-660.
- [21] Oomah, B.D.; Mazza, G. (1996) Flavonoids and antioxidative activities in buckwheat. *Journal of Agricultural and Food Chemistry*, 44(7), 1746-1750.
- [22] Molyneux, P. (2004) The use of the stable free radical diphenylpicrylhydrazyl (DPPH) for estimating antioxidant activity. *Songklanakarin Journal of Science & Technology*, 26(2), 211-219.
- [23] Thaipratum, R. (2014) evaluation of antioxidant activities of cabbage (*Brassica oleracea* L. var. Capitata L.). *International Journal of Biological, Agricultural, Food and Biotechnological Engineering*, 8(6), 591-593.
- [24] Pliszka, B.; Mielezko, E.; Huszcza-Ciolkowska, G.; Wroblewska-wierzicka, B. (2007) Content of anthocyanins and their antioxidative properties in various cultivars of red head cabbage (*Brassica oleracea* L. var. capitata L. f. rubra). *Journal of Elementology*, 12(3), 191-198.
- [25] Köksal, E.; Gülçin, İ. (2008) Antioxidant activity of cauliflower (*Brassica oleracea* L.). *Turkish Journal of Agriculture & Forestry*, 32, 65-78.
- [26] Heimler, D.; Vignolini, P.; Dini, M.G.; Vincieri, F.F.; Romani, A. (2006) Antiradical activity and polyphenol composition of local *Brassicaceae* edible varieties. *Food Chemistry*, 99, 464-469.
- [27] Jacob, J.A.; Mahal, H.S.; Mukherjee, T.; Kapoor, S. (2011) Free radical reactions with the extract of brassica family. *Food Chemistry*, 129, 1132-1138.
- [28] Ismail, A.; Marjan, Z.M.; Foong, C.W. (2004) Total antioxidant activity and phenolic content in selected vegetables. *Food Chemistry*, 8, 581-586.
- [29] Leja, M.; Kaminska, I.; Kolton, A. (2010) Phenolic compounds as the major antioxidants in red cabbage. *Folia Horticulturae*, 22(1), 19-24.
- [30] Karadeniz, F.; Burdurlu, H.S.; Koca, N.; Soyer, Y. (2005) Antioxidant activity of selected fruits and vegetables grown in Turkey. *Turkish Journal of Agriculture and Forestry*, 29, 297-303.
- [31] Marinova, D.; Ribarova, F.; Atanassova, M. (2005) Total phenolics and total flavonoids in Bulgarian fruits and vegetables. *Journal of the University of Chemical Technology and Metallurgy*, 40(3), 255-260.
- [32] Mariko, N.; Hassimotto, M.; Genovese, I.M.; Lajolo, F.M. (2005) Antioxidant activity of dietary fruits, vegetables and commercial frozen pulps. *Journal of Agricultural and Food Chemistry*, 53, 2928-2935.
- [33] Singh, J.; Upadhyay, A.K.; Bahadur, A.; Singh, B.; Singh, K.P.; Mathura, R. (2006) Antioxidant phytochemicals in cabbage (*Brassica oleracea* L. var capitata). *Scientia Horticulturae*, 108, 233-237.
- [34] Gorinstein, S.; Park, Y. S.; Gu Heo, B.; Namiesnik, J.; Leontowicz, M.; Sik-Ham, K.; Cho, J.; Kang, S. (2009) A comparative study of phenolic compounds and antioxidant and antiproliferative activities in frequently consumed raw vegetables. *European Food Research and Technology*, 228, 903-911.
- [35] Sun, T.; Powers, J.R.; Tang, J. (2007) Evaluation of the antioxidant activity of Asparagus, Broccoli and their juices. *Food Chemistry*, 105, 101-106.

Received: 31.08.2016
Accepted: 03.05.2017

CORRESPONDING AUTHOR

Okan Erken

Çanakkale Onsekiz Mart University, Faculty of Agriculture, Department of Agricultural Structures and Irrigation, Terzioğlu Kampusü Çanakkale, Turkey.

e-mail: oyerken@comu.edu.tr

COMPARISON OF CHLORAMPHENICOL ADSORPTION BEHAVIOR ON BIOCHARS DERIVED FROM REED STRAWS AND MUNICIPAL SEWAGE SLUDGE

Hanyu Zhang, Zhaowei Wang, Xiaoyun Xie*, Junhong Gao, Junmin Zhu, Chaoran Xie

College of Earth and Environmental Sciences, Lanzhou University, Key Laboratory for Environment Pollution Prediction and Control, Gansu Province, Lanzhou 730000, P.R. China

ABSTRACT

This work studied the adsorption of chloramphenicol (CAP) on two types of biochars derived from reed straw (RSB) and municipal sewage sludge (SSB), which were prepared by pyrolyzing at 500°C. The biochars were characterized by scanning electron microscope, Fourier transform infrared spectroscopy, energy dispersive spectroscopy and Brunauer-Emmett-Teller. It revealed that RSB had a higher surface area (125.04 m²/g) than SSB (7.14 m²/g) and the adsorption of chloramphenicol on SSB ($q_m=1.171$ mg/g, 308.15K) was much less than that on RSB ($q_m=6.586$ mg/g, 308.15K). Adsorption kinetics of CAP on biochars followed pseudo second order kinetic model, and adsorption isotherm fitted well with Sips model. The adsorption kinetics and thermodynamics demonstrated that the adsorption of CAP on two biochars squinted towards chemical adsorption. The π - π electro-donor-acceptor interaction between nitro group, benzene ring in CAP and π electron on the surface of biochars played an important role in the adsorption of CAP on biochars, while the hydrogen bonding interaction also contributed to the adsorption of CAP on biochars synchronously.

KEYWORDS:

Chloramphenicol, Biochar, Adsorption kinetics, Adsorption thermodynamics, π - π electro-donor-acceptor

INTRODUCTION

Chloramphenicol (CAP) is a broad-spectrum antibiotic against various microorganisms, and it may lead to severe side effect on human health. The World Health Organization (WHO) had proclaimed that CAP should not be permitted in animals used for human food in 1969 [1]. However, CAP is still used just for its low cost and high efficiency in the treatment of disease [2]. From 2009 to 2015, it was listed that 53 exporters from China, Vietnam, Malaysia and India to USA had detected CAP in shrimps and frog legs products [3]. Besides, it has been reported that

residua of antibiotics can also directly cause ecological harm in organisms and promote antibiotic resistance genes (ARGs). Li et al. [4] have investigated CAP from four reservoirs in the Luan River of Tianjin, China, and the detection frequency high than 60%. The pollution of CAP is still an environment problem which can't be overlooked.

Adsorption is a common process in water treatment, the adsorbent is varied [5]. Biochar is a kind of carbon-rich solid obtained by the thermochemical conversion of biomass in a zero or low oxygen environment [6]. Due to its large specific surface area, rich surface functional groups, high hydrophobicity and aromaticity, biochar may interact with contaminants in aqueous effectively [7, 8]. Lots of studies have focused on remediation of organic contaminants in aqueous like dyes, antibiotics, pesticides by biochar [9-11].

Reed and dry municipal sewage sludge are common biomass material, both of them have large yield but are not easy to degrade [12, 13], so the management of them presents difficult environmental challenges. In this study, these two different materials were used to produce biochars, and the adsorptive behavior of CAP by RSB and SSB from aquatic environment were investigated and compared.

MATERIALS AND METHODS

Chemicals. CAP with a purity of 98% was purchased from J&K Scientific Co., and its properties are listed in Table 1. The CAP was dissolved into distilled water with CaCl₂ and NaN₃ to prepare the CAP stock solution. All other chemicals used in the experiment were analytical grade.

Preparation of biochars. Reed straws were collected from the bank of Yellow River in Lanzhou, China; municipal sewage sludge (dewatered sludge) obtained from Anning Municipal Sewage Treatment Plant in Lanzhou, China. The reed straws were rinsed with distilled water. Both reed straws and municipal sewage sludge were air dried at room temperature for 2 to 5 days. When biomass materials dried enough to grind to powder without stickiness, two

materials were ground by an electric grinder or a mortar. The powder of biomass materials passed 0.25 mm sieve and encased in crucibles respectively. Pyrolysing under Oxygen-limited condition was absolutely necessary for producing biochars [14], so every crucible was covered with a fitting lid. Then the crucibles were put in a muffle furnace for pyrolysing. Pyrolysis temperature was raised to 500 °C at a rate about 20 °C/min and with a residence time for 6 h, subsequently cooled to room temperature. The obtained biochars were ground again and passed through a 0.15 mm sieve.

Characterizations of the biochars. Surface area of biochars was measured at 77 K using a surface area analyzer (Tristar II 3020, USA) and determined by Brunauer-Emmet-Teller (BET) equation. Pore size distribution was calculated by using Barret-Joyner-Haleda model. Surface morphology was investigated by using scanning electron microscope (SEM) (JSM-5600LV, JEOL, Japan). Surface elemental composition of biochars was determined by energy dispersive spectroscopy (EDS) (IE250, Oxford Instrument, England). Fourier transform infrared spectroscopy (FTIR) (Nexus 670, Nicolet, USA) was used to characterize functional groups of two different biochars.

Analysis of chloramphenicol. Concentration of CAP in the solution was determined with UV spectrophotometer (UNICAM UV300, Thermo Spectronic, USA) at wavelength of 278 nm. A technical calibration curve was obtained from known concentrations of CAP ranging from 0.0 to 10.0 mg/L before analyzing samples.

Batch adsorption experiment. Three types of adsorption experiments were conducted in this study: a) adsorption equilibrium of CAP on RSB and SSB, b) adsorption isotherms of CAP to two biochars, and c) effect of pH on adsorption.

Adsorption equilibrium of CAP to RSB and SSB: RSB and SSB of 30 mg were weighed into 50 mL centrifuge tubes, 25 mL of CAP (5.0 and 10.0 mg/L) solution were added into each tube. All samples were shaken without light in a constant-temperature shaker at 25 ± 1 °C, then the samples were taken out at 10, 30 min and 1, 2, 4, 8, 12, 24, 36, 48 h, respectively. After taking out, the samples were centrifuged to separate the solid and aqueous phase at

4000 rpm for 5 min. The aqueous phase was filtered with 0.46 µm filter membrane.

Adsorption isotherms of CAP to RSB and SSB: two biochars of 30 mg were weighed into 50 mL centrifuge tubes, 25 mL of CAP solution with different concentrations ranging from 2.0 to 10.0 mg/L was added into each tube. All samples were shaken without light in a constant-temperature shaker at 288.15 K, 298.15 K and 308.15 K. Then the samples were centrifuged, filtered to separate the solid and aqueous phase.

Effect of pH on adsorption of CAP: 25 mL of CAP solution (5.0 mg/L) was added to 50 mL centrifuge tubes, and then 30 mg of RSB or SSB was added into each tube respectively. The pH was adjusted with HCl or NaOH solution in the range 2.0-11.0. Then the samples were shaken without light for 24 h at 25 ± 1 °C. After shaking, the samples were centrifuged, filtered to determine spectrophotometrically at 278 nm.

Amount of CAP adsorbed at time q_t (mg/g) and equilibrium adsorption amounts of CAP, q_e (mg/g) were calculated according to the following equations (Eq. (1) and (2)):

$$q_t = \frac{v(C_0 - C_t)}{w} \quad (1)$$

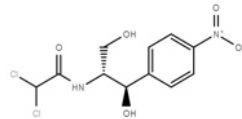
$$q_e = \frac{v(C_0 - C_e)}{w} \quad (2)$$

where C_0 and C_e are the initial and equilibrium concentrations of the CAP in aqueous solution (mg/L). C_t is the CAP concentration at time (mg/L). v is the volume of solution (L), w is the mass of biochars (g).

RESULTS AND DISCUSSION

Materials characteristics. The surface elemental compositions, surface area, and pore volume of the two biochars are compared in Table 2. The surface elemental compositions dates indicate that the surface of all biochars mainly consisted by C, O and Si, but their elemental ratios are different. Surface C content of RSB is 85.00%, whereas SSB only contains 40.27% and surface O and Si content of RSB are less than SSB. Since municipal sewage sludge is more complicate than reed straws, the component of them may decide the different elemental ratios of biochars. In Table 2 inorganic minerals content on the surface can be negligible.

TABLE 1
Structure and properties of CAP

Compound	CAS number	Chemical formula	Molecular mass	Log K_{ow}	pKa	Molecular structure
Chloramphenicol	56-75-7	$C_{11}H_{12}Cl_2N_2O_5$	323.13	1.14	n/a ^a	

^a not available.

TABLE 2
Basic physico-chemical characteristics of biochars

Biochar	Surface elemental composition ^a			BET surface area ^b (m ² g ⁻¹)	Micropore area ^b (m ² g ⁻¹)	Micropore volume ^c (cm ³ g ⁻¹)	Average pore diameter ^d (nm)
	C%	O%	Si%				
RSB	85.01	11.95	1.69	125.04	48.09	0.02000	2.43
SSB	40.27	43.43	7.05	7.14	1.86	0.00009	10.67

^a Determined by energy dispersive spectroscopy (EDS).

^b BET surface area and micropore area calculated in the relative pressure region $P/P_0=0.300$.

^c Micropore volume determined at $P/P_0=0.998$.

^d Average pore diameter obtained from BJH equation using N₂ isotherms.

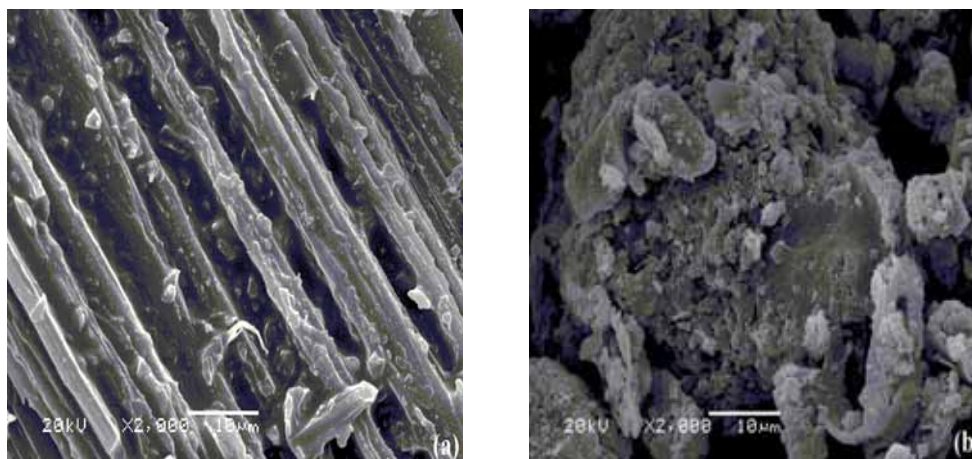


FIGURE 1
SEM images of RSB and SSB

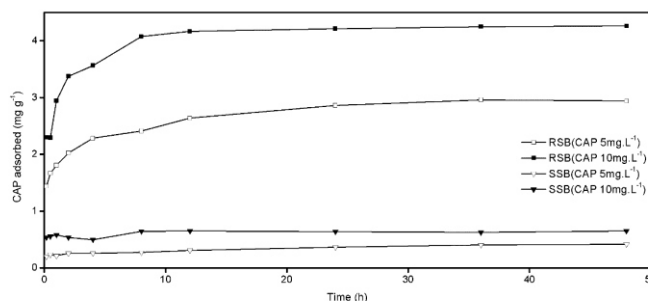


FIGURE 2
Equilibrium profiles of CAP on RSB and SSB

Figure 1 shows the surface morphology of RSB and SSB at 2000× magnifications. The RSB (Figure 1(a)) exhibits arrays of hollow channels structure. The hollow channels may be caused by the thermal degradation of organic compounds and celluloses in the channels [15]. Municipal sewage sludge contains a great quantity of microbes, organic compounds and volatile matters, which can be removed by thermo-chemical decomposition at temperature of 500 °C. However, irregular structure of sludge and inorganic compounds may hinder the forming of pores; thus, the SSB exhibits irregular flakes or sphere with few pores. The difference of surface structure may affect

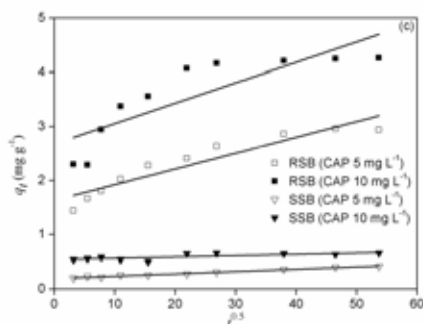
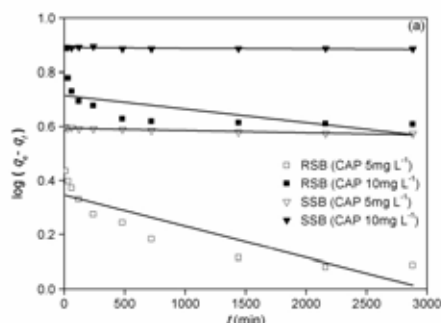
the surface area of material, the data of surface area, and pore volume of the two biochars. The Table 2 shows the BET surface area, micropore area and average pore of RSB are much higher than SSB. The average pore diameter of RSB and SSB are 2.43 and 10.67 nm, respectively. The hollow channels may increase the surface area of RSB, whereas less of pore structure and low BET surface area of SSB may due to the poor surface morphology.

Adsorption study. Adsorption kinetics describes the removal rate of adsorbate with the contact

time [16]. The influence of contact time on the adsorption of CAP (5.0 mg/L and 10.0 mg/L) on RSB and SSB is shown in Figure 2. The CAP adsorption on RSB can be divided into two steps. At the beginning 12 h, the adsorption rate was rapid and over 40% of the total CAP was adsorbed. Then the adsorption rate grew slowly and the curve shape became a flat horizontal line. The adsorption equilibrium was achieved after 24h. The adsorption of CAP on SSB was few, only 8.38% and 6.53% of the total CAP (5.0 mg/L and 10.0mg/L) were adsorbed, and the variation trend of adsorption rate was not obviously from adsorption processes began to end. Additionally, the Figure 2 shows that the adsorption of CAP on RSB was more effective than that on SSB. The possible reason is that the higher BET surface area, micropore area and average pore of RSB may have allowed the CAP molecules into the adsorbent easier.

Four well-known kinetic equations: pseudo-first-order model Eq. (3) [17], pseudo-second-order model Eq. (4) [18], intraparticle diffusion model Eq. (5) [19] and Elovich model Eq. (6) [20] were used to discuss the adsorption kinetics. The four models are presented as follows:

$$\log(q_e - q_t) = \log q_e - k_1 t / 2.303 \quad (3)$$



where q_t (mg/g) and q_e (mg/g) are the adsorption capacities of CAP adsorbed at time t (min) and at equilibrium, respectively; k_1 (min^{-1}) is the rate constant of the pseudo-first-order model. The fitting curves of the pseudo-first-order models for adsorption of CAP onto RSB and SSB are given in Figure 3 (a).

$$t/q_t = 1/k_2 q_e^2 + t/q_e \quad (4)$$

where, k_2 ($\text{g}/(\text{mg} \cdot \text{min})$) is the pseudo-second-order rate constant and it mainly depends on the applied operating conditions, initial antibiotic concentration, temperature and pH of solution [20]. The linear plot of the pseudo-second-order model is given in Figure 3 (b).

$$q_t = k_{id} t^{0.5} \quad (5)$$

where k_{id} ($\text{mg}/(\text{g} \cdot \text{min}^{0.5})$) is the rate constant of intraparticle diffusion equation and the fitting curves of the intraparticle diffusion is given in Figure 3 (c).

$$q_t = \beta \ln(\alpha\beta) + \beta \ln t \quad (6)$$

where α and β are the Elovich constants which represent the initial adsorption rate ($\text{g}/(\text{mg} \cdot \text{min}^2)$) and the desorption constant ($\text{mg}/(\text{g} \cdot \text{min})$), respectively. Figure 3(d) is the linear plot for the Elovich model of CAP onto RSB and SSB.

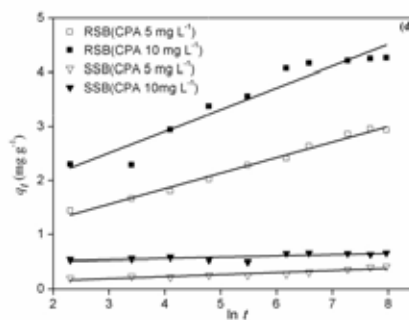
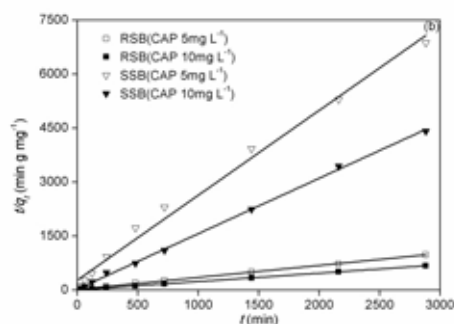


FIGURE 3
Different kinetic plots for the adsorption of CAP onto RSB and SSB

TABLE 3
Kinetic model parameters for adsorption of CAP onto RSB and SSB.

Kinetic models	Parameters	RSB		SSB	
		5.0mg/L	10.0mg/L	5.0mg/L	10.0mg/L
Pseudo-first-order	$q_e(\text{exp})$ (mg/g)	2.940	4.261	0.419	0.653
	k_1 (min^{-1})	0.000265	0.000116	0.000019	0.000005
	$q_e(\text{calc})$ (mg/g)	2.218	5.201	3.932	7.770
	R^2	0.762	0.485	0.918	0.376
Pseudo-second-order	k_2 ($\text{g}/(\text{mg} \cdot \text{min})$)	0.0061	0.0083	0.0201	0.0867
	$q_e(\text{calc})$ (mg/g)	2.952	4.301	0.424	0.649
	R^2	0.999	0.999	0.990	0.999
Intra-particle diffusion	k_{id} ($\text{mg}/(\text{g} \cdot \text{min})$)	0.029	0.038	0.004	0.002
	R^2	0.878	0.688	0.977	0.483
Elovich	α ($\text{mg}/(\text{g} \cdot \text{min})$)	38.993	66.304	233.105	8.996×10^{10}
	β (g/mg)	0.288	0.4	0.038	0.022
	R^2	0.988	0.923	0.849	0.468

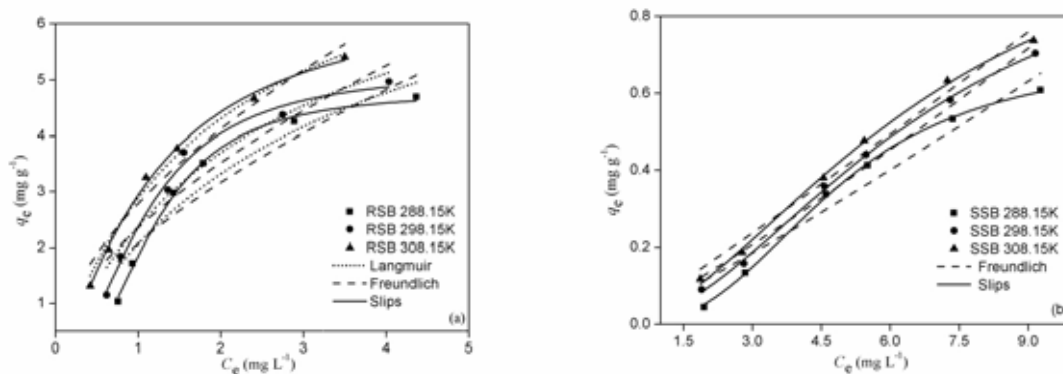


FIGURE 4
Adsorption isotherms of CAP on RSB and SSB

The parameters of adsorption kinetics are summarized in Table 3. The values of the rate correlation coefficients (R^2) for the pseudo-first-order, intra-particle diffusion and Elovich were low, showed that the adsorption of CAP deviated considerably from these three models. The R^2 for the pseudo-second-order model was >0.99 which demonstrated the fittest curves and all predicted points were marginally scattered from the actual experimental values. Additionally, the theoretical equilibrium adsorption capacities ($q_e(\text{calc})$) were in good agreement with the experimental equilibrium adsorption capacities ($q_e(\text{exp})$), which calculated by the pseudo-second-order kinetic model. Therefore the adsorption of CAP by RSB and SSB followed the pseudo-second-order kinetic model appropriately.

Some other studies also have proved that the pseudo-second-order kinetic model could described the antibiotic adsorption accurately, such as Din et al. [21] showed that the adsorption of CAP on ordered mesoporous carbon followed the pseudo-second-order kinetic model. This model assumes that the rate-limiting step is chemical adsorption or

chemisorptions through exchanging or sharing electrons between adsorbent and adsorbate [22, 23].

Adsorption isotherms reflect the interaction between adsorbates and adsorbents and the capacity of the adsorbents. The most widely used model is the Langmuir adsorption model [24], Freundlich model [25] and Sips model [26]. The adsorption isotherms expressions are represented by Eq. (7), Eq. (8) and Eq. (9):

$$q_e = K_1 q_m C_e / (1 + K_1 C_e) \quad (7)$$

$$q_e = K_f C_e^{1/n} \quad (8)$$

$$q_e = \frac{q_m K_s C_e^{1/n}}{1 + K_s C_e^{1/n}} \quad (9)$$

where q_m (mg/g) is the maximum adsorption amount; q_e (mg/g) is the adsorption amount of CAP onto RSB and SSB at equilibrium; C_e (mg/L) is the equilibrium aqueous CAP concentration; K_1 (L/mg) is the Langmuir bonding term related to interaction energies; K_f ($\text{mg}^{1-1/n} \text{L}^{1/n} / \text{g}$) represents the Freundlich

affinity coefficient; K_s (L/mg) is the Sips isotherm constant; n is model constants for corresponding models.

The simulated results for the adsorption of CAP onto RSB and SSB are shown in Figure 4, and calculate models parameters are listed in Table 4. The Sips model produced better fit for the nonlinear adsorption of CAP onto RSB and SSB at different temperature. It can be found that the Sips isotherm had higher correlation coefficient (RSB: $R^2 > 0.980$ and SSB: $R^2 > 0.990$) than the Langmuir and Freundlich isotherms. The q_m for RSB at 288.15, 298.15, 308.15K were 4.792, 5.209 and 6.586 mg/g respectively, which were higher than that for SSB (0.697, 1.055 and 1.171 mg/g). Therefore, the adsorption of CAP onto two type biochars can be well described by the Sips isotherm model. The Sips model is a combination of the Langmuir and Freundlich models and incorporates the advantages of both two models. It can be applied either to homogeneous or heterogeneous surface. The exponent $1/n$ values for CAP onto RSB and SSB were all bigger than unity, which mean that the adsorption of CAP onto RSB and SSB may more occur on heterogeneous adsorbent surface.

The adsorption thermodynamic parameters such as change in Gibbs free energy (ΔG), enthalpy (ΔH) and entropy (ΔS) were calculated by the following Eq. (10) and Eq. (11) [27].

$$\Delta G = -RT \ln K \quad (10)$$

$$\Delta G = \Delta H - T\Delta S \quad (11)$$

where R (8.314 J/(mol·K)) is the universal gas constant; T (K) is the absolute temperature; K (L/mg) is the adsorption coefficient which is defined by the ratio between equilibrium solid-phase concentrations and aqueous-phase concentrations (q_e/C_e). The ΔH and ΔS can be determined from the slope and intercept of the linear plot of ΔG versus T .

Table 5 shows the parameters of thermodynamics the adsorption of CAP onto RSB and SSB. A decrease in the negative ΔG values suggested that CAP adsorption onto RSB isotherm dynamically spontaneous and more favorable at higher temperature. Due to the mobility of adsorbate in the solution increase with the increase of temperature so that the affinity of adsorbate on the adsorbent is higher at high temperature. On the contrary, the ΔG values for SSB are positive indicate that the adsorption is non-spontaneous, which may lead to low adsorption capacity. The values of ΔH determine the nature of adsorption: physical adsorption (2.1-20.9 KJ/mol) or chemical adsorption (20.9-418.4 KJ/mol) [28]. The values of ΔH for RSB and SSB were found to be 31.341 and 27.034 KJ/mol respectively, which illustrate that the adsorption on two biochars is chemical adsorption. The positive values of ΔH suggest that adsorption of CAP on the biochars is an endothermic process [29]. Positive values of ΔS for RSB and SSB (0.113 and 0.065 J/(mol·K)) indicate an increase of randomness that possibly originated from the growth of entropy of the solvent.

TABLE 4
Model parameters for adsorption isotherms of CAP onto RSB and SSB

isotherms models	Parameters	RSB			SSB		
		288.15K	298.15K	308.15K	288.15K	298.15K	308.15K
Langmuir	K_i (L/mg)	0.323	0.403	0.511	—	—	—
	q_m (mg/g)	8.476	8.298	8.533	—	—	—
	R^2	0.907	0.933	0.989	—	—	—
Freundlich	K_f (mg ^{1-1/n} L ^{1/n} /g)	2.083	2.359	2.792	0.054	0.06	0.074
	$1/n$	0.607	0.579	0.563	1.116	1.128	1.058
	R^2	0.841	0.878	0.953	0.932	0.978	0.98
Sips	K_s (L/mg)	0.630	0.836	0.809	0.012	0.024	0.032
	q_m (mg/g)	4.792	5.209	6.586	0.697	1.055	1.171
	$1/n$	2.582	2.063	1.347	2.809	1.987	1.810
	R^2	0.996	0.983	0.996	0.999	0.999	0.998

TABLE 5
Thermodynamic parameters for the adsorption of CAP onto RSB and SSB at different temperatures

Adsorbent	T (K)	$\ln K$ (L/mg)	ΔG (KJ/mol)	ΔH (KJ/mol)	ΔS (J/(mol·K))
RSB	288.15	0.630	-1.509	31.341	0.113
	298.15	0.968	-2.399		
	308.15	1.477	-3.784		
SSB	288.15	-3.485	8.349	27.034	0.065
	298.15	-2.988	7.407		
	308.15	-2.750	7.045		

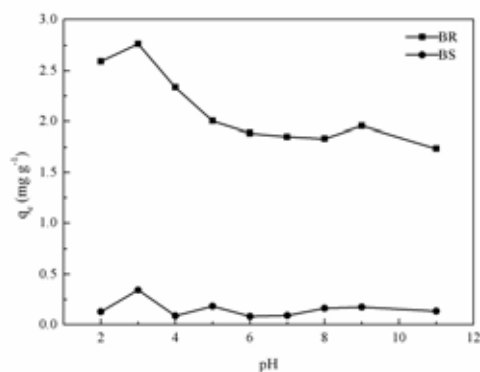


FIGURE 5
Effect of pH for the adsorption of CAP on RSB and SSB

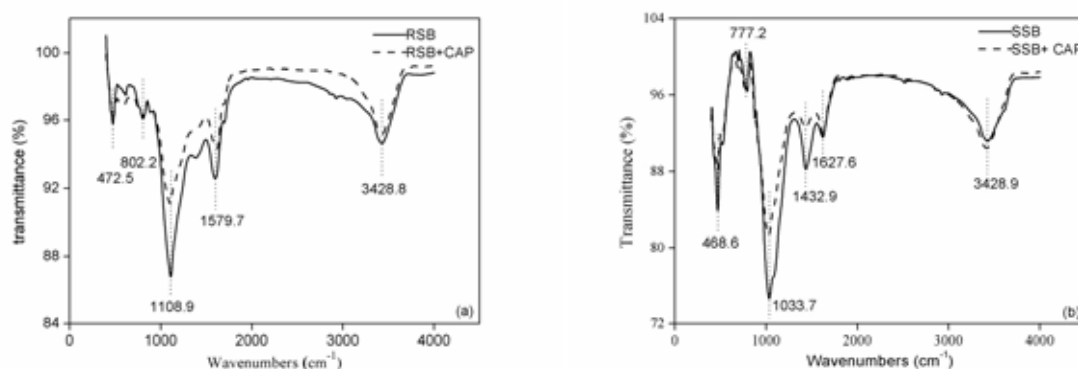


FIGURE 6
FTIR spectra of RSB and SSB before and after CAP adsorption

Effect of pH on adsorption. The pH of solution is one of the important factors for the adsorption of CAP on biochars. Figure 5 describes the dependency of CAP adsorption amount by RSB and SSB at different pH value (2.0-11.0). It can be observed the adsorption of CAP on RSB and SSB was roughly similar and strongly pH-dependent. The higher q_e appeared at acid condition. At acid condition, the hydroxyls could dissociate from CAP, the positive charge of CAP was attracted by the negative charge of biochar. Their electrostatic attraction consequently caused a higher adsorption. However, under neutral pH condition, the adsorption amount for CAP on RSB decreased obviously. The increased pH might increase ionization, solubility and hydrophilicity, which led to the reduced of H-bonding formation when biochar carboxylic groups were ionized at higher pH conditions. On the other hand, a trend of small increment of adsorption at basicity condition was attributed to enhanced π - π electron-donor-acceptor (EDA) interaction [30]. The same result was observed by Din et al., they found that the CAP adsorption was higher under low acidity and high basicity conditions [21].

Adsorption mechanisms. The mechanisms of CAP adsorption onto RSB and SSB probable included: (i) H-bonding interaction between the ionic or polar functional groups of CAP and the O-containing functional groups of biochars [31], and (ii) π - π EDA interaction between the positively charged carbon surface and the nitro group in CAP [32].

The surface chemistry of RSB and SSB are presented in Figure 6. The bands at 1579.7 cm^{-1} for RSB and 1627.6 cm^{-1} for SSB are assigned to aromatic groups and carbonyl/carboxyl C=O stretching vibration [33]. The band at 1432.9 cm^{-1} for SSB is assigned to the -COOH and -CHO [34]. The -OH stretching vibration of RSB and SSB can be observed at 3428.8 and 3428.9 cm^{-1} [16]. The functional groups such as N-H, O-H-NO₂ in the CAP could act as H acceptor interacting with the O-containing groups on the surface of biochars such as -OH, C=O and -COOH via H-bonding. However, water molecules could also interact with functional groups on two biochars by forming H-bonds, which will compete with CAP for adsorption sites and effectively decrease the adsorption of CAP [35]. Thus, the H-bonding could affect the adsorption of CAP on

BR and SSB, but it was not the primary interaction mechanism.

Besides H-bonding, π - π EDA interaction was another factor which influenced chemical adsorption. Biochars surface were rich in π electron which could act as the electron-donor, the nitro group and benzene ring of CAP were strong π -acceptor (Table 1). Therefore, the molecule structure of CAP might interact with biochars via the π - π EDA interaction. Zhu et al. [36] revealed that the adsorption intensity of the polar compounds (such as nitroaromatic compounds) were greater than that of the apolar compound possibly because of the π - π EDA interaction.

In this study, both H-bonding interaction and π - π EDA interaction were existed in adsorption processes. Whereas, the experiments of adsorption kinetics and thermodynamics illustrated that the adsorption of CAP on two biochars tended to chemical adsorption, this demonstrated that there was a chemical bond between CAP with two biochars, so π - π EDA interaction was the main mechanisms for the adsorption. A similar observation was found by Liao, who revealed that chemical bond such as π - π EDA interaction was the main mechanisms for the adsorption of tetracycline and CAP on bamboo charcoal [37]. Fan et al. [38] also reported that increase of adsorption for CAP on NaOH modified bamboo charcoal was mainly ascribed to the π - π EDA interaction.

CONCLUSIONS

The adsorption of CAP on RSB and SSB were investigated and compared. The pseudo second order kinetic model was appropriate for describing the adsorption of CAP onto RSB and SSB. The adsorption of CAP on SSB was very slight, meanwhile the adsorption on RSB was satisfactory and the maximum adsorption amount increased with the raising of temperature. It is proposed that RSB was more effective for the adsorption of CAP than SSB. The study of adsorption kinetics and thermodynamics indicated that the adsorption of CAP on two biochars squinted towards chemical adsorption. The adsorption isotherms both fitted the Sips model well. The H-bonding and π - π EDA interaction all contributed to the adsorption of CAP on biochars, while the π - π EDA interaction played an important role in the adsorption mechanism.

ACKNOWLEDGEMENTS

This research was supported by the National Natural Science Foundation of China (Grants 21307050), and the Fundamental Research Funds for the Central Universities (lzujbky-2016-162).

REFERENCES

- [1] Akhtar, M., Croteau, L., Dani, C., AbouElSooud, K. (1997) Development and validation of microwave-assisted extraction of fortified and incurred chloramphenicol residues in egg albumen and yolk. *Spectrosc-Int J.* 13, 33-40.
- [2] Chen, H.L., Rao, H.H., He, P.Z., Qiao, Y.X., Wang, F., Liu, H.J., Cai, M.M., Yao, J. (2014) Potential toxicity of amphenicol antibiotic: binding of chloramphenicol to human serum albumin. *Environ Sci Pollut Res.* 21, 11340-11348.
- [3] Import Alert 16-124 [Internet]. U.S. Food and Drug Administration [cited 2015 Jun 11], Available from: http://www.accessdata.fda.gov/cms_ia/importalert_27.html.
- [4] Li, N., Zhang, X.B., Wu, W., Zhao, X.H. (2014) Occurrence, seasonal variation and risk assessment of antibiotics in the reservoirs in North China. *Chemosphere.* 111, 327-335.
- [5] Zafarani, H.R., Gactha-Bandjun, N., Tsamo, C., Bahrololoom, M.E., Noubactep, C., Tashkhourian, J. (2014) Evaluating the suitability of the testing procedures for alternative adsorbing materials in wastewater treatment. *Fresen. Environ. Bull.* 23(6), 1438-1442
- [6] Shackley, S., Carter, S., Knowles, T., Middelink, E., Haefele, S., Sohi, S., Cross, A., Haszeldine, S. (2012) Sustainable gasification-biochar systems? A case-study of rice-husk gasification in Cambodia, Part I: Context, chemical properties, environmental and health and safety issues. *Energy Policy.* 42, 49-58.
- [7] Chen, C.P., Zhou, W.J., Lin, D.H. (2015) Sorption characteristics of N-nitrosodimethylamine onto biochar from aqueous solution. *Bioresource technol.* 179, 359-366.
- [8] Uchimiya, M., Klasson, K.T., Wartelle, L.H., Lima, I.M. (2011) Influence of soil properties on heavy metal sequestration by biochar amendment: 1. Copper sorption isotherms and the release of cations. *Chemosphere.* 82, 1431-1437.
- [9] Liu, P., Liu, W.J., Jiang, H., Chen, J.J., Li, W.W., Yu, H.Q. (2012) Modification of biochar derived from fast pyrolysis of biomass and its application in removal of tetracycline from aqueous solution. *Bioresource technol.* 121, 235-240.
- [10] Xun R.K., Xiao, S.C., Yuan, J.H., Zhao, A.Z. (2011) Adsorption of methyl violet from aqueous solutions by the biochars derived from crop residues. *Bioresource technol.* 102, 10293-10298.
- [11] Yang, X.B., Ying, G.G., Peng, P.A. (2010) Influence of biochars on plant uptake and

- dissipation of two pesticides in an agricultural soil. *J Agr Food Chem.* 58, 7915-7921.
- [12] Brix, H., Sorrell, B.K., Lorenzen, B. (2001) Are Phragmites-dominated wetlands a net source or net sink of greenhouse gases? *AquatBot.* 69, 313-324.
- [13] Melero, J.A., Sanchez-Vazquez, R., Vasilliadou, I.A., Castillejo, M., Bautista, L.F., Iglesias, J., Morales, G., Molina, R. (2015) Municipal sewage sludge to biodiesel by simultaneous extraction and conversion of lipids. *Energy Conversion Manage*l. 03, 111-118.
- [14] Li, T.Q., Han, X., Liang, C.F., Shohag, M.J., Yang, X. (2015) Sorption of sulphamethoxazole by the biochars derived from rice straw and alligator flag. *Environ Technol.* 36, 245-253.
- [15] Ahmad, M., Rajapaksha, A.U., Lim, J.E., Zhang, M., Bolan, N., Mohan, D., Vithanage, M., Lee, S.S., Ok, Y.S. (2014) Biochar as a sorbent for contaminant management in soil and water: a review. *Chemosphere.* 99, 19-33.
- [16] Kong J.J., Yue, Q.Y., Sun, S.L., Gao, B.Y., Kan, Y.J., Li, Q., Wang, Y. (2014) Adsorption of Pb(II) from aqueous solution using keratin waste – hide waste: Equilibrium, kinetic and thermodynamic modeling studies. *Chem Eng J.* 241:393-400.
- [17] Kamari, A., Yusoff, S.N.M., Abdullah, F., Putra, W.P. (2014) Biosorptive removal of Cu(II), Ni(II) and Pb(II) ions from aqueous solutions using coconut dregs residue: Adsorption and characterisation studies. *J Environ Chem Eng.* 2, 1912-1919.
- [18] Ho, Y.S., McKay, G. (2003) The kinetics of sorption of divalent metal ions onto sphagnum moss peat. *Water Res.* 34, 735-742.
- [19] Weber, W.J., Morris, J.C. (2015) Kinetics of Adsorption on Carbon from Solution American Society of Civil. *J Sanit Eng Div Asec.* 89, 53-55.
- [20] Ghasemi, M., Naushad, M., Ghasemi, N., Khosravi, F.Y. (2014) Adsorption of Pb(II) from aqueous solution using new adsorbents prepared from agricultural waste: Adsorption isotherm and kinetic studies. *J Ind Eng Chem.* 20, 2193-2199.
- [21] Din, A.T.M., Ahmad, M.A., Hameed, B.H. (2015) Ordered mesoporous carbons originated from non-edible polyethylene glycol 400 (PEG-400) for chloramphenicol antibiotic recovery from liquid phase. *Chem Eng J.* 260, 730-739.
- [22] Oliveira, E.A., Montanher, S.F., Andrade, A.D., Nobrega, J.A., Rollemberg, M.C. (2005) Equilibrium studies for the sorption of chromium and nickel from aqueous solutions using raw rice bran Process. *Biochemistry.* 40, 3485-3490.
- [23] Zhu, Y.N., Wang, D.Q., Zhang, X.H., Qin, H.D. (2009) Adsorption removal of methylene blue from aqueous solution by using bamboo charcoal. *Fresen. Environ. Bull.* 18(3), 380-387.
- [24] Dobaradaran, S., Kakuee, M., Nabipour, I., Pazira, A., Zazouli, M.A., Keshtkar, M., Khorsand, M. (2015) Fluorid removal from aqueous solutions using moringa oleifera seed ash as an environment friendly and cheap biosorbent. *Fresen. Environ. Bull.* 24(4), 1269-274.
- [25] Chen, C.P., Zhou, W.J., Yang, Q., Zhu, L.F., Zhu, L.Z. (2014) Sorption characteristics of nitrosodiphenylamine (NDPhA) and diphenylamine (DPhA) onto organo-bentonite from aqueous solution. *Chem Eng J.* 240, 487-493.
- [26] Zhou, Q., Deng, S.B., Yu, Q., Zhang, Q.Y., Yu, G., Huang, J., He, H.P. (2010) Sorption of perfluorooctane sulfonate on organo-montmorillonites. *Chemosphere.* 78, 688-694.
- [27] Fei, L., Sun, B.B., Song, Z.G., Zhu, L.Y., Qi, X.H., Xing, B.S. (2014) Physicochemical properties of herb-residue biochar and its sorption to ionizable antibiotic sulfamethoxazole. *Chem Eng J.* 248, 128-134.
- [28] Sag, Y., Kutsal, T. (2000) Determination of the biosorption heats of heavy metal ions on *Zoogloea ramigera* and *Rhizopus arrhizus*. *Biochem Eng J.* 6, 145-151.
- [29] Huang, W., Weber, W.J. (1997) Thermodynamic Considerations in the Sorption of Organic Contaminants by Soils and Sediments. 1. The Isothermic Heat Approach and Its Application to Model Inorganic Sorbents. *Environ Sci Technol.* 31, 3238-3243.
- [30] Pan, B., Xing B.S. (2008) Adsorption Mechanisms of Organic Chemicals on Carbon Nanotubes. *Environ Sci Technol.* 42:9005-9013.
- [31] Hickey, J.P., Passino-Reader DR. (1991) Linear solvation energy relationships: Rules of thumb' for estimation of variable values. *Environ Sci Technol.* 25(10),1753-1760.
- [32] Chen, W., Duan, L., Wang, L.L., Zhu, D.Q. (2008) Adsorption of hydroxyl- and amino-substituted aromatics to carbon nanotubes. *Environ Sci Technol.* 42, 6862-6868.
- [33] Chen, B.L., Chen, Z.M., Lv, S.F. (2001) A novel magnetic biochar efficiently sorbs organic pollutants and phosphate. *Bioresource technol.* 102, 716-723.
- [34] Chun, Y., Sheng, G.Y., Chiou, C.T., Xing, B.S. (2004) Compositions and Sorptive Properties of Crop Residue-Derived Chars. *Environ Sci Technol.* 38, 4649-4655.
- [35] Lin, D.H., Xing, B.S. (2008) Adsorption of Phenolic Compounds by Carbon Nanotubes: Role of Aromaticity and Substitution of Hydroxyl Groups. *Environ Sci Technol.* 42, 7254-7259.
- [36] Zhu, D., Kwon, S., Pignatello, J.J. (2005)

Adsorption of Single-Ring Organic Compounds to Wood Charcoals Prepared under Different Thermochemical Conditions. *Environ Sci Technol.* 39, 3990-3998.

- [37] Liao, P., Zhan, Z.Y., Dai, J., Wu, X.H., Zhang, W.B., Wang, W.B., Wang, K., Yuan, S.H. (2013) Adsorption of tetracycline and chloramphenicol in aqueous solutions by bamboo charcoal: A batch and fixed-bed column study. *Chem Eng J.* 228, 496-505.
- [38] Fan, Y., Wang, B., Yuan, S.H., Wu, X.H., Chen, J., Wang, L.L. (2010) Adsorptive removal of chloramphenicol from wastewater by NaOH modified bamboo charcoal. *Bioresour technol.* 101, 7661-7664.

Received: 14.09.2016

Accepted: 25.05.2017

CORRESPONDING AUTHOR

Xiaoyun Xie

College of Earth and Environmental Sciences
Lanzhou University
Key Laboratory for Environment Pollution
Prediction and Control,
Gansu Province, Lanzhou 730000 – P.R. CHINA

E-mail : xiexiaoyun@lzu.edu.cn

MOLECULAR APPROACHES TO EVALUATE ACTINOMYCETE DIVERSITY IN THE CRUDE OIL-CONTAMINATED SOIL

Haijun Liu^{1,*}, Zhenzhen Wan¹, Chun Hu¹, Baohua Zhou¹, Kanaji Masakorala², Jun Yao³

¹School of Resources and Environment, Anqing Normal University, 1318 Jixian North Road, Anqing 246133, P.R. China

²Department of Botany, Faculty of Science, University of Ruhuna, Sri Lanka

³School of Water Resource and Environmental Engineering, Sino-Hungarian Joint Laboratory of Environmental Science and Health, China University of Geosciences (Beijing), 100083, P.R. China

ABSTRACT

This research was conducted to investigate effects of crude oil contamination stress on soil chemical properties and actinomycete diversity based on molecular approaches. In this study, there was a higher contamination level of petroleum hydrocarbon of 26.6 mg g⁻¹ in the soil. And its total abundance of actinomycete had a lower order of magnitude than in the pristine soil on the basis of both the conventional cultivation and real-time quantitative PCR analysis. Furthermore, the actinomycete structure showed a significant difference in the two soils. Constructing 16S rRNA gene clone library analysis, it found that diversity indices of OTUs and Shannon index were significantly less than in the pristine soil, and there were eight genera of actinomycete identified in oil-contaminated soil, which were *Streptomyces* (31.9%), *Mycobacterium* (20.9%), *Nocardioidea* (19.8%), *Microbacterium* (9.9%), *Leifsonia* (2.2%), *Blastococcus* (2.2%), *Georgenia* (2.2%), *Marmoricola* (2.2%) and some other unidentified genera (8.8%), respectively. Moreover, it is interesting that genera of *Mycobacterium*, *Nocardioidea* and *Microbacterium* with a potential for hydrocarbon degradation have higher abundance in the oil-contaminated soil. Those findings suggested oil contamination seriously influences soil ecosystem, while give an insight into actinomycete structure and provide effective information for bioremediation of hydrocarbon contaminations.

KEYWORDS:

oil contamination, actinomycete, community diversity, clone library analysis

INTRODUCTION

Crude oil as a non renewable energy source plays an important role in the modern industrial development. It mainly consists of saturated and aromatic hydrocarbons, resins and asphaltenes, which are considered as serious contaminants for natural ecosystem [1]. Oil contamination occurs frequently

during all processes of crude oil recovery, transportation, refining and storage, and it has turned out to be a global environmental issue, such as in China [2], Brazil [3], Russia [4] and the United States [5]. Oil contaminants usually have the capability of migrating among soil, water and gas, thus pose a serious threat to the ecosystem and to human beings. Soil contamination by crude oil is negatively influence on structure and physic chemical properties of soil [6]. Previous studies have shown that oil contamination not only restricts oxygen and water movements in the pores of soil, but also disturbs nutrient cycling of nitrogen, phosphorus and potassium [7, 8]. Meanwhile, oil contamination also shows an obvious toxicity to organisms in soil. Studies have revealed that the clear decreasing trends of abundance of bacteria, archaea and fungi in soil and their functional genes such as *pgl*, *rbcL* and *nifH*, along the increasing contaminated gradient based on the GeoChip analysis [7].

Microbial communities are given more attention in the soil remediation of crude oil contaminated environmental matrices due to their potential to inhabit adverse habitats and degrading hydrocarbon contaminants [9]. When soil ecosystem is contaminated by crude oil, the microbial communities are quickly responded. Due to the natural selecting pressure of oil contaminants, it is interesting that parts of hydrocarbon-degrading microorganisms could dominate in the overall microbial community. Especially to various specific bacterial communities, there are tremendous systematical studies of their characterizations and hydrocarbon-degrading mechanisms. For example, genus *Acinetobacter* [10], genus *Pseudomonas* [11], and genus *Dietzia* [12] are capable of utilizing petroleum hydrocarbons as the sole carbon sources. And certain alkane hydroxylase genes are also cloned and detected from those bacteria such as *alk B*, *CYP153* and *alk M* [12, 13]. Further, responses of bacterial communities in oil-impacted environments have been investigated widely using DGGE fingerprinting, terminal restriction fragment length polymorphism analysis (T-RFLP), construction of 16S rRNA clone library and microarray analysis [14, 15, 16].

However, due to the complicated composition

of crude oil and severe limitations of single populations, synergistic effect among different kinds of microorganism should be an effective strategy for hydrocarbon degradation in oil contaminated habitats. As one of the important member of the soil microflora, actinomycete is a special subdivision of gram-positive bacteria based on the high guanine and cytosine in their DNA structures [17]. Furthermore, these taxa belong to chemoorgano-trophic microorganisms and are capable of degrading a wide range of substances such as paraffin, chitin and cellulose, thus play a significant role in the energy flow and nutrient cycling [18, 19]. At present, there are very few systematic researches focused on the whole actinomycete community in crude oil contaminated soil. Therefore the present work was carried out with the methods of actinomycete abundance analysis by real-time quantitative PCR, and actinomycete diversity analysis by constructing the 16S rRNA gene clone library with the aim to better understand the specific actinomycete community properties and their responses to crude oil contamination in soil.

MATERIALS AND METHODS

Soil samples were collected from the surface (10 cm depth) at Dagang oilfield, China, and they were transported to our laboratory immediately for storing at 4 °C. The contaminated soil was sampled beside the oil production well, while the negative control was chosen far from those production wells. Soil samples were divided into duplicate for chemical and biological analysis. The total petroleum hydrocarbon (TPH) was measured with the gravimetric method. And soil pH, water content, total nitrogen (TN), phosphorus, and organic matter (OM) were measured with the related soil testing procedures, respectively [20]. The abundance of culturable actinomycetes in soils was estimated using the spread plate method of Gause's synthetic agar medium containing 20.0 g of soluble starch, 1.0 g of KNO₃, 0.5g of K₂HPO₄, 0.5g of MgSO₄·7H₂O, 0.5g of NaCl, 0.01g of FeSO₄·7H₂O and 20.0 g of agar per liter, with the pH adjusted to 7.4-7.6 and sterilized under 121 °C for 30 min.

Total DNA of soil samples were extracted with the PowerSoil™ DNA Isolation Kit (MoBio, USA) and checked by running a 1% agarose gel electrophoresis for actinomycete diversity analysis. The abundance of soil actinomycete community was quantified using real-time quantitative PCR analysis (Fast 7500 instrument, USA) with 243F primer (5'-GGATGAGCCCGCGGCTA-3') and 513R primer (5'-CGGCCGCGGCTGCTGGCACGTA-3') [18]. PCR mixture of 20 µl contained 10 µl of SYBR mixture, 1.0 µl of template DNA, 0.1 µl of each primer and 8.8 µl of sterile deionized water. The amplification protocol was as follows: initial denaturation for

20 s at 95 °C followed by 60 cycles (30 s at 95 °C, annealing for 30 s at 60 °C, and extension for 1 min at 72 °C). Each reaction for real-time PCR was performed in triplicate. Standard curves for calculating the abundance of actinomycete were established as the previous method [21].

Amplification was carried out with initial denaturation for 5 min at 95 °C, 35 cycles of 30 s at 94 °C, 1 min at 53 °C, and 2 min at 72 °C, and final extension for 10 min at 72 °C. The reaction was conducted in a total volume of 25 µl. The amplified fragments were purified using the AxyPrep PCR purification kit (Axygen, USA), and cloned to the pMD®18-T vector using the PCR cloning kit (TaKaRa, Japan). Clones harboring recombinant plasmids grew overnight on the solid LB medium (LB contains 10 g of NaCl, 10 g of tryptone, 5 g of yeast extract, 1.8 g of agar, and pH 7.0) with ampicillin (100 µg/ml) at 37 °C. One hundred clones were chosen and verified using PCR amplification. Thus culturable positive clones in liquid LB medium with ampicillin were sequenced and constructed the 16S rRNA clone libraries of actinomycete in soils.

Sequences of actinomycete were edited using the software Oligo Version 7.37 and alignment was generated with the method of ClustalW multiple alignment by the software MEGA 5.05. Then 16S rRNA sequences were searched against the NCBI database (<http://blast.ncbi.nlm.nih.gov/Blast.cgi>) for establishing 16S rRNA clone libraries. Softwares Mothur v.1.33.0 and Estimates 8.2.0 were applied to calculate operational taxonomic units (OTUs), the Shannon-Wiener index and Evenness index for each clone library of actinomycete.

RESULTS AND DISCUSSION

The biogeochemical parameters were measured to show the real inhabiting condition of the actinomycete community in the oil contaminated soils as summarized in table 1. It found that the total petroleum hydrocarbon was up to 26.6 mg g⁻¹ nearby the selected oil production well. Furthermore, the organic matter of oil contaminated soil reached to 57.2 mg g⁻¹ due to the crude oil contamination, and it apparently indicated a higher increase compared with the negative control. Other geochemical values such as total nitrogen, phosphorus, potassium, pH and water content also varied considerably between the investigated two samples. These objective changes of all those geochemical values suggested that oil contamination enable to influence the soil ecosystem, not only change the physico-chemical properties, but also might bring serious toxicity to their organisms. Previous reports revealed a decrease in earthworm survival and seed germination, and also in the microbial activity at

TABLE 1
Biogeochemical parameters of soil samples from Dagang oilfield

	TPH mg g ⁻¹	OM mg g ⁻¹	pH	Water %	TN mg kg ⁻¹	P mg kg ⁻¹	K mg kg ⁻¹	Actinomycete ^a cfu/g	Actinomycete ^b copies/g
Control	0.0±0.0	3.5±0.2	7.7±0.2	18.2±0.6	440.6±16.7	25.6±2.8	54.4±3.1	(2.1±0.4)×10 ⁴	(2.0±0.1)×10 ⁷
Contaminated	26.6±1.3	57.2±2.5	7.3±0.3	10.3±0.4	590.3±19.6	14.3±1.6	65.6±2.5	(1.6±0.3)×10 ³	(1.1±0.1)×10 ⁶

OM—organic matter; TN—total nitrogen; P—phosphorus; K—potassium;

^a—abundance of culturable actinomycete measured by the conventional cultivation method;

^b—abundance of unculturable actinomycete measured by real-time quantitative PCR analysis.

more than 10 mg g⁻¹ of the petroleum hydrocarbon. In this study, the abundance of actinomycete communities was numbered with the conventional cultivation method and the real-time quantitative PCR analysis for investigating the possible eco-toxicity of petroleum hydrocarbons. They were about 1.6 × 10³ cfu g⁻¹ and 1.1 × 10⁶ copies g⁻¹ measured in oil-contaminated soil, respectively, which emerged a lower order of magnitude than the fresh soil sample. Those results suggested that actinomycete could survive, although there was a serious high hydrocarbon contamination level. However, petroleum contamination was able to decrease the abundance of actinomycete in soil compared with the two samples. On the basis of the two methods, it is better to show the accurate condition by the real-time quantitative PCR on the molecular level, which could exhibit those uncultivable parts of actinomycete communities in soil. As a sensitive and active molecular technique, real-time quantitative PCR could offer qualitative information of actinomycete in the complicated ecological environment.

Actinomycete communities play an important role in the material cycling and energy transformation. Evaluation of actinomycete's response to extrinsic contaminants will better understand the environmental behaviors of those contaminants and possess an effective control tactics. Using the terminal restriction fragment length polymorphism (T-RRLP), Liu et al. revealed there was an obvious increase in the actinomycete community diversity by planting *Paulownia fortunei* in heavy metal-contaminated soils [19]. Meanwhile, they were capable of enhancing the retention of heavy metals such as Pb, Zn, Cu and in soils. Polti et al. also investigated chromium (VI) resistance using isolated actinomycetes from the waste water of a copper filter plant and found that most of them were genera *Streptomyces* with the highest Cr(VI) specific removal value up to 75.5 mg g⁻¹ cell [22]. Other similar results could also show a great potential of actinomycete communities to remediate the heavy metal contaminated environments [23, 24]. However, it is clear that the previous studies have mainly focused on the abundance variation, especially based on the conventional cultivation method, or on some special functional microorganisms. Therefore there is a scarcity of relevant information in the existing literature on systematic investigation of microbial community structures in the complicated soil ecosystems. Thus to better under-

stand the populations community structure of the actinomycete community in different types of environments, some molecular approaches such as real-time quantitative PCR, T-RRLP and denaturing gradient gel electrophoresis (DGGE) were extensively applied. Those molecular approaches were more fast and effective than the conventional cultivation ones, and able to investigate unculturable parts of actinomycete communities. On the basis of DGGE analysis, presence of five genera of actinomycetes containing *Geodermatophilus*, *Actinokineospora*, *Actinoplanes*, *Streptomyces* and *Kocuria* have been recorded in soil and roots of four rice cultivars [25]. Therefore it gives a clear picture of the actinomycete community structure. Further, those molecular approaches could provide insight into information of actinomycete communities in a variety of subjects investigated.

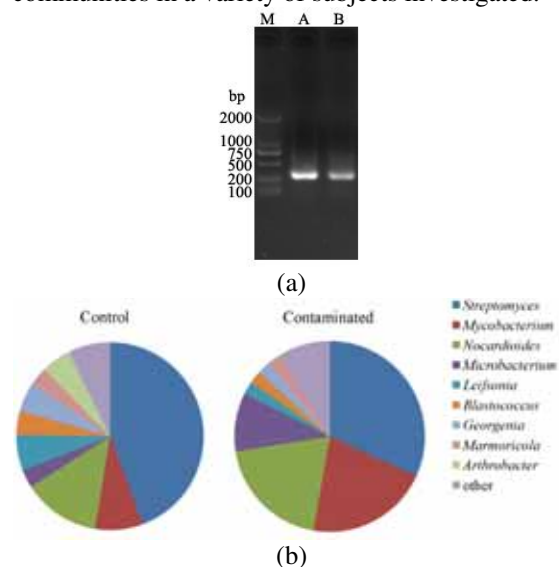


FIGURE 1

Constructing 16S rRNA gene clone libraries of actinomycete in the pristine and crude oil-contaminated soils: (a) 16S rRNA gene amplification of actinomycete using the total extracted DNA from soils (M: D2000 Ladder; A: pristine soil as control; B: crude oil-contaminated soil); (b) Relative abundance of actinomycete on the genus level based on constructing 16S rRNA gene clone libraries, and the positive clone numbers were 97 and 91 in clone libraries of the pristine and crude oil-contaminated soils, respectively.

Many studies have shown that all sorts of contaminants might disturb metabolic activities of actinomycetes, especially such as heavy metals. Nevertheless, the impact on them from crude oil contaminants still remains a leakage. Actinomycetes are very important organisms in hydrocarbon contaminated environments as they are capable of producing all kinds of metabolite compounds, and enhancing the biogeochemical cycle. For instance, they are able to solubilize phosphate and fix nitrogen [26]. And at the same time, actinomycetes as genus *Mycobacteria*[27] and genus *Gordonia*[28] have a potential for degradation of alkane and aromatic hydrocarbon. Hence, they are vitally important in the remediation of hydrocarbon-contaminated environments. However, high contamination levels of hydrocarbon have demonstrated the negative influence on ecosystems. As Liang et al. reported an apparent decrease in actinomycete abundance with a high oil contamination level from the angle of microbial functional genes using the microarray-based analysis [14]. Thus systematic study on the behaviors of actinomycetes in hydrocarbons contaminated soil ecosystems will be highly propose an effective remedying tactics for petroleum contamination.

TABLE 2
Co-existing order, family, OTUs and its relative abundance of the clone libraries of actinomycete in the pristine and crude oil contaminated soils

Co-existing Order	Co-existing Family	Relative abundance		Co-existing OTUs
		Pristine (OTUs)	Contaminated (OTUs)	
Streptomiv-	Streptomyceta- ceae			
	<i>Streptomyces</i>	22.6%(7)	18.2% (4)	3
Coryne-	Mycobacteri-			
	<i>Mycobacterium</i>	12.9% 4)	13.6% (3)	3
Propionibacte-	Nocardioideaceae			
	<i>Nocardioideae</i>	25.8% 8)	27.3% (6)	5
Geodermat	Geodermatophi- laceae			
	<i>Blastococcus</i>	3.2% (1)	4.5% (1)	1
Micrococcales	Microbacteri- aceae			
	<i>Georgenia</i>	6.5% (2)	4.5% (1)	1
	<i>Mycobacterium</i>	3.2% (1)	4.5% (1)	1
	<i>Leifsonia</i>	3.2% (1)	4.5% (1)	1
	<i>Arthrobacter</i>	3.2% (1)	0	0
Unidentified	unidentified	19.4%(6)	22.7% (5)	

In this study, the 16S rRNA gene PCR product of actinomycetes in pristine and oil-contaminated soils was amplified with conserved primers of 243F and 513R. This primer successfully generated a product size of about 270 bp as shown in Fig. 1(a). The targeted products were cut from the agarose gel and purified, and then carried out to construct 16S rRNA gene clone libraries of actinomycete as exhibited in Fig. 1(b). The results revealed that most actinomycete communities of the pristine and oil contaminated soils were co-existing in both clone libraries at the hydrocarbon level of 26.6 mg g⁻¹, which

seem to indicate that most actinomycetes have a potential of hydrocarbon resistance to a certain degree. However, it was interesting that the ratio of operational taxonomic units still emerged an apparent diversity in both clone libraries suggesting they suffer from hydrocarbon toxicity, as shown in table 2. In addition, all the identified microorganisms of the two clone libraries belonged to the phylum of actinobacteria using the conserved primers. The co-existing orders were Streptomycetales, Corynebacteriales, Propionibacteriales, Geodermatophilales and Micrococcales, while the co-existing families were Streptomycetaceae, Mycobacteriaceae, Nocardioideaceae, Geodermatophilaceae and Microbacteriaceae, respectively. Although there were the same co-existing orders and families in the two subjects investigated of the pristine and oil-contaminated soils, actinomycete communities in both appeared divergent partially based on the common OTUs analysis. The non-homogeneity of co-existing OTUs in the clone libraries indicated that hydrocarbon contamination could influence the actinomycete diversity. Especially, there was no trace of genus *Arthrobacter* in oil-contaminated soil.

As drawn in Fig. 1(b), the findings revealed that the identified genera had a basic similarity including of *Streptomyces*, *Mycobacterium*, *Nocardioideae*, *Mycobacterium*, *Leifsonia*, *Blastococcus*, *Georgenia* and *Marmoricola* in the two studied soil samples. In both clone libraries, it was found that genus *Streptomyces* has the highest proportion in soils, and they were 44.3% and 31.9% in pristine and oil contaminated soils, respectively. This result has a sealed accordance with a fact that actinomycetales contains more than eighty genera identified, and dominant genus *Streptomyces* has a widespread distribution. Genus *Streptomyces* is part of the family *Streptomycetaceae*, and it has been thoroughly explored in detail for its bioactive metabolites. Meanwhile, it is interesting that numbers of genus *Streptomyces* have the potential of degrading hydrocarbons such as alkane, nitroalkane, polyester and naphthalene [29]. But at the same time, genus *Streptomyces* emerged an apparent inhibition from oil contamination comparing oil-contaminated and pristine soils, indicating that crude oil contamination will cause the physiological toxicity to this specific microorganism to a certain extent. Furthermore, it found that the relative abundance of genus *Mycobacterium* increased significantly in the oil-contaminated soil, and which has reported with a great potential of hydrocarbon degradation such as pyrene and benzo[a] pyrene [7, 30]. Genus *Mycobacterium* is from the family *Mycobacteriaceae*, and they are usually aerobic and non-motile bacteria. The relative abundance of this population was 8.2% in pristine and 20.9% in oil-contaminated soils, indicating the potential of this genus to survive in the extreme condition with a higher crude oil concentration. Previous studies reported that

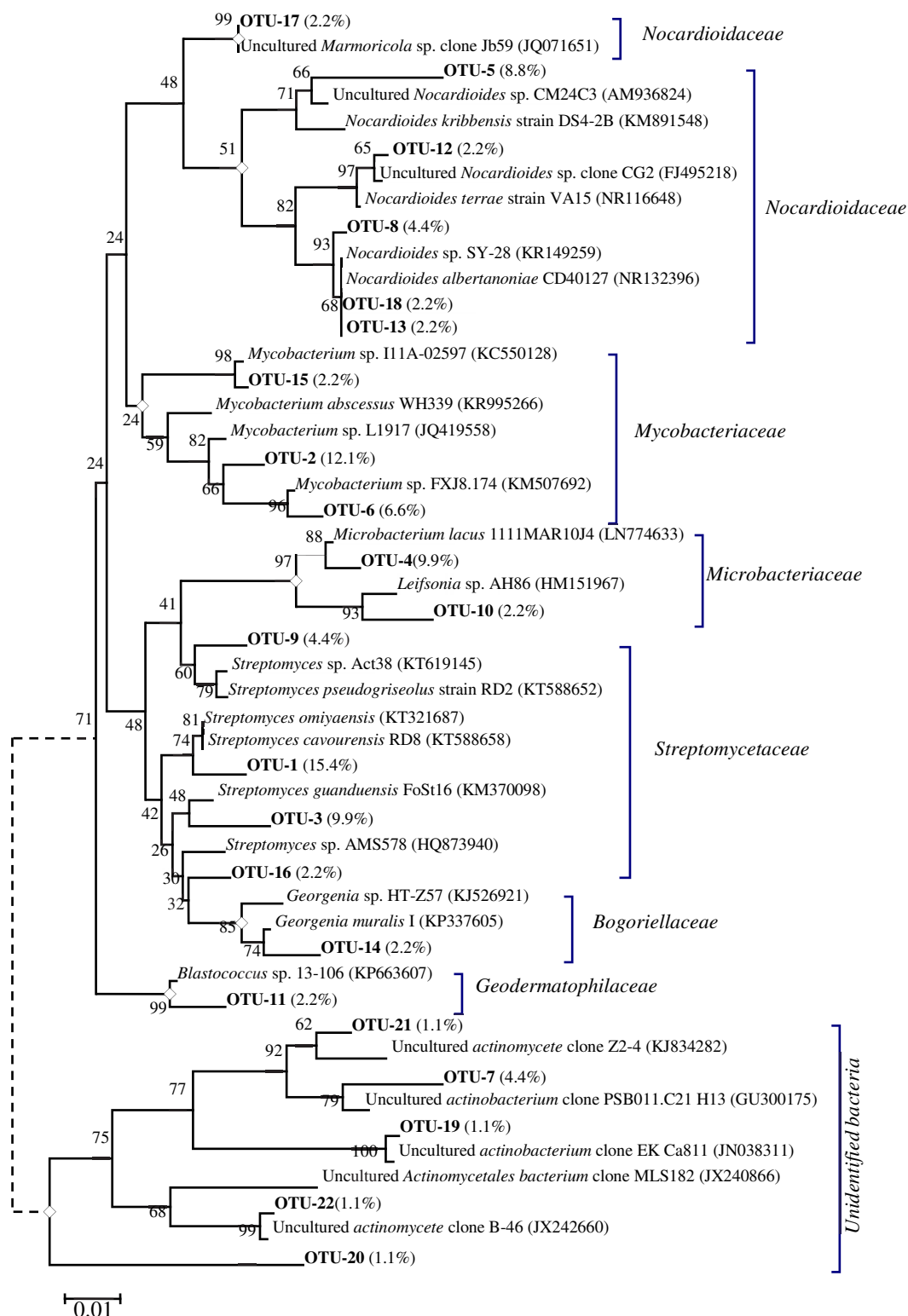


FIGURE 2

Phylogenetic analysis using the Neighbor-Joining method with software Mega 5.05 based on partial 16S rRNA gene of actinomycete in the crude oil-contaminated soil. And there are 1000 replicate runs for the bootstrap values. The relative percentage of each OTUs was calculated here.

gene *pdo A2* encoded a subunit of a PAH ring-hydroxylating dioxygenase [31] and genes *nidA* and *nidB* for subunits of a pyrene dioxygenase [32] were

discovered from genus *Mycobacterium*, which constructed a basic foundation for their survival in oil-contaminated environments. As an important population in soil ecosystems, genus *Nocardioide*s also

showed a higher relative abundance of 19.8% in the contaminated soil, which belongs to the family *Nocardioideae* as depicted in Fig. 2. Some bacteria such as *Nocardioides* sp. KP7 and *Nocardioides* sp. DF412 have the ability to phenanthrene and dibenzofuran due to their own dioxygenases [33, 34]. Meanwhile, strain *Nocardioides* sp. JS1661 plays an important role in the mineralization of 2,4-dinitroanisole via the 2,4-dinitrophenol pathway [35]. Furthermore, genus *Microbacterium* had a widespread distribution with a higher ratio of 9.9% in the oil-contaminated soil, which is from the family *Microbacteriaceae* of the order *Micrococcales*. Chen et al. reported that strain *Microbacterium* sp. ZD-M2 has the capability of dibenzothiophene desulfurization [36]. And strain *Microbacterium* E19 enables to degrade oxyethylated fatty alcohols, which was isolated from crude oil contaminated soil [37]. Moreover, the ratio of genus *Leifsonia* from the family *Microbacteriaceae*, genus *Blastococcus* from the family *Geodermatophilaceae*, genus *Georgenia* from the family *Bogoriellaceae* and genus *Marmoricola* from the family *Nocardioideae* was all 2.2% in the oil-contaminated soil based on the 16S rRNA clone library analysis, and genus *Arthrobacter* from the family *Micrococcaceae* even was not detected. Those actinomycetes in contaminated soil all emerged a lower distribution ratio compared with the pristine soil suggesting that crude oil contamination show toxicity to actinomycetes in soil ecosystems in fact. Better investigating actinomycete community structure will help us for achieving available species resources and carrying out bioremediation of contaminated environments. However, there were some bacteria identified invalidly based on the actinomycete 16S rRNA clone library analysis in this study. In this study, the relative abundance of those unidentified bacteria was up to 7.2% and 8.8% in pristine and oil-contaminated soils, respectively.

Constructed clone libraries were evaluated using indices of operational taxonomic units (OTUs) and shannon index calculated from rarefaction curves and shannon index curves in this study. One hundred clones for each sample were selected for sequencing analysis. The number of positive clones was $N=97$ in pristine sample and $N=91$ in the oil-contaminated sample, respectively. Softwares Mothur v.1.33.0 and estimates 8.2.0 were carried out to calculate OTUs and shannon index. In the pristine sample, OTUs number and shannon index were 31 and 3.12, while they were 22 and 2.76 in the oil-contaminated sample as depicted in Fig. 3. Evenness of both actinomycetes clone libraries was also calculated based on above data, and they were 0.91 and 0.89, respectively. Diversity indices revealed that there is higher actinomycete diversity in the pristine soil suggesting crude oil contamination will disturb actinomycetes community structure in soil environments. Furthermore, the trend of both rarefaction curves nearly reached to the saturation condition

demonstrating that both two constructed 16S rRNA clone libraries could represent the major information of actinomycete community structure in soil samples summarized in Fig. 3a. However, on account of those unidentified bacteria above in both pristine and oil-contaminated soils, clone library analysis of actinomycetes using homologous conserved primers of 243F and 513R based on 16S rRNA gene still prove a slight limitation. This approach can represent the major constituents of actinomycetes, but relatively less abundant or non-homologous ones may not be visible. Thus in order to investigate or exploit actinomycetes resources in complex soils, a combined approach of biological methods should be considered carefully. For instance, Heuer et al. detected actinomycetes in environments using PCR-DGGE analysis combined with a nested PCR served as template for the PCR amplification on the basis of 16S rRNA gene [18]. And Mahyarudin et al. evaluated actinomycetes diversity in soil and roots of rice with PCR-DGGE analysis based on 16S rRNA and *nifH* genes [25].

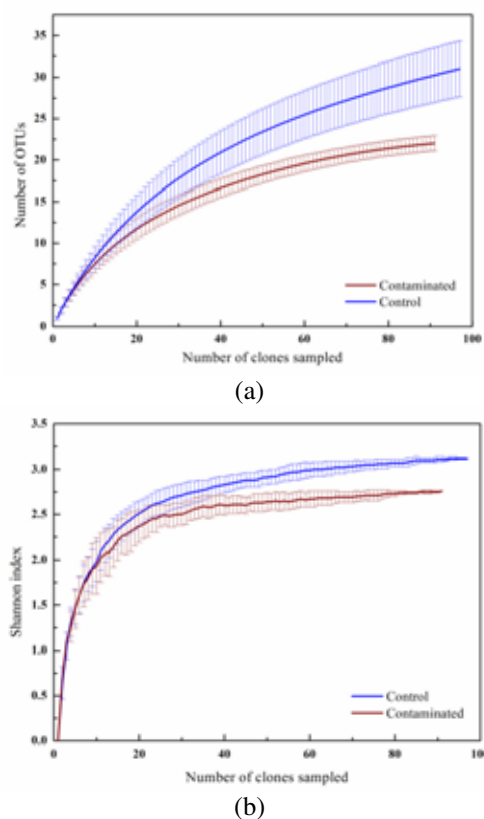


FIGURE 3

Rarefaction curves (a) and shannon index curves (b) of 16S rRNA gene positive clones for actinomycete clone libraries in pristine ($N=97$) and oil-contaminated soils ($N=91$). Number of OTUs and shannon index were calculated using Softwares Mothur v.1.33.0 and Estimates 8.2.0.

In conclusion, results of this study revealed that crude oil contamination not only changed the physico-chemical properties in soil, but also influenced

on the actinomycetes community. Molecular approaches of the real-time PCR and clone library analysis showed that crude oil contamination cause apparent physiological toxicity to the actinomycetes community in soil. And it also found that valuable species resources such as genus *Streptomyces*, genus *Mycobacterium*, genus *Nocardioide*s and genus *Mycobacterium* reported with a potential of hydrocarbon degradation survive in oil-contaminated condition. This study will give us an insight into the actinomycetes structure in oil-contaminated soil and provide valuable information for the bioremediation of hydrocarbon contaminated sites.

ACKNOWLEDGEMENTS

This work is supported in part by grants from Key project from National Science Foundation of China (41430106), National Natural Science Foundation of China (41603083, 41573080 and 41273060), Public welfare project of Chinese Ministry of Environmental Protection (201509049), Key Project Supported by the Natural Science Foundation of the Higher Education Institutions of Anhui Province (KJ2016A432). We gratefully acknowledge all the supports provided.

REFERENCES

- [1] Sugiura K, Ishihara M, Shimauchi T, Harayama S. (1997) Physicochemical properties and biodegradability of crude oil. *Environmental Science & Technology* 31, 45-51.
- [2] Liang YT, Van Nostrand JD, Deng Y, He ZL, Wu LY, Zhang X, Li GH, Zhou JZ. (2011) Functional gene diversity of soil microbial communities from five oil-contaminated fields in China. *ISME Journal* 5, 403-413.
- [3] Azevedo JS, Lopes B, Katsumiti A, Braga ES, Roche H, Ribeiro CAO, Bebianno MJ. (2012) Evidence of contamination by oil and oil Products in the Santos-Sao vicente estuary, Sao Paulo, Brazil. *Brazilian Journal of Oceanography* 60, 117-126.
- [4] Hosokawa R, Nagai M, Morikawa M, Okuyama H. (2009) Autochthonous bioaugmentation and its possible application to oil spills. *World Journal of Microbiology & Biotechnology* 25, 1519-1528.
- [5] Brody TM, Di Bianca P, Krysa J. (2012) Analysis of inland crude oil spill threats, vulnerabilities, and emergency response in the midwest United States. *Risk Analysis* 32, 1741-1749.
- [6] Wang Y, Feng J, Lin QX, Lyu XG, Wang XY, Wang GP. (2013) Effects of crude oil contamination on soil physical and chemical properties in Momoge wetland of China. *Chinese Geographical Science* 23, 708-715.
- [7] Schneider J, Grosser RK, Xue W, Warshawsky D. (1996) Degradation of pyrene, benz[a]anthracene, and benzo[a]pyrene by *Mycobacterium* sp strain rjgii-135, isolated from a former coal gasification site. *Applied & Environmental Microbiology* 62, 13-19.
- [8] Beznosikov VA, Lodygin ED. (2010) Ecological-geochemical assessment of hydrocarbons in soils of Northeastern European Russia. *Eurasian Soil Science* 43, 550-555.
- [9] Whyte LG, Smits THM, Labbe D, Witholt B, Greer CW, van Beilen JB. (2002) Gene cloning and characterization of multiple alkane hydroxylase systems in *Rhodococcus* strains Q15 and NRRL B-16531. *Applied and Environmental Microbiology* 68, 5933-5942.
- [10] Liu HJ, Yao J, Yuan ZM, Shang YF, Chen HL, Wang F, Masakorala K, Yu C, Cai MM, Blake RE, Choi MMF. (2014) Isolation and characterization of crude-oil-degrading bacteria from oil-water mixture in Dagang oilfield, China. *International Biodeterioration & Biodegradation* 87, 52-59.
- [11] Masakorala K, Yao J, Cai MM, Chandankere R, Yuan HY, Chen HL. (2013) Isolation and characterization of a novel phenanthrene (PHE) degrading strain *Pseudomonas* sp. USTB-RU from petroleum contaminated soil. *Journal of Hazardous Materials* 263, 493-500.
- [12] Wang XB, Chi CQ, Nie Y, Tang YQ, Tan Y, Wu G, Wu XL. (2011) Degradation of petroleum hydrocarbons (C6-C40) and crude oil by a novel *Dietzia* strain. *Bioresource Technology* 102, 7755-7761.
- [13] Rojo F. (2009) Degradation of alkanes by bacteria. *Environmental Microbiology* 11, 2477-2490.
- [14] Liang Y, Li G, Van Nostrand JD, He Z, Wu L, Deng Y, Zhang X, Zhou J. (2009) Microarray-based analysis of microbial functional diversity along an oil contamination gradient in oil field. *FEMS Microbiology Ecology* 70, 324-333.
- [15] Powell SM, Bowman JP, Ferguson SH, Snape I. (2010) The importance of soil characteristics to the structure of alkane-degrading bacterial communities on sub-Antarctic Macquarie Island. *Soil Biology & Biochemistry* 42, 2012-2021.
- [16] Reis I, Almeida CMR, Magalhaes CM, Cochofel J, Guedes P, Basto MCP, Bordalo AA, Mucha AP. (2014) Bioremediation potential of microorganisms from a sandy beach affected by a major oil spill. *Environmental Science and Pollution Research* 21, 3634-3645.
- [17] Monciardini P, Sosio M, Cavaletti L, Chiocchini C, Donadio S. (2002) New PCR primers for the selective amplification of 16S rDNA from different groups of actinomycetes. *FEMS Microbiology Ecology* 42, 419-429.
- [18] Heuer H, Krsek M, Baker P, Smalla K,

- Wellington EM. (1997) Analysis of actinomycete communities by specific amplification of genes encoding 16S rRNA and gel-electrophoretic separation in denaturing gradients. *Applied and Environmental Microbiology* 63, 3233-3241.
- [19] Liu W, Wang J, Zhang C. (2013) Evaluation of soil chemical properties and actinomycete community structure following a temporal sequence of revegetation through *Paulownia Fortunei* in the heavy metal-contaminated soil. *Water, Air, & Soil Pollution* 224, 1-10.
- [20] Liu HJ, Chen HL, Yao J, Yuan ZM, Wang F, Doni S, Choi MMF. (2015) Molecular detection and microcalorimetric analysis of soil microbial community along an oil contamination gradient. *Fresen. Environ. Bull.* 24, 451-459.
- [21] Song M, Shin SG, Hwang S. (2010) Methanogenic population dynamics assessed by real-time quantitative PCR in sludge granule in upflow anaerobic sludge blanket treating swine wastewater. *Bioresource Technology* 101, S23-S28.
- [22] Polti MA, Amoroso MJ, Abate CM. (2007) Chromium(VI) resistance and removal by actinomycete strains isolated from sediments. *Chemosphere* 67, 660-667.
- [23] Gremion F, Chatzinotas A, Harms H. (2003) Comparative 16S rDNA and 16S rRNA sequence analysis indicates that actinobacteria might be a dominant part of the metabolically active bacteria in heavy metal-contaminated bulk and rhizosphere soil. *Environmental Microbiology* 5, 896-907.
- [24] Kothe E, Dimkpa C, Haferburg G, Schmidt A, Schmidt A, Schütze E. (2010) Streptomycete heavy metal resistance: extracellular and intracellular mechanisms. in: soil heavy metals. Springer Berlin Heidelberg, Berlin, Heidelberg, p 225-235.
- [25] Mahyarudin, Rusmana I, Lestari Y. (2015) Metagenomic of actinomycetes based on 16S rRNA and *nifH* genes in soil and roots of four Indonesian rice cultivars using PCR-DGGE. *HAYATI Journal of Biosciences* 22, 113-121.
- [26] Gonzalez Perez P, Ye J, Wang S, Wang X, Huang D. (2014) Analysis of the occurrence and activity of diazotrophic communities in organic and conventional horticultural soils. *Applied Soil Ecology* 79, 37-48.
- [27] Cheung P-Y, Kinkle BK. (2001) *Mycobacterium* diversity and pyrene mineralization in petroleum-contaminated soils. *Applied and Environmental Microbiology* 67, 2222-2229.
- [28] Xue Y, Sun X, Zhou P, Liu R, Liang F, Ma Y. (2003) *Gordonia paraffinivorans* sp. nov., a hydrocarbon-degrading actinomycete isolated from an oil-producing well. *International Journal of Systematic and Evolutionary Microbiology* 53, 1643-1646.
- [29] Ferradji FZ, Mnif S, Badis A, Rebbani S, Fodil D, Eddouaouda K, Sayadi S. (2014) Naphthalene and crude oil degradation by biosurfactant producing *Streptomyces* spp. isolated from Mitidja plain soil (North of Algeria). *International Biodeterioration & Biodegradation* 86, 300-308.
- [30] Zeng J, Lin X, Zhang J, Li X. (2010) Isolation of polycyclic aromatic hydrocarbons (PAHs)-degrading *Mycobacterium* spp. and the degradation in soil. *Journal of Hazardous Materials* 183, 718-723.
- [31] Pagnout C, Frache G, Poupin P, Maunit B, Muller JF, Féraud JF. (2007) Isolation and characterization of a gene cluster involved in PAH degradation in *Mycobacterium* sp. strain SNP11: Expression in *Mycobacterium smegmatis* mc² 155. *Research in Microbiology* 158, 175-186.
- [32] Stingley RL, Khan AA, Cerniglia CE. (2004) Molecular characterization of a phenanthrene degradation pathway in *Mycobacterium vanbaalenii* PYR-1. *Biochemical and Biophysical Research Communications* 322, 133-146.
- [33] Saito A, Iwabuchi T, Harayama S. (1999) Characterization of genes for enzymes involved in the phenanthrene degradation in *Nocardioidea* sp. KP7. *Chemosphere* 38, 1331-1337.
- [34] Fukuda M, Sukda P, Kasai D, Masai E, Miyauchi K. (2009) Dibenzofuran degradation system in a *Nocardioidea* sp. DF412. *Journal of Bioscience and Bioengineering* 108, Supplement 1:S76.
- [35] Karthikeyan S, Spain JC. (2016) Biodegradation of 2,4-dinitroanisole (DNAN) by *Nocardioidea* sp. JS1661 in water, soil and bioreactors. *Journal of Hazardous Materials* 312, 37-44.
- [36] Chen H, Zhang W-J, Cai Y-B, Zhang Y, Li W. (2008) Elucidation of 2-hydroxybiphenyl effect on dibenzothiophene desulfurization by *Microbacterium* sp. strain ZD-M2. *Bioresource Technology* 99, 6928-6933.
- [37] Nowicka D, Ginter-Kramarczyk D, Holderna-Odachowska A, Budnik I, Kaczorek E, Lukaszewski Z. (2013) Biodegradation of oxyethylated fatty alcohols by bacteria *Microbacterium* strain E19. *Ecotoxicology and Environmental Safety* 91, 32-38.

Received: 27.05.2016
Accepted: 31.05.2017

CORRESPONDING AUTHOR

Haijun Liu, Doctor

School of Resources and Environment, Anqing Normal University, 1318 Jixian North Road, Anqing 246133, P.R. China

e-mail: liuhj@aqnu.edu.cn

PHTHALATE ESTERS MIGRATION FROM TWO KINDS OF PLASTIC FILMS AND THE ENRICHMENT IN PEANUT PLANT

Kairong Wang*, Ningning Song, Mingming Cui, Yanxi Shi

Qingdao Engineering Research Center for Rural Environment, Qingdao Agricultural University, Qingdao 266109, China

ABSTRACT

Agricultural plastic films are widely used as an important measure to promote peanut yield; however, pollution by phthalate esters (PAEs) subsequently migrating from agricultural plastic films is not well understood. The present study investigated the migration of PAEs from two kinds of agricultural plastic films (white polyethylene film and black recycled plastic film) as well as the absorption and accumulation characteristics of dibutyl phthalate (DBP) and di-(2-ethylhexyl) phthalate (DEHP) by two peanut varieties in pot experiments. The results showed:

a. DBP and DEHP concentrations in soils increased with the increase in amount of agricultural plastic films applied.

b. residual concentrations of DBP and DEHP in soils with black recycled plastic film applied were greater than with white polyethylene film treatment, and

c. regardless of the type of film applied, DBP and DEHP residual concentrations were reduced significantly with time in all treatments except for the control.

The proportion of DBP accumulated by two peanut varieties relative to the total amount DBP applied in soils was 0.01%–0.03%, and that of DEHP was 0.02%–0.04%. DBP and DEHP concentrations in peanut kernels were significantly higher than those of root, but not pods, showing that PAE absorption by roots, but not pods, was an important mechanism in determining PAE accumulation.

KEYWORDS:

phthalate esters (PAEs); plastic films; migration; accumulation; peanut

INTRODUCTION

Phthalate esters (PAEs) are widely used in the manufacture and the processing of plastics as plasticizers to improve the softness and flexibility of plastic materials [1][2]. Chemically, they linked together by hydrogen bonds and Van Der Waal forces and do not form covalent bonds with plastic substrates [3].

Hence, with time, PAEs can migrate into the soil and subsequently into other parts of the ecosystem [4][5]. PAEs are hazardous substances that can interfere with endocrine systems and procreation ability [6][7].

Previous studies showed that application of agriculture films might be a significant pollution source of phthalates in arable soils of China [8]. There is an increase in the pollution level of PAEs along with increased use of agriculture films, which can affect the quality of agricultural production [3][9][10]. Peanut (*Arachis hypogaea* L.) is one of the most important oil crops in China and has a large production area. As an important effective measure for improving production, plastic film mulching is widely used in the main peanut-producing areas in China. PAEs such as dibutyl phthalate (DBP) and di-(2-ethylhexyl) phthalate (DEHP), can migrate from agricultural plastic and be released into agricultural soils, transfer to peanut crops and thus directly or indirectly into the human food chain. However, there is little published information on the toxicity and accumulation of PAEs in peanut.

The present work evaluated the migration of PAEs from two kinds of agricultural plastic films (white polyethylene film and black recycled plastic film) as well as the absorption and accumulation characteristics of DBP and DEHP by two peanut varieties in pot-culture experiments. This study provides reliable data for risk assessment of PAE pollution in peanut crops *via* the application of agricultural plastic films, which are of great significance in agricultural production.

MATERIALS AND METHODS

Soil characterization. Soil used in this study was collected from Qingdao, Shandong Province, China. The soil was classified as sandy loam with the following properties: soil pH 7.3 (soil:water ratio, 1:2.5), 7.4 g·kg⁻¹ of organic matter, 36.6 cmol·kg⁻¹ of cation exchange capacity, 8.0 mg·kg⁻¹ of total nitrogen (N), 9.0 mg·kg⁻¹ of Olsen-phosphorus (P) and 61.4 mg·kg⁻¹ of NH₄OAc-potassium (K).

Agricultural films. Two kinds of agricultural plastic films, white polyethylene film (white film) and black recycled plastic film (black film), were

chosen to evaluate the migration of PAEs. Both films are widely used for increasing agricultural production and for the covering crops and greenhouse vegetables in winter. The thickness of white and black film was 0.01 and 0.008 mm, respectively. The white film was obtained from Shandong Laizhou Yuqiang Film Factory, and the black film from a local market in Qingdao, China. The concentrations of six kinds of PAEs in the films are shown in Table 1.

TABLE 1
Concentration of six PAEs in two agricultural films (mg·kg⁻¹)

Film type	DBP	DEHP	BBP	DOP	DMP	DEP
White film	80.04	3.08	1.85	0.71	0.68	ND
Black film	653.41	17.39	ND	1.82	8.82	ND

DBP-di-n-butyl-phthalate; DEHP-di-(2-ethylhexyl) phthalate; BBP-benzyl butyl phthalate; DOP- di-n-octyl-phthalate; DMP-dimethyl phthalate; DEP- diethyl phthalate. ND-not detectable.

Plants. Two peanut genotypes were considered, *Fenghua-3* and *Baisha-1016*. Previous study showed that *Baisha-1016* had a strong root system that accumulated heavy metals such as cadmium, and its root length, biomass, total surface area and total absorption area exceeded those of *Fenghua-3*.

Experiment design. The pot experiment consisted of a control and three concentrations of white and black plastic film, respectively: I, no plastic film (control); II, 36 mg·kg⁻¹ (equivalent to one year period of average plastic film residue in the field); III, 178 mg·kg⁻¹ (equivalent to 5 years of residue); and IV, 356 mg·kg⁻¹ (equivalent to 10 years of residue). Each treatment had three replicates. Each 500-g dry soil sample was placed in a 500-ml glass beaker. The white and black plastic films were cut into 1–2 mm² square pieces and then mixed into soils. Soils were maintained at 60–70% maximum water holding capacity (MWHC) during the 180-d incubation period. The DBP and DEHP concentrations in soils were both determined at 90 and 180 d.

The pot experiment of peanut PAE absorption consisted of eight treatments with four respective levels of DBP and DEHP: 0, 12.5, 25 and 50 mg·kg⁻¹. Each treatment had three replicates. DBP and DEHP were dissolved in acetone, applied into 15 kg of dry soils in each pot at 10 d before peanuts were sown. The soils were then fertilized with 93.2 mg N kg⁻¹, 65.5 mg P kg⁻¹ and 166 mg K kg⁻¹, and watered to 70% of MWHC. Six kernels of peanuts were sown in each pot, and thinned to three seedlings per pot after germination. After 127 d of growth, the vines, roots, pods and kernels of plants were harvested separately. After harvest, soil samples were dried,

sieved and stored at 4°C.

Sample extraction and fractionation. DBP and DEHP in soil and peanut plants were extracted by shaking and fractionated using a Florisil silica column [11]. Each aliquot of 5 g of peanut kernels was pulverized with a glass mortar. After adding a small amount of anhydrous sodium sulfate (Na₂SO₄), the sample was transferred into a 250-ml iodine flask with 90 ml of acetonitrile and shaken for 45 min, then filtered through a glass funnel. The four supernatants were all filtered into a round bottom flask after another three extractions with 60 ml of acetonitrile. The approximately 150 ml of liquid in the flask was reduced by rotary evaporation to 3–5 ml.

Column chromatography was carried out in a glass column (1.2 × 30 cm) with 10 mm of Na₂SO₄, 70 mm of magnesium tri-silicate and 10 mm of Na₂SO₄ (from bottom to top). Pre-washing was with 15 ml of hexane before sample loading and elution with 90 ml of hexane. All washing solutions were collected and reduced to less than 1 ml by rotary evaporation as described above.

High performance liquid chromatography (HPLC) analysis. Analysis of individual PAEs was performed using an Inertsil HPLC system (LC-20AT with UV detector, Shimadzu Corporation, Chiyodaku, Tokyo, Japan) with an Inertsil ODS-SP column (4.6 × 250 mm, 5 μm; Shimadzu Corporation). The temperature of the column oven was maintained at 32°C. The derived samples (10 μl) were run with a linear gradient elution. Solvent A was water and solvent B was methanol. The flow rate was 0.8 ml·min⁻¹. The gradient profile was 0–25 min, 70–100% B; 25–33 min, 100% B; 33–40 min, 70% B, and total analysis time was 40 min. The wavelength of detector was 228 nm.

Control and guarantee of quality. The detection limits of DBP and DEHP were 4.868 and 4.100 μg·l⁻¹, respectively. The specific measures of quality control during the experiment process were previously published [11]. The blank levels for the liquid chromatogram instrument, solvent and the whole test method were all lower than detection limits. The adding standard recovery rates for DBP and DEHP were 84.2%–131.8 and 70.8–105.1%, respectively. In the process of real sample detection, the range of the recovery rate of benzyl benzoate that acted as an indicator was 70.0%–136.2%.

Statistical analysis. Data were treated with analysis of variance using SPSS version 17.0 (SPSS Inc.). Significant differences between means were determined using least significant difference ($p < 0.05$).

TABLE 2
Concentrations of DBP and DEHP in different parts of peanut plants ($\text{mg}\cdot\text{kg}^{-1}$)

Variety	Adding Level	Root		Vine		Pod		Kernel	
		DBP	DEHP	DBP	DEHP	DBP	DEHP	DBP	DEHP
<i>Fenghua-3</i>	0	1.76 ^c	0.94 ^c	1.67 ^b	1.67 ^c	1.25 ^b	1.08 ^c	0.23 ^c	0.24 ^c
	12.5	4.42 ^b	3.39 ^b	1.63 ^b	2.14 ^a	2.67 ^a	1.97 ^b	0.50 ^b	0.55 ^b
	25	4.59 ^b	3.36 ^b	1.76 ^b	1.85 ^b	2.70 ^a	2.14 ^{ab}	0.57 ^b	0.60 ^b
	50	6.58 ^a	13.4 ^a	2.40 ^a	2.52 ^a	2.91 ^a	2.28 ^a	1.22 ^a	4.34 ^a
<i>Baisha-1016</i>	0	4.84 ^c	3.36 ^d	1.84 ^b	1.13 ^c	0.61 ^d	0.59 ^c	0.39 ^c	0.66 ^d
	12.5	5.32 ^c	4.71 ^c	2.35 ^a	1.88 ^b	1.14 ^c	1.00 ^b	1.09 ^b	1.74 ^c
	25	8.14 ^b	8.41 ^b	2.19 ^{ab}	2.13 ^b	1.44 ^b	1.39 ^a	1.25 ^b	2.72 ^b
	50	15.1 ^a	20.4 ^a	2.38 ^a	3.32 ^a	1.94 ^a	1.43 ^a	2.09 ^a	4.49 ^a

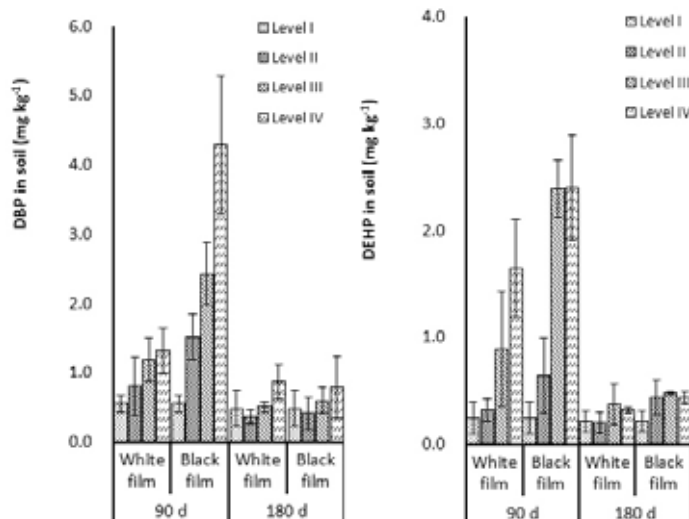


FIGURE 1
Migration of DBP and DEHP from two kinds of agricultural plastic films.

RESULTS

Migration of PAEs from agricultural plastic films. The migration of PAEs from the two kinds of agricultural plastic films is shown in Fig. 1. The concentrations of DBP and DEHP in soils increased after 90 d with the increase in amount of agricultural plastic films applied to soils. The residual concentrations of DBP and DEHP in soils with black film applied were significantly ($p < 0.05$) more than for white film. There were significant correlations between soil DBP and DEHP concentrations and the amounts of white film ($R^2 = 0.991$ and 0.999 , respectively) and of black film ($R^2 = 0.973$ and 0.993 , respectively) (all $p < 0.01$).

Regardless of whether white or black film was applied, the residual concentration of DBP and DEHP in soils was reduced significantly in all treatments except for level I after 180 d, with orders of level IV > III > II \approx I and IV \approx III > II \approx I for residual DBP and DEHP concentrations in the soils with white film, respectively; for black film the corresponding orders were level IV > III > II \approx I and IV \approx III \approx II > I. The maximum residual concentration of DBP was 0.879 and 0.799 $\text{mg}\cdot\text{kg}^{-1}$ in soils with

white and black film under level IV treatment, respectively; and maximum residual concentration for DEHP was 0.374 and 0.478 $\text{mg}\cdot\text{kg}^{-1}$ in soils with white and black film under level III treatment, respectively.

DBP and DEHP in peanut. The DBP and DEHP concentrations in different parts of peanut plants are shown in Table 2. Compared with controls, the concentrations of DBP and DEHP in the root, vine, pod and kernel of *Fenghua-3* and *Baisha-1016* were significantly increased in soils with DBP and DEHP. The maximum DBP and DEHP concentrations were 20.4 and 15.1 $\text{mg}\cdot\text{kg}^{-1}$ in the root of *Baisha-1016* at the DBP or DEHP level of 50 $\text{mg}\cdot\text{kg}^{-1}$, respectively. The DBP and DEHP concentrations in pod of *Fenghua-3* were significantly higher than in *Baisha-1016* ($p < 0.05$). The concentrations of DEHP in the kernels of both peanut varieties were higher than that of DBP for all treatments. There was a significant correlation between DBP and DEHP concentrations in the root, vine, pod and kernel of the peanut varieties and the concentration of DBP or DEHP applied to soils (Figs. 2 and 3).

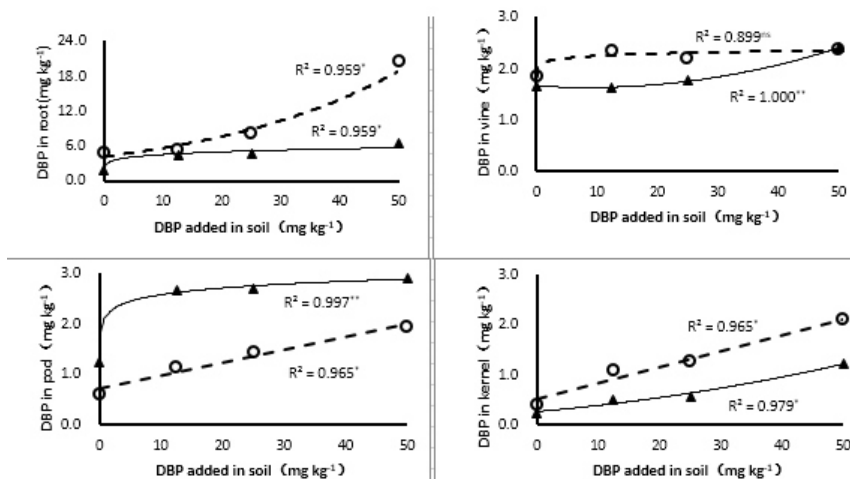


FIGURE 2
Relationships between DBP concentrations in the root, vine, pod and kernel of two peanut varieties and the concentration of DBP applied to soil
 (--○-- *Baisha-1016*; —▲— *Fenghua-3*; * $p < 0.05$; ** $p < 0.01$; ^{ns} $p > 0.05$).

TABLE 3
Accumulative Amounts of DBP/DEHP in Different Parts of Peanut Plants (mg·pot⁻¹)

Variety	Adding Level	Root		Vine		Pod		Kernel	
		DBP	DEHP	DBP	DEHP	DBP	DEHP	DBP	DEHP
<i>Fenghua-3</i>	0	0.015 ^c	0.008 ^c	0.067 ^b	0.067 ^c	0.021 ^c	0.018 ^b	0.008 ^b	0.009 ^c
	12.5	0.027 ^b	0.021 ^b	0.073 ^b	0.096 ^{ab}	0.053 ^a	0.039 ^a	0.020 ^a	0.022 ^b
	25	0.028 ^{ab}	0.021 ^b	0.075 ^{ab}	0.079 ^{bc}	0.047 ^{ab}	0.038 ^a	0.025 ^a	0.026 ^b
	50	0.035 ^a	0.071 ^a	0.096 ^a	0.101 ^a	0.037 ^b	0.030 ^a	0.027 ^a	0.098 ^a
<i>Baisha-1016</i>	0	0.023 ^c	0.016 ^d	0.078 ^{ab}	0.048 ^c	0.011 ^c	0.010 ^c	0.013 ^c	0.022 ^c
	12.5	0.030 ^{bc}	0.028 ^c	0.104 ^a	0.083 ^b	0.009 ^c	0.008 ^c	0.015 ^c	0.025 ^c
	25	0.048 ^b	0.052 ^b	0.067 ^b	0.065 ^{bc}	0.023 ^b	0.021 ^b	0.038 ^b	0.082 ^b
	50	0.099 ^a	0.073 ^a	0.108 ^a	0.151 ^a	0.042 ^a	0.031 ^a	0.078 ^a	0.169 ^a

Different small letters in same variety of the same column meant significant difference at 0.05 level.

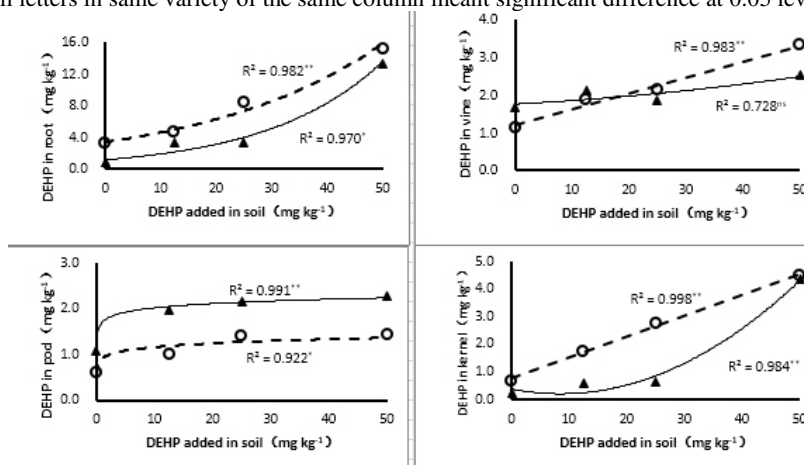


FIGURE 3
Relationships between DBP concentrations in the root, vine, pod and kernel of two peanut varieties and the concentration of DBP applied to soils (--○-- *Baisha-1016*; —▲— *Fenghua-3*; * $p < 0.05$; ** $p < 0.01$; ^{ns} $p > 0.05$).

Total uptake of DBP and DEHP in different parts of the peanut varieties is shown in Table 3. Increasing the concentrations of DBP and DEHP in soils increased the corresponding concentrations in plants. There was a significant correlation between DBP or DEHP accumulated in the root and kernel of

peanut varieties and the corresponding concentrations in soil ($p < 0.05$). The maximum accumulation of DBP was 0.099 mg·pot⁻¹ in the root, and that of DEHP was 0.169 mg·pot⁻¹ in the root and kernel of *Baisha-1016*.

The proportion of DBP accumulated by both varieties relative to the total amount of DBP applied

in soil was 0.01%–0.03%, and that of DEHP was 0.02%–0.04%. The DBP distribution proportions of root, vine, pod and kernel were 15.6%–17.9%, 42.2%–49.2%, 19.0%–30.6% and 11.6%–14.3% for *Fenghua-3*, respectively, and correspondingly 19.0%–30.3%, 33.0%–65.8%, 5.7%–13.1% and 9.5%–23.9% for *Baisha-1016*. The corresponding proportions for DEHP were 11.8%–23.7%, 33.7%–53.9%, 10.0%–23.2% and 12.4%–32.7% for *Fenghua-3* and 17.2%–23.6, 29.5%–57.6%, 5.6%–9.5% and 17.4%–39.9% for *Baisha-1016*. The DEHP distribution proportion was higher than of DBP in kernels of both varieties.

Residual DBP and DEHP in soil. The residual concentrations of DBP and DEHP in soils after harvest decreased significantly in soils with DBP and DEHP applied, compared with the initial concentrations (i.e. levels II, III and IV; Fig. 4). The residual proportions of DBP and DEHP were 3.2%–4.4% and 6.5%–16.1% in soils with *Fenghua-3*, respectively, and correspondingly 1.6–4.2 and 3.1%–5.8% in soils with *Baisha-1016*.

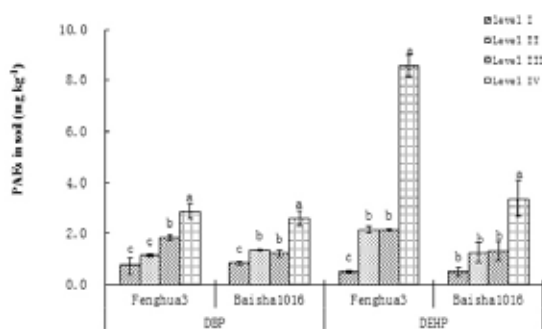


FIGURE 4
Residual concentrations of DBP or DEHP in soil after harvest of peanuts.

DISCUSSION

Agricultural film is one of the main sources of PAEs in soils in rural areas, and the content of PAEs released is determined by the type of film. In the present study, both DBP and DEHP were detected after 90 d in soils with 356 mg.kg⁻¹ of agricultural film applied, which was equivalent to the average amount of residue of mulching plastic film after 10 years of use in northern China. The concentrations of DBP and DEHP in soils with black film applied were 223 and 46.1% higher compared with white film, respectively. Black recycled plastic films are produced from old plastics and plastic film materials, with large amounts of plasticizers added in the process, thus causing higher DBP and DEHP pollution. The concentrations of DBP and DEHP in soils after 90 d with 356 mg.kg⁻¹ of agricultural film applied were lower than the concentration thresholds proposed by the United States Environmental Protection Agency

in 2007: 4.35 and 50 mg.kg⁻¹, respectively. However, the detected concentrations were significantly higher than those in agricultural soils in China, reaching the level of light pollution [8][10].

In the present study, the residue concentrations of DBP in soils after 180 d decreased by 64.3%, 66.3% and 57.7% compared with after 90 d for the plastic film treatments of levels II, III and IV, respectively; and by 33.8%, 69.1% and 81.2% for DEHP in levels II, III and IV, respectively. The average daily rates of DBP and DEHP decrease were 0.54% and 0.65%, and 0.85% and 0.72% for the white and black plastic film treatments, respectively (Fig. 1). Interestingly, the average daily decrease rates of DBP and DEHP were 0.71% and 0.67% during the plant growth process, respectively (Fig. 4). Further analysis revealed that the absorption and accumulation amounts of DEHP and DBP in the mature stage of peanut were only 0.01%–0.03% and 0.02% to 0.04% of soil applied amounts, respectively. These data indicated that there was no obvious effect on PAE degradation by peanut plants. Previous studies demonstrated that microbial and chemical processes were the principal mechanisms for degradation of DBP and DEHP in the environment [12][13]. It can be inferred that the main mechanism of rapid reduction of PAE levels in soil was not absorption by peanut, but photochemical and microbial degradation [14][15].

The absorption and accumulation of organic pollutants in soils are influenced by the synergistic effect of the confluence of factors such as environmental conditions and the nature of pollutants [16]. In this study, concentrations of DEHP and DBP in two peanut cultivars were closely related to the level of PAE contamination in soils (Fig. 2 and 3), although the bioavailability of PAEs in soils released from standard dilution in acetone may differ from that resulting from application of plastic sheets. In addition, PAE concentrations in peanut kernel were significantly higher than those of root and vine, but PAE concentrations in pods was not significantly correlated. It is apparent that PAEs absorbed by roots but not pods was an important mechanism in determining PAE accumulation in peanuts. The root system, root biomass, total length, total surface area and total absorption area of *Baisha-1016* were higher than those of *Fenghua-3*, thus resulting in a stronger absorption capacity and cumulative efficiency for soil PAEs (Table 2). The DEHP distribution proportion in kernels of the two peanut varieties was higher than that of DBP (Table 3). DBP and DEHP are high molecular weight organic compounds that are relatively easy for the crop to take up and accumulate; however, the higher octanol–water partition coefficient, stability and lipophilicity of DEHP causes a higher accumulation level of DEHP compared with DBP.

CONCLUSION

Agricultural plastic film is an important source of soil PAE pollution in China. Concentrations of DBP and DEHP in soils with black recycled film applied were 223 and 46.1% higher compared with white polyethylene film applied, respectively. Black recycled plastic films are produced from old plastics and plastic film materials, with large amounts of plasticizers added in the process, resulting in higher DBP and DEHP pollution. Whether white or black film was applied, the residual concentrations of DBP and DEHP in soils were reduced significantly in all treatments except for the control. Further analysis revealed no obvious effect on PAE degradation by peanut plants, indicating that the main mechanism of rapid reduction of PAE levels in soil was not absorption by peanut, but photochemical and microbial degradation. The DBP and DEHP concentrations in peanut plants increased with increases in concentrations of DBP and DEHP in soils. DBP and DEHP concentrations of peanut kernels were significantly correlated with that of root, but not pods, showing that PAE absorption by roots, but not pods, was an important mechanism in determining PAE accumulation in peanuts. Compared with *Fenghua-3*, *Baisha-1016* had a stronger root system and higher root biomass, thus exhibiting a higher risk for PAE pollution.

ACKNOWLEDGEMENTS

This work was financially supported by the Special Funding Project of Yellow and Blue District Construction of Shandong Province (No. 2011-Yellow-19) and the National Natural Science Foundation of China (No. 40871224). The authors are deeply grateful to Dr. Robert D. Cameron at the Pennsylvania State University for modifying the manuscript.

REFERENCES

- [1] Net, S., Delmont, A., Sempere, R., Paluselli, A., Ouddane, B. (2015) Reliable quantification of phthalates in environmental matrices (air, water, sludge, sediment and soil), A review. *Sci. Total Environ.*, 515-516, 162-180.
- [2] Wang, J., Luo, Y., Teng, Y., Ma, W., Christie, P., Li, Z. (2013) Soil contamination by phthalate esters in Chinese intensive vegetable production systems with different modes of use of plastic film. *Environ. Pollut.*, 180, 265-273.
- [3] Zhang, Y., Wang, P., Wang, L., Sun, G., Zhao, J., Zhang, H., Du, N. (2015) The influence of facility agriculture production on phthalate esters distribution in black soils of northeast China. *Sci. Total Environ.*, 506-507, 118-125.
- [4] Yin, R., Lin, X.G., Wang, S.G., Zhang, H.Y. (2003) Effect of DNBP/DEHP in vegetable planted soil on the quality of capsicum fruit. *Chemosphere*, 50, 801-805.
- [5] Kong, S., Ji, Y., Liu, L., Chen, L., Zhao, X., Wang, J.J., Bai, Z.P., Sun, Z.R. (2013) Spatial and temporal variation of phthalic acid esters (PAEs) in atmospheric PM 10 and PM 2.5 and the influence of ambient temperature in Tianjin, China. *Atmos. Environ.*, 74, 199-208.
- [6] Guo, Y., Kannan, K. (2011) Comparative assessment of human exposure to phthalate ethers from house dust in China and the United States. *Environ. Sci. Technol.*, 45, 3788-3794.
- [7] Higuchi, T.T., Palmer, J.S., Gray, L.E., Jr. Veeramachaneni, D.N.R. (2003) Effects of dibutyl phthalate in male rabbits following in utero, adolescent, or postpubertal exposure. *Toxicol. Sci.*, 72, 301-313.
- [8] Hu, X.Y., Wen, B., Shan, X.Q. (2003) Survey of phthalate pollution in arable soils in China. *J. Environ. Monitor.*, 5, 649-653. (In Chinese)
- [9] Fu, X.W., Du, Q.Z. (2011) Uptake of di-(2-ethylhexyl) phthalate of vegetables from plastic film greenhouses. *J. Agr. Food Chem.*, 59, 11585-11588
- [10] Yang, H.J., Xie, W.J., Liu, Q., Liu, J.T., Yu, H.W., Lu, Z.H. (2013) Distribution of phthalate esters in topsoil, A case study in the Yellow River Delta, China. *Environ. Monit. Assess.*, 185, 8489-8500.
- [11] Cui, M.M., Wang, K.R., Wang, L.L., Shi, Y.X. (2013) Distribution characteristics of phthalic acid esters in soils and peanut kernels in main peanut producing areas of Shandong Province, China. *J. Appl. Ecol.*, 24, 3523-3530. (In Chinese)
- [12] Juneson, C., Ward, O.P., Singh, A. (2002) Biodegradation of dimethyl phthalate with high removal rates in a packed-bed reactor. *World J. Microb. Biot.*, 18, 7-10.
- [13] Di, Gennaro, P., Collina, E., Franzetti, A., Lasagni, M., Luridiana, A., Pitea, D., Bestetti, G. (2005) Bioremediation of diethylhexyl phthalate contaminated soil, a feasibility study in slurry- and solid-phase reactors. *Environ. Sci. Technol.*, 39, 325-330.
- [14] Cartwright, C.D., Thompson, I.P., Burns, R.G. (2000) Degradation and impact of phthalate plasticizers on soil microbial communities. *Environ. Toxicol. Chem.*, 19, 1253-1261.
- [15] Xu, G., Li, F.S., Wang, Q.H. (2008) Occurrence and degradation characteristics of dibutyl phthalate (DBP) and di-(2-ethylhexyl) phthalate (DEHP) in typical agricultural soils of China. *Sci. Total Environ.*, 393, 333-340.

- [16]Chen, Y., Wang, C.X., Wang, Z.J. (2005) Residues and source identification of persistent organic pollutants in farmland soils irrigated by effluents from biological treatment plants. *Environ. Int.*, 31, 778-783.

Received: 24.10.2016

Accepted: 18.04.2017

CORRESPONDING AUTHOR

Kairong Wang

Qingdao Engineering Research Center for Rural Environment, Qingdao Agricultural University, Qingdao 266109, China

e-mail: krwang1@163.com

ANALYSIS OF ADSORPTION AND KINETIC OF LIPASE ENZYME ON KAOLINITE

Salih Alkan*, Umit Turgut

Ordu University, Faculty of Arts and Science, Department of Chemistry, 52200, Ordu, Turkey

ABSTRACT

The properties of the clay kaolinite as a support for enzyme immobilization were studied using the enzyme lipase. Lipases are biocatalysts of great importance due to their ability to catalyze diverse reactions. They are extensively used for the catalysis in organic solvents, which leads to multiple industrial applications. Studies have been done at different (pH 4,0- 10,0) and in the temperature range of 20-80° C. Taking into the account the Lagergren first-order equation for adsorption kinetics, q_1 and k_1 values, are a measure of absorbance strength were obtained. The values adsorption enthalpy (ΔH^0), Gibbs free enthalpy (ΔG^0) and adsorption entropy (ΔS^0) were thermodynamics parameters. These studies indicate that kaolinite is a valuable support for the simple adsorption of enzymes.

KEYWORDS:

Kaolinite, lipase enzyme, immobilization, adsorption, kinetic.

INTRODUCTION

Kaolinite is a clay which has the highest absorbent capacity of and minerals clay as well as a high adsorptive capacity [1]. Its advantages over other minerals, especially with regards to its low density and high specific surface, have been accepted for a long time, and the account for most of the current uses kaolinite [2]. Recently, clay and its modified forms have been efficiently used as adsorbents. Since clay has great specific surface area, excellent physical and chemical stability and several other structural and surface properties [3]. Lipases (E.C.3.1.1.3) can be broadly defined as enzymes that catalyze the hydrolysis of ester bonds in substrates such as vitamin esters, phospholipids, triglycerides and cholesterol esters [4]. For various applications, lipase enzymes are preferably used in an immobilized state in order to ease separation of the catalyst from the product stream [5]. Lipases have been immobilized on various supports either by physical adsorption, covalent binding, ionic interactions or by entrapment [6]. Lipases remain active in slightly hydrated organic solvents, enabling them to be used as

biocatalysts in organic synthesis [7]. Lipases preferably hydrolyze insoluble triglycerides, while esterases usually hydrolyze water-soluble esters. Since lipases and esterases act in a wide range of substrates, they have many applications [8], such as degradation of fats and oils through detergents [9], paper bleaching, bio-diesel and bio lubricants [10], the food industry and the resolution of racemic mixtures in drug production [11]. It was the aim of this to adapt an adsorption assay p-nitrophenyl butyrate (pNPB) as the substrate for the rapid quantification of lipase activity in kaolinite.

MATERIALS AND METHODS

Solid support. Kaolinite used in this study as parent clay was provided from Eczacıbaşı Co. in Turkey. In order to prepare the support, the kaolinite was dispersed, by vigorous stirring for 60 min, in an equilibration buffer and further prepared at 25 mg.ml⁻¹. These suspensions exhibited considerable stability, with no sedimentation after 24 h. In this study for standard purpose, solutions of lipase (0,1 mg.ml⁻¹) in 0,1M sodium phosphate buffer, pH 7,25 were added to 25 mg.ml⁻¹ suspensions kaolinite, in a 1:4 volume ratio. The lipase-kaolinite complex was removed by centrifugation at 3500 g for 15 min and then washed 4 times with 5 ml of phosphate buffer.

Enzyme. Lipase (E.C.3.1.1.3) from wheat germ TypI. Lyophilized powder 5-15 units/ mg.protein. the product of USA.

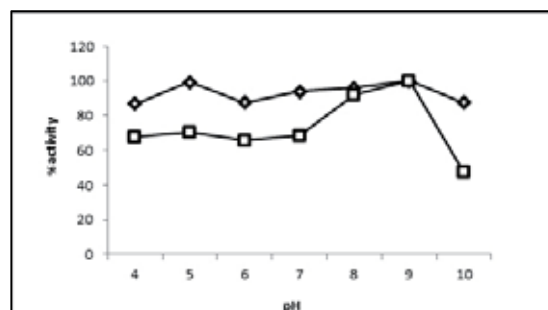


FIGURE 1
Effect of pH on the enzyme activity of (◇) kaolinite-supported lipase and (□) free Lipase.

Lipase assay. Kaolinite 0,1g was weighed into polypropylene centrifuge tubes mixed with 5 ml 100 mM NaH₂PO₄/NaOH buffer, pH 7,25 and pre-warmed at 30°C in a water bath for 10 min. Then 50 µl of substrate solution (100 mM pNPB diluted in 2-propanol and stored -20°C) were added. The contents were mixed and the tubes were incubated in the water bath 30°C for exactly another 10 min. In order to measure the p-nitrophenol (pNP) released from the substrate a control was prepared without soil [12].

RESULT AND DISCUSSION

Optimum pH stability was continued with p-nitrophenyl butyrate as a substrate. Free and supported lipase preparations were incubated at 30°C, for 24 h at different pH in appropriate 0,1 M phosphate buffer pH 4,0-10,0 and the relative activity was measured under standard conditions [13]. Enzyme gave better results at alkaline pH values such as pH 9,0.

Generally, of lipase show their enzyme activity at alkaline pH. Enzyme takes place in the wide range of pH values.

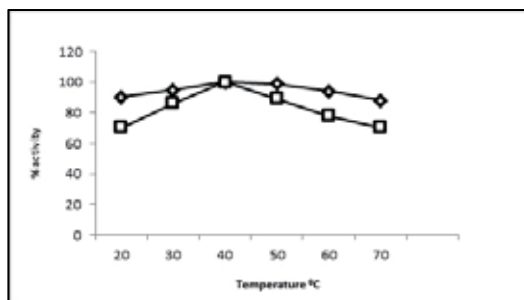


FIGURE 2

Effect of temperature on the activity of (◊)kaolinite-supported lipase and (◻) free lipase.

Thermal stability studies of free and immobilized lipase were performed by measuring the residual activity of the enzyme after exposure to three different temperatures (20-80°C) in 0,1 M phosphate buffer (pH 7,25) for 2 and 5h. Over 40°C, the absorbance values of lipase assay fluctuated and enzyme lost its activity. Optimum temperature value promotes binding potential of enzyme and substrates.

Substrate concentration. Varying the substrate concentration showed that the concentration adopted (0,02 mM-0,001 mM pNPB was used in the reaction mixture) was satisfactory for booty enzymes [14].

The Lineweaver-Burk plots were linear indicated that hydrolysis of various kaolinite the lipase followed kinetics parameters, K_m and V_{max} which show the substrate affinity of enzyme. The smaller K_m value indicate the higher enzyme affinity to sub-

strates [15]. The enzyme activity was determined using substrate solutions in different concentrations to obtain the 1/S and 1/V values. The K_m and V_{max} values were determined by means of the Lineweaver-Burk plot. The Michaelis-Menten equation is written and correlated to determine the K_m and V_{max}

$$1/V = K_m/V_{max} \cdot 1/S + 1/V_{max}$$

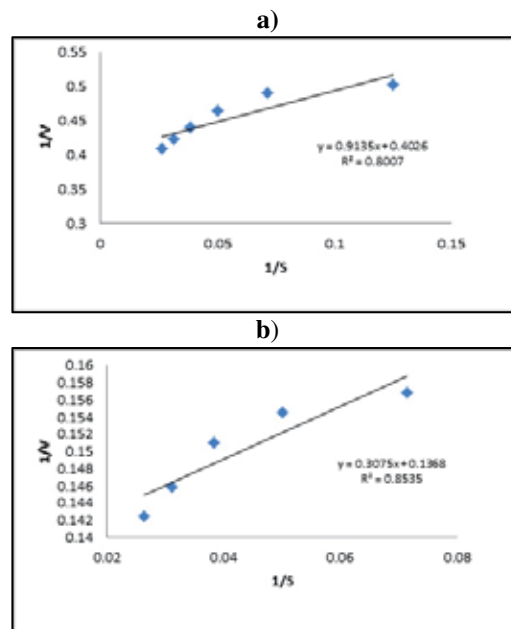


FIGURE 3

Lineweaver-Burk plots,(a) free lipase and (b) immobilize lipase.

The value of K_m was found to be 2.23 mM whereas the V_{max} was calculated as 2.50 µmol.min⁻¹ for free lipase. The K_m value was found to be 2.24 mM and the V_{max} value was found to be 7.69 µmol.min⁻¹ for the immobilized lipase [16].

TABLE 1
For immobilized enzymes ln(q_e-q_t)-t

t (min)	10	20	30	40	50
ln (q _e -q _t)	-1.7147	-1.8388	-1.9105	-2.7333	-3.5065
Enzyme unit	0.267	0.288	0.299	0.382	0.417

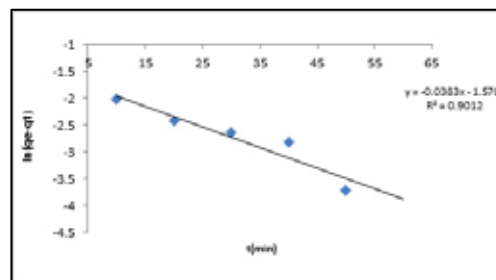


FIGURE 4

Enzyme adsorption related Lagergren pseudo-first-order equation

The first order equation is described by Lagergren as follows

$$\log(q_e - q_t) = \log q_e - k_1 t / 2.303$$

Where q_t refers to the amount of lipase enzyme adsorbed per unit weight of adsorbent ($\text{mg} \cdot \text{g}^{-1}$) at time t (min). The value of q_e and first order rate constant (k_1) can be calculated from the plot of $\log(q_e - q_t)$ versus t . Table 1. displayed the first order parameters of lipase enzyme onto kaolinite as well as the linear equation of the plot of $\log(q_e - q_t)$ versus t [17].

TABLE 2

Lagergren pseudo first-order velocity equation

q_e	k_1 (1/min)	linear equation	R^2
37.2	0.088	$y = -0.0383x - 1.5708$	0.9012

Thermodynamic Studies. The type of adsorption can be determined through the quantities of thermodynamic parameters such as Gibbs free energy ΔG^0 , standard enthalpy ΔH^0 and entropy change ΔS^0 for the adsorption of lipase enzyme onto the of kaolinite. These parameters are given Table 3. ΔG^0 was calculated using the following equation

$$\Delta G^0 = -RT \ln K_1$$

Where, K is equilibrium constant, R is ideal gas constant (8.314 J/molK), " G and " H are in J/mol ," " S is in J/molK were calculated respectively from the slope and intercept of the plots of $1/T$ versus $\ln K$ using the Van't Hoff equation

$$\ln K = \Delta S^0 / R - \Delta H^0 / RT$$

The standard free energy (ΔG^0) is computed as follows:

$$\Delta G^0 = \Delta H^0 - T\Delta S^0$$

TABLE 3

Kaolinite and of lipase different concentrations ΔG^0 , ΔH^0 , ΔS^0 , R^2 values

Concentration(M)	0.05	0.1	0.25	0.5	1
Equation	$y = -0.8276x + 10.293$	$y = -6.8829x + 13.91$	$y = -4.6078x + 7.4936$	$y = -3.1911x + 3.7131$	$y = -2.8077x + 2.7744$
R^2	0.9537	0.9723	0.9855	0.9934	0.9470
ΔH^0	48.45	57.226	38.30	26.53	23.27
ΔS^0	85.57	115.64	62.30	30.87	29.06
ΔG^0_{313}	-26763	-36140	-19461	-9635	-7199
ΔG^0_{323}	-27590	-37281	-20084	-9944	-7406
ΔG^0_{333}	-28446	-38450	-20707	-10253	-7636
ΔG^0_{343}	-29302	-39388	-21330	-10561	-7866
ΔG^0_{353}	-30157	-40763	-21953	-10870	-8096

The negative values of ΔG^0 showed that, the adsorption process was spontaneous thermodynamically. However the decrease of the values of ΔG^0 with increase temperatures [18].

Proved that, the adsorption was not favorable at higher temperatures. The positive value of ΔH^0 indi-

cated the endothermic nature of the adsorption process. The ΔS^0 take the positive values of entropy change may be due to some structural changes between adsorbent and adsorbed substance [19].

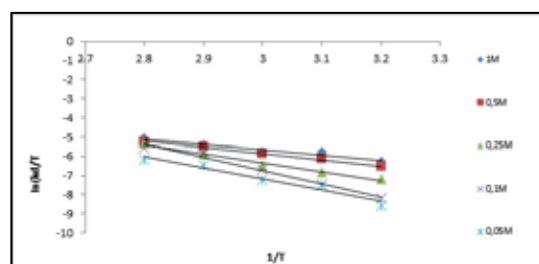


FIGURE 5

Kaolinite-lipase enzyme different concentration ($\ln k_a/T - 1/T$)

REFERENCES

- [1] Robertson, R.H.S. (1957) Sepiolit:A versalit raw material. Chem.Ind.5,1492-1495
- [2] Robertson RHS(1954)Mineralogy of kaolin clays from pugu American Mineralogist. 39,118-138
- [3] Yavuz, Ö. And Aslan, H. (2002) Removal of cadmium from aqueous solution by natural and thermally activated kaolinite. Fresen. Environ. Bull. 11(4) 194-197.
- [4] Kurtovic, J., Marshall, S.N., Zhao, X and Simpson, B.K. (2009) Lipases from mammals and fishes. Reviews in Fisheries Science, 17(1):18-40.
- [5] Pereira, E.B., Zanin, G.M. and Castro, H.F. (2003) Immobilization and catalytic properties of lipase on chitosan for hydrolysis and esterification reactions. Brazil. J. Chem. Eng., 20:343-355
- [6] Nair, D., Coşkun, A., Derya, Y.I., Mahmut, B., Aziz, T and Bülent, K. (2009) Biodiesel production from sun ower soybean and waste cooking oils by transesterication using lipase immobilized onto a novel microporous polymer. Bioresour. Technol., 100: 1983-1991.
- [7] Roberts, S.M. (1993) Biocatalysis for Fine Chemical Synthesis, Wiley and sons, New York.
- [8] Casas, G.L., Duguesne, S., Bordes, F., Marty, A. (2012) An overview. In Lipases and Phospholipases SE-E;Sandoval,G.Ed; Humane Press: NewYork, NY, USA. Volume 861, pp.3-30.
- [9] Fariha, H., Aamer, A.S., Sundus, J., Abdul, H. (2010) Enzymes used in detergents: Lipases.Afr.J.Biotechnol 9,4836-4844.
- [10] Nguyen, D.J., Zhang, ZH., Dudet, A., Renaud, S. (2008) Bleaching of kraft pulp by a commercial lipase: Accessory enzymes degrade hexenuronic acids. Enzyme Microb. Technol.

- 43,130-136
- [11] Fan, X., Nrehus, X., Sandoval, G. (2012) *Lipases and Phospholipases: Methods and Applications*; New York, NY, USA: pp.471-483
- [12] Ferreira, D.S., Sandoval, G., Plow, F. (2013) The potential use of lipases in the production of fatty acid derivatives for the food and nutraceutical industries. *Electron.J.Biotechnol.*, 16.1-38.
- [13] Margesin, R., Feller, G., Hammerle, M., Stegner, U and Schinner, F.A. (2002) Colorimetric method for the determination of lipase activity in soil. *Biotechnology letters* 24:27-33.
- [14] Alkan, S., Ceylan, H and Arslan, O. (2005) Bentonite-Support catalase. *J. Serb. Chem. Soc.* 70(5) 721-726.
- [15] Feller, G., Thiry, M., Arpigny, J.L., Gerday, C. (1991) Cloning and expression in *Escherichia Coli* of three lipase-encoding genes from the psychrotrophic antarctic strain *Moraxella TA 144* *Gene* 102:111-115.
- [16] Cornis-Bowden, H. (1976) *Principles of Enzyme Kinetics*, Butterworths, London, p.142.
- [17] Fengfeng, M., Boawer, Z., Jingiu, D., Hongtao, Q., Jinkui, Z. (2016) Sorption of Cd by biochar produced from pyrolysis of cattle manure in aqueous solution. *Fresen. Environ. Bull.*, 25, 5226-5236.
- [18] Depçi, T., Alkan, S., Kul, A.R., Önal, Y., Alacabey, İ., Dişli, E. (2011) Characteristic properties of adsorbed catalase onto activated carbon based Adıyaman lignite. *Fresen. Environ. Bull.*, 9, 2371-2378.
- [19] Panayotova, M. (2001) Kinetics and thermodynamics of Removal of Nickel Ions from Wastewater by Use Of Natural and Modified Zeolite, *Fresen. Environ. Bull.* 10 (3) 267-272.

Received: 26.09.2016

Accepted: 07.04.2017

CORRESPONDING AUTHOR

Salih Alkan

Ordu University, Faculty of Arts and Science,
Department of Chemistry, 52200, Ordu, Turkey

e-mail: salihalkan@odu.edu.tr

EVALUATION OF THE WOUND HEALING AND ANTI-INFLAMMATORY ACTIVITIES AND PHYTOCHEMICAL ANALYSIS OF *MYRTUS COMMUNIS* L.

Ibrahim Tumen^{1,3}, Esra Kupeli Akkol^{2*}, Ipek Suntar², Guler Erbey¹, Mehmet Kurtca³, Hikmet Keles⁴, Markku Reunanen⁵, Andrey Pranovich⁵

¹Department of Forest Products Chemistry, Faculty of Forestry, Bartın University, 74100, Bartın, Turkey

²Department of Pharmacognosy, Faculty of Pharmacy, Gazi University, Etiler 06330, Ankara, Turkey

³Vocational School of Health Services, Bartın University, 74100, Bartın, Turkey

⁴Department of Pathology, Faculty of Veterinary Medicine, Afyon Kocatepe University, 03200, Afyonkarahisar, Turkey

⁵Department of Wood and Paper Chemistry, Åbo Akademi University, 20500, Turku, Finland

ABSTRACT

This study evaluates wound healing activities of *n*-hexane and acetone extracts, as well as the essential oils obtained from the berries and leaves of *Myrtus communis* L., (Myrtaceae), using excision and incision wound models. Ulcerations of the skin tissues, re-epithelization, fibroblast proliferation, mono/polymorphonuclear cells, vascularization and collagen increase were qualitatively evaluated by the histopathological analysis. An acute anti-inflammatory activity method based on the inhibition of the increase in vascular permeability was used to determine the anti-inflammatory effect of the extracts and essential oils. Oils' yields and chemical profiles were also determined. Volatile oil, obtained from *M. communis* berries, provided a contraction rate of 60.08% in the circular excision wound model and a tensile strength ratio of 39.1% in the linear incision wound model. The *n*-hexane extract of *M. communis* berries was found to possess significant activity in the circular excision wound model with a ratio of 49.2%. However, it did not provide a significant increase in wound tensile strength. Berries' essential oils provided significant inhibition (28.5%). Particularly the essential oil of *M. communis* berries and its extracts can be used wound healing and anti-inflammatory purposes.

KEYWORDS:

Myrtus communis, Myrtaceae, Essential oil, Wound Healing, Anti-inflammatory

INTRODUCTION

Myrtle (*Myrtus communis* L.) is an evergreen shrub belonging to the Myrtaceae family. It grows throughout the Mediterranean area [1] and called as mersin, murt, hambeles. It is used in folk medicine in Turkey and other Mediterranean countries [2-4]. Its essential oil is used as an antiseptic and hemostatic, in the synthesis of perfum components and fla-

voring additives, and to treat common cold and diabetes mellitus. However, an overdose essential oil can cause an irritation in the respiratory system as well as abortus due to the induction of uterine contraction [5].

The plant contains fibres, sugars and many biologically active compounds, such as flavonoids [6] and anthocyanins, as the major phytochemicals of the berries [7]. Seeds yield 12- 15% fatty oil (fixed oil) consisting of glycerides of oleic, linoleic, myristic, palmitic, linolenic and lauric acid. Studies that analyze fatty acid in myrtle berries revealed 14 fatty acids; oleic acid being the dominant one (67.07%), followed by palmitic (10.24%) [8] and stearic acids (8.19%) [9]. Leafs, berries and flowers were reported to have terpenoid compounds [10]. Some compositions of essential oil were: 1,8-cineole, α -pinene, β -pinene, myrcene, sabinene, eugenol, α -terpineole, β -caryophyllene, p-cymene, 3-carene, phellandrene, limonene, linalool and myrtenol. Berries were reported to contain resin, tannin, sugars, flavonoids, anthocyanin, quercetin, myricetin-3-*O*-glucoside, caffeic acid, hesperetin-7-*O*-rhamnoglucoside, [10-14]. Leaves contain tannins, flavonoids, coumarins, myrtucommulone, galloyl-glucosides, caffeic, gallic and ellagic acids. Finally, the roots contain tannins, alkaloids, glycosides, reducing sugars, gallic acids, phenolic acids, quercetin and patuletin [15].

Several studies have been conducted on the biological activity of *M. communis*, including its antifungal and antibacterial effects on *Escherichia coli*, *Pseudomonas aeruginosa* and *Candida lipolytica* [16-20], as well as its antimolluscicidal [21], insecticidal [22,23], narcotic analgesic [24], anti-inflammatory [25], antioxidant [13], antidiabetic [26-28], antimutagenic [7,29], antiulcerogenic [30] and cholesterol [31]. In the light of the ethnobotanical data, this study was designed to reveal the wound healing activity potential of *Myrtus communis* through *in vivo* bioassays.

MATERIALS AND METHODS

Plant Material. The leaves and berries of *M. communis* L. were collected from Silifke town in Mersin, Turkey, using the conventional method for the plant at its maturity period and stored at -24°C until the laboratory analyses were performed. Voucher specimens were deposited in the Herbarium of the Faculty of Forestry, Bartın University (BOF 516). The specimens were authenticated by Dr. Barbaros Yaman (Bartın University, Faculty of Forestry, Department of Forest Botany, Bartın/Turkey).

Hydrodistillation. The essential oils (EOs) of the leaves and berries of *M. communis* L. were obtained by hydrodistillation using a Clevenger apparatus (ILDAM CAM Ltd. Ankara-Turkey). A portion of 500 g fresh samples were used and the EOs were collected for 3 h. The samples were dried over anhydrous sodium sulphate in a sealed vial until they were used [32-34].

GC and GC-MS analysis. The EO samples were analyzed using an HP 6890-5973 GC-MSD instrument (Agilent Technologies Canada Inc., Mississauga, ON, Canada) equipped with an HP-5 capillary column (25 m/0.25 mm i.d., 0.11 µm film thickness). Helium was used as the carrier gas at 1.0 mL/min flow rate. The column oven temperature was programmed starting from 50 °C (0.5 min) to 250 °C, at a heating rate of 4°C/min. After 10 min of hold time at 250°C the temperature program was continued at 10 °C/min to 290 °C for 15 min. The split-injector and MS-transfer line were at 260 °C and 280 °C, respectively. The MSD was operated in electron impact ionization mode at 70 eV electron energy. Samples were injected by splitting at a ratio of 1:10 [32]. Compounds were identified based on mass spectra, referring to NIST98 and WILEY275 mass spectral libraries, and by comparing measured retention index (RI) values of components with literature data [35]. The quantitative area-percent measurements were based on peak-areas from the GC-MS data [33].

Dynamic Headspace (SPME). A 65 µm Stableflex DVB/CAR/PDMS fiber assembly was pre-conditioned for SPME by desorbing in the GC injector for a few hours. The conditioning process was repeated if residual contaminant peaks were seen in blank analyses. Headspace SPME was performed on a commercially available sampling stand (Supelco, Inc., USA) equipped with a revolver-type vial receptacle and a holder cartridge for the manual SPME device, which was placed on a hot plate. The 4 ml vials with fresh 0.8 g samples were placed in the receptacle. After the samples were equilibrated for 60 min at the desired temperature (about 55 °C), they were extracted by headspace with an SPME fiber for 30 min. After extraction, the

SPME fiber was retracted, the manual holder was removed from the cartridge, and the fiber was inserted into the GC injector for 5-min of desorption. The SPME-extracted VOCs were analyzed by GC and GC-MS. The capillary GC-FID analyses were performed using a Varian 3400 model gas chromatograph. Hydrogen was used as the carrier gas (1 mL/min). An HP-5 capillary column (30 m x 0.32 mm i.d.; 0.25 µm film thickness) was used to separate the compounds. The column oven temperature for the dynamic-headspace (SPME) analyses was programmed as follows: starting temperature 50 °C (1 min), 4°C/ min heating rate to 250 °C for 10 min and, finally, increased to 270 °C at 10°C/min and held isothermally for 10 min. Injector and detector temperatures were 250°C and 270°C, respectively [32-36].

Biological activity tests. Animals. Male, Sprague-Dawley rats (160-180 g) and Swiss albino mice (20–25 g) were purchased from the animal breeding laboratory of Kobay (Ankara, Turkey).

The animals left under room conditions for 3 days to ensure acclimatization. They followed on standard pellet diet and water *ad libitum* throughout the experiment. A minimum of six animals were used in each group. The study was approved by the Institutional Animal Ethics Committee and was performed pursuant to the international rules on animal experiments and biodiversity right.

Preparation of test samples for bioassay. Test samples were prepared in an ointment base consisting of glycol stearate, 1,2 propylene glycol, liquid paraffin (3:6:1) in 1% concentration. Test ointments were topically applied (0.5 g) to the wounded site. The vehicle group animals were treated only with the ointment base, and the reference group animals were treated with 0.5 g of Madecassol® (Bayer, 00001199).

Test samples were orally given to test animals after being suspended in a mixture of distilled H₂O and 1% Tween 80 in the anti-inflammatory activity assay. In the control group, the drug treatment was replaced with appropriate volumes of dosing vehicle. Indomethacin (10 mg/kg) in 1% Tween 80 was used as a reference drug.

Wound healing activity. Circular excision wound model. The animals were anaesthetized with 0.02 cc Xylazine (%2 Alfazyne®) and 0.08 cc Ketamin (%10 Ketamol®). The mice's back hairs were depilated and a circular wound was created on the dorsal interscapular region of each animal by excising the skin with a 5-mm biopsy punch (Nopa instruments, Germany). The wounds were left open [37]. Test samples, the reference drug (Madecassol®, Bayer) and the vehicle ointments were topically applied daily until the wound completely healed. The

progressive changes in the wound area were monitored by a camera (Fuji, S20 Pro, Japan) every two days, and the wound evaluated using AutoCAD program. Wound contraction was calculated in proportion to the reduction in the wound area. A sample of the wounded tissue was isolated from the healed skin in each group for histopathological examination [38,39].

Linear incision wound model. The animals were anaesthetized with 0.05 cc Xylazine (%2 Alfazyne®) and 0.15 cc Ketamin (%10 Ketazol®) [40]. The hairs on the dorsal part were shaved and cleaned with 70% alcohol. Two 5cm-length linear-paravertebral incisions were made using a sterile blade on the shaved skin at a distance of 1.5 cm from the dorsal midline on each side. Three surgical sutures were placed at 1 cm intervals. The ointments were topically applied on the wounds daily throughout 9 days. All the sutures were removed on the final day and tensile strength of treated skin was measured using a tensiometer (Zwick/Roell Z0.5, Germany) [39-42].

Histopathology. Skin specimens were collected at the end of the experiment. Samples were fixed in 10% buffered formalin, and processed and blocked using paraffin. Then they were divided into 5 µm sections and stained with hematoxylin & eosin (HE) and Van Gieson (VG) stains. The tissues were examined by light microscope (Olympus CX41 attached Kameram® Digital Image Analyze System) and graded as mild (+), moderate (++) and severe (+++) for epidermal or dermal re-modeling. Re-epithelization or ulcer in epidermis, fibroblast proliferation, mononuclear and/or polymorphonuclear cells, and neo-vascularization and collagen depositions in dermis were analyzed for epidermal or dermal re-modeling. Van Gieson-stained sections were analyzed for collagen deposition. At the end of the examination, all the wound healing processes were combined and staged for wound healing phases as inflammation, proliferation, and re-modeling in all groups.

Anti-inflammatory activity. Acetic acid-induced increase in capillary permeability. The effect of the test samples on the increased vascular permeability induced by acetic acid in mice was determined using Whittle method [43], with some modifications [44]. Test samples were orally applied to the mice in 0.2 ml/20 g body weight. Thirty minutes after the administration, Evans blue in saline solution was injected (i.v.) to the tails of each animal, held for 10 min, and then 0.5% (v/v) acetic acid was injected (i.p.). After 20 min, the mice were killed by dislocation of the neck, and their viscera were exposed to and irrigated with distilled water. 0.1 N NaOH solution was added and absorption of the final solution

was measured at 590 nm (Beckmann Dual Spectrometer; Beckman, Fullerton, CA, USA). A mixture of distilled water and 0.5% CMC was orally given to the control groups, and they were treated as described above.

Statistical data analysis. The data were analyzed using the one-way analysis of variance (ANOVA). The significance threshold was determined to be $p \leq 0.05$. No statistical tests were performed for the histopathologic data since they were nonparametric.

RESULTS

Table 1 volumetrically and gravimetrically shows the essential oil yields of *M. communis* obtained by hydro-distillation. The highest rate of oil yield (0.55%) was obtained from the berries.

TABLE 1
Essential oil yields of berries and leaves of *M. communis* (%)

Sample	Oil Yields (%)	
	Volumetric (mL/100 g)	Gravimetric (w/w)
<i>M. communis</i> L. Berries	0.55	0.29
<i>M. communis</i> L. Leaves	0.36	0.34

Table 2 shows the composition of the essential oil obtained from myrtle berries and leaves using hydro-distillation. The main compounds were α -pinene, β -myrcene, limonene, eucalyptol, linalool, α -terpineol and geranyl acetate. A major compound, α -Pinene, is contained most abundantly in leaves with a rate of 34.85%. On the other hand, the highest amounts of limonene (9.76%), eucalyptol (5.94%), linalool (18.47%) and geranyl acetate (5.87%) in leaves. Berries were found to contained α -pinene (5.64%), eucalyptol (35.73%), linalool (20.20%) and α -terpineol (20.93%). Table 2 lists the characteristics of 34 compounds, constituting between 92.50% and 95.87% of the chromatogram area. Chromatograms areas of the unidentified compounds were between 4.13% and 7.50%.

Table 3 shows the total composition of the essential oils found in the berries and the leaves of *M. communis* by SPME. The major compounds were α -pinene, β -myrcene, Δ^3 -carene, cymene, limonene, eucalyptol, α -ocimene, β -ocimene and linalool. The rate of eucalyptol was higher in the berries (30.79%) than in the leaves (6.16%). In addition, the rate of α -pinene was higher in the berries (24.24%) than in the leaves (13.31%). A total of 43 compounds were

identified during SPME. The total amount of the uncharacterized compounds varied between 2.82% and 6.86%.

TABLE 2

Composition¹⁾ rates of essential oils of *M. communis* obtained by the hydrodistillation method

Nr.	RI	Compounds ²⁾	Berries	Leaves
1	918	isobutyl isobutanoate	0.26	0.71
2	926	α -thujene	-	0.17
3	936	α -pinene	5.64	34.85
4	948	α -fenchene	-	0.03
5	949	camphene	-	0.05
6	978	β -pinene	-	0.19
7	989	β -myrcene	0.48	1.42
8	999	α -phellandrene	-	0.16
9	1010	3-carene	0.22	0.27
10	1019	α -terpinene	0.35	0.14
11	1021	cymene	0.23	0.28
12	1029	limonene	1.16	9.76
13	1031	eucalyptol	35.73	5.94
14	1039	α -ocimene	-	0.51
15	1045	Phenylacetaldehyde ²⁾	2.51	-
16	1046	β -ocimene	1.06	1.28
17	1056	χ -terpinene	0.47	0.40
18	1087	α -terpinolene	0.79	0.88
19	1088	cymenene	0.51	-
20	1099	linalool	20.20	18.47
21	1177	4-terpineol	1.27	0.10
22	1190	α -terpineol	20.93	3.33
23	1193	estragole	-	0.47
24	1263	linalyl acetate	0.64	3.55
25	1290	anethole	-	0.06
26	1332	myrtenyl acetate	-	0.12
27	1334	methyl geranate	-	0.19
28	1349	2-hydroxycineole acetate	-	0.05
29	1356	α -terpinyl acetate	0.55	0.83
30	1371	neryl acetate	-	1.44
31	1391	geranyl acetate	1.26	5.87
32	1413	methyl eugenol	0.28	0.36
33	1420	caryophyllene	0.53	0.30
34	1448	α -caryophyllene ³⁾	0.22	0.32
Total identified compounds			95.87	92.50
Total unidentified compounds			4.13	7.50

- 1) peak area percents from total eluted components on GC-MS
- 2) identified by MS and retention index (RI) data from the literature [35]
- 3) identification was based on MS-data only

This study investigated the wound healing activity of the *n*-hexane and acetone extracts and essential oils obtained from the berries and leaves of *M. communis* using linear incision and circular excision wound models to verify the claimed traditional use of the plant on a scientific base. It also assessed the histopathologic examination of the tissues treated with the extracts and essential oils. As shown in Table 4, a significant wound healing activity was observed in the group of animals treated with the *n*-hexane extract and essential oil of the fruit of *M. com-*

munis in the circular excision wound model. The closure of wound was significant for the animals treated using this *n*-hexane extract with a rate of 49.19% on day 10, and using the essential oil from the fruit with a rate of 32.48% on day 8, and with a rate of 60.08% on day 10, respectively.

TABLE 3

Percent composition¹⁾ of EOs of *M. communis* obtained by the SPME method

Nr.	RI	Compounds ²⁾	Berries	Leaves
1	779	Toluene	-	0.07
2	800	hexanal	-	0.28
3	844	2-hexenal	0.14	2.71
4	848	3-hexen-1-ol	0.42	0.75
5	858	2-hexen-1-ol	0.65	0.93
6	861	1-hexanol	1.08	0.68
7	918	isobutyl isobutanoate	0.93	0.97
8	926	α -thujene	0.31	0.15
9	936	α -pinene	24.24	13.31
10	949	camphene	0.44	0.05
11	961	benzaldehyde	-	0.05
12	978	β -pinene	0.32	0.11
13	985	2,2,4,6,6-pentamethylheptane	0.29	0.53
14	988	α -myrcene	-	0.10
15	989	β -myrcene	4.71	8.00
16	999	α -phellandrene	0.45	0.42
17	1010	3-carene	1.29	0.25
18	1019	α -terpinene	0.54	0.49
19	1021	cymene	3.85	1.30
20	1029	d-limonene	7.97	13.74
21	1031	eucalyptol	30.79	6.16
22	1039	α -ocimene	1.45	2.92
23	1045	benzeneacetaldehyde	0.18	-
24	1046	β -ocimene	2.55	4.90
25	1056	χ -terpinene	0.74	0.49
26	1087	α -terpinolene	1.28	1.33
27	1088	isopropenyl toluene	0.46	-
28	1099	linalool	4.33	13.12
29	1109	1,3,8-p-menthatriene	-	0.06
30	1141	allo-ocimene	-	0.7
31	1177	4-terpineol	0.34	-
32	1190	α -terpineol	0.89	0.61
33	1193	estragol	0.34	1.92
34	1263	linalyl acetate	0.68	15.69
35	1290	anethole	-	0.11
36	1332	myrtenyl acetate	-	0.09
37	1334	methyl geranate	-	0.17
38	1356	α -terpinenyl acetate	0.26	0.30
39	1371	neryl acetate	0.15	0.69
40	1391	geranyl acetate	0.67	2.26
41	1413	methyleugenol	0.12	0.31
42	1420	caryophyllene	0.33	0.25
43	1448	α -caryophyllene ³⁾	0.18	0.21
Total identified compounds			93.14	97.18
Total unidentified compounds			6.86	2.82

- 1) peak area percents from total eluted components on GC-MS
- 2) identified by MS and retention index (RI) data from the literature [35]
- 3) identification was based on MS-data only

The increase in wound tensile strength reveals

an enhanced healing by indicating the collagen content deposition [45]. The tensile strength of the incised wound was remarkably increased in the animals treated with the ointment prepared with the essential oil of *M. communis* berries. A moderate but insignificant enhancement was observed in tensile

strength of the animals treated with the fruit-n-hexane extract and leaf-essential of *M. communis* (Table 5). The animals treated with the essential oil from the fruit of *M. communis* demonstrated an increase by 39.1% in tensile strength. On the other hand, the reference drug Madecassol® demonstrated an increase by 50.3%.

TABLE 4
The effect of the extracts and essential oils from *M. communis* on circular excision wound model

Material	Wound area ± S.E.M. (Contraction %)						
	0	2	4	6	8	10	
Vehicle	21.03 ± 2.43	19.62 ± 2.43	15.82 ± 1.89 (0.6)	11.27 ± 1.74 (8.5)	7.39 ± 1.35 (7.9)	4.96 ± 0.49 (4.8)	
Negative Control	20.86 ± 2.29	19.35 ± 2.08	15.91 ± 1.93	12.31 ± 1.44	8.02 ± 1.55	5.21 ± 1.06	
Fruit	<i>n</i> -Hexane	20.45 ± 2.35	18.49 ± 2.27 (5.8)	13.96 ± 2.05 (11.8)	9.06 ± 1.65 (19.6)	5.23 ± 1.48 (29.2)	2.52 ± 0.63 (49.2)*
	Acetone	20.36 ± 2.49	18.45 ± 1.80 (5.9)	14.25 ± 1.95 (9.9)	9.23 ± 1.88 (18.0)	5.82 ± 1.74 (21.2)	3.97 ± 0.72 (19.9)
	Essential oil	20.53 ± 2.27	17.48 ± 1.46 (10.9)	13.38 ± 1.74 (15.4)	8.97 ± 1.27 (20.4)	4.99 ± 1.18 (32.5)*	1.98 ± 0.41 (60.1)**
Leaf	<i>n</i> -Hexane	20.26 ± 2.50	19.75 ± 2.52	14.17 ± 2.14 (10.4)	9.89 ± 1.81 (12.2)	6.38 ± 1.46 (13.7)	4.06 ± 0.56 (18.2)
	Acetone	20.37 ± 2.39	19.71 ± 2.43	15.09 ± 2.21 (4.6)	10.16 ± 1.68 (9.9)	6.73 ± 1.40 (8.9)	4.64 ± 0.33 (6.5)
	Essential oil	20.19 ± 2.41	18.64 ± 2.16 (4.9)	14.07 ± 1.92 (11.1)	9.71 ± 1.81 (13.8)	5.74 ± 1.44 (22.3)	3.72 ± 0.38 (25.0)
Madecassol®	20.49 ± 2.23	16.43 ± 1.28 (16.3)	10.21 ± 0.96 (35.5)*	4.02 ± 0.63 (64.3)**	1.50 ± 0.51 (79.7)***	0.00 ± 0.00 (100.0)***	

* p < 0.05; ** : p < 0.01; *** : p < 0.001; S.E.M.: Standard error of the mean

Percentage of contraction values: Vehicle group was compared with Negative control group; Test groups and the reference material were compared with vehicle group

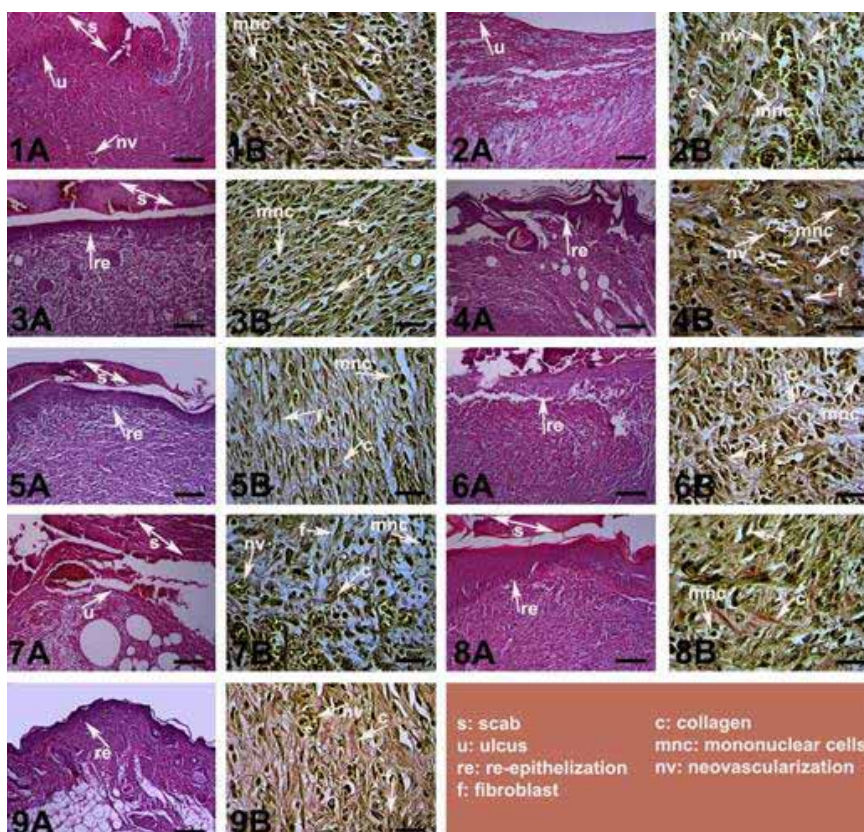


FIGURE 1
Histopathological view of wound healing and epidermal/dermal re-modeling in the test material administered animals

Figure 1 shows the results of the histopathological analysis. The histological examination showed that the rate of original tissue regeneration was much higher in the skin wound treated with essential oil ointment and Madecassol® without any edema, congestion or inflammation. In the vehicle and negative control groups, the speed of dermal modeling was very slow.

This study also examined the effect of the extracts and essential oils from the fruit and leaves from *M. communis* on the inflammatory phase of wound healing. As shown in Table 6, an inhibitory activity was observed for the essential oil at the dose of 100 mg/kg obtained from the fruit of *M. communis*, with the highest inhibitory value of 28.5%.

TABLE 5

Effect of the extracts and essential oils from *M. communis* on linear incision wound model

Material		Statistical	(Tensile
		Mean ± S.E.M.	strength %)
Vehicle		10.13 ± 1.91	8.2
Negative Control		11.04 ± 2.17	-
Fruit	<i>n</i> -Hexane	12.97 ± 2.09	28.0
	Acetone	12.53 ± 2.18	23.7
	Essential oil	14.09 ± 1.77	39.1***
Leaf	<i>n</i> -Hexane	12.18 ± 2.25	20.2
	Acetone	12.11 ± 2.16	19.5
	Essential oil	12.30 ± 2.15	21.4
Madecassol®		15.23 ± 1.45	50.3***

* : $p < 0.05$; ** : $p < 0.01$; *** : $p < 0.001$; S.E.M.: Standard error of the mean

Percentage of tensile strength values: Vehicle group was compared to Negative control group; Test groups and the reference material were compared to vehicle group

TABLE 6

Inhibitory effect of the test materials on acetic acid-induced capillary permeability model

Material	Dose (mg/kg)	Evans blue concentration (µg/ml) ± S.E.M.	Inhibition (%)
Control		12.28 ± 1.36	-
Fruit	<i>n</i> -Hexane	100	10.61 ± 1.51
	Acetone	100	10.17 ± 1.24
	Essential oil	100	8.78 ± 1.08
Leaf	<i>n</i> -Hexane	100	11.13 ± 1.29
	Acetone	100	10.40 ± 1.48
	Essential oil	100	9.96 ± 1.19
Indometasin	10	7.17 ± 0.81	41.6***

* : $p < 0.05$; ** : $p < 0.01$; *** : $p < 0.001$;

S.E.M.: Standard error of the mean

Skin sections show the hematoxylin & eosin (HE) stained epidermis and dermis in A, and the dermis stained with Van Gieson (VG) in B. The original magnification was x 100 and the scale bars represent

120 µm for figures in A, and the original magnification was x 400 and the scale bars represent 40 µm for B. The data represent 6 animals per group: 1) Vehicle group, 2) Negative Control group, 3) *M. communis* fruit *n*-hexane extract, 4) *M. communis* fruit acetone extract, 5) *M. communis* fruit essential oil, 6) *M. communis* leaf *n*-hexane extract, 7) *M. communis* leaf acetone extract, 8) *M. communis* leaf essential oil 9) Madecassol®

Arrows are pointing the events during wound healing: s= scab, u= ulcer, re= re-epithelization, f= fibroblast, c= collagen, mnc= mononuclear cells, nv= neovascularization.

DISCUSSION AND CONCLUSIONS

Maxia et al. [46], reported the topical anti-inflammatory effect of *M. communis* essential oil. They indicated that essential oil acted as an anti-inflammatory by reducing leukocyte migration to the damaged tissue. This activity was demonstrated using croton oil induced ear edema and myeloperoxidase (MPO) activity in mice, as well as cotton pellet induced granuloma, and serum tumor necrosis factor-alpha (TNF-alpha) and interleukin-6 (IL-6) in rats [46]. The *M. communis* extracts were also indicated to have an antioxidant effect [47]. Both activities were proven to contribute to the wound healing process.

Essential oils are known for their antimicrobial potential. A recent research reported that *M. communis* essential oil was an effective antimicrobial agent against persistent endodontic microorganisms [48]. Antimicrobial activity is very important to prevent microbial infections in the wound healing phases. The essential oil of *M. communis* can have an antimicrobial effect on the wound area and contribute to a proper healing. Eucalyptol, the major compound of the essential oil in the berries of *M. communis* in the present study, was previously reported to be the major compound of the essential oil of a plant with a wound healing activity, *Croton adamanthinus* Müll. Arg., which is traditionally used as wound healing agent in Brazil [49]. A more recent study on eucalyptol demonstrated its anti-inflammatory and antioxidant activities, indicating its preventive effects on chronic inflammatory diseases [50].

The previously published articles emphasized the roles of monoterpenoid compounds such as α -pinene, limonene and α -terpineol, regarding their wound healing potential [36,51,52]. In this study, the α -Terpineol showed wound healing [53] and anti-inflammatory activities by inhibiting the COX enzyme and IL production [54] and NF-Kb, promoting the down-regulation of IL-1 β expression [55] and IL-6 formation [56] and decreasing the TNF- α and NO production [57]. This study revealed that the terpenoid compounds in the essential oil of *M. communis* can accelerate the wound healing process.

ACKNOWLEDGEMENT

A part of the study was presented as a poster at European Non-Wood Forest Products (NWFPs) Network COST Action FP1203 4th Workshop Meeting, February, 17-19 April 2016, Antalya, TURKEY.

REFERENCES

- [1] Hsouna, B.A., Hamdi, N., Miladi, R. and Abdelkafi, S. (2014) *Myrtus communis* essential oil: chemical composition and antimicrobial activities against food spoilage pathogens, *Chem Biodivers.*, 11(4), 571-80.
- [2] Davis, P.H. (1982) *Flora of Turkey and the East Aegean Islands*, Vol. 7., Edinburgh University Press, Edinburgh, 947s.
- [3] Boelens, M.H. and Jimenez, R. (1992) The chemical composition of Spanish myrtle oils, *J Essential Oil Res*, 4, 349-353.
- [4] Özek, T., Demirci, F. and Başer, K.H.C. (2009) Chemical composition of Turkish myrtle oil, *J Essential Oil Res*, 12, 541-544.
- [5] Baytop, T. (1999) *Türkiye'de Bitkiler ile Tedavi (Therapy with Medicinal Plants in Turkey, past and present)*, second ed. Nobel Tip Kitapevi, İstanbul.
- [6] Miguel, M., Bouchmaa, N., Aazza, S., Gaamoussi, F. and Lyoussi, B. (2014) Antioxidant, Anti-Inflammatory and Anti-Acetylcholinesterase Activities of Eleven Extracts of Moroccan Plants, *Fresen. Environ. Bull.*, 23(6), 1379-1392.
- [7] Hayder, N., Bouhleb, I., Skandrani, I., Kadri, M., Steiman, R., Guiraud, P., Mariotte, A.M., Ghedira, K., Dijoux-Franca, M.G. and Chekir-Ghedira, L. (2008) *In vitro* antioxidant and antigenotoxic potentials of myricetin-3-*O*-galactoside and myricetin-3-*O*-rhamnoside from *Myrtus communis*: Modulation of expression of genes involved in cell defence system using cDNA microarray, *Toxicol In Vitro*, 22(3), 567-581.
- [8] Karatas, M., Dogan, M., Emsen, B. and Aasim, M. (2015) Determination of *In Vitro* Free Radical Scavenging Activities of Various Extracts from *In Vitro* Propagated *Ceratophyllum demersum* L., *Fresen. Environ. Bull.*, 24(9a), 2946-2952.
- [9] Serce, S., Ercisli, S., Sengul, M., Gunduz, K. and Orhan, E. (2010) Antioxidant activities and fatty acid composition of wild grown myrtle (*Myrtus communis* L.) fruits, *Phcog Mag.*, 6, 9-12.
- [10] Jerkovic, I., Radionic, A. and Borcic, I. (2002) Comparative study of leaf, fruit and flower essential oils of Croatian *Myrtus communis* Linn. during a one year vegetative cycle, *J. Essent Oil Res*, 14(4), 266-270.
- [11] Rastogi, R.P. and Mehrotra, B.N. (1993) *Compendium of Indian Medicinal Plants (1980-1984)*, Central Drug Research Institute Lucknow, Vol. 3, Publications and Information Directorate, CSIR, New Delhi, p. 444.
- [12] Martin, T., Rubio, B., Villaescusa, L., Fernandez, L. and Diaz, A.M. (1999) Polyphenolic compounds from pericarps of *Myrtus communis*, *Pharmaceut Biol*, 37(1), 28-31.
- [13] Montoro, P., Tuberoso, C.L., Piacente, S., Perrone, A., Feo, V.D., Cabras, P. and Pizza, C. (2006) Stability and Antioxidant activity of Polyphenols in extracts of *Myrtus communis* L., *J Pharm Biomed Anal*, 41, 1614-1619.
- [14] Akin, M., Aktumsek, A. and Nostro, A. (2010) Antibacterial activity and composition of the essential oils of *Eucalyptus camaldulensis* Dehn. and *Myrtus communis* L. growing in Northern Cyprus, *Afr. J. Biotechnol.*, 9(4), 531-535.
- [15] Diaz, A.M. and Abeger, A. (1987) Phenolic compounds of the seeds of *Myrtus communis* L., *Plant Med Phytother*, 21(4), 317-322.
- [16] Alem, G., Mekonnen Y., Tiruneh, M. and Mulu, A. (2008) *In vitro* antibacterial activity of crude preparation of myrtle (*Myrtus communis*) on common human pathogens, *Ethiop Med J*, 46(1), 63-69.
- [17] Al-Saimary, I.E., Bakr, S.S., Jaffar, T., Al-Saimary, A.E., Salim, H. and Al-Muosawi, R. (2002) Effects of some plant extracts and antibiotics on *Pseudomonas aeruginosa* isolated from various burn cases, *Saudi Med J*, 23(7), 802-805.
- [18] Antonella, D., Giovanna, B., Paola, M., Antonio Mario, P.G., Mario, C., Bruno, T., Bianca, P., Antonio, M., Leonardo Antonio, S., Guido, F. and Anna Lucia, Z.S. (2007) *In vitro* activity of essential oil of *Myrtus communis* L. against *Helicobacter pylori*, *Int J Antimicrob Agents*, 30(6), 562-563.
- [19] Curini, M., Bianchi, A., Epifamo, F., Bruni, R., Torta, L. and Zambonelli, A. (2003) *In vitro* antifungal activity of essential oils of *Erigeron Canadensis* and *Myrtus communis* from France, *Chem Nat Comp*, 30(2), 191-194.
- [20] Vatan Oztopcu, P., Savaroglu, F., Iscen Filik, C., Kabadere, S., Ilhan, S. and Uyar, R. (2011) Antimicrobial and Antiproliferative Activities of *Homalothecium sericeum* (Hedw.) Schimp. Extracts, *Fresen. Environ. Bull.*, 20 (2a), 461-466.
- [21] Deuruaz, D. and Raynaud, J. (1993) Evaluation of the molluscicidal properties of *Myrtus communis* Linn., *Phytother Res*, 7(6), 428-430.
- [22] Traboulsi, A.F., Taoubi, K., El-Haj, S., Bessiere, J.M. and Rammal, S. (2002) Insecticidal properties of essential plant oils against the mosquito *Culex pipiens molestus* (Diptera: Culicidae), *Pest Manag Sci.*, 58(5), 491-495.
- [23] Ayvaz, A., Sagdic, O., Karaborklu, S. and

- Ozturk, I. (2008) Insecticidal activity of the essential oils from different plants against three stored-product insects, *J Insect Sci.*, 10(21), 1-13.
- [24] Twaij, H. and El-Jalil, H.A. (2009) Evaluation of Narcotic (Opioid like) analgesic activities of medicinal plants, *Europ J Sci Res.*, 33(1), 179-182.
- [25] Al-Hindawi, M.K., Al-Deen, I.H., Nabi, M.H. and Ismail, M.A. (1989) Anti-inflammatory activity of some Iraqi plants using intact rats, *J Ethnopharmacol*, 26(2), 163-168.
- [26] Sepici, A., Gurbuz, I., Cevik, C. and Yesilada, E. (2004) Hypoglycaemic effects of myrtle oil in normal and alloxan-diabetic rabbits, *J Ethnopharmacol*, 93(2-3), 311-318.
- [27] Dineel, A.S., Acikgoz, S., Cevik, C., Sengelen, M. and Yesilada, E. (2007) Effects of *in vivo* antioxidant enzyme activities of myrtle oil in normoglycemic and alloxan diabetic rabbits, *J Ethnopharmacol*, 110 (3), 498-503.
- [28] Fahim, A.B., El-Ghathai, M., Amesh, S. and Dhayabaran, D. (2009) Biochemical studies on the effect of phenolic compounds extracted from *Myrtus communis* in diabetic rats, *Tamilnadu J Vet Anim Sci.*, 5(3), 87-93.
- [29] Dukić, N.M., Bugarin, D., Grbović, S., Čulafić, D.M., Gačić, B.V., Orčić, D., Jovin, E. and Couladis, M. (2010) Essential Oil of *Myrtus communis* L. as a Potential Antioxidant and Antimutagenic Agents, *Molecules*, 15, 2759-2770.
- [30] Sumbul, S., Ahmad, M.A., Asif, M., Saud, I. and Akhtar, M. (2010) Evaluation of *Myrtus communis* Linn. berries (common myrtle) in experimental ulcer models in rats, *Hum Exp Toxicol*, 29(11), 935-944.
- [31] Elfellah, M.S., Akhter, M.H. and Khan, M.T. (1984) Antihyperglycaemic effect of an extract of *Myrtus communis* in streptozotocin-induced diabetes in mice, *J Ethnopharmacol*, 11(3), 275-281.
- [32] Tumen, I., Hafizoglu, H., Kilic, A., Donmez, I.E., Sivrikaya, H. and Reunanen, M. (2010) Yields and Constituents of Essential Oil from Cones of *Pinaceae* spp. Natively Grown in Turkey, *Molecules*, 15 (8), 5797-5806.
- [33] Tumen, I. and Reunanen, M. (2010) A comparative study on turpentine oils of oleoresins of *Pinus sylvestris* L. from three districts of Denizli, *Rec. Nat. Prod.*, 4, 224-229.
- [34] Ceker, S., Agar, G., Alpsoy, L., Nardemir, G. and Kizil, H.E. (2013) Protective Role of Essential Oils of *Calamintha nepeta* L. on Oxidative and Genotoxic Damage Caused by Aflatoxin B1 In Vitro, *Fresen. Environ. Bull.*, 22 (11), 3265-3270.
- [35] Adams, R.P. (2007) Identification of Essential Oil Components by Gas Chromatography/Mass Spectrometry, Allured Publishing: Carol Stream, IL, USA
- [36] Tumen, I., Suntar, I., Keles, H. and Küpeli Akkol, E. (2012) A therapeutic approach for wound healing by using essential oils of *Cupressus* and *Juniperus* species growing in Turkey, *Evid. Based Complement. Alternat. Med.*, Vol. 2012, Article ID 728281, 7 pages.
- [37] Tramontina, V.A., Machado, M.A., Nogueira Filho Gda R., Kim, S.H., Vizzioli, M.R. and Toledo, S. (2002) Effect of bismuth subgallate (local hemostatic agent) on wound healing in rats. Histological and histometric findings, *Brazilian Dental Journal*, 13, 11-16.
- [38] Sadaf, F., Saleem, R., Ahmed, M., Ahmad, S.I. and Navaid-ul, Z. (2006) Healing potential of cream containing extract of *Sphaeranthus indicus* on dermal wounds in guinea pigs, *J Ethnopharmacol*, 107, 161-163.
- [39] Süntar, I., Küpeli Akkol, E., Keles, H., Yesilada, E. and Sarker, S.D. (2013) Exploration of the wound healing potential of *Helichrysum graveolens* (Bieb.) Sweet: Isolation of apigenin as an active component, *J Ethnopharmacol*, 149, 103-110.
- [40] Shetty, B.S., Udupa, S.L., Udupa, A.L. and Somayaji, S.N. (2006) Effect of *Centella asiatica* L (Umbelliferae) on normal and dexamethasone-suppressed wound healing in wistar albino rats, *The International Journal of Lower Extremity Wounds*, 5, 137-143.
- [41] Suguna, L., Singh, S., Sivakumar, P., Sampath, P. and Chandrakasan, G. (2002) Influence of *Terminalia chebula* on dermal wound healing in rats, *Phytother Res*, 16, 227-31.
- [42] Lodhi, S., Pawar, R.S., Jain, A.P. and Singhai, A.K. (2006) Wound healing potential of *Tephrosia purpurea* (Linn.) Pers. in rats, *J. Ethnopharmacol*, 108, 204-210.
- [43] Whittle, B.A. (1964) The use of changes in capillary permeability in mice to distinguish between narcotic and non-narcotic analgesics, *Brit J Pharmacol*, 22, 246-253.
- [44] Yesilada, E. and Küpeli, E. (2007). *Clematis vitalba* L. aerial part exhibits potent anti-inflammatory, antinociceptive and antipyretic effects, *J Ethnopharmacol*, 110, 504-515.
- [45] Madden, J.W. and Peacock, E.E. (1971) Studies on the biology of collagen during wound healing. 3. Dynamic metabolism of scar collagen and remodeling of dermal wounds, *Ann Surg.*, 174(3), 511-520.
- [46] Maxia, A., Frau, M.A., Falconieri, D., Karchuli, M.S. and Kasture, S. (2011). Essential oil of *Myrtus communis* inhibits inflammation in rats by reducing serum IL-6 and TNF-alpha. *Nat Prod Commun.*, 6(10), 1545-8.
- [47] Romani, A., Coinu, R., Carta, S., Pinelli, P., Galardi, C., Vincieri, F.F. and Franconi, F. (2004) Evaluation of antioxidant effect of different extracts of *Myrtus communis* L., *Free Radic Res.*, 38(1), 97-103.

- [48] Nabavizadeh, M., Abbaszadegan, A., Gholami, A., Sheikhi, R., Shokouhi, M., Shams, M.S. and Ghasemi, Y. (2014) Chemical constituent and antimicrobial effect of essential oil from *Myrtus communis* leaves on microorganisms involved in persistent endodontic infection compared to two common endodontic irrigants: An *in vitro* study, *J Conservative Dentistry*, 17(5), 449-453.
- [49] Ximenes, R.M., de Moraes Nogueira, L., Cas-sundé, N.M., Jorge, R.J., dos Santos, S.M., Magalhães, L.P., Silva, M.R., de Barros Viana, G.S., Araújo, R.M., de Sena, K.X., de Albuquerque, J.F. and Martins, R.D. (2013) Antinociceptive and wound healing activities of *Croton adamantinus* Müll. Arg. essential oil, *J Nat Med.*, 67(4), 758-64.
- [50] Juergens, U.R. (2014) Anti-inflammatory properties of the monoterpene 1.8-cineole: current evidence for co-medication in inflammatory airway diseases, *Drug Res*, 64 (12), 638-646.
- [51] Adams, S. and Thrash, T.P. (2010) Methods for wound treatment and healing using limonene-based compositions. International Application WO2010/062933 A1, Patent Cooperation Treaty.
- [52] Amirghofran, Z., Hashemzadeh, R., Javidnia, K., Golmoghaddam, H. and Esmaeilbeig, A. (2011) In vitro immunomodulatory effects of extracts from three plants of the Labiatae family and isolation of the active compound, *J. Immunotoxicol.*, 8, 265-273.
- [53] Villegas, L.F., Marçalo, A., Martin, J., Fernández, I.D., Maldonado, H., Vaisberg, A.J. and Hammond, G.B. (2001) (+)- α -Bisbolol is the wound-healing principle of *Peperomia galioides*: Investigation of the in vivo wound-healing activity of related terpenoids, *J. Nat. Prod.*, 64, 1357-1359.
- [54] Kawata, J., Kameda, M., and Miyazawa, M. (2008) Cyclooxygenase-2 inhibitory effects of monoterpenoids with a p-methane skeleton, *Int. J. Essent. Oil Ther.*, 2, 145-148.
- [55] Hassan, S.B., Gali-Muhtasib, H., Göransson, H. and Larsson, R. (2010) Alpha terpineol: A potential anticancer agent which acts through suppressing NF- κ B signaling, *Anticancer Res.*, 30, 1911-1919.
- [56] Held, S., Schieberle, P. and Somoza, V. (2007) Identification of α -terpineol as an anti-inflammatory component of orange juice by in vitro and ex vivo studies. In *Recent Highlights in Flavor Chemistry & Biology*, 8th ed.; In Proceedings of the Wartburg Symposium on Flavor Chemistry and Biology, Eisenach, Germany, 27 February-2 March 2007; Deutsche Forschungsanstalt für Lebensmittelchemie: Garching, Germany, pp. 239-244.
- [57] Barreto, R.S.S., Albuquerque-Júnior, R.L.C., Araújo, A.A.S., Almeida, J.R.G.S., Santos, M.R.V., Barreto, A.S., DeSantana, J.M., Siqueira-Lima, P.S., Quintans, J.S.S. and Quintans-Júnior, L.J. (2014) A Systematic Review of the Wound-Healing Effects of Monoterpenes and Iridoid Derivatives, *Molecules*, 19, 846-862.

Received: 25.11.2016
Accepted: 12.06.2017

CORRESPONDING AUTHOR

Esra Akkol

Gazi University, Faculty of Pharmacy, Department of Pharmacognosy, 06330, Ankara, Turkey

e-mail: esrak@gazi.edu.tr

FIXED-BED COLUMN SORPTION OF ANTIMONY(III) BY POROUS COMPOSITE OF IRON OXIDES AND CARBON WITH EUCALYPTUS WOOD MICROSTRUCTURE

Yanhong Li^{1,2}, Xuehong Zhang^{1,2}, Yinian Zhu^{2,*}, Zongqiang Zhu², Liwei Xie²

¹College of Light Industry and Food Engineering, Guangxi University, Nanning, Guangxi 530004, P.R. China

²College of Environmental Science and Engineering, Guilin University of Technology, Guilin, Guangxi 541004, P.R. China

ABSTRACT

The fixed-bed column sorption-desorption of antimony(III) by porous composite of iron oxides and carbon with eucalyptus wood microstructure was experimentally studied. The breakthrough curves indicated that a larger sorbent mass and a smaller sorbent grain size prolonged the column life span. The increased influent concentration and flow rate caused the column exhaustion to occur earlier. The solution pH and operating temperature had negligible influence. All breakthrough curves could be well predicted with the Thomas, Yoon–Nelson and Clark models. The equilibrium sorption capacity reached 18.47 mg/g, which was near the predicted value of 18.64 mg/g according to the Thomas model. The sorption capacity of the unpulverized material as a novel filtration sorbent is comparable to fine particles of the pulverized material, synthetic and natural iron oxides.

KEYWORDS:

Fixed-bed column sorption; Antimony (III); Biomorph-genetic magnetic composite; Iron oxide; Carbon; Eucalyptus wood microstructure

INTRODUCTION

Antimony (Sb) is an important industrial material and is widely used as additives in the manufacture of chemicals ceramic enamels, retardant paint, battery grids, glassware, etc. [1-4]. Nevertheless, significant antimony pollution in surface water has been caused by its excessive exploitation and overuse [5, 6]. It exists widely in environment due to diverse industries and natural processes [3, 7], and is a potentially harmless and carcinogenic heavy metal [8]. The toxic effect of Sb is generally dependent on its oxidation state [7, 9]. In environments, Sb occurs in different valence states (3-, 0, 3+, and 5+), and mainly as inorganic Sb⁵⁺ and Sb³⁺ in water. The toxicity of Sb³⁺ is ten times bigger than that of Sb⁵⁺ [4, 9]. Some compounds of antimony are harmful to human body and long-term exposure to such antimony compounds can stimulate respiratory tract then cause

pneumoconiosis [1-3]. Due to antimony's toxicity, antimony and its compounds have been listed as priority pollutants early in the 1970's by the European Union [10] and the United States Environmental Protection Agency [11], which should be eliminated and controlled [1, 2, 8]. For antimony in drinking water, the maximum permissible concentrations are 6 and 10 µg/L according to the USEPA and EU standards, respectively. The China drinking water standard for antimony is 5 µg/L, which is the same as the value recommend by the World Health Organizations (WHO) [8, 12].

For centuries, the largest emission source into the environment is the antimony mining and smelting. China is one of the biggest country in the antimony reserves and production in the world [5, 6], and large amount of antimony has been discharged into the environment as a consequence of inappropriate treatment and disposal of antimony-containing solid wastes and wastewaters in mining and smelting, which has caused serious environmental pollution [6, 12]. Environment and human health problems caused by Sb have been also reported in Australia, Bangladesh and Japan [5, 6]. Antimony is one of the least investigated toxic metals and researches on antimony pollution control are also very lack [7].

Different technologies, such as sorption, sorption in a fixed-bed column, ion exchange, reduction and precipitation, membrane filtration, reverse osmosis, etc., have been developed to treat antimony-containing wastewaters [4, 7, 13-20]. Due to its simplicity and a lesser amount of harmful byproducts, the sorption technology is usually considered as one of the most efficient methods to separate and remove antimony from wastewaters [21-24]. One of the difficulties faced by the sorption technique is to develop effective and low cost sorbents that could remove antimony from aqueous solutions [25]. Knowledge about the application of the sorption technology in the removal of Sb from wastewater is also very little in literatures [7, 26-40]. Generally, grinding of sorbents can increase their sorption capacity and speed. However, due to potential clogging, extremely fine particles of sorbents are not applicable to be used in column sorption. Therefore, an objective of many researches is to find the optimal sorbent that can be packed in column to remove toxic metals

[41-44].

The porous composite of $\text{Fe}_3\text{O}_4/\text{Fe}_2\text{O}_3/\text{C}$ (PC-Fe/C) has been developed using eucalyptus wood as microstructural biotemplate and confirmed to be effective for sorption of antimony through batch experiments [45]. Nevertheless, the sorption parameters gained from batch experiments are usually not applicable to column operations. And so, it is still needed to carry out equilibrium studies by using fixed-bed columns [46]. The main purpose of the present work is to investigate the effectiveness of using PC-Fe/C for the column sorption of Sb(III) from aqueous solution. The effects of influent initial concentration, flow rate, influent pH, sorbent mass, sorbent grain size and operating temperature on antimony(III) sorption by the PC-Fe/C-packed column were studied. The Thomas, Yoon–Nelson, Adams–Bohart, Wolborska and Clark models were used to fit the performance.

MATERIALS AND METHODS

Sorbent preparation and characterization.

To increase the connectivity among cellular and pores of the bio-templates effectively, *Eucalyptus* wood chips ($30 \times 10 \times 3 \text{ mm}^3$) as biotemplates were firstly boiled in 5% ammonia solution for six hours to extract fats, fatty acid, tropolones, gums, etc. The wood chips were washed with pure water and dried at 80°C for one day. After that, the wood chips after extraction treatment were soaked in a precursor solution of $1.2 \text{ mol/L Fe}(\text{NO}_3)_3$ in a binary (1:1) water/ethanol solvent mixture at 60°C for 3 days. The soaked wood chips were then taken out from the precursor and dried at 80°C for one day. This soaking-drying process was repeated three times. The soaked-dried wood chips were finally heated in a muffle furnace gradually to 600°C at $4^\circ\text{C}/\text{min}$ and then kept at 600°C for 3 hours. After cooling to room temperature, the porous composite of $\text{Fe}_3\text{O}_4/\text{Fe}_2\text{O}_3/\text{C}$ (PC-Fe/C) with eucalyptus wood hierarchical microstructure was obtained.

An Element Analyzer (EA2400II, PerkinElmer) was used to determine the chemical composition of the prepared $\text{Fe}_3\text{O}_4/\text{Fe}_2\text{O}_3/\text{C}$ sorbent (PC-Fe/C). The specific surface area of PC-Fe/C was measured by the Brunauer-Emmett-Teller (BET) method using a Quantachrome NOVAe1000. The prepared PC-Fe/C sorbent was also analyzed with an X-ray diffractometer (X'Pert PRO, PANalytical B.V.) and identified by comparing the obtained pattern to the standards of the International Center for Diffraction Data (ICDD). The FT-IR spectra from 4000 to 400 cm^{-1} were recorded in a form of KBr pellets using a FT-IR spectrophotometer (Nicolet Nexus 470, Thermo Fisher Scientific Inc.). Additionally, the morphology of the prepared PC-Fe/C sorbent was observed by using a scanning electron

microscopy (Jeol JSM-6380LV, Japan Electron Optics Ltd.).

Column experiments. Sorption. For the rapid small-scale column test (RSSCT), four columns with a length of 140 mm and an inner diameter of 12.8 mm were employed. A plastic mesh and fibre glass were put at the column bottom and top to support the sorbent, avoid the sorbent loss and maintain dense degree of the sorbent during the sorption process. A predesigned weight of the PC-Fe/C sorbent was packed into each column. Before the experiment started, the sorbent packed in the column was wetted with ultrapure water in downward flow direction to withdraw the trapped air among the particles. Stock solution of 200 mg/L Sb(III) was prepared by dissolving 0.274 g potassium antimony tartrate ($\text{KSbO} \cdot \text{C}_4\text{H}_4\text{O}_8$) in 500 mL of water. The Sb(III) working solution was continuously fed downward into the column by a peristaltic pump (BL100-DG, Changzhou PreFluid Technology Co., Ltd., China). At regular time intervals (20 min) in all the sorption, the effluent was collected and filtered through a $0.22 \mu\text{m}$ membrane filter. The sampled effluent was then preserved with acidification and stored at 4°C until metal analysis. The residual Sb concentration was determined by using an atomic fluorescence spectrometry (SA-20, Beijing Titan Instruments Co., Ltd., China).

The sorption experiments were carried out with predesigned PC-Fe/C columns and different influent Sb(III) concentrations to investigate the influence of the operating condition on sorption removal capacity. The effects of influent flow rate, initial Sb(III) concentration, influent pH, sorbent mass, sorbent grain size and operating temperature were studied. The stock solution of Sb(III) was diluted to 10 , 20 , 30 and 50 mg/L and the influent pH was adjusted to 2 , 5 and 8 to investigate the ability of PC-Fe/C in removing Sb(III) from different solutions. The flow rate of Sb(III) solution was adjusted to 3.434 , 5.136 , 10.27 and 15.41 mL/min to examine the influence of influent flow rate. For evaluation of the effect of sorbent mass, the PC-Fe/C amounts were varied according to different weights (1 , 2 , 3 , and 4 g or 0.85 , 1.69 , 2.54 and 3.38 cm in bed depth) and were packed in separate columns. The PC-Fe/C sorbent was ground and sieved to the various sizes of $20\sim 40$ mesh ($0.841\sim 0.4\text{mm}$), $40\sim 60$ mesh ($0.4\sim 0.25\text{mm}$), $60\sim 80$ mesh ($0.25\sim 0.177\text{mm}$), $80\sim 100$ mesh ($0.177\sim 0.149\text{mm}$) or <100 mesh ($<0.149\text{mm}$) to investigate the effect of sorbent grain size. 25°C , 35°C or 45°C were chosen to study the effect of temperature.

Desorption. 0.50 g of the PC-Fe/C material (<100 mesh) was first agitated (150 rpm) with 50 mL of 20mg/L Sb(III) solution of pH 8 by a thermostatic water bath oscillator for 1 h at 35°C . And then, the Sb(III)-saturated sorbent was taken out and agitated

(150 rpm) for 1h at room temperature with 50 mL of 0.1mol/L desorption solvent (NaOH, NaHCO₃, NaCl or H₂O). Based on the result, the optimized desorption solvent was chosen for further column investigation. In each stage, the liquid was decanted from the settled solid material and analyzed for Sb(III). Three sorption–desorption cycles were accomplished in a continuous fixed-bed column. The Sb(III) working solution was first continuously fed downward into the column by a peristaltic pump. The influent initial concentration, the influent flow rate, the influent, the sorbent mass, the sorbent grain size and temperature were controlled at 20 mg/L, Q=5.136 mL/min, pH=8, m=2 g, <100 mesh and T=35°C, respectively. At the time interval of 20min, the effluent was collected, filtered and analyzed. When the effluent reached the exhaustion point (the exhaustion concentration = 18mg/L), the feeding of the Sb(III) working solution was stopped. Then, 0.1mol/L NaOH solution as desorption solvent was continuously fed upward into the column by a peristaltic pump. At the time interval of 20min, the effluent was also collected, filtered and analyzed. The effect of desorption solvent concentration, influent rate and temperature was studied.

Mathematical description of fixed-bed column studies. The total sorbed Sb(III) (q_{total}) by the column can be calculated by integrating the plot of the sorbed Sb(III) concentration ($C_{\text{ad}}=C_0-C_t$) against the flow time (t). The area (A) under this integrated plot is substituted in Eq.(1) to determine q_{total} .

$$q_{\text{total}} (\text{mg}) = \frac{QA}{1000} = \frac{Q}{1000} \int_{t=0}^{t=t_{\text{total}}} C_{\text{ad}} dt \quad (1)$$

The total amount of Sb(III) flowing through the column (m_{total}) can be calculated with Eq.(2).

$$m_{\text{total}} (\text{mg}) = \frac{C_0 Q t_{\text{total}}}{1000} \quad (2)$$

where, the t_{total} and Q represent the total flow time (min) and the volumetric flow rate (mL/min), respectively.

The total removal percentage of Sb(III) can be used to evaluate the column performance, as expressed in Eq.(3).

$$\text{Total removal percentage (Y)} = \frac{q_{\text{total}}}{m_{\text{total}}} \times 100 \quad (3)$$

The column maximum sorption capacity, also known as the equilibrium metal ion uptake (q_e), is calculated using Eq.(4).

$$q_e (\text{mg/g}) = \frac{q_{\text{total}}}{x} \quad (4)$$

in which, x is the unit mass of sorbent packed in the column.

Sorption modeling for fixed bed column studies. Generally, the breakthrough curve of the continuous fixed bed system can be expressed as C/C_0 versus the flow time (t), in which C_0 and C_t

represent the influent and effluent Sb(III) concentrations, respectively [46, 47]. The application of the column sorption kinetic models is essential to provide further description of the column performance or to evaluate the strengths and weaknesses for the current sorbent and column design. The column parameters show the most important effects on the column performance and optimum operation factors that contributed to the effective removal of Sb(III) ions. Hence, suitable parameters are important for the column operation to achieve optimum performance. Additionally, the theoretical models can be applied to the experimental data to further describe the sorption mechanism. Because the sorption process is not at a steady state as the influent flows through the fixed-bed column under predesigned operating conditions, it is not easy to express the dynamic behavior of sorbate in the column. However, the modeling of data has been made in this work using the mathematical models such as the Thomas, Yoon–Nelson, Adams–Bohart, Wolborska and Clark models, which were constructed to describe and predict the dynamic behavior of the break through curves and have been used by various authors [48]. The theoretical predicted points (lines) with the five models were superposed on the breakthrough curves of the experimental results (points).

The Thomas model is among the models commonly selected to conduct prediction of the breakthrough results [49]. The Thomas model has the following linearized form:

$$\ln \left[\frac{C_0}{C_t} - 1 \right] = \frac{k_{\text{Th}} q_e m}{Q} - k_{\text{Th}} C_0 t \quad (5)$$

where k_{Th} is the Thomas rate constant (mL/min·mg) and q_e is the column maximum sorption capacity (mg/g), which can be determined from a plot of $\ln[(C_0/C_t)-1]$ against t at a given flow rate.

The Yoon–Nelson model is known to be a simple theoretical model because less column data is needed to construct the model, and it is suitable for the single component system [49]. The linearized equation can be described as:

$$\ln \left[\frac{C_t}{C_0 - C_t} \right] = k_{\text{YN}} t - \tau k_{\text{YN}} \quad (6)$$

in which, k_{YN} is the rate constant (1/min) and τ is the time required for 50% sorbate breakthrough (min), which can be obtained from the plot of $\ln[C_t/(C_0-C_t)]$ versus t . The linearized Yoon–Nelson equation is similar to the linearized form of the Thomas model.

The Clark model combines the mass transfer concept with the Freundlich equation:

$$\ln \left[\left(\frac{C_t}{C_0} \right)^{1-n} - 1 \right] = \ln A - rt \quad (7)$$

TABLE 1
Parameters of the Thomas model and the Yoon–Nelson model using linear regression analysis and the equilibrium Sb(III) uptake (q_e) and the total removal percentage (Y) for Sb(III) sorption to PC-Fe/C under different conditions.

Operating condition					Thomas model				Yoon–Nelson model								R ²	
In-flu-ent concn. C ₀	Flow rate Q	Sorbent mass x	Sorbent grain size	Op-erating temp. T	In-flu-ent pH	k _{Th}	q _{e,calc}	q _{e,exp}	Y	k _{YN}	τ _{calc}	τ _{exp}	Δτ/τ _{exp}	t _{1,calc}	t _{1,exp}	t _{2,calc}		t _{2,exp}
mg/L	mL/min	g	mesh	°C		mL/min·mg	mg/g	mg/g	%	min ⁻¹	min	min	%	min	min	min	min	
10	5.136	2	<100	35	8	0.00203	11.38	11.33	80.96	0.0203	442	449	1.49	298	312	551	531	0.9785
20	5.136	2	<100	35	8	0.00112	18.64	18.47	74.16	0.0224	363	366	0.95	199	166	461	469	0.9479
30	5.136	2	<100	35	8	0.00094	19.92	19.13	68.03	0.0283	259	238	8.67	115	106	336	346	0.9584
50	5.136	2	<100	35	8	0.00076	12.58	12.33	58.19	0.0379	98	105	6.63	-23	<5	156	141	0.9182
20	3.434	2	<100	35	8	0.00112	14.56	14.35	76.67	0.0224	424	419	1.22	260	255	522	531	0.9876
20	5.136	2	<100	35	8	0.00112	18.64	18.47	74.16	0.0224	363	366	0.95	199	166	461	469	0.9479
20	10.27	2	<100	35	8	0.00112	26.58	25.71	68.03	0.0225	259	249	3.95	96	112	357	357	0.9719
20	15.41	2	<100	35	8	0.00142	27.48	25.79	58.19	0.0283	178	155	15.05	49	53	256	266	0.9399
20	5.136	1	<100	35	8	0.00147	21.73	21.06	67.23	0.0293	212	198	6.84	87	85	287	289	0.9798
20	5.136	2	<100	35	8	0.00112	18.64	18.47	74.16	0.0224	363	366	0.95	199	166	461	469	0.9479
20	5.136	3	<100	35	8	0.00097	16.45	16.12	77.82	0.0193	480	463	3.76	291	293	594	600	0.9768
20	5.136	4	<100	35	8	0.00079	14.56	14.29	76.74	0.0158	567	545	4.02	335	372	706	701	0.9889
20	5.136	2	20-40	35	8	0.00151	8.66	8.30	60.98	0.0302	169	146	15.53	47	42	241	249	0.9649
20	5.136	2	40-60	35	8	0.00125	10.74	10.13	60.69	0.0250	209	192	8.91	63	66	297	310	0.9455
20	5.136	2	60-80	35	8	0.00125	12.09	11.73	66.20	0.0250	235	212	11.06	89	87	323	330	0.9767
20	5.136	2	80-100	35	8	0.00107	15.72	15.10	66.07	0.0213	306	289	5.89	134	127	409	433	0.9677
20	5.136	2	<100	35	8	0.00112	18.64	18.47	74.16	0.0224	363	366	0.95	199	166	461	469	0.9479
20	5.136	2	<100	25	8	0.00096	19.51	18.83	69.84	0.0192	380	341	11.42	188	198	495	502	0.9779
20	5.136	2	<100	35	8	0.00112	18.64	18.47	74.16	0.0224	363	366	0.95	199	166	461	469	0.9479
20	5.136	2	<100	45	8	0.00091	18.99	18.67	71.98	0.0180	370	355	4.16	167	184	491	483	0.9857
20	5.136	2	<100	35	2	0.00096	17.96	17.79	74.49	0.0192	350	365	4.22	159	161	464	453	0.9596
20	5.136	2	<100	35	5	0.00099	19.00	18.59	71.68	0.0198	370	365	1.35	185	175	481	489	0.9807
20	5.136	2	<100	35	8	0.00112	18.64	18.47	74.16	0.0224	363	366	0.95	199	166	461	469	0.9479

Note: the subscripts ‘exp’ and ‘calc’ show the experimental and calculated values.

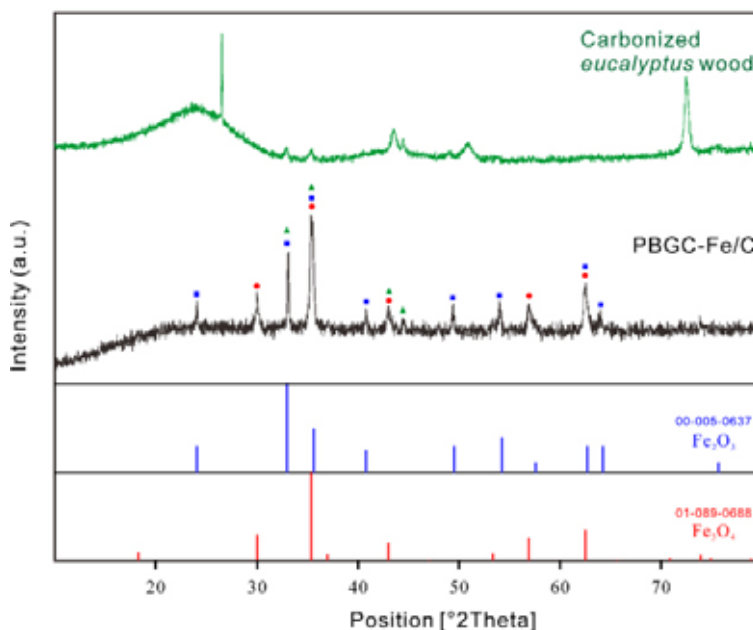


FIGURE 1
XRD patterns of the PC-Fe/C sorbent prepared with eucalyptus wood biotemplate.

where n is the Freundlich constant, A is the constant of the Clark model (min) and r is the sorption rate (mg/L·min).

The Adams–Bohart model is usually selected for the prediction of the breakthrough for the initial part of the sorption process. The model can be described as Eq.(8):

$$\ln \left[\frac{C_t}{C_0} \right] = k_{AB} C_0 t - k_{AB} N_0 \frac{Z}{U_0} \quad (8)$$

where the k_{AB} represents the Adams–Bohart kinetic constant (L/mg min). The Z and N_0 are the bed depth of column (cm) and the saturation concentration (mg/L), respectively. The U_0 is the linear velocity (cm/min) determined from the calculation of volumetric flow rate over the bed section area.

The Wolborska model can also be used to describe the breakthrough for the initial part of the sorption dynamics with Eq.(9):

$$\ln \left[\frac{C_t}{C_o} \right] = \frac{\beta_a C_o}{N_o} t - \frac{\beta_a Z}{U_o} \quad (9)$$

where β_a is the kinetic coefficient of the external mass transfer (1/min). The Wolborska expression is the same as the Adams–Bohart equation when $k_{AB} = \beta_a / N_o$.

RESULTS AND DISCUSSION

Characterization of the sorbent. The elemental compositions of Fe, O, C and H for the prepared $Fe_3O_4/Fe_2O_3/C$ (PC-Fe/C) material were determined to be about 62.51~65.37%, 20.46~20.52%, 10.73~10.96% and 3.04~5.52%, respectively. The BET surface area of the unpulverized PC-Fe/C was determined to be 59.2 m²/g, which was comparable to those for synthetic or naturally occurring iron oxides [50]. The XRD characterization indicated that the PC-Fe/C sorbent was composed of magnetite (Fe_3O_4), hematite ($\alpha-Fe_2O_3$) and carbon (Figure 1).

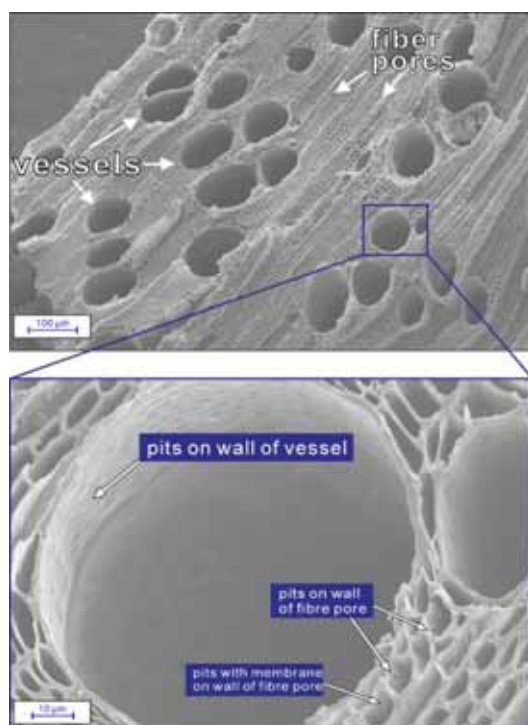


FIGURE 2
SEM result of the PC-Fe/C sorbent prepared with eucalyptus wood biotemplate.

The PC-Fe/C sorbent preserved the microstructure of eucalyptus wood perfectly (Figure 2). Pores of three different sizes were retained from the wood biotemplate, i.e., macropores, mesopores and micropores, which originated from vessels (widths 70~120 µm), fibre pores (widths 4.1~6.4 µm) and pits on the walls of the vessels and fibre pores

(widths 0.1~1.3 µm), respectively (Figure 2). The extracting pre-treatment could obviously increase the interpore connectivity.

Column sorption. Effect of influent concentration. The initial concentrations of Sb(III) were varied to 10, 20, 30 and 50 mg/L to find the optimum performance of the continuous fixed-bed column at 5.136 mL/min flow rate. With the increase in initial Sb(III) concentrations, the equilibrium uptake of Sb(III) ions was observed to increase (Figure 3, Table 1). The un-sorbed metal concentrations at the equilibrium also showed increased values along with the higher initial concentrations. This indicated that the bed saturated faster when a large amount of Sb(III) ions were introduced to the sorbent column. In the plot of the Sb(III) breakthrough curve, all four initial concentrations experienced exhaustion. From the observation, the PC-Fe/C is likely to be favorable for Sb(III) sorption. For the higher load of metal ions, the column performances were rapid initially and remained constant at the equilibrium after the removal efficiency started to decrease.

The breakthrough happened gradually and the breakthrough curves were dispersed at smaller influent Sb(III) concentrations. The sharper breakthrough curves appeared as the influent Sb(III) concentrations increased (Figure 3). The breakthrough ($C_t = 0.5$ mg/L) at an influent Sb(III) concentration of 50 mg/L occurred after <5min (<25.68mL of effluent solution) while the breakpoint time ($C_t = 0.5$ mg/L) at an influent Sb(III) concentration of 10mg/L appeared after 312min (1602.43mL of effluent solution) (Table 1). The breakthrough time increased with decreasing influent Sb(III) concentration since the sorption sites in the fixed-bed became more slowly saturated. A increased influent Sb(III) concentration caused an early breakpoint time and the treated volume was the smallest at the highest influent Sb(III) concentration because the higher concentration gradient resulted in a faster transport as a consequence of an increased mass transfer coefficient or increased diffusion coefficient, i.e., the difference between the Sb(III) concentration in the solution and the Sb(III) concentration on the sorbent is the driving force for sorption [51]. A larger concentration difference gives a larger driving force for sorption and results in a larger sorption capacity of the column fed. Additionally, the availability of the Sb(III) ions for the sorption sites was more at larger influent Sb(III) concentration.

The equilibrium Sb(III) uptake (q_e) and the total Sb(III) removal percentage (Y) are also showed in Table 1. The initial Sb(III) concentration in the influent can affect the sorption to some extent. The equilibrium sorption capacities ($q_{e,exp}$) were 11.33 mg/g, 18.47 mg/g, 19.13 mg/g and 12.33 mg/g for the influent Sb(III) concentrations of 10 mg/L, 20 mg/L, 30 mg/L and 50 mg/L, respectively. The total Sb(III) removal percentages decreased from 80.96%

to 58.19% with the increasing influent Sb(III) concentration from 10 to 50 mg/L. This indicated that the equilibrium Sb(III) uptake ($q_{e,exp}$) increased from 11.33 mg/g to 19.13 mg/g with the increasing influent Sb(III) concentration from 10 to 30 mg/L. While a further increase of the influent Sb(III) concentration to 50mg/L negatively affected the sorption capacity. At a lower Sb(III) concentration in the feed, the inflow sorbate molecules were commensurate to the active sites on the surface of the sorbent. While on the contrary, outrageous inflow of Sb(III) ions (>30 mg/L) outstripped the limited available active sites on the sorbent surface. Increase in the influent Sb(III) concentration increased the concentration gradient which has also been found by other researchers to overcome mass transfer resistance as well as increasing the sorption capacity [52, 53].

This indicated that the bed has been saturated faster when higher amounts of Sb(III) ions were introduced into the column reactor [46, 47, 54].

Effect of influent flow rate. The flow rate of metal solution into the column is among the parameters that influence the removal capacity of the bed column [49, 54]. An increase in the influent flow rate into the sorption column was synonymous with an increase in mass flow [53]. The flow rates (Q) were varied to 3.434, 5.136, 10.27 and 15.41 mL/min for the column. The sorption data versus flow rate were plotted in Figure 4, and the equilibrium Sb(III) uptake (q_e) and the total Sb(III) removal percentage (Y) are showed in Table 1.

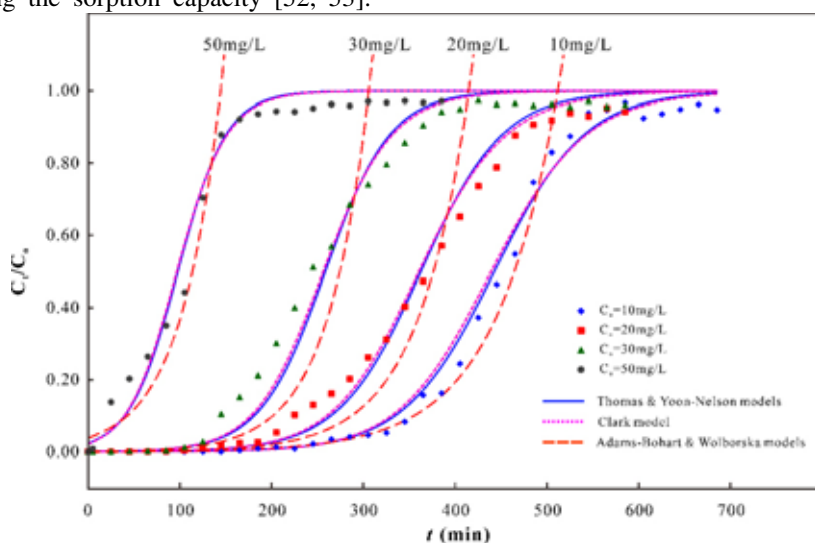


FIGURE 3

Effect of influent concentration on breakthrough curve for Sb(III) sorption removal by the PC-Fe/C sorbent prepared with eucalyptus wood template (flow rate: 5.136 mL/min; pH: 8; sorbent mass: 2g; sorbent grain size: <100mesh; operating temperature: 35°C).

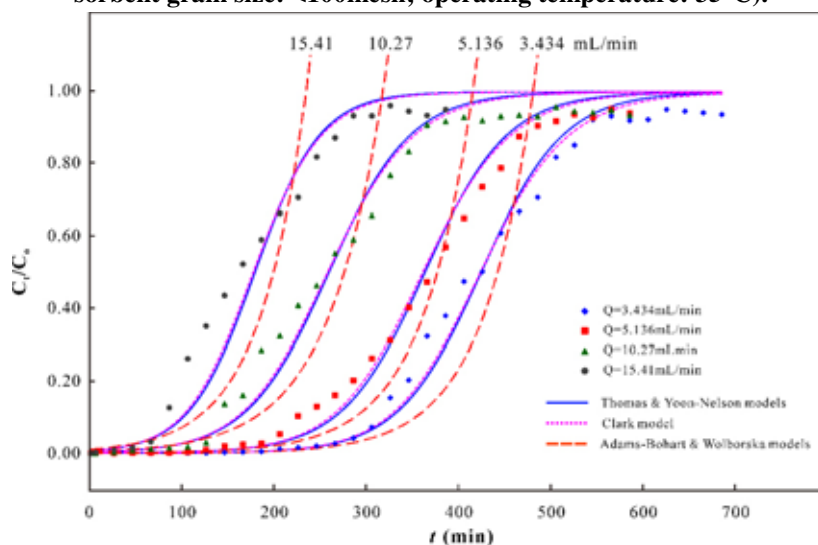


FIGURE 4

Effect of influent flow rate on breakthrough curve for Sb(III) sorption removal by the PC-Fe/C sorbent prepared with eucalyptus wood template (influent Sb(III) concentration: 20 mg/L; pH: 8; sorbent mass: 2g; sorbent grain size: <100mesh; operating temperature: 35°C).

For the lowest flow rate applied in the columns system, 3.434 and 5.136 mL/min, the breakthrough curves in the column (C_t/C_0) were observed to have a gradual curve than the 10.27 and 15.41 mL/min. While for the highest flow rate, 15.41 mL/min, the breakthrough curve (C_t/C_0) of Sb(III) was seen to increase drastically at the initial part of the operation (Figure 4). The maximum sorption capacity of the columns decreased with the decreased influent flow rates. At the equilibrium, the un-sorbed Sb(III) concentrations were seen to be high and increased according to the flow rates. The influent flow rate significantly influenced the contact time between the sorbate and sorbent, which was comparatively long

with the decreased flow rate. Hence, at the beginning of operation, the sorption was incomplete and led to steep breakthrough result [49, 54].

As indicated in Figure 4 and Table 1, at the lowest flow rate of 3.434 mL/min, comparatively the larger equilibrium Sb(III) uptake value (q_e) was observed for Sb(III) sorption to the PC-Fe/C at the beginning of operation. However, as the operation progressed, the effluent Sb(III) concentration would quickly rise to the influent Sb(III) concentration and the bed in the PC-Fe/C column became saturated with Sb(III). The breakpoint time decreased with increasing flow rate. Much sharper breakthrough

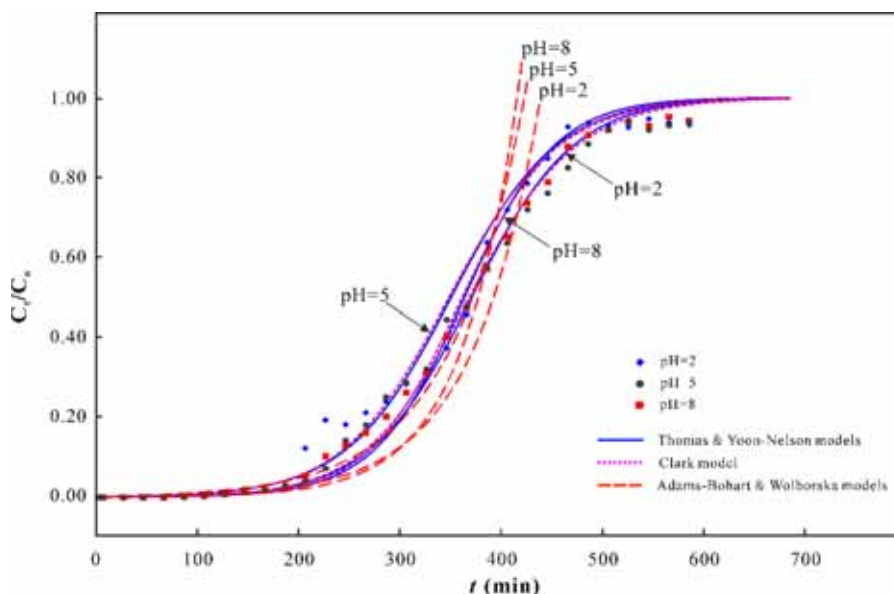


FIGURE 5

Effect of influent pH on breakthrough curve for Sb(III) sorption removal by the PC-Fe/C sorbent prepared with eucalyptus wood template (influent Sb(III) concentration: 20 mg/L; flow rate: 5.136 mL/min; sorbent mass: 2g; sorbent grain size: <100mesh; operating temperature: 35°C).

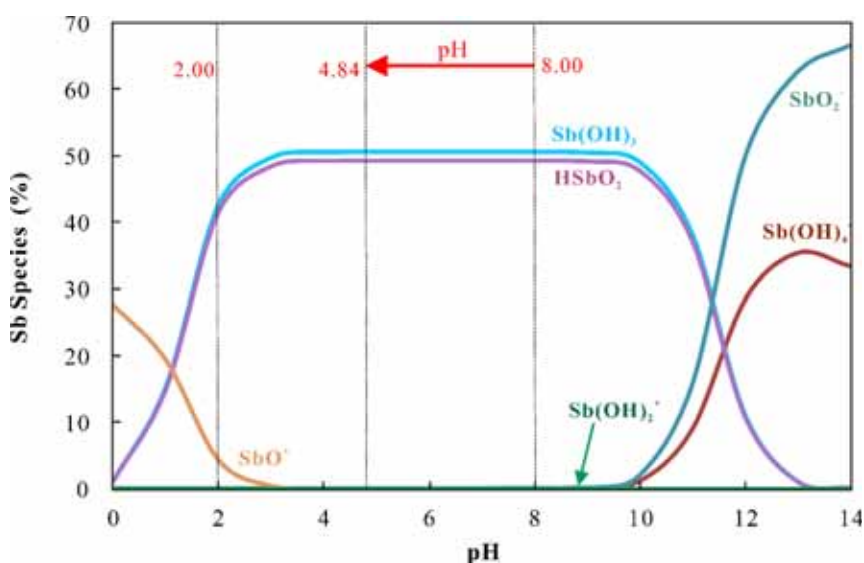


FIGURE 6

Variation of the Sb(III) species distribution with solution pHs (Sb=20mg/L, 35°C).

curve was obtained by the PC-Fe/C at a higher flow rate. At the slow flow rate of 3.434 mL/min, the breakthrough time was elongated as compared to the higher flow rate of 15.41 mL/min. Although longer residence time experienced at lower flow rates allow for diffusion of the Sb(III) ions, the q_e value rose from 14.35 mg/g to 25.79 mg/g with the flow rate increasing from 3.434 mL/min to 15.41 mL/min, because the total Sb(III) influent volume at the exhausting point $C_t/C_0=0.9$ increased from 1823 mL to 4099 mL, i.e., the total amounts of inlet Sb(III) were 36.47, 48.18, 73.33 and 81.98 g at the flow rates of 3.434, 5.136, 10.27 and 15.41 mL/min, respectively. Early saturation of sorption column sorbent bed was associated with higher mass transfer coefficient emanating from higher flow rate. So lower flow rate would enhance the sorption of Sb(III) on the PC-Fe/C bed and slower the breakthrough, i.e., a decrease in the flow rate would significantly increase the breakthrough time reaching saturation (Figure 4, Table 1).

Figure 4 and Table 1 indicated also that the removal efficiency was higher at lower flow rate. Sb(III) had a longer time in contact with sorbent at a low influent flow rate, which caused a greater removal of Sb(III) ions in the PC-Fe/C column. The total sorbed Sb(III) quantity also decreased from 76.67% to 58.19% with increasing flow rate from 3.434 mL/min to 15.41 mL/min. Meanwhile, the breakthrough curves become steeper and the column operation reached the breakthrough rapidly. The reason is that the contact time between the sorbate and the sorbent was decreased and the rate of mass transfer increased at a higher flow rate, i.e. the amount of Sb(III) sorbed onto unit bed depth (mass transfer zone) increased with increase in flow rate resulting in faster saturation and early breakthrough [46, 51].

The speed of the influent remarkably affected the contact between the sorbate and sorbent. This can be described by the fact that the residence of the sorbate was more at lower flow rate and so, the sorbent had longer time to bind metal ions effectively [49, 54]. In other words, the Sb(III) influent might leave the column before the equilibrium reached, if the residence time of Sb(III) ions in the PC-Fe/C column was not long enough to reach the sorption equilibrium at a particular flow rate. The sorbent attained saturated easily at a high flow rate. Hence, the sorption was incomplete and resulted in steep breakthrough curves at the beginning of operation [54, 55].

Effect of influent pH. The influent pH is one of the most important parameters affecting the sorption capacity and efficiency. The sorption mechanism from aqueous solution onto the sorbent surface is related to the solution pH, which reflects the character of the physico-chemical interaction between the adsorptive sites of sorbent and the species in solution [34, 56]. The Sb(III) sorption experiment was made

at various pH values of 2.0, 5.0 and 8.0 to investigate the effects of the pH variation on Sb(III) sorption in the PC-Fe/C column using a plot of dimensionless concentration (C_t/C_0) versus time (t) (Figure 5). The variations of the equilibrium Sb(III) uptake (q_e) and the total Sb(III) removal percentage (Y) with the influent pH obtained from the column system researches were also given in Table 1. The sorption removal of Sb(III) was more efficient at the influent pHs of 5 and 8 than pH 2. The equilibrium Sb(III) uptakes were 17.79 mg/g at influent pH 2, 18.59 mg/g at the influent pH 5 and 18.47 mg/g at pH 8, respectively. As shown in Figure 5 and Table 1, the times needed for the 50% sorbate breakthrough (τ_{exp}) were 365 min, 365 min and 366 min at the influent pHs of 2, 5 and 8, respectively. This means that the breakthrough curves were not affected by the influent pH, i.e., the breakthrough curves shifted not obviously with an increasing influent pH in the present work.

The sorption of Sb(III) ions was greatly dependent on the solution pH because it can affect not only the solubility of the metal ions, but also the ionization state of all functional groups existing on the sorbent surface at the same time. It was observed from the graph of the variation of the concentrations of the antimony(III) species with pH obtained using the PHREEQC program that Sb(III) exists as neutral molecules, i.e., HSbO_2^0 and Sb(OH)_3^0 species, at the comprehensive region of pH 3~10, accounting for more than 99 per cent of the total Sb(III) in solution (Figure 6). In more acidic solution of pH<3 Sb(III) exists as monovalent ions [SbO^+ , Sb(OH)_2^+] while in more alkaline solution of pH>10, it exists as antimonic ions [H_2SbO_3^- or Sb(OH)_4^-] [31, 38]. Additionally, when Fe^{2+} and Fe^{3+} are present in water, they will hydrolyze as follows: $\text{Fe}^{2+} + \text{H}_2\text{O} = \text{Fe(OH)}_2 + \text{H}^+$ or $\text{Fe}^{3+} + \text{H}_2\text{O} = \text{Fe(OH)}_3 + \text{H}^+$. Consequently, with the increase in the concentration of H^+ , the pH decreased from 8.00 to 4.84 (Figure 6), which will in turn make the balance of the reactions from the right to the left. Since ion hydroxides are colloids, and it is benefit to purify the wastewater, so the removal efficiency decreased as the concentration of ion hydroxides decreased, which is also one reason for the low sorption capacity at pH 2 [38]. The competition for the sorption sites between H^+ and the cationic Sb species [SbO^+ and Sb(OH)_2^+] might also result in a lower sorption capacity at pH<2~3 [31]. On the other hand, the competition for the binding to the sorbent surface between OH^- and the dominant anionic Sb species [SbO_2^- and Sb(OH)_4^-] might cause a slightly decrease in sorption capacity at higher pH (pH 8) [31]. Similar results have also been reported for Sb sorption on some other sorbents [31, 57-59]. The sorption of Sb(III) shows no noteworthy variation in the pH range between 3 and 8. A similar pH-dependence of Sb(III) sorption on Fe-oxide-rich red earth soils in the pH range of 3~10 was also reported [40, 60].

Speciation of antimony in solution showed that it existed as oxyanions like $\text{Sb}(\text{OH})_3^0$ in the pH range of 2–12. Surface charge of Fe_3O_4 powder became positive under such pH. Sorption of oxyanions on oxide/hydroxide surfaces in acidic aqueous environment is primarily driven by coulombic attraction between positively charged surface of oxides/hydroxides and negatively charged oxyanions.

Clearly, the solution pH of 3–10 had negligible

influence on the removal of $\text{Sb}(\text{III})$. Previous researches also indicated that the uptake of $\text{Sb}(\text{III})$ by hydroxyapatite (at pH from 5 to 10) [28] or by goethite (at pH from 2 to 12) or by the hematite modified magnetic nanoparticles (at pH from 3 to 11) was not obviously affected by solution pH. Thus, considering the surface sites as Lewis acids, the interaction of $\text{Sb}(\text{III})$ with magnetite and hematite in the PC-Fe/C sorbent would be strong and thus the complexation could remain stable over a broader pH range [35].

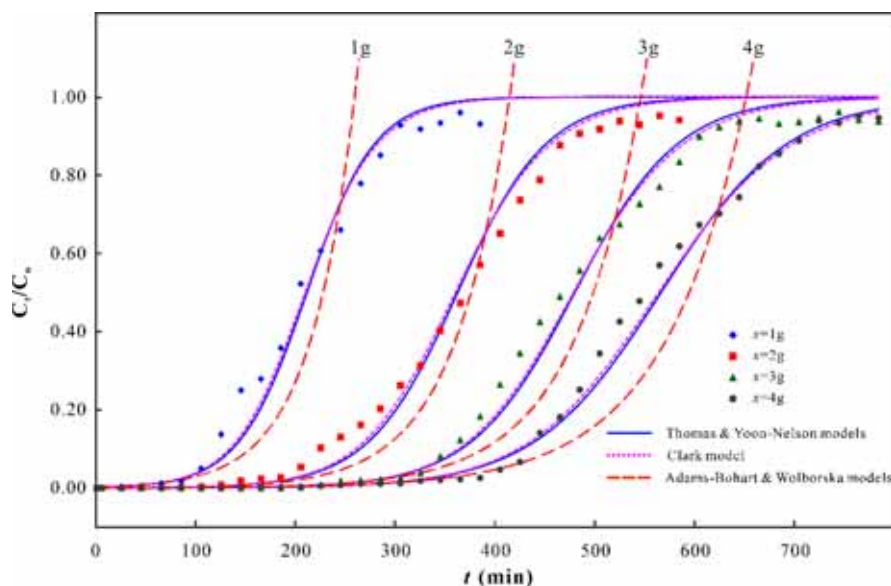


FIGURE 7

Effect of sorbent mass on breakthrough curve for $\text{Sb}(\text{III})$ sorption removal by the PC-Fe/C sorbent prepared with eucalyptus wood template (influent $\text{Sb}(\text{III})$ concentration: 20 mg/L; flow rate: 5.136 mL/min; pH: 8; sorbent grain size: <100mesh; operating temperature: 35°C).

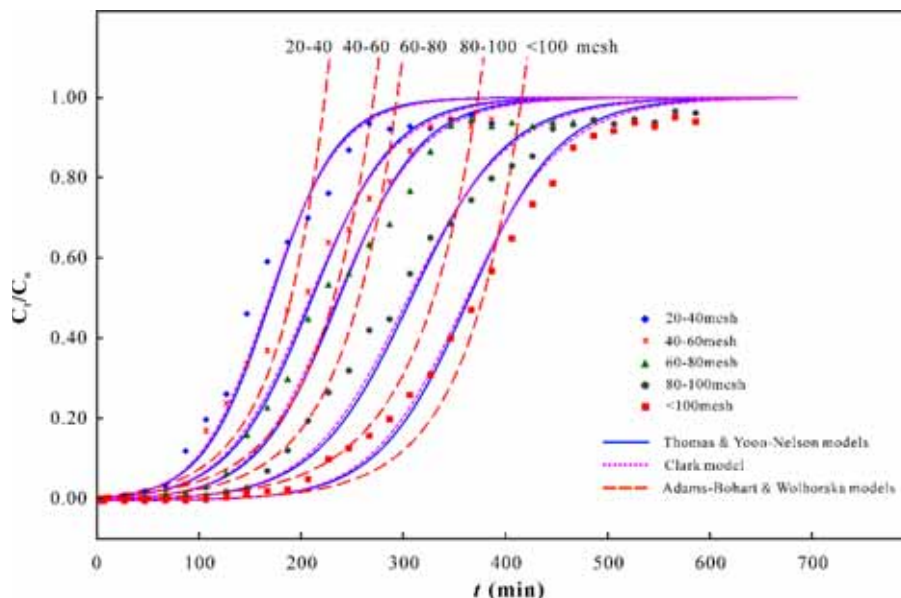


FIGURE 8

Effect of sorbent grain size on breakthrough curve for $\text{Sb}(\text{III})$ sorption removal by the PC-Fe/C sorbent prepared with eucalyptus wood template (influent $\text{Sb}(\text{III})$ concentration: 20 mg/L; flow rate: 5.136 mL/min; pH: 8; sorbent mass: 2g; operating temperature: 35°C).

Effect of sorbent mass (bed depth). Less amount of sorbent corresponds to small bed depth. The contact time of treated water sample withdrawn at sorbent mass (bed depth) along the bed of the column reactor varies, though the flow rates of the influents keep same [54]. To investigate the influence of sorbent mass (bed depth) on the breakthrough time, 20mg/L Sb(III) solution of pH 8.0 was passed through the PC-Fe/C column at a flow rate of 5.136 mL/min by varying the sorbent mass (bed depth). The breakthrough for both metals occurred faster and the bed column exhausted rapidly with the decreasing bed depth, i.e., the column breakthrough time and the sorbent bed performance were strongly affected by the bed depth [49]. The increase of Sb(III) uptake capacity with the increase in the sorbent mass might be due to the increased surface area of the sorbent that would provide more binding sites for sorption [46, 54]. The larger sorbent mass could delay its exhaustion time, which indicated that the PC-Fe/C bed could work for a longer time without replacing the sorbent [54, 55].

The breakthrough curves for variation in the amount of the PC-Fe/C (sorbent mass: 1, 2, 3, 4 g or bed depth: 0.85, 1.69, 2.54, 3.38 cm) loaded into the sorption column on Sb(III) sorption are plotted in Figure 7. As the sorbent mass or the bed depth was increased, Sb(III) ions had a long time to be sorbed onto PC-Fe/C with a higher removal efficiency. Therefore the larger sorbent mass could result in a decrease in the effluent Sb(III) concentration in the same operating time. The slope of the breakthrough curve increased with the decreasing sorbent mass resulting in a broadened mass transfer zone [46].

The sorption data were evaluated and the equilibrium Sb(III) uptake (q_e) and the total Sb(III) removal percentage (Y) with respect to sorbent mass are presented in Table 1. Both of the q_e and Y values increased with the increasing sorbent mass. As the sorbent mass (bed depth) decreased, the bed column exhausted quicker and the breakthrough for Sb(III) occurred faster. The increase in sorbent mass simultaneously improved the column operation and continued to reduce the effluent concentration at the end of the system (Table 1). The results indicated that the throughput amount of the Sb(III) solution decreased with decrease in sorbent mass or bed depth because of the accessibility of more sorption sites [51]. The equilibrium Sb(III) uptake (q_e) increased with decrease in sorbent mass. This means that at larger sorbent mass the effluent Sb(III) concentration ratios decreased more quickly than for a smaller sorbent mass. Furthermore, the bed was saturated in more time for a larger sorbent mass [51]. An increase in the amount of sorbent was accompanied with subsequent increase in the service area of the sorbent [53]. The operation area increase enhanced more contact between Sb(III) ions and the active sites on PC-Fe/C, thus increasing the sorption capacity. It is also interesting to note that enlarged service area increased the

treatment volume of the Sb(III) influent as well as gave a prolonged breakthrough point attainment.

Effect of sorbent grain size. Effect of sorbent grain size was investigated with various sorbent grain sizes, while the other conditions were kept constant (Figure 8, Table 1). The sorption of antimony was highly dependent on the sorbent grain size. The equilibrium sorption capacities [$q_{e,exp}$] were 8.30mg/g, 10.13mg/g, 11.73mg/g, 15.10mg/g and 18.47mg/g for the sorbent grain sizes of 20~40mesh (0.841~0.4mm), 40~60mesh (0.4~0.25mm), 60~80mesh (0.25~0.177mm), 80~100mesh (0.177~0.149mm) and <100mesh (<0.149mm), respectively. The total Sb(III) removal percentages increased from 60.98% to 74.16% with the decreasing sorbent grain sizes. As the sorbent grain sizes decreased, flatter breakthrough curves were obtained. A decreased sorbent grain size resulted a later breakthrough time and the influent volume treated was the largest for the smallest grain size (<100mesh or <0.149mm). The breakpoint time increased with decreasing grain size because the sorbent surface area increased and the sorption sites were more slowly to be occupied in the PC-Fe/C column. The times required for 50% Sb(III) breakthrough (τ_{exp}) were found to be 146 min, 192 min, 212 min, 289 min and 366 min for the sorbent grain sizes of 20~40mesh, 40~60mesh, 60~80mesh, 80~100mesh and <100mesh, respectively (Table 1).

Effect of operating temperature. The breakthrough curves for the Sb(III) sorption by PC-Fe/C at different temperatures and their sorption capacities are depicted in Table 1. The equilibrium sorption capacities ($q_{e,exp}$) were 18.83mg/g, 18.47mg/g and 18.67mg/g at the temperatures of 25, 35 and 45°C, respectively. The times required for 50% sorbate breakthrough (τ_{exp}) were 341 min, 366 min and 355 min at the temperatures of 25, 35 and 45°C, respectively. This means that the breakthrough curves were not significantly affected by the operating temperature, i.e., the breakthrough curve shifted not obviously with the variation of the operating temperature. The temperature had no significant influence on Sb(III) sorption, which has also been observed for the sorption removal of Sb(III) from water by using grey and red Erzurum clay at different temperatures between 10 and 40°C [34]. Therefore, the PC-Fe/C sorbent could be used for Sb(III) removal over a wide range of temperature.

Sorption modeling for breakthrough curve. The Thomas model and the Yoon–Nelson model. The Thomas rate constant (k_{Th}) and the equilibrium Sb(III) uptake ($q_{e,calc}$) were determined by fitting the column experimental data to the Thomas model (Table 1). Along with the experimental data points, the curves predicted by the Thomas equation under different experimental conditions are also illustrated in

Figure 3 ~ Figure 8, respectively. The Thomas rate constants and coefficients (R^2) were determined by using linear regression (Table 1). The R^2 values ranged from 0.9182 to 0.9889, which indicated that the correlation between C_t/C_0 and t was significant. The increase in the influent Sb(III) concentration and sorbent mass (bed depth) tended to decrease the Thomas rate constant (k_{Th}). As the influent flow rates were lower than 10.27 mL/min, the flow rates had no effect on the k_{Th} values, while the k_{Th} values increased with the increasing flow rates when they were >10.27 mL/min. The reason was that the concentration difference between Sb(III) in the solution and Sb(III) on the sorbent was the driving force for sorption. Therefore, the higher driving force caused by the higher influent Sb(III) concentration could cause a better column performance. So lower flow rate and higher influent Sb(III) concentration would increase the Sb(III) sorption in the PC-Fe/C column. Although longer residence time experienced at lower flow rates allow for diffusion of the Sb(III) ions, the value of q_e increased from 14.35 mg/g to 25.79 mg/g and the value of k_{Th} increased from 0.00112 mL/min·mg to 0.00142 mL/min·mg with the flow rate increasing from 3.434 mL/min to 15.41 mL/min, because the total Sb(III) influent volume at the exhausting point $C_t/C_0=0.9$ increased from 1823 mL to 4099 mL. The increase in the sorbent mass in the column identically increased the bed depth. As the sorbent mass increased from 1g to 4g or the bed depth increased from 0.85cm to 3.38cm, the equilibrium Sb(III) uptake (q_e) increased notably while the Thomas rate constant (k_{Th}) decreased from 0.00147 to 0.00079 significantly. For given experimental conditions, the equilibrium Sb(III) uptake value determined from calculation ($q_{e,calc}$) was very close to that obtained from experiment ($q_{e,exp}$) (Table 1). It was obvious that the predicted and the experimental data were plotted with great consistency (Figure 3 ~ Figure 8). The Thomas model is appropriate to describe the sorption process where the limiting step will not be the external and internal diffusions.

The Yoon–Nelson model, which is considered to be a simple theoretical model since less column data is required to construct the model, was used to explore the breakthrough character of the Sb(III) sorption onto PC-Fe/C. The Yoon–Nelson rate constants (k_{YN}) and the times required for 50% Sb(III) breakthrough (τ) were calculated (Table 1). As seen in the table, the constants (k_{YN}) increased with the increasing Sb(III) influent concentration, influent pH and flow rate. With the increase in the sorbent mass, the τ values increased while the rate constants (k_{YN}) decreased. Additionally, the rate constants (k_{YN}) increased with the increase in the sorbent grain size. The results show that the 50% breakthrough time (τ) was shortened with the increase in the influent Sb(III) concentration and the influent flow rate, and was extended with the increase in the sorbent mass.

The calculated τ values (τ_{calc}) were close to the experimental results (τ_{exp}). The deviation of τ_{calc} from τ_{exp} ($\Delta\tau/\tau_{exp}$) was 15.05% at the influent flow rate of 15.41 mL/min, while the deviation was less than 4% under other conditions (Table 1). In comparison to the experimental points under various experimental conditions, the predicted curves with the Yoon–Nelson model are simultaneously illustrated in Figure 3 ~ Figure 8.

The increase of the rate constant (k_{YN}) and the sorption capacity (q_e) with the increase in the influent Sb(III) concentration is considered to be due to the increasing competition of Sb(III) ions for the sorption sites on the PC-Fe/C surface, which finally results in the increase of the Sb(III) uptake rate [51]. High correlation coefficients ($R^2=0.9182\sim 0.9889$) indicate that the experimental data could be well fitted by using the Yoon and Nelson model. According to the correlation coefficients (R^2) for the Thomas and Yoon–Nelson equations, it can be inferred that the selected two classical models can reasonably describe the process of morph-genetic composite materials of Fe/C to sorb Sb(III). Table 1 show that the correlation coefficient (R^2) of Yoon–Nelson equation is same as that of Thomas equation.

The Yoon–Nelson rate constants (k_{YN}) decreased with the increase of the sorbent mass. Because of the high values of linear regression coefficients for the plotted curves of the influent flow rate or sorbent mass (x) versus the Yoon–Nelson model parameters [τ_{Theo} , t_1 and t_2], the breakthrough time and failure time of the sorption breakthrough curves can be calculated by the equations in the studied sorbent mass range. It also can be calculated that while the sorbent masses were 1g, 2g, 3g and 4g, the dynamic sorption capacity were respectively 9.54 mg/g, 14.91 mg/g, 18.62 mg/g and 21.60 mg/g. It is obvious that dynamic sorption capacity were arising with the increase in the sorbent mass, indicating that active site on the sorbent, which was conducive to the sorption of Sb(III), increased with the sorbent mass increase from 1g to 4g, making an extended time as well as a sufficient reaction for the sorption.

The Clark model. It was confirmed that the Freundlich model could be used to describe the Sb(III) sorption on the PC-Fe/C powder in a previous batch research [45]. Therefore, the parameters of the Clark model was estimated with the Freundlich constant $1/n$ (0.5359, 35°C) determined in the batch experiments. The values of A and r of the Clark model were calculated by Eq.(7) using linear regression analysis. As the influent Sb(III) concentration and the influent flow rate increased, the constant of the Clark model (A) decreased and the values of the sorption rate (r) increased. However, the constant (A) increased and the sorption rate (r) decreased with the increase in the sorbent mass and the decrease in the sorbent grain size. The increase in the influent pH could result in the increase in r and the decrease

in A. The breakthrough curves predicted by the Clark model according to Eq.(7) were also plotted in Figure 3 ~ Figure 8. A comparison of the data regression with the experimental results showed that the Clark model gave good correlation on the effects of the flow rate ($R^2=0.9498\sim 0.9912$), the influent Sb(III) concentration ($R^2=0.9267\sim 0.9730$), the sorbent mass ($R^2=0.9571\sim 0.9887$) and the sorbent grain size ($R^2=0.9544\sim 0.9817$), i.e., the fact shows that the forecast values are almost equal to the measured ones.

The Adams–Bohart model and the Wolborska model. The Adams–Bohart and Wolborska sorption models could be used to describe the initial part of the breakthrough curves (Figure 3~ Figure 8). As the influent Sb(III) concentrations increased from 10 mg/L to 50 mg/L, the kinetic constants k_{AB} of the Adams–Bohart model decreased from 0.001470 L/mg·min to 0.000452 L/mg·min and the kinetic coefficients of the external mass transfer (β_a) of the Wolborska model decreased from 0.0178 to 0.0077 1/min. As the sorbent mass (bed depth) increased from 1 to 4g (0.85 to 3.38cm), the kinetic constants k_{AB} of the Adams–Bohart model decreased from 0.001095 to 0.000605 L/mg·min and the kinetic coefficients of the external mass transfer (β_a) of the

Wolborska model decreased from 0.0268 to 0.0093 1/min. The kinetic constants (k_{AB}) increased with the increasing influent pH. The kinetic coefficients (β_a) increased with the increase in the influent flow rate and pH, but with the decrease in the sorbent grain size. This indicated that the external mass transfer was the dominant kinetics in the initial part of sorption in the column system. The corresponding experimental data under various experimental conditions were compared with the predicted curves using the Adams–Bohart model in Figure 3 ~ Figure 8. There was a good correlation between the predicted values and the experimental data in the initial part of the column sorption. The Adams–Bohart and Wolborska models were valid only for the relative concentration up to 60% breakthrough.

Comparison of the five models. Among the five models, the correlation coefficients (R^2) for the Thomas model were the same as those for the Yoon–Nelson model and the correlation coefficients (R^2) for the Adams–Bohart model were the same as those for the Wolborska model. In a comparison of the experimental data and the predicted curves, the

TABLE 2

Comparison of the sorption capacity of the PC-Fe/C and various sorbents for Sb(III) removal from water.

Sorbent	pH	Initial Sb (III) concentr. (mg/L)	Surface area (m ² /g)	Grain size	T (°C)	Capacity (mg/g)	Ref.
PC-Fe/C	8	20	59.2	<0.149	35	14.35- 25.79	This study
Granular PVA–Fe ⁰	7.0±0.2	0~20	11.3	2.04 mm	15~35	6.99~9.40	Zhao et al., 2014 [39]
MnOOH	<7	0.12~1.58	-	-	25	19.48	Thanabalasingam and Pickering, 1990 [26]
Al(OH) ₃	6~7	0.12~1.58	-	-	25	5.48	Thanabalasingam and Pickering, 1990 [26]
FeOOH	6~7	0.12~1.58	-	-	25	4.02	Thanabalasingam and Pickering, 1990 [26]
Bentonite (Sigma-Aldrich, USA)	6	0.05~ 4	99	-	15~35	0.37~0.56	Xi et al., 2011 [61]
Kaolinite (Sigma-Aldrich, USA)	6.0±0.1	0.5~3	15.8	-	5~45	0.13~0.22	Xi et al., 2016 [40]
Fe–Mn Binary Oxide (FMBO)	3.0±0.1	24.35~243.52	231	<50 nm	20 ± 1	237.43	Xu et al., 2011 [63]
FeOOH	3.0±0.1	24.35~243.52	261	<50 nm	20 ± 1	96.19	Xu et al., 2011 [63]
MnO ₂	3.0±0.1	24.35~243.52	117	<50 nm	20 ± 1	93.76	Xu et al., 2011 [63]
Graphene	3~4	1~10	154.43	-	30	10.919	Leng et al., 2012 [32]
Goethite (α-FeOOH)	7.0±0.3	0.05~15	106	-	25	7.05~20.68	Xi et al., 2013 [62]
Goethite (α-FeOOH)	3.94±0.6	4.79~47.93	40.1	-	25	53.0~70.1	Watkins et al., 2006 [29]
Goethite (α-FeOOH)	9	1.22~36.53	27.39	-	20.5	53.45	Guo et al., 2014 [36]
Akaganéite (β-FeOOH)	9	1.22~36.53	32.79	-	20.5	34.09	Guo et al., 2014 [36]
Hematite α-Fe ₂ O ₃	9	1.22~36.53	19.89	-	20.5	31.41	Guo et al., 2014 [36]
MNP@hematite	7±0.1	1~20	-	10~30 nm	25	36.7	Shan et al., 2014 [35]
Fe ₃ O ₄	7±0.1	1~20	-	< 50 nm	25	19.9	Shan et al., 2014 [35]
MWCNTs	7	4	89.2	20~40 nm	25	0.33	Salam and Mohamed, 2013 [7]
Fe ₂ O ₃ -modified carbon nanotubes	7	1.5	90.4	10~20 nm	25	6.23	Yu et al., 2013 [37]
Carbon nanotubes (CNTs)	7	1.5	101.7	10~20 nm	25	3.01	Yu et al., 2013 [37]
Pyrogallol bonded sorbent (ICAA-PPG)	6.2	192.8	-	-	~20	21.60	Deorkar and Tavlarides, 1997 [27]
Diatomite (SiO ₂ ·nH ₂ O)	6	10~500	-	-	20	35.2	Sarı et al., 2010 [31]
Freshwater cyanobacteria	4	10~500	-	powder	25	4.88	Wu et al., 2012 [33]
Grey and red Erzurum clay	natural water's	10~50	-	500 mesh	25~40	8.58~9.15	Targan et al., 2013 [34]
GAC	7.03	0.91~3.74	940.00	0.5~0.8	25	0.54	Yu et al., 2014 [38]
FAC-0.02	7.03	0.91~3.74	940.38	0.5~0.8	25	2.44	Yu et al., 2014 [38]
FAC-0.05	7.03	0.91~3.74	940.03	0.5~0.8	25	2.64	Yu et al., 2014 [38]
Hydroxyapatite	5~8	0.05~50	-	-	room	17.05	Leyva et al., 2001 [28]
Iron oxide composite [>70% Fe ₂ O ₃ and 90.1% α-FeOOH]	6.0~8.0	0.065	120~200	0.5~2	room	0.0278	Ilavský, 2008 [30]
Granulated ferric hydroxide [52-57% Fe(OH) ₃ and β-FeOOH]	5.5~9.0	0.065	250~300	0.32~2	room	0.0850	Ilavský, 2008 [30]

Thomas, Yoon–Nelson and Clark models could be used to describe the behavior of the sorption process, but the Adams–Bohart and Wolborska models did not give the best results. Comparing the correlation coefficients (R^2) for the Thomas, Yoon–Nelson and Clark models, the correlation coefficients (R^2) for the Thomas and Yoon–Nelson models were lower under all conditions except at the low influent Sb(III) concentration of 10mg/L, which were 0.9785 and 0.9730, respectively. Therefore, the Clark model was better in describing the Sb(III) sorption process in a PC-Fe/C column. Regarding the Adams–Bohart and Wolborska models, they could be used to predict only the initial part of breakthrough curves (C_t/C_0 less than 0.15). But in the present work, the predicted range was up to 0.6, and the correlation coefficients (R^2) were a little lesser than those for the Thomas, Yoon–Nelson and Clark models under the same experimental conditions.

Comparison of sorption capacity. A comparison of sorption capacity of the PC-Fe/C sorbent with those of various sorbents reported in literatures is presented in Table 2. As shown in the table, the PC-Fe/C sorbent has a significant potential for the sorption removal of Sb(III) from aqueous solution.

Sb(III) removal from water has been reported in only a few researches, and for the antimony sorption on pure iron (hydro-)oxides, the sparsity of data is noticeably evident. The sorption capacity of the PC-Fe/C sorbent for Sb(III) (14.35~25.79 mg/g) was larger than that of a polyvinyl alcohol-stabilized granular sorbent with nanoscale Fe^0 (Granular PVA- Fe^0 , 8.84~9.40 mg/g) [39], hydrous oxide of Al (5.48

mg/g) [26], bentonite (0.37~0.56 mg/g) [61], kaolinite (0.13~0.22 mg/g) [40], graphene (10.92 mg/g) [32], multi-walled carbon nanotubes (MWCNTs, 0.33 mg/g) [7], carbon nanotubes (3.01 mg/g) [37], Fe_2O_3 -modified carbon nanotubes (6.23 mg/g) [37], cyanobacteria *Microcystis* biomass (4.88 mg/g) [33], grey and red Erzurum clay (8.58~9.15 mg/g) [34], granular activated carbon (GAC, 0.54 mg/g) [38], and FeCl_3 -modified granular activated carbon (FAC, 2.44~2.64 mg/g) [38]. Based on the results of the column tests at the Sb concentration of 65 $\mu\text{g/L}$ and the filtration rate of 5.3 m/h, the sorption capacities of the iron oxide composite [$>70\%$ Fe_2O_3 and 90.1% $\alpha\text{-FeOOH}$] and granulated ferric hydroxide [52-57% $\text{Fe}(\text{OH})_3$ and $\beta\text{-FeOOH}$] were observed to be 27.78 $\mu\text{g/g}$ and 85.04 $\mu\text{g/g}$, respectively [30].

The PC-Fe/C had a same sorption capacity as hydrous oxide of Mn (MnOOH , 19.48 mg/g) [26], goethite ($\alpha\text{-FeOOH}$) (7.05~20.68 mg/g) [62], Fe_3O_4 nanopowder (19.9 mg/g) [35], pyrogallol bonded sorbent (ICAA-PPG, 21.60 mg/g) [27], and hydroxapatite (17.05 mg/g) [28]. Its sorption capacity was only smaller than that of Fe-Mn Binary Oxide (FMBO, 237.43mg/g) [63], MnO_2 (93.76 mg/g) [63], goethite ($\alpha\text{-FeOOH}$, 96.19 mg/g) [63], goethite ($\alpha\text{-FeOOH}$, 53.0~70.1 mg/g) [29], goethite ($\alpha\text{-FeOOH}$, 53.45 mg/g) [36], akaganéite ($\beta\text{-FeOOH}$, 34.09 mg/g) [36], hematite ($\alpha\text{-Fe}_2\text{O}_3$, 31.43 mg/g) [36], hematite modified magnetic nanoparticles (MNP@hematite, 36.7 mg/g) [35], and diatomite ($\text{SiO}_2 \cdot n\text{H}_2\text{O}$, 35.2 mg/g) [31], most of which were nanoparticles and are not suitable for the use as an appropriate sorption material in a fixed-bed sorption column. Normally, the finer the grain size the greater the sorption capacity. Nevertheless, very small particle can clump together. Hence, the hierarchical porous microstructure of the PC-Fe/C prepared with

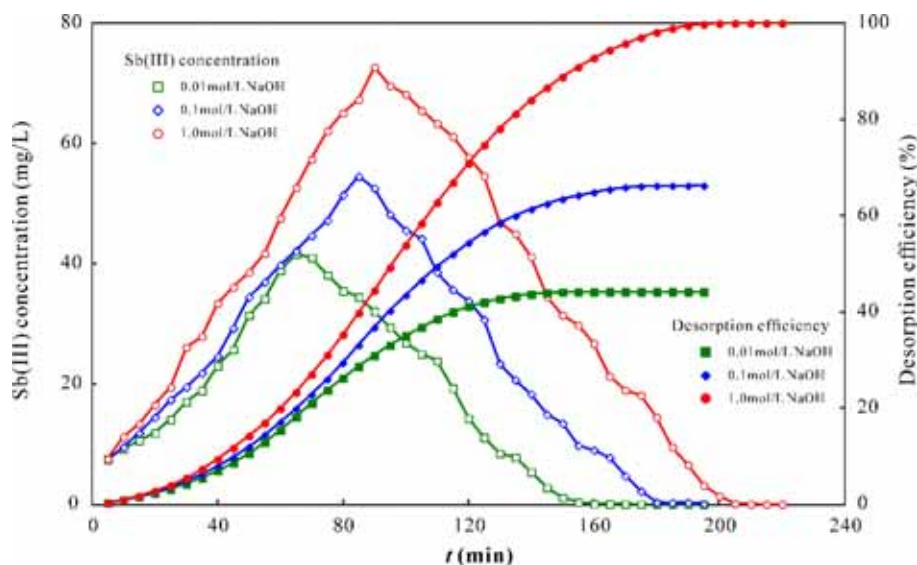


FIGURE 9

Effect of eluent concentration on the Sb(III) desorption efficiencies (flow rate: 5.136 mL/min; sorbent mass: 2g; sorbent grain size: <100mesh; operating temperature: 35°C).

eucalyptus wood template can have a beneficial effect on the overall sorption when the sorbent is used without additional grinding to nanoparticles.

Column desorption and regeneration. Effect of desorption eluent. Elution of the Sb(III) (sorbate) from the PC-Fe/C sorbent was done using four different eluents, i.e., 0.1 mol/L NaOH, 0.1 mol/L NaHCO₃, 0.1 mol/L NaCl and 0.1 mol/L H₂O. The results obtained with four different eluents indicated that the use of 0.1 mol/L NaOH appeared to be more effective than others. The desorption efficiencies were 65.73%, 50.52%, 6.23% and 6.09% for 0.1 mol/L NaOH, 0.1 mol/L NaHCO₃, 0.1 mol/L NaCl and 0.1 mol/L H₂O, respectively. Of the reagents tested in the batch study to desorb Sb(III) that was already sorbed on the PC-Fe/C sorbent, 0.1 M NaOH was found to be the most suitable one. The high effectiveness of 0.1 M NaOH in desorbing Sb(III) is due to the lowest Sb(III) sorption at very high pHs (pH>10) produced by this alkaline reagent [45]. As indicated previously (Figure 6), Sb(III) exists as antimonite ions [H₂SbO₃⁻ or Sb(OH)₄⁻] in more alkaline solutions at pH>10 [31-38], while a negative surface of the PC-Fe/C sorbent formed at the same time, which resulted in a desorption of Sb(III) from the PC-Fe/C sorbent. Therefore, NaOH is used as desorption solution in the following column regeneration study.

Effect of desorption eluent concentration. The column desorption of Sb(III) from the PC-Fe/C sorbent was tested at various inlet concentrations of NaOH, i.e., 0.01, 0.1 and 1.0 mol/L under the identical conditions of the influent flow rate of 5.136 mL/min, the sorbent mass of 2g, the sorbent grain size of <100mesh and the operating temperature of 35°C. The result obtained for three different NaOH concentrations is plotted in Figure 9. The maximum Sb(III) concentrations in the effluent appeared to be 72.71 mg/L for 1.0M NaOH, 54.55 mg/L for 0.1M NaOH and 41.63 mg/L for 0.01M NaOH after operating for 90, 85 and 65 min, respectively. From comparison of the elution curves, it was noted that the total regeneration efficiencies after the desorption operating for 200min amounted to be 99.79% for 1.0M NaOH, 66.25% for 0.1M NaOH and 44.17% for 0.01M NaOH, respectively, i.e., the regeneration efficiencies increase with the increasing eluent concentration. This increase may be due to the fact that during the time of desorption with 1M NaOH the surfaces of the sorbents became more negative, and the percentage of H₂SbO₃⁻ or Sb(OH)₄⁻ species of Sb(III) in more alkaline solutions also increased. Nevertheless, 0.1M NaOH may be more suitable as eluent in terms of the amount of eluent used in the real elution process and severe problems caused by disposal of a higher basic waste.

Effect of flow rate. The column elution of

Sb(III) from the PC-Fe/C sorbent was done at three influent flow rates, i.e., 3.43mL/min, 5.14mL/min and 10.27mL/min, under the identical conditions of the eluent concentration of 0.1 mol/L NaOH, the sorbent mass of 2g, the sorbent grain size of <100mesh and the operating temperature of 35°C. The maximum concentrations of Sb(III) in the effluent solution appeared to be 72.29 mg/L at the influent flow rates of 3.43mL/min, 54.55 mg/L at 5.14mL/min and 37.75 mg/L at 10.27mL/min after operating for 125, 85 and 40 min, respectively. From comparison of the elution curves, it was noted that the total regeneration efficiencies amounted to be 80.63% at the eluent flow rates of 3.43mL/min after the desorption operating for 240min, 66.25% at 5.14mL/min after 200min and 51.60% at 10.27mL/min after 120min, respectively, i.e., the regeneration efficiencies decrease with the increasing eluent flow rates, while a longer desorption time was also needed at lower flow rate.

Effect of operating temperature. The column elution of Sb(III) from the PC-Fe/C sorbent was done at three temperatures, 25°C, 35°C and 45°C, under the identical conditions of the eluent concentration of 0.1 mol/L NaOH, the influent flow rate of 5.136 mL/min, the sorbent mass of 2g and the sorbent grain size of <100mesh. The maximum Sb(III) concentrations in the effluent appeared to be 58.46 mg/L at the temperature of 25°C, 54.55 mg/L at 35°C and 55.70 mg/L at 45°C after operating for 80, 85 and 80 min, respectively. From comparison of the elution curves, it was noted that the total regeneration efficiencies amounted to be 67.85% at the temperature of 25°C after the desorption operating for 200min, 66.25% at 35°C after 200min and 64.99% at 45°C after 200min, respectively, i.e., the regeneration efficiencies increased only slightly with the decreasing operating temperature. Obviously, the operating temperature had negligible effect on the desorption of Sb(III).

CONCLUSIONS

The PC-Fe/C sorbent can be employed to remove Sb(III) from wastewater efficiently. The increase in sorbent mass (bed depth) and the decrease in sorbent grain size considerably affected the column performance by decelerating the exhaustion time and improved the column quality. The total removal percentage of Sb(III) could be increased with the increase in sorbent mass. However, the increase in the influent flow rate and the influent Sb(III) concentration tended to accelerate the column exhaustion. The solution pH and operating temperature had negligible effects on the column removal of Sb(III).

The Thomas, Yoon–Nelson and Clark models showed a very good correlation for the Sb(III) experimental data ($R^2>0.9$), which shows that the models

can accurately forecast the operation status of the sorbing poles under the conditions of different initial concentration, flow rate, sorbent mass and temperature. The trends of both the experimental and theoretical data were strongly and significantly correlated involving the column parameters q_e , τ , t_1 and t_2 . The time required for 50% breakthrough (τ) decreased with increase in flow rate, sorbent mass (bed depth) and initial Sb(III) ion concentration. The Adams–Bohart and Wolborska models were found only suitable to describe the initial part of the breakthrough curves. Under the condition of the influent flow rate of 5.136 mL/min, the influent Sb(III) concentration of 20 mg/L, the influent pH of 8, the sorbent mass of 2g, the sorbent grain size of <100mesh, and the operating temperature of 35°C, the equilibrium sorption capacity reached 18.47 mg/g, which was near the predicted value of 18.64mg/g according to the Thomas model.

The column desorption of the sorbed Sb(III) from PC-Fe/C were strongly depended on the eluent concentration and flow rate, while the operating temperature had negligible effect on the desorption. The sorbed Sb(III) ion could be effectively eluted by using 1M NaOH at inflow rate of 5.136 mL/min with the regeneration efficiency >99% after the desorption operating for 200min.

ACKNOWLEDGEMENTS

The authors thank the Guangxi Key Laboratory of Environmental Pollution Control Theory and Technology for the research assistance. This research was financially assisted by the National Natural Science Foundation of China (NSFC 51638006), the Guangxi Science and Technology Development Project (GuiKeGong 14124004-3-3) and the Provincial Natural Science Foundation of Guangxi (2014GXNSFBA118054).

REFERENCES

- [1] Filella, M., Belzile, N., Chen, Y.W. (2002) Antimony in the environment: a review focused on natural waters: I. Occurrence. *Earth-Science Reviews* 57, 125-176.
- [2] Filella, M., Belzile, N., Lett, M.C. (2007) Antimony in the environment: a review focused on natural waters. III. Microbiota relevant interactions. *Earth-Science Reviews* 80, 195-217.
- [3] Filella, M., Williams, P.A., Belzile, N. (2009) Antimony in the environment: knowns and unknowns. *Environmental Chemistry* 6, 95-105.
- [4] Dong, S., Dou, X., Mohan, D., Pittman Jr., C.U., Luo, J. (2015) Synthesis of graphene oxide/schwertmannite nanocomposites and their application in Sb(V) adsorption from water. *Chemical Engineering Journal* 270, 205-214.
- [5] He, M. (2007) Distribution and phyto-availability of antimony at an antimony mining and smelting area, Hunan, China. *Environmental Geochemistry and Health* 29, 209-219.
- [6] He, M., Wang, X., Wu, F., Fu, Z. (2012) Antimony pollution in China. *Science of the Total Environment* 421-422, 41-50.
- [7] Salam, M.A. and Mohamed, R.M. (2013) Removal of antimony (III) by multi-walled carbon nanotubes from model solution and environmental samples. *Chemical Engineering Research & Design* 91, 1352-1360.
- [8] Du, X., Qu, F., Liang, H., Li, K., Yu, H., Bai, L., Li, G. (2014) Removal of antimony (III) from polluted surface water using a hybrid coagulation–flocculation–ultrafiltration (CF–UF) process. *Chemical Engineering Journal* 254, 293-301.
- [9] Smichowski, P. (2008) Antimony in the environment as a global pollutant: a review on analytical methodologies for its determination in atmospheric aerosols. *Talanta* 75, 2-14.
- [10] Council of the European Communities (1976) Council Directive 76/464/EEC of 4 May 1976 on pollution caused by certain dangerous substances discharged into the aquatic environment of the Community. *Official Journal L* 129, 23-29.
- [11] USEPA, Water related fate of the 129 priority pollutants 1., Washington, 1979.
- [12] Guo, X., Wu, Z., He, M. (2009) Removal of antimony(V) and antimony(III) from drinking water by coagulation–flocculation–sedimentation (CFS). *Water Research* 43, 4327-4335.
- [13] Gannon, K. and Wilson, D.J. (1986) Removal of antimony from aqueous solutions. *Separation Science & Technology* 21, 475-493.
- [14] Mok, W.M. and Wai, C.M. (1990) Distribution and mobilization of arsenic and antimony species in the Coeur D’Alene River, Idaho. *Environmental Science & Technology* 24, 102-108.
- [15] Perez-Corona, T., Madrid, Y., Camara, C. (1997) Evaluation of antimony selective uptake of selenium (Se(IV) and Se(VI)) and (Sb(III) and Sb(V)) species by baker’s yeast cells (*Saccharomyces cerevisiae*). *Analytica Chimica Acta* 345, 249-255.
- [16] Guin, R., Das, S.K., Saha, S.K. (1998) The anion exchange behavior of Te and Sb. *Journal of Radioanalytical & Nuclear Chemistry* 230, 269-271.
- [17] Kang, M., Kawasak, M., Tamada, S., Kamei, T., Magara, Y. (2000) Effect of pH on the removal of arsenic and antimony using reverse osmosis membranes. *Desalination* 131, 293-298.
- [18] Saito, T., Tsuneda, S., Hirata, A., Nishiyama, S., Saito, K., Saito, K., Sugita, K., Uezu, K., Tamada, M., Sugo, T. (2004) Removal of

- antimony (III) using polyol-ligand-containing porous hollow-fiber membranes. *Separation Science & Technology* 39, 3011-3022.
- [19] Tomko, J., Bačkor, M., Štofko, M. (2006) Biosorption of heavy metals by dry fungi biomass. *Acta Metallurgica Slovaca* 12, 447-451.
- [20] Bakir, A., McLoughlin, P., Tofail, S.A.M., Fitzgerald, E. (2009) Competitive sorption of antimony with zinc, nickel, and aluminum in a seaweed based fixed-bed sorption column. *CLEAN – Soil, Air, Water* 37, 712-719.
- [21] Chang, P., Yu, S., Chen, T., Ren, A., Chen, C., Wang, X. (2007) Effect of pH, ionic strength, fulvic acid and humic acid on sorption of Th(IV) on Na-rectorite. *Journal of Radioanalytical & Nuclear Chemistry* 274, 153-160.
- [22] Srivastava, V.C., Mall, I.D., Mishra, I.M. (2007) Adsorption thermodynamics and isosteric heat of adsorption of toxic metal ions onto bagasse fly ash (BFA) and rice husk ash (RHA). *Chemical Engineering Journal* 132, 267-278.
- [23] Demirbas, E., Dizge, N., Sulak, M.T., Koby, M. (2009) Adsorption kinetics and equilibrium of copper from aqueous solutions using hazelnut shell activated carbon. *Chemical Engineering Journal* 148, 480-487.
- [24] Sheng, G., Shao, D., Fan, Q., Xu, D., Chen, Y., Wang, X. (2009) Effect of pH and ionic strength on sorption of Eu(III) to MX-80 bentonite: batch and XAFS study. *Radiochimica Acta* 97, 621-630.
- [25] Zhao, Z., Wang, X., Zhao, C., Zhu, X., Du, S. (2010) Adsorption and desorption of antimony acetate on sodium montmorillonite. *Journal of Colloid and Interface Science* 345, 154-159.
- [26] Thanabalasingam, P. and Pickering, W.F. (1990) Specific sorption of antimony (III) by the hydrous oxides of Mn, Fe, and Al. *Water, Air, & Soil Pollution* 49, 175-185.
- [27] Deorkar, N.V. and Tavlarides, L.L. (1997) A chemically bonded adsorbent for separation of antimony, copper and lead. *Hydrometallurgy* 46, 121-135.
- [28] Leyva, A.G., Marrero, J., Smichowski, P., Cicerone, D. (2001) Sorption of antimony onto hydroxyapatite. *Environmental Science & Technology* 35, 3669-3675.
- [29] Watkins, R., Weiss, D., Dubbin, W., Peel, K., Coles, B., Arnold, T. (2006) Investigations into the kinetics and thermodynamics of Sb(III) adsorption on goethite (α -FeOOH). *Journal of Colloid and Interface Science* 303, 639-646.
- [30] Ilavský, J. (2008) Removal of antimony from water by sorption materials. *Slovak Journal of Civil Engineering* 2, 1-6.
- [31] Sarı, A., Çıtak, D., Tuzen, M. (2010) Equilibrium, thermodynamic and kinetic studies on adsorption of Sb(III) from aqueous solution using low-cost natural diatomite. *Chemical Engineering Journal* 162, 521-527.
- [32] Leng, Y., Guo, W., Su, S., Yi, C., Xing, L. (2012) Removal of antimony(III) from aqueous solution by graphene as an adsorbent. *Chemical Engineering Journal* 211-212, 406-411.
- [33] Wu, F., Sun, F., Wu, S., Yan, Y., Xing, B. (2012) Removal of antimony(III) from aqueous solution by freshwater cyanobacteria microcystis biomass. *Chemical Engineering Journal* 183, 172-179.
- [34] Targan, Ş., Tirtom, V.N., Akkuş, B. (2013) Removal of antimony(III) from aqueous solution by using grey and red Erzurum clay and application to the Gediz river sample. *ISRN Analytical Chemistry* 2013, Article ID 962781.
- [35] Shan, C., Ma, Z., Tong, M. (2014) Efficient removal of trace antimony(III) through adsorption by hematite modified magnetic nanoparticles. *Journal of Hazardous Materials* 268, 229-236.
- [36] Guo, X., Wu, Z., He, M., Meng, X., Jin, X., Qiu, N., Zhang, J. (2014) Adsorption of antimony onto iron oxyhydroxides: Adsorption behavior and surface structure. *Journal of Hazardous Materials* 276, 339-345.
- [37] Yu, T., Zeng, C., Ye, M., Shao, Y. (2013) The adsorption of Sb(III) in aqueous solution by Fe₂O₃-modified carbon nanotubes. *Water Science and Technology* 68, 658-664.
- [38] Yu, T., Wang, X., Li, C. (2014) Removal of antimony by FeCl₃-modified granular-activated carbon in aqueous solution. *Journal of Environmental Engineering* 140, A4014001.
- [39] Zhao, X., Dou, X., Mohan, D., Pittman Jr., C.U., Ok, Y.S., Jin, X. (2004) Antimonate and antimonite adsorption by a polyvinyl alcohol-stabilized granular adsorbent containing nanoscale zero-valent iron. *Chemical Engineering Journal* 247, 250-257.
- [40] Xi, J., He, M., Kong, L. (2016) Adsorption of antimony on kaolinite as a function of time, pH, HA and competitive anions. *Environmental Earth Sciences* 75, 136.
- [41] Hua, M., Zhang, S., Pan, B., Zhang, W., Lv, L. (2012) Heavy metal removal from water/wastewater by nanosized metal oxides: A review. *Journal of Hazardous Materials* 211-212, 317-331.
- [42] Mahapatra, A., Mishra, B.G., Hota, G. (2013) Electrospun Fe₂O₃-Al₂O₃ nanocomposite fibers as efficient adsorbent for removal of heavy metal ions from aqueous solution. *Journal of Hazardous Materials* 258-259, 116-123.
- [43] Han, R., Wang, Y., Zou, W., Wang, Y., Shi, J. (2007) Comparison of linear and nonlinear analysis in estimating the Thomas model parameters for methylene blue adsorption onto natural zeolite in fixed-bed column. *Journal of Hazardous Materials* 145, 331-335.
- [44] Mahmoud, M.E., Abdelwahab, M.S., Fathallah,

- E.M. (2013) Design of novel nano-sorbents based on nano-magnetic iron oxide-bound-nano-silicon oxide-immobilized-triethylenetetramine for implementation in water treatment of heavy metals. *Chemical Engineering Journal* 223, 318-327.
- [45] Wei, W., Zhu, Z., Zhu, Y., Qin, H., Liang, M. (2013) Adsorption of Sb(III) from aqueous solution by the porous biomorph-genetic composite of Fe₂O₃-Fe₃O₄/C prepared with eucalyptus wood template. *Technology of Water Treatment* 39, 69-72. (in Chinese)
- [46] Han, R., Wang, Y., Yu, W., Zou, W., Shi, J., Liu, H. (2007) Biosorption of methylene blue from aqueous solution by rice husk in a fixed-bed column. *Journal of Hazardous Materials* 141, 713-718.
- [47] Goel, J., Kadirvelu, K., Rajagopal, C., Garg, V.K. (2005) Removal of lead(II) by adsorption using treated granular activated carbon: batch and column studies. *Journal of Hazardous Materials* B125, 211-220.
- [48] Ghosh, A., Chakrabarti, S., Ghosh, U.C. (2014) Fixed-bed column performance of Mn-incorporated iron(III) oxide nanoparticle agglomerates on As(III) removal from the spiked groundwater in lab bench scale. *Chemical Engineering Journal* 248, 18-26.
- [49] Lim, A.P. and Aris, A.Z. (2014) Continuous fixed-bed column study and adsorption modeling: Removal of cadmium (II) and lead (II) ions in aqueous solution by dead calcareous skeletons. *Biochemical Engineering Journal* 87, 50-61.
- [50] Zhu, Z., Zhu, Y., Qin, H., Y, Li., Liang, Y., Deng, H., Liu, H. (2015) Preparation and properties of porous composite of hematite/magnetite/carbon with eucalyptus wood biotemplate. *Materials and Manufacturing Processes* 30, 285-291.
- [51] Nwabanne, J. T. and Igbokwe, P. K. (2012) Adsorption performance of packed bed column for the removal of lead (II) using oil palm fibre. *International Journal of Applied Science & Technology* 2, 106-115.
- [52] Chen, N., Zhang, Z., Feng, C., Li, M., Chen, R., Sugiura, N. (2011) Investigations on the batch and fixed-bed column performance of fluoride adsorption by Kanuma mud. *Desalination* 268, 76-82.
- [53] Auta, M., Amat Darbis, N.D., Mohd Din, A.T., Hameed, B.H. (2013) Fixed-bed column adsorption of carbon dioxide by sodium hydroxide modified activated alumina. *Chemical Engineering Journal*, 233, 80-87.
- [54] Podder, M.S. and Majumder, C.B. (2016) Fixed-bed column study for As(III) and As(V) removal and recovery by bacterial cells immobilized on sawdust/MnFe₂O₄ composite. *Biochemical Engineering Journal* 105, 114-135.
- [55] Xu, X., Gao, B., Tan, X., Zhang, X., Yue, Q., Wang, Y., Li, Q. (2013) Nitrate adsorption by stratified wheat straw resin in lab-scale columns. *Chemical Engineering Journal* 226, 1-6.
- [56] Aksu, Z. and Gönen, F. (2004) Biosorption of phenol by immobilized activated sludge in a continuous packed bed: prediction of breakthrough curves. *Process Biochemistry* 39, 599-613.
- [57] Xu, Y., Ohki, A., Maeda, S. (2001) Adsorption and removal of antimony from aqueous solution by an activated alumina 1. Adsorption capacity of adsorbent and effect of process variable. *Toxicological & Environmental Chemistry* 80, 133-144.
- [58] Biswas, B.K., Inoue, J., Kawakita, H., Ohto, K., Inoue, K. (2009) Effective removal and recovery of antimony using metal-loaded saponified orange waste. *Journal of Hazardous Materials* 172, 721-728.
- [59] Khalid, N., Ahmad, S., Toheed, A., Ahmed, J. (2000) Potential of rice husks for antimony removal. *Applied Radiation and Isotopes* 52, 31-38.
- [60] Vithanage, M., Rajapaksha, A.U., Dou, X., Bolan, N.S. (2013) Surface complexation modeling and spectroscopic evidence of antimony adsorption on iron-oxide-rich red earth soils. *Journal of Colloid and Interface Science* 406, 217-224.
- [61] Xi, J., He, M., Lin, C. (2011) Adsorption of antimony(III) and antimony(V) on bentonite: kinetics, thermodynamics and anion competition. *Microchemical Journal* 97, 85-91.
- [62] Xi, J., He, M., Wang, K., Zhang, G. (2013) Adsorption of antimony(III) on goethite in the presence of competitive anions. *Journal of Geochemical Exploration* 132, 201-208.
- [63] Xu, W., Wang, H., Liu, R., Zhao, X., Qu, J. (2011) The mechanism of antimony(III) removal and its reactions on the surfaces of Fe-Mn binary oxide. *Journal of Colloid and Interface Science* 363, 320-326.

Received: 09.09.2016

Accepted: 27.05.2017

CORRESPONDING AUTHOR

Yinian Zhu

College of Environmental Science and Engineering,
Guilin University of Technology, Guilin, Guangxi
541004, P.R. China

e-mail: zhuyinian@glut.edu.cn

α -AMYLASE FROM *BACILLUS SIMPLEX*- PRODUCTION, CHARACTERIZATION AND PARTIAL PURIFICATION

Veysi Ortakaya¹, Sema Aguloglu Fincan^{1,*}, Baris Enez²

¹Department of Biology, Faculty of Science, Dicle University, Diyarbakir, Turkey

²Veterinary Health Department, Vocational School of Technical Sciences, Bingöl University, Bingöl, Turkey

ABSTRACT

In this study, some bacteria were isolated from the soil obtained from Ergani Makam Mountain. The isolated bacteria were defined as *Bacillus simplex* with the biochemical tests and 16S rRNA analysis. The optimum conditions for bacterial growth were determined as the 32nd hour, 37°C and pH 7.0. While the maximum amylase activity was observed of the 72nd hour, the optimum temperature and pH of the enzyme were determined to be 37°C and 7.0 reciprocally. It was observed that the enzyme production increased with ammonium sulfate and ammonium nitrate from nitrogen sources and decreased with the addition of carbon sources. Amylase was partially purified with 70% ammonium sulfate precipitations and dialysis. When the effect of detergents was examined on the partially purified enzyme it was determined that SDS considerably inhibited and the other detergents increased the enzyme activity. It was also determined that while CaCl₂ increased the activity whereas FeCl₂, CuCl₂, ZnCl₂ and HgCl₂ considerably inhibited the enzyme activity.

KEYWORDS:

Bacillus simplex; α -amylase; isolation; production; partial purification; characterization

INTRODUCTION

Microorganisms in particular have been regarded as treasure of useful enzymes [1]. The reason is that microorganism-based enzymes can easily be obtained, do not constitute unwanted waste product, are more stable and economic, can be obtained in high purity and high quantity [2,3]. Among microorganisms, mostly, some *Bacillus* species and subspecies that can be found widely in the nature are used. α -Amylase, β -amylase, xylanase, alkaline phosphatase, β -glucanase (cellulase), glucose isomerase, β -lactamase, neutral protease and pullulanase can be counted among the primary enzymes synthesized by *Bacillus* [4].

The enzyme industry as we know it today is the result of a rapid development seen primarily over the past four decades thanks to the evolution of

modern biotechnology [5,6]. The first enzyme produced industrially was α -amylase that was used for medicinal purposes. α -Amylase (EC 3.2.1.1,1,4- α -D-glucan-glucanohydrolase) is an extracellular enzyme that hydrolyzes starch and glycogen molecules [7]. It breaks the α -1,4 bonds in starch molecule into glucose, maltose, maltotriose and α -limit dextrine. It is primarily used in food industry for preparation of maltose syrup, purification and clarification of various drinks and production of bread and beer. Besides, it has a wide area of usage like paper, detergent and textile industries and pharmaceuticals [8,9,10,11].

α -Amylase, which has economical, industrial importance was produced from *Bacillus simplex* which is isolated from soil. Characterization of the partially purified enzyme has been performed.

MATERIAL AND METHODS

Microorganism and Culture Conditions. *Bacillus simplex*, isolated from the soil was produced in 120 rpm, pH 7.0 37°C and NB environment for 72 hours.

Morphological and Biochemical Tests. A test for the morphological and physiological identification of the obtained isolation was conducted. Gram, and spore staining methods and motility tests were used in order to determine the characteristics of the bacterium. Through biochemical tests (starch, gelatin and casein hydrolysis, catalase, urease and lipase activities, etc.) some characteristics of the isolates were determined and comparison was made.

α -Amylase Activity Assay. The enzyme activity was measured by DNS according to the method described by Bernfeld using 0.5% starch dissolved in a 0.1 M Tris-HCl buffer pH 7.0, for 30 min at 37°C. One unit of amylase activity was defined as the amount of enzyme that released 1 μ mol of reducing end groups per minute at 37°C [12].

Determination of Protein Content. The protein content was determined by the method of Lowry [13].

Effect of Temperature, pH and Incubation

Time on Microorganism and Amylase Production. Temperature values increasing from 15°C to 55°C with 5°C intervals were tried to investigate the effect of temperature on the production of bacteria and enzyme. Samples obtained were measured in spectrophotometer. Bacteria and enzyme production was made in various pH ranges from pH 2.0 to pH 11.0 for pH effect. For the effect of incubation time on microorganism development and enzyme production; bacteria were cultivated in NB (Nutrient broth) and measured in spectrophotometer between 4th and 96th hours at 4 hours intervals.

Effect of pH and Temperature on Enzyme Activity. Incubated culture of *Bacillus simplex* in NB was centrifuged for the pH effect. To define the optimum pH of α -amylase in the obtained supernatant; enzyme activity was measured with the usage of substrate prepared in 0.1 M citric acid (pH 4.0-6.0), 0.1 M Tris-HCl buffer (pH 7.0-9.0) and 0.1 M carbonate/bicarbonate (pH 10.0-11.0) buffers. Besides, the effect of temperature on amylase activity was investigated with enzyme activity measurement in various temperatures from 25°C to 55°C at 5°C intervals.

Effect of Carbon and Nitrogen Sources on Enzyme and Bacteria Production. Glucose, galactose, fructose, lactose, soluble starch, maltose and sucrose from the carbon sources at a concentration of 1% were added to 25 ml NB in 100 ml erlenmeyers. The effect of carbon sources on enzyme and bacteria production was determined by incubation in optimal conditions with spectrophotometric measurements.

After adding peptone, tryptone, urea, ammonium sulfate, ammonium chloride, ammonium nitrate, sodium nitrate, beef extract, yeast extract, it was incubated in optimal conditions and measured in spectrophotometer.

Partial Purification of α -Amylase. Bacteria cultivation was made in NB and incubated in 37°C temperature for 72 hours. After the incubation, it was centrifuged in 10 000 rpm for 15 minutes. Two following processes were applied in the partial purification of the enzyme. The processes were precipitated with ammonium sulfate and dialysis.

Ammonium Sulfate Precipitation. Ammonium sulfate [(NH₄)₂SO₄] of 40% and 70% respectively added to the supernatant in a sterile beaker. Afterwards, the mixture was centrifuged in a refrigerative centrifuge in 10 000 rpm for 15 minutes.

Dialysis. Pellet was dissolved in 0.1 M pH 7.0 Tris-HCl buffer, transferred to the dialysis tube and dialyzed against the same buffer in +4°C for overnight.

Determination of Thermal Stability and pH

Stability. For the determination of pH stability of α -amylase enzyme, 0.1 M citric, 0.1 M Tris-HCl, 0.1 M carbonate / bicarbonate (10.0 and 11.0) were prepared. The enzyme was pre-incubated in different buffers for 180 minutes. After the pre-incubation, substrate was added and the enzyme activity was measured under the experimental conditions.

To determine the temperature stability (thermal stability) of partially purified α -amylase enzyme, enzyme alone was pre-incubated in 30°C, 40°C and 50°C temperature values for 15-120 minutes. After pre-incubation, enzyme activity specification was made.

Effect of Some Metals on Enzyme Activity. In order to determine the effect of some metals on enzyme activity, 1.5 mM concentration in overall volume from the 50 mM-stock solutions of CaCl₂, CuCl₂, ZnCl₂, MgCl₂, HgCl₂, MnCl₂ ve FeCl₂ were prepared in 0.1 M pH 7.0 Tris-HCl buffer. After 30 minutes of pre-incubation, substrate was added and α -amylase activity was tested.

Effect of Some Detergents on Enzyme Activity. To investigate the effect of some detergents on partially purified enzyme activity, in the ratio of %0.5 SDS, Tween-40, Tween-80 and TritonX-100 were used. These detergents were prepared in 0.1 M pH 7.0 Tris-HCl buffer and pre-incubated for 30 minutes. Then, substrate was added and left to α -amylase activity.

TABLE 1
Morphological, Physiological and Biochemical Tests

Characteristics	<i>Bacillus simplex</i>
Gram painting	+
Cell form	rod shape
Temperature range (°C)	20-45
Optimum temperature (°C)	35
pH range	5.0-10.0
Optimum pH	7.0
Hemolysis	+
Motility	-
Hydrolysis of:	
Starch	++
Activity of:	
Urease	+
Catalase	+

+, positive result or growth; -, negative result or no growth.

RESULTS AND DISCUSSION

In this study, *Bacillus simplex* was isolated from the soil obtained from Ergani Makam Mountain and α -amylase production, partial purification and characterization were performed.

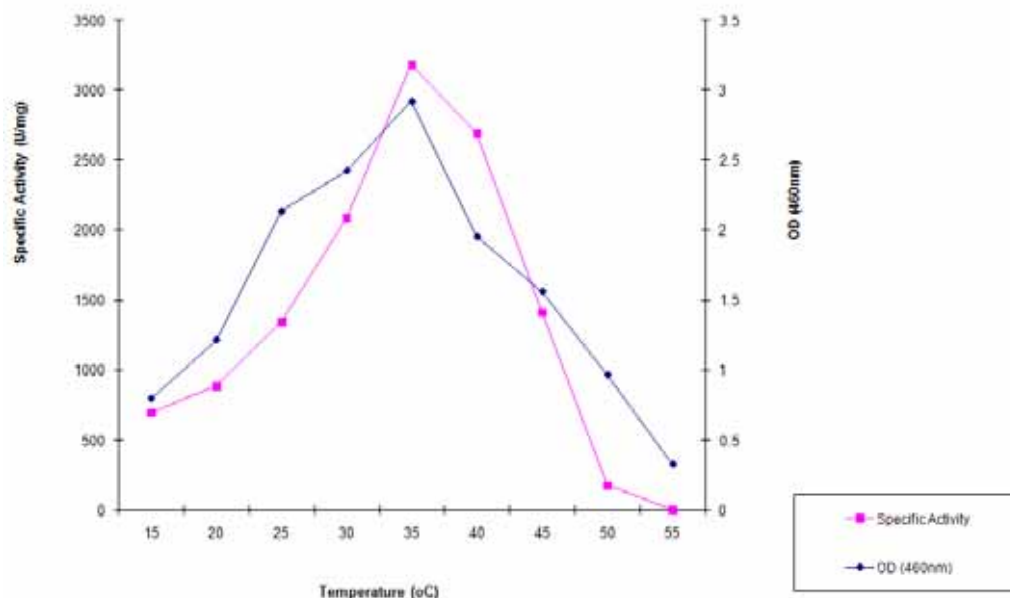


FIGURE 1
Effect of temperature on bacterial growth and enzyme activity

Morphological and Biochemical Tests. It was determined that the obtained isolate is gram-positive and has rod-shaped cells with the ability to form spores (Table 1).

The microorganism was identified by biochemical tests and 16S rRNA sequence. The 16S rRNA analyses of the obtained isolates were conducted by Ref-Gen (METU Technocity/Ankara). The 16S rRNA sequence of this strain is:

```

CCCACTGGCGGCGTGCTATACTGCAGT
CGAGCGAATCGATGGGAGCTTGCTCCCTGA
GATTATTCGGCGGACGGGTGAGTAACACGT
GGGCAACCTGCCTATAAGACTGGGATAACT
TCGGGAAACCGGAGCTAATACCGGATACGT
TCTTTTCTCGCATGAGAGAAGATGGAAAGA
CGGTTTACGCTGTCACTTATAGATGGGCC
GCGGCGCATTAGCTAGTTGGTGAGGTAATG
GTCACCAAGGCGACGATGCGTAGCCGAC
TGAGAGGGTGATCGGCCACACTGGGACTGA
GACACGGCCAGACTCCTACGGGAGGCAGC
AGTAGGGAATCTTCCGCAATGGACGAAAGT
CTGACGGAGCAACGCCGCGTGAACGAAGA
AGGCCTTCGGGTCGTAAAGTTCTTTGTTAGG
GAAGAACAAGTACCAGAGTAACTGCTGGTA
CCTTGACGGTACCTAACCAGAAAGCCACGG
CTAACTACGTGCCAGCAGCCGCGGTAATAC
GTAGGTGGCAAGCGTTGTCCGGAATTATTG
GGCGTAAAGCGCGCGCAGGTGGTTCCTTAA
GTCTGATGTGAAAGCCACGGCTCAACCGT
GGAGGGTCATTGGAAACTGGGGAACCTTGAG
TGCAGAAGAGGAAAGTGGAAATCCAAGTGT
AGCGGTGAAATGCGTAGAGATTTGGAGGAA
CACCAGTGGCGAAGGCCACTTTCTGGTCTG
TAACTGACACTGAGGCGCGAAAGCGTGGGG
AGCAAACAGGATTAGATACCCTGGTAGTCC
ACGCCGTAAACGATGAGTGCTAAGTGTTAG

```

```

AGGGTTTCCGCCCTTTAGTGCTGCAGCTAAC
GCATTAAGCACTCCGCTGGGGAGTACGGC
CGCAAGGCTGAAACTCAAAGGAATTGACGG
GGGCCCCGACAAGCGGTTGGAGCATGGTGG
ATTTAATTTCGAAGCAACGCGAAGAACCTTA
CAGGTCTTGACATCCTCTGACAACCCTAGA
GATAGGCTTCCCTTCGGGGACAGAGTGAC
AGGTGGTGCATGTTGTCGTCAGCTCTGTTCT
GGAATGTTGGGTTAAGTCCCCACGAGCCAC
CTTGATCTTAGTTGCAACATTCAGTTGGCAC
TCTAAGGTGACTGGCTGTGACAACGGAGAA
AGGTGGATAGACGTCATCTTCATGCCTTT
GACTGGCTAACCGGTCTAATGATGTTAAA
GGTTGCAACCTGCAGTAGGATCCTTAAGCA
C

```

Effect of Temperature, pH and Incubation Time on Microorganism and Amylase Production. To investigate the effect of temperature on bacteria reproduction and enzyme production, it was incubated between 15°C and 55°C. It was determined that maximum bacteria reproduction and enzyme production were observed at 37°C (Fig.1).

Temperature is related with microorganism growth and therefore, α -amylase production. Wide temperature range (35-80°C) was given for the optimum bacterial growth and α -amylase production by many researchers.

In the bacteria culture produced in various pH at 37°C, the best bacteria reproduction and amylase production was determined at pH 7.0 (Fig. 2).

pH of the growth environment among the physical parameters has an important role for the morphological changes of microorganism, therefore the increase of enzyme syntheses.

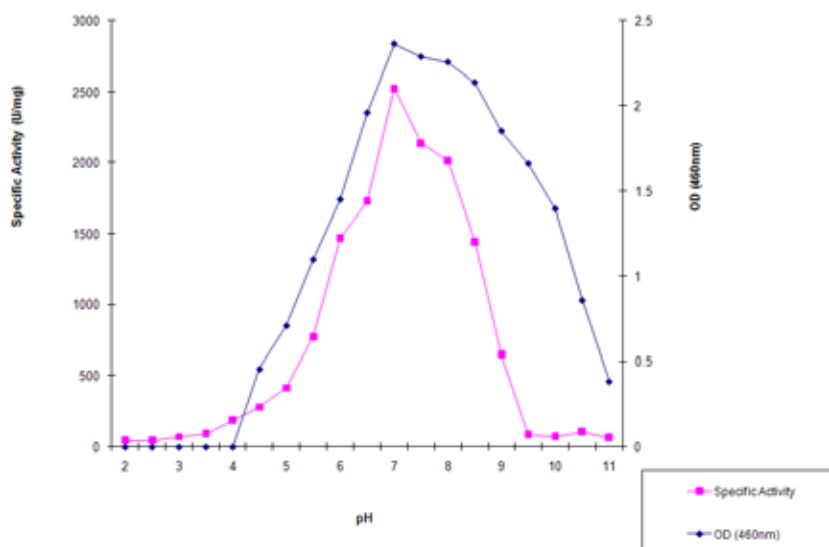


FIGURE 2
Effect of pH on bacterial growth and enzyme activity

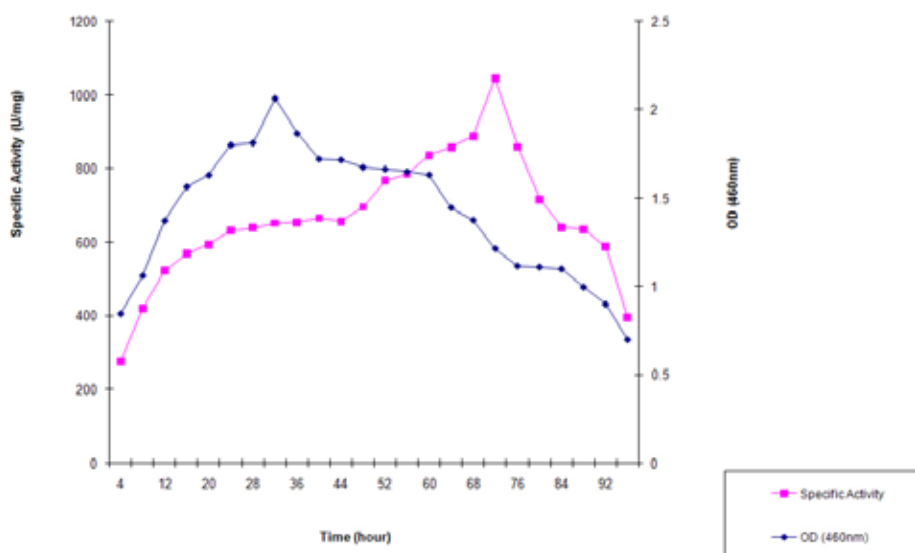


FIGURE 3
Effect of time on bacterial growth and enzyme production

For the effect of incubation time on microorganism development and enzyme production, a sample was taken at 4 hour intervals from the bacteria culture that was produced in 37°C NB, between 4th and 96th hours. As seen in the Fig. 3, the optimum incubation time for *Bacillus simplex* was determined to be 72 hours.

Hamilton et al. [14] determined the optimum incubation time at 41 hours, and temperature to be 40°C for *Bacillus sp.* IMD 43 production. Asgher et al.[15] determined incubation time to be 48 hours, temperature to be 50°C and pH to be 7.0 of thermophilic *Bacillus subtilis* JS-2004.

Effect of Temperature and pH on Enzyme Activity. To investigate the effect of temperature on α -amylase enzyme secreted by *Bacillus simplex*; bacteria were incubated in NB (pH 7.0) at 37°C that

was the optimum incubation temperature for 72 hours that was the optimum incubation time. α -Amylase activity was measured with temperature increase in the obtained supernatant from 25 °C to 55°C, according to Bernfeld method [12]. The highest α -amylase activity of *Bacillus simplex* was determined between 35°C and 40°C, the optimum temperature of the enzyme was determined at 37°C (Fig. 4).

It was determined that the enzyme obtained from the bacteria produced in optimum conditions were active between pH 5.0 and pH 11.0. Increase of the enzyme activity was observed starting from pH 5.0 whereas decrease of the enzyme activity was determined up to 7.0. As seen in the Figure 5, the optimum pH of α -amylase enzyme was determined to be 7.0.

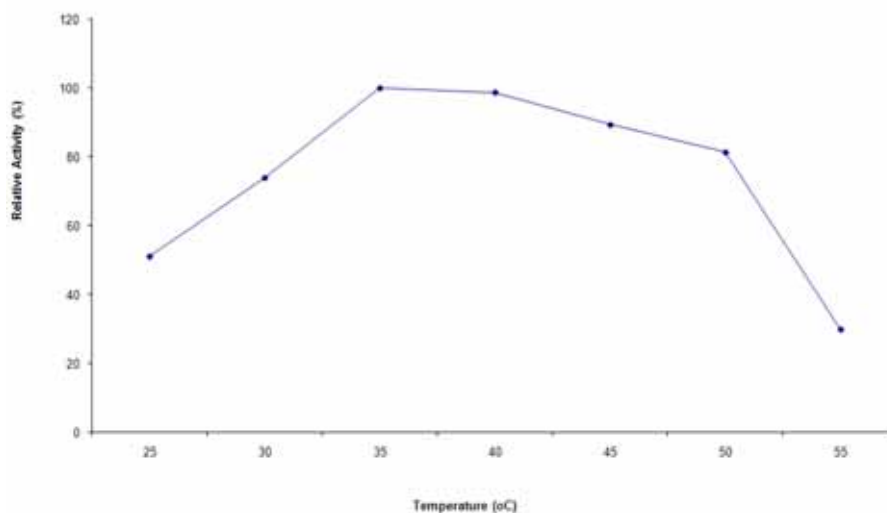


FIGURE 4

Effect of temperature on amylase activity

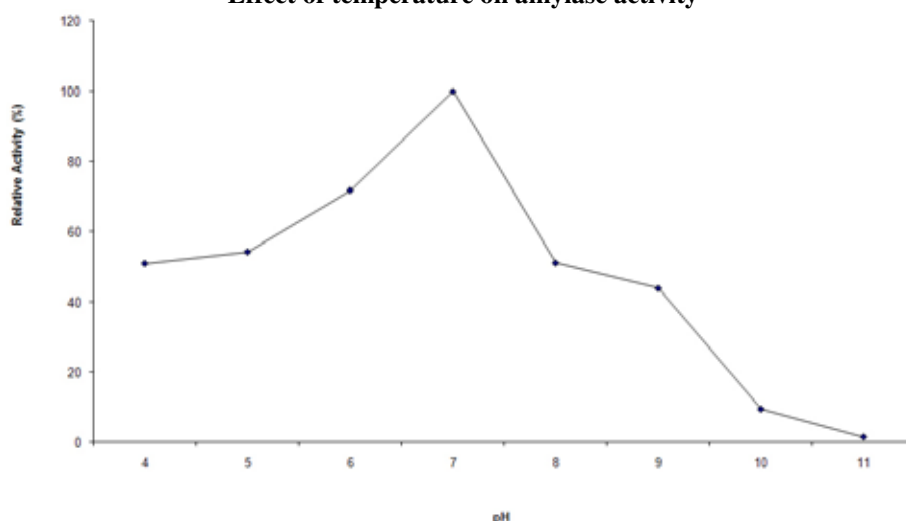


FIGURE 5

Effect of pH on amylase activity

Similar results were also implied by some other researchers. Noman et al. [16] studied on the purification of α -amylase enzyme from *Pachyrhizus erosus* L. They determined the optimum pH of the enzyme at 7.3 and temperature to be 37°C. Sudharhsan et al. [17] investigated the psychical and nutritional factors that affect the amylase production in the *Bacillus* species isolated from rotten food garbage, analyzed the effects of temperature and pH factors psychically and stated that the maximum enzyme activity was observed at pH 7.0 and 37°C.

The optimum pH of extracellular α -amylases varies between 3.0 and 10. In many studies, the optimum pH of α -amylases obtained from bacteria and fungi are stated as acidic and neutral [2]. Due to its usage in the areas such as liquefaction of starch, food industry and dry cleaning, the neutral pH is essential in such processes. The fact that α -amylase of *Bacillus simplex* exhibit maximum activity in neutral conditions that means it is usable in industrial processes.

Effect of Carbon and Nitrogen Sources on Enzyme and Bacteria Production. In the conducted research, when control was compared with other carbon sources, it was determined that glucose and galactose showed close activity to control while the amylase activity importantly reduced in other carbon sources. For bacteria reproduction, when control was compared to other carbon sources, it was determined that reproduction in all carbon sources was higher than control (Fig. 6).

As seen in the Fig. 7, when control was compared with other nitrogen sources, lower amylase activity was obtained in all nitrogen sources than control. The highest specific activity among nitrogen sources was obtained in the culture environment with ammonium nitrate and ammonium sulfate. In bacterial reproduction, an increase was observed in all nitrogen sources with regards to control.

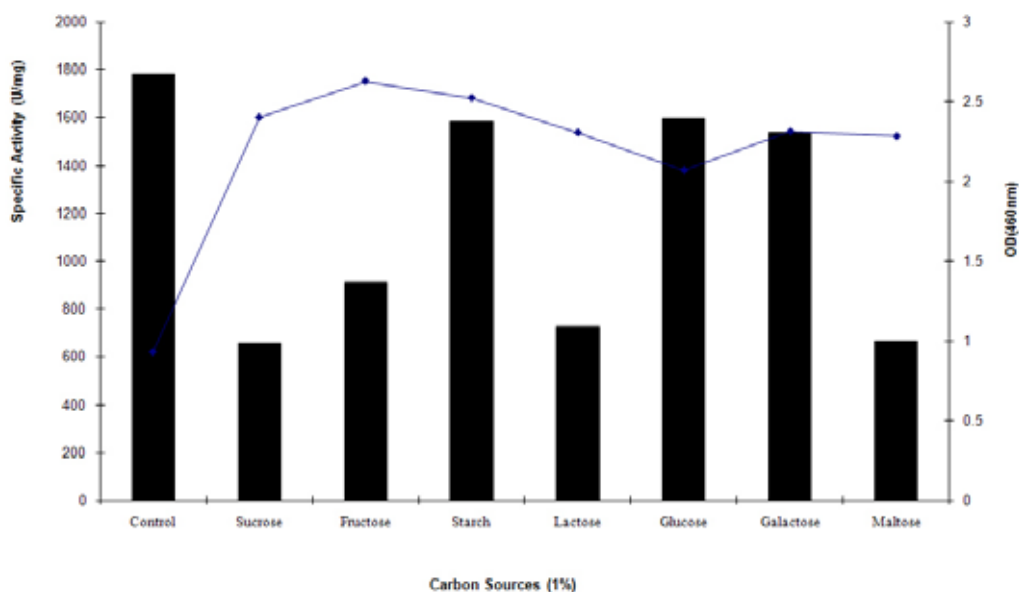


FIGURE 6
Effect of carbon sources on bacterial growth and amylase production

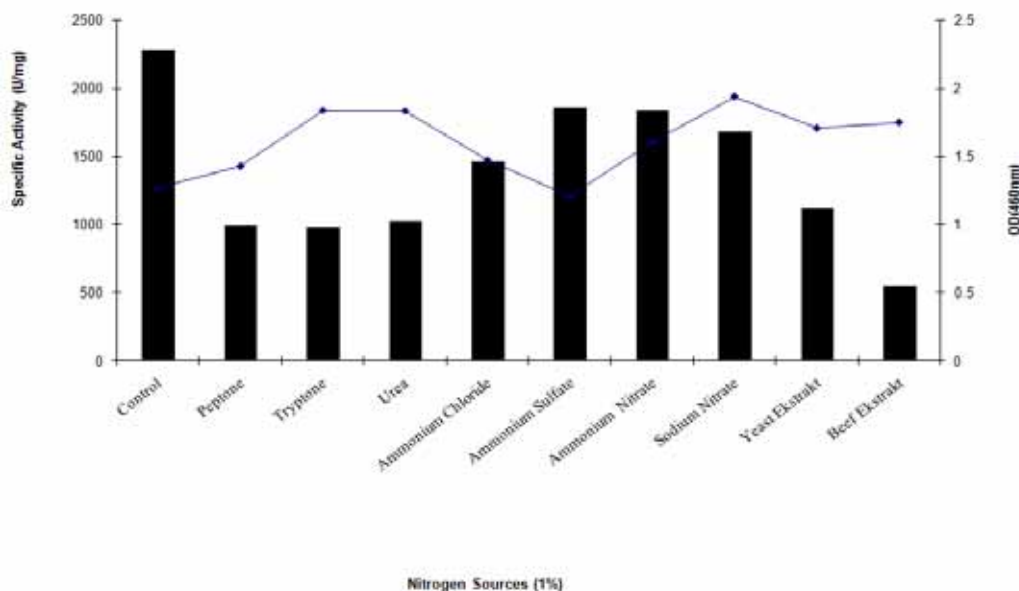


FIGURE 7
Effect of nitrogen sources on bacterial growth and amylase production

Behal et al. [18] produced α -amylase from *Bacillus* sp. AB 04 in nutrient media that has 1% fructose of carbon sources and %1 beef extract of nitrogen sources. Saxena et al. [19] acquired maximum specific activity in nutrient media that has (%) 0.6 starch, and 0.5 peptone 0.3 yeast extract for high thermostable amylase produced from *Bacillus* sp. PN5. Carvalho et al. [20] implemented the maximum production from thermophilic *Bacillus* sp. SMIA-2 in nutrient media with peptone as the nitrogen source and soluble starch as the carbon source. Prakash et al. [21] determined the best α -amylase production from halophilic *Chromohalobacter* sp. TVSP 101 bacteria in the media with tripton as the nitrogen source.

Partial Purification of Amylase. After the determination of optimum conditions of *Bacillus simplex* α -amylase, enzyme was partially purified. Bacteria culture produced in optimum conditions was centrifuged in a frigorific centrifuge in 10 000 rpm for 10 minutes. Ammonium sulfate $[(NH_4)_2SO_4]$ in 70% saturation level was added with stirring to the supernatant in a sterile beaker. Subsequently the mixture was centrifuged in 10 000 rpm for 15 minutes. Obtained pellet was dissolved in 0.1 M pH 7.0 Tris-HCl buffer, transferred to the dialysis tube and was dialyzed over night.

Effect of Metals. When the effect of some metals on partially purified enzyme activity was analyzed, it was determined that $CaCl_2$ (113%)

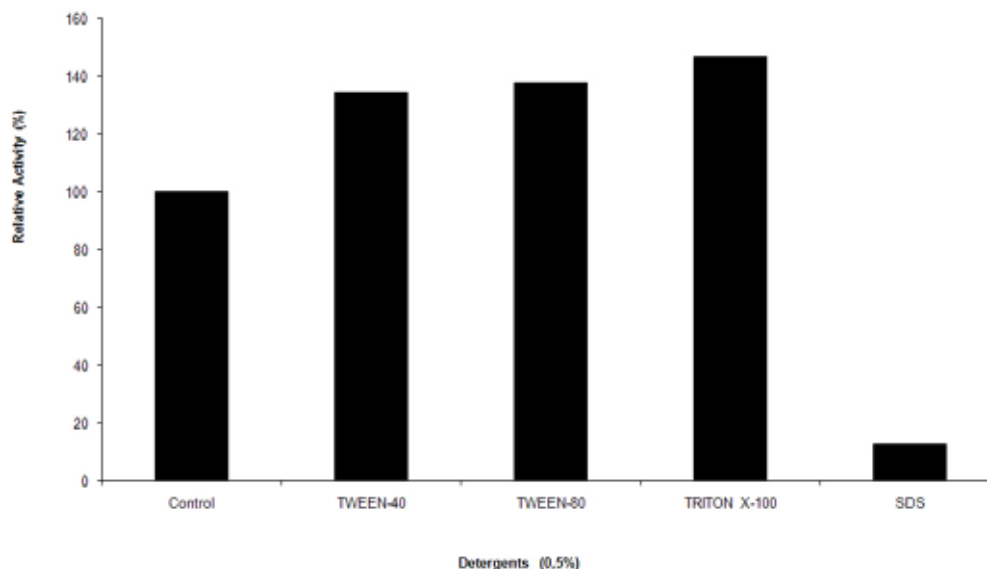


FIGURE 8

Effect of detergents on amylase activity

increased the activity; no change was observed after adding $MnCl_2$ (100%) and $MgCl_2$ (92%); $FeCl_2$ (61%) partially inhibited and $CuCl_2$ (22%), $ZnCl_2$ (24%), $HgCl_2$ (16%) strongly inhibited the enzyme activity (Table 2).

TABLE 2

Effect of cations on α -amylase activity

Effectors (1,5 mM)	Relative enzyme activity (%)
Control	100
Mn^{+2}	100
Fe^{+2}	61
Zn^{+2}	24
Mg^{+2}	92
Hg^{+2}	16
Cu^{+2}	22
Ca^{+2}	113

Shafiei et al. [22] biochemically characterized the amylase enzyme excreted from *Nesterenkonia* sp. F strain. They determined that Zn^{2+} , Fe^{3+} , Cu^{2+} and Al^{3+} ions inhibited the amylase activity while Ca^{2+} increased the it. Noman et al. [16] determined that Zn^{2+} , Fe^{2+} and Cu^{2+} ions make inhibition effect in high rate while Li^{+} , Hg^{+} and Cd^{2+} , Ag^{+} , Mg^{2+} and K^{+} ions have low effects on activity. Srivastava [23] determined that Cu^{2+} , Fe^{3+} , Ni^{2+} , Hg^{2+} , Pb^{2+} and Ag^{1+} ions completely inhibited the activity of purified amylase, but Ca^{2+} , Ba^{2+} , Sr^{2+} and K^{+} ions increased it. The results obtained from conducted studies support the findings we obtained from our study.

Effect of Detergents. To investigate the effect of some detergents on partially purified α -amylase enzyme activity, SDS in the ratio of 0.5%, Tween-40, Tween-80 and TritonX-100 were used. Rest of the enzymes were compared with the control and their relative activities were calculated. According to

the control, the amount of rest of the enzymes were determined to be; SDS 12%, Tween-40 134%, Tween-80 138% and TritonX-100 140% (Fig. 8). While the inhibition was observed only with the SDS effect, the inhibition having not been observed with other detergents shows the the resistance to detergents.

Asoodeh et al. [24] determined that α -amylase activity they purified from thermophilic *Bacillus* sp. *ferdowsicus* increased with Triton X-100. Shafiei et al. [22] determined that amylase was considerably stable to SDS, Triton X-100, Tween 80 and Tween 20 detergents.

In the literature, because disulfide bonds are found in the enzyme and becoming unstable to oxidation due to the amino acids undergoing a change by oxidation; it is stated that the thermostability of the enzyme increases and thus the enzyme is not affected by the oxidizing agents.

This result obtained suggests that the enzyme is not affected by oxidant agents, the amino acids change with heat and cause resistance.

pH and Temperature Stability. 25 μ l enzyme and various buffers prepared in 50 μ l were left and pre-incubation was done for 60 minutes. α -Amylase activity specification was made with substrate adding after pre-incubation. It was observed that pH stability of enzyme activity increased after pH 5.0 and started to decrease after pH 7.0. As seen in the Fig. 9, pH stability was found to be 7.0. To determine the temperature stability of partially purified enzyme, enzyme was pre-incubated in 30°C, 40°C and 50°C temperature values for 15, 30, 45, 60 and 120 minutes. After pre-incubation, enzyme activity specification was made. Partially purified enzyme was determined to be stable in 30°C, 40°C and 50°C after 2 hours (Fig.10).

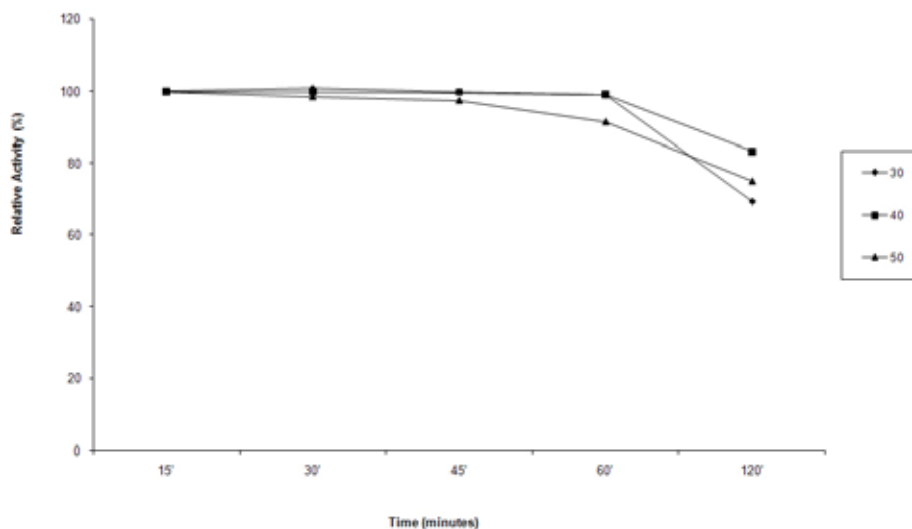


FIGURE 9
Effects of pH on amylase stability

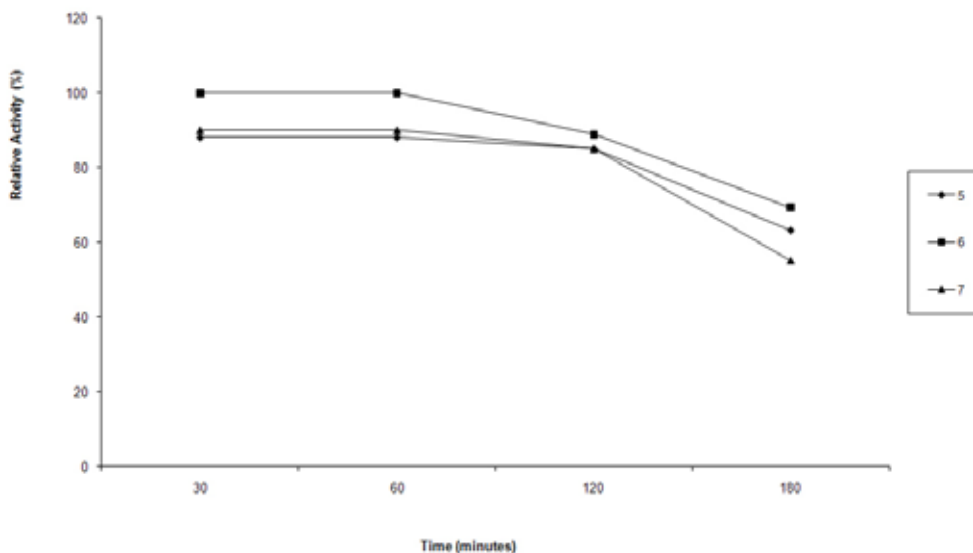


FIGURE 10
Effects of temperature on amylase stability

Bernhardsdotter et al. [25] detected that when the isolated amylase was pre-incubated in 37°C, between pH 7.0 and 11.0 for 1 hour, it lost the 20% percent of its original activity.

Wang et al. [26] detected that the purified amylase's pH stability was between 6.0 and 11.0 and its temperature stability was under 60°C

CONCLUSION

Studies about industrial enzymes are becoming more important since the enzyme technology is developing. Therefore, in our study, amylase which has a great industrial importance was produced easily and economic processes and was partially purified in optimum conditions.

REFERENCES

- [1] Agüloğlu, S., Ensari, N.Y., Uyar, F., Otludil, B. (2000). The effects of amino acids on production and transport of α -amylase through bacterial membranes. *Starch/Stärke*, 52:290–295.
- [2] Gupta, R., Gigras, P., Mohapatra, H., Goswami, V.K. (2003) Chauhan, B. Microbial α -amylase: a biotechnological perspective. *Process. Biochem*, 38:1599–1616.
- [3] Agüloğlu Fincan, S., Enez, B. (2014) Production, purification, and characterization of thermostable α -amylase from thermophilic *Geobacillus stearothermophilus*. *Starch/Stärke*, 66:182–189.
- [4] Boyce, A., Walsh, G. (2007) Production, purification and application-relevant characterization of an endo-1,2 (4)- β -glucanase from

- Rhizomucor miehei. Appl. Microbiol. and Biotechnol,76:835– 841.
- [5] Kirk, O., Borchert, T.V., Fuglsang, C.C. (2002) Industrial enzyme applications. Curr. Opin. Biotechnol, 3:345–35.
- [6] Enez, B., Ağuloğlu Fincan, S. (2016) Isolation, partial purification and characterization of thermostable xylanase from thermophilic *Anoxybacillus* sp. isolated from hot springs. Fresen. Environ. Bull, 25, 3028–3038.
- [7] Ağuloğlu Fincan, S., Enez, B., Özdemir, S., Matpan Bekler, F. (2014) Purification and characterization of thermostable α -amylase from thermophilic *Anoxybacillus flavithermus*. Carbohydr. Polym, 102:144– 150.
- [8] Kumagai, Y., Satoh, T., Inoue, A., Ojima, T. (2013) Enzymatic properties and primary structures of two α -amylase isozymes from the Pacific abalone *Haliotis discushannai*. Comp. Biochem. Physiol. B Biochem, Mol. Biol.164:80–88.
- [9] Lama, L., Nicolaus, B., DiDonato, P., Poli, A., Toksoy, Oner, E., Finore, I. (2009) A raw starch digesting α -amylase from the thermophilic *Anoxybacillus amylolyticus*. Purification and characterization. New Biotechnol, 25:91–92.
- [10] Wiseman, A. (1987) The application of enzyme in industry. Handbook of Enzyme Biotechnol, 3:275–373.
- [11] Alamri, S.A. (2010) Isolation, phylogeny and characterization of new α - amylase producing thermophilic *Bacillus* sp. from the Jazan Region, Saudi Arabia Int. J. Biotechnol. Biochem, 6:537–547.
- [12] Bernfeld, P. (1955) Enzymes Carbohydrate Metabolism. In Methods In Enzymol. Acad. Press,17:149–158.
- [13] Lowry, O.H., Rosebrough, N.J., Farr, A.L., Randall, R.J. (1951) Protein measurement with the folin-phenol reagent. J. Biol. Chem, 193:265–275.
- [14] Hamilton, L.M., Kelly, C.T., Fogarty, W.M. (1999) Production and properties of the raw starch digesting α -amylase of *Bacillus* sp. IMD 435. Process Biochem, 35:27–31.
- [15] Asgher, M., Asad, M.J., Rahman, S.U., Legge, R.L. 2007. A thermostable α -amylase from a moderately thermophilic *Bacillus subtilis* strain for starch processing. J. Food. Eng, 79:950–955.
- [16] Noman, A.S.M., Hoque, M.A., Sen, P.K., Karim, M.R. (2006) Purification and some properties of α -amylase from post-harvest *Pachyrhizus erosus* L. tuber. Food Chem,99: 444–449.
- [17] Sudharhsan, S., Senthilkumar, S., Ranjith, K. (2007) Physical and nutritional factors affecting the production of amylase from species of bacillus isolated from spoiled foodwaste. Afr. J. Biotechnol, 6:430-435.
- [18] Behal, A., Singh, J., Sharma, M.K., Puri, P., Batra, N. (2006) Characterization of alkaline α -amylase from *Bacillus* sp. AB 04. Int. J. Agric. Biol., 8:80–83.
- [19] Saxena, R.K., Dutt, K., Agarwal, L., Nayyar, P. (2007) A highly thermostable and alkaline amylase from a *Bacillus* sp. PN5. Bioresour. Technol, 98:260–265.
- [20] Carvalho, R.V., Córrea, T.L.R., Silva, J.C.M., Mansur, L.R.C.O., Martins, M.L.L. (2008) Properties of an amylase from thermophilic *Bacillus* sp. Braz. J. Microbiol, 39:102–107.
- [21] Prakash, B., Vidyasagar, M., Madhukumar, S., Muralikrishna, G., Sreeramulu, K. (2009) Production, purification, characterization of two extremely halotolerant, thermostable, and alkalistable α -amylases from *Chromo halobacter* sp. TVSP 101. Process Biochem, 44:210–215.
- [22] Shafiei, M., Ziaee, A.A., Amoozegar, M.A. (2010) Purification and biochemical characterization of a novel SDS and surfactant stable, raw starch digesting and halophilic α -amylase from a moderately halophilic bacterium *Nesterenkonia* sp. strain F. Process Biochem, 45:694–699.
- [23] Srivastava, R.A.K. (1987) Purification and chemical characterization of thermostable amylase produced by *Bacillus stearothermophilus*. Enzyme Microb. Technol, 9:749–755.
- [24] Asoodeh, A., Chamani, J., Lagzian, M. (2010) A novel thermostable, acidophilic alpha-amylase from a new thermophilic "*Bacillus sp. Ferdowsicus*" isolated from Ferdows hot mineral spring in Iran: Purification and biochemical characterization. Int. J. Biol. Macromol, 46:289–297.
- [25] Bernhardsdotter, E.C.M.J., Josepli, D., Garriott, O.K., Pusey, M.L. (2005) Enzymic properties of an alkaline chelator-resistant α -amylase from alkaliphilic *Bacillus* sp. isolate L1711. Process Biochem, 40:2401–2408.
- [26] Wang, S.L., Liang, Y.C., Liang, T.W. 2011. Purification and characterization of a novel alkali stable α -amylase from *Chryseobacterium taeanense* TKU001, and application in antioxidant and prebiotic. Process Biochem, 46:745–750.

Received: 08.02.2017
Accepted: 26.04.2017

CORRESPONDING AUTHOR

Sema Aguloglu Fincan
Department of Biology, Faculty of Science, Dicle
University, Diyarbakir, Turkey

e-mail: semaguloglu@hotmail.com

RESPONSE TO HEAVY METALS ON POLLEN VIABILITY, GERMINATION AND TUBE GROWTH OF SOME APPLE CULTIVARS

Ferhad Muradoglu^{1,*}, Omer Beyhan², Ferit Sonmez³

¹Department of Horticulture, Faculty of Agriculture and Natural Sciences, Abant Izzet Baysal University, Bolu,

²Pamukova Vocational School, Sakarya University, Pamukova, Turkey

³Department of Seed Science and Technology, Faculty of Agriculture and Natural Sciences, Abant Izzet Baysal University, Bolu,

ABSTRACT

Heavy metal toxicity is one of the major abiotic stresses leading to hazardous effects in plants and pollen are among the most sensitive to atmospheric pollution. Both pollen germination and tube length are inhibited by adverse environmental conditions. Pollen grains from three apple (Gala, Fuji and Braeburn) cultivars were tested for determination of pollen quality (pollen viability, germination ability and tube length) and five types of Heavy metals (Cd, Co, Pb, Hg and Zn). Viability of the pollens were determined by TTC test. The pollen germination experiments were conducted in petri dishes in 10% sucrose, 0.01% boric acid and 22°C temperature for 3 hours. Among the cultivars highest pollen viability were recorded in Braeburn with 81.85%. Heavy metals lead to a significant decrease in pollen germination and tube length of apple cultivars. It was found that there were different cultivars with variable sensitivity to heavy metals on pollen germination and tube length. In general, increasing heavy metal treatments inhibited pollen germination and tube length in all cultivars. Among heavy metals mercury (Hg) had the highest toxic effect on pollen growth and tube length of all cultivars. Heavy metals have negative effect on reproduction of plant due to inhibition of pollen viability and germination.

KEYWORDS:

Apple, heavy metal, pollen viability, tetrazolium

INTRODUCTION

Metal toxicity of air and agricultural are serious environmental problems on world at increasing level due to natural and human activities [1]. In last years many researchers all over world studied on heavy metals toxicity contraption, its accumulation and their harmful effect in plants. The studies have been focusing on biochemical-physiological process such as seed germination, photosynthesis, transpiration, leaf senescence. The over production of reactive oxygen species (ROS), which may result in damage the

proteins and lipids membrane are indicators of oxidative stress in plant [2, 3, 4, 5]. Pollens are male reproductive cells and travel through air for pollination. Industrial development and consumption of petroleum products leads to increase air pollution levels especially in urban and industrial areas. Pollens are considered to be more sensitive to pollutants than vegetative parts of the plants. Pollen germination and tube growth are sensitive plant indicators used to detect pollution such as air pollution, pesticides, heavy metals and acid rain [6, 7]. During pollinations pollens are exposed to air pollutants and the viability of pollens are also affected by air metal toxicity and some species leading to deterioration of their fertility. Apples have hermaphrodite flower structure and great majority of the cultivars are self-incompatible [8]. After flowers pollination, pistil fertilization is necessary for fruit set [9]. For successful pollination the high quantity and quality pollen must be transferred to the stigma when it is receptive [10]. The viability, tube growth and morphological homogeneity related to pollen quality are the most important properties in fruit trees. These properties are useful for plant breeders, geneticists, and growers [11]. Therefore, many researchers studied on inhibition of viability, tube growth and pollen morphology such as, effect of methyl jasmonat in apricot by Muradoğlu et. al., [12], bioregulators (brassinolide, gibberellic acids and kinetin) in almond by Maita and Sotomoyar [13], jasmonic acid, ACC and ethephon in strawberry by Yıldız and Yılmaz [14] and Hg (mercury) in apple by Munzur and Gür [15], Pb (lead) *Picea wilsonii* by Sheng et. al., [16] and Cd (cadmium) *Picea wilsonii* by Wang et. al., [17]. So far, many studies with relevant heavy metal influence was conducted on physiological and biochemical processes in plants. But the effects of heavy metal toxicity on sexual reproduction and their physiological and biochemical mechanisms under multiple heavy metal stress in plants is very limited, despite this complex process is extremely important. In the present study, response of pollen germination and tube length from three apple cultivars were evaluated under five heavy metals.

MATERIALS AND METHODS

This study was undertaken in the Lake Van region of Eastern Turkey on cultivars of Gala, Fuji and Braeburn grafted onto M9 rootstocks. The study conducted at an altitude of 1675 m, with 377 mm precipitation, a continental climate and under standard growing conditions such as irrigations, fertilization and pest control. The flowers were collected from 8 years old trees of the apple cultivars. Before petals opened, they were kept at the room temperature for 24 hours. In this study, firstly, pollen viability was tested according to Eti [18] in 1% TTC (2, 3, 5-triphenyl tetrazolium chloride). After pollen viability, pollens were germinated in liquid media containing 10% sucrose and 0.01% boric acid [19, 15]. Sterile 3 microscopic slides were used for each treatment. Heavy metals solutions and culture medium at the same volumes were used. At first, 50 μ L liquid media were dropped on microscopic slides. Then, 50 μ L heavy metals solutions and were dripped on to slides. Heavy metals solutions prepared with distilled water were 50, 100, 250, 300, 400 and 500 μ M for Cd ($\text{CdSO}_4 \cdot 8 \text{H}_2\text{O}$), Co ($\text{CoCl}_2 \cdot 6\text{H}_2\text{O}$) and Pb [$\text{Pb}(\text{NO}_3)_2$]. Also for Hg (HgCl_2) and Zn (ZnCl_2), 25, 50, 75, 100, 125 and 150 μ M and for control group, 50 μ L distilled water was dropped instead of heavy metal solutions. Pollens were shed in this liquid culture media under Olympus light microscope with aid of sterile pin. The microscopic slides with pollens were placed in petri dishes with a moist filter paper lining the lower plate, serving as an improvised humidity chamber. Then, the petri dishes were settled in incubator at $22 \pm 2^\circ\text{C}$ for 3 hours under dark conditions. After incubation, a few drop of 10% ethanol was added to the microscopic slides for fixations and then placed cover slip. Germination percentages of pollens were determined by examining grain and tube lengths of pollens were measured by using an ocular micrometer under Olympus light microscope [20]. In the study, a completely randomized design with three replications was used.

STATISTICAL ANALYSIS

The experiment was designed as a complete random block design and all measurements were replicated four times. The statistical analysis of the data was performed using SPSS (22.0) program. The results were statistically evaluated by ANOVA using and error bars in table shows \pm standard error.

RESULTS AND DISCUSSION

Pollen viability and germination is very significant in fruit trees for regular and quality yield. En-

vironmental conditions such as acid rain, temperature, heavy metals, medium culture, precipitation and heavy wind negatively affect pollination. The viability, germination and tube length of apple cultivars is investigated in this study. The results of TTC test for pollen viability are shown Figure 1. Comparison between pollen viability indicate that the highest viability percentage was obtained from Braeburn cultivars with 81.32% and followed Gala cultivars with 74.32% and Fuji cultivars with 70.67% (Figure 1). Similar results were obtained by Petrisor et al., [21], who reported that pollen viability of apple cultivars was recorded between 52.55 and 89.92%. Similar to this study, TTC test analysis is commonly used in many fruits for pollen viability. Derin and Eti [22] reported that the rate of pollen viability in pomegranate cultivars changed between 68.61 and 75.24% using TTC test. Similarly, Bolat and Pirlak [11] reported that the pollen viability ranged from 75.67 to 85.75% (apricot) and varied between 67.35 and 80.95 (sweet cherry) using TTC test analysis.

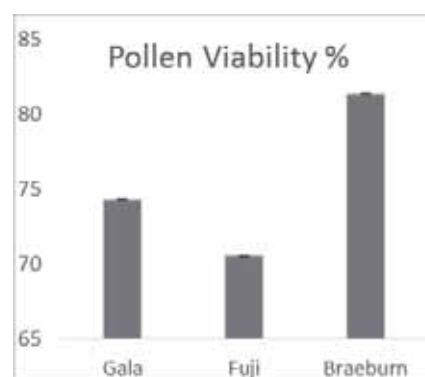


FIGURE 1
Pollen viability level of tested (TTC) apple cultivars.

Pollen germination and pollen tube growth are key events in the sexual reproduction of plants and successful fertilization need high germination rates and fast tube growth because low rates may lead to low fruit set [23, 24]. In this study, pollen of three apple cultivars were exposed different concentration of heavy metals showed different response to pollen germination rate and tube growth length. Results indicated pollen germination and tube growth was significantly inhibited by increasing heavy metal concentration (Table 1). In control, both pollen germination rate and pollen tube length was found higher in Braeburn cultivar 73.23% and 524.93μ than Gala 66.13% and 487.20μ and Fuji 64.20% and 327.39μ cultivars. These results were in agreement in with previously study by Petrisor, et al.,[21] and Munzuroğlu and Gür [15] they have shown pollen germination and tube length of Golden cultivars between 92.3 and 96.5% arranged from 593.4 to 642.3μ and on ten apple cultivars ranged from 52.55 to 89.92% and between 99.65 and $153.62\mu\text{m}$ respectively.

TABLE 1
The effect of Cadmium (Cd) treatment on pollen germination rates (%) and tube length (μ) in apple cultivars

Treatments (μ M)	Apple cultivars					
	Gala		Fuji		Braeburn	
	PG	PTL	PG	PTL	PG	PTL
Control	66.13 \pm 4.67	487.20 \pm 34.19	64.20 \pm 3.53	327.39 \pm 14.74	73.23 \pm 3.11	524.93 \pm 22.37
Cd50	73.28 \pm 4.05	256.16 \pm 19.54	63.98 \pm 3.45	274.39 \pm 10.16	76.66 \pm 3.13	318.09 \pm 19.13
Cd100	67.98 \pm 3.11	157.89 \pm 6.85	56.11 \pm 2.82	225.49 \pm 10.26	67.98 \pm 3.10	283.21 \pm 19.52
Cd250	46.66 \pm 3.56	102.72 \pm 9.29	41.43 \pm 2.68	157.74 \pm 9.73	39.70 \pm 2.63	69.46 \pm 9.74
Cd300	41.29 \pm 2.84	79.17 \pm 5.11	38.52 \pm 2.80	114.67 \pm 7.09	32.73 \pm 2.56	37.50 \pm 8.78
Cd400	37.63 \pm 3.43	65.07 \pm 5.56	23.58 \pm 2.36	84.13 \pm 8.55	11.16 \pm 1.92	15.47 \pm 6.72
Cd500	27.08 \pm 2.85	36.46 \pm 6.71	17.76 \pm 1.89	56.88 \pm 4.51	6.72 \pm 1.81	6.52 \pm 3.31

TABLE 2
The effect of Lead (Pb) treatment on pollen germination (%) and tube length (μ) in apple cultivars

Treatments (μ M)	Apple cultivars					
	Gala		Fuji		Braeburn	
	PG	PTL	PG	PTL	PG	PTL
Control	66.13 \pm 4.67	487.20 \pm 34.19	64.20 \pm 3.53	327.39 \pm 14.74	73.23 \pm 3.11	524.93 \pm 22.37
Pb50	59.63 \pm 3.73	386.36 \pm 22.28	58.19 \pm 3.69	288.89 \pm 13.83	63.80 \pm 3.47	354.21 \pm 22.32
Pb100	48.81 \pm 5.76	316.36 \pm 20.34	53.31 \pm 3.26	227.62 \pm 12.69	55.87 \pm 2.78	232.30 \pm 18.32
Pb250	25.24 \pm 3.22	78.98 \pm 12.44	33.97 \pm 2.66	148.20 \pm 11.68	45.60 \pm 2.69	103.22 \pm 10.77
Pb300	18.76 \pm 3.07	48.71 \pm 12.14	28.35 \pm 2.61	129.75 \pm 10.94	38.72 \pm 2.31	83.62 \pm 8.42
Pb400	9.33 \pm 2.96	31.75 \pm 7.98	14.39 \pm 2.80	112.65 \pm 6.57	33.87 \pm 2.08	70.11 \pm 5.35
Pb500	1.32 \pm 0.53	15.39 \pm 4.21	10.41 \pm 1.89	89.98 \pm 6.23	23.62 \pm 1.88	26.15 \pm 4.60

TABLE 3
The effect of Cobalt (Co) treatment on pollen germination (%) and tube length (μ) in apple cultivars

Treatments (μ M)	Apple cultivars					
	Gala		Fuji		Braeburn	
	PG	PTL	PG	PTL	PG	PTL
Control	66.13 \pm 4.67	487.20 \pm 34.19	64.20 \pm 3.53	327.39 \pm 14.74	73.23 \pm 3.11	524.93 \pm 22.37
Co50	79.14 \pm 4.40	430.29 \pm 31.92	63.15 \pm 4.72	355.16 \pm 16.59	77.20 \pm 4.00	540.66 \pm 24.84
Co100	70.34 \pm 3.21	406.04 \pm 28.28	59.92 \pm 3.21	336.38 \pm 16.63	75.57 \pm 3.32	468.40 \pm 21.33
Co250	68.77 \pm 4.44	389.14 \pm 26.50	56.52 \pm 3.91	312.49 \pm 12.83	74.78 \pm 2.98	454.71 \pm 17.63
Co300	56.94 \pm 4.45	303.62 \pm 24.80	54.13 \pm 2.96	232.52 \pm 11.34	70.71 \pm 2.15	409.97 \pm 14.94
Co400	53.85 \pm 4.62	258.80 \pm 23.35	50.94 \pm 2.42	215.61 \pm 9.93	69.60 \pm 2.08	306.15 \pm 13.22
Co500	46.16 \pm 4.53	237.90 \pm 22.83	46.56 \pm 1.90	211.72 \pm 8.39	68.22 \pm 1.90	225.01 \pm 12.00

In exposed to cadmium (Cd), the lowest treatment seem to have no significant effect on pollen germination rate but both pollen germination and tube length was inhibited with increase of Cd treatment. In cultivars, the high inhibition of pollen germination with 90.82% and tube length with 98.76% was determined in Braeburn cultivar compared to control. This cultivar followed by Fuji (72.34% with pollen germination and 82.63% with tube length) and Gala (59.05% with pollen germination and 92.52% tube length).

Relative pollen germination rates and tube length of three cultivars exposed to different lead (Pb) treatments are listed to Table 2. Pollen germination and tube length of three cultivars were decreased due to Pb toxicity and rate of decrease ranged from 67.75 (in Braeburn) to 98.00% (in Gala) and from 72.53 (in Fuji) to 96.84% (in Fuji) over controls at 500 μ M Pb respectively. However, the percent decrease in pollen germination was found relatively less in Braeburn cultivar than Fuji and

Gala cultivars but tube length was found less in Fuji cultivar than Braeburn and Gala cultivars.

The results of different Cobalt (Co) treatments on pollen germination and tube length are shown in Table 3. In Gala and Braeburn cultivars pollen germination were monitored increased by 19.67% and 5.42% (50 μ M), 6.37% and 3.20 (100 μ M) and 3.99% and 2.12 (250 μ M) respectively. On the other hand, an inhibition in PG was monitored after 250 μ M (in Gala and Braeburn cultivars) and the pollen germination inhibition was decline nearly 30.20% (in Gala), 27.48% (in Fuji) and 6.84% (in Braeburn) as compare to control over 500 μ M cobalt treatment. The pollen tube length increased considerably within Gala (50 μ M) and Fuji (50 μ M and 100 μ M) but decreased about 51.17% in Gala, 35.33% in Fuji and 57.14% in Braeburn under 500 μ M treatment of cobalt.

As shown in Table 4. In Fuji cultivars, increasing zinc (Zn) treatments were increased pollen germination 3.18% up to 50 μ M and tube length

TABLE 4
The effect of Zinc (Zn) treatment on pollen germination (%) and tube length (μ) in apple cultivars

Treatments (μM)	Apple cultivars					
	Gala		Fuji		Braeburn	
	PG	PTL	PG	PTL	PG	PTL
Control	66.13±4.67	487.20±34.19	64.20±3.53	327.39±14.74	73.21±3.11	524.93±22.37
ZN25	62.21±3.32	407.19±25.09	66.24±3.53	500.94±30.31	74.10±3.16	440.53±19.80
ZN50	54.06±3.48	296.71±11.82	63.90±3.89	442.75±24.17	73.15±2.43	405.76±17.47
ZN75	41.80±2.99	238.04±11.02	53.63±3.72	405.67±23.34	72.25±2.60	399.81±16.41
ZN100	39.18±1.02	199.37±10.90	49.12±3.14	312.95±15.81	70.21±2.61	285.41±16.41
ZN125	35.70±1.29	187.61±9.74	38.97±2.89	263.42±14.16	65.40±2.54	265.17±12.48
ZN150	31.84±1.70	143.53±6.96	30.63±1.96	223.13±12.88	61.22±2.11	250.13±10.45

TABLE 5
The effect of Mercury (Hg) treatment on pollen germination (%) and tube length (μ) in apple cultivars

Treatments (μM)	Apple cultivars					
	Gala		Fuji		Braeburn	
	PG	PTL	PG	PTL	PG	PTL
Control	66.13±4.67	487.20±34.19	64.20±3.53	327.39±14.74	73.23±3.11	524.93±22.37
Hg25	49.81±5.70	412.36±29.24	62.26±2.67	287.43±17.16	70.56±3.65	259.32±21.72
Hg50	40.46±4.49	379.83±23.96	57.82±2.53	216.42±15.47	56.68±3.15	231.79±17.08
Hg75	19.76±4.89	185.72±21.36	52.11±3.06	208.03±14.46	31.54±2.82	168.75±15.50
Hg100	9.50±2.49	123.89±11.44	23.62±2.15	111.68±10.78	20.77±2.42	41.76±13.43
Hg125	5.67±0.76	49.83±7.66	9.49±2.46	64.59±10.90	5.81±1.22	22.51±10.09
Hg150	2.42±0.22	23.73±4.06	4.13±1.68	26.37±7.82	2.20±1.00	10.57±5.91

was show regularly increased from 53.01, 35.24 to 23.91% Zn treatments respectively. In tube length was show an inhibition after 100 μM Zn treatments and this inhibition was continued to 500 μM Zn treatments that this decline was higher than the control by 31.85% in Fuji cultivars. Conversely of Fuji cultivars, Zn treatments were inhibited pollen germination and tube length approximately 51.85% and 70.54% (in Gala) and 16.38% and 52.35% (in Braeburn) as compared with control respectively.

This study shows that an increase in mercury (Hg) treatments inhibited of pollen germination and tube length all apple cultivars. In Gala, Fuji and Braeburn apple cultivars, pollen germination rate and tube length was decreased sharply varied from 96.34% to 95.13% (in Gala), from 93.36% to 91.95% (in Fuji) and from 97.00% to 97.99% (in Braeburn) with increasing Hg treatments from control to 150 μM respectively (Table 5).

In this study heavy metals was the most effective in inhibiting pollen growth and tube length in different rates. Gala cultivar was found very sensitive than Braeburn and Fuji cultivars. In general the most toxicity effect prevent to pollen germination and tube length was found copper from among heavy metals. Many studies have shown that heavy metals adversely affected vegetative and generative growth in different plant species and cultivars. Similar to results of this study Munzuroğlu and Gür [15], reported that heavy metals effected pollen germination and tube length rates and mercury (Hg) show the highest toxic effect among heavy metals. Similar negative effect of heavy metals on pollen germination and tube length have been reported by Sabrina et al., [3] in pea (*Pisum sativum* L.) found that pollen

germination inhibited by Cd 78% and Cu 72%. Previous report indicated that in *M. sylvester* and *C. Vulgaris* plant, pollen germination and tube length strongly inhibited by Cd and Cu [25]. According to Cox [6] Pollen germination and tube length are considered to be among sensitive botanical indicators of air pollution. Pollen is considered to be more sensitive to pollutants than the vegetative parts of plant. In plant, pollen germination and pollen tube growth depend on various factors such as pollen species, nutrition conditions, and air pollutants as well as on the pollutants and their concentration, the exposure time, relative humidity, light, temperature, pH, storage, biochemical processes and among some environmental factors the one of the most environmental factors is heavy metal affecting plant growth and productivity. Understanding apple pollination and fertilization, primarily pollen tube growth rates and tube length, can help crop load management and fruit quality. In this study we tested the pollen viability, germination and tube length of different apple cultivars and also determined effect of different heavy metals treatments which can be used for further studies. In conclusion, it is found that heavy metals have toxicity effect on plant, when the concentration is increased to high level, pollen germination and tube length was seriously inhibited and reducing their reproductive ability. We suggested that future research on pollen should be done on different morphological, biochemical and cytological aspects of heavy metal stress in new apple cultivars.

REFERENCES

- [1] Thounaojam, T.C., Panda, P., Mazumdar, P Kumar, D., Sharma, G.D., Sahoo, L. and Panda, S.K. (2012) Excess copper induced oxidative stress and response of antioxidants in rice. *Plant physiol. Biochem.* 53: 33-39.
- [2] Panda S.K. and Choudhury, S. (2005) Chromium stress in plants. *Braz. J. Plant Physiol.*, 17:95-102.
- [3] Sabrine, H., Afif, H., Mohamed, B., Hamadi, B. and Maria, B. (2010). Effects of cadmium and copper on pollen germination and fruit set in pea (*Pisum sativum* L. *Scientia Horticulturae* 125:551-555
- [4] Hassan, M. and Mansoor S. (2014) Oxidative stress and antioxidant defence mechanism in mung bean seedlings after lead and cadmium treatments. *Turk J. Agric. For.* 38:55-61
- [5] Muradoğlu, F., Encu, T., Gündoğdu, M and Canal, S.B. (2016) Influence of lead stress on growth, antioxidative enzyme activities and ion change in root and leaf of strawberry. *Fresen. Environ. Bull.*, 25(2):623-632.
- [6] Cox, R.M. (1988) The sensitive of pollen from various coniferous and broad-leaved trees to combinations of acidity and trace metals. *New phytol.* 109:193-201.
- [7] Gür, N. and Topdemir, A. (2005) Effect of heavy metals (Cd, Cu, Pb, Hg) on pollen germination and tube growth of Quince (*Cydonia oblonga* M) and Plum (*Prunus domestica* L.) *Fresen. Environ. Bull.*, 14:36-39.
- [8] Broothaerts, W. (2003). New findings in apple S-genotype analysis resolve previous confusion and request the renumbering of some Salleles. *Theor. Appl. Genet.*, 106: 703-714.
- [9] Calzoni, GL., Speranza A. and Bagni, N. (1979) In vitro germination of apple pollens. *Scientia Horticulturae*, 10:49-55.
- [10] Dekers, T. and Porreye, W. (1984) Influence of the temperature on pollen germination of different cultivars of apple and pear trials in vitro. *Acta Hort*, 149: 123-130.
- [11] Bolat, I. and Pirlak, L. (1999) An Investigation on Pollen Viability, Germination and Tube Growth in Some Stone Fruits. *Tr. J. of Agriculture and Forestry*, 23:383-388.
- [12] Muradoğlu, F., Yıldız, K. and Balta, F. (2010) Methyl jasmonate influences of pollen germination and pollen tube growth of apricot (*Prunus armeniaca* L.) *YYU. J Agr Sci.* 20(3):183-188.
- [13] Maita, S. and Sotomayer, C. (2015) The effect of three plant bioregulators on pollen germination, pollen tube growth and fruit set in almond [*Prunus dulcis* (Mill.) D.A. Webb] cvs. Non Pareil and Carmel. *Electronic Journal of Biotechnology.* 18(5):381-386.
- [14] Yıldız, K. and Yılmaz, H. (2002) Effect of jasmonic acid, ACC and ethephon on pollen germination in strawberry. *Plant Growth Regulation* 38:145-148.
- [15] Munzuroğlu, O. and Gur, N. (2000) The effects of heavy metals on the pollen germination and pollen tube growth of apples (*Malus sylvestris* Miller cv. Golden). *Turk J Biol* 24:677-84.
- [16] Sheng, X., Zhang, S., Jiang, L., Li, K., Gao, Y. and Li, X. (2012) Lead stress disrupts the cytoskeleton organization and cell wall construction during *Picea wilsonii* pollen germination and tube growth. *Biol Trace Elem Res* 146: 86-93.
- [17] Wang, X., Gao, Y., Feng, Y., Li, X., Wei, Q. and Sheng, X. (2014) Cadmium stress disrupts the endomembrane organelles and endocytosis during *Picea wilsonii* pollen germination and tube growth. *PLoS One.* 9(4).
- [18] Eti, S. (1991) Determination of pollen viability and germination capability of some fruit species and cultivars by different in vitro test *J. Agric. Faculty Çukurova Univ.* 6:69-80
- [19] Brewbaker, J.L. and Kwack, B.H. (1963) The Essential role of calcium ion in pollen germination and pollen tube growth. *Amer. J. Botany* 50 (9): 859-865.
- [20] Shivanna, K.R. and Rangaswamy, N.S. (1992) *Pollen Biology Laboratory Manual.* Druckerei Kutschbach, Berlin.
- [21] Petrisor, C., Mitre, V., Mitre, I., Jantschi, L. and Balan, M. (2012) The Rate of Pollen Germination and the Pollen Viability at Ten Apple Cultivars in the Climatic Conditions of Transylvania. *Bulletin UASVM Horticulture*, 69(1): 1843-5254.
- [22] Derin, K. and Eti, S., (2001) Determination of pollen quality, quantity and effect of cross pollination on the fruit set and quality in pomegranate. *Turk J. Agric. For.* 25:169-173
- [23] Wu, J., Qin, Y. and Zhao, J. (2008) Pollen tube growth is affected by exogenous hormones and correlated with hormone changes in styles in *Torenia fournieri* L. *J. Plant Growth Regulation.* 55:137-148.
- [24] Shafari, Y. (2011) Investigation on pollen viability and longevity in *Malus pumila* L. *Pyrus comminus* L. and *Cydonia oblonga* L. in vitro. *J. Med. Plant. Res.* 5(11):2232-2236
- [25] Topdemir, A., Gür, N. and Koçak, K. (2015) Several heavy metals (Cu⁺⁺, Pb⁺⁺, Cd⁺⁺) *Malus Sylvestris* Miller (Apple) and *Cerasus Vulgaris* Miller (Cherry) plant germination and pollen tube growth effects. *Journal of Anatolian Natural Sciences* 2:108-112.

Received: 28.10.2016
Accepted: 09.06.2017

CORRESPONDING AUTHOR

Ferhad Muradoglu

Department of Horticulture, Faculty of Agriculture
and Natural Sciences, Abant Izzet Baysal University,
Bolu, Turkey

e-mail: muradogluf@ibu.edu.tr

BIOLOGICAL PRE-TREATMENT OF SOFT-WOOD *LARIX KAEMPFERI* USING THREE WHITE-ROT FUNGI - *CORTICIUM CAERULEUM*, *HETEROBASIDION INSULARE* AND *PSEUDOTRAMETES GIBBOSA*

Zhang Yue-Hua¹, Yu Jing-Ni², Zhao Cheng-Cheng¹, Li Jia-Lin^{2,*}

¹Institute of Agricultural and Environmental Biotechnology, Jiamusi University, Jiamusi, Heilongjiang Province, 154007, China

²School of Public Health, Jiamusi University, Jiamusi, Heilongjiang Province, 154007, China

ABSTRACT

The impact of the bio-pretreatment for *Larix kaempferi* was assessed after its exposure to three white-rot fungi, namely *Corticoid caeruleum*, *Heterobasidion insulare*, and *Pseudotrametes gibbosa*. Their changes in chemical composition and micro-structure, as well as their predisposition to enzymatic saccharification and wood decomposition were investigated. Three white-rot fungi were tested. *H. insulare* selectively reduced this wood lignin and cellulose, instead of the whole assembly. After an 8-week pretreatment with *H. insulare*, the weight loss was 10.7%, and the test sample of lignin lost 14.52%. In comparison, all cellulose was lost due to *C. caeruleum* and *P. gibbosa* by 7.81% or less. Data show that the enzyme secreted outside exhibits cellulase from *H. insulare* concentrations higher than other strains of white-rot fungi. Thus, lignin and cellulose activities depend on the total weight loss of *L. kaempferi* and other chemical composition of the sample with three white-rot fungi showing good correlation. According to the experimental analysis, X-ray diffraction (XRD) and pore size distribution of the sample timber obtained from the degradation of the physical data reported an optimistic forecast of *H. insulare*; these could be processed using potential fungal strain targets through woody biomass pretreatment. Compared with the non-disaccharide yield, pretreatment with a control sample greatly increased to 21.01%. Experimental results also show that white-rot fungal strain *H. insulare* in the lignin degradation process does not provide the necessary biomass. Nevertheless, disaccharide provides an effective method.

KEYWORDS:

Biodegradable; pretreatment; lignin; white-rot fungi; enzymatic saccharification; ligninase

INTRODUCTION

With increases in both the population and energy consumption worldwide, the demand for substitutes of fossil fuel resources will also increase. In order to solve this problem, many researchers have tried to convert biomass into ethanol fuel [1]. Some countries with advanced technology, such as the United States and Japan, have promoted and disseminated policies to support alternative energy. Biomass of new materials, especially woodiness materials, is regarded an alternative energy source, which has received special attention. For example, lignocellulosic biomass is a promising renewable energy, as it is rich in carbohydrates [2,3]. However, it has a complex structure with hemi-cellulose and lignin. It is difficult for the saccharification of cellulose and hemi-cellulose to occur without any loss of carbohydrates. Therefore, efficient preprocessing or acid cellulose enzyme saccharification is a necessary process. Effective pretreatment not only reduces the lignin content and crystallinity of cellulose fibers, but also increases its surface area and the material of the aperture. Due to the lignin degradation of cellulose enzymes [4,5], removing the lignin is a necessary process. Various pretreatment methods, such as steam explosion of dilute acid [6], organosolvent extraction, and the biological treatment of white-rot fungus, have been extensively researched [7]. In recent years, super-critical and subcritical water treatments have attracted great attention. This is because the induced potential biomass resources directly converted into sugar would not require the saccharification step [8]. Most biological pretreatments need expensive instruments or sophisticated technology. In particular, the physical and thermal chemical processes require a lot of biomass energy conversion. In the case of steam explosion, the release of grapes' cellulose degradation for 5-HMF, levulinic acid and formic acid enzyme saccharification and alcoholic fermentation inhibitors is necessary [9]. The application of white-rot fungi and biological treatment

could ensure safety and protect the environment from pollution. It is not necessary in long-term lignin degradation, despite the high lignocellulose biomass removal of lignin [10]. White-rot fungi degrade lignin through lignin degrading enzymes such as peroxidase and laccase. These enzymes are composed of carbon and nitrogen sources. In this study, the red pine *Pinus densiflora* enzyme saccharification and biological pretreatment requires three white-rot fungi, namely *H. Insulare*, white-rot fungus, and peanut blue fungus. These fungi were chosen because of their effective degradation of lignin and lignin compounds with chlorinated aromatic compounds such as endocrine disruptors [11]. Additionally, the quantity and structural changes of the components following *L. kaempferi* pre-treatment as well as the characteristics of the enzyme solution were studied.

MATERIALS AND METHODS

Woody biomass and white rot fungi. We selected *Larix kaempferi* wood aged 15-20 years old as the raw-material test samples. These test samples with a slicer-cut specification for an inner diameter of $1 \times 1 \times 0.5$ cm were stored at 4°C in a refrigerator until further processing. *C. caeruleum* (CCJ-1030) was provided by the Institute of Microbiology Application of Jiamusi University in Heilongjiang Province, China. *H. Insulare* (HIJ-2234) and *Pseudotrametes gibbosa* (PGJ-0610) were obtained from the Key Laboratory of Forest Protection, Northeast Forestry University, Heilongjiang Province, China. White-rot fungal strains were grown in modified PDA (potato-dextrose) at 28°C for 7 days. The same amounts of cell blocks inoculated in modified PDB (potato-dextrose-) were taken for liquid inoculation.

Biological pretreatment using white-rot fungi. Here, 150 µg of prefabricated chips and 200 ml of distilled water in a flask were autoclaved at 120°C for 20 minutes. Then, 0.5 g (dry weight) of each of 3 strains of rot fungi was separated and inoculated with mycelium. Then, they were placed in an incubator at 30°C for 6 weeks continuously. For the mycelia mass, pure PDB medium was utilized for a 1-week incubation period and then 4 hours in an oven to achieve dry weight at 120°C. After incubation, the chips with adhering mycelium were washed with distilled water, oven-dried and weighed to calculate weight loss. The dried samples were evacuated to chips and ground to analyze the chemical composition and physical properties of 40 mesh powders.

Chemical properties analysis of woody biomass. With the TAPPI test method, pulp testing was utilized to determine the chemical composition of the test samples. The holocellulose and klason lignin were measured through an acidic process. Lignin was dissolved in an acidic solution, which was then measured using UV-spectroscopy at 205 nm. Humidity, total cellulose content, and insoluble ash contents were assessed in alkali extracts. Klason lignin content was analyzed after biological pre-treatment with the TAPPI method. Data were statistically analyzed, and comparative variance was analyzed with SPSS. 16.

Physical properties analysis of woody biomass. Measurement of the crystallinity of woody biomass was carried out using powder High Resolution X-ray diffractometry (HR-XRD, Bruker D8 DISCOVER, Germany) [12]. Crystallinity (%) was defined as $[(I_{002}-I_{am})/I_{002}] \times 100$, where I_{002} is the crystalline peak of the maximum intensity at 2θ between 22°C and 23°C for cellulose I, and I_{am} is the minimum intensity at 2θ between 18°C and 19°C for cellulose I. The measurement was conducted under the condition of 40 KV, 40 mA, and 0.75L/min (scanning speed).

The lignin from the vacuum-dried sample was milled with powder prepared with a conventional method of measuring nitrogen adsorption surface area and internal pore. Through nitrogen adsorption (Microtrac BEL Instruments, BELCAT II, Japan), data were measured in low-temperature settings. Assay conditions were as follows: The sample vessel temperature was set at 81.28K. Then, 1.0 g of sample was taken to assess quality, temperature and pressure stability at intervals of 15 seconds. The volumes of the measuring space and the cooling space for temperature measurement were 9.6136 and 29.2568 cm³, respectively. The total volume was estimated on the basis of nitrogen adsorption under a volume of 0.99 and relative pressure.

Enzymatic assay of white-rot fungi. The wood samples, as a carbon source, were placed in shallow static culture (SSC) medium. Three fungi [13] were determined by spectrophotometry lignin enzyme activity. Manganese oxide peroxidase activity, and pyrogallol-1,3-dimethyl ether-Syringol ($\epsilon_{469}=27500/\text{M}/\text{cm}$ 2,6-DMP) were measured. The reaction mixture contained 50mM of MDA sodium buffer solution (pH4.5), 0.1 m mol of 2,6-DMP, 0.5 mm of magnesium sulfate, and H₂O 0.1mM of catalase as the extracellular fluid. The reaction was started by adding H₂O₂. Absorbance was monitored at 469 nm for 3 minutes [14]. This served as a substrate. Laccase activity was assessed. 2,2'-azino-bis(3-ethyl-benzo-thiazole-6-sulfonic acid) ($\epsilon_{420}=36000/\text{M}/\text{cm}$ ABTS) assay was obtained. The

reaction mixture contained 2.55 ml of 0.2M lactic acid buffer solution (pH4.5), 150 μ l of ABTS, and 300 μ l of enzyme solution outside the cell, and the increase in absorption at 420nm was monitored for 3 minutes. Endo-1,4- β -glucanase activity was measured using ostazin-red hydroxycellulose (Sigma Chemical Company, USA). The reaction mixture (750 L) contained 25 L of 2.5 mg OBR/ml and 10 L of 50mM citrate-phosphate buffer (pH 4.8) enzyme solution. It was incubated at 40°C for 15 min. The reaction was initiated by adding three volumes of ethanol/acetone termination (2:1, v/v). The product released from the polymeric substrate was assessed at 550nm to monitor the increase in absorbance [15].

Cellobiohydrolase enzyme content can be determined as follows. The reaction mixture consists of 0.4 ml/5mM nitrophenyl- β -D-amino- galactosidase (Merck & Co., Inc., Canada), 0.4 ml of enzyme solution and 0.8 ml of 50mM sodium acetate buffer (pH 5.0) in solution. The mixture was incubated at 40°C for 60 minutes. Then, 2.0ml of 1% sodium carbonate solution was added to the reaction mixture released from the substrate p-nitrophenol at 420nm based on chroma estimates [16]. β -glucosidase activity was induced by glucoside (Merck & Co., Inc., Canada) to monitor the release of p-nitrophenol from p-nitrophenyl- β -D-pyran. Enzyme solution (100 μ l) was incubated in 10mM sodium acetate buffer (pH 5.0) at 30°C for 5 minutes with 1mM p-nitrophenyl- β - D'Glucopyranoside. The enzyme reaction caused by the addition of 100 μ l of 2M sodium carbonate was terminated. The released amount of nitrophenol β -glucosidase enzyme was calculated using the same method, and cellobiohydrolase was determined [12]. By using RBB xylan (Merck & Co., Inc., Canada) as a substrate, xylanase activity was measured. In order to measure the activity of the mixture, 50 μ l of RBB xylan solution (10 mg/ml) was added to 100 μ l of enzyme solution. Then, 150 μ l of 50mM sodium acetate buffer (pH 4.5) was composed. After 30 minutes of incubation at 30°C, the reaction was stopped by the addition of two volumes of 95% ethanol. The samples were centrifuged at 620nm for determination of the supernatant containing soluble xylan digestion, resulting in distinct fractions [17].

Enzymatic saccharification. To compare the white-rot fungi used during the pretreatment period with cellobiose production, Celluclast adopted a culture tank with a volume of 1.5 liters (Solutia Inc., Denmark) for the preparation of β -glucosidase and cellulose. Here, 0.50g of the bio-pretreatment samples of woody biomass was transferred to a 100 ml conical flask. Then, 20 ml of 50mM acetate buffer (pH 5.0) was added to the components. Then, a suitable amount of cellulase (120EGU/g) and an appropriate amount of β -glucosidase (84IU/g) was added.

The 250ml Erlenmeyer flask was placed in a shaking incubator at 49°C, and incubated for 12, 24, 36, and 48 hours at 125rpm. After hydrolyzing the sample, 4.0 ml of culture supernatant was filtered with a 0.30 μ m centrifugal filter and stored in a refrigerator at 4°C. Subsequently, these samples were analyzed using a high-performance liquid chromatograph (HPAEC) (ESSEN-TIA LC-15C; Shimadzu Japan). Cellulose sugar solution was decomposed with 3.0 mm NaOH for 50 minutes for the analysis. The mobile phase was set at 0.8 ml/min.

RESULTS AND DISCUSSION

Chemical components analysis of pretreated woody biomass. After eight weeks of biological pretreatment process analysis, timber ingredients were presented in Tables 1 and 2. The weight losses of the sample woods were 10.6% and 9.8% after decomposition with *H. insulare* and *P. gibbosa*, respectively. In addition, mechanized weight losses were 7.7% and 10.5%, respectively. Fully-induced loss of cellulose by *H. insulare* was at a similar level. This implied that the use of its own secreted hydrolytic enzymes would degrade cellulose-wide; for *C. caeruleum* and *P. gibbosa*, there were difficulties with low weight loss of holocellulose. According to statistical analysis, there is a difference between the lignin degradation rates per fungi. However, there is no significant difference in weight loss after treatment for the entire cellulose content with *C. caeruleum* and *H. insulare* ($P < 0.05$).

The results show that *H. insulare* lignin degradation was significantly higher than that of other fungi. The reason for the decrease in the lignin content of insoluble acids may be that white-rot fungi degrades lignin enzymes with low molecular phenol compounds at a low capacity. Acid-soluble lignin was slightly higher than all fungi (See Table 2). According to the results regarding the weight loss of lignin and hemicellulose, only *H. insulare* could selectively degrade lignin and cellulose. This result can also be confirmed by the alkaline content of the extract. Compared with the control sample, the content of alkaline extract increased from 16.12% to 18.14% and from 17.25% and 16.87% corresponding to *H. insulare*, *P. gibbosa* and *C. caeruleum*, respectively. This implies that carbohydrate and lignin degradation products have low molecular weights, which means that degradation starts from the outside during the culture of these cells in the production of fungal enzymes. Based on the comparison and statistical analysis of results, the chemical composition is statistically significantly different compared with the control

TABLE 1

Weight loss and changes in chemical components of *Larix kaempferi* in biological pretreatment with white-rot fungi

White rot	Weight loss (%)	Lignin loss (%)	Fungi holocellulose loss (%)
<i>C. lacerata</i>	9.5±0.5	13.1±0.4	8.0±0.5
<i>P. gibbosa</i>	9.9±0.4	11.6±0.3	10.6±0.3
<i>H. Insulare</i>	10.7±0.7	14.5±0.4	7.8±0.3

TABLE 2

Changes in the chemical components after biological pretreatment with white-rot fungi

Biological pretreatment	Acid soluble lignina	Alkali extractive (%) ^a	Ash (%)
Control	10.68	15.74	0.45
<i>C. lacerata</i>	0.95	17.16	0.32
<i>P. gibbosa</i>	0.91	16.52	0.32
<i>H. Insulare</i>	0.95	18.85	0.33

Note: Values are expressed as percent decrease based on the oven-dried weight of original wood; a signifies the average of triplicate experimental results under each condition

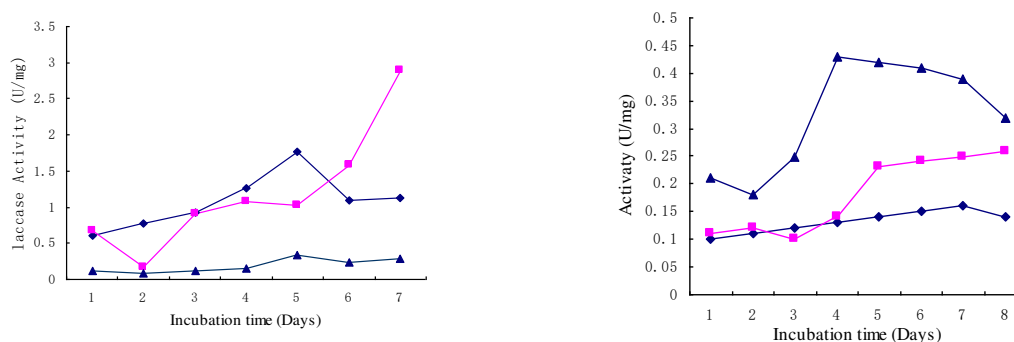


FIGURE 1

Changes in the ligninase activities of white-rot fungi during the cultivation on *Larix kaempferi* wood powder as a carbon source. (A) laccase, (B) manganese peroxidase, (▲) *P. gibbosa*, (◆) *H. insulare*, (▼) *C. lacerata*.

($P \leq 0.05$). Instead, there is no significant difference between the control and acid soluble lignin and ash contents with three fungi

Based on earlier studies, softwood cellulose and lignin treated with other white-rot fungi would suffer higher losses compared with those treated with *H. insulare*. After 40 days of solid-state fermentation, experimental samples of lignin and hemicellulose contents were reduced by 20% and 15%, respectively [18]. For saccharification enzymes, fungi should be based upon their impacting lignin, and the smallest cellulose degradation ability should be chosen. It is indicated that *H. insulare* is considered to be more suitable for biological preprocessing, compared with the fungi *P. gibbosa* and *C. caeruleum*.

Assay of the active enzyme in white-rot fungus. Throughout the incubation period, *H. Insulare* laccase and manganese peroxidase showed the highest living rate (See Fig. 1 A and B). Nevertheless, *C. lacerata* laccase activity was detected in *C. lacerata* laccase and lignin peroxidase liquid culture based on

this discovery and previous results [19]. Accordingly, *H. insulare* (See Fig. 1) activity may contribute to the highest lignin and the maximum significant loss (See Table 1). The variety of cellulolytic enzymes produced in the culturing process using three white-rot fungi are shown in Fig. 2. β -glucosidase and endoglucanase activities as well as incubation time are shown in Fig. 2 A and C. Chemical changes in the results are listed in Table 1, which are consistent with the gradual increase.

In endoglucanase and xylanase activities, the random degradation of cellulose and hemicellulose backbones were higher than that of β -glucosidase, and that of cellobiohydrolase was significantly higher (See Figure 2). For another aspect, low or undetected cellobiohydrolases in all three fungi were incubated for 15 days. Following 20 cultivation days, slight cellobiohydrolase activities in *P. gibbosa* and *H. insulare* were detected. Nonetheless, they were still far below the intensity reported in *C. caeruleum*. As a consequence, they were considered negligible (See Fig 2B). However, the xylanase activity was 2

times higher in *C. caeruleum* than in *H. insulare* (See Fig. 2D). Although xylanase and endoglucanase took on the highest activity in *C. caeruleum*, the fungus could not effectively lead to the degradation of hemicellulose (See Table 1 and Fig. 2). On the contrary, *P. gibbosa* exhibited β -glucosidase and cellobiohydrolase activities with the highest endoglucanase and xylanase activity level, resulting in the most significant loss of whole cellulose (See Table 1 and Fig. 2).

Physical properties of woody biomass pre-treatment. Through X-ray diffraction (XRD), the structures of the original samples and pretreated

wood powder were obtained. The crystallinity of the non-pretreated timber was 68.4%, while those of the pre-treated flour kinds were between 64% and 65.9% (See Fig 3). Therefore, the biological pre-treatment with three white-rot fungi did not show a significant effect on the degree of crystallinity (See Fig.3). Crystallization has previously been proven to influence different celluloses, especially cellobiohydrolases [20]. The element which causes minimal crystallinity was used in this study (See Fig 2B). The low cellobiohydrolase activity in three white-rot fungi may be determined for use (See Fig 3).

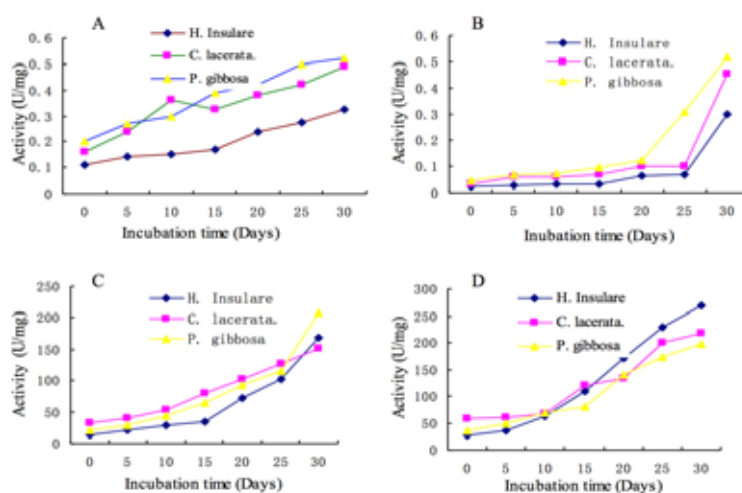


FIGURE 2

Changes in the cellulolytic enzyme activities of white-rot fungi during cultivation on Japanese red pine wood powder as a carbon source. (\blacktriangle) *P. gibbosa*, (\blacklozenge) *H. insulare*, (\blacktriangledown) *C. lacerata*. (A) β -glucosidase, (B) cellobiohydrolase, (C) endoglucanase, (D) xylanase. Values shown are the averages from triplicate experiments with each condition.

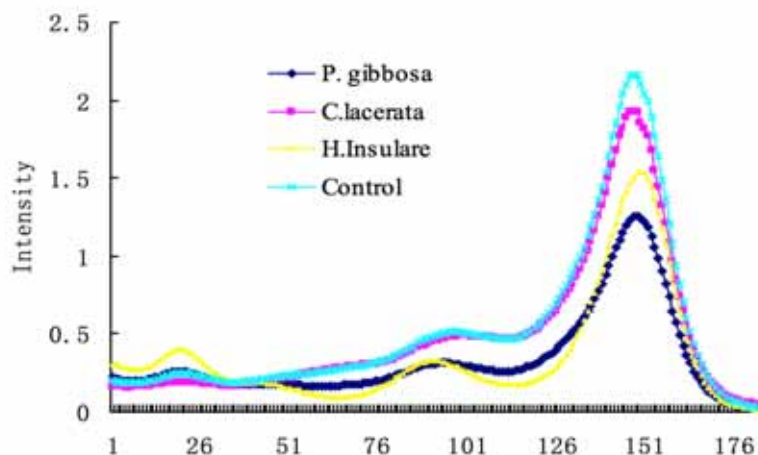


FIGURE 3

Changes in the crystallinity of lignocellulosic biomass after biological pretreatment

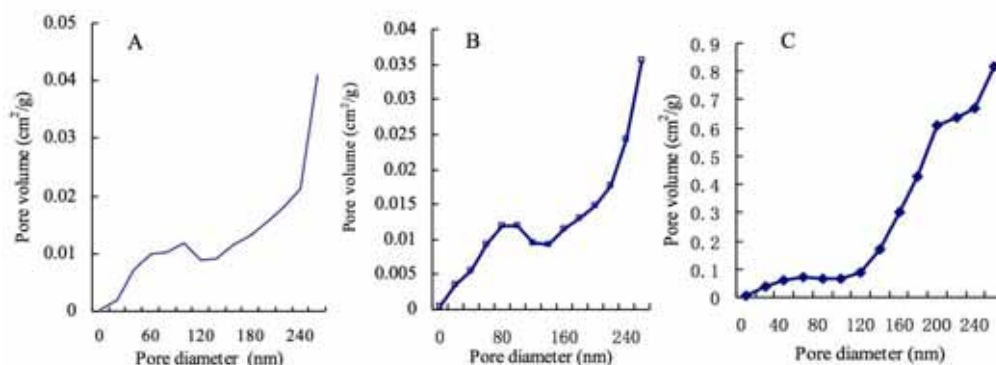


FIGURE 4

Pore size distribution for non-treated and pretreated wood powders. (A) untreated wood powder, (B) wood powder pretreated with *H. insulare*, (C) wood powder pretreated with *P. gibbosa*.

TABLE 3

Monosaccharides and total sugar yields of woody biomasses non-treated and pretreated by commercial enzymes

Carbon source	Time (h)	Monomeric sugars (%)					Sugar yield (%)
		Arabinose	Galactose	Glucose	Xylose	Mannose	
CON	24	0.20	0.08	1.68	0.29	0.14	2.38
	48	0.87	0.44	6.70	1.18	1.15	10.34
	72	1.11	0.62	8.83	2.11	1.93	14.60
STH	24	0.38	0.13	7.67	1.48	0.42	10.07
	48	0.77	0.27	11.83	2.68	1.71	17.26
	72	1.01	0.41	13.56	3.26	2.77	21.01
POB	24	0.45	0.14	6.23	1.01	0.33	8.16
	48	0.71	0.26	8.47	1.61	1.15	12.21
	72	0.95	0.43	9.68	1.96	1.90	14.91
CEL	24	0.46	0.18	8.94	1.44	0.65	11.67
	48	0.53	0.25	9.91	1.70	1.22	13.61
	72	0.56	0.28	10.78	1.82	1.56	15.03

Note: CON, non-treated *Larix kaempferi* (JRP); STH, JRP pretreated with *P. gibbosa*; POB, JRP pretreated with *H. insulare*; CEL, JRP pretreated with *C. lacerata*. The values shown in the table are the averages of triplicate experiment results under each condition.

In normal circumstances, pore diameter and specific surface area are very important for the adsorption of enzymes and accessibility. Research has suggested that the available surface area of a substrate and protein binding are positively correlated. The pore size distributions of wood flour that is untreated and pretreated with white-rot fungi are shown in Fig. 4. The nitrogen adsorption and desorption values were 1.039 m²/g and 1.213 m²/g, respectively. Similarly, the values of adsorption and desorption determine the reliability of indicators obtained in this study's test data. Compared with an acid pretreatment for wood powder, it shows a different distribution curve [21]. Cellulose was reported to have a spherical diameter of 24-74 nm [22]. The available aperture was less than 120 nm, and the possibility that the enzyme *H. insulare* would access pretreated flour rather than untreated wood flour increased dramatically. The results suggest that efficiency can be increased by the saccharification of the available specific surface area and pore size as the prediction

based on the recommendations [23]. Previous studies have noted that hydrolysis and usable area are closely linked [24]. The increase in the available aperture of *P. gibbosa* and *S. hirsutum* was degraded by wood, and lignin degradation enzymes secreted by these fungi from hemicellulose caused a small part.

Sugar yield. For the yields of glucose and other monosaccharides after conventional calibration, a standard international saccharification enzyme assay was practiced (See Table 3). Wood saccharification was different when woody biomass was pretreated with *H. insulare* for 72 hours and saccharified at 49°C. Under this condition, we obtained the highest sugar production (i.e.22.10%). Meanwhile, woody biomass saccharification enzymes pretreated with *P. gibbosa* and *C. lacerata* were utilized in sugar production under the same conditions (14.89% and 15.10%, respectively). The most abundant glucose can be produced in all circumstances. Xylose and mannose, as the main ingredients of glucomannan

production, were from arabinose and glucuronic acid derivatives of softwood hemicellulose in biomass. Through the enzymatic hydrolysis of pretreated wood biomass, we obtained high xylose and mannose yields. As a result, it is widely regarded that hemicellulose is a white-rot fungus with an easily degradable structure. In particular, *H. insulare* becomes the preferred fungal strain for biological pretreatment in a suitable timber preprocessor.

ACKNOWLEDGEMENTS

The work has been supported by the Natural Science Foundation of Heilongjiang Province, China. №: C201451.

REFERENCES

- [1] Ayas, N., Asci, Y., & Yurdakul, M. (2016). Using of Fe/ZrO₂ catalyst to remove direct orange 26 from water by Fenton oxidation at wide pH values. *Fresen. Environ. Bull.*, 25, 3272-3279
- [2] Stocker, M. (2008) Biofuels and biomass to liquid fuels in the biorefinery: Catalytic conversion of lignocellulosic biomass using porous materials. *Angewandte Chemie International Edition*, 47(48), 9200-9211.
- [3] Ho, S. H., Huang, S. W., Chen, C. Y., Hasunuma, T., Kondo, A., & Chang, J. S. (2013). Bioethanol production using carbohydrate-rich microalgae biomass as feedstock. *Bioresource Technology*, 135, 191- 198.
- [4] Acarbabacan, S., Vergili, I., Kaya, Y., Demir, G., & Barlas, H. (2002). Removal of color from textile wastewater containing azodyes by Fenton's reagent. *Fresen. Environ. Bull.*, 11(10), 840-843.
- [5] Eriksson, K. E. L., Blanchette, R. A. and Ander, P. (1990). *Microbial and Enzymatic Degradation of Wood and Wood Components*. Springer Berlin Heidelberg. DOI: 10.1007/ 978-3-642-466687-8.
- [6] Emmel, A., Mathias, A. L., Wypych, F., & Ramos, L. P. (2003). Fractionation of *Eucalyptus grandis* chips by dilute acid-catalyzed steam explosion. *Bioresource Technology*, 86(2), 105-115.
- [7] Taniguchi, M., Takahashi, D., Watanabe, D., Sakai, K., Hoshino, K., Kouya, T., & Tanaka, T. (2010). Effect of steam explosion pretreatment on treatment with *Pleurotus ostreatus* for the enzymatic hydrolysis of rice straw. *Journal of Bioscience and Bioengineering*, 110(4), 449- 452.
- [8] Bokinsky, G., Peralta-Yahya, P. P., George, A., Holmes, B. M., Steen, E. J., Dietrich, J., & Keasling, J. D. (2011). Synthesis of three advanced biofuels from ionic liquid-pretreated switchgrass using engineered *Escherichia coli*. *Proceedings of the National Academy of Sciences*, 108(50), 19949-19954.
- [9] Almeida, J. R., Modig, T., Petersson, A., Hähn Hägerdal, B., Lidén, G., & Gorwa-Grauslund, M. F. (2007). Increased tolerance and conversion of inhibitors in lignocellulosic hydrolysates by *Saccharomyces cerevisiae*. *Journal of Chemical Technology and Biotechnology*, 82(4), 340-349.
- [10] Clark, J. H., Luque, R., & Matharu, A. S. (2012). Green chemistry, biofuels, and biorefinery. *Annual Review of Chemical and Biomolecular Engineering*, 3, 183-207.
- [11] El-Rahim, W. M., Moawad, H., & Khalafallah, M. (2003). Enhancing the growth of promising fungal strains for rapid dye removal. *Fresen. Environ. Bull.*, 12(7), 764-770.
- [12] Rahmani, A., Barjasteh Askari, F., & Asgari Gh, S. M. (2012). Degradation of reactive red 198 dye by catalytic ozonation using pumice and copper coated pumice. *Fresen. Environ. Bull.*, 21(9), 2810-2817.
- [13] Tassi, F., Venturi, S., Cabassi, J., Capecciacci, F., Nisi, B., & Vaselli, O. (2015). Volatile organic compounds (VOCs) in soil gases from Solfatara crater (Campi Flegrei, southern Italy): Geogenic source (s) vs. biogeochemical processes. *Applied Geochemistry*, 56, 37-49.
- [14] Varela, E., Mester, T., & Tien, M. (2003). Culture conditions affecting biodegradation components of the brown-rot fungus *Gloeophyllum trabeum*. *Archives of Microbiology*, 180(4), 251-256.
- [15] Korkmaz, M., Özmetin, C., Fil, B. A., Özmetin, E., & Yaşar, Y. (2013). Methyl violet dye adsorption onto clinoptilolite (natural zeolite): Isotherm and kinetic study. *Fresen. Environ. Bull.*, 22(5a), 15, 24-33.
- [16] Singh, P., Suman, A., Tiwari, P., Arya, N., Gaur, A., & Shrivastava, A. K. (2008). Biological pretreatment of sugarcane trash for its conversion to fermentable sugars. *World Journal of Microbiology and Biotechnology*, 24(5), 667-673.
- [17] Dinis, M. J., Bezerra, R. M., Nunes, F., Dias, A. A., Guedes, C. V., Ferreira, L. M., & Rodrigues, M. A. (2009). Modification of wheat straw lignin by solid state fermentation with white-rot fungi. *Bioresource Technology*, 100(20), 4829-4835.
- [18] Sambusiti, C. (2013). Physical, chemical and biological pretreatments to enhance biogas production from lignocellulosic substrates, PhD-work. Politecnico di Milano.

- [19] Zhou, J., Wang, Y. H., Chu, J., Zhuang, Y. P., Zhang, S. L., & Yin, P. (2008). Identification and purification of the main components of cellulases from a mutant strain of *Trichoderma viride* T 100-14. *Bioresource Technology*, 99(15), 6826-6833.
- [20] Teramoto, Y., Tanaka, N., Lee, S. H., & Endo, T. (2008). Pretreatment of eucalyptus wood chips for enzymatic saccharification using combined sulfuric acid-free ethanol cooking and ball milling. *Biotechnology and Bioengineering*, 99(1), 75-85.
- [21] Chithrani, B. D., Ghazani, A. A., & Chan, W. C. (2006). Determining the size and shape dependence of gold nanoparticle uptake into mammalian cells. *Nanoletters*, 6(4), 662-668.
- [22] Reardon, S. A., Davis, M. R., & Doe, P. E. (1999). Construction of an analytical model of paper drying. *Drying technology*, 17(4-5), 655-690.
- [23] Rahmani, A., Barjasteh Askari, F., & Asgari Gh, S. M. (2012). Degradation of reactive red 198 dyes by catalytic ozonation using pumice and copper coated pumice. *Fresen. Environ. Bull.*, 21(9). 2810-2817

Received: 07.11.2016

Accepted: 03.05.2017

CORRESPONDING AUTHOR

Li Jia-Lin

School of Public Health, Jiamusi University, Jiamusi,
Heilongjiang Province, 154007 – CHINA

e-mail: zhangyaohua_2008@163.com

EFFECTS OF LEAD APPLICATION ON GROWTH AND NUTRIENT ACCUMULATIONS IN *MIRABILIS JALAPA* L.

Muhittin Dogan¹, Mustafa Pehlivan^{2*}, Oguz Gumus Inan¹, Hasan Akgul³

¹Department of Biology, Faculty of Arts and Sciences, Gaziantep University 27310 Gaziantep-Turkey

²Nurdağı Vocational School, Gaziantep University, Nurdağı-Gaziantep-Turkey

³Department of Biology, Faculty of Sciences, Akdeniz University, Antalya-Turkey

ABSTRACT

In the present study, effects of Pb application on the accumulation of nutrients (K, Ca, Mg, Fe, Zn, Cu and Mn) and its effects on the growth in *M. jalapa* were investigated. *M. jalapa* seedlings were treated with 0, 10, 100 and 1000 mg/L Pb concentrations. Absorbed Pb were not uniformly distributed throughout the plant. Among plant parts, higher Pb accumulation capability determined in roots compared to stems and leaves, exception of 10 mg/L Pb concentration. Growth and development of *M. jalapa* were adversely affected by Pb toxicity. Root and stem lengths and their Pb contents showed negative correlations. Similarly, dry weights of root, stem and leaves were decreased as well. In general, contents of Fe, Zn, Mn and Mg were decreased by Pb. In roots, Cu contents changed insignificantly at 10 and 100 mg/L concentrations, but decreased significantly at 1000 mg/L concentration. Despite the fact that Cu contents were risen with Pb applications in stems, the content decreased with increasing Pb concentrations in leaves. In root and leaves, Ca contents were decreased. Moreover Ca content in stems was increased up to 19.7% at 100 mg/L Pb concentration, then decreased up to 10.0% at 1000 mg/L Pb concentration. K accumulations were increased up to 34.7% at 100 mg/L in roots, 26.9% at 1000 mg/L in stems and 10.3% at 10 mg/L in leaves. However, K accumulation in leaves was significantly decreased at 1000 mg/L as 34.1%. As a results, Pb toxicity disturbed the uptake and translocation of nutrients and induced its nutrient imbalance.

KEYWORDS:

Lead, growth, mineral nutrients, *Mirabilis jalapa*

INTRODUCTION

A wide variety of contaminants enter into environment due to extensive industrial production, energy and fuel production and intensive agriculture. Heavy metals are one of the most dangerous of these contaminants. They have been

considered to be major environmental pollutants and their toxicity on plants is well established [1]. Among heavy metals, Pb is one of the hazardous heavy metal pollutants of the environment that originates from various sources like mining and smelting of lead-ores, burning of coal, effluents from storage battery industries, automobile exhausts, metal plating and finishing operations, fertilizers, pesticides and from additives in pigments and gasoline [2]. Lead is one of the most widely distributed heavy metals and is toxic to plants [3]. Responses of plants to Pb exposure include decrease in root elongation and biomass [4,5], inhibition of chlorophyll biosynthesis and chlorophyll content [6,7], and induction or inhibition of several enzymes [8,9].

Mirabilis jalapa (Nyctaginaceae) is an ornamental plant commonly known as the 'four o'clock flower' because its flowers open from late afternoon and onwards. Plants produce fragrant flowers in a range of colours from white to red over the course of a few months. It is a multi-branched perennial plant in southern and warm western regions, and an annual in cooler northern regions, of its native tropical South America [10]. *M. jalapa* has been cultivated in many parts of the world, including Turkey. It has long been used for medicinal purposes [11]. In addition to that, it can be applied to remediation of Cd and Pb contaminated soils [12,13].

The present study is an attempt to determine the effects of Pb application on the accumulation of nutrients (K, Ca, Mg, Fe, Zn, Cu and Mn) and its effects on the growth in *M. jalapa*.

MATERIALS AND METHODS

Plant exposure. *M. jalapa* seeds were obtained at the campus of Gaziantep University. The seeds were soaked in water for 10 h. Then, two seeds were sown in each pot (8.5 cm × 13.5 cm) filled with perlite. After germination, seedlings were watered to 10% nutrient solution. The nutrient solution consisted of 0.88 mM K₂SO₄, 2 mM Ca(NO₃)₂, 0.25 mM KH₂PO₄, 1 mM MgSO₄, 0.11 mM KCl, 100 μM Fe-EDTA, 10 μM H₃BO₃, 5 μM MnSO₄, 10 μM ZnSO₄, 2 μM CuSO₄, and 0.2 μM

(NH₄)₆Mo₇O₂₄. The seedlings were grown in a climate chamber (Snijders Scientific, Netherlands) under light/dark regimes of 16/8 h, light level of 120 μE m⁻². s⁻², and at 28±1 °C. Three weeks after, seedlings were treated with 0, 10, 100 and 1000 mg/L Pb as Pb(NO₃)₂. Each treatment had four pots. All solutions were prepared with distilled water. The seedlings were harvested after 25 days; then, seedling roots were carefully washed with deionized water three times.

Measurement and calculation. Roots and stems of the plant were measured using a ruler. After determination of fresh weight of root, stem and leaves using precision scales, all plant parts were dried in an electric furnace at 80 °C. Tolerance index of plant parts were calculated as follows [14]:

$$\text{Tolerance index} = \frac{\text{Dry weight of Pb applied plant part (g)}}{\text{Dry weight of Pb unapplied plant part (g)}} \times 100 - 100$$

Determination of lead accumulation. To determine Pb and nutrient accumulations, the dried samples were pulverized using mortar and pestle. The samples were dissolved in 14 M HNO₃ and residues were dissolved in 1 M HCl. After mineralization, metals were determined using an atomic absorption spectrometer (Perkin Elmer Analyst 400, USA). Measurements of Pb, Fe, Zn, Mn, Cu, Ca, K and Mg were carried out at 283.31, 248.33, 213.86, 279.48, 324.75, 422.67, 766.19 and 285.21 nm, respectively. Metal contents of plant parts were calculated on dry weight basis.

Bioconcentration factor (BCF) was calculated as follows [15]:

$$\text{BCF} = \frac{\text{Average Pb accumulation in plant tissues (root+stem+leaf)}}{\text{Pb concentration added in solution}}$$

Transportation index of stem and leaf (BCF) was calculated as follows [16]:

$$\text{Transportation index} = \frac{\text{Pb accumulation stem or leaves}}{\text{Pb accumulation in root}} \times 100$$

Statistical analysis. All analyses were carried out with four replicates. Data were analyzed with the analysis of variance (ANOVA) using SPSS 11.0 for Windows. The significance of differences was determined with the least significant difference (LSD) test. Pearson's correlation was analyzed between Pb accumulation and mineral accumulations.

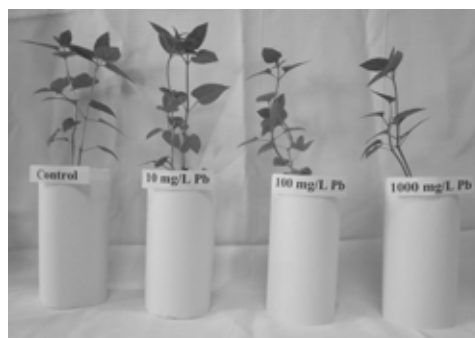


FIGURE 1
Growth of *M. jalapa* after 25-days Pb applications.

TABLE 1
Lead accumulation of different parts of *M. jalapa* after 25-days Pb applications

Pb concentration (mg/L)	Pb contents (mg/kg d wt.)		
	Root	Stem	Leaf
0	82.5±10.4a, x	48.2±8.0a,x	30.3±3.2a,x
10	1075.4±150.8a,x	1711.0±46.6b,y	204.6±14.0b,z
100	22078.6±1543.8b,x	3551.8±185.1c,y	973.3±32.1c,z
1000	12842.6±675.4c,x	898.7±124.9d,y	549.1±40.9d,y

Values expressed as mean ± standard deviation. Letters a, b, c and d show the differences among exposure concentrations; letters x, y and z show the differences among plant parts (p<0.05).

TABLE 2
Bioconcentration factor and transportation factors of *M. jalapa* after 25 days Pb applications

Pb concentration (mg/L)	BCF	Transportation factor	
		Stem	Leaf
10	299.1	159.1	19.0
100	266.0	16.1	4.4
1000	14.3	7.0	4.3

RESULTS AND DISCUSSION

Influence of different Pb applications (0, 10, 100 and 1000 mg/L) were investigated on *M. jalapa*. Shoot growths of plant was visually observed after 25 days Pb treatments (Figure 1). At 10 mg/L and 100 mg/L concentrations, the Pb accumulations were increased in all plant parts while it was interestingly decreased at 1000 mg/L compared to other Pb applications. The rate of respective Pb increases in different tissues for 10, 100 and 1000 mg/L Pb applications can be calculated from the data presented in Table 1 as 13, 268 and 156-fold in root tissue, 35, 74 and 19-fold in stem tissue, and 7, 32 and 18-fold in leaf tissue compared to that found in control tissues. Absorbed Pb were not uniformly distributed throughout the plant, so that different parts may vary in their ability to concentrate Pb. Among plant parts, higher Pb accumulation capability determined in roots compared to stems and leaves, exception of 10 mg/L Pb concentration. The BCF, defined as the concentration ratio of Pb in the plant to that in the

tested solution, is used to measure the effectiveness of the plant in concentrating Pb in its biomass. While the highest BCF was calculated on 10 mg/L Pb-treated seedlings, the lowest BCF was measured on 1000 mg/L Pb-treated ones. (Table 2) This indicates that roots of *M. jalapa* have high Pb accumulation capability at low Pb concentrations. Similarly, transportation indexes of stem and leaves were decreased with increasing external Pb concentrations (Table 2). The translocation index, defined as the ratio of the metal concentration in the stem and leaves to that in the roots. It is used to evaluate the effectiveness of a plant in translocating metal from roots to stem and leaves. Our findings show that roots of *M. jalapa* play a crucial role in Pb storage by blocking Pb translocation from root to upper tissues as protection mechanism from deleterious effects of high Pb accumulation. These findings are in agreement with those of Sayyed et al. [17] in safflower and wheat plants subjected to Pb, Cd, Cu, and Zn contamination and showed that heavy metal treatment decreased metal translocation from the roots to the shoots. A similar mechanism was found in roots of peanut seedling for Pb in response to high external Pb concentrations [7]. The mechanism of this blockage may be similar to that reported by Marschner [18] as Pb can adhere to root cell wall, in pyrophosphate form.

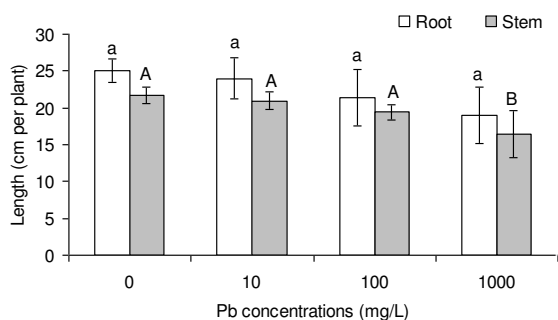


FIGURE 2

Root and stem lengths of *M. jalapa* after 25-days Pb applications. Error bars represent the standard deviation of means. Means with different letters are significantly different from one another according to LSD test ($p < 0.05$).

TABLE 3

Tolerance index of different parts of *M. jalapa* after 25 days Pb applications

Pb concentration(mg/L)	Tolerance index		
	Root	Stem	Leaf
10	-1.0	-16.8	-14.6
100	-15.8	-21.4	-17.3
1000	-24.9	-24.4	-30.1

In all tested Pb concentrations development was adversely affected with respect to control (Figure 2). The decreases at 10, 100 and 1000 mg/L concentrations for root lengths were calculated as 4.0%, 14.4% and 24.3%, respectively. Root lengths

and their Pb contents showed a negative correlation ($r = -0.425$; $p = 0.084$). Similarly, decreases of stem lengths were not significant for 10 and 100 mg/L concentration of Pb as 3.5% and 10.6%, respectively ($p > 0.05$). However, the decrease was significant at 1000 mg/L as 24.2% ($p < 0.05$). Relationship between Pb accumulation of stems and their lengths was negative ($r = -0.017$; $p = 0.479$). Due to the application of Pb, dry weights of root, stem and leaves were decreased as well. (Figure 3) Root dry biomass was found to be negatively correlated with root Pb accumulation ($r = -0.501$; $p = 0.048$). Similarly, There were negative correlations between Pb accumulation in stem and leaves tissues and their dry biomass ($r = -0.402$; $p = 0.098$ for stem, and $r = -0.476$; $p = 0.059$ for leaf). As can be seen in Table 3, tolerance indexes of *M. jalapa* parts are negative as well. In roots, the index was maximum (24.9%) at the highest Pb level (1000 mg/L) followed by 15.8% at 100 mg/L and 1% at 10 mg/L. The minimum tolerance for stem and leaf was calculated as 24.4 and 30.1, respectively, at 1000 mg/L Pb application. There are many researches on adverse effects of Pb on plant growth and development [4,5,19]. On the contrary high Pb accumulation in roots, growth inhibition was stronger in aerial parts of *M. jalapa*. Tolerance index is an integrated calculation of particular parameter and makes for a summary assessment of effect of Pb on the plant growth. The indexes were negatives all plant parts. Growth retardation of *M. jalapa* from Pb treatments may be attributed to nutrient metabolic disturbances as determined our findings.

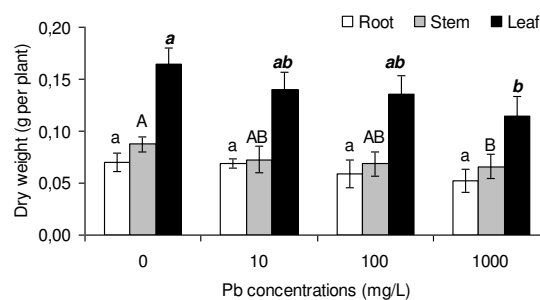


FIGURE 3

Dry weights of different part of *M. jalapa* after 25-days Pb applications. Error bars represent the standard deviation of means. Means with different letters are significantly different from one another according to LSD test ($p < 0.05$).

Iron contents in roots of *Amaranthus* species showed gradual increase over control with all rates of Pb and the lowest values were obtained with the highest rate of Pb in both the species [20]. However, the contents in the shoots and roots of canola cultivars were reduced with increase in exogenous Pb from 0 to 90 mg kg⁻¹ soil [21]. In our study, Fe accumulations were decreased up to 28.1% ($p < 0.05$) at 10 mg/L for roots, 34.6%

TABLE 4
Nutrient accumulations of *M. jalapa* after 25 days Pb applications

Nutrient	Plant part	Pb concentrations (mg/L)			
		Control	10	100	1000
Fe (mg/kg d.wt.)	Root	619.3±22.2ac	445.1±13.9bd	570.4±35.9c	502.9±6.9d
	Stem	111.9±12.9a	102.0±5.6ab	82.6±6.5bc	73.2±7.4c
	Leaf	320.6±26.3a	311.1±16.9 a	287.9±14.0ab	241.0±8.5b
Zn (mg/kg d.wt.)	Root	673.6±12.2ad	477.5±24.7b	802.9±49.3cd	723.6±17.8d
	Stem	455.9±17.2a	424.5±10.6a	437.4±23.2a	408.9±14.0a
	Leaf	324.7±11.7a	316.6±9.3a	248.2±23.8bc	234.2±15.3c
Cu (mg/kg d.wt.)	Root	140.8±4.5a	138.8±4.5 a	152.3±10.3a	107.2±5.6b
	Stem	126.1±8.3acd	175.2±10. b	146.3±6.7cd	129.7±12.3d
	Leaf	70.5±4.9a	58.7±4.7bc	53.2±2.6c	42.7±1.9d
Mn (mg/kg d.wt.)	Root	43.8±2.6a	38.4±3.6ab	43.5±2.1a	33.3±1.1b
	Stem	30.0±2.8a	26.2±4.1a	26.1±2.9a	29.0±4.2a
	Leaf	92.7±5.3 a	73.9±5.8bc	70.0±2.9c	26.6±7.6d
Ca (%)	Root	7.32±0.13 a	6.68±0.14bc	6.42±0.07c	4.21±0.14d
	Stem	7.63±0.07ab	7.45±0.32ab	9.13±1.44a	6.87±0.27b
	Leaf	5.54±0.20 a	4.62±0.23b	3.87±0.21c	3.03±0.13d
K (%)	Root	2.02±0.04ac	1.96±0.19ac	2.72±0.26b	2.21±0.02c
	Stem	2.27±0.08a	2.49±0.09b	2.79±0.05cd	2.88±0.07d
	Leaf	1.26±0.04a	1.39±0.03a	1.28±0.06a	0.83±0.07b
Mg (%)	Root	1.21±0.04a	1.16±0.23a	1.32±0.18a	1.01±0.14a
	Stem	1.22±0.14a	1.17±0.02a	1.16±0.04a	1.13±0.01a
	Leaf	0.87±0.08a	0.89±0.01a	0.59±0.25ab	0.38±0.06b

Values expressed as means ± standard deviation. Means with different letters in the same line are significantly different from one another according to LSD test ($p < 0.05$).

TABLE 5
Relationships between Pb and nutrient accumulations in different parts of *M. jalapa*

Relations in root								
	Pb	Fe	Zn	Cu	Mn	Ca	K	Mg
Pb	1							
Fe	0.13	1						
Zn	0.79 *	0.65*	1					
Cu	0.07	0.40	0.04	1				
Mn	-0.02	0.60	0.18	0.80**	1			
Ca	-0.44	0.38	-0.29	0.83**	0.83**	1		
K	0.90**	0.35	0.79**	0.38	0.27	-0.14	1	
Mg	0.15	0.28	0.14	0.64*	0.84**	0.57	0.34	1
Relations in stem								
Pb	1							
Fe	-0.40	1						
Zn	-0.09	0.72*	1					
Cu	0.42	0.23	-0.17	1				
Mn	-0.54	0.18	0.28	-0.34	1			
Ca	0.70*	0.08	0.54	0.09	-0.43	1		
K	0.53	-0.86**	-0.59	-0.05	-0.28	0.13	1	
Mg	-0.23	0.65	0.54	0.08	0.45	-0.01	-0.39	1
Relations in leaf								
Pb	1							
Fe	-0.51	1						
Zn	-0.80**	0.72*	1					
Cu	-0.63*	0.80**	0.86**	1				
Mn	-0.42	0.92**	0.77**	0.91**	1			
Ca	-0.70*	0.85**	0.91**	0.99**	0.92**	1		
K	-0.21	0.80**	0.67*	0.68**	0.85**	0.70*	1	
Mg	-0.64*	0.83**	0.80**	0.78**	0.81**	0.82**	0.82**	1

* and ** significant at 0.05 and 0.01 levels, respectively.

($p < 0.05$) at 1000 mg/L for stems and 24.8% ($p < 0.05$) at 1000 mg/L for leaves. (Table 4) Although there is positive and insignificant correlation between Pb accumulation in root tissues and their Fe accumulation, there are negative correlation between Pb accumulation in stem and leaves tissues and their Fe accumulations (Table 5). Moreover, interaction between Fe accumulation and

other nutrient accumulations in all plant parts are positives, exception of K accumulation in stems.

Zinc accumulation of *M. jalapa* roots decreased significantly at 10 mg/L Pb concentration as 29.1% ($p < 0.05$), but increased at 100 and 1000 mg/L Pb concentrations as 19.2% ($p < 0.05$) and 7.4% ($p < 0.05$), respectively. (Table 4). On the contrary, Zn accumulations in stem and leaves

decreased by Pb treatment, with respect to their controls. The data clearly revealed that translocation of Zn inhibited by Pb. Correlation analysis confirmed the findings as well. (Table 5) According to the Lopez et al. [22], Zn contents were decreased by Pb application in alfalfa plants. Zinc content of shoots and roots *Amaranthus* species decreased significantly with increasing rate of Pb application showing a negative relation between Pb and Zn [20].

Copper accumulations in all plant parts were differently affected by Pb (Table 4). In roots, Cu levels changed insignificantly at 10 and 100 mg/L concentrations ($p > 0.05$), but decreased significantly at 1000 mg/L concentration ($p < 0.05$). Despite the fact that Cu contents were risen with Pb applications in stems, the content decreased with increasing Pb concentrations in leaves. Positive and insignificant relation between Cu and Pb accumulations were estimated in roots and stems. (Table 5) In addition these, correlations between Cu accumulation and other nutrient accumulations in all plant parts are positives, exception of Mn, K and Zn accumulation in stems.

In general, all parts of *M. jalapa* showed to decrease in Mn accumulations with the increase of Pb application. (Table 4) With respect to their controls, the highest reduction rates of Mn in roots, stems and leaves were estimated as 24.0% ($p < 0.05$) at 1000 mg/L, 13.0% ($p > 0.05$) at 100 mg/L and 71.3% ($p < 0.05$) at 1000 mg/L, respectively. There are negative and insignificant correlations between Pb and Mn accumulations in all plant parts. (Table 5) Moreover positive interactions were observed between Mn and other element accumulations in all plant parts, exception of Cu, Ca and K accumulation in stems.

In root and leaves, Ca accumulations decreased up to 42.5% ($p < 0.05$) and 45.3% ($p < 0.05$) at 1000 mg/L, respectively. (Table 4) Moreover Ca content in stems was increased up to 19.7% ($p > 0.05$) at 100 mg/L Pb concentration, then decreased up to 10% ($p > 0.05$) at 1000 mg/L Pb concentration. Although there are negative correlation between Pb accumulations in root and leaves tissues and their Ca accumulations, there is positive and significant correlation between Pb accumulation and Ca accumulation in stem (Table 5).

According to study of Azhar et. al. [21], K contents in canola shoots and roots showed a similar decreasing trend with increasing Pb concentration in the growth medium. On the other hand, Pb application significantly increased K concentrations in both shoots and roots of *Amaranthus oleracea* [20]. In our study, K concentrations were differently affected by Pb treatment (Table 4). The accumulations were increased up to 34.7% ($p < 0.05$) at 100 mg/L in roots, 26.9% ($p < 0.05$) at 1000 mg/L in stems and

10.3% ($p > 0.05$) at 10 mg/L in leaves. However, K accumulation in leaves was significantly decreased at 1000 mg/L as 34.1% ($p < 0.05$). No significant correlations estimated between Pb and K accumulations in stems and leaves, but there was positive and significant interaction in roots. (Table 5)

Mg accumulations were significantly decreased in shoots of corn and ragweed after two week Pb application [23]. According to a study, however, there was no definite effect on Mg content of rice plant which is treated with Pb [24]. Similarly, Pb treatment insignificantly changed Mg concentration in roots and stems of *M. jalapa* (Table 4). However, Mg content of leaves was decreased up to 56.3% ($p < 0.05$) at 1000 mg/L. There are negative relationships between Pb and Mg contents in stems and leaves. (Table 5) Apart from this, Mg contents all plant parts are positively correlated with other nutrient accumulations.

As a results, Pb toxicity can disturb the uptake and translocation of macro and micronutrients in *M. jalapa* and induce its nutrient imbalance. It is known that changes in nutrient contents as well as in internal ratios of nutrients occur in plants under Pb toxicity. Although data are insufficient to allow a definitive conclusion to be drawn, it is known that Pb affects nutrient uptake [23,25,26]. But, it is not possible to conclude if this decrease results from blockage of root absorption, a decrease in translocation from roots to aerial plant parts, or a change in distribution of these elements in the plant [22,26,27]. According to Pourrut et al. [28] two mechanisms for decreased uptake of micro and macronutrients under Pb toxicity have been suggested. The first mechanism, termed physical, relies on the size of metal ion radii, whereas the second mechanism, which is a chemical one, relies on the metal-induced disorder in the the cell metabolism leading to changes in membrane enzyme activities and membrane structure. Nutrient imbalances of *M. jalapa* due to Pb application may also result from competition, as obtained our study.

REFERENCES

- [1] Ross, S.M. (1994) Toxic Metals in Soil-Plant Systems, John Wiley and Sons, Chichester, 469 pp.
- [2] Eick, M.J., Peak, J.D., Brady, P.V. and Pesek J.D. (1999) Kinetics of lead absorption/desorption on goethite: residence time effect. Soil Sci. 164, 28-39.
- [3] Kosobrukhov, A., Knyazeva, I. and Mudrik, V. (2004) *Plantago major* plants responses to increase content of lead in soil: growth and photosynthesis. Plant Growth Regul. 42, 145-151.
- [4] Fargasova, A. (1994) Effect of Pb, Cd, Hg, As

- and Cr on germination and root growth of *Sinapis alba* seeds. Bull. Environ. Contam. Toxicol. 52, 452-456.
- [5] Dogan, M. and Colak, U (2009) *Triticum aestivum* L. cv. Tosunbey'e Uygulanan Kurşunun Bazı Fizyolojik Özelliklere Etkisi. Ekoloji 19, 73, 98-104.
- [6] Miranda, M.G. and Ilangovan, K. (1996) Uptake of lead by *Lemna gibba* L. influence on specific growth rate and basic biochemical changes. Bull. Environ. Contam. Toxicol. 56, 1000-1007.
- [7] Dogan M., Akgul, H. and Tozcu, I. (2013) Lead Accumulation and toxicity in peanut (*Arachis hypogaea* L.) seedlings. Fresen. Environ. Bull., 22, 2350-2356.
- [8] Van Assche, F. and Clijsters, H. (1990) Effects of metal on enzyme activity in plants. Plant Cell Environ. 13, 195-206.
- [9] Demirors Saygıdeger, S., Keser, G. and Dogan, M. (2013) Effects of lead on chlorophyll content, total nitrogen, and antioxidant enzyme activities in duckweed (*Lemna minor*). International Journal of Agriculture and Biology, 15, 145-148.
- [10] Sobolev, I., Weintraub, P.G., Gera, A., Tam, Y. and Spiegel, S. (2007) Phytoplasma infection in the four o'clock flower (*Mirabilis jalapa*). Bulletin of Insectology 60, 281-282.
- [11] Le Duc, A. (1986) A revision of *Mirabilis* section *Mirabilis* (Nyctaginaceae). Sida Contrib. Bot., 16, 613-648.
- [12] Carucci, A., Cao, A., Fois G. and Muntoni, A. (2005) Phytoremediation of lead and zinc contaminated soils using *Mirabilis Jalapa*. In Contaminated Soils, Sediments and Water: Science in the Real World, Vol. 9, chapter 21, pp. 329-338, Springer Science, USA.
- [13] Yu, Z. and Zhou, Q. (2009) Growth responses and cadmium accumulation of *Mirabilis jalapa* L. under interaction between cadmium and phosphorus. Journal of Hazardous Materials, 167, 38-43.
- [14] Hund, A., Fracheboud, Y., Soldati, A. and Stamp, P. (2008) Cold tolerance of maize seedlings as determined by root morphology and photosynthetic traits. Europ. J. Agronomy 28, 178-185.
- [15] Zayed, A., Gowthaman, S. and Terry, N. (1998) Phytoaccumulation of trace elements by wetland plants: I. Duckweed. J. Environ. Qual. 27, 715-721.
- [16] Ghosh, M. and Singh, S.P. (2005) Comparative uptake and phytoextraction study of Soil induced chromium by accumulator and high biomass weed species. Appl. Ecol. Environ. Res. 3, 67-79.
- [17] Sayyad, G., Afyuni, M., Mousavi, S.F., Abbaspour, K.C., Hajabbasi, M.A., Richards, B.K. and Schulin, R. (2009) Effects of cadmium, copper, lead, and zinc contamination on metal accumulation by safflower and wheat. Soil Sediment Contamin., 18, 216-228.
- [18] Marschner, H. (1995) Mineral Nutrition of Higher Plants. 2nd Edn., Academic Press, New York.
- [19] Dogan, M., Demirors Saygıdeger, S. and Colak, U. (2009) Effect of lead toxicity on aquatic macrophyte *Elodea canadensis* Michx. Bull. Environ. Contam. Toxicol. 83, 249-254.
- [20] Kibria, M.G., Islam, M.S. and Osman, K.T. (2009) Effects of lead on growth and mineral nutrition of *Amaranthus gangeticus* L. and *Amaranthus oleracea* L. Soil and Environment 28, 1-6.
- [21] Azhar, N., Ashraf, M., Hussain M. and Arshad, M. (2011) Influence of lead on growth and nutrient accumulation in canola (*Brassica napus* L.) cultivars. J. Environ. Biol. 32, 659-666.
- [22] Lopez, M.L., Peralta-Videa, J.R., Benitez, T., Duarte-Gardea, M. and Gardea-Torresdey, J.L. (2007) Effects of lead, EDTA, and IAA on nutrient uptake by alfalfa plants. J. Plant Nutr. 30, 1247-1261.
- [23] Huang, J.W., and Cunningham, S.D. (1996) Lead phytoextraction: species variation in lead uptake and translocation. New Phytol. 134, 75-84.
- [24] Chatterjee, C., Dube, B.K., Sinha, P. and Srivastava, P. (2004) Detrimental effects of lead phytotoxicity on growth, yield and metabolism of rice. Commun. Soil Sci. Plant Anal. 35, 255-265.
- [25] Seregin, I.V., Shpigun, L.K. and Ivanov, V.B. (2004) Distribution and toxic effects of cadmium and lead on maize roots. Russ. J. Plant Physiol. 51, 525-533.
- [26] Gopal, R. and Rizvi, A.H. (2008) Excess lead alters growth, metabolism and translocation of certain nutrients in radish. Chemosphere 70, 1539-1544.
- [27] Kopittke, P.M., Asher, C.J., Kopittke, R.A. and Menzies, N.W. (2007) Toxic effects of Pb²⁺ on growth of cowpea (*Vigna unguiculata*). Environ. Pollut 150, 280-287.
- [28] Pourrut, B., Shahid, M., Dumat, C., Winterton, P. and Pinelli, E. (2011) Lead uptake, toxicity, and detoxification in plants. Rev. Environ. Contam. Toxicol. 213, 113-136.

Received: 17.10.2016

Accepted: 09.06.2017

CORRESPONDING AUTHOR

Mustafa Pehlivan

Nurdağı Vocatinal School, Gaziantep University,
Nurdağı-Gaziantep-Turkey

e-mail: mphehivan@gantep.edu.tr

YIELD AND FIBER TECHNOLOGICAL TRAITS OF ADVANCED COTTON LINES DEVELOPED BY LINE TESTER MATING DESIGN

Cetin Karademir^{1,*}, Emine Karademir¹, Ugur Sevilmis²

¹Siirt University, Agriculture Faculty, Field Crops Department, Siirt, Turkey

²Eastern Mediterranean Agricultural Research Institute, Adana, Turkey

ABSTRACT

The purpose of this study was to determine yield and fiber technological characteristics of advanced cotton lines developed by crossing parents which were selected in terms of their genetic diversity and genetic distances and comparing them with controls. The research has been carried out in GAP International Agricultural Research and Training Center's experimental area during 2013 and 2014 cotton growing season. Developed 10 advanced lines and 2 cotton cultivars (GW Teks and Stoneville 468) were used as material. The study was conducted in randomized complete block design with four replications. The statistical results showed that there were significant differences between lines/varieties in terms of all observed characteristics. The effect of year was significant for seed cotton yield, fiber yield, first picking percentage, ginning percentage, fiber fineness and fiber elongation. Year x variety interaction was significant for seed cotton yield, fiber yield, fiber uniformity index and short fiber index. According to the results of this study it was determined that Fiber Max 832 x Stv 453; Fiber Max 832 x Stv 453/2 for seed cotton yield and fiber yield; Stoneville 453, Tam 94 L 25 x Stv 453 and Fiber Max 832 x Stv 453 for ginning percentage; Tam 94 L 25 x Stv 453/2 for fiber fineness and fiber length; GW Teks, Giza 45 x Sayar 314 and GW Teks x Stv 453 for fiber strength were promising varieties.

KEYWORDS:

Cotton, genetic diversity, origin, yield, fiber technological properties

INTRODUCTION

Genetic diversity and genetic distance between parents is crucial for developing novel varieties in cotton and it is known that superior varieties have been developed by crossing varieties which are genetically far from each other [1, 2, 3]. An investigation has been carried out in order to determine genetic differences among some registered cotton

genotypes of Turkey, the results indicated that there were 8-26% genetic differences among genotypes, the highest differences (26%) were among Suregrow 125 variety and Sayar 314 and Maraş 92 [4]. Genetic differences among genotypes belong to *Gossypium hirsutum* L. species changed from 6-34%, while it was 12-42% for *Gossypium barbadense* species. The highest genetic differences (42%) obtained between GB-4 and Bahar 2482 genotypes, while the lowest genetic differences (12%) was between Bahar 82 and Aşkabat 91 genotypes. A study carried out for evaluating the genetic diversity and relationships among commercial *Gossypium hirsutum* species registered in Turkey from 1964 to 2014, 96 cotton cultivars were examined using morphological and molecular markers. The morphological analysis was scrutinized based on 4 fiber quality characteristics including fiber length, strength, fineness, and uniformity. It was reported that Turkish cotton cultivars had a good genetic diversity with high fiber quality, when taking into account upland cotton's narrow genetic structure [5]. Additionally, it was reported that within the upland cotton cultivars, the Egyptian cotton cultivar Giza 70 (*G. barbadense* L.) was distinctly separated from commercial cotton cultivars of Turkey (*G. hirsutum* L.) [6]. The main hindrance for providing simultaneously genetic progress between seed cotton yield and fiber quality is the existing negative correlation between lint yield and lint quality parameters and narrowing of cotton varieties in terms of genetic diversities [7, 8, 9, 10].

This study was carried out with aim to develop novel cotton varieties which have high yielding capacity, meeting textile sector's demands in terms of fiber quality parameters and have superior characteristics than present varieties by using cotton varieties which are genetically far from each other.

MATERIALS AND METHODS

The plant material used in this study was obtained by Line x Tester crossing. Ten upland cotton genotypes (FiberMax 832, Tam 94 L 25, GW Teks, Aşkabat 71, Giza 45, Bahar 14, Gedera 236, Stoneville 453, Maraş 92 and Sayar 314) were used

TABLE 1
Summary of chemical properties of soils of experimental area at GAP International Agricultural and Research Center.

Texture	Salinity (%)	PH	CaCO ₃ (%)	P ₂ O ₅ (kg/da)	Organic Mat. (%)	Water Saturation (%)
Clay-Loamy	0.013	7.03	9.57	2.48	1.57	74

GAP International Agricultural Research and Training Center's laboratory analysis, Diyarbakır

TABLE 2
Climatic data of experimental area during two years (2013 and 2014) and long term period (1950-2013).

Months	Minimum Temperature (°C)			Average Temp. (°C)			Maximum Temp. (°C)			Rainfall (mm)		
	2013	2014	Long Term	2013	2014	Long Term	2013	2014	Long Term	2013	2014	Long Term
April	6.9	6.9	7.1	14.4	14.7	13.9	21.9	22.0	20.3	39.4	39.9	73.5
May	11.4	11.1	11.3	19.1	19.8	19.3	27.3	28.1	26.5	98.0	48.8	40.8
June	17.1	17.6	16.4	26.8	26.6	25.9	34.9	34.1	33.2	2.8	21.4	8.2
July	22.8	21.9	21.6	31.3	31.6	31.0	38.4	39.3	38.2	0.0	0.6	0.7
August	21.4	21.2	20.9	30.5	31.1	30.3	38.1	39.6	38.0	0.0	0.0	0.6
September	15.9	16.5	15.9	24.4	24.7	24.9	32.1	32.2	33.3	0.0	27.4	2.6
October	9.0	11.0	9.8	16.9	17.5	17.1	25.0	24.2	25.2	0.0	34.2	30.8

Turkish State Meteorological Service.

TABLE 3
Average values and statistical groups of seed cotton and fiber yields

Variety/Line	Seed Cotton Yield (kg ha ⁻¹)			Fiber Yield (kg ha ⁻¹)		
	2013	2014	Mean	2013	2014	Mean
1.FiberMax832 x Stv 453	3589.2 b-g	4071.4 a	3830.3 ab	1510.6 a-g	1708.8 a	1609.7 a
2.FiberMax832 x Stv 453/2	3736.9 a-f	3989.9 ab	3863.4 a	1522.0 a-g	1653.8 a-c	1587.9 ab
3.GW Teks x Maraş 92	3500.7 c-g	3661.4 a-g	3581.1 a-d	1434.1 d-g	1521.6 a-g	1477.9 a-d
4.GW Teks x Maraş 92/2	3626.4 a-g	3840.4 a-d	3733.4 a-c	1476.8 b-g	1604.4 a-d	1540.6 a-c
5.GW Teks x Stv 453	3296.1 fg	3569.9 b-g	3433.0 c-e	1344.3 g	1500.4 b-g	1422.4 c-e
6.GW Teks x Stv 453/2	3401.0 d-g	3936.7 a-c	3668.8 a-c	1399.6 e-g	1673.5 ab	1536.6 a-c
7.Tam 94 L 25 x Stv 453	3408.8 d-g	3462.4 d-g	3435.6 c-e	1452.3 d-g	1471.7 c-g	1462.0 b-d
8.Tam 94 L 25 x Stv 453/2	2460.9 h	3800.9 a-e	3130.9 ef	1003.3 h	1595.2 a-e	1299.2 ef
9.Aşkabat 71 x Stv 453	3272.3 g	3281.2 fg	3276.7 de	1359.0 g	1384.2 fg	1371.6 de
10.Giza 45 x Sayar 314	2272.3 h	3542.7 b-g	2907.5 f	920.0 h	1509.8 a-g	1214.9 f
11.STV 468 (Kontrol)	3362.3 e-g	3566.9 b-g	3464.6 cd	1438.7 d-g	1574.6 a-f	1506.6 a-d
12.GW Teks (Kontrol)	3375.0 e-g	3667.4 a-g	3521.2 b-d	1421.9 d-g	1559.7 a-f	1490.8 a-d
Mean	3275.3 B	3699.3 A		1356.9 B	1563.2 A	
CV (%)	9.38			9.65		
LSD (0.05)						
Variety/Line	32.55**			14.02 **		
Year	39.67*			15.68 *		
Variety x Year	46.04 **			19.84 **		

ns: non significant; * and **, significantly different from zero at $P \leq 0.05$ and $P \leq 0.01$, respectively.

as parents. According to this method, seven lines (FiberMax 832, Tam 94 L 25, GW Teks, Aşkabat 71, Giza 45, Bahar 14, Gedera 236) and three testers (Stoneville 453, Maraş 92 and Sayar 314) were crossed as 21 combinations under field conditions, in GAP International Agricultural Research and Training Center's experimental field, Turkey in 2006. The seven cultivars used as lines were selected due to different origin and genetically far from each other, and three testers were selected from prevalently planted *Gossypium hirsutum* L. cultivars of region. Within 21 combinations 8 combinations (FiberMax 832 x Sayar 314, FiberMax 832 x Stoneville 453, GW Teks x Maraş 92, GW Teks x Stoneville 453, Tam 94 L 25 x Maraş 92, Tam 94 L

25 x Stoneville 453, Aşkabat 71 x Stoneville 453 and Giza 45 x Sayar 314) had high specific combining ability (SCA) effect, therefore, the breeding program for developing new varieties were continued with these hybrid combinations.

Ten advanced cotton lines obtained by selection from within the scope of this breeding program and two control varieties, totally 12 genotypes used as plant material in this study. The study was carried out in GAP International Agricultural Research and Training Center's experimental area in 2013 and 2014 cotton growing seasons. The soil characteristics of the experimental area are shown in Table 1.

Some climatic data belong to experiment 2013, 2014 and long term years are shown in Table 2. From the Table 2, max temperature in July and August of 2014 is higher than both 2013 and long term period. In 2013 at May, which is cotton sowing-time, 98 mm rainfall was recorded, this amount was higher than both 2014 and long term period.

Seeds of cotton were planted with combined cotton drilling machine on 8th May, 2013 and on 5th May, 2014. The experiments have been conducted in randomized complete block design with 4 replications. The plots consisted of four rows of 12 m length. Between and within the rows were 0.7 and 0.2 m, respectively. All plots received 140 kg ha⁻¹ N and 80 kg ha⁻¹ P₂O₅. 80 kg ha⁻¹ N and all of the P₂O₅ were applied at planting time remaining N (60 kg ha⁻¹) was applied at pre-flowering time. All of the cultivation process and irrigation have been performed at necessary periods. Insects and weeds were monitored throughout experiment. In 2013 insecticide was used at early growing phase against to thrips (*Thrips tabaci*) and at the boll forming periods against to the red spider mite (*Tetranychus urticae*). In 2014, two times insecticides were applied against to the *Empoasca*, *Heliothis armigera* and *Earias insulana*. The experiment was harvested by hand on 21th October 2013 and second on 14th November 2013. In the 2014 harvesting was done on 24th October and second on 13th November. The fiber quality characteristics were analyzed by High Volume Instrument (HVI) and the observations and differences were tested for significance by using LSD_(0.05).

RESULTS AND DISCUSSION

The average values and significance groups of observed characteristics were given as tables. The seed cotton yield and fiber yields of lines and varieties were given in Table 3. From the Table 3, it can be seen that there were significant differences in terms of variety, year and variety x year interactions for seed cotton yield. Seed cotton yield changed from 2907.5 kg ha⁻¹ (Giza 45 x Sayar 314) to 3863.4 kg ha⁻¹ (FiberMax 832 x Stv 453/2). As seen in Table the year differences is significant, the mean seed cotton yield of 2013 is 3275.3 kg ha⁻¹, while it is 3699.3 kg ha⁻¹ for 2014. The yield of 2014 is higher than 2013. The June's rainfall amount of 2014 is more than 2013 one reason of the difference can be that, the other reason can be due to the cultivation maintenance processes. Variety x year interaction is significant at 1% level, the highest yield was obtained from FiberMax 832 x Stv 453(4071.4 kg ha⁻¹) in 2014, while the lowest yield obtained from Giza 45 x Sayar 314 (2272.3 kg ha⁻¹) in 2013. The significance of the variety x year interaction has been indicating that the yield of genotypes used

in experiment can be changed year by years. The results of this study was compromised with previous researches. It was reported that the yield is affected from many factors such as, climate conditions, plant vegetation period, high temperature, the soil's pH, moisture, organic matter and textures [11]. Previous researcher reported that 70% of the yield variation is stemming from environmental differences which are occurring year by years and the other 30% is stemming from management process differences [12]. It was expressed that yield gain is found to be attributed by variety, i.e. genetics 48% management 28% and cultivar x management 24% [13].

It can be seen that there were significant differences in terms of variety, year and variety x year interactions for fiber yield (Table 3). According to the combined two years statistical analysis fiber yield changed from 1214.9 kg ha⁻¹ (Giza 45 x Sayar 314) to 1609.7 kg ha⁻¹ (FiberMax 832 x Stv 453). When comparing years the average fiber yield was 1356.9 kg ha⁻¹ in 2013, while it was 1563.2 kg ha⁻¹ in 2014. Variety x year interaction is significant at 1% level, the highest yield was obtained from FiberMax 832 x Stv 453 (1708.8 kg ha⁻¹) in 2014, while the lowest yield obtained from Giza 45 x Sayar 314 (920.0 kg ha⁻¹) in 2013. The significance of the variety x year interaction has indicated that the yield of lines and varieties used in experiment can be changed year by years. It was reported that environment is the dominant factor governing fiber yield (96.1% environment, 1.2% genotype) [14]. The significance of genotype x year interactions for fiber yield was reported by number of researchers [15]. The mean values of first picking percentage was given in Table 4. As seen from the table, variety and year differences were significant for this trait, but the variety x year interaction was not. The first picking percentage values of genotypes changed from 84.75% to 91.75. The highest first picking percentage obtained from Tam 94 L 25 x Stv 453 (91.75%) and Tam 94 L 25 x Stv 453/2 (91.60%).

From the Table 4, it can be seen that there were significant differences for varieties and years, but variety x year interaction was non-significant for ginning percentage. According to the combined two years statistical analysis for ginning percentage changed from 41.14% to 43.51. The highest values obtained from Stoneville 468 (43.51%), Tam 94 L 25 x Stv 453 (42.56%), GW Teks (42.35%) and FiberMax832 x Stv 453 (42.02%). As seen in table the year differences is significant, when comparing years the average ginning percentage was 41.39% for 2013, while it was 42.30% for 2014. Variety x year is non-significant it means that the ginning percentage is not changing from years. It was reported that lint percentage was impacted more by

TABLE 4
Average values and statistical groups of first picking percentage and ginning percentage

Variety/Line	First Picking Percentage (%)			Ginning Percentage (%)		
	2013	2014	Mean	2013	2014	Mean
1.FiberMax832 x Stv 453	88.23	91.10	89.66 a-c	42.06	41.99	42.02 bc
2.FiberMax832 x Stv 453/2	86.03	91.63	88.82 a-d	40.78	41.52	41.14 c
3.GW Teks x Maraş 92	86.50	83.01	84.75 f	40.94	41.59	41.26 c
4.GW Teks x Maraş 92/2	89.00	91.38	90.19 ab	40.78	41.78	41.28 c
5.GW Teks x Stv 453	87.81	90.51	89.15 a-d	40.77	42.02	41.39 bc
6.GW Teks x Stv 453/2	86.63	92.60	89.61 a-c	41.16	42.49	41.82 bc
7.Tam 94 L 25 x Stv 453	89.87	93.64	91.75 a	42.64	42.48	42.56 ab
8.Tam 94 L 25 x Stv 453/2	91.42	91.79	91.60 a	40.75	41.95	41.35 bc
9.Aşkabat 71 x Stv 453	87.93	88.34	88.13 b-e	41.51	42.22	41.86 bc
10.Giza 45 x Sayar 314	83.62	87.83	85.72 ef	40.49	42.70	41.59 bc
11.STV 468 (Kontrol)	86.46	87.20	86.83 c-f	42.71	44.31	43.51 a
12.GW Teks (Kontrol)	86.85	85.61	86.23 d-f	42.14	42.58	42.35 a-c
Mean	87.53 B	89.55 A		41.39 B	42.30 A	
CV (%)	3.40			2.91		
LSD (0.05)						
Variety/Line	3.04 **			1.21 **		
Year	1.61 *			0.85 *		
Variety x Year	ns			ns		

ns: non significant; * and **, significantly different from zero at $P \leq 0.05$ and $P \leq 0.01$, respectively.

TABLE 5
Average values and statistical groups of fiber fineness and fiber length

Variety/Line	Fiber Fineness (micronaire)			Fiber Length (mm)		
	2013	2014	Mean	2013	2014	Mean
1.FiberMax832 x Stv453	4.35	4.76	4.55 b-d	27.52	28.89	28.20 ab
2.FiberMax832 x Stv 453/2	4.94	5.13	5.03 a	26.35	26.55	26.45 de
3.GW Teks x Maraş 92	4.28	4.45	4.36 cd	28.86	28.19	28.52 ab
4.GW Teks x Maraş 92/2	4.46	4.66	4.55 b-d	28.58	28.05	28.32 ab
5.GW Teks x Stv 453	4.26	4.85	4.55 b-d	27.73	28.17	27.95 a-c
6.GW Teks x Stv 453/2	4.21	4.83	4.51 b-d	27.68	27.90	27.79 a-c
7.Tam 94 L 25 x Stv 453	4.50	4.73	4.61 bc	27.44	27.38	27.41 b-d
8.Tam 94 L 25 x Stv 453/2	3.99	4.64	4.31 d	28.72	29.02	28.87 a
9.Aşkabat 71 x Stv 453	4.29	4.78	4.53 b-d	26.41	27.62	27.01c-e
10.Giza 45 x Sayar 314	4.08	4.60	4.33 d	28.68	27.79	28.23 ab
11.STV 468 (Kontrol)	4.43	4.94	4.68 b	25.07	26.89	25.98 e
12.GW Teks (Kontrol)	4.21	4.57	4.39 cd	28.45	28.94	28.70 a
Mean	4.33 B	4.74 A		27.62	27.94	
CV (%)	5.73			4.21		
LSD (0.05)						
Variety/Line	0.25 **			1.15 **		
Year	0.34 *			ns		
Variety x Year	ns			ns		

ns: non significant; * and **, significantly different from zero at $P \leq 0.05$ and $P \leq 0.01$, respectively.

genotype (51.5%) than by environment (38.8%) [14]. Investigations indicated that environmental conditions lesser affects the trait which has high heritability [16].

From the Table 5, it can be seen that there were significant differences for varieties and years, but variety x year interaction was non-significant for fiber fineness. According to the combined two years statistical analysis for fiber fineness values changed from 4.31 to 5.03 micronaire. The lowest micronaire values obtained from Tam 94 L 25 x Stv

453/2 (4.31 mic.) and Giza 45 x Sayar 314 (4.33 mic.). As seen in table the year differences is significant, when comparing years the average fiber fineness was 4.33 micronaire for 2013, while it was 4.74 micronaire for 2014. The obtained results of this study compromises with the previous researches, i.e; It was reported that the environment was the dominant factor governing micronaire (63.8% environment, 9.9% genotype) [14]. Previous researchers reported that the genetic control of cotton fiber quality was significantly affected from general

TABLE 6
Average values and statistical groups of fiber strength and fiber elongation

Variety/Line	Fiber Strength (g tex ⁻¹)			Fiber Elongation (%)		
	2013	2014	Mean	2013	2014	Mean
1.FiberMax832 x Stv453	32.73	31.70	32.21 bc	6.00	6.38	6.18 e
2.FiberMax832 x Stv 453/2	31.03	31.00	31.01 cd	6.23	6.90	6.56 de
3.GW Teks x Maraş 92	33.48	31.93	32.70 bc	6.70	7.08	6.88 b-d
4.GW Teks x Maraş 92/2	32.83	32.00	32.41 bc	6.30	7.00	6.65 c-e
5.GW Teks x Stv 453	34.00	32.95	33.47 ab	6.75	7.85	7.30 ab
6.GW Teks x Stv 453/2	33.58	32.25	32.91 b	7.05	6.95	7.00 b-d
7.Tam 94 L 25 x Stv 453	33.10	31.70	32.40 bc	6.70	6.83	6.76 b-d
8.Tam 94 L 25 x Stv 453/2	29.63	28.83	29.22 d	6.70	7.15	6.92 b-d
9.Aşkat 71 x Stv 453	30.33	29.65	29.99 d	7.47	7.80	7.63 a
10.Giza 45 x Sayar 314	33.50	33.90	33.70 ab	6.68	7.13	6.90 b-d
11.STV 468 (Kontrol)	30.25	29.95	30.10 d	7.03	7.28	7.15 a-c
12.GW Teks (Kontrol)	35.83	34.45	35.13 a	6.38	7.08	6.72 c-e
Mean	32.52	31.69		6.66 B	7.11 A	
CV (%)	5.57			7.98		
LSD (0.05)						
Variety/Line	1.77 **			0.54 **		
Year	ns			0.26 **		
Variety x Year	ns			ns		

ns: non significant; * and **, significantly different from zero at $P \leq 0.05$ and $P \leq 0.01$, respectively.

TABLE 7
Average values and statistical groups of fiber uniformity and short fiber index

Variety/Line	Fiber Uniformity (%)			Short Fiber Index (%)		
	2013	2014	Mean	2013	2014	Mean
1.FiberMax832 x Stv453	81.70 c-f	82.82 c-e	82.26 cd	11.1 a-c	8.57 ef	9.83 a-d
2.FiberMax832 x Stv 453/2	80.63 ef	81.82 c-f	81.22 d	11.4 a	7.67 f	9.55 b-d
3.GW Teks x Maraş 92	82.72 c-f	82.82 c-e	82.77 b-d	9.45 a-f	8.25 f	8.85 cd
4.GW Teks x Maraş 92/2	86.60 a	82.55 c-f	84.57 ab	8.76 d-f	10.7 a-e	9.77 b-d
5.GW Teks x Stv 453	81.77 c-f	83.05 b-e	82.41 cd	10.7 a-e	9.40 a-f	10.0 a-d
6.GW Teks x Stv 453/2	83.42 b-d	82.52 c-f	82.97 b-d	9.82 a-f	8.92 c-f	9.37 b-d
7.Tam 94 L 25 x Stv 453	83.37 b-d	82.80 c-e	83.08 a-c	9.07 b-f	10.7 a-e	9.90 a-d
8.Tam 94 L 25 x Stv 453/2	82.40 c-f	82.40 c-f	82.40 cd	10.6 a-e	11.0 a-d	10.8 ab
9.Aşkat 71 x Stv 453	80.13 f	83.17 b-e	81.65 cd	11.5 a	11.2 ab	11.4 a
10.Giza 45 x Sayar 314	83.30 b-d	83.02 b-e	83.16 a-c	9.45 a-f	10.9 a-d	10.1 a-c
11.STV 468 (Kontrol)	81.10 d-f	83.62 b-d	82.38 cd	10.8 a-e	9.32 a-f	10.0 a-d
12.GW Teks (Kontrol)	85.62 ab	84.17 a-c	84.90 a	9.32 a-f	7.62 f	8.47 d
Mean	82.73	82.90		10.17	9.54	
CV (%)	2.24			16.24		
LSD (0.05)						
Variety/Line	1.85 **			1.59 *		
Year	ns			ns		
Variety x Year	2.60 *			2.24 **		

ns: non significant; * and **, significantly different from zero at $P \leq 0.05$ and $P \leq 0.01$, respectively.

differences between years [17]. In contrast, the effect of environment was not significant on fiber fineness [18].

As shown in Table 5, it can be seen that there were significant differences at 1% level between genotypes for fiber length, but not for years and genotype x year interaction. The length values of genotypes changed from 25.98 mm to 28.87 mm. The highest fiber length obtained from Tam 94 L 25 x Stv 453/2 (28.87 mm) and GW Teks (28.70 mm). Although fiber length is a genetic trait it is affected by management, soil moisture, the frequency of

irrigation and amount of water and temperature variations [19, 20, 21].

From the Table 6, it can be seen that there were significant differences among varieties for fiber strength. In contrast, there were non-significant relations in terms of years and variety x year interaction. The fiber strength values of genotypes changed from 29.22 to 35.13 g tex⁻¹. The highest values obtained from GW Teks (35.13 g tex⁻¹), Giza 45 x Sayar 314 (33.70 g tex⁻¹) and GW Teks x Stv 453 (33.47 g tex⁻¹). The insignificance of years and genotype x year interaction means that

the varieties have the same values in different years and also indicate that the effect of genotype was more than environment in terms of this trait. The results of this study is compromise with the results of previous researchers who reported the effect of genotypes more than environment [18 , 20 , 21].

It can be seen that there was significant differences at 0.01 probability level between genotypes and years for fiber elongation, but the differences in terms of genotype x year interaction was non-significant (Table 6). The elongation values changed from 6.18% to 7.63. The highest values obtained from Aşkabat 71 x Stv 453 (7.63%) and GW Teks x Stv 453 (7.30%). The elongation values changed year by year. In 2013 the average of the genotypes were 6.66%, while it was 7.11% in 2014. Elongation is affected from genotype, environment and genotype x environment interaction [22]. Elongation was affected from night temperature, by decreasing the night temperature elongation decreased [23].

The high volume instrument's (HVI) results showed that there were significant differences among varieties at 1% level and at %5 level in terms of variety x year interaction for fiber uniformity. On the other hand, year differences were non-significant for this trait (Table 7). The uniformity values changed from 81.22% to 84.90. The highest values obtained from GW Teks (84.90%) and GW Teks x Maraş 92/2 (84.57%). For varieties x years the highest uniformity was obtained in 2013 as 86.60% from GW Teks x Maraş 92/2, while the lowest value was obtained in 2013 as 80.13% from Aşkabat 71 x Stv 453.

From the Table 7, there were significant differences for short fiber index (SFI) in terms of all investigated traits except years. The SFI values changed from 8.47 to 11.4%, the highest result obtained from Aşkabat 71 x Stv 453 (11.4%) and the lowest obtained from GW Teks (8.47%). When comparing varieties x years interaction the lowest result obtained in 2014 from GW Teks (7.62%), while the highest value obtained in 2013 from Aşkabat 71 x Stv 453 (11.5%). SFI was affected from genotype, management, harvesting, ginning and crop process [20].

CONCLUSION

In this breeding study different varieties came from different origin and genetically far from each other have been used as parent and the advanced lines obtained from this breeding program compared with varieties which prevalently planted in the region during two years. It was determined that there were significant differences among varieties and advanced lines in terms of yield, first picking percentage, ginning percentage and all investigated quality parameters.

The year differences were significant for seed cotton yield, first picking percentage, fiber fineness and elongation, while variety x year interaction was significant for seed cotton yield, fiber uniformity ratio and short fiber index. The results showed that Fiber Max 832 x Stv 453; Fiber Max 832 x Stv 453/2 had highest values for seed cotton yield and fiber yield; Tam 94 L 25 x Stv 453 and Fiber Max 832 x Stv 453 for ginning percentage; it was determined that Tam 94 L 25 x Stv 453/2 lines were promised lines for fiber fineness and fiber length; GW Teks, Giza 45 x Sayar 314 and GW Teks x Stv 453 were promised lines for fiber strength. All of the genotypes had more than 80% uniformity index values.

ACKNOWLEDGEMENT

This work was supported by General Directorate of Agricultural Research and Policies (TAGEM).

REFERENCES

- [1] Esbroeck, G.V and Bowman, D.T. (1998) Cotton Germplasm Diversity and Its Importance to Cultivar Development. *The Journal of Cotton Science* 2, 121-129.
- [2] El-Zik, K.M and Thaxton, P.M. (1998) Genetic Improvement of Cotton Utilising the Multi-Adversity Resistance (MAR) System. *Proceedings of the World Cotton Conference-2, Athens, Greece, September, 6-12, p.10-19*
- [3] Kuraparthi, V and Bowman, D.T. (2013) Gains in Breeding Upland Cotton for Fiber Quality. *The Journal of Cotton Science* 17:157-162.
- [4] Bardak, A. (2007) Genetic diversity of diploid and tetraploid cottons determined by SRR markers and its relationship with fiber quality traits. *University of Kahramanmaraş Sutcu Imam, Institute of Natural and Applied Sciences Department of Field Crops, MSc Thesis, Kahramanmaraş.*
- [5] Akışcan, Y. (2012) Determination of Genetic Improvement on Fiber Quality Traits in Some Cotton Cultivars released between 1980 and 2009 in Turkey. *SDU Journal of the Faculty of Agriculture* 7 (2):32-40.
- [6] Elçi, E., Akışcan, Y. and Akgöl, B. (2014) Genetic diversity of Turkish commercial cotton varieties revealed by molecular markers and fiber quality traits. *Turk J Bot.* 38, 1274-1286.
- [7] Ulloa, M. and Meredith, J.W.R. (2000) Genetic Linkage Map and QTL Analysis of Agronomic and Fiber Quality Traits in an Intraspecific Population. *The Journal of Cotton Science* 4:161-170.

- [8] Desalegn, Z., Ratanadilok, N. and Kaveeta, R. (2009) Correlation and Heritability for Yield and Fiber Quality Parameters of Ethiopian Cotton (*Gossypium hirsutum* L.) Estimated from 15 (diallel) Crosses. *Kasetsart J. (Nat. Sci.)* 43 : 1 – 11.
- [9] Bourland, F. M. (2013) Novel Approaches used to breed and evaluate cotton. editorialexpress.com/cgi-bin/conference/download.cgi?db_name=AGRAR2013&paper_id=114
- [10] Zeng, L. (2014) Broadening the Genetic Base of Upland Cotton in U.S. Cultivars – Genetic Variation for Lint Yield and Fiber Quality in Germplasm Resources. <http://cdn.intechopen.com/pdfs-wm/46501.pdf>
- [11] Elms, M.K., Green, C. J., Johnson, F. N. (2001) Variability of Cotton Yield and Quality. *Commun. Soil Sci. Plant Analy*, 32 (3&4), 351–368.
- [12] Krieg, D.R (1997) Genetic and environmental factors affecting productivity of cotton. *Proceedings of the Beltwide Cotton Conference*, 7-10 January, National Cotton Council of America, New Orleans, LA, 2:1347.
- [13] Liu, S.M., Constable, G.A., Reid, P.E., Stiller, W.N. and Cullis, B.R. (2013) The interaction between breeding and crop management in improved cotton yield. *Field Crops Research*, 148, 48-60.
- [14] Snider, J.L., Collins, G.D., Whitaker, J., Davis, J.W. (2013) Quantifying Genotypic and Environmental Contributions to Yield and Fiber Quality in Georgia: Data from Seven Commercial Cultivars and 33 Yield Environments. *The Journal of Cotton Science* 17:285–292.
- [15] Elayan Sohair, E. D., Abdallah Amany, M., Abd El-Gawad Nadia, S. and Younies Shimaa, S. A. (2014) Evaluation of Some Long Staple Cotton Genotypes Cultivated Under Different Environmental Conditions. *American-Eurasian J. Agric. & Environ. Sci.*, 14 (6): 546-554.
- [16] Mukoyi, F., Mubvekeri, W., Kutwayo, D., Muripira, V. and Mudada, N. (2015) Development of elite medium staple cotton (*G. hirsutum*) genotypes for production in middleveld upland ecologies. *African Journal of Plant Science*, 9 (1), 1-7.
- [17] Paterson, A.H., Saranga, Y., Menz, M., Jiang, C.X. and Wright, R.J. (2003) QTL analysis of genotype × environment interactions affecting cotton fiber quality. *Theor Appl Genet*, 106:384–396.
- [18] Green, C.C., and Culp, T.W. (1990) Simultaneous improvements of yield, fiber quality, and yarn strength in upland cotton. *Crop Sci.* 30:66–69.
- [19] Reddy, K.R., Davidonis, G.H., Johnson, A.S., Vinyard, B.T. (1999) Temperature regime and carbon dioxide enrichment alter cotton boll development and fiber properties. *Agronomy Journal*, 91 (5): 851-858.
- [20] Bradow, J.M. and Davidonis, G.H. (2000) Quantitation of fiber quality and the cotton production-processing interface: A physiologist's perspectives, *The Journal of Cotton Science* 4:34-64.
- [21] May, O.L. (2000) Genetic variation in fiber quality. p. 183–220. In A.S. Basra (ed) *Cotton fibers developmental biology, quality improvement, and textile processing* Food Products Press, New York.
- [22] Campbell, B.T and Jones, M.A. (2005) Assessment of genotype × environment interactions for yield and fiber quality in cotton performance trials. *Euphytica*, 144: 69–78.
- [23] Gipson, J.R and Ray, L.L. (1969) Fiber elongation rates in five varieties of cotton (*Gossypium hirsutum* L.) as influenced by night temperature. *Crop Science*. 9:339–341.
- [24] Anonymous (2013a). GAP International Agricultural Research and Training Center. The results of soil laboratory analysis, Diyarbakır
- [25] Anonymous, 2013b. Turkish State Meteorological Service.

Received: 02.11.2016

Accepted: 09.06.2017

CORRESPONDING AUTHOR

Cetin Karademir

Siirt University, Agriculture Faculty, Field Crops Department, Siirt, Turkey

e-mail: cetinkarademir@siirt.edu.tr

KINETICS AND EQUILIBRIUM ADSORPTION STUDY OF LEAD(II) ONTO ACTIVATED CARBON PREPARED FROM PUMPKIN SEED SHELL

Ilknur Demiral*, Canan Aydın Samdan, Hakan Demiral

Department of Chemical Engineering, Engineering and Architecture Faculty, Eskişehir Osmangazi University, Meşelik Campus, 26480 Eskişehir, Turkey

ABSTRACT

In this study, activated carbon was prepared from pumpkin seed shells by $ZnCl_2$ (chemical) activation at an impregnation ratio of 3/1 and a carbonization temperature of 500 °C. The prepared activated carbon was used to remove lead(II) ions from aqueous solutions. The BET surface area and micropore volume of the obtained activated carbon was 1564 m^2/g and 0.526 cm^3/g , respectively. Optimum adsorption conditions were determined as a function of initial pH, contact time, temperature, adsorbent dosage and initial lead(II) concentration. Langmuir isotherm provided the best fit to the equilibrium data with maximum adsorption capacity of 36.33 mg/g . The kinetic data were found to follow closely the pseudo-second-order model. The thermodynamic parameters such as ΔG° , ΔH° and ΔS° were calculated for predicting the nature of adsorption.

KEYWORDS:

Pumpkin seed shell, chemical activation, activated carbon, adsorption, lead(II) removal

INTRODUCTION

Unregulated and rapid industrialization, which is widely encountered in many developing countries, results in increasing environmental pollution via discharge of industrial waste water, without any treatment, into receiving water body such as rivers, streams or lakes. Heavy metal pollution is a serious environmental problem due to the toxic effects of the heavy metal ions on human health and living organisms [1].

Heavy metal contamination exists in aqueous wastes of many industries and these metal ions do not degrade into harmless end products. Heavy metals like As, Cd, Cu, Hg, Zn, Pb, Cd, Ni, Cr, etc. make a waste hazardous in case of any contamination [2]. Lead is one of the potentially toxic heavy metals [3]. The presence of high levels of lead in the environment may cause long-term health risks to humans and ecosystems [4]. Hence, it becomes essential to control and reduce the levels of these lead ions in

wastewaters and bring them to allowable values. The allowable level for lead in drinking water is 0.05 $mg L^{-1}$ according to the US Environmental Protection Agency (EPA) [5].

Manufacture of storage batteries, painting pigments, ammunition, solder, plumbing fixtures, automobiles, cable coverings, radioactivity shields, bearings and caulking are some of the lead pollution sources [6]. Lead ions are taken into body via inhalation, ingestion or skin adsorption. Lead can act as a cumulative poison when the body is exposed to it. Lead accumulates mainly in bones, brain, kidney and muscles and may cause many serious disorders like anemia, kidney diseases, nervous disorder and sickness and even death [7].

Oxidation, chemical coagulation, precipitation, flotation, solvent extraction, membrane filtration, reverse osmosis, ion exchange, adsorption, etc. are used to remove the heavy metals from wastewaters. One of the effective methods used for removing lead ions from aqueous solutions is adsorption. In recent years, carbon materials have been used widely in water treatment technology [8,9]. Activated carbon is one of the most commonly used adsorbents for the adsorption process. High surface area, micro-porous nature, high adsorption capacity, high purity and easy availability are the most important advantages of the activated carbons [10]. Another advantage is their low cost when the activated carbon is prepared from waste materials [11]. Any carbonaceous material high in carbon content with low ash can be used as a raw material for the preparation of activated carbon. Several factors are considered when selecting an appropriate raw material. Industrially, an inexpensive material with high density and sufficient volatiles, available in high amounts, is usually preferred [12]. Several studies have been reported on lead adsorption with activated carbon produced from alternative materials such as hazelnut husk [1], cotton stalk [10], scrap tires [13], sewage sludge [14], woody biomass [15] and apple pulp [16].

Physical and chemical activation are used for preparing an activated carbon. In the physical activation, a raw material is first carbonized and the carbonized material is secondarily activated by an activation agent such as steam or carbon dioxide. In the chemical activation, a raw material is impregnated

with an activating reagent and the impregnated material is heat-treated under an inert atmosphere. The carbonization and activation steps simultaneously progress in the chemical activation [17]. The most widely used chemicals are zinc chloride (ZnCl_2), phosphoric acid (H_3PO_4), potassium hydroxide (KOH) and sodium hydroxide (NaOH) [10, 18-21]. The higher yield, simplicity, lower activation temperature and shorter activation time and good development of the porous structure are the advantages of the chemical activation [22-23].

In this study, activated carbon was produced from pumpkin seed shells by zinc chloride activation and the produced activated carbon was used to remove lead(II) ions from aqueous solutions by adsorption. The effects of initial pH, contact time, temperature, adsorbent dosage and initial concentration of the solution on the adsorption of lead ions were investigated. The equilibrium, kinetic and thermodynamic data of the adsorption were studied to describe the adsorption process.

MATERIALS AND METHODS

Materials. The pumpkin seed shell used in this study was obtained from pumpkin seed process waste of Peyman Company in Eskişehir, Turkey. The dried sample was crushed and sieved to obtain 0.850 mm to 1 mm grain size by a high-speed rotary cutting mill. The proximate analysis of the pumpkin seed shell gave 7.6% moisture, 3.90% ash, 70.97% volatile matter and 17.53% fixed carbon. The C, H, N, and O contents of the pumpkin seed shell were found as 48.79 %, 7.52 %, 3.97 %, 39.72 %, respectively.

Activated carbon preparation. The impregnation ratio of 3/1 and carbonization temperature of 500 °C were determined as the optimum conditions in a previous study [24]. Therefore, these parameters were used in the activated carbon preparation. The activated carbon production method is as follows.

The chemical activation of pumpkin seed shell was carried out using zinc chloride (ZnCl_2). The impregnation ratio was calculated as the ratio of the weight of ZnCl_2 in solution to the weight of the used pumpkin seed shell. In the first step of activation, 60 g of ZnCl_2 were dissolved in 200 ml of distilled water, and then 20 g of dried pumpkin seed shell was mixed with the zinc chloride solution and stirred at approximately 75 °C for 6 h. The mixtures were then filtered and the remaining solids were dried at 105 °C for about 24 h. In the second step, 10 g of the impregnated sample was placed in a stainless steel boat and carbonized in a vertical furnace at desired temperatures (500 °C) under the nitrogen flow of 100 ml/min. The carbonization process was initiated by heating the sample with a heating rate of 10 °C/min

starting from room temperature until the desired temperature was reached. The samples were held at the desired temperature for 1 h. Then, the temperature of the reactor was cooled down to the room temperature under nitrogen atmosphere. The activated carbon was washed with a 0.5 N HCl solution. Subsequently, the samples were repeatedly washed with hot distilled water until the pH of the solution reached a value between 6 and 7. Finally, the wet samples were dried at 105 °C for 24 h.

Characterization of activated carbons. The activated carbon characterization was carried out by nitrogen adsorption-desorption isotherms measured at 77 K using Quantachrome, Autosorb 1C device. Prior to the gas adsorption measurement, the samples were degassed at 300 °C under vacuum for 3 h. The adsorption data were obtained in a relative pressure, P/P_0 , range of 10^{-5} to 1. The BET surface area was calculated from N_2 adsorption isotherm by using the Brunauer–Emmett–Teller (BET) equation within the 0.01-0.15 relative pressure range. The t-plot method was applied to calculate the micropore volume. The total pore volume was calculated at a relative pressure of 0.995. The pore size distribution of the activated carbon was determined by DFT (Density Functional Theory) method.

Adsorption studies. The adsorption of lead(II) ions onto the produced activated carbon was carried out by batch experiments. The lead(II) ions dissolved from $\text{Pb}(\text{NO}_3)_2$ (1000mg/L) were used in the adsorption experiments. The concentration of lead(II) ions was determined by using a UV spectrophotometer (Thermo Electron Corporation, Aquamate) at 340 nm. The effects of initial pH, temperature, contact time and adsorbent dosage were investigated.

Effect of the initial pH. The study of the influence of the initial pH on the adsorption was carried out in a pH range of 2–6. The solution pH was adjusted by the addition of HCl or NaOH solutions after the mixing of lead(II) solutions with activated carbon. The amount of adsorbent (0.1 g), volume of solution (50 mL), initial concentration of solution (100 mg/L) and temperature (25 °C) were kept constant. After adsorption, the solutions were centrifuged and the concentrations of the solutions were determined.

Kinetic studies. The rate of adsorption of lead was studied at different time intervals. In kinetic studies 50 ml lead(II) solution (100 mg/L) and 0.1 g activated carbon were placed into glass vials. The bottles were agitated using isothermal bath shaker at 25 °C until reaching the adsorption equilibrium. Batch experiments were repeated for different periods. The concentration of lead(II) remaining in the solution was measured.

Adsorption isotherms. In order to determine the adsorption isotherms and thermodynamic parameters, the adsorption of lead from aqueous solutions by activated carbon was carried out at different temperatures (25, 35 and 45 °C). In the experiments, 0.1 g activated carbon samples were mixed with 50 mL solutions of various lead(II) concentrations ranging from 30 mg/L to 200 mg/L. After adsorption, the lead(II) ions concentrations in the solution were determined.

RESULTS AND DISCUSSION

Characterization of the activated carbon.

The results of ultimate analysis and surface properties of the pumpkin seed shell and activated carbon are given in Table 1. Activated carbon has higher carbon content than raw pumpkin seed shell and this makes it a more carbonaceous material. The carbon content increased after the activation process, and the hydrogen, nitrogen and oxygen contents indicated the opposite change trend. This is due to the release of volatiles during carbonization that results in the elimination of the non-carbonaceous species and enrichment of carbon [25].

TABLE 1
Characteristics of the pumpkin seed shell and activated carbon

Characteristics	Pumpkin seed shell	Activated carbon
<i>Ultimate analysis</i>		
Carbon	48.79	75.71
Hydrogen	7.52	3.07
Nitrogen	3.97	2.70
Oxygen (by differ-	39.72	18.52
<i>Surface properties</i>		
BET surface area (m ² /g)	7.96	1564
Micropore area (m ² /g)	-	878
Total pore volume (cm ³ /g)	-	0.965
Micropore volume (cm ³ /g)	-	0.526
Average pore diameter (nm)	-	2.47

The adsorption of N₂ is essential for identifying the pore structure of adsorbents before liquid sorption experiments. Figure 1 shows the N₂ adsorption isotherm of the activated carbon prepared from pumpkin seed shell by chemical activation. As can be seen from Figure 1, a rapid increase is observed in the adsorption–desorption isotherm at low relative pressures, which is followed by a nearly horizontal plateau at higher relative pressures, indicating type I of the isotherm based on the classification of the Brunauer, Deming, Deming and Teller (BDDT) [26].

The type I isotherm represents a material with microporous structure. The major uptake occurs at low relative pressures indicating the formation of highly porous materials with narrow pore size distribution.

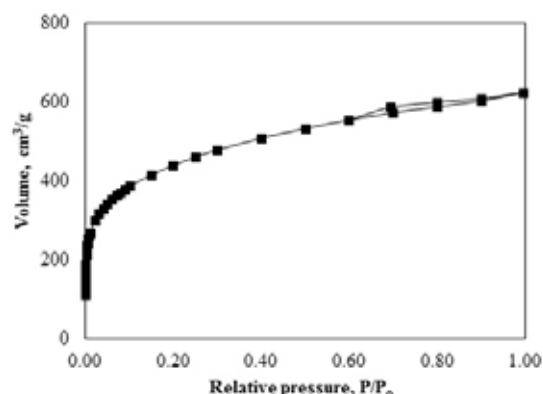


FIGURE 1

The adsorption-desorption isotherm of the produced activated carbon.

Specific surface area, pore volume and pore size distribution identify the adsorptive capacity of the activated carbon. Generally, as the surface area of the activated carbon increases, its adsorptive capacity also increases. These surface areas are generated gradually during the activation processes [27]. The BET surface area of activated carbon is important because differences in the surface area and porosity within the material can greatly influence its performance characteristics in the purification process.

The high surface area is probably due to the opening of the restricted pores with the help of activating reagents. The BET surface area of the pumpkin seed shell was found to be about 7.96 m²/g. The surface area of the activated carbon was obtained as 1564 m²/g with ZnCl₂ having 3:1 impregnation ratio. This is a relatively high surface area for an activated carbon [24].

Table 1 shows the physical properties including BET surface area (S_{BET}), micropore volume, total pore volume and average pore diameter. The data given in Table 1 show that using ZnCl₂ as an activating agent is very efficient to produce activated carbon with high porosity and high surface area. It is well known that activation with zinc chloride prevents the accumulation of tar on the carbon surface and provides further decompositions, and thus, develops the microporosity when using cellulosic and lignocellulosic precursor in the manufacture of activated carbon [28].

The structural heterogeneity of a porous material is generally characterized in terms of pore size distribution. The pore size distribution represents a model of a solid internal structure. The pore size distribution of the prepared activated carbon is shown in Figure 2. The activated carbon prepared in this study exhibits two peaks around 7–20 Å and 20–60 Å. As seen from Fig. 2, the activated carbon includes both micropores and mesopores.

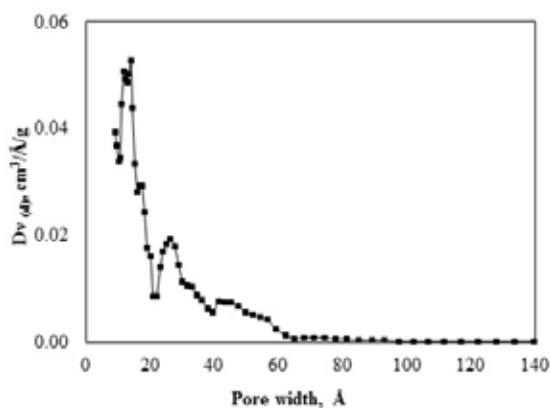


FIGURE 2

Pore size distribution of the produced activated carbon.

Adsorption studies. Effect of the initial pH on the adsorption of lead(II). The pH of the solution is one of the most important factors to determine the adsorption property of an adsorbent due to its effect not only on surface charge of the adsorbent, but also on the degree of ionization and speciation of adsorbate [29]. The effect of the initial pH on the adsorption of lead(II) on the produced activated carbon was studied by changing the initial pH of the solution from 2.0 to 6.0 and the results are shown in Figure 3. It is apparent that the uptake is quite low at a lower pH (2.0); however, with increased pH, a significant enhancement in adsorption is recorded. At low pH, there is a high concentration of H^+ that has high mobility compared to metal ions and the competition between H^+ and metal ions decreases the adsorption of the metal ions. With an increase in the pH, the negative charge density on the activated carbon surface increases due to the deprotonation of the metal binding sites and thus increases the adsorption [5]. When the initial pH of the adsorption medium was adjusted to a higher value of pH=6, lead precipitation as $(Pb(OH)_2)$ was observed due to the existence of OH^- ions in the adsorption medium. Therefore, the effect of higher pH values than 6 were not studied.

All the other adsorption experiments in this study were carried out at the original solution pH of 5.0.

Adsorption kinetics. Every adsorption process may follow one of the different patterns such as chemical reaction, diffusion control and mass transfer or some combination of them. Analysis of the experimental data at various time intervals make possible to calculate the kinetic parameters and to get some information for designing and modelling the adsorption processes. In this study, pseudo- first order, pseudo-second order and intraparticle diffusion kinetic models were analyzed with the adsorption data. The accordance between the experimental data and the model-predicted values were expressed by the correlation coefficients and the average relative error (ARE).

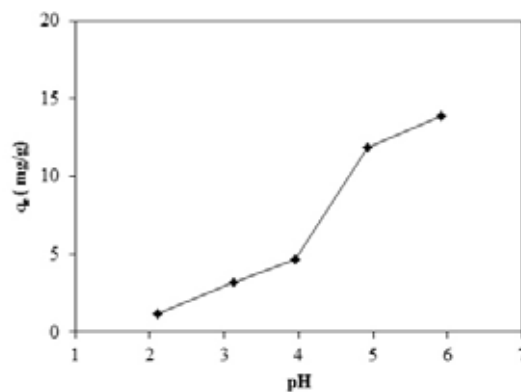


FIGURE 3

Effect of initial pH on adsorption of lead (II).

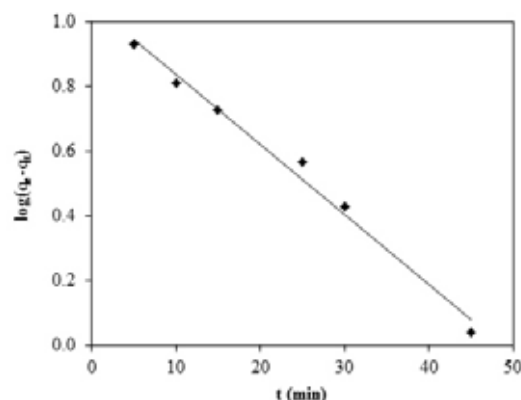


FIGURE 4

Pseudo-first order kinetics plot for the removal of lead(II).

A pseudo-first order equation of Lagergren is generally expressed as [30]:

$$\log(q_e - q_t) = \log q_e - \frac{k_1 t}{2.303} \quad (1)$$

in which q_e and q_t (mg/g) are the amounts of lead(II) adsorbed at equilibrium and at time t , respectively, t (min) is the contact time, and k_1 (L/min) is the rate constant for this equation. The values of k_1 and q_e can be calculated from a plot of $\log(q_e - q_t)$ against t (Figure 4).

The linear pseudo-second order rate equation is expressed as follows [31-32]:

$$\frac{t}{q_t} = \frac{1}{k_2 q_e^2} + \frac{t}{q_e} \quad (2)$$

where k_2 is the pseudo-second order rate constant (g/mg min), q_e and q_t are the amounts of lead(II) adsorbed (mg/g) at equilibrium and at time t (min), respectively. The values of k_2 and q_e can be calculated from the plot of t/q_t against t (Figure5).

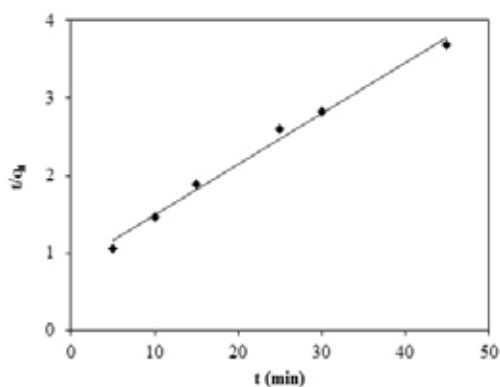


FIGURE 5

Pseudo-second order kinetics plot for the removal of lead(II).

An intraparticle diffusion model is of major concern because it is the rate-determining step in the liquid–solid adsorption systems. During the batch adsorption process, there is a possibility of transport of sorbate species into the pores of sorbent, which is often a rate-controlling step. An intraparticle diffusion model, based on the theory proposed by Weber and Morris, was used to identify the diffusion mechanisms [33]. The intraparticle diffusion can be stated by the following equation [4, 33]:

$$q_t = k_p t^{1/2} + C \quad (3)$$

where k_p is the intraparticle rate constant ($\text{g mg}^{-1} \text{min}^{-0.5}$) and C is the constant that gives an idea about the boundary layer thickness (mg g^{-1}). They are obtained from the slope of the straight line of q_t versus $t^{1/2}$ (Figure 6).

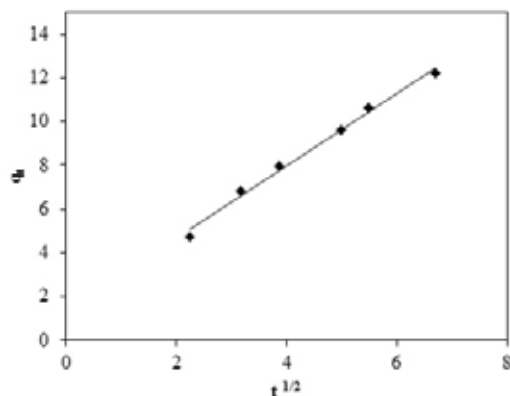


FIGURE 6

Intraparticle diffusion kinetics for lead(II) adsorption .

To evaluate the fitness of kinetic and isotherm equations to the experimental data, the average relative error (ARE) calculated using Equation (4) was used to determine the kinetic and isotherm constants. ARE can be expressed as [34]

$$\text{ARE (\%)} = \frac{100}{n} \sum_i^n \left| \frac{q_{i,\text{cal}} - q_{i,\text{exp}}}{q_{i,\text{exp}}} \right| \quad (4)$$

where n is the number of data points, $q_{i,\text{exp}}$ (mg.g^{-1}) is the equilibrium value obtained from the experiment and $q_{i,\text{cal}}$ (mg.g^{-1}) is the calculated value using the isotherm model.

The fit of these models was checked by comparing the regression coefficients and the average relative error (ARE) for each expression. The rate constants, calculated equilibrium uptakes, the corresponding correlation coefficients and average relative errors were given in Table 2.

TABLE 2

Kinetic parameters for the adsorption of lead(II) onto activated carbon

Kinetic models	Kinetic parameters		R ²	ARE (%) =
Pseudo-first order	k_1 (L min^{-1}) = 0.049	q_e (mg/g) = 11.29	0.97	26.14
Pseudo-second order	k_2 ($\text{g mg}^{-1} \text{min}^{-1}$) = 0.005	q_e (mg/g) = 15.24	0.99	4.36
Intraparticle diffusion	k_p ($\text{g mg}^{-1} \text{min}^{-0.5}$) = 1.644		0.99	11.73

According to Table 2, the pseudo-second order kinetic model was suitably fitted with the kinetic data by presented little ARE values and also high R^2 . The calculated q_e value (15.24 mg/g) close to the experimental data (13.75 mg/g) indicated that Pb(II) adsorption onto the produced activated carbon can be approximated more favourably by the pseudo-second order model than the pseudo-first order one. The pseudo-second order kinetic model assumes that the rate limiting step may be chemisorption involving valency forces through the sharing or exchange of electrons between the adsorbent and adsorbate as covalent forces, and ion exchange. According to the experimental results, chemisorption is the predominant process in our system. Similar results were also reported by other workers [30, 35].

Film diffusion, pore diffusion and intra-particle diffusion are the three steps of the adsorption mechanism. The slowest of the three steps controls the overall rate of the process. Generally, pore diffusion and intra-particle diffusion are often rate-limiting in a batch adsorption system. The adsorption rate parameter which controls the batch process for most of the contact time is the intra-particle diffusion.

According to the intraparticle diffusion model, a plot of q_t versus $t^{1/2}$ should be linear if intraparticle diffusion is involved in the adsorption process, and if this line passes through the origin then intraparticle diffusion is the rate controlling step. When the plot does not pass through the origin, this is indicative of some degree of boundary layer control and this further show that the intraparticle diffusion is not the only rate limiting step, but other kinetic models may also control the rate of adsorption, all of which may be operating simultaneously [36]. As can be seen from Fig. 6, a linear relationship was observed but

the trend did not pass through the origin which revealed that the intraparticle diffusion is part of the adsorption but is not the only rate-controlling step. Some other mechanisms such as ion exchange may also be controlling the rate of adsorption. Fitting of the pseudo-second order kinetic model to the adsorption data supported this assumption.

Adsorption isotherms. The adsorption isotherm indicates how the molecules subjected to adsorption distribute between the liquid phase and the solid phase when the adsorption process reaches an equilibrium state. The analysis of the isotherm data by fitting them to different isotherm models is an important step to find the suitable model that can be used for design purposes [37, 38]. Adsorption isotherm studies were carried out on three isotherm models such as Langmuir, Freundlich and Temkin.

The Langmuir treatment is based on the assumption that a maximum adsorption corresponds to a saturated monolayer of solute molecules on the adsorbent surface, that the energy of adsorption is constant, and that there is no transmigration of adsorbate in the plane of the surface [30]. The Langmuir isotherm model can be represented by the following equation [35, 39]:

$$\frac{C_e}{q_e} = \frac{1}{bQ_m} + \frac{C_e}{Q_m} \quad (5)$$

where q_e is the amount of lead(II) adsorbed on activated carbon (mg/g), C_e is the equilibrium concentration (mg/l), b is the adsorption equilibrium constant (l/mg) and Q_m is the maximum adsorption capacity. A plot of C_e/q_e versus C_e (Figure 7) gives the adsorption coefficients.

The basis of a dimensionless equilibrium parameter, R_L , also known as the separation factor, is given by [40]

$$R_L = \frac{1}{1+bC_0} \quad (6)$$

where b is the Langmuir constant and C_0 is the initial lead(II) concentration (mg/L). If the average of the R_L values for each of the different initial concentrations used is between 0 and 1, it indicates the favourable adsorption. The adsorption coefficients and the correlation coefficients are given in Table 3.

The Freundlich isotherm describes multilayer adsorption of lead(II) ions on mesoporous carbons, relating the concentration of a solute on the surface of the adsorbent to the concentration of the solute in solution, as shown in the following equation [35]:

$$\log q_e = \log k_f + \frac{1}{n} \log C_e \quad (7)$$

where q_e is the amount of lead(II) ion adsorbed (mg/g), C_e is the equilibrium concentration of lead in solution (mg/L), and the constants k_f and n are the factors affecting the adsorption capacity and intensity of adsorption, respectively. The Freundlich constants were determined from the slope and intercept of a plot of $\log q_e$ versus $\log C_e$ (Figure 8).

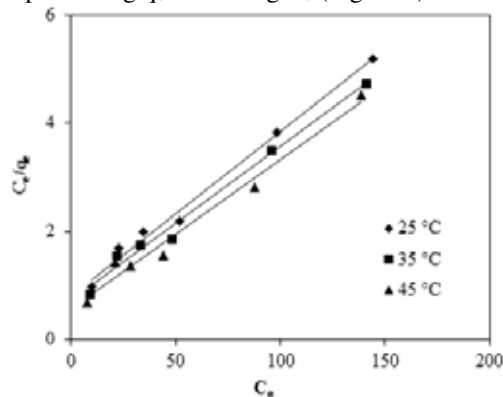


FIGURE 7

Langmuir isotherm model for lead(II) adsorption.

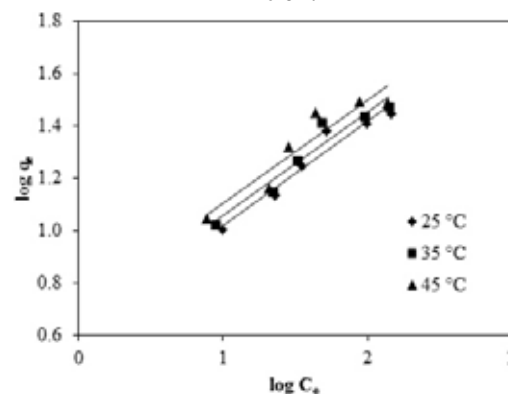


FIGURE 8

Freundlich isotherm model for lead(II) adsorption.

The Temkin isotherm can be used to study the effect of indirect adsorbent–adsorbate interactions on the adsorption, and it suggests that the heat of adsorption of all the molecules in the layer would decrease linearly with the coverage due to these interactions. This model also assumes that adsorption is characterized by a uniform distribution of binding energies upto some maximum binding energy [32, 41]. The linear form of Temkin isotherm is expressed as follows:

$$q_e = B \ln K_t + B \ln C_e \quad (8)$$

where $B = RT/b$, K_t is the equilibrium binding constant (L/mg), and B is related to the heat of adsorption. A plot of q_e versus $\ln C_e$ (Figure 9) enables the determination of the isotherm constants.

TABLE 3
Adsorption constants for the sorption of lead(II) at various temperatures

Isotherms	Temperature (K)	Constants				
		Q_m (mg/g)	b (L/mg)	R_L	R^2	ARE (%)
Langmuir	298	33.01	0.037	0.26	0.99	5.34
	308	34.96	0.039	0.25	0.99	5.04
	318	36.33	0.049	0.21	0.98	7.84
Freundlich	298		k_f (mg/g)	n (L/mg)	R^2	ARE (%)
	308		4.13	2.50	0.95	6.17
	318		4.54	2.52	0.93	6.80
Temkin	298		B (mg/g)	K_t (L/mg)	R^2	ARE (%)
	308		7.12	0.38	0.95	6.34
	318		7.46	0.42	0.93	7.85
						9.98

TABLE 4
Comparison of lead(II) adsorption results of Pumpkin seed shell based activated carbon with other adsorbents

Adsorbents	pH	Q_m (mg/g)	Fitted isotherm model	Fitted kinetic model	Reference
Areca waste	6.6	3.37	Freundlich-Langmuir	Pseudo-second order	[31]
Aspergillus versicolor	5	44.80	Redlich-Peterson	Pseudo-second order	[42]
Bentonite	5.5	142.9	Langmuir	Pseudo-second order	[6]
Pine cone activated carbon	5	27.53	Langmuir	Pseudo-second order	[40]
Cow bone activated carbon	4	47.61	Langmuir	Pseudo-second order	[43]
Papaya peel activated carbon	6	38.31	Langmuir	Pseudo-second order	[44]
Dinde stones activated carbon	6	30.37z	Langmuir, Freundlich,	Bangham model	[13]
Citrus limettioides peel carbon	6	166.6	Langmuir	Pseudo-second order	[30]
Broadleaf hardwood	5	47.66	Langmuir	Pseudo-second order	[45]
Cotton stalk activated carbon	6.5	119.95	Langmuir	-	[10]
Pumpkin seed shell activated carbon	5	36.33	Langmuir	Pseudo-second order	This study

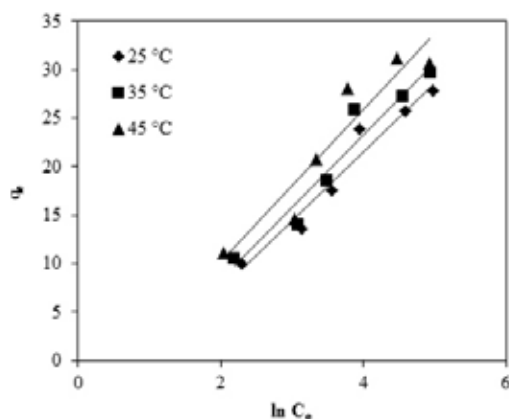


FIGURE 9

Temkin isotherm model for lead(II) adsorption.

The isotherm constants, correlation coefficients and average relative error (ARE) values are given in Table 3. Comparison of the R^2 values shows that the Langmuir isotherm fitted quite well with the experimental data with a high correlation coefficient. The Langmuir monolayer adsorption capacity (Q_m) increased from 33.01 to 36.33 mg/g as the temperature increased from 25 to 45 °C, indicating that the adsorption is an endothermic process. According to the

Langmuir isotherm, metal ions are chemically adsorbed at a fixed number of well-defined sites; each site can hold only one ion; all sites are energetically equivalent, and there is no interaction between the ions. When the initial metal concentration rises, adsorption increases while the binding sites are not saturated. A good fit of the experimental results to this equation reflects monolayer adsorption.

The k_F constant is concerned with the tendency of the adsorbent to adsorb and the n constant is concerned with the ability of the adsorbate to be adsorbed. As noticed in Table 3, the values of n were larger than 1 which means favourable adsorption of lead(II) on the activated carbon.

The Temkin isotherm constant in Table 3 shows that the heat of adsorption (B) increases with increase in temperature, indicating endothermic adsorption.

According to the ARE and R^2 values, the adsorption of lead(II) ions on the activated carbon follow Langmuir type adsorption isotherms. The Langmuir isotherm model describes quantitatively about the formation of a monolayer adsorbate on the outer surface of the adsorbent and after that no further adsorption takes place. The Langmuir model represents the equilibrium distribution of adsorbate between the

solid and liquid phases. Adsorption takes place at specific homogeneous sites on the adsorbent. Once a pollutant occupies a site, no further adsorption can take place in that site. All sites are identical and energetically equivalent. Several studies have been carried out using different types of adsorbents for lead(II) adsorption. A comparison of the adsorption results of Pumpkin seed shell based activated carbon with some other adsorbents reported in literature is given in Table 4. It can be seen from the table that the pumpkin seed shell activated carbon shows the comparable adsorption capacity with respect to other adsorbents. This indicates that it could be considered as a promising material for the removal of lead(II) ions from aqueous solutions.

Thermodynamic parameters. The changes in standard free energy (ΔG), standard enthalpy change (ΔH) and standard entropy change (ΔS) were used to speculate on the adsorption mechanism. These thermodynamic parameters are determined by using the following equations [46-47]:

$$K_c = \frac{C_A}{C_e} \quad (9)$$

$$\Delta G^\circ = -RT \ln K_c \quad (10)$$

$$\ln K_c = \frac{\Delta S^\circ}{R} - \frac{\Delta H^\circ}{RT} \quad (11)$$

where K_c is the equilibrium constant, C_A is the solid phase concentration at equilibrium (mg/L) and C_e is the equilibrium concentration in solution (mg/L). The respective ΔH° and ΔS° values were obtained from the slope and intercept of linear Van't Hoff plots of $\ln K_c$ versus $1/T$ (figure not shown). Table 5 shows the calculated values of the thermodynamic parameters for the adsorption of lead on activated carbon.

TABLE 5
Thermodynamic parameters for the adsorption of lead(II).

T (K)	ΔG	ΔH (kJ/mol)	ΔS
298	-9.76		
308	-10.09	26.26	0.052
318	-10.42		

The values of ΔG suggest the spontaneous nature of the adsorption process and give the information about the type of adsorption. The increase in ΔG with increasing temperature showed that adsorption was favourable at high temperatures. The positive value of ΔH suggests that the interaction of lead(II) ions adsorbed by activated carbon is an endothermic process, which supported by the increasing adsorption of lead(II) ions with the increase in temperature. The positive value of ΔS indicates that there is an increase in the randomness in the system solid/solution interface during the adsorption process. Similar results have been reported by other researchers working on the removal of lead ions from

aqueous solutions by activated carbon [4, 10].

The effect of adsorbent dosage. The effect of adsorbent dosage on the removal of lead(II) by the obtained activated carbon is shown in Fig. 10.

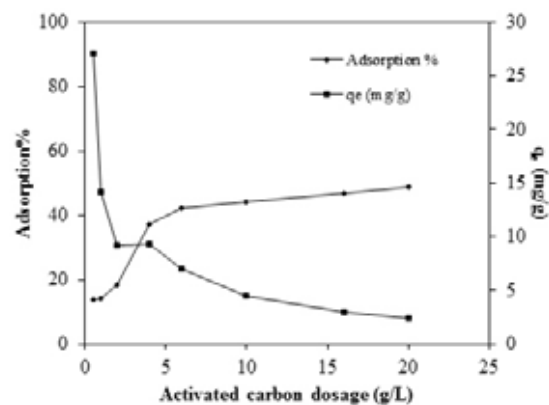


FIGURE 10
The effect of adsorbent dosage on adsorption of lead(II).

The removal efficiency of lead(II) was calculated by the difference between the initial and final lead(II) concentrations. It is clear that the lead(II) ion removal percentage increases sharply from 13.54% to 44.14% with increasing activated carbon dose from 0.5 to 6 g/L. This may be due to the greater adsorbent surface area and pore volume available at higher adsorbent dosage providing more functional groups and active adsorption sites that result in a higher lead(II) ion removal percentage [29]. The removal of lead(II) ions did not increase considerably with further increase in adsorbent dosage from 6 to 10g/L. It is due to the fact that all active sites on the adsorbent surface are entirely occupied and the increase in the adsorbent dosage do not provide a higher uptake of lead(II) ions.

CONCLUSION

In this study activated carbon was produced from pumpkin seed shells by zinc chloride activation. The specific surface area and total pore volume of the activated carbon were obtained as 1564 m²/g and 0.526 cm³/g, respectively. Batch adsorption studies for the removal of lead(II) from aqueous solutions were carried out using the produced activated carbon. It was shown that the pseudo-second order kinetic model better described the sorption data; this suggests that the rate-limiting step may be chemical sorption rather than diffusion. The adsorption isotherm studies showed that the Langmuir adsorption isotherm model adequately described the adsorption of lead(II) onto activated carbon and the maximum adsorption capacity was found to be 36.23 mg/g. The thermodynamic parameters ΔG , ΔH and ΔS showed a spontaneous and endothermic adsorption.

ACKNOWLEDGEMENT

This study was financially supported by Eskişehir Osmangazi University Scientific Research Foundation (Project No: 201315A103).

REFERENCES

- [1] İmamoğlu, M., Şahin, H., Aydın, Ş., Tosunoğlu, F., Yılmaz, H. and Yıldız, S.Z. (2016) Investigation of Pb(II) adsorption on a novel activated carbon prepared from hazelnut husk by K_2CO_3 activation. *Desalination and Water Treatment* 57, 4587-4596.
- [2] Jusoh, A., Shiung, L.S., Ali, N. and Noor, M.J.M.M. (2007) A simulation study of the removal efficiency of granular activated carbon on cadmium and lead. *Desalination* 206, 9-16.
- [3] Goel, J., Kadirvelu, K., Rajagopal, C. and Garg, V.K. (2005) Removal of lead(II) by adsorption using treated granular activated carbon: Batch and column studies. *Journal of Hazardous Materials* 25, 211-220.
- [4] Acharya, J., Sahu, J.N., Mohanty, C.R. and Meikap, B.C. (2009) Removal of lead (II) from wastewater by activated carbon developed from Tamarind wood by zinc chloride activation. *Chemical Engineering Journal* 149, 249-262.
- [5] Gerçel, Ö. and Gerçel, H.F. (2007) Adsorption of lead(II) ions from aqueous solutions by activated carbon prepared from biomass plant material of *Euphorbia rigida*. *Chemical Engineering Journal* 132, 289-297.
- [6] Özcan, A.S., Gök, Ö. and Özcan, A. (2009) Adsorption of lead(II) ions onto 8-hydroxy quinoline-immobilized bentonite. *Journal of Hazardous Materials* 161, 499-509.
- [7] Özdeş, D., Gündoğdu, A., Kemer, B., Duran, C., Senturk, H.B. and Soylak, M. (2009) Removal of Pb(II) ions from aqueous solution by a waste mud from copper mine industry: Equilibrium, kinetic and thermodynamic study. *Journal of Hazardous Materials* 166, 1480-1487.
- [8] Ozdemir, K. (2016) Experimental investigation of trihalomethanes removal in chlorinated drinking water sources with carbon nanomaterials. *Fresen. Environ. Bull.*, 25, 6202-6214.
- [9] Dai, Y., Zhang, B., Liu, T. and Tanaka, S. (2016) Development of carbon materials entrapped in konjac glucomannan gel beads for the removal of nitrobenzene. *Fresen. Environ. Bull.*, 25, 3234-3237.
- [10] Li, K., Zheng, Z. and Li, Y. (2010) Characterization and lead adsorption properties of activated carbons prepared from cotton stalk by one-step H_3PO_4 activation. *Journal of Hazardous Materials* 181, 440-447.
- [11] Largette, L., Brudey, T., Tant, T., Couespel Dumesnil, P. and Lodewyckx P. (2016) Comparison of the adsorption of lead by activated carbons from three lignocellulosic precursors. *Microporous and Mesoporous Materials* 219, 265-275.
- [12] Girgis, B.S., Attia, A.A. and Fathy, N.A. (2007) Modification in adsorption characteristics of activated carbon produced by H_3PO_4 under flowing gases. *Colloids and Surfaces A: Physicochemical and Engineering Aspects* 299, 79-87.
- [13] Rahmani, A.R., Asgari, G., Askari, F.B. and Torbaghan, A.E. (2015) Adsorption of lead metal from aqueous solutions using activated carbon derived from scrap tires. *Fresen. Environ. Bull.*, 24, 2341-2347.
- [14] Song, M., Yu, L., Wang, K. and Jin, B. (2017) The preparation and adsorption performance of sewage sludge based carbon adsorbents by one step fluidized bed pyrolysis methods. *Environmental Bulletin* 26, 1883-1890
- [15] Dai, Y., Du, C., Yu, H., Zhang, D. and Tanaka, S. (2016) Effect of contact time, solution pH, dosage of adsorbent, and regeneration on adsorption behavior of lead using nitric acid treated carbon material. *Fresen. Environ. Bull.*, 9, 3513-3517.
- [16] Depci, T., Kul, A.R. and Önal, Y. (2012) Competitive adsorption of lead and zinc from aqueous solution on activated carbon prepared from Van apple pulp: Study in single- and multi-solute systems. *Chemical Engineering Journal* 200, 224-236.
- [17] Hayashi, J., Horikawa, T., Takeda, I., Murayama, K. and Ani, F.N. (2002) Preparing activated carbon from various nutshells by chemical activation with K_2CO_3 . *Carbon* 40, 2381-2386.
- [18] Timur, S., Kantarlı, I.C., Onenc, S. and Yanik, J. (2010) Characterization and application of activated carbon produced from oak cups pulp. *Journal of Analytical and Applied Pyrolysis* 89, 129-136.
- [19] Rostamian, R., Heidarpour, M., Mousavi, S.F. and Afyuni, M. (2015) Preparation, characterization and sodium sorption capability of rice husk carbonaceous adsorbents. *Fresen. Environ. Bull.*, 24, 1649-1658.
- [20] Tseng, R.L. (2007) Physical and chemical properties and adsorption type of activated carbon prepared from plum kernels by NaOH activation. *Journal of Hazardous Materials* 147, 1020-1027.
- [21] Demiral, H., Demiral, İ., Tümsük, F. and Karabacakoglu, B. (2008) Pore structure of activated carbon prepared from hazelnut bagasse by chemical activation. *Surface and Interface Analysis* 40, 616-619.
- [22] Ahmed, M.J. and Theydan, S.K. (2012) Physical and chemical characteristics of activated carbon prepared by pyrolysis of chemically treated date Stones and its ability to absorb organics. *Powder*

- Technology 229, 237–245.
- [23] Lim, W.C., Srinivasakannan, C. and Balasubramanian N. (2010) Activation of palm shells by phosphoric acid impregnation for high yielding activated carbon. *Journal of Analytical and Applied Pyrolysis* 88, 181-186.
- [24] Demiral, İ., Aydın Şamdan, C. and Demiral, H. (2016) Production and characterization of activated carbons from pumpkin seed shell by chemical activation with ZnCl₂. *Desalination and Water Treatment* 57, 6, 2446-2454.
- [25] Aygün, A., Yeniso-y-Karakaş, S. and Duman, I. (2003) Production of granular activated carbon from fruit stones and nutshells and evaluation of their physical, chemical and adsorption properties. *Microporous and Mesoporous Materials* 66, 189-195.
- [26] Lowell, S. and Shields, J.E. (1991) *Powder Surface Area and Porosity*, Chapman and Hall, Third Edition.
- [27] Önal, Y., Akmil-Başar, C., Sarıcı-Özdemir, C. and Erdoğan, S. (2007) Textural development of sugar beet bagasse activated with ZnCl₂. *Journal of Hazardous Materials* 142, 138–143.
- [28] Özdemir, I., Şahin, M., Orhan, R. and Erdem, M. (2014) Preparation and characterization of activated carbon from grape stalk by zinc chloride activation. *Fuel Processing Technology* 125, 200–206.
- [29] Li, Y., Dua, Q., Wang, X., Zhang, P., Wang, D., Wang, Z. and Xia, Y. (2010) Removal of lead from aqueous solution by activated carbon prepared from *Enteromorpha prolifera* by zinc chloride activation. *Journal of Hazardous Materials* 183, 583-589.
- [30] Sudha, R. and Srinivasan, K. (2016) Lead(II) removal from aqueous solution using Citrus limettioides peel and its modified form: isotherms, kinetics and thermodynamic studies. *Desalination and Water Treatment* 57, 13690-13700.
- [31] Li, X., Zheng, W., Wang, D., Yang, Q., Cao, J., Yue, X., Shen, T. and Zeng, G. (2010) Removal of Pb(II) from aqueous solutions by adsorption onto modified areca waste: Kinetic and thermodynamic studies. *Desalination* 258, 148-153.
- [32] Demiral, İ. (2011) Methylene Blue adsorption from aqueous solution using activated carbon prepared from olive bagasse. *Fresen. Environ. Bull.*, 2, 127-134.
- [33] Chen, C., Zhao, P., Li, Z. and Tong, Z. (2016) Adsorption behaviour of chromium(VI) on activated carbon from eucalyptus sawdust prepared by microwave-assisted activation with ZnCl₂. *Desalination and Water Treatment* 57, 12572-12584.
- [34] Rajabi, M., Mirza, B., Mahanpoor, K., Mirjalili, M., Najafi, F., Moradi, O., Sadegh, H., Shahryari, R., Asif, M., Tyagi, I., Agarwal, S. and Gupta, V.K. (2016) Adsorption of malachite green from aqueous solution by carboxylate group functionalized multi-walled carbon nanotubes: Determination of equilibrium and kinetics parameters. *Journal of Industrial and Engineering Chemistry* 34, 130-138.
- [35] Burke, D.M., Morris, M.A. and Holmes, J.D. (2013) Chemical oxidation of mesoporous carbon foams for lead ion adsorption. *Separation and Purification Technology* 104, 150-159.
- [36] Arami, M., Limaee, N.Y. and Mahmoodi, N.M. (2008) Evaluation of the adsorption kinetics and equilibrium for the potential removal of acid dyes using a biosorbent. *Chemical Engineering Journal* 139, 2-10.
- [37] Demiral, H. and Gündüzoğlu, G. (2010) Removal of nitrate from aqueous solutions by activated carbon prepared by sugar beet bagasse. *Bioresource Technology* 101, 1675-1680.
- [38] Tan, I.A.W., Ahmad, A.L. and Hameed, B.H. (2008) Adsorption of basic dye on high surface area activated carbon prepared from coconut husk: equilibrium, kinetic and thermodynamic studies. *Journal of Hazardous Materials* 154, 337-346.
- [39] Dai, Y., Yan, H., Fu, H. and Tanaka S. (2016) Elimination of nitrobenzene by konjac glucomannan gel beads with entrapped carbon materials. *Fresen. Environ. Bull.*, 3238-3242.
- [40] Momcilovic, M., Purenovic, M., Bojic, A., Zarubica, A. and Randelovic, M. (2011) Removal of lead(II) ions from aqueous solutions by adsorption onto pine cone activated carbon. *Desalination* 276 (2011) 53-59.
- [41] Zhong, Z.Y., Yang, Q., Li, X.M., Luo, K., Liu, Y. and Zeng, G.M. (2012) Preparation of peanut hull-based activated carbon by microwave-induced phosphoric acid activation and its application in Remazol Brilliant Blue R adsorption. *Industrial Crops and Products* 37, 178-185.
- [42] Bairagi, H., Khan, M.M.R., Raya, L. and Guha, A.K. (2011) Adsorption profile of lead on *Aspergillus versicolor*: A mechanistic probing. *Journal of Hazardous Materials* 186, 756-764.
- [43] Cechinel, M.A.P., Souza, S.M.A.G.U. and Souza, A.A.U. (2014) Study of lead (II) adsorption onto activated carbon originating from cow bone. *Journal of Cleaner Production* 65, 342-349.
- [44] Abbaszadeh, S., Alwi, S.R.W., Webb, C., Ghasemi, N. and Muhamad, I.I. (2016) Treatment of lead-contaminated water using activated carbon adsorbent from locally available papaya peel biowaste. *Journal of Cleaner Production* 118, 210-222.
- [45] Shen, Z., Jin, F., Wang, F., McMillan, O. and Al-Tabbaa, A. (2015) Sorption of lead by Salisbury biochar produced from British broadleaf hardwood. *Bioresource Technology* 193, 553–556.
- [46] Ding, L., Zou, B., Gao, W., Liu, Q., Wang, Z.,

Guo, Y., Wang, X. and Liu, Y. (2014) Adsorption of Rhodamine-B from aqueous solution using treated ricehusk-based activated carbon. *Colloids and Surfaces A: Physicochemical and Engineering Aspects* 446, 1-7.

[47] Morcali, M.H., Zeytuncu, B., Baysal, A., Akman, S. and Yuce, O. (2014) Adsorption of copper and zinc from sulfate media on a commercial sorbent. *Journal of Environmental Chemical Engineering* 2, 1655-1662.

Received: 09.11.2016

Accepted: 03.05.2017

CORRESPONDING AUTHOR

Ilknur Demiral

Department of Chemical Engineering, Engineering and Architecture Faculty, Eskişehir Osmangazi University, Meşelik Campus, 26480 Eskişehir, Turkey

email: idemiral@ogu.edu.tr

OPTIMIZATION OF SLUDGE DEWATERING PERFORMANCE THROUGH RESPONSE SURFACE METHODOLOGY COMBINED WITH ULTRASONIC AND CALCIUM OXIDE

Wen-Jun Liang*, Xiu-Juan Shi, Yi-Li Li, Yan-Ling Li, Rui Shi

Key Laboratory of Beijing on Regional Air Pollution Control, Beijing University of Technology, Beijing 100124, China

ABSTRACT

The high moisture content of sludge is harmful to the environment during the process of disposal such as water pollution or the large area. Therefore, sludge pretreatment is very important before the mechanical dewatering. In this paper, sludge specific resistance (SRF) and moisture content of the cake were regarded as the evaluation parameters of sludge dewatering. Optimum range of the effect factors was obtained through single factor experiment. The effect of ultrasonic and Calcium oxide on sludge dewatering performance was investigated. Multiple quadratic regression equation models of SRF and moisture content of sludge cake were established by Box-Behnken experimental design. The optimum parameters of co-conditioning demonstrated that ultrasonic combined with Calcium oxide could significantly improve sludge dewatering performance. The optimum conditions for ultrasonic time, ultrasonic density and Calcium oxide dosage were 2.53 min, 0.33 W/mL and 0.97 g/100mL, respectively. Calibration experiment was conducted under the optimal conditions, SRF being of $(2.33 \pm 0.37) \times 10^{12}$ m/kg and moisture content of the cake being of $(65.07 \pm 0.57)\%$ could be achieved, which coincided with model predictions.

KEYWORDS:

Calcium oxide, Parameters optimization, Response surface methodology, Sludge dewatering, Ultrasonic

INTRODUCTION

Sludge is the main solid waste during the treatment of municipal sewage. It is estimated that dry sludge emissions of municipal sewage treatment plant about 30 million tons per year in China [1]. However, the sludge contains a lot of moisture and organic matter, in which the sludge particles present colloidal structure, super-hydrophilicity and easy combination with different forms of water molecules, so the sludge dewatering is very difficult. Therefore, in order to achieve the reduction and recovery of

sludge, appropriate sludge pretreatment technologies should be chosen prior to dewatering [2-4]. At the present stage, many methods of the sludge treatment have been investigated, such as ultrasonic treatment [5], Fenton treatment [6], flocculants treatment [7] and microbial flocculants [8]. But sludge dewatering performance may not perform as expected when single technology is being used. So, in order to improve sludge dewatering performance, many researchers employ the combination technology for sludge conditioning, such as a variety of conditioning agents, a variety of techniques and combination conditioning agents and other technical means. There are some combined methods, for example, ultrasonic-micro-wave [9], alkaline-thermal hydrolysis [10-11], combine Fenton process with chemical coagulation and precipitation [12].

In recent years, scholars have generated considerable research interest of ultrasonic technology due to its non-pollution, simple operation and strong ability of penetrating. As a pretreatment means for improving sludge dewatering performance, it has been applied to the sludge treatment [13]. After ultrasonic treatment, the total solid content of sludge could be increased by 16.2%, average size of sludge floc about 22.3 μm , floc size decrease rate above 60.9% and the sludge viscosity was reduced, so sludge dewatering performance improved [14]. Gonze [15] concluded that the low input power and shorter ultrasonic time could improve sludge dewatering performance. This viewpoint was confirmed by Na [16], whose research showed that with the increase of ultrasonic power and energy, the sludge floc size showed a trend of decrease after the first increase. The synergetic effects of the ultrasonic technology and Fenton reagent on sludge dewatering performance have been investigated [17]. Guo [18] used agricultural waste such as wheat straw powder and corn stalk powder to condition sludge after ultrasonic treatment. The results indicated that sludge dewatering performance could be improved. Xie [19] reported that sludge dewatering performance could be obvious improved by combining ultrasonic technology with FeCl_3 . At the same time, the combination ultrasonic and inorganic coagulant PAFs also could improve sludge dewatering performance [20].

Calcium oxide, a coagulant aid, acted as filling material during the process of sludge dewatering. It can form a porous, strong permeability and rigid lattice structure in the sludge cakes and sludge floc structure become more granulation [21]. Su [22] studied the synergetic effect of combination ultrasonic with Calcium oxide on sludge dewatering performance. The results indicated that ultrasonic coupled with Calcium oxide could obviously improve sludge dewatering performance. But the report of this aspect was less.

Response surface method (RSM) refers to an experimental design method for optimal experimental conditions by using statistical methods. RSM could reduce the effect of single factor experiment and consider interaction between different factors. So, in our experiment, RSM was used to optimize the parameters of sludge dewatering performance. In previous paper, it was highlighted the importance of the co-conditioning by ultrasonic and chemical method in the processes of sludge dewatering [22,23]. However, there were few reports about the parameters optimization of sludge co-conditioning by ultrasonic and Calcium oxide based on RSM in the process of sludge dewatering. The aim of this paper was to optimize the parameters of sludge co-conditioning by ultrasonic and Calcium oxide based on RSM and obtained the optimum parameters.

MATERIALS AND METHODS

Sludge materials and experimental equipment. The sludge samples of the experiment were collected from secondary sedimentation tank from Beijing Gaobeidian wastewater treatment plant. The sludge samples were dewatered by mechanical method and were stored at 4°C. Basic properties of sludge samples were presented as follows: moisture content being of (79.3±2)%, organic content being of (56.9±1)% and pH value being of (6.45±0.1).

The ultrasonic treatment of sludge was realized by an ultrasonic cleaner (KQ3200, Kunshan Inc., China), which could produce ultrasound with a frequency 40 kHz. The ultrasonic density could be changed by adjusting the volume of sludge.

Experimental procedures. The experiments were performed using the following procedures. (1)

Preparation of the sludge. A given amount of sludge was added into deionized water to achieve a moisture content of 97%. (2) Ultrasonic conditioning. 500 mL sludge samples were treated with ultrasonication for 1, 3, 5, 7, 9 and 11 min, respectively. The effect of the ultrasonic density (0.15, 0.30, 0.45, 0.60, 0.75, 0.90 W/mL, respectively) on sludge dewatering performance was investigated under the optimal ultrasonic time [13]. (3) Co-conditioning using ultrasonic and Calcium oxide. Firstly, the sludge was treated by the optimum condition of the ultrasonic (ultrasonic time of 3 min and ultrasonic density of 0.30 W/mL). Secondly, a given amount of sludge was mixed with Calcium oxide, which dosage was 0.30, 0.60, 0.90, 1.20, 1.50 and 1.80 g per 100 mL sludge, respectively [22]. The effects of the co-conditioning on sludge dewatering performance were discussed.

After the above treatments, all conditioned sludge samples were analyzed for SRF and moisture content of the cake. According to the results of single-factor experiment, SRF and moisture content of the cake were selected as the response variable, Y_1 , Y_2 marked as variables, respectively. Ultrasonic time (A), ultrasonic density (B) and Calcium oxide dosage (C) were chosen as three independent variables. In order to realize the response surface design, 17 experiments were designed. The range and levels of response variables and the experimental results were shown in Table 1 and Table 2. The verification test was carried out under the condition of the optimal.

Analytical methods. SRF and moisture content of the cake were selected as the evaluation parameters of sludge dewatering performance in this paper. SRF was calculated according to the following equation:

$$SRF = \frac{2PA^2b}{\omega\mu} \quad (1)$$

where SRF is the sludge specific resistance of sludge, m/kg; P is the filtration pressure, N/m²; A is filtration area, m²; b is the slope of t/V versus V under the condition of constant pressure, m/s⁶; μ is the viscosity of the filtrate, Pa·s and ω is the weight of dry solids per unit volume of filtrate in the process of filtering, kg/m³. Moisture content of the cake is measured in accordance with the standard methods. Changes of sludge surface morphologies of different samples are confirmed by scanning electron microscope (SEM).

TABLE 1
Response variables and coding standards

Variables	Code	Level of the code		
		-1	0	1
A: Ultrasonic time (min)	X_1	1	3	5
B: Ultrasonic density (W/mL)	X_2	0.15	0.30	0.45
C: Calciumoxide dosage (g/100mL)	X_3	0.60	0.90	1.20

TABLE 2
Response surface design and experimental results

Number	Ultrasonic time (min)	Ultrasonic density (W/mL)	Calciumoxide dosage (g/100mL)	SRF (10^{12} m/kg)		Moisture content of the cake (%)	
				Experimental value	Predicted value	Experimental value	Predicted value
1	1	0.15	0.9	6.79	6.97	75.07	74.10
2	5	0.15	0.9	10.63	10.19	72.77	71.70
3	1	0.45	0.9	6.15	6.59	66.37	67.44
4	5	0.45	0.9	10.05	9.87	73.24	74.21
5	1	0.3	0.6	6.35	6.58	72.82	73.03
6	5	0.3	0.6	9.73	10.58	70.29	70.60
7	1	0.3	1.2	6.97	6.12	67.03	66.73
8	5	0.3	1.2	8.85	8.62	73.74	73.53
9	3	0.15	0.6	4.16	3.75	77.67	78.44
10	3	0.45	0.6	4.23	3.56	73.49	72.21
11	3	0.15	1.2	2.04	2.71	71.32	72.60
12	3	0.45	1.2	1.79	2.20	75.45	74.68
13	3	0.3	0.9	6.70	7.88	77.85	75.26
14	3	0.3	0.9	9.55	7.88	75.06	75.26
15	3	0.3	0.9	7.32	7.88	75.07	75.26
16	3	0.3	0.9	9.69	7.88	74.49	75.26
17	3	0.3	0.9	6.14	7.88	73.85	75.26

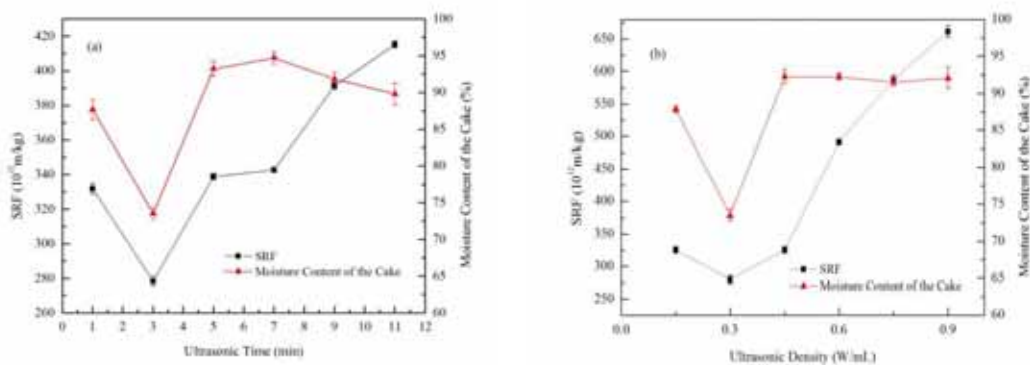


FIGURE 1
Effect of ultrasonic treatment on sludge dewatering performance
(a) ultrasonic time; (b) ultrasonic density

RESULTS AND DISCUSSION

Effect of ultrasonic treatment on sludge dewatering performance. Fig.1 illustrated the effects of ultrasonic treatment on sludge dewatering performance. With the increasing of ultrasonic intensity, SRF decreased firstly and then increased. Moisture content of the cake decreased firstly, then increased gradually and achieved a smooth in the end. A possible explanation for this result is that the surface of sludge can generate many channels on account of the sponge effect by the ultrasonic treatment, which can prompt the internal moisture of sludge transfer to the floc particles outside. On the other hand, extracellular polymers (EPS) and the network structure of the sludge flocs can be easily destroyed and result in the decrease of resistance between particles. However, the ultrasonic energy input is too large to lead to the breakage of sludge floc. Furthermore, the water molecules tightly adsorbed on the surface of particles

and the dehydration performance reduced [24].

Fig.1(a) showed when the ultrasonic time was increased to 3 min, SRF gradually reduced from 331.86×10^{12} m/kg to 278.41×10^{12} m/kg, moisture content of the cake decreased from 87.68 % to 73.53 %. Fig.1(b) illustrated when the ultrasonic density was 0.30 W/mL, SRF and moisture content of the cake could get the minimum values. These results showed that ultrasonic treatment could improve sludge dewatering performance effectively.

Effect of Calcium oxide dosage on sludge dewatering performance. Fig.2 showed the effect of Calcium oxide dosage (from 0.30 to 1.80 g/100 mL) on sludge dewatering performance. With the increasing of Calcium oxide dosage, SRF decreased firstly and then increased. Moisture content of the cake decreased firstly, then increased gradually and achieved a smooth in the end. And there was a minimum at 0.90 g/100 mL sludge. When the Calcium oxide dosage increased to 0.90 g/100 mL, SRF and

moisture content of the cake decreased to 4.42×10^{12} m/kg, 68.75%, respectively. This result attributed to the presence of the ultrasonic and Calcium oxide. Firstly, ultrasonic treatment can adjust the sludge structure and improve sludge dewatering performance at a certain extent. Secondly, Calcium oxide, a coagulant aid in the process of sludge dewatering, acts as filling material to improve the sludge structure. It can form a porous, strongly permeability and rigid lattice structure in the sludge cakes and sludge floc structure become more granulation [21], which improve sludge dewatering performance. At the same time, combination Calcium ionic with organic

matter of sludge can improve particle density [22], and result in SRF decrease with increasing Calcium oxide dosage. However, when the Calcium oxide dosage was higher than 0.90 g/100 mL, the sludge dewatering performance was decreased.

Microscopic structure of sludge. The morphological changes of the raw sludge could be seen in Fig.3 (a). From Fig.3 (a), the pore size distribution on the sludge surface was not obvious and floc particles were aggregated together. Fig.3 (b) illustrated the findings of the morphological changes of the sludge after the ultrasonic treatment. The SEM

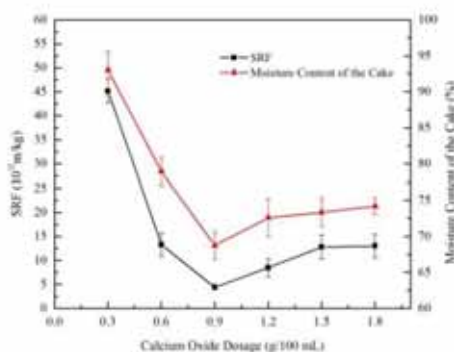


FIGURE 2
Effect of Calcium oxide dosage on sludge dewatering performance

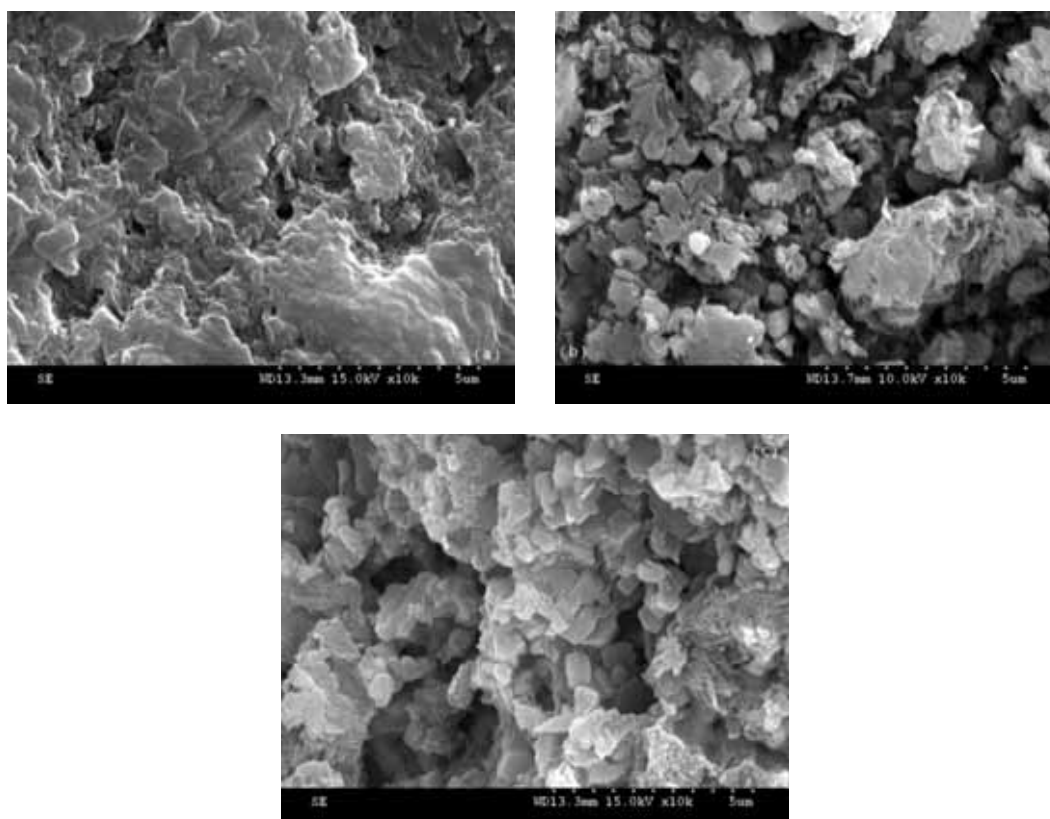


FIGURE 3
SEM images of sludge
(a) raw sludge; (b) ultrasonic treatment; (c) combine ultrasonic with Calcium oxide treatment

TABLE 3
Variance analysis for regression equation of SRF

Source	Sum of squares	df	Mean square	F	P (Prob>F)	
Model	102.48	9	11.39	5.69	0.0160	Significant
A	21.13	1	21.13	10.55	0.0141	
B	0.24	1	0.24	0.12	0.7368	
C	2.90	1	2.90	1.45	0.2676	
AB	9.000E-004	1	9.000E-004	4.496E-004	0.9837	
AC	0.56	1	0.56	0.28	0.6125	
BC	0.026	1	0.026	0.013	0.9131	
A ²	31.21	1	31.21	15.59	0.0055	
B ²	20.33	1	20.33	10.16	0.0153	
C ²	29.07	1	29.07	14.52	0.0066	
Residual	14.01	7	2.00			
Lack of Fit	3.22	3	1.07	0.40	0.7631	Not significant
Pure Error	10.80	4	2.70			
Cor Total	116.50	16				

A, Ultrasonic time; B, Ultrasonic density; C, Calcium oxide dosage; $R^2=0.8797$; $R^2_{adj}=0.7250$

photos showed that sludge flocs were broken, which led to the roughness on the sludge surface and abundant irregular porous structure. Therefore, sludge dewatering performance could be improved by ultrasonic treatment. Fig.3 (c) showed that the effect was obvious for the sludge samples by co-conditioning ultrasonic and Calcium oxide. Compared to the sludge treated by ultrasonic, the morphological changes of the sludge after co-conditioning ultrasonic and Calcium oxide was remarkable, which could present a lot of bumps and different apertures on the surface of the sludge.

Analysis of variance of SRF and moisture content of the cake model. The experimental results were analyzed with statistical analysis method, fitting with a quadratic response surface equation, which could describe the relationship between response variable and values. The quadratic response surface equation of SRF and moisture content of the cake (MCC) could be seen in Equation 2 and 3, where A, B and C represented ultrasonic time, ultrasonic density and Calcium oxide dosage, respectively. Variance analysis for regression equation of SRF was shown in Table 3.

$$\text{SRF}(Y_1) = 7.88 + 1.63A - 0.17B - 0.60C + 0.015AB - 0.38AC - 0.080BC + 2.72A^2 - 2.20B^2 - 2.63C^2 \quad (2)$$

$$\text{MCC} = 65.26 + 1.09A - 1.03B - 0.84C + 2.29AB + 2.31AC + 2.08BC + 1.54A^2 + 5.06B^2 + 4.16C^2 \quad (3)$$

In the process of variance analysis, F and p values were chosen to represent the significant degree of correlation coefficient. If $F > F_{0.01}$ or $p < 0.01$, which it indicated the impact of factors was very obvious on the characterization of indices. When $F_{0.05} < F < F_{0.01}$ or $0.01 < P < 0.1$, it showed significant effect on the characterization of indices, otherwise the impact of factors on the experiment index was not significant. The F and p values of the model were 5.69, 0.0160, respectively, which indicated that response surface equation was significant and the value of the Lack of Fit was 0.3980, which indicated that reliability of the response surface equation was significant. A and A², B², C² were above 95% confidence level, which proved that they were more outstanding.

Otherwise, the interaction of AB, BC and AC were not obvious. The regression equation was expressed by the coefficient of determination (R^2). This parameter indicated 88% of the response variability for SRF could be explained with the model. The coefficient (R^2_{adj}) being of 0.7250 and $R^2 - R^2_{adj}$ being of $0.1547 < 0.2$, which indicated that the credibility and precision of model was higher and the correlation of predicted values and measured values were better [23]. The variance analysis results for quadratic response surface of SRF showed that the regression model had been reached significance level within the scope of the research. Therefore, sludge dewatering performance parameters could be predicted with the model analysis of ultrasonic coupled with Calcium oxide.

Table 4 showed that the variance analysis results for moisture content of the cake. The variance analysis results for quadratic response surface of moisture of the cake showed that the regression model had been reached significant level within the scope of the research. Therefore, sludge dewatering performance parameters could be predicted with the model analysis of ultrasonic and Calcium oxide.

Analysis of the response surface for the SRF.

When the SRF was chosen to the response, the response surfaces of polynomial regression model with one variable at the optimal level and the other two changing within the experimental ranges were reported in Fig.4. The minimum value of the response surfaces indicated that the interactive effects on SRF between ultrasonic time and ultrasonic density, ultrasonic time and Calcium oxide dosage were significant, as shown in Fig.4 (a) and 4(b), respectively. When the optimal ultrasonic density was 0.30W/mL, the ultrasonic time was 1-5 min, and the Calcium oxide dosage were within the range of 0.60-1.20g/100 mL, the SRF was lower, just shown in Fig.4(b). In conclusion, the appropriate ultrasonic density during the ultrasonic sludge treatment pro-

cess was in a range of 0.10-4.00 W/mL. The low ultrasonic density and short ultrasonic time could enhance the sludge dewatering performance [15]. Likewise, under the condition of the optimal Calcium oxide dosage, the ultrasonic time was within the range of 1-5 min and ultrasonic density was 0.15-0.45

W/mL (Fig.4a). At the optimal ultrasonic time, the peak value of the response surfaces was reported in Fig.4c. Therefore, the optimize for ultrasonic time, ultrasonic density and Calcium oxide dosage are necessary in order to obtain a minimum of SRF and achieve the best dewatering performance.

TABLE 4
Variance analysis for regression equation of moisture content of the cake

Source	Sum of squares	df	Mean square	F	P (Prob>F)	
Model	291.76	9	32.42	12.42	0.0016	Significant
A	9.57	1	9.57	3.67	0.0971	
B	8.57	1	8.57	3.28	0.1129	
C	5.66	1	5.66	2.17	0.1843	
AB	21.02	1	21.02	8.05	0.0251	
AC	21.34	1	21.34	8.18	0.0244	
BC	17.26	1	17.26	6.61	0.0369	
A ²	10.02	1	10.02	3.84	0.0909	
B ²	107.61	1	107.61	41.22	0.0004	
C ²	72.97	1	72.97	27.95	0.0011	
Residual	18.27	7	2.61			
Lack of Fit	8.91	3	2.97	1.27	0.3980	Not significant
Pure Error	9.37	4	2.34			
Cor Total	310.03	16				

A, Ultrasonic time; B, Ultrasonic density; C, Calcium oxide dosage; $R^2=0.9411$; $R^2_{adj}=0.8653$

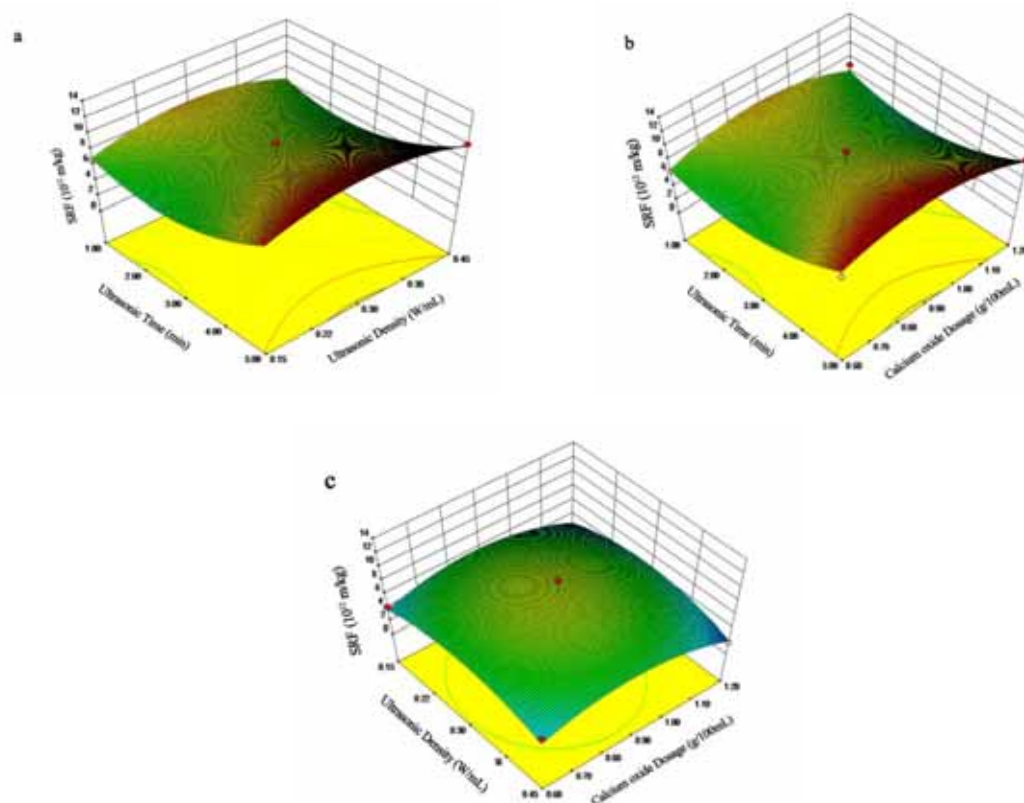


FIGURE 4
Response surface graphs and contour plot of SRF
(a) X₁-X₂; (b) X₁-X₃; (c) X₂-X₃

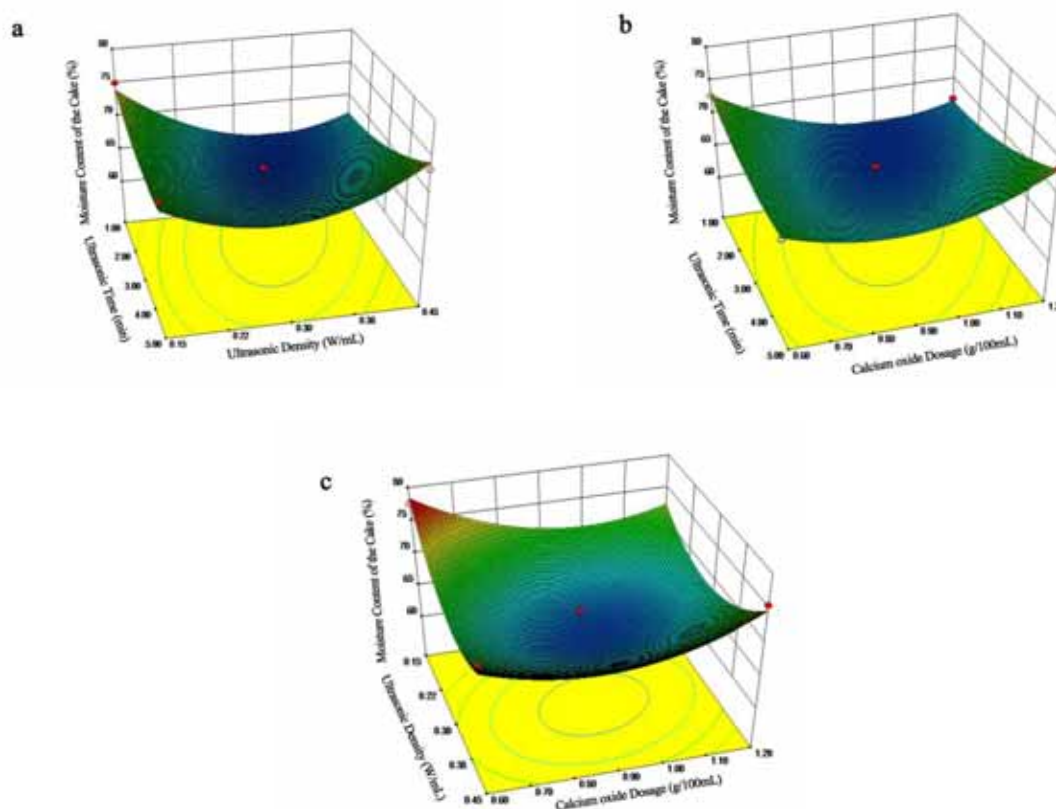


FIGURE 5
Response surface graphs and contour plot of moisture content of the cake
 (a) X₁-X₂; (b) X₁-X₃; (c) X₂-X₃

Analysis of the response surface for moisture content of the cake. With the moisture content of the cake being the response, the response surfaces of the quadratic regression model with one variable at the optimal level and the other two changing within the experimental ranges could be seen in Fig.5. The elliptical contour plots in Fig.5(a), 5(b) and 5(c) indicated that there were obvious interactive effects between ultrasonic time and Calcium oxide dosage, ultrasonic density and Calcium oxide dosage, ultrasonic time and ultrasonic density. From Fig.5, we could see that the moisture content of the cake reduced at the center of the three regions. It was proved by the significant minimum in the response surfaces, in which the optimal conditions were exactly located inside the design boundary.

In the sludge treatment process by ultrasonic and Calcium oxide, ultrasonic played a role of adjusting the structure of the sludge and Calcium oxide acted as coagulant, which was used to build a skeleton structure and improve the effect of coagulation. The coagulant in our experiment was Calcium oxide in order to prompt sludge granulation, reduce sludge viscosity and make free water pass through easily [22]. A given amount of sludge treated by ultrasonic was mixed with Calcium oxide, which increased the chances of the coagulant approaching to the different

forms of water in the sludge. Therefore, the sludge treated by ultrasonic and Calcium oxide could contribute to the formation of aperture on the surface of sludge flocs, which led to the water separation from the sludge. Therefore, smaller SRF and moisture content of the cake could be obtained.

Determination of the optimal conditions and model validation. According to the results of the response surface analysis and the optimization of the experiment conditions, there was a best response quantity under the optimum conditions. Through the researches of the optimization of SRF, the SRF could be 2.05×10^{12} m/kg under the condition of ultrasonic time being 2.53min, ultrasonic density being 0.30W/mL, and Calcium oxide dosage being 1.20g/100mL. The moisture content of the cake could be 64.68% under the condition of ultrasonic time being 1.62 min, ultrasonic density being 0.33 W/mL, and Calcium oxide dosage being 0.97 g/100mL. The best conditions of sludge dewatering performance were as follows: ultrasonic time, ultrasonic density and Calcium oxide dosage were 2.53 min, 0.33 W/mL and 0.97 g/100mL, respectively. In order to verify the accuracy and practicability for the optimal conditions of the polynomial regression equation model, several experiments were carried

out with SRF being $(2.33 \pm 0.37) \times 10^{12}$ m/kg and moisture content of the cake being $(65.07 \pm 0.57)\%$. That was consistent with the results obtained by model prediction. Therefore, the operating conditions could be optimized and the optimal process parameters could be obtained using response surface method.

CONCLUSIONS

(1) The sludge dewatering performance could be obvious improved by ultrasonic / Calcium oxide and the optimum conditions of the ultrasonic time, ultrasonic density and Calcium oxide dosage were 3 min, 0.30 W/mL and 0.90 g/100mL, respectively.

(2) The response surface method was used to analyze and optimize joint working parameters. The results showed that regression equation model could be reached at the significant level. The optimum conditions of the ultrasonic time, ultrasonic density and Calcium oxide dosage were 2.53 min, 0.33 W/mL and 0.97 g/100mL, respectively.

(3) SRF and moisture content of the cake were $(2.33 \pm 0.37) \times 10^{12}$ m/kg, $(65.07 \pm 0.57)\%$ under the optimum conditions. That was consistent with the results obtained by model prediction.

ACKNOWLEDGEMENTS

This work was financially supported by the Fundamental Research Funds for the Beijing University of Technology (X4005013201501).

REFERENCES

- [1] Mu, J. (2014) Analyses of the present state and development of the sludge industry in our country. <http://news.bjx.com.cn/html/20140626/521940.shtml>.
- [2] Xie, H.H., Ma, H.L., Chi, Y. and Ma, Z.Y. (2012) The measurement of sludge bound water and moisture distribution characteristics. *Journal of Zhejiang University (Engineering Science)*, 46, 503-508.
- [3] Malgorzata, F. and Lidia, B. (2014) Sorption of heavy metal ions from aqueous solution by glauconite. *Fresen. Environ. Bull.* 23, 825-839.
- [4] Joanna, F., Maja, R. and Zbigniew, M. (2015) Copper removal from contaminated groundwater using natural and engineered limestone sand in permeable reactive barriers. *Fresen. Environ. Bull.* 24, 228-234.
- [5] Xu, H.C., He, P.J., Yu, G.H. and Shao L.M. (2011) Effect of ultrasonic pretreatment on anaerobic digestion and its sludge dewater ability. *J. Environ. Sci.* 23, 1472-1478.
- [6] Mo, R.S., Huang, S.S., Dai, W.C., Liang, J. L. and Sun, S.Y. (2015) A rapid Fenton treatment technique for sewage sludge dewatering. *Chem. Eng. J.* 269, 391-398.
- [7] Wang, J.P., Yuan, S.J., Wang, Y. and Yu, H.Q. (2013) Synthesis, characterization and application of a novel starch based flocculent with high flocculation and dewatering properties. *Water Res.* 47, 2643-2648.
- [8] Ye, H.L., Ye, J.S., Zheng, Z.J., Yin, H. Peng, H. and Zhang, N. (2009) Study on sludge dewatering using microbial feculent. *Environ. Chem.* 28, 414-417.
- [9] Anteneh, M.Y., Chong, S.H., Sen, T.K., Ang, H.M. and Ahmet, K. (2011) Effect of ultrasonic, microwave and combined microwave-ultrasonic pretreatment of municipal sludge on anaerobic digester performance. *Water Air. Soil. Poll.* 224, 2-9.
- [10] Zhang, S.T., Guo, H.G., Du, L.Z., Liang, J.F., Lu, X.B., Li, N. and Zhang, K.Q. (2015) Influence of NaOH and thermal pretreatment on dewatered activated sludge solubilisation and subsequent anaerobic digestion: Focused on high-solid state. *Bioresour. Technol.* 185, 171-177.
- [11] Fatma, B. and Sener, A. (2010) The effect of salinity on growth and nutrient composition in broad bean (*Vicia faba* L.) seedlings. *Fresen. Environ. Bull.* 19, 2910-2019.
- [12] Apostolos, G.V., Haralampos, N.L., Panagiotis, K.K., Elli Maria, P.B. and Sofia, T.M. (2004) Olive mill wastewater detoxification by applying ph related fenton oxidation process. *Fresen. Environ. Bull.* 13, 501-504.
- [13] Liu, J., Liu, Y.D., Zhao, J.H., Wang, M.M. and Wang, X. (2011) Study on factors of sludge reduction in continuous flow system by ultrasonic waves. *China water wastewater.* 27, 58-60.
- [14] Hernando, M.R., Elorza, G.M., Labanda, J. and Llorens, J. (2013) Dewater ability of sewage sludge by ultrasonic, thermal and chemical treatments. *Chem. Eng. J.* 230, 102-110.
- [15] Gonze, E., Pillot, S., Valette, E., Gothier, Y. and Bernis, A. (2003) Ultrasonic treatment of an aerobic activated sludge in a batch reactor. *Chem. Eng. Process: Process Intensification*, 42, 965-975.
- [16] Na, S., Kim, Y.U. and Khim, J. (2007) Physicochemical properties of digested sewage sludge with ultrasonic treatment. *Ultrason. Sonochem.* 14, 281-285.
- [17] Jiang, J.G., Gong, C.X., Tian, S.C., Yang, S.H. and Zhang, Y.J. (2014) Impact of ultrasonic treatment on dewater ability of sludge during Fenton oxidation. *Environ. Monit. Assess.* 186, 8081-8088.
- [18] Guo, S.D., Qu, F.S., Ding, A., He, J.G., Yu, H.R. and Bai, L.M. (2015) Effects of agricultural waste-based conditioner on ultrasonic-aided activated sludge dewatering. *RSC Adv.* 5, 43065-43073.



- [19] Xie, J.L., Li, C.F., Liu, L., Peng, Z. and Wang, F.H. (2014) Effect of ultrasonic combined with Ferric Chloride on different sludge dewatering process. *Bulleting of sci. technol.* 30, 203-207.
- [20] Li, D.L., Zhang, Z. X., Shen, J. J., Ma, J. F. and Feng, S. (2011) Effect of ultrasonic and inorganic coagulants on sludge dewatering process. *Environ. Sci. Technol.* 34, 20-22.
- [21] Yu, Z.R., Yu, Y.C., Gao, T. Y. and Zhou, Z.Y. (1989) The application and mechanism of lime in sludge conditioning. *China Water and Wastewater*, 5, 7-11.
- [22] Su, J.W., Zhang, H., Wang, C.D., Wang, J.C., Xu, S.Y. and Shi, Y.H. (2014) Individual or combined effect of ultrasonic and Calcium oxide on performance of sludge dewatering. *Water Purification technol.* 33, 48-51,57.
- [23] Li, L., Zhang, Z., Zhang, S. and Pan, S.X. (2010) Study on technological parameters of the treatment of landfill leachate by MAP method using response surface methodology. *Chin. J. Chem. Eng.* 4, 1289-1295.
- [24] Qi, J., Chen, L. and Chen, D.H. (2005) The

study on the intensifying of sludge dewater ability in ultrasonic processing. *Proceedings of the 2nd national environmental chemistry academic report*, Shanghai, 721-722.

Received: 16.11.2016

Accepted: 03.05.2017

CORRESPONDING AUTHOR

Wen-Jun Liang

Key Laboratory of Beijing on Regional Air Pollution Control

Beijing University of Technology

Beijing 100124 – CHINA

E-mail: liangwenj@bjut.edu.cn

GUIDELINES FOR EIA OF A FISHING PORT IN A SEMI-ENCLOSED WATER BODY

Mohammed Rasheed^{1,2,*}, Saima Mian³, Mohamad Almasri³, David Aubrey³

¹Department of Chemistry, The University of Jordan, Amman, Jordan

²Mote Marine Laboratory - Mote Aquaculture Research Park, 12300 Fruitville Road, Sarasota, FL 34240, USA

³Woods Hole Group, 81 Technology Park Drive, East Falmouth, MA 02536, USA

ABSTRACT

The development or expansion of marine fishing ports is considered as a significant urban stress on the surrounding environment. Construction activities usually include dredging, filling, soil excavation or replacement; whereas the operations phase involves anchoring, shading, as well as extensive human activity in a small scale area. These activities may impact the marine environment through physical and chemical disturbances including an increase in the rate of sedimentation, discharge of chemicals, nutrient enrichment, increased wastewater, oil spills, increase in organic matter and heavy metals loads as well as solid waste generation, etc. This paper provides guidelines for conducting an EIA of a fishing port in a semi-enclosed water body, such as the Arabian Gulf or the Red Sea. The purpose of the guidelines is to outline issues that may be relevant to the design and construction of the port and to identify important factors for consideration in an EIA study. Elements to be studied in depth include impacts on water quality, sediment and habitat loss. The paper also provides suggested mitigation measures for minimizing potential impacts along with key aspects to be considered in the development of an adequate Environmental Management and Monitoring Plan.

KEYWORDS:

EIA, Fishing Port, Marine Water.

INTRODUCTION

Ports are the gateway for industry, services and support the security and safety needs of humans in any countries. Although ports generally contribute significantly in economic growth of any country, port activities may however, have adverse activities on air water and sediment of the ecosystem being in contact with the ports [e.g. 1, 2], particularly those often located in sensitive environmental areas.

The development or expansion of marine fishing ports is considered as a significant urban stress on the surrounding environment [e.g. 3]. Construc-

tion phase activities usually include dredging, filling, soil excavation or replacement; whereas the operations phase involves anchoring, shading, as well as extensive human activity in a small scale area. These activities may impact the marine environment through physical and chemical disturbances including an increase in the rate of sedimentation, discharge of chemicals, nutrient enrichment, increased wastewater, oil spills, increase in organic matter and heavy metals loads as well as solid waste generation, etc. Any country undertaking a fishing port development project should ensure that the project is compatible with national economic, social and environmental development goals, and an Environmental Impact Assessment (EIA) should be conducted in the early stages of the project.

This paper focuses on EIA guidelines for fishing port projects in the Kingdom of Saudi Arabia (KSA) which is bordered by both the Arabian Gulf and the Red Sea. The Presidency of Meteorology and Environment (PME) is responsible for environmental protection and management activities in KSA. Regulatory requirements for an EIA are addressed in the General Environmental Regulations and Rules for Implementation (15 October 2001). Additional EIA requirements apply to the industrial cities of Jubail and Yanbu which are listed in the Royal Commission Environmental Regulations [4]. As environmental regulation in Middle East, especially KSA, is still evolving, often guidelines are needed to assist environmental practitioners in addressing specialized topics. For example, the Saudi Geological Survey has issued EIA guidelines for mining activities in KSA. Similarly, Saudi Aramco has its own requirements, in addition to the national regulations, for projects in the oil and gas industry. The authors of this paper have previously provided EIA guidelines for hatcheries in semi-enclosed water bodies such as the Arabian Gulf and Red Sea [5]. Such guidelines are needed to assist EIA practitioners in KSA and other countries bordering the two water bodies in identifying and evaluating potential impacts associated with new development projects. The purpose of this paper is to outline issues that may be relevant to the design and construction of a port development and to identify important factors for consideration in an EIA study.

MATERIALS AND METHODS

The EIA would need to follow requirements set forth in the applicable national regulatory framework. Steps recommended in the overall study are as follows:

Document review Data collection. An extensive literature review should be conducted to compile information on the legislative requirements and environmental conditions at the project site. In addition, a typical description of the project activities, within the project area relevant to the environmental assessment, should be compiled with the help of the Project Proponent and Conceptual Design Team.

Site specific field investigations are recommended to augment and validate any available baseline data at the proposed marine site including physiochemical and biological properties [5]. Field investigations may also include a terrestrial survey of the area where construction of support facilities will take place.

Analysis of alternatives. An analysis of alternatives is an essential component of a comprehensive EIA project. Alternatives considered can include: no project/action, site location, different design elements, etc. Elements to be considered in site location include elevation, existing land use, potentially impacted habitats and existing infrastructure.

Impact assessment. The environmental information collected in the previous phases should be used to assess the potential impacts of the project activities. Various predictive techniques can be used to determine the nature and extent of the impacts identified. The significance of each impact needs to be determined and rated taking into account the nature of the impact and the existing environmental conditions.

Legislative requirements need to be consulted to ensure that evaluated parameters comply with regulations.

Development of environmental management and monitoring plan. Project specific environmental management plans should be developed to reduce and mitigate all significant adverse environmental impacts to acceptable levels. The management plan will typically cover construction and operational phases of the project and include necessary pollution control and treatment systems identified based on a review of potentially feasible alternatives. A monitoring program can help ensure proper implementation of the environmental management plan.

Documentation. At the end of the assessment, a report should be prepared based on regulatory requirements. This report will include the findings of the assessment, project impacts, and mitigation

measures to be implemented during the execution of project activities.

RESULTS AND DISCUSSION

Potential Impact Evaluation. This section identifies the potential environmental impacts associated with typical fishing port development in a semi-enclosed water body.

(1) Construction Phase. (a) Water and Sediment. Construction activities for the expansion of the ports, including possible landfilling, may lead to a temporary deterioration in seawater quality, which can directly or indirectly impact marine flora and fauna in the area. Factors that may affect water quality include discharge of heavy metals, organic and inorganic matter, inorganic nutrients, solid waste, and accidental spillage of oil, chemicals etc. Each factor is discussed below in detail.

Heavy metals and organic matter may be released into the seawater and seabed during construction activities near the coast. The sources of these compounds are mainly construction materials and filling activities at the bottom of the sea. Bottom sediments are known to contain much higher concentrations of heavy metals, organic matter, oil residue and some other toxic materials compared to the water body such as those of Red Sea and Arabian Gulf [e.g. 6, 7]. Contamination by heavy metals affects seawater quality significantly as once released into the environment, they do not readily convert into harmless components and often tend to accumulate in the tissues of living organisms [8, 9]. Heavy metals in general, and lead, chromium, arsenic, zinc, cadmium, copper and mercury in particular can cause significant damage to the environment and human health as a result of their mobility and solubility [10, 11].

Filling activities and construction materials may also release organic matter into the sea. Bacterial breakdown of these organic materials may deplete dissolved oxygen from water leading to adverse impacts on marine life. In oxygen depleted environments, non-aerobic process start taking place for the breakdown of organic matter that in turn results in the production of toxic compounds such as methane, hydrogen sulfide and ammonia [12,13].

Some inorganic nutrients, such as silicates, may also be discharged into the water through construction activities. This would impact the nutrient cycle and nutrient enhancement (eutrophication) may simulate growth of certain harmful algae e.g. dinoflagellates, which can be toxic to marine organisms and humans [14, 15].

Accidental spillage of oil and oil compounds may be another cause of adverse impacts on water quality. Although oil is not soluble in water, photo-

chemical oxidation is capable of transforming a variety of oil components into oxygenated derivatives that are fairly water soluble and show significant toxicity to algae, bacteria, marine invertebrates and fish [16]. The effects of oil pollution are exacerbated by the use of dispersants and wave action, which cause the oil to enter the water column rather than floating on the surface [17]. Oil spills can harm marine ecosystems and poison marine animals that ingest or inhale its many toxins [18]. Spillage of other chemicals and hazardous materials during construction can cause toxicity to flora and fauna in the impacted area leading to community shifts in the ecosystem.

Landfilling may cut across the existing sedimentation patterns and disturb the existing current regime. In addition, filling activities may cause an increase in suspended solids and floating particles. This may lead to the formation of sediment plumes that in turn increase water turbidity. In addition, dust arising from construction works will end up in the sea, thereby increasing the turbidity of seawater as well as increasing the rate of sedimentation, which may impact the sea habitat including corals directly or indirectly (Table 1). The effect of sedimentation rate and suspended particles will not be localized; it may affect other water bodies located at a distance due to movement of suspended particles by water currents.

(b) Marine Habitat. Excavation, transportation and disposal of soft-bottom material may lead to numerous impacts on the marine environment [20]. Filling activities may impact the seagrass patches, if present, directly and displace benthic habitat in the areas where it takes place [21]. This can affect the general benthic community structure of the seagrass beds such as an initial reduction in the abundance, species biodiversity, nursery grounds and larval settlement of different marine organism including polychaetes, mollusks, shrimps, sea cucumbers, sea urchins and even some species of fish. In addition, filling can cause temporal damage to sandy bottoms in the area, which can ultimately lead to the partial destruction of fauna and flora in the affected area. An

indirect impact of filling is a possible rise in suspended solids and floating particles in water, which can lead to an increase in turbidity and prevent sunlight from reaching underwater plant life and thus affecting the growth and productivity of seagrasses and other flora [22].

Accidental spillage of oil during construction works may lead to oil and petroleum compound deposits on the seagrass patches. This factor combined with an increase in sediments released in to the water can affect the proper growth of the seagrass and the associated benthic organisms such as polychaetes, mollusks and other sea bottom dwelling organisms. In addition, the risk of toxicity to these organisms from direct oil spillage is also possible [23].

Other potential impacts include the discharge of heavy metals and toxic pollutants from construction activities leading to inhibition of photosynthesis and subsequent adverse impacts on the overall food web. Marine flora may also suffer from the shadow effect of the sediment plumes, and fauna species in the near zone may disappear due to filling activity or will be buried due to high sedimentation.

(c) Terrestrial Habitats. Terrestrial habitats may be disturbed due to land based construction including direct disturbance or nuisance from increased noise levels associated with various equipment and machinery.

(d) Solid Waste. An increase in solid waste generated by human activities and construction debris such as plastics, metal, wood, rubber, and glass will occur. These substances may have adverse impacts on the fauna and flora. The solid wastes are usually non-degradable and cause physical damage [24].

(e) Sewage. Sewage from temporary sanitary facilities for workers, if allowed to drain directly into the sea, may impact the water quality and cause eutrophication.

TABLE 1
Sedimentation rate and the degree of impact [19]

1-10 (mg cm ⁻² d ⁻¹)	10-50 (mg cm ⁻² d ⁻¹)	> 50 (mg cm ⁻² d ⁻¹)
<i>Slight to moderate</i>	<i>Moderate to severe</i>	<i>Severe to catastrophic</i>
Decreased abundance	Greatly decrease abundance	Severely decreased abundance
Altered growth forms	Greatly decrease growth rate	Severe deterioration of communities
Decreased growth rates	Reduce growth rate	Most species excluded
Possible reduction in number of species	Predominance of altered growth forms	Most colonies die
Possible reduction in recruitment	Reduce recruitment	Recruitment severely reduced
	Decrease number of species	Regeneration slowed or stopped
	Possible invasions of opportunistic species	Invasions of opportunistic species

(f) Ambient Air Quality. Sources of air emission during the construction phase include engine driven construction machinery and vehicular emissions, barges offshore, etc. Dust generation from construction activities such as site preparation, movement of heavy equipment and earthwork machines is also expected. These factors may lead to a temporary and insignificant deterioration in the local ambient air quality.

(g) Noise and Vibration. The noise and vibration during excavation and filling will affect marine life, and many organisms including fish may get disoriented in a noisy environment and move away from their preferred habitat to an area where they are exposed to various threats.

(h) Traffic. An increase in the number of construction vehicles and workers will have some influence on local traffic-related congestion, noise, and dust. However, heavy equipment use, such as that of cement and dump trucks, should be limited to daylight hours. In the interest of safety, the ports will need to be closed to visitors during construction.

(i) Health and Safety. Health and safety concerns are mainly related to the accidental spillage of hazardous substances during construction or machinery related accidents. In addition, an increase in road traffic for transport of materials and labor force is likely to give rise to safety concerns; therefore, proper signs will be required within the site and nearby to enable drivers, construction workers and road users to avoid any traffic related accidents. Digging and construction activities on the shore may pose a hazard for people attempting to use the old jetty especially at night. To prevent any danger to the public, the construction site will need to be cordoned off and protective measures undertaken to prevent any accidents.

(j) Fisheries/Tourism/Recreation. Impact on commercial fishing may occur as access to fishing boats, docking and mooring facilities can be hampered during the construction phase of the project. Alternative ports can be used during the construction phase.

The construction activities may also have a temporary impact on tourism, recreational fishing, entertainment and other beach related activities. Such impacts will be limited to the duration of the construction activity only and alternative sites for recreational fishing and beach related activities need to be identified.

(k) Employment. The construction of the ports will benefit the local economy and provide employment opportunities for unskilled labor. This phase is likely to see the arrival of large number of construction workers, which can lead to stress on the existing

public infrastructure. Adequate provisions will be required for the workers at the project site to minimize conflicts over resource sharing with the local community.

(l) Infrastructure Facilities. Development of the ports in previously undeveloped areas can result in improvement of local infrastructure such as roads, transport facilities, communication linkages, and market facilities.

(2) Operations Phase. (a) Water Quality. In the operations phase, hypoxic water conditions can occur in the semi enclosed ports due to insufficient water exchange. The level of hypoxia, however, can be greatly reduced by design measures such as an enhanced circulation design. Hypoxia is defined as $< 2\text{-}3 \text{ mg l}^{-1}$ of dissolved oxygen [25]. In confined areas much of the water body is stagnant as water mixing is minimized and oxygen content is generally low. In addition, water is warmer during summer holding less oxygen and marine organisms are stressed by the low oxygen levels. The de-oxygenated zone is usually found in bottom waters near sediment, and if severe, is devoid of most life. Although fish probably leave dead zones, less mobile, bottom-dwelling organisms may be killed. This can lead to loss of valued biological resources in the affected area. A hypoxic-stressed benthos is typified by short-lived, smaller surface deposit feeding polychaetes and the absence of marine invertebrates such as crustaceans, bivalves and gastropods [26].

Solid and liquid wastes from boats and other human activities, either dumped directly or leached into water, can cause significant damage to water quality, and subsequently to marine life and ecosystems [24]. These effects may include bacterial and viral contamination of commercial fish and shellfish, depletion of oxygen in water, and bioaccumulation of certain toxins in fish. Other pollutants from boats are the antifouling additives used in paints to prevent the growth of barnacles and other marine organisms on vessel surfaces. Some of these additives contain tributyltin (TBT), a toxic chemical that can leach into water. TBT is absorbed by organisms and bioaccumulates in marine life [27].

Any discharge of heavy metals from construction activities such as filling may elevate levels of lead, mercury or copper in bivalves and fish, and increase levels of cadmium, vanadium, and zinc in sediments. Phytoplankton growth may be inhibited resulting in a lack of zooplankton, a major food source for fish and corals [28].

Other potential sources of impacts on the water quality include oil spills from boats and engine oil change, and an increase in solid waste from industrial and human activity.

(b) Marine Habitat. A potential impact on marine habitats will be the shading of benthic habitats,

which will prevent sunlight from reaching the bottom organisms and lead to reduced photosynthesis and growth rates for benthic flora in the impacted areas. This effect is mainly caused by the presence of jetties, floating jetties and boats moored for long periods of time during the day [e.g. 29].

Operation of the ports may also increase the potential for disruption of the life cycle pattern, spawning, and migration of various marine species including marine birds. Artificial lights at ports, sometimes in operation for nearly twelve hours during the night, can also have negative effects on the wildlife including disorientation, confusion of biological rhythms that are adapted to a day/night alternation, and an overall deterioration of habitat quality. In general, bright nighttime lights and the flashing lights of straddle carriers are likely to disrupt biological rhythms and cause stress to all forms of marine life in and around the area [30]. Boat noise is another factor that may adversely impact marine life.

Marine habitats are likely to be impacted by oil spills from boats and port operations. A large share of oil contamination is the result of "chronic" pollution from such sources as port runoff, unloading and loading of oil tankers, and removal of bilge water. Oil spills can harm marine ecosystems and poison marine animals that ingest or inhale toxins. The spillage of other hydrocarbon compounds, chemicals and hazardous materials through ports operation can also cause direct toxicity to different fauna and flora in the area and serious threats to the marine life located in the vicinity [23].

Other potential impacts include an increase in solid wastes through industrial and human activities; accumulation of nutrients leading to eutrophication

in the water and an increase in primary production and biomass at both phytoplankton level and benthic algal populations; oxygen depletion that negatively affects the living organisms; and introduction of oil compounds, heavy metals and other organic and inorganic chemicals that can influence the benthic community in the sandy habitats.

(c) Traffic. Post-construction traffic to the ports is expected to be higher than pre development conditions. Anticipated increases in total fish production may also result in an increase in vehicular traffic to and from the ports. Visitation to the ports by the public may also rise.

(d) Fisheries. The development of fishing ports may help enhance the safety of the fishing fleet; provide more modern facilities to allow an increased number of boats to operate safely; improve the hygiene and thus health of fish catch by providing more modern offloading facilities.

(e) Employment. The operations phase will also help provide employment opportunities for local fishing vessel owners and in maintenance and waste management areas.

(3) Impact Evaluation. The significance of the predicted positive and negative impacts has been evaluated using well defined criteria as described by Rasheed et al. [5]:

Table 2 provides an assessment of the significance of the impacts during the construction phase, and Table 3 deals with the assessment for the operations phase.

TABLE 2
Significance of impacts generated during the construction phase of the project

<i>Impact Area</i>	<i>Description of Impact</i>	<i>Reversibility</i>	<i>Duration</i>	<i>Significance before mitigation</i>
Water and Sediment	Release of pollutants e.g. heavy metals due to filling and construction materials			
	Increase in organic matter load due to filling and construction materials			
	Increase in turbidity and particle suspension in water because of filling			
	Increase in nutrient concentration levels leading to eutrophication			
	Accidental spillage of oil and oil compounds			
Marine Habitat	Increase in solid wastes from construction activities and a risk of buildup of these wastes on seafloor			
	Physical removal of benthic habitat such as seagrasses and direct impact on polychaetes due to construction activities			
	Deterioration of fauna and flora in the area due to an increase in solid waste and water turbidity			
	Risk of toxicity and growth rate reduction from oil and other toxic spills			
Terrestrial Habitat	Burial and shadow effect of sediment plumes			
	Disturbance to habitat due to land based construction including nuisance from increased noise levels			
Socio-economic	Generation of employment opportunities			
	Expansion of infrastructure facilities			
	Access to recreational ground/ fishing			
	Traffic generation			

(-) = Potential adverse impact; (+) = Potential positive impact

1= Low significance; 2= Moderate significance; 3= High significance

TABLE 3
Significance of potential impacts generated during the project operations

<i>Impact Area</i>	<i>Description of Impact</i>	<i>Reversibility</i>	<i>Duration</i>	<i>Significance before mitigation</i>
Water and Sediment	Hypoxia in the semi enclosed ports Release of pollutants such as heavy metals Increase in water turbidity and particle suspension due to boat traffic Increase in nutrient concentration levels resulting in eutrophication Accidental spillage of oil and oil compounds Reduced water quality as a result of contaminants washing into the sea Increase in solid wastes and a risk of buildup of these wastes on seafloor			
Marine Habitat	Potential positive impact on certain fish species due to increased shelter and protection under newly constructed areas Physical removal of benthic habitat such as seagrasses and polychaetes due to anchoring Adverse effects on the fauna and flora in the area as a result of increase in solid waste and turbidity Risk of toxicity and growth rate reduction from oil and other toxins spillage especially antifouling additives Disruption of marine species and birds life cycle pattern, spawning, and migration due to increased port activities Burial and shadow effect of the boats and sediment plumes Disorientation, disruption of biological rhythms by artificial light Spread of disease in some habitats due to oxygen deficient environment			
Socio-economic	Improved access to port facilities Fisheries Generation of employment opportunities Traffic generation			

(-) = Potential adverse impacts; (+) = Potential positive impact

1= Low significance; 2= Moderate significance; 3= High significance

Mitigation Measures. (1) Construction Phase. In order to avoid or minimize impacts during construction, the following mitigation measures are proposed:

(a) Health and Safety. The construction contractor should ensure that health and safety procedures are in place for all workers on site prior to the start of construction activities. Safe working practices should be adopted for all works and use of correct protective gear enforced. All personnel should be fully briefed on work site access procedures including safety briefings prior to entering any site. Key areas need to be fenced off by warning tape or other suitable hazard warning signs. If necessary, security guards should be employed to ensure no unauthorized persons gain entry.

(b) Benthic Habitat. Construction activities can be carefully programmed and managed to prevent significant deterioration of marine flora and fauna. Filling near sensitive habitats should be avoided and activities restricted to the immediate vicinity of the construction sites.

(c) Sediment Suspension and Dispersal. Dumping, filling and other construction activities will increase the rate of sedimentation and concentration of suspended particles in water. This may lead to a temporary deterioration in water quality and have negative impacts on benthic communities by smothering and blanketing as well as decreasing sunlight penetration and causing damage to light dependent photosynthetic organisms. The impacts can be reduced through the following measures:

- Appropriate construction equipment of a high quality should be used along with techniques that minimize sediment suspension and dispersal.
- Suction and confined equipments and bulldozers with turbidity reduction measures should be used for filling. Grab bulldozers should be avoided; instead screens with grab and backhoe bulldozers should be used.
- The marine consultant should be asked to provide recommendations regarding a suitable limit to turbidity. Work should be temporarily prohibited if the recommended value is exceeded.
- Tidal currents should be taken into consideration during landfilling. Landfilling should not occur in open water if the currents are high enough to induce significant sediment transport away from the

immediate construction vicinity. Therefore, currents should be monitored on site and landfilling as well as other construction activities should be carried out during low tide.

- Installation of protective silt curtains or screens near and along the dredging and filling sites should be considered.

- Environmental monitoring needs to be conducted during the construction phase to make sure that mitigation measures are effective.

- Exposed surfaces during site preparation and land excavation should be visibly moist in order to reduce the spread of dust and suspended solids.

- Prior to landfilling, the relevant construction workers should be briefed on mitigation measures for reducing environmental impacts.

- No landfilling at sea should be permitted without a license from the competent authority.

(d) Air Quality & Dust Control. Dust is produced mainly during land excavation, filling, and transport of construction materials. The best achievable control measures may include all of the following as applicable to the project site:

- Active construction areas should be watered daily;

- All trucks hauling soil, sand, and other loose materials should be covered or required to maintain at least two feet of freeboard;

- Non-toxic soil stabilizers should be applied on all unpaved access roads, parking areas and staging areas at construction sites;

- The construction site entrance must be posted with visible speed limit signs;

- All construction vehicles should enter the construction site through the graveled roadways, unless an alternative route is submitted to and approved for use by the local authorities.

(e) Nutrients, Organic Matter and Heavy Metals Enrichment. Nutrients, organic matter and heavy metal enrichment would result mainly during landfilling as sediments are considered reservoirs for nutrients, organic and other toxic materials. Impacts can be reduced by sucking mud and sediment plumes through special machines and disposing off at proper facilities inland to prevent the release of pollutants present in mud or sediment into the water body.

(f) Oil Spills. Oil, paints and fuelling residues may be discharged into the water body during construction activities. This can be avoided or minimized by adopting the following measures:

- Preventing any discharge of oil, oil sludge, domestic refuse, engine room waste, and wastewater into the sea. All liquids containing oil should pass into the sea only via an oil separation system, and the sludge and the separated oil residues need to be either incinerated on board the concerned vessel or in

special furnaces or discharged to oil collecting facilities;

- All equipments and machinery need to be properly serviced and maintained in accordance with manufacturer's specifications to prevent any leaks, equipment breakdown or accidents that may cause hazardous material spills;

- Equipment operators should follow proper safety procedures to avoid accidents and spills;

- TBT based anti-fouling paints should not be used and boat maintenance needs be restricted to approved areas to prevent the accumulation of anti-fouling agents that harm marine life.

(g) Solid Waste and Garbage Disposal. Solid waste and various left over materials are expected to be thrown in the water body during construction activities. The waste may accumulate over time or be driven to the deep sea by local currents and consequently have adverse impacts on the environment. In order to reduce these impacts, the following actions are recommended:

- Solid waste should be collected in dustbins and disposed in approved landfill sites. Under no circumstances should solid wastes be disposed in the water body;

- Organic wastes except plastic should be burnt in incinerators, whereas the rest of the solid wastes should be stored for proper disposal out of the area;

- Good site practices should be adopted to collect the rubbish and litter from the construction sites and to prevent rubbish from spreading away from the site area. It is necessary to clean the construction site regularly. Scavenging service for collecting any waste loss from the site into the sea should be provided as needed;

- Notices should be posted at the construction sites to remind workers not to discharge any sewage and wastewater into the nearby environment;

- Public awareness campaigns on proper disposal of solid waste should be organized;

- Cleanup diving campaigns should be conducted periodically for cleaning inland and underwater.

(h) Noise and Vibration. The various sources of noise and vibration at ports include traffic, heavy machinery and equipment used for construction activities. Noise impacts can be mitigated by using silencers or mufflers on equipment, reducing duration of activities, switching off equipment when not in use, and using well serviced equipment.

(i) Traffic. Construction access should be along the existing right-of-way via paved road connecting the project site to the main road. Construction should be generally conducted during daylight hours and water should be sprayed on access roads

to control dust. Adjacent landowners need to be informed of the construction schedule to minimize traffic-related disturbances. Appropriate cautionary signs should be installed along the main road during the construction period.

(2) Operations Phase. (a) Water Quality. Impacts on water quality include possible hypoxia in the semi-enclosed ports in addition to accidental spill of oil and other hazardous materials. Mitigation measures suggested to reduce impacts include:

- Use of external power such as pumps for improving circulation;
- Provision of measures to clean the marine basin. These will include measures to skim the surface of the floating deposits, as well as equipment to remove debris from the sea bed;
- In the event of a spill, all fluids in the containment area should be removed and treated/disposed in an appropriate manner according to applicable regulations;
- All workers and Coast Guards must be adequately trained to recognize the hazards associated with accidental spills;
- Facilities designs must include some controls and monitoring systems to minimize the potentials for conditions in which accidental spills could occur.

(b) Waste Management. A detailed waste management plan should be prepared in advance to ensure proper storage, labeling, packaging, record keeping, and disposal of all wastes. The waste management plan should include:

- A description of each waste stream;
- Handling, transport, treatment, and disposal procedures for each waste;
- Preparedness, prevention, contingency, and emergency procedures;
- Personnel training especially for the Coast Guards;
- Implementation of best practices for fueling and cleaning boats;
- Public awareness of proper waste disposal measures;
- Sorting and recycling of scrap materials such as paper, packing materials, glass, metal, and plastics. Non-recyclable inert wastes should be stored in covered trash bins in accordance with local ordinances and picked up by an authorized local trash hauler on a regular basis for transport and disposal in suitable landfill.

(c) Marine Boats. Local authorities should create financial incentives for the cleanup of boats as well as the replacement of old marine vessels and conduct training courses for the Coast Guards to manage the behavior/actions of fishermen. Restricted regulations should be applied for boat cleaning, oil replacing, and maintenance of the boats.

These regulations should be communicated to the fishermen through written documents. In addition, use of diesel engine fuel should be minimized to the extent possible.

(d) Legislation Traffic. Increase in post construction traffic can be managed by clearly marking alternative access routes and Regulation. In order to minimize adverse environmental impacts, there is a need to regulate effluent disposal, chemical use, and waste generation, storage and disposal. The following regulatory measures will improve the effectiveness of the mitigation measures proposed earlier:

- Enforcement by government through criminal prosecution; and
- Economic incentives or disincentives by government through charges and forfeits.

Environmental Management and Monitoring. A comprehensive Environmental Management and Monitoring Plan (EMMP) for the mitigation and management of potential adverse impacts during the construction and operations phases of the project is highly recommended. The EMMP should include specific mitigation measures and monitoring for each adverse impact identified and feed directly into a Health Safety and Environment (HSE) management system to be implemented by the project contractor. The ultimate responsibility for environmental management during all phases of the project rests with the Project Proponent. However, the contractor for the project also bears responsibility for the implementation of the EMMP. A sample EMMP is shown in Table 4 and Table 5.

The Project Proponent should have a representative on site to ensure that the project activities are carried out in accordance with the work program. The representative's duties usually cover monitoring the sufficiency of equipment to carry out the work (pre-mobilization check), ensuring safety requirements are covered and auditing the operations. The representative can also perform the duties of an Environmental Auditor (EA) during the construction activities. The EA would be familiar with construction activities, associated environmental impacts, mitigation measures and monitoring techniques and will ensure compliance with the EMMP, national and international laws. The EA will work closely with the contractor during construction and subsequent operations (for example repairs) to monitor the methods used by the contractor in construction as per the expectations of the EIA and proposed mitigation measures.

During construction, close liaison should be maintained between the EA and the contractor to ensure that all aspects of the construction are monitored. The contractor should be prepared to provide method statements to the EA as required and make the construction program available to the auditor as

early as possible. The contractor should give adequate warning to the auditor of any changes in the program. The EA must maintain good communication with local authorities and relevant interest

groups. Reporting progress and environmental performance and maintaining contact with the Project

TABLE 4
Environmental management for construction phase

Area of Impact	Activity	Impact	Proposed Control and Mitigation Measures	Proposed Monitoring Plan
Water	Handling and disposal of wastewater	Seepage of wastewater discharged on land into the sea	<ul style="list-style-type: none"> Collect sewage from onsite camps in adequate size holding tanks and transport to municipal facilities. Cover stockpiles to reduce run off materials entering the marine waters. Adequately label storage areas indicating the nature, quantity of hazardous material and safety measures required. Regularly inspect storage areas to identify leaks or spills. Prevent any discharge of oil, oil sludge, domestic refuse, engine room waste into the sea. All liquids containing oil should pass into the sea only via an oil separation system, and the sludge and separated oil residues need to be either incinerated on board the concerned vessel or in special furnaces or discharged to oil collecting facilities. 	<ul style="list-style-type: none"> Water monitoring of pH, DO, TSS, turbidity, inorganic nutrients (ammonium, nitrate, nitrite, phosphate, and silicate), chlorophyll <i>a</i>, BOD, COD, oil and grease, some heavy metals, and bacterial enterococcus. Monitoring should be performed in compliance with national standards.
	Handling, storage and transportation of hazardous material/waste	Spills and leakages (oil, hazardous chemicals)	<ul style="list-style-type: none"> Service all equipment and machinery in accordance with manufacturer's specifications to prevent any leaks, equipment breakdown or accidents that may cause hazardous material spill. Ensure equipment operators follow proper safety procedures to avoid accidents and spills. Avoid use of TBT based anti-fouling paints. Boat maintenance needs be restricted to approved areas to prevent the accumulation of anti-fouling agents that harm marine life. Use appropriate equipment of a high quality along with techniques that minimize sediment suspension and dispersal. Use suction and confined bulldozers with turbidity reduction measures. Avoid use of grab bulldozers; instead backhoe should be used. 	
	Landfilling	Sediment disturbance causing turbidity	<ul style="list-style-type: none"> Use closed or sealed bucket clamshell bulldozers to minimize the effect of increased turbidity. Install protective silt curtains or screens near and along the construction site. Carryout landfilling and other construction activities during low tide. 	
Waste	Generation of solid waste	Increase in solid waste	<ul style="list-style-type: none"> Provide suitable storage areas adequately designed and sized. Define disposal procedures for waste generated on site during onshore construction. Segregate any hazardous waste from nonhazardous. Define procedures for dealing with any potential hazardous waste. Recycle to extent possible; dispose of non-recyclable waste to municipal landfill sites. Comply with all national and international regulations. Train and monitor all personnel/workers to avoid intentional discharges. Review and monitor procedures to prevent accidental discharge of pollution stream. 	<ul style="list-style-type: none"> Visual inspection and monitoring of the storage materials to Check for any possible spillage or leakage. Visual observations of waste management on site during construction. Solid waste monitoring for all waste materials in land and seawater. Monitoring should be performed in compliance with national standards.
	Civil works	Discharges form works, equipment	<ul style="list-style-type: none"> Avoid impacts to marine ecological resources as much as possible during construction activities. Avoid filling near sensitive habitats and restrict activities to the immediate vicinity of construction site. No landfilling at sea should be permitted without a license from the competent authority. 	
Marine Habitat	Landfilling and pollutant discharges	Habitat damage	<ul style="list-style-type: none"> Use barriers to protect sensitive receivers from works. Use silencers/mufflers on equipment. Provide personal protective devices to workers in high noise areas. 	Monitor noise levels during construction to ensure that they Comply with the international standards.
Noise and Vibration	Onshore construction and offshore landfilling	Disturbance of marine life	<ul style="list-style-type: none"> Water all active construction areas daily. Cover all trucks hauling soil, sand, and other loose materials or require all trucks to maintain at least two feet freeboard. Apply non-toxic soil stabilizers on all unpaved access roads, parking areas and staging areas at construction sites. Provide entry for all construction vehicles through the graveled roadways, unless an alternative route is submitted to and approved for use by the local authorities. 	<ul style="list-style-type: none"> Visual inspection of the construction materials to determine if there are any conditions which would require further testing of the materials before disposal. Visual monitoring of the sediment curtain at all times during construction; stop work if visible breaches of the curtain occur. Water monitoring of pH, DO, TSS, turbidity, inorganic silicate, chlorophyll <i>a</i>, and heavy metals.
Air Quality & Dust Control	Onshore construction and landfilling	Dust generation	<ul style="list-style-type: none"> Provide alternative mooring facilities to the fishermen. Provide access along the existing right-of-way via paved road. Install appropriate cautionary signs along the road in the project vicinity during construction. 	Visual monitoring of traffic jams.
Socio-economic	Construction works Transport of construction materials, labor	Restricted access Increased traffic		

TABLE 5
Environmental management for operations phase

Area	Activity	Description of Impact	Proposed Control and Mitigation Measures	Proposed Monitoring Plan
Water	Increased release of nutrients	Eutrophication	<ul style="list-style-type: none"> Design some holes in the breaking water according to the dominant current in order to increase the flow of water from inside to outside. Provide means to clean the marine basin. These will include measures to skim the surface of the floating deposits, as well as means to remove debris from the sea bed. Adequately train all workers and Coast Guards to recognize the hazards associated with accidental spills. Provide controls and monitoring systems in facilities designs to minimize the potential for conditions in which accidental spills could occur. Remove and treat all fluids in the containment area in an appropriate manner in the event of a spill. 	<ul style="list-style-type: none"> Conduct water monitoring including pH, DO, TSS, turbidity, inorganic nutrients (ammonium, nitrate, nitrite, phosphate, and silicate), chlorophyll <i>a</i>, BOD, COD, oil and grease, some heavy metals, and bacterial enterococcus measurements. Carry out sediment monitoring once a year for the following parameters: TOC, TN, TP, H₂S, oil and grease and some heavy metals Monitoring should be performed in compliance national standards.
	Accidental spillage of oil or chemicals	Deterioration in water quality	<ul style="list-style-type: none"> Prepare a detailed waste management plan to ensure minimization, proper storage, labeling, packaging, record keeping, and disposal of all wastes. The waste management plan should include: <ul style="list-style-type: none"> A description of each waste stream. Handling, transport, treatment, and disposal procedures for each waste. Preparedness, prevention, contingency, and emergency procedures. Personnel training. Comply with all national and international regulations. Train all personnel/workers to avoid intentional discharges. Review procedures to prevent accidental discharge of pollution stream from vessel. 	<ul style="list-style-type: none"> Visual inspection and monitoring of the storage materials to check for any possible spills or leakage. Visual observations of waste management on site during operations. Solid waste monitoring for all waste materials in land and seawater. Monitoring should be performed in compliance with national standards.
Ecology	Oil and chemical spills, solid waste discharge	Habitat disturbance	<ul style="list-style-type: none"> Implement appropriate solid and liquid waste management plan. Conduct public awareness programs. 	<ul style="list-style-type: none"> Monitor marine habitat once a year for seagrass, fish, other fauna (sea urchin, sponges, etc.), and substrata (rocky, rubles and sandy). Conduct a comprehensive study every year to compare between the results of the monitoring and to detect any change in marine habitat status.
Socio-economic	Increase in traffic	Congestion	Develop and implement a traffic management plan.	Monitor traffic changes and modify management plans to accommodate any changes.

Proponent will also be an important part of the EA's responsibilities. Monitoring requirements during different phases of the project are explained in below. Areas to be considered for monitoring include health and safety, waste, dust, noise, water quality, sediment and marine habitat.

(a) Health and Safety. Occupational safety of the workers at the construction site should be the responsibility of the contractor. A detailed Health, Safety and Environment (HSE) plan should be developed by the contractor, which should be approved

by the Project Proponent. Moreover, reporting of any health and safety violations should be mandatory.

(b) Waste Management. A detailed waste management plan should be prepared for construction and operations to ensure minimization, proper storage, and disposal of all wastes.

- The contractor should remove all solid waste materials from the sea bed during the construction period. This should be inspected by divers or by visual checks by the Proponent;

- Visual inspection and monitoring of the storage materials should be carried out to check for any possible spillage or leakage;

- Visual observations of waste management on site need to be made during construction;

- Training programs should be conducted for the workers during construction and operations of the project;

- Solid waste monitoring should be performed during construction and operations on land and in seawater;

- The monitoring should cover all the possible waste materials, such as bags, construction materials, floating materials, food residual, chemical spillage, etc.; and

- The monitoring should be performed in compliance with national standards and guidelines.

(c) Dust and Noise. Dust generation from construction activities should be in compliance with national standards for the total suspended solids and turbidity or transparency.

- Visual inspection of the construction materials should be carried out to determine if there are any conditions which would require further testing of the materials before disposal;

- Visual monitoring of dust levels should be maintained at all times during construction and work stopped if visible breaches occur; and

- Noise levels should be monitored during construction to ensure that they comply with international standards and work stopped in case of violations of good practices.

(d) Water Quality.

- Seawater should be monitored during construction and operations (once a month) for the following parameters; pH, DO, TSS, turbidity, inorganic nutrients (ammonium, nitrate, nitrite, phosphate, and silicate), chlorophyll *a*, BOD, COD, oil and grease, some heavy metals, and bacterial enterococcus.

- The monitoring should be performed in compliance with national standards.

Sediment.

- Sediment should be monitored during construction and operations (once a year) for the following parameters: TOC, TN, TP, H₂S, oil and grease and some heavy metals.

- The monitoring should be performed in compliance with national standards.

(e) Marine Habitat. If any rare or threatened fauna species are encountered within 50 m of works during the construction phase, all nearby construction activities should cease and the site supervisor should be notified. Work will only continue if either

the threatened species leaves the site or the environmental consultants can carry out an assessment and recommend a course of action.

In the operations phase, the following measures are recommended:

- Marine habitat should be monitored once a year for corals, seagrass cover, fish, other fauna (sea urchin, sponges, etc.), and substrata (rocky, rubles and sandy).

- A comprehensive study should be done every year to compare between the results of the monitoring and to detect any change in marine habitat status.

(f) Inspections. Visual and operational inspections should be executed by the competent authority once a year on all port processes. This is to ensure that the ports are operating in accordance with all environmental regulatory requirements; and to check adequate implementation of the monitoring plan.

In addition, annual auditing of all activities and monitoring programs should be carried out.

CONCLUSIONS

Overall, fishing port projects can help improve the socio-economic condition of fishermen by enhancing the safety of the fishing fleet; providing more modern facilities to allow an increased number of boats to operate safely and improving the hygiene and thus health of fish catches by providing more modern offloading facilities.

Potential adverse impacts during project construction and operations of fishing port projects in a semi-enclosed water body include possible deterioration in water quality, damage to some local benthic habitats, waste generation, dust, noise, health and safety concerns, and traffic congestion.

An Environmental Management and Monitoring Plan is proposed to minimize the adverse impacts associated through suggested mitigation measures and a monitoring program to oversee the implementation of the mitigation measures during the different phases of the development.

ACKNOWLEDGEMENTS

This work was conducted while a Sabbatical Fellow from The University of Jordan to Mohammed Rasheed to be spent at the Mote Marine Laboratory in Florida USA. Fulbright scholarship was also awarded to Mohammed Rasheed during this period.

REFERENCES

- [1] Dinwoodie, J., Tuck, S., Knowles, H., Benhin, J. and Sansom, M. (2012) Sustainable development of maritime operations in ports. *Business Strategy Environment*, 21, 111–126.
- [2] Chanchang, C., Sithisarankul, P. and Supanitayanon, T. (2016) Environmental and health impact assessment for ports in Thailand. *International Maritime Health*, 67, 112–116.
- [3] Kasprzak, K. (2011) Environmental impact of Mrzezyno fishing port modernization within the NATURA 2000 area. *Journal of Coastal Research*, 64, 1238–1244.
- [4] RCER (2010) Royal Commission Environmental Regulations, vol. 1, Regulations and Standards.
- [5] Rasheed, M., Mian S. and Aubrey, D. (2011) Guidelines for EIA of fish and shrimp hatcheries in a semi-enclosed water body. *Ocean Coastal Management*, 54, 678–688.
- [6] Banat, I.M., Hassan, E., El-Shahawi, M. and Abu-Hilal, A. (1998) Post-gulf-war assessment of nutrients, heavy metal ions, hydrocarbons, and bacterial pollution levels in the United Arab Emirates coastal waters. *Environment International*, 24, 109–116.
- [7] Hassn, M., Heba, M. and Al Edresi, A. (2004) Background level of heavy metal in Dissolved particulate passes of water and sediment of Al Hodeidah Rea Sea coast of Yemen, Faculty of marine science and Environment Alhodeidah university city republic of Yemen JKAU. *Marine Science*, 15, 53–71.
- [8] Akpan, E., Ekpe, U. and Ibok, U. (2002) Heavy metals trends in the Calaber River, Nigeria. *Environmental Geology*, 42, 47–51.
- [9] Bazzi, A. (2014) Heavy metals in seawater, sediments and marine organisms in the Gulf of Chabahr, Oman Sea. *Journal of Oceanography and Marine Science*, 5, 20–29.
- [10] Mulligan, C., Yong, R. and Gibbs, B. (2001) Remediation technologies for metal contaminated soils and groundwater: An evaluation. *Engineering Geology*, 60, 193–207.
- [11] Tchouwou, P., Yedjou, C., Patlolla, A. and Sutton, J. (2012) Heavy metals toxicity and environment. *EXS*, 101, 133–64.
- [12] Holmes, M., Wristen, K. and Bonner, M. (1999) The National Sewage Report Card (Number Two). Sierra Legal Defence Fund. Vancouver, Canada.
- [13] Rasheed, M., Badran, M. and Huettel, M. (2003) Influence of sediment permeability and mineral composition on organic matter deterioration in three sediments from the Gulf of Aqaba, Red Sea. *Estuarine Coastal shelf Science*, 57, 369–38.
- [14] Anderson, D., Glibert, P. and Burkholder, J.M. (2002) Harmful algal blooms and eutrophication: nutrient sources, composition and consequences. *Estuaries*, 25, 562–584.
- [15] Heisler, J., Glibert, P., Burkholder, J., Anderson, D., Cochlan, W., Dennison, W., Gobler, C., Dortch, Q., Heil, C., Humphries, E., Lewitus, A., Magnien, R., Marshall, H., Sellner, K., Stockwell, D. Stoecker, D. and Suddleson, M. (2008) Eutrophication and harmful algal blooms: A scientific consensus. *Harmful Algae*, 8, 3–13.
- [16] Sydnese, L., Hemmingsen, T., Skare, S. and Hansen, S. (1985) Seasonal variations in weathering and toxicity of crude oil in seawater under arctic conditions. *Environmental Science and Technology*, 19, 1076–1081.
- [17] Singer, M., George, S., Lee, I., Jacobson, S., Weetman, L., Blondina, G., Tjeerdema, R., Aurand, D. and Sowby, M. (1998) Effects of dispersant treatment on the acute aquatic toxicity of petroleum hydrocarbons. *Archive of Environmental Contamination and Toxicology*, 34, 177–187.
- [18] Capuzzo, J. (1987) Chapter 8: Biological effects of petroleum hydrocarbons: Assessments from experimental results. In: Boesch and Rabalais (eds.). Long-term environmental effects of offshore oil and gas development. Elsevier Applied Science, New York, NY. 343–410.
- [19] Pastorok, R. and Bilyard, G. (1985) Effect of sewage pollution on coral-reef communities. *Marine Ecology Progress Series*, 21, 175–189.
- [20] ABP Research (1999) Good practice guidelines for ports and harbours operating within or near UK European marine sites. English Nature, UK Marine SACs Project, 20 pp.
- [21] Erfemeijer, P. and Lewis III, R. (2006) Environmental impacts of dredging on seagrasses: A review. *Marine Pollution Bulletin*, 52, 1553–1572.
- [22] Hitchcock, D. and Bell, S. (2004) Physical impacts of marine aggregate dredging on seabed resources in coastal deposits. *Journal of Coastal Research*, 20, 101–114.
- [23] Taylor, H. and Rasheed, M. (2011) Impacts of a fuel oil spill on seagrass meadows in a subtropical port, Gladstone, Australia – The value of long-term marine habitat monitoring in high risk areas. *Marine Pollution Bulletin*, 63, 431–437.
- [24] Abu-Hilal, A. and Al-Najjar, T. (2004) Litter Pollution on the Jordanian shores of the Gulf of Aqaba (Red Sea). *Marine Environmental Research*, 58, 29–63.
- [25] Vaquer-Sunyer, R. and Duarte, C. (2008) Thresholds of hypoxia for marine biodiversity. *Proceedings of the National Academy Sci.*, 105, 15452–15457.
- [26] Rabalais N., Turner, R. and Wiseman, W. (2002) Gulf of Mexico hypoxia, A.K.A. "the

dead zone". Annual Review of Ecology, Revolution and Systematics, 33, 235-263.

- [27] Dwivedi, J. and Trombetta, L. (2006) Acute toxicity and bioaccumulation of tributyltin in tissues of *Urolophus jamaicensis* (yellow sting-ray). Journal of toxicology and Environmental Health, 69, 1-13.
- [28] Pilcher, N. (2000) Corals and human disturbance. *Al-Sanbouk*, 12.
- [29] Rogers, C (1979) The effects of shading on coral reef structure and function. Journal of Experimental Marine Biology and Ecology, 41, 269-288.
- [30] Chepesiuk, R. (2009) Missing the Dark: Health Effects of Light Pollution. Environmental Health and Perspective, 117: A20-A27.

Received: 17.11.2016

Accepted: 06.06.2017

CORRESPONDING AUTHOR

Mohammed Rasheed

Mote Marine Laboratory
Mote Aquaculture Research Park
12300 Fruitville Road
Sarasota, FL 34240 – USA

E-mail: m.rasheed@ju.edu.jo
marsheed@mote.org

ADVANCED TREATMENT OF COAL CHEMICAL INDUSTRY WASTEWATER BY EXPANSIVE FLOW BIOLOGICAL AERATED FILTER

Baolin Hou*, Zhi Li, Renjian Deng, Bozhi Ren

Hunan Provincial Key Laboratory of Shale Gas Resource Utilization, School of civil engineering, Hunan University of Science and Technology, Xiangtan, 411201, China

ABSTRACT

Treatment efficiency was investigated for advanced treatment of coal chemical industry wastewater by expansive flow biological aerated filter. Removal efficiencies of COD and total phenols rose with the prolonging of hydraulic retention time (HRT). The removal efficiencies of COD and total phenols increased from 56.3% to 66.7% and from 63.8% to 74.2% respectively when HRT expanded from 6 h to 12 h. $\text{NH}_4^+\text{-N}$ removal efficiency decreased with the augment of HRT. Shorter HRT induced higher hydraulic loading rate, which could promote mass transfer between biofilm and wastewater, accelerating the reaction rate. Turbidity and chroma in effluent were 3.66 NTU and 26.22 at the HRT of 9 h, with the removal efficiency of 98.03% and 91.67% respectively. The optimal backwashing time was 6 minutes in pulse manner with air and water intensity of $8.0 \text{ L}/(\text{s}\cdot\text{m}^2)$ and $2.5 \text{ L}/(\text{s}\cdot\text{m}^2)$, according to the amount of suspended solid and recovery time.

KEYWORDS:

Expansive flow biological aerated filter; Coal chemical industry wastewater; Advanced treatment; Backwashing

INTRODUCTION

Biological aerated filter (BAF) is an efficient biofilm technology for wastewater treatment[1]. It has been the hot issue to be studied due to such advantages as high quality in effluent, rapid start up, high efficiency, small occupation and low cost[2]. It shows great advantages in terms of new sewage treatment plant and transformation of old sewage treatment plant, especially in the treatment of industrial wastewater, the amount of which is less comparing to domestic sewage[1]. BAF integrates the functions of physical filtration and biodegradation, including the effects of absorption and retention in filter, biological oxidation and hierarchical predation of the food chain along with the height of the filter bed[3-5]. Recently studies on BAF focused on the mechanism of retention, biodegradation, oxygen

transfer and optimization of backwashing[6, 7]. The further study provides the basis for the wide application of BAF. BAF could be served as secondary treatment or advanced treatment of wastewater[8]. Expansive flow BAF was the modified process of traditional BAF based on optimizing the hydraulic condition, showing better removal efficiency and hydraulic condition both in treatment operation and backwashing. Expansive flow BAF was a new pool type with potential of widely application.

Coal chemical industry wastewater was considered to be one kind of refractory industrial wastewater with poor biodegradability. The composition of coal chemical industry wastewater was very complex, containing high concentration of phenols, tar, polycyclic aromatic hydrocarbons, ammonia as well as refractory and toxic compounds such as cyanide and thiocyanate[9]. Traditional activated sludge process was widely used in coal chemical plants for wastewater treatment[10, 11]. However, the effectiveness of traditional activated sludge process was unsatisfactory with the disadvantages of high energy consumption, poor removal efficiency[12, 13]. Biofilm processes had been proved to be an available method to treat coal chemical industry effluent by overcoming some of the problems in traditional activated sludge process, especially in the treatment of wastewater with low concentrations of pollutants[14]. The contents of contaminants in the effluent after traditional treatment were still high, a great distance between the requirement of zero emission of coal chemical industry wastewater. Therefore, advanced treatment was essential for coal chemical industry wastewater[15]. In this study, expansive flow BAF was adopted for the advanced treatment of coal chemical industry wastewater and the treatment performance was investigated. Parameters of backwashing were also optimized based on the amount of suspended solid in backwashing effluent and recovery time.

MATERIALS AND METHODS

Experimental apparatus. The expansive flow BAF was a circular truncated cone shaped plexiglas reactor, with the bottom diameter of 80 mm and the

top diameter of 240 mm (Fig. 1). The effective volume was 16 L, with the height of 800 mm. The filter media was made of ceramisite, the average diameter of which was 3.0 mm. The density of the filter element was about 1.46 g/cm³, and the bulk density was 0.84 g/cm³, with the porosity of 42.5%.

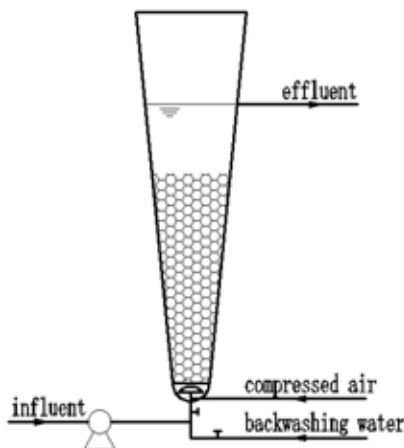


FIGURE 1

Schematic diagram of bench-scale apparatus

Inoculum and wastewater characteristics.

Inoculum sludge was obtained from a full-scale coal chemical wastewater facility, which has been running for two years. The inoculum sludge was gray-black with good settling characteristic, the SVI of which was 80. There was 30 days batch cultivation before experimental operation. The real coal chemical industry wastewater used in the experiment was collected from the effluent of secondary settling tank of the coal chemical wastewater treatment plant. The main characteristics of the wastewater were shown in Table 1.

TABLE 1
Main characteristics of wastewater

Item	COD (mg/L)	Total phenol (mg/L)	NH ₄ ⁺ -N (mg/L)	pH	Turbidity (NTU)	Chroma (degree)
Range	80-150	10-50	15-60	6.96-7.97	100-250	200-400
Mean	122	34	28	7.82	185	314

Analysis methods. During the experiment, samples were taken from the influent and effluent of the expansive flow BAF everyday and analyzed immediately after filtered through filter paper of 0.45 μm. COD, total phenols, NH₄⁺-N, NO₃⁻-N, NO₂⁻-N, turbidity and chroma were measured in accordance with standard methods. DO and pH were measured using IntelliCAL multifunction meter (HACH, USA). For organic analysis, the samples were firstly filtered through a 0.45 μm membrane filter and then extracted with methyl tert-butyl ether at neutral, basic and acid phase (repeated three times for each phase), following concentrated by evaporating in a water bath at 40°C. The concentrated samples were used for GC-MS analysis.

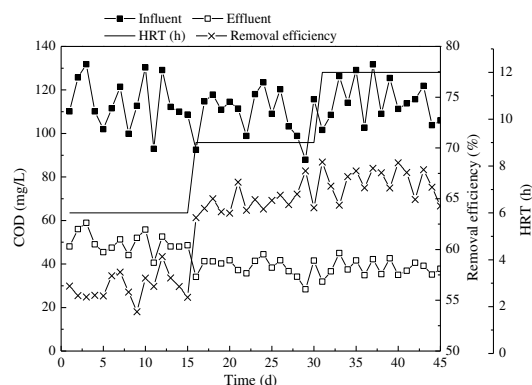


FIGURE 2

Performance of COD removal

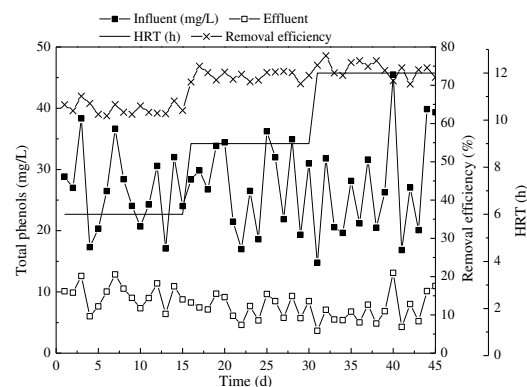


FIGURE 3

RESULTS AND DISCUSSION

COD and total phenols removal. The evolutions of COD and total phenols in influent and effluent were illustrated in Fig. 2 and Fig. 3. Influent COD concentration was in the range of 87.90 - 131.80 mg/L, with the average concentration of 112.60 mg/L. The average effluent concentration was 49.73 mg/L when the HRT was 6 h, with the average removal efficiency of 56.3% (Fig. 2). COD average removal efficiencies were 64.72% and 66.74% respectively when HRT increased to 9 h and 12 h. The performance of total phenols removal was similar to that of COD removal. The average total phenols concentration in the influent was 26.9 mg/L, and the average concentrations in effluent were 9.50, 7.53 and 6.98 mg/L respectively, with the average removal efficiency of 63.84%, 72.49% and 74.20%, when HRT were 6 h, 9 h and 12 h (Fig. 3). The removal efficiency only ascended 2.02% and 1.71% in forms of COD and total phenols when HRT extended from 9 h to 12 h, indicating that contact and reaction time were not the restricting factors for further degradation of pollutants in the expansive flow BAF.

Performance of total phenols removal. Pollutants in the biologically pretreated coal chemical industry wastewater were refractory compounds, the

biodegradation rates of which were very low. In addition, the first step of degradation was the contact between microorganism and pollutants, more time would be required when the COD concentration was not high[16, 17]. Therefore, COD removal efficiency ascended with the prolonging of HRT. It was detected that BOD₅/COD in the effluent was less than 0.1 when the HRT was 12 h, suggesting that pollutants in the effluent could hardly be degraded in biological way.

NH₄⁺-N removal. NH₄⁺-N removal in expansive flow BAF was illustrated in Fig. 4. The average NH₄⁺-N concentrations in the influent and effluent were 36.40 mg/L and 6.51 mg/L respectively when HRT was 6 h, with the removal efficiency of 81.27%. NH₄⁺-N removal efficiency dropped to 79.14% and 72.63% respectively when HRT increased to 9 h and 12 h. NH₄⁺-N removal efficiency decreased with the augment of HRT. The higher the HRT was, the lower the hydraulic loading rate. The mass transfer resistances of oxygen and substrate were poor when hydraulic loading was low, and an uneven distribution of gas and wastewater would emerge in the reactor[18, 19]. The mass transfer resistance was larger when the NH₄⁺-N concentration was lower. High hydraulic loading rate promoted mass transfer and hydraulic condition[20]. Therefore, NH₄⁺-N removal efficiency declined with the augment of HRT in expansive flow BAF.

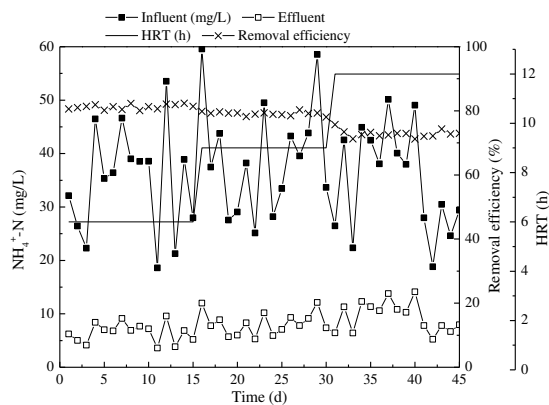


FIGURE 4
Performance of NH₄⁺-N removal

TABLE 2
Turbidity and chroma removals in expansive flow BAF

	Influent	Effluent	Removal efficiency
Turbidity (NTU)	185.58±12.16 ^a	3.66±0.83	98.03%
Chroma (Degree)	314.95±24.38	26.22±1.63	91.67%

^a Values represent the average values ± standard deviation from two weeks' data at the steady operation stage

Turbidity and chroma removal. According to the effect of HRT on COD, total phenols and NH₄⁺-

N removals, turbidity and chroma removals were inspected at the HRT of 9 h.

Table 2 shows the average turbidity and chroma concentrations in the influent and effluent of expansive flow BAF. The average concentrations of turbidity and chroma in effluent were 3.66 NTU and 26.22, indicating expansive flow BAF was an available process to remove turbidity and chroma from coal chemical industry wastewater.

TABLE 3
Main organic composition in the influent and effluent by GC-MS analysis

Organic compounds	Influent	Effluent	Organic compounds	Influent	Effluent
Phenol	25.31 ^a	- ^b	Pyridine	2.24	-
Phenol, 2-methyl-	8.92	-	Pyridine, 3-methyl-	1.94	+
Phenol, 3-methyl-	30.26	-	Quinoline	6.54	-
Phenol, 2,3-dimethyl-	5.49	-	Isoquinoline	0.84	+
Phenol, 2,4-dimethyl-	2.16	-	Quinoline, 2-methyl-	0.48	-
Phenol, 3,4-dimethyl-	1.53	-	Indole	5.98	-
Hydroquinone	0.41	+	Diethyl phthalate	4.34	-
Heptadecanoyl	0.36	+	Others	2.63	-
Eicosane	0.57	+			

^a Values represent the relative percentage of total peak area.

^b +, detected. -, not detected.

Organics removal. The organic compositions of influent and effluent were analyzed by GC-MS. The main organic compositions in the influent and effluent by GC-MS analysis were shown in Table 3. The main organic composition in the influent included phenolic compounds such as phenol, methylphenol, dihydroxybenzene, and nitrogen-containing heterocyclic compounds such as pyridine, quinoline, indole and aromatic hydrocarbons. Phenolic compounds were the main pollutants in the wastewater, accounting for about 73% of the total organic contaminant in the influent. Nitrogen-containing heterocyclic compounds (pyridine, quinoline and indole) constituted about 18%. A significant reduction was observed in terms of organic compound amount and kind in effluent by the treatment of expansive flow BAF. Phenols were almost completely degraded, while some nitrogen-containing heterocyclic compounds, aromatic hydrocarbons and long-chain hydrocarbons were refractory to be degraded or removal in expansive flow BAF. Nitrogen-containing heterocyclic compounds comprised the majority in the effluent. The results suggested that those compounds were recalcitrant to be removal by biological method, and the effect of absorption and interception in expansive flow BAF had little effect on the removal of those compounds.

Backwashing. Backwashing was conducted after 96 hours operation of expansive flow BAF. Backwashing was an important measure to maintain the purification of BAF and activity of biofilm. Pulse backwashing was used in this study, which was the combination of pulse air and continuous water backwashing. The air intensity was $8.0 \text{ L}/(\text{s}\cdot\text{m}^2)$ and water intensity was $2.5 \text{ L}/(\text{s}\cdot\text{m}^2)$.

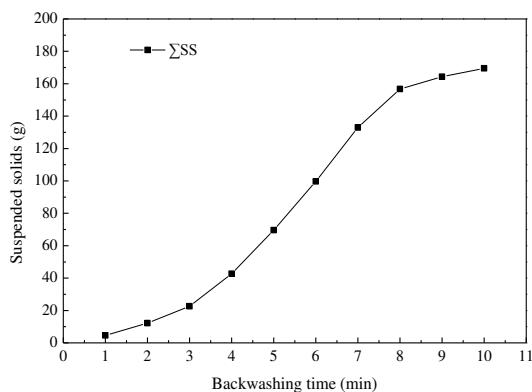


FIGURE 5

Relation between backwashing time and accumulative SS in backwashing liquor

The accumulative suspended solids (SS) content ascended with the prolonging of backwashing time (Fig. 5). The accumulative SS content achieved steady after 10 min backwashing. SS in backwashing liquor rose faster in the first 8 minutes than that in the later 2 minutes. When backwashing began, aging biofilm was washed out of the system along with the backwashing water firstly. Then, the outer biofilm began to be eroded by the effect of shear and friction. When the above two kinds of biofilm had been washed out, the inner active biofilm became the object to be rinsed. The adhesion between inner active biofilm and filter media was firm, therefore inner active biofilm was not easy to fall off. An appropriate backwashing was not only to purify filter layer, but also to update the biofilm, guaranteeing the activity of biofilm and effectiveness of expansive flow BAF for wastewater treatment.

Recovery time of the filter bed after backwashing was another item to evaluate the effect of backwashing. The recovery time was about 5 h when backwashing durations were 6, 7 and 8 minutes (Fig. 6). The recovery time rose to 10 h and 15 h respectively when backwashing time prolonged to 9 minutes and 10 minutes. The appropriate backwashing time was 6-8 minutes, according to the accumulative SS content in backwashing liquor (Fig. 5), and the backwashing time was set to be 6 minutes in this study.

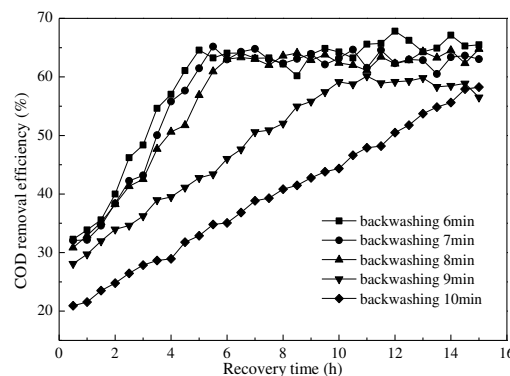


FIGURE 6

Relation between COD removal and filter bed recovery time

CONCLUSIONS

Advanced treatment of coal chemical industry wastewater by expansive flow BAF was performed to remove COD, total phenols, $\text{NH}_4^+\text{-N}$, turbidity and chroma. The high organics removal efficiency demonstrated that expansive flow BAF was an available process for the advanced treatment of coal chemical industry wastewater. The operated cycle was 96 hours. The appropriate backwashing time was 6-8 minutes, with the air intensity of $8 \text{ L}/(\text{s}\cdot\text{m}^2)$ and water intensity of $2.5 \text{ L}/(\text{s}\cdot\text{m}^2)$ in pulse manner.

ACKNOWLEDGEMENTS

This study was financially supported by the open foundation of Hunan Provincial Key Laboratory of Shale Gas Resource Utilization, Hunan University of Science and Technology (No. E21721), the National Science Foundation of China Hunan Province (No. 2016JJ2057).

REFERENCES

- [1] Farabegoli, G., Chiavola, A., Rolle, E. (2009) The Biological Aerated Filter (BAF) as alternative treatment for domestic sewage. Optimization of plant performance. *Journal of Hazardous Materials*, 171(1-3), 1126.
- [2] Jia, X., Zhou, L., Li, Y., Wang, Y., Yue, Y., Wang, G. (2012) Comparative Study of Laboratory-Scale Biological Aerated Filters Based on Macroporous Polyurethane and Haydite Carrier Materials. *Environmental Engineering Science*, 29(5), 350.
- [3] Ji, G., Tong, J., Tan, Y. (2011) Wastewater treatment efficiency of a multi-media biological aerated filter (MBAF) containing clinoptilolite and bioceramsite in a brick-wall embedded design. *Bioresource Technology*, 102(2), 550.
- [4] Gao, X.-Y., Xu, Y., Liu, Y., Liu, Z.-P. (2011)

- Bacterial diversity, community structure and function associated with biofilm development in a biological aerated filter in a recirculating marine aquaculture system. *Marine Biodiversity*, 42(1), 1.
- [5] Feng, Y., Yu, Y., Qiu, L., Zhang, J., Gao, L. (2012) The characteristics and application of grain-slag media in a biological aerated filter (BAF). *Journal of Industrial and Engineering Chemistry*, 18(3), 1051.
- [6] Feng, Y., Qi, J., Chi, L., Wang, D., Wang, Z., Li, K., Li, X. (2013) Production of sorption functional media (SFM) from clinoptilolite tailings and its performance investigation in a biological aerated filter (BAF) reactor. *Journal of Hazardous Materials*, 246-247, 61.
- [7] Liu, Y., Du, F., Yuan, L., Zeng, H., Kong, S. (2010) Production of lightweight ceramsite from iron ore tailings and its performance investigation in a biological aerated filter (BAF) reactor. *Journal of Hazardous Materials*, 178(1-3), 999.
- [8] Seker, D.Z., Yucel, U. (2017) Gis Based Multi-Criteria Decision Analysis for Site Selection of a Wastewater Treatment Plant. *Fresen. Environ. Bull.*, 26(1), 399.
- [9] Hou, B.L., Ren, B.Z., Deng, R.J., Zhu, G.C., Wang, Z.H., Li, Z. (2017) Three-dimensional electro-Fenton oxidation of N-heterocyclic compounds with a novel catalytic particle electrode: high activity, wide pH range and catalytic mechanism. *Rsc Advances*, 7(25), 15455.
- [10] Gargosova, H.Z., Urminska, B. (2017) Assessment of the Efficiency of Wastewater Treatment Plant Using Ecotoxicity Tests. *Fresen. Environ. Bull.*, 26(1), 56.
- [11] Kuriqi, A., Kuriqi, I., Poci, E. (2016) Simulink Programing for Dynamic Modelling of Activated Sludge Process: Aerator and Settler Tank Case. *Fresen. Environ. Bull.*, 25(8), 2891.
- [12] Ai, H.N., Wang, Y.L., Huang, W., He, Q., Zhang, D.J., Lu, P.L. (2015) Pso-Based Parametric Analysis of Slowly Biodegradable Cod Kinetics. *Fresen. Environ. Bull.*, 24(1), 84.
- [13] Wang, Q., Lv, Y.K., Zhang, R., Bi, J.C. (2013) Decomposition of Dyeing Wastewater by Supercritical Water Oxidation. *Fresen. Environ. Bull.*, 22(12), 3588.
- [14] Hou, B., Han, H., Zhuang, H., Xu, P., Jia, S., Li, K. (2015) A novel integration of three-dimensional electro-Fenton and biological activated carbon and its application in the advanced treatment of biologically pretreated Lurgi coal gasification wastewater. *Bioresource Technology*, 196, 721.
- [15] Hou, B.L., Han, H.J., Jia, S.Y., Zhuang, H.F., Xu, P., Li, K. (2016) Three-dimensional heterogeneous electro-Fenton oxidation of biologically pretreated coal gasification wastewater using sludge derived carbon as catalytic particle electrodes and catalyst. *Journal of the Taiwan Institute of Chemical Engineers*, 60, 352.
- [16] Ji, G., Wu, Y., Wang, C. (2012) Analysis of microbial characterization in an upflow anaerobic sludge bed/biological aerated filter system for treating microcrystalline cellulose wastewater. *Bioresource Technology*, 120, 60.
- [17] Chen, Y.-H., Wang, Y.-T., Dai, J.-L., Wang, R.-Q. (2017) Prokaryotic Community Structure And Composition In A Full-Scale Wastewater Treatment System For The High-Efficiency Biodegradation Of Polyvinyl Alcohol. *Fresen. Environ. Bull.*, 26(3), 1847.
- [18] Albuquerque, A., Makinia, J., Pagilla, K. (2012) Impact of aeration conditions on the removal of low concentrations of nitrogen in a tertiary partially aerated biological filter. *Ecological Engineering*, 44, 44.
- [19] Abu Hasan, H., Sheikh Abdullah, S.R., Tan Kofli, N., Kamarudin, S.K. (2012) Effective microbes for simultaneous bio-oxidation of ammonia and manganese in biological aerated filter system. *Bioresource Technology*, 124, 355.
- [20] Sun, F., Sun, W.-L. (2012) A simultaneous removal of beryllium and ammonium–nitrogen from smelting wastewater in bench- and pilot-scale biological aerated filter. *Chemical Engineering Journal*, 210, 263.

Received: 20.11.2016
Accepted: 20.05.2017

CORRESPONDING AUTHOR

Baolin Hou

Hunan Provincial Key Laboratory of Shale Gas Resource Utilization, School of civil engineering, Hunan University of Science and Technology, Xiangtan, 411201, China

e-mail: paishuigou2016@163.com

ADSORPTION BEHAVIOR OF NEUTRAL RED FROM AQUEOUS SOLUTION ONTO NaOH-MODIFIED PEANUT SHELL

Xia Du¹, HongYan¹, Yingjie Dai^{2,*}

¹Key Laboratory of Green Chemical Technology of College of Heilongjiang Province, College of Chemical and Environmental Engineering, Harbin University of Science and Technology, Harbin 150040, China

²Laboratory of Environmental Remediation, College of Resources and Environment, Northeast Agricultural University, No.59 Mucai Street Xiangfang District, Harbin 150030, China

ABSTRACT

Adsorption of neutral red (NR) on the raw peanut shell (PS) and NaOH-modified peanut shell (NaOH-PS) was examined and its' effects of pH was investigated. The removal ratios of NR on PS and NaOH-PS after 2 h were 95.0 and 98.1%, respectively. The removal ratio of NR is increased by increasing the pH value. Equilibrium data fitted very well in a Langmuir isotherm equation, the adsorption capacity of NR onto PS and NaOH-PS were 126.58 mg/g and 192.31 mg/g, respectively. The adsorption mechanisms can be contributed by hydrophobicity interaction at the interface occurs between NR and PS and NaOH-PS. The present study shows that the NaOH-modified peanut shell can be used as an inexpensive, effective and easily used adsorbent for the removal of neutral red from its aqueous solutions.

KEYWORDS:

Neutral red, Langmuir and Freundlich isotherm, Kinetics, Distribution.

INTRODUCTION

Peanuts are a widely planted legume commodity crop worldwide. Peanut shell is an abundant and low cost agricultural waste residue and is easily available in large quantity and its weight reach 10.3 million tons in 2008 all over the world [1]. Most of peanut shells are discarded as solid waste or burned off, resulting in environmental pollution and lost resources. Thus peanut shells are a need to convert these by-products to useful, value-added products. The peanut shell were reported as an adsorbent in the removal of organic and inorganic pollutants. Powder prepared from peanut hull was used for biosorption of three anionic dyes such as amaranth (Am), sunset yellow (SY) and fast green FCF (FG) [2]. The effects of various experimental parameters including initial concentration, pH,

contact time, particle size and ion strength were examined. The study results showed that the maximum adsorption capacities were 14.90 mg/g for Am, 13.99 mg/g for SY and 15.60 mg/g for FG, respectively. The adsorption processes conformed to the pseudo-first-order rate kinetics. Peanut shells were used as a precursor to prepare activated carbon via physical activation with CO₂ for remove methylene blue and phenazone were estimated [3]. The maximum adsorption capacities of methylene blue and phenazone were 225.8 mg/g and 421.5 mg/g, respectively at 5 h (activation time) and 900 °C (activation temperature). The kinetic adsorption model of methylene blue was a pseudo-second-order. Carboxyls and hydroxyls groups on the surface of activated carbon from peanut shells were able to interact with protons and metal or positive dye ions; therefore, the adsorption capacity of the activated carbon from peanut shells was mainly due to the interactions between the positive ions of carboxyls and hydroxyls groups and positive dye ions. Adsorption study of neutral red (NR) onto peanut husk in aqueous solutions was investigated at 22 °C [4]. The adsorption capacity of NR onto peanut husk was determined. The maximum adsorption capacity of NR was 37.5 mg/g. The potential feasibility of peanut hull particle for removal of methylene blue, brilliant cresyl blue and NR from aqueous solution was investigated [5]. The adsorption processes followed the pseudo-first-order rate kinetics. The maximum adsorption capacity of NR was 87.72 mg/g with the *Langmuir* adsorption model. Adsorption of Cr(III) and Cu(II) ions from aqueous solutions by raw peanut shell was investigated [6]. The experimental data were analyzed using Redlich-Peterson and Sips models. The equilibrium biosorption isotherms showed that peanut shells possess high affinity and adsorption capacity was 25.39 mg/g for Cu(II) and 27.86 mg/g for Cr(III) ions, respectively. In this research, to the best of our knowledge, the removal of a NR (a cationic dye, used as an adsorbate) on NaOH-modified peanut shell as an adsorbent have not been reported.

The objective of this study was to investigate the removal of NR onto NaOH-modified peanut shell. The influences of contact time and pH were analyzed. In addition, the kinetics, adsorption isotherms and thermodynamics of NR onto NaOH-modified peanut shell were investigated.

MATERIALS AND METHODS

Materials. The peanut shell (PS) used in this work was obtained from a local market. The PS was washed in running tap water for 1–2 h to remove soil and dirt, and then washed with distilled water several times before drying. In order to investigate the effect of functional groups on the surface of PS, NaOH-modified PS was prepared according to the reported method [7]. PS (10 g) was maintained for 24 h in 250 mL 20% NaOH solution with a stirring speed of 165 rpm and at ambient temperature. The modified PS by NaOH was labeled NaOH-PS. The dried samples were crushed and milled into powder. The particle sizes were less than 25 μm . NR was supplied by Guangfu Institute of Fine Chemical Industry, Tianjin, China. The chemical structures of NR is shown in Fig. 1. Chemical formula of NR and molar mass are $\text{C}_{15}\text{H}_{16}\text{N}_4\text{HCl}$ and 288.78 g/mol, respectively. A stock solution (500 mg/L) was pre-prepared by dissolving NR in deionized water; desired concentrations were obtained when needed by diluting the stock solution with deionized water. All chemicals used in this study were of analytical grade, which solutions were being prepared using deionized and distilled water. To adjust the pH, HCl (0.1M) and NaOH (0.1M) solutions were used.

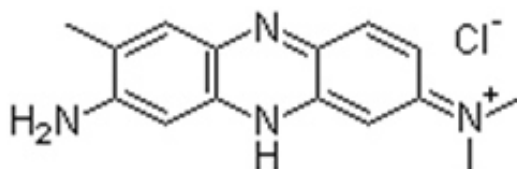


FIGURE 1
The chemical structures of neutral red

Physical and Chemical Characteristics. The surfaces of PS and NaOH-PS were observed by using a Scanning Electron Microscope (SEM), S-3400N (Hitachi Ltd. Tokyo, Japan). The numbers of acidic functional groups and basic sites on the surface of PS and NaOH-PS were determined by using the method developed by Boehm [8]. Acidity was determined by mixing 0.6 g of PS or NaOH-PS with 15 mL of NaHCO_3 (0.1 M), Na_2CO_3 (0.05 M) or NaOH (0.1 M) solution in a well-sealed flask. The mixture was then shaken for 48 h at 25 $^\circ\text{C}$ and 165 rpm. An aliquot of the solution for each sample was back titrated with HCl (0.1 M). The NaHCO_3 neutralizes only the carboxylic groups on the carbon surface, whilst the Na_2CO_3 does the carboxylic and

lactonic, and NaOH reacts with the carboxylic, lactonic and phenolic groups. Accordingly, the difference between the groups neutralized by NaHCO_3 and Na_2CO_3 are lactones, whereas the difference between those neutralized by Na_2CO_3 and NaOH are the phenolic groups. The same procedure was carried out for the mixtures of 0.5 g of the PS or NaOH-PS and 15 mL of HCl (0.1 M) solution to determine the basic sites of the sample surface. The remaining HCl solution was titrated with NaOH (0.1 M) after neutralization. The point of zero charge (pH_{PZC}) for the PS and NaOH-PS were determined using the pH drift method [9]. A 0.01 M NaCl solution was aliquoted (50 mL) into a series of flasks. The initial pH (pH_i) was adjusted from 2 to 12 by the addition of 0.1 M NaOH or HCl. A 0.1 g sample of PS or NaOH-PS was added to each flask, followed by agitation for 48 h. Then, the final pH (pH_f) of the mixtures was measured. The pH_{PZC} was defined as the point at which the curve determined by $\text{pH}_f - \text{pH}_i$ crossed the axis $\text{pH}_i = \text{pH}_f$.

Adsorption experiments. The adsorption features of the adsorbents (PS and NaOH-PS) were investigated as a function of contact time, and initial pH. The adsorption equilibrium and kinetics were obtained from batch experiments, using 100 mL flasks containing 25 mL of NR solutions. After shaking the flasks for predetermined time intervals, the mixture was filtered, and the concentration of NR in the filtrate was determined from the absorbance at 530 nm measured with an ultraviolet visible spectrophotometer V-560 (Jasco Co., Tokyo, Japan). Three replicate runs were carried out for each experimental treatment. The NR amounts on the adsorbents were calculated by difference between the initial and the equilibrium NR concentrations in the solution. The removal ratio was calculated by dividing the amount of NR adsorbed on PS and NaOH-PS by the initial amount of NR in the solution.

Adsorption Kinetics. The controlling mechanism of the adsorption process was investigated using two kinetic models; which were pseudo-first-order and pseudo-second-order models, respectively. The kinetic rate equations can be written as follow,

$$\frac{dq_t}{dt} = (q_e - q_t)^n \quad (1)$$

Where, q_e and q_t correspond to the amount of NR adsorbed per unit mass of adsorbent (mg/g) at equilibrium and at time t , respectively. k_n is the rate constant for nth order adsorption (k_n units are 1/min for $n=1$ and g/mg min for $n=2$). The linearized integrated forms of the equations are shown as follow,

First-order kinetics ($n=1$) and second-order kinetics ($n=2$):

$$\ln(q_e - q_t) = \ln q_e - k_1 t \quad (2)$$

$$\frac{t}{q_t} = \frac{1}{k_2 q_e} + \frac{t}{q_e} \quad (3)$$

The straight-line plots of $\ln(q_e - q_t)$ against t and of t/q_t against t were used to determine the rate constants and correlation coefficients (R^2) for the first and second-order kinetic models, respectively. The fitting equation was selected based on both linear regression R^2 and the calculated q_e values.

RESULTS AND DISCUSSIONS

Physical and Chemical Characteristics of PS and NaOH-PS. The SEM image of PS and NaOH-PS are shown in Fig. 2. There are a few larger surface voids on the surface of PS, however, it's surface have irregular porous and convex structure, while the distribution of a large number of grooves and pores after modified by NaOH solution. Modified sample is more conducive to the internal absorption of NR in water, the adsorption capacity is stronger.

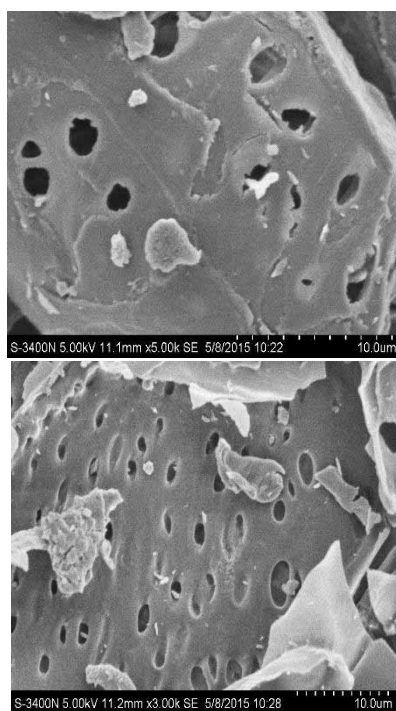


FIGURE 2

SEM photos of PS (up) and NaOH-PS (down).

The functional groups of acidic and basic were measured, and the pH_{PZC} value of PS and NaOH-PS are shown in Table 1. The amount of basic functional groups on NaOH-PS (3.26 mmol/g) was significantly increased than that of untreated PS (1.88 mmol/g). However, the amount of acidic functional groups on NaOH-PS (0.44 mmol/g) was decreased by the treatment of NaOH. The number of

acidic functional groups on NaOH-PS was found to be less than that of untreated PS. Therefore, the surface polarity of NaOH-PS is low, making this material more hydrophobic than that of PS. The pH_{PZC} value of PS and NaOH-PS were 6.99 and 11.75, respectively. The surface charge of samples is depending on the pH of the solution.

Adsorption Kinetics. Fifty milliliter mixtures of NR (50 mg/L) and PS (50 mg) or NaOH-PS (15 mg) were shaken at 165 rpm. Fig. 3 shows the removal ratios of NR on PS and NaOH-PS after 2 h were 95.0 and 98.1%, respectively. The removal ratio of NR on PS and NaOH-PS was reached a plateau after 1h.

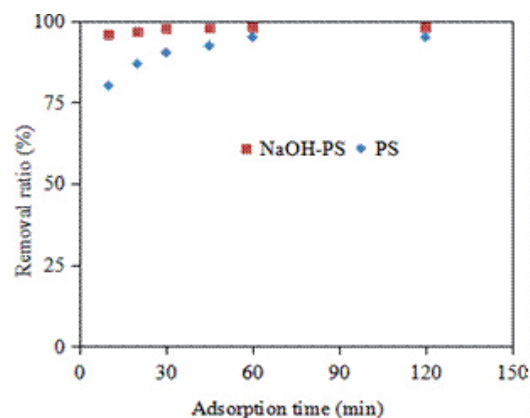


FIGURE 3

Effect of adsorption time on NR adsorption on PS and NaOH-PS

TABLE 1

Physical and chemical properties of PS and NaOH-PS		
	PS	NaOH-PS
Acidic functional groups (mmol/g)	2.18	0.44
carboxylic groups(-COOH)	1.25	0.07
lactonic groups(-COO-)	0.43	0.18
phenolic groups(-OH)	0.50	0.19
Basic functional groups (mmol/g)	1.88	3.26
pH_{PZC} value	6.99	11.75

The controlling mechanism of NR adsorption by PS and NaOH-PS was investigated by fitting first-order models and second-order models. The results of pseudo-second-order kinetic plots are displayed in Fig. 4. The parameter in equation (2) and (3), which was determined from kinetic constants of NR on PS and NaOH-PS are summarized in Table 2. The pseudo-first-order model data do not fall on straight lines. Besides, the calculated q_e values determined from the models differs substantially from those determined experimentally, suggest that the studied adsorption NR on PS and NaOH-PS is not a pseudo-first-order reaction. On the other hand, the R^2 for the pseudo-second-order kinetic model are nearly equal to 1 (see Table 2), and

the calculated q_e values (129.85 mg/g for PS and 196.26 mg/g for NaOH-PS) are acceptable compared to the experimental data (126.58 mg/g for PS and 192.31 mg/g for NaOH-PS). So, this suggests that the adsorption NR on PS and NaOH-PS seems to be more of a pseudo-second-order.

	k_1	Calculated	R^2	Experience
	(1/min)	q_e (mg/g)		q_e (mg/g)
Pseudo-first-order model				
PS	0.2674	48.56	0.9376	126.58
NaOH-PS	1.1866	63.84	0.9583	192.31
Pseudo-second-order model				
	k_2 (g/mg min)			
PS	0.0100	129.85	0.9999	126.58
NaOH-PS	0.0480	196.26	1.0000	192.31

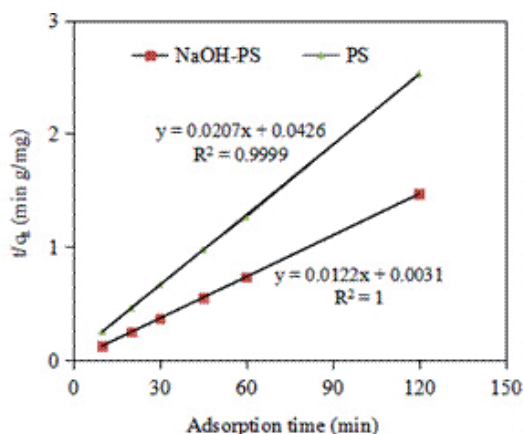


FIGURE 4
Pseudo-second-order kinetic plots of NR on PS and NaOH-PS

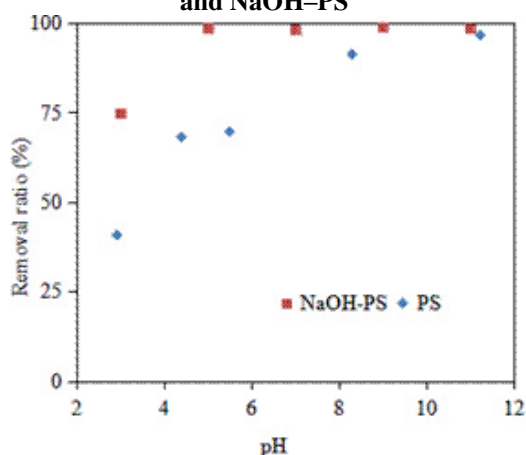


FIGURE 5
Effect of pH for NR adsorption on PS and NaOH-PS

Effect of initial pH. As elucidated in Fig. 5, the NR removal ratios were increased with the increasing of pH in the solution. At low pH values area (about pH 3), the removal ratio of PS and NaOH-PS for NR were 40.7 % and 74.7%, res-

pectively, while at high pH values area (about pH 11) the removal ratio of PS and NaOH-PS for NR were 96.5 % and 98.8%, respectively. There are a few reasons may be attributed to the NR adsorption behavior relative to the solution pH. The surface of samples (PS and NaOH-PS) may contain a large number of active sites and the NR ions uptake can be related to the active sites. At $pH \leq 6.99$, the surface charges of PS and NaOH-PS were positively, thus making H^+ ions compete effectively with positive cations, which results in a decrease in the amount of NR adsorbed. At $pH \geq 6.99$, the surface of PS and NaOH-PS were negatively charged, which enhances the positively charged NR cations with electrostatic attraction.

Adsorption isotherm. Langmuir and Freundlich isotherm models were commonly used to analyze the isotherm data. The relationship between the reciprocal of the amount of NR adsorbed on PS and NaOH-PS and the reciprocal of the equilibrium concentration of NR in the solution was linear.

The parameter in equation (4) and (5), which was determined from the adsorption isotherms of PS and NaOH-PS are summarized in Table 3.

$$q_e = \frac{Q_0 K_L C_e}{1 + K_L C_e} \quad (4)$$

Here, q_e (mg/g) is the amount adsorbed at equilibrium; Q_0 (mg/g), the saturated adsorption amount; K_L (L/mg), the adsorption equilibrium constant of Langmuir isotherm; and C_e (mg/L), the adsorption equilibrium concentration.

$$q_e = K_F C_e^{1/n} \quad (5)$$

where K_F (L/mg) is the empirical constant of Freundlich isotherm; and the constant n is the empirical parameter related to the intensity of adsorption. When $1/n$ values are in the range of 0.1–1, the adsorption process is favorable.

Compared with Freundlich isotherm model, the Langmuir isotherm model yielded a higher correlation coefficient, which was higher than 0.98. Consequently, the Langmuir isotherm fitted the experimental data well, which illuminated that the adsorption mechanism was involved in this NR adsorption process, the surface adsorption sites and adsorption energies of adsorbent was homogenous in its distribution.

The adsorption isothermal curve for NR on PS and NaOH-PS is shown in Fig. 6. Table 3 showed the values of parameters obtained for NR from the Langmuir isotherm Q_0 and K_L were 192.31 mg/g, and 0.8125 L/mg for NaOH-PS and 126.58 mg/g, and 0.1276 L/mg for PS, respectively.

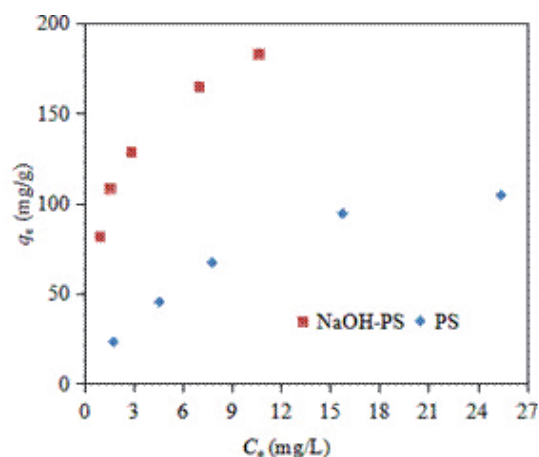


FIGURE 6

Adsorption isothermal curve of NR on the PS and NaOH-PS ($C_0 = 25$ to 150 mg/L, shaking time 2 h, at pH 7.0 and 25 °C).

Langmuir isotherm			
	Q_0 (mg/g)	K_L (L/mg)	R^2
PS	126.58	0.1276	0.9981
NaOH-PS	192.31	0.8125	0.9861
Freundlich isotherm			
	K_F (L/mg)	$1/n$	R^2
PS	21.38	0.4615	0.9674
NaOH-PS	89.68	0.3021	0.9195

The hydrophobic interaction of the adsorbent surface is one of the important determinants of adsorption capacity because water molecules can compete with the adsorbate at the adsorption sites [10, 11]. In order to clarify the effect of functional groups on the surface of samples, the numbers of acidic functional groups and basic sites on the surface of PS and NaOH-PS were determined. The number of acidic functional groups on NaOH-PS was found to be about 20% that of PS (Table 1). The results of the adsorption equilibrium isotherm of NaOH-PS showed that Q_0 and K_L were larger than that of PS (Table 3). NaOH-PS (0.44 mmol/g) has fewer acidic functional groups than PS (2.18 mmol/g). Therefore, the surface polarity of NaOH-PS is low, making this material more hydrophobic. The strong hydrophobicity of the NaOH-PS surface might explain the high adsorption capacity for NR.

The adsorption capacity of adsorbents in this work are compared with various adsorbents in the literature [4, 5, 12–15] as shown in Table 4. The results obtained from this study were found to be higher than that of some adsorbents such as Fe_3O_4 hollow nanospheres (105 mg/g), peanut hull (87.72 mg/g), halloysite nanotubes (54.85 mg/g), peanut husk (37.46 mg/g). Therefore, compared with these materials in Table 4, NaOH-PS used in this study has higher adsorption ability for NR.

Adsorbents	Uptake capacity	References
	(mg/g)	
Mn-impregnated activated carbons prepared from <i>Typha orientalis</i>	198.32	[12]
NaOH-PS	192.31	This study
Spent cottonseed hull substrate	166.70	[13]
PS	126.58	This study
Fe_3O_4 hollow nanospheres	105.00	[14]
Peanut hull	87.72	[5]
Halloysite nanotubes	54.85	[15]
Peanut husk	37.46	[4]

CONCLUSIONS

We examined the adsorption capacity of neutral red from aqueous solution on PS and NaOH-PS. The removal ratio of NR is increased by increasing the pH value. The removal ratios of NR (50 mg/L) on PS and NaOH-PS after 2 h were 95.0 and 98.1%, respectively. Equilibrium data fitted very well in a Langmuir isotherm equation, the adsorption capacity of NR onto PS and NaOH-PS were 126.58 mg/g and 192.31 mg/g, respectively. The adsorption mechanisms can be contributed by hydrophobicity interaction at the interface occurs between NR and PS or NaOH-PS. The present study shows that the NaOH-modified peanut shell can be used as an inexpensive, effective and easily used adsorbent for the removal of neutral red from its aqueous solutions.

ACKNOWLEDGEMENT

The many precious and helpful comments provided by the reviewers of this manuscript are gratefully acknowledged. The authors are grateful for the financial support from the Natural Science Foundation of China (21406043) and the National Science Foundation of Heilongjiang Province of China (C201301).

REFERENCES

- [1] Li, C.G., Dong, L.Y., Ji, Y.Y., Zhu, Y.F., Fang, S.S., (2010) Study on extraction of cellulose and removal of hemicelluloses and lignin from peanut hull, *Chinese Agr. Sci. Bull.*, 26, 350–354
- [2] Gong, R., Ding, Y., Li, M., Yang, C., Liu, H., Sun, Y., (2005) Utilization of powdered peanut hull as biosorbent for removal of anionic dyes from aqueous solution, *Dyes Pig.*, 64, 187–192
- [3] Wu, M., Guo, Q., Fu, G., (2013) Preparation and characteristics of medicinal activated carbon powders by CO_2 activation of peanut shells, *Powder Technol.*, 247, 188–196

- [4] Han, R., Han, P., Cai, Z., Zhao, Z., Tang, M., (2008) Kinetics and isotherms of neutral red adsorption on peanut husk, *J. Environ. Sci.*, 20, 1035–1041
- [5] Gong, R., Li, M., Yang, C., Sun Y., Chen, J., (2005) Removal of cationic dyes from aqueous solution by adsorption on peanut hull, *J. Hazard. Mater.*, B 121, 247–250
- [6] Witek-Krowiak, A., Szafran, R. G., Modelski, S., (2011) Biosorption of heavy metals from aqueous solutions onto peanut shell as a low-cost biosorbent, *Desalination*, 265, 126–134
- [7] Selatnia, A., Bakhti, M. Z., Madani, A., Kertous, L., Mansouri, Y., (2004) Biosorption of Cd²⁺ from aqueous solution by a NaOH-treated bacterial dead *Streptomyces rimosus* biomass. *Hydrometallurgy*, 75, 11–24
- [8] Boehm, H.P., (2002) Surface oxides on carbon and their analysis: a Critical Assessment. *Carbon*, 40, 145–149
- [9] Al-Degs, Y.S., Ei-Barghouthi, M.I., El-Sheikh A.H., Walker, G.M., (2008) Effect of solution pH, ionic strength, and temperature on adsorption behavior of reactive dyes on activated carbon, *Dyes Pig.*, 77, 16–23
- [10] Dai, Y., Zhang, D., Yan, H., Ji, Y., Wu, W., Tanaka, S., (2016) Effects of contact time, solution pH, dosage of adsorbent, ionic strength and regeneration on adsorption behavior of methylene blue on spent coffee grounds, *Fresen. Environ. Bull.*, 25(9), 3417–3422.
- [11] Dai, Y., Zhang, D., Yan, H., Ji, Y., Wu, W., Tanaka, S., (2016) Study on the mechanism of methylene blue adsorption on spent coffee grounds, *Fresen. Environ. Bull.*, 25(9), 3423–3429
- [12] Zhang, J., Shi, Q., Zhang, C., Xu, J., Zhai, B., Zhang, B., (2008) Adsorption of neutral red onto Mn-impregnated activated carbons prepared from typha orientalis, *Bioresource Technol.*, 99, 8974–8980
- [13] Zhou, Q., Gong, W., Xie, C., Yang, D., Ling, X., Yuan, X., Chen, S., Liu, X., (2011) Removal of neutral red from aqueous solution by adsorption on spent cottonseed hull substrate, *J. Hazard. Mater.*, 185, 502–506
- [14] Irama, M., Guo, C., Guan, Y., Ishfaq A., Liu, H., (2010) Adsorption and magnetic removal of neutral red dye from aqueous solution using Fe₃O₄ hollow nanospheres, *J. Hazard. Mater.*, 181, 1039–1050
- [15] Luo, P., Zhao, Y., Zhang, B., Liu, J., Yang, Y., Liu, J., (2009) Study on the adsorption of neutral red from aqueous solution onto halloysite nanotubes, *Water Res.*, 44, 1489–1497

Received: 22.11.2016

Accepted: 23.04.2017

CORRESPONDING AUTHOR

Yingjie Dai

Laboratory of Environmental Remediation, College of Resources and Environment, Northeast Agricultural University, No.59 Mucai Street Xiangfang District, Harbin 150030, China

e-mail: dai5188@hotmail.com

PHOTODEGRADATION OF ENROFLOXACIN UNDER DIFFERENT CONDITIONS IN AQUEOUS SYSTEMS: KINETICS, PRODUCTS AND QUANTUM YIELD

Zheng Wenxiu^{1,2}, Deng Huanhuan^{1,2}, Wang Lan³, Ge Liyun^{1,2,*}, Chen Libo¹

¹School of Public Health and Management, Wenzhou Medical University, Wenzhou, Zhejiang, 325035, China

²Southern Zhejiang Water Research Institute (iWATER), Wenzhou, Zhejiang, 325035, China

³School of Stomatology, Wenzhou Medical University, Wenzhou, Zhejiang, 325035, China

ABSTRACT

The kinetics and products of enrofloxacin (ENR) direct photocatalytic degradation in aqueous solution under high pressure mercury lamp (HPML) were systematically investigated in this paper. The effects of different ENR initial concentrations, pH and light sources and products were explored in this study to assess its ecological fate. The high-performance liquid chromatography (HPLC) - fluorescence detector (FLD) was used to detect the ENR concentrations in the study. And the mass spectrometer (MS) was developed to characterize the main constituents of photodegradation products of ENR. The results showed that ENR degraded fast under the condition that the ENR initial concentration of $2\text{mg}\cdot\text{L}^{-1}$, $\text{pH}=6$ and artificial light with the degradation rate constant (k) of $7.30 \times 10^{-3} \text{ min}^{-1}$, $1.21 \times 10^{-3} \text{ min}^{-1}$ and $4.50 \times 10^{-3} \text{ min}^{-1}$, respectively. Furthermore, according to the analysis of ENR photocatalytic degradation products, the reaction process might include the defluorination, depiperazining, deethylation and methylation. Quantum yield of ENR was measured to be 9.30×10^{-3} in pure water under the irradiation by light emitting diode (LED) lamps. These results would reveal the direct photodegradation kinetics systematically under some reaction conditions in the lab and understand the hydrolysis characteristic to provide primary evidences to further researches.

KEYWORDS:

Enrofloxacin, photodegradation, kinetics, pathways

INTRODUCTION

The widespread and continual application of medicine in the aquatic environment has led to an increasing concern on their fate and risk to the environment in the last decades [1-5]. Antibiotics are also used in aquaculture to inhibit fungal growth and enhance the growth of animals in sub-therapeutic doses [6-9]. According to the researches about pharmaco-

kinetic and pharmacodynamic parameters, the antibiotics could be discharged into waters in the form of parent compounds or metabolites through different pathways [10, 11]. And they have been confirmed to be ubiquitous in surface water bodies [12-15]. In recent years, researches have been reported about the detection of antibiotics in water bodies in China with low concentrations [12-14]. Therefore, the detrimental effects of the antibiotics both on environment and health have raised concerns, and the degradation process of drugs has been the research focus during the last years. Conventional wastewater treatment methods alone are not able to remove pharmaceuticals. Therefore, advanced treatment methods along with conventional methods are essential for removing these contaminants. For this to happen, several advanced treatment methods are used, namely photolysis and chemical oxidation [16, 17].

With the character of broad activity spectrum, fluoroquinolones (FQs), a representative kind of antibiotic medicine, have been widely applied in human medicines, veterinary medicines, and aquaculture [18, 19]. While because of the inefficient elimination by treatment plants, FQs are considered as important aqueous micropollutants [20]. Some investigations about biodegradation of FQs also revealed that they are not readily biodegradable in water [21, 22]. Thus, FQs are defined as 'pseudo persistent' contaminants [23]. But previous studies have demonstrated that photodegradation is considered as an important removal pathway of FQs in waters [24-27].

As a representative FQs, ENR is most frequently used in aquaculture. Its original drug and degradation products can flow into the surface water and soil through rain and irrigation to pose potential threats to human health, environment and ecology. Researches showed that ENR could be accumulated in crop plants, and then transformed into ciprofloxacin both in crop plants and livestock, which was of better antibacterial activity than the original medicine (ENR) [28-31]. What's more, in chicken feces, it had a long half-life at the low concentration of original drug [32]. The photochemical fate of ENR, known to be present in surface waters, was investigated in aqueous solution by exposure to solar light

(summer), and followed first-order kinetics. Studies reported that ENR can effectively be photodegraded by solar light in environmental waters, and the solar quantum yield for ENR was studied at 290–420 nm in pure water [33–36]. The photolysis of ENR involved three main pathways: decarboxylation, defluorination, and piperazinyl N⁴-dealkylation [37].

In this paper, the direct photodegradation behavior of ENR in pure water was systematically investigated. Indirect photochemical behavior of ENR has been investigated in previous studies [32, 38], while direct photocatalytic degradation behavior in aqueous system has not been adequately characterized. Therefore, the photodegradation kinetics, products and quantum yield were measured in this study, aimed to reveal the direct photodegradation kinetics systematically under some reaction conditions in the lab and understand the hydrolysis characteristic to provide primary evidences to further researches.

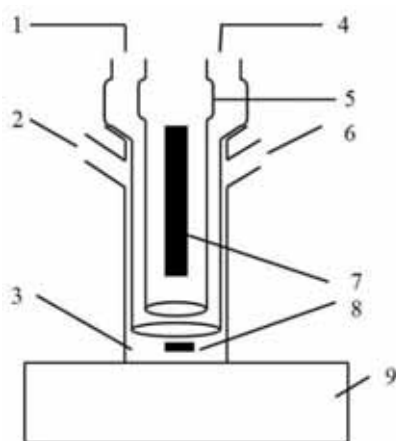


FIGURE 1

Schematic diagram of the photo reactor system: (1) cooling water inlet; (2) injection port; (3) reaction solution; (4) cooling water outlet; (5) cold trap; (6) sample outlet port; (7) lamp; (8) stirring shelf; (9) magnetic stirrer.

MATERIALS AND METHODS

Reagents and materials. Enrofloxacin (C₁₉H₂₂FN₃O₃) (≥ 98%) was purchased from Sigma Chemical Corporation. HPLC grade acetonitrile and methanol were supplied by Aladdin. Phosphoric acid and other reagents used for photolysis studies were of analytical grade. Double distilled water was used in this experiment.

Photodegradation. As shown in Figure 1, reaction was carried out in the photochemical reaction system which consisted of a 250 W high pressure mercury lamp, a stirring shelf and a cooling water jacket. The stirring shelf was controlled by a magnetic stirrer with a counter clock wise rotation. There was a cooling water inlet in the upper port of vessel

for a continuous stream of water. A high pressure mercury lamp (250 W) placed in the center of the reactor was used to be the light source. During the photoreaction, the cooling water pump was set up at 5°C. Samples were gathered at regular intervals of time.

As referred in the previous study [39], quantum yield experiment was conducted in a 250 mL beaker, where the 200 mL solution was placed. Around the beaker, four 15 cm × 15 cm light-emitting diode (LED) lamps were used to irradiate in the near-UV (NUV) region, which average intensity of emitted light was about 0.13 mW•cm⁻². Since the lamps were not calorogenic, the reactions did not require the use of cooling water. Experiment was conducted at room temperature about 25°C.

Sample preparation. The working solutions of ENR were prepared by dilution of the 100 mg•L⁻¹ stock solution with distilled water. Light sources, pH and ENR initial concentrations were investigated for their effects on the photodegradation of ENR. The intensity of illumination of sunlight was determined as 7.89 × 10² Lux in this study. And the light intensity of artificial lamp was 250 W.

Instrumental analysis. ENR concentrations were determined by an Agilent 1260 HPLC with a fluorescence detector (FLD). The column was ZORBAX SB-C18 (4.6 × 150 mm, 5 μm) and the oven temperature was kept at 40°C. The mobile phase was a 10: 20: 70 (V: V: V) mixture of acetonitrile, methanol and acidified water (0.6% phosphoric acid, pH 3.0 adjusted by triethylamine) with a flow rate of 0.8 ml•min⁻¹. The injection volume was 20 μL.

A triple quadrupole (TQD) mass spectrometer with an electrospray ionization (ESI) source coupled to a UPLC system was used in positive ESI mode. Chromatographic separation was carried out using a CSH column (2.1 × 100 mm, 1.7 μm) with the temperature of 45°C. The injection volume and mode were 0.5 μL and full loop, respectively. An optimized gradient was used at a flow rate of 0.3 ml•min⁻¹ using 0.1% formic acid in water (A) and acetonitrile (B). The capillary was set at 3.0 kV. The source and desolvation temperature were set at 100°C and 400°C, respectively. The cone and desolvation gas flow were at 50 L•h⁻¹ and 500 L•h⁻¹, respectively.

RESULTS AND DISCUSSION

Effect of initial concentrations. The effect of initial concentrations on the degradation rate was investigated at different ENR concentrations with solution pH = 8 (Fig. 2). As shown in Figure 2, at the initial concentration of 1 mg•L⁻¹ in dark conditions, ENR was observed to decrease from 1 mg•L⁻¹ to 0.90 mg•L⁻¹. But when exposed to the mercury lamp,

ENR degraded rapidly, with the concentration changing from $1 \text{ mg}\cdot\text{L}^{-1}$ to $0.34 \text{ mg}\cdot\text{L}^{-1}$. Based on the curve in Figure 2, ENR degraded most rapidly at the concentration of $2 \text{ mg}\cdot\text{L}^{-1}$. And the degradation rate decreased with the increasing of initial concentrations.

Correlation coefficients (r^2) for the linear regression of C_t and time were more than about 0.95, which indicated that photodegradation process followed pseudo-first-order kinetics. In order to assess the degradation half lives ($t_{1/2}$) in water, the photodegradation rate constants (k) were further calculated in this experiment system (Table 1), which ranged from $0.6 \times 10^{-3} \text{ min}^{-1}$ to $7.3 \times 10^{-3} \text{ min}^{-1}$. Under the irradiation of artificial illumination, with the increasing of initial concentration from $1 \text{ mg}\cdot\text{L}^{-1}$ to $6 \text{ mg}\cdot\text{L}^{-1}$, degradation rates increased firstly and then decreased with the peak value at $2 \text{ mg}\cdot\text{L}^{-1}$.

As for the negative effect of initial concentration on the kinetics, the reason was proposed that light transmission was attenuated when the concentration was high enough [39]. Another study attributed this phenomenon to self sensitization via ROS (reactive oxygen species), such as hydroxyl radical ($\cdot\text{OH}$) [41]. H_2O and dissolved O_2 play the

role of quenchers of triplet excited FQs and are transformed into $\cdot\text{OH}$ to inhibit direct photodegradation [42]. Therefore, the competitive reactions may lead to the negative effect of initial concentration.

Influence of pH. With respect to the kinetics, the pH greatly affects the photolysis of FQs [43]. The effect of pH on the fate of ENR in the environment was investigated in this study at the concentration of $2 \text{ mg}\cdot\text{L}^{-1}$. Results in Table 2 demonstrated that pH could significantly influence the photolytic rate constant (k). Along with the change of pH of the initial solution from 6 to 10, the k value of ENR decreased from 1.21×10^{-2} to $7.20 \times 10^{-3} \text{ min}^{-1}$.

In this experiment, as shown in Figure 3, the photo degradation behavior of ENR with different pH indicated that the ENR degradation rate decreased with the increasing of pH. In view of the chemical characteristic, ENR is an amphoteric compound. The pK_a values of its acidic and basic functional groups were 5 and 9, respectively [44]. So this result highlighted that the state of ionization of ENR could be an important factor to affect the photo degradation process.

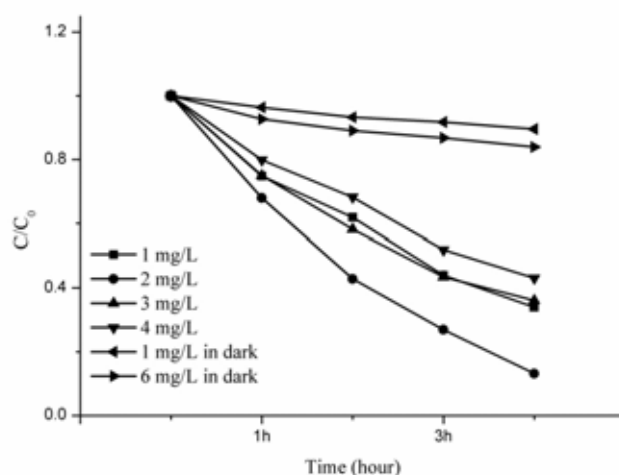


FIGURE 2
ENR photocatalytic degradation at different initial concentrations

TABLE 1
ENR photocatalytic degradation at different initial concentrations

Initial concentrations ($\text{mg}\cdot\text{L}^{-1}$)	First order reaction kinetic equation	k (min^{-1})	$t_{1/2}$ (min)
1	$C_t = e^{-0.0045t}$	0.0045	154.03
2	$C_t = 2e^{-0.0073t}$	0.0073	94.95
4	$C_t = 4e^{-0.0045t}$	0.0045	154.03
6	$C_t = 6e^{-0.0035t}$	0.0035	198.04
1 (in dark)	$C_t = e^{-0.0006t}$	0.0006	1155.25
6 (in dark)	$C_t = 6e^{-0.0010t}$	0.0010	693.15

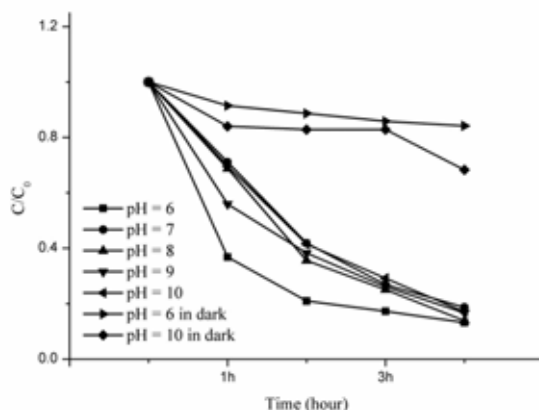


FIGURE 3
ENR photocatalytic degradation with different pH

TABLE 2
ENR photocatalytic degradation with different pH

pH	reaction kinetic equation	k (min^{-1})	$t_{1/2}$ (min)
6	$C_t = 2e^{-0.0121t}$	0.0121	57.28
7	$C_t = 2e^{-0.0072t}$	0.0072	96.27
8	$C_t = 2e^{-0.0075t}$	0.0077	90.02
9	$C_t = 2e^{-0.0077t}$	0.0082	84.53
10	$C_t = 2e^{-0.0082t}$	0.0072	96.27
6 (in dark)	$C_t = 2e^{-0.0072t}$	0.0008	866.43
10 (in dark)	$C_t = 2e^{-0.0014t}$	0.0014	495.11

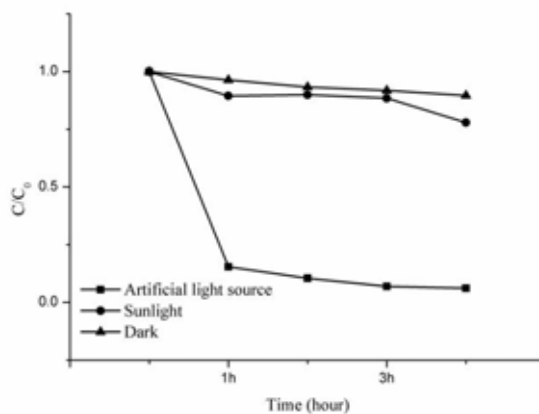


FIGURE 4
ENR photocatalytic degradation under different irradiation conditions

TABLE 3
ENR photocatalytic degradation under different irradiation conditions

Light source	reaction kinetic equation	k (min^{-1})	$t_{1/2}$ (min)
Sunlight	$C_t = e^{-0.0011t}$	0.0011	630.13
Mercury lamp	$C_t = e^{-0.0045t}$	0.0045	154.03
dark	$C_t = e^{-0.0006t}$	0.0006	1155.25

Light sources. The results showed in Figure 4 indicated that the presence of light significantly accelerated the degradation process of ENR. As shown in Table 3, the k value was $0.6 \times 10^{-3} \text{ min}^{-1}$ in dark, while which were $1.1 \times 10^{-3} \text{ min}^{-1}$ and $4.5 \times 10^{-3} \text{ min}^{-1}$ under sunlight and high pressure mercury lamp (250 W), respectively. Artificial illumination in this experiment was of higher intensity than sunlight, which partly showed that the photo degradation rate had a positive effect with light intensity. Furthermore, in view of the structure of ENR, benzene ring and carboxyl consist of a group which is of great photon absorption ability. Due to the stronger intensity of light leading to higher photon absorption, the drugs degraded more rapidly [45]. So the intensity of the light source played a crucial role in the degradation process of ENR. Hence, the photodegradation was not only affected by the initial concentration and pH, but also the light intensity, which could be influenced by the geography and climate across the globe.

LC/MS analysis. Since previous work gave no evidence for ENR photodegradation products for 4 hours, data of this study showed the existence of only one identifiable product after 4 hours irradiation, based on the analysis of the total ion chromatogram (TIC) and the corresponding mass spectra.

The reaction process might include the defluorination, depiperazining, deethylation and methylation. As a representative FQs, the pathways were corresponding to the main process in the hydrolytic reaction of FQs [46]. In the defluorination process of FQs in position 6, the mechanism was the photo-induced nucleophilic substitution reaction, which also happened in ENR photodegradation. Quantum yield of ENR in defluorination was higher than other FQs, which was of a positive effect with the defluorination ability [47]. The proposed pathways of ENR photodegradation were inferred in Figure 6 [48, 49].

According to the previous reported pathways, the following interpretations were provided [24]. Firstly, defluorination destroyed the core structures to generate product A, which induced decreased antibacterial activity. It was also the primary process according to the open literature related FQs, and could be followed by oxidative degradation of ethylpiperazine side chain, leading to product C, E and B. What's more, product B and product E were generated through parallel paths. Side-chain oxidation of A generated product C. Mentioned above were consumed within 1 hour. Further degradation involved the stepwise degradation of the side chain with the oxidation of the benzo ring and pyridone ring. Reduction and substitution processes were showed in Fig. 6. According to these pathways, the final product was proposed to be product 5 (Fig. 6).

However, the product showed in Figure 5 in this study with m/z 278 was far different from product 5. It could result from *ipso* attack (the attachment

to a position in an aromatic compound already carrying a substituent group) by $\bullet\text{OH}$, and next hydroxylation [48].

MS data of ultimate products after 4 hours were detected but the structures need to be further studied in next works.

Quantum yield. Φ value is defined as the number of photons emitted (at all wavelengths) divided by the number of photons absorbed by the fluorescing system, and reflects the efficiency of photodegradation process that takes place in a system. For determination of photodegradation quantum yield, the equations were employed as below [39]:

$$\Phi = \frac{N_s}{N_{Abs}} = \frac{N_s}{I_{irr} \cdot f_{Abs}} \quad (1)$$

$$f_{Abs} = \frac{I_{irr} - I_{out}}{I_{irr}} = 1 - e^{-Abs} \quad (2)$$

$$\Phi = \frac{N_s}{I_{irr}} \frac{1}{1 - e^{-Abs}} \quad (3)$$

$$N_s = N_A \times v \quad (4)$$

v ($\mu\text{M} \cdot \text{min}^{-1}$) is the photodegradation rate of ENR. Avogadro's constant N_A is $6.02 \times 10^{23} \text{ mol}^{-1}$. Because the main peak wavelength of LED lamps (λ_{max}) is at 394 nm, Abs is the absorption value of sample at 394 nm. I_{irr} is the light quantum of incident light. The Radiometer was used to measure radiation intensity. The photo flux emitted by the lamp, measured by a radiometer leaned against the external wall of the photo reactor was $6.125 \times 10^3 \text{ mW} \cdot \text{m}^2$.

According to the measurement results of the photodegradation, quantum yield of ENR in this experiment was calculated to be 9.30×10^{-2} .

CONCLUSIONS

The impact factors on ENR direct photodegradation kinetics in pure water and product analysis were investigated in this research. The results showed that due to the self-sensitization via ROS (reactive oxygen species), such as hydroxyl radical ($\bullet\text{OH}$), ENR degraded fastest at the concentration of $2 \text{ mg} \cdot \text{L}^{-1}$ in this study. When the concentration of ENR exceeded $2 \text{ mg} \cdot \text{L}^{-1}$, the k value showed a negative effect with initial concentrations.

The relationship between pK_a of ENR functional groups and the k value indicated that the state of ionization of ENR was an important factor to affect the photo degradation rate by the change of pH of the reaction solution.

Under the irradiation of mercury lamp, the k value of ENR was four times as much as the value in the sunlight, and even eight times as in dark condition. Hence, photolysis could be considered as an effective removal pathway of ENR in pure water.

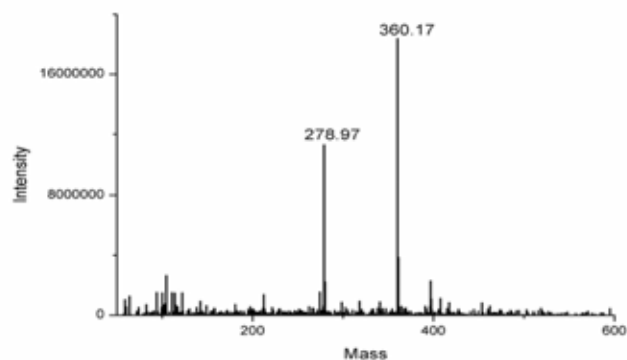


FIGURE 5
Mass spectra of photodegradation products of ENR

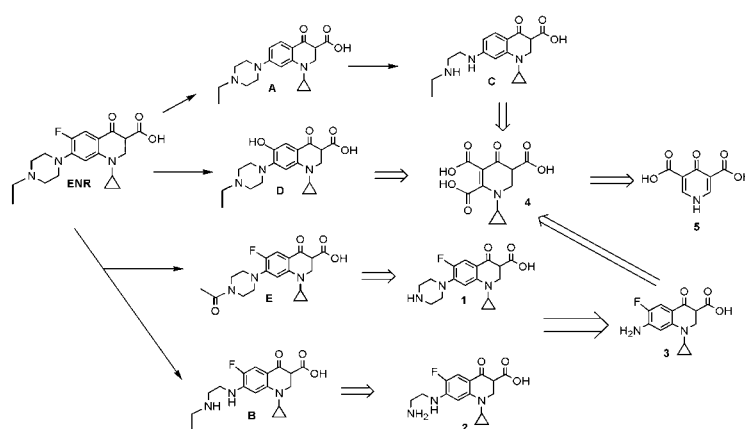


FIGURE 6
Analysis of ENR photocatalytic degradation pathways

Furthermore, according to the product analysis of ENR photocatalytic degradation, the reaction process might include the defluorination, depiperazine ring, deethylation and methylation. And the structures of products need further analysis in next studies. Quantum yield of ENR was calculated to be 9.30×10^{-2} in the system of pure water in this experiment.

ACKNOWLEDGEMENTS

This work was financed by the National Natural Science Foundation of China (Grant No.: 51108351 and 51108350) and Zhejiang Provincial Natural Science Foundation (LY14D060009, LY17E090006), Wenzhou Municipal Science and Technology Bureau (S20140034, S20140036).

REFERENCES

- [1] An, T., Yang, H., Li, G., Song, W., Cooper, W.J. and Nie, X. (2010) Kinetics and mechanism of advanced oxidation processes (AOPs) in degradation of ciprofloxacin in water. *Applied Catalysis B*, 94(3-4), 288-294.
- [2] Sturini, M., Speltini, A., Maraschi, F., Pretail, L., Profumo, A., Fasani, E., Albini, A., Migliavacca, R. and Nucleo, E. (2012) Photodegradation of fluoroquinolones in surface water and antimicrobial activity of the photoproducts. *Water Research*, 46(17), 5575-5582.
- [3] Lin, J.S., Pan, H.Y., Liu, S.M. and Lai, H.T. (2010) Effects of light and microbial activity on the degradation of two fluoroquinolone antibiotics in pond water and sediment. *Journal of Environmental Science and Health, Part B*, 45(5), 456-465.
- [4] Kim, Y., Jung, J., Kim, M., Park, J., Boxall, A.B.A. and Choi, K. (2008) Prioritizing veterinary pharmaceuticals for aquatic environment in Korea. *Environmental Toxicology and Pharmacology*, 26(2), 167-176.

- [5] Pico, Y. and Andreu, V. (2007) Fluoroquinolones in soil-risks and challenges, *Analytical and Bioanalytical Chemistry*, 387(4), 1287-1299.
- [6] Martinsen, B. and Horsberg, T.E. (1995) Comparative single-dose pharmacokinetics of four quinolones, oxolinic acid, flumequine, sarafloxacin, and ENR, in Atlantic salmon (*Salmo salar*) held in seawater at 10 degrees C. *Antimicrobial Agents and Chemotherapy*, 39(5), 1059-1064.
- [7] Schilling, J.B., Cepa, S.P., Menacherry, S.D., Bavda, L.T., Heard, B.M. and Stockwell, B.L. (1996) Liquid chromatography combined with tandem mass spectrometry for the confirmation of sarafloxacin in catfish tissue. *Analytical Chemistry*, 11(68), 1905-1909.
- [8] Thiele-Bruhn, S. (2003) Pharmaceutical antibiotic compounds in soils - a review. *Journal of Plant Nutrition and Soil Science*, 2(166), 145-167.
- [9] Halling-Sorensen, B., Nors Nielsen, S., Lanzky, P. F., Ingerslev, F., Holten Lutzhof, H.C. and Jorgensen, S.E. (1998) Occurrence, fate and effects of pharmaceutical substances in the environment - A review. *Chemosphere*, 2(36), 357-394.
- [10] Heinen, E. (2002) Comparative serum pharmacokinetics of the fluoroquinolones ENR, difloxacin, marbofloxacin, and orbifloxacin in dogs after single oral administration. *Journal of Veterinary Pharmacology and Therapeutics*, 1(25), 1-5.
- [11] Kemper, N. (2008) Veterinary antibiotics in the aquatic and terrestrial environment. *Ecological Indicators*, 1(8), 1-13.
- [12] Liang, X., Chen, B., Nie, X., Shi, Z., Huang, X. and Li, X. (2013) The distribution and partitioning of common antibiotics in water and sediment of the Pearl River Estuary, South China. *Chemosphere*, 11(92), 1410-1416.
- [13] Chen, K. and Zhou, J.L. (2014) Occurrence and behavior of antibiotics in water and sediments from the Huangpu River, Shanghai, China. *Chemosphere*, 95(5), 604-612.
- [14] Luo, Y., Xu, L., Rysz, M., Wang, Y., Zhang, H. and Alvarez, P.J. (2011) Occurrence and transport of tetracycline, sulfonamide, quinolone, and macrolide antibiotics in the Haihe River Basin, China. *Environmental Science and Technology*, 45(5), 1827-1833.
- [15] Schwarzenbach, R.P., Escher, B.I., Fenner, K., Hofstetter, T.B., Johnson, C.A., von Gunten, U. and Wehrli, B. (2006) The challenge of micropollutants in aquatic systems. *Science*, 313(5790), 1072-1077.
- [16] Dolar, D., Kosutic, K., Perisa, M. and Babic, S. (2013) Photolysis of enrofloxacin and removal of its photodegradation products from water by reverse osmosis and nanofiltration membrane. *Separation and Purification Technology*, 115, 1-8.
- [17] Keisuke, I., Naghashkar, J. N. and Gamal El-Din, M. (2006) Degradation of aqueous pharmaceuticals by ozonation and advanced oxidation processes: A review. *Ozone: Science and Engineering*, 28(6), 353-414.
- [18] Paul, T., Miller, P.L. and Strathmann, T.J. (2007) Visible-Light-Mediated TiO₂ photocatalysis of Fluoroquinolone Antibacterial Agents. *Environmental Science and Technology*, 41(13), 4720-4727.
- [19] Zhang, H. and Huang, C.-H. (2005) Oxidative transformation of fluoroquinolone antibacterial agents and structurally related amines by manganese oxide. *Environmental Science and Technology*, 39(12), 4474-4483.
- [20] Chen, C., Zhang, H., Ying, G. and Jones, K.C. (2013) Evidence and recommendations to support the use of a novel passive water sampler to quantify antibiotics in wastewaters. *Environmental Science and Technology*, 47(23), 13587-13593.
- [21] Kummerer, K. (2003) Significance of antibiotics in the environment. *Journal of Antimicrobial Chemotherapy*, 52(1), 5-7.
- [22] Alexy, R., Kumpel, T. and Kummerer, K. (2004) Assessment of degradation of 18 antibiotics in the closed bottle test. *Chemosphere*, 57(6), 505-512.
- [23] Hu, X., Luo, Y. and Zhou, Q. (2010) Simultaneous analysis of selected typical antibiotics in manure by microwave-assisted extraction and LC-MS. *Chromatographia*, 71(3), 217-223.
- [24] Sturini, M., Speltini, A., Maraschi, F., Profumo, A., Pretali, L., Fasani, E. and Albini, A. (2010) Photochemical degradation of marbofloxacin and ENR in natural waters. *Environmental Science and Technology*, 44(12), 4564-4569.
- [25] Li, Y., Niu, J. and Wang, W. (2011) Photolysis of ENR in aqueous systems under simulated sunlight irradiation: Kinetics, mechanism and toxicity of photolysis products. *Chemosphere*, 85(5), 892-897.
- [26] Lam, M.W. and Mabury, S.A. (2005) Photodegradation of the pharmaceuticals atorvastatin, carbamazepine, levofloxacin, and sulfamethoxazole in natural waters. *Aquatic Sciences*, 67(2), 177-188.
- [27] Andreozzi, R., Raffaele, M. and Nicklas P. (2003) Pharmaceuticals in STP effluents and their solar photodegradation in aquatic environment. *Chemosphere*, 50, 1319-1330.
- [28] Intorre, L., Mengozzi, G., Bertini, S., Bagliacca, M., Luchetti, E. and Soldani, G. (1997) The plasma kinetics and tissue distribution of ENR and its metabolite ciprofloxacin in the Muscovy duck. *Veterinary Research Communications*, 21(4), 240.
- [29] Migliore, L., Cozzolino, S. and Fiori, M. (2003) Phytotoxicity to and uptake of enrofloxacin in

- crop plants. *Chemosphere*, 52(7), 1233-1244.
- [30] Dosogne, H., Meyer, E., Sturk, A., van Loon, J., Massart-Leen, A.M. and Burvenich, C. (2002) Effect of enrofloxacin treatment on plasma endotoxin during bovine *Escherichia coli* mastitis. *Inflammation Research*, 51(4), 201-205.
- [31] Otero, J.L., Mestorino, N. and Errecalde, J.O. (2009) Pharmacokinetics of enrofloxacin after single intravenous administration in sheep. *Revue Scientifique et Technique*, 28, 1129.
- [32] Wu, Y., Wang, Z. and Liao, X. (2005) Study on the excretion of enrofloxacin and its degradation in chicken feces. *Acta Veterinaria Et Zootechnica Sinica*, 36(10), 1069-1074 (in Chinese)
- [33] Wammer, K.H., Korte, A.R. Lundeen, R.A., Sundberg, J.E., McNeill, K. and Arnold, W.A. (2013) Direct photochemistry of three fluoroquinolone antibacterials: Norfloxacin, ofloxacin, and enrofloxacin. *Water Research*, 47(1), 439-448.
- [34] Ge, L., Chen, J., Wei, X., Zhang, S., Qiao, X., Cai, X. and Xie, Q. (2010) Aquatic Photochemistry of Fluoroquinolone Antibiotics: Kinetics, Pathways, and Multivariate Effects of Main Water Constituents. *Environ. Sci. Technol.*, 44(7), 2400-2405.
- [35] Sturini, M., Speltini, A., Maraschi, F., Profumo, A., Tarantino, S.C., Gualtieri, A.F. and Zema, M. (2016) Removal of fluoroquinolone contaminants from environmental waters on sepiolite and its photo-induced regeneration. *Chemosphere*, 150, 686-693.
- [36] Sturini, M., Speltini, A., Maraschi, F., Profumo, A., Pretali, L., Fasani, E. and Albini, A. (2010) Photochemical Degradation of Marbofloxacin and Enrofloxacin in Natural Waters. *Environmental Science and Technology*, 44(12), 4564-4569.
- [37] Li, Y., Niu, J. and Wang, W. (2011) Photolysis of Enrofloxacin in aqueous systems under simulated sunlight irradiation: Kinetics, mechanism and toxicity of photolysis products. *Chemosphere*, 85(5), 892-897.
- [38] Sturini, M., Speltini, A. and Maraschi, F. (2015) Sunlight photodegradation of marbofloxacin and ENR absorbed on clay minerals. *Journal of Photochemistry and Photobiology. A: Chemistry*, 299(15), 103-109.
- [39] Xu, J., Li, J., Wu, F. and Zhang, Y. (2014) Rapid Photooxidation of As (III) through Surface Complexation with Nascent Colloidal Ferric Hydroxide. *Environmental Science and Technology*, 48(1), 272-278.
- [40] Lau, T.K., Chu, W. and Graham, N.J.D. (2005) The degradation of endocrine disruptor di-n-butyl phthalate by UV irradiation: A photolysis and product study. *Chemosphere*, 60(8), 1045-1053.
- [41] Li, K., Zhang, P., Ge, L., Ren, H., Yu, C., Chen, X. and Zhao, Y. (2014) Concentration - dependent photodegradation kinetics and hydroxyl-radical oxidation of phenicol antibiotics. *Chemosphere*, 111(20), 278-282.
- [42] Ji, Y., Zhou, L., Zhang, Y., Ferronato, C., Brigante, M., Mailhot, G., Yang, X. and Chovelon, J.-M. (2013) Photochemical degradation of sunscreen agent 2-phenylbenzimidazole-5-sulfonic acid in different water matrices. *Water Research*, 47(15), 5865-5875.
- [43] Fasani, E., Rampi, M. and Albini, A. (1999) Photochemistry of some fluoroquinolones: effect of pH and chloride ion. *Journal of the Chemical Society*, 30(52), 1901-1907.
- [44] Wan, M. and Hong, H. (2013) Determination of solubility of Enrofloxacin Hydrochloride in water. *Journal of Domestic Animal Ecology*, 34(12), 45-49.
- [45] Prabhakaran, D., Sukul, P., Lamshoft, M., Maheswari, M.A., Zühlke, S. and Spittler, M. (2009) Photolysis of difloxacin and sarafloxacin in aqueous systems. *Chemosphere*, 77(6), 739-746.
- [46] Ge, L., Chen, J. and Zhang, S. (2009) Effects of Aqueous Dissolved Matter on Photodegradation of Phenicol and Fluoroquinolone Antibiotics. Dalian: Dalian. University of Technology, 71-104.
- [47] Albini, A. and Monti, S. (2003) Photophysics and photochemistry of fluoroquinolones. *Chemical Society Reviews*, 32(4), 238-250.
- [48] Santoke, H., Tong, A.Y.C., Mezyk, S.P. and Peake, B.M. (2015) UV Photodegradation of Enoxacin in Water: Kinetics and Degradation Pathways. *Journal of Environmental Engineering*, 141(10), 04015027.
- [49] Sturini, M., Speltini, A., Maraschi, F., Profumo, A., Pretali, L., Fasani, E. and Albini, A. (2012) Sunlight-induced degradation of soil-adsorbed veterinary antimicrobials Marbofloxacin and Enrofloxacin. *Chemosphere*, 86(2), 130-137.

Received: 26.11.2016

Accepted: 27.05.2017

CORRESPONDING AUTHOR

Ge Liyun

Wenzhou Medical University
 School of Public Health and Management
 Southern Zhejiang Water Research Institute
 (iWATER)
 325035, Wenzhou, Zhejiang – CHINA

E-mail: glymail@163.com

REMOVAL OF Hg⁰ FROM SIMULATED FLUE GAS BY MAGNETIC SILVER-LOADED FIBER

Ru Yang, Jinghong Wang, Yongfa Diao*, Yan Zhao, Zhannan Lian

College of Environmental Science and Engineering, Donghua University, Shanghai 201620, China

ABSTRACT

The magnetic silver-loaded polytetrafluoroethylene (PTFE) fiber was employed to remove mercury (Hg⁰) in simulated flue gas. Factors affecting Hg⁰ removal efficiency (including inlet Hg concentration, reaction temperature and partial flue gas components) were studied. Results showed that the Hg⁰ removal efficiency showed nonlinear trend with the increasing inlet Hg concentration. Besides, the Hg⁰ removal efficiency increased from 52.6% to 76.5% when the reaction temperature increased from 25°C to 160°C, but had a negative effect with further reaction temperature increase. When 100ppm and 300ppm of NO were added to the N₂ gas stream, the Hg⁰ removal efficiency increased from 70.5% to around 71.8% and 73.2%, however, in the presence of 4% O₂, the efficiency to around 74.8%. When 15ppm and 45ppm of HCl were added to the pure N₂ gas stream, the Hg⁰ removal efficiency increased from 70.5% to 80.5% and 81.4%, the efficiency to around 85.6% when the presence of 4% O₂. When 200ppm and 500 ppm of SO₂ to the pure N₂ gas stream, the Hg⁰ removal efficiency decreased from 70.5% to 62.4% and 49.5%, the efficiency was around 65.8% when added 4% O₂. Therefore, NO and HCl could enhance the mercury removal efficiency, but SO₂ hindered Hg⁰ removal. Furthermore, the magnetic silver-loaded PTFE fiber could be regenerated and repeatedly used for about five times.

KEYWORDS:

Magnetic silver-loaded polytetrafluoroethylene fiber, Hg⁰, Removal efficiency, Regeneration

INTRODUCTION

One of the major sources of atmospheric mercury deposition is the flue gas from coal-fired plant, choosing a cheap but efficient sorbent for mercury removal is critical. Nowadays, the regenerable sorbents for mercury removal can be classified into noble metals and transition metals, etc. Pd was loaded on the adsorbent [1, 2], Ag and Au were also loaded on the adsorbent [3-8]. Solution impregnation and thermal decomposition were used to remove

mercury [9-12]. At higher temperatures, Hg⁰ removal efficiency and adsorption capacity of most of the adsorbent materials will be lower, they are non-renewable and deactivated when they react with the flue gas components [13].

Many researchers [14, 15] have studied Hg⁰ removal efficiency of different sorbents in the simulated flue gas, they found it was closely related to the temperature and composition of gases like O₂, HCl, NO, and SO₂. However, they have not reached a consensus about the removal mechanism. It is considered that O₂ and HCl could promote the conversion of Hg⁰ in the flue gas [16], the HgSO₄ may be formed at low concentration of SO₂ [17]. Therefore, in order to improve the efficiency of Hg⁰ removal from a coal-fired power plants flue gases, it is very important to study the mechanism of oxidation and adsorption of Hg⁰ under different conditions.

In this work, we used magnetic silver-loaded fiber as the sorbent for Hg⁰ removal, which the fiber was used in bag filter. Studying the efficiency of the fiber in simulated flue gas under different conditions, such as different inlet Hg concentrations, reaction temperatures, gas compositions (HCl, NO, SO₂), as well as the adsorption and influence mechanism was discussed.

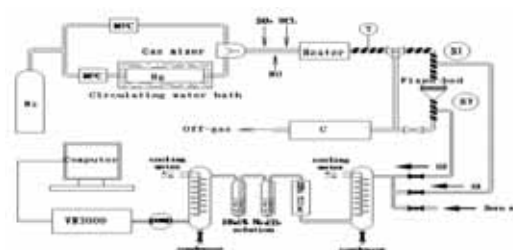


FIGURE 1
Schematic diagram of mercury fixed-bed experimental setup

MATERIALS AND SETUP

Experimental setup. The experimental device setup, as shown in Figure 1, uses a mercury fixed-bed system consisting of Hg⁰ vapor production system, mass flow control system, flue gas heating system, a fixed bed reaction system, and exhaust gas

treatment system, etc.

A constant flow rate in various gas components was maintained by using a flow controller with a valve and a mass flow controller. The temperature was provided by an electric heating element (K-type thermocouple, accuracy was $\pm 1^\circ\text{C}$). Reactor outlet gas was detected online by mercury concentration detector (VM3000 mercury concentration detector, the accuracy was $0.1\mu\text{g}/\text{m}^3$, Mercury Instruments company, Germany). The mercury vapor setup produced the desired mercury vapor under constant water bath heating conditions. Nitrogen gas (N_2) was used as the carrier gas to carry the elemental mercury vapor into the experimental system piping. An adsorption tank equipped with activated charcoal filter element was used as an exhaust gas treatment section to prevent the mercury from being adsorbed to the environment. An adsorption tank equipped with activated carbon was used as the tail gas treatment section for adsorbing mercury which was not adsorbed.

The mercury removal efficiency could be calculated by comparison between inlet and outlet total mercury concentration as following equation:

$$\eta = \frac{[\text{Hg}^0]_{\text{in}} - [\text{Hg}^0]_{\text{out}}}{[\text{Hg}^0]_{\text{in}}} \quad (1)$$

Where η is mercury removal efficiency (%), $[\text{Hg}^0]_{\text{in}}$ and $[\text{Hg}^0]_{\text{out}}$ stands for the inlet and outlet concentration of mercury (Hg^0 and Hg^{2+}), respectively.

Experimental materials. Electing 1g glass fiber, 1g polyphenylene sulfone terephthalamid (PSA) fiber, 1g polyimide (P84) fiber, 1g Polyphenylene sulfide(PPS) fiber, and 1g Polytetrafluoroethylene(PTFE) fiber as adsorbents. All the fibers used in the experiment were pretreated with HCl and loaded with magnetic silver [18].

RESULTS AND DISCUSSION

Hg^0 removal efficiency of different magnetic silver-loaded fibers. Electing 1g glass, PSA, PPS, P84 and PTFE as adsorbents, simulated flue gas temperature was 160°C , flue gas flow rate was 3L/min and mercury inlet concentration was about $45\mu\text{g}/\text{m}^3$. Effects of various magnetic silver-loaded fibers on Hg^0 removal efficiency is shown in Fig. 2.

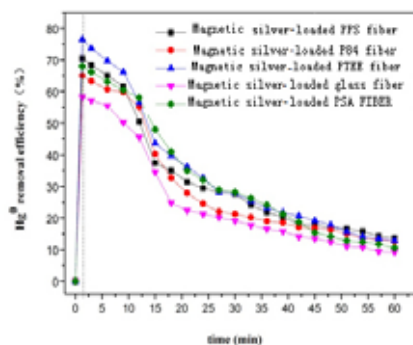


FIGURE 2
Effect of different magnetic silver-loaded fibers on Hg^0 removal efficiency

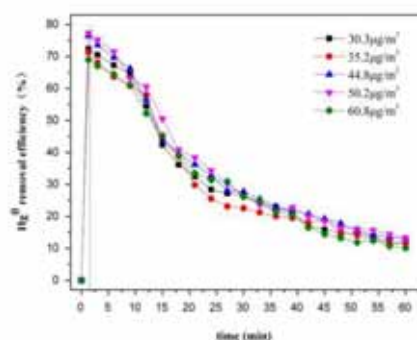


FIGURE 3
Effect of inlet Hg concentration on Hg^0 removal efficiency of PTFE fiber

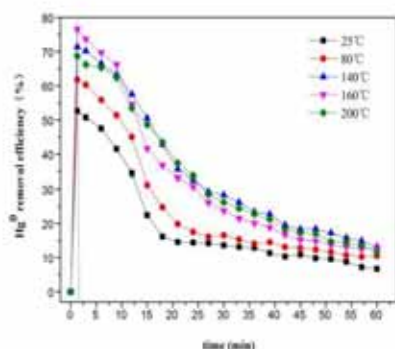


FIGURE 4
Effect of reaction temperature on Hg^0 removal efficiency of PTFE fiber

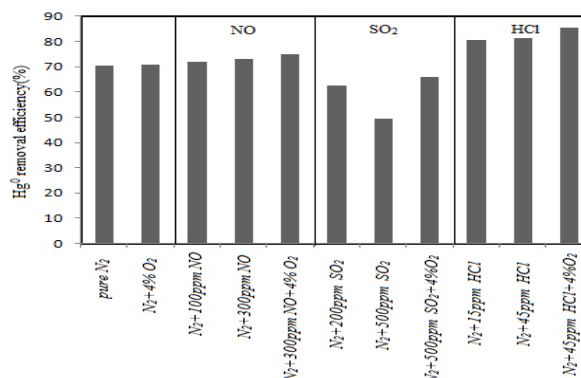


FIGURE 5
Effect of gas composition on Hg^0 removal efficiency of PTFE fiber

The Hg^0 removal efficiency of all fibers was very high at the beginning as shown in FIGURE 2. Of all the fibers tested magnetic silver-loaded PTFE fiber shows the highest Hg^0 removal efficiency of 76.5%, followed by the magnetic silver-loaded glass fiber 58.3%, then the Hg^0 removal efficiency decreased. After 45 minutes the Hg^0 removal efficiency remained stable. From results shown in figure 2, we can conclude that the Hg^0 removal efficiency of the magnetic silver-loaded PTFE fiber was higher than the other fibers in most of the time.

Effect of mercury inlet concentration on Hg^0 removal efficiency. Electing 1g PTFE fiber as adsorbents, simulated flue gas temperature was 160°C , flue gas flow rate was 3L/min. Adjusting mercury inlet concentration ($[\text{Hg}^0]_{\text{in}}$) by varying the water bath temperature of the mercury vapor generator.

According to Fig. 3, the Hg^0 removal efficiency reached the highest under the corresponding conditions in the initial stage of the adsorption process. When the $[\text{Hg}^0]_{\text{in}}$ increased from $30.3 \mu\text{g}/\text{m}^3$ to $35.2 \mu\text{g}/\text{m}^3$, the Hg^0 removal efficiency decreased from 72.4% to 71.2%. However, when the $[\text{Hg}^0]_{\text{in}}$ increased from $35.2 \mu\text{g}/\text{m}^3$ to $44.8 \mu\text{g}/\text{m}^3$, the Hg^0 removal efficiency also increased from 71.2% to 76.5%. All the five curves showed a similar trend of nonlinear trend in Hg^0 removal efficiency, because as more mercury enters the system more active sites and adsorption vacancies were required to adsorb Hg^0 . This resulted a reduction in adsorption in the corresponding space and active sites. However, the Hg^0 removal efficiency and the $[\text{Hg}^0]_{\text{in}}$ were not in a linearly proportional relationship as the adsorption site and space were limited.

Effect of reaction temperature on the Hg^0 removal efficiency. Electing 1g PTFE fiber as adsorbent, simulated flue gas temperature was 160°C , flue gas flow rate was 3L/min, mercury inlet concentration was about $45 \mu\text{g}/\text{m}^3$.

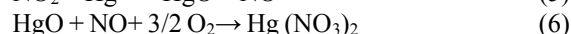
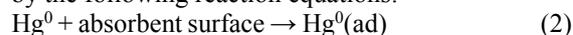
Fig. 4 showed the adsorption curves under different flue gas temperatures. As can be seen from figure 4, the reaction temperature influenced the Hg^0 removal efficiency significantly. When the reaction temperature increased from 25°C to 160°C , the Hg^0 removal efficiency of the magnetic silver-loaded PTFE fiber also increased from 52.6% to 76.5%. However, the Hg^0 removal efficiency decreased from 76.5% to 68.7% when the temperature increased from 160°C to 200°C . After reaction time of 25 minutes the Hg^0 removal efficiency was almost stable. The H_2O molecules on the surface of the sorbent and the oxygen functional groups also played a significant role in Hg^0 adsorption [19]. Water molecules also reacted from the increase, allowing the oxygen functionalities to change, when the temperature exceeded a certain value. The H_2O molecules on the surface of the sorbent evaporated, and some oxygen functionalities also decreased due to

decomposition. Therefore, it is necessary to control the reaction temperature during the Hg^0 adsorption process.

Effect of different gas compositions on the Hg^0 removal efficiency. Electing 1g PTFE as adsorbents, simulated flue gas temperature was 160°C , flue gas flow rate was 3L / min, mercury inlet concentration was about $45 \mu\text{g}/\text{m}^3$.

Fig. 5 showed the adsorption curves under different gas compositions.

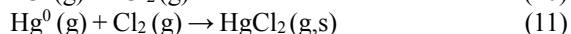
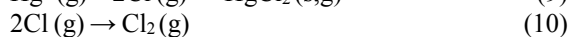
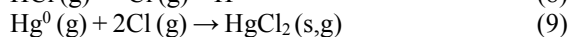
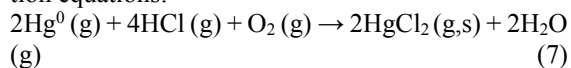
(1) Effect of NO on Hg^0 removal efficiency. As shown in Fig. 5, the Hg^0 removal efficiency under pure N_2 were around 70.5%. When 100ppm of NO was added to the N_2 gas stream, the Hg^0 removal efficiency increased from 70.5% to around 71.8%, and further increase in NO concentration to 300ppm increased the efficiency to around 73.2%. However, in the presence of 4% O_2 , the efficiency to around 74.8%. NO had little effect on Hg^0 removal. NO would be weakly adsorbed on the surface of the magnetic silver-loaded PTFE fiber [20, 21], and a part of NO would react to generate NO^+ , NO^{3-} and NO^{2+} intermediate species [22]. On the other hand, the simulated flue gas contained trace O_2 , it was also possible that NO and O_2 formed NO_2 , and NO_2 was a strong oxidant, which could oxidize Hg^0 to HgO and finally formed $\text{Hg}(\text{NO}_3)_2$. This could be interpreted by the following reaction equations:



(2) Effect of SO_2 on the Hg^0 removal efficiency. In this experiment, it was observed that addition of SO_2 lowered Hg^0 removal under pure N_2 . As can be seen from Fig. 5, addition of 200ppm of SO_2 to the pure N_2 gas stream, decreased the Hg^0 removal efficiency from 70.5% to 62.4%, while further increase in SO_2 to 500 ppm decreased the Hg^0 removal efficiency to 49.5%. The efficiency was around 65.8% when added 4% O_2 . The possible reason was the competitive adsorption of SO_2 and Hg^0 on the surface of the magnetic silver-loaded PTFE fiber; which inhibited the Hg^0 adsorption and the formation of Ag-amalgam. Therefore, Hg^0 adsorption could not be enhanced by SO_2 .

3) Effect of HCl on Hg^0 removal efficiency. As can be seen from Fig. 5, the addition of HCl could bring a significant enhancement in Hg^0 removal efficiency. When 15ppm of HCl was added to the pure N_2 gas stream, the Hg^0 removal efficiency increased from 70.5% to 80.5% and further raised to 81.4% with the concentration of HCl increased to 45ppm, the efficiency to around 85.6% when the presence of 4% O_2 . There are two possible reasons for this result,

on one hand, when HCl entered the magnetic silver-loaded PTFE fiber, a part of HCl attended the chemical reaction, active areas increased, so the Hg^0 removal efficiency increased; on the other hand, HCl and Hg^0 reacted to form HgCl_2 , which promoted Hg^0 removal efficiency. When HCl gas entered into the adsorbent layer, HCl and Hg^0 will react to form HgCl and finally will form stable HgCl_2 , thereby enhancing the adsorption of the adsorbent. The possible chemical reactions are shown in the following reaction equations:



ADSORPTION-REGENERATION CYCLES EFFECT OF THE MAGNETIC SILVER-LOADED PTFE FIBER

After the magnetic silver-loaded PTFE fiber was adsorbed, which was heated in N_2 for 2h to regenerate, the Ag-amalgam was decomposed and Hg^0 was released from the surface of the sorbent. The reaction conditions were: the mass of the adsorbent was 1g, the adsorption temperature was 160°C , $[\text{Hg}^0]_{\text{in}}$ was $45 \mu\text{g}/\text{m}^3$, the regeneration temperature was 150°C , 200°C and 250°C , respectively.

The mercury removal efficiency of the sorbent at different regeneration temperatures. Fig. 6 indicated that the Hg^0 removal efficiency of the magnetic silver-loaded PTFE fiber decreased significantly at the fifth cycle compared to the first four cycles. Therefore, the magnetic silver-loaded PTFE fiber could be recycled for about 5 times.

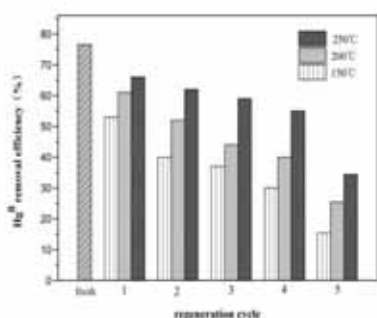


FIGURE 6

Hg^0 removal efficiency of the magnetic silver-loaded PTFE fiber in 5 adsorption-regeneration-adsorption cycles at different regeneration temperatures

The mercury adsorption capacity of the sorbent at different regeneration temperatures. The Hg^0 adsorption capacity of the fresh sorbent was about $10.1 \mu\text{g}/\text{g}$. As can be seen from figure 7, after 5 cycles of adsorption-regeneration-adsorption the adsorption capacities were about 5.3, 4.6, and $3.2 \mu\text{g}/\text{g}$ at regeneration temperatures of 250°C , 200°C and 150°C respectively. This indicated that higher temperature would accelerate the release of Hg^0 and increase the adsorption capacity. But the higher temperature could also have an adverse effect on the sorbent structure, as the structure of the sorbent could be damaged by overheating. The morphology of the Ag⁰ nanoparticle was affected, the magnetic property of the magnetic particles would become damaged, as a result, the adsorption performance of the adsorbent decreased. Therefore, it was very important to select a relatively reasonable regeneration temperature for achieving a better adsorption and regeneration.

FTIR-ATR spectra. Fig. 8 shows that the C=O absorption peaks on the surface of the magnetic silver-loaded PTFE fiber became weaker after 5 cycles of adsorption-regeneration-adsorption, indicating the C=O groups on the fiber surface decreased. The peak at 3282 cm^{-1} was the C-H stretching vibration peak, the C = O group had higher oxidability, which could be used as the active center for the Hg^0 oxidation and adsorption [23]. The infrared absorption band drifted at 1305 cm^{-1} and absorption peak was generated at 1308 cm^{-1} , further indicating the formation of chemical bonds between Fe_3O_4 and sorbent. These oxygen-containing functional groups on the surface of the silver-loaded fibers acted as the active sites that accept the electrons provided by Hg^0 and oxidize Hg^0 , then adsorbed by the chemical adsorption, the adsorption capacity of the sorbent decreased with the decreasing amount of oxygen functional groups.

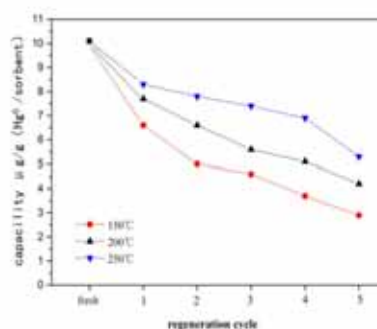


FIGURE 7

Hg^0 adsorption capacity of the magnetic silver-loaded PTFE fiber in 5 adsorption-regeneration-adsorption cycles at different regeneration temperatures

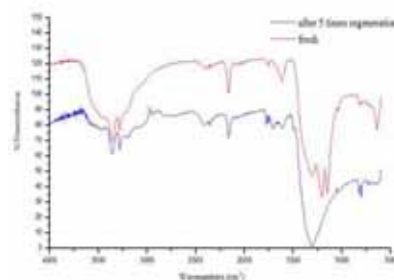


FIGURE 8
FTIR-ATR spectra of the magnetic silver-loaded PTFE fiber before and after 5 adsorption-regeneration-adsorption cycles

CONCLUSIONS

The effect of reaction conditions of the magnetic silver-loaded PTFE fiber in simulated flue gas was investigated in this study. The Hg^0 removal efficiency showed an irregular change with an increase in inlet Hg concentration. In addition, below 160°C an increase in reaction temperature had shown an increase in removal efficiency but further increase resulted in a decline in efficiency. Besides, experimental results of the effect of gas components on mercury removal indicated that NO and HCl enhanced mercury removal, but SO_2 hindered Hg^0 removal. Finally, the magnetic silver-loaded PTFE fiber was testified which could be regenerated and repeatedly used for about five times. The results of this finding will provide a theoretical guidance in high-efficiency Hg^0 removal.

ACKNOWLEDGEMENTS

This work is financially supported by the Project of Shanghai Excellent Technical Leader in China (14XD1424700), the Central University Basic Research Service Cost Key Project Fund (11D11315) and the Doctoral Innovation Fund of Donghua University in China (16D11013).

REFERENCES

- [1] Presto A.A., Granite E.J. (2008) Noble metal catalysts for mercury oxidation in utility flue gas gold, palladium, platinum formulations. *Platinum Met. Rev.* 52 (3), 144.
- [2] Wenhui Hou, Jinsong Zhou, Chunjiang Yu, Shulin You, Zhongyang Luo. (2014) $\text{Pd}/\text{Al}_2\text{O}_3$ sorbents for elemental mercury capture at high temperatures in syngas. *Ind, Eng, Chem, Res.* 53, 9909-9914.
- [3] Haomiao Xu, Zan Qu, Wenjun Huang, Naiqiang Yan. (2015) Regenerable $\text{Ag}/$ graphene sorbent for elemental mercury capture at ambient temperature. *Colloids and Surfaces A: Physicochem. Eng. Aspects*, 476, 83-89.
- [4] Magdalena Wdowin, Małgorzata M. Wiatros-Motyka, Rafał Panek, Colin E. Snape. (2014) Experimental study of mercury removal from exhaust gases. *Fuel*, 128, 451-457.
- [5] Jie Dong, Zhenghe Xu, Feng Wang. (2008) Engineering and characterization of mesoporous silica-coated magnetic particles for mercury removal from industrial effluents. *Applied Surface Science*, 254, 3522-3530.
- [6] Zhao Y, Mann MD, Pavlish JH, Mibeck BA, Dunham GE, Olson ES. (2006) Application of gold catalyst for mercury oxidation by chlorine. *Environ. Sci. Technol*, 40 (5), 1603.
- [7] Ballester D., Gomez-Gimenez C., Garcia-Diez E., Teresa Izquierdo M. (2013) Influence of temperature and regeneration cycles on Hg capture and efficiency by structured Au/C regenerable sorbents. *Journal of Hazardous Materials*, 260, 247-254.
- [8] Rodriguez-Perez J, Lopez-Anton MA, Diaz-Somoano M, Garcia R, Martinez-Tarazona MR. (2013) Regenerable sorbents for mercury capture in simulated coal combustion flue gas. *Journal of Hazardous Materials*, 260, 869-877.
- [9] Jianping Yang, Yongchun Zhao, Junying Zhang, Chuguang Zheng. (2014) Regenerable cobalt oxide loaded magnetosphere catalyst from fly ash for mercury removal in coal combustion flue gas. *Environ. Sci. Technol*, 48, 14837-14843.
- [10] Xie Yine, Caiting Li, Lingkui Zhao, Shasha Tao. (2015) Experimental study on Hg^0 removal from flue gas over columnar $\text{MnO}_x\text{-CeO}_2$ /activated coke. *Applied Surface Science*, 333, 59-67.
- [11] Xiaopeng Fan, Caiting Li, Guangming Zeng, Xing Zhang, Shasha Tao, Pei Lu, Ya Tan, Diqiang Luo. (2012) Hg^0 Removal from Simulated Flue Gas over $\text{CeO}_2/\text{HZSM-5}$. *Energy Fuels*, 26, 2082-2089.
- [12] Scala F., Cimino S. (2015) Elemental mercury capture and oxidation by a regenerable manga-

- nese-based sorbent: The effect of gas composition. *Chemical Engineering Journal*, 278, 134-139.
- [13] Yan Liu, Zhenghe Xu, Steven M. Kuznicki. (2010) Development of a novel mercury cartridge for mercury analysis. *Energy & Fuels*, 24, 10-17.
- [14] Min Kuang., Guohua, Yang, Wujun Chen, Zhixue Zhang. (2008) Studies on heat removal characteristics of activated carbon with and without Ag for Hg adsorption. *Academic journal of fuel chemistry*, 36(4), 465-473.
- [15] Diamantopoulou I., Skodras G. and Sakellaropoulos G.P. (2010) Sorption of mercury by activated carbon in the presence of flue gas components. *Fuel Process Technol.*, 91(2), 158-164.
- [16] Yanqun Zhu, Jinsong Zhou, Xiaoshu Cai, Kefa Cen. (2007) Effect of flue gas composition on Hg morphology change during coal combustion. *Zhejiang University Academic Journal (Engineering)*, 41(2), 356-360.
- [17] Li Y.H., Lee C.W., Gullett B.K. (2002) The effect of activated carbon surface moisture on low temperature mercury adsorption. *Carbon*, 40(1), 65-72.
- [18] Shangdi Wang, Junquan Sun. (2001) Introduction catalyst engineering. Beijing: Chemical Industry Press, 38-70.
- [19] Mercedes Maroto-Valer, Yinzhi Zhang, Evan J. Granite, Henry W. Pennline. (2005) Effect of porous structure and surface functionality on the mercury capacity of a fly ash carbon and its activated sample. *Fuel*, 84, 105-108.
- [20] Scala F., Cimino S. (2015) Elemental mercury capture and oxidation by a regenerable manganese-based sorbent: The effect of gas composition. *Chemical Engineering Journal*, 278, 134-139.
- [21] Shaohua Qiao, Jie Chen, Jianfeng Li, Zan Qu, Ping Liu, Naiqiang Yan, Jinping Jia. (2009) Adsorption and catalytic oxidation of gaseous elemental mercury in flue gas over MnOx/alumina. *Ind. Eng. Chem. Res.*, 48(7), 3317.
- [22] Jiangkun Xie, Zan Qu, Naiqiang Yan, Shijian Yang, Wanmiao Chen, Linguang Hu, Wenjun Huang, Ping Liu. (2013) Novel regenerable sorbent based on Zr-Mn binary metal oxides for flue gas mercury retention and recovery. *Journal of Hazardous Materials*, 261, 206-213.
- [23] Allia C.O., Parra J.B., Pis J.J. (2002) Influence of oxygen-containing functional groups on active carbon adsorption of selected organic compounds. *Fuel Processing Technology*, 79(3), 265-271.

Received: 03.12.2016

Accepted: 27.05.2017

CORRESPONDING AUTHOR

Yongfa Diao

College of Environmental Science and Engineering
Donghua University
Shanghai 201620 – CHINA

E-mail: diaoyongfa@dhu.edu.cn

LEACHING CHARACTERISTICS AND CHANGE OF BIOAVAILABILITY OF HEAVY METALS IN MSWI-FLY ASH DURING VARIOUS WASHING PROCESSES

Lei Wang^{1,2}, Li-ao Wang^{1,2,*}, Xue Zhao^{1,2}, Xiang Wang^{1,2}, Yifu Li^{1,2}, Chaochao Hu^{1,2}

¹State Key Laboratory of Coal Mine Disaster Dynamics and Control, Chongqing University, Chongqing 400044, China

²College of Resources and Environmental Science, Chongqing University, Chongqing 400044, China

ABSTRACT

Municipal solid waste incineration fly ash from Chongqing has been sampled and investigated the phase composition, major elements composition and content of heavy metal. Water-leaching, acid-leaching and multiple-step nitric acid-water-leaching process was applied to leach the MSWI fly ash, sequential extraction procedure was used to monitor the fraction and bioavailability change of heavy metals. Water-leaching process showed low efficiency on remove of heavy metals but high efficiency on reduce the bioavailability of heavy metals from fly ash. Acid leaching process can remove the heavy metal efficiency but changed the fraction distribution of heavy metals which activated the heavy metal. Multiple-step leaching process was the most efficient process to achieve double effect that reduced the content and potential availability of heavy metal in fly ash in the meantime.

KEYWORDS:

Heavy metal; Fly ash; Leach; Bioavailability.

INTRODUCTION

With such features as small floor area, harmlessness, effective recycle and prolong the service life of the landfill, incineration can eliminate a large number of MSW continuously, stably, safely and reliably, which makes incineration become one of the important MSW harmless treatment methods[1-3]. MSWI procedure produced two kinds of by-product-bottom ash and fly ash, in which the weight of fly ash was usually 3 to 5 percent of municipal solid waste[4]. MSWI fly ash contained dioxin[5-6]and heavy metals for the complex compose of solid waste which can be the secondary pollution to environment. With the higher concentration and leaching toxicity of heavy metals, fly ash is considered high potential risk to creature.

MSWI fly ash has great harm to the environment and the treatment methods, utilization and the potential risk assessment of MSWI fly ash has been attracted more and more attention. To handle

MSWI fly ash, solidification/stabilization, thermal process, secure landfill and wet treating process were usually proposed[3, 7-9]. Wet treating process is a economic and safe method to treat MSWI fly ash while the heavy metal and salts can be retrieved at the same time. Acid, alkali, water and biological were the prevalent extractant in the MSWI fly ash wet treating process[10-13]. Water leaching was usually used to promote the formation of hydrate phases and remove significant amounts of soluble salts such as sodium chloride, potassiumchloride from fly ash[14-16]. Nitric acid and sulfuric acid can remove the heavy metal from MSWI fly ash effectively[17-18].

In general, the concentration of heavy metals can't reflect the ecological effect and environmental behavior, the eco-environment risk was relied on the available forms of pollutant. The bioavailability of heavy metals is mainly due to the active chemical forms of metals. Researchers have found that significant positive correlations between the availability of heavy metals to creature and the chemical fraction of heavy metals. Speciation analysis is one of the most important methods to analysis the mobility, toxicity and portability of heavy metals. Sequential extraction schemes such as Tessier extraction, Modified Tessier extraction and BCR extraction were introduced to represent the fraction and speciation of heavy metals[19-21]. Based on the speciation analysis, bioavailability index can be used to evaluate the availability of heavy metals in the field of environmental biogeochemistry and it can reflect the migration patterns and toxicity of heavy metal clearly[22-25].

The management and utilization of MSWI fly ash were studied numerously recently, while few researches was carried out on the bioavailability of heavy metals during the leaching process. Therefore, the current study introduces the leaching characteristics and change of bioavailability of heavy metals in MSWI fly ash during various washing processes.

MATERIALS AND METHODS

Sample collection and preparation. Municipal Solid Waste Incineration fly ash was sampled in a typical incineration plant in Chongqing, China. Fly ash was air dried and grinded into powder samples with particle size $<150\ \mu\text{m}$. To analysis the concentration of heavy metals in MSWI fly ash, samples were digested in acid-cleaned microwave vessels with 8 ml of aqua regia and 4ml ultra pure, concentrated hydrofluoric acid (HF). The digested samples were separately diluted for analysis by AAS with 2% of nitric acid. Pb, Cd, Zn, Cu and Hg were measured by atomic absorption spectrometry (AAS) made by Shimadzu, Japan. Analysis of major elements composition of MSWI fly ash was carried out by using X-ray fluorescence spectrophotometer (XRF) made by Shimadzu, Japan. The phase composition of MSWI fly ash was measured by X-ray diffraction(XRD) made by Shimadzu, Japan.

Leaching process. Water-leaching process, nitric acid-leaching process and multiple-step nitric acid-water-leaching process were conducted to determine the leaching ratio and bioavailability of heavy metals in MSWI fly ash.

Water-leaching process. To get a better view on the repartition of heavy metals remaining in the washed MSWI fly ash, 20g of dried raw MSWI fly ash was put into a 1-L beaker and mixed with de-ionized water at an L/S ratio of 10/1 by magnetic stirring at the temperature of 25°C . The leaching time was 5, 10, 30, 60, 120, 240min, separately. The leached fly ash was filtered and freeze dried to analysis the concentration and fraction of heavy metal quantitatively.

Acid-leaching process. 20g of dried raw MSWI fly ash was put into a 1-L beaker and mixed with nitric acid ($c=1.0\ \text{mol/L}$) at an L/S ratio of 10/1 by magnetic stirring at the temperature of 25°C . The leaching time was 5, 10, 20, 40, 80min, respectively. The after leached fly ash was filtered and freeze dried to analysis the concentration and fraction of heavy metal quantitatively.

Multiple-step nitric acid-water-leaching process. The optimal water leaching time and acid leaching time were determined by analyzing the remove ratio of heavy metals in MSWI fly ash during the water and acid leaching process. 10g of filtered and freeze dried acid-leached fly ash in the batch of the optimal acid leaching time was put into a 1-L beaker and mixed with deionized water at an L/S ratio of 10/1 by magnetic stirring at the temperature of 25°C . The leaching time was the same as the optimal water leaching time. The multiple-step leached fly ash was filtered and freeze dried to

analysis the concentration and fraction of heavy metal quantitatively. Flowcharts for three different processes above are shown in Fig. 1.

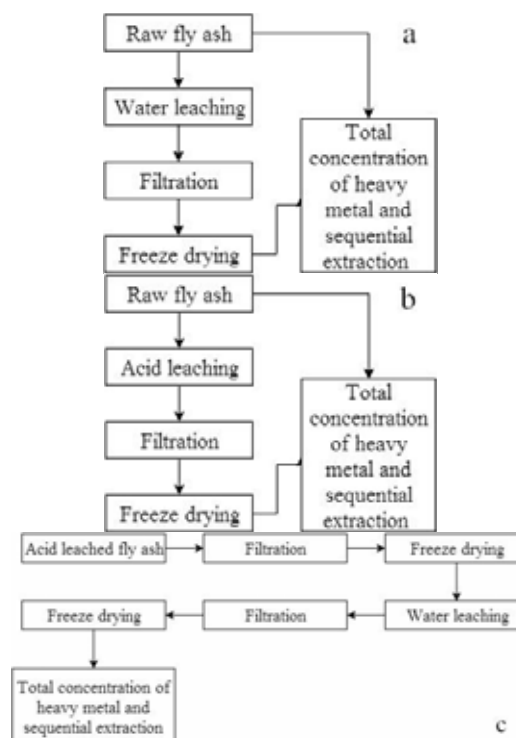


FIGURE 1

(a) Flow charts for water leaching process; (b) Flow charts for acid leaching process; (c) Flow charts for multiple-step nitric acid-water-leaching process;

Sequential extraction procedures and bioavailability index. Sequential extraction was performed using a five-step procedure as adopted by Tessier [26] which fractionated the heavy metals into five fractions: exchangeable fraction(F1), bound to carbonates fraction(F2), bound to Fe-Mn oxides fraction(F3), bound to organic matter fraction(F4) and residual fraction(F5). The sequence extraction procedures were shown in Table 1:

TABLE 1
Sequence extraction procedures

Extraction stage	Tessier method
F1	8 ml, 1 M MgCl_2 , pH 7
F2	8 ml, 1 M Sodium Acetate, pH 5 with 25% v/v Acetic Acid
F3	20 ml, 0.04 M Hydroxyl ammonium chloride in 25% v/v acetic acid
F4	5 ml, 30% v/v H_2O_2 and 3 ml, 0.02 M HNO_3 . Extracted with 5 ml, 3.2 M ammonium acetate
F5	Conc. 15 ml, HF and 4 ml, HClO_4 . Repeated and residue taken up in 5 ml HNO_3

Bioavailability index (BI), which can be introduced to evaluate the potential harm and the degree of exploitation of heavy metal, has been widely recommended to calculate the accumulated extent in creature. There was an algorithm based on the

fractions of heavy metals in Tessier to calculate the BI of heavy metals in MSWI fly ash, the equation is as follows:

$$BI = (F1+F2+F3) / (F4+F5)$$

Data analysis. All data analysis was performed through the help of OriginLab OriginPro for Windows software version 8.5.1.

RESULT AND DISCUSSION

Characteristics of raw MSWI fly ash.

MSWI fly ash is a mixture of different compounds for the diversity of municipal solid waste. The phase composition of MSWI fly ash was shown in Fig 2 and the chemical composition and contents of heavy metal in fly ash were shown in Table 2 and Table 3, respectively. The MSWI fly ash was mainly consisted of calcium compounds and chloride compounds. The content of heavy metals was in the order of Zn, Pb, Cu, Cd and Hg, which was outdistances both the background value of soil and the value of the third level of National Soil Environmental Quality Standard of China. Compared with previously reports, the heavy metal in this study had as close content with that in Taiwan and Korea[27-28]. With the high content of chlorine from municipal solid waste, the metal chloride such as PbCl₂ and ZnCl₂ which had a low-boiling point could volatilize and be adsorbed by fly ash, making for the high concentration of Zn and Pb in the fly ash[19].

TABLE 2

Chemical composition of Fly Ash(%)

Element	O	Ca	Cl	Na	K	Si	S
Composition	31	28	8.1	5.3	4.69	4.2	3.54
Element	Fe	Mg	Al	Zn	P	Ti	Pb
Composition	1.5	1.5	1.1	0.7	0.55	0.4	0.21
	8	1	7	1		8	

TABLE 3

Contents of heavy metals in fly ash (mg/kg)

Heavy metal	Cd	Cu	Pb	Zn	Hg
Fly ash	194.	842.	2130.	7126.	25.52
Background value of soil	0.13	21.5	23	5	0.05
GB15618-1995	≤1.0	≤40	≤500	≤500	≤0.5
		0			

Notes: The background value of soil came from “The Atlas of Soil Environmental Background Value in the People’s Republic of China” and GB15618-1995 was the third level of National Soil Environmental Quality Standard[29].

The fraction and bioavailability index(BI) of heavy metals in raw fly ash was shown in Fig 3, Hg was mainly existed in bound to organic matter fraction and residual fraction while the main fraction of the other heavy metals was the residual fraction. The relative amounts of easily dissolved phase of

heavy metals in the fly ash were in the order of Cd>Cu>Hg>Zn>Pb, suggested that Cd posed a higher potential risk to the ecosystem for its higher BI and it could easily enter the environment and pose serious threat to the ecosystem due to its high-toxicity and availability.

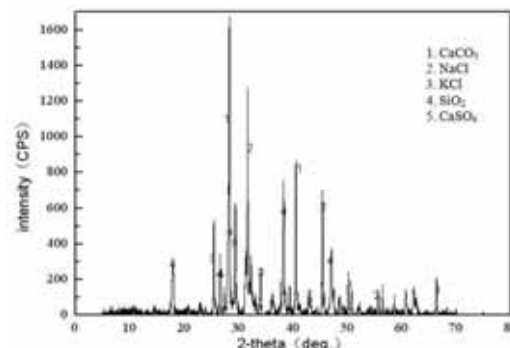


FIGURE2

XRD spectrum of fly ash

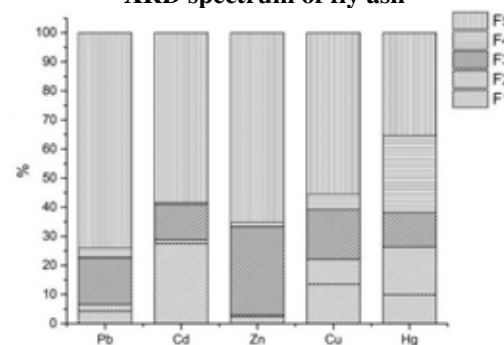


FIGURE3

Fraction of heavy metals in raw fly ash

TABLE 4

Bioavailability index(BI) of heavy metals in raw fly ash

Heavy metal	Pb	Cd	Zn	Cu	Hg
BI	0.2926	0.6947	0.4993	0.6470	0.6180

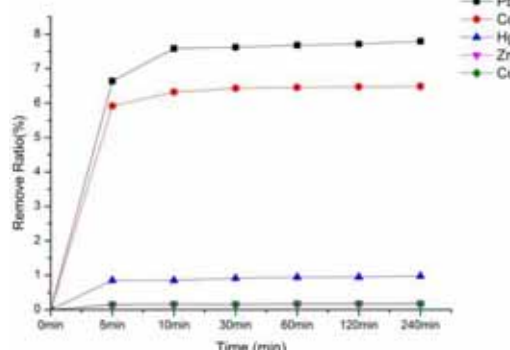


FIGURE4

Remove ratio of heavy metals during the water leaching process

Water-leaching characteristics and change of bioavailability of heavy metal. Heavy metals in fly ash would be dissolved out during the water leaching process and it was a complex physical and

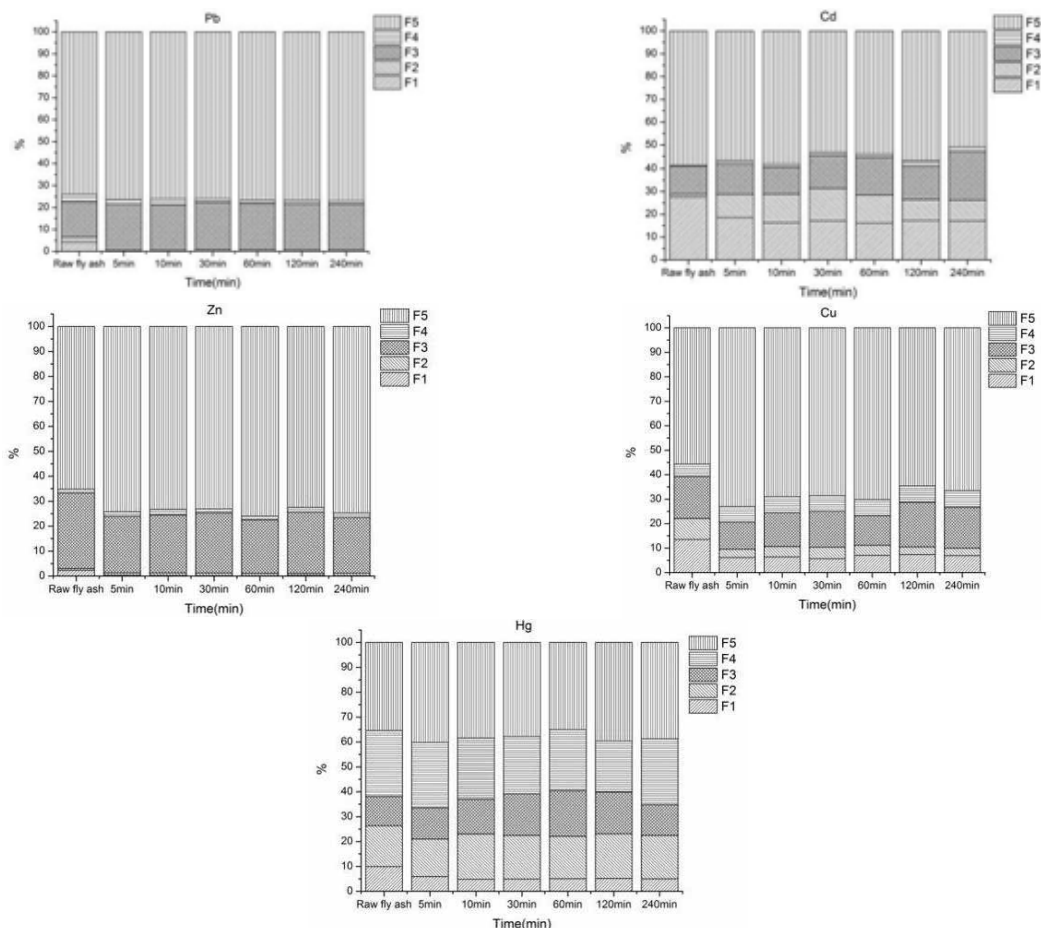


FIGURE 5
Fraction of heavy metals in fly ash during water-leaching process

chemical processes which consisted of desorption and ion exchange. The remove ratio of heavy metals during the water leaching process was shown in Fig 4.

Water leaching can dissolve little part of heavy metal while the remove ratio was less than 10%. Pb and Cd in fly ash can be removed in a short time and the remove ratio increased little after 10 min, the remove ratio was 7.58% and 6.32% while the remove ratio of the other three heavy metals was less than 1%. 10 min was selected to be the optimal leaching time by water.

The fraction and the change of bioavailability of heavy metals between raw and leached fly ash during water-leaching process was revealed in Fig 5 and 6. Water-leaching did not change the fraction of heavy metals, but decreased the proportion of exchangeable fraction which was absorbed on the surface of MSWI fly ash and would exchange with ionic composition in neutral solution compared to raw fly ash. With the time went on, BI of heavy metals first descended then rose to a dynamic equilibrium. Bioavailability of heavy metals in the leached fly ash was less than that in raw fly ash which resulted from the elution of exchangeable fraction.

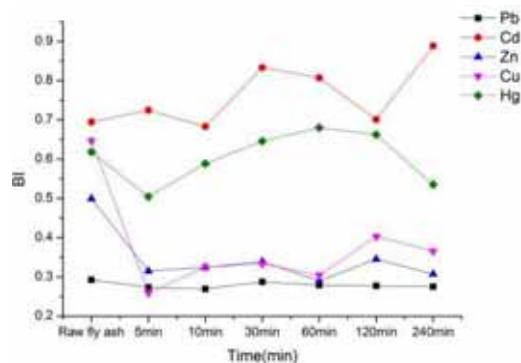


FIGURE 6
Change of bioavailability of heavy metals during water-leaching process

Acid-leaching characteristics and change of bioavailability of heavy metal. Acid leaching was a more complex process than water leaching, apart from desorption and ion exchange, chemical reaction occurred during the acid leaching process. Under the acid condition, heavy metals migrate to the liquid phase from acid-soluble material or salt with heavy metal such as carbonate. The remove ratio of heavy metals during the water leaching process was shown in Fig 7.

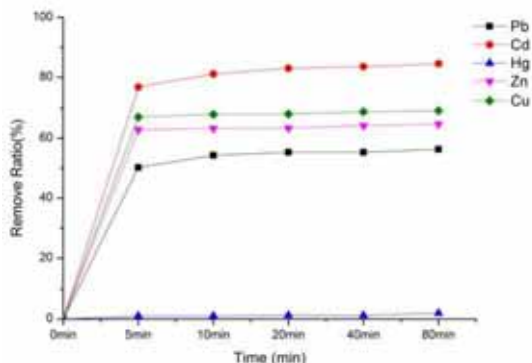


FIGURE 7

Remove ratio of heavy metals during the acid leaching process

Compared by water-leaching process, remove ratio of heavy metals during the acid leaching process was much higher, Cd was the most sensitive heavy metal leached by nitric acid and nearly 83% of the total cadmium could be dissolve out of fly ash. Due to the change of remove ratio, 10 min was also the optimal leaching time by nitric acid and the remove ratio of Pb, Cd, Zn and Cu was 54.29%, 81.07%, 63.23% and 67.94%. The leaching efficiency of Hg by nitric acid was not obvious which the highest remove ratio was less than 2%.

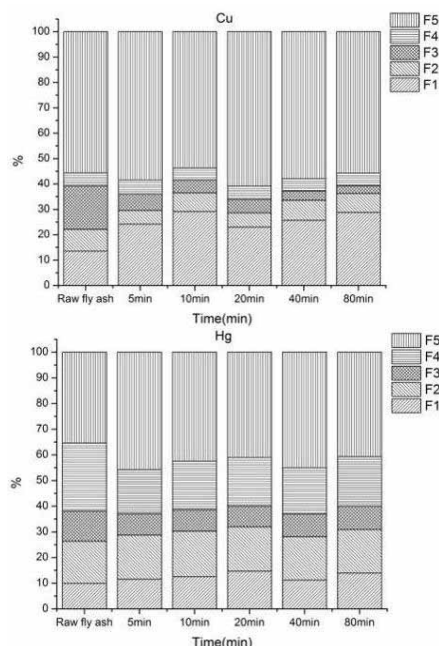


FIGURE 8

Fraction of heavy metals in fly ash during acid-leaching process

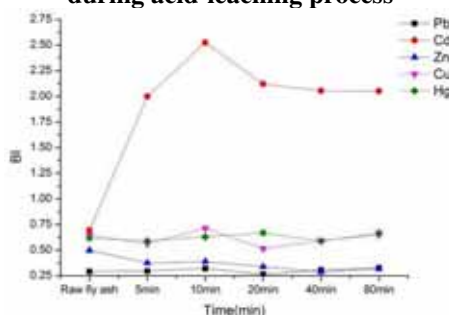


FIGURE 9

Change of bioavailability of heavy metals during acid-leaching process

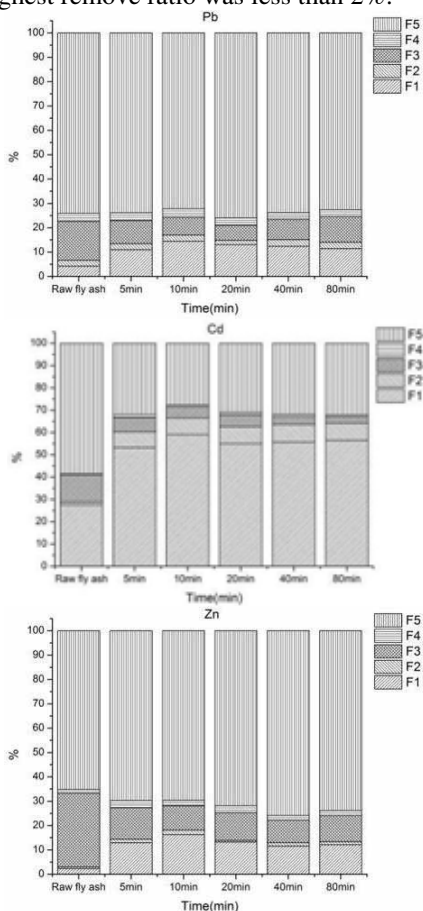


Fig 8 and 9 showed the change of fraction and bioavailability of heavy metals during during acid-leaching process. Nitric acid has changed the fraction distribution of heavy metals in fly ash. The ratio of exchangeable fraction increased rapidly while the fraction bounded to carbonates and fraction bounded to Fe-Mn oxides decreased at the same time. Part of heavy metal bounded to carbonates and Fe-Mn oxides was dissolved by nitric acid to more active fraction which increase the risk of the heavy metal entered the environment and resorbed by the creature. The effect of nitric acid to Cd fraction was more distinct than the other heavy metals, the proportion of exchangeable fraction raised to 49.49% to 59.10, indicated that Cd posed the best mobility to leach out from the fly ash.

According to the variation curve of BI, after leached by nitric acid, BI of Cd was much larger than that in raw fly ash and the peak was 2.52 at the time of 10min. BI of Zn was steady decline during the acid-leaching process, meanwhile, BI of the other three heavy metals changed slight and reached

a dynamic equilibrium. At the optimal leaching time, BI of heavy metals in leached fly ash was in the order of Cd>Zn >Hg >Cu >Pb.

Multiple-step leaching process characteristics and change of bioavailability of heavy metal. Multiple-step nitric acid-water-leaching process was a promotion of water-leaching and acid-leaching process, acid-leaching can remove the heavy metal efficiently to reduce the total concentration of heavy metal while water-leaching remove the heavy metal in active fraction. Multiple-step leaching process imbibed advantages of both two processes. Change of remove ratio and BI of heavy metal was shown below:

TABLE 5
Remove ratio of heavy metal by different leaching process

	Pb	Cd	Zn	Cu	Hg
Water leaching	8.69	6.60	0.28	0.26	1.20
Acid leaching	61.62	63.70	71.41	58.94	13.38
Multi-step leaching	63.51	67.33	71.94	59.63	13.78

TABLE 6
BI of heavy metals by different leaching process

	Pb	Cd	Zn	Cu	Hg
Raw fly ash	0.29	0.69	0.50	0.65	0.62
Water-leached fly ash	0.27	0.68	0.32	0.32	0.59
Acid-leached fly ash	0.32	2.52	0.39	0.71	0.63
Multiple-step leached fly ash	0.11	0.55	0.12	0.39	0.48

As is seen in Table 5 and 6, the removal capacity of heavy metals was in the order of multiple-step leaching, acid leaching and water leaching process, indicated that multiple-step leaching process was the most efficiency wet-way to remove the heavy metals from MSWI fly ash. Compared to BI of heavy metals in raw fly ash, water-leaching process removed the heavy metals in exchangeable fraction and reduced the availability of them. With the exception of Zn, acid-leaching process motivated the transformation to active fractions and raised the BI value, Zn dissolved into the liquid phase which led to the decreased the transferability. Multiple-step leaching process was the most efficient process to achieve double effect that reduced the content and potential availability of heavy metal in fly ash in the meantime.

CONCLUSION

This study investigated the composition of heavy metal, the leaching characteristics and change of bioavailability during the leaching process by water, nitric acid and multiple-step nitric acid-water, the research achievement was as fol-

lows:

The MSWI fly ash was mainly consisted of calcium compounds and chloride compounds. The content of heavy metals was in the order of Zn, Pb, Cu, Cd and Hg, Hg was mainly existed in bound to organic matter fraction and residual fraction while the main fraction of the other heavy metals was the residual fraction, Cd posed a higher potential risk to the ecosystem. Water leaching can dissolve little part of heavy metal and 10 min was selected to be the optimal leaching time by water. Water-leaching did not change the fraction of heavy metals, but decreased the proportion of exchangeable fraction to reduced the BI. Apart from Hg, nitric acid leaching process posed high remove ratio to the heavy metals in fly ash and 10 min was also the optimal leaching time. Nitric acid has changed the fraction distribution of heavy metals that accelerated the fraction bounded to carbonates and bounded to Fe-Mn oxides transformed to more active fraction and dissolved out. Multiple-step leaching process achieved double effect that lowered the total content and potential availability of heavy metal in the meantime.

REFERENCES

- [1] Yang, F, Wu, G, Q. and Jin, Z.F. (2006) Municipal waste incineration fly ash physical and chemical properties and processing technology[J]. *Journal of Chongqing University (Natural Science Edition)*, 29(9): 56-59.
- [2] Gonzálezcorrochano, B, Alonsozcarate, J and Rodas, M. (2009) Characterization of light-weight aggregates manufactured from washing aggregate sludge and fly ash.[J]. *Resources Conservation & Recycling*, 53(10):571-581.
- [3] Sun, X, Li, J, Zhao, X, Zhu, B and Zhang, G. (2016) A Review on the Management of Municipal Solid Waste Fly Ash in American [J]. *Procedia Environmental Sciences*, 31:535-540.
- [4] Yu, J, Yu, Q, Li, M J, Ma C and Paterson, N. (2015) Removal of toxic and alkali/alkaline earth metals during co-thermal treatment of two types of MSWI fly ashes in China. *Waste Management*, 46: 287-297.
- [5] Pan, Y, Yang, L, Zhou, J, Liu, J and Qian, G. (2013) Characteristics of dioxins content in fly ash from municipal solid waste incinerators in China.[J]. *Chemosphere*, 92(7):765-771.
- [6] Zhou, J, Yun, P, Zhang, J and Zhang, L. (2016) Dioxin distribution characteristics and health risk assessment in different size particles of fly ash from MSWIs in China[J]. *Waste Management*, 50:113-120.
- [7] Zhang, G and Cheng, J. (2011) Progress on treatment of municipal solid waste incineration (MSWI) fly ash[J]. *Xiandai Huagong/modern Chemical Industry*, 31(8):31-34.

- [8] Cai, K, Peng, X, Yang, R, Wu, Y and Hu, X. (2012) Progress of Disposal and Utilization of Fly Ash from MSW Incineration[J]. *Environmental Science & Management*, 37(4): 30-34.
- [9] Yao, G. (2014) Status and Prospect of the Treatment Technologies of MIWS Fly Ash[J]. *Chemical Industry Times*, 28(7): 45-48.
- [10] Wang, Q, Jie, Y, Qi, W and Wu, T. (2009) Effects of water-washing pretreatment on bioleaching of heavy metals from municipal solid waste incinerator fly ash[J]. *Journal of Hazardous Materials*, 162(2-3):812-8.
- [11] Komonweeraket, K, Cetin, B, Benson, C H, Aydilek, A H and Edil, T B. (2014) Leaching characteristics of toxic constituents from coal fly ash mixed soils under the influence of pH[J]. *Waste Management*, 38(1):174-184.
- [12] Jiao, F, Zhang, L, Dong, Z, Namioka, T, Yamada, N and Ninomiya, Y. (2016) Study on the species of heavy metals in MSW incineration fly ash and their leaching behavior[J]. *Fuel Processing Technology*, 152:108-115.
- [13] Luan, J, Chai, M and Li, R. (2016) Heavy Metal Migration and Potential Environmental Risk Assessment During the Washing Process of MSW Incineration Fly Ash and Molten Slag[J]. *Procedia Environmental Sciences*, 31:351-360.
- [14] Yang, R, Liao, W P and Wu, P H. (2012) Basic characteristics of leachate produced by various washing processes for MSWI ashes in Taiwan.[J]. *Journal of Environmental Management*, 104(16):67-76.
- [15] Chen, X, Bi, Y, Zhang, H and Wang, J. (2016) Chlorides Removal and Control through Water-washing Process on MSWI Fly Ash [J]. *Procedia Environmental Sciences*, 31:560-566.
- [16] Wang, X, Li, A and Zhang, Z. (2016) The Effects of Water Washing on Cement-based Stabilization of MWSI Fly Ash [J]. *Procedia Environmental Sciences*, 31:440-446.
- [17] Zhang, H Y and Ma, G X. (2012) Leaching of Heavy Metals from Municipal Solid Waste Incineration (MSWI) Fly Ash Using Nitric Acid[J]. *Applied Mechanics & Materials*, 249-250:922-926.
- [18] Zhao, X, Wang, L A, Wang, L and Zhang W. (2016) Distribution of remaining Cd in MSWI fly ash washed with nitric acid[J]. *Journal of Material Cycles & Waste Management*:1-8.
- [19] Pan, Y, Wu, Z, Zhou, J, Zhao J, Ruan, X, Liu, J and Qian, G. (2013) Chemical characteristics and risk assessment of typical municipal solid waste incineration (MSWI) fly ash in China.[J]. *Journal of Hazardous Materials*, 261(20):269-276.
- [20] Ibrahim, L A A. (2015) Chemical characterization and mobility of metal species in fly ash – water system[J]. *Water Science*, 29(2):109-122.
- [21] Zhang, B, Zhou, W, Zhao, H, Tian, Z, Li, F and Wu, Y. (2016) Stabilization/solidification of lead in MSWI fly ash with mercapto functionalized dendrimer Chelator.[J]. *Waste Management*, 50:105-112.
- [22] Qiu, N. (2012) Speciation Analysis and Biological Availability of Heavy Metals in Municipal Solid Waste Incineration Ashes[J]. *Shandong Chemical Industry*, 41: 32-35.
- [23] Xiong, Y, Zhu, F and Zhao, L. (2014) Heavy metal speciation in various types of fly ash from municipal solid waste incinerator[J]. *Journal of Material Cycles and Waste Management*, 16(4):608-615.
- [24] Xiao, Z, Yuan, X, Li, H, Leng, L, Chen, X, Zeng, G, Li, F and Cao, L. (2015) Chemical speciation, mobility and phyto-accessibility of heavy metals in fly ash and slag from combustion of pelletized municipal sewage sludge.[J]. *Science of the Total Environment*, 536:774-783.
- [25] Zheng, L, Wang, W and Gao, X. (2016) Solidification and immobilization of MSWI fly ash through aluminate geopolymerization: Based on partial charge model analysis.[J]. *Waste Management*, 58: 270-279.
- [26] Tessier, A, Campbell, PGC and Bisson, M. (1979) Sequential extraction procedure for the speciation of particulate trace metals.*Anal. Chem*; 51:844-851.
- [27] Chou, S.Y, Lo, S.L, Hsieh, C.H and Chen, C L. (2009) Sintering of MSWI fly ash by microwave energy[J]. *Journal of Hazardous Materials*, 163(1):357-62.
- [28] Shim, Y.S, Rhee, S.W and Lee, W.K. (2005) Comparison of leaching characteristics of heavy metals from bottom and fly ashes in Korea and Japan.[J]. *Waste Management*, 25(5):473-80.
- [29] Wu, S. (1994) The Atlas of Soil Environmental Background Value in the People's Republic of China[M]. China Environmental Science Press.

Received: 04.12.2016

Accepted: 31.05.2017

CORRESPONDING AUTHOR

Li-ao Wang

State Key Laboratory of Coal Mine Disaster Dynamics and Control, Chongqing University, Chongqing 400044, China

E-mail: wangliao@cqu.edu.cn

METAL CONCENTRATIONS IN TISSUES OF TWO FISH SPECIES (*MYSTUS MACROPTERUS* AND *CYPRINUS CARPIO*) FROM THE CHISHUI RIVER, A PROTECTED AREA IN CHINA

Shenwen Cai^{1,*}, Jinhua Gan², Bin Liu¹, Jiazhen Wang³

¹Department of Resources and Environment, Zunyi Normal College, Zunyi 563000, Guizhou, China

²Yangtze River Fisheries Research Institute, Chinese Academy of Fishery Sciences, Wuhan 430072, Hubei, China

³Department of Life Science, Zunyi Normal College, Zunyi 563000, Guizhou, China

ABSTRACT

Concentrations of copper, zinc, lead, cadmium, manganese, arsenic, and mercury were measured in the muscle, gill, liver, and kidney of *Mystus macropterus* and *Cyprinus carpio* collected from the Chishui River which is the last undammed first tributary of the upper Yangtze River. The concentrations of zinc were the highest in all tissues of the two fish species. Metal concentrations were found to be tissue- and species-specific. There were no identical relationships between metal concentrations and fish length. The Pb concentrations in muscle of some individuals were higher than that recommended by the Ministry of Health of China and European Commission.

KEYWORDS:

Metal, *Mystus macropterus*, *Cyprinus carpio*, Chishui River

INTRODUCTION

Heavy metal pollution in rivers has become a problem of increasing concern. Metals and metalloids from natural and anthropogenic sources can enter the freshwater ecosystems and cause threat because of their toxicity, long persistence, bioaccumulation and biomagnification. Metals such as Cu, Zn, and Mn are biologically essential elements. However, they are regarded as potential hazards if the concentrations above the permissible level. Pb, Cd, As, and Hg are non-essential elements and can be toxic even at quite low concentrations [1]. Fish accumulate metals directly from the water or through the diet, and the contaminants can be biomagnified in tissues [2]. So, fish have been widely used as bioindicator for the evaluation of metal pollution in aquatic ecosystems [3, 4]. Generally, the muscle was chosen as target tissue to evaluate the consumption safety for humans, the gill represents the metal levels in the aquatic environment where the fish lives, the levels in the liver and kidney reflect the long term

accumulation of metals in the fish [5].

The purpose of the present study is to evaluate Cu, Zn, Pb, Cd, Mn, As, and Hg concentrations in different tissues of two fish species *Mystus macropterus* and *Cyprinus carpio* from Chishui River, which located in the rare and endemic fish nature reserve in the upper reaches of the Yangtze River, China. The Chishui River is the last undammed first tributary of the upper Yangtze River and play important roles in fish conservation [6], especially for the rare and endemic fish species. This nature reserve is established in 2006 to protect the resource of these fish species, as well as prevent water environmental contamination under the tendency of intense industrial development [7]. Although the populations of fish species in this river are currently in rapid decline because of water environment degradation, overfishing, laxity in law enforcement, mismanagement, and indifferent consciousness to environment, it appears that not much attention has been paid towards contamination studies of fish inhabiting in this river. The data dealing with metal pollution in this area is extremely limited. *M. macropterus* and *C. carpio* are two important commercial and widely consumed fish species by lots of people who living in the Chishui River basin. Thus, it is necessary to assess the safety of fish for human consumption. The results obtained from present study will provide background information about the metal concentrations of two fish species in Chishui River, contributing to the effective monitoring of both environmental quality and the health of the organisms inhabiting in the river ecosystem. Also, Gaining information of metal levels in tissues of fish is essential both respecting river management and fish conservation.

MATERIALS AND METHODS

Study Area and Samplings. Two fish species (*M. macropterus* and *C. carpio*) which appear to have great economic and ecological importance in the Chishui River were taken from special fisher-

TABLE 1
Number, length and weight ranges of the two fish species

Fish	Number	Length ranges (cm)	Weight ranges (g)
<i>M. macropterus</i>	22	12.5–33.9	18.8–189.0
<i>C. carpio</i>	20	14.4–21.7	40.8–153.2

TABLE 2
Measurements of standard sample of prawn constituent (mg/kg wet wt)

	Cu	Zn	Pb	Cd	Mn	As	Hg
Certified values	10.3 ± 0.7	76 ± 4	0.20 ± 0.05	0.039 ± 0.002	8.9 ± 0.3	1.4 ± 0.3	0.049 ± 0.008
Measured values	10.7 ± 0.1	75 ± 2	0.17 ± 0.02	0.038 ± 0.001	9.0 ± 0.2	1.3 ± 0.1	0.053 ± 0.002

men in 2015~2016 (Fig. 1). All the fish samples used in present study were measured to the nearest 0.1 cm and weighed to the nearest 0.1 g (Table 1). Accurate weighed samples (0.40–0.65 g) of muscle (under dorsal fin without skin), gill, liver, and kidney were taken from each fish and stored in glass vials at -20 °C before analysis. Each sample was pre-digested overnight with 10 mL of digestion solution HNO₃-HClO₄ (9:1 v/v), 4 mL of digestion solution was then added and the mixture was heated at 150 °C on a hot plate until the sample solution became clear and nearly dry. After cooling, the solution was quantitatively transferred to 25 mL glass tube with ultrapure water (Milli-Q, 18.2 MΩ cm). Then the solution was filtered using 0.45 μm nitrocellulose membrane filter.

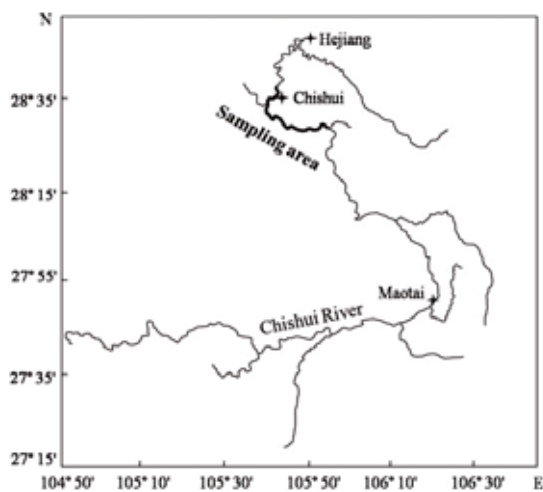


FIGURE 1

Map of the Chishui River with the sampling area

Determination of Metals. Levels of Cu, Zn, Pb, Cd, and Mn were analyzed using inductively coupled plasma atom emission spectrometry (ICP-AES; Thermo ICAP6300-duo, USA). The As and Hg concentrations were measured by the KCHG AFS-230E atomic fluorophotometer. The detection limits of Cu, Zn, Pb, Cd, Mn, As, and Hg were 2 μg/L, 0.6 μg/L, 4 μg/L, 0.5 μg/L, 0.5 μg/L, 0.04 μg/L, and 0.3 μg/L, respectively. Recovery rates ranged from 93%

to 105% for all investigated elements. The accuracy of the applied analytical procedure was tested using certified reference materials (GBW10050 and GBW10051, standard samples of biological constituent) provided by the National Research Center for Certified Reference Materials of China. They were analyzed at regular time intervals throughout the measurement together with the studied fish samples (Table 2).

Statistical Analysis. All statistical calculations were performed using SPSS 19.0 for Windows. One-way analysis of variance (ANOVA) and Duncan's Multiple Comparison Test ($p = 0.05$) were used to access whether metal concentrations varied significantly between fish species. Two-way ANOVA was performed to test the effects of fish species and tissue on metal concentrations. Pearson's correlation coefficient (r) was used to examine the relationship between metal concentrations and fish length. The metal concentrations in fish tissues were reported in mg/kg (wet weight), as mean ± standard deviation (SD).

RESULTS AND DISCUSSION

Metal Concentrations in Fish Tissues. The metal concentrations in the tissues of *M. macropterus* and *C. carpio* from the Chishui River are showed in Table 3. The mean concentrations of Cu, Zn, Pb, Cd, Mn, As, and Hg in the two fish species were 0.34 ± 0.05 , 10.38 ± 2.69 , 0.35 ± 0.29 , 0.02 ± 0.02 , 0.30 ± 0.07 , 0.09 ± 0.01 , 0.07 ± 0.02 mg/kg for muscle, 0.80 ± 0.18 , 17.75 ± 3.88 , 1.01 ± 0.64 , 0.10 ± 0.06 , 2.05 ± 1.69 , 0.12 ± 0.03 , 0.06 ± 0.01 mg/kg for gill, 6.74 ± 6.15 , 67.57 ± 57.99 , 0.40 ± 0.17 , 0.22 ± 0.16 , 1.45 ± 0.35 , 0.10 ± 0.01 , 0.07 ± 0.02 mg/kg for liver, 1.46 ± 0.60 , 90.37 ± 74.62 , 0.48 ± 0.20 , 0.55 ± 0.39 , 0.77 ± 0.27 , 0.11 ± 0.03 , 0.07 ± 0.02 mg/kg for kidney, respectively. The Zn concentrations were much higher than other metals in all tissues. The concentrations of Cd were the lowest in muscle and gill of *M. macropterus* and muscle of *C. carpio*. The concentrations of Hg were the lowest in liver and kidney of *M. macropterus* and in gill, liver, and kidney of *C. carpio*. The most

TABLE 3
Concentrations of seven metals (Cu, Zn, Pb, Cd, Mn, Hg, and As) in tissues (muscle, gill, liver, and kidney) of two fish species (*M. macropterus* and *C. carpio*) from the Chishui River (mean \pm SD, mg/kg wet wt)

Fish	Tissue	Cu	Zn	Pb	Cd	Mn	As	Hg
<i>M. macropterus</i>	Muscle	0.35 \pm 0.06 ^a	9.23 \pm 3.04 ^a	0.41 \pm 0.38	0.03 \pm 0.03 ^a	0.27 \pm 0.04 ^a	0.09 \pm 0.01 ^a	0.06 \pm 0.01
	Gill	0.70 \pm 0.14 ^{ab}	15.26 \pm 2.64 ^b	0.53 \pm 0.23	0.05 \pm 0.03 ^a	0.60 \pm 0.12 ^b	0.10 \pm 0.01 ^{bc}	0.06 \pm 0.01
	Liver	2.73 \pm 1.25 ^c	21.47 \pm 4.21 ^c	0.43 \pm 0.23	0.29 \pm 0.19 ^b	1.35 \pm 0.32 ^c	0.10 \pm 0.01 ^{ab}	0.07 \pm 0.02
	Kidney	1.06 \pm 0.25 ^b	27.56 \pm 5.39 ^d	0.50 \pm 0.26	0.47 \pm 0.32 ^c	0.58 \pm 0.17 ^b	0.11 \pm 0.04 ^c	0.07 \pm 0.02
<i>C. carpio</i>	Muscle	0.33 \pm 0.04 ^a	11.65 \pm 1.46 ^a	0.28 \pm 0.10 ^a	0.01 \pm 0.01 ^a	0.34 \pm 0.07 ^a	0.09 \pm 0.02 ^a	0.07 \pm 0.02
	Gill	0.91 \pm 0.16 ^a	20.49 \pm 3.11 ^a	1.54 \pm 0.53 ^c	0.14 \pm 0.05 ^b	3.64 \pm 1.04 ^d	0.13 \pm 0.03 ^c	0.06 \pm 0.01
	Liver	11.14 \pm 6.40 ^b	118.75 \pm 45.53 ^b	0.36 \pm 0.04 ^{ab}	0.15 \pm 0.08 ^b	1.55 \pm 0.36 ^c	0.10 \pm 0.01 ^{ab}	0.06 \pm 0.01
	Kidney	1.90 \pm 0.57 ^a	159.47 \pm 48.87 ^c	0.47 \pm 0.11 ^b	0.63 \pm 0.45 ^c	0.97 \pm 0.20 ^b	0.12 \pm 0.03 ^{bc}	0.07 \pm 0.02

Different letters indicate significant differences between different tissues ($p < 0.05$).

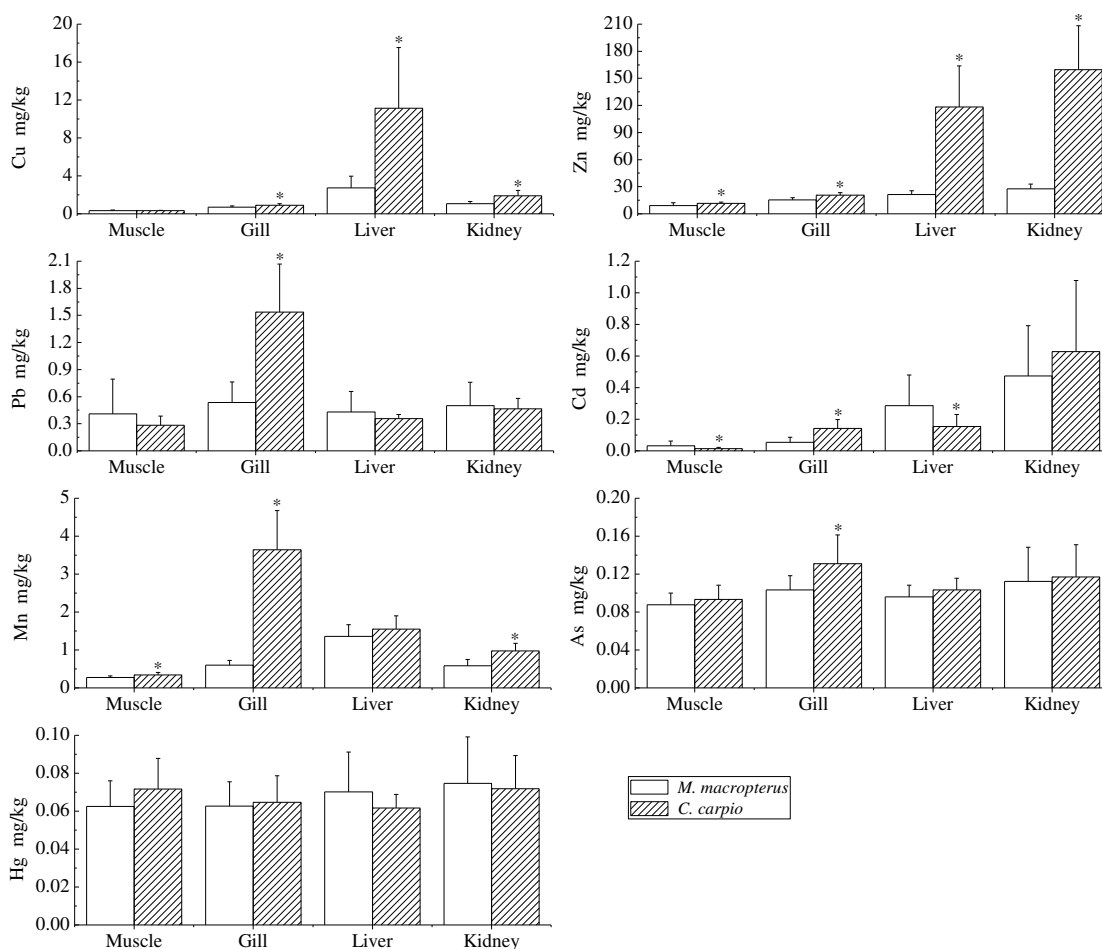


FIGURE 2

Comparison of mean concentrations of Cu, Zn, Pb, Cd, Mn, Hg, and As (mg/kg wet wt.) in the muscle, gill, liver, and kidney between *M. macropterus* and *C. carpio*. * $p < 0.05$, significant difference between the two fish species.

possible reason for that may be related to different capabilities of metal accumulation, as well as with the background values in the aquatic ecosystems.

It is generally accepted that the metal bioaccumulation pattern was mainly associated with tissue and species [8]. Metal concentrations in fish tissues not only reflect exposure to elements but also the elemental excretion from various organs by metabolic

processes [9]. Compared with the gill, liver, and kidney, muscle typically contains low metal concentrations. The muscle was not an active tissue for metal bioaccumulation [10]. Consistent with this hypothesis, the lowest Cu, Zn, Pb, Cd, Mn, and As concentrations were found in muscle tissue of the two fish species. However, the Hg concentration showed no significant difference between muscle and other tissues ($p < 0.05$). It suggests that Hg can accumulate

TABLE 4
Relationships between tissues metal concentrations and fish length for *M. macropterus* and *C. carpio* (Pearson's correlation coefficient, *r*).

Fish species	Tissues	Cu	Zn	Pb	Cd	Mn	As	Hg
<i>M. macropterus</i>	Muscle	0.11	-0.75**	0.66**	0.65**	-0.30	-0.13	-0.32
	Gill	-0.22	0.00	0.16	-0.10	0.18	0.38	-0.37
	Liver	-0.20	-0.16	-0.04	0.06	0.11	-0.16	-0.07
	Kidney	0.03	-0.16	-0.04	0.29	-0.18	-0.01	-0.03
<i>C. carpio</i>	Muscle	-0.18	0.26	0.17	-0.30	-0.09	-0.13	-0.05
	Gill	-0.30	-0.32	-0.07	-0.01	0.26	0.04	0.47*
	Liver	-0.02	-0.20	0.12	-0.16	0.30	0.20	-0.36
	Kidney	-0.07	-0.15	-0.60**	-0.54*	-0.36	-0.20	-0.34

* $p < 0.05$, ** $p < 0.01$

easily in muscle [11]. Gill is an important tissue to uptake metals from the water due to the metal-binding sites located at the tissue's surface [12]. Liver and kidney are the most important tissues for metal detoxification and metabolism in fish [13]. The liver and kidney appear to have a significantly higher tendency for the accumulation of most of the metals [14]. In present study, the Pb concentrations were highest in the gills of both fish species. The As concentration was highest in the gills of *C. carpio*. The Cu and Mn concentrations were highest in the livers of both fish species. The Zn and Cd concentrations were highest in the kidneys of both fish species (Table 3). According to these results, it could be concluded that the Pb and As are mainly accumulated in gill, the Cu and Mn are mainly accumulated in liver, the Cd and Zn are mainly accumulated in kidney. Similar results were demonstrated in other studies [9, 11].

Metal concentrations in fish are usually species specific [15]. Differences in metal concentrations between fish species might be a result of different habitat environment, diet, characteristic behavior, lifespan and metabolic activities [16, 17]. *M. macropterus* and *C. carpio* are both omnivorous fish feeding on mollusks, larva of aquatic insect, organism detritus, and some kinds of algae. *M. macropterus* is living in the gravel-bottom of river, whereas *C. carpio* is living in the soft-bottom of river. The concentrations of Cu in gill, liver, and kidney, Zn in all tissues, Pb in gill, Cd in muscle, gill, and liver, Mn in muscle, gill, and kidney, As in gill of *C. carpio* were significant higher than that of *M. macropterus* ($p < 0.05$) (Fig. 2). Bottom sediment is a sink and source of metals in water system [18, 19]. So, *C. carpio* could be easily exposed to higher concentrations of metals. The concentrations of Cd in muscle and liver of *M. macropterus* were significant higher than that of *C. carpio*. ($p < 0.05$). This might be related to the differences in metabolic activities and metals accumulation abilities between them. Differences in geographic distribution of life stages could be additional possible explanations for the variation observed in metal concentration between different fish species [20].

Relationships between Metal Concentrations and Fish Length. The relationships between metal concentrations and fish length in different tissues of *M. macropterus* and *C. carpio* are showed in Table 4. No identical relationships between metal concentrations and fish length were showed in present study. Significant relationships between metal concentrations and fish length were negative except in a few cases [21-23]. The possible reason for the negative correlation in the concentration-length relationships might be explained by the fact that the smaller fish need more energy for growth, less energy might be available for detoxification [23]. In present study, significant negative correlations were found between metal concentrations and fish length for Zn in muscle of *M. macropterus* ($p < 0.01$), Pb ($p < 0.01$) and Cd ($p < 0.05$) in kidney of *C. carpio*, while significant positive correlations were observed between concentrations and fish length for Pb and Cd in muscle of *M. macropterus* ($p < 0.01$), and Hg in gill of *C. carpio* ($p < 0.05$). Positive relationships between metal concentrations in fish and length were also reported in other studies [24, 25]. Larger fish can consume larger prey and are functionally at a higher trophic level than smaller fish of the same species [2]. Although negative or positive correlations were observed between metal concentrations in some tissues and length of the species, metal concentrations in some other tissues showed no significant correlations with fish length [26], what is in agreement with the results of present study where the concentrations of all metals in gill, liver and kidney of *M. macropterus* and in muscle and liver of *C. carpio* showed no significant correlations with fish length. The relationship between metal concentration and length seems to be dependent on numerous factors such as the specific metal, the degree of pollution in water, the species, the physiological condition of the fish, as well as the tissue concerned [25].

Health Risk Assessment for Fish Consumption. The muscle of fish is the main edible part that can directly affect human health if carries metals beyond standards [27]. There are no maximum limits of Cu, Zn, and Mn in fish in Chinese standard. The mean concentrations of Pb, Cd, As and Hg in muscle

were below the tolerance limit levels (Pb: 0.5 mg/kg; Cd: 0.1 mg/kg; As: 0.1 mg/kg; Hg: 0.5 mg/kg) assigned by the Ministry of Health of China. The concentrations of Pb in some individuals, however, were above the tolerance limit level. The mean concentration of Pb in *M. macropterus* was also above the European Commission's maximum permissible level (0.3 mg/kg) [28]. It indicates that the fish from this study area could be not safe for human consumption. The results of present study provide baseline data for metal accumulations in fish species from the Chishui River, and also indicate that strict protection and long-term monitoring of metal pollution are essential in this area.

CONCLUSIONS

The results from the present study indicated that the muscle was not an active tissue for metal bioaccumulation. Differences in metal concentrations between *M. macropterus* and *C. carpio* from the Chishui River might be a result of different bottom types, metabolic activities, and geographic distribution of life stages. There were no identical relationships between metal concentrations and fish length. Potential human health risk may be present due to high Pb concentration in some individuals exceeding the tolerance limit level assigned by the Ministry of Health of China and EC. The present study provided baseline data for metal accumulations in fish species from the Chishui River. Strict protection and long-term monitoring of metal pollution in this area are needed.

Conflict of Interest Statement. All authors declare no conflict of interest.

ACKNOWLEDGEMENTS

This study was funded by the Natural Science Foundation of the Education Department of Guizhou Province (No. QJHKY [2014]321) and the Science and Technology Department of Guizhou Province (No. QKHJ [2015]2148).

REFERENCES

- [1] Duran, A, Tuzen, M, Soylak, M. (2014) Assessment of trace metal concentrations in muscle tissue of certain commercially available fish species from Kayseri, Turkey. *Environ Monit Assess* 186:4619-4628
- [2] Burger, J, Gochfeld, M, Batang, Z, Alikunhi, N, Al-Jahdali, R, Al-Jebreen, D, Aziz, M.A.M, Al-Suwailem, A. (2014) Interspecific and locational differences in metal levels in edible fish tissue from Saudi Arabia. *Environ Monit Assess* 186:6721-6746
- [3] Bergek, S, Ma, Q, Vetemaa, M, Franzen, F, Appelberg, M. (2012) From individuals to populations: Impacts of environmental pollution on natural eelpout populations. *Ecotoxicol Environ Saf* 79:1-12
- [4] Yi, Y, Yang, Z, Zhang, S. (2011) Ecological risk assessment of heavy metals in sediment and human health risk assessment of heavy metals in fishes in the middle and lower reaches of the Yangtze River basin. *Environ Pollut* 159:2575-2585
- [5] Ahmed, M, Ahmad, T, Liaquat, M, Abbasi, KS, Farid, IBA, Jahangir, M. (2016) Tissue specific metal characterization of selected fish species in Pakistan. *Environ Monit Assess* 188:212
- [6] Liu, F, Cao, W, Wang, J. (2014) Length-weight relationships of 77 fish species from the Chishui River, China. *J Appl Ichthyol* 30:254-256
- [7] Cai S, Ni Z, Li Y, Shen Z, Xiong Z, Zhang Y, Zhou, Y. (2012) Metals in the tissues of two fish species from the rare and endemic fish nature reserve in the upper reaches of the Yangtze river, China. *Bull Environ Contam Toxicol* 88:922-927
- [8] Monroy, M, Maceda-Veiga, A, de Sostoa, A. (2014) Metal concentration in water, sediment and four fish species from Lake Titicaca reveals a large-scale environmental concern. *Sci Total Environ* 487:233-244
- [9] Wei, Y, Zhang, J, Zhang, D, Tu, T, Luo, L. (2014) Metal concentrations in various fish organs of different fish species from Poyang Lake, China. *Ecotoxicol Environ Saf* 104:182-188
- [10] Alcorlo, P, Otero, M, Crehuet, M, Baltanás, A, Montes, C. (2006) The use of the red swamp crayfish (*Procambarus clarkii*, Girard) as indicator of the bioavailability of heavy metals in environmental monitoring in the River Guadiana (SW, Spain). *Sci Total Environ* 336:380-390
- [11] Has-Schön E, Bogut I, Kralik G, Bogut S, Horvatić J, Čačić I (2008) Heavy metal concentration in fish tissues inhabiting waters of "Buško Blato" reservoir (Bosnia and Herzegovina). *Environ Monit Assess* 144:15-22
- [12] Wang, W.X, Rainbow, P.S. (2008) Comparative approaches to understand metal bioaccumulation in aquatic animals. *Comp Biochem Physiol C Toxicol Pharmacol* 148:315-323
- [13] Onsanit, S, Ke, C, Wang, X, Wang, K.J, Wang, W.X. (2010) Trace elements in two marine fish cultured in fish cages in Fujian province, China. *Environ Pollut* 158:1334-1342
- [14] Dhanakumar, S, Solaraj, G, Mohanraj, R. (2015) Heavy metal partitioning in sediments and bioaccumulation in commercial fish species of three major reservoirs of river Cauvery delta region, India. *Ecotoxicol Environ Saf* 113:145-151

- [15] Gaspic, Z.K, Zvonaric, T, Vrgoc, N, Odzak, N, Baric, A. (2002) Cadmium and lead in selected tissues of two commercially important fish species from the Adriatic Sea. *Water Res* 36:5023-5028
- [16] Andres, S, Ribeyre, F, Tourencq, J.N, Boudou, A. (2000) Interspecific comparison of cadmium and zinc contamination in the organs of four fish species along a polymetallic pollution gradient (Lot River, France). *Sci Total Environ* 248:11-25
- [17] Mdegela, R.H, Braathen, M, Pereka, A.E, Moshia, R.D, Sandvik, M, Skaare, J.U. (2009) Heavy metals and organochlorine residues in water, sediments, and fish in aquatic ecosystems in urban and peri-urban areas in Tanzania. *Water Air Soil Pollut* 203:369-379
- [18] Dalman, Ö, Demirak, A, Balci, A. (2006) Determination of heavy metals (Cd, Pb) and trace elements (Cu, Zn) in sediments and fish of the Southeastern Aegean Sea (Turkey) by atomic absorption spectrometry. *Food Chem* 95:157-162
- [19] Liu, J.L, Xu, X.R, Ding, Z.H, Peng, J.X, Jin, M.H, Wang, Y.S, Hong, Y.G, Yue, W.Z. (2015) Heavy metals in wild marine fish from South China Sea: levels, tissue- and species-specific accumulation and potential risk to humans. *Ecotoxicology* 24:1583-1592
- [20] Allen-Gil, S, Martynov, V. (1995) Heavy metal burdens in nine species of freshwater and anadromous fish from the Pechora River, northern Russia. *Sci Total Environ* 160-161:653-659
- [21] Canli, M, Atli, G. (2003) The relationships between heavy metal (Cd, Cr, Cu, Fe, Pb, Zn) levels and the size of six Mediterranean fish species. *Environ Pollut* 121:129-136
- [22] McKinley, A.C, Taylor, M.D, Johnston, E.L. (2012) Relationships between body burdens of trace metals (As, Cu, Fe, Hg, Mn, Se, and Zn) and the relative body size of small tooth flounder (*Pseudorhombus jenynsii*). *Sci Total Environ* 423:84-94
- [23] Merciai, R, Guasch, H, Kumar, A, Sabater, S, García-Berthou, E. (2014) Trace metal concentration and fish size: Variation among fish species in a Mediterranean river. *Ecotoxicol Environ Saf* 107:154-161
- [24] Monikh, F.A, Safahieh, A, Savari, A, Ronagh, M.T, Doraghi, A. (2013) The relationship between heavy metal (Cd, Co, Cu, Ni and Pb) levels and the size of benthic, benthopelagic and pelagic fish species, Persian Gulf. *Bull Environ Contam Toxicol* 90:691-696
- [25] Yi, Y.J, Zhang, S.H. (2012) Heavy metal (Cd, Cr, Cu, Hg, Pb, Zn) concentrations in seven fish species in relation to fish size and location along the Yangtze River. *Environ Sci Pollut R* 19:3989-3996
- [26] Niri, A.S, Sharifian, S, Ahmadi, R. (2014) Assessment of metal accumulation in two fish species (*Tenualosa ilisha* and *Otolithes ruber*), captured from the north of Persian Gulf. *Bull Environ Contam Toxicol* 94:71-76
- [27] Ozparlak, H, Sanda, M.A, Arslan, G. (2016) Some heavy metal levels in muscle tissue of seven fish species from the Sugla and Beysehir lakes, Turkey. *Fresen. Environ. Bull.* 25: 2090-2098
- [28] EC (2006) Commission Regulation (EC) No. 1881/2006 of 19 December 2006 setting maximum levels for certain contaminants in foodstuffs. *Official J Euro Union* 364:5-24

Received: 05.12.2016
Accepted: 06.06.2017

CORRESPONDING AUTHOR

Shenwen Cai

Department of Resources and Environment, Zunyi Normal College, Zunyi 563000, Guizhou, China

e-mail: caishenwen@163.com

THE COMPARATIVE ECONOMIC ANALYSIS OF ORGANIC AND CONVENTIONAL DRIED APRICOT PRODUCTION: A CASE STUDY FOR TURKEY

Kubilay Ucar^{1,*}, Gamze Saner¹, Sait Engindeniz¹

¹Ege University, Faculty of Agriculture, Department of Agricultural Economics, 35100 Bornova, Izmir, Turkey

ABSTRACT

The aim of this study is to comparative analyse economic aspects of the production of organic and conventional dried apricot in Malatya Province of Turkey. Data was collected at farmer level by the production year of 2009-2010 have been obtained as the result of interviews made with 38 organic apricot farmers and with 40 conventional apricot farmers selected from the districts of Akcadag, Darende and Hekimhan in Malatya Province where apricot production is carried out intensively. The fresh and dried organic apricot yield per hectare were determined as 5,969.90 kg and 1,680.90 kg in this research. The fresh and dried apricot yield per hectare were 4,688.60 kg and 1,586.40 kg in the conventional farms. Gross production value per hectare is found as €6,597.25 in the farms producing organic dried apricot and this value is found as €5,197.49 in the farms producing conventional dried apricot. While variable costs per hectare in the organic apricot farms is found as €2,285.32. It is found as €1,812.97 in the farms producing conventional dried apricot. Fixed costs per hectare in the organic and conventional apricot farms are found as €1,005.89 and €996.77, respectively. Gross margin per hectare is determined as €4,311.93 in the farms producing organic apricot and it is determined as €3,384.52 in the farms of conventional apricot production. Net profit per hectare in the organic and conventional apricot farms are found as €3,306.04 and €2,387.75, respectively.

KEYWORDS:

Apricot, Organic farming, Profitability analysis, Economic analysis, Market analysis, Sustainable agriculture.

INTRODUCTION

Turkey is the most important dried apricot producer in the world. Dried apricot production is one of major part of agricultural economy in Turkey.

Dried apricot production in the world is 239,018 tons and Turkey provides 73.93% of it by

176,718 tons [1]. Apricot is produced mainly in the province of Malatya and partially in Elazığ, Erzincan, Sivas, Kars and Iğdir provinces with Aegean, Mediterranean, Central Anatolia and Marmara Regions in Turkey. Total fresh apricot production of Turkey is reached 7.6 million tons and yield per tree is reached to 54 kg in 2012 [2]. The apricot of Malatya is a product having geographical mark. 90% of the total apricot production in Malatya province of Turkey is being allocated for drying. Dried apricot production plays an important role in the export of agricultural products. The amount of dried apricot oriented to export is decreased as 9.62% from 99.04 million tons to 89.75 million tons during 2001-2010 period. Export value of dried apricot is increased from \$ 89.14 million to \$ 347.58 million with an increase of 290% in the same period. Turkey exports dried apricots to 90 countries. It is known that it directs more than 50% of its export to USA, Russian Federation and some EU countries (Germany, England and France). The increase of demand in the world for organic products in recent years is caused the increase of production and export of organic products in Turkey as starting from 1985. Organic apricot production is increased from 1.12 million tons to 1.17 million tons with an increase of 4% in between the years of 1998-2008. The export value of organic dried apricot is increased by 23.70% from \$ 3.15 million to \$ 3.90 million. The production of organic dried apricot is rapidly increased in the recent ten years within Malatya province due to its high price and market guarantee. The total number of organic apricot farmers is reached to 371 farmers in 12 districts including the central district of Malatya in 2010 [3]. In recent years, some studies have been made on economics of apricot production in Turkey. [4,5,6,7,8,9,10,11,12,13,14,15,16,17,18]. But, there is still need for study, especially in local level. The aim of this study is to comparative analyse economic aspects of organic and conventional dried apricot production in Malatya Province of Turkey.

MATERIALS AND METHODS

In this research, the data was collected through face-to-face interviews with selected farmers from

the districts of Central, Akcadag, Darende and Hekimhan at the Malatya province in the production year of 2009-2010. These farmers were willing for their data to be recorded. Data and observations were recorded throughout the production period. Moreover, the results of researches previously made in the region regarding the subject. Data obtained from directorates of provinces and counties reports and statistics published by TurkStat. Turkish Ministry of Food, Agriculture and Livestock and relevant web sites had been used as secondary data sources. According to Malatya farmer registration system 2009, it is determined that 88,457 parcels of apricot exists in Malatya. In the previous studies, the number of conventional farmers is determined as 22,114 as the average number of parcels of the farms is 4. It is also determined that the number of organic apricot farmers in Malatya was 371 in 2009 [3]. Thus, it is started from the number of organic and conventional farmers in the selection of samples. Proportional sample volume formula is used in the determination of the number of conventional farmers with whom it will be met and it is based on 90% probability and 12% error margin [19].

$$n = \frac{Np(1-p)}{(N-1)\sigma_{\hat{p}}^2 + p(1-p)}$$

In formula:

n = sample size.

N = population.

p = proportion of record keeping apricot farmers (1-p):0.50

= Variance of proportion

In this calculation, the number of farmers performing conventional apricot production within the districts of Central, Akcadag, Darende and Dogansehir of with whom it will be met have been calculated as 40 within the 90% confidence interval. Moreover, it is planned to make reserve questionnaire at a rate of 10%. In the determination of the number of organic farmers with whom it will be met. Sample size is determined considering 90% confidence interval and 12% error margin. Sample size is found as 38. At the end, the total number of farmers whom will be interviewed have been determined as 78.

In this study, the cost items of organic and conventional apricot production was classified into variable costs and fixed costs. The variable costs associated with the growing of organic and conventional apricots were all inputs that directly related to the production of organic and conventional, and which covered the costs of labor, fertilizer, pesticide, electricity, fuel oil, etc. Variable costs were calculated by using current input prices and labor costs. Variable costs also included the interest on variable costs. Interest on the total variable costs was calculated by charging a simple

interest rate of 4% (annual savings deposits interest rates on the €). But, the interest on the total variable costs was calculated for six months and the interest rate was 2%, since the apricot production and market period were approximately six months. In this study, fixed costs included administrative costs, annual depreciation costs, rent equivalent of land, interest of variable costs. In this study, administrative costs were estimated to be 3% of the total variable costs [20, 21]. Fixed costs plus variable costs equal the total production costs. The total costs were subtracted from the total gross production value to calculate the net profit.

First Kolmogorov-Smirnov test and normal distribution test is performed with the continuous data obtained from the research area [22]. According to the result of this test, technical and economical variables had been separated as variables showing and non-normal distribution. One-Way Anova test is applied for variables showing normal distribution and Mann Whitney-U test is applied for the ones not showing normal distribution. One-way Anova test (one-way variance analysis) intends to test whether two or more groups is taken from normal distributed populations with similar average by using common variance. Mann Whitney-U test is being used to test the equality of two averages. It is known and implemented more extensively compared to other tests as it is the most powerful one among the non-parametric tests [23].

RESULT AND DISCUSSION

Socio-economic characteristics of farmers. It is found that average farmer age at farms producing organic apricot is 51.37, education level of the farmer is 8.37 years, the experience period in agricultural activity was 29.61 years, the experience period of only apricot cultivation is 27.24 years and it is determined that these farms were performing organic apricot production since 8.34 years. Average farmer age is found as 51.56, educational level as 7.22 years and agricultural experience period as 30.38 years in the farms of conventional production. Average land of organic and conventional farms were determined as 4.06 and 3.62 hectare (Table 1).

Organic and conventional apricot production. Mainly Hacıhaliloglu variety and Hacıhaliloglu and Kabaasi varieties are being preferred at farms performing organic and conventional apricot production. Yield of apricot is at low levels within Malatya province due to the frost damage in March of 2010. At the investigated farms, average organic apricot area is 4.06 hectares and conventional apricot area is 3.62 hectares. When the number of apricot trees per hectare are calculated, the same findings were obtained in the organic and conventional farms and it is determined that about

TABLE 1
Farmer's age, education and agricultural experience

<i>Characteristics of farmers</i>	<i>Organic Farms</i>	<i>Conventional Farms</i>
<i>Farm Groups</i>	<i>(38 farms)</i>	<i>(40 farms)</i>
Age (year)	51.37	51.56
Education level (year)	8.37	7.22
Agricultural experience (year)	29.61	32.26
Apricot production experience (year)	27.24	30.38
Organic apricot production experience (year)	8.34	-
Land (ha)	4.06	3.62

TABLE 2
Average variable costs of farms (€)

<i>Variable Costs</i>	<i>Organic Farms</i>	<i>Conventional Farms</i>
	<i>(38 farms)</i>	<i>(40 farms)</i>
Fertilizer costs	1,712.42	1,371.42
Pesticide costs	1,026.93	592.48
Fuel oil costs	2,040.82	2,038.27
Labour costs	2,397.27	1,563.67
Irrigation costs	258.55	258.35
Electricity costs	1,842.40	738.78
Total variable costs	9,278.39	6,562.97
Total variable costs (per hectar)	2,285.32	1,812.97

nine trees exists per hectar. While fresh apricot yield per tree is found as 63.85 kg at organic farms and this amount is found as 51.52 kg at conventional farms in this study. Organic apricot production per tree is found as 60.00 kg in another study in Turkey [5]. While dried apricot yield per tree is found as 17.98 kg at organic farms and it is found as 17.43 kg at conventional farms. While one kg dried apricot is being obtained from three kilograms of conventional fresh apricot. More fresh apricot is being required in order to obtain one kg organic dried apricot. While fresh apricot yield per hectar is found as 5,969.90 kg at organic farms, It is found as 4,688.60 kg at conventional farms. While dried apricot yield per hectar is found as 1,680.90 kg at organic farms, it is found as 1,586.40 kg at conventional farms.

Production costs. Production costs covers variable costs and fixed costs. Variable costs at the investigated farms are given in Table 2. Variable costs per hectar is found as €2,285.32 at farms producing organic dried apricot and it is found as €1,815.97 at farms producing conventional dried apricot. Labour pesticide and fertilizer among variable cost factors occupy a significant place in both of the farm groups except organic certification cost. Organic certification cost is paid by the firms and exporter. The higher variable costs of organic apricot farms are caused mainly by the usage of excessive labor [10]. Statistically significant differences have been determined in respect of pesticide, labour and water costs. ($p < 0.05$). In the

One Way Anova test made according to cultivation type. Significant difference is not found in respect of variable costs per hectar ($p > 0.05$).

Average fixed costs per hectar are given in Table 3. While fixed costs per hectar is 996.77 €/hectar at conventional apricot farms and the average value of fixed costs per hectar at organic apricot farms are calculated as 1,005.89 €/ha. It is been determined that there is no statistically significant difference in respect of total fixed costs and fixed costs per hectar as the result of One Way Anova test made according to apricot cultivation types. But statistically significant results are obtained as the result of One Way Anova test made according to apricot area ($p < 0.05$).

Gross production value. Gross production value consists of the monetary value of apricot production obtained as the result of one year's productive activity in the farms. Apricot pit also had monetary value as by product of apricot production. Thus the pit value is added to gross production value of apricot production. While total gross production value at farms producing organic dried apricot is calculated to be € 26,784.82. Gross production value per hectar is calculated as € 6,597.25. Total gross production value is found to be €18,814.93 and gross production per hectar is found to be € 5,197.49 in conventional dried apricot farms (Table 4). According to One Way Anova test made according to apricot cultivation type. The difference in between the farms performing organic and conventional.

TABLE 3
Average fixed costs of farms (€)

<i>Fixed Costs</i>	<i>Organic Farms (38 farms)</i>	<i>Conventional Farms (40 farms)</i>
Administrative costs (3%)	2,783.52	1,968.89
Annual depreciation costs (*)	7,877.86	7,595.21
Rent equivalent of land (5%)	28,281.93	25,216.28
Interest of variable costs (2%)	1,855.68	1,312.59
Total fixed costs	40,798.99	36,092.97
Total fixed costs (per hectar)	1,005.89	996.77

(*) The economic life of plantations was estimated as 30 years.

TABLE 4
Gross production value of farms

<i>Items</i>	<i>Organic Farms (38 farms)</i>	<i>Conventional Farms (40 farms)</i>
Sold fresh apricots (kg)	6,656.67	5,066.10
Fresh apricot price (€/kg)	0.64	0.62
Dried apricot production (kg)	6,817.74	5,744.64
Dried apricot price (€/kg)	3.12	2.60
Pit (kg)	2,124.07	1,272.22
Pit price (€/kg)	0.59	0.58
Total gross production value (€)	26,784.82	18,814.93
Gross production value (per hectar)	6,597.25	5,197.49

apricot production in respect of gross production value per hectar had been found statistically significant

Gross margin and net profit. Net profit and gross margin are being used in measuring the success of farms during farms analysis. Gross margin is obtained by deducting the total variable costs from the total gross production value of investigated farms. Net profit is calculated by deducting the total costs from the total gross production value. Gross production value, variable costs, gross margin and net profit of farms has shown in Table 5. While gross margin per hectar at farms producing organic dried apricot had been found to be 4,311.93 €/ha. It had been found as 3,384.52 €/ha at farms producing conventional dried apricot. Net profit per hectar at farms producing organic dried apricot had been found to be 3,306.04 €/ha. It had been found as 2,387.75 €/ha at farms producing conventional dried apricot. Due to provision of premium to organic products at organic farms, it can be said that gross

margin per hectar is higher. The difference in between farms performing organic and conventional apricot production in respect of gross margin and net profit per hectar is found to be statistically significant according to the result of One-Way Anova test ($p < 0.05$).

CONCLUSION

This research has been successful in determining profitable of organic and conventional dried apricot production. In apricot production, success depends on how well the farmer can manage the crop and make the right decisions. Usage of chemical fertilizer and pesticide is intense in the production of conventional cultivated dried apricot. On the contrary, pesticide usage is lower and fertilizer usage is higher at farms producing organic

TABLE 5
Net profit and gross margin per hectare of farms (€)

<i>Items</i>	<i>Organic Farms (38 farms)</i>	<i>Conventional Farms (40 farms)</i>
Gross production value (1)	6,597.25	5,197.49
Variable costs (2)	2,285.32	1,812.97
Variable + fixed costs (3)	3,291.21	2,809.74
Gross margin (4=1-2)	4,311.93	3,384.52
Net profit (5=1-3)	3,306.04	2,387.75

dried apricot. Thus, it is specified by the farmers that improvement is observed in the nature and environment since the start of organic cultivation. As the result of the research made, it had been determined that the organic dried apricot is more profitable than the conventional dried apricot due to price superiority despite the lower level of yield per tree.

Some suggestions for improving organic and conventional production in the region should be presented. For example; farmers should be informed about Integrated Pest Management. Contract farming systems should be developed. Irrigation cooperatives should be improved. Producers should be informed about crop insurance. Sales cooperatives should be established. Credit limits should be increased and credit interest should be decreased. As a conclusion; organic dried apricot growing is an profitable activity in Turkey compare to conventional dried apricot growing. But farmers should gather all the economic data about organic dried apricot growing and market conditions before planting apricot. Although, cost and return estimates are believed to be typical and realistic, individual farmers should adjust these values to their own specific situations and circumstances.

REFERENCES

- [1] International Nut and Dried Fruit Council (2012) Annual Reports. Spain
- [2] TurkStat. (2012) Agricultural Production Statistics-2012, Ankara
- [3] Turkish Ministry of Food, Agriculture and Animal Husbandry, Directorate of Malatya (2010) Annual Records, Malatya.
- [4] Dellal, I. and Koc, A. (2003) An econometric analysis of apricot supply and export demand in Turkey. *Turk. J. Agric For.* 27, 313-321.
- [5] Demirtas, B. and Gul, A, (2003) Socio-economic structure and problems of fresh apricot producers in Mersin province. *Journal of Aegean Agricultural Research Institute*, 13(1), 158-175.20.
- [6] Gezer, I., Acaroglu, M. and Haciseferogullari, H. (2003) Use of energy and labour in apricot agriculture in Turkey. *Biomass Bioenerg*, 24(3), 215–219.
- [7] Peker, K. (2004) Comparative economic analysis between chemical pesticides and bacterium using in apricot production. *Die Bodenkultur, Austrian Journal of Agricultural Research*. 55(2), 47-51.
- [8] Gultekin, U. and Adanacioglu, H. (2004) Production and marketing of organic dried apricot in Turkey. *The Market for Organic Products in the Mediterranean Region. Cahiers Options Méditerranéennes*, pp:287-294.
- [9] Olgun, A. and Adanacioglu, H. (2006) Production and Marketing of Organic Dried and the Tendences of Apricot Producers for the Future in Turkey: Case Study of Malatya. *Acta Horticulturae*, 717, 271-280.
- [10] Gundogmus, E. (2006) A comparative analysis of organic and conventional dried apricot production on small households in Turkey, *Asian Journal of Plant Sciences*, 5(1), 98-104.
- [11] Asma, B. (2007) Malatya: World's capital of apricot. *Chronica Horticulture*. 47(1), 20-24.
- [12] Esengun, K., Gunduz, O. and Erdal, G. (2007) Input-output energy analysis in dry apricot production of Turkey. *Energy Conversion and Management*. 48, 592-598.
- [13] Cukur, F., Saner, G., Cukur, T. and Ucar, K. (2008) The Evaluation of apricot farmers' behaviours toward agricultural insurance for risk transfer in Malatya province: the case study of Doğanşehir district, Polatdere village. *Journal of Ege Universty Faculty of Agriculture*. 45(2), 191-198.
- [14] Ercisli, S. (2009) Apricot culture in Turkey. *Scientific Research and Essay*, 4. 715-719.
- [15] Gunduz, O. (2010) Effect of exchange rate on dried apricot export in Turkey: A vector autoregression (VAR) analysis, *African Journal of Agricultural Research*, 5(18), 2485-2490.
- [16] Gunduz, O., Ceyhan, V. and Esengun, K. (2011) Measuring the technical and economic efficiencies of the dry apricot farms. *Journal of Food, Agriculture and Environment*, 9(1), 319-324.
- [17] Saribas, E.B. (2012) Economic Analysis of Turkish Apricot Industry: A Case Study on Malatya Province, Msc. Thesis, Istanbul University, Turkey. 117p.
- [18] Ucar, K. and Saner, G. (2013) Analaysis of investment projects oriented to organic and convantional apricot orchard in Malatya Province *Journal of Ege Universty Faculty of Agriculture*. 50(2), 191-198.
- [19] Newbold, P. (1995) *Statistics for Business and Economics*. Prentice-Hall International. New Jersey. 867p.
- [20] Engindeniz, S., Cukur, F. and Engindeniz, Y. (2003) Alternative opportunities for small farms: a case study on technical and economic analysis of peach growing in Turkey, *Journal of Agricultural & Food Information*, 5(4), 47-58.
- [21] Engindeniz, S., Cukur, F. and Engindeniz, Y. (2006) Factor afecting the profitability of peach in Turkey. *Agricultura Tropica et Subtropica*, 39(4), 227-232.
- [22] Pazarlioglu, V. and Akkaya, P. (1995) *Econometrics I*, 3rd Edition, Anadolu Printing, Izmir, 581p
- [23] Basturk, R. (2010) *With All Aspects SPSS-Sample Nonparametric Statistical Methods*, Ani Publishing. Ankara. 251 p.

- [24] Demirtas, M.N., Atay, S. and Aslan, A. (2011)
Apricot growing and problems in Malatya. GAP
VI. Agriculture Congress, Sanliurfa, May 9 -12,
14-19.

Received: 15.12.2016
Accepted: 20.05.2017

CORRESPONDING AUTHOR

Kubilay Ucar
Ege University
Faculty of Agriculture
Department of Agricultural Economics
35100 Bornova, Izmir – TURKEY

E-mail: kubilay82ucar@hotmail.com

NANO-BIOLOGICAL MODIFICATION OF THE ELECTRODES IN MICROBIAL FUEL CELL

Farzad Sadri¹, Alireza Khodavandi², Ali Shamsazar³, Masoud Negahdary⁴, Ghasem Rahimi^{5,*}

¹Young Researchers and Elite Club, Yasooj Branch, Islamic Azad University, Yasooj, Iran

²Department of Biology, Gachsaran Branch, Islamic Azad University, Gachsaran, Iran

³Department of Biochemistry, Payame Noor University, Tehran, Iran

⁴Yazd Cardiovascular Research Center, Shahid Sadoughi University of Medical Sciences, Yazd, Iran

⁵Young Researchers and Elite Club, Marvdasht Branch, Islamic Azad University, Marvdasht, Iran

ABSTRACT

Recently, renewable energy with the ability to replace traditional energy such as fossil fuels, has attracted the attention of many researchers. In this study, the amount of the produced electricity in the presence of modified graphite electrode with biological synthesized silver nano particles was evaluated. In the first stage microbial fuel cell (MFC) system was designed; subsequently, synthesized silver NPs through biological method and their properties were investigated using UV-vis spectroscopy, Fourier transform infrared spectroscopy (FTIR) and particle size analysis (PSA). Scanning electron microscope (SEM) was used for exploring the modified electrodes with silver NPs and valid modification status. Eventually, the modified graphite electrode with used NPs and the amount of produced electricity in the presence of electrodes were evaluated. Our results showed that the modified graphite electrode with NPs has high potential for electricity generation that was more than bare graphite electrode. Indeed, the generated maximum power and current density for bare graphite electrode were 82 mW/m⁻³ and 1100 mA/m⁻³ respectively but the generated maximum power and current density for modified electrode with silver NPs were 160 mW/m⁻³ and 1400 mA/m⁻³ respectively.

KEYWORDS:

Nano-biological Modification, Microbial Fuel Cell, silver NPs

INTRODUCTION

Recently, due to the reduction of fossil fuel resources and the destructive effects of global warming, the use of biomasses as a safe, sustainable and optimal resource has been considered. In this regard, various studies have been conducted and different methods have been introduced [1]. MFC, considering the catabolic ability of microorganisms for gen-

erating electricity, is one of the most optimal approaches which was introduced for first time by Potter in 1911[2]. MFC is a combination of microbiology, electrochemistry and other compatible sciences such as nanotechnology that lead to transformation of chemical energy to electrical energy. In this system anaerobic microorganisms, by attaching to the electrode surface, create a complex structure that called biofilm. In biofilm structure, microorganisms are creating electrons by oxidizing organic matter. The produced electrons move among respiratory enzymes and participate in energy generation as ATP form. Then, after passing among the electrolyte in the cell, the electrons are transferred to electron acceptor (anode) and subsequently to electron acceptor in cathode. In addition, the produced positive ions in anode are conducted towards cathode by passing through the membrane (electrolyte); in the presence of catalyst, react with the oxygen and electron that reach the cathode section from the external circuit and are turned into water molecules (figure1) [3,4,5]. Different and complex parameters such as the type of cathode and anode, the rate of transfer electron, microbial biofilm anode, the rate of transfer electron from the anode to the cathode, the substrate used for biofilm formation, ohmic resistance of the electrolyte and the other factor chemical can be involved in MFC performance[6]. However, one of these parameters that have a direct connection with the level and speed of electron transfer from microorganism to anode and the transfer of electron in circuit, and in other words have a significant role in MFC performance is electrode surface area because it creates limitation in the number of microorganisms that can reach to anode. Electrode surface area is one of the factors on which a few studies have been conducted. Recently some researchers have tried to increase the performance of MFC to some extent by increasing coating electrodes with Nps [7]. The unique characteristics of Nps such as the increased surface to volume ratio are found in them that act in order to increase the performance of MFC. In this study, biosynthesized silver NPs were used for modifying electrode to increase MFC performance.

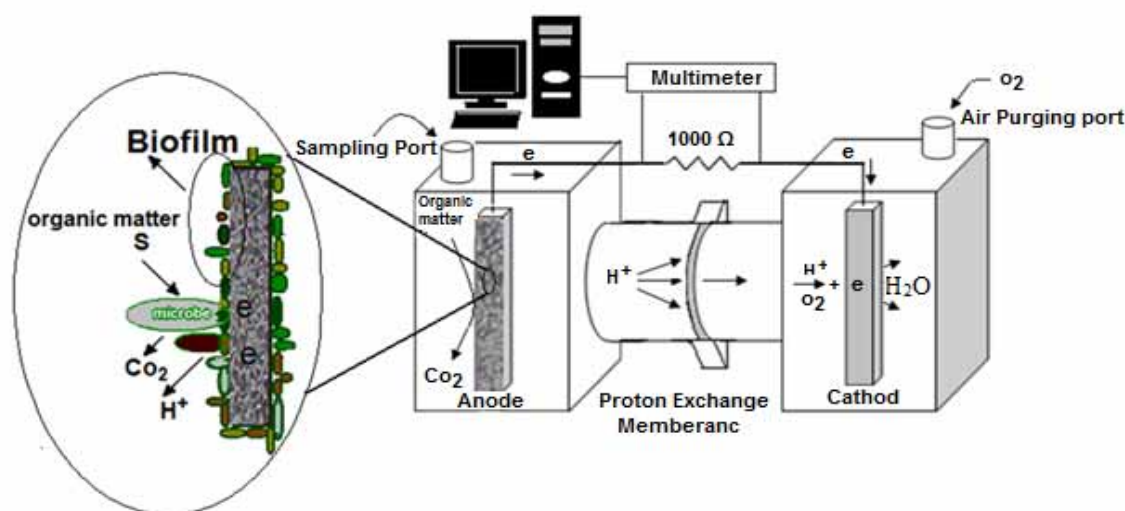


FIGURE 1
Microbial fuel cell system

MATERIALS AND METHODS

Materials. All chemicals that were used in this study such as NH_4Cl , $\text{NaH}_2\text{PO}_4 \cdot \text{H}_2\text{O}$, MnSO_4 , MgSO_4 and culture medium (used for growing of yeast) were obtained from Merck company, Germany. In all experiments, a graphite (10cm x 10cm) was used which was purchased from Arvin Danesh Arian Company, Iran.

Designing microbial fuel cell. For designing MFC, two cylindrical chambers that were connected by a polyethylene tube were used. For separating the content of cylindrical chambers, a proton exchange membrane (PEM) Nafion 117cs (Sigma, USA) was used. PEM pretreatment started with boiling the film in 3% H_2O_2 for 1h, washing with deionized water, 0.5 M H_2SO_4 , and washing with deionized water respectively. Total volume of each chamber was 2 liter and the useful volume was 1.5 liter. The used graphite electrode was modified with biosynthesized silver Nps. In the anode chamber a small pump for circulation of substrate was used. Before performing the test, washing steps with 30% H_2O_2 , 0.5M H_2SO_4 , and deionized water were done exactly [8,9]. Table 1 shows the properties of PEM.

TABLE 1
Properties of proton exchange membrane

Description	Unit	Nafion 117cs
Average grain size	cm ²	100
Width	μm	183
Proton conductivity	mS/cm	83

Preparation of microorganism and medium.

In this study *Saccharomyces cerevisiae* PTCC 5269 was used for electricity generation in MFC. This

yeast was supplied by Centre for Scientific and Industrial Research of Iran. *Saccharomyces cerevisiae* was grown in an anaerobic condition. In MFC, the medium that added to anodic chamber of MFC was contained NH_4Cl (130 mg L⁻¹), $\text{NaH}_2\text{PO}_4 \cdot \text{H}_2\text{O}$ (7400 mg L⁻¹), MnSO_4 (50 mg L⁻¹), MgSO_4 (20 mg L⁻¹), glucose (500 mg L⁻¹) and yeast extract (10 mg L⁻¹). For the cathodic chamber, all the mentioned constituents except yeast extract and glucose were used [10].

Synthesis of silver NPs. In order to perform synthesizing procedure, the clinical isolates of *Candida albicans* were cultured on Saborad Dextrose agar medium (Merck .co). 3.5 mM silver nitrate was used in order to detect and isolate yeast resistant against silver nitrate. After 24 h incubation at 37 ° C, plates that were contained of grown colonies of *Candida albicans* were isolated for next usage. In order to obtain cell mass, colonies grown were cultured in Meyer flask containing 250 ml of Saborad Dextrose broth medium (Merck .co) and also were maintained in Shaking incubator at 200 rpm for 24 h at 37 ° C. After this time, the cells were separated using centrifugation in 6000 rpm and then washed 3 times with phosphate buffer saline medium pH 7.4. Then, 5 g of wet weight yeast was removed and transferred to sterile flask containing 100 ml of 1.5 mM silver nitrate. This flask was kept in dark conditions in shaking incubator at 37 ° C. After a long time (2h); along with observed color change, biomass was maintained in shaking incubator for 48 h in order to find separated cell. In the next step, the separated cell biomass was centrifuged in 6000 rpm due to achieve the optimized condition for synthesizing of silver Nps. The yeast biomass that had ability to produce silver Nps

was isolated via centrifugation in 6000 rpm and was divided into three parts for the purpose of FTIR investigation, PSA analysis and UV-vis spectroscopy [11].

Characterization of silver NPs. UV-Vis spectroscopy. Ultraviolet-visible spectroscopy was used to explore the absorption spectrum of the biosynthesized Nps. For this purpose, 50 μ l of obtained solution and 50 μ l of distilled water were added and analyzed with this technique at the wave length of 300-800nm [11].

FTIR investigation. FTIR spectroscopy is one of preferred spectrophotometric methods. FTIR was used due to approve accurate identification and also more exploring about features of synthesized NPs.

PSA investigation. Determining the exact size and distribution of silver Nps was also performed through PSA. In order to do this experiment, 1 ml of resulted admixed solution (the interaction of silver nitrate and cells biomass with 10 ml of distilled water) was analyzed by PSA.[12]

Modifying graphite electrode. In this study two graphite electrode types were used. Bare graphite electrode was provided through desired carbon powder and modified graphite electrode was prepared based on mixing a 3: 1 ratio of carbon powder and biosynthesized silver Nps (C) respectively. [13]

Measurements of voltage and current. Data analysis. The current produced in this study was calculated and recorded according to equation 1 and system power was calculated based on equation 2. Through dividing the values of power density and current density by the surface of electrode, the values of these two factors were calculated and recorded. The data obtained in this stage were used for plotting the polarization curve and also for the diagram of voltage change in each loading cycle. Voltage (V) changing with the external resistance in the MFC was recorded by a data acquisition system connected to a computer every 20 min. Furthermore, 10 Ω , 100 Ω , 1000 Ω , 10000 Ω and 100000 Ω resistances were used for indicating the relation between power density and resistance in modified electrode state and basic electro state. [14]

$$I=V/R \quad (1)$$

$$P=V \times I. \quad (2)$$

RESULT AND DISCUSSION

The characteristics of the synthesized NPs.

According to the macroscopic observations, the change of color in produced biosynthesis process in the Nps indicated the existence of Nps in the reaction

solution. As shown in figure 2, after adding silver nitrate salt to the yeast cell biomass, the color of the reaction mixture was changed from white to reddish-brown after 2 h. This change in color verifies the ability of *Candida albicans* in biosynthesizing of Nps.

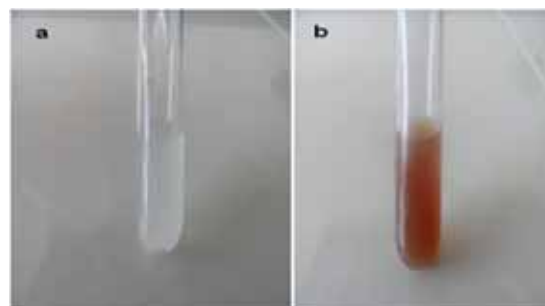


FIGURE 2

The resulted change in color after biosynthesizing of Nps

Study of UV-visible spectroscopy. Figure 3 Shows the UV- visible spectrum of synthesized silver Nps by yeast; an absorption peak found in range of 800-300 nm that was related to silver Nps and indicates shifts and surface plasmon at 420 nm. Previous researches showed that the peak absorption of silver Nps was in the range of 450-400 nm [11].

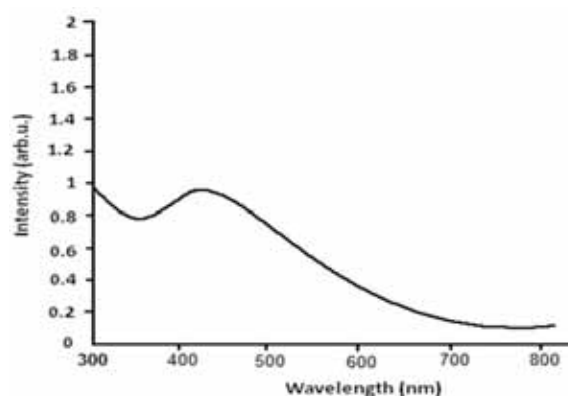


FIGURE 3

UV- visible spectrum of the synthesized silver Nps by candida albicans

FTIR Absorption spectrum. Figure 4 show colloid FTIR spectrum of biosynthesized silver Nps in the 500-4000 CM^{-1} range. The created peaks, especially the peaks 1 and 2 were created in the 2500-4000 CM^{-1} range that indicate the existence of proteins around the synthesized particles; on the other hand, the mentioned created peaks indicate the preservation of the second protein structure after interaction with silver NPs. Therefore, it can be find that the fungal proteins are reducing agents for silver nitrate solution and responsible for the synthesis of silver NPs; the recommended mechanism for biological synthesis of silver Nps is also related to these proteins. This mechanism suggests that

enzymes of a type of nitrogen reducing proteins (nitroreductases) act as reducing agents.

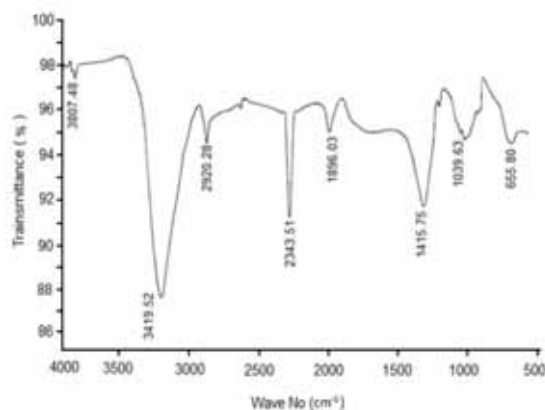


FIGURE 4

Fourier transform infrared spectroscopy of silver Nps

Determination the exact size and distribution of silver Nps via particle size analysis. Figure 5 shows the synthesized silver Nps that have average size of about 10 - 70 nm and most produced particles have a size 20 nm. This distribution of synthesized silver Nps in the nanometer range captured certain special physical and chemical properties that have many applications in various fields such as biology and medicine.

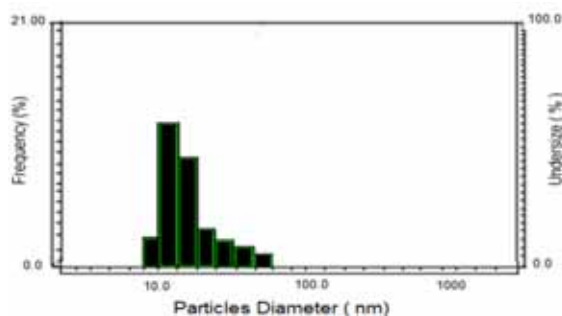


FIGURE 5

Particle size analysis of silver Nps

Figure 6 shows the SEM images of the used electrode in two conditions: before (a) and after (b) modification with biosynthesized silver Nps. Figure 6b indicates that the used electrode in this study is completely covered with biosynthesized silver NPs with special spherical morphology and average size of 10 to 70 nm. Considering the unique properties of mentioned NPs including the increased surface to volume ratio, it can be concluded that the electrode coated with biosynthesized NPs create very higher surface on the electrode for attachment, contacting and transmission of electrons.

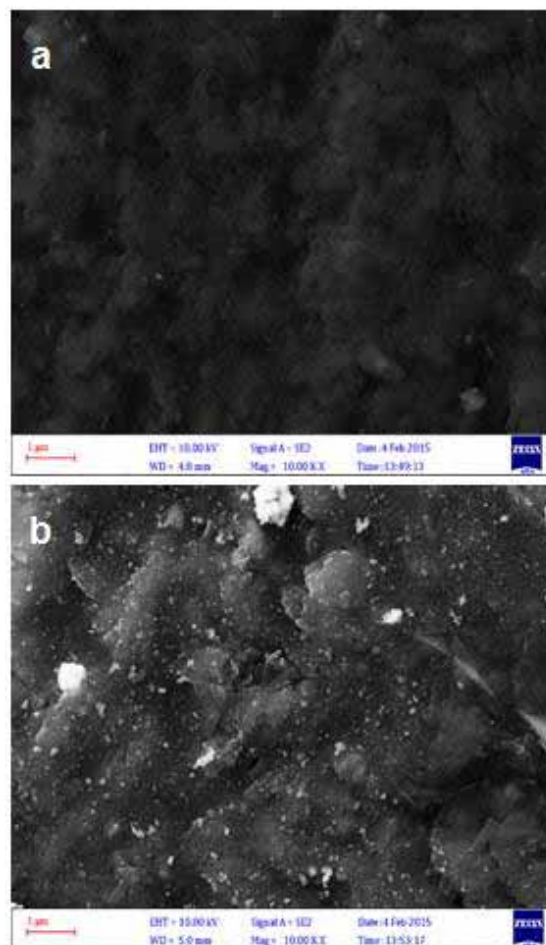


FIGURE 6

SEM images of graphite electrode; a) Before modification with biosynthesized silver Nps and b) after modification with biosynthesized silver Nps.

Figure 7 shows the energy-dispersive X-ray spectroscopy (EDX) spectrum of the modified electrode with biosynthesized silver NPs. This figure is also considered as verification for the existence of biosynthesized silver NPs and purity of them on the surface of graphite electrode.

Current and power density. The data analyzing in this study indicated that voltage for bare graphite electrode is recorded as 710 mV while for the modified graphite electrode with silver Nps it was recorded as 950 mV (figure 8). The current and power profiles for graphite electrode and modified graphite electrode by biological silver NPs are shown in figure 9. As shown in this figure the power and current density were decreased. This decrease may be due to membrane resistance, the distance between the anode and cathode or applied type of electrolyte used in the experiments. Our results showed that maximum power and current density generated for bare graphite electrode were 82 mW/m^{-3} and 1100 mA/m^{-3} respectively while the maximum generated power and current density for the modified

electrode by biological silver NPs were 160 mW/m^3 and 1400 mA/m^3 respectively. Here, the obtained maximum power density and the level of voltage changes using polarization curve are considered to assessment the performance of MFC.

Efficiency of a MFC is depends on several factors such as type of electrode, the rate of electron transfer from microbial biofilm (cathod) to anode, the rate of electron transfer from anode to cathod, substrate used for biofilm formation, ohmic resistance of the electrolyte and other chemical factors [3]. Many studies have been conducted to improve the performance microbial fuel cell using metal materials [15]. Nanoparticles are useful materials that can have ameliorative impact on performance of a MFC [16]. Overall, the increasing

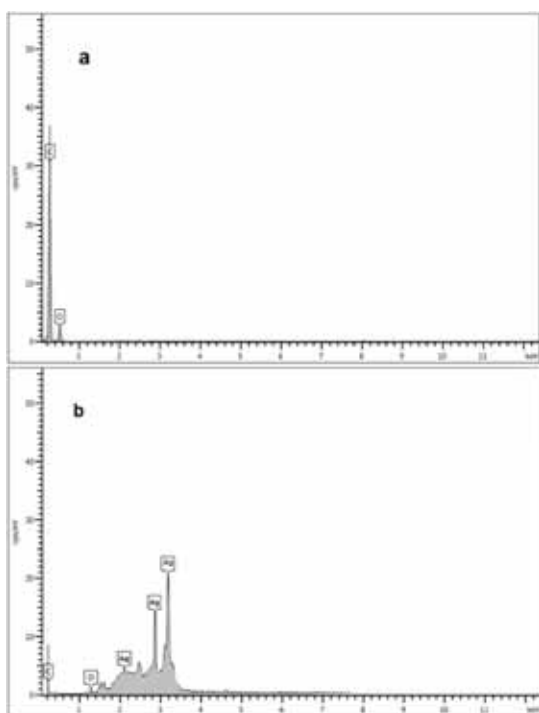


FIGURE 7

EDX spectrum. a: Basic electrode: b: Modified electrode with biosynthesized silver NPs

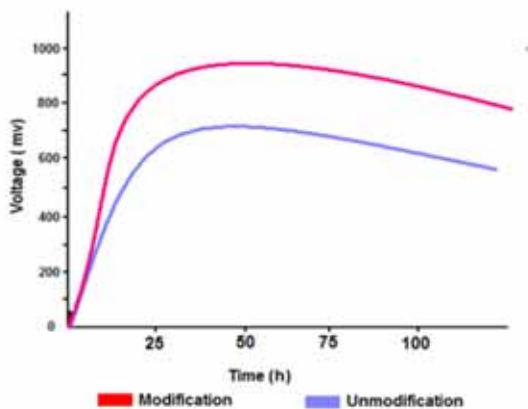


FIGURE 8

Voltage changes in designed MFC

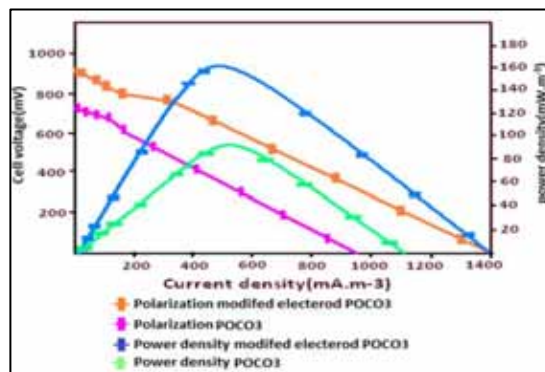


FIGURE 9

Polarization and power density in designed MFC

surface area to volume ratio that occurs gradually with the reduction of particles size results in the domination of behavior of atoms on the particle size on the behavior of the internal atoms. This phenomenon impacts the particle properties as isolated form and in interaction of materials. High surface area is a key factor in the performance of catalysts and structures of electrodes. The efficiency of chemical catalysts and electrodes can be effectively improved using this property [17].

This study has tried to improve the MFC performance by modification of electrode with biosynthesized silver Nps for the first time. These results showed the increase of efficiency of MFC with the electrode modified with silver Nps. In a study, reported output power of MFC was increased from 0.65 mW/m^2 to 788 mW/m^2 in the yeast *Saccharomyces* and modified electrodes with Mn^{4+} [18]. In contrast to mentioned study, our results showed that output power of MFC in the presence of *Saccharomyces* and modified electrode with biosynthesized silver NPs increased from 82 to 160 mW/m^3 . Our result showed that the electrode modified with silver Nps increases output power 2.7 times higher than bare graphite electrode. In a study, after modification graphite electrode with Mn^{4+} , the output power of MFC was increased from 0.02 mW/m^2 to 10.2 mW/m^2 . Our result showed that when graphite electrode is coated and modified by biological silver Nps, its output power is increased from 82 to 160 mW/m^3 . [20]. Alatraktchi et al used gold NPs with an average size of 50 to 100 nm for the assessment of MFC performance. By using modified electrode with these NPs, they concluded that the performance of MFC was significantly increased. Also, in our study the performance of MFC was significantly increased but this matter should be considered that the used nanoparticles in our study were synthesized via a biological method and their size was between 20 - 70 nm [20]. In another study, Wen et al explored the MFC performance in the presence of TiO_2 NPs [21]. The results of their research indicated that voltage, power density and current density were increased during using of the modified electrode with these

Nps. Also, in the presented study, the using of modified electrodes with biosynthesized silver Nps led to increasing the power density, current density and voltage. However, the Nps in the present study were synthesized using a biological method that can be considered as an important advantage.

CONCLUSION

Technology of biological fuel cells is one of the newest methods for electricity generation from microbial biomass. Designing of fuel cell system is considered as one of the most important and hot approaches due to achieving to related advanced technology using microbial fuel cell systems. In this study we used of microbiology, nanotechnology and electrochemistry to obtain new microbial form of electricity. Along with increasing of generated power and current density in the presence of modified graphite electrode against bare graphite electrode, it can be concluded that silver Nps provide more surface for electron transfer from anode to cathode pole.

REFERENCES

- [1] Lewis, N.S and Nocera, D.G. (2006). Powering the planet: chemical challenges in solar energy utilization", *PNAS* 103(43) 15729-15735.
- [2] Potter, M.C. (1911). Electrical effects accompanying the decomposition of organic compounds. *Proc. Roy. SOC. London Ser. B* 84 260-276.
- [3] Logan, B.E. Hamelers, B. Rozendal, R. Schröder, U. Keller, J. (2006). Microbial fuel cells: methodology and technology. *Environ Sci Technol* 40: 5181-5192.
- [4] Chaudhuri, S. K.; Lovley, D. R. (2003). Electricity generation by direct oxidation of glucose in mediatorless microbial fuel cells. *Nat. Biotechnol.* 21, 1229-1232.
- [5] Logan, B.E., "Microbial Fuel Cell", John Wiley & Sons, 2008.
- [6] Logan, B. E, Regan, J.M. (2006). Microbial fuel cells--challenges and applications. *Environ Sci Technol* 40: 5172-5180.
- [7] Rahimnejad, M. Mokhtarian, N. Nagafpour, G.h. Ghorayshi, A. Ghasemi, M. and Sharifzadeh M. (2008). Generation of electric using *Saccharomyces cerevisiae* in microbial fuel cell. 1th Conference of H₂ Aand fuel cell.2008
- [8] Kim, H.J., Hyun, M.-S., Chang, I.S. and Kim, B.H. (1999). A microbial fuel cell type lactate Biosensor using a metal-reducing bacterium, *Shewanella putrefaciens*", *J. Microbiol. Biotechnol.* 9(3): 365-367.
- [9] Wilkinson, S. (2000). "Gastrobots" benefits and challenges of microbial fuel cells in food powered robot applications. *Auton Robot* 9:99-111.
- [10] Gil, G.C. Chang, I.S. Kim, B.H. Kim, M. Jang, J.Y, Park, H.S. (2003). Operational parameters affecting the performance of a mediatorless microbial fuel cell. *Biosens Bioelectron.* 18:327-34.
- [11] Ghasem, R. Fahimeh, A. and Alireza K. (2016). Mycosynthesis of Silver Nanoparticles from *Candidaalbicans* and its Antibacterial Activity against *Escherichia coli* and *Staphylococcus aureus*. *Tropical Journal of Pharmaceutical Research.* 15 (2): 371-375
- [12] Farahnaz, B., Masoud N. Ali, A. Sahar, M., Roya, M. Yazdan, M and Ghasem, R. (2016). Eco-Friendly Synthesis Of Cadmium Oxide Nanoparticles Using *Salvia Officinalis* Plant And Investigate Its Anti-Fungal Biofilm Effects, In Single Form And In Combination With Fluconazole Against *Candida Albicans*. *Fresen. Environ. Bull.*, 25(4): 3507-3511.
- [13] Tashkhouria, J. Hormozi Nezhad, M.R, Khodavesi, J. Javadi, S. (2009). Silver nanoparticles modified carbon nanotube paste electrode for simultaneous determination of dopamine and ascorbic acid. *Journal of Electro analytical Chemistry* 633 (2009) 85-91
- [14] Morteza, K. Zinat, M. Mojtaba, K. Maryam, B. Sahar, M. Yazdan, M. and Ghasem, R. (2016). Improvement of the Performance of Microbial Fuel Cell with Modification of Electrode using Copper Nanoparticles. *Journal Of Pure And Applied Microbiology*, 10(1), 355-361
- [15] Zhao, F. Harnisch, F. Schroder, U. Scholz, F. Bogdanoff, P. Herrmann, I. (2005). Application of pyrolysed iron (II) phthalocyanine and CoT-MPP based oxygen reduction catalysts as cathode materials in microbial fuel cells. *Electrochemistry Communications.* 7(12): 1405-1410
- [16] Wen, Zh. Suqin, C. Mao, Sh. Cui, Sh. Lu, G. Kehen, Y. Shenglian, L. Zhen, H. Chen, J. (2013). TiO₂ nanoparticles-decorated carbon nanotubes for significant improved bioelectricity generation in microbial fuel cells. *Power Sources.* 234, 100-106.
- [17] Junqiu, J. Qingliang, Z., Guodong, Z., Duu-Jong, L., (2010). Electricity generation from bio-treatment of sewage sludge with microbial fuel cell. *Bio resource Technology.* 100, 5808-5812.
- [18] Rahimnejad, M. Mokhtarian, N. Nagafpour, Gh. Ghorayshi, A. Ghasemi, M and Sharifzadeh, M. (2008). Generation of electric using *Saccharomyces cerevisiae* in microbial fuel cell. 1th Conference of H₂ Aand fuel cell.2008.
- [19] Beliaev, A.S. and Saffarini, D.A. (1928). *Shewanellaputrefaciens mtrB* encodes an outer membrane protein required for Fe (III) and Mn(IV) reduction", *J. Bacteriol.* 180(93) 6293-6297.
- [20] Fatima, A. Yifeng, Z. Irini, A. (2014) Nanomodification of the electrodes in microbial fuel cell:

Impact of nanoparticle density on electricity production and microbial community. *Applied Energy*, 116. 216-222.

- [21] Zhenhai, W. Suqin, C. Shun, M. Shumao, C. Ganhua, L. Kehan, Y. Shenglian, L. Junhong, C. (2013). TiO₂nanoparticles-decorated carbon nanotubes for significantly improved bioelectricity generation in microbial fuel cells. *Journal of Power Sources*. 234. 100-106

Received: 16.12.2016

Accepted: 23.04.2017

CORRESPONDING AUTHOR

Ghasem Rahimi

Young Researchers and Elite Club, Marvdasht Branch, Islamic Azad University, Marvdasht, Iran

E-mail: rahimighasem75@yahoo.com

TWO DIFFERENT MOLECULAR MARKERS (SSR AND IPBS) ASSESSMENT ON *CORIANDRUM SATIVUM L.* WITH CAPILLARY ELECTROPHORESIS

Furan M Alp*, Merve Dilek Gebologlu

Yuzuncu Yil University, Faculty of Agriculture, Department of Plant Biotechnology, Van, Turkey

ABSTRACT

Coriandrum sativum L. is the spices plant that using as medicinal plant including essential oil, belonging to the family Umbelliferae/Apiaceae. Its various chemical components in different parts are useful as antibacterial, antifungal and antioxidative. Therefore, plays an important role in preserving the shelf life of foods by preventing their spoilage. Leaves and seeds of coriander mostly used in folk medicine and its essential oil used for pharmaceutical products and as an ingredient in perfumes cause of non-toxic to humans. Coriander has not much defined as molecularly. It has not gone far enough investigated in that way yet. Breeding studies will probably result in more or less genetically identical varieties of coriander. The acceptability of the genotypes is determined by the amount of genetic variability in the germplasm. In this study, genetic variation between most known twelve coriander genotypes was investigated using two types of molecular markers; Sixteen iPBS primers and Eight SSR primers selected for polymorphism across the twelve coriander genotypes. The maximum PIC for a dominant marker is 0.49 for $f = 0.5$ and co-dominant marker is 0.43 for each primer; the PIC value was the mean of calculated PIC of all loci.

KEYWORDS:

Coriander, Genetic diversity, SSR, iPBS-retrotransposon

INTRODUCTION

The aromatic plants and spices have been used in many different areas like food preservation, pharmaceuticals, folk medicine and natural therapies, all over the world [1]. The most important constituents are the essential oil and the fatty oil [2, 3]. Coriander fruits are still used in medicine and it is still placed in the list of German and Austrian official pharmaceutical plant drugs [4, 5]. Also, coriander used as fresh green herbs because of its flavor distinct from ripe fruits. It is used on a large scale as green herb in India, China, Thailand, Malaysia, Indonesia, and the American Midwest and in

the Near East [6, 7, 8]. The exception, of commercial production areas, coriander mostly is to be found in gardens rather than in large fields. It is difficult to assess its genetic resources because of the less information about coriander available on the occurrence of the wild species [9]. Using microsatellites have been proven as valuable markers for various applications in numerous gene identification, genetic mapping and genetic variability studies [10]. The long terminal repeat (LTR) retrotransposons are suitable to use as molecular markers [11, 12]. Inter primer binding site is an ideal marker system as a PCR-based method for “orphan crops” and other species in itself proper and for the rapid isolation of retrotransposon termini and full-length elements [11, 13]. There exist various local names for coriander (Table 1). These diverse names bear witness to the role that this plant has played since ancient times [14, 15]. This research aimed to DNA analysis using SSR and iPBS technique together to determine the genetic divergence of most known twelve genotypes.

MATERIALS AND METHODS

Plant materials. Plant materials of this study consist of Six Turkish certified coriander varieties and 1 mixed population collected from Turkey, three genotypes from France, 1 India and 1 from Albania were used for iPBS and SSR analysis (Table 1).

DNA extraction. Fresh leaves samples of all twelve genotypes collected from germinated in petri dishes and stored in 2ml eppendorf tubes and kept at -80 C for a night to grind to samples. It was used in the polypropylene sample pestle for each tube to a fine powder. Fine powdered leaf samples were used only for isolation of genomic DNA using CTAB (hexadecyl trimethyl ammonium bromide) method [16]. The genomic DNA was extracted from approximately 2 gr of leaf tissue of each variety of coriander. The extraction procedure was the CTAB as reported by Doyle [16]. DNA was quantified using NanoDrop 2000 versions (Thermo Scientific) by measuring A260/A280.

TABLE 1
Coriander genotypes used in this study

Genotype	Origin
Pelmus	Turkish certified
Gurbuz	Turkish certified
Erba	Turkish certified
Arslan	Turkish certified
Kerkuk	Turkish certified
Kudret-K	Turkish certified
France-1	Gondiam
France-2	Vilmorin
France-3	Vilmorin
Antakya	Turkish mixed population
Albania	Koriander fura
India	Dubai

SSR PCR amplification. Eight SSR primers were used that previously published from Gatersleben wheat microsatellite and Beltsville agricultural research center and listed in table 3. The polymerase chain reaction was performed as described by Roder [17]. The PCR program initially started at 95 °C for 3 min, 35 cycles of denaturation at 94 °C for 30 s, annealing at 45–50 °C for 30 s and extension at 72 °C for 2 minutes, afterwards 72 °C final extension for 5 minutes before the program was terminated by holding at 4 °C [18]. The amplified products were analyzed by electrophoresis in capillary system and results were screened by Qiagene ScreenGel 1.4 software.

iPBS PCR amplification. Sixteen primers were selected from 80 iPBS primer pairs after screening because of their band profiles (Table 2). DNA amplification were performed in Applied Biosystem 96 well Thermal Cycler and it was carried out 25 µl reaction mixture containing 25 ng DNA, 1 µM of primer for 12–13 nt primers and 0.6 µM of primer for 18–19 nt, primers, 0.2 mM dNTPs and 1 unit Taq DNA polymerase according to [11]. The PCR products were electrophoresis on 1.7%

(w/v) of agrose gel containing 6-µl ethidium bromide, at 110 volts for 3 hours and screened using Vilber Lourmart Quantum ST4 system.

Data scoring and analysis. DNA bands were screened by Quantum ST4 software and two or three times checked with eye exam; just clear bands were taken into account and pale bands were ignored. Bands that having the same size were assumed to offer a single locus. For the presence of a band as locus data were calculated '1' and '0' for the absence of the band. Binary data were entered the computer as an excel sheet using for further analysis both NTSYS-pc version 2.2 and SPSS statistics to occur with distance matrices and construction of dendrogram. Phylogenetic dendrogram was constructed on a Dice genetic similarity coefficient [19, 20]. Using the Unweighted Pair Group Method of Arithmetic means (UPGMA) and the binary data were imported into SPSS statistical software to build a similarity matrix. Genetic distance built on the Jaccard coefficient [21] was calculated by making hierarchical clustering employing agglomerative, proximity matrix. The goodness of fit of the clustering compared with the basic data matrix was checked.

RESULTS

iPBS marker system. Sixteen primers selected for polymorphism across the twelve coriander genotypes (2077, 2079, 2085, 2095, 2232, 2239, 2242, 2249, 2295, 2298, 2375, 2377, 2378, 2394, 2395, 2415) from initially screened 80 iPBS primers for PCR amplifications. The number of polymorphic bands and number of bands, percentage of polymorphism and mean PIC value from these 16 iPBS primers are presented in Table 2.

TABLE 2
Sixteen iPBS primers to detection of polymorphism among 12 Coriander (*Coriandrum sativum L.*) genotypes.

iPBS primers	Sequence (5'–3')	Ta(°C)	Number of bands ^a	Number of polymorphic bands	Percentage of polymorphism (%)	Mean PIC value
2077	CTCACGATGCCA	46.1	8	6	75	0.4444
2079	AGGTGGGCGCCCA	56.6	2	2	100	0.2778
2085	ATGCCGATACCA	43.8	10	8	80	0.4911
2095	GCTCGGATACCA	44.8	6	6	100	0.3457
2232	ACTTGGATGCTGATACCA	56.6	6	6	100	0.4861
2239	ACCTAGGCTCGGATGCCA	60.4	10	8	80	0.4911
2242	GCCCCATGGTGGGCGCCA	69.2	4	4	100	0.3750
2249	AACCGACCTCTGATACCA	54.7	12	10	83.3	0.4550
2295	AGAACGGCTCTGATACCA	55.0	2	2	100	0.2778
2298	AGAAGAGCTCTGATACCA	51.6	6	6	100	0.1975
2375	TCGCATCAACCA	45.1	7	5	71	0.2133
2377	ACGAAGGGACCA	47.2	8	8	100	0.4922
2378	GGTCCTCATCCA	44.2	2	2	100	0.3750
2394	GAGCCT AGGCCA	48.5	2	2	100	0.2778
2395	TCCCCAGCGGAGTCGCCA	66.0	2	2	100	0.2778
2415	CATCGTAGGTGGGCGCCA	62.5	4	4	100	0.2778

^aTotal accounted bands appearing in two or three times repeated experiments.

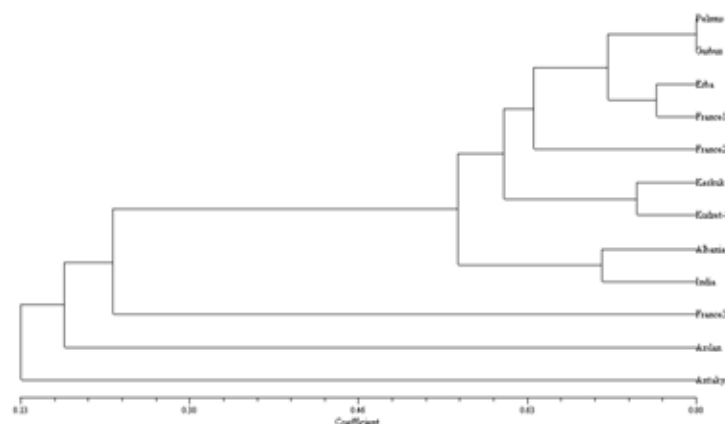


FIGURE 1

Dendrogram of 12 coriander genotypes generated with data from sixteen iPBS primers

TABLE 3

Eight SSR primers to detection of polymorphism among 12 Coriander (*Coriandrum sativum L.*) genotypes.

SSR primer	Forward primer	Reverse primer	Ta (°C)	^a Alleles	Mean PIC value
XBAC 137	AGAGGACGCTGAGAAC TTAGAGAA	GCGATCTTTGTAATGCATGGTGAAC	53	17	0.4029
XBARC186	GGAGTGTGCGAGATGATGTGGA AAC	CGCAGACGTCAGCAGCTCGAGAGG	68	17	0.3328
XBARC187	GTGGTATTTTCAGGTGGAGTTGTTTA	CGGAGGAGCAGTAAGGAAGG	63	14	0.3157
XBARC263	GGAAGCGCTCAGCACTAGGCAAC	GGCTTCTAGGTGCTGCGGCTTTTGT C	70	13	0.2946
XGWM113	ATTCGAGGTTAGGAGGAAGAGG	GAGGGTCTGCCTATAAGACC	55	10	0.4266
XGWM156	CCAACCGTGCTATTAGTCATT	CAATGCAGGCCCTCCTAAC	60	17	0.3153
XGWM257	AGAGTGCATGGTGGGACG	CCAAGACGATGCTGAAGTCA	60	16	0.4132
XGWM630	GTGCCTGTGCCATCGTC	CGAAAGTAACAGCGCAGTGA	60	22	0.2778

^a Number of bands from two or three times repeated experiments.

Polymorphic Information Content (PIC) for dominant markers was determined as: $PIC = 1 - [f^2 + (1-f)^2]$, meantime for the co-dominant markers as: $PIC = 1 - \sum p_i^2$. PIC value is calculated as where “f” is the frequency of the marker in the data set. The maximum PIC for a dominant marker is 0.49 for $f = 0.5$ [22] and co-dominant marker is 0.43. For each primer, the PIC value was the mean of calculated PIC of all loci. We used sixteen primers amplified a total of 338 countable bands with 58% mean ratio of polymorphism indicating the rank of genetic variability. Knowledge of these sixteen primers, with the inclusion of mean polymorphism information content (PIC) values and band polymorphism is presented in Table 2. Primer 2249 produced the highest number of bands (12) and whereas obtained the highest PIC value (0.4922) from primer 2377. Primer 2298 has the lowest (0.1975). These results indicated that these 16 iPBS markers used during this study displayed an extensive range of genomic DNA diversity in coriander genotypes. Binary matrices of the DNA results produced by the 16 iPBS primers used for twelve coriander genotypes were imported into the NTSYS-pc v2.2 software package and SPSS statistics [23] to take place with distance matrices and construction of dendrogram. The UPGMA dendrogram has set out in Fig. 1.

Figure 1 indicates that 12 genotypes distributed themselves into four major groups and the fourth group had subgroups contained 9 other coriander genotypes. Antakya variety in the first group clearly kept separate from the other genotypes. Similarly, the Arslan variety in the group 2 and the France genotype in the group 3 were completely taken placed differently. Gurbuz and Pelmus varieties had found the most similar varieties with 80% similarity ratios. These results also showed that iPBS markers could make desirable distinguishing power in determining genetic diversity and relationships.

SSR marker system. Six Turkish varieties, 1 mixed population collected from Turkey, 3 genotypes from France, 1 India and 1 from Albania genotype to be totally 12 coriander genotypes, were used for SSR analysis. Eight primers were amplified to screen the 12 corianders for determining the genetic similarities and their alleles and mean PIC values are presented in Table 3. Significant molecular variability was detected among all genotypes.

The unique banding patterns from these genotypes suggest that SSR markers could provide an opportunity to determine genetic similarities among coriander genotypes. 8 SSR primers amplified 126 alleles, with frequencies of 13–22 per locus and an average 15.7. Primer Xgwm630 produced the larg-

est number of bands (22) whereas Xgwm113 primer produced the smallest number of bands (10). PICs varied from 0.2778 to 0.4266 with an average of 0.3474 each locus. These results showed us that microsatellite markers could be helpful in the assessment of genetic relationship between coriander genotypes. The dendrogram was generated from binary data screening eight SSR primers for twelve coriander genotypes were imported into the NTSYS-pc v2.2 [24] software package and SPSS statistics to identify genetic relationships between them. The UPGMA dendrogram has set forth in Fig. 2.

Figure 2 indicates that 12 genotypes distributed themselves into two major groups that completely separated each other and these groups consisted of some subgroups. First group containing 4 coriander varieties, second group had 8 coriander geno-

types. While Turkish coriander varieties were mostly placed in the same group, Antakya and Pelmus varieties were placed in the second group being separate from the other Turkish varieties. According to observation from different phylogenetic tree (İPBS and SSR) indicated that some of Turkish genotypes clearly separated from each other. Antakya and Arslan varieties showed that more resembles in both two dendrograms. Gurbuz and Kerkuk varieties had found the most similar varieties with 34% similarity ratios. Also this presented study revealed that specific SSR markers could develop to determine genetic relationships with *Coriandrum sativum* L. species in future. All binary data were also used to generate combine dendrogram to see the variations between two different dendrogram (Figure 3).

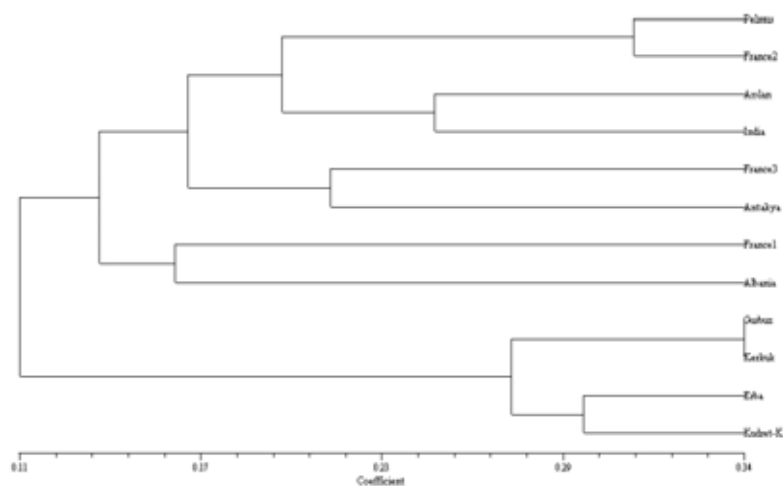


FIGURE 2

Dendrogram of 12 coriander genotypes generated with data from eight SSR primers

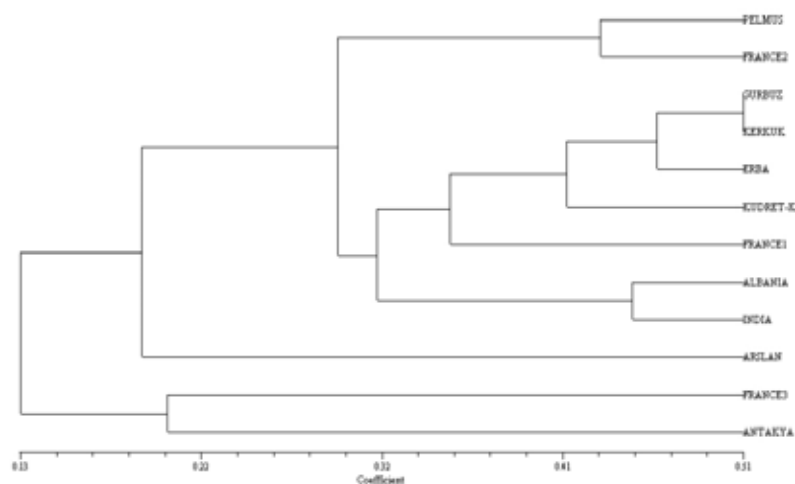


FIGURE 3

Dendrogram of 12 coriander genotypes generated with combined all binary data from both primers.

Figure 3 showed that 12 genotypes distributed

themselves into three major groups. Antakya varie-

ty has been placed completely different from other genotypes and Pelmus variety has located in the same way with France2 genotype as in the second dendrogram (Fig.2). On the other hand, Arslan variety has located close to Antakya variety as in the first dendrogram (Fig.1). Still of Turkish varieties Gurbuz and Kerkuk have been placed together as in the second dendrogram that generated from SSR markers data. Also other two Turkish varieties Erba and Kudret-K were close to each other. All the Turkish coriander varieties were in groups close to each other. Built on the observation from two different dendrogram and their combined phylogenetic tree indicated that Turkish coriander genotypes are mostly similar genotypes except some differences. To be genetically, the most divergent variety has been observed the Antakya genotype and Arslan varieties showed most resembles with it in both two dendrograms.

DISCUSSION

This research is vital to show the importance of investigation genetically relationships of the coriander plant. There are limited number of study has been carried out for genetic relationships of the coriander plant at the DNA level. Using molecular markers is highly effective for estimation of genetic diversity and genetic relationships in plant breeding. In this study two different molecular markers were used to identifications of genetic similarities of some coriander varieties. İPBS markers as a new universal method developed for DNA fingerprinting by [11] that is based on location of specific inter primer-binding sites (İPBS) of the LTR retrotransposons that they are found in all major eukaryotic divisions and comprise major fragments of the genomes of plants [25] and also simple sequence repeat (SSR) markers tested on coriander (*Coriandrum sativum L*) that are valuable because of their higher level of transferability to related species, and they can be used as leading markers for comparative mapping and evolutionary studies [26]. Preferred marker method should access a very large number of polymorphisms that are distributed within the genome. At the same time preferred markers should be as cheap as effectively as possible to use, and the analytical method should be easy to perform [27]. Most of researches on coriander varieties have been based on morphological traits and it's also known that many of those traits are influenced by environmentally effects. In this study has been presented an approach to investigate the genetic variability in selected coriander genotypes including Six Turkish certified coriander varieties and 1 mixed population collected from Turkey, three genotypes from France, 1 India and 1 from Albania using two different molecular markers by SSR and İPBS marker methods. The study also gave a

chance to compare two distinct marker molecular analyses on coriander for the first time.

CONCLUSION

The results obtained from this research indicate that the marker-assisted characterization can be applied to develop the coriander breeding programs. It's obvious that genetic observations on coriander is limited, and applying molecular methods can offers opportunities to improve desirable selection of proper coriander genotypes and it may help to make appropriate choices for market demands in the future.

ACKNOWLEDGEMENTS

Any company or institution did not fund this study. The authors declare that they have no conflict of interest.

REFERENCES

- [1] Mandal, S. and Mandal, M. (2015) Coriander (*Coriandrum sativum L.*) essential oil: Chemistry and biological activity. Asian Pacific Journal of Tropical Biomedicine, 5(6), 421-428.
- [2] Diederichsen, A. (1996) Coriander: *Coriandrum Sativum L.*, 3. Bioversity International.
- [3] Tuncturk, R. (2011) Effects of different row spacings on the yield and quality in coriander (*Coriandrum sativum L.*) cultivars. Yuzuncu Yil University Journal of Agricultural Sciences (Turkey).
- [4] Ebert, K. and Mechler, E. (1982) Arznei-und Gewurzpflanzen: ein Leitfaden fur Anbau und Sammlung. Wissenschaftliche Verlagsgesellschaft.
- [5] Purseglove, J.W., Brown, E., Green, C., and Robbins, S. (1981) Spices, 2., Longman Group Ltd.
- [6] Prakash, V. (1990) Leafy spices. CRC Press, Inc.
- [7] Coskuner, Y. and Karababa, E. (2007) Physical properties of coriander seeds (*Coriandrum sativum L.*). Journal of Food Engineering, 80(2), 408-416.
- [8] Kalemba, D. and Kunicka, A. (2003) Antibacterial and antifungal properties of essential oils. Current medicinal chemistry, 10(10), 813-829.
- [9] Singh, S.P, Katiyar, R.S., Rai, S.K., Tripathi, S.M. and Srivastva, J.P. (2005) Genetic divergence and its implication in breeding of

- desired plant type in coriander-*Coriandrum sativum* L. *Genetika*, 37(2), 155-163.
- [10] Ince, A.G., Karaca, M. and Elmasulu, S.Y. (2014) New microsatellite and CAPS-microsatellite markers for clarifying taxonomic and phylogenetic relationships within *Origanum* L. *Molecular breeding*, 34(2), 643-654.
- [11] Kalendar, R., Antonius, K., Smykal, P. and Schulman, A.H. (2010) iPBS: a universal method for DNA fingerprinting and retrotransposon isolation. *Theor Appl Genet*, 121(8), 1419-30.
- [12] Schulman, A.H., Flavell, A.J., and Noel Ellis, T.H., (2004) The application of LTR retrotransposons as molecular markers in plants. *Mobile Genetic Elements: Protocols and Genomic Applications*, 145-173.
- [13] Shedlock, A.M. and Okada, N. (2000) SINE insertions: powerful tools for molecular systematics. *Bioessays*, 22(2), 148-160.
- [14] Li, H.H. (1969) Chinese medicine. *Chin Cult*, 10, 67-79.
- [15] Ivanova, K.V. and Stoletova, E.A., (1990) The history of culture and intraspecific taxonomy of *Coriandrum sativum* L. *Russ. Eng. Bot. Genisel*, 133, 26-40.
- [16] Doyle, J.J. (1987) A rapid DNA isolation procedure for small quantities of fresh leaf tissue. *Phytochem bull.*, 19, 11-15.
- [17] Roder, M.S., Korzun, V., Wendehake, K., Plaschke, J., Tixier, M.H., Leroy, P. and Ganal, M.W. (1998) A microsatellite map of wheat. *Genetics*, 149(4), 2007-23.
- [18] Mehmood, A., Luo, S., Ahmad, N.M., Dong, C., Mahmood, T., Sajjad, Y., Jaskani, M.J., and Sharp, P. (2016) Molecular variability and phylogenetic relationships of guava (*Psidium guajava* L.) cultivars using inter-primer binding site (iPBS) and microsatellite (SSR) markers. *Genetic Resources and Crop Evolution*, 63(8), 1345-1361.
- [19] Dice, L.R. (1945) Measures of the amount of ecological association between species. *Ecology*, 26, 297-302.
- [20] Nei, M. and Li, W.H. (1979) Mathematical model for studying genetic variation in terms of restriction endonucleases. *Proc Natl Acad Sci U S A*. 76(10), 5269-73.
- [21] Jaccard, P. (1908) Nouvelles recherches sur la distribution florale. *Bull Soc Vaud Sci Nat*, 44, 223-270.
- [22] De Riek, J., Calsyn, E., Everaert, I., Van Bockstaele, E. and De Loose, M., (2001) AFLP based alternatives for the assessment of distinctness, uniformity and stability of sugar beet varieties. *TAG Theoretical and Applied Genetics*, 103(8), 1254-1265.
- [23] Pierrakos, D., Paliouras, G., Papatheodorou, C. and Spyropoulos, C.D. (2003) Web usage mining as a tool for personalization: A survey. *User modeling and user-adapted interaction*, 13(4), 311-372.
- [24] Rohlf, F.J. (2000) Statistical power comparisons among alternative morphometric methods. *Am J Phys Anthropol*, 111(4), 463-78.
- [25] Mehmood, A., Jaskani, M.J., Ahmad, S., and Ahmad, R. (2013) Evaluation of genetic diversity in open pollinated guava by iPBS primers. *Pak. J. Agri. Sci*, 50(4), 591-597.
- [26] Varshney, R.K., Graner, A. and Sorrells, M.E. (2005) Genic microsatellite markers in plants: features and applications. *TRENDS in Biotechnology*, 23(1), 48-55.
- [27] Queen, R.A., Gribbon, B.M., James, C., Jack, P., and Flavell, A.J. (2004) Retrotransposon-based molecular markers for linkage and genetic diversity analysis in wheat. *Molecular Genetics and Genomics*, 271(1), 91-97.

Received: 18.12.2016

Accepted: 05.06.2017

CORRESPONDING AUTHOR

Furan M Alp

Yuzuncu Yil University

Faculty of Agriculture

Department of Plant Biotechnology

Van – TURKEY

E-mail: alpfuran@hotmail.com

THE INFLUENCE OF SOIL CONFIGURATION OF RICE PADDY IN THE YELLOW RIVER BEACH ON THE RICE YIELD AND SOIL HYDRAULIC CHARACTERISTIC

Daiwen Zhu^{1,2}, Jichang Han^{1,2,*}, Miao Cai^{1,2}, Yang Wei^{1,2}, Gang Li^{1,2}, Bo Yan^{1,2}, Nan Lu^{1,2}

¹Shaanxi Provincial Land Engineering Construction Group Co., Ltd., Xi'an city, Shaanxi Province, China

²Institute of Land Engineering and Technology, Shaanxi Provincial Land Engineering Construction Group Co., Ltd., Key Laboratory of Degraded and Unused Land Consolidation Engineering, the Ministry of Land and Resources, Shaanxi Provincial Land Consolidation Engineering Technology Research Center, China

ABSTRACT

Field experiment was conducted in Yellow River Beach and soil column experiment was conducted in lab to evaluate the optimal soil configuration suited for rice growth. Yellow River Beach soils were formed from sandy parent material with high air-filled porosity and poor water retention of the soil and cannot support the rice growth. Therefore, the artificial soil configuration was composed of the plow pan and the plough layer. The plough layer was formed by the covering loess, and the plow pan was constituted by the mixture of sand and FA (fly ash), which could be because that FA could amend soil by improving the soil water retention. In the field experiment, the influence of thickness of the plough layer on the rice yield and quality was explored. In the lab experiment, the influence of the constitution (i.e., ratio of FA to sand and compactness degree) of the plow pan on the hydraulic characteristic of the soil was studied. Based on our result, the optimal soil configuration in the yellow river beach appropriated for rice growth could be the constituted by the 30-cm thickness of covering loess and plow pan with 1:2 ratio of FA to sand and 1.8g/cm³ bulk density, considering the engineering cost. In view of serious problem of arable land resources in China, the study of the optimal soil configuration of rice paddy soil in the Yellow River Beach was necessary, considering such remediation method could be applied in large area to improve the soil productivity in the Yellow River Beach.

KEYWORDS:

Yellow River Beach; Fly ash; loess; Plow pan; Plough layer; Hydraulic characteristic.

INTRODUCTION

The Yellow River, the most sediment-laden river in the world, carries about 1.6 billion tons of sediment yearly [1]. Yellow River Beach is areas of

sandy land where large amount of depositional layers of sand are produced by transporting sand and sediment in the Yellow River [2]. As an important part of the river course, the Yellow River beach plays a key role on reducing flood peaks and depositing sediments [3]. The increased global population growth and increased demand for food suggest that larger areas of floodplain land will need to be cropped in the future. It is unavoidable imperative to use the river beach land for agriculture and other purpose [4]. However, the effective utilization of floodplain land and reasonable land development for agriculture is a problem, since the floodplain is a barren land resource [5].

Over the past century, site-specific remediation practices or control measures for remediation of floodplain land have been developed. One practice is to use the floodplain for forest land [6]. Utilization of floodplain for tourism was also reported [7]. The utilization of floodplain for farmland is perhaps one of the most economic and practical approach in Yellow River beach, which could be due to the abundant water resource [8]. The underground water level is high, mainly controlled by the Yellow River water level and the need of crop irrigation could be met by groundwater extraction [9]. Therefore, the rice could be planted in this area. However, its application was limited owing to large amount of depositional layers of sand in this area. And the water retention of sand is poor [10], thus is not conducive to the rice survival. Therefore, it is of great significance to improve sand water retention and water conservation for rice growth in the Yellow River Beach.

Fly ash (FA) generated by the thermal power station, is compatible with soil in chemical composition and particle diameter [11]. FA could improve soil structure, soil bulk density and increase water retention [12]. It was reported that FA was to improve water retention to remediate soils for several crops growth including rice, cabbage, barley and corn [13]. Therefore, FA could be used in this experiment to improve the water retention of sand in Yellow River Beach. But heavy metals, especially Cd and Pb are abundant in FA, which may cause the soil

pollution [14]. Lots of documents have been reported that excessive use of FA to remediate soil could lead to high content of heavy metal in plants and even affect the plant growth [15]. Consequently, the amount of FA used in this experiment should be explored.

Soil is the matrix and nutrient provider for plant growth, yet sand cannot provide a favorable situation for rice growth for lacking the nutrient and element [16]. It is generally accepted that certain soil thickness of reclamation or artificial land is required used as farmland [17]. Since the loess is available around the Yellow River Beach, the loess was selected as the covering soil in this experiment. But there is not unified standard on the thickness of covering loess. Considering the fact that the thickness loess used to cover on the sand above could affect the engineering quantity and expense input, thickness of artificial plough layer was explored in this experiment.

In this study, FA and sand from Yellow River Beach were mixed and compacted in a certain bulk density as plow pan, and the loess was covered above on the plow pan to support the nutrient for crop growth. The ratio of FA to sand and the compaction degree of the plow pan was explored by the soil core experiment using constant-head permeameter method to measure saturated hydraulic conductivity (Ks) value [18]. Soil Ks is an important soil physical property, especially for determining infiltration rate, which is an important parameter for rice paddy soil [19]. In the present, in terms of rice paddy soil, the research on soil Ks has been reported [20]. Consequently, the optimal ratio of FA to sand and its degree of compactness could be obtained according the soil Ks, which is suitable for rice growth. Meanwhile, the influence of loess thickness on the rice yield and quality was explored by the field experiment. In this way, the optimal soil configuration in the Yellow River Beach was explored in this experiment for rice growth.

The remediation method to improve the soil productivity in view of Yellow River Beach could be summarized through this experiment. Also, the land in the Yellow River Beach could be used effectively in order to achieve the aim for protecting ecological environment and cultivated land area on the condition that this method could be applied and promoted in a large scale.

MATERIAL AND METHOD

Materials and chemical analysis. Loess and sand were collected from Yellow River Beach. Fly ash was purchased from power plant. The soil samples (with FA) were air-dried, ground, and sieved through a 150 μm mesh before use.

The soil pH was measured with a digital pH meter (pHS-3C). The electrical conductivity (EC) of soil samples ($\mu\text{S}/\text{cm}$) was determined by a digital

conductivity meter (DDS-307A). Organic matter (OM) content of samples was determined by potassium dichromate in acid medium [21]. Total nitrogen (TN) content was estimated by the Kjeldahl method [22]. Available phosphorus contents (AP) was determined with spectrophotometer [23]. Available potassium contents (AK) was determined by Flame Atomic Absorption Spectrometry [24]. Available Boron contents (AB) was determined with azomethine-h colorimetric method [25]. The total concentrations of Cd, Cu, Pb, Zn, Cr and As in the soil and brown rice were determined by digesting the samples with HNO_3 (EPA method 3052) in a micro wave oven (MARS-X; CEM) and analyzing them with inductively coupled plasma-optical emission spectrometry (ICP-MS, Angilent, 7700e).

Field experiment. Field experiments were conducted in Yellow River Beach, Hancheng city ($35^{\circ}31'02''\text{N}$, $110^{\circ}30'34''\text{E}$), Northwest China. The area is characterized by the continental monsoon climate with a long-term average annual temperature of 13.7°C , and the annual mean precipitation of 555.2 mm, over 50% of which falls between June and September. The average annual sunshine is 2436 h and the annual total radiation is 121.24 kcal/cm^2 . The annual accumulated temperature (the sum of temperature that exceeds 10°C) is about 4000°C , which exceeds the base line (2000°C) for cultivating rice in north China. Soils of the experiment sites were sandy loam texture.

50cm depth of plot was dug at the Yellow River Beach and different thickness of loess (10, 20, 30, 40 cm) was covered on different plot. The area of each plot is 50m^2 . Then 50 day-old rice seedlings of Huangjingqing were planted. 2cm^3 manure and 2.5 kg compound fertilizer (the ratio of N: P: K was 16:16:8) was added in each plot as a basal fertilizer. Addition of nitrogenous fertilizer was added at panicle initiation stage (5kg), heading stage (10kg) and filling stage (10kg). And rice plants were grown for 122 days (June 23 to October 23, 2015).

Soils were sampled at the end (the day of rice harvest) of the growing period. Soil was sampled from the plow layer (0-20 cm) of a paddy field and dried. Then the soil pH, EC, OM, TN, available phosphorus, available potassium and available boron value were measured.

At harvest, plants in 1m^2 were randomly harvested in the center of the plot. In details, rice plants were cut 4 cm above the soil surface, and separated into rice grain sand stems. Plant samples were rinsed thoroughly with deionized water, dried at 40°C and weighed. The aboveground biomass was calculated by summing the dry weights of rice grains and stems. Then grain yield in 1m^2 , actual rice yield and unfilled grain rates were calculated. Rice grains were dehulled manually, and the obtained brown rice samples were ground in a ceramic mortar and sieved to less than 150 μm . And the contents of Cr, Cu, Zn, As,

Cd and Pb in the brown rice was measured. At last, all the rice plants in different plot were harvested and the actual rice yield was measured.

Hydraulic conductivity laboratory. The plow pan was prepared by mixing FA and sand at different ratio (1:1, 1:2, 1:3, 1:4, 1:5) thoroughly and compacted to different bulk density (1.65, 1.7, 1.8g•cm⁻³). Then its Ks was measured by using the stainless steel rings under constant-head [26]. According to the result of the Ks of plow pan, the soil core experiment was conducted to simulate the soil configuration in the Yellow River Beach consolidation. The soil column was prepared by the 10-cm depth plow pan (FA and sand were mixed at different ratio and were compacted to different bulk density) at the bottom and loess (depth was decided by the field experiment) in the above. The soil column experiment apparatus consists of standpipe with suitable diameter, PVC tub, soil sample core. The tub was 50 cm high and the prepared soil column was placed in an empty PVC tub, which has a coarse mesh. The tube was then connected to a constant head standpipe, which has previously been filled with water. Then the columns were saturated slowly over a 7-day period and the Ks of soil core in different treatment were measured.

RESULTS AND DISCUSSION

Fly ash and soil background. The composition of loess (Table 1 and Table 2) is as follows: sand, 26.0%; silt, 73.4%; clay, 0.6%; and pH, 8.5. Its amounts of elements are (mg/kg): Pb, 8.7; Zn, 21.2; Cu, 10.9; Cr, 24.0; As, 1.1 and Cd, 0.01. The composition of sand is as follows: sand, 95.2%; silt, 4.8%; and pH, 8.7. Its amounts of elements are (mg/kg): Pb, 9.7; Zn, 33.7; Cu, 18.5; Cr, 20.7; As, 6.3 and Cd, 0.07. The composition of FA is as follows: sand, 48.1%; silt, 51.5%; clay, 0.3%; and pH, 9.13. Its amounts of elements are (mg/kg): Pb, 99.9; Zn, 47.7; Cu, 24.4; Cr, 29.99; As, 7.4 and Cd, 2.58. According to the environment quality standard for soils (GB 15618-1995), the FA contained excessive level of Cd. Loess and FA texture were silty loam, and sand texture was sandy soil. Soil and FA were weakly alkaline (8.47-9.13). Fly ash's EC (681 us/cm) were much higher than that of loess (134.40 us/cm) and sand (138.50 us/cm). Soil organic contents and soil N, K, P fertility varied a lot in three samples. And the organic content and fertility of FA were much higher than that of loess and sand.

TABLE 1
Chemical properties of materials used in this experiment

Material	pH	EC (us/cm)	Texture	OM (%)	TN (%)	AK (mg/kg)	AP (mg/kg)
Loess	8.5	134.40	silty loam	0.18	0.03	75	4.0
sand	8.7	138.50	sandy soil	1.76	0.05	2	1.4
FA	9.1	681.00	silty loam	6.41	0.006	190	95.0

FA, Fly ash; EC, Electrical conductivity, OM, Organic Matter contents, TN, total nitrogen contents, AP, Available phosphorus contents, AK, Available potassium contents, AB, Available boron contents.

TABLE 2
Background metal contents of materials used in this experiment

Material	Cr (mg/kg)	Cu (mg/kg)	Zn (mg/kg)	As (mg/kg)	Cd (mg/kg)	Pb (mg/kg)
Loess	23.99	10.92	21.22	1.05	0.09	8.71
sand	20.71	18.50	33.74	6.26	0.07	9.74
FA	29.91	24.40	47.72	7.44	2.58	99.90

TABLE 3
Chemical properties of rice soil in different covering thickness treatments

Treatments	pH	EC (us/cm)	OM (%)	TN, (%)	AP (mg/kg)	AK (mg/kg)	AB (mg/kg)
10cm	7.9 ^a	180.47 ^a	1.12	0.30	29.37 ^{ab}	127.37 ^a	0.20
20cm	7.8 ^a	186.40 ^a	1.28	0.32	21.83 ^a	129.96 ^{ab}	0.28
30cm	7.8 ^a	211.25 ^b	1.11	0.35	37.17 ^b	135.10 ^b	0.25
40cm	8.1 ^b	200.48 ^b	1.22	0.36	33.90 ^{ab}	126.70 ^a	0.27

FA, Fly ash; EC, Electrical conductivity; OC, Organic carbon; N, total nitrogen, AP, Available phosphorus, AK, Available potassium, AB, Available boron

Significant differences between treatments at P ≤ 0.05 level indicated by different letters.

Field experiment. The soil pH, electric conductivity (EC), OM, TN, available phosphorus, available potassium, and available boron content of plow layer soil at different treatments (i.e., 10cm-depth, 20cm-depth, 30cm-depth and 40cm-depth loess) was shown in Table 3. Although the sand and loess was weakly alkaline, but the soil in four treatment were near neutral (7.85-8.05), which signified that the secretions from rice root may alter the soil properties in some extent. The EC varied a lot in four treatments (180.47-211.25), but their all meet the soil environmental quality standard for agricultural land (EC value ≤ 2000 us/cm). It was found from a two-way analysis of variance (ANOVA; as shown in Table 1) that the available phosphorus and potassium of the soil samples collected at the different treatment were different. However, there was no significant difference at the different treatment in terms of OM, TN and available boron. According to the nation classification criterion of soil nutrient, the soil in all treatment was in deficiency of OM. Also, the soil in all treatments was in high content of TN. The contents of available phosphorus and potassium in all treatments were high and medium. Meanwhile, the soil of all treatment was in deficiency of boron according to the classification criterion of soil trace elements (DB21/T 1437-2006). Therefore, during the rice cultivation, it was necessary to apply potassium and boron fertilizer and to promote rice growth in all treatments.

The grain yields, rice yield, and potential rice yield increased gradually through from loess thickness gradation (Table 4). And higher aboveground biomass was obtained at 40cm-depth treatment than other treatment. However, there were no significant differences between the 20cm-depth and 30cm-depth plough layer treatments in terms of biomass of

aboveground, grain yield and rice yield. Also the unfilled grain rates decreased significantly with the loess thickness. It could be concluded that loess thickness caused major improvements in rice growth, rice yield and rice quality. Similarly, it was reported that the elevated plough layer thickness could improve spring maize yield within range of 50cm [27]. However, considering the fact that engineering cost would significantly increase with the elevated thickness of the plough layer and the plough layer thickness should be more than 20cm to ensure the root normal growth [28], the 20cm and 30cm covering thickness would be selected to plant rice plants in the practice. Meanwhile, the heavy metal levels remained almost the same in four treatments (Table 5), which could be attribute that there is no significant difference of the heavy metal contents among different treatment, implicating no increase of pollution by loess.

Lab experiment. The Ks of different ratio plow pan was shown in table 6. With the increased proportion of sand in the plow pan, the Ks significantly increased, which suggested that addition of FA could significantly increase the water retention of plow pan. This could be due to the low permeability of FA [11]. Meanwhile, the increasing degree of compactness of the plow pan significantly decreased the saturated hydraulic conductivity, indicating that the degree of compactness also was an important factor for water retention of plow pan [29]. It was reported that the Ks of the plow pan ranging from $0.74 \cdot 10^{-4}$ - $6.22 \cdot 10^{-4}$ cm/s could meet the soil water retention for rice paddy field [20]. Therefore, the ratio of FA to sand (1:2 and 1:3) was selected in the soil column experiment to further explore the optimal soil configuration suitable for rice growth in the Yellow River Beach.

TABLE 4
Aboveground biomass, yield and unfilled grain rates of rice grown in different covering thickness treatments

Treatments	Above ground Biomass (kg/m ²)	Rice yield(kg/ha)	Grain yield (g/m ²)	Unfilled grain rates (%)
10cm	1.98 ^a	8154 ^a	0.86 ^a	33 ^a
20cm	2.39 ^{ab}	8450 ^b	1.00 ^b	30 ^a
30cm	2.20 ^{ab}	8590 ^b	1.04 ^b	18 ^b
40cm	3.02 ^b	8926 ^c	1.33 ^c	14 ^b

Significant differences between treatments at $P \leq 0.05$ level indicated by different letters.

TABLE 5
Metal uptake by rice grains in different covering thickness treatments

Treatments	Cr (mg/kg)	Cu (mg/kg)	Zn (mg/kg)	As (mg/kg)	Cd (mg/kg)	Pb (mg/kg)
10cm	38.25	35.53	151.49	2.41	0.13	5.92
20cm	45.90	31.03	161.23	2.52	0.12	5.72
30cm	44.11	32.11	161.64	2.25	0.07	5.40
40cm	44.53	37.67	172.81	2.34	0.07	5.10

Significant differences between treatments at $P \leq 0.05$ level indicated by different letters.

TABLE 6
Saturated hydraulic conductivity (K_s , cm/s) of different ratios of sand to FA treatments and sand treatments

Treatments	1.80 g•cm ⁻³	1.7g•cm ⁻³	1.65 g•cm ⁻³
1:1	/	/	/
1:2	1.92•10 ⁻⁴ aA	6.19•10 ⁻⁴ aB	8.24•10 ⁻⁴ aC
1:3	2.92•10 ⁻⁴ aA	6.73•10 ⁻⁴ aB	11.17•10 ⁻⁴ bC
1:4	5.24•10 ⁻⁴ bA	9.09•10 ⁻⁴ bB	12.00•10 ⁻⁴ bC
1:5	12.56•10 ⁻⁴ cA	14.95•10 ⁻⁴ cB	16.00•10 ⁻⁴ cB
CK(sand)	0.05 ^d	0.05 ^d	0.06 ^d

Significant differences between treatments at $P \leq 0.05$ level indicated by different letters. Small letter in column for applications, capital letter in row for periods.

TABLE 7
Saturated hydraulic conductivity (K_s , cm/s) of different treatments with varied plough layer thickness and plow pan with varied bulk density and ratios of sand to FA

Treatments	20cm-depth loess			30cm-depth loess		
	1.80 g•cm ⁻³	1.7 g•cm ⁻³	1.65 g•cm ⁻³	1.80 g•cm ⁻³	1.7 g•cm ⁻³	1.65 g•cm ⁻³
1:2	0.33•10 ⁻⁴ aA	0.43•10 ⁻⁴ aC	0.62•10 ⁻⁴ aE	0.37•10 ⁻⁴ aB	0.43•10 ⁻⁴ aC	0.53•10 ⁻⁴ aD
1:3	0.56•10 ⁻⁴ bC	0.59•10 ⁻⁴ bD	0.60•10 ⁻⁴ bE	0.46•10 ⁻⁴ bA	0.49•10 ⁻⁴ bB	0.58•10 ⁻⁴ bD

Significant differences between treatments at $P \leq 0.05$ level indicated by different letters. Small letter in column for applications, capital letter in row for periods

TABLE 8
Water infiltration rate (cm/min) of different treatments with varied plough layer thickness and plow pan with varied bulk density and ratios of sand to FA

Treatments	20cm-depth loess			30cm-depth loess		
	1.80 g•cm ⁻³	1.7 g•cm ⁻³	1.65 g•cm ⁻³	1.80 g•cm ⁻³	1.7 g•cm ⁻³	1.65 g•cm ⁻³
1:2	0.195 ^{aB}	0.245 ^{aD}	0.364 ^{aF}	0.176 ^{aA}	0.230 ^{aC}	0.276 ^{aE}
1:3	0.456 ^{bD}	0.509 ^{bE}	0.523 ^{bF}	0.259 ^{bA}	0.303 ^{bB}	0.315 ^{bC}

Significant differences between treatments at $P \leq 0.05$ level indicated by different letters. Small letter in column for applications, capital letter in row for periods

The K_s of different soil column was shown in Table 7 and Table 8. The distance of wetting front, cumulative infiltration and water infiltration amount of different soil column was shown in Figure 1. And it was found that the thickness of the plough layer could not significant affect the K_s (Table7) and distance of wetting front (Figure1, upper panel), but play important role on the cumulative infiltration (Figure1, middle panel) and water seepage amount (Figure1, lower panel) and water seepage rate (Table 8). It was reported that the thickness of covering soil posed little effect on the wetting front, but could significantly affect the cumulative infiltration [30]. The water seepage amount in treatment of 20cm thickness of the plough layer (Figure1, lower left panel) was more than that of 30cm thickness (Figure1, lower right panel), which indicated that the increased covering thickness could significantly decrease the water seepage amount. The water seepage rate increased with decrease of the plough layer thickness. Similarly, Rodrick et al. found that the soil thickness layer could not significantly alter its K_s but could reduce the water seepage rate and water seepage [31]. Also the increase of the covering thickness

increased the cumulative infiltration (Figure1 middle panel). Similar findings have been found [32].

The ratio of FA to sand and the degree of compactness in the plow pan not only affect the K_s (Table7) but also have effect on the cumulative infiltration (Figure 1 middle panel), water seepage amount (Figure 1 lower panel) and water seepage rate (Table 8). In details, the incremental proportion of the sand in the plow pan increased the cumulative infiltration (Figure1 middle panel) and water seepage amount (Figure 1 lower panel) and water seepage rate (Table 8), which suggested that the sand could significantly increase the infiltration ability of the soil column. Also, the degree of the compactness significantly decreased the infiltration ability, which could be attributed to the increase of the cumulative infiltration and water seepage amount and rate with the elevated bulk density [33].

In order to decrease the water seepage amount to save water irrigation, the treatments of 30cm covering thickness and the bulk density of 1.8 g•cm⁻³ of plow pan should be selected in the practice engineering.

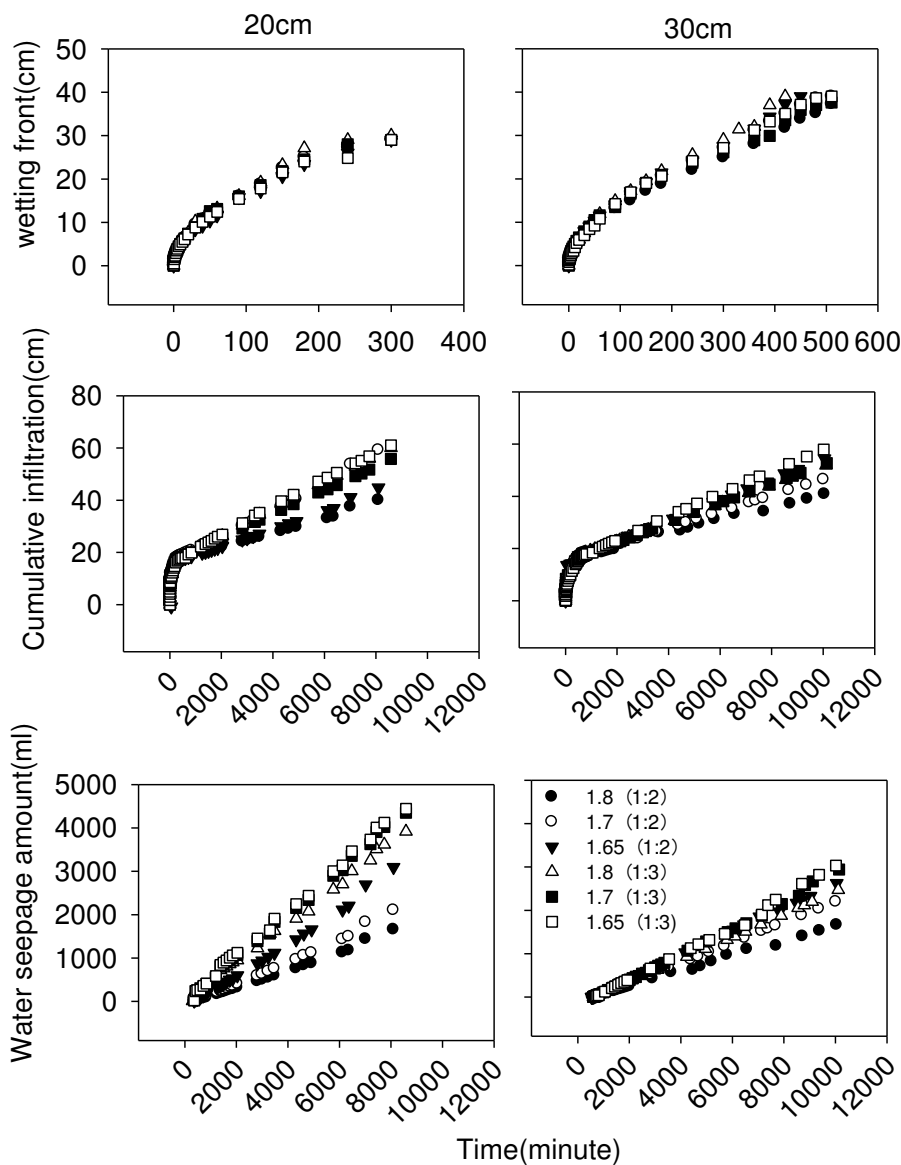


FIGURE1

The hydraulic characteristic in different treatments with varied plough layer thickness and plow pan with varied bulk density and ratios of sand to FA.

CONCLUSION

In general, in order to cultivate rice plant in the Yellow river beach, the optimal soil configuration was study in our experiment. In details, the plow pan with different ratio of sand to FA was constructed to decrease water penetration, and the loess was covered above the plow pan acting as plough layer, to support the rice plants growth. In our experiment, the influence of varied plough layer (i.e., covering thickness) on the rice yield and rice quality was studied. It was found that the elevated plough layer thickness could significantly increase the rice yield and decrease the rice unfilled rates. However, considering the engineering cost could significantly increased with the elevated covering thickness, and the 20cm

and 30cm plough layer thickness with higher rice yield and rice quality was selected. Meanwhile, the influence of plow pan constitution and the plough layer thickness on soil hydraulic characteristic was studied. Result showed that increased covering thickness could significantly decrease water seepage amount and water seepage rate. Our study also reported that the ratio of sand to FA and the degree of compactness of plow pan play a role on the saturated hydraulic conductivity, water seepage and cumulative infiltration. The increase proportion of FA and the elevated degree of compactness of plow pan in the plow pan significantly decreased the Ks the water seepage and cumulative infiltration. Based on our results, the optimal soil configuration should be constituted with plow pan with 1:2 ratio of sand to FA

and 30cm thickness covering loess, and the plow pan should be compacted into $1.8 \text{ g}\cdot\text{cm}^{-3}$.

Further studies should be carried out to investigate the influence of ratio of FA to sand on rice grains metal uptake, since the heavy metal in FA could be absorbed by the rice root, and then transferred into rice grains, posing potential risks to human health. Also, the results of the optimal soil configuration of rice paddy soil in the Yellow River Beach should be verified by field experiment.

In view of the scarcity of arable lands in China, it would mitigate serious problem of land resources on condition that Yellow River Beach soil could be effectively used for agricultural land. Therefore, the study of the optimal soil configuration of rice paddy soil in the Yellow River Beach was necessary, considering such remediation method could be applied and promoted in large area to improve the soil productivity in the Yellow River Beach, achieving the aim for protecting ecological environment and cultivated land area.

ACKNOWLEDGEMENTS

This work was funded by the Shaanxi Province Key Program for Science Innovation Team, No. 2016KCT-23.

REFERENCES

- [1] Wu, B., Wang, Z. and Changzhi, L.I. (2004) Yellow River Basin management and current issues, *Journal of Geographical Sciences*. 14, 29-37.
- [2] Zhang, P.Y., Ren, X., Qin, M.Z., Chen, L. and Li, X.L. (2013) Ecological protection and safety utilization of beaches based on the Xiaolangdi Reservoir flood control of the Yellow River lower reach: Kaifeng area as a case study, *Journal of Food Agriculture & Environment*. 11, 2302-2308.
- [3] Qin, M., Cheng, J., Zhang, P., Yan, J., Liu, X. and Wang, X. (2011) Research on ecological safety and utilization pattern on the lower reaches wetland of the Yellow River in Kaifeng city, *Procedia Environmental Sciences*. 10, 2654-2658.
- [4] Opperman, J.J., Galloway, G.E., Fargione, J., Mount, J.F., Richter, B.D. and Secchi, S. (2009) Land use. Sustainable floodplains through large-scale reconnection to rivers, *Science*. 326, 1487-8.
- [5] Opperman, J.J., Luster, R., Mckenney, B.A., Roberts, M. and Meadows, A.W. (2010) Ecologically functional floodplains: connectivity, flow regime, and scale 1. Jawra, *Journal of the American Water Resources Association*. 46, 211-226.
- [6] Lee, L.C. and Gosselink, J.G. (1988) Cumulative impacts on wetlands: Linking scientific assessments and regulatory alternatives, *Environmental Management*. 12, 591-602.
- [7] Taffs, K.H., Farago, L.J., Heijnis, H. and Jacobsen, G. (2008) A diatom-based Holocene record of human impact from a coastal environment: Tuckean Swamp, eastern Australia, *Journal of Paleolimnology*. 39, 71-82.
- [8] Mao, W., Kang, S., Wan, Y., Sun, Y., Li, X. and Wang, Y. (2014) Yellow River sediment as a soil amendment for amelioration of saline land in the Yellow River Delta, *Land Degradation & Development*.
- [9] Qin, M., Jackson, R.H., Yuan, Z., Jackson, M.W. and Sun, B. (2007) The effects of sediment-laden waters on irrigated lands along the lower Yellow River in China, *Journal of Environmental Management*. 85, 858-65.
- [10] Min, Y., Liu, S., Yang, Z., Tao, S., Degloria, S.D. and Holt, K. (2009) Effect on soil properties of conversion of Yellow River Delta ecosystems, *Wetlands*. 29, 1014-1022.
- [11] Wang, S. and Wu, H. (2006) Environmental-benign utilisation of fly ash as low-cost adsorbents. *J Hazard Mater, Journal of Hazardous Materials*. 136, 482-501.
- [12] Singh, R.P., Gupta, A.K., Ibrahim, M.H. and Mittal, A.K. (2010) Coal fly ash utilization in agriculture: Its potential benefits and risks, *Reviews in Environmental Science & Bio/technology*. 9, 345-358.
- [13] Mishra, M., Sahu, R.K. and Padhy, R.N. (2007) Growth, yield and elemental status of rice (*Oryza sativa*) grown in fly ash amended soils, *Ecotoxicology*. 16, 271-8.
- [14] Padhy, R.N., Nayak, N., Dash-Mohini, R.R., Rath, S. and Sahu, R.K. (2016) Growth, metabolism and yield of rice cultivated in soils amended with fly ash and cyanobacteria and metal loads in plant parts, *Rice Science*. 23, 22-32.
- [15] Padhy, R.N., Nayak, N., Dash-Mohini, R.R., Rath, S. and Sahu, R.K. (2016) Growth, yield and metabolism of rice grown in soil amended with fly ash and cyanobacteria and metal loads in plant parts, *Rice Science*. 23, 22-32.
- [16] Zhang, X., Shan, Y., Zhang, J.P., Xiang rong, L.U. and Fu guo, L.I. (2006) Effect of fertilization on rice cultivated in film-bottomed sandy land and applying techniques, *Journal of Soil & Water Conservation*. 20, 139-142.
- [17] Feng, Q.Z. (2009) Determination of the thickness and medium of covering soil for land reclamation, *Agricultural Science & Technology*, 04, 189-194.
- [18] Durner, W. and Lipsius, K. (2006) Determining soil hydraulic properties, *John Wiley & Sons, Ltd*.

- [19] Reynolds, W.D., Bowman, B.T., Brunke, R.R., Drury, C.F. and Tan, C.S. (2000) Comparison of Tension Infiltrometer, Pressure Infiltrometer, and Soil Core Estimates of Saturated Hydraulic Conductivity, *Soil Science Society of America Journal*. 64, 478-484.
- [20] Hua-Shan, W.U., Chen, X.M., Min-Biao, Y.E. and Hua-Qiang, W.U. (2006) Study on the soil saturated hydraulic conductivity and the infection factors of the main paddy soils in Tai-lake region, *Journal of Irrigation & Drainage*. 25, 46-49.
- [21] Aj, W. and Black, I.A. (1933) An examination of degradation method for determining soil organic matter: A proposed modification of the chromic acid titration method, *Soil Science*. 1934, 37, 29-38.
- [22] Parkinson, J. A., and Allen, S. E. (1975) A wet oxidation procedure suitable for the determination of nitrogen and mineral nutrients in biological material, *Communications in Soil Science & Plant Analysis*, 6(1), 1-11.
- [23] Olsen, S. R. (1954) Estimation of available phosphorus in soils by extraction with sodium bicarbonate, *United States Department Of Agriculture; Washington*.
- [24] Yang, X., Wang, J., Wang, L. and Yongjie, Y.U. (2012) Determination of available potassium in tobacco planting soil by flame atomic absorption spectrometry, *Tobacco Science & Technology*. 10, 67-69. (Chinese).
- [25] Chen, S. (2009) Determination of soil available boron with azomethine-h method, *Geophysical Research Letters*. 03, 167-170. (Chinese).
- [26] Amoozegar, A. (2015) A compact constant-head permeameter for measuring saturated hydraulic conductivity of the vadose zone, *Soil Science Society of America Journal*. 53, 1356-1361.
- [27] Juan, L.I. (2013) Effects of different depth of soil thickness on soil chemical properties and spring maize yield on barren gravel land for land reclamation, *Journal of Anhui Agricultural Sciences*. 05, 169-171, 192. (Chinese).
- [28] Chen, C.L., Zhang, Y.L., Jiang, A.F., Xi-Qiao, H.U., Chen, L.M., Chen, W.X., Lan, H.P. and Sheng-Liang, W.U. (2007) Investigation on the nutrient contents in plough layers in the major soils of Henan Province, *Journal of Henan Agricultural Sciences*. 02, 62-64. (Chinese).
- [29] Suzuki, L.E.A.S., Reichert, J.M., Reinert, D.J. and de Lima C.L.R. (2015) Degree of compactness and mechanical properties of a subtropical alfisol with eucalyptus, native Forest, and grazed pasture, *Forest Science*. 61, 716-722.
- [30] Yi, L.I. and Shao, M.A. (2006) Effects of rainfall intensity on rainfall infiltration and redistribution in soil on Loess slope land, *Chinese Journal of Applied Ecology*. 17, 2271-2276.
- [31] Lentz, R.D. (2007) Inhibiting water infiltration into soils with cross-linked polyacrylamide: seepage reduction for irrigated agriculture, *Soil Science Society of America Journal*. 71, 1352-1362.
- [32] Bhattacharjee, D. and Mallick, S. (2004) Behaviour and prediction of infiltration in layered soils, *Journal of the Indian Society of Soil Science*.
- [33] Ma, J., Sun, X., Bi, Y. and Guo, X. (2009) Changes of topsoil bulk density and saturated hydraulic conductivity under infiltration condition of water storage pit, *Nongye Gongcheng Xuebao/transactions of the Chinese Society of Agricultural Engineering*. 25, 39-43.

Received: 19.12.2016

Accepted: 18.05.2017

CORRESPONDING AUTHOR

Jichang Han

Shaanxi Provincial Land Engineering Construction Group Co., Ltd.

Xi'an city, Shaanxi Province – CHINA

E-mail: wsz99108@gmail.com

ION-EXCHANGE PREPARATION OF NiFe₂O₄-CuFe₂O₄ COMPOSITE WITH ENHANCED VISIBLE-LIGHT PHOTOCATALYTIC PERFORMANCE FOR DEGRADATION

Kuili Liu, Hongqiang Shen, Weidong Shi*

School of Chemistry and Chemical Engineering, Jiangsu University, Xuefu Road 301, Zhenjiang, 212013, P. R. China

ABSTRACT

A series of magnetically separable NiFe₂O₄-CuFe₂O₄ composite photocatalysts were synthesized through ion-exchange via a facile hydrothermal method. The difference of solubility products (K_{sp}) of NiFe₂O₄ and CuFe₂O₄ is the main driving force for the formation of these NiFe₂O₄-CuFe₂O₄ nanocomposites. The prepared sample was characterized by X-ray diffraction (XRD), scanning electron microscopy (SEM), energy dispersive spectrometer (EDS), UV-vis diffuse reflectance spectra (DRS) and photoluminescence (PL). The photocatalytic activity of NiFe₂O₄-CuFe₂O₄ photocatalysts was evaluated by the degradation of Rhodamine B under visible-light irradiation. The as-prepared NiFe₂O₄-CuFe₂O₄ composite exhibited an enhanced photocatalytic performance compared to the single NiFe₂O₄. The significant enhancement of photoactivity could be ascribed to the formation of heterogeneous structures fabricated by ion-exchange growth method.

KEYWORDS:

NiFe₂O₄; Magnetism; photocatalytic; ion-exchange

INTRODUCTION

Currently photocatalytic technology has become a green and potential method to degrade pollutants due to its simplicity, low cost and high efficiency. In the past decades, though a large number of photocatalysts have been investigated and show a good photocatalytic activity, most of them are ultraviolet-light-driven photocatalysts, such as TiO₂, SrTiO₃, NaNbO₃ [1-9], etc. As is known to all, visible light occupies nearly half of the sunlight, while ultraviolet light only accounts for 4% of the solar spectrum. Thus, it is attractive and challenging to search for a suitable visible-light-driven photocatalysts to achieve the effective degradation of Rhodamine B (RhB).

The spinel ferrites (MFe₂O₄, M=Co, Ni, Cu or Zn) have attracted increasingly attention in the field of photocatalytic pollutants elimination due to their chemical stabilities, excellent electrical and magnetic properties [10-13]. And their narrow band gaps

(ca. 2.0 eV) allow them to be excited in the visible light region. However, most of ferrites such as NiFe₂O₄ suffer from the rapid recombination of photo-generated electron-hole pairs, which lead to a poor photocatalytic performance. Thus, a large number of methods have been explored to improve their photocatalytic activities, such as adjusting morphologies [14-18], constructing heterojunctions [19-23], doping metal ions [24-29], etc. Jing synthesized new promising magnetic CuFe₂O₄ nanotubes via the electrospinning technique, and the CuFe₂O₄ nanotubes showed a huge enhancement of photocatalytic degradation for AF dye [14]. Cheng prepared a new type of CuFe₂O₄/g-C₃N₄ composite photocatalyst by a facile one-pot calcinations approach using urea and a CuFe₂O₄ gel as precursors, which is about 3 times that on pure g-C₃N₄ obtained from urea [30].

Herein, a series of magnetically separable NiFe₂O₄-CuFe₂O₄ composite photocatalysts were first synthesized through ion-exchange via a hydrothermal method. The photocatalytic performance of as-synthesized NiFe₂O₄-CuFe₂O₄ photocatalyst was evaluated via the degradation of RhB with visible light illumination. The effect of Ni/Cu mass ratio on photocatalytic performance was systematically investigated in this system. The possible mechanism for the enhancement of dye photocatalytic degradation on NiFe₂O₄-CuFe₂O₄ nanocomposite was also analyzed.

EXPERIMENTAL

Synthesis of NiFe₂O₄. First of all, Ni(NO₃)₃·6H₂O (1.16 g) and Fe(NO₃)₃·9H₂O (3.22 g) were dissolved in distilled water (30 mL) and the solution was continuously stirred for 30 minutes. Next, pH of the solution was adjusted to 14 by adding 6 M NaOH solution and the suspension was also continuously stirred for another 30 minutes. Then the brown mixture was transferred to a 50 mL Teflon-lined stainless steel autoclave and heated in high temperature oven maintained at 220 °C for 24 h. Finally, the brown product was collected by centrifugation, washed with distilled water and absolute ethanol three times and dried at 80 °C.

Synthesis of NiFe₂O₄-CuFe₂O₄. Firstly, the obtained NiFe₂O₄ precursor (0.2 g) and Cu(NO₃)₃·3H₂O (0.02 g) were dissolved by ultrasound in distilled water (30 mL). Secondly, pH of the NiFe₂O₄ suspension was adjusted to 5 with 0.1 M HNO₃ solution and the suspension was also continuously stirred for 30 minutes. Next the mixture was transferred to a 50 mL Teflon-lined stainless steel autoclave and heated at 180 °C for 12 h. Finally, the product was collected by centrifugation, washed with distilled water and absolute ethanol three times and dried at 80 °C. The samples 2-7 were obtained by the different addition (0.02 g, 0.04 g, 0.06 g, 0.08 g, 0.010 g and 0.012 g) of Cu(NO₃)₃·3H₂O.

Characterization. The X-ray diffraction (XRD) patterns were obtained with a D/MAX-2500 X-ray powder diffractometer with Cu K α radiation and a scan rate of 7° min⁻¹ for 2 θ measurements over the range of 5–80°. The morphology of NiFe₂O₄-CuFe₂O₄ samples were observed by scanning electronic microscopy (SEM) on an S-4800field emission SEM (SEM, Hitachi, Japan). The energy dispersive spectrometer (EDS) analysis of the samples was also performed during the SEM measurements. The UV-vis diffused reflectance spectra (DRS) of the samples were acquired using an UV-vis spectrophotometer (UV-2450, Shimadzu, Japan). The photoluminescence (PL) spectra of samples were recorded on a Perkin-Elmer LS 55 at room temperature using a fluorescence spectrophotometer.

Photocatalytic tests. The photocatalytic activities of the NiFe₂O₄-CuFe₂O₄ composites were evaluated by the degradation of RhB under visible-light irradiation. A 150 W xenon lamp with a cutoff filter ($\lambda > 420$ nm) was used as a light source in this degradation experiment. Typically, 50 mg NiFe₂O₄-CuFe₂O₄ catalyst, 90 mL distilled water and 10 mL of 100 mg/L TC aqueous solution were added into a special quartz bottle. Before snapping the light on, the reaction suspension must be stirred in the dark for 40 min to achieve the balance between adsorption and desorption. Next, 5 mL of the suspension was sampled, centrifugal and measured with ultraviolet spectrophotometer at 554 nm, and its concentration and absorbance were marked as C₀ and A₀, respectively. Then, the above operation was repeated at 20-minute intervals and degradation time was 3 hours until the degradation time reached 3 hours. Finally, the photocatalytic degradation rate (DR%) was estimated by the following formula:

$$DR\% = [1 - (C/C_0)] \times 100\% = [1 - (A/A_0)] \times 100\% \quad (1)$$

RESULTS AND DISCUSSION

The crystal structure and phase purity of the as-

prepared samples were characterized by XRD analysis. Fig 1 shows the XRD patterns of the pure NiFe₂O₄ (sample 1) and NiFe₂O₄-CuFe₂O₄ photocatalysts. It can be seen that all samples are indexed to cubic spinel structure of NiFe₂O₄ (JCPDS No. 03-0875). The observed peaks at 18.41°, 30.31°, 35.71°, 37.21°, 43.51°, 53.91°, 57.51° and 62.71° can be assigned to the reflections of (111), (220), (311), (222), (400), (422), (511) and (440) crystal planes [17-18], respectively. No peaks of other compounds, such as CuO and Cu(OH)₂, can be observed, indicating that CuFe₂O₄ is successfully synthesized on the basis of the pure NiFe₂O₄ by the ion-exchange with Cu²⁺. Moreover, because the CuFe₂O₄ has a crystal structure similar to that of NiFe₂O₄, NiFe₂O₄-CuFe₂O₄ composites maintain a good crystallinity.

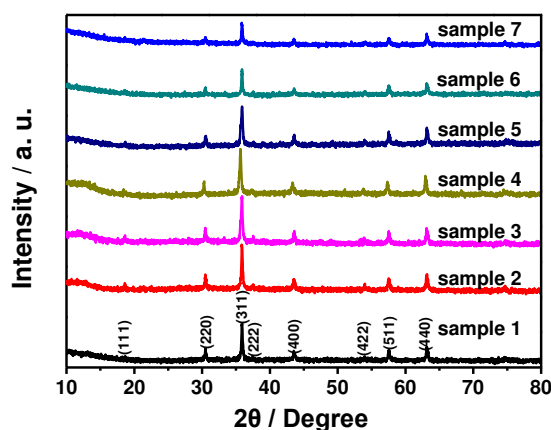


FIGURE 1

XRD patterns of NiFe₂O₄-CuFe₂O₄ composite.

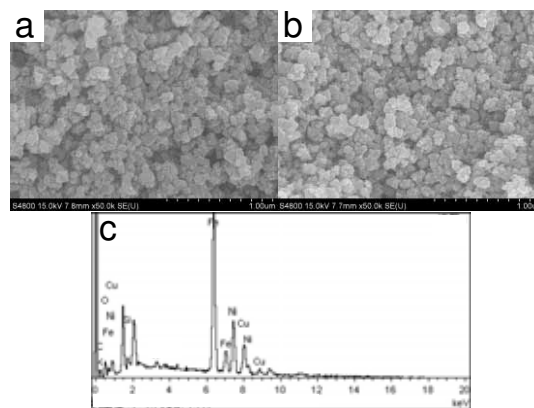


FIGURE 2

SEM images of (a) NiFe₂O₄ and (b) NiFe₂O₄-CuFe₂O₄ composite and EDS spectrum of (c) NiFe₂O₄-CuFe₂O₄ composite.

SEM and EDS analysis. The morphology of sample 1 and sample 5 are displayed by SEM, as shown in Fig 2a and Fig 2b. Fig 2a shows the morphology of the sample 1 is formed of NiFe₂O₄ congeries particles, every of which was about 50-150 nm. And it can be seen from Fig 2b that the second

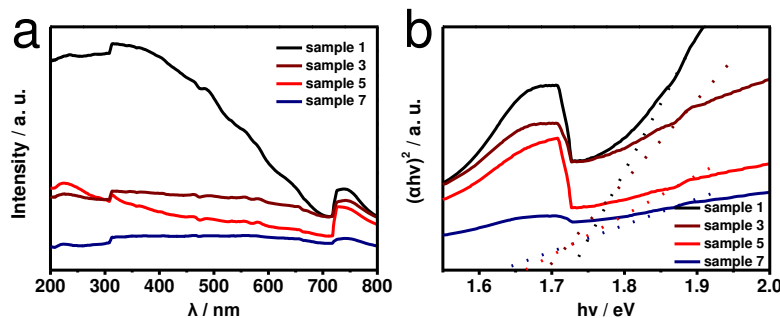


FIGURE 3

(a) UV-vis DRS of the as-synthesized samples and (b) the corresponding band gap energy of sample 1-7.

hydrothermal process has little effect on the morphology of sample 5, which is prepared by the ion-exchange with Cu^{2+} . Moreover, the chemical composition of sample 5 is also analyzed by using EDS. Besides Si, there are only Ni, Cu, Fe and O elements detected in Fig 2c, which indicates that $\text{NiFe}_2\text{O}_4\text{-CuFe}_2\text{O}_4$ composite is successfully synthesized in the presence of Cu^{2+} .

UV-vis absorption was used to determine the optical properties of $\text{NiFe}_2\text{O}_4\text{-CuFe}_2\text{O}_4$ composites. Fig 3a shows the UV-vis diffuse reflectance spectra of sample 1, sample 3, sample 5 and sample 7. It can be found that all samples exhibit absorption in the visible light region from 400 nm to 700 nm, and $\text{NiFe}_2\text{O}_4\text{-CuFe}_2\text{O}_4$ samples exhibit the better visible-light absorption compared to NiFe_2O_4 (Fig. 3a). The band gap (E_g) of the as-prepared samples can be achieved by the calculation from the equation (1) [31-33], as shown in Fig 3.

$$\alpha hv = A(hv - E_g)^{n/2} \quad (1)$$

The α , A and hv are defined as absorption coefficient, transition constant and photon energy, respectively. The value of n belonging to NiFe_2O_4 is 4, demonstrating that the transition of NiFe_2O_4 is a direct transition, which is different from indirect transition ($n=1$). Fig 3b shows the extrapolation of the plots of $(\alpha hv)^2$ vs hv , where the E_g of the four samples are assessed at 1.73, 1.69, 1.66 and 1.63 eV. The E_g of NiFe_2O_4 was nearly equal to that had reported in the past [17-18]. The value of E_g decreases with the increase of the copper, which further indicates Cu^{2+} successfully entered into NiFe_2O_4 via ion-exchange.

The photocatalytic performance of $\text{NiFe}_2\text{O}_4\text{-CuFe}_2\text{O}_4$ samples was assessed by the degradation of RhB with visible-light illumination. Apparently, due to the fast recombination of photoinduced electron-hole pairs of NiFe_2O_4 , the pure NiFe_2O_4 (Fig 4) showed a poor photocatalytic performance on the degradation of RhB, which was just about 7%. With Ni^{2+} being replaced by Cu^{2+} , the content of NiFe_2O_4 continues to decrease, the photocatalytic activity was gradually increased. The sample 5 reached the maximum degradation rate (68%), which is nearly ten times the efficiency of NiFe_2O_4 . When the content of

Cu^{2+} was excess, the degradation effectiveness became worse. These results exhibited that the ion-exchange plays a significant role in the enhancement of photocatalytic performance for the single NiFe_2O_4 [34-36].

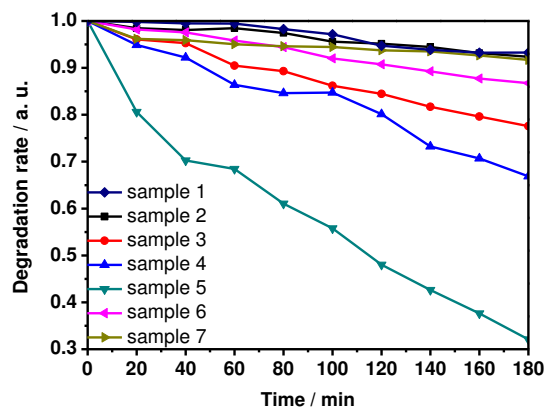


FIGURE 4

Photocatalytic performance of as-synthesized samples for Rh B degradation.

The photocatalytic activity of the semiconductors is mainly handicapped by on separation and migration ability of photon-generated carrier. Because the main energy of fluorescence is from the recombination of photoinduced electron-hole pairs, the photocatalytic performance is often associated with the fluorescence intensity. Fig 5 shows PL emission spectra of the sample 1 and sample 5 detected at an excitation wavelength of 310 nm. As illustrated in Fig 5, the PL emission intensity of sample 5 is weaker than that of NiFe_2O_4 , which suggested that the $\text{NiFe}_2\text{O}_4\text{-CuFe}_2\text{O}_4$ composite has an accelerated separation of photoinduced electrons and holes, exhibiting the enhanced photocatalytic ability.

The major reactive species acting on the degradation of RhB in this system were detected by the trapping experiments. The benzoquinone (BQ), ethylene diamine tetraacetic acid (EDTA), and isopropanol (IPA) were chose as scavengers to capture $\cdot\text{O}_2^-$, h^+ and $\cdot\text{OH}$, respectively, The results are shown in Fig 6a. It can be seen that the maximal change on photocatalytic degradation occurred in the group using BQ and the groups using EDTA and IPA still

maintained the considerable performance, suggesting that $\cdot\text{O}_2^-$ played a key role in the degradation of RhB under visible light irradiation.

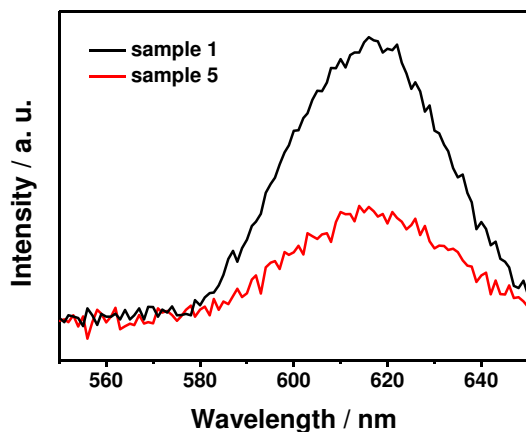


FIGURE 5
PL spectra of NiFe_2O_4 and $\text{NiFe}_2\text{O}_4\text{-CuFe}_2\text{O}_4$ ($\lambda=300$ nm).

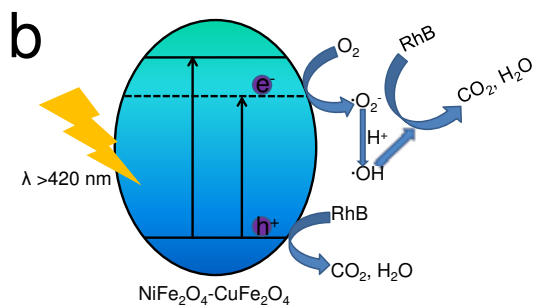
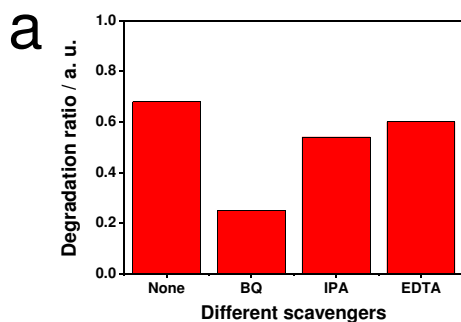


FIGURE 6
(a) photodegradation of RhB on $\text{NiFe}_2\text{O}_4\text{-CuFe}_2\text{O}_4$ composite with different scavengers;
(b) the schematic diagram of separation and migration for electron-hole pairs in $\text{NiFe}_2\text{O}_4\text{-CuFe}_2\text{O}_4$ composite

Fig 6b shows the schematic diagram of separation and migration for electron-hole pairs in $\text{NiFe}_2\text{O}_4\text{-CuFe}_2\text{O}_4$ composite [37-38]. The conduction band (CB) potential and valence band (VB) potential have been reported in previous literatures [18], which are -0.6 and 1.10 eV, respectively. And as is known to all, the reduction potential of $\text{O}_2/\cdot\text{O}_2^-$ is more negative than -0.33 eV and the oxidation potential of $\cdot\text{OH}/\text{OH}^\cdot$ is more positive than 2.4 eV.

Thus, based on the trapping experiments, electrons are excited from the VB to CB in $\text{NiFe}_2\text{O}_4\text{-CuFe}_2\text{O}_4$ system and react with O_2 to form $\cdot\text{O}_2^-$, where some of $\cdot\text{O}_2^-$ are converted to hydroxyl radical. Then, pollutant RhB is digested by $\cdot\text{O}_2^-$, h^+ and $\cdot\text{OH}$, in which $\cdot\text{O}_2^-$ is the main reactive species for the degradation of RhB in $\text{NiFe}_2\text{O}_4\text{-CuFe}_2\text{O}_4$ system.

CONCLUSION

In summary, a series of magnetically separable $\text{NiFe}_2\text{O}_4\text{-CuFe}_2\text{O}_4$ composite photocatalysts were first synthesized by ion-exchange between NiFe_2O_4 and Cu^{2+} ions in solution via a hydrothermal method. The different solubility products (K_{sp}) contributed to the successful construction of $\text{NiFe}_2\text{O}_4\text{-CuFe}_2\text{O}_4$ heterogeneous structures. The addition of Cu can directly affect the photocatalytic performance of $\text{NiFe}_2\text{O}_4\text{-CuFe}_2\text{O}_4$ composites. The $\text{NiFe}_2\text{O}_4\text{-CuFe}_2\text{O}_4$ photocatalysts exhibited tremendous enhancements on the photocatalytic degradation ratio of RhB with visible-light illumination. The sample 5 showed the highest degradation rate (68%), which was 10 times than that of the pure NiFe_2O_4 sample. The UV-vis and PL results demonstrated that the formation of $\text{NiFe}_2\text{O}_4\text{-CuFe}_2\text{O}_4$ heterojunction by ion exchange reduced the nickel ferrite band gap and accelerated separation of photogenerated electron-hole pairs. This work showed great potential of ion-exchange in situ growth method in the field of structuring ferrites heterogeneous.

ACKNOWLEDGEMENTS

This work was supported by the National Natural Science Foundation of China (21477050, 21522603), Excellent Youth Foundation of Jiangsu Scientific Committee (BK20140011), Chinese-German Cooperation Research Project (GZ1091). Program for High-Level Innovative and Entrepreneurial Talents in Jiangsu Province. Program for New Century Excellent Talents in University (NCET-13-0835), Henry Fok Education Foundation (141068) and Six Talents Peak Project in Jiangsu Province (XCL-025).

REFERENCES

- [1] Lin, H.F. and Wang, X. (2016). Epitaxy of radial high-energy-faceted ultrathin TiO_2 nanosheets onto nanowires for enhanced photoreactivities. *Advanced Functional Materials*. 26, 1580-1589.
- [2] Sordello, F., Odorici, E., Hu, K., Minero, C., Cerruti, M. and Calza, P. (2016). Shape controllers enhance the efficiency of graphene- TiO_2 hybrids in pollutant abatement. *Nanoscale*. 8, 3407-3415.

- [3] Lin, X., Chen, Y.N., Liu, N., Cao, Y.Z., Xu, L.X., Zhang, W.F. and Feng, L. (2016). In situ ultrafast separation and purification of oil/water emulsions by superwetting TiO₂ nanocluster-based mesh. *Nanoscale*. 8, 8525-8529.
- [4] Yu, K., Zhang, C.X., Chang, Y., Feng, Y.J., Yang, Z.Q., Yang, T., Lou, L.L. and Liu, S.X. (2017). Novel three-dimensionally ordered macroporous SrTiO₃ photocatalysts with remarkably enhanced hydrogen production performance. *Applied Catalysis B-Environmental*. 200, 514-520.
- [5] Tan, H.Q. et al. (2014). Oxygen vacancy enhanced photocatalytic activity of perovskite SrTiO₃. *Acs Applied Materials & Interfaces*. 6, 19184-19190.
- [6] Kuang, Q. and Yang, S.H. (2013). Template synthesis of single-crystal-like porous SrTiO₃ nanocube assemblies and their enhanced photocatalytic hydrogen evolution. *Acs Applied Materials & Interfaces*. 5, 3683-3690.
- [7] Yu, Q.N., Zhang, F., Li, G.Q. and Zhang, W.F. (2016). Preparation and photocatalytic activity of triangular pyramid NaNbO₃. *Applied Catalysis B-Environmental*. 199, 166-169.
- [8] Katsumata, K., Cordonier, C.E.J., Shichi, T. and Fujishima, A. (2009). Photocatalytic activity of NaNbO₃ thin films. *Journal of the American Chemical Society*. 131, 3856-+.
- [9] Shi, H.F., Chen, G.Q., Zhang, C.L. and Zou, Z.G. (2014). Polymeric g-C₃N₄ coupled with NaNbO₃ nanowires toward enhanced photocatalytic reduction of CO₂ into renewable fuel. *Acs Catalysis*. 4, 3637-3643.
- [10] Sharma, R., Bansal, S. and Singhal, S. (2015). Tailoring the photo-Fenton activity of spinel ferrites (MFe₂O₄) by incorporating different cations (M = Cu, Zn, Ni and Co) in the structure. *Rsc Advances*. 5, 6006-6018.
- [11] Guo, Y.L., Zhang, L.L., Liu, X.Y., Li, B., Tang, D., Liu, W.S. and Qin, W.W. (2016). Synthesis of magnetic core-shell carbon dot@MFe₂O₄ (M = Mn, Zn and Cu) hybrid materials and their catalytic properties. *Journal of Materials Chemistry A*. 4, 4044-4055.
- [12] Gao, X., Liu, X.X., Zhu, Z.M., Wang, X.J. and Xie, Z. (2016). Enhanced photoelectrochemical and photocatalytic behaviors of MFe₂O₄ (M = Ni, Co, Zn and Sr) modified TiO₂ nanorod arrays. *Scientific Reports*. 6.
- [13] Chen, J., Zhao, D.M., Diao, Z.D., Wang, M. and Shen, S.H. (2016). Ferrites boosting photocatalytic hydrogen evolution over graphitic carbon nitride: a case study of (Co, Ni)Fe₂O₄ modification. *Science Bulletin*. 61, 292-301.
- [14] Yang, H., Yan, J.H., Lu, Z.G., Cheng, X. and Tang, Y.G. (2009). Photocatalytic activity evaluation of tetragonal CuFe₂O₄ nanoparticles for the H₂ evolution under visible light irradiation. *Journal of Alloys and Compounds*. 476, 715-719.
- [15] Cheng, C.K., Kong, Z.Y. and Khan, M.R. (2015). Photocatalytic-Fenton Degradation of Glycerol Solution over Visible Light-Responsive CuFe₂O₄. *Water Air and Soil Pollution*. 226.
- [16] Golsefidi, M.A., Abrodi, M., Abbasi, Z., Dashtbozorg, A., Rostami, M.E. and Ebadi, M. (2016). Hydrothermal method for synthesizing ZnFe₂O₄ nanoparticles, photo-degradation of Rhodamine B by ZnFe₂O₄ and thermal stable PS-based nanocomposite. *Journal of Materials Science-Materials in Electronics*. 27, 8654-8660.
- [17] Zhao, H., Dong, Y.M., Jiang, P.P., Wang, G.L., Zhang, J.J. and Li, K. (2014). An insight into the kinetics and interface sensitivity for catalytic ozonation: the case of nano-sized NiFe₂O₄. *Catalysis Science & Technology*. 4, 494-501.
- [18] Peng, T.Y., Zhang, X.H., Lv, H.J. and Zan, L. (2012). Preparation of NiFe₂O₄ nanoparticles and its visible-light-driven photoactivity for hydrogen production. *Catalysis Communications*. 28, 116-119.
- [19] Khedr, M.H., Bahgat, M. and El Rouby, W.M.A. (2008). Synthesis, magnetic properties and photocatalytic activity of CuFe₂O₄/MgFe₂O₄ and MgFe₂O₄/CuFe₂O₄ core/shell nanoparticles. *Materials Technology*. 23, 27-32.
- [20] Zhu, Z.R., Li, X.Y., Zhao, Q.D., Li, Y.H., Sun, C.Z. and Cao, Y.Q. (2013). Photocatalytic performances and activities of Ag-doped CuFe₂O₄ nanoparticles. *Materials Research Bulletin*. 48, 2927-2932.
- [21] Zhu, Z.R., Liu, F.Y., Zhang, H.B., Zhang, J.F. and Han, L. (2015). Photocatalytic degradation of 4-chlorophenol over Ag/MFe₂O₄ (M = Co, Zn, Cu, and Ni) prepared by a modified chemical co-precipitation method: a comparative study. *Rsc Advances*. 5, 55499-55512.
- [22] Singh, C., Devika, Malik, R., Kumar, V. and Singhal, S. (2015). CdS nanorod-MFe₂O₄ (M = Zn, Co and Ni) nanocomposites: a heterojunction synthesis strategy to mitigate environmental deterioration. *Rsc Advances*. 5, 89327-89337.
- [23] Zhang, G.S., Qu, J.H., Liu, H.J., Cooper, A.T. and Wu, R.C. (2007). CuFe₂O₄/activated carbon composite: A novel magnetic adsorbent for the removal of acid orange II and catalytic regeneration. *Chemosphere*. 68, 1058-1066.
- [24] Nasrallah, N., Kebir, M., Koudri, Z. and Trari, M. (2011). Photocatalytic reduction of Cr(VI) on the novel hetero-system CuFe₂O₄/CdS. *Journal of Hazardous Materials*. 185, 1398-1404.
- [25] Zhao, W., Jin, Y., Gao, C.H., Gu, W., Jin, Z.M., Lei, Y.L. and Liao, L.S. (2014). A simple method for fabricating p-n junction photocatalyst CuFe₂O₄/Bi₄Ti₃O₁₂ and its photocatalytic

- activity. *Materials Chemistry and Physics*. 143, 952-962.
- [26] Chen, H., Yan, J.Q., Wu, H., Zhang, Y.X. and Liu, S.Z. (2016). One-pot fabrication of NiFe₂O₄ nanoparticles on alpha-Ni(OH)₂ nanosheet for enhanced water oxidation. *Journal of Power Sources*. 324, 499-508.
- [27] Ansari, F., Bazarganipour, M. and Salavati-Niasari, M. (2016). NiTiO₃/NiFe₂O₄ nanocomposites: Simple sol-gel auto-combustion synthesis and characterization by utilizing onion extract as a novel fuel and green capping agent. *Materials Science in Semiconductor Processing*. 43, 34-40.
- [28] Ji, H.Y., Jing, X.C., Xu, Y.G., Yan, J., Li, Y.P., Huang, L.Y., Zhang, Q., Xu, H. and Li, H.M. (2016). Synthesis of magnetic BiOBr-NiFe₂O₄ hybrids and the efficient photocatalytic activity. *Fresen. Environ. Bull.*, 25, 3083-3091.
- [29] Lu, Z.F., Wang, H.M., Zhou, D.P., Liu, D. and Chen, Z. (2016). The preparation of Ag/Cu₂O hollow nanospheres for enhanced photocatalytic activity. *Fresen. Environ. Bull.*, 25, 391-400
- [30] Cheng, R.L., Fan, X.Q., Wang, M., Li, M.L., Tian, J.J. and Zhang, L.X. (2016). Facile construction of CuFe₂O₄/g-C₃N₄ photocatalyst for enhanced visible-light hydrogen evolution. *Rsc Advances*. 6, 18990-18995.
- [31] Gao, N.L. et al. (2016). Enhanced photocatalytic activity of a double conductive C/Fe₃O₄/Bi₂O₃ composite photocatalyst based on biomass. *Chemical Engineering Journal*. 304, 351-361.
- [32] Bai, Y., Chen, T., Wang, P.Q., Wang, L. and Ye, L.Q. (2016). Bismuth-rich Bi₄O₅X₂ (X = Br, and I) nanosheets with dominant {101} facets exposure for photocatalytic H₂ evolution. *Chemical Engineering Journal*. 304, 454-460.
- [33] Ye, Z.F., Li, J.Z., Zhou, M.J., Wang, H.Q., Ma, Y., Huo, P.W., Yu, L.B. and Yan, Y.S. (2016). Well-dispersed nebula-like ZnO/CeO₂@HNTs heterostructure for efficient photocatalytic degradation of tetracycline. *Chemical Engineering Journal*. 304, 917-933.
- [34] Hong, Y.Z., Ren, A., Jiang, Y.H., He, J.H., Xiao, L.S. and Shi, W.D. (2015). Sol-gel synthesis of visible-light-driven Ni_{1-x}Cu_xFe₂O₄ photocatalysts for degradation of tetracycline. *Ceramics International*. 41, 1477-1486.
- [35] Shi, W.D., Shi, J.Q., Yu, S. and Liu, P. (2013). Ion-exchange synthesis and enhanced visible-light photocatalytic activities of CuSe-ZnSe flower-like nanocomposites. *Applied Catalysis B-Environmental*. 138, 184-190.
- [36] Gao, P.Z., Hua, X., Degirmenci, V., Rooney, D., Khraisheh, M., Pollard, R., Bowmand, R.M. and Rebrov, E.V. (2013). Structural and magnetic properties of Ni_{1-x}Zn_xFe₂O₄ (x=0, 0.5 and 1) nanopowders prepared by sol-gel method. *Journal of Magnetism and Magnetic Materials* 348, 44-50.
- [37] Xu, D.B., Chen, M., Song, S.Y., Jiang, D.L., Fan, W.Q. and Shi, W.D. (2014). The synthesis of a novel Ag-NaTaO₃ hybrid with plasmonic photocatalytic activity under visible-light. *Crystengcomm*. 16, 1384-1388.
- [38] Xu, D.B., Yang, S.B., Jin, Y., Chen, M., Fan, W.Q., Luo, B.F. and Shi, W.D. (2015). Ag-Decorated ATaO₃ (A = K, Na) Nanocube Plasmonic Photocatalysts with Enhanced Photocatalytic Water-Splitting Properties. *Langmuir*. 31, 9694-9699.

Received: 26.12.2016

Accepted: 20.06.2017

CORRESPONDING AUTHOR

Weidong Shi

School of Chemistry and Chemical Engineering,
Jiangsu University, Xuefu Road 301, Zhenjiang,
212013, P. R. China

e-mail: swd1978@ujs.edu.cn

PREPARATION OF SULPHOALUMINATE CEMENT WITH RESIDUE OF MANGANESE DIOXIDE ORE LEACHED BY SO₂

Bo-zhi Wang, Shi-jun Su, Sang-lan Ding, Wei-yi Sun*

College of Architecture and Environment, Sichuan University, Chengdu, 610065, China

ABSTRACT

In this study, the physical and chemical properties of residue of manganese dioxide ore (RMDO), a type of solid waste derived from the reductive leaching of manganese by SO₂, were analyzed. Subsequently, RMDO was used as a raw material for the preparation of sulphoaluminate cement mixed with limestone and bauxite, according to the formula calculated by the three rates (Cm, P, N). The effect of sintering time, holding time, plaster addition on alkalinity, mechanical properties and setting time of cement were investigated. The findings demonstrate the feasibility of sulphoaluminate cement preparation using RMDO, since the various indicators of the prepared sulphoaluminate cement all reached the national standard of sulphoaluminate cement (GB20427-2006). The changing regularity of cement's alkalinity and setting times was within a control range, compared to traditional cement. In the same formulation of raw material, sintering temperature and plaster addition were found to have a great impact on clinker strength, whereas the holding time had little impact on strength.

KEYWORDS:

Residue of manganese dioxide ore; Sulphoaluminate cement; Compressive strength; Alkalinity

INTRODUCTION

Reduction of sulfur dioxide emissions [1,2] and resource utilization of low-grade manganese dioxide ores [3,4] are two major issues which must be urgently addressed in China. The reductive leaching of manganese dioxide ores by various SO₂ waste gases is a means for reducing SO₂ emissions [5] and pro-

duces a leaching solution containing manganese sulfate [6] which can then be used to prepare manganese sulfate [7], electrolytic manganese [8], manganese carbonate [9] and other products. Reserves of low-grade manganese dioxide ore resources (containing 20%–25% Mn) are abundant in China. Due to the low content of Mn in manganese dioxide ores, recovery of Mn inevitably results in a large number of residues [10]. If these residues are not adequately processed, they will become a new source of environmental pollution.

In order to reduce the potential hazard of the residue of manganese dioxide ore (RMDO), researchers have investigated the resource utilization of RMDO as an adsorbent to remove a number of pollutants such as hexavalent chrome [11], congo red [12] and methylene blue (MB) [13]. This paper had studied that RMDO were used as a raw material for the preparation of sulphoaluminate cement which possesses the advantageous features of steady strength, high strength, early strength and rapid hardening, [14] as well as good corrosion and freezing resistance [15,16]. Being a relatively new technology, the study outlined in this publication investigated the feasibility of sulphoaluminate cement. The performance of sulphoaluminate cement was explored, including the influencing factors, alkalinity, sintering temperature, holding time, plaster addition and setting time.

EXPERIMENTAL PROGRAM

Material. The following materials were used in the study:

(1) MRDO was produced by reductive leaching of manganese dioxide ore by SO₂ [8]. The residue pH was tested to be 6.23, and the packing density was approximately 0.68g/m³.

TABLE 1
Chemical composition of MRDO wt/%

Composition	SO ₃	SiO ₂	CaO	K ₂ O	Al ₂ O ₃	TiO ₂
content	13.3	39.1	4.9	3.0	14.2	3.7

TABLE 2
Particle size distribution of RMDO

Size range (µm)	<38	38~75	75~105	105~150	150~300	>300
Cumulative sieve residue (%)	100	97.87	88.27	87.3	76.3	66.3

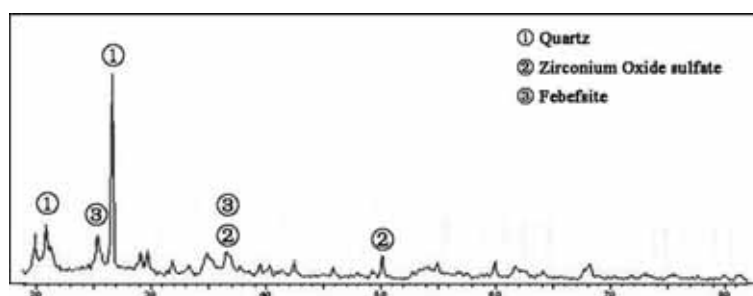


FIGURE 1
X-ray diffraction pattern of RMDO

TABLE 3
Analysis of bauxite composition

component	Al ₂ O ₃	SiO ₂	K ₂ O	TiO ₂	SO ₃	Fe ₂ O ₃
content	64.0	17.8	6.5	6.2	3.1	2.4

TABLE 4
Composition of raw material

Lime wt/%	Bauxite wt/%	desulfurization residue wt/%	Cm	P	N
48	23	29	0.95	3.37	1

The compositions of residue are shown in Table 1, as determined by X-ray photoelectron spectroscopy (XPS). Particle size distribution of RMDO is listed in Table 2, as determined by a manual screening method. To identify the phases of the residue, the results of X-ray diffraction are shown in Figure 1.

From the results shown in Figure 1, it is evident from the peaks at 20.89° and 26.71° that the main mineral was quartz. The peak at 50.18° indicates the presence of magnetite in the residue. Therefore, the residue was not a pure mineral phase, and its X-ray diffraction pattern is very similar to manganese modified sand. The results in Table 1 and Table 2 demonstrate that SiO₂, Al₂O₃ and SO₃ accounted for the vast majority of the RMDO composition, which corresponds to the composition of general silicate materials. Moreover, particle size was less than 150 µm. The residues used in this experiment had the basic conditions amenable to preparation of sulphoaluminate cement, according to the standard of sulphoaluminate cement clinker [17].

(2) Lime was used as the laboratory chemical reagent CaO, with a purity of about 99%.

(3) Parget was used as the laboratory chemical reagent CaSO₄, with a purity of about 99%.

(4) Bauxite used in this study was collected from Sichuan Neijiang. The composition of the bauxite is shown in Table 3.

Experimental Apparatus. The following equipment was used to conduct the study:

JSM-7500F scanning electron microscope (Japan's electronics production);

HCTP12A pallet scales with 0.1 g precision (Beijing Medical Balance Factory);

Standard consistency and setting time of measuring instrument, CHN-2 (HebeiBrightChina);

X-ray photoelectron spectrometer, XSAM800 (British Kratos company);

RIX-12-16 type high temperature box resistance furnace (Beijing City Yong Guangming medical Instrument Co. Ltd.);

SX-8-10 type muffle furnace (Shanghai experimental instrument factory production);

X'Pert Pro MPD X-ray diffraction (the PHILIPS company, Holland).

Experimental principle. According to the three rates, the proportions of the raw materials of lime, bauxite and RMDO could be determined with regards to being placed in a high temperature furnace

for sintering sulphoaluminate cement. The three rates [18] were expressed as follows:

$$C_m = \frac{w(\text{CaO}) - 0.7w(\text{TiO}_2)}{0.73[w(\text{Al}_2\text{O}_3) - 0.64w(\text{Fe}_2\text{O}_3)] + 1.4w(\text{Fe}_2\text{O}_3) + 1.87w(\text{SiO}_2)} \quad (1)$$

$$P = \frac{w(\text{Al}_2\text{O}_3) - 0.64w(\text{Fe}_2\text{O}_3)}{w(\text{SO}_3)} \quad (2)$$

$$N = \frac{w(\text{Al}_2\text{O}_3) - 0.64w(\text{Fe}_2\text{O}_3)}{w(\text{SiO}_2)} \quad (3)$$

The rate of C_m refers to the CaO raw material needed for the generation of useful mineral clinker; this can be calculated using equation (1). The rate of P refers to the ratio of sulfur to aluminum, and indicates that the amount of Al_2O_3 formed after the formation of iron phase and CaSO_4 can meet the degree of formation of $3\text{CaO} \cdot 3\text{Al}_2\text{O}_3 \cdot \text{CaSO}_4$. It can be calculated using equation (2). The rate of N is the ratio of aluminum and silicon, in detail it is the ratio of $\text{C}_4\text{A}_3\text{S}$ to C_2S . In order to make the clinker mineral form well, the three rates must be in certain ranges. The rate of C_m should be as close to 1 as possible, though not equal to 1; the rate of P may be ≤ 3.82 , the rate of N should generally be between 1 to 3, though it is preferable that this should be as close to 1 as possible.

Experimental procedure. With manual screening of particles with a particle size of less than $150\mu\text{m}$, raw meal was prepared according to the composition shown in Table 4, which is the best ratio based on experimental principle calculations. Subsequently, the raw meal and 10% water are placed in a porcelain crucible and mixed well. The porcelain crucible is then placed in a high temperature furnace, with a temperature rising to the preset temperature. After a certain time duration, the test block will be taken out and placed in the air to allow it to cool under ambient conditions. After grinding with a uniform ceramic mortar and passing through a 200 mesh sieve (aperture $75\mu\text{m}$), the cement clinker is prepared. Subsequently, the alkalinity and mechanical properties of the cement can be determined.

Analysis method. The sieve distribution of RMDO was tested by sieve analysis (manual sieve analysis method) according to the 1345-2005 GB/T "cement fineness test method". The measurement of cement alkalinity was undertaken with reference to the GB5086.2-1997 "solid waste leaching toxicity leaching method the level of vibration method". In detail, a standard solution was initially prepared and subsequently leached for the measurement of cement alkalinity. The cement clinker was powdered in a ball mill under different conditions and sieved at $120\mu\text{m}$. The sieved clinker was mixed with water according to a certain ratio (water : clinker = 3 : 10), and then pressed using a pressure machine to obtain samples with the dimensions, $4\text{ cm} \times 4\text{ cm} \times 1\text{ cm}$. After the prepared samples were placed in air for 7, 14 and 28 days, the mechanical properties were evaluated using a universal material testing machine. All the data

were provided from a testing center in SiChuan University.

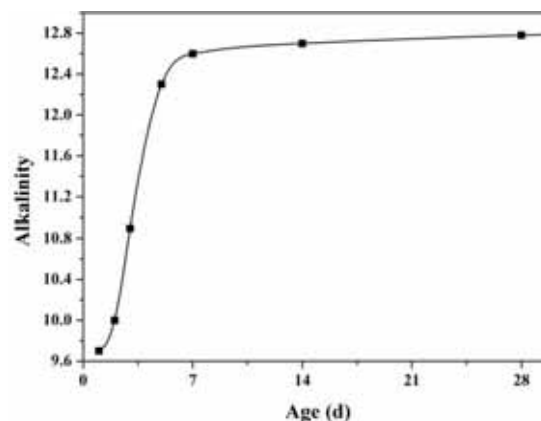


FIGURE 2
Alkalinity of clinker

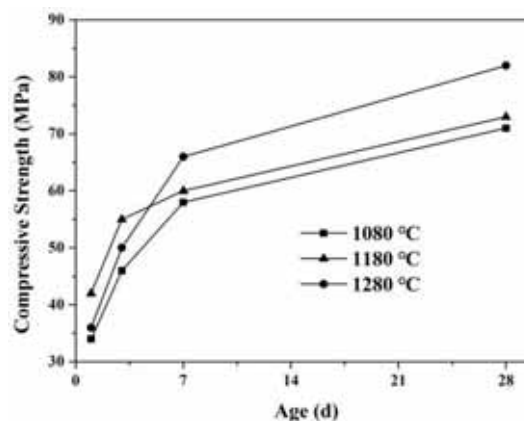


FIGURE 3
Compressive strength of sintering temperature

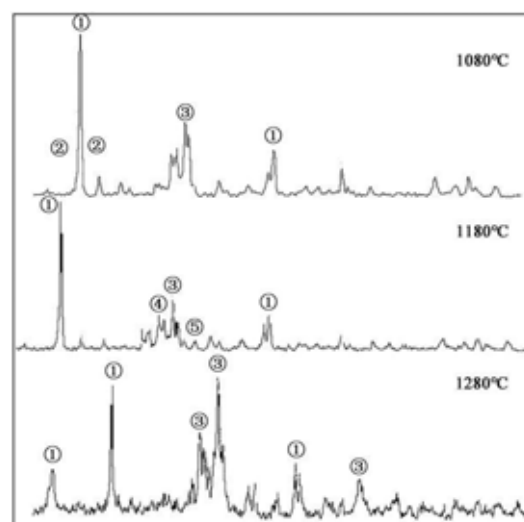


FIGURE 4
XRD of different sintering temperature

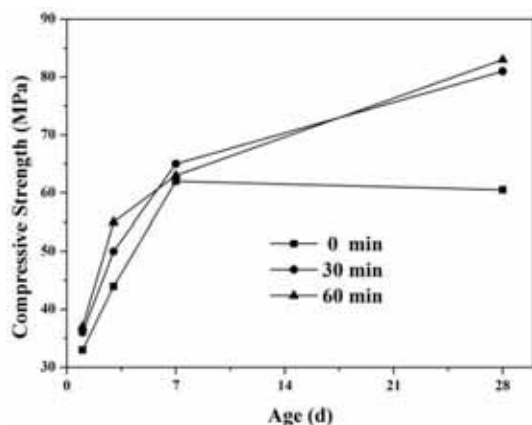


FIGURE 5
Compressive strength of holding time

RESULTS AND DISCUSSION

Alkalinity of cement. Alkalinity [19] of cement is determined by the ability to bind protons, and is proportional to the corrosion resistance property of cement. In short, the higher the alkalinity of the cement is, the better the corrosion resistance. Therefore, alkalinity of cement is one of the important indices of cement performance, which determines the active substance content in the cement matrix. The result of cement clinker alkalinity is presented in Figure 2.

The variation trend of the alkalinity can be divided into three stages (see Figure 2) as follows. In stage 1, the value of the cement alkalinity greatly increases between 0 and 7 days, which is closely related to the growth starting point and growth rate. After seven days, the alkalinity reached approximately 12.5. In stage two, the change in alkalinity experienced a tendency to rise slightly in the process of hydration from day 7 to day 28. In stage 3, the cement alkalinity is stable from day 14 to 28. In general, the main variation of alkalinity was experienced before 7 days, and the span of its value increased from 9.65 to 12.55. After 56 days, the alkalinity of cement is stable. This is in line with national standards [17].

Mechanical property. (1) **Influence of sintering temperature on compressive strength.** Figure 3 showed compressive strength of cement clinker at different temperatures and the corresponding XRD patterns are listed in Figure 4. The compressive strength of all samples increased with increasing time durations. Before 3 days, the compressive strength of clinker sintered at 1180°C is higher than others, due to the interim phase gehlenite appearing in linker phase composition, which revealed the high early compressive strength. From 3 to 7 days, the compressive strength of clinker sintered at 1280°C exhibited a rapid rising rate, and its specific value at

7 days reached 60 MPa, which was beyond that of the clinker at 1180°C. This is because gehlenite disintegrated and calcium aluminate reacted with residual dissociative CaO to form the $C_4A_3\bar{S}$. Under this formula, the cement clinker at 1280°C results in great development of mineral phases.

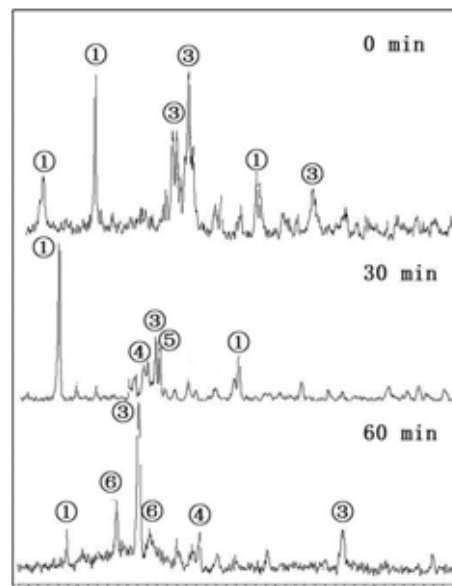


FIGURE 6
XRD of different holding time

(2) **Influence of holding time on compressive strength.** Figure 5 shows the variation of compressive strength for the samples after various holding times. The phase composition of clinker after being maintained for various times was identified by XRD. Evidently, the compressive strength of the clinker after 30 and 60 min holding times was higher than the value of the control group, especially between 7 and 28 days. The increased holding time may accelerate the rate of mass transfer to improve the strength. Meanwhile, comparing between the clinkers after 30 and 60 min holding times, there was no substantial difference in the compressive strengths. In detail, the compressive strength of the clinker after holding for 60 min was slightly higher than the strength of clinker after 30 min holding time. From the XRD results shown in Figure 6, it is evident that the diffraction peak of C_3S became narrower for the sample after holding for 60 min, which indicates the good crystallinity of C_3S in the clinker matrix. The reason for higher compressive strength is that the long holding times (60 min) could offer more energies for the formation of C_3S phase than the short holding time (30 min), which could contribute to the mechanical strength of clinker. However, C_3S is not favorable to formation of $C_4A_3\bar{S}$ [20] because excessive holding

time could cause a proportion of calcium sulphoaluminate minerals to decompose and react with the rest of the mineral phase, forming the excessive phase material, gehlenite, which is an impurity resulting from the clinker burning process. Moreover, the distinction in compressive strength caused by the different holding time (30 min and 60 min) is slight. Besides, the shorter holding time results in lower production costs and energy consumption, which is beneficial to the environment. In this study, 30 min was selected as the optional holding time.

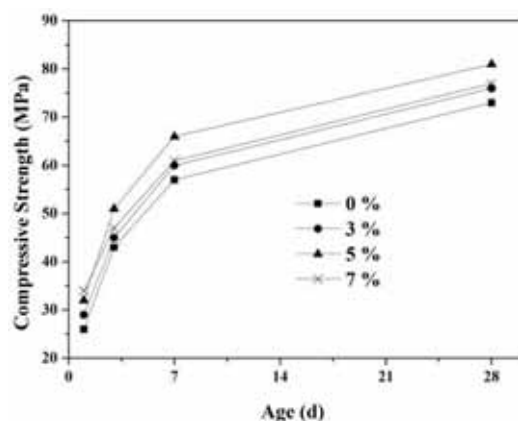


FIGURE 7
Compressive strength of plaster addition

(3) Influence of plaster addition on compressive strength. The effect of plaster on the setting time of cement is listed in Table 5. It is obvious that the plaster was of great significance in improving the setting time. The initial and final setting time of doped-plaster groups was largely higher than non-doped one. The initial and final setting times of all doped samples complied with the requirement of GB20427-2006 (initial times ≥ 25 min and final times ≤ 180 min). The setting time of cement increased with the doped content of plaster, because the plaster could accelerate the rate of ettringite formation, and the formed phases would rapidly cover the surface of C_2S and unhydrated $C_4A_3\bar{S}$ to reduce the incidence of the reaction between unhydrated ions and plaster, and the hydrated rates for the adjustment of setting times[21].

Nonetheless, considering the effect of plaster on the compressive strength (Figure 7), the content of plaster should be limited within a certain range. The sample doped with the 5% plaster exhibited the highest compressive strength at 7 and 28 days, and the setting time was in accordance with the GB20427-2006. Hence, the optional plaster doping is 5%.

Through this investigation into the effect of various factors on compressive strength, it is demonstrated that manipulation of appropriate process pa-

rameters can confer cement with excellent performances. In the same formulation of raw material, sintering temperature and plaster addition had a great impact on clinker strength, whereas the holding time had little effect on strength. The mineral phases may be altered due to different sintering temperatures, which were primary reasons for the change in compressive strength. A series of reactions would happen under inadequate temperature addition, characterized with the formation of incomplete or complex phases and the decomposition of mineral phases. The plaster is a normal mineralized agent [21] which played a major role in production of cement. Then plaster did not only reduce the viscosity of liquid formation, but also enhanced the liquid content. These promoted the spread and movement of phases. The plaster can interact with C_2S to form the main compositions of cement ($CaSO_4$ and thaumasite). Considering the economic factors, the optimum sintering temperature is $1280^\circ C$, the optimum holding time is 30 min, and the best plaster addition is 5%.

Setting time. Setting time was divided into initial setting and final setting. The initial setting time meant that the slurry began to lose plasticity and flow reduced since the water mixed with cement. The final setting time meant that the slurry loses plasticity completely and began to have certain structural strength since the water mixed with cement [22, 23]. So setting time was an important characteristic of cement. The setting time of the cement with the plaster addition of 5% is shown in table 6.

TABLE 6
Setting time of the cement

sintering temperature	Initial setting/min	Final setting/min
$1180^\circ C$	35	48
$1280^\circ C$	33	49

Table 6 demonstrates that regardless of the temperature, the initial and final setting times of the cement are in line with national standards. The initial setting at $1280^\circ C$ is earlier than that at $1180^\circ C$, validating that $1280^\circ C$ is the more favorable temperature for sintering of cement.

Through the study of the alkalinity, sintering temperature, holding time, plaster addition and setting time of cement, performance parameters compared with the national standards are shown in Table 7. The performance parameters that were determined all indicate favorable stability performance of the cement preparation from RMDO, demonstrating the feasibility of this technology, and highlight the potentially broad prospects of industrial application.

TABLE 7
Main performance parameters compared with National standard (GB2042-2006)

Performance parameter	Alkalinity	Compressive strength			Setting time	
		1d	3d	28d	Initial	Final
Experimental	12.8	32	51	81	33	49
GB2042-2006	≥10.5	≥30	≥42.5	≥45	≥25	≤180

CONCLUSIONS

This study has demonstrated the feasibility of this new technology. The cement preparation by RMDO has stability performance, and the main performance parameters, including alkalinity, compressive strength and setting time, reached the national standard of sulphoaluminate cement (GB20427-2006). The changing regularity of cement's alkalinity and setting times was within a controlled range, compared with traditional cement. For the same formulations, sintering temperature and plaster addition had a great impact on clinker strength, whereas the holding time had little effect on strength.

Through the research on preparation of sulphoaluminate cement by RMDO, the study outlined in this publication has explored a novel approach for resource utilization. This study has demonstrated a reasonable application of RMDO in a way that reduces the environmental impact of RMDO waste. Furthermore, building materials with excellent properties were prepared. This approach is conducive to the sustainable development of China's environmental economy.

ACKNOWLEDGEMENTS

This project is supported by the National Natural Science Foundation of China (NSFC-51374150 and NSFC-51304140) and the Science and Technology Plan Projects of Sichuan Province, China (2014SZ0146 and 2015HH0067).

REFERENCES

- [1] Gao, C., Yin, H., Ai, N. and Huang, Z. (2009) Historical analysis of SO₂ pollution control policies in China. *Environmental management*, 43, 447-457.
- [2] Zhang, J.J. and Smith, K.R. (2007) Household air pollution from coal and biomass fuels in China: measurements, health impacts, and interventions. *Environmental Health Perspectives*, 115, 848-855.
- [3] Tong-qing, L. (2008) Technology of Low Grade Pyrolusite Ore Reduction Process and Recent Advances [1]. *China's Manganese Industry*, 2, 143-144
- [4] Haifeng, S., Huaikun, L., Fan, W., Xiaoyan, L. and Yanxuan, W. (2010) Kinetics of reductive leaching of low-grade pyrolusite with molasses alcohol wastewater in H₂SO₄. *Chinese Journal of Chemical Engineering*, 18, 730-735.
- [5] Shifeng, H., Jun, C., Futian, L., Lingchao, L., Zhengmao, Y., Xin, C. (2004) Poling process and piezoelectric properties of lead zirconate titanate/sulphoaluminate cement composites. *Journal of materials science*, 39, 6975-6979.
- [6] Jiang, T., Yang, Y., Huang, Z., Zhang, B. and Qiu, G. (2004) Leaching kinetics of pyrolusite from manganese-silver ores in the presence of hydrogen peroxide. *Hydrometallurgy*, 72, 129-138.
- [7] Sahoo, R., Naik, P. and Das, S. (2001) Leaching of manganese from low-grade manganese ore using oxalic acid as reductant in sulphuric acid solution. *Hydrometallurgy*, 62, 157-163.
- [8] Sun, W.-y., Su, S.-j., Wang, Q.-y. and Ding, S.-l. (2013) Lab-scale circulation process of electrolytic manganese production with low-grade pyrolusite leaching by SO₂. *Hydrometallurgy*, 133, 118-125.
- [9] Lin, Q.-q., Gu, G.-h., Wang, H., Zhu, R.-f., Liu, Y.-c., Fu, J.-g. (2016) Preparation of manganese sulfate from low-grade manganese carbonate ores by sulfuric acid leaching. *International Journal of Minerals, Metallurgy, and Materials*, 23, 491-500.
- [10] Zhou-chu, H., Ai-guo, P., Zheng, X.-f., Changyan, Y. and Yu-ling, L. (2004) A Study on the two-ores Method of Leaching Low Grade Pyrolusite [J]. *China's Manganese Industry* 2: 010.
- [11] Sun, W.-Y., Shen, W., Wang, Q.-Y., Ding, S.-L. and Su, S.-J. (2013) Adsorption of chromium (VI) from aqueous solution onto aluminum pillared pyrolusite leaching residue. *Fresen. Environ. Bull.*, 22, 2645-2650.
- [12] Shen, W., Liao, B., Sun, W., Su, S. and Ding, S. (2013) Adsorption of Congo red from aqueous solution onto pyrolusite reductive leaching residue. *Desalination and Water Treatment*, 52, 3564-3571.
- [13] Liao, B., Shen, W., Sun, W., Wu, B., Su, S., Ding, S. (2014) Adsorption of Methylene Blue from Aqueous Solution Onto Pyrolusite Leaching Residue And Degradation In H₂O₂/H₂SO₄ System. *Fresen. Environ. Bull.*, 23, 1618-1625.
- [14] Korhonen J, Wihersaari M, Savolainen I (2001)

- Industrial ecosystem in the Finnish forest industry: using the material and energy flow model of a forest ecosystem in a forest industry system. *Ecological Economics* 39: 145-161.
- [15] Wang, Y., Su, M. and Zhang, L. (1999) Sulphoaluminate cement. Publication of Beijing University of Technology, 1st edition, Beijing.
- [16] Xin, C., Shifeng, H., Jun, C., Ronghua, X., Futian, L., Zengmao, Y., Xiude, W. (2005) Piezoelectric and dielectric properties of piezoelectric ceramic-sulphoaluminate cement composites. *Journal of the European Ceramic Society*, 25: 3223-3228.
- [17] AQSIQ, GB20472-2006 Sulphoaluminate cement [S]. Beijing: Standards Press of China, 2001.
- [18] Kolovos, K., Tsvivilis, S. and Kakali, G. (2002) The effect of foreign ions on the reactivity of the CaO-SiO₂-Al₂O₃-Fe₂O₃ system: Part II: Cations. *Cement & Concrete Research*, 32, 463-469.
- [19] Juenger, M.C.G. and Jennings, H.M. (2001) Effects of high alkalinity on cement pastes. *Materials Journal*, 98, 251-255.
- [20] Li, B., Li, Y., Wu, Y. (2011) The influence of C3S content on the calcining and properties of alite-sulphoaluminate cement clinker. *ShuiNi*, 3, 9-12
- [21] Moussavi, G. and Khosravi, R. (2011) The removal of cationic dyes from aqueous solutions by adsorption onto pistachio hull waste. *Chemical Engineering Research and Design*, 89, 2182-2189.
- [22] Uchikawa, H., Hanehara, S., Shirasaka, T. and Sawaki, D. (1992) Effect of admixture on hydration of cement, adsorptive behavior of admixture and fluidity and setting of fresh cement paste. *Cement and Concrete Research*, 22, 1115-1129.
- [23] Bortoluzzi, E.A., Broon, N.J., Bramante, C.M., Felipe, W.T., Tanomaru Filho, M., et al. (2009) The influence of calcium chloride on the setting time, solubility, disintegration, and pH of mineral trioxide aggregate and white Portland cement with a radiopacifier. *Journal of endodontics*, 35, 550-554.

Received: 26.12.2016

Accepted: 16.06.2017

CORRESPONDING AUTHOR

Wei-yi Sun

College of Architecture and Environment

Sichuan University

Chengdu, 610065 – CHINA

E-mail: swylscu@163.com

PRECURSOR-CONTROLLED SYNTHESIS OF GRAPHENE-LIKE CARBON NITRIDE FOR MC-LR DEGRADATION UNDER VISIBLE LIGHT

Jiahui Ma, Liping Wang*, Chengjie Song, Shaomang Wang, Fan Zhang

School of Environmental and Safety Engineering, Changzhou University, Changzhou, 213164, P.R. CHINA

ABSTRACT

The increasing occurrence of algal blooms with harmful algae-derived organic matters as microcystin-LR (ML-LR) has become an urgent public health issue. In this study, the preparation of g-C₃N₄ with changing the ratio of urea to melamine in the precursor was studied for MC-LR degradation under visible light. The prepared photocatalysts were characterized by scanning electron microscopy (SEM), X-ray diffraction (XRD), Fourier transform infrared spectrometry (FTIR) and UV-vis diffuse reflection spectroscopy (DRS) methods. The results show that the prepared photocatalysts exhibit the different structure and properties with the different mass ratio of urea to melamine. The photocatalyst CN(32) with porous structure and high photocatalytic activity has improved the degradation rate of MC-LR compared with other photocatalysts. It shows that the degradation rate of MC-LR to CN(32) is 23.68% which is 1.8 and 2.2-folds higher than that of CN(10) and CN(01), respectively. This finding can guide us to prepare photocatalysts with high activity based g-C₃N₄ for degrading microcystins

KEYWORDS:

precursor; visible light; MC-LR; degradation

INTRODUCTION

In recent years, with the development of industry and agriculture, a large number of wastewater containing N, P drains into freshwater which resulting in the increasingly serious eutrophication in water [1]. Especially in the summer, the cyanobacterial blooms will release microcystins (MCs) which damages the liver of animals and human even leading to death by inhibiting protein phosphatase 2A (PP2A) and 1 (PP1A) [2, 3]. Microcystins are biologically active cyclic-peptides compound with a unique group D-amino acids, β-linked erythro-β-methylaspartic acid, γ-linked glutamic acid, the two unusual amino acids (N-methyldehydroalanine and 3-amino-9-methoxy-10-phenyldeca-2,6,8-trimethyl-4,6-dienoic acid (Adda), and two L-amino acids). It is the special existence of Adda side chain in the structure

that determines its toxicity [4]. MC-LR, MC-RR and MC-YR are the most common microcystins among 80 types of identified and MC-LR is most prevalently available [5].

Due to their cyclic structure and spacer double bonds microcystins are highly stable under visible light and resist to be decomposed even under high temperature, UV irradiation and general peptide hydrolase [6]. From some studies can be found that the Adda side chain in the microcystin structure contains β, γ double bonds which can be oxidized, photodegraded and biodegraded [7, 8]. Among the studies on photocatalytic degradation of microcystins a majority of them are degraded under UV irradiation.

Considering visible light accounting for about 43% in solar radiation, the photocatalysts under visible light has great potential as a renewable and sustainable water treatment technique [9]. To overcome this drawback, numerous studies have been performed to enhance the photocatalytic efficiency and to make the most use of solar energy. Recently, as a new metal-free material, graphite-like carbon nitride (g-C₃N₄) with good visible light response has attracted wide attention due to its high thermal and chemical stabilities in the photocatalysts field.

However, the g-C₃N₄ prepared by conventional methods has the problems of small specific surface area and low quantum yield which limits its application in practical treatment [10]. During the photocatalytic reaction, g-C₃N₄ is required to have good adsorption performance and proper energy band position for the degradation of target pollutants. Therefore, the micro-morphology of g-C₃N₄ is also the important factor affecting the photocatalytic performance. So far, it has been shown that the microstructure of g-C₃N₄ can be porous and low-dimensional by improving the experimental process or further treatment. As porous-nano particles, nanorods and nano-thin layer, the g-C₃N₄ with these structures has a large specific surface area, high crystallinity and significantly improved photocatalytic performance [11, 12].

EXPERIMENTAL

Materials. Methanol and sequanal-grade trifluoroacetic acid (TFA) were purchased from Anpel. Sep-pak C₁₈ solid phase extraction cartridge was purchased from Waters (USA). The standard of microcystin-LR (>95%) was purchased from Enzo (USA). Urea and melamine were both extra pure purchased from Sinopharm Chemical Reagent Co.Ltd (China). Deionized-distilled water was purified using Milli-Q ultra-pure water system.

Synthesis. After adequately grinding the mixture of urea and melamine with different mass ratio (urea: melamine = 1: 0, 4: 1, 3: 2, 1: 1, 2: 3, 1: 4, 0: 1), the powders were put into alumina crucibles with cover for further calcination treatment at a heating rate of 2.3 °C/min in a muffle furnace and maintained at 550 °C for 4h. After the reaction, the alumina crucibles were cooled to room temperature. The resultant g-C₃N₄ were turned into fine powders. Samples prepared from different precursor masses were named as CN(10), CN(41), CN(32), CN(11), CN(23), CN(14) and CN(01), respectively.

Apparatus. Morphological characteristics were analyzed by using a scanning electron microscopy (SEM) with an SUPRA55 field emission SEM (Zeiss, Germany). X-ray diffraction (XRD) patterns was performed on a D/max-2500 PC with a high-power Cu-K α radioactive source ($\lambda=0.15406\text{nm}$) at 60 kV/30mA to determine the crystal phase of the obtained samples (Rigaku, Japan). Fourier transform infrared spectra (FTIR) were performed on a Nicolet iS50 spectrometer using KBr as reference sample within wavelength range of 400-4000cm⁻¹ (Thermo fisher, USA). UV-vis diffuse reflection spectroscopy (DRS) was performed on a UV-3600 spectrometer was using BaSO₄ as a reference within scanning range of 200-800 nm (Shimadzu, Japan). The photocatalytic reaction was carried out by XPA-2 photochemical reaction apparatus (Nanjing Xujiang, China). The microcystin was monitored by LC-UV with liquid chromatograph (Wufeng, China).

Analytical procedures. *Microcystis aeruginosa* was purchased from the Institute of Hydrobiology, Chinese Academy of Sciences (Wuhan, China). The axenic *Microcystis aeruginosa* cultures were cultured in BG-11 medium in Erlenmeyer flasks placed in an incubation at the 25 °C with aeration [13]. The sunshine was simulated by using fluorescent lamps as light source with an automatic light/dark cycle of every 12 h during the lighting phase [14]. Cultures were sequentially subjected to repeated freezing and heating three times after a 30-day incubation. Then the algae cell solution in charreuse was ultrasonically shaken for 60 min by ultrasonic system. For further pretreatment, the supernatant obtained after high-speed centrifugation of the

algae cell solution was filtered through a membrane filter. The resulting solution was subjected to solid phase extraction and nitrogen stripping to obtain purified microcystins. Liquid chromatography (LC) analysis was performed on a Wufeng liquid chromatograph with a C₁₈ chromatographic column (LK-C18, 4.6x150 mm, 5 μm). The mobile phase consisted of deionized water with 0.1% TFA: methanol (V/V) =48:52. The flow rate was 5mL/min and the injection volume was 20 μL [15, 16].

Photocatalytic degradation of MC-LR. The photocatalytic activities of g-C₃N₄ were evaluated with its degradation of MC-LR under visible light irradiation. The photocatalytic reaction was carried out in a visible light photo-degradation apparatus at a constant temperature of 26 °C. A certain amount of photocatalyst was weighed and added into 50 mL reaction solution. For eliminating the influence of adsorption, the suspension was magnetically stirred in the dark for 60min before irradiation to reach the adsorption-desorption equilibrium. The xenon lamp (350W, 360nm-760nm) as light source was then switched on to initiate the photocatalytic reaction. The UV beam was cut off by adopting a UV cut-off filter (420nm). The NaNO₂ solution was added into quartz cold trap to filter out ultraviolet light [17]. During irradiation, the sampling was taken every 30 minutes periodically and filtrated after centrifugation to remove the catalyst particles. The solubility of MC-LR in the solution was measured by liquid chromatography.

RESULTS AND DISCUSSION

Morphology and structure. The typical scanning electron microscopy images of as-prepared photocatalysts are presented in Fig.1. It can be seen that g-C₃N₄ is a block formed by stacking many irregular nanosheets with each other, which has a typical graphite lamellar structure. Fig.1 (a) and (g) show that the g-C₃N₄ nanosheets prepared with pure urea and pure melamine exhibits layered structure and the surface is very smooth. In Fig.1 (b), (c), (d), (e) and (f), the bulk g-C₃N₄ prepared with the mixture of urea and melamine have relatively rough surface and hierarchical porous structure compared with CN(10) and CN(01). Fig. 1(b) shows that as-prepared g-C₃N₄ exhibits a graphene-like morphology with some porous structure. Many small pores are clustered on the rough surface of large nanosheets which is beneficial to the adsorption performance of photocatalysts [18]. It can be seen in Fig.1 (b) and (c), the photocatalysts have porous graphene morphology with porous structure in the nano-lamellar and the existence of porous structure may be due to the decomposition and

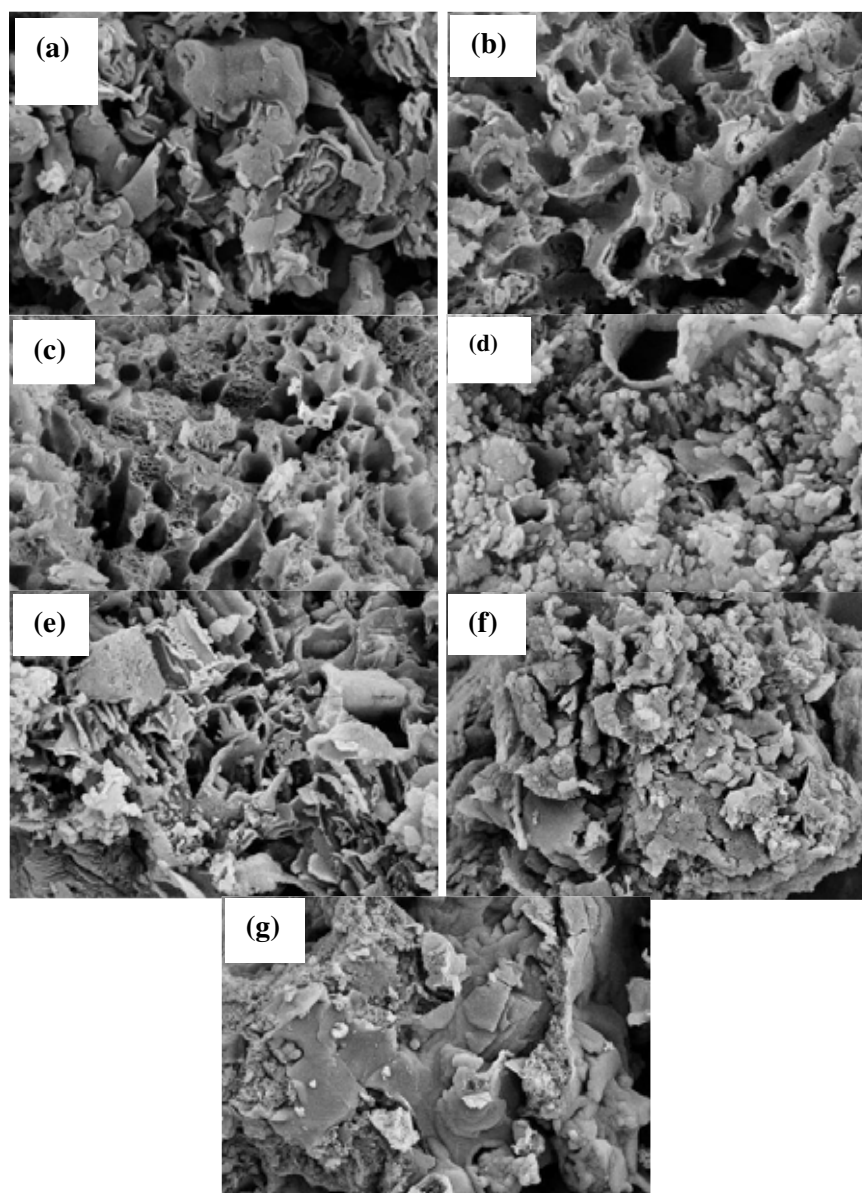


FIGURE 1
SEM images of $g\text{-C}_3\text{N}_4$. (a) CN(10); (b) CN(41); (c) CN(32); (d) CN(11); (e) CN(23); (f) CN(14) and (g) CN(01).

combustion of precursor during the calcination reaction which causes the short-term gas generation. This is the typical combustion synthesis catalyst reaction conducive to catalytic reaction [19].

XRD was used to analyze the crystal structure and phase composition of the prepared photocatalysts. Fig. 2 (a) shows the XRD patterns of the prepared CN (10), CN (41), CN (32), CN (11), CN (23), CN (14) and CN (01). It can be seen that two typical diffraction peaks of $g\text{-C}_3\text{N}_4$ photocatalysts with different mass ratio of urea to melamine mixture highlighting that the crystal structure of $g\text{-C}_3\text{N}_4$ is well maintained. All the characteristic peaks of the samples can be well indexed to the hexagonal phase of $g\text{-C}_3\text{N}_4$ (JCPDS 087-1526; lattice parameters: $a=b=4.74\text{\AA}$, $c=6.72\text{\AA}$) [20]. The dif-

fraction peak at 13.1° indexed to (100) plane corresponds to the in-plane structural packing motif of tri-s-triazine units. The intensive diffraction peak at 27.4° is an interlayer stacking peaking of aromatic systems as indexed as the (002) plane [21]. Fig. 2 (b) shows the enlarged view of (002) peak. It can be seen that the diffraction peak of the (002) plane of sample CN (32) shows a significant shift leftward to a lower angle of 27.3° with an inter-planar distance of $d=0.326\text{ nm}$ indicating the packing aggregates getting loose.

The chemical structure of the samples were further evaluated by the FTIR analysis. Fig. 3 shows the typical FTIR patterns of $g\text{-C}_3\text{N}_4$. All the diffraction peaks were similar for CN (10), CN (41), CN (32), CN (11), CN (23), CN (14) and CN (01). The broad

peak at $3000\text{--}3600\text{ cm}^{-1}$ is derived from the stretching vibration of NH_2 at the end of the NH group which is at the aromatic ring defect site. The peak at $1240\text{--}1635\text{ cm}^{-1}$ is the typical vibration of aromatic ring. The peak around 1635 cm^{-1} is mainly attributed to the stretching vibration of $\text{C}=\text{N}$ bond, while the three around 1576 cm^{-1} , 1458 cm^{-1} and 1420 cm^{-1} are derived from typical stretching vibration mode of $\text{C}=\text{N}$ and $\text{C}-\text{N}$ heterocycles [22]. The peaks around 1319 cm^{-1} and 1243 cm^{-1} correspond to the stretching vibration of connected units of $\text{C}-\text{NH}-\text{C}$. And these sharper peaks are supported by the ordered packing of hydrogen-bonding interactions. In addition, the peak around 810 cm^{-1} is the characteristic typical bending vibration of the tri-s-triazine ring [23]. FTIR results show that the main structure of $\text{g}-\text{C}_3\text{N}_4$ prepared with the mixture of urea and melamine did not change.

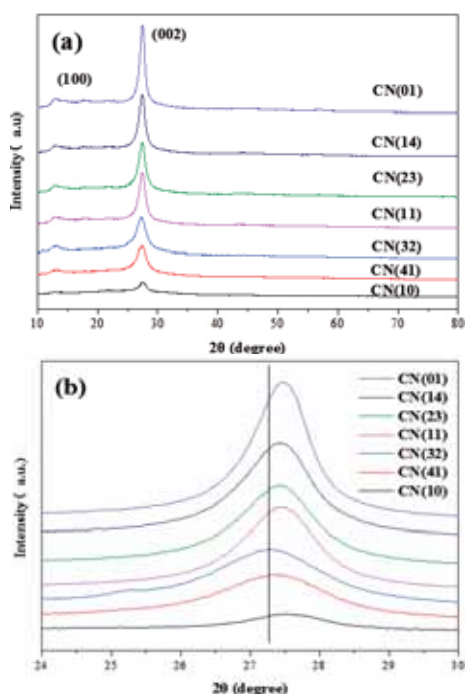


FIGURE 2

XRD patterns of $\text{g}-\text{C}_3\text{N}_4$ (a) and enlarged view of (002) peak (b).

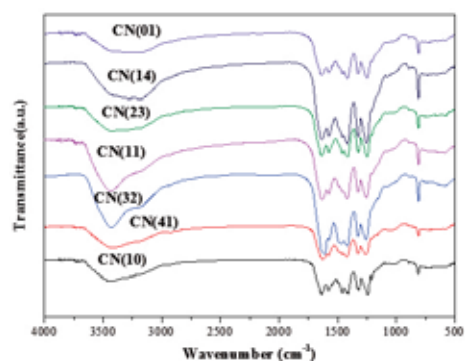


FIGURE 3

FT-IR spectra of $\text{g}-\text{C}_3\text{N}_4$.

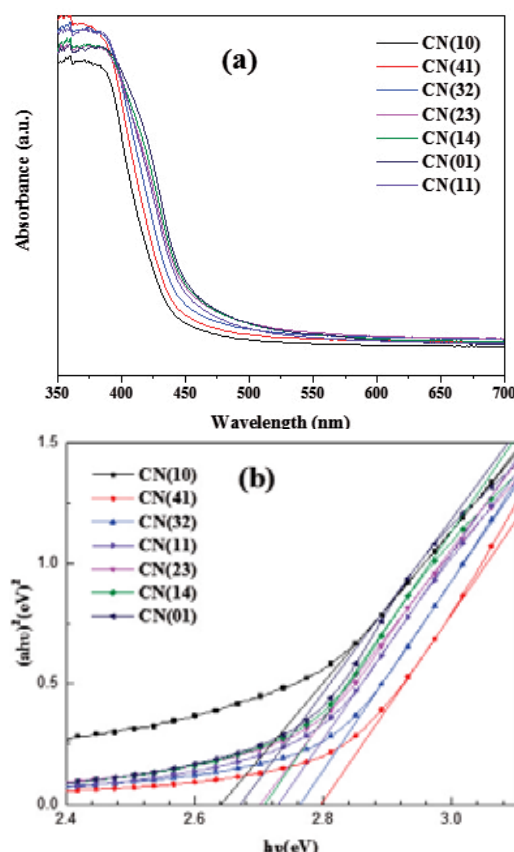


FIGURE 4

UV-vis DR spectra (a) and plots of $(ah\nu)^2$ versus photon energy (b) of $\text{g}-\text{C}_3\text{N}_4$.

The as-prepared $\text{g}-\text{C}_3\text{N}_4$ samples were optically absorbed by UV-Vis diffuse reflectance spectroscopy to measure the optical properties of photocatalysts in Fig. 4. From Fig. 4 (a), it can be seen that photo adsorption edge of $\text{g}-\text{C}_3\text{N}_4$ in visible light region is estimated at about 450 nm . All the samples feature an intrinsic semiconductor absorption in the blue region of the visible spectra. With respect to the other samples, the photo absorption edge of CN(10) shows a remarkable blue shift and the derived band gap of the light absorbed is 2.66 eV as shown in Fig. 4(b). It deserved to note that the diffuse reflectance absorption spectra of CN(01) and the $\text{g}-\text{C}_3\text{N}_4$ prepared with mixture are stronger than CN(10). In addition, the absorbance edge of samples have took place distinct red-shift up to of 448 nm with the increasing of the specific gravity of melamine in the precursor. The enhanced light absorption ability will enhance the photocatalytic activity [24]. The band-gap energy of the semiconductors can be calculated from the relationship of $(ah\nu)^2$ and $h\nu$ which is shown in the followed equation [25]:

$$ah\nu = A (h\nu - E_g)^{n/2} \quad (1)$$

Where a , $h\nu$, ν , A and E_g represent the absorbance, Planck's constant, emission frequency, constant and photonic energy band gap, respectively. The n is constant whose values depend on the type of semiconductor (the direct conductor is $n = 1$ and

the indirect conductor is $n = 4$). The n value is 4 because the $g\text{-C}_3\text{N}_4$ is indirect-allowed transitions. The band gap of CN (10), CN (41), CN (32), CN (11), CN (23), CN (14) and CN (01) were calculated to be 2.66 eV, 2.84 eV, 2.78 eV, 2.72 eV, 2.71 eV, 2.69 eV and 2.73 eV, respectively. The increasing band gap of CN (41) may be caused by the high crystallinity and the increase of lamellar thickness and the nanoplates of CN (41) tends to be planarized causing the blocked transition of $n \rightarrow \pi$ broadening band [26].

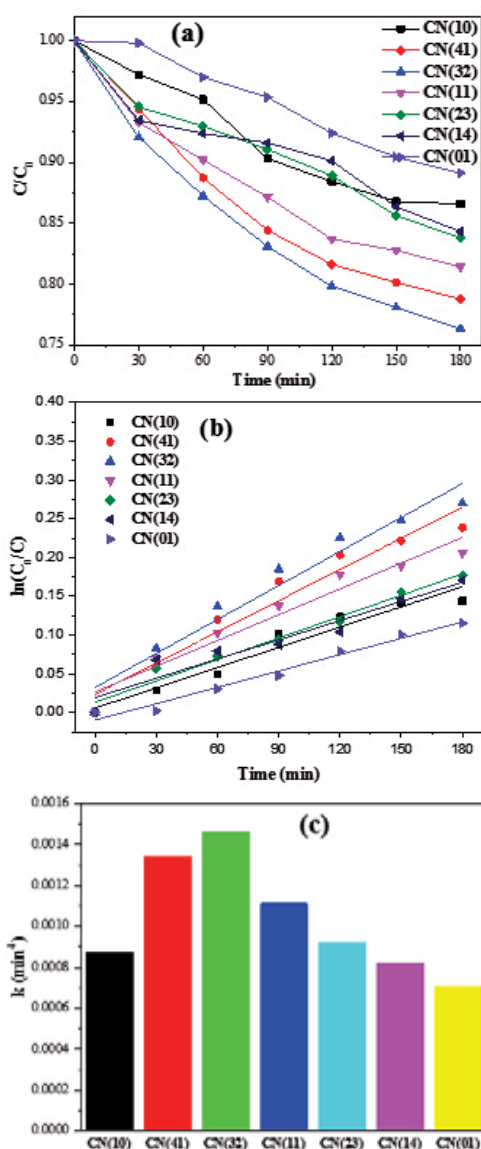


FIGURE 5

Photocatalytic activities (a) and (b) of samples for MC-LR degradation under visible light (c) the comparison of apparent rate constant k .

Photocatalytic degradation of MC-LR. Fig. 5 shows the degradation rate and degradation kinetics of MC-LR under visible light using different photocatalysts at various irradiation times. As shown in Fig. 5 (a), $g\text{-C}_3\text{N}_4$ exhibited photocatalytic activity in degrading MC-LR under visible light. After 180 min of visible irradiation, the degradation rate of MC-LR

using CN (10), CN (41), CN (32), CN (11), CN (23), CN (14), CN (01) were 13.41%, 21.24%, 23.68%, 18.60%, 16.19%, 15.68%, 10.89%, respectively. The CN (32) exhibits the highest photo-degradation efficiency, which is 1.8 and 2.2-folds higher than that of CN(10) and CN(01), respectively.

In order to further validate the photocatalytic principle, the Langmuir-Hinshelwood equation is used to describe the reaction and simplified to a pseudo first order kinetic equation which is shown as followed [27]:

$$\ln(C_0/C) = kt \quad (2)$$

Where C_0 and C represent MC-LR concentrations in solution at time 0 and t respectively, k is the apparent first-order rate constant, and t is the irradiation time. Fig. 5 (b) shows the degradation of MC-LR with different photocatalysts under the visible light accords with the pseudo first order kinetic equation. The results suggested that the photocatalytic degradation rate and apparent first-order rate constant for $g\text{-C}_3\text{N}_4$ catalyst increased up to maximum as a function of the melamine to urea and tended to decrease upon further higher value of this melamine to urea ratio. The highest photocatalytic degradation rate of was obtained at when the mass ratio of urea to melamine was 3:2 and the calculated k value was 0.00146. The suitable melamine content in precursor cause its well pore structure in the nano-lamellar, which favored the adsorption, transfer and separation of the charge carriers for MC-LR degradation. However, at contents higher than 60 wt.%, photocatalytic activity of the $g\text{-C}_3\text{N}_4$ photocatalysts was declined as shown in Fig.5 (c).

CONCLUSIONS

In this study, the effect of different precursors on the structure of $g\text{-C}_3\text{N}_4$ after calcination was verified. The results of characterization show that the surface and structure of $g\text{-C}_3\text{N}_4$ are affected by changing the mass ratio of urea and melamine in the precursors. It is apparent that $g\text{-C}_3\text{N}_4$ was a feasible and effective photocatalyst in degrading the MC-LR under visible light. Compared with other photocatalysts, CN(32) with porous fluffy structure performs significant enhancement in the photocatalytic activity for MC-LR degradation under visible light irradiation. The enhanced photocatalytic activity is closely associated with the surface of $g\text{-C}_3\text{N}_4$ which can promote the transferring of electron-hole and annihilate the electrons and holes generated from $g\text{-C}_3\text{N}_4$. The enhanced $g\text{-C}_3\text{N}_4$ here developed could provide new perspective for sustainable utilization of solar irradiation and constructing other functionalized $g\text{-C}_3\text{N}_4$ heterostructure to promote high performance photocatalysts for the degradation of microcystins.

ACKNOWLEDGEMENTS

The authors are grateful for national natural Science Foundation of China (NO.51308078), Natural Science Foundation of Jiangsu Province, China (NO. BK20130252), International Scientific and Technological Cooperation in Changzhou (CZ20140017).

REFERENCES

- [1] Gehringer, M. M., & Wannicke, N. (2014). Climate change and regulation of hepatotoxin production in Cyanobacteria. *FEMS microbiology ecology*, 88(1), 1-25.
- [2] Hitzfeld, B. C., Lampert, C. S., Späth, N., Mountfort, D., Kaspar, H., & Dietrich, D. R. (2000). Toxin production in cyanobacterial mats from ponds on the McMurdo Ice Shelf, Antarctica. *Toxicon*, 38(12), 1731-1748.
- [3] Dahlmann, J., Rühl, A., Hummert, C., Liebezeit, G., Carlsson, P., & Graneli, E. (2001). Different methods for toxin analysis in the cyanobacterium *Nodularia spumigena* (Cyanophyceae). *Toxicon*, 39(8), 1183-1190.
- [4] Tsuji, K., Naito, S., Kondo, F., Ishikawa, N., Watanabe, M. F., Suzuki, M., & Harada, K. I. (1994). Stability of microcystins from cyanobacteria: effect of light on decomposition and isomerization. *Environmental Science & Technology*, 28(1), 173-177.
- [5] Jia, J., Luo, W., Lu, Y., & Giesy, J. P. (2014). Bioaccumulation of microcystins (MCs) in four fish species from Lake Taihu, China: Assessment of risks to humans. *Science of the Total Environment*, 487, 224-232.
- [6] Martins, J. C., & Vasconcelos, V. M. (2009). Microcystin dynamics in aquatic organisms. *Journal of Toxicology and Environmental Health, Part B*, 12(1), 65-82.
- [7] Liu, I., Lawton, L. A., & Robertson, P. K. (2003). Mechanistic studies of the photocatalytic oxidation of microcystin-LR: an investigation of by-products of the decomposition process. *Environmental science & technology*, 37(14), 3214-3219.
- [8] Antoniou, M. G., Shoemaker, J. A., Cruz, A. A. D. L., & Dionysiou, D. D. (2008). Unveiling new degradation intermediates/pathways from the photocatalytic degradation of microcystin-LR. *Environmental science & technology*, 42(23), 8877-8883.
- [9] Zou, Z., Ye, J., Sayama, K., & Arakawa, H. (2001). Direct splitting of water under visible light irradiation with an oxide semiconductor photocatalyst. *Nature*, 414(6864), 625-627.
- [10] Huang, L., Xu, H., Li, Y., Li, H., Cheng, X., Xia, J., Cai, G. (2013). Visible-light-induced WO₃/g-C₃N₄ composites with enhanced photocatalytic activity. *Dalton Transactions*, 42(24), 8606-8616.
- [11] Dong, G., & Zhang, L. (2012). Porous structure dependent photoreactivity of graphitic carbon nitride under visible light. *Journal of Materials Chemistry*, 22(3), 1160-1166.
- [12] Xu, J., Wang, Y., & Zhu, Y. (2013). Nanoporous graphitic carbon nitride with enhanced photocatalytic performance. *Langmuir*, 29(33), 10566-10572.
- [13] Rippka, R., Deruelles, J., Waterbury, J. B., Herdman, M., & Stanier, R. Y. (1979). Generic assignments, strain histories and properties of pure cultures of cyanobacteria. *Microbiology*, 111(1), 1-61.
- [14] Pinho, L. X., Azevedo, J., Brito, Â., Santos, A., Tamagnini, P., Vilar, V. J., ... & Boaventura, R. A. (2015). Effect of TiO₂ photocatalysis on the destruction of *Microcystis aeruginosa* cells and degradation of cyanotoxins microcystin-LR and cylindrospermopsin. *Chemical engineering journal*, 268, 144-152.
- [15] Pflugmacher, S. (2015). Toxin resistance in aquatic fungi poses environmentally friendly remediation possibilities: A study on the growth responses and biosorption potential of *Mucor hiemalis* EH5 against cyanobacterial toxins. *Int J Water and Wastewater Treatment*, 1(1).
- [16] Xu, H., Wang, H., Xu, Q., Lv, L., Yin, C., Liu, X., Yan, H. (2015). Pathway for biodegrading microcystin-YR by *Sphingopyxis* sp. USTB-05. *PloS one*, 10(4), e0124425.
- [17] Moon, J., Yun, C. Y., Chung, K. W., Kang, M. S., & Yi, J. (2003). Photocatalytic activation of TiO₂ under visible light using Acid Red 44. *Catalysis Today*, 87(1), 77-86.
- [18] Li, F. T., Zhao, Y., Liu, Y., Hao, Y. J., Liu, R. H., & Zhao, D. S. (2011). Solution combustion synthesis and visible light-induced photocatalytic activity of mixed amorphous and crystalline MgAl₂O₄ nanopowders. *Chemical engineering journal*, 173(3), 750-759.
- [19] Furfori, S., Bensaïd, S., Russo, N., & Fino, D. (2009). Towards practical application of lanthanum ferrite catalysts for NO reduction with H₂. *Chemical Engineering Journal*, 154(1), 348-354.
- [20] Xiao, X., Wei, J., Yang, Y., Xiong, R., Pan, C., & Shi, J. (2016). Photoreactivity and Mechanism of g-C₃N₄ and Ag Co-Modified Bi₂WO₆ Microsphere under Visible Light Irradiation. *ACS Sustainable Chemistry & Engineering*, 4(6), 3017-3023.
- [21] Bojdys, M. J., Müller, J. O., Antonietti, M., & Thomas, A. (2008). Ionothermal synthesis of crystalline, condensed, graphitic carbon nitride. *Chemistry—A European Journal*, 14(27), 8177-8182.

- [22] Zhang, J., Chen, X., Takanahe, K., Maeda, K., Domen, K., Epping, J. D., & Wang, X. (2010). Synthesis of a Carbon Nitride Structure for Visible - Light Catalysis by Copolymerization. *Angewandte Chemie International Edition*, 49(2), 441-444.
- [23] Tan, L., Xu, J., Zhang, X., Hang, Z., Jia, Y., & Wang, S. (2015). Synthesis of g-C₃N₄/CeO₂ nanocomposites with improved catalytic activity on the thermal decomposition of ammonium perchlorate. *Applied Surface Science*, 356, 447-453.
- [24] Fu, J., Tian, Y., Chang, B., Xi, F., & Dong, X. (2012). BiOBr-carbon nitride heterojunctions: synthesis, enhanced activity and photocatalytic mechanism. *Journal of Materials Chemistry*, 22(39), 21159-21166.
- [25] Tauc, J. (1970). Absorption edge and internal electric fields in amorphous semiconductors. *Materials Research Bulletin*, 5(8), 721-729.
- [26] Fan, X., Xing, Z., Shu, Z., Zhang, L., Wang, L., & Shi, J. (2015). Improved photocatalytic activity of g-C₃N₄ derived from cyanamide-urea solution. *RSC Advances*, 5(11), 8323-8328.
- [27] Li, F. T., Zhao, Y., Hao, Y. J., Wang, X. J., Liu, R. H., Zhao, D. S., & Chen, D. M. (2012). N-doped P25 TiO₂-amorphous Al₂O₃ composites: One-step solution combustion preparation and enhanced visible-light photocatalytic activity. *Journal of Hazardous materials*, 239, 118-127.

Received: 27.12.2016
Accepted: 27.05.2017

CORRESPONDING AUTHOR

Liping Wang

School of Environmental and Safety Engineering
Changzhou University Changzhou, 213164 P.R.
CHINA

e-mail: wlp@cczu.edu.cn

YIELD REDUCTION ANALYSIS OF BREAD WHEAT UNDER HEAT STRESS AT TWO DIFFERENT ENVIRONMENTS IN PAKISTAN

Muhammad Jamil^{1,*}, Aamir Ali¹, Abdul Ghafoor², Alvina Gul³, Khalid Farooq Akbar⁴, Humayun Bashir¹, Adeel Ijaz¹, Rameez Hussain¹, Ahmed Muneeb¹, Naima Huma Naveed¹, Nasim Ahmad Yasin⁶, Abdul Aziz Napar⁵, Abdul Mujeeb Kazi⁷

¹Department of Botany, University of Sargodha

²Plant Genetic Resources Institute (PGRI), National Agriculture Research Center (NARC), Islamabad, Pakistan

³Atta-ur-Rehman School of Applied Biosciences (ASAB), National University of Science and Technology (NUST), Islamabad, Pakistan

⁴Department of Botany, University of Lahore (UOL), Sargodha campus, Sargodha, Pakistan

⁵Department of Plant sciences, Quaid-i-Azam University, Islamabad, Pakistan

⁶Horticulture wing, University of the Punjab, Pakistan

⁷Soil and crop Sciences, Texas A & M University, USA.

ABSTRACT

Terminal heat stress has become an alarming threat for bread wheat in warm humid zones. Heat susceptibility index (HSI) of 51 genotypes from diverse parentage was calculated for estimation of yield reduction for two consecutive years. In the field experiment, terminal heat stress was provided through late sowing during the years 2014 and 2015. Mean heat susceptibility index (HSI) was 1.02 and 0.97 for both the years. Overall 50% yield reduction was observed due to terminal heat stress. Treatment results were significant with 9.928 mean square. On the basis of HSI of two years, the best tolerant nine genotypes were sorted out for the breeding purposes. This might be one of the effective strategies toward production of heat tolerant wheat germplasm. Heat sensitivity index parameter allowed the selection of best varieties and such germplasm can also be used for gene pyramiding for climate change resilience.

KEYWORDS:

Heat Susceptibility Index (HSI), Wheat, Yield Reduction

INTRODUCTION

Previous two decades were of prime importance in obtaining the attention of researchers toward the global warming. A serious problem of enhanced temperature is being faced during grain ripening stages of wheat. Constantly high temperature exposure during floret formation period of the wheat crop can cause severe influence on diverse morphological, physiological and biochemical malfunctions in plant thus ultimately causing immense yield reduction. Wheat that is most widely grown cereal crop is vital as staple food, so underlying its importance under changing environment due to increasing temperature. About

40 % irrigated land, where wheat is grown sternly influenced by heat stress [1]. Bread wheat (*Triticum aestivum* L.) faces severe heat stress that is a main yield reduction threat in Pakistan. Globally in non-temperate zones, terminal heat stress is limiting the bread wheat production [2, 3]. Grain weight and grain number are the major yield component have been influenced directly from heat stress [4]. This high temperature may damage the anthers thus reducing the embryo development. So grain filling rate is affected causing the reduction in grain yield [5]. Present study was designed to evaluate the effects of terminal heat stress on wheat yield.

MATERIALS AND METHODS

Present experiment was designed to assess the yield reduction under heat stress. A total of 51 entries from Cereal Systems Initiative for South Asia (CSISA) were provided by wheat program of Crop Science Institute (CSI) at National Agriculture Research Center (NARC), Islamabad. Study was performed in two different environments in Pakistan; first at the field of NARC in 2013-14 and the second at the field of University of Sargodha (UOS) in 2014-15.

A plot of four meter four rows with 10cm row distance was specified for each entry. Sowing was at the optimal condition (second week of November 2013) and this was declared Normal sown. Second complete set of 51 entries with same plot specifications was sown on first week of January 2014 at NARC. Same practice with changed location was repeated in 2014-15 at University of Sargodha (UOS). Normal irrigation and other agronomic practices were performed for both timely sown and late sown trials.

Yield (Kg/plot) was estimated for each entry in normal sowing and late sowing conditions for two consecutive years making four observations for each

there was a total of $51 \times 4 = 204$ observations in the experiment under completely randomized block design (RCBD). Heat susceptibility index (H S I) for yield was calculated as done by Paliwal [6].

$$HSI (Yield) = \frac{[1 - Yield_{(Stress)} / Yield_{(Control)}]}{[1 - X_{(stress)} / X_{(control)}]}$$

Where $X_{(stress)}$ and $X_{(Control)}$ is the average yield of all 51 genotypes under stress and normal conditions respectively.

Descriptive statistics was performed on the yield measurements in normal and late sown during years 2014 and 2015. Data was subjected to analysis of variance and the mean squares have been dissected with respect to two sowing dates (Normal and Late), two years (2014 and 2015) and 51 genotypes as a source of variation.

RESULTS AND DISCUSSION

Mean yield per plot was observed 0.92 Kg/plot and 0.93 Kg/plot under normal conditions during the years 2014 and 2015. About 41% and 54 % yield reduction was estimated in both years due to heat stress. Heat susceptibility index (H S I) for yield was 1.02 and 0.97 during 2014 and 2015 respectively (Table 1). Summary of descriptive statistics of phenotypic evaluation revealed the diverse pattern of cultivar response to thermal stress. HSIs values ranges from moderate to high divided the germplasm

panel in to distinct resistant and susceptible genotypes.

Analysis of Variance (Table 2) is indicating that there was no significant difference among genotype, year and their interactions as well. Mean square of sowing dates (Treatment MS: 9.928) was significant. As the mean squares of HSI for both the years was non- significant across the years so mean HSI was calculated to draw the histogram (Fig 1) with the help of which 51 genotypes were grouped into six classes. The level of variation examined in yield reduction depicted in the histogram (Fig 1) under heat stress influence. Out of 51 genotypes, two were found highly tolerant, 10 tolerant, 17 moderately tolerant, 6 moderately susceptible, 13 susceptible and 4 were found highly susceptible. In the histogram H S I for yield was spread from 0.26 to 1.69. Maximum frequency (17 genotypes i.e. 33%) was observed in the histogram.

Nine Genotypes lowest in heat susceptibility index (< 0.71) were declared as heat tolerant genotypes (Table 3). Genotypes with heat susceptibility index above 0.98 were mentioned to be heat susceptible. Development of thermal resilient wheat cultivar and further characterization of cereal crop will be helpful to better understand the basis of tolerance to temperature fluctuations during plant growth stages [7]. Genetic resources establishment is surely required to address the abiotic stress resilience. Because heat stress is complex quantitative trait driven by multiple pathways of gene regulation hence it requires a major focus on phenotypic evaluation of the stress in more than one environments as done in the present study.

TABLE 1
Yield (kg/plot) expression of 51 genotypes Normal and late sown (heat stress) along with parentage of top performing nine genotypes and heat susceptibility index (H S I) of yield in the years 2014 and 2015.

Description	2014				2015			
	NORMAL	LATE	Red %	HSI	NORMAL	LATE	Red %	HSI
MEAN	0.92	0.55	40.66	1.02	0.93	0.41	54.20	0.97
MAX.	1.30	1.09	82.50	2.06	1.51	0.85	83.93	1.50
MIN.	0.09	0.07	1.18	0.03	0.57	0.15	1.16	0.02
Range	1.21	1.03	81.32	2.03	0.94	0.70	82.76	1.48
SD	0.23	0.24	19.99	0.50	0.21	0.15	17.77	0.32
CV %	24.78	43.91	49.16	49.16	23.08	35.83	32.78	32.78
SE	0.03	0.03	2.80	0.07	0.03	0.02	2.49	0.04
GEN ID	Mean HSI	Parentage						
6702	0.26	1447/PASTOR//KRICHAUFF/5/2*SERI*3//RL6010/4*YR/3/PASTOR/4/BAV92						
6709	0.44	T.DICOCCON PI254157/AE.SQUARROSA (879)/4/MILAN/KAUZ//PRINIA/3/BAV92/5/2*SKAUZ/BAV92						
6717	0.60	KACHU/KINDE						
6720	0.61	ND643/2*TRCH//MUTUS/3/SUP152						
6740	0.64	DANPHE #1/3/HUW234+LR34/PRINIA//PFAU/WEAVER						
6714	0.65	BABAX/LR42//BABAX*2/3/KUKUNA/4/2*MUNAL #1						
6742	0.65	ATTILA/3*BCN//BAV92/3/PASTOR/4/TACUPETO F2001*2/BRAMBLING/5/PAURAQ						
6741	0.70	PBW65/2*PASTOR/3/KIRITATI//ATTILA*2/PASTOR/4/DANPHE #1						
6739	0.71	WEAVER/TSC//WEAVER/3/WEAVER/4/2*SERI.1B*2/3/KAUZ*2/BOW//KAUZ/5/WHEAR/VIVITSI//WHEAR						

Red %: Percentage of reduction in yield due to heat stress.

HSI: Heat susceptibility index for yield.

TABLE 2
Analysis of Variance for yield and H S I across two years under heat stress

SOV	df	MS	F	P
Genotypes	50	0.072	0.036	1.000
Year	1	0.201	0.100	0.753
Treatments	1	9.928	4.968	0.030
Genotype*Year	50	0.063	0.032	1.000
Genotype*Treatments	50	0.026	0.013	1.000
Year*Treatments	1	0.312	0.156	0.694
Error	51	1.998		

HSI(YIELD)				
Genotypes	50	0.218	0.002	1.000
Year	1	0.061	0.001	0.984
Genotype*Year	50	0.140	0.001	1.000

p-value: <0.05 = significant

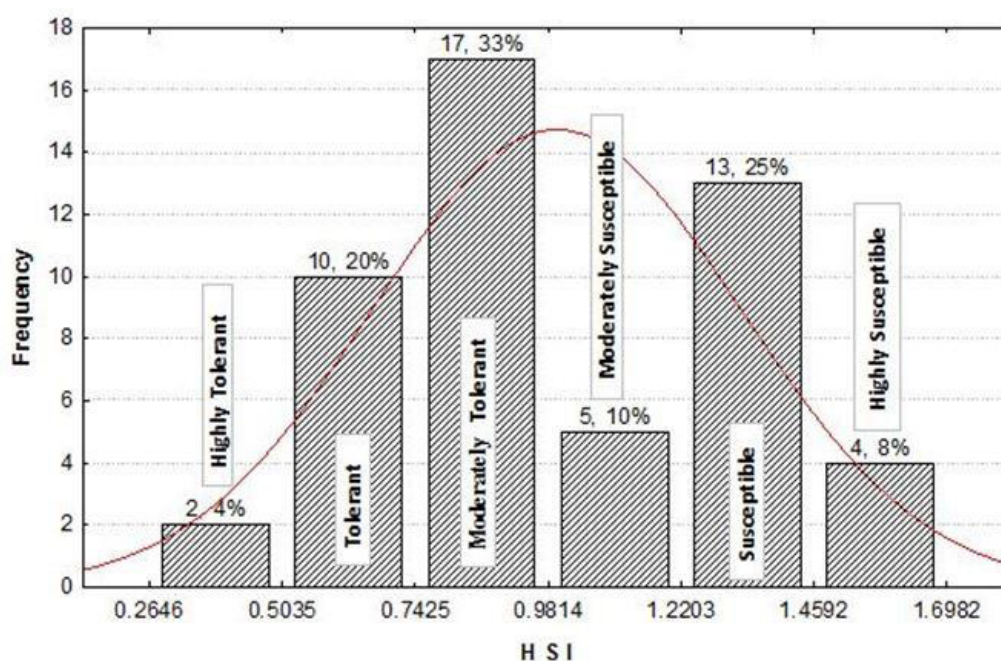


FIGURE 1
Histogram showing frequency distribution of 51 genotypes for heat susceptibility index (HSI) of Yield

TABLE 3
Top Nine, best heat tolerant lines and their attributes arranged

Gen ID	2014				2015				MEAN H S I
	NORMAL	LATE	RED %	H S I	NORMAL	LATE	RED %	H S I	
6702	0.97	0.85	12.89	0.32	0.69	0.61	11.59	0.21	0.26
6709	1.11	1.09	1.18	0.03	0.64	0.33	47.81	0.85	0.44
6717	1.11	0.59	47.06	1.18	0.86	0.85	1.16	0.02	0.60
6720	1.17	0.95	18.89	0.47	1.35	0.78	42.22	0.75	0.61
6740	0.91	0.60	34.29	0.86	0.59	0.45	24.07	0.43	0.64
6714	0.91	0.72	21.43	0.54	0.92	0.53	42.61	0.76	0.65
6742	0.85	0.68	20.00	0.50	1.15	0.63	45.03	0.80	0.65
6741	1.11	0.86	22.35	0.56	0.67	0.36	46.57	0.83	0.70
6739	1.04	0.90	13.75	0.34	0.75	0.30	60.27	1.08	0.71

RED%: Percentage of reduction in yield due to heat stress.

HSI: Heat susceptibility index for yield

Best performing nine genotypes across two years were selected on the basis of lowest HSI for yield (Table 1). Genotype (6702) with PASTOR double inheritance and SERI in its parentage expressed highest tolerance for heat stress. Synthetic bread wheat [8] line (6709) having *Aegilops squarrosa* a wild wheat relative in its ancestor making it tolerant for abiotic stresses as well as resistant for biotic stress [8]. Genotype (6717), (6720) and (6740) were tolerant might be due to KIND, MUTUS and WEAVER in their inheritance. Genotype (6714), (6742) and (6739) having BABAX, ATTILA, PASTOR and WEAVER might be genetic resources for heat tolerance. This identification of heat tolerant genotypes would be important for the breeding programs to cope with the severe effects of thermal stress. Use of genotypes with inherent resistance potential can also be helpful in pyramiding the stress resilience.

CONCLUSION

Yield under heat stress is significantly affected and causes threat to the global food security. Germplasm with the synthetic wheat proved heat tolerant due to the introgression of D-genome progenitor. To use such cultivars in breeding program will be helpful to minimize the losses due to heat stress. In such a way the climate-resilient varieties can be produced so that the yield minimizing risks can be overcome.

REFERENCES

- [1] Reynolds, M.P., Nagarajan, S., Razzaque, M.A. and Ageeb, O.A.A. (2001) Heat tolerance. In: Reynolds MP, Ortiz-Monasterio I, McNab A (eds) Application of physiology in wheat breeding. CIMMYT, Mexico, DF.
- [2] Mason, R.E., Mondal, S., Beecher, F.W., Pacheco, A., Jampala, B., Ibrahim, A.M. and Hays D.B. (2010) QTL associated with heat susceptibility index in wheat (*Triticum aestivum* L.) under short-term reproductive stage heat stress. *Euphytica*. 174, 423-436.
- [3] Pinto, R.S., Reynolds, M.P., Mathews, K.L., McIntyre, C.L., Olivares-Villegas, J.J. and

Chapman S.C. (2010) Heat and drought adaptive QTL in a wheat population designed to minimize confounding agronomic effects. *Theoretical and Applied Genetics*. 121, 1001-1021.

- [4] Tiwari, C., Wallwork, H. Kumar, U., Dhari, R. Arun, B., Mishra, V.K. and Joshi, A.K. (2013) Molecular mapping of high temperature tolerance in bread wheat adapted to the Eastern Gangetic Plain region of India. *Field Crops Research*. 154, 201-210.
- [5] Mondal, S., Singh, R.P., Crossa, J., Huerta-Espino, J., Sharma, I., Chatrath, R. and Kalappanavar, I.K. (2013) Earliness in wheat: a key to adaptation under terminal and continual high temperature stress in South Asia. *Field Crops Research*. 151, 19-26.
- [6] Chopra, R., Burow, G., Burke, J.J., Gladman, N. and Xin, Z. (2017) Genome-wide association analysis of seedling traits in diverse Sorghum germplasm under thermal stress. *BMC BMC Plant Biology*. 17(1), 12.
- [7] Mujeeb-Kazi, A., Gul, A., Farooq, M., Rizwan, S. and Ahmad, I. (2008) Rebirth of synthetic hexaploids with global implications for wheat improvement. *Crop and Pasture Science*. 59, 391-398.
- [8] Paliwal, R., Roder, M.S., Kumar, U., Srivastava, J.P. and Joshi, A.K. (2012) QTL mapping of terminal heat tolerance in hexaploid wheat (*T. aestivum* L.) *Theoretical and Applied Genetics* 125, 561-575.

Received: 04.01.2017

Accepted: 01.05.2017

CORRESPONDING AUTHOR

Muhammad Jamil

Department of Botany

University of Sargodha

Sargodha, Punjab – PAKISTAN

E-mail: jshahid80@yahoo.com

THE EFFECT OF MAGNETIC FIELD APPLICATIONS TO CHEMICAL CONTENT OF STRATIFIED SEEDS OF ORIENTAL BEECH (*Fagus orientalis* Lipsky.)

Nezahat Turfan¹, Esra Nurten Yer², Sezgin Ayan^{2,*}

¹Faculty of Science, Biology Department, Kastamonu University, 37150, Kastamonu, Turkey

²Faculty of Forestry, Silviculture Department, Kastamonu University, 37150, Kastamonu, Turkey

ABSTRACT

The effects of magnetic field (MF) applied with cold-wet pre-treatment on the chemical components of the oriental beech seeds with physiological deep dormancy are researched in this study. The seeds were subjected to various MF application periods (20, 60 and 120 min) and different MF intensities (200 and 400 mT). Total soluble protein, lipid peroxidation level (malondialdehyde-MDA), total soluble sugars and starch quantities as well as antioxidants such as CAT, SOD, APX and GuPX and α -amylase activity of the seeds were examined. MF application affected protein, lipid, α -amylase and sucrose values positive, starch, glucose and fructose values of the seed negatively. Furthermore, MF applications were found to have an increasing effect on CAT and SOD enzyme activities while having reducing effect on APX and GuPX antioxidant enzymes. It was reached to the conclusion that magnetic field application processes with 400 mT intensity generally increase the seed physiology parameters.

KEYWORDS:

Oriental beech, antioxidant, abiotic stress, oxidative balance

INTRODUCTION

Oriental Beech (*Fagus orientalis* Lipsky.) is the only broad-leaved tree species which is subject to the National Tree Breeding program basing on the spreading area in Turkey and silvicultural importance thereof. In Turkey, oriental beech forests have been transformed into offshoot-rooted forest form both due to anthropogenic influences and the application of mismanagement techniques. However, enhancement of quality and quantity of oriental beech stands is basically possible through generative production. It will be possible to establish forests with large gene pools resistant to biotic and abiotic effects and with high adaptation to climate change effects in this way. 33%, 48% and 19% of the forests in Turkey consist of broad-leaved, nee-

dle-leaved (coniferous) and both broad-leaved and needle-leaved trees respectively. In Turkey, it is not possible to regeneration most of the oriental beech forests, which are allocated for the regeneration block in the Forestry Management Plans, due to silvicultural interventions implemented in a wrong way. Optimum beech forests are largely devastated and these fields have left their places to young beeches coming from the root offshoots. Furthermore, beech is beaten by the rhododendron in competition in the areas where rhododendrons are common. Beech cultures, a species resistant to shadow due to their biology, are affected by early and late frosts in the first years in addition to extreme temperatures.

Artificial rejuvenation works, as an alternative to natural rejuvenation activities, for the oriental beech is of great importance for the establishment and sustainability of high quality forests. To this end, it is important to investigate the chemical composition of the beech seed. Different techniques are utilized physically and chemically with an eye to produce high quality production material, develop inadequate features of varieties and increase the rate of germination. Numerous researchers apply magnetic field applications in seed germination tests and for determination of plant growth and development occurrences in recent years. Accordingly, Ozel et al. [1]; Mousavizadeh et al. [2]; Vashisth and Nagarajan [3]; Danilov et al. [4], Samy, [5]; Podlesny et al. [6]; Bilalis et al. [7]; Duarte Diaz et al [8]; Agustrina et al. [9]; Florez et al. [10]; Turfan et al. [11], Mousavizadeh et al. [2]; Rady et al. [12]; Qi et al. [13]; Jiang et al. [14]; Mousavizadeh et al. [2]; Atak et al. [15]; Jajte [16]; Agustrina et al. [17] have expressed that MF applications affect, germination percentage and rate of plants; earliness; receipt and transport of mineral substances from the soil; seedling growth rate; α -amylase activity; amount of chlorophyll and total soluble protein content and enzyme activities such as ascorbate peroxidase, catalase, guaiacol peroxidase and superoxide dismutase; increase the level of lipid peroxidation (MDA); and increase the dimensions of parenchymatic cells, transmission bundles and stoma cells in young plants respectively. The responses of the plants to the MF may vary

according to the seed characteristics such as genotype, seed quality, germination ability, vitality or seed power as well as seed preparation methods and the degree of being effected of the chemical content of the seed from the applications in addition to the strength, duration, and frequency of MF [18]. However, it is also expressed that MF applications are not effective on plant growth and development [19] or affect foregoing negatively [20]. As such, it needs to be continued to researches on the nature of MF stimulation.

Seed quality has vital significance for the success of plantation forestry. The most important quality criteria for the plants are high vitality and seed strength in addition to physical and genetic purity [21, 22]. Seed viability and seed power depend on the chemical content of the seed in addition to genetic factors. The chemical content of the seed mainly comprises carbohydrates, fats and proteins. Further, there are small amounts of compounds such as hormones, alkaloids, lectins, proteinase inhibitors, phytin and raffinose in the seeds [23]. The ratio of these compounds in the seed varies according to the plant species, age and nutritional status of the plant, treatments applied during and after the harvest period, mechanical damage during the harvest, postharvest storage conditions and treatments used for germinating [24, 21]. The inadequacy resulting from any of the mentioned factors may cause quality degradation by affecting the chemical composition of the seed and may also cause a reduction of approximately 75% in seed germination ability [25]. As such, studies on the effects of MF applications on the chemical content of seed storage materials of forest trees, deterioration of cellular integrity (lipid peroxidation), ascorbate peroxidase, guaiacol peroxidase, catalase and superoxide dismutase enzyme activities as well as α -amylase enzyme activity are of great significance. The effects of different MF applications made to the beech seeds showing different physiological profound dormancy [26, 27, 28, 29] on chemical content of seed (Protein, starch, soluble sugar, etc.), lipid peroxidation level (malondialdehyde), ascorbate peroxidase, guaiacol peroxidase, catalase and superoxide dismutase and α -amylase enzyme activities are examined in this study.

MATERIALS AND METHODS

MA Application in Seeds. In the research, oriental beech seeds of 2015 harvest year originated from Bartin-Devrek-Akcasu were utilized. Cold-wet stratifying was applied to the seeds at +4°C for 60 days. Seeds were soaked in water for 8 hours before being stratified. Agricultural perlite was used as stratifying medium. The seeds were placed in a 15 x 10 x 5 cm perforated plastic container as one layer of wet perlite and as one layer of seed and

kept in a cold air storage at a temperature of 4 ± 1 °C.

The seeds were exposed to different application periods (20, 60 and 120 min) and different MF intensities (200 and 400 mT) for magnetic field (MF) treatment of stratified seeds.

Chemical Analysis Methods. 0.5 g of seeds were taken and homogenized with 50 mM (pH 7.6) phosphate buffer solution (5 mL) containing 0.1 mM Na-EDTA in the sample for the preparation of enzyme extracts. Subsequently, homogenized samples were centrifuged for 15 min at 15000 g and +4° C, the enzyme activities in the resulting supernatant were measured (SOD, APX, GuPX and CAT). Ascorbate peroxidase activity (APX) was measured spectrophotometrically by the method utilized through Nakano and Asada (1981) [30]; 290 nm by measuring the oxidation rate of ascorbate ($E = 2.8 \text{ mm cm}^{-1}$) and catalase (CAT) activity was measured spectrophotometrically by virtue of the method utilized through Bergmeyer [31] while superoxide dismutase (SOD) enzyme activity was measured according to the method applied by Cakmak [32] and guaiacol peroxidase enzyme (GuPX) activity was measured according to Birecka et. [33]. The total amount of soluble protein in the samples was determined according to the method utilized by Bradford [34] while lipid peroxidation (MDA) was found as per the method employed by Lutts et al. hand. [35]. Determination of α -amylase activity was performed according to the method of Morais and Takaki [36]. The absorbance of the seed samples homogenized in 0.2 M (pH 5.5) citrate buffer was read at 620 nm and the amount causing the 0.1 change in absorbance was considered as 1 enzyme unit. The α -amylase activity was calculated according to Bradford [34] method, where BSA is used as standard, as the amount of starch hydrolyzed per mg protein. Determination of the total carbohydrate amount was made according to the method utilized by Pearson et al. [37] using Anthron separator. The samples incubated in 80% ethanol for 24 hours at +4 °C were filtered and the obtained filtrate was used for glucose determination. The remaining pulp was incubated in pure water for 24 hours at +4 °C and filtered again and used for fructose assay. The final pulp was incubated with 52% perchloric acid for 24 hours at +4 °C and filtered. This sample was utilized to determine the sucrose amount. The amount of starch was determined by the equation obtained from glucose standard curve. Glucose obtained from glucose standards was determined from fructose standard curve and sucrose amount was determined from sucrose standard curve (mg/g TA).

Statistical analyzes. The experiments were done in three replicates. Statistical analyzes of the obtained data were performed through employment of the statistical program named SPSS for Windows

20.0 Evaluation Version. Differences between control and treatment groups were analyzed through utilization of one-way ANOVA. After the variance analysis, Tukey multiple test was employed with an eye to determine differences in significance value of $P < 0.05$.

RESULTS

Wet stratification was conducted in cold for 60 days at +4 °C and data as to activities of MF applications in different duration and intensity applied to the beech seeds as to total protein content, lipid peroxidation level (malondialdehyde-MDA), glucose, fructose, sucrose and starch amount and α -amylase, ascorbate peroxidase (APX), guaiacol peroxidase (GuPX), catalase (CAT) and superoxide dismutase (SOD) are given in Tables 1, 2 and 3. According to the results of analyses applied to data MF applications showed a statistically significant effect ($P < 0.05$) in all chemical components measured on seeds.

Soluble Protein Content Changes. The total soluble protein content of the seeds increased compared to the control depending on the increased duration and intensity of MF. Compared to the control, high protein was determined in MF applications with intensity dose of 400 mT in 60 min (16.49%) ($P < 0.05$) (Table 1).

Level Changes in Lipid Peroxidation. The concentration of lipid peroxidation (malondialdehyde-MDA) showed a statistically significant increase compared to the control due to the increased duration and intensity of MF. The highest MDA concentration compared to control was observed at following doses as at intensity of 200 mT in 60 min with 316.59 $\mu\text{mol/g}$ (5.36 times more), at intensity of 400 mT in 120 min with 298.19 $\mu\text{mol/g}$ (5.04 times more), at intensity of 400 mT in 20 min with 218.56 $\mu\text{mol/g}$ (3.7 times more), at intensity of 200 mT in 120 min with 202.56 $\mu\text{mol/g}$ (4.43 times), at intensity of 400 m in 60 with 187 $\mu\text{mol/g}$ to min (3.17 times more) and at intensity of 200 mT in 60 min with 120.58 $\mu\text{mol/g}$ (2-times more) ($P < 0.05$) (Table 1).

Soluble Sugar Content Changes. Effect of MF applications on the amount of soluble sugars in seeds were found to be statistically significant ($P < 0.05$) (Table 2). As the duration and intensity of MF increased, the amount of glucose decreased significantly. The lowest amount of glucose compared to control was recorded as 120 min (16.4 times more) and 20 min (6.3 times more) at intensity of 400 mT, 120 min (5.57 times more) at intensity of 200 mT, 60 min (4.66 times more) and 20 min (4.53 times more) in MF applications ($P < 0.05$,

Table 2). Fructose content also decreased significantly compared to control. Especially 20 min at intensity of 400 mT (66.77%) and 60 min at intensity of 200 mT (66.58%) had the lowest fructose content in ME applications is ($P < 0.05$, Table 2). The sucrose content was increased in all groups with intensity of 400 mT MF and increased compared to control in 20 min and 120 min applications at intensity of 200 mT MF (Table 2).

Changes in Starch Content. Changes in starch quantities were in parallel with glucose values. As MF duration and intensity increased in seeds, decreases in the total amount of starch was observed ($P < 0.05$). The lowest starch content compared to control was 120 min (16.4 times more) and 20 min (6.3 times more) with intensity of 400 mT, 120 min (5.57 times more), 60 min (4.66 times more) and 20 min it is recorded in the application ($P < 0.05$, Table 2).

Changes in α -amylase Enzyme Activity of Seeds. Total α -amylase activity of seeds (EU/mg Protein) was significantly increased in all treatment groups compared to control. Compared to the control, process of 120 min at intensity of 400 mT MF increased the α -amylase activity by 38.60% (Table 2, $P < 0.05$). It can be said in line with current analysis that 400 m MF applications in general increase enzyme activity of the seeds more.

Antioxidant Enzyme Activity Changes. Applied MF effect on antioxidant enzyme activity levels were statistically significant as well ($P < 0.05$, Table 3).

APX activity increased compared to control in 20 min with intensity of 400 mT (26.94%) and in 60 min at intensity of 200 mT (5.81%) MF treatments, but decreased in other MF applications. 60 min at intensity of 400 mT (84.24%), 200 mT to 120 minutes (78%) and in 60 min with 400 mT activity in practice is the lowest ($P < 0.05$, Table 3). GuPX activity in seeds was adversely affected in all treatments compared to control in MF applications. The lowest GuPX activity at intensity of 200 mT MF was found in 60 min (81.68%) and 120 min (72.45%). In 400 mT MF application, GuPX activity increased with increasing duration (respectively 80.48%, 75.47%, 48.39%) ($P < 0.05$; Table 3). MF applications had a significant effect on CAT activity in seeds ($P < 0.05$, Table 3). CAT activity increased in the 200 mT MF administration group compared to 20 min (80.3%) and 60 min (55.26%) control, but decreased in 120 min (14.49%). In 400 mT MF application it is seen that the enzyme activity increases with increasing time ($P < 0.05$, Table 3). In 400 mT application highest CAT activity compared to the control application was detected in 120 minutes (2 times more), 60 min (56.83%) and 20 min (19%) ($P < 0.05$, Table 3). It was de-

terminated that MF applications caused an increase in SOD activity in seeds (Table 3). The highest SOD activity compared to the control was determined at intensity of 200 mT in 60 min (52.55%), 20 min (31.74%) and at intensity of 400 mT in 120 min (28.3%) ($P < 0.05$; Table 3).

DISCUSSION

Plants can be exposed to abiotic stress factors such as drought, low/high temperature, UV light, high light, heavy metals, nutritional deficiencies and magnetic field within their living environment. In these conditions, the amount of toxic compounds

known as free radicals or reactive oxygen derivatives in tissues and cells, which causes events such as inhibition of enzyme activities, proteins, DNA and RNA denaturation, increases. Furthermore, lipid peroxidation in the membranes results also in excessive MDA accumulation. The plants have developed various antioxidant systems against free radicals and reactive oxygen species such as SOD, CAT, APX, GuPX and GR [38, 39]. Antioxidant compounds are effective in protecting the balance between oxidant and antioxidant systems by cleaning free radicals and oxygen derivatives, repressing their reactions or repairing the damage they create. Tissues and cells are not affected by free radicals, as long as oxidative stability is provided [40, 41].

TABLE 1
Effects of different intensity and periods of magnetic field applications on total soluble protein and lipid peroxidation level (malondialdehyde-M)¹.

Intensity (mT)	Exposure Period (min)	Protein (mg/g)	MDA (nmol/g)
	Control	96.65±0.12a	59.13±0.06a
200	20	111.59±0.18e	316.59±0.13g
	60	102.53±0.23c	120.58±0.12b
	120	97.66±0.16b	202.56±0.13d
400	20	102.53±0.19c	218.56±0.16e
	60	112.59±0.21f	187.41±0.13c
	120	104.57±0.12d	298.20±0.07f

¹Statistically there is a significant difference with confidence level $p < 0.05$

TABLE 2
Effects of different intensity and periods of magnetic field applications on glucose, fructose, sucrose, starch amounts and α -amylase activity¹.

Intensity (mT)	Exposure Period (min)	Glucose mg/g	Fructose mg/g	Sucrose mg/g	Starch mg/g	A-amylase EU/mg Protein
	Control	45.60±0.12g	2.33±0.01f	1.96±0.01ab	4.35±0.011g	38.75±0.12a
200	20	24.84±0.05e	1.35±0.03d	2.06±0.04bc	2.37±0.005e	48.77±0.13d
	60	9.79±0.06d	0.78±0.01a	1.90±0.01a	0.94±0.006d	39.36±0.21ab
	120	8.19±0.11c	1.01±0.01b	2.19±0.06c	0.78±0.011c	44.24±0.11c
400	20	7.25±0.11b	0.78±0.01a	2.52±0.01d	0.69±0.010b	39.63±0.15b
	60	28.91±0.20f	1.64±0.02e	2.76±0.03e	2.76±0.019f	48.67±0.05d
	120	2.78±0.02a	1.20±0.02c	2.87±0.03e	0.27±0.002a	53.70±0.13e

¹Statistically there is a significant difference with confidence level $p < 0.05$

TABLE 3
The effect of magnetic field applications on APX, CAT and GuPX and SOD activity¹.

Intensity (mT)	Exposure Period (min)	APX EU/mg Protein	GuPX EU/mg Protein	CAT EU/mg Protein	SOD EU/mg Protein
	Control	0.085±0.0003cd	0.054±0.0001g	0.082±0.001b	82.36±0.11a
200	20	0.063±0.0001bc	0.020±0.0001e	0.148±0.001e	108.50±0.17f
	60	0.090±0.0001cd	0.010±0.0001a	0.127±0.001d	125.64±0.09g
	120	0.019±0.0001a	0.015±0.0001d	0.070±0.001a	104.47±0.17d
400	20	0.110±0.0002d	0.011±0.0002b	0.093±0.001c	102.50±0.15c
	60	0.0133±0.0002a	0.013±0.0001c	0.128±0.001d	101.34±0.06b
	120	0.028±0.0002ab	0.031±0.0002f	0.165±0.001f	105.67±0.15e

¹Statistically $p < 0.05$ significantly different confidence level

The seeds have two group proteins as "structural proteins and biologically active proteins" [42]. These proteins, which are accumulated during seed development in order to be used in a metabolic active phase in the future, are called "storage proteins" [43]. These proteins are not enzymatic and their task is to provide support as a source of nitrogen and sulfur that is necessary during germination and new plant formation [44, 45, 46].

Although MF has increased protein content compared to control in stratified-applied oriental beech seeds, the protein content in seeds Bewley, [46] varied depending on the intensity and duration of MA. The highest protein was observed at intensity of 400 mT in 60 min and at intensity of 200 mT in 20 min MF with and the lowest protein was observed in the control seed seeds (Table 1). According to the data; The MF application resulted in an increase in protein content in the beech seeds (Table 1). It is thought that the high protein value in the seeds of the oriental beech may be due to the high SOD and CAT activity, the water intake of the seeds causing accumulation of soluble proteins by stimulating the metabolic reactions, and also the increase in the total soluble protein amount caused by MF causing stress in the seeds. This is because McDonald [47], Bewley and Marcus [48] state that protein synthesis is stimulated after 30 minutes following water ingestion in seeds and that protein levels are maintained at a high level after 6 hours. Eraslan et al. [49]; Bartels and Sunkar [50], report that the amount of proline, soluble protein and sugars that work in the maintenance of the integrity of cellular membranes under stress conditions increase. Furthermore, researchers also report that the extent to which proteins are affected by stress conditions can vary according to the amino acid content, and proteins are less sensitive to stress conditions than to membranes (peroxidation of lipids in membranes) [51, 52, 53]. The amino acid sequence of the seed storage proteins varies according to the plant species. Some researchers have shown that the amino acid content affects the susceptibility of proteins to free radicals and that they are more susceptible to the radical effects of amino acid cysteine, cystine, methionine, histidine and tyrosine-rich proteins [54, 55]. Kristensen et al. [56] found that bean seeds are dominant in glutamylphenylalanine and willardiinin, as well as being rich in amino acid fractions such as hydroxyproline, alanine, glutamic acid, glutathione and glutamyltyrosine and Ayaz et.al. [23] found that beech seeds are rich in glutamic acid, arginine and leucine. This information and protein data have led to the thought that bean seeds may have amino acid-rich proteins may be less affected by possible damage to MF.

Many investigators have reported that membrane integrity is lost in the seeds as a result of lipid peroxidation [57, 53] and electrolyte leakage from

tissues and cells increase while, color, odor and appearance are deteriorated and chemical content is changed, and seed viability and strength are reduced because the aging is accelerated. MDA concentration is low in the control group and quite high in other application groups in this study. 200 mT intensity in 20 and 120 min and 400 mT intensity in 20 and 120 min of MF have significantly increased the amount of MDA in seeds (Table 1). These data demonstrate that the MF application and the stratification process applied to the seeds had a negative effect on the maintenance of cellular integrity in the seed. Sure enough, Yilmaz [58] has stated in his study on the determination of the chemical components of different oriental beech origins that seeds contained 48.69% fat, 29.04% protein, 3.16% starch and 4.10% ash, and the fats consisted predominantly of unsaturated fatty acids; Ratajczak and Pukacka [51] stated that the storage conditions of beech seeds above 0 °C have caused them lose their vitality due to ambient humidity, mainly due to the loss of membrane integrity due to peroxidation of unsaturated fatty acids. The results of the study are in parallel with the results obtained by Sahebamei [59]; Tian et al. [60], Saha and Sultana [61] and McDonald [22].

These investigators found that the amount of free radicals and reactive oxygen species increased in seeds due to cellular membranes and organelles being damaged in MF applied seeds and in line with this the structures of lipids, proteins, carbohydrates and nucleic acids in the cells deteriorated; and MDA concentration in the cells increased in line with the degree of deterioration of cellular structures. Furthermore, Mittler [62] and Allen [63] reported that MF applications increased the radical synthesis by stimulating oxidative stress in the organism and Majd et al. [64] reported that external magnetic field applications are more effective than geomagnetic field applications while Ishisaka et al. [65] and Garcia et al. [66] have reported that MF can cause electrolyte leakage by increasing membrane permeability and this occurrence impairs the functions of ions involved in enzyme activation, the water balance and osmotic potential of the seed.

Assimilates are found as starch in the insoluble form and as sucrose, glucose, fructose, myoinositol and raffinose and sugars in the soluble form in the endosperm [67, 68]. These compounds work in important physiological processes such as regulation of growth and development, maintenance of osmotic balance, maintenance of membrane integrity, protection of protein, DNA and RNA structure, prevention of water loss, resistance to environmental factors such as low temperature, drought, germination events and food mobilization [68, 69, 70]. Sure enough, Murata et al. [71], Nomura et al. [72], Palmiano and Juliano, [73], Matsukura et al. [74] have reported that starch in the endosperm was degraded by α and β amylase enzymes, mainly to

glucose and, to a lesser extent to reducing sugars such as maltose as well as non-reducing sucrose units. The same researchers have also reported that glucose is converted to sucrose by being transported to scutellum and used as a carbon source in the embryonic axillary. Glucose and fructose contents are lower in stratified and MF applied oriental beech seeds compared to control. The sucrose content increased with increasing time in the 400 mT application group whereas it higher in the 200 mT application group in 120 min and 20 min in MF compared to control. The starch content is higher in the control group and significantly lower in the other application groups (Table 2). The data on the sugars in the seeds indicate that wetness and different durations and severities of MF application during the stratification, stimulates the enzymatic degradation of starch in the beech seeds and also that glucose units are transported to scutellum and converted to sucrose units.

Slewinski and Braun [75], Aoki et al. [76], Bewley [46]; Jacobsen et.al. [77] reported that the activity of the α -amylase enzyme increased with the water intake of seed in their studies and that the respiratory substrate of starch converted into soluble sugars such as glucose and fructose [78, 79, 80] and a decrease in the total carbohydrate level in the endosperm, and this decrease persisted during germination. The researchers also stated that sucrose is high in scutellum while glucose and fructose are high in embryonic axillary and this occurrence proves that sucrose is not deposited in embryonic axes and that it is used as a carbon source by degrading to hexoses such as glucose and fructose, α -amylase and β -amylase are enzymes which degrade starch molecules in endosperms to simple sugars such as glucose, fructose and sucrose [46, 81]. Metabolic reactions are accelerated after the seeds take water and storage materials. They are degraded enzymatically and mobilized to the embryonic axes. The MF applied to stratification applied oriental beech seeds generally has increased the α -amylase activity. The highest enzyme activity was found respectively as 200 in 20 min and 120 min, while the lowest enzyme activity was found in the control group seeds (Table 2). It was thought that there was combined effect of water intake during stratification, stratification application and MF on increase in α -amylase activity in beech seeds. As such, Vashisth and Nagarajan [3], Pintilie et al. [82] and Atak et al. [83] have reported that water intake in seeds increased the degradation of starch to simple sugars by stimulating the activity of α -amylase enzyme while Rochalska and Grabowska [84] expressed that there were changes in α -amylase and β -amylase and glutation S-transferase enzymes during germination of wheat seeds exposed to MA and Agustrina et al. [9] stated that low levels of MF increased the α -amylase activity in leguminous seeds, but did not affect soybeans and Rochalska

and Grabowska [84] mentioned that MF reduced α -amylase activity in wheat seeds while Turfan et al. [11] reported that MF applications reduced the α -amylase activity in oriental beech seeds that were not subjected to stratification.

Seed quality, vitality and germination power are largely based on the activity of antioxidant compounds found in the seed, such as SOD, CAT, APX and GuPX, which protect the seed from damage by radicals and active oxygen derivatives. APX and GuPX activity in the stratification-applied oriental beech seeds are high in the control group and very low in the other MF applied seeds. In particular, applications of 200 mT intensity in 60 min, 400 mT intensity in 20 and 60 min of MF significantly reduced APX and GuPX activity compared to control and other applications. CAT has the lowest value in 200 mT 120 min operation and the highest value at 400 mT intensity in 120 min and 200 mT in 20 min. SOD activity is low only in the control group seeds (Table 3). MF increased SOD activity in all other treatment groups except control, while APx and CAT activities were increased in other treatment groups except control; CAT activity was adversely affected only at intensity 200 mT in 120 min. Based on these results, it was concluded that MF treatments stimulated SOD and CAT activity, whereas APX and GuPX inhibited activity. The findings of the studies on the enzyme activity are consistent with the results of studies in this field. Sure enough Celik et al. [87] has reported that MF increased the SOD and CAT activities, while in dampened seed peroxidase groups such as ascorbate peroxidase reduce the enzyme activity in their study investigated the effects of MF applications on the SOD activity in soybean roots.

Furthermore, Radhakrishnan and Kumari [88] and Huang et al. [89] stated that their applications increased the SOD and CAT activities in the seeds, and Majd and Shabrang of [90] reported that MF and Mousavizadeh et al. [2] reported that high intensity and long-lasting MF reduces the peroxidase activity in lettuce seeds. Researchers report that various metabolic reactions such as protein, DNA and RNA synthesis and degradation of macromolecules are initiated in the seeds together with water intake and MF applications and the activity of antioxidants such as SOD, CAT, APX and GuPX are stimulated and also lipid peroxidation in membranes are effective in deterioration of seed viability [40, 47, 85, 86, 91, 92, 93].

CONCLUSION

It was concluded that MF application of different intensity and duration, affected the chemical content of stratified oriental beech seeds differently depending on the intensity and duration, and made

the MDA amount of MF seed increasing and gave damage mostly to membranes and this case may arise from the diversity of chemical composition of the seeds stratification time and effect of MF as well as factors like seed harvest time and storage conditions. Furthermore, it will be possible to provide more accurate and descriptive results to determine the effects of the magnetic field applications on beech seeds with further studies to be held on seeds with different harvest years, different storage conditions and populations. As such, it is needed to conduct studies regarding the nature of the MF stimulation.

REFERENCES

- [1] Ozel, H.B., Kirdar, E. and Bilir, N. (2015) The effects of magnetic field on germination of the seeds of oriental beech (*Fagus orientalis* Lipsky) and growth of seedlings. *Agriculture & Forestry*, 61, 195-206.
- [2] Mousavizadeh, S.J., Sedaghatpour, S., Rahimi, A. and Haydeh Mohammadi, H. (2013) Germination parameters and peroxidase activity of lettuce seed under stationary magnetic field. *International Journal of Biosciences*. 3(4), 199-207.
- [3] Vashisth, A. and Nagarajan, S. (2010) Characterization of water distribution and activities of enzymes during germination in magnetically-exposed maize (*Zea mays* L.) Seeds. *Indian Journal of Biochemistry and Biophysics*. 47, 311-38.
- [4] Danilov, V., Bas, T., Eltez, M. and Rizakulyeva, A. (1994) Artificial magnetic field effects on yield and quality of tomatoes. *Acta Hort.* 366, 279-285.
- [5] Samy, C. G. (1998) Magnetic seed treatment. I. Influence on flowering, siliquae and seed characteristics of cauliflower. *Orissa J. Hort.* 26, 68-69.
- [6] Podlesny, J., Pietruszewski, S. and Podlesna, A. (2005) Influence of magnetic stimulation of seeds on the formation of morphological features and yielding of the pea. *International Agrophysics* 19, 61-68.
- [7] Bilalis, D.J., Katsenios, N., Efthimiadou, A., Karkanis, A., Khah, E.M. and Mitsis, T. (2013) Magnetic field pre-sowing treatment as an organic friendly technique to promote plant growth and chemical elements accumulation in early stages of cotton. *Aust J Crop Sci.* 7, 46-50.
- [8] Duarte Diaz, C.E., Riquenes, J.A., Sotolongo, B., Portuondo, M.A., Quintana, E.O. and Perez, R. (1997) Effects of magnetic treatment of irrigation water on the tomato crop. *Hortic. Abst.*, 69. p. 494.
- [9] Agustrina, R., Handayani, T.T., Wahyuningsih, S. and Prasetya, O. (2012) Pertumbuhan tanaman tomat (*Lycopersicum esculentum* Mill.) di bawah perlakuan medan magnet 0,2 mT. In the *Proceedings of the 2012. SNSMAIP III*, 277-281.
- [10] Florez, M., Carbonell, M.V. and Martinez, E. (2007) Exposure of maize seeds to stationary magnetic fields: Effects on germination and early growth. *Environ Exp Botany* 59, 68-75.
- [11] Turfan, N., Yer, E.N., Ayan, S., Hasdemir, B. and Hancerliogullari, A. (2016) The effect of magnetic field application on chemical composition in *Fagus orientalis* Lipsky. seed. *Biological Diversity and Conservation*. 9/2 (S1), 75-83.
- [12] Rady, M.M. (2012) A novel organo-mineral fertilizer can mitigate salinity stress effects for tomato production on reclaimed saline soil. *S. Afr. J. Bot.* 81, 8-14.
- [13] Qi, B., Doughty, J. and Hooley, R. (2013) A Golgi and tonoplast localized S-acyl transferase is involved in cell expansion, cell division, vascular patterning and fertility in *Arabidopsis*. *New Phytologist* 200, 444-456.
- [14] Jiang, Y. and Huang, B. (2002) Protein alterations in tall fescue in response to drought stress and abscisic acid. *Crop Science* 42, 202-207.
- [15] Atak, C., Celik, O., Olgun, A., Alikamanoglu, S. and Rzakoulieva, A. (2007) Effect of agnetic field on peroxidase activities of soybean tissue culture. *Biotechnol. & Biotechnol. EQ.* 21 (2), 166-171.
- [16] Jajte, J.M. (2000) Programmed cell death as a biological function of electromagnetic fields at a frequency of (50/60 Hz). *Medycyna Pracy*. 51, 383-389.
- [17] Agustrina, R., Tripeni, T. and Ernawati, E. (2011) Anatomi kecambah tomat yang diberi perlakuan medan magnet 0,2 mT. In: *In the Proceedings of the 2012 Seminar Nasional Sains & Teknologi - IV*, pp: 632-646.
- [18] Dhawi, F. and Al-Khayri, J.M. (2009) Magnetic fields induce changes in photosynthetic pigments content in Date Palm (*Phoenix dactylifera* L.) seedlings. *Open Agri J.* 3, 1-5.
- [19] Magnusson, M. (1984) Magnetic treatment of the nutrient solution for tomatoes and the influence of a magnetic field on water and plants. *Rapport Ins. For Tradgardsvetenskap, Sveriges, Lant Bruksuniversite*, 30, 42.
- [20] Dunlop, D.W. and Schmidt, B.L. (1965) Biomagnetics II. Anomalies found in the root of *Allium cepa* L. *Hort. Abst.* 36, 563.
- [21] Guney, D., Bak, Z. D., Aydinoglu, F., Turna, I. and Ayaz, F.A. (2013) Effect of geographical variation on the sugar composition of the oriental beech (*Fagus orientalis* Lipsky). *Turk J Agric For:* 7, 221-230.

- [22] McDonald, M.B. (1999) Seed deterioration: physiology, repair and assessment. *Seed Sci. Technol.* 27, 177-237.
- [23] Ayaz, F.A., Glew, R.H., Turna, I., Guney, D., Chuang, L.T., Chang, Y.C., Andrews, R., Power, L., Presley, J., Torun, H. and Sahin, N. (2011) *Fagus orientalis* (Oriental beechnut) seeds are a good source of essential fatty acids, amino acids and minerals. *Food* 5, 48–51.
- [24] Prasad, P.V.V., Boote, K.J., Allen, Jr, L.H. and Thomas, J.M.G. (2002) Effects of elevated temperature and carbon dioxide on seed-set and yield of kidney bean (*Phaseolus vulgaris* L.). *Global Change Biol.* 8, 710–721.
- [25] McDonald, M.B. (2004) Orthodox seed deterioration and its repair. In: Benech-Arnold, R.L. and Sanchez, R.A. (Eds.) *Handbook of seed physiology: Applications to Agriculture*, Food Products Press, New York, 273-304.
- [26] Yilmaz, M. (2005) The researches on the physiology of oriental beech (*Fagus orientalis* Lipsky.) seeds. PhD thesis, Istanbul University, Faculty of Forestry, Istanbul, Turkey, 170 p.
- [27] Gezer, A. and Yucedag, C. (2006) Forest tree seeds and techniques of seedling propagation from seed originated. Suleyman Demirel University, Faculty of Forestry, Pub. No: 56, Isparta, Turkey, 140 p.
- [28] Rezaei, A., Nasery, B., Yazdian, F. and Mhedayati, M. (2011) A study of gibberalic acid effect on oriental beech (*Fagus orientalis* L.) nuts dormancy removal. In: Wagner, S., Fahlvik, N., Fischer, H. (eds.) *Proceedings of the 9th IUFRO International Beech Symposium organized by IUFRO working party 1.01.07 "Ecology and Silviculture of Beech"* Dresden/Gottingen, Germany, 1217 September 2011. Institute for Silviculture and Forest Protection, Dresden, Germany, 61-63.
- [29] Ertekin, M., Kirdar, E. and Ayan, S. (2015). Effects of tree ages, exposures and elevations on some seed characteristics of Oriental beech (*Fagus orientalis* Lipsky.) *SEEFOR - South-east European Forestry*, 6(1) 15-23.
- [30] Nakano, Y. and Asada, K. (1981) Hydrogen peroxide is scavenged by ascorbate specific peroxidase in spinach chloroplasts. *Plant Cell Physiol.* 22, 867– 880.
- [31] Bergmeyer, H.U. (ed.) (1970) *Methoden der enzymatischen analyse*, Akademie Verlag, 1, 636-562.
- [32] Cakmak I., Graham R. and Welch R.M. (2002) Agricultural and molecular genetic approaches to improving nutrition and preventing Micronutrient malnutrition globally. In *Encyclopedia of Life Support Systems* (Section eds. Cakmak, I. and Welch, R.M.), UNESCO-EOLSS Publishers Co. Ltd., UK, 1075-1099.
- [33] Birecka, H., Briber, K.A. and Catalfamo, J.L. (1973) Comparative studies on tobacco pith and sweet potato root isoperoxidases in relation to injury, indoleacetic acid, and ethylene effects. *Plant Physiol.* Jul; 52(1), 43–49.
- [34] Bradford, M.M. (1976) A rapid sensitive method for the quantitation of micro program quantities of protein utilizing the principle of protein-dye binding. *Anal Biochem.* 72, 248-254.
- [35] Lutts, S., Kinet, J.M. and Bouharmont, J. (1996) NaCl-Induced senescence in leaves of rice (*Oryza sativa* L.) cultivars differing in salinity resistance. *Annals of Botany.* 78, 389-398.
- [36] Morais, G.A. and Takaki, M. (1998) Determination of amylase activity in cotyledons of *Phaseolus vulgaris* L. cv. carioca. *Brazilian Archives of Biology and Technology*, 41, 17-25.
- [37] Pearson, D., Melon, H.K. and Ronald, S. (1976) *Chemical analysis of Food*, 8th edition. Churchill Livingstone. 5-63.
- [38] Mojovic, M., Vuletic, M., Bacic, G.G. and Vucinic, Z. (2004) Oxygen radicals produced by plant plasma membranes: an EPR spin-trap study. *J Exp Bot*; 55, 2523-2531.
- [39] Gechev, T., Willekens, H. and Van Montagu, M. (2003) Different responses of tobacco antioxidant enzymes to light and chilling stress. *J Plant Physiol*, 160, 509-515.
- [40] Wang, H.Y., Chen, C.L. and Sung, J.M. (2003) Both warm water soaking and matriconditioning treatments enhance anti-oxidation of bitter gourd seeds germinated at suboptimal temperature. *Seed Sci. & Technol.* 31: 47-56.
- [41] Sung, J.M. (1996) Lipid peroxidation and peroxide scavenging in soybean seeds during ageing. *Physiologia Plantarum*, 97, 85-89.
- [42] Fukushima, D. (1991) Recent progress of soybean protein foods: Chemistry, technology, and nutrition. *Food Reviews International*, 7, 323–351.
- [43] Derbyshire, E. Wright, D.J. and Boulter, D. (1976) Legumin and vicilin, storage proteins of legume seeds. *Phytochemistry*, 15(1), 3-24.
- [44] Alvarez, J.B. Toledo, M.J. Abellanas, B. and Martin, L.M. (2004) Use of megagametophyte storage proteins as markers of the genetic diversity in stone pine (*Pinus pinea* L.) in Andalusia, Spain. *Genetic Resources and Crop Evolution*, 51, 621-627.
- [45] Kumar, J. Agarwal R.L. Mani, S.C. Sing, Y. Pandey, I.D. and Kumar, A. (2001) Variability in seed storage proteins of sunflower. *Physiol Mol Biol Plants*, 7, 89-91.
- [46] Bewley, J.D. (2001) Seed germination and reserve mobilization. J Derek Bewley, University of Guelph, Guelph, Ontario, Canada. *Encyclopedia of Life Sciences & 2001 Nature Publishing Group / www.els.net.*
- [47] McDonald, M. B. (2000) Seed priming. In Black, M. and Bewley, J.D. (eds.) *Seed Tech-*

- nology and Its Biological Basis. Sheffield Academic Press, Sheffield. pp. 287-325.
- [48] Bewley, J. D. and Marcus, M. (1990) Gene expression in seed development and germination. *Progress in Nucleic Acids Research and Molecular Biology* 38, 165–193.
- [49] Eraslan, F., Inal, A., Savasturk, O. and Gunes, A. (2007) Changes in antioxidative system and membrane damage of lettuce in response to salinity and boron toxicity. *Sci Hortic.*, 114(1), 5–10.
- [50] Bartels, D. and Sunkar, R. (2005) Drought and salt tolerance in plants. *Crit Rev Plant Sci.*, 24, 23–58.
- [51] Ratajczak, E. and Pukacka, S. (2005) Decrease in beech (*Fagus sylvatica*) seed viability caused by temperature and humidity conditions as related to membrane damage and lipid composition. *Acta Physiol Plant*, 27, 3–11
- [52] Nordberg, J. and Arner, E.S.J. (2001) Reactive oxygen species, antioxidants, and the mammalian thioredoxin system. *Free Radical Biology and Medicine*, 31, 1287-1312.
- [53] Wilson, D.O. and McDonald, M.B. (1986) The lipid peroxidation model of seed ageing. *Seed Science and Technology*, 14, 269-300.
- [54] Aricioglu, A. (1994) Free oxygen radicals and cell damage. *Doktor.* 2/3 May, 238-242.
- [55] Kaneko, J.J. (1980) *Clinical Biochemistry of Domestic Animals*. Third Edition. Academic Press. Inc. (London) Ltd.
- [56] Kristensen, I., Larsen, P.O. and Sorensen, H. (1974) Free amino acids and γ -glutamyl peptides in seeds of *Fagus sylvatica*. *Phytochemistry*, 13(12), 2803-2811.
- [57] Sung, J.M. and Chiu, C.C. (1995) Lipid peroxidation and peroxide-scavenging enzymes of naturally aged soybean seed. *Plant Science*, 110(1), 45-52.
- [58] Yilmaz, M. (2008) Dogu Kayini (*Fagus orientalis* Lipsky.) Tohumlarının Kimyasal Bileşimi. *KSU Fen ve Mühendislik Dergisi*, 11(1), 64-68.
- [59] Sahebamei, H., Abdolmaleki, P. and Ghanati, F. (2007) Effects of magnetic field on the antioxidant enzyme activities of suspension-cultured Tobacco cells. *Bioelectromagnetics*, 28, 42-47.
- [60] Tian, X., Song, S. and Lei, Y. (2008) Cell death and reactive oxygen species metabolism during accelerated ageing of soybean axes. *Russ. J. Plant Physiol.*, 55(1), 33-40.
- [61] Saha, R. R. and Sultana, W. (2008) Influence of seed ageing on growth and yield of soybean. *Bangla J Bot* 37, 21-26.
- [62] Mittler, R. (2002) Oxidative stress, antioxidants and stress tolerance. *Trends in Plant Science*, 7, 405-410.
- [63] Allen, R.D. (1995) Dissection of oxidative stress tolerance using transgenic plants. *Plant Physiol.*, 107, 1049-1054.
- [64] Majd, A., Farzpourmachiani, S. and Dorrani, D. (2010) Evaluation of the effect of magnetic fields on seed germination and seedling ontogenesis of vetch (*Vicia sativa* L.). *Journal of Plant Science Research*, 18, 1-9.
- [65] Ishisaka, R., Kanno, T., Inai, Y., Nakahara, H., Akiyama, J., Yoshioka, T. and Utsumi, K. (2000) Effects of magnetic fields on the various functions of subcellular organelles and cells. *Pathophysiology* 7, 149–52.
- [66] Garcia, R.F., Arza, P.L. and Almanza, F.L. (2001) Influence of a stationary magnetic field on water relations in lettuce seeds. Part II: Experimental results *Bioelectromagnetics*, 22, 596-602.
- [67] Garcia, I.S., Souza, A., Barbedo, C.J., Dietrich, S.M. and Figueiredo-Ribeiro, R.C.L. (2006) Changes in soluble carbohydrates during storage of *Caesalpinia echinata* LAM. (Brazilwood) seeds, an endangered leguminous tree from the Brazilian Atlantic Forest. *Braz. J. Biol.*, 66, 739-745.
- [68] Borges, I.F., Barbedo, C.J., Richter, A.A. and Figueiredo-Ribeiro, R.C.L. (2006) Variations in sugars and cyclitols during development and maturation of seeds of brazilwood (*Caesalpinia echinata* Lam., Leguminosae). *Braz. J. Plant Physiol.* 18(4), 475-482.
- [69] Nkang, A. (2002). Carbohydrate composition during seed development and germination in two sub-tropical tree species (*Erythrina caffra* and *Guilfoylia monostylis*). *J. Plant Physiol.* 159, 473-483.
- [70] Francisco Arenas-Huertero, A. A., Zhou, L., Sheen, J. and Leon, P. (2000) Analysis of *Arabidopsis* glucose insensitive mutants, gin5 and gin6, reveals a central role of the plant hormone ABA in the regulation of plant vegetative development by sugar. *Genes Dev*, 14(16), 2085-2096.
- [71] Murata, T., Akazawa, T. and Fukuchi, S. (1968) Enzymic mechanism of starch breakdown in germinating rice seeds. I. An analytical study. *Plant Physiology* 43, 1899–1905.
- [72] Nomura, T., Kono, Y. and Akazawa, T. (1969) Enzymic mechanism of starch breakdown in germinating rice seeds. II. Scutellum as the site of sucrose synthesis. *Plant Physiology* 44, 765-769.
- [73] Palmiano, E.P. and Juliano, B.O. (1972) Biochemical changes in the rice grain during germination. *Plant Physiology* 49, 751–756.
- [74] Matsukura, C.A., Saitoh, T., Hirose, T., Ohsugi, R., Perata, P. and Yamaguchi, J. (2000) Sugar uptake and transport in rice embryo: expression of companion cell-specific

- sucrose transporter (OsSUT1) induced by sugar and light. *Plant Physiology* 124, 85–93.
- [75] Slewinski, T.L. and Braun, D.M. (2010) Current perspectives on the regulation of whole-plant carbohydrate partitioning. *Plant Sci.* 178, 341–349. doi:10.1016/j.plantsci.2010.01.010.
- [76] Aoki, N., Scofield, G.N., Wang, X.D., Patrick, J.W., Offler, C.E. and Furbank, R.T. (2006) Expression studies indicate sugar transporters play key roles in germinating wheat seeds. *Plant Physiology* 141, 1255–1263.
- [77] Jacobsen, J.V., Gubler, F. and Chandler, P.M. (1995) Gibberellin and abscisic acid in germinating cereals, in Davies P.J. (ed.) *Plant Hormones: Physiology, Biochemistry and Molecular Biology*, (Boston, MA: Kluwer), 246–271.
- [78] Price, J., Li, T.C., Kang, S.G., Na, J.K. and Jang, J.C. (2003) Mechanisms of glucose signaling during germination of *Arabidopsis*. *Plant Physiol.* 132, 1424–1438.
- [79] Winter, H., Huber, J. L. and Huber, S. C. (1997) Membrane association of sucrose synthase: changes during the gravity response and possible control by protein phosphorylation, *FEBS Lett.* 430, 151–155.
- [80] Weber, H., Borisjuk, L., and Wobus, U. (1997) Sugar important metabolism during seed development. *Trends Plant Sci.* 2, 169–174. doi:10.1016/S1360-1385(97)85222-3.
- [81] Rochalska, M. and Orzeszko-Rywka, A. (2005) Magnetic field treatment improves seed performance. *Seed Science and Technology*, 33(3), 669–674. <https://doi.org/10.15258/sst.2005.33.3.14>.
- [82] Pintilie, M., Oprica, L., Surleac, Dragutivan, M. S. and Creanga, D. E. (2006) Enzyme Activity in Plants Treated with magnetic solution. *Rom. Journal Phys.*, 51(1–2) 239–244.
- [83] Atak, C., Celik, O., Olgun, A., Alikamanoglu, S. and Rzakoulieva, A. (2007) Effect of magnetic field on peroxidase activities of soybean tissue culture. *Biotechnol. & Biotechnol. EQ.* 21(2), 166–171.
- [84] Rochalska, M. and Grabowska, K. (2007) Influence of magnetic fields on the activity of enzymes: α - and β -amylase and glutathione S-transferase (GST) in wheat plants. *Int. Agrophysics*, 21, 185–188.
- [85] Ak, A., Yucel, E. and Ayan, S. (2012) Relationship between seed germination and catalase enzyme activity of *Abies* taxa from Turkey, Kastamonu Univ., *Journal of Forestry Faculty*, 12(3), 185–188.
- [86] Bailly, C. (2004) Active oxygen species and antioxidants in seed biology. *Seed Sci Res.* 14:93–107.
- [87] Celik, O., Buyukuslu, N., Atak, C. and Rzakoulieva, A. (2009) Effects of magnetic field on activity of superoxide dismutase and catalase in glycine max (L.) Merr. *Roots. Polish Journal of Environmental Studies* 18 (2), 175–182.
- [88] Radhakrishnan, R. and Kumari, B.D.R. (2012) Pulsed magnetic field: A contemporary approach offers to enhance plant growth and yield of soybean. *Plant Physiology and Biochemistry*, 51, 139–144.
- [89] Huang, R., Sukprakarn, S., Phavaphutanon, L., Juntakool, S. and Chaikul, C. (2006) Changes in antioxidant enzyme activity, lipid peroxidation and seedling growth of cucumber seed induced by hydro priming and electric field treatments. *Kasetsart J. (Nat. Sci.)* 40, 825–834.
- [90] Majd, A. and Shabrangi, A. (2009) Effect of seed pretreatment by magnetic fields on seed germination and ontogeny growth of agricultural plants. In the Proceeding of 2009 Electromagnetics Research Symposium, Beijing, China, 1137–1141.
- [91] Yasar, F., Uzal, O. and Yasar, O. (2016) Antioxidant enzyme activities and lipid peroxidation amount of pea varieties (*Pisum sativum* sp. *arvense* L.) under salt stress. *Fresen. Environ. Bull.*, 25(1), 37–42.
- [92] Cekic, F.O., Yilmaz, S. and Karagoz, A. (2016) Combined effects of salinity and peg-induced osmotic stress on antioxidant defence system in endemic halophyte *Salvia halophila* hedge. *Fresen. Environ. Bull.*, 25(8), 3179–3185.
- [93] Parlak, K.U. (2016) Differential response of growth, photosynthetic pigments and antioxidant enzymes to UV-B radiation in tomato (*Solanum lycopersicum* L.) seedlings. *Fresen. Environ. Bull.*, 25(10), 4192–4196.

Received: 09.01.2017

Accepted: 09.06.2017

CORRESPONDING AUTHOR

Sezgin Ayan

Siviculture Department

Faculty of Forestry

Kastamonu University

37150, Kastamonu – TURKEY

E-mail: sezginayan@gmail.com

EFFECTS OF VARIOUS MULCH MATERIALS ON FRUIT QUALITY CHARACTERISTICS ON ORGANICALLY GROWN STRAWBERRIES

Sevinc Sener^{1,*}, Nurgul Fetiye Turemis²

¹University of Akdeniz, Vocational School of Technical Sciences, Antalya, Turkey.

²University of Cukurova, Faculty of Agriculture, Department of Horticulture, Adana, Turkey

ABSTRACT

The present experiment was carried out during 2011 - 2013 open-field cultivation in order to determine the effects of black plastic, agro-textile and sawdust mulches on ascorbic acid (AA), total phenolic content (TPC) and antioxidant activity (DPPH test) of organically grown strawberries (*Fragaria x ananassa* Duch.) cv. Monterey, Albion, Aromas, Camarosa and Sweet Charlie. TPC was determined by Folin - Ciocalteu (FCR) method, while antioxidant activity was determined by DPPH radical scavenger. The AA, TPC and DPPH of strawberry fruits were significantly influenced by genotypes difference and mulch types. Camarosa cultivar was found superior in terms of AA (61.49 mg/100 gr), TPC content (2140.45 mg GAE/kg w) and DPPH radical scavenger (3.76 µg/mL). In addition, sawdust mulch had a higher impact on TPC (1820.60 mg GAE/kg fw) and DPPH radical (4.56 µg/mL) while agro-textile mulch had a higher impact on AA content (58 mg/100 gr).

KEYWORDS:

Antioxidant, ascorbic, mulch, organic agriculture, phenolics, strawberry.

INTRODUCTION

In recent years, people desire of consuming healthy and environmentally friendly grown food has increased the popularity of organic agriculture [1]. Organic strawberry production commercially increased in the world [2]. According to 2013 data of FAO, 274.927 tons of strawberries are grown in a 13.549 hectares field, in our country [3]. 3.857 tones of the production are organic [4]. Compared to other fruits, strawberry has a higher antioxidant activity, which is reported to be related to phenolic compounds, anthocyanins [5], flavonoids, ascorbic acid, vitamins and carotenoids [6]. The fruit quality and antioxidant activity of strawberries can be influenced by ecological conditions, genetic factors and growing conditions [7, 8, 9, 10, 11]. The use of mulch is common in strawberry cultivation, as it keeps the

fruit clean by preventing contact with the soil, conserves soil moisture and temperature, increase the yield, control weeds [12, 13] in addition to this using plastic mulch is a common practice in cultivation of strawberry [7]. Some studies report that mulch material influences fruit quality [14, 15]. Compared to plastic mulch, sawdust and agro-textile mulches are more advantageous in permeable to air and water and decomposition [16, 17].

Organically grown strawberries are reported to have a higher phenolic content and higher quality in terms of some fruit characteristics [18, 19, 20]. Anticarcinogen [21] and chronicle illness preventing characteristics of phenolic compounds are reported in some studies [22]. In this paper, it was aimed to determine the effects of different mulch types on ascorbic acid (AA), total phenolic content (TPC) and antioxidant activity (DPPH test) of three neutral ('Monterey', 'Albion' and 'Aromas') and two short day strawberry (*Fragaria x ananassa* Duch.) cultivars ('Camarosa' and 'Sweet Charlie') under central Anatolia conditions in summer growing season.

MATERIALS AND METHODS

Plant materials and experimental design.

The experiment was conducted between 2011 - 2012 and 2012 - 2013 growing seasons in Nevsehir (Turkey) under open-field conditions and 1150 m above sea level. The treatments consisted of 5 strawberry cultivars and 3 mulch types. The cultivars used in the experiment were as follows: three neutral 'Monterey, Albion, Aromas' and two short-day strawberries (*Fragaria x ananassa* Duch.) 'Camarosa, Sweet Charlie' cultivars which grown organic seedling conditions. Mulch materials were black plastic mulch, agro-textile mulch and sawdust mulch. Seedlings planted in a 30 x30 cm spacing arrangement into 100 cm beds. Through the experiment plants were watered by sprinkling water and drip irrigation. Seedlings were transplanted 19 May 2012. Organic agriculture certificated products were used during the experiment for fertilization and plant production. The treatments were arranged in a randomized block design (RBD) using a 5 x 3 factorial arrangement with 4 replications and 30 plants per parcel. A total

of 600 plants were used in experiment. Black plastic and agro-textile mulches were applied before seedling and sawdust mulch was applied 15 days after the seedling as 10 cm's denseness.

Chemicals. The list of chemicals used in experiments are; oxalic acid, ascorbic acid, 2,6 dichlorophenolyn, 2,2-Diphenyl-1-picrylhydrazyl (DPPH), acetic acid, folin celteau (FCR), sodium carbonate (Na_2CO_3), and gallic acid. All reagents used were of analytical grade.

Sample preparation. Ripen fruit from each treatment was harvested throughout the experimental period. Strawberry fruits were graded for size, external color and sorted to eliminate damaged fruits and transported under refrigeration to the laboratory. Post-harvest evaluations assessed 500 g randomly selected marketable fruits per replication. Samples, homogenized by food processor, were extracted. Samples, extracted with methanol, were centrifuged and supernatants were subjected - 20 °C in a deep freezer to further analysis.

Antioxidant characteristics. AA, TPC and DPPH were determined once every 15 days through the experiment.

Ascorbic acid. Vitamin C content was determined by spectrophotometric method, according to Pearson [23]. The results are expressed as mg ascorbic acid/100 g of fresh weight. Cary 100 Bio UV/VIS spectrophotometer was used in the study. Interpretation was done in 15 seconds after samples were prepared and dye solution was added.

Total phenolic content. Total phenolic content concentration was measured by FCR as described by Singleton & Rossi [24]. The phenol content was representing as kg of gallic acid equivalent per one kilogram fresh weight tissue.

Fruit samples were homogenized by food processor. Homogenized fruit samples were added as 3g's into a 70% methanol solution (29.5 ml pure water + 70 ml methanol + 0.5 ml acetic acid) and homogenized for 5 minutes and preserved in a dark environment for 18 hours. Samples were centrifuged for 20 minutes at 4 °C; supernatants were extracted and preserved in - 20 °C until the analyze. 0.01 ml of the sample was gathered and added into 0.5 ml of 10% FCR solution and incubated in room temperature 6 - 8 minutes. Afterwards, 1.5 ml of 20% Na_2CO_3 solution was added and incubated in room temperature for 2 hours. At the end of the process it was interpreted in a spectrometer at 750 nm. 0, 50, 100, 200, 400, 800 and 1600 mg/L of gallic acid concentrations were prepared and interpreted in a spectrometer at 750 nm. Total phenolic concentration was measured by standard curve.

Radical scavenging activity indication. For antioxidant activity measurement, a methanol soluble free radical (DPPH; - 2,2 dipheyl-1-picrylhydrazyl) was used [25]. Solvent (methanol) was lyophilized and evaporated from extracted samples with rotary evaporator. Extracts were prepared in several different concentrations (500, 250, 100, 50, 25, 10, 5 ppm) and DPPH solution was added. After vortexing for 30 minutes, absorbance was interpreted as 515 nm. Control value was determined by using 1 ml methanol instead of using sample and standard substance. EC_{50} value was measured with a graphic that was formed by placing % radical scavenger activity values against concentrations and results were presented as $\text{EC}_{50} = \mu\text{g/mL}$.

% DPPH radical scavenger activity was measured according to the formula given below.

$$\text{DPPH radical inhibition (\%)} = [(A1 - A2 / A1)] \times 100$$

A1: Absorbance of Control Sample (non-antioxidant) at 515 nm.

A2: Absorbance of sample (antioxidant) at 515 nm.

Statistical analysis/ Data analyzes were performed using SPSS software version 23. Mean values of application were compared with Duncan test after variance analysis. Differences between means at 5% ($P < 0.05$) and 1% ($P < 0.01$) level were considered significant. Correlations were obtained by Pearson correlation coefficient in bivariate correlations.

RESULTS AND DISCUSSION

In strawberry plantation, plants may be influenced by environmental conditions and thereby antioxidant level of fruits may be influenced [8]. In this study, effects of different cultivars and mulching methods on antioxidant characteristics of strawberries were determined by AA, TPC and DPPH methods. AA, TPC and DPPH methods, which were used in our study are in accordance with previous studies [26, 27, 28, 29].

Effects of cultivars. The study was conducted under certified organic agricultural practices. Albion, Aromas, Camarosa and Sweet Charlie are common commercial strawberry cultivars grown in Turkey [9]. However, Monterey is a less known and grown cultivar compared to the four cultivars above. Different strawberry cultivars' AA, TPC and DPPH test results took place in this study are presented in Table 1. According to the some studies AA, TPC and DPPH test results may vary depending on characteristics of cultivars [30, 31]. As can be seen in Table 1, the effects of cultivar on AA, TPC and DPPH were found be statistically significant. As for Table 1, fruit which were harvested from Camarosa, had the highest AA (61.49 mg/100g), than those harvested from

other cultivars. Similar values were found between Monterey (53.13 mg/100g) and Aromas (53.51 mg/100g). AA values obtained from the studies are in accordance with some reports [8, 32, 33]. Samec et al., [32] has reported 57.96 mg/100 g fw for Abion and 53.48 mg/100 g fw for Monterey cultivar while Tiwari et al., [33] has reported 54.75 mg/100 g fw value for Sweet Charlie Cultivar. However, Gani et al., [34] has reported a higher level of ascorbic acid for Chandler cultivar as 78.54 - 80.12 mg/100 g fw. The difference between the results may be due to the climate and growing conditions.

Total phenolic method, used in this study, is based on electron transfer from phenolic compounds and other reductant compounds to molybdenum. Complex blue formation is determined at 750 - 765 nm spectrophotometrically [35]. As seen in Table 1, the highest TPC concentration (2140.45 mg GAE/kg fw) has occurred in Camarosa cultivars same as AA concentration, and the line is followed by Monterey cultivar (2109.06 mg GAE/kg fw). The lowest content was found in Sweet Charlie cultivar (1306.33 mg GAE/kg fw). It was a previously reported that, similar TPC values were obtained [32] and TPC content of Camarosa cultivar is higher than other cultivars [36] just as in our study.

A substance's antioxidant effect depends on its ability to remove the free radicals in the environment [37]. An absorbance change, which is based on fading of compounds due to free radicals, were measured at 517 nm and EC₅₀ values of these were measured according to the calibration graphic of DPPH radical scavenger. In this regard, the lower EC₅₀ values, the higher antioxidant potential. Different cultivars DPPH scavenger, based on EC₅₀ values, are presented in Table 1. DPPH test results of all cultivars are found significantly different ($P < 0.05$) and mean value has ranged between 3.76 µg/mL (Camarosa) and 6.87 µg/mL (Sweet Charlie) (Table 1).

It is reported that, differences of genotypes influence the fruit's AA, TPC, DPPH results [32, 36]. Considering the results, the highest data was obtained by Camarosa cultivar compared to other cultivars (Table 1). Similarly, Hernanz et al., [38] have also obtained higher values from Camarosa cultivar, compared to other cultivars.

Effects of Mulches. Antioxidant characteristics of strawberry fruits may get influenced by agronomic techniques such as open or protected system, sort of sole type or different mulch materials [39, 40]. Plants were grown by getting mulched with black plastic mulch, agro-textile mulch and sawdust mulch and AA, TPC and DPPH values of obtained samples were measured and presented in Table 2. AA content of strawberries grown in different types ranged between 54.46 mg/100 g (sawdust mulch) and 58 mg/100 g (agro-textile mulch). As seen in Table 2, AA content of agro-textile mulch (58 mg/100 gr) was found significantly higher ($P < 0.05$) than other mulch types. Moor et al., [41] has also reported AA content of strawberry 61 mg/100 g fw⁻¹, in plastic mulched parcels and 55 mg/100 g fw⁻¹ in straw mulched parcels.

As showed in Table 2, there was a significant difference ($P < 0.05$) between all mulch types in terms of TPC contents. The highest values were obtained from sawdust mulch (1820.60 mg GAE/kg fw). The highest DPPH value (5.21 µg/mL) (the lowest is EC₅₀) was found in agro-textile mulch, as same as AA. Mean DPPH value of sawdust mulch was found different and lower (4.56 µg/mL) than two other mulch types.

It is reported in the literature that, when strawberries grown with plastic mulch have higher anthocyanin content than the ones grown up with straw mulch due to high soil temperature [7, 41]. In our study, AA, TPC and DPPH content of fruits, grown in plastic mulched parcels were not significantly higher than sawdust mulched parcels. The reason is thought to be that, growing was conducted in summer months and therefore sawdust mulched parcels were also highly temperature.

Correlations. Extracts obtained from five different strawberry cultivars, grown in different mulch types, were analyzed and correlations between their antioxidant characteristics were presented in Table 3. Considering the results in Table 3, AA and TPC were positively correlated ($R^2 = 0.502$, $P < 0.01$), on the other hand, AA content and DPPH test results are negatively correlated ($R^2 = -0.547$, $P < 0.01$). Moreover a negative correlation was also found between DPPH and TPC ($R^2 = -0.839$, $P < 0.01$). This reveals the effect of total phenolic content in strawberries on

TABLE 1
Ascorbic acid (AA), total phenolic contents (TPC) and antioxidant activity (DPPH) in the five strawberry cultivars

Cultivar	AA (mg/100 gr fw)	TPC (mg GAE/kg fw)	EC ₅₀ (DPPH) (µg/mL)
Monterey	53.13 b	2109.06 c	4.32 b
Abion	58.82 c	1864.20 b	4.68 c
Aromas	53.51 b	1350.25 a	5.26 d
Camarosa	61.49 d	2140.45 c	3.76 a
Sweet Charlie	51.88 a	1306.33 a	6.87 e
Mean	55.77	1754.06	4.98

Values in the same column followed by a different small letter are significantly different ($P < 0.05$).

TABLE 2

Ascorbic acid (AA), total phenolic contents (TPC) and antioxidant activity (DPPH) in three mulch types

Mulch type	AA (mg/100 gr fw)	TPC (mg GAE/kg fw)	EC ₅₀ (DPPH) (µg/mL)
Black plastic	54.83a	1747.79b	5.16b
Agro-textile	58.00b	1693.80a	5.21b
Sawdust	54.46a	1820.60c	4.56a

Values in the same column followed by a different small letter are significantly different (P < 0.05).

TABLE 3

Correlations between ascorbic acid (AA), total phenol contents (TPC) and antioxidant activity (DPPH)

	AA (mg/100 gr fw)	TPC (mg GAE/kg fw)	EC ₅₀ (DPPH) (µg/mL)
AA	1	,502**	-,547**
TPC	,502**	1	-,839**
DPPH	-,547**	-,839**	1

** Correlation is significant at the 0.01 level (2-tailed).

TABLE 4

Correlations between ascorbic acid (AA), total phenolic content (TPC) and antioxidant activity (DPPH) of different strawberry cultivars

	Cultivar	AA (mg/100 gr fw)	TPC (mg GAE/kg fw)	EC ₅₀ (DPPH) (µg/mL)
AA	Monterey	1	-,627*	,757**
	Abion	1	-,389	,687*
	Aromas	1	-,535	,581*
	Camarosa	1	-,446	,166
	Sweet Charlie	1	-,494	-,203
TPC	Monterey	-,627*	1	-,615*
	Abion	-,389	1	-,292
	Aromas	-,535	1	-,010
	Camarosa	-,446	1	-,734**
	Sweet Charlie	-,494	1	-,118
DPPH	Monterey	,757**	-,615*	1
	Abion	,687*	-,292	1
	Aromas	,581*	-,010	1
	Camarosa	,166	-,734**	1
	Sweet Charlie	-,203	-,118	1

* Correlation is significant at the 0.05 level, ** 0.01 level.

TABLE 5

Correlations between ascorbic acid (AA), total phenol contents (TPC) and antioxidant capacity (DPPH) in different mulch types

	Mulch type	AA (mg/100 gr fw)	TPC (mg GAE/kg fw)	EC ₅₀ (DPPH) (µg/mL)
AA	Black plastic	1	,651**	-,759**
	Agro-textile	1	,537*	-,606**
	Sawdust	1	,621**	-,690**
TPC	Black plastic	,651**	1	-,766**
	Agro-textile	,537*	1	-,842**
	Sawdust	,621**	1	-,910**
DPPH	Black plastic	-,759**	-,766**	1
	Agro-textile	-,606**	-,842**	1
	Sawdust	-,690**	-,910**	1

* Correlation is significant at the 0.05 level, ** 0.01 level.

antioxidant activity. Indeed, it is reported in some studies that, plants total phenolic content is related with antioxidant activity [42].

Correlations of different strawberry cultivars, resulted from AA, TPC and DPPH test results, were presented in Table 4. Correlations between AA and TPC of cultivars were not found significantly different negatively, except Monterey cultivar ($R^2 = 0.627$, $P < 0.05$). On the correlations of AA and DPPH test results, a positive correlation was found between Monterey ($R^2 = 0.757$, $P < 0.01$), Albion ($R^2 = 0.687$, $P < 0.05$) and Aromas ($R^2 = 0.581$, $P < 0.05$) cultivars. Considering the correlation between TPC and DPPH test results, any significant negative correlation was not found, except Monterey ($R^2 = 0.615$, $P < 0.05$) and Camarosa ($R^2 = 0.734$, $P < 0.01$) (Table 4).

Positive correlation between AA and TPC contents in different mulch types and a negative correlation between AA and DPPH values was determined. There were negative correlations between TPC and DPPH test results in all mulch types as presented in Table 5.

CONCLUSIONS

The present study indicates that the strawberry cultivar Camarosa is an extremely rich source of ascorbic acid, total phenolic compounds and antioxidant capacity, demonstrating its potential use as a food additive.

Moreover, ascorbic acid content of agro-textile mulch was found higher than black plastic mulch and textile much while total phenolic content and antioxidant characteristics of sawdust mulch was found higher. Black plastic mulch was not found favorable in terms of characteristics determined in this study.

It was determined that, AA had a positive correlation with TPC test results and a negative correlation with DPPH test results. A negative correlation between TPC and DPPH test results was also determined.

ACKNOWLEDGEMENTS

This study was supported by Cukurova University Scientific Research Project Intuitional Unit (Project no: ZF2011D17). I would like to thank Assistant Professor Nilda Ersoy and Assistant Professor Sahlan Ozturk. This article is a part of doctoral dissertation by Sevinc Ates.

REFERENCES

[1] Nandwani, D. and Nwosisi, S. (2016) Organic Farming for Sustainable Agriculture. In: Nandwani, D. (Ed.) Global Trends in Organic

Agriculture. 9, International Publishing, Switzerland, 1-36.

- [2] Hakala, M., Lapvetelainen, A., Huopalahti, R., Kallio, H., and Tahvonon, R. (2003) Effects of varieties and cultivation conditions on the composition of strawberries. *Journal of Food composition and analysis*, 16(1), 67-80.
- [3] FAOSTAT (2015) Food and Agriculture Organization of the United Nations Cropping Database Production of Strawberry. (Accessed 15 March 2016). URL <http://faostat3.fao.org/download/Q/QC/E>.
- [4] TUIK (2015) Turkish Statistical Institute. Organic Crop Production. (Accessed 20 March 2016) URL. <http://www.turkstat.gov.tr/Ust-Menu.do?metod=temelist>
- [5] Oszmianski, J. and Wojdylo, A. (2009) Comparative study of phenolic content and antioxidant activity of strawberry puree, clear, and cloudy juices. *European Food Research and Technology*, 228(4), 623-631.
- [6] Kelebek, H. and Selli, S. (2011) Characterization of phenolic compounds in strawberry fruits by RP-HPLC-DAD and investigation of their antioxidant capacity. *Journal of Liquid Chromatography & Related Technologies*, 34(20), 2495-2504.
- [7] Anttonen, M.J., Hoppula, K.I., Nestby, R., Verheul, M.J., and Karjalainen, R.O. (2006) Influence of fertilization, mulch color, early forcing, fruit order, planting date, shading, growing environment, and genotype on the contents of selected phenolics in strawberry (*Fragaria x ananassa* Duch.) fruits. *Journal of Agricultural and Food Chemistry*, 54(7), 2614-2620.
- [8] Crespo, P., Bordonaba, J.G., Terry, L.A. and Carlen, C. (2010) Characterization of major taste and health-related compounds of four strawberry genotypes grown at different Swiss production sites. *Food Chemistry*, 122(1), 16-24.
- [9] Kafkas, E. (2016) Strawberry growing in Turkey: Current status and future prospects. *Proceeding of VIII th International Strawberry Symposium, Quebec, Canada. Acta Horticulturae*, 1156(2), 903-908.
- [10] Baran, M.F., Oguz, H.I., and Gokdogan, O. (2017) Determination of Energy Input-Output Analysis in Organic Strawberry Production. *Fresen. Environ. Bull.*, 26(3), 2076-2081.
- [11] Yasar, F., Uzal, O. and Yasar, O. (2016) Antioxidant Enzyme Activities and Lipidperoxidation Amount of Pea Varieties (*Pisum Sativum* Sp. *Arvense* L.) Under Salt Stress. *Fresen. Environ. Bull.*, 25(1), 37-42.
- [12] Birkeland, L., Doving, A., and Sonstebly, A. (2000) Yields and quality in relation to planting bed management of organically grown strawberry cultivars. *Proceeding of IV International*

- Strawberry Symposium, Tampere, Finland. 567(2), 519-522.
- [13] Plekhanova, M.N., and Petrova, M.N. (2000) Influence of black plastic soil mulching on productivity of strawberry cultivars in Northwest Russia. *Proceeding of IV International Strawberry Symposium, Tampere, Finland.* 567(2), 491-494.
- [14] Wang, S.Y., Zheng, W. and Galletta, G.J. (2002) Cultural system affects fruit quality and antioxidant capacity in strawberries. *Journal of Agricultural and Food Chemistry*, 50(22), 6534-6542.
- [15] Jin, P., Wang, S.Y., Wang, C.Y. and Zheng, Y. (2011) Effect of cultural system and storage temperature on antioxidant capacity and phenolic compounds in strawberries. *Food Chemistry*, 124(1), 262-270.
- [16] Skroch, W.A., Powell, M.A., Bilderback, T.E., and Henry, P.H. (1992) Mulches: durability, aesthetic value, weed control, and temperature. *Journal of environmental horticulture*, 10(1), 43-45.
- [17] Berglund, R., Svensson, B. and Gertsson, U. (2006) Impact of plastic mulch and poultry manure on plant establishment in organic strawberry production. *Journal of plant nutrition*, 29(1), 103-112.
- [18] De Jesus Ornelas-Paz, J., Yahia, E.M., Ramirez-Bustamante, N., Perez-Martinez, J.D., del Pilar Escalante-Minakata, M., Ibarra-Junquera, V., Acosta-Muniz, C., Guerrero-Prieto, V. and Ochoa-Reyes, E. (2013) Physical attributes and chemical composition of organic strawberry fruit (*Fragaria X ananassa* Duch, Cv. Albion) at six stages of ripening. *Food chemistry*, 138(1): 372-381.
- [19] Turemis, N., Kafkas, E., Zarifikhoshorahi, M., Birgili, B., Burgut, A. and Saygi H. (2016). Fruit quality characteristics of organically grown strawberry. *Proceeding of 3 rd International Symposium on Organic Greenhouse Horticulture, Izmir, Turkey.* 68.
- [20] Kafkas, E., Turemis, N., Birgili, B., Kafkas, S., Burgut, A. and Zarifikhoshorahi, M. (2016). Aroma profiles of organically grown Benicia and Albion strawberries. *Proceeding of VIII th International Strawberry Symposium, Quebec, Canada. Acta Horticulturae*, 1156(2), 703-708.
- [21] Kuroda, Y. and Hara, Y. (1999) Antimutagenic and anticarcinogenic activity of tea polyphenols. *Mutation Research/Reviews in Mutation Research*, 436(1), 69-97.
- [22] Muller, H., Bub, A., Watzl, B., and Rechkemper, G. (1999) Plasma concentrations of carotenoids in healthy volunteers after intervention with carotenoid-rich foods. *European journal of nutrition*, 38(1), 35-44.
- [23] Pearson, D.A. (1976) *Chemical analysis of foods*. 7th ed. Vol 1, Church Hill Livingstone, New York, 422-511.
- [24] Singleton, V.L. and Rossi, J.A. (1965) Colorimetry of total phenolics with phosphomolybdic-phosphotungstic acid reagents. *American journal of Enology and Viticulture*, 16(3), 144-158.
- [25] Blois, M.S. (1958) Antioxidant determinations by the use of a stable free radical. *Nature*, 181(4617), 1199-1200.
- [26] Yang, Z., Zheng, Y. and Cao, S. (2008) Effect of high oxygen atmosphere storage on quality, antioxidant enzymes, and DPPH-radical scavenging activity of Chinese bayberry fruit. *Journal of agricultural and food chemistry*, 57(1), 176-181.
- [27] Patras, A., Brunton, N.P., Da Pieve, S. and Butler, F. (2009) Impact of high pressure processing on total antioxidant activity, phenolic, ascorbic acid, anthocyanin content and colour of strawberry and blackberry purées. *Innovative Food Science & Emerging Technologies*, 10(3), 308-313.
- [28] Floegel, A., Kim, D.O., Chung, S.J., Koo, S.I. and Chun, O.K. (2011) Comparison of ABTS/DPPH assays to measure antioxidant capacity in popular antioxidant-rich US foods. *Journal of food composition and analysis*, 24(7), 1043-1048.
- [29] Huang, W.Y., Zhang, H.C., Liu, W.X. and Li, C.Y. (2012) Survey of antioxidant capacity and phenolic composition of blueberry, blackberry, and strawberry in Nanjing. *Journal of Zhejiang University-Science B*, 13(2), 94-102.
- [30] Wojdylo, A., Figiel, A. and Oszmiannski, J. (2009) Effect of drying methods with the application of vacuum microwaves on the bioactive compounds, color, and antioxidant activity of strawberry fruits. *Journal of agricultural and food chemistry*, 57(4), 1337-1343.
- [31] Pineli, L.D.L.D.O., Moretti, C.L., dos Santos, M.S., Campos, A.B., Brasileiro, A.V., Cordova, A.C., and Chiarello, M.D. (2011) Antioxidants and other chemical and physical characteristics of two strawberry cultivars at different ripeness stages. *Journal of Food Composition and Analysis*, 24(1), 11-16.
- [32] Samec, D., Maretic, M., Lugaric, I., Mesic, A., Salopek-Sondi, B. and Duralija, B. (2016) Assessment of the differences in the physical, chemical and phytochemical properties of four strawberry cultivars using principal component analysis. *Food chemistry*, 194, 828-834.
- [33] Tiwari, V., Maji, S., Kumar, S., Prajapati, G. and Yadav, R. (2016) Use of kitchen waste based bio-organics for strawberry (*Fragaria x ananassa* Duch) production. *African Journal of Agricultural Research*, 11(4), 259-265.
- [34] Gani, A., Baba, W.N., Ahmad, M., Shah, U., Khan, A.A., Wani, I.A., Masoodi, F.A. and

- Gani, A. (2016) Effect of ultrasound treatment on physico-chemical, nutraceutical and microbial quality of strawberry. *LWT-Food Science and Technology*, 66, 496-502.
- [35] Magalhaes, L.M., Segundo, M.A., Reis, S. and Lima, J.L. (2008) Methodological aspects about in vitro evaluation of antioxidant properties. *Analytica chimica acta*, 613(1), 1-19.
- [36] Mandave, P.C., Pawar, P.K., Ranjekar, P.K., Mantri, N. and Kuvalekar, A.A. (2014) Comprehensive evaluation of in vitro antioxidant activity, total phenols and chemical profiles of two commercially important strawberry varieties. *Scientia Horticulturae*, 172, 124-134.
- [37] Tekeli, Y., Sezgin, M. and Sanda, M.A. (2008) Determination of phenolic content and antioxidant effect of *Centaurea Pterocaula truatv.* in Konya Suleyman Demirel University Journal of Science, 3(1), 35-41.
- [38] Hernanz, D., Recamales, A.F., Melendez-Martinez, A.J., Gonzalez-Miret, M.L., and Heredia, F.J. (2007) Assessment of the differences in the phenolic composition of five strawberry cultivars (*Fragaria x ananassa* Duch.) grown in two different soilless systems. *Journal of agricultural and food chemistry*, 55(5), 1846-1852.
- [39] Wang, S.Y., and Millner, P. (2009) Effect of different cultural systems on antioxidant capacity, phenolic content, and fruit quality of strawberries (*Fragaria x ananassa* Duch.). *Journal of agricultural and food chemistry*, 57(20), 9651-9657.
- [40] Bordonaba, J.G., and Terry, L.A. (2010) Manipulating the taste-related composition of strawberry fruits (*Fragaria x ananassa*) from different cultivars using deficit irrigation. *Food Chemistry*, 122(4), 1020-1026.
- [41] Moor, U., Karp, K., Poldma, P. and Pae, A. (2005) Cultural systems affect content of anthocyanins and vitamin C in strawberry fruits. *European Journal of Horticultural Science*, 70, 195-201.
- [42] Schempp, H., Christof, S., Mayr, U. and Treutter, D. (2016) Phenolic compounds in juices of apple cultivars and their relation to antioxidant activity. *Journal of Applied Botany and Food Quality*, 89, 11-20.

Received: 01.11.2017
Accepted: 08.06.2017

CORRESPONDING AUTHOR

Sevinc Sener
University of Akdeniz
Vocational School of Technical Sciences
Antalya – TURKEY

E-mail: svncsener@gmail.com

COMPREHENSIVE REVIEWS ON ADVERSE HEALTH EFFECTS OF HUMAN EXPOSURE TO ENDOCRINE-DISRUPTING CHEMICALS

Hussein Kehinde Okoro^{1,2,*}, Julius Oluwafunso Ige², Oluyinka Ajibola Iyiola³, Sadanand Pandey¹, Isiaka Ayobamidele Lawal¹, Caliphs Zvinowanda¹, Catherine Jane Ngila¹

¹Analytical-Environmental and Membrane Nanotechnology Research Group, Department of Applied Chemistry, University of Johannesburg, P.O. Box 17011, Doornfontein 2028, Johannesburg, Republic of South Africa.

²Material and Environmental-Analytical Research Group, Department of Industrial Chemistry University of Ilorin, P.M.B. 1515, Ilorin, Nigeria.

³Cell Biology and Genetics Unit, Department of Zoology, University of Ilorin, P.M.B. 1515, Ilorin, Nigeria.

ABSTRACT

Endocrine disruption refers to the ability of chemicals or substances at a certain dose to interfere with hormonal systems in the body. This has brought genuine concern globally in recent years. Endocrine disruptive chemicals (EDCs) represent a serious health risk to human and wildlife and have the tendency to impact human health negatively. This review focuses on the health impact of EDCs. There is growing interest from researchers, scientists and standard organization across the globe on the possible health threat posed by endocrine disrupting chemicals (EDCs), which are substances we get exposed to on a daily basis in our environment, food, drinks and consumer products (creams, drugs, addictive, plastics, children toy etc.) that interfere with hormone biosynthesis, action resulting in a deviation from normal homeostatic control or reproduction and metabolism. Moreover, EDCs represent a broad class of molecules such as industrial chemicals and organo-chlorinated pesticides, plasticizers and plastics, fuels, and many more chemicals that are present in the environment or are in extensive use. This article focuses on making suggestions to broaden society knowledge of the health risk of EDCs, including enhancing increased basic and clinical research, invoking the precautionary principle, and advocating involvement of individual and scientific society stakeholders in communicating and implementing changes in public policy and awareness.

KEYWORDS:

Endocrine Disruptive Chemicals, Endocrine disruptor, DDTs, PCBs, Health impact

INTRODUCTION

The production of chemicals and their introduction into the environment is turning out to be

progressively on a worldwide premise because of urbanization and industrialization. Some of these chemicals act as endocrine disruptors as they disturb endogenous hormone signaling pathways. Endocrine disruptors are chemicals that at a certain dose can interfere with the body's endocrine system and produce adverse developmental, reproductive, neurological, and immune effects in both humans and wildlife. Some of different reviews indicate an association with cancer, diabetes, endometriosis and other ailments. There is confirmation that the rate of endocrine-related issue in people has expanded in recent years. Numerous causes underlie this pattern; however, confirmation is mounting that chemical exposure is involved. Close to 800 chemicals are known or suspected to be capable of interfering with hormone receptors, hormone synthesis or hormone conversion.

An extensive variety of substances, both natural and man-made, are thought to cause endocrine disruption, including dioxin and dioxin-like compounds, pharmaceuticals, polychlorinated biphenyls, organotin compounds, plasticizers such as bisphenol, DDT and other pesticides. Endocrine disruptors may be found in most of the products which we use every day including flame retardants, food, toys, plastic bottles, detergents, cosmetics, metal food cans, and pesticides [1]. The NIEHS studies help to determine whether exposure to endocrine disruptors may result in human health effects including male and female lowered fertility and an increased incidence of endometriosis and some cancers [2]. Research shows that endocrine disruptors may pose the greatest risk during prenatal and early postnatal development, when organ and neural systems are forming.

Endocrine disrupting chemicals (EDCs) and potential EDCs are usually man-made, discover in various materials such as additives or contaminants in food, pesticides, metals, and personal care products. EDCs have been suspected to be associated with altered reproductive function in males and females; increased incidence of breast cancer, ab-

normal growth patterns and neuro-development delays in children, as well as changes in immune function.

HISTORY OF ENDOCRINE DISRUPTORS

The first evidence of endocrine disruption was disclosed almost 40 year ago through observations of uncommon vagina adenocarcinoma in daughters born 15–22 year earlier to women treated with the potent synthetic estrogen Diethylstilboestrol (DES) during pregnancy [3]. The term endocrine disruptor was coined at the Wingspread Conference Centre in Wisconsin, in 1991. One of the early papers on the developmental effects of endocrine-disrupting chemicals in wildlife and humans was proposed by Colborn and co worker [4]. In the paper, she stated that environmental chemicals disrupt the development of the endocrine system, and that effects of exposure during development are often permanent. Although the endocrine disruption has been disputed by some, work sessions from 1992 to 1999 have generated consensus statements from scientists regarding the hazard from endocrine disruptors, particularly in wildlife and also in humans [5-8].

The Endocrine Society released a scientific statement outlining mechanisms and effects of endocrine disruptors on “male and female reproduction, breast development and cancer, prostate cancer, neuroendocrinology, thyroid, metabolism and obesity, and cardiovascular endocrinology,” and showing how experimental and epidemiological studies converge with human clinical observations “to implicate EDCs as a significant concern to public health.” The statement noted that it is difficult to show that endocrine disruptors cause human diseases, and it recommended that the precautionary principle should be followed [9]. A concurrent statement expresses policy concerns [10].

Endocrine disrupting compounds encompass a variety of chemical classes, including drugs, pesticides, compounds used in the plastics industry and in consumer products, industrial by-products and pollutants, and even some naturally produced botanical chemicals. Some are pervasive and widely dispersed in the environment and may bioaccumulate. Some are persistent organic pollutants (POP's), and can be transported long distances across national boundaries and have been found in virtually all regions of the world, and may even concentrate near the North Pole, due to weather patterns and cold conditions [11]. Others are rapidly degraded in the environment or human body or may be present for only short periods of time [12]. Health effects attributed to endocrine disrupting compounds include a range of reproductive problems (reduced fertility, male and female reproductive tract abnormalities, and skewed male/female sex ratios, loss of foetus, menstrual problems [13];

changes in hormone levels; early puberty; brain and behaviour problems; impaired immune functions; and various cancers.

TYPES OF EDCS

Endocrine disruptors are chemicals, or chemical mixtures, that interfere with normal hormone function. EDCs are highly heterogeneous [14] and can be classified in the following two ways.

1. They can be classified in two categories [10]:

- (i) Those that occur naturally
 - . Natural chemicals found in human and animal food (e.g. Phytoestrogen: genistein and coumestrol) and
 - (ii) Those that are synthesized. These can be further grouped as follows
 - Synthetic chemicals used as industrial solvents or lubricants and their by-products (e.g. polychlorinated biphenyls(PCBs), polybrominated biphenyls (PBBs), dioxins)
 - Plastics [e.g. bisphenol A (BPA), organotin compounds]
 - Plasticizers Pesticides [e.g. dichlorodiphenyltrichloroethane (DDT)]
 - Fungicide (e.g. vinclozolin) and some pharmaceutical agents [e.g. diethylstilboestrol (DES)].

2. The EDCs can also be grouped according to their origins [15]:

- (i) Natural and artificial hormones (e.g. fitoestrogens, 3-omegafatty acids, contraceptive pills and thyroid medicines).
- (ii) Drugs with hormonal side effects (e.g. naproxen, metoprolol and clofibrate).
- (iii) Industrial and household chemicals (e.g. Phthalates, alkylphenoletoxilate detergents, fire retardants, plasticizers, solvents, 1, 4-dichlorobenzene and polychlorinated bis-phenols (PCBs, organotin compounds).
- (iv) Side products of industrial and household processes (e.g. polycyclic aromatic hydrocarbons (PAHs), dioxins, pen-tachlorobenzene, organotin compounds).

Some other examples of putative EDCs are polychlorinated dibenzo-dioxins (PCDDs) and -furans (PCDFs), phenol derivatives and a number of pesticides (most prominent being organochlorine insecticides like endosulfan, Kepone (chlordecone) and DDT and its derivatives, the herbicide atrazine, and the fungicide vinclozolin), the contraceptive 17-alpha ethinylestradiol, as well as naturally occurring phytoestrogens such as genistein and mycoestrogens such as zearalenone [16]. Tributyltin (TBT) are organotin compounds that was used as a biocide in anti-fouling paint, commonly known as bottom paint [17,18].

TABLE 1
Some well-known EDCs and their uses
adapted from [19]

Category/Use	Example EDCs
Pesticides	DDT, chlorpyrifos, atrazine, 2,4-D, glyphosate, triphenyltins (TPT)
Children's products	Lead, phthalates, cadmium
Food contact materials	BPA, phthalates, phenol, organotin
Electronics and Building materials	Brominated flame retardants, PCBs
Personal care products, medical tubing	Phthalates
Antibacterial	Triclosan
Textiles, clothing	Perfluorochemicals
Product Cleaner	Fragrances, cyclosiloxanes
Surfactants-certain kinds of detergents used for removing oil and their metabolites	Nonylphenol (alkylphenols)
Contraceptive	Ethinyl estradiol (Synthetic steroid)

SELECTED EDCS IN THIS REVIEW ARTICLE

Organotin Compounds (OTCs). Tributyltin (TBT) are organotin compounds that was used as a biocide in anti-fouling paint, commonly known as bottom paint. TBT has been shown to impact invertebrate and vertebrate development, disrupting the endocrine system, resulting in masculinization, lower survival rates, as well as many health problems in mammals [17,18,20,21]. High toxicity of tri-substituted organotin (effects seen in the aquatic environment at $<1 \text{ ngL}^{-1}$)(R_3SnX) has led to the ban of organotin compounds as a marine antifouling under the international convention on the control of harmful antifouling systems on ships [1,22]. Basically, there are numerous effects of TBT which are well reported in organotin compounds produce various effects when aquatic life are exposed to these chemicals. These effects include; larva mortality, growth impairment, developmental and reproductive effects [1,17,22]. Among other effects of organotin compounds which includes immune toxicity, carcinogenicity etc. Apparently, TBT and TPT have reported to induce toxic effects in both male and female reproductive organs of rodents, these contaminants have been confirmed to cause tumors I organs of rodents and may results in endocrine disruption [23].

Recent studies have released a significant reduction by TBT along coastlines as well as the biological recovering of many marine species [24]. In a study carried out by Okoro and his co-workers on Cape Town harbour, organotin compounds were

detected in Cape Town harbour in both sediments and seawater samples [25]. The observed values recorded for TBT could be the result of an increase or decrease in traffics of ships and boats. Ship reparations is one of the reasons suggested for TBT detection in sediments samples [25]. Tributyltin has been demonstrated by Okoro and co-workers to have effects on the stability of hemocytic lysosome membrane of the mussel, (*Mytillus galloprovincialis*), they found out that the two exposed groups of mussels exhibited appreciably increased whole body TBT concentration with decreases in Neutral Red Retention (NRRT) for lower and higher exposure groups. NRRT assay was found useful in this study for early warning and cellular biomarker of stress due to TBT exposure in *Mytillus galloprovincialis* [26], a similar trend was reported in *Tapes philippinarum* and *Mytilus galloprovincialis* [27,28].

Dichloro-Diphenyl-Trichloroethane (DDT).

DDT was first used as a pesticide against Colorado potato beetles on crops beginning in 1936 [29]. An increase in the incidence of malaria, epidemic typhus, dysentery, and typhoid fever led to its use against the mosquitoes, lice, and houseflies that carried these diseases [29]. It became used worldwide to increase monoculture crop yields that were threatened by pest infestation, and to reduce the spread of malaria which had a high mortality rate in many parts of the world. As early as 1946, the harmful effects of DDT on bird, beneficial insects, fish, and marine invertebrates were seen in the environment. The most infamous example of these effects was seen in the eggshells of large predatory birds, which did not develop to be thick enough to support the adult bird sitting on them [30].

Further studies found DDT in high concentrations in carnivores all over the world, the result of biomagnification through the food chain [31]. Twenty years after its widespread use, DDT was found trapped in ice samples taken from Antarctic snow, suggesting wind and water are another means of environmental transport [32]. Recent studies show the historical record of DDT deposition on remote glaciers in the Himalayas [[33]. More than sixty years ago when biologists began to study the effects of DDT on laboratory animals, it was discovered that DDT interfered with reproductive development [34,35]. Recent studies suggest DDT may inhibit the proper development of female reproductive organs that adversely affects reproduction into maturity [36]. Additional studies suggest that a marked decrease in fertility in adult males may be due to DDT exposure [37]. Most recently, it has been suggested that exposure to DDT in utero can increase a child's risk of childhood obesity [38]. DDT is still used as anti-malarial insecticide in Africa and parts of South East Asia in limited quantities.

Polychlorinated Biphenyls (PCBs). Polychlorinated biphenyls (PCBs) are a class of chlorinated compounds used as industrial coolants and lubricants. PCBs are created by heating benzene, a by-product of gasoline refining, with chlorine [39]. They were first manufactured commercially by the Swann Chemical Company in 1927. In 1933, the health effects of direct PCB exposure were seen in those who worked with the chemicals at the manufacturing facility in Alabama. In 1935, Monsanto acquired the company, taking over US production and licensing PCB manufacturing technology internationally. General Electric (GE) was one of the largest US companies to incorporate PCBs into manufactured equipment. Between 1952 and 1977, the New York GE plant had dumped more than 500,000 pounds of PCB waste into the Hudson River. PCBs were first discovered in the environment far from its industrial use by scientists in Sweden studying DDT [40]. The effects of acute exposure to PCBs were well known within the companies who used Monsanto's PCB formulation who saw the effects on their workers who came into contact with it regularly. Direct skin contact results in a severe acne-like condition called chloracne [41]. Exposure increases the risk of skin cancer [42], liver cancer [43] and brain cancer [42,44]. Monsanto tried for years to downplay the health problems related to PCB exposure in order to continue sales [45]. The detrimental health effects of PCB exposure to humans became undeniable when two separate incidents of contaminated cooking oil poisoned thousands of residents in Japan and Taiwan [46], leading to a worldwide ban on PCB use in 1977.

Recent studies show the endocrine interference of certain PCB congeners is toxic to the liver and thyroid [47]; increases childhood obesity in children exposed prenatally [38] and may increase the risk of developing diabetes [48,49]. PCBs in the environment may also be related to reproductive and infertility problems in wildlife. In Alaska it is thought that they may contribute to reproductive defects, infertility and antler malformation in some deer populations. Declines in the populations of otters and sea lions may also be partially due to their exposure to PCBs, the insecticide DDT, other persistent organic pollutants. Bans and restrictions on the use of EDCs have been associated with a reduction in health problems and the recovery of some wildlife populations [50].

Polybrominated Diphenyl Ethers (PBDEs). Polybrominated diphenyl ethers (PBDEs) are a class of compounds found in flame retardants used in plastic cases of televisions and computers, electronics, carpets, lighting, bedding, clothing, car components, foam cushions and other textiles. Potential health concern: PBDE's are structurally very similar to Polychlorinated biphenyls (PCBs), and

have similar neurotoxic effects [51,52]. Research has correlated halogenated hydrocarbons, such as PCBs, with neurotoxicity [47]. PBDEs are similar in chemical structure to PCBs, and it has been suggested that PBDEs act by the same mechanism as PCBs [47]. In 1972, in response to this situation, the National Commission on Fire Prevention and Control was created to study the fire problem in the US. In 1973 they published their findings in *America Burning*. Most of the recommendations dealt with fire prevention education and improved building engineering, such as the installation of fire sprinklers and smoke detectors.

The Commission expected that with the recommendations, a 5% reduction in fire losses could be expected each year, halving the annual losses within 14 years. Historically, treatments with alum and borax were used to reduce the flammability of fabric and wood, as far back as Roman times [53]. Since it is a non-absorbent material once created, flame retardant chemicals are added to plastic during the polymerization reaction when it is formed. Organic compounds based on halogens like bromine and chlorine are used as the flame retardant additive in plastics, and in fabric based textiles as well.

The widespread use of brominated flame retardants may be due to the push from Great Lakes Chemical Corporation (GLCC) to profit from its huge investment in bromine. In 1992, the world market consumed approximately 150,000 tonnes of bromine-based flame retardants, and GLCC produced 30% of the world supply [54]. PBDEs have the potential to disrupt thyroid hormone balance and contribute to a variety of neurological and developmental deficits, including low intelligence and learning disabilities [54]. Many of the most common PBDE's were banned in the European Union in 2006 [54]. Studies with rodents have suggested that even brief exposure to PBDEs can cause developmental and behaviour problems in juvenile rodents [55] and exposure interferes with proper thyroid hormone regulation [56].

Phthalates. Phthalates are found in some soft toys, flooring, medical equipment, cosmetics and air fresheners. They are of potential health concern because they are known to disrupt the endocrine system of animals, and some research has implicated them in the rise of birth defects of the male reproductive system [57-59]. Although an expert panel has concluded that there is "insufficient evidence" that they can harm the reproductive system of infants [60], California [61] and Europe have banned them from toys. One phthalate, Bis(2-ethylhexyl) phthalate (DEHP), used in medical tubing, catheters and blood bags, may harm sexual development in male infants [58]. In 2002, the Food and Drug Administration released a public report which cautioned against exposing male babies to

DEHP. Although there are no direct human studies the FDA report states: "Exposure to DEHP has produced a range of adverse effects in laboratory animals, but of greatest concern are effects on the development of the male reproductive system and production of normal sperm in young animals. In view of the available animal data, precautions should be taken to limit the exposure of the developing male to DEHP [62]. Similarly; phthalates may play a causal role in disrupting masculine neurological development when exposed [57].

Perfluorooctanoic Acid. PFOA exerts hormonal effects including alteration of thyroid hormone levels. Blood serum levels of PFOA were associated with an increased time to pregnancy or "infertility. PFOA exposure is associated with decreased semen quality. PFOA appeared to act as an endocrine disruptor by a potential mechanism on breast maturation in young girls. A C8 Science Panel status report noted an association between exposure in girls and a later onset of puberty.

Bisphenol A (BPA). Of the approximately 85,000 chemicals in use, 1000 have been identified as having the ability to disrupt normal endocrine function. Exposure to endocrine disrupting chemicals (EDCs) during critical period in brain differentiation (prenatal and neonatal life) via the mother can alter the course of the development of sexually dimorphic behaviours. Bisphenol A (BPA) has estrogenic activity and is one of the most studied EDCs. Jones and co worker [63] review evidence from studies in rodents using dose levels relevant to human exposure. BPA alters behaviour and eliminates or in some cases reverses sexually dimorphic behaviours observed in unexposed animals.

Other Suspected Endocrine Disruptors. Some other examples of putative EDCs are polychlorinated dibenzo-dioxins (PCDDs) and -furans (PCDFs), polycyclic aromatic hydrocarbons (PAHs), phenol derivatives and a number of pesticides (most prominent being organochlorine insecticides like endosulfan, Kepone (chlordecone) and DDT and its derivatives, the herbicide atrazine, and the fungicide vinclozolin), the contraceptive 17-alpha ethinylestradiol, as well as naturally occurring phytoestrogens such as genistein and mycoestrogens such as zearalenone. The molting in crustaceans is an endocrine-controlled process. In the marine penaeid shrimp (*Litopenaeus vannamei*), exposure to endosulfan result increased susceptibility to acute toxicity and increased mortalities in the postmolt stage of the shrimp [64]. Many sunscreens contain oxybenzone, a chemical blocker that provides broad-spectrum UV coverage, yet is subject to a lot of controversy due its potential estrogenic effect in humans [18].

ROUTES OF EXPOSURE

Food is a major mechanism by which people are exposed to pollutants. Diet is thought to account for up to 90% of a person's PCB and DDT body burden [65]. In a study of 32 different common food products from three grocery stores in Dallas, fish and other animal products were found to be contaminated with PBDE [66]. Since these compounds are fat soluble, it is likely they are accumulating from the environment in the fatty tissue of animals which we eat. Some suspect fish consumption has a major source of many environmental contaminants. Indeed, both wild and farmed salmon from all over the world have been shown to contain a variety of man-made organic compounds [67].

With the increase in household products containing pollutants and the decrease in the quality of building ventilation, indoor air has become a significant source of pollutant exposure [68]. Residents living in homes with wood floors treated in the 1960s with PCB-based wood finish have a much higher body burden than the general population [69]. A study of indoor house dust and dryer lint of 16 homes found high levels of all 22 different PBDE congeners tested for in all samples [70]. Recent studies suggest that contaminated house dust, not food, may be the major source of PBDE in our bodies [71,72]. One study estimated that ingestion of house dust accounts for up to 82% of our PBDE body burden [73].

Consumer goods are another potential source of exposure to endocrine disruptors. An analysis of the composition of 42 household cleaning and personal care products versus 43 "chemical free" products was performed by [74]. The products contained 55 different chemical compounds: 50 were found in the 42 conventional samples representing 170 product types, while 41 were detected in 43 "chemical free" samples representing 39 product types. Parabens, a class of chemicals that has been associated with reproductive-tract issues, were detected in seven of the "chemical free" products, including three sunscreens that did not list parabens on the label.

Vinyl products such as shower curtains were found to contain more than 10% by weight of the compound DEHP, which when present in dust has been associated with asthma and wheezing in children. The risk of exposure to EDCs increases as products, both conventional and "chemical free," are used in combination. "If a consumer used the alternative surface cleaner, tub and tile cleaner, laundry detergent, bar soap, shampoo and conditioner, facial cleanser and lotion, and toothpaste would potentially be exposed to at least 19 compounds: 2 parabens, 3 phthalates, MEA, DEA, 5 alkylphenols, and 7 fragrances [74]. An analysis of the endocrine disrupting chemicals in old Mennonite women in mid-pregnancy determined that they

have much lower levels in their systems than the general population. Menonites eat mostly fresh, unprocessed foods, farm without pesticides, and use few or no cosmetics or personal care products. One woman who had reported using hairspray and perfume had high levels of monoethyl phthalate, while the other women all had levels below detection.

Three women who reported being in a car or truck within 48 hours of providing a urine sample had higher levels of diethylhexyl phthalate which is found in polyvinyl chloride, and is used in car interiors [75]. Additives added to plastics during manufacturing may leach into the environment after the plastic item is discarded; additives in micro plastics in the ocean leach into ocean water and in plastics in landfills may escape and leach into the soil and then into groundwater [76]. Esteban and co worker [77] determine the presence and origin of 30 substances of anthropogenic origin considered to be, or suspected of being, endocrine disruptors in the continental waters of the Antarctic Peninsula region.

HOW ENDOCRINE DISRUPTORS WORK

There are various mechanisms of ED action, one of which is their interference in the action of 11 β -hydroxysteroid dehydrogenase (11 β HSD) that maintains a balance between active and inactive glucocorticoids on the intracellular level. This enzyme has two isoforms and is expressed in various tissues. Inhibition of 11 β HSD in various tissues can have different consequences. Vitku and co worker [78] review on the effects of 11 β HSD inhibitors in the testis, colon, adipose tissue, kidney, brain and placenta. Clinical evidence, experimental models, and epidemiological studies suggest that EDC have major risks for human by targeting different organs and systems in the body. Multiple mechanisms are involved in targeting the normal system, through estrogen receptors, nuclear receptors and steroidal receptors activation. Maqbool and co worker [79] review summarize all evidence regarding different physiological disruptions in the body and possible involved mechanisms, to prove the association between endocrine disruptions and human diseases.

From animal studies, researchers have learned much about the mechanisms through which endocrine disruptors influence the endocrine system and alter hormonal functions.

HARMFUL EFFECTS OF ENDOCRINE DISRUPTORS ON HUMAN HEALTH

- Mimic or partly mimic naturally occurring hormones in the body like estrogens (the female sex hormone), androgens (the male sex hormone), and thyroid hormones as shown in Fig. 1B, potentially producing overstimulation.

- Bind to a receptor within a cell and block the endogenous hormone from binding. The normal signal then fails to occur and the body fails to respond properly. Examples of chemicals that block or antagonize hormones are anti-estrogens and anti-androgens.

- Fig. 1C explains the Interfering or blocking the way natural hormones or their receptors are made or controlled, for example, by altering their metabolism in the liver.

When absorbed in the body, an endocrine disruptor can decrease or increase normal hormone levels (left), mimic the body's natural hormones (middle), or alter the natural production of hormones (right).

Many endocrine-related diseases and disorders are on the rise [80-82], For example:

- Large proportions (up to 40%) of young men in some countries have low semen quality, which reduces their ability to father children.

- The incidence of genital malformations, such as non-descending testes (cryptorchidisms) and penile malformations (hypospadias), in baby boys has increased over time.

- Neurobehavioural disorders associated with thyroid disruption affect a high proportion of children in some countries.

- Global rates of endocrine-related cancers (breast, endometrial, ovarian, prostate, testicular and thyroid) have been increasing in past decade.

- The prevalence of obesity and type 2 diabetes has dramatically increased worldwide.

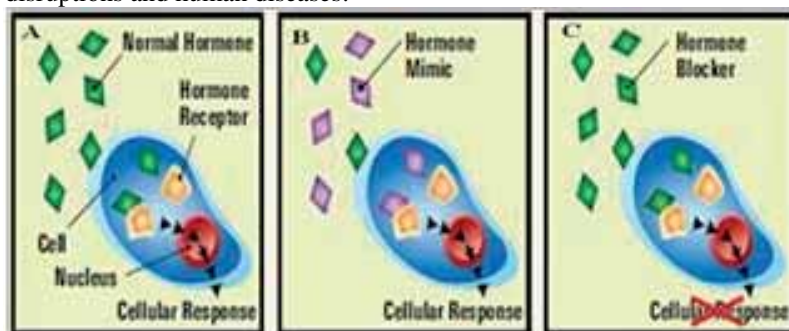


FIGURE 1
EDCs mechanisms

TABLE 2
Examples of EDC routes of exposures in humans

Exposure to EDCs	EDCs come from	EDC example(s)
Oral consumption of contaminated food or water	Industrial waste/ pesticides contaminating soil/ groundwater	PCBs, dioxins, perfluorinated compounds, DDT
Oral consumption of contaminated food or water	Leaching of chemicals from food/ beverage containers; pesticide residues in food/beverage	BPA, phthalates, chlorpyrifos, DDT
Contact with skin and/or inhalation	Household furniture treated with flame retardants	BFRs
Contact with skin and/or inhalation	Pesticides used in agriculture, homes/ for public disease vector control	DDT, chlorpyrifos, vinclozolin, pyrethroids
Intravenous	Intravenous tubing	Phthalates
Application to skin	Some cosmetics, personal care products, anti-bacterials, sunscreens, medications	Phthalates, triclosan, Parabens, insect repellants
Biological transfer from placenta	Maternal body burden due to prior/current exposures	Numerous EDCs can cross the placenta
Biological transfer from mother's milk	Maternal body burden due to prior/current exposures	Numerous EDCs are detected in milk

KEY: BFR: brominated flame retardant; BPA: bisphenol A; PCBs: polychlorinated biphenyls

EDCs are global and ubiquitous problem. People and animals are exposed to EDCs by a variety of routes (Table 2), including consumption of food and water, through the skin, by inhalation, and by transfer from mother to fetus (across the placenta) or mother to infant (via lactation) if a woman has EDCs in her body. Pregnant mothers and children are the most vulnerable populations to be affected by developmental exposures, and the effect of exposures to EDCs may not become evident until later in life. Research also shows that it may increase the susceptibility to non-communicable diseases. It was observed that increasing chemical production and use is related to the growing incidence of endocrine-associated paediatric disorders over the past 20 years, including male reproductive problems (cryptorchidism, hypospadias, and testicular cancer), early female puberty, leukaemia, brain cancer, and neurobehavioral disorders. Chemicals such as polychlorinated biphenyls (PCBs), BPA, and phthalates, are now detectable in serum, fat, and umbilical cord blood in humans around the globe.

One example of the consequences of the exposure of developing animals, including humans, to hormonally active agents is the case of the drug diethylstilbestrol (DES), a non-steroidal estrogen and not an environmental pollutant. Prior to its ban in the early 1970s, doctors prescribed DES to as many as five million pregnant women to block spontaneous abortion, an off-label use of this medication prior to 1947.

It was discovered after the children went through puberty that DES affected the development of the reproductive system and caused vaginal cancer. The relevance of the DES saga to the risks of exposure to endocrine disruptors is questionable, as the doses involved are much higher in these individuals than in those due to environmental exposures [83]. Aquatic life subjected to endocrine disruptors in an urban effluent have experienced decreased levels of serotonin and increased feminiza-

tion [84].

Childhood neuropsychiatric disorders are increasing in prevalence with as many as 1 in 6 children in the US now diagnosed with at least one [85]. These disorders include attention deficit hyperactivity disorder (ADHD) and Autism Spectrum Disorder (ASD), as well as depression and other mood disorders, learning disabilities, executive function deficits, and conduct disorders. PCBs have the strongest and longest-known associations with neurological disorders. In humans, there is evidence for impaired neurodevelopment [80,86], lower IQ, and problems with attention, memory, and fine motor skills such as writing. Similarly, polybrominated diphenyl ethers (PBDEs) are associated with reduced IQ, and other cognitive deficits [87]. PBDEs affect neurotransmitter activity, synaptic organization, and neuron viability suggesting that they impact not only brain development but also brain aging.

Brominated flame retardants, perfluorinated compounds, and pesticides (organophosphates such as chlorpyrifos and organochlorines), are linked to ADHD, ASD, and related learning disabilities [88]. Obesity rates are rising rapidly globally. Chemicals referred to as "Obesogens" are thought to enhance weight gain by altering or reprogramming key parts of the endocrine system governing metabolism, energy balance, and appetite, resulting in obesity and its related adverse health outcomes [89-92]. A brominated flame retardant, Firemaster 550, was shown to alter thyroid hormone levels in pregnant rats and their offspring, with the pups growing up to develop obesity, cardiac disease, early puberty and insulin resistance [93].

The increase in early puberty in girls, maybe attributed to many factors which includes; nutrition, stress, and ethnicity. Also, it may be due to exposures to estrogenic EDCs [94,95]. Such estrogenic compounds are also associated with uterine fibroids, ovarian dysfunction, and subfertility in humans and in animal models [96-98]. Several

chemicals, most notably phthalates, are associated with a variety of adverse effects on the male urogenital tract, including cryptorchidism, hypospadias, prostate disease and testicular cancer [99].

The list of known chemical carcinogens is long and includes metals [100,101], vinyl chloride, benzidine (used in dyes), solvents such as benzene, polycyclic aromatic hydrocarbons (PAHs), dioxins, fibers and dust (silica, asbestos, etc.), some pesticides including those on the Stockholm Convention's list of Persistent Organic Pollutants, and numerous pharmaceuticals including the synthetic estrogens. It was observed that estrogenic and other hormone-active chemicals such as BPA, phthalates and some pesticides, are thought to contribute to carcinogenic risk [102].

Vitku and co worker [78] reported the stimulatory effects of combined endocrine disruptors on MA-10 Leydig cell steroid production and lipid homeostasis. The author investigated direct effects and mechanisms of toxicity of Genistein (GEN) and plasticizer DEHP, MA-10 mouse tumor Leydig cells were exposed in-vitro to varying concentrations of GEN and MEHP, the principal bioactive metabolite of DEHP. The results suggest a deregulation of MA-10 Leydig function in response to a combination of GEN + MEHP. Hampl and co worker [103] provided the overview of the levels and sites at which endocrine disruptors (EDs) affect steroid actions. An important target for EDs is also steroid acute regulatory protein (StAR), responsible for steroid precursor trafficking to mitochondria. EDs influence receptor-mediated steroid actions at both genomic and non-genomic levels. This article is mainly focus on Endocrine disruptors & steroids.

Maqbool and co worker [79] reported the impact of environmental factors including the possible role of nutrition; stress and endocrine disruptors on the individual variations in pubertal timing and the possible underlying mechanisms. Estrogenic endocrine disruptors (EDs) were detected in 80% of 116 sports supplements investigated by biological in vitro reporter gene assays (RGAs). Palanza and co worker [104] quantify the hormonal activity in 50 of these sports supplement samples using a validated estrogen RGA and perform an exposure and risk assessment for human health. Palanza and co worker [104] investigated the highest activity samples presented a potential to influence the human daily exposure to 17 β -estradiol like activity in various risk groups with a predicted hormonal impact of greatest concern in young boys and postmenopausal women. Thus in conclusion, consumers of sports supplements may be exposed to high levels of estrogenic EDs.

Endocrine disruptors (EDs) are a class of environmental toxic molecules able to interfere with the normal hormone metabolism. Numerous studies involve EDs exposure to initiation and development of cancers, including prostate cancer. Bedia and co

worker [105] investigated three different EDs (aldrin, aroclor 1254 and chlorpyrifos (CPF)) were investigated as potential inducers of a malignant phenotype in DU145 prostate cancer cells after a chronic exposure. Epithelial to mesenchymal transition (EMT) induction, proliferation, migration, colony formation and release of metalloproteinase 2 (MMP-2) were analysed in 50-day exposed cells to the selected EDs. As a result, aldrin and CPF exposure led to an EMT induction (loss of 16% and 14% of E-cadherin levels, respectively, compared to the unexposed cells).

Aroclor and CPF presented an increased migration (134% and 126%, respectively), colony formation (204% and 144%, respectively) and MMP-2 release (137% in both cases) compared to the unexposed cells. Thus Bedia and co worker [105] concluded that some lipid compounds and lipid metabolic pathways could be involved in the acquisition of the malignant phenotype in exposed prostate cancer cells to the selected EDs. Milk and dairy products are a major component of our diet, thus it is important to monitor them for EDs. However, most methods developed to date are devoted to one group of compounds at a time. Wielogórska and co worker [106] described UHPLC/MS/MS method has been validated according to EC decision 2002/657/EC and allows simultaneous extraction, detection, quantitation and confirmation of 19 EDs in milk. This method facilitates fast, reliable, quantitative and confirmatory analysis of sub mg kg⁻¹ levels of a range of EDs in milk.

Corticoid hormonal function can be affected by endocrine disruption. For example, hexachlorobenzene induces oxidative stress, disruption of arachidonic acid metabolism and porphyria [107] PPAR α is present in liver and when associated with the presence of endocrine disruptors mainly causes the metabolic disorders [108]. PCBs reduce the thyroxin and thyroid stimulating hormone(TSH) in response to thyrotropin releasing hormone which result in hypothalamic and pituitary deregulation [19]. The diseases of female reproductive system that might be associated with EDC include precocious puberty, polycystic ovary syndrome and premature ovarian failure [109]. EDC may interfere with the hormonal regulation of menstruation cycle and thereby causing irregularities, such as long cycles which may reduce fecund ability (ability to conceive in a menstrual cycle) [109]. Certain EDC such as estrone (E₁), 17 β -estradiol (E₂), diethylstilbestrol (DES), nonylphenol (NP), octylphenol(OP), Biphenol A (BPA),dibutyl phthalate (DBP), and di-(2-ethylhexyl)phthalate (DEHP) was determined in lakes and rivers of Wuhan city, China [110]. Dun and co worker [111] establish the behavior and potential risks of phenolic endocrine disrupting chemicals in surface water and suspended particle matter of the Xiaohe river, north china plain , china.

In response to these concerns, WHO published

several publications, including the latest information on the subject in the State of the Science of Endocrine Disrupting Chemicals 2012, which was done in collaboration with UNEP and key scientific experts? A resolution to include EDCs as an emerging issue under Strategic Approach to International Chemicals Management (SAICM) which was adopted in September 2012 by the third International Conference on Chemicals Management (ICCM) in Nairobi during which WHO and UNEP jointly raised public awareness on EDC issues during a side-event and technical briefing session (partially supported by the National Institute of Environmental Health Sciences). Since endocrine disrupting chemicals (EDCs) are substantially diverse in character, vary widely in physical and chemical properties, how they are used, as well as how they exist in the environment, discussion of fate and transport is very difficult unless the chemicals are categorized in some manner [112].

CONCLUSION AND RECOMMENDATIONS

Daily use of chemicals is an essential part of modern society. Yet with the exponentially increased production and release of synthetic chemicals, an unwanted effect includes introduction of toxic and persistent substances into the environment. Today, humans and wildlife are constantly exposed to thousands of chemical residues, through air, food, and water. However, scientific information regarding the long-term effects of this chronic, low-dose exposure to complex mixtures of chemicals is very limited. The literature provides highlights and insights to the fate, history and health impact of EDCs on both human and wildlife. The overview was not meant to be an exhaustive review of the evidence, but rather a synthesis of the current knowledge in an ever-changing field of inquiry and discovery. Although there is current scientific, public, and governmental interest in the potential health risks of exposure to EDCs, the human evidence of EDCs with altered human and wildlife health endpoints remains limited and, in certain instances, inconsistent across studies. This highlights the need for further research on these classes of EDCs, more comprehensive testing methods are required to identify other possible endocrine disruptors, their sources, and routes of exposure, more scientific evidence is needed to identify the effects of mixtures of EDCs on humans and wildlife (mainly from industrial by-products) to which humans and wildlife are increasingly exposed, many sources of EDCs are not known because of insufficient reporting and information on chemicals in products, materials and goods, more data sharing between scientists and between countries can fill gaps in data, primarily in developing countries and emerging economies.

ACKNOWLEDGEMENTS

We would like to express our gratitude to the global excellence and stature (GES), National Research foundation (NRF) South Africa and University of Johannesburg (UJ) for financial support. The authors also acknowledge University of Johannesburg (UJ), (South Africa) for UJ Database and laboratory facility.

REFERENCES

- [1] Okoro, H.K, Fatoki, O.S, Adekola, F.A, Ximba, B.J, Snyman, R.G. Opeolu, B. (2011a) Human exposure, biomarkers, and fate of organotins in the environment. *Reviews of Environmental Contamination and Toxicology* Volume 213: Springer. pp. 27-54.
- [2] Crisp, T.M, Clegg, E.D, Cooper, R.L, Wood, W.P, Anderson, D.G. (1998) Environmental endocrine disruption: an effects assessment and analysis. *Environmental health perspectives* 106: 11.
- [3] Herbst, A.L, Ulfelder, H, Poskanzer, D.C. (1971) Adenocarcinoma of the vagina: association of maternal stilbestrol therapy with tumor appearance in young women. *New England journal of medicine* 284: 878-881.
- [4] Colborn, T, Vom Saal F.S, Soto, A.M. (1993) Developmental effects of endocrine-disrupting chemicals in wildlife and humans. *Environmental health perspectives* 101: 378.
- [5] Colborn, T. (1995) Statement from the work session on environmentally induced alterations in development: a focus on wildlife. *Environmental Health Perspectives*: 3-5.
- [6] Alleva, E, Brock, J, Brouwer, A, Colborn, T, Fossi, M. (1998) Statement from the work session on environmental endocrine-disrupting chemicals: Neural, endocrine and behavioural effects. *Toxicol Ind Health* 14: 1-8.
- [7] Colborn, T, Clement, C. (1992) *Chemically-induced alterations in sexual and functional development: the wildlife/human connection*: Princeton Scientific Pub. Co.
- [8] Rolland, R, Gilbertson, M, Peterson, R.E. (1997) *Chemically induced alterations in functional development and reproduction of fishes*. SETAC Press.
- [9] Short, P. (1999) Statement from the work session on health effects of contemporary-use pesticides: the wildlife/human connection. *Toxicology and Industrial Health* 15: 1-5.
- [10] Diamanti-Kandarakis, E, Bourguignon, J-P, Giudice, L.C, Hauser, R, Prins, G.S. (2009) *Endocrine-Disrupting Chemicals: An Endo-*

- crine Society Scientific Statement. *Endocrine Reviews* 30: 293-342.
- [11] Visser, M.J. (2007) *Cold, clear, and deadly*: Michigan State University Press.
- [12] Damstra, T, Barlow, S, Bergman, A, Kavlock, R, Van Der Kraak, G. (2002) *Global assessment of the state-of-the-science of endocrine disruptors*. Geneva: World Health Organization.
- [13] Harrison, P, Humfrey, C, Litchfield, M, Peakall, D, Shuker, L. (1995) *Environmental oestrogens: consequences to human health and wildlife*: Institute for Environment and Health.
- [14] Grun, F, Blumberg, B. (2009) Minireview: the case for obesogens. *Molecular Endocrinology* 23: 1127-1134.
- [15] Caliman, F.A, Gavrilesco, M. (2009) Pharmaceuticals, personal care products and endocrine disrupting agents in the environment—a review. *CLEAN—Soil, Air, Water* 37: 277-303.
- [16] Tumburu, L, Shepard, E.F, Strand, A.E, Browdy, C.L. (2012) Effects of endosulfan exposure and Taura Syndrome Virus infection on the survival and molting of the marine penaeid shrimp, *Litopenaeus vannamei*. *Chemosphere* 86: 912-918.
- [17] Okoro, H.K, Fatoki, O.S, Adekola, F.A, Ximba, B.J, Snyman, R.G. (2011b) Sources, environmental levels and toxicity of organotin in marine environment—a review. *Asian Journal of Chemistry* 23: 473.
- [18] Burnett, M.E, Wang, S.Q. (2011) Current sunscreen controversies: a critical review. *Photodermatology, photoimmunology & photomedicine* 27: 58-67.
- [19] Gore, A.C. (2010) Neuroendocrine targets of endocrine disruptors. *Hormones (Athens, Greece)* 9: 16.
- [20] Grun, F, Blumberg, B. (2006) Environmental obesogens: organotins and endocrine disruption via nuclear receptor signaling. *Endocrinology* 147: s50-s55.
- [21] Grün F, Watanabe H, Zamanian Z, Maeda L, Arima K, Cubacha R, Gardiner DM, Kanno J, Iguchi T, Blumberg B. (2006) Endocrine-disrupting organotin compounds are potent inducers of adipogenesis in vertebrates. *Molecular Endocrinology* 20: 2141-2155.
- [22] Bedia, C, Dalmau, N, Jaumot, J, Tauler, R. (2015) Phenotypic malignant changes and untargeted lipidomic analysis of long-term exposed prostate cancer cells to endocrine disruptors. *Environmental research* 140: 18-31.
- [23] Okoro, HK, Fatoki, OS, Adekola, FA, Ximba, BJ, Snyman, RG. (2014) Organotin Compounds, In Wexler, P. (Ed). *Encyclopedia of Toxicology*, 3rd edition. Vol 3 Elsevier Inc., Academic Press. pp. 720-725.
- [24] Langston, W, Pope, N, Davey, M, Langston, K, O'Har,a S. (2015) Recovery from TBT pollution in English Channel environments: A problem solved? *Marine pollution bulletin* 95: 551-564.
- [25] Okoro, HK, Fatoki, OS, Adekola, FA, Ximba, B.J, Snyman, R.G. (2016) Spatio-temporal variation of organotin compounds in seawater and sediments from Cape Town harbour, South Africa using gas chromatography with flame photometric detector (GC-FPD). *Arabian Journal of Chemistry, Elsevier*. 9: 95-104.
- [26] Okoro, HK, Snyman, RG, Fatoki, OS, Adekola, FA, Ximba, BJ, MY, Slabber. (2015) Lysosomal Membrane Stability of the Mussel, *Mytilus galloprovincialis* (L), as a Biomarker of Tributyltin exposure. *Bulletin Environmental Contamination and Toxicology, Springer Media*. 94(5): 609-613.
- [27] Pagliarani A, Bandiera P, Ventrella V, Trombetti F, Pirini M, Borgatti AR. (2006) Response to alkyltins of two Na⁺-dependent ATPase activities in Tapes philippinarum and *Mytilus galloprovincialis*. *Toxicology in vitro* 20: 1145-1153.
- [28] Fiorini R, Pagliarani A, Nesci S, Pirini M, Tucci E, Ventrella V. (2012) Structural and functional changes in gill mitochondrial membranes from the Mediterranean mussel *Mytilus galloprovincialis* exposed to tri- n- butyltin. *Environmental Toxicology and Chemistry* 31: 877-884.
- [29] Davis, K.S. (1971) *The Deadly Dust: The Unhappy History of DDT*: American Heritage Publishing Company, Incorporated.
- [30] Lundholm, C. (1997) DDE-induced eggshell thinning in birds: effects of p, p'-DDE on the calcium and prostaglandin metabolism of the eggshell gland. *Comparative Biochemistry and Physiology Part C: Pharmacology, Toxicology and Endocrinology* 118: 113-128.
- [31] Szlinder-Richert, J, Barska, I, Mazerski, J, Usydus, Z. (2008) Organochlorine pesticides in fish from the southern Baltic Sea: levels, bioaccumulation features and temporal trends during the 1995–2006 period. *Marine Pollution Bulletin* 56: 927-940.
- [32] Peterle, T.J. (1969) DDT in Antarctic snow. *Nature* 224: 620-620.
- [33] Daly, G.L, Wania, F. (2005) Organic contaminants in mountains. *Environmental science & technology* 39: 385-398.
- [34] Tauber, O.E, Hughes, A.B (1950) Effect of DDT Ingestion on Total Cholesterol Content of Ovaries Of White Rat.*. *Proceedings of the Society for Experimental Biology and Medicine* 75: 420-422.

- [35] Stoner, H. (1953) Effect of 2, 2-bis (Parachlorophenyl)-1, 1-Dichloroethane (DDD) on the Adrenal Cortex of the Rat. *Nature* 172: 1044-1045.
- [36] Tiemann, U. (2008) In vivo and in vitro effects of the organochlorine pesticides DDT, TCPM, methoxychlor, and lindane on the female reproductive tract of mammals: a review. *Reproductive Toxicology* 25: 316-326.
- [37] Hallegue, D, Rhouma, K.B, Tebourbi, O, Sakly, M. (2003) Impairment of testicular endocrine and exocrine functions after dieldrin exposure in adult rats. *Polish Journal of Environmental Studies* 12: 557-562.
- [38] Verhulst, S.L, Nelen, V, Den Hond, E, Koppen, G, Beunckens, C. (2009) Intrauterine exposure to environmental pollutants and body mass index during the first 3 years of life. *Environmental health perspectives* 117: 122.
- [39] Francis, E. (1994) Conspiracy of Silence: The story of how three corporate giants—Monsanto, GE, and Westinghouse—covered their toxic trail. *Sierra Magazine*.
- [40] Jensen, S. (1969) DDT and PCB in marine animals from Swedish waters. *Nature* 224: 247-250.
- [41] Tang, N-J, Liu, J, Coenraads, P, Dong, L, Zhao, L-J. (2008) Expression of AhR, CYP1A1, GSTA1, c-fos and TGF- α in skin lesions from dioxin-exposed humans with chloracne. *Toxicology letters* 177: 182-187.
- [42] Loomis, D, Browning, S.R, Schenck, A.P, Gregory, E, Savitz, D.A. (1997) Cancer mortality among electric utility workers exposed to polychlorinated biphenyls. *Occupational and Environmental Medicine* 54: 720-728.
- [43] Brown, D.P. (1987) Mortality of workers exposed to polychlorinated biphenyls—an update. *Archives of Environmental Health: An International Journal* 42: 333-339.
- [44] Sinks, T, Steele, G, Smith, A.B, Watkins, K, Shults, R.A. (1992) Mortality among workers exposed to polychlorinated biphenyls. *American journal of epidemiology* 136: 389-398.
- [45] Grunwald, M. (2002) Monsanto hid decades of pollution. *Washington Post* 1.
- [46] Organization, W.H. (1976) Environmental Health Criteria 2. Poly chlorinated biphenyls and terphenyls: United Nations Environment Programme/WHO, Geneva, Switzerland.
- [47] Kodavanti, P.R.S. (2005) Neurotoxicity of persistent organic pollutants: possible mode (s) of action and further considerations. *Nonlinearity in Biology, Toxicology, Medicine* 3: dose-response. 003.003. 002.
- [48] Uemura, H, Arisawa, K, Hiyoshi, M, Satoh, H, Sumiyoshi, Y. (2008) Associations of environmental exposure to dioxins with prevalent diabetes among general inhabitants in Japan. *Environmental research* 108: 63-68.
- [49] Mullerova, D, Kopecky, J, Matejkova, D, Muller, L, Rosmus, J. (2008) Negative association between plasma levels of adiponectin and polychlorinated biphenyl 153 in obese women under non-energy-restrictive regime. *International Journal of Obesity* 32: 1875-1878.
- [50] Organization, W.H. (2013) Effects of human exposure to hormone-disrupting chemicals examined in landmark United Nations report. *ScienceDaily*.
- [51] Daso, A.P, Fatoki, O.S, Odendaal, J.P, Olujimi, O.O. (2013) Polybrominated diphenyl ethers (PBDEs) and 2, 2', 4, 4', 5, 5'-hexabromobiphenyl (BB-153) in landfill leachate in Cape Town, South Africa. *Environmental monitoring and assessment* 185: 431-439.
- [52] Eriksson, P, Fischer, C, Fredriksson, A. (2006) Polybrominated diphenyl ethers, a group of brominated flame retardants, can interact with polychlorinated biphenyls in enhancing developmental neurobehavioral defects. *Toxicological Sciences* 94: 302-309.
- [53] Organization WH (1997) Flame retardants: a general introduction. *Environmental Health Criteria*.
- [54] Ether, D. (2008) Toxicological Review Of Decabromodiphenyl Ether (BDE-209).
- [55] Costa, L.G, Giordano, G. (2007) Developmental neurotoxicity of polybrominated diphenyl ether (PBDE) flame retardants. *Neurotoxicology* 28: 1047-1067.
- [56] Lema, S.C, Dickey, J.T, Schultz, I.R, Swanson, P. (2008) Dietary exposure to 2, 2', 4, 4'-tetrabromodiphenyl ether (PBDE-47) alters thyroid status and thyroid hormone-regulated gene transcription in the pituitary and brain. *Environmental health perspectives* 116: 1694.
- [57] Swan, S, Liu, F, Hines, M, Kruse, R, Wang, C. (2010) Prenatal phthalate exposure and reduced masculine play in boys. *International journal of andrology* 33: 259-269.
- [58] Fisher, J.S. (2004) Environmental anti-androgens and male reproductive health: focus on phthalates and testicular dysgenesis syndrome. *Reproduction* 127: 305-315.
- [59] Barrett, J.R. (2005) Phthalates and baby boys: potential disruption of human genital development. *Environmental health perspectives* 113: A542.
- [60] Kaiser, J. (2005) Panel finds no proof that phthalates harm infant reproductive systems. *Science* 310: 422-422.
- [61] Bette, H. (2007) California bans phthalates in

- toys for children. *Chemical and Engineering News* 12.
- [62] Feigal, D. (2002) PVC Devices Containing the Plasticizer DEHP. FDA Public Health Notification (12 July 2002).
- [63] Jones, S, Boisvert, A, Naghi, A, Hullin-Matsuda, F, Greimel, P. (2016) Stimulatory effects of combined endocrine disruptors on MA-10 Leydig cell steroid production and lipid homeostasis. *Toxicology* 355: 21-30.
- [64] Knobeloch, L, Turyk, M, Imm, P, Schrank, C, Anderson, H. (2009) Temporal changes in PCB and DDE levels among a cohort of frequent and infrequent consumers of Great Lakes sportfish. *Environmental research* 109: 66-72.
- [65] Fürst, P. (2006) Dioxins, polychlorinated biphenyls and other organohalogen compounds in human milk. Levels, correlations, trends and exposure through breastfeeding. *Molecular nutrition & food research* 50: 922-933.
- [66] Schechter, A, Pöpke, O, Tung, K-C, Staskal, D, Birnbaum, L. (2004) Polybrominated diphenyl ethers contamination of United States food. *Environmental science & technology* 38: 5306-5311.
- [67] Hites, R.A, Foran, J.A, Carpenter, D.O, Hamilton, M.C, Knuth, B.A. (2004) Global assessment of organic contaminants in farmed salmon. *Science* 303: 226-229.
- [68] Weschler, C.J. (2009) Changes in indoor pollutants since the 1950s. *Atmospheric Environment* 43: 153-169.
- [69] Rudel, R.A, Seryak, L.M, Brody, J.G (2008) PCB-containing wood floor finish is a likely source of elevated PCBs in residents' blood, household air and dust: a case study of exposure. *Environmental Health* 7: 2.
- [70] Stapleton, H.M, Dodder, N.G, Offenberg, J.H, Schantz, M.M, Wise, S.A. (2005) Polybrominated diphenyl ethers in house dust and clothes dryer lint. *Environmental science & technology* 39: 925-931.
- [71] Anderson, H.A, Imm, P, Knobeloch, L, Turyk, M, Mathew, J. (2008) Polybrominated diphenyl ethers (PBDE) in serum: findings from a US cohort of consumers of sport-caught fish. *Chemosphere* 73: 187-194.
- [72] Morland, K.B, Landrigan, P.J, Sjödin, A, Gobeille, A.K, Jones, R.S. (2005) Body burdens of polybrominated diphenyl ethers among urban anglers. *Environmental health perspectives*: 1689-1692.
- [73] Lorber, M. (2008) Exposure of Americans to polybrominated diphenyl ethers. *Journal of Exposure Science and Environmental Epidemiology* 18: 2-19.
- [74] Dodson, R.E, Nishioka, M, Standley, L.J, Perovich, L.J, Brody, J.G. (2012) Endocrine disruptors and asthma-associated chemicals in consumer products. *Environmental health perspectives* 120: 935.
- [75] Martina, C.A, Weiss, B, Swan, S.H. (2012) Lifestyle behaviors associated with exposures to endocrine disruptors. *Neurotoxicology* 33: 1427-1433.
- [76] Teuten, E.L, Saquing, J.M, Knappe, D.R, Barlaz, M.A, Jonsson, S. (2009) Transport and release of chemicals from plastics to the environment and to wildlife. *Philosophical Transactions of the Royal Society of London B: Biological Sciences* 364: 2027-2045.
- [77] Esteban, S, Moreno-Merino, L, Matellanes, R, Catalá, M, Gorga, M. (2016) Presence of endocrine disruptors in freshwater in the northern Antarctic Peninsula region. *Environmental research* 147: 179-192.
- [78] Vitku, J, Starka, L, Bicikova, M, Hill, M, Heracek, J. (2016) Endocrine disruptors and other inhibitors of 11 β -hydroxysteroid dehydrogenase 1 and 2: Tissue-specific consequences of enzyme inhibition. *The Journal of steroid biochemistry and molecular biology* 155: 207-216.
- [79] Maqbool, F, Mostafalou, S, Bahadar, H, Abdollahi, M. (2016) Review of endocrine disorders associated with environmental toxicants and possible involved mechanisms. *Life sciences* 145: 265-273.
- [80] Winneke, G. (2011) Developmental aspects of environmental neurotoxicology: lessons from lead and polychlorinated biphenyls. *Journal of the neurological sciences* 308: 9-15.
- [81] Porte, C, Janer, G, Lorusso, L, Ortiz-Zarragoitia, M, Cajaraville, M.P. (2006) Endocrine disruptors in marine organisms: approaches and perspectives. *Comparative Biochemistry and Physiology Part C: Toxicology & Pharmacology* 143: 303-315.
- [82] Giulivo, M, de Alda, M.L, Capri, E, Barceló, D. (2016) Human exposure to endocrine disrupting compounds: Their role in reproductive systems, metabolic syndrome and breast cancer. A review. *Environmental Research* 151: 251-264.
- [83] Golden, R.J, Noller, K.L, Titus-Ernstoff, L, Kaufman, R.H, Mittendorf, R. (1998) Environmental endocrine modulators and human health: an assessment of the biological evidence. *Critical reviews in toxicology* 28: 109-227.
- [84] Willis, I.C (2007) *Progress in Environmental Research*: Nova Science Publishers.
- [85] Boyle, C.A, Boulet, S, Schieve, L.A, Cohen, R.A, Blumberg, S.J. (2011) Trends in the prevalence of developmental disabilities in US children, 1997–2008. *Pediatrics* 127: 1034-1042.
- [86] Stein, J, Schettler, T, Wallinga, D, Valenti, M.

- (2002) In harm's way: toxic threats to child development. *Journal of Developmental & Behavioral Pediatrics* 23: S13-S22.
- [87] Dingemans, M.M, van den Berg, M, Westerink, R.H (2011) Neurotoxicity of brominated flame retardants:(in) direct effects of parent and hydroxylated polybrominated diphenyl ethers on the (developing) nervous system. *Environmental health perspectives* 119: 900.
- [88] De Cock, M, Maas, Y.G, van de Bor, M. (2012) Does perinatal exposure to endocrine disruptors induce autism spectrum and attention deficit hyperactivity disorders? Review. *Acta paediatrica* 101: 811-818.
- [89] Casals-Casas, C, Desvergne, B. (2011) Endocrine disruptors: from endocrine to metabolic disruption. *Annual review of physiology* 73: 135-162.
- [90] Grün, F, Blumberg, B. (2007) Perturbed nuclear receptor signaling by environmental obesogens as emerging factors in the obesity crisis. *Reviews in Endocrine and Metabolic Disorders* 8: 161-171.
- [91] Kirchner, S, Kieu, T, Chow, C, Casey, S, Blumberg, B. (2010) Prenatal exposure to the environmental obesogen tributyltin predisposes multipotent stem cells to become adipocytes. *Molecular endocrinology* 24: 526-539.
- [92] Baillie-Hamilton, P.F. (2002) Chemical toxins: a hypothesis to explain the global obesity epidemic. *The Journal of Alternative & Complementary Medicine* 8: 185-192.
- [93] Patisaul, H.B, Roberts, S.C, Mabrey, N, McCaffrey, K.A, Gear, R.B (2013) Accumulation and endocrine disrupting effects of the flame retardant mixture Firemaster® 550 in rats: an exploratory assessment. *Journal of biochemical and molecular toxicology* 27: 124-136.
- [94] Biro, F.M, Greenspan, L.C, Galvez, M.P, Pinney, S.M, Teitelbaum, S. (2013) Onset of breast development in a longitudinal cohort. *Pediatrics* 132: 1019-1027.
- [95] Mouritsen, A, Aksglaede, L, Sørensen, K, Mogensen, S.S, Leffers, H. (2010) Hypothesis: exposure to endocrine-disrupting chemicals may interfere with timing of puberty. *International journal of andrology* 33: 346-359.
- [96] Crain, D.A, Janssen, S.J, Edwards, T.M, Heindel, J, Ho, S-m. (2008) Female reproductive disorders: the roles of endocrine-disrupting compounds and developmental timing. *Fertility and sterility* 90: 911-940.
- [97] Jefferson, W.N, Patisaul, H.B, Williams, C. (2012) Reproductive consequences of developmental phytoestrogen exposure. *Reproduction: REP-11-0369*.
- [98] Newbold, R.R. (2008) Prenatal exposure to diethylstilbestrol (DES). *Fertility and sterility* 89: e55-e56.
- [99] Skakkebaek, N.E, Meyts, E.R, Main, K. (2001) Testicular dysgenesis syndrome: an increasingly common developmental disorder with environmental aspects. *Apmis* 109.
- [100] Titretir, S, Sakar, M.K. (2007) Determination of some metals in medicinal plants by flame atomic absorption spectrometry after different digestion procedures. *Fresen. Environ. Bull.* 16: 216-222.
- [101] Turner, E.A, Pye, C.C, Singer, R.D. (2003) Use of ab initio calculations toward the rational design of room temperature ionic liquids. *The Journal of Physical Chemistry A* 107: 2277-2288.
- [102] Soto, A.M, Sonnenschein, C. (2010) Environmental causes of cancer: endocrine disruptors as carcinogens. *Nature Reviews Endocrinology* 6: 363-370.
- [103] Hampl, R, Kubátová, J, Stárka, L. (2016) Steroids and endocrine disruptors—History, recent state of art and open questions. *The Journal of steroid biochemistry and molecular biology* 155: 217-223.
- [104] Palanza, P, Nagel, S.C, Parmigiani, S, vom Saal, F.S. (2016) Perinatal exposure to endocrine disruptors: sex, timing and behavioral endpoints. *Current opinion in behavioral sciences* 7: 69-75.
- [105] Bedia, A, Bedia, F.Z, Aillerie, M, Maloufi, N, Benyoucef, B. (2015) Morphological and Optical properties of ZnO thin films prepared by spray pyrolysis on glass substrates at various temperatures for integration in solar cell. *Energy Procedia* 74: 529-538.
- [106] Wielogórska, E, Elliott, C, Danaher, M, Chevallier, O, Connolly, L. (2015) Validation of an ultra high performance liquid chromatography–tandem mass spectrometry method for detection and quantitation of 19 endocrine disruptors in milk. *Food control* 48: 48-55.
- [107] Lelli, S.M, Ceballos, N.R, Mazzetti, M.B, Aldonatti, C.A, de Viale, L.C.S.M. (2007) Hexachlorobenzene as hormonal disruptor—studies about glucocorticoids: their hepatic receptors, adrenal synthesis and plasma levels in relation to impaired gluconeogenesis. *Biochemical pharmacology* 73: 873-879.
- [108] Feige, J.N, Gelman, L, Michalik, L, Desvergne, B, Wahli, W. (2006) From molecular action to physiological outputs: peroxisome proliferator-activated receptors are nuclear receptors at the crossroads of key cellular functions. *Progress in lipid research* 45: 120-159.
- [109] Costa, E.M.F, Spritzer, P.M, Hohl, A, Bachega, T.A (2014) Effects of endocrine

- disruptors in the development of the female reproductive tract. *Arquivos Brasileiros de Endocrinologia & Metabologia* 58: 153-161.
- [110] Xue, X, Wu, F, Zhang, X, Deng, N. (2008) Occurrence of endocrine disrupting compounds in rivers and lakes of Wuhan City, China. *Fresen. Environ. Bull.* 17: 203.
- [111] Dun, Y, Tang, C, Zhang, Y. (2014) Characteristics, behavior and potential risks of phenolic endocrine-disrupting chemicals in surface water and suspended particle matter of the Xiaohe River, North China Plain, China. *Fresen. Environ. Bull.* 23: 620-629.
- [112] Organization, W.H. (2012) *State of the Science of Endocrine-Disrupting Chemicals*. Geneva: International Programme on Chemical Safety.

okoroowo@yahoo.com

Received: 12.01.2017
Accepted: 10.03.2017

CORRESPONDING AUTHOR

Hussein Kehinde Okoro

Analytical-Environmental and Membrane Nanotechnology Research Group, Department of Applied chemistry, University of Johannesburg, P.O. Box 17011, Doornfontein 2028, Johannesburg, Republic of South Africa.

E-mail: hkoadeola@gmail.com;

OVERVIEW OF PEST MANAGEMENT PRACTICES IN TURKISH FOOD PROCESSING FACILITIES

Eyyup Mennan Yildirim^{1,*}, Ayse Demet Karaman², Huseyin Yerlikaya³

¹Department of Agricultural Biotechnology, College of Agriculture, Adnan Menderes University, Aydın, Turkey.

²Department of Dairy Technology, College of Agriculture, Adnan Menderes University, Aydın, Turkey.

³Sultanhisar Vocational School, Adnan Menderes University, Aydın, Turkey.

ABSTRACT

This study analyzes the effectiveness of and confidence in pest management practices and systems in Turkish food processing facilities. Results suggest that most of the food facilities had sufficient infrastructure, kept significantly reliable pest practices records, and were knowledgeable about pest applications. However, when it came to sanitation practices, some facilities had less hygienic pest management practices and development. Our findings suggest that facility infrastructure and sanitation practices, as well as employing pest management operators, are important in the successful adoption and implementation of efficient pest management in food facilities. Accordingly, Turkish food safety management training programs, especially in different processing facilities, should maximize the efficacy of pest management practices.

KEYWORDS:

Food safety, pest management, food facility, Turkey.

INTRODUCTION

Food-borne illnesses are persistent problems worldwide, causing both morbidity and mortality. The US Centers for Disease Control and Prevention (CDC) estimates that 1 in 6 Americans gets sick, 128,000 people are hospitalized, and 3,000 people die from by consuming contaminated foods or beverages each year [1]. Similarly, the US Department of Agriculture estimates that food-borne illnesses cost the US \$10-83 billion each year [2,3]. Contamination can come from many food sources, harmful chemicals, and insect infestations [4]. Accordingly, many federal governments are trying to reduce food-borne illnesses by improving the safety of their food supplies [5]. In September 2016, the US Food and Drug Administration (FDA) passed the Preventative Controls for Human Food rule, which includes an analysis of hazards and risk-based preventative controls, as well as a rigorous pest management program with increased documentation [1]. Similarly, to address food safety concerns the Turkish government has required food-processing facili-

ties to implement food safety management systems (FSMSs), such as the internationally recognized risk-based Hazard Analysis Critical Control Points (HACCP) system. This requirement likewise encourages facilities to follow prerequisite programs (PRPs) such as Good Hygiene Practices (GHPs) or Good Manufacturing Practices (GMPs), which are the foundation of HACCP.

European Union food law incorporated HACCP principles in the early 1990s, and added enhanced regulations in 2004. Turkey, in its bid for EU inclusion, integrated European legislative requirements on food hygiene within Turkish Law 5996, which mandates the implementation and maintenance of an HACCP system for all food businesses. Other food and quality standards such as the International Food Standards (IFS) and the British Retail Consortium Food Standard (BRC), classified under the International Organization for Standardization (ISO) as policy ISO 22000:2005, are applied voluntarily in Turkey, although the government promotes food safety implementation and certification. According to Law 5996, the ultimate responsibility for food safety lies with a business. Each business has a legal and ethical duty to apply a food safety system based on risk assessment and HACCP, to produce safe food and to protect consumer health [6,7]. Prior to designing a HACCP plan, food producers are expected to demonstrate ongoing compliance with GMPs, GHPs, and Turkish regulations on sanitation and pest management, as named prerequisite programs [8]. Within this legal context, it is critical that all food processing facilities have effective sanitation programs and infrastructure to implement risk-based HACCP programs and pest management practices.

Food contamination caused by pests is more widespread than most people think. Often times consumers' stomach problems and mild illnesses can be avoided if food is properly handled and stored to protect against pests [9]. Food facilities are typically large, complex structures with many locations vulnerable to insect infestation. They differ from each other in function (e.g., warehouse, mill, food processing), commodity (e.g., cereals, animal-based materials, spices), product generated (e.g., flour, whole grain, human food or pet food), structure type (e.g., old or new, construction mate-

rial), equipment, geographic location, and surrounding landscape, among other factors. This makes generalizations about pest management difficult [10].

Pests can be kept out by using effective Integrated Pest Management (IPM) as part of a food facility's sanitation and prerequisite programs. IPM has basic rules designed to prevent pests' access to the establishment, and to deny them food, water and a place to hide or nest. These facilities should also partner with licensed and qualified pest management professionals called Pest Control Operators (PCOs), in order to ensure that their products are pest-free [10,11,1]. However, the direct impact of Pest Control Operators (PCOs) on pest management in food processing facilities is not well-understood, especially in terms of how collaboration with a PCO may impact the overall PRPs and effectiveness of a facility's pest management program. Improving this understanding may encourage facility managers to adopt sanitation and prerequisite programs.

The aim of this study was to evaluate and determine the level of general practice at different kinds of food facilities in western Turkey, including those focusing on dried vegetables & fruits, catering, table olive/vegetable oil, dairy, and baked goods, focusing on the professional pest management service they have received. To our knowledge, this is the first survey of food facility handling practices in Turkey and in the broader field. The results from this study will support food facilities and pest control operators, by providing information about what influences the effective implementation of a pest management and food safety program.

MATERIALS AND METHODS

Data collection. This study surveyed food processing facilities with current production licenses from the Aydın Local Food, Agriculture, and Livestock Organization, all of which are located in Aydın, in western Turkey. All 112 food processing facilities in the region were visited, and data was collected via in-plant observations by members of the research team and 30-45 minute oral interviews with the pest manager. The observations all used a standardized questionnaire, described below. One observation and one interview were conducted at each facility, between February and July 2016.

Documentation design. A questionnaire was developed with a total of 57 questions, divided into five category sections, relating to the facility, its pest management sanitation programs, and its managers' knowledge. Five-point Likert scales were used to score the answers: Strongly Agree = 5, Agree = 4, Neither Agree nor Disagree = 3, Disa-

gree = 2, and Strongly Disagree = 1 (for agreements) or Always = 5, Often = 4, Sometimes = 3, Rarely = 2, and Never = 1 (for frequency). The first section (9 questions) consisted of general questions about the facility's demographic structure, including food safety certifications, number of employees, legal structure, and basic pest management data. The second section (13 questions) evaluated the facility's documentation practices in pest management. The third section (20 questions) related to elements of the facility's structure which affect effective pest management. The fourth section (14 questions) dealt with hygiene practices which could be important in implementing the facility's PRPs. These four sections were related to observers' suggestions. Finally, for the last question the observers asked facility managers about barriers they encountered in implementing the facility's pest management systems.

TABLE 1
Demographics of food facilities (n=112)

<i>Variables</i>	<i>n</i>	<i>%</i>
Age of facility (years)		
- 1-10	66	58.9
- 11-20	28	25.0
- 20-30	10	8.9
- More than 30	8	7.1
Facility's legal structure		
- Joint-stock company	12	10.7
- Limited	34	30.4
- Private	66	58.9
Food sector		
- Dried vegetables & fruits	21	18.8
- Catering	30	26.8
- Table olive/vegetable oil	18	16.1
- Baked goods	37	33.0
- Milk and milk products	6	5.4
Number of employees		
- 1-50	101	90.2
- 51-100	5	4.5
- 101-150	1	0.9
- More than 150	5	4.5
Years of experience of interviewed personnel		
- 0-5	59	52.7
- 6-10	24	21.4
- 11-15	14	12.5
- 16-20	5	4.5
- More than 20	10	8.9
FSMS Certificate		
- None	72	64.3
- ISO 22000	28	25.0
- ISO 9001	9	8.0
- BRC	2	1.8
- Other	1	0.9
IPM application in facility		
- Yes	82	73.2
- No	30	26.8
Outsourced IPM service		
- Yes	99	88
- No	13	11
License		
- Yes	99	88
- No	13	11

Data analysis. All the data were analyzed with SPSS for Windows (Version 16.0, SPSS Inc,

Chicago, IL). Descriptive statistics were computed, including frequencies and standard deviations. Cronbach's alpha was used to determine construct validity [13], and a threshold of 0.70 was used to demonstrate consistency.

RESULTS

Characteristics of respondents. The demographic characteristics of the surveyed food processing facilities are described in Table 1. Overall, most of the food processing facilities were 1-20 years old (83.9%) and had 1-50 employees (90.2%). These facilities represented five different food sectors: dried vegetables & fruits, catering, table olive/vegetable oil, baked goods, and dairies. While 72 food facilities don't have any management system applications such as ISO 9001, ISO 22000, or BRC, most (73.2%) had some sort of Integrated Pest Management (IPM) application. Although this IPM implementation percentage is high, 88% of the facilities outsourced the service.

Pest management documentation and practices. Table 2 characterizes observations related to pest management documentation and practices at the surveyed facilities. Overall, most facilities scored above 70% ("agree" and "strongly agree")

on all the measures. Specifically, almost 90% of food facilities had detailed reporting, material safety data sheets (MSDS), and complete documentation of all pest activities in their files. This could be because the pest management operators had licenses and worked in food facilities. As predicted, 93.8% of food facilities "agree" and "strongly agree" that they had licensed pest management operators. However, 13.4% of facilities, the highest negative score in the results, did not show all their traps in their monitoring maps. 22.3% had a neutral score ("neither agree nor disagree") regarding emergency plans for pest infestations or pest findings.

Facility infrastructure scores. Table 3 presents observations about specific pest management practices. Scores related to facility infrastructure average more than 80%, and generally relate to preventing animals and pests from entering the facility and to avoiding food contamination. The lowest positive scores relate to closed spaces, slots and blanks (35.7%), and to inappropriate in-facility storage of pest chemicals (43.8%). However, it is interesting that the question related to closed spaces had a high percentage (58.0%) of neutral responses. The question about preventing rodent climbing also had a fairly high neutral score, 26.8%. Similarly, 48.2% of facilities demonstrated inappropriate in-plant storage of pest chemicals.

TABLE 2
Observations regarding pest management documentation and practices (n=112).

Variable	Standard deviation	Reliability	Strongly disagree %	Disagree %	Neither agree nor disagree %	Agree %	Strongly agree %
1 Pest management operator has a license and it involves food facilities.	0.85		2.7	1.8	1.8	27.7	66.1
2 Material safety data sheet (MSDS) is sufficient.	0.87		3.6	0	3.6	32.1	60.7
3 All traps are shown in monitoring maps.	1.24	0.95	6.3	7.1	15.2	19.6	51.8
4 If pheromones and pest traps with lights are used in the facility, they are effectively controlled (e.g. date control)	1.09		4.5	2.7	14.3	19.6	58.9
5 Feeding traps (stations) are durable, resistant, and steady, and also located to protect food from contamination.	1.02		4.5	1.8	10.7	26.8	56.3
6 Responsible staff has sufficient experience in pest management.	0.86		1.8	1.8	11.6	40.2	44.6
7 Pest management practices are detailed in reports.	0.80		1.8	0.9	6.3	35.7	55.4
8 Emergency plans are in place for pest infestation and pest findings.	1.00		1.8	6.3	22.3	30.4	39.3
9 The facility has sufficient training/information related to pest management.	1.02		1.8	8.0	17.0	33.0	40.2
1 All corrective actions related to pest management are documented and recorded.	0.85		1.8	1.8	8.9	38.4	49.1
1 Top management supports pest management.	0.78		1.8	0	8.0	40.2	50.0
1 All pest activities are documented completely in the file.	0.75		1.8	0	5.4	37.5	55.4
1 Pest activities are monitored and pest management practices/activities are reported periodically to top management.	0.96		1.8	2.7	17.0	24.1	54.5

TABLE 3
Observations related to facility infrastructure and pest management (n=112).

Variable	Standard deviation	Reliability	Strongly disagree %	Disagree %	Neither agree nor disagree %	Agree %	Strongly agree %
1 Pest chemicals are stored in warehouse in-plant.	0.79		2.7	1.8	5.4	51.8	38.4
2 During pest management practices, preventative actions for food, food making surfaces and food packaging are adequate.	0.74		1.8	0	6.3	52.7	39.3
3 Pest chemicals are not stored appropriately in-plant.	1.49		32.1	16.1	8	18.8	25
4 Insect screens on doors, windows, and ventilation are sufficient.	0.82	0.94	1.8	6.3	14.3	41.1	36.6
5 Facilities are well kept and durable to prevent pest entry.	0.82		1.8	2.7	12.5	49.1	33.9
6 Drainage and ports are insulated.	0.75		1.9	0.9	9.8	54.5	33.0
7 Food in storage does not contact the floor or wall.	0.81		1.8	1.8	2.7	51.8	42.0
8 Preventative actions are taken in-plant related to pest nidus/slots.	0.88		1.8	2.7	4.5	54.5	36.6
9 All spaces 0.6 cm or wider are closed (e.g., door strips, ventilators)	0.81		1.8	0.9	12.5	48.2	36.6
0 Rodent climbing prevention actions are adequate.	0.93		1.8	1.8	26.8	36.6	33.0
1 When not in use, all doors and windows are closed.	0.92		4.5	1.8	2.7	33.9	57.1
1 If windows are open, they have swatters.	0.91		1.8	5.4	9.8	40.2	42.9
2 Door strips have skirts and combs.	1.24		4.5	18.8	23.2	26.8	26.8
3 Entries to plants have PVC bands and/or air curtains.	1.13		3.6	15.2	10.7	34.8	35.7
4 All spaces, slots, and blanks are closed.	0.76		0	6.3	58.0	33.9	1.8
5 There are spaces between storage floor and wall, and there is a hole straight to the wall.	0.79		1.8	0	8.9	44.6	44.6
6 There are no wreck yards or junk on the outdoor facility grounds.	1.06		7.1	5.4	2.7	35.7	49.1
7 Warehouses are clean and have no pests or animals.	1.02		4.5	4.5	4.5	49.1	37.5
8 Preventative actions to keep pests away from food preparation, handling, and storage places.	0.82		1.8	0.9	3.6	32.1	61.6
9 If storage is outside the plant, materials are protected from weather conditions and pest infestation.	0.81		2.7	0	10.7	41.1	45.5

Facility sanitation practices (Table 4). Most of the facilities scored highly on sanitation practices related to effective pest management: the “often” and “always” scores typically totaled above 80%, while the “never” score ranged from 0.9% to 3.6%. The highest average score was for “food particles

cleaned off floor and floor mopped” at 93.8%. However, 25% of facilities only sometimes performed deep cleaning or cleaned “invisible spots” (e.g. closets, behind machines & stands) on a daily basis.

TABLE 4
Observations related to hygiene practices and pest management (n=112).

Variable	Standard deviation	Reliability	Never %	Rarely %	Sometimes %	Often %	Always %
1 Food particles cleaned off floor and floor mopped.	0.71		0.9	0.9	4.5	38.4	55.4
2 Clean greasy surfaces.	0.73		0.9	0.9	7.1	46.4	44.6
3 Invisible spots, closets, & areas behind machines and stands cleaned daily.	0.94	0.89	0.9	5.4	25.0	34.8	33.9
4 Deep cleaning is important.	0.93		0.9	3.6	25.0	33.0	37.5
5 Outlets cleaned.	0.94		0.9	6.3	25.9	36.6	30.4
6 Dead birds, mice, or rats thrown away.	1.17		3.6	11.6	4.5	24.1	56.3
7 Residual dirtiness in equipment cleaned.	0.87		0.9	3.6	13.4	38.4	43.8
8 Cleaning equipment (e.g. brooms, mops) left clean when not in use, and stored upside-down.	0.85		0.9	1.8	14.3	33.0	50.0
9 Trash bags used, and full bags thrown in a designated dumpster.	0.92		3.6	0	8.9	33.9	53.6
0 Dumpster emptied at least weekly.	0.70		0.9	0	6.3	35.7	57.1
1 Garbage containers are washed out and area around dumpsters are mopped during every cleaning session.	1.09		2.7	6.3	23.2	23.2	44.6
1 External packaging, boxes, etc. removed directly from production area.	0.72		0.9	0	9.8	47.3	42.0
2 All outdoor areas cleaned.	0.94		2.7	4.5	13.4	47.3	32.1
3 When pests or infestations are found, all hygienic practices and operations used to eliminate the hazard are determined and recorded.	1.07		2.7	8.9	11.6	35.7	41.1

Barriers to pest management. Table 5 characterizes managers' opinions about barriers to effective pest management practices in their facilities. These opinions are analyzed relative to significance level. The data indicate that managers believed that a lack of facility infrastructure is the main barrier to improvement (2.96), though some managers also cited other reasons related to the pest management operators (1.83).

TABLE 5
Barriers to implementing pest management systems, according to facility managers(n=112).

<i>Variable</i>	<i>Significance level (Mean±Std.Deviation)^a</i>
Lack of knowledge of staff	2.63±1.0
Lack of budget	2.59±1.1
Lack of infrastructure in facility	2.96±0.9
Other reasons related to pest management operators	1.83±1.2

^a Answer options range from 1 (not important) to 4 (important).

Limitations of the study. Because the population of this study consisted of food facilities in Aydın, the results should not be generalized to all food facilities in Turkey. Another limitation is related to study participation: some of the food processing facilities did not want to respond to the questionnaire or to allow us to visit their indoor facilities.

DISCUSSION

Our study investigated whether the surveyed food facilities used effective pest management practices. We found that although most of the food facilities were less than 20 years old and were privately owned, they typically had established integrated pest management (IPM) practices (73.2%, Table 1). The presence of IPM did not vary by food sector diversity or by whether the facility had other food or quality management system practices in place. High levels of IPM application in food facilities (82%) are related to Turkish governmental regulations, which require preventative pest infections to be effective during the food safety chain (8). Additionally, almost all facilities had outsourced and licensed their IPM services (99%). This could be due to legal regulations involving public health and pest management services. Turkish law requires that pest management services have a license from the Turkish Ministry of Health [14].

HACCP requires consistent documentation and record keeping [25]. This supports a transparent system and enables government, auditors, and certification authorities to evaluate food safety in that business, which increases consumer and market confidence in the plant's products [26]. Turkish Law 5996 stipulates that food facilities document

their activities related to hygiene rules, risk assessments, and traceability for critical control points and food, and for pest monitoring [6]. Our results indicated that almost 90% of food facilities had consistent documentation and record-keeping in their facilities related to pest management practices (Table 2). Additionally, 93.8% of food facilities had pest management operators with licenses. A pest control operator (PCO) is a vital team member in any effective pest management program [12], and their preventative or corrective actions and recommendations should be documented, especially in food facilities [17]. However, contrary to our findings, Xiong et al. [18] found that pork slaughter plants in China failed to implement monitoring records on time, violating procedures for good manufacturing practices such as pest control and product contamination control.

Our data also indicate that almost all of the top management (90%) in the surveyed food facilities support pest management practices, and perhaps as a result, these facilities have effective and continuous pest management monitoring, training, practices, and documentation (Table 2). In another context, Kalmar et al. [19] reported a general lack of managerial awareness about pest management in child care centers. This suggests the necessity of training senior management in pest management. After attending a pest management education workshop, Kalmar et al. reported, all the managers felt more capable of dealing with pest infestation.

One effective approach to food safety practices and implementing a risk based system such as HACCP in food facilities involves various basic prerequisite programs (PRPs), including proper facility-design practices, pest control, equipment-maintenance, supplier selection, cleaning and sanitation programs, staff training, and specification programs (cross-contamination control) [7,20]. These programs ensure that the premises, equipment, transportation, and employees don't become or contribute to food safety hazards [21]. As our data show, facility infrastructure and design scores are very high-quality, with more than 80% (Table 3) overall adherence for all food facilities, except for practices involving non-closed spaces, slots and blanks (35.7%) and inappropriate storage of pest chemicals in plants (43.8%). All of these results affirm that better infrastructure would help effective pest management monitoring (Table 2) and facility sanitation practices (Table 4) in these food facilities. Therefore, effective pest control involves 'building them out' by eliminating pests' access to structures from doors, windows, screens and any other openings [17], along with other basic prerequisite programs [22].

Food processing facilities face many challenges while developing and implementing PRPs and risk-based HACCP systems in their facilities. A number of studies have identified these challenges

in different kind of food businesses in a number of countries [21, 23, 24, 25, 26, 27, 28]. A lack of basic hygienic practices is the most important challenge [6, 18, 21, 29]. Moreover, some researchers [30, 31] have described sanitation as the first step of pest management in food processing facilities. Sanitation involves the proper storage and handling of food materials and refuse, and the elimination of shelter that pests use for hiding, resting, and nesting [17]. However, our data indicate that food processing facilities have generally effective and high-level (more than 80%) sanitation practices in pest management (Table 4). This may be why the managers in our study believed that lack of sanitation is not the main barrier to pest management effectiveness (Table 5). Similarly, facility sanitation may not be the sole factor influencing successful pest management [4].

Based on the existing literature, the main managerial barriers to pest management program maintenance and implementation are related to lack of control regarding building maintenance, repair and sanitation, lack of money, and lack of staff communication [19]. Our respondents' opinions about these barriers are presented in Table 5. All the food managers agreed that the greatest barrier to implementing pest management in their respective facilities was insufficient infrastructure. However, reasons related to pest management operators (1.83) were cited least often. This is consistent with our observations of good pest management recording and other practices related to pest management operators (Table 2), and that top management as well as staff knows their responsibilities for effective pest management. It is clear that the employment of experienced and technically qualified personnel or pest management operators is critical to effective pest practices, because of their practical responsibilities in the implementation and maintenance of pest management systems.

Although our findings are significant and contribute to national discussions about food safety, certain parameters of this study limit the generalizability of its findings. First, only a modest number of food processing facilities were studied in Aydin province, so the data do not represent all the facilities in Turkey. In addition, facility visits were made with managers and some of them didn't want us to visit their indoor plants. Interviews with these managers were therefore not included in the data analysis. It is important that these limitations be considered when interpreting and discussing the study's results. Overall, this study explored the characteristics of pest management systems and attitudes of managers in different food processing facilities in western Turkey. Results suggest that most of the food facilities kept significantly reliable pest practice records and knew a lot about pest applications and good sanitation practices. They also suggest that effective facility infrastructure and sanitation

practices are important in the successful and more convenient adoption and implementation of an efficient pest management in food facilities. This study also documents that food processing facilities had greater PRPs and more consistent documentation and record-keeping activities than other researchers found.

Based on these results, it is clear that outsourced license pest management operators are important in the successful adoption and implementation of an efficient pest management in food facilities within risk based management systems, at least within the surveyed food sectors (dried vegetables & fruits, catering, table olive/vegetable oil, baked goods, and dairy) in western Turkey. However, our data don't confirm previous findings regarding a lack of documentation and sanitation practices for PRPs in food facilities. Therefore, to improve pest management practices, HACCP compliance, and food safety in Turkey, we suggest more sectorial HACCP and food safety management training programs, as well as further research to maximize the efficacy of pest prevention practices in Turkey and as well as in other countries.

REFERENCES

- [1] Fredericks, J., and Mannes, C. (2016) Integrating Pest Management Procedures to Protect Food Safety. *Food Safety Magazine*, Available at: August/September 2016, <http://www.foodsafetymagazine.com/magazine-archive1/augustseptember-2016/integrating-pest-management-procedures-to-protect-food-safety/> Accessed 07 November 2016.
- [2] Abdul-Mutalib, N.A., Abdul-Rashid, M.F, Mustafa, S., Amin-Nordin, S., Hamat R.A, and Osman, M. (2012) Knowledge, attitude and practices regarding food hygiene and sanitation of food handlers in Kuala Pilah, Malaysia. *Food Control* 27:289-293.
- [3] Arpanutud, P., Keeratipibul, S., Charoensupaya, A., and Taylor, E. (2009) Factors influencing food safety management system adoption in Thai food-manufacturing firms. *Brit. Food J.* 111(4):364-375.
- [4] Williams, S.B., Alexander, C.E., and Mason, L.J., (2015). Sanitation's impact on the effectiveness of the pest management programs of food processing facilities. *Journal of stored products research* 60:48-53.
- [5] Banati, D., and Lakner, Z. (2012) Managerial attitudes, acceptance and efficiency of HACCP systems in Hungarian catering. *Food Control* 25:484-492.
- [6] Bas, M., Ersun, S.A., and Kivanc, G. (2006) Implementation of HACCP and prerequisite programs in food businesses in Turkey. *Food Control* 17:118-126.

- [7] Bas, M., Yuksel, M., and Cavusoglu, T. (2007) Difficulties and barriers for the implementing of HACCP and food safety systems in food businesses in Turkey. *Food Control* 18:124-130.
- [8] M.F.A.L. (2008) Ministry of food, agriculture and livestock, Gıda güvenliği ve kalitesinin denetimi ve kontrolüne dair yönetmelik. Turkish Republic Official Journal, 28 September 2008, issue: 27009.
- [9] Kolożyn-Krajewska, D. and Sikora, T. (1999) HACCP-Koncepcja I System zapewnienia bezpieczeństwa Zdrowotnego Żywności. SIT SPOZ, Warszawa.
- [10] Trematerra, P. (2013) Aspects related to decision support tools and Integrated Pest Management in food chains. *Food Control* 34:733-742.
- [11] Mannes C., Sheperdigianis, M.S., and Sargent, J. E. (2003) Keys to Effective Pest Management in the Food Industry. *Food Safety Magazine*, August/September 2003, Available at: <http://www.foodsafetymagazine.com/magazine-archive1/augustseptember-2003/keys-to-effective-pest-management-in-the-food-industry/> Accessed 07 November 2016.
- [12] IPM, (2013) Pest management for food professionals. Available at: [www.wichita.gov/ Government/Departments/PWU/Pages/Food-Tobacco.aspx](http://www.wichita.gov/Government/Departments/PWU/Pages/Food-Tobacco.aspx). Accessed 07 September 2016
- [13] Cronbach, L. (1951) Coefficient alpha and the internal structure of tests. *Psychometrika* 16 (3): 297–334.
- [14] M.H. (2005) Ministry of Health, Halk sağlığı alanında haşereler karşı ilaçlama usul ve esasları hakkında yönetmelik. Turkish Republic Official Journal, 27 January 2005. Issue: 25709.
- [15] Stevenson, K.E (1990). Implementing HACCP in the food industry. *Food Tech.* 44, 179-180.
- [16] Taylor, E. (2001) HACCP in small companies: benefit or burden? *Food Control* 12, 217-222.
- [17] Ignatowicz, S. (2010) Rodent and insect pest control according to the requirements of IFS/BRC standards. Pula-DD I ZUPP 2010. 239-245.
- [18] Xiong, C., Liu, C., Chen, F., and Xheng, L. (2017) Performance assessment of food safety management system in the pork slaughter plants of China. *Food Control* 71:264-272.
- [19] Kalmar E., Ivey, S.L., Bradman, A., Leonard, V., and Alkon, A. (2014) Implementing an integrated pest management (IPM) program in childcare centers: A qualitative study. *Early Childhood Research Quarterly* 29:245–254.
- [20] Walker, E., Pritchard, C., and Forsythe, S. (2003) Hazard analysis critical control point and prerequisite programme implementation in small and medium size food businesses. *Food Control* 14:169-174.
- [21] Khalid, S.M.N. (2015) How and why to implement HACCP in food businesses in developing countries? Suggestions to Afghan Government and private sector. *Turkish Journal of Agriculture-Food Science and Technology* 3(6):459-465.
- [22] Seward, S. (2000) Application of HACCP in food service. *Irish journal of agriculture and food research* 39:221-227.
- [23] Azanza, M., and Zamora-Luna, M. (2005) Barriers of HACCP team members to guideline adherence. *Food Control* 16:15-22.
- [24] Cusato, S., Gameiro, A.H., Corassin, C.H., Cruz, A.G., and de Alveira, C.A.F. (2013) Food safety systems in a Small dairy factor: Implementation, major challenges and assessment of systems' performances. *Food Borne Pathogens and Disease* 10:6-12.
- [25] Gilling, S.J., Taylor, E.A., Kane, K., and Taylor, Z.J. (2001) Successful hazard analysis critical control point implementation in the United Kingdom: Understanding the barriers through the use of a behavioral adherence model. *J. Food Prot.* 64:710-715.
- [26] Panisello P.J. and Quantick, P.C. (2001) Technical barriers to Hazard Analysis Critical Control Point (HACCP). *Food Control* 12(3):165–173.
- [27] Sözen B.U. and Hecer, C. (2013) Is HACCP a Difficult food safety system to implement? *Journal of biological and environmental science* 7:33-38.
- [28] Vela, A.R. and Fernandez, J.M. (2003) Barriers for the developing and implementing of HACCP plans: results from a Spanish regional survey. *Food Control* 14:333-337.
- [29] Domenech, E., Amoros, J.A., Perez-Gonzalvo, M., and Escriche, I. (2011) Implementation and effectiveness of the HACCP and pre-requisites in food establishments. *Food Control* 22: 14119-1423.
- [30] Campbell, J.F., Arthur, F.H., and Mullen, M.A. (2004) Insect management in food processing facilities. *Adv. Food Nutr. Res.* 48:1-57.
- [31] Phillips, T.W., and Thorne, J. (2009) Biorational approaches to managing stored-products insects. *Annu. Rev. Entomol.* 55:375-397.

Received: 16.01.2017
Accepted: 09.06.2017

CORRESPONDING AUTHOR

Eyyup Mennan Yildirim

Department of Agricultural Biotechnology, College
of Agriculture, Adnan Menderes University, Aydın,
Turkey.

e-mail: emennan78@hotmail.com

PERFORMANCE OF GROWTH AND NUTRIENT CONTENT IN *MELIA AZEDARACH* L. UNDER WASTEWATER IRRIGATION

Hayssam M Ali^{1,2}, Saud A Alamri¹, Manzer H Siddiqui^{1,*}, Mutahhar Y Y Al-Khaishany¹, Mohammed A Al-Qutami¹, Khaled A Alakeel³

¹Department of Botany and Microbiology, College of Science, King Saud University, Riyadh, 2455, Kingdom of Saudi Arabia

²Department of Timber Trees Research, Sabahia Horticulture Research Station, Horticulture Research Institute, Agriculture Research, Alexandria, Egypt

³Center of Excellence for Wildlife Research, Life Sciences & Environment Research Institute, King Abdulaziz City for Science and Technology, Riyadh, 11442, Kingdom of Saudi Arabia

ABSTRACT

Due to scarcity of water globally, wastewater has become an alternative source of water for irrigation to minimize the pressure of fresh water demand. Therefore, the aim of the present study was to investigate the influence of wastewater on the performance of *Melia azedarach* L. grown for three consecutive years. The pooled data of three years reveal that wastewater irrigation markedly increased plant height, stem diameter, leaf area, fiber length, leaf fresh weight, leaf dry weight, stem fresh weight, stem dry weight, root fresh weight and root dry weight except specific gravity as compared to the tap water irrigation. Also, plants irrigated with wastewater exhibited higher concentration of nutrients (nitrogen, phosphorus and potassium). Although, continuous irrigation of plants with wastewater may cause heavy metal accumulation, (especially by lead, cadmium and nickel). The use of wastewater for irrigation of *Melia azedarach* might be an important and alternative source of water and nutrients for better growth and development of tree plant.

KEYWORDS:

Wastewater, *Melia azedarach*, nutrients content, plant growth

INTRODUCTION

The discharge of wastewater is constantly increasing with the increasing world's population [1]. Globally, the demand of wastewater in agriculture is increasing in many countries particularly in arid and semi-arid regions due to the scarcity of water, and also high quality water is not enough for irrigation and even shrinking by fulfilling the demand of increasing urban population [2]. Therefore, wastewater can be used in the alleviation of surface water contamination problem and not only help in

the conservation of water resources but it also provides the nutrients and organic matters to grow agricultural plants [2-4]. However, according to a new report of FAO that wastewater use is very limited practice worldwide, and also only 20 million ha in around 50 countries (i.e. 10% of the world's irrigated land) has been used reclaimed wastewater for irrigation [5]. Therefore, it is an important way to overcome shortage of fresh water problem caused by urbanization, agriculture industries by adopting sustainable alternative approach that can minimize the dependency on surface fresh water resources.

As we know that the demand of wood is increased with increasing urbanization and demand of wood products, such as construction timber, plywood, and furniture. According to Meyfroidt and Lambin [6] tropical deforestation is very critical issue worldwide. Globally, almost 3.4 billion cubic meters of wood were reaped from forest in 2010 [7]. Environmental contaminant like sewage discharge that causes harmful effects on living bodies resulting in economic loss [8]. Therefore, it is an important approach to minimize wastewater discarding problem, risk of environmental and public health and ground water pollution by irrigating forest species with wastewater. Use of wastewater in agriculture improves soil properties by improving nutrient content. Irrigation of plants (*Eucalyptus*, *Populus* spp., *Pinus* spp., *Bambusa arundinacea*, *Acacia mangium*, and Indian *Azadirachta indica* and *Dalbergia sissoo*) provides a safe and alternative approach for disposal of wastewater [9]. Wastewater increases growth characteristic of plants [10]. Matheyarasu et al. [11] reported that wastewater treatments increased biomass yields and nutrient content in *Pennisetum purpureum*, *Medicago sativa*, *Sinapis alba* and *Helianthus annuus*.

Melia azedarach L., belongs to Meliaceae family, known as bread tree. It has been used in the treatment of various diseases, such as fungal infection, leprosy, cystitis, scrofula, ulcerative wounds, syphilitic ulcer and uterine illnesses because it has good medicinal properties [12, 13]. Also, wood of this plant is resistant to termites and is used in

TABLE 1
Average composition of water used in irrigation treatments in the experiment

Parameter	Wastewater	Tap water	Limits of wastewater for agric. reuse (FAO, 1992)
pH	6.62	6.60	6.50 – 8.40
E.C ds/m	1.40	0.48	3.00 – 7.00
Soluble Cations (meq/L)			
Ca ⁺⁺	2.73	1.20	--
Mg ⁺⁺	2.41	1.80	--
K ⁺	0.33	0.10	--
Na ⁺	12.95	3.60	--
Soluble Anions (meq/L)			
CO ₃ ²⁻	--	--	--
HCO ₃ ⁻	4.93	2.50	1.50 – 8.50
Cl ⁻	8.63	3.92	--
DO (mg/L)	0.00	--	--
BOD ₅ (mg/L)	230	--	40 - 500
COD (mg/L)	422	--	80 - 600
TSS (mg/L)	1035	--	--
Available N (ppm)	1.38	0.12	--
Available P (ppm)	0.41	0.01	--
Total heavy metals (ppm)			
Cd	0.04	0.003	0.01
Ni	0.03	0.001	0.20
Pb	0.29	0.02	5.00

making of boxes, poles, and other tools [14]. Therefore, keeping in view the use of alternative source of water for the irrigation of plants, the aim of the present study was to investigate the effect of wastewater treatment on growth and nutrient content in *Melia azedarach* L.

MATERIAL AND METHODS

Taken sewage effluent in the present the study, was collected from oxidation ponds of the Sewage Effluent Treatment Station, New Borg El-Arab City, Alexandria, Egypt. The characteristics of wastewater are presented in Tables 1. Analysis of wastewater was performed according to the analytical methods given in Standard Methods for the Examination of Water and Wastewater [15]. Chemical Oxygen Demand (COD) and Dissolved Oxygen (DO) were measured by the standard method of azide modification of winkler and dichromate oxidation respectively. Five days Biochemical Oxygen Demand (BOD) was performed by measuring the amount of oxygen lost after incubation for 5 days in the dark at 20°C.

This study was conducted for three consecutive years at the Horticultural Research Station at Alexandria, Egypt. Wastewater was applied, and data were collected at every end of the year, and pooled data were given in Tables. One-year old seedlings of *Melia azedarach* L. were irrigated with wastewater up to the field capacity of the soil to maintain optimum water conditions.

Sampling was done at every end of the year,

and the performance of the plant was assessed on the basis of plant height (PH), stem diameter (SD), leaf area (LA), fiber length (FL), specific gravity (SG), leaf fresh weight (LFW), Leaf dry weight (LDW), stem fresh weight (SFW), stem dry weight (SDW), root fresh weight (RFW) and root dry weight (RDW). SFW and SDW were noted after detaching leaves from the plants. PH by scale, SD by vernier caliper and LA by leaf area meter (CI-203 Portable Laser Area Meter, USA) were measured. LDW, SDW and RDW were taken after drying samples in an oven at 80°C for 72h. Dried plant materials were stored for further chemical study. SG of each sample was determined according to the method of Smith [16]. FL was measured as described by Burley et al. [17].

Dried samples of each treatment were powdered to pass through a 2 mm sieve and digested with triacid mixture (HNO₃ : H₂SO₄ : HClO₄ in 10:4:1 ratio) [18]. The content of N and P was analyzed after wet-digestion with H₂SO₄ by adopting the methods of Jackson [19] and Singh et al. [20], respectively. The content of K was determined according to the method of Page et al. [21]. The content of heavy metals [Cd, Pb and Ni (ppm)] was measured with the help of Atomic Absorption Spectrophotometer (Perkin Elmer, 3300, USA).

Statistical analysis. Each pot was treated as one replicate, and six replicates were taken for all the treatments. The data were collected each year. The combined data were subjected to one-way analysis of variance (ANOVA) using SAS version 8.2 (SAS, 2001)

TABLE 2
Effect of wastewater on the growth performance of *Melia azedarach* L.

Treatments	Parameters				
	Plant height (cm)	Stem diameter (cm)	Leaf area (cm ²)	Fiber length (mm)	Specific gravity
Tapwater	43.4	0.73	55.92	0.92	0.44
Wastewater	152.8	2.44	74.28	0.95	0.36

TABLE 3
Effect of wastewater on the growth performance of *Melia azedarach* L.

Treatments	Parameters					
	LFW (g)	LDW (g)	SFW (g)	SDW (g)	RFW (g)	RDW (g)
Tapwater	80.47	13.58	89.66	43.87	75.24	38.21
Wastewater	655.28	39.87	1755.24	1243.71	235.87	119.82

TABLE 4
Effect of wastewater on the nutrients and heavy metals content in *Melia azedarach* L.

Treatments	Parameters					
	N (g/Kg DM)	P (g/Kg DM)	K (g/Kg DM)	Cd (mg/Kg DM)	Pb (mg/Kg DM)	Ni (mg/Kg DM)
Tapwater	22.74	0.40	19.81	0.01	4.75	2.01
Wastewater	30.65	1.14	28.93	1.38	14.20	9.76

RESULTS AND DISCUSSION

Data given in Table 1 showed that the pH and EC of tap water were recorded lower than wastewater. The concentration of nutrients (N, P and K) and heavy metals (Cd, Pb and Ni) was also lower than wastewater (Table 1). However, Food and Agriculture Organization of the United Nations [22] reported that the acceptance limit of pH of waters for irrigation is ranged from 6.50 to 8.40. Also, according to the FAO [22] the dissolve oxygen (DO), biological oxygen demand (BOD), chemical oxygen demand (COD) and total suspended solids (TSS) of wastewater were below the range of the tolerance limit [22].

Performance of the growth characteristics of *Melia azedarach* was assessed on the basis of PH, SD, LA, FL, LFW, LDW, SFW, SDW, RFW and RDW (Tables 2 and 3). All growth parameters were found to be significantly increased with the irrigation of wastewater as compared to the tap water irrigation except SG. The irrigation of wastewater enhanced PH by 252.07%, SD by 234.25%, LA by 32.83%, FL by 3.26%, LFW by 714.32%, LDW by 193.59%, SFW by 1857.66%, SDW by 2734.99%, RFW by 213.49% and RDW by 213.58% over the tap water irrigation. A decrease in SG might be due to the accumulation of heavy metals in plant by continuous irrigation of wastewater. This result agrees with the findings of Al-Mefarrej [23]. We found very interesting from this study that wastewater irrigation was proved beneficial in enhancement of growth attributes for *Melia azedarach*. In this study, improved growth and dry matter production might be due to the better orientation of leaves that may capture more

solar energy by improving PH, SD and LA (Tables 2 and 3). This results were supported by the previous studies of Ali et al. [2]; Siddiqui et al. [24]. Also, the improved growth performance might be due to the sufficient availability of nutrients that help in the regulation of many physiological processes in plants [25].

The irrigation of wastewater was found to be more effective than the tap water by improving the contents of N, P and K in *Melia azedarach* (Table 4). Wastewater irrigation increased N by 34.78%, P by 184.99% and K by 46.04% as compared to the tap water. The improved nutrients concentration in plants might be due to continue addition of nutrient rich-wastewater, which could be the major factors to improve plant growth attributes because they play an important role in the synthesis macromolecules [26]. We know that wastewater is, rich source of organic and inorganic nutrients, very useful for plants. Irrigation of wastewater also improves ecological balance and environmental quality. Improved uptake of nutrients could have enhanced biomass production (Tables 2 and 3). On the other hand, wastewater irrigation significantly increased heavy metals concentrations in plants (Table 4). The irrigation of wastewater increased accumulation of Cd by 13699.99%, Pb by 198.95% and Ni by 385.57% as compared to the tap water. These results substantiate with the previous findings of Ali et al. [2] and Karata et al. [27].

CONCLUSION

It is concluded that the irrigation with wastewater exhibited beneficial effects on plant growth performance of *Melia azedarach* by improving growth characteristics, such as PH, SD, LA, FL, SG, LFW, LDW, SFW, SDW, RFW and RDW. Also, it improved the concentration of nutrients *i.e.* N, P and K. An increase in uptake of nutrient may be the reason of improved growth parameters. Therefore, wastewater could be considered as an alternative source of water for irrigation for *Melia azedarach*. Also, it may minimize the risk of public health and the ground water pollution by its safe disposal.

REFERENCES

- [1] Gargosova, H.Z., Urminska B. (2017). Assessment of the efficiency of wastewater treatment plant using ecotoxicity tests. *Fresen. Environ. Bull.*, 26, 56-62.
- [2] Ali, H.M., Siddiqui, M.H., Khamis, M.H., Hassan, F.A., Salem, M.Z.M. and El-Mahrouk E.M. (2013). Performance of forest tree *Khaya senegalensis* (Desr.) A. Juss. under sewage effluent irrigation. *Ecological Engineering*, 61, 117-126.
- [3] Pescod, M.B. (1992). Wastewater treatment and use in agriculture. F.A.O. Irrigation and Drainage Paper 47.
- [4] Al Zabir, A., Zaman, M.W., Hossen, M.Z., Uddin, M.N., Biswas, M.J.H. and Al Asif A. (2016). Impact of wastewater irrigation on major nutrient status in soil near Bhaluka industrial area of Bangladesh. *Asian Journal of Medical and Biological Research*, 2, 131-137.
- [5] Winpenny, J., Ingo H. and Sasha (2010). *The Wealth of Waste: The Economics of Wastewater Use in Agriculture*. FAO Water Reports 35, Rome, Italy.
- [6] Meyfroidt, P. and Lambin, E.F. (2011). Global forest transition: Prospects for an end to deforestation. *Annual Review of Environment and Resources*, 36, 343-371.
- [7] Elias, P. and Boucher, D. (2014). *Planting for the Future: How Demand for Wood Products Could Be Friendly to Tropical Forests*. Union of Concerned Scientists: Science for a Healthy Planet and Safer World, October, 2014.
- [8] Seker, D.Z., Yucel, U. (2017). Gis based multi-criteria decision analysis for site selection of a wastewater treatment plant. *Fresen. Environ. Bull.*, 26, 399-404.
- [9] Yadav, R.K., Minhas, P.S., Khajanchi-Lal and Dagar J.C. (2016). Potential of Wastewater Disposal Through Tree Plantations. In: Dagar, J.C. and Minhas, P.S. (eds.), *Agroforestry for the Management of Waterlogged Saline Soils and Poor-quality Waters*, Advances in Agroforestry Vol. 13, Springer, India.
- [10] Alghobar, M.A., Suresha, S. (2016). Effect of wastewater irrigation on growth and yield of rice crop and uptake and accumulation of nutrient and heavy metals in soil. *Applied Ecology and Environmental Sciences*, 4, 53-60.
- [11] Matheyarasu, R., Bolan, N.S. and Naidu, R. (2016). Abattoir wastewater irrigation increases the availability of nutrients and influences on plant growth and development. *Water, Air, & Soil Pollution*, 227, 253.
- [12] AL-Rubae, A.Y. (2009). The potential uses of *Melia azedarach* L. as pesticidal and medicinal plant, review. *Journal: American-Eurasian Journal of Sustainable Agriculture*, 3, 185-194.
- [13] Khatoon, A., Mohapatra, A. and Satapathy, K.B. (2016). Studies on evaluation of in-vitro antifungal activities of *Melia azedarach* L. Bark. *International Journal of Pharmaceutical Sciences and Research*, 7, 331-335.
- [14] Rind, N.A., Aksoy, O., Dahot, M.U., Dikilitas, S., Rafiq, M., Tütünoglu, B., (2016). Evaluation of genetic diversity among melia azedarach l. (meliaceae) with rapd markers. *Fresen. Environ. Bull.*, 25, 2374-2382.
- [15] APHA-AWWA-WPCF (1995). *Standard Methods for the Examination of Water and Wastewater*, 19th ed. American Public Health Association, Washington, DC.
- [16] Smith, D.M. (1954). Maximum moisture content method for determining specific gravity of small wood samples. *USDA Forest Prod. Lab. Rep.* 2014:8.
- [17] Burley, J., Posner, T. and Waters, P. (1970). Sampling techniques for measurement of fiber length in Eucalyptus Species. *Wood Science and Technology*, 4, 240-245.
- [18] Jones, Jr., J.B. and Case, V.W. (1990). Sampling, handling and analyzing plant tissue samples. In: Westerman, R.L. (Ed.), *Soil testing and Plant Analysis*, 3rd ed. Soil Science Society of America Inc, Madison, WI, pp. 389-427.
- [19] Jackson, M.L. (1973). *Soil Chemical Analysis*. Prentice-Hall of India, Private Limited, New Delhi, pp. 38-82.
- [20] Singh, G., Bhati, M., and Rathod, T. (2010). Use of tree seedlings for the phytoremediation of a municipal effluent used in dry areas of North-Western India: plant growth and nutrient uptake. *Ecological Engineering*, 36, 1299-1306.
- [21] Page, A.L., Miller, R.H., and Keeny, D.R. (1982). *Methods of Soil Analysis, Part II*. In: *Agronomy Monogr.*, 2nd ed. ASA and SSSA, Madison, WI, pp. 539-579.
- [22] FAO (1992). *Wastewater treatment and use in agriculture*. Pescod M.B. *Irrigation and Drainage*. Paper 47. FAO, Rome.
- [23] Al-Mefarrej, H.A. (2013). Growth characteristics and some wood quality of *Tamarix aphylla* seedlings irrigated with primary treated

wastewater under drought stress. Asian Journal of Plant Sciences, 12, 109-118.

- [24] Siddiqui, M.H., Khan, M.N., Mohammad, F. and Khan, M.M.A. (2008). Role of nitrogen and gibberellic acid (GA₃) in the regulation of enzyme activities and in osmoprotectant accumulation in *Brassica juncea* L. under salt stress. Journal of Agronomy and Crop Science, 194, 214–224.
- [25] Maathuis, F. (2009). Physiological functions of mineral nutrients. Current Opinion in Plant Biology, 12, 250-258.
- [26] Marschner, H. (1995). Mineral Nutrition of Higher Plants, 2nd ed. Academic Press, London.
- [27] Karatas, M., Dursun, S., Guler, E., Ozdemir, C., Argun, M.E. (2006). Heavy metal accumulation in wheat plants irrigated by waste water. Cellulose Chemistry and Technology, 40, 575–579.

Received: 24.01.2017

Accepted: 25.04.2017

CORRESPONDING AUTHOR

Manzer H Siddiqui

Department of Botany and Microbiology, College of Science, King Saud University, Riyadh, 2455, Kingdom of Saudi Arabia

e-mail:manzerhs@yahoo.co.in

NEXT GENERATION SEQUENCING TECHNOLOGIES AND USAGE IN FORENSIC GENETICS

E Hulya Yukseloglu¹, Umut Kara², S Sibel Ramadanoglu¹, Faruk Asicioglu¹

¹Institute of Forensic Sciences, Istanbul University, Istanbul 34098, Turkey

²Department of Morgue Specialty, The Council of Forensic Medicine (ATK), Istanbul 34186, Turkey

ABSTRACT

DNA sequence analysis applications, which started, all the way back in the 90s and have stepped up with the Human Genome Project, has reached a completely different level with the techniques and methods developed nowadays. Almost all fields of application have taken advantage of these developments where single base level and genome distributed DNA sequence differences can be detected in maternal twins [1]. Forensic Genetics did not keep distance from these developments that started with clinical purpose and with the New Generation Sequencing techniques developed in recent years, it is stated that a new era in this field has begun. Particularly the convenience provided by the analysis of mix samples containing DNA of multiple persons and due to presenting more than one genetic markers in a single analysis, these technologies have brought great dynamism to the field. Once the foremost disadvantages of New Generation Sequencing methods situated as the cost that comes with high technology and analysis errors of high amounts of information produced are overcome, a paradigm shift is inevitable in where “length polymorphism” dominates the field of forensic genetics [2].

KEYWORDS:

New Generation Sequencing (NGS), DNA analysis, Single Nucleotide Polymorphism (SNP), Forensic Genetics

INTRODUCTION

DNA sequencing studies go a long way back in the field of forensic molecular biology and forensic genetics. A new era in DNA analysis has begun in the 70s with the first use of Sanger Sequencing method. Important steps were taken when it came to cracking criminal cases, such as a series of encountered complications based upon identification in the field of forensics have been overcome with mtDNA sequencing done by the end of 80s and at the start of 90s. DNA sequencing technologies have made

great progress from past to present numerous fields of the scientific community [2, 3]. This article aims to inform on the working principle of certain sequencing systems on the market after emphasizing the basics of sequence analysis and the innovations that new generation sequencing brought.

SEQUENCE ANALYSIS METHOD FROM PAST TO PRESENT

DNA sequence analysis is defined as determining the order of nucleotides A, C, G, and T that belong in DNA fragments. The order determination of these nucleotides are used in, data acquisition on what protein the DNA section will be able to code, discovering the exon and introns by comparing sequence data from genomic DNA and complementary DNA, and imprinting of zones that control gene activity with DNA sequence analysis. This method is also applied during recognition of evolutionary kinship relations by identification in the forensic genetics field and specific DNA sequence determinations [4, 5].

Since Watson and Crick showed the double helix structure back in 1953, the most critical point for molecular biology and genetics have been the DNA sequence and detectability of the structure and order of bases of this sequence. The study in this field with the widest impact is the one developed by Frederick Sanger in 1977 and took part in literature as *Sanger Sequencing Method*. This method, is based on the replication stage that occurs in a cell, is carried out in a test tube. In the DNA synthesis; the 5’“P” atom recently added to deoxynucleotide (dNTP), react to the last nucleotides 3’-OH group at the end of the chain and forms a “phospho-diester” bond. Thus, a nucleotidic extension is provided in the chain synthesized. If dideoxynucleotide (ddNTP) is added to the chain, the chain expansion will terminate. The basic approach in the chain termination method can be summarized as follows: Part of the bases (dNTP) added to the medium during a classic PCR process, lose the ability to add a new base to one end and change with another fluorescent featured base type (ddNTP) and thus terminated in different lengths

and fluorescence emitting DNA's that become visible depending on the terminal-base. Each base (A, T, G and C) have two axis similar to magnets (these axis are named 5' and 3') and thus a bases one terminal can connect to another bases other terminal. So, the 5' end of a base ready to bond will be added to a 3' terminal of a DNA chain. If the 3' terminal of a base is disrupt, this base can still bond with a DNA chain, however this DNA chain cannot extend any longer, due to the binding point being no longer available for a new base to connect. Therefore, DNA chains with various lengths can be aligned and depending on this order, it is apprehensible that which chain ends with which base [2, 4].

There are a few points to be considered related to their technical details. The first of these, the first 15 to 40 bases of this DNA sequence is low quality; the second, starting from 700 to 900 bases the quality of the sequence goes below acceptable levels. The third point, the time required to read approximately 800 bases is too long; and the fourth point, consumables used per base is relatively expensive. It is a whole other story, especially when considering time and cost estimations for the sequencing of the human genome that has approximately 3 billion base pairs rather than an 800 base DNA sequence. That said, this method is used for sequencing small regions of the genome [6]. However, conventional Sanger sequencing technology is insufficient when it comes to more specific and complicated genome analysis, due to low process volume, high-cost and challenges encountered during analysis. With the use of new generation sequencing technologies, high process volumes have been acquired, and with advantages such as increased yield, many of the challenges caused by the method aforesaid have been overcome. In addition, this technology is used for identification in the field of forensic genetics, diagnostics of medical genetic diseases and genome studies of various organisms such as yeast, fungus and viruses [7].

Researchers have initially worked on improving the Sanger method before new generation sequencing technologies. The main objective was to perform a faster sequencing with less consumables. While the classic Sanger method indicated the gel electrophoresis stage, automatic equipment accelerated the process with the capillary electrophoresis method. In addition, the number of bases sequenced in unit of time has increased by using more than one capillary electrophoresis. This period, which may be named as a transition period, has actually provided a basis for the emerging of the first models of new generation sequencing [8, 9].

New generation DNA sequencing methods in general, divide into 3 main groups as follows; *sequencing via synthesis*, *sequencing through ligation* and *single molecule sequencing*. These procedural differences create variation in key studies such as

reading length, productivity and error rate. New generation sequencing technology has entered the scientific community commercially for the first time in the year 2005 with the use of 454 pyrosequencing technology. From that day forward a few different sequencing methods have been developed [8, 10]. New generation sequencing analysis technologies such as 454 GS20 pyrosequencing (Roche Applied Science), Solexa 1G (Illumina, Inc.), SOLID (Applied Biosystems), Heliscope (Helicos, Inc.), Ion Torrent and The MiSeq FGx Forensic Genomics System (Illumina, Inc.) are commercially available [11].

NEW GENERATION SEQUENCING TECHNOLOGIES AND FORENSIC GENETICS

There are many innovations brought to the field of forensic genetics by new generation sequencing analysis techniques. The most important significance of this technology is that it provides assurance to the base sequence of the DNA we are analyzing. This very valuable advantage not only ensures the forensic separation by drabs and drabs of mutations of twins that are almost identical in terms of DNA, but also overcome some of the deficiencies of the STR analysis that is a principal technique in genetic identification. For example, it is not possible to separate two people with the same sequence length by the same locus with the STR technique used on a mix DNA profile obtained from a stain that contains more than one source of DNA. This is because the STR technique is based on length polymorphism. It is unable to reveal the sequence variations in that length. New generation sequencing, however, determines the DNA sequence in question with a high accuracy rate and enables to separate alleles by revealing the variations between sequences even if they have the same length. Due to this situation named as "isoallele", this technology simplifies the analysis of mix samples that is perhaps one of the most challenging fields situated in forensic genetics for the forensic genetics specialist [10, 12].

Another highly substantial advantage of new generation sequencing techniques is that it offers the forensic genetics specialist numerous information in a single analysis by using more than one genetic markers all together. New generation sequencing techniques can transform biological findings obtained from the crime scene into hair or eye color or even into bio-geographical ancestry information by SNP analysis along with the STR marker. Arguments go on as to prove how this great advantage will be utilized, putting forward the ethical extent of the issue [13].

One other advantage of new generation sequencing technologies is that it lowers the DNA

source measures down to a satisfactory level from what the routine techniques require. This is, as we explained above, because it enables us to separate even the sequences that are close to each other lengthwise. Therefore, it will be possible to prepare reference sequences in desired length and the sequence length necessary for the targeted DNA section will decrease. However, as with any new technology, many parameters must be delicately fictionalized to be able to utilize this advantage for new generation technologies [13, 14].

The most important contribution to paternity tests by new generation sequencing technologies is that it is a considerable guide for the specialists on the subject of mutations. By scanning more than hundreds of DNA sections using SNP and STR markers, it will provide an insight towards the estimations of mismatches detected among DNA profiles fit to be a data regarding whether it is a mutation or a case of dismissal of mother-fatherhood [15].

Of course there are some disadvantages in question when it comes to new generation sequencing technologies that we mentioned as assuring many advantages to forensic genetics specialists. It draws attention that according to many forensic genetics specialists whom approach the subject theoretically, the most important limitation of this technique is the emphasis of time and cost. Nevertheless, the most important advantage of new generation sequencing technology is in the meantime the most important handicap of this technique. To clarify this statement; it is clear that the greatest innovation this technology has brought alongside is that it provides the possibility that nearly all of the DNA can be analyzed with high accuracy rates. However, this situation brings along with it a massive knowledge generation as well. Forensic genetics specialists may encounter some difficulties due to lack of experience while analyzing this information. Although the world's leading biotechnology companies who are aware of this situation are eager to prepare software to help analyze this information, it is clear that this will cause specialists to be more bound to kit manufacturers. Even though the open source software in this area has made a breakthrough in the last 5 years, it has not yet reached the desired level. In today's technology where kit manufacturers bring into use the process steps that can be summarized as "library construction-sequencing and analysis" that are so to speak reduced into a "pill", the effort of open source software is nevertheless noteworthy. However this stance does not change the fact that there is a need for advanced computer software for the interpretation of the high amount of data acquired [16].

Systems in the Market. Few of the new generation sequencing systems used nowadays in fo-

rensic sciences and manufactured kits related to the field are mentioned below.

Roche 454 GS Genome Sequencing System.

The principle of pyrophosphate detection has been defined in 1985 and using this principle a new method for DNA sequencing was notified in 1988. The first new generation sequencing technology, the 454 technology has gained a place in the market in 2005. The 454 technology, is the most commonly used and published research in regard to new generation sequencing technology. Pyrosequencing strategy is used in this system. Pyrosequencing is a simultaneous sequencing strategy based upon the release of pyrophosphate (Ppi) during enzymatic DNA synthesis [7, 17].

Solexa System. Soelxa sequencing platform was commercialized in the year 2006. The basis of this technique is the sequencing-synthesis of four reversible terminal nucleotides all labeled with a different fluorescent dye. In the Solexa method, on one end of a single DNA molecule an adaptor is used to hybridize molecules bound on a stable surface with the use of a complementary adaptor and synthesize complementary strings. Patterns are massive parallel-aligned using DNA synthesis-sequencing approach, re-tachable fluorescent parts and special DNA polymerases with recyclable terminals can be included in to the oligonucleotide chain. Terminators are mark with four different colors and are differed by the length of base [2, 18].

New Generation Sequence – PGM (Personal Genome Machine) SNP applications for criminal purpose. These came into effect in the following fields: genetic identification, determination of kinship, phenotype specification, bio-geographical ancestry analysis and Mitochondrial DNA Identification. It can be used on degraded difficult samples and mixture samples. Three different kit panels have become available for these studies [16, 19].

Ion Torrent PGM Systems. It is a system that allows the determination of bases by using hydrogen ions oscillating during the nucleotide binding. The most important advantage of Personal Genome Machine (PGM) System for forensic purposes is the potential it carries to provide assistance to cases that cannot be cracked with traditional DNA sequencing technologies. Even though capillary electrophoresis method may still be the golden standard for laboratories that work with STR, the Ion PGM System enhances the capability of laboratories to acquire DNA results from challenging materials [5, 20]. The system in question converts chemical information into digital data and combines natural biochemical analysis and semi-conductive sequencing technology to provide accessibility of

the sequence information acquired from any laboratory or research center. The system in question combines the semi conductive sequencing technology with natural biochemical analysis to translate chemical information into digital data and to ensure the accessibility of the sequencing information acquired from any laboratory or research center [10]. The basic natural sequencing structure of the system rules out the need for costly optic material also reduces the complex structures required for the measurement of the natural DNA. Direct real time sequencing analysis enables to gain results in a single day as from sampling.

Ready panels (Ion Ampliseq Human Identity Panel-Identification Panel, HID-Ion AmpliSeq™ Ancestry Panel- Phenotype and Bio-geographical Ancestry Analysis Panel and Mitochondrial DNA Panel) or design panels created with special genes by laboratories demand can be worked using chips fit for the study intended along with the Ion Torrent™ system [19, 21].

Mitochondrial DNA Panel for PGM. “Ion AmpliSeq™ Whole Mt Genome Sequencing” kit unique to new generation sequence systems; is a product developed for the purpose of research on missing persons, mass grave cases and identification of body parts of disaster victims. Mitochondrial DNA’s advantages to nuclear DNA provides important benefits in terms of genetic identification.

Disaster Victim Identification expressed as DVI (Disaster Victim Identification), is imposed upon mitochondrial DNA analysis to match families from combined body parts and residues obtained from the scene of disaster. Meanwhile, Mitochondrial DNA enables the examination regarding origin in affinity-ancestry research due to its inheritance from maternal lineage. The bone residues from the mass grave found in Russia in 1978 that was detected to be related to the Romanov Dynasty and the identification of King Richard III were all done with the help of Mitochondrial DNA analysis [22, 23]. Purposefully, the kit allows sequencing of the whole Mitochondrial DNA. The kit can sequence the whole gene in 2 multi analysis as MPX1 and MPX2. As is known, the gene sequencing process which takes too long with the Sanger method is possibly downhill all the way with the new generation sequencing system.

New Generation Sequence Based Human Identification Kit: HID-Ion AmpliSeq™ Identification Panel. The SNP based identification kit specific to new generation sequence system, “HID-Ion AmpliSeq™ Identity Panel”, is especially designed to be used on samples with unobtainable or semi-obtainable profiles. It allows working with up to 100 pg of DNA. It is appropriate to work with any type of biological sample. The kit contains a

total of 124 multiplex SNP Points. Results with 99.99% compliance may be given with these SNP points. An average of 27 SNP is supposed to be studied in order to capture resolution for a single STR locus, thereby 27 SNP were chosen when designing the kit to capture 99.99% resolution. These 124 SNP contains 90 autosomal SNP, and 34 Y chromosome specific SNP points. 45 of the 90 autosomal SNPs are the SNPs identified by Dr. Kenneth Kidd at the Yale University and were chosen by the SNP identification consortium [7]. These are biallelic and are areas with low mutation rates and small amplicon sizes (132-141 nucleotides). Thus the kit allows to study degraded or trace amounts of samples. Phenotypic attributes were determined using SNP points from samples that belonged to King Richard III using this kit and these attributes overlapped with the descriptions in history [22, 24].

Biogeographical Ancestry and Phenotype Indication Kit for the purpose of Human Identification: HID-Ion AmpliSeq™ Ancestry Panel.

“HID-Ion AmpliSeq™ Ancestry Panel”, the SNP based biogeographical ancestry indication and phenotype identification kit specific for the new generation sequence system; is a kit developed for the use of uncovering phenotypic attributes (hair color, eye color, skin color) that define a person and may direct the investigation in the case of the suspect DNA profile acquired from the crime scene does not match any database [11, 25]. The kit allows studying the 165 SNP points as multiplex. The kit is fit to study all types of biological samples including degraded samples, and enables to study with samples with amplicon sizes of 122-133 nt. 123 of the 165 SNPs are points that Dr. Michael Seldin developed. 53 of them are points developed by Dr. Kenneth Kidd. Software by the name of ALFRED (Allele Frequency Database) is used along with the kit. This software has data specific to all populations, and determines what population the sample is statistically near to in each dispatch for each sample. The SNP points that the kit contains have a resolution of 99.77% [12, 20].

The MiSeq FGx (Forensic Genomics System).

MiSeq FGX Forensic Genomics System is the first validated sequencing system that was designed to be used in forensic genomic applications. This system uses specially designed library preparation kits, customized equipment control software and analytical software packages to carry on reliable analysis of challenging forensic samples encountered during routine work. MiSeq FGX system is a part of the new generation sequencing system integrated in to the field of forensic genetics [11, 18].

CONCLUSION

DNA analysis has come into prominence with the rapid progress of molecular biology and genetics dating from the 1950's. Studies driven by DNA sequencing techniques have come a long way in the past 10-15 years and is rapidly proceeding at present. Various new generation sequencing platforms for both medical and forensic purposes are within reach. Since the beginning of 2000 the methods and equipment used for DNA sequence analysis has progressed rapidly. These sequencing methods with different sequencing pathways, various sample preparation strategies, immobilization and nucleic acid chemistry are currently improving. By bringing in new generation sequencing systems for forensic purposes in to forensic laboratories located in Turkey, it will be possible to acquire profiles in challenging forensic events and confirm mutation cases. Additionally, using these systems along with the evaluation of mix samples (mixtures) that cause a great problem in the STR system will considerably simplify the specialists work.

Finally, in cases where there is not a single data aside from the DNA profile of the suspect, phenotype attributes that may describe the suspect will be determined along with these systems. Thus the contribution of new generation sequencing techniques on the provision of justice in the field of genetic identification will reach a new level and together with all these developments the new generation sequencing techniques will take its place among the essential methods in forensic genetic laboratories in the near future.

REFERENCES

- [1] Sanchez JJ, Phillips C, Børsting C, Balogh K, Bogus M, Fondevila M, Harrison CD, Musgrave-Brown E, Salas A, Syndercombe-Court D, Schneider PM, Carracedo A, Morling N. (2006) A multiplex assay with 52 single nucleotide polymorphisms for human identification, *Electrophoresis* 27: 1713–1724.
- [2] Yaran Yang, Bingbing Xie, Jiangwei Yan (2014) Application of Next Generation Sequencing Technology in Forensic Science, *Genomics Proteomics Bioinformatics*; 12:190-197
- [3] Coble M. D. Butler J. M. (2005), "Characterization of New MiniSTR Loci to Aid Analysis of Degraded DNA", *J Forensic Science*; Vol. 50: 43-53.
- [4] Michael L. Metzker (2010) Sequencing Technologies – The Next Generation, *Applications of Next Generation Sequencing*, *Nature Reviews*; 11: 31-46
- [5] Parson W., Strobl C, Huber G, Zimmermann B, Gomes SM, Souto L, Fendt L, Delpont R, Langit R, Wootton S, Lagace R, Irwin J. (2013) Evaluation of next generation mtGenome sequencing using the Ion Torrent Personal Genome Machine (PGM), *Forensic Sci Int Genet.*7(5):543-9
- [6] Seo S.B, King J.L, Warshauer D.H, Davis C.P, Ge J, Budowle B. (2013) Single nucleotide polymorphism typing with massively parallel sequencing for human identification, *Int J. Legal Med.* 127:1079-1086
- [7] Dicle Dönmez, Özhan Şimşek, Yıldız Aka Kaçar (2015) Yeni Nesil DNA Dizileme Teknolojileri ve Bitkilerde Kullanımı, *Türk Bilimsel Derlemeler Dergisi*; 8:30-37
- [8] Turi E. King, Fortes GG, Balaesque P, Thomas MG, Balding D, Maisano Delser P, Neumann R, Parson W, Knapp M, Walsh S, Tonasso L, Holt J, Kayser M, Appleby J, Forster P, Ekserdjian D, Hofreiter M, Schürer K. (2014) Identification of the remains of King Richard III, *Nature Communications*,
- [9] Weber J. L., May P. E. (1989) Abundant class of human DNA polymorphisms which can be typed using the polymerase chain reaction, *Am J Hum Genet*; 44: 388-96.
- [10] Claus Børsting, Niels Morling (2015) Next Generation Sequencing and It's Applications in Forensic Genetics, *Forensic Science International Genetics*; 18:7 8-89
- [11] <http://www.illumina.com/NextGen/>
- [12] Kidd KK, Kidd JR, Pakstis AJ, Speed WC. (2012) Better SNPs for Better Forensics: Ancestry, Phenotype, and Family Identification. Poster presented at the National Institute of Justice (NIJ) annual meeting, Arlington VA.
- [13] Pakstis AJ, Speed WC, Fang R, Hyland FC, Furtado MR, Kidd JR, Kidd KK. (2010) SNPs for a universal individual identification panel. *Hum Genet* 127:315–324.
- [14] Edwards A., Hammond H. A., Jin L., Caskey T., Chakraborty R. (1992) Genetic variation at five trimeric and tetrameric tandem repeats, *Genomics*; 12: 241-53.
- [15] Kosoy R, Nassir R, Tian C, White PA, Butler LM, Silva G, Kittles R, Alarcon-Riquelme ME, Gregersen PK, Belmont JW, De La Vega FM, Seldin MF. (2009) Ancestry informative marker sets for determining continental origin and admixture proportions in common populations in America. *Hum Mutat* 30(1)69–78.
- [16] Fordice SL, Mogensen HS, Børsting C, Lagacé RE, Chang CW, Rajagopalan N, Morling N. (2015) Second-generation sequencing of forensic STRs using the Ion Torrent™ HID STR 10-plex and the Ion PGM™, *Forensic Science International: Genetics*; vol(14):132-140
- [17] <http://www.appliedbiosystems.com/home/>
- [18] <http://www.thermofisher.com/home/>
- [19] <http://www.nanoporetech.com/>

- [20] Ralf, A, van Oven M, Zhong K, Kayser M. (2014) Simultaneous Analysis of Hundreds of Y-Chromosomal SNPs for High-Resolution Paternal Lineage Classification using Targeted Semiconductor Sequencing, Hum Mutat doi: 10.1002/humu.22713
- [21] <http://www.pacb.com/>
- [22] Coble, M.D. “Mystery solved: The identification of the two missing Romanov children using DNA analysis”, Plos One, Vol 4, p: 3, s. e4838
- [23] Coble M.D. (2011) The identification of the Romanovs: Can we (finally) put the controversies to rest? Investigative Genetics, Coble Investigative Genetics, 2:20.
- [24] Demircan, K. (2013) Rusya İmparatorluğu’nu 300 Yıl Yöneten Romanov Ailesi’nin 100 Yıllık Efsanesi: ANASTASYA, Bilim Teknik, Ocak: 58:61
- [25] <http://www.fbi.gov>lab>codis>

Received: 26.01.2017

Accepted: 24.05.2017

CORRESPONDING AUTHOR

E Hulya Yukselglu

Istanbul University, Institute of Forensic Sciences,
Fatih-Istanbul 34098, Turkey

e-mail: emelhulyayukselglu@gmail.com

A COST EFFECTIVENESS APPROACH FOR CONFIGURATION OF FEASIBLE SKYLINE YARDER FOR SPECIFIC FOREST REGIONS

Selcuk Gumus^{1,*}, Taha Yasin Hatay²

¹Department of Forest Engineering, Faculty of Forestry, Karadeniz Technical University, Trabzon, Turkey

²Forest Engineering, Faculty of Forestry, Kastamonu University, Kastamonu, Turkey.

ABSTRACT

The skyline yarder usage is the main extraction system in developed countries especially on steep terrains depending on cost effectiveness. Despite the availability of skyline yarder in many different types and characteristics it is extremely important choosing the feasible skyline yarder that will best meet the wood extraction requirements of any particular forest area, whether it is purchased or manufactured. It was aimed to configure the feasible forest skyline yarder by determining the technical and economic characteristics, which will be needed according to the qualifications of wood extraction operations of the Eastern Black Sea region of Turkey. The configuration is based on determining the technical specifications (skyline cable length, max. cycle load capacity and daily productivity) of the skyline yarder according to the extraction distance and the carrying capacity to be determined depending on the load to be carried at carriage cycle time. Technical specifications were evaluated by the cost of skyline yarder operation and the cost of the alternative extracting system by cost-effectiveness analysis method. The study showed that a feasible skyline yarder's technical specification must have at least 700 m yarding distances, ten cycles per a working day and 2.2 t carriage load capacity per cycle. This skyline yarders can be operated at the cost of 16.70 €/m³ if the daily productivity amount 30 m³ is. The work machine companies produce in a wide range of technical specifications, for this reason, the feasibility analysis should be made for selection of a logging machine, especially for local usage. Also, if domestic machinery production is considered, this scientific data will be the starting point.

KEYWORDS:

Cable Extraction, Configuration, Cost-effectiveness, Feasibility, Productivity, Skyline Yarder

INTRODUCTION

Timber extraction operation is one of the most dangerous, difficult and expensive logging operations. These operations are realised depending on many factors. Different logging systems may lead different processes costs as well as fragmentation on technological logging lines [1]. In the stump-to-truck timber harvesting analysis, primary transport activities such as skidding and yarding consumed the largest amount of cost. It is also greatest environmental impacts such as compaction of forest soils and damages on resident trees occurred compared with the other harvesting stages (felling, processing, and loading) [2, 3].

Cable yarding is a common harvesting technique of extracting timber from a steep slope or poorly accessible sites worldwide [4-6]. A great many different types of cable extraction systems developed recently. Cable systems fall into the category of "Skyline" systems, also called cable-crane systems [7]. On steep terrain, cable yarding is the cost-effective alternative to building an extensive network of skidding trails and results in a much lower site impact compared to ground-based logging [8].

The uses of the skyline systems enable more easy and low cost of logging operations. However, winching machines with power capabilities that are appropriate for the terrain and the size of logs extracted should be selected [7, 9]. Many logging site parameters have to be taken into account [10, 11]. In this stage, to consider which skyline systems to use is a very important issue according to the technical specifications. Talbot and his friends used economics, versatility and productivity for evaluating the skyline yarding systems [12].

Approximately 99% of the forests in Turkey are state-owned and operated by the state. Forest villagers who are not professional workers realise wood extraction. These workers do not have the means to invest in forestry machinery. They can use general farming machines owned by the forest villagers. These machines are not sufficient capacity in logging. For this reason, machines such as skylines yarders and skidders are purchased by the state and

rented to forest workers. The state charges workers for their extracted wood amount. The government pays these fees at the unit prices determined according to the nature of the business. Unit costs determine unit price in logging works. Machine rental rates are applied according to unit costs.

In 1985, the most recent purchase of skyline yarders was carried out in Turkey from various countries. Today, almost all of the machines have completed their physical lives. Skyline yarders, like they used to be, have to go into the extraction of timber again, with the purchase from the abroad or with the domestic production. However, according to past experiences, instead of purchasing or producing machines in many different types, it is necessary to determine the feasible machine specifications according to the local forestry needs and to act accordingly.

It has been put forth that the cable systems design studies were only 7 of 172 scientific research around the world, between from 2000 to 2011. Most of the studies have been made on skyline efficiency [13]. Skyline systems are being started to use since 1970 in Turkey. There are many studies on the skyline yarding efficiency, although none of them is for the choosing feasible skyline systems according to harvesting conditions. In many studies, the productivity value has been studied in the region [14-21]. At the same time, comparisons were made with each other according to the productivities.

Technical, economic, social and environmental elements that interact with each other must be evaluated in the feasibility analysis for forestry machinery. The optimum method of timber extraction is not always the cheapest. The feasible skyline yarders must be meet transportation needs and economics. Those requirements may be fulfilled by the identification of the forestry operations, infrastructure and terrain specifications (e.g. labour cost, line length, tree size, removal, etc.). It has been determined that the right logging method can reduce costs by 60-80% [10, 22, 23].

Cost-effectiveness analysis (CEA) is one of the methods used for cost evaluation. In a generic sense, CEA is a technique for identifying the least-cost option for meeting a specific physical objective/outcome [24-26]. Cost-effectiveness analysis can be a useful and powerful tool for resource allocation, decisions, uniform cost-effectiveness criterion [27]. The choice of a cost-effectiveness threshold depends on who is making the decision; what the purpose of the analysis is; how the decision maker values health, money, and risk; and what the available resources are [28, 29].

The objective of this study is the configuration of the feasible skyline yarder by using the specifications of yarding distance, carriage payload capacity and cycle time deal with daily productivity and operational costs for any specific forest region with examples of forestry and forest land conditions in Eastern Black Sea region of Turkey.

MATERIALS AND METHODS

To determine the technical specifications of the forest skyline yarder which is most suitable for the forests of Eastern Black Sea Region (EBSR), production systems and logging data was handled primarily. This was done by examining the records of forest operations in the forest enterprises. Then, according to the obtained technical data, a cost-effectiveness analysis based on efficiency and cost comparison was used to configure the most compatible skyline yarder. The manual gravity sliding method and the skyline yarder were compared in the cost-effectiveness analysis due to the steepness of the forest land structure of the area. Tractor winching does not have an effective use even if it is in the records. Tractor winching can be used only in limited to the cable distance.

For the determination of the extraction technical specifications, cutting quantities for extraction operations applied in the region were taken from logging records and cost value records from forest offices. Also, Google Earth software was used to measure the extraction distance and average slope for skyline extraction.

It was provided with a series of conditions which would assure approximately identical work premises for the two extraction systems to realise a technical and economic comparison regarding the involved costs for timber extraction using the manual gravity sliding and the skyline yarder.

Study Area and Logging Data Handling. The study was realised in Artvin, Giresun and Trabzon Forest Regional Headquarters (FRH) in the EBSR of Turkey. The total forest land surface area of the FRH's located on the study site is 1.398.588 ha. The study area is cover 6.45% of the whole Turkey's forest land [30]. This region has the most difficult transportation conditions, with an important place in the country's forests.

Logging sites data like as forest enterprises, compartment numbers, tree species, total logging volumes (m^3), log pieces numbers, surface slope (%), stump to road extraction distance (m), logging systems, transport direction (up to hill or down) and road interval data derived from Google Earth, were obtained and used to determining the skyline yarder specifications. Logging sites records were obtained by sampling on region forestry enterprises. The number of total logging compartments of the FRH's was determined. The number of logging sites on Artvin RFH was 424, Giresun FRH 324 and Trabzon FRH 341. The total logging site number was 1089.

The sampling numbers in the study area were estimated with the 95 % confidence level [31]. The minimum sampling number was calculated 285. Totally 301 sampling logging sites were accepted for sampling (120 in Artvin FRH, 91 in Giresun FRH and 90 in Trabzon FRH) by taking into account of

weighted average. The selection of the logging records was made randomly.

Extraction distance is one of the most important factors at logging operations. Extraction distances were acquired from site records and also from Google Earth digital globe by using its measurement tool. The 3D forest road interval distances were used for the extraction distance. This enabled us to compare the above mentioned two data sets each other. The measurement of the extraction distance was realised at sampling points of the whole region according to the 20x10 km grid spacing. A 10x10 km sample has been tried primarily. However, because there is many data and it makes the job harder, 20x10 km range is preferred. Totally 183 points were determined from the 207 sampling points, by the election of none forest lands on stand type maps. At each point, the nearest roads were used for the measurement. The road interval distance and site slope were measured at these points by drawing a line from a road to the nearest road directly and getting the elevation profile.

These measured extraction distance and slope values were discussed with the obtained data by the logging site records to get more accurate technical data.

Determining of the Technical Specifications and Configuration. The setting-up and operation of skylines used in forest operations represent a complex activity [32]. Log diameter, volumes cut per acre and average slope yarding distances have been used by LeDoux (1986) to simulate delay-free yarding cost for uphill cable yarders.

In this study, average yarding (extraction) distance, extraction direction according to the slope surface, cutting unit volume (m^3), number of log piece and total volume for per cycle and total logs weight per cycle were used for configuration of the skyline yarder operations. The obtained data from the region FRH's logging records were evaluated to determine the skyline yarder technical specifications. Technical specifications are the skyline cable length, max

cycle load capacity and daily productivity. The most important factor is the operational cost per m^3 .

Cost calculations were conducted according to the guidelines for machine rate estimation [33]. Cost calculations were made using cycle volume (m^3), cycle weight (t), cycle time (hour), daily yarder volume (m^3/day), average cutting unit volume (m^3), machine workday, worker day, worker fee ($₺/day$), machine amortization cost ($₺$), insurance costs ($₺$), maintenance and spare parts costs ($₺$), daily fuel expenses ($₺$) (€/₺ exchange rate was used 2.2161 according to data of the Central Bank of the Republic of Turkey for the study periods of 2010-2012 years).

The costs of different skyline yarder configurations are calculated according to daily productivity values according to max cycle load capacity and related items. By the way, the technical specifications of the skyline yarder were determined and feasible configuration according to the cost-effectiveness analysis regarding cost and productivity. The cost of the skyline yarders system, which is equivalent to the average cost of manual gravity sliding system that is one of the alternative extraction systems, is determined as the economic threshold point. The configuration has been carried out by using the economic threshold point level that showed the minimum carriage cycle load capacity according to log weight, daily productivity and skyline cable length.

RESULTS AND DISCUSSION

Harvesting Operations. Total log volume of sampled 120 number logging sites was found 56 339.509 m^3 at Artvin RFH while average log volume per logging site was 469.495 m^3 . These values were 25 927.133 m^3 and 284.913 m^3 at 91 cutting unit at Giresun while 27 428.514 m^3 and 304.765 m^3 at 90 cutting unit at Trabzon. Cutting units average log volume is 364.44 m^3 . The other data derived from the region RFH's is summarized at bellow table (Table 1).

TABLE 1
Logging sites harvesting data

Regional Forest Headquarters	Extraction system	Cutting unit number	Volume (m^3)	Total log pieces number (n)	Site slope (%)	Average extraction distance(m)	Volume per piece (m^3)
Artvin	Manual ground sliding	47	19 590	14 753	74	216.17	1.328
	Tractor winching	34	14 200	11 758	73	228	1.208
	Skyline yarding	39	22 549	15 557	79	534.1	1.449
Giresun	Manual ground sliding	28	2 119	1 801	73	168.2	1.177
	Tractor winching	55	19 717	15 914	74	367	1.239
	Skyline yarding	8	4 091	7 454	76	1385	0.549
Trabzon	Manual ground sliding	37	4 345	3 452	70	173.5	1.259
	Tractor winching	53	23 083	22 131	74	370.5	1.043
	Skyline yarding	-	-	-	-	-	-
Total		301	109 695	92 820	-	-	-
Average			364.44	308	74.1	334.9	1.125

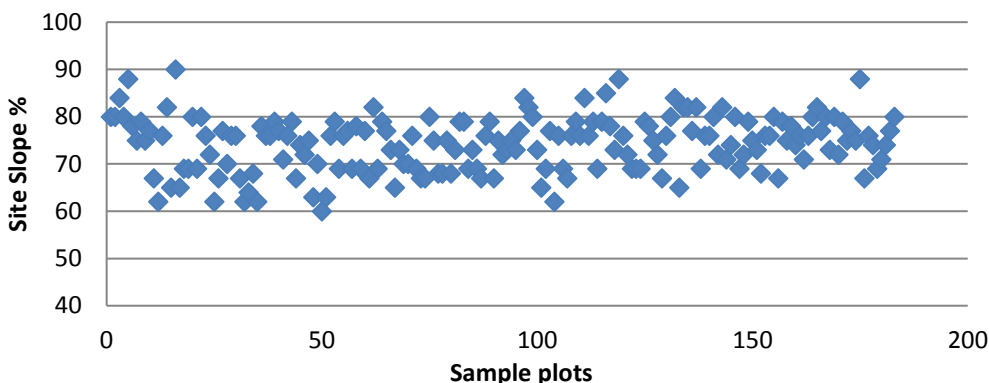


FIGURE 1
Cluster graph of the measured site slope at sample points

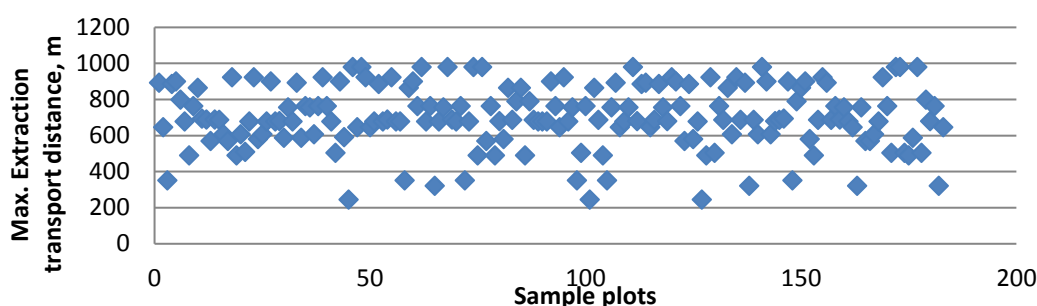


FIGURE 2
Cluster graph of the measured maximum extraction distances

TABLE 2
Site slope and extraction distance values from Google Earth virtual globe

RFH	Sample plot number	Ave. site slope, %	Maximum extraction distance, m	Ave. extraction distance, m
Artvin RFH	43	76	688	344
Trabzon RFH	84	75	696	348
Giresun RFH	56	72	724	362
Average		74.33	703	351.5

TABLE 3
Skyline yarder cost analysis table (summarised)

Yarding capacity per cycle (hardwood)		Daily Productivity (m ³)	Work days (day)	Worker costs (€/m ³)	Amortization + insurance costs (€/m ³)	Fuel, repair and maintain cost (€/m ³)	Total cost (€/m ³)
(m ³)	(t)						
1.042	0.7	10	36	21.28	8.37	11.28	40.93
2.083	1.5	20	18	12.93	4.19	5.64	22.76
3.125	2.2	30	12	10.15	2.79	3.76	16.70
4.167	2.9	40	8	8.24	2.77	2.48	13.49
5.208	3.6	50	7	7.92	2.21	2.26	12.39
6.250	4.4	60	6	7.36	2.44	1.88	11.68
7.292	5.1	70	5	6.87	2.09	1.55	10.51

Eastern Black Sea region site slope range is 60-90 %, extraction distance between 245 and 980 m according to the Google Earth measurements as shown in Figure 1, Figure 2 and Table 2).

The region has a steep terrain also long extraction distance. Skyline yarders usage gets importance for extraction of logs in this region. The extraction

distance is one of the most important specifications of the yarder specifications.

Skyline Technical Specifications. Extraction costs were calculated for according to the logging operation specifications for determining of skyline yarder technical specifications. For this, manual

workmanship costs and skyline yarder operational costs paired each other according to the cost-effectiveness threshold for determining economic skyline usage level and skyline yarder technical specifications.

The cost of manual ground gravity sliding was calculated 16.34 €/m³ where the conditions are in average maximum extraction distance 700 m (average extraction distance 351.5 m) and cutting unit average log volume 364.44 m³ according to the FRH's logging site data records. Daily extraction productivity is 9.508 m³ for five workers.

Skyline yarder cost calculation was made taking into account operational cost components such as total work time according to the max yarding distance (700 m), yarding capacity per cycle (log volume (m³) and weight (t)), average cycle time (50 min.), daily productivity (day=productive system hours as 8 hours), average log volume per logging site (364.440 m³), setup and uninstallation period time (10 days), work crew (5 workers) workmanship costs (€16.34), machine amortization, machine annual maintenance and repair costs, fuel usage and total operating expenses including insurance costs. Some used values were taken from the earlier studies [2, 8, 19, 23, 34-38].

The summary of the cost calculations was presented in Table 3. Daily work productivity was assumed from 10 to 70 m³ according to possible carriage cycle load capacity.

Workmanship cost is one of the most effective factors in the cost components. The number of working days depends on the daily productivity due to cycle yarding load capacity. Total cost decreases with daily productivity increasing. If the skyline yarder can be operated for 30 m³/day performance, the yarding cost will be 16.70 €/m³. If the daily productivity reaches to 70 m³/day, the yarding cost can be reduced to 10.51 €/m³. These performances are reachable values according to the carriage load capacity and skyline main power unit.

Daily productivity values were calculated in many earlier studies for different skyline yarder models in Turkey. The daily work productivity varied from 34.144 m³ to 62.976 m³ for different yarding distance up to maximum 600 m in these studies at the region [14-21]. It was found that the daily productivity and operational cost varied from 19.2 to 74.4 m³ and 4.57 to 30 €/m³ respectively at other studies were made on European countries [8, 32-42]. The results of the cost analysis show that the configuration gives average values according to the recent studies.

Cost-effectiveness analysis of the manual gravity sliding and skyline yarders used in the region was realized by productivity pairing them each other. P ratio varies from 49.98 to -0.10, but the change is mainly between 0.61 and -0.10. The ratio was calculated 0.00 at the 30.5 m³/day productivity value. There is no obvious consensus about how small the

cost-effectiveness ratio should be evaluated [24, 25]. The point (p=0.00) was accepted as economic threshold point. This point was evaluated the lowest daily productivity value that the skyline yarder should have. This productivity value also revealed other technical specifications which are based on the cost calculation and configuration of the skyline yarder.

Logs can be extracted 9.508 m³/day with the cost of €16.34 by manual gravity sliding system, whereas approximately 30 m³ logs can be yarded at the same cost value by skyline yarder according to results. The skyline yarder system is approximately 3 times productive than the manual gravity sliding system.

Configured Skyline Yarder Specifications.

The feasible skyline yarder productivity must be over 30 m³/day due to ensure profitable against the manual sliding system on Eastern Black Sea region. In this frame, the technical specifications of the feasible yarder are: 700 m yarding distance, 2.2 t carriage load capacity for per cycle and 50 min/cycle compatible carriage speed for the yarding distance according to the cost calculation method used in this study. These three values should define the other specifications. This type of skyline yarder can be realized ten cycles per a workday.

When the carriage load capacity reaches to 5.1 t, it can be yard 70 m³/day. This productivity is a reachable limit and it can improve the logging productivity at a significant level. "The limited average extracted volume may have depended on the work method employed rather than the machine capacity. It is known that the preparation of loads has an important effect on the efficiency of load extraction [42]".

CONCLUSION

Many scientific studies were made about skyline yarders which have being used since 1970 in Turkey. These were the case studies about determining the productivity of skyline yarders. There was not any study about the configuration of feasible skyline yarder specifications in this region. Skyline yarders were not used feasibly because of the scientific knowledge absence.

Cost-effectiveness analysis was found capable of decision making about the evaluation of alternative extraction systems. Feasible skyline yarder daily productivity according to cycle payload, yarding cycle time and extraction distance were determined for configuration of the feasible skyline yarder minimum technical specifications.

Skyline yarder technical specifications should be determined by using the method described in the study for skyline yarder use, as required for each region separately. Therefore, forest logging data, road

network and alternative transportation systems costs should be evaluated. Google Earth was found a useful tool to measure derive terrain and road network data.

This study results will be guidance to manufacturers and forest workers in sustainable timber extraction operations. Until now there is not any skyline yarder procurement in Turkey. Configured skyline yarder technical specifications will make it possible increasing extraction productivity with the profitable usage of the skyline yarders or provide data for possible skyline yarder producing in Turkey also. At the same time, a maximum cost effective usage can be established even if the machines are being imported.

ACKNOWLEDGEMENTS

We thanks to Artvin, Trabzon and Giresun Regional Forest Headquarters staff for kind cooperations for a while data handling. Special thanks to Dr. Sezgin Hacisalihoglu for his support.

REFERENCES

- [1] Birda, M., and Borz, S.A. (2012) A comparison between tractor based and skyline based mechanized systems for timber logging, *Bulletin of the Transilvania University of Brasov Series II* 5(54), 19-24.
- [2] Holmes, T.P., Blate, G.M., Zweede, J.C, Pereira, R., Barreto, P, Boltz, F. and Bauch, R. (2002) Financial and ecological indicators of reduced impact logging performance in the Eastern Amazon, *Forest Ecol Manag* 63, 93-110.
- [3] Han, H., O'Neil, E., Bergman, R.D., Eastin, I.L. and Johnson, L.R. (2015) Cradle-to-gate life cycle impacts of redwood forest resource harvesting in northern California, *Journal of Cleaner Production* 99, 217-229.
- [4] Bont, L. and Heinimann, H.R. (2012) Optimum geometric layout of a single cable road, *Eur J Forest Res* 131, 1439-1448.
- [5] Spinelli, R., Maganotti, N. and Visser, R. (2015) Productivity models for cable yarding in Alpine forests, *Eur J Forest Eng* 1, 9-14.
- [6] Talbot, B., Stampfer, K. and Visser, R. (2015) Machine function integration and its effect on the performance of a timber yarding and processing operation, *Biosystems Engineering* 135, 10-20.
- [7] Dykstra, D.P. and Heinrich, R. (1996) *FAO Model Code of Forest Harvesting Practice*. Rome, Italy: FAO.
- [8] Spinelli, R., Magagnotti, N. and Lombardini, C. (2010) Performance, capability and costs of small-scale cable yarding technology, *Small-scale Forestry* 9, 123-135.
- [9] Worrell, W.C., Bolding, M.C. and Aust, W.M. (2011) Potential soil erosion following skyline yarding versus tracked skidding on bladed skid trails in the Appalachian region of Virginia, *Southern Journal of Applied Forestry* 35, 131-135.
- [10] LeDoux, C.B. (1986) Stump-to-truck cable logging cost equations for young-growth douglas-fir. *Western Journal of Applied Forestry* 1: 19-22.
- [11] Magaud, P. (2011) SIMULCABLE, a new software to optimise the line implantation for cable yarding. Pushing the boundaries with research and innovation in forest engineering FORMEC 2011, In: Kanzian, C. (ed.) *Proceedings of the 44th International Symposium on Forestry Mechanisation*, 9-13 October 2011; Graz, Austria: University of Natural Resources and Life Sciences. 1-8.
- [12] Talbot, B., Tarp, P. and Nitteberg, M. (2014) Selecting an appropriate excavator-based yarder concept for Norwegian conditions through the analytic hierarchy process, *International Journal of Forest Engineering* 25, 113-123.
- [13] Cavalli, R. (2012) Prospects of research on cable logging in forest engineering community, *Croat J for Eng* 33, 339-356.
- [14] Acar, H.H. and Erdas, O. (1992) Comparison of Long-distance Crane skyline yarders and Forest Road Alternatives in Terms of wood extraction on Artvin region, *Turk J Agric for* 16, 549-558.
- [15] Aykut, T., Acar, H.H. and Senturk, N. (1997) An investigation on the comparison of Koller K 300, Urus M III and Gantner skylines used for extraction from compartment in Artvin region (article in Turkish with an abstract in English), *Review of the Faculty of Forestry, Istanbul University Series A* 47(2), 29-54.
- [16] Ozturk, T. (2003) The research on transporting forest products with varied forest skylines in mountainous forest zone of Turkey. PhD, Istanbul University, Istanbul, Turkey.
- [17] Degermenci, K.V. (2007) A study on the logging operations using cableway in Atila forest, MSc. Kafkas University, Kars, Turkey.
- [18] Erdas, O. (2008) *Transport Teknigi*, Kahramanmaraş Turkey: Kahramanmaraş University.
- [19] Gumus, S. and Acar, H.H. (2010) Evaluation of consecutive skylines yarding and gravity skidding systems in primary forest transportation on steep terrain, *J Environ Biol* 31, 213-218.
- [20] Bektas, C. (2011) Examination of extraction methods in terms of transport technique in the sample of Devrek Forest Enterprise, MSc. Bartın University, Bartın, Turkey.
- [21] Caglar, S. and Acar, H.H. (2011) An investigation on the time study and productivity of Koller K300 mobile yarder, *Artvin Coruh University Journal of Forestry Faculty* 6, 113-120.

- [22] Frutig, F., Fahrni, F., Stettler, A. and Egger, A., (2007) La recolte mecanisee des bois sur terrain en pente, *Technique Forestiere* 6, 16-21.
- [23] Spinelli, R., Visser, R., Thees, O., Sauter, U.H., Krajnc, N., Riond, C. and Magagnotti, N. (2015) Cable logging contract rates in the Alps: the effect of regional variability and technical constraints, *Croatian Journal of Forest Engineering* 36, 195-203.
- [24] Azimi, N.A. and Welch, H.G. (1998) The effectiveness of cost-effectiveness analysis in containing costs, *J Gen Intern Med* 13, 664.
- [25] Edejer, T.T., Baltussen, R., Adam, T., Hutubessy, R., Acharya, A., Evans, D.B. and Murray, C.J.L. (2003) WHO guide to cost-effectiveness analysis, Geneva, Italy: World Health Organization.
- [26] Balana, B.B., Vinten, A. and Slee, B. (2011) A review on cost-effectiveness analysis of agri-environmental measures related to the EU WFD: Key issues, methods, and applications, *Ecological Economics* 70, 1021-1031.
- [27] Garber, A.M. and Phelps, C.E. (1997) Economic foundations of cost-effectiveness analysis, *Journal of Health Economics* 16, 1-31.
- [28] Douglas, K. and Owens, M.D. (1998) Interpretation of Cost-Effectiveness Analyses, *Journal of General Internal Medicine* 13, 716-717.
- [29] Elia, M., Lovreglio, R., Ranieri, N.A., Sanesi, G. and Laforzezza, R. (2016) Cost-Effectiveness of fuel removals in Mediterranean wildland-urban interfaces threatened by wildfires, *Forests* 7, 149.
- [30] GDF. (2013) Forestry statistics, General Directorate of Forestry, Ankara, Turkey: Turkish Statistical Institute.
- [31] Demirutku, K., Okay, N.C., Yaman, A., Kivanc, F.E., Muratoglu, B. and Yeniceri, Z. (2005) *Statistical Formulas and Tables*. Ankara, Turkey: Baskent University, Faculty of Economics and Administrative Sciences, Creative Thinking and Behavioural Research Laboratory.
- [32] Duta, I.C. and Ignea, G.H. (2011) Traf - new software for skylines design for forest purposes, *Bulletin of the Transilvania University of Brasov Series II* 5.54, 57-62.
- [33] Hoffmann, S., Jaeger, D., Lingenfelder, M. and Schoenherr, S. (2016) Analyzing the efficiency of a start-up cable yarding crew in Southern China under new forest management perspectives, *Forests* 7, 188.
- [34] Park, S.J., Kim, J.W., Park, M.S., Song, T.Y. and Cho, K.H. (2006) An analysis of the yarding operation system with a mobile tower-yarder in Korea, In: Chung W, Han HS, editors. *Proceedings of the 29th Council on Forest Engineering (COFE)*, July 22-Aug 2, 2006; Coeur d'Alene, Idaho, USA: Council on Forest Engineering (COFE), 1-11.
- [35] Borz, S.A., Birda, M, Ignea, G. and Oprea, I. (2011) Technological aspects regarding timber exploitation using Mounty 4100 cable yarder. *Bulletin of the Transilvania University of Brasov Series II*, 4(53), 1-6.
- [36] Dimitrov, D. (2012) Investigation on work time and productivity of forest skyline Koller K 300 in Orgazhden Mountain. *Forestry Ideas* 18, 92-96.
- [37] Ghaffariyan, M.R., Stampfer, K. and Sessions, J. (2013) Production Equations for Tower Yarders in Austria, *International Journal of Forest Engineering* 20, 17-21.
- [38] Spinelli, R., Visser, R., Thees, O., Sauter, U.H., Krajnc, N., Riond, C. and Magagnotti, N. (2015) Cable logging contract rates in the Alps: the effect of regional variability and technical constraints, *Croatian Journal of Forest Engineering* 36, 195-203.
- [39] Devlin, G. and Klvac, R. (2014) How Technology Can Improve the Efficiency of Excavator-Based Cable Harvesting for Potential Biomass Extraction—A Woody Productivity Resource and Cost Analysis for Ireland, *Energies* 7, 8374-8395.
- [40] Hoffmann, S., Jaeger, D., Schoenherr, S. and Talbot, B. (2015) Challenges in mechanization efforts of small diameter Eucalyptus harvesting operations with a low capacity running skyline yarder in Southern China, *Forests* 6, 2959-2981.
- [41] Campbell, T. (2016) Assessment of the Opportunity of Modern Cable Yarders for Application in New Zealand. MSc, University of Canterbury, Christchurch, New Zealand.
- [42] Proto, A.R., Skoupy, A., Macri, G. and Zimbalatti, G. (2016) Time consumption and productivity of a medium size mobile tower yarder in downhill and uphill configurations: a case study in Czech Republic, *Journal of Agricultural Engineering* 47, 216-221.

Received: 04.02.2017

Accepted: 31.05.2017

CORRESPONDING AUTHOR

Selcuk Gumus

Department of Forest Engineering
Faculty of Forestry
Karadeniz Technical University
Trabzon – TURKEY

E-mail: sgumus@ktu.edu.tr

EMISSION CHARACTERISTICS OF BIOMASS COMBUSTION IN A DOMESTIC HEATING BOILER FED WITH WOOD AND VIRGINIA MALLOW PELLETS

Grzegorz Zajac, Joanna Szyszlak-Bargłowicz*, Tomasz Słowik, Jacek Wasilewski, Andrzej Kuranc

Department of Power Engineering and Transportation, Faculty of Production Engineering, University of Life Sciences in Lublin, Głęboka 28, 20-612 Lublin, Poland

ABSTRACT

The presented research was aimed at analysing the emission characteristics of a domestic heating boiler fed with Virginia mallow pellets (*Sida hermaphrodita* Rusby) and wood pellets available on the market. A 32 kW boiler with automatic fuel load adapted to wood pellets combustion was used in the research. The installation used in the research was a typical installation used to heat single-family houses. Timelines of changes in O₂, CO, CO₂, NO, NO_x, and SO₂ concentrations were registered at the boiler's outlet throughout the study. Analyses of mallow pellets and wood pellets combustion in a boiler with automatic fuel load adapted to wood pellets combustion showed that CO, NO, NO_x and SO₂ emissions were higher during mallow pellets combustion.

KEYWORDS:

combustion, biomass, pellets, CO, CO₂, NO, NO_x, SO₂ emission

INTRODUCTION

The systematic increase in renewable fuels use results mainly from environmental conditions which are the outcome of specific climate policies imposed on Member States of the European Union [1] and the need for sustainable energy supply [2]. Using the potential of biomass energy for heating households based on locally available biomass resources is the most effective in the Polish climate (also typical of many regions in Europe) [3]. To facilitate the use of biomass for energetic purposes (transport, storage and combustion), it is processed into the form of pellets and briquettes [4].

The ecological aspects and threats of contamination indicate that wood pellets should be used first and foremost in low-power boilers used in household heating. The lack of affordable, good quality wood pellets, which are currently used in Poland in the commercial power generation, has aroused an interest in agricultural biomass pellets as the fuel for low-power boilers [5]. The acquisition of biomass from

plantations of perennial native species and these introduced to Poland may complete the biomass supply balance in the energy market [6,7]. Attempts have also been undertaken of combustion of the pellets produced from different types of biomass, including waste pellets, in the systems which enable the controlled conduct of the process [8–11].

The process of biomass combustion is determined by fuel properties, especially the granulation, moisture content, density and nitrogen and sulphur contents as well as the design, nature and type of the furnace. These factors are predominantly independent, nevertheless, because of the complexity of the combustion processes, they are often subject to interaction, which complicates the optimization of the combustion process [12]. The fuel supply rate and air supply are the control parameter of the combustion process. Each combustion process is accompanied by the emission of pollutants such as: carbon monoxide and soot, nitrogen oxides, sulphur oxides, hydrocarbons and metals in varying quantities [13]. The quantity and type of contamination produced in the process of biomass combustion depend not only on the process-related factors, but also on the type of the burnt biomass [14–18]. The problem of emission of incompletely combusted products is particularly pronounced during biomass combustion in the low-power boilers. Only approx. 20% of volatiles by weight are produced in the first stage of hard coal combustion, whereas in the case of biomass, the amount ranged from 70% to 80% [19].

The research was aimed at analysing the emission characteristics of low-power boiler fuelled with mallow pellets (*Sida hermaphrodita* Rusby) and wood pellets available on the market. A 32 kW boiler with automatic fuel load adapted to wood pellets combustion was used in the research. In the course of the research, timelines of changes in O₂, CO, CO₂, NO, NO_x, SO₂ concentrations were recorded at the boiler's outlet.

RESEARCH METHODOLOGY

A 32 kW boiler with automatic fuel load adapted to wood pellets combustion was used to carry out tests on Virginia mallow pellets and wood

pellets combustion. The boiler is equipped with a burner, to which the fuel is fed by a screw feeder from a container. The air for combustion is supplied by a fan to a system of nozzles in the burner. The operation of the boiler is controlled through a programmed electronic controller. In the course of the tests, 28.9 kg of Virginia mallow pellets were used in a 4.8 kg·h⁻¹ stream of fuel weight and 44.8 kg of wood pellets in a 7.4 kg·h⁻¹ stream of fuel weight.

The combustion tests were carried out in specified conditions of the boiler operation at rated settings; the tests lasted 6 hours. Differences were observed in the value of the coefficient of air excess λ . In the case of combustion of Virginia mallow pellets it was 1.8 and during combustion of wood pellets it was 1.5. This difference may be due to the difficulty in adjusting the furnace control to the conditions of combustion. Thermal power of 20.2 kW and 33.5 kW respectively was achieved in the combustion with 90% and 91.1% thermal efficiency of the boiler.

Pellets of Virginia mallow biomass, which is one of the energy crops with a satisfactory yield potential and advantageous characteristics of energy parameters, and wood pellets available on the market were the tested fuel [20,21]. Physical and chemical properties of Virginia mallow pellets and wood pellets are presented in Table 1.

TABLE 1
Physical and chemical properties of Virginia mallow pellets and wood pellets

Parameter	Unit	Virginia mallow pellets	Wood pellets
Total moisture content	wt. [%]	7.7	5.7
Ash	wt. [%]	2.9	0.3
Content of volatile materials	wt. [%]	82.68	84.45
Carbon	wt. [%]	48.1	49.5
Hydrogen	wt. [%]	5.79	6.06
Sulphur	wt. [%]	0.07	0.02
Nitrogen	wt. [%]	0.42	0.17
Heat of combustion	[kJ·kg ⁻¹]	19 084	19 953
Calorific value	[kJ·kg ⁻¹]	16 804	17 893

The composition of emission at the broiler's outlet was measured the system of analysers manufactured by SIEMENS. The system included ULTRAMAT 23 analysers enabling measurements of CO concentrations within the ranges of 0-5% and 0-50%, CO₂ within the range of 0-50%, SO₂ within the range of 0-2500 ppm; and two NO analysers within the range of 0-1000 ppm, including one operating with NO₂ converter to NO. NO₂ concentration was very low during the experiment and was included by

the flue gas analyser in NO_x concentration value. Those measurements were carried out using the IR reference method. The O₂ concentration in the gas was measured using an OXYMAT 5 analyser operating on the basis of a reference method using the phenomenon of paramagnetism and within O₂ range of 0-25%. The emissions were sampled in a continuous way by means of a heated probe with a ceramic filter, a heated hose and a gas conditioning system.

The installation used in the research was a typical installation used for heating one-family houses and designed for the combustion of pellets. During the combustion tests, its rating settings were not interfered. The study results are not strict data, but only examples of one-time measurements indicating the level of emission of particular compounds.

RESEARCH FINDINGS AND DISCUSSION

Figures from 1 to 6 present the results of measurements of O₂, CO₂, CO, SO₂, NO and NO_x emissions that accompany Virginia mallow pellets and wood pellets combustion. The average concentrations of the measured exhaust components, calculated on the basis of the timelines of their changes, are listed in Table 2. In addition, their emissions of during the combustion of the tested fuels are compared in Table 3.

TABLE 2
Average concentrations of the measured exhaust components.

Specification	Unit	Virginia mallow pellets	Wood pellets
O ₂	[%]	9.66	6.71
CO ₂	[%]	10.7	13.73
CO	[%]	0.21	0.00
NO	[ppm]	324.81	256.24
NO _x	[ppm]	328.18	256.39
SO ₂	[ppm]	0.33	0.00

TABLE 3
Emissions of the determined exhaust components (converted per 10% O₂ content)

Specification	Unit	Virginia mallow pellets	Wood pellets
Z _{CO2}	[%]	10.41	10.57
C _{CO}	[mg·m _n ⁻³]	2525.2	47.2
C _{NO}	[mg·m _n ⁻³]	421.7	263.7
C _{NOx}	[mg·m _n ⁻³]	664.8	519.4
C _{SO2}	[mg·m _n ⁻³]	0.9	0

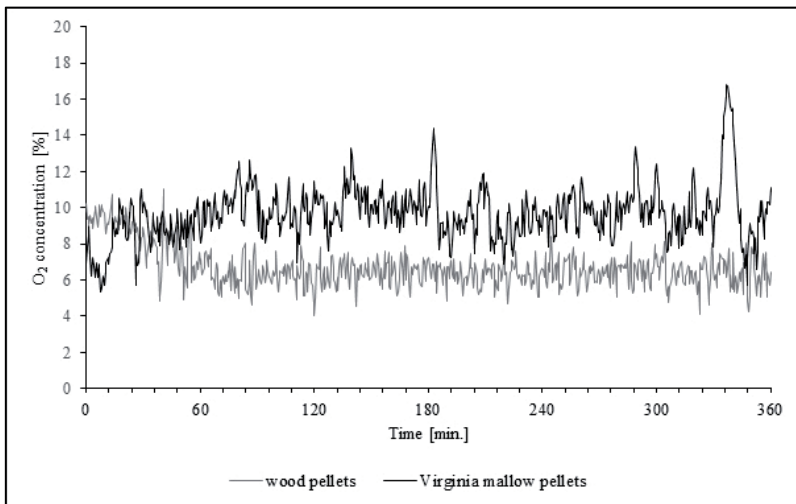


FIGURE 1
Timeline of changes in O₂ concentration in combustion tests of Virginia mallow pellets and wood pellets

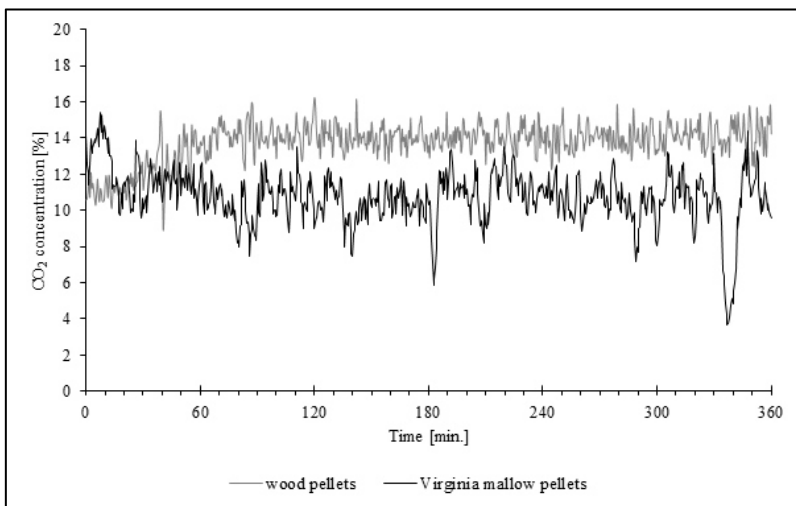


FIGURE 2
Timeline of changes in CO₂ concentration in combustion tests of wood pellets and Virginia mallow pellets

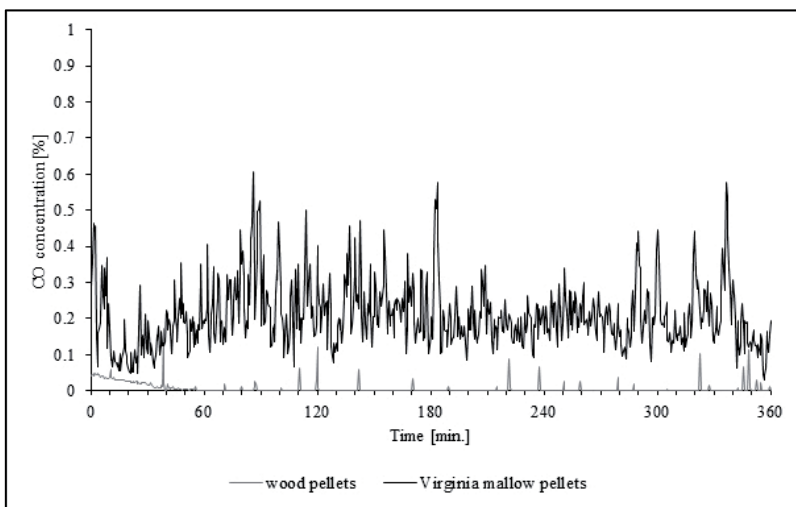


FIGURE 3
Time line of changes in CO concentration in combustion tests of wood pellets and Virginia mallow pellets

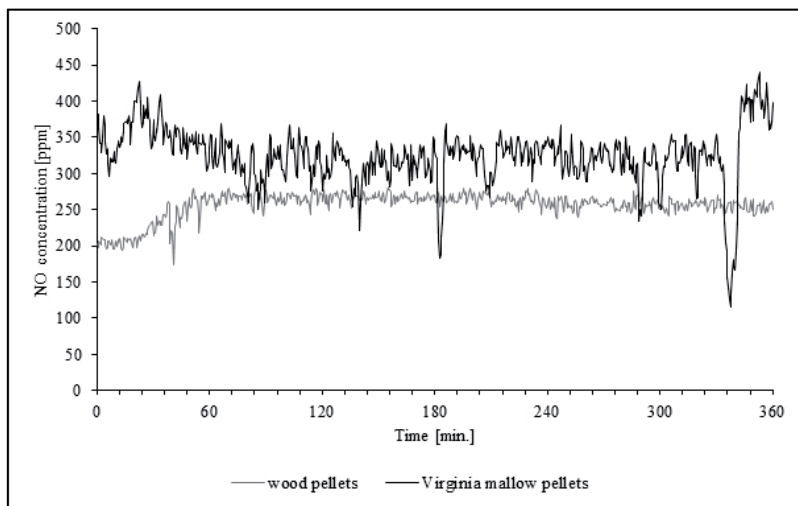


FIGURE 4

Time line of changes in NO concentration in combustion tests of on wood pellets and Virginia mallow pellets

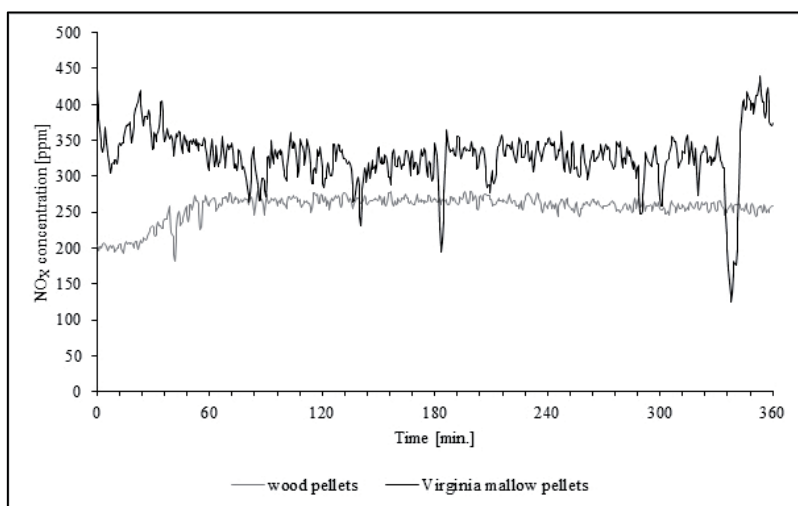


FIGURE 5

Time line of changes in NOx concentration in combustion tests of wood pellets and Virginia mallow pellets

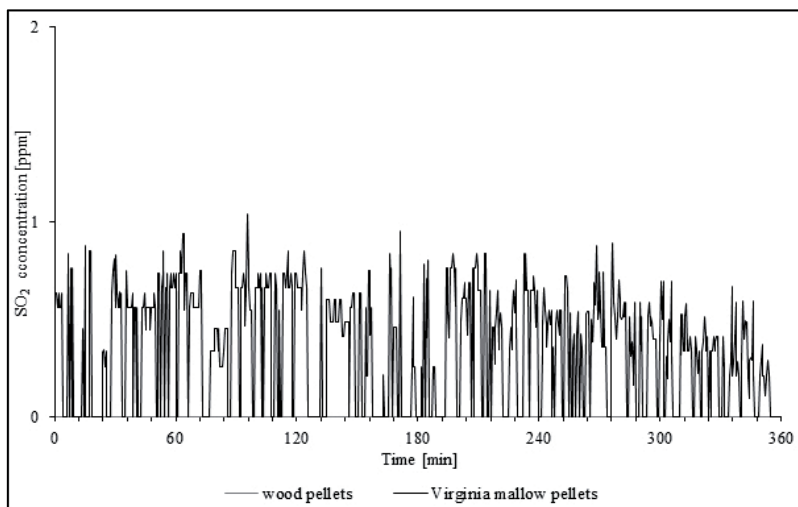


FIGURE 6

Time line of changes in SO2 concentration in combustion tests of wood pellets and Virginia mallow pellets

Higher O₂, CO, NO, NO_x, SO₂ concentrations were observed during Virginia mallow pellets combustion when comparing the concentrations of each of the measured exhaust component presented in Figures from 1 to 6. High CO emission (2525.2 mg·m_n⁻³) during Virginia mallow pellets combustion resulted from an incomplete combustion and a poor organization of the process. The higher CO concentration was influenced by a reduction of the temperature in the combustion chamber caused by difficulties in supplying fuel. High dust content in the fuel hindered the movement of pellets in feeder containers, in addition, rough surface of Virginia mallow pellets caused blockages in the containers (despite the use of moving parts), which resulted in temporary interruptions in the feeding of the desired amount of pellets into the burner. This was not observed in the case of wood pellets. Juszczak [22] in his studies on concentrations of pollutants emitted from a boiler fuelled with wood pellets in a periodic and continuous way noticed an increase in the CO concentration above the minimum value as a result of temperature reduction in the combustion chamber at pellets feeding interruption. In the case of combustion of the fuel fed in a periodic way, the CO concentration was much higher in the setting with a long break in pellets feeding (from 312 mg·m_n⁻³ in a continuous fuel supply to 1604 mg·m_n⁻³ in fuel supply with the longest break). The CO emission observed by Dias et al. [23] during the combustion of pellets from various biomass types, in specified conditions of the boiler operation, usually amounted to less than 1500 mg·m_n⁻³.

The combustion process of incomplete-combustion products is complex but it needs to be resolved because of the unsatisfactory oxidation of CO. Low-power boilers have a compact structure, which poses a difficulty in creating an extra space serving as an after-combustion chamber. Because of that it is difficult to design this type of units and optimize the combustion process in terms of reducing air pollutants emissions [13].

When comparing the results of the nitrogen content in Virginia mallow pellets (Tab. 1) with typical values for wood biomass, which according to the literature are less than 0.2% [24,25], a higher content of this element can be observed in Virginia mallow pellets. This may be due to the use of mineral fertilizers containing nitrogen in the growing of Virginia mallow, which had a negative influence on the level of NO and NO_x emissions during the combustion of the studied biomass. This is supported by the findings of the energy and emission analyses (NO 421.7 mg·m_n⁻³, NO_x 664.8 mg·m_n⁻³) (Tab. 2-3, Fig. 4-5). In the above-mentioned publication, Juszczak [22] observed an increase in the concentration of nitrogen oxides NO and NO_x with an increase of oxygen concentration and a decrease of those concentrations with an increase of the temperature in the combustion chamber. The NO_x concentration determined by

the author did not exceed 400 mg·m_n⁻³. If the temperature in the furnace is relatively low, NO and NO_x concentrations depend mainly on the stream of nitrogen fed to the furnace with the fuel, and nitrogen oxides are formed from the nitrogen contained in the fuel [26]. In low-power boilers, the combustion temperature often does not exceed 1300°C and no formation of thermal NO_x occurs (because of the oxidation of atmospheric nitrogen) [27–29]. In such a case, NO_x emissions should be directly connected with nitrogen content in the fuel. However, because of the very high ash content in the agricultural biomass, the influence of catalytic effects of ash surface should also be taken into account when considering the formation of NO_x during the combustion of this type of biomass. Different NO_x emissions during the combustion of pelleted agricultural biomass may result from the variable contents of nitrogen and ash, catalysing the formation of NO_x in the biofuel [14].

SO₂ emission was very low (0.9 mg·m_n⁻³) in the case of Virginia mallow pellet combustion and in the tests on wood pellets combustion it was zero. During the tests on wood pellets and hay pellets combustion, Roy et al. [30] also observed a very low emission of SO₂ within the range of 0-26 mg·m_n⁻³. Sulphur content is one of the parameters indicating the usefulness of biomass for energy purposes. The sulphur content in the biomass of plant origin is minimal; it is only derived from amino acids and vitamins which have sulphur in their structure. The content of this macroelement in plants is determined by both plant species and by its content in the soil [31]. Verma et al. [32] observed the lowest emissions of SO_x during wood pellets combustion (0-3.5 mg·m_n⁻³) and the highest one during straw pellets combustion (185.52-245.59 mg·m_n⁻³). They also confirmed that SO_x emission was dependent on sulphur content in the biofuels subjected to combustion. An in-depth discussion on the research findings obtained in the course of similar experiments can be found in publications [33,34].

The results of analysis of concentrations in fumes of air pollutants using a boiler with retort furnace of the capacity of 15 kW, which is often used for heating detached houses, were presented by Hardy et al. [35]. The studies were conducted in similar temperature ranges and using the excessive air factor on pellets of wood, wheat straw and rape straw along with miscanthus. The highest concentration of CO was determined while feeding the boiler with pellets made of rape straw (1.65-3.0%). The concentration was slightly lower, but still comparably high, during the combustion of wheat straw pellets (0.75-1.2%), lower during the combustion of miscanthus pellets (0.18-0.3%) and the lowest during the combustion of wood pellets, (0.1-0.16%). The concentration of NO was fluctuating within the range of 100-200 ppm, whereas the lowest one was determined during the combustion of rape straw pellets (100-130 ppm) and the highest one while burning the wheat straw pellets (150-200 ppm). By contrast, Magdziarz

and Wilk [36], who were burning standardized wood pellets, determined CO concentrations at 0.005–0.02% (i.e. 57–230 mg·m⁻³). The NO_x concentration detected by these authors proved to be within the lower range of NO_x concentrations generated from fuel combustion and amounted to 170–220 ppm (270 mg·m⁻³ and 208 mg·m⁻³). Literature data provide different concentrations of NO_x in the exhaust gases, which range from 170 to 920 mg·m⁻³, as affected by the types of fuel and furnace [19].

The cutting-edge wood pellet furnaces with oxygen probe and continuous fuel delivery are characterised by CO concentrations from 10 to 50 mg·m⁻³ [37,38] (however, these were the studies conducted in stationary conditions, on research posts, at high thermal power). Whereas, in the case of the most common boilers with periodic distribution of pellets and without the oxygen stream regulation nor probe, the values of CO concentration achieved in the boiler room, in the near real-life environment, often amount to 300–1200 mg·m⁻³ (calculated in respect to the 10% concentration of oxygen), depending on the quality of pellets and the type of burner [2, 38–40]. In addition, the parameters of the emissions from the pellet furnaces, measured in accordance with the technical standards, do not provide representative data in relation to the actual use. These differences result from the different operating conditions of the boiler and combustion, as well as the exclusion of phases during transient operating conditions (e.g. the ignition phase) at the time of the standard measurement.

Toscano et al. [42] conducted the stimulation of the real-life exploitation conditions of the boiler for burning pellets and made more representative measurements of the actual impact exerted by these devices on the environment. The maximum values of CO concentration have always been connected to the ignition phase and exceeded 5000 mg·m⁻³.

In many countries, the residues from agricultural and food production are used for the energy-related purposes, for example, the dried residues of tomatoes [43], grapes [44], or olives [45]. However, the concentration of CO obtained from their combustions often reaches up to several thousand mg·m⁻³ (10% of the oxygen content in the exhaust gas), and is significantly higher compared to the combustion of wood pellets (in top-quality furnaces, they amount to less than 1000 mg·m⁻³ [2]).

It is particularly important to consider the attempt to determine the balance between NO_x and CO using low-power boilers for gradual biomass combustion in order to control the emission of NO_x. It is considered that optimised designs of furnaces, boilers and secondary air mixing and combustion products of the root zone can provide both low emissions of NO_x and CO even from the low-power boilers fuelled by biomass [46].

SUMMARY AND CONCLUSIONS

Based on the survey, the following conclusions were formulated:

1. The tests in which the pellets produced from Virginia mallow and wood pellets were burnt in a boiler with automatic feed of fuel adapted to burn wood pellets indicated the higher emissions of CO, NO, NO_x and SO₂ in the case of combustion of pellets from Virginia mallow.

2. The increased emission of CO during the combustion of pellets produced from Virginia mallow resulted from incomplete combustion and poor organisation of the process due to the large heterogeneity of Virginia mallow pellets and the lack of adaptation of the control system for this specific fuel.

3. The adverse level of nitrogen oxides emission in the process of burning Virginia mallow pellets was caused by the high content of nitrogen in the fuel. This may be related to the use of mineral fertilizers containing nitrogen in growing Virginia mallow.

4. The emission of sulphur dioxide during the combustion of Virginia mallow pellets was very low, and it amounted to zero at the time of burning wood pellets.

5. Burning pellets produced from agricultural biomass in low-power boilers designed to burn wood pellets may be connected with higher emissions of toxic components in relation to the basic fuel, i.e. wood pellets. It may result from the fact that other fuels and fuel feeding systems are adapted merely to the combustion of wood pellets.

ACKNOWLEDGEMENTS

The research was financed by the Ministry of Science and Higher Education (Project no. NN313444737)

REFERENCES

- [1] Grudziński, Z. (2013) Environmental Costs Resulting from the Use of Coal in the Power Sector. *Rocznik Ochrona Środowiska*, 15(3), 2249–2266.
- [2] Kjällstrand, J. and Olsson, M. (2004) Chimney emissions from small-scale burning of pellets and fuelwood—examples referring to different combustion appliances. *Biomass and Bioenergy*, 27(6), 557–561.
- [3] Gula, A. and Goryl, W. (2014) Toward a More Environmentally Friendly Use of Biomass for Energy Purposes in Poland. *Polish Journal of Environmental Studies*, 23(4), 1377–1380.
- [4] Obidziński, S. (2014) Pelletization of biomass waste with potato pulp content. *International Agrophysics*, 28(1), 85–91.

- [5] Juszczak, M. (2012) Concentrations of carbon monoxide and nitrogen oxides from a 15 kW heating boiler supplied periodically with a mixture of sunflower husk and wood pellets. In *Ochrona powietrza atmosferycznego – wybrane zagadnienia*, pp 123–129, PZITS nr 898, Sienna – Czarna Góra (k. Stronia Śląskiego) 13–16 czerwca 2012 r.
- [6] Niedziółka, I., Szpryngiel, M., Kachel-Jakubowska, M., Kraszkiewicz, A., Zawiślak, K., Sobczak, P. and Nadulski, R. (2015) Assessment of the energetic and mechanical properties of pellets produced from agricultural biomass. *Renewable Energy*, 76, 312–317.
- [7] Stolarski, M.J., Krzyżaniak, M., Śnieg, M., Słomińska, E., Piórkowski, M. and Filipkowski, R. (2014) Thermophysical and chemical properties of perennial energy crops depending on harvest period. *International Agrophysics*, 28(2), 201–211.
- [8] Olsson, M. and Kjällstrand, J. (2004) Emissions from burning of softwood pellets. *Biomass and Bioenergy*, 27(6), 607–611.
- [9] Czop, M. and Kajda-Szcześniak, M. (2013) Environmental impact of straw based fuel combustion. *Archives of Environmental Protection*, 39(4), 71–80.
- [10] Carvalho, L., Wopienka, E., Pointner, C., Lundgren, J., Verma, V.K., Haslinger, W. and Schmidl, C. (2013) Performance of a pellet boiler fired with agricultural fuels. *Applied Energy*, 104, 286–296.
- [11] Qiu, G. (2013) Testing of flue gas emissions of a biomass pellet boiler and abatement of particle emissions. *Renewable Energy*, 50, 94–102.
- [12] Szkarowski, A. and Janta-Lipińska, S. (2013) Examination of boiler operation energy-ecological indicators during fuel burning with controlled residual chemical underburn. *Rocznik Ochrona Środowiska*, 15, 981–995.
- [13] Janicki, M., Bąk, A. and Wróbel, R. (2013) The effect of applying aluminosilicate ceramics in combustion chamber on the amount of ash produced from the combustion of grains of oats and wooden pellets. *Archives of Waste Management and Environmental Protection*, 15(4), 47–56.
- [14] Verma, V., Bram, S. and De Ruyck, J. (2009) Small scale biomass heating systems: standards, quality labelling and market driving factors—an EU outlook. *Biomass and bioenergy*, 33(10), 1393–1402.
- [15] Zajemska, M., Musiał, D., Radomiak, H., Poskart, A., Wyleciał, T. and Urbaniak, D. (2014) Formation of Pollutants in the Process of Co-Combustion of Different Biomass Grades. *Polish Journal of Environmental Studies*, 23(4), 1445–1448.
- [16] Rajczyk, R., Bień, J., Palka, H., Pogodziński, A. and Smorąg, H. (2014) Co-Combustion of Municipal Sewage Sludge and Hard Coal on Fluidized Bed Boiler WF-6. *Archives of Environmental Protection*, 40(3), 101–113.
- [17] García-Maraver, A., Popov, V. and Zamorano, M. (2011) A review of European standards for pellet quality. *Renewable Energy*, 36(12), 3537–3540.
- [18] Kraszkiewicz, A. and Przywara, A. (2016) Correct Combustion Black Locust (*Robinia Pseudo-acacia* L.) Wood in Boiler a Low-Temperature Low-Power. *Fresen. Environ. Bull.*, 25(7), 2436–2443.
- [19] Kordylewski, W. (2000) *Combustion and fuel*, Ofic. Wyd.Polit. Wroc., Wrocław.
- [20] Szyszlak-Bargłowicz, J., Zajac, G. and Piekarski, W. (2012) Energy biomass characteristics of chosen plants. *International Agrophysics*, 26(2), 175–179.
- [21] Maj, G., Piekarski, W., Kowalczyk-Jusko, A. and Lukaszczuk, A. (2014) Waste from agri-food sector, communal and targeted crops as a source of biogas. *Przemysł Chemiczny*, 93(5), 732–736.
- [22] Juszczak, M. (2013) Concentrations of carbon monoxide and nitrogen oxides (NO, NO_x) from a 25 kW boiler supplied periodically and continuously with wood pellets. *Archives of Waste Management and Environmental Protection*, 15(3), 17–24.
- [23] Dias, J., Costa, M. and Azevedo, J. L. T. (2004) Test of a small domestic boiler using different pellets. *Pellets 2002. The first world conference on pellets*, 27(6), 531–539.
- [24] Król, D., Łach, J. and Poskrobko, S. (2010) About some problems with the use of non-forest biomass in the energy sector. *Energetyka*, 1, 53–62.
- [25] Demirbas, A. (2004) Combustion characteristics of different biomass fuels. *Progress in energy and combustion science*, 30(2), 219–230.
- [26] Juszczak, M. (2014) Concentrations of carbon monoxide and nitrogen oxides from a 15 kW heating boiler supplied periodically with a mixture of sunflower husk and wood pellets. *Environment Protection Engineering*, 40(2), 65–74.
- [27] Zhao, W., Li, Z., Wang, D., Zhu, Q., Sun, R., Meng, B. and Zhao, G. (2008) Combustion characteristics of different parts of corn straw and NO formation in a fixed bed. *Bioresource technology*, 99(8), 2956–2963.
- [28] Li, Z. (2010) *Corn Straw and Biomass Blends: Combustion Characteristics and NO Formation*, Nova Science Publishers Inc, Hauppauge, N.Y.
- [29] Houshfar, E., Skreiberg, Ø., Løvås, T., Todorović, D. and Sørum, L. (2011) Effect of excess air ratio and temperature on NO_x emission from grate combustion of biomass in the staged air combustion scenario. *Energy & Fuels*, 25(10), 4643–4654.
- [30] Roy, M.M., Dutta, A. and Corscadden, K.

- (2013) An experimental study of combustion and emissions of biomass pellets in a prototype pellet furnace. *Applied Energy*, 108(0), 298–307.
- [31] Fabjańska-Świeca, G., Hrabak, J., Zapala, E. and Patyna, I. (2013) Determination of sulfur content in power biomass using selected analytical methods. *Karbo*, 2(2), 190–195.
- [32] Verma, V.K., Bram, S., Delattin, F., Laha, P., Vandendael, I., Hubin, A. and De Ruyck, J. (2012) Agro-pellets for domestic heating boilers: Standard laboratory and real life performance. *Energy Solutions for a Sustainable World, Special Issue of International Conference of Applied Energy, ICA2010, April 21-23, 2010, Singapore*, 90(1), 17–23.
- [33] Verma, V.K., Bram, S., Gauthier, G. and De Ruyck, J. (2011) Evaluation of the performance of a multi-fuel domestic boiler with respect to the existing European standard and quality labels: Part-1. *Biomass and Bioenergy*, 35(1), 80–89.
- [34] Verma, V.K., Bram, S., Gauthier, G. and De Ruyck, J. (2011) Performance of a domestic pellet boiler as a function of operational loads: Part-2. *Biomass and Bioenergy*, 35(1), 272–279.
- [35] Hardy, T., Musialik-Piotrowska, A., Ciołek, J., Mościcki, K. and Kordylewski, W. (2010) Adverse effects associated with combustion and co-combustion of biomass in boilers, pp 145–152, PZITS, Polanica-Zdrój 16–19 czerwca 2010 r.
- [36] Magdziarz, A. and Wilk, M. (2012) Ecological aspect of biomass combustion in grate boiler. *Rynek Energii*, 2, 99–105.
- [37] Wieselburg, F. (2009) Test Report 223/08 for pellets heating boiler: Pellets Unit ETAPU15.
- [38] Wieselburg, F. (2010) Test Report 213/09 for pellets heating boiler: Pellets Compact ETAPC 25.
- [39] Johansson, L. S., Leckner, B., Gustavsson, L., Cooper, D., Tullin, C. and Potter, A. (2004) Emission characteristics of modern and old-type residential boilers fired with wood logs and wood pellets. *Atmospheric Environment*, 38(25), 4183–4195.
- [40] Öhman, M., Boman, C., Hedman, H., Nordin, A. and Boström, D. (2004) Slagging tendencies of wood pellet ash during combustion in residential pellet burners. *Biomass and Bioenergy*, 27(6), 585–596.
- [41] Juszcak, M. (2011) Pollutant concentrations from deciduous wood fuelled heat station. *Chemical and Process Engineering*, 32(1), 41–55.
- [42] Toscano, G., Duca, D., Amato, A. and Pizzi, A. (2014) Emission from realistic utilization of wood pellet stove. *Energy*, 68(0), 644–650.
- [43] González, J.F., González-García, C.M., Ramiro, A., González, J., Sabio, E., Gañán, J. and Rodríguez, M.A. (2004) Combustion optimisation of biomass residue pellets for domestic heating with a mural boiler. *Biomass and Bioenergy*, 27(2), 145–154.
- [44] Mediavilla, I., Fernández, M. and Esteban, L. (2009) Optimization of pelletisation and combustion in a boiler of 17.5 kW th for vine shoots and industrial cork residue. *Fuel Processing Technology*, 90(4), 621–628.
- [45] Lajili, M., Jeguirim, M., Kraiem, N. and Limousy, L. (2015) Performance of a household boiler fed with agropellets blended from olive mill solid waste and pine sawdust. *Fuel*, 153, 431–436.
- [46] Liu, H., Chaney, J., Li, J. and Sun, C. (2013) Control of NOx emissions of a domestic/small-scale biomass pellet boiler by air staging. *Fuel*, 103, 792–798.

Received: 13.02.2017

Accepted: 27.05.2017

CORRESPONDING AUTHOR

Joanna Szyszlak-Bargłowicz

Department of Power Engineering and Transportation, Faculty of Production Engineering, University of Life Sciences in Lublin, Głęboka 28, 20-612 Lublin, Poland

e-mail: joanna.szyszlak@up.lublin.pl

IN VITRO SCREENING OF PRECONDITIONED PLUMULAR APICES EXPLANTS OF PEANUT (*ARACHIS HYPOGAEAE*) TO DIFFERENT SALTS CONCENTRATION

Sibel Day^{1,*}, Muhammad Aasim²

¹Department of Field Crops, Faculty of Agriculture, Ankara University, 06110 Diskapi, Ankara, Turkey

²Department of Biotechnology, Faculty of Science, Necmettin Erbakan University, Konya, Turkey.

ABSTRACT

High salinity level in soil or irrigation water limits the plant growth and yield due to altering the metabolic processes, enzymes contents and activities. Peanut is sensitive plant to salinity and salinity level above EC of 8 dS m⁻¹ which hindered the germination rate and plant growth. *In vitro* screening method using plant tissue culture techniques could be employed to identify salt tolerance of explant, cultivar or plant without exposing to soil or climate. In this study, preconditioned plumular apices explants were cultured on agar solidified MS medium supplemented with 1.0 mg l⁻¹ BAP and 5-20 µS cm⁻¹ salinity level of NaCl and KCl for two months. 100% callus induction and shoot regeneration frequency was recorded along with browning or necrosis on callus or regenerated shoots on all mediums irrespective of salty type or concentration. Increased salt concentrations significantly inhibited the number of shoots and shoot length compared to control. Regenerated shoots (≤ 0.5 cm) were rooted on rooting medium enriched with 0.25-2.0 mg l⁻¹ IBA or 1.0 mg l⁻¹ IBA with 0.15-0.6% sucrose concentrations. Rooted plantlets were successfully acclimatized in the pots containing peat moss or coarse sand: peat moss soil mix (1:1) in the growth room. Results revealed that preconditioned plumular explants can be used for modern biotechnological techniques like *in vitro* selection or genetic transformation studies.

KEYWORDS:

In vitro, KCl, NaCl, salinity, EC, BAP, preconditioning

INTRODUCTION

Peanut (*Arachis hypogea*) is one of the important oil seed legume plant that shows wide distribution and compatibility with climates varied from semi arid to sub-tropical regions [43]. The ideal pH is around 6-6.5 but can tolerate pH range of 5.5-7.0. High salinity is not suitable for peanut

growth and it results in decreased growth indices and pod or seed size [36]. Peanut is an important edible legume plant due to its high nutritional value, byproducts and medicinal uses [11, 33].

Salinity is one of the most challenging problem for growers and breeders [15, 26] and area affected with salinity is increasing continuously due to improper agronomic practices [17, 28]. Although, plants generally show variable tolerance to salinity but ultimate result is decrease in yield and plant growth [44]. Introduction of plants to salt stress conditions under *in vitro* conditions significantly affects the *in vitro* regeneration behaviour [14]. NaCl or KCl are the important salts that can be used for screening of plants for salinity both under *in vitro* or *ex vitro* conditions. NaCl affects plant growth by decreasing plant length/height [24]; reduced leaf area [30]; osmotic stresses [18]; biochemical processes [39] or protein contents [21]. On the other hand, higher concentration of KCl may lead to reduced shoots [7] or necrosis [34]. It has been also recorded that salt stress has negative effects on nutrient uptake of plants [40].

Biotechnological tools like *in vitro* tissue culture provides an alternate way of screening of plants under *in vitro* conditions by exposing seeds, embryos or other explants to mediums provided with salts at different concentrations, without any interference with soil or climate [42]. In this study, preconditioned plumular apices of Halisbey cv. of peanut were exposed to different concentrations of NaCl and KCl under *in vitro* conditions with the objective to screen the explants that could tolerate with minimum loss in their activity and *in vitro* regeneration.

MATERIALS AND METHODS

Peanut seeds of cv. Halisbey were collected from Department of Field Crops, Cukurova University, Adana, Turkey. Seeds were surface sterilized with 100 % commercial bleach (containing 5 % NaOCl) for 10 min [14]. The

mature embryos were isolated from sterilized seeds under sterile conditions and preconditioned with 20.0 mg l⁻¹ BAP for 10 days on agar solidified MS medium [27] enriched with 3.0 % sucrose in Magenta GA7 vessels.

EC of regeneration medium without any external provision of salts was recorded 5.0 $\mu\text{S cm}^{-1}$ and used as control. Whereas, three different salinity levels (10, 15, 20 $\mu\text{S cm}^{-1}$) of NaCl and KCl were tested for screening of explants. Plumular apices explants extracted from preconditioned embryos were cultured on MS medium containing 1.0 mg l⁻¹ BAP, also aided with KCl and NaCl salts. The salinity level of culture medium to 10, 15 and 20 $\mu\text{S cm}^{-1}$ was adjusted by using WTW 3.15 conductivity meter.

For rooting of regenerated shoots, two experiments were performed. In first experiment, randomly selected shoots from all culture mediums were cultured on rooting medium containing 0.25, 0.50, 1.00 and 2.00 mg l⁻¹ IBA. In second experiment, the best rooting medium from 1st experiment was selected and enriched with different sucrose concentrations (15-60 g l⁻¹). Each treatment had 3 replications with 8-10 shoots and were kept at 24±2°C. Rooting percentage was recorded after 4 weeks of culture. *In vitro* rooted plants were washed under tap water to remove agar and kept submerged in water for 10-15 min prior to transplantation in pots containing peat moss or coarse sand: peat moss soil mix (1:1) placed in growth rooms for acclimatization. Pots were covered with polythene bags for 7-10 days to keep 80-90 % humidity followed by gradual opening of these bags under ambient conditions of temperature [14].

pH of all media was adjusted to 5.6 - 5.8 before autoclaving at 104 kPa atmospheric pressure, 120 °C for 20 min. All cultures were incubated under 16 h light (35 $\mu\text{mol photons m}^{-2} \text{ s}^{-1}$) photoperiod provided by Philips® cool white fluorescent tubes at 24±2 °C. All chemicals (agar, MS, sucrose, KCl, NaCl) used in this study were purchased from Duchefa Biochemie B.V. (Haarlem, the Netherlands) and Sigma-Aldrich Co. (St. Louis, MO, USA).

Data pertaining to callus induction (%), shoot regeneration (%), number of shoots per explant and shoot length were scored after 8 weeks of culture. Each treatment contained 36 explants of 6 replicated groups (6 explants per replication). Data were subjected to One Way analysis of variance (Anova: SPSS17 for Windows, SPSS Inc., Chicago, IL, USA). Means were compared with Duncan's multiple range test (DMRT) at 0.05 level of significance. The treatments were arranged in a completely randomized design and data given in percentages were subjected to arcsine (\sqrt{X}) transformation [37] before statistical analysis.

RESULTS

Preconditioned plumular apices with 20.0 mg l⁻¹ BAP followed by post conditioning with 1.0 mg l⁻¹ BAP was used to screen peanut against various types and concentrations of salts and their effects were compared. Callus induction with shoot regeneration was obvious within two weeks of culture irrespective of salts type or concentration. However, sign of chlorosis on shoots and callus appeared which increased with the passage of time and it was more prominent on NaCl based medium compared to KCl based mediums. After 8 weeks of culture, data regarding callus induction frequency (%), shoot regeneration (%), shoots per explant and shoot length were scored and analyzed statistically. It was noted that all explants induced callus (100 %) and shoot regeneration (100 %) irrespective of salt type and concentration.

TABLE 1
Effects of Different salts types and concentrations on number of shoots per explant and shoot length of preconditioned plumular apices of peanut.

Treatment	($\mu\text{S cm}^{-1}$)	Shoots per explant	Shoot length (cm)
Control	5	4.95ab	1.03b
	10	5.33a	0.95bc
	15	4.11bc	1.34a
KCl	20	3.50c	0.70cd
	10	4.06bc	0.80bcd
	15	4.00bc	0.60de
NaCl	20	4.11bc	0.43e

Means followed by different small letters within columns are significantly different using DMRT test at $P < 0.005$

Results revealed statistically significant impact of salts type and concentration on number of shoots and shoot length. Comparing salt type, explants responded to both salts in statistically similar way, but, it was shoot length which was affected more by salt type. NaCl was more suppressive and regenerated shorter shoots compared to KCl. Comparing salts concentration, increased salt concentrations inhibited significantly the number of shoots and shoot length compared to control. Average number of 3.50-5.33 and 4.00-4.11 shoots per explant were obtained from KCl and NaCl based mediums respectively (Table 1). Maximum number of 5.33 shoots were scored on MS medium with 10 $\mu\text{S cm}^{-1}$ KCl followed by sharp decline and minimum of 3.50 shoots per explant were obtained from 20 $\mu\text{S cm}^{-1}$ KCl medium (Table 1). On the other hand, explant response to different concentrations of NaCl showed statistically similar effects of NaCl concentration. Results regarding response of explants to shoot length for KCl and NaCl based mediums ranged 0.70-1.34 cm and

0.53-0.80 cm respectively. Results further revealed that all concentrations of NaCl were more suppressive for shoot length compared to KCl. This difference was almost double at $15 \mu\text{S cm}^{-1}$ which was recorded 1.34 cm on KCl compared to 0.60 cm at $15 \mu\text{S cm}^{-1}$ NaCl based medium (Table 1). On the other hand, shoots per explant and shoot length was recorded 4.95 and 1.03 cm respectively for control medium.

TABLE 2
Effects of different IBA concentrations on rooting of *in vitro* regenerated shoots from preconditioned plumular apices of peanut

IBA (mg l^{-1})	Frequency of Rooting (%)
0.25	56.67c
0.50	63.33b
1.00	78.67a
2.00	75.67a

Means followed by different small letters within columns are significantly different using DMRT test at $P < 0.005$

TABLE 3
Effects of different sucrose concentrations on rooting of *in vitro* regenerated shoots from preconditioned plumular apices of peanut

Sucrose (%)	Frequency of Rooting (%)
0.15	73.00 ns
0.30	78.67
0.45	73.33
0.60	74.33

Means followed by different small letters within columns are significantly different using DMRT test at $P < 0.005$

Rooting of *in vitro* regenerated shoots from all culture medium were performed on medium containing 0.25 to 2.00 mg l^{-1} IBA that resulted in 56.67-78.67 % rooting frequency (Table 2). *In vitro* regenerated shoots obtained from salty medium took relatively more time to develop into plantlets. In another experiment, regenerated shoots cultured on rooting medium containing 1.00 mg l^{-1} IBA enriched with 0.15, 0.30, 0.45 and 0.60 % sucrose concentrations resulted in 73.00-78.67 % rooting frequency (Table 3). Results showed that sucrose concentration had no effect on rooting frequency. Higher concentration of sucrose however promoted the callus induction which ultimately hindered the successful acclimatization of plants. It was noteworthy that shoots less than 0.50 cm were also rooted at reasonable rate irrespective of salt type or concentration used for regeneration and were successfully acclimatized employing procedure used for normal rooted plantlets. For acclimatization, rooted plantlets were transferred to pots containing different substrate, covered with polyethylene bags and kept at growth room conditions. Polyethylene bags were removed after

10-12 days and rooted plantlets showed high survival rate and set seed in growth room conditions.

DISCUSSION

High salinity level in soil or irrigation water is major environmental stress factor which limits plant growth and crop productivity by altering a wide array of metabolic processes, enzymes contents and activities [32]. Inhibitory effects of salinity on the yield and crop productivity due to physiological processes disorders and chemical aspects is well established [6]. In general, peanut cannot tolerate high salinity levels exceeding 8 dS m^{-1} and difficult to germinate and grow [25]. Evans [16] reported 1.1 dS m^{-1} tolerance level and 10 % yield reduction at 1.4 dS m^{-1} for peanut. Although, peanut can tolerate higher salinity level but salinity adversely affects the pod growth.

Several promising strategies can be employed to check the screening of plants to salinity level. *In vitro* screening method can be employed to identify salt tolerance of explant, cultivar or plant. In present study, preconditioned plumular apices explants were subjected to 5-20 $\mu\text{S cm}^{-1}$ salinity level of NaCl and KCl in order to check the efficacy to salinity. Results revealed 100 % callus induction and shoot regeneration frequency irrespective of salt type or concentration. The results are contrary to the findings of Zinnah et al. [46], who reported low callus weight and decreased regeneration frequency of rice with increase of NaCl concentration. On the other hand, Day et al. [14] achieved 100% callus induction from preconditioned plumular apices explants of Osmaniye cv. of peanut exposed to different concentrations of KCl. Variable effects of salinity in different crops has been reported by other researchers [8, 23, 29, 35].

Results further revealed browning or necrosis of callus or regenerated shoots due to continuously exposing of explants to different salts and concentration level for two months. NaCl was more detrimental than KCl at all concentrations. Khorami and Safarnejad [23] reported browning of calli of *Foeniculum vulgare* followed by death at 100 and 150 mM NaCl in the culture medium. Zia et al. [45] also reported sign of necrosis on calli of *Thymus vulgaris* (L.) after transferring them to salty medium containing different concentration of NaCl. Similarly, necrosis due to KCl has been reported in sunflower [34] and peanut [14].

Results also revealed that preconditioned explants tolerated well and generated shoots at all levels of salinity. However, salt type affected the shoot length as NaCl was more suppressive than KCl compared to control [9]. Explants behaved in

similar fashion to different concentrations of NaCl and generated statistically similar number of shoots with stunted shoots compared to control ($5 \mu\text{S cm}^{-1}$). Mungala et al. [25] screened 123 peanut cultivars to 1.5, 2.0 and 2.5 % NaCl medium using cotyledonary node explant and recorded decreased survival rate with increase of NaCl concentration by continuously browning and drying up of shoots. Suppressive effects of NaCl on shoot regeneration and shoot length might be due to negative effects of NaCl resulted in suppressed cell division and restricted growth activities [12] by accumulation of Na^+ and Cl^- in tissues led to toxicity [22, 41] in the cells' cytoplasm that affects different biochemical and physiological processes [20].

KCl responded totally different from NaCl and $10 \mu\text{S cm}^{-1}$ KCl enhanced the number of shoots compared to control ($5 \mu\text{S cm}^{-1}$) or NaCl. Ahire et al. [7] reported reduced shoots per culture and shoot length with increasing KCl concentration compared to control. Contrarily, Sabir et al. [31] reported better shoot and calli culture on NaCl and KNO_3 containing culture medium compared to KCl, NaNO_3 , and CaCl_2 . Results also revealed that further increase of KCl concentration (above $10 \mu\text{S cm}^{-1}$) was detrimental and resulted in decreased shoots per explant. Contrarily, insignificant effects of 0-40 mM KCl on shoots per explants of prunus rootstocks (GF677 and Nemared) was reported by Sotiropoulos et al. [38]. Results on mean shoot length showed that $15 \mu\text{S cm}^{-1}$ KCl concentration induced maximum longer shoots than all KCl concentrations. Similarly, longer shoots in response to KCl has been reported by Ahire et al. [7] and Day et al. [14].

In vitro rooting of regenerated shoots is an important step for acclimatization under external conditions of greenhouse or field conditions. Auxins are generally employed for *in vitro* rooting and previous reports on *in vitro* rooting reports low rooting percentage. Hassan et al. [19] reported that rooting of *in vitro* regenerated shoots of peanut is difficult under *in vitro* conditions. Successful rooting of preconditioned explants has been reported in cowpea [1, 2] and grasspea [10]. However, low rooting percentages after preconditioning has been reported in chickpea [3] and lentil [4]. In this study, we achieved high rooting frequency at different IBA concentrations. Day et al. [14] achieved 100% rooting of peanut obtained from different KCl concentrations.

In order to improve rooting frequency, Aasim et al. [5] used increased sucrose concentration for rooting in chickpea and obtained 100 % rooting frequency with hardening of plants. However, in this study, increased sucrose concentrations slightly increased the rooting frequency with callus induction at higher concentration of sucrose. Callus induction from basal end of legumes in response to

IBA is unknown phenomenon and creates problem for acclimatization [5]. Callus induction also hindered the acclimatization of rooted plantlets of peanut that might be due to induction of adventitious roots emerged from the callus that failed to transfer water and mineral uptaken from soil.

It was positive to note that regenerated shoots obtained from these high salts concentrations containing mediums were also rooted successfully. Even shoots less than 0.5 cm were rooted in the rooting media containing different concentrations of IBA but took more time than normal rooting experiments which might be due to neutralizing the carry over effects of preconditioning and salts concentration. Contrarily, negative effects of NaCl on root growth has been reported [13, 23] in different plant species. Plants acclimatized well in pots containing coarse sand, clay and organic matter soil mix (1:1:1) under growth room conditions [1-5, 10].

CONCLUSION

The present work presents the first ever report of using plumular apices for screening to salt type and concentrations. Screening of explants to different concentrations of NaCl and KCl and their response to culture conditions also show the supremacy of plumular apices explants. This protocol can be easily employed for screening of other economic plants by using plumular apices explant.

REFERENCES

- [1] Aasim, M., Khawar, K.M. and Ozcan, S. (2009) *In vitro* micropropagation from plumular apices of Turkish cowpea (*Vigna unguiculata* L.) cultivar Akkiz. Sci. Hortic. 122, 468-471.
- [2] Aasim, M., Khawar, K. M. and Ozcan, S. (2010) Efficient *in vitro* propagation from preconditioned embryonic axes of Turkish cowpea (*Vigna unguiculata* L.) cultivar akkiz. Arch. Biol. Sci. 62, 1047-1052.
- [3] Aasim, M., Day, S., Rezai, F., Hajyzadeh, M., Mahmud, S.T. and Ozcan, S. (2011) *In vitro* shoot regeneration from preconditioned explants of chickpea (*Cicer arietinum* L.) cv. Gokce. Afr. J. Biotechnol. 10, 2020-2023.
- [4] Aasim, M. (2012) Micropropagation of lentil (*Lens culinaris* Medik.) using pulse treatment of immature plumular apices. Pak. J. Agric. Sci. 49, 149-154.
- [5] Aasim, M., Day, S., Rezaei, F. and Hajyzadeh, M. (2013) Multiple shoot regeneration of

- plumular apices of chickpea. Turk. J. Agric. For. 37, 33-39.
- [6] Abou-Hussien, E.A., El-Shinnawi, M.M., Abo-El-Fadl, M.A. and El-Fishy, M.A. (2010) Growth of corn plants cultivated in differently manured arid soils and irrigated with various water quality. Minufiya, J. Agric. Res. 35, 235-255.
- [7] Ahire, M.L., Laxmi, S., Walunji, P.R., Kavi Kishore, P.B. and Nikam, T.D. (2013) Effect of potassium chloride and calcium chloride induced stress on *in vitro* cultures of *Bacopa monnieri* (L.) Pennell and accumulation of medicinally important bacoside A. J. Plant Biochem. Biot. DOI:10.1007/s13562-013-0220-z.
- [8] Al-Forkan, M., Rahim, M.A., Chowdhury, T., Akter, P. and Khaleda, L. (2005) Development of highly *in vitro* callogenesis and regeneration system for some salt tolerant rice (*Oryza sativa* L.) cultivars of Bangladesh. Biotechnol. 4, 230-234.
- [9] Arıcı, Ş.E. and Eraslan, F. (2012) Effect of salt-stress on shoot growing, chlorophyll and minerals content sweet cherry rootstock colt (*Prunus avium* X *Prunus pseudocerasus*) cultured *in vitro*. SDÜ Zir. Fak. Derg. 7, 41-48.
- [10] Barpete, S., Aasim, M., Özcan S.F., Khawar, K.M. and Özcan, S. (2014). Preconditioning effect of cytokinins on *in vitro* multiplication of embryonic node of grass pea (*Lathyrus sativus* L.) cultivar Gürbüz. Turkish Journal of Biology 38, 485-492.
- [11] Blomhoff, R., Carlsen, M.H., Andersen, L.F. and Jacobs, DR.Jr. (2008) Health benefits of nuts: potential role of antioxidants. Br. J. Nutr. 99, 447-44.
- [12] Bohnert, H.J. and Jensen, R.G. (1996) Metabolic engineering for increased salt tolerance- the next step. Aust. J. Plant Physiol. 59, 661-667.
- [13] Cano, E.A., Perez-Alfocea, F., Moreno, V., Caro, M. and Bolarin, M.C. (1998) Evaluation of salt tolerance in cultivated and wild tomato species through *in vitro* shoot apex culture. Plant Cell Tiss. Org. Cult. 53, 19-26.
- [14] Day, S., Aasim, M. and Bakhsh, A. (2016) Effects of preconditioning, plant growth regulators and KCl on shoot regeneration of peanut (*Arachis hypogea*). Journal of Animal and Plant Sciences. 26, 294-300.
- [15] Demirbas, S. and Acar, O. (2017). Physiological and biochemical defense reactions of *Arabidopsis Thaliana* to *Phelipanche Ramosa* infection and salt stress. Fresen. Environ. Bull., 26, 2277-2284.
- [16] Evans, L. (2006) Salinity tolerance in irrigated crops [http://www.dpi.nsw.gov.au/agriculture/resources/soils/salinity/crops/tolerance-](http://www.dpi.nsw.gov.au/agriculture/resources/soils/salinity/crops/tolerance-irrigated)
- irrigated
- [17] Flowers, T.J. (2004). Improving crop salt tolerance. J. Exp. Bot. 55, 307- 319.
- [18] Gama, P.B.S., Tanaka, K., Eneji, A., Eltayeb, A.E. and Elsiddig, K. (2009). Salt induced stress effects on biomass, photosynthetic rate and reactive oxygen species scavenging enzyme accumulation in common bean. J. Plant Nutr. 32, 837–854.
- [19] Hassan, M.U., Akram, Z., Ajmal, S., Mukhtar, T., Nasim, S., Shabbir, G. and Zafar, Y. (2013) Highly efficient *in vitro* root induction in peanut by mechanical stress method. J. Anim. Plant Sci. 23, 425-429.
- [20] Jampeetong, A. and Brix, H. (2009) Effects of NaCl salinity on growth, morphology, photosynthesis and proline accumulation of *Salvinia natans*. Aquat. Bot. 91, 181-186.
- [21] Kapoor, K. and Srivastava, A. (2010) Assessment of salinity tolerance of *Vinga mungo* var. Pu-19 using ex vitro and *in vitro* methods. Asian J. Biotechnol. 2, 73–85.
- [22] Karimi, E., Abdolzadeha, A. and Sadeghipour, H.R. (2009) Increasing salt tolerance in olive, *Olea europaea* L. plants by supplemental potassium nutrition involves changes in ion accumulation and anatomical attributes. Int. J. Plant Prod. 3, 49-60.
- [23] Khorami, R. and Safarnejad, A. (2011) *In vitro* selection of *Foeniculum vulgare* for salt tolerance. Not. Sci. Biol. 3, 90-97.
- [24] Memon, S.A., Hou X. and Wang, L.J. (2010) Morphological analysis of salt stress response of pak Choi. EJEAFChe. 9, 248–254.
- [25] Mungala, A.J., Radhakrishnan, T. and Dobarra, J.R. (2008) *In vitro* screening of 123 Indian peanut cultivars for sodium chloride induced salinity tolerance. World J. Agric. Sci. 4, 574-582.
- [26] Munns, R. (2005) Genes and salt tolerance: bringing them together. New Phytologist 167, 645–663.
- [27] Murashige, T. and Skoog, E.A. (1962) Revised medium for rapid growth and bioassays with tobacco tissue cultures. Physiol. Plant. 15, 473–497.
- [28] Priya, A.M., Pandian, S.K. and Ramesh, M. (2011). Effect of NaCl on *in vitro* plant regeneration from embryogenic callus cultures of 'cv IR 64' indica rice (*Oryza sativa* L.). African Journal of Biotechnology 10, 6947-6953.
- [29] Rudra, B., Khaleda, L. and Al-Forkan, M. (2013) Screening of salt tolerant potentiality and development of *in vitro* tissue culture system for some local rice (*Oryza sativa* L.) varieties. Int. J. Biotechnol. 2, 193-205.
- [30] Rui, L., Wei, S., Mu-xiang, C., Cheng-jun, J., Min, W. and Bo-ping, Y. (2009) Leaf

- anatomical changes of *Burquiera gymnorhiza* seedlings under salt stress. J. Trop. Subtrop. Bot. 17, 169–175.
- [31] Sabir, F., Sangwan, R., Kumar, R. and Sangwan, N. (2012) Salt stress-induced responses in growth and metabolism in callus cultures and differentiating *in vitro* shoots of Indian ginseng (*Withania somnifera* Dunal). J. Plant Growth Regul. 31, 537-548.
- [32] Salwa, A.R., Hammad, Kh.A., Shaban, F. and Manal, F. (2010) Studies on salinity tolerance of two peanut cultivars in relation to growth, leaf water content. Some Chemical Aspects and Yield. Journal of Applied Sciences Research 6, 1517-1526.
- [33] Sanders, T.H., McMichael, Jr.R.W. and Hendrix, K.W. (2000) Occurrence of resveratrol in edible peanuts. J. Agr. Food Chem. 48, 1243-1246.
- [34] Santos, V.C.L., Campos, A., Azevedo, H. and Caderia, G. (2001). In situ and *in vitro* senescence induced by KCl stress: nutritional imbalance, lipid peroxidation and antioxidant metabolism. J. Exp. Bot. 52, 351-360.
- [35] Shankhdhar, D., Shankhdhar, S.C., Mani, S.C. and Pant, R.C. (2000) *In vitro* selection for salt tolerance in rice. Bio. Plant. 43, 477-480.
- [36] Smart, J. (1994) The groundnut crop: A scientific basis for improvement". London. Chapman & Hall, pp734.
- [37] Snedecor, G.W. and Cochran, W.G. (1967) Statistical Methods. The Iowa State Univ. Press, Iowa, USA, pp. 327–329.
- [38] Sotiropoulos, T.E., Dimassi, K.N., Tsirakoglou, V. and Therios, I.N. (2006). Responses of two prunus root stocks to KCl induced salinity *in vitro*. Biologia Plant 50, 477-480.
- [39] Taffouo, V.D., Wamba, O.F., Yombi, E., Nono, G.V. and Akoe, A. (2010). Growth, yield, water status and ionic distribution response of three bambara groundnut (*Vigna subterranean* (L.) verdc.) landraces grown under saline conditions. Int. J. Bot. 6, 53–58.
- [40] Temel, S., Keskin B., Şimşek U. and Yılmaz, İ.H. (2016). The effect of soils having different salt content on mineral accumulations of some forage legume species. Fresen. Environ. Bull., 25, 1038-1050.
- [41] Tester, M. and Devenport, R. (2003) Na⁺ tolerance Na⁺ transport in higher plants. Annal Bot. 91, 503-527.
- [42] Troncoso, J., Liñán, J., Cantos, M., García, J.L. and Troncoso, A. (2004). *In Vitro* Selection of Salt-Tolerant Olive Clones. Acta Horticulturae (ISHS) 791, 217-223.
- [43] Venkatachalam P. and Jayabalan, N. (1997). Effect of auxin and cytokinins on efficient plant regeneration and multiple-shoot formation from cotyledonary-node explants of groundnut (*Arachis hypogaea* L.) by *in vitro* culture technology. App. Biochem. Biotechnol. 67, 237-247.
- [44] Vicente, G., Martinez, M. and Aracil, J. (2004). Integrated biodiesel production: a comparison of different homogeneous catalysts systems. Bioresour. Technol. 92, 297-305.
- [45] Zia, A., Rezanejad, F. and Safarnejad, A. (2010) *In vitro* selection for NaCl tolerance in *Thymus vulgaris* L. J. Cell Mol. Res. 2, 86-92.
- [46] Zinnah, K.M.A., Zobayer, N., Sikdar, S.U., Liza, L.N., Chowdhury, M.A.N. and Ashrafuzzaman, M. (2013) *In Vitro* regeneration and screening for salt tolerance in rice (*Oryza sativa* L.). Int. Res. J. Biol. Sci. 2, 29-36.

Received: 22.02.2017

Accepted: 18.05.2017

CORRESPONDING AUTHOR

Sibel Day

Department of Field Crops, Faculty of Agriculture, Ankara University, 06110 Diskapi, Ankara, Turkey

e-mail: siday957@gmail.com

IN VITRO EFFECTS OF SOME HEAVY METAL IONS ON CYTOSOLIC THIOREDOXIN REDUCTASE PURIFIED FROM RAINBOW TROUT GILL TISSUES

Hatice Akyol¹, Muslum Kuzu^{2,*}

¹Department of Chemistry, Institute of Natural & Applied Sciences, İbrahim Çeçen University of Ağrı

²Faculty of Pharmacy, İbrahim Çeçen University of Ağrı

ABSTRACT

Thioredoxin system is formed of thioredoxin reductase (E.C 1.6.4.5.; TrxR), thioredoxin (Trx) and nicotinamide adenine dinucleotide phosphate (NADPH), and participates in cell growth, apoptosis, antioxidant defense, redox signaling, etc. In this study, cytoplasmic TrxR enzyme was purified by using heat denaturation and 2',5'-ADP Sepharose 4B affinity chromatograph techniques from rainbow trout gill tissues. The purity and the monomer molecular weight of the enzyme were determined with SDS-PAGE. K_M values for NADPH and 5,5'-Dithio-bis (2-nitrobenzoic acid), the substrates of the enzyme were calculated by means of Lineweaver-Burk graphic. Optimal pH and optimal ionic strength values were determined as 7.75 and 300 mM, respectively. Then, *in vitro* effects of the Ni^{2+} , Cu^{2+} , Pb^{2+} , Cd^{2+} , Sr^{2+} , Zn^{2+} , Mg^{2+} , Cr^{3+} , Fe^{3+} , Al^{3+} and Ag^+ metal ions on the enzyme activity were analyzed. IC_{50} values were determined for the ones showing inhibition effect and their K_i values were calculated by means of Cheng-Prusoff equation.

KEYWORDS:

Thioredoxin Reductase, Purification, Heavy Metal, Inhibition

INTRODUCTION

The thioredoxin system consists of thioredoxin (Trx), NADPH, and thioredoxin reductase (TrxR). The TrxR enzyme belongs to the family of flavoprotein disulfide reductase that contains enzymes such as trypanothione reductase, lipoamide dehydrogenase, mycothione reductase, mercuric reductase and alkyl hydroperoxide reductase [1]. TrxR reduces Trx with electrons from NADPH. Reduced mammal Trx is essential for functions such as thiol redox control of transcription factors, ribonucleotide reductive electron transport, defense against oxidative stress, and apoptosis [2]. Interaction of Trx with transcription factors makes this molecule the key regulator of pro-inflammatory cytokine expression. Trx performs an important role in both reactive oxygen species

(ROS) scavenger and cofactor of antioxidant enzymes. And, Trx functions in the reactivation of oxidatively damaged proteins [3]. In addition to this, the thioredoxin system also functions in metabolic events such as DNA synthesis, glucose metabolism, selenium metabolism and vitamin C reversal [4]. The importance of Trx is that it immediately allows a cell to regenerate an oxide substrate. TrxR is the only known enzyme capable of reducing Trx. This makes TrxR an integral component of the thioredoxin function [5].

The definition of heavy metals refers to relatively high density ($3.5-7 \text{ g / cm}^3$). These metals are widely found on the earth and do not undergo biodegradation in nature [6]. In certain environmental conditions, heavy metals reach toxic concentrations and cause ecological damage [7]. The presence of heavy metals in nature can be due to natural causes as well as from industrial waste. Fish are usually at the top of the aquatic food chain and may be exposed to metal deposits from their environment. As a result, these metals are transmitted to the human body through food. Due to the bioaccumulative features in biotic systems, the presence of metals in different foods creates serious health problems according to their levels [6,8].

MATERIAL AND METHOD

Chemicals. Sodium dodecyl sulfate (SDS), sodium chloride, sodium acetate, hydrochloric acid, phosphoric acid, ethanol, methanol, isopropanol, acetic acid, sodium acetate and potassium chloride were obtained from E. Merck AG, ethylenediaminetetraacetic acid (EDTA), β -mercaptoethanol, silver nitrate and formaldehyde Fluka, and other chemicals used in the study were obtained from Sigma Chemical Co.

Fish Samples. Rainbow trout was brought alive from the rainbow trout farm in Taşlıçay, then brought to the laboratory according to the cold chain principles. The fish brought to the laboratory was decapitated and the gill tissues were taken.

Lysate Preparation and Heat Denaturation.

The gill tissues were washed with 10 mM Tris / HCl buffer (pH 7.5) containing 1 mM ethylenediaminetetraacetic acid (EDTA), then the cartilage was separated and divided as small as possible using a knife. Lysate was prepared in the same buffer with homogenizer. The prepared lysate was centrifuged at 12700 rpm for 30 min. The resulting precipitate was discarded and the supernatant was removed. The resulting supernatant was stored at 60 ° C for 6-7 minutes, then centrifuged again at 12700 rpm for 30 min to remove supernatant and precipitate. The resulting supernatant was filtered using filter paper and then applied to the 2', 5'-ADP Sepharose 4B affinity column.

2',5'-ADP Sepharose 4B affinity chromatography. A column (1 × 10 cm) of 10 mL in bed volume was made using 2 g of dried 2',5'-ADP Sepharose 4B. The gel was washed with 300 mL of distilled water to remove foreign bodies and air, suspended in 10 mM Tris/HCl buffer containing 1 mM EDTA (pH 7.5), and packed in the column. After precipitation of the gel, the column was equilibrated with the same buffer by means of a peristaltic pump. The flow rates for washing and equilibration were adjusted to 30 mL/h. For purification of TrxR enzyme, the sample was loaded onto the 2',5'-ADP Sepharose 4B affinity column and the column was washed with equilibration buffer and 0.15 M K-phosphate buffer containing 2 mM EDTA, pH 7.5 until the final absorbance difference became 0.05 at 280 nm. TrxR was eluted with a gradient of 0 to 10 mM NADP⁺ in equilibration buffer. Active fractions were collected and dialyzed with equilibration buffer.

Sodium dodecyl sulfate polyacrylamide gel electrophoresis. After the purification of TrxR enzyme, sodium dodecyl sulfate polyacrylamide gel electrophoresis (SDS-PAGE) with 3%-10% batch was conducted in accordance with the method of Laemmli [9]. Purity grade and monomer molecular mass of the enzyme were determined.

Optimal pH studies. In order to determine the optimal pH of the TrxR enzyme of the rainbow trout gill, 0.5 M K-phosphate (pH ranging from 6.5 to 8.0) buffers were prepared. Enzyme activity was determined separately in each buffer using an appropriate substrate solution.

Optimal ionic strength studies. In order to determine the optimal ionic strength of the TrxR, K-phosphate buffers (pH 7.75) were prepared in different ionic strength ranging from 50 mM to 550 mM. Enzyme activity was determined separately in each buffer and so, the optimal ionic strength was determined for the enzyme.

Protein determination. The amount of quantitative protein in the prepared homogenate and all purification steps was determined according to the Bradford method [10]. Bovine serum albumin was used as standard.

Activity determination. TrxR activity was determined spectrophotometrically with a Shimadzu spectrophotometer (UV-1800) at 412 nm. This assay is based on the NADPH dependent reduction of the artificial substrate DTNB. The reaction mixture contained, in a final volume of 1 mL, 200 μM NADPH, 2 mM DTNB, and 1mM EDTA in 300mM K-phosphate buffer (pH 7.75). A value of 13.6 mM⁻¹ cm⁻¹ for the extinction coefficient of DTNB was used in the calculations.

Kinetic studies and in vitro inhibition assay.

In order to determine the K_M values for the substrates of the TrxR enzyme, activity measurements were made at constant concentration of the other substrate using five different concentrations of the K_M value to be calculated. Lineweaver-Burk graphs were drawn using the obtained values. The K_M values are calculated from the drawn Lineweaver-Burk graphs [11]. In order to determine the effects of heavy metals on enzyme activity, enzyme activity was measured with saturated substrate concentration and five different heavy metal concentrations. The heavy metal concentrations causing up to 50% inhibition (IC₅₀) were determined by constructing % activity-heavy metal concentration graphs. Results are reported as IC₅₀ values. Ki constants is calculated using the Cheng-Prusoff equation [12].

RESULTS AND DISCUSSION

Rapid urbanization and industrial developments in recent years have caused some environmental problems. Natural aquatic systems are subject to large-scale contamination due to household, industrial and other man-made activities. Heavy metal contamination in rivers is one of these problems in rapidly growing cities. Current acute damage assessment procedures for chemical contaminants are based on persistence, bioaccumulation and toxicity. However, it is difficult to determine the critical levels of these values for metals. Because metals naturally remain in the environment, both essential and non-essential metals naturally undergo bioaccumulation. Furthermore, toxicities of metals are highly affected by geochemical properties [13-15]. Heavy metal contamination has devastating effects on the ecological balance and diversity of aquatic organisms. Among animal species, fish are living creatures which cannot escape the harmful effects of these pollutants. Studies on various fish species have shown that heavy metals could alter both biochemical parameters and physiological activities in both

TABLE 1
Purification of Thioredoxin reductase from rainbow trout gill tissue.

Fractions	Activity (EU/ml)	Volume (ml)	Protein (mg/ml)	Total Ac-tivity	Specific Activity (EU/mg)	Recovery %	Purification Fold
Lysate	0.042	12	7.41	0.504	0.0057	100	1
Heat Denaturation	0.04	10	1.27	0.4	0.0315	79.37	5.6
2',5'-ADP Sepharose 4B affinity chromatography	0.024	5.5	0.023	0.132	1.0435	26.19	184.1

tissues and blood. The gill is an important part of the body for the entry of heavy metals and this causes some lesions and gill damage [15].

The TrxR enzyme is required for all metabolic events in which Trx acts as a reducing substrate. This includes the events of detoxification of oxidants and radicals by the reduction of ribonucleotides to deoxyribonucleotides. It has also been reported to play a role in various physiological and pathological conditions such as apoptosis, cancer, parasitoses, chronic inflammatory, autoimmune diseases and neurodegenerative diseases [16].

Previous studies have emphasized the necessity of studies to determine the effects of heavy metal toxicity on changes in antioxidant enzyme systems [8]. For example, the Glutathione S-transferase enzyme involved in detoxification was purified from the gill tissue of Ağrı Balık Lake trout and it was determined that the enzyme inhibited by Hg^{2+} , Cu^{2+} , Zn^{2+} and Se^{4+} ions [17]. It was stated in another study that cytochrome P450 reductase, one of the NADPH-dependent enzymes, was purified from the liver tissue of the Van Lake fish and some metal ions such as Hg^{2+} , Ag^+ and Cu^{2+} inhibited the enzyme [18]. In another study, it was observed that the number of erythrocytes decreased significantly in the *Oreochromis niloticus* species exposed to Pb^{2+} and Cu^{2+} metals [19], glutathione peroxidase, catalase and superoxide dismutase levels decreased and MDA levels increased in the rainbow trout gill tissues exposed to Cd^{2+} and Cr^{3+} [20]. However, very limited information is available in the literature on the effects of heavy metals on thioredoxin reductase enzyme in particular. In a recent study, mitochondrial TrxR enzyme was purified and characterized from trout liver tissues to investigate the in vitro effects of some heavy metals on enzyme activity [21]. In this study, the cytosolic TrxR enzyme was purified for the first time from the gill tissue of a fish species in the electrophoretic purity. Purification was carried out in two steps using heat denaturation and 2',5'-ADP Sepharose 4B affinity chromatography techniques (Table 1).

The purity of the enzyme obtained from the affinity column was checked by SDS-PAGE and a single band was observed (Figure 1). Using the Rf-log MW graph obtained using standard proteins, the monomer molecular weight of the enzyme was cal-

culated as ~ 64.1 kDa. In previous studies, the mitochondrial TrxR enzyme was purified from bovine adrenal cortex and the monomer molecular weight was given as 56 kDa [22]. This value was given as approximately 70 kDa for the TrxR of trout liver [21] for the human placenta TrxR, 55.2 kDa [23] and 58 kDa for the rat liver TrxR enzyme [24]. Therefore, it can be said that the molecular weight of the trout gill cytosolic TrxR enzyme is in accordance with the literature.

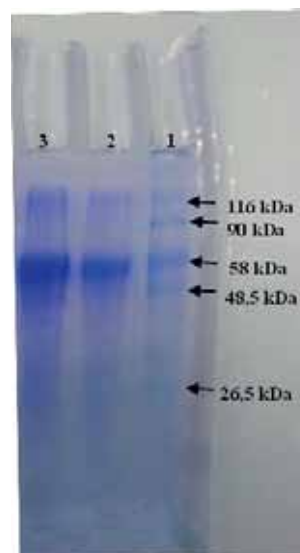


FIGURE 1

Line 1 standard proteins (b-galactosidase from *E. Coli* 116 kDa, lactoferrin from human milk 90 kDa, pyruvate kinase from rabbit muscle 58 kDa, fumarase from porcine heart 48.5 kDa and triosephosphate isomerase from rabbit muscle 26.6 kDa), Line 2 and Line 3 purified rainbow trout gill TrxR.

Activity measurements were performed to determine optimum pH and optimal ionic strength for the purified enzyme. As a result of the studies conducted, it was found that the enzyme retained its activity at a certain level after pH 7.0, with the highest activity exhibited in the pH 7.75 K⁻ phosphate buffer. However, in the activity measurements made with Tris/HCl buffer at pH 7.75 and 8.0, the activity was found to be very low compared to the measurements made with K-phosphate buffer (Figure 2A). It was also determined that enzyme activity was the highest in the 300 mM cuvette concentration in the

activity measurements made in the K-posfat buffer at different concentrations (Figure 2B).

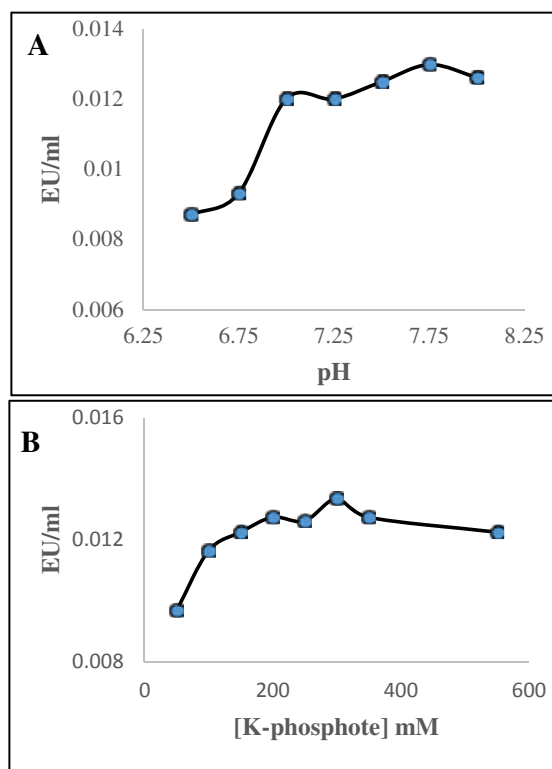


FIGURE 2

Effect of pH (A, the buffers used were 300 mM K-phosphate, pH 6.5, 6.75, 7.0, 7.25, 7.5, 7.75, 8.0) and ionic strength (B, the buffers used were 50-550 mM K-phosphate, pH 7.75) on activity of TrxR.

However, the activity was found to be relatively stable up to a concentration of 550 mM after the concentration of 150 mM. In the previous study, the optimum pH for the trout mitochondrial TrxR enzyme was 7.50 and the optimum ionic strength was 500 mM [21]. For the E. coli enzyme, it was reported that the optimum pH was 7.7 and the activity in measurements made with K-phosphate was 2-fold higher than the measurements made with Tris/HCl [25]. Lineweaver-Burk plots were drawn by measuring activity at five different substrate concentrations to calculate the K_M values that are of interest to enzyme substrates. Accordingly, the K_M values of the enzyme for NADPH and DTNB were calculated to be 7.88 μM and 0.25 mM, respectively. These values were 6 μM and 0.66 mM for rat liver TrxR, respectively [24], 3.9 mM for bovine adrenal cortex TrxR enzyme [24], 18 μM for human placental TrxR enzyme, respectively [23]. Compared to these values, it can be said that the enzyme is similar to rat liver

TrxR in terms of the affinity against its substrates.

The TrxR enzyme is a component of the thioredoxin system, which has a key role in protecting against oxidative damage, cellular stress response and protein repair, and becomes susceptible to oxidation due to the structural cysteine residues it contains [26]. It has also been reported that due to selenol and thiol groups, the enzyme may be inhibited by complexing with divalent metal ions [21]. For example, it has been emphasized that the toxic effect of mercury can be demonstrated by inhibiting selenoenzymes such as glutathione peroxidase and TrxR, which are necessary for antioxidant regulation [27]. For this reason, in vitro effects of Ni^{2+} , Cu^{2+} , Pb^{2+} , Cd^{2+} , Sr^{2+} , Zn^{2+} , Mg^{2+} , Cr^{3+} , Fe^{3+} , Al^{3+} , Ag^+ on purified TrxR were investigated in order to determine how the thioredoxin system affected by heavy metals in fish gill tissues (Table 2).

TABLE 2

Inhibition data of the metal ions on TrxR activity.

Metal Ion	Concentration range μM	IC_{50} μM	K_i μM
Ag^+	0.0005-0.015	0.00582	0.000647
Ni^{2+}	5-80	40	4.44
Pb^{2+}	10-240	149	16.56
Fe^{3+}	100-2000	561	62
Cu^{2+}	100-1200	720	80
Cr^{3+}	500-1500	871	97
Cd^{2+}	500-10000	Not inhibited	
Sr^{2+}	1000-15000	Not inhibited	
Zn^{2+}	500-5000	Not inhibited	
Mg^{2+}	500-20000	Not inhibited	
Al^{3+}	10-300	Not inhibited	

As a result of the measurements, it was determined that Ni^{2+} , Cu^{2+} , Pb^{2+} , Cr^{3+} , Fe^{3+} , Ag^+ ions inhibited TrxR. A graph of % Activity-metal ion concentration for each ion was drawn by using the results and the IC_{50} value was found from the graph (Figure 3). K_i values were then calculated using the Cheng-Prusoff equation. Ag^+ ion showed the strongest inhibitory effect among the other metals. However, Ni^{2+} ion showed inhibition effect at μM level. Previous studies have shown that enzyme activity is strongly inhibited by divalent metal ions such as Cu^{2+} , Fe^{2+} , Mn^{2+} , Zn^{2+} while weakly inhibited by Ca^{2+} and Mg^{2+} ions (22). Studies by Özgençli and Çiftci have also examined the effects of Se^{4+} , Cu^{2+} , Co^{2+} , Ni^{2+} , Fe^{3+} , and Al^{3+} ions on mitochondrial TrxR purified from trout liver tissue. Though, Se^{4+} activated the enzyme activity, the other metal ions inhibited the enzyme activity in mM range [21]. It has also been reported that sodium selenite increases levels of antioxidant enzymes such as glutathione peroxidase and superoxide dismutase in rainbow trout liver

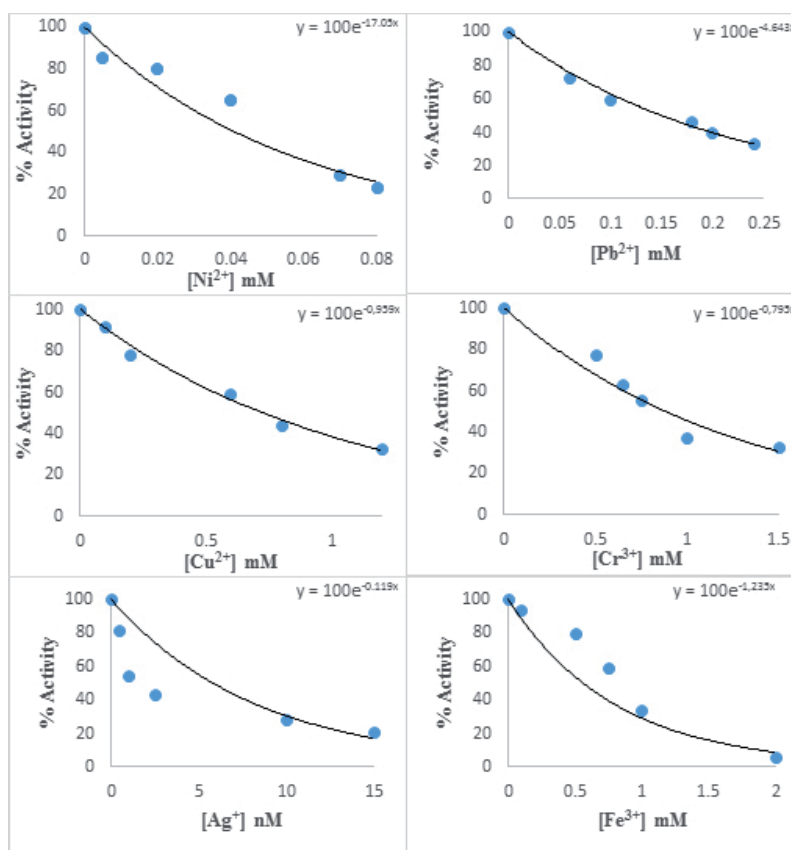


FIGURE 3

% Activity–[I] plots for metal ions having inhibition effect.

tissues [28]. Bioaccumulation properties of heavy metals were studied on *Cyprinus carpio* species and it was stated that metals tend to accumulate in the order of $Cd > Pb > Ni > Cr$ in gill tissues [15]. Therefore, it can be said that the thioredoxin system in fish species exposed to heavy metals will affect this situation and this effect may increase with time due to bioaccumulation. This can be said to be one of the mechanisms of the toxic effects of heavy metals.

Here, the inhibition effect of Ag^+ ion is quite remarkable. The IC_{50} value for this ion is calculated to be 5.82 nM. The reason for this is thought to be the presence of cysteine amino acid in the active site of the enzyme. It has been reported that the human cytosolic TrxR enzyme contains three structural cysteine residues (Cys^{62} , Cys^{69} and Cys^{73}) and that these residues constitute the second disulfide bond which causes the loss of activity between Cys^{62} and Cys^{69} , rendering them resistant to enzyme oxidation [26]. Enzymes containing Cys in active and catalytic regions have been reported to inhibit by forming mercaptans via the $-SH$ group with heavy metal ions such as Ag^+ and Hg^{2+} [29].

CONCLUSION

In conclusion, the TrxR enzyme, a component of the thioredoxin system involved in many physiological events, was purified for the first time from the

gill tissues of a fish species in electrophoretic purity. The monomer molecular mass of the enzyme was then determined by SDS-PAGE. In addition, optimum pH and ionic strength values of the enzyme were determined. After finding the K_M values that are of interest to the substrate of the enzyme, the effects of some heavy metal ions on the enzyme activity were examined in vitro. It has been observed that Ni^{2+} , Cu^{2+} , Pb^{2+} , Cr^{3+} , Fe^{3+} , Ag^+ ions inhibited the enzyme, however, Ag^+ possesses the strongest inhibitory properties. Considering that some salt forms of silver metal are used in the production of photographic materials and alkaline batteries and soluble silver compounds are used as external antiseptic agents, bacteriostatic agents and as disinfectants [30], it is thought to be useful to control the use of silver salts.

REFERENCES

- [1] Argyrou, A. and Blanchard, J. S. (2004) Flavo-protein disulfide reductases: advances in chemistry and function. *Progress in nucleic acid research and molecular biology*, 78, 89-142.
- [2] Sandalova, T., Zhong, L., Lindqvist, Y., Holmgren, A. and Schneider, G. (2001) Three-dimensional structure of a mammalian thioredoxin reductase: implications for mechanism

- and evolution of a selenocysteine-dependent enzyme. *Proceedings of the National Academy of Sciences*, 98, 9533-9538.
- [3] Pacitti, D., Wang, T., Martin, S. A. M., Sweetman, J. and Secombes, C. J. (2014) Insights into the fish thioredoxin system: Expression profile of thioredoxin and thioredoxin reductase in rainbow trout (*Oncorhynchus mykiss*) during infection and in vitro stimulation. *Developmental & Comparative Immunology*, 42, 261-277.
- [4] Witte, A. B., Anestål, K., Jerremalm, E., Ehrsson, H. and Arnér, E. S. (2005) Inhibition of thioredoxin reductase but not of glutathione reductase by the major classes of alkylating and platinum-containing anticancer compounds. *Free Radical Biology and Medicine*, 39, 696-703.
- [5] Arnér, E. S. and Holmgren, A. (2000) Physiological functions of thioredoxin and thioredoxin reductase. *European Journal of Biochemistry*, 267, 6102-6109.
- [6] Gautam, R. K., Sharma, S. K., Mahiya, S. and Chattopadhyaya, M. C. (2014) Contamination of heavy metals in aquatic media: transport, toxicity and technologies for remediation
- [7] Gümgüm, B., Tez, Z. and Gülsün, Z. (1994) Heavy metal pollution in water, sediment and fish from the Tigris River in Turkey. *Chemosphere*, 29, 111-116.
- [8] Mansour, S. A. and Sidky, M. M. (2002) Ecotoxicological studies. 3. Heavy metals contaminating water and fish from Fayoum Governorate, Egypt. *Food Chemistry*, 78, 15-22.
- [9] Laemmli, U. K. (1970) Cleavage of structural proteins during the assembly of the head of bacteriophage T4. *Nature*, 227, 680-685.
- [10] Bradford, M. M. (1976) A rapid and sensitive method for the quantitation of microgram quantities of protein utilizing the principle of protein-dye binding. *Analytical biochemistry*, 72, 248-254.
- [11] Lineweaver, H. and Burk, D. (1934). The determination of enzyme dissociation constants. *Journal of the American Chemical Society*, 56(3), 658-666.
- [12] Yung-Chi, C. and Prusoff, W. H. (1973) Relationship between the inhibition constant (K_i) and the concentration of inhibitor which causes 50 per cent inhibition (I₅₀) of an enzymatic reaction. *Biochemical pharmacology*, 22, 3099-3108.
- [13] Reza, R. and Singh, G. (2010). Heavy metal contamination and its indexing approach for river water. *International Journal of Environmental Science & Technology*, 7, 785-792.
- [14] DeForest, D. K., Brix, K. V. and Adams, W. J. (2007). Assessing metal bioaccumulation in aquatic environments: the inverse relationship between bioaccumulation factors, trophic transfer factors and exposure concentration. *Aquatic toxicology*, 84, 236-246.
- [15] Vinodhini, R. and Narayanan, M. (2008) Bioaccumulation of heavy metals in organs of fresh water fish *Cyprinus carpio* (Common carp). *International Journal of Environmental Science & Technology*, 5, 179-182.
- [16] Saccoccia, F., Angelucci, F., Boumis, G., Carotti, D., Desiato, G., E Miele, A. and Bellelli, A. (2014) Thioredoxin reductase and its inhibitors. *Current Protein and Peptide Science*, 15, 621-646.
- [17] Çomaklı, V., Kuzu, M. and Demirdağ, R. (2015). Characterization and Purification of Glutathione S-Transferase from the Liver and Gill Tissues of Ağrı Balık Lake Trout *Salmo trutta labrax* and the Effects of Heavy Metal Ions on Its Activity. *Journal of aquatic animal health*, 27, 145-151.
- [18] Kuzu, M. and Ciftci, M. (2015) Purification and characterization of NADPH-cytochrome P450 reductase from Lake Van fish liver microsomes and investigation of some chemical and metals' effects on the enzyme activity. *Turkish Journal of Chemistry*, 39, 149-158.
- [19] Çiftçi, N., Karayakar, F., Ay, Ö., Cicik, B. and Erdem, C. (2015) Effects of Copper and Lead on Some Hematological Parameters of *Oreochromis niloticus*. *Fresen. Environ. Bull.*, 24, 2771-2775.
- [20] Orun, I., Talas, Z. S. and Alkan, A. (2011) Modulating effect of selenium on gills of fish exposed to heavy metals. *Fresen. Environ. Bull.*, 20, 104-108.
- [21] Özgençli, İ. and Çiftci, M. (2016) Purification and characterization of mitochondrial thioredoxin reductase enzyme from rainbow trout (*Oncorhynchus mykiss*) liver and investigation of the in vitro effects of some metal ions on the enzyme. *Turkish Journal of Chemistry*, 40, 174-183.
- [22] Watabe, S., Makino, Y., Ogawa, K., Hiroi, T., Yamamoto, Y. and Takahashi, S. Y. (1999) Mitochondrial thioredoxin reductase in bovine adrenal cortex. *European Journal of Biochemistry*, 264, 74-84.
- [23] Gromer, S., Arcsott, L. D., Williams, C. H., Schirmer, R. H. and Becker, K. (1998) Human placenta thioredoxin reductase isolation of the selenoenzyme, steady state kinetics, and inhibition by therapeutic gold compounds. *Journal of Biological Chemistry*, 273, 20096-20101.
- [24] Luthman, M. and Holmgren, A. (1982) Rat liver thioredoxin and thioredoxin reductase: purification and characterization. *Biochemistry*, 21, 6628-6633.
- [25] Moore, E. C., Reichard, P. and Thelander, L. (1964) Enzymatic synthesis of deoxyribonucleotides V. Purification and properties of thioredoxin reductase from *Escherichia coli* B. *Journal of Biological Chemistry*, 239, 3445-3452.

- [26] Carvalho, C. M., Chew, E. H., Hashemy, S. I., Lu, J. and Holmgren, A. (2008) Inhibition of the human thioredoxin system a molecular mechanism of mercury toxicity. *Journal of Biological Chemistry*, 283, 11913-11923.
- [27] Branco, V., Canário, J., Lu, J., Holmgren, A. and Carvalho, C. (2012) Mercury and selenium interaction in vivo: effects on thioredoxin reductase and glutathione peroxidase. *Free Radical Biology and Medicine*, 52, 781-793.
- [28] C) Orun, I., Ates, B., Selamoglu, Z., Yazlak, H., Ozturk, E. and Yilmaz, I. (2005) Effects of various sodium selenite concentrations on some biochemical and hematological parameters of rainbow trout (*Oncorhynchus mykiss*). *Fresen. Environ. Bull.*, 14, 18-22.
- [29] Keha, E. E., & Küfrevioğlu, Ö. İ. (2010). *Biyokimya. Aktif Yayınevi, Erzurum*,
- [30] Guidelines for drinking-water quality (1996) 2nd ed. Vol. 2. Health criteria and other supporting information. World Health Organization, Geneva.

Received: 27.02.2017

Accepted: 10.05.2017

CORRESPONDING AUTHOR

Muslum Kuzu

Ibrahim Cecen University of Agri, Faculty of Pharmacy 04100, Agri – TURKEY

e-mail: mkuzu@agri.edu.tr

DETERMINATION OF THE EFFECTS OF LIGHT INTENSITY AND LIGHT CYCLE PARAMETERS IN THE CULTIVATION OF *CHLORELLA PROTOTHECOIDES* MICROALGAE SPECIES

Ahmet Konuralp Elicin*

Agricultural Machinery and Technology Engineering Department, Faculty of Agriculture, University of Dicle, Diyarbakir, Turkey

ABSTRACT

Intensive studies are being conducted to improve alternative energy resources due to a significant increase in the risks arising from the use of oil based energy in recent years. Biomass, ethanol and biodiesel are the most important alternative energy resources are renewable, recyclable and non-polluting. Biodiesel has caused an increase in food prices and has made it difficult to obtain food in some less developed countries, due to the allocation of agricultural land for the cultivation of oil crops rather than food production, to gain more profit. Therefore, microalgae, which can grow easily in fields not used for agriculture and for which per hectare yield is very high when compared with other biodiesel resources; appear to be a new biodiesel resource.

In this study, the *Chlorella protothecoides* species belonging to the class *Chlorophyceae* were examined, suitability for biofuel production, large amount of oil, different temperature requirements. The effect of some growing parameters of this species, on different light intensity (172 lux, 186 lux and 265 lux) and different light cycles (12/12, 18/6, 6/18 and 24/0) on cell numbers, pH and conductivity values, has been investigated. According to the results of this study, it was determined that the effect of both light cycles and light intensity are important for cell numbers, pH, conductivity and salinity values.

KEYWORDS:

Renewable energy, microalgae, biodiesel, *Chlorella protothecoides*.

INTRODUCTION

The starvation problem keeps on making itself be felt increasingly every day thus forcing humankind to rearrange its relationship with nature in a world where agricultural areas continue to decrease and population increment cannot be controlled [1]. Air pollution, resulting from the consumption of petroleum derived fuels, the greenhouse effect and furthermore, difficulties in supplying petroleum, has

significantly increased the search for alternative fuels [2]. One of these alternative fuels is biodiesel whose production was accelerated after 2000s in our country and in the World [3]. Because of its properties, for example being similar to diesel fuels, being liquid and usable with current fuels in an admixture, it has great advantages; however, as the raw material for biodiesel were selected from agricultural products, it has led to the excessive use agricultural land. Thus, it is predicted that it will result in scarcity, price rises for food products, erosion and biodiversity loss and, due to the excessive use of fertilizers and pesticides, land and ground water pollution [4]. Algae are known to be comparatively sensitive to many chemicals, and the inclusion of these organisms in test batteries has been shown to improve the capacity of the battery to predict the most sensitive ecosystem responses [5].

Microalgae are unicellular organisms. They convert carbon dioxide into carbohydrates and form the basic oxygen supply for the atmosphere [6]. It is estimated that some species produce between 18.700 and 46.750 liters of oil per hectare per year; however, although 468 liters of oil can be obtained when soybean is sown, this value corresponds to 1% of the total oil production of microalgae. Furthermore, it is seen as a way of producing biofuel without competing with agriculture. Some freshwater algae can be produced in wastewater and marine algae in a mixture of sea water and wastewater. As a result, the wastewater will be purified. In these circumstances, the need for fresh water and fertilizer is eliminated.

Animal oils and the oil of herbal products, such as soybean, corn and sunflower, are used for biodiesel production. Microalgae are much more advantageous than soybean and corn plants for biodiesel production. Algae can be grown in large quantities on much smaller areas of land. In addition, algae do not need special conditions, such as fresh water and fertile soil and it can be harvested many times during the year [7]. Algae can practically be grown in any location where there is enough light. Some can also grow in salty water [8].

It seems that microalgae is a unique source for biodiesel and in the future has the potential to replace

diesel. Unlike other oil crops, microalgae grow extremely fast and some of them are very rich in terms of oil. Indeed, microalgae are the fastest growing photosynthetic organism. Every few days they can complete their entire growth cycle. Approximately, 46 tons per hectare per year can be produced from single-celled marine algae. Different species of algae produce oil in varying amounts [9]. A microalga often doubles the amount of biomass within 24 hours. The doubling time of biomass during growth is usually a little short of 3.5 hour. The oil content of microalgae may exceed 80% of their dry biomass [10]. According to some assessments, the oil yield derived from algae is 200 times more than the yield of vegetable oil, the performance of which is the best. Biodiesel was produced from heterotrophic micro algal oil.

Several different types of renewable biofuel can be obtained from microalgae. These are methane production by anaerobic degradation of algal biomass, obtaining biodiesel from micro algal oil and photo biologically bio hydrogen production [11]. Biodiesel is obtained by the transesterification of animal and vegetable oil. Furthermore, at the end of the transesterification process, a valuable by-product glycerol is obtained.

Micro algal oils differ from many vegetable oils, as it is rich in four or more double bound polyunsaturated fatty acids; for example, eicosapentaenoic acid (EPA, C20: 5N3; five double bonds) and docosahexaenoic acid (DHA, C22: 6n-3; six double bonds) are usually formed in oils from algae. During four or more double bound fatty acids and storage on fatty acid methyl ester, it is very sensitive to oxidation and this reduces the acceptability of these oils for use in biodiesel production.

Depending on the species, microalgae produce many different types of lipid, hydrocarbon and other complex oils. Although not all algal oils are suitable for producing biodiesel, many suitable oils are found [10]. Microalgae, owing to fatty acids such as oleic acid (C18:1) and palmitoleic acid (C16:1) in their structure, in amounts of more than 80%, contain high energy; therefore, converting microalgae into fuel is very advantageous [12].

MATERIAL AND METHODS

Chlorophyceae generally is well known to be one of the most promising candidates for commercial lipid production [13, 14]. In the study, the *Chlorella protothecoides* species belonging to the class *Chlorophyceae* was selected, due to its factors, such as including larger amounts of oil, its availability and durability to contamination.

Chlorella protothecoides was grown in the Department of Agricultural Machine of Faculty of Agriculture of Dicle University and cultivation param-

eters have been examined. The reason for the determination of cultivation parameters is its accessibility in nature and being little affected by external factors. (Figure 1). Before being distributed to the flasks, the species to be studied were produced in a large lantern. After they had been produced in sufficient quantities they were distributed to the flasks in the same volume (300 ml) (Figure 2). As can be seen in Table 1, Bold-Basal Medium (BBM) was applied to the grown microalga as the nutrient.



FIGURE 1
Chlorella protothecoides microscope image



FIGURE 2
Chlorella protothecoides growth medium

TABLE 1
Composition of Bold Basal Medium (BBM)

Content	Amount	Amount
NaNO ₃	30 ml / l	10 g / 400ml
CaCl ₂ ·2H ₂ O	10 ml / l	1 g / 400ml
MgSO ₄ ·7H ₂ O	10 ml / l	3 g / 400ml
K ₂ HPO ₄	10 ml / l	3 g / 400ml
KH ₂ PO ₄	10 ml / l	7 g / 400ml
NaCl	10 ml / l	0,4 g / 400ml
P-IV Metal Solution	6 ml / l	0,1 g / 400ml
Soil water: GR+ Medium	40 ml / l	1,5 g / 400ml
Vitamin B ₁₂	1 ml / l	2 g / 400ml
Biotin Vitamin Solution	1 ml / l	0,9 g / 400ml
Thiamine Vitamin Solution	1 ml / l	0,1 g / 400ml

Experiments were planned in two different sections after the cultivation of algae. Since light intensity and light cycle will be examined, a light-proof box made of polystyrene was made for each volumetric flask where algae were grown (Figure 3).

At the beginning of the experiment, the number of cells, pH and conductivity values of the alga species were measured using White light under 24 hours' light, 18 hours light – 6 hours dark and 12 hours light – 12 hours dark. At the second and final section of the experiment, the changes of light intensity provided by respectively 256 lux, 186 lux and 172 lux light sources on the same parameters were determined by following the experiments, the obtained data was evaluated in randomized blocks according to experimental design and analysis of variance. Groupings were calculated according to the Duncan test.

numbers values obtained in the experiments under different light intensities in *Chlorella protothecoides* microalga species is given in Tables 2. As shown in Table 2, light intensity x day and light intensity 15-day interaction is significant ($p < 0.01$).

RESULTS AND DISCUSSION

Statistical results belongs to different light intensity. Variance analysis results and average values regarding to salinity, conductivity, pH and cell



FIGURE 3
Protective boxes

TABLE 2
Variance analysis results for pH, salinity, conductivity and cell numbers of different light intensity

Variance source	Degrees of Freedom	pH		Salinity (mg/L)		Conductivity ($\mu\text{S}/\text{cm}$)		Cell number (pcs/mm^3)	
		Mean Square	Probability	Mean Square	Probability	Mean Square	Probability	Mean Square	Probability
Replication	2	0.06		697.874		242.985		1.265E10	
Light intensity	2	3.219	$P < 0.01$	259627.941	$P < 0.01$	24.763	$P < 0.05$	2.763E12	$P < 0.01$
Error	4	0.002		270.163		2.430		1.720E9	
Day	14	0.637	$P < 0.01$	23139.550	$P < 0.01$	6621.347	$P < 0.01$	5.981E11	$P < 0.01$
Intensity x day	28	0.127	$P < 0.01$	8168.568	$P < 0.01$	101.144	$P < 0.01$	9.018E10	$P < 0.01$
Error	84	0.001		6.146		1.996		1.435E9	
Cv (%)		0.32		0.63		0.22		3.60	

TABLE 3
The values determined under 265 lux light intensity

Days	ph	Salinity (mg/L)	Conductivity ($\mu\text{S}/\text{cm}$)	Cell number (pcs/mm^3)
1	8.338	302.3	597.7	1056000
2	8.345	328.7	605.0	1112000
3	8.404	356.7	607.3	1157000
4	8.459	388.0	610.7	1225000
5	8.561	415.0	615.7	1288000
6	8.643	438.7	619.0	1407000
7	8.706	456.3	626.3	1485000
8	8.791	477.3	637.7	1576000
9	8.843	503.7	645.7	1499000
10	8.733	551.3	652.0	1392000
11	8.583	556.3	660.3	1303000
12	8.395	577.3	667.0	1205000
13	8.337	600.7	676.3	1056000
14	8.237	628.0	684.3	983300
15	8.141	652.0	689.0	820000
Mean	8.501^a	482.2^a	639.6^a	1238000^a

TABLE 4
The values determined under 186 lux light intensity

Days	pH	Salinity (mg/L)	Conductivity ($\mu\text{S/cm}$)	Cell number (pcs/mm ³)
1	8.382	325.3	597.0	1157000
2	8.418	330.7	603.0	1197000
3	8.455	329.7	607.0	1248000
4	8.501	330.0	611.7	1309000
5	8.538	337.3	614.3	1509000
6	8.617	343.3	621.0	1537000
7	8.658	351.0	626.7	1425000
8	8.596	358.3	632.3	1368000
9	8.504	365.3	642.3	1239000
10	8.389	368.3	649.3	1104000
11	8.304	369.7	657.7	1021000
12	8.197	380.3	668.3	929300
13	8.109	384.7	675.3	821300
14	8.050	387.7	681.3	714700
15	7.943	390.0	686.3	624700
Mean	8.377^b	356.^b	638.2^b	1147000^b

TABLE 5
The values determined under 172 lux light intensity

Days	pH	Salinity (mg/L)	Conductivity ($\mu\text{S/cm}$)	Cell number (pcs/mm ³)
1	8.303	314.3	608.0	1153000
2	8.355	320.3	613.7	1153000
3	8.438	325.3	619.3	1129000
4	8.444	327.7	624.0	1110000
5	8.365	331.7	626.0	1059000
6	8.269	336.3	628.3	993300
7	8.196	341.3	631.0	954700
8	8.114	344.0	635.0	909300
9	8.064	347.3	640.3	774700
10	8.008	354.7	646.3	645300
11	7.914	375.3	653.0	584000
12	7.689	359.0	659.3	509300
13	7.446	363.0	663.0	397300
14	7.220	366.3	668.7	159300
15	7.002	371.0	675.7	22930
Mean	7.989^c	345.2^b	639.4^a	770300^c

TABLE 6
Variance analysis results for pH, salinity, conductivity and cell numbers of different light cycles

Variance source	pH		Salinity (mg/L)		Conductivity ($\mu\text{S/cm}$)		Cell number (pcs/mm ³)		
	Degrees of Freedom	Mean Square	Probability	Mean Square	Probability	Mean Square	Probability	Mean Square	Probability
Replication	2	0.007		42.022		67.606		7.851E9	
Light/dark time	3	5.079	p<0.01	88001.354	p<0.01	113163.511	p<0.01	4.596E12	p<0.01
Error	6	0.013		70.659		158.006		7.414E9	
Day	14	0.495	p<0.01	746.165	p<0.01	3965.006	p<0.01	4.667E11	p<0.01
Light/dark time x day	42	0.207	p<0.01	2090.278	p<0.01	5359.206	p<0.01	2.212E11	p<0.01
Error	112	0.006		0.911		9.435		6.300E8	
Cv (%)	0.94			0.28		0.48		2.89	

The largest pH value was 8.8 at 265 lux on the 9th day and the smallest was 8.14 on the 15th day. It is understood that pH values tend to increase within the first 10 days and then start to decline (Table 3). While salinity reaches the highest value with 652.0 mg/L depending on light intensity of 256 lux, it has the smallest value with 302.3 mg/L on the first day. Salinity values showed an upward tendency during the following days. When average values were examined in terms of conductivity, the highest value

obtained on the 15th day at 265 lux intensity and similar trends emerged in pH and salinity. However, unlike the others, while the number of cells increased up to 8th day, significant decreases were recorded over the following days. The highest cell number was seen on the 8th day with 1576000 pcs/mm³ at 265 lux (Table 3). Depending on the different light intensities, an increase was observed in pH values up to the 8th day with the highest pH value being determined as 8.65 on the 7th day. But, as the number of observation days increased, decreases were observed

and the lowest pH value was determined as 7.94 on the 15th day. This is in agreement with the reports of Solovchenko et al. [15].

In contrast to pH, salinity values at 186 lux indicated an increase in parallel with the increasing number of days. Accordingly, the lowest salinity value was recorded on the 1st day as 325.3 mg/L while the highest value was on the 15th day as 390.0 mg/L. In the light intensity trial, an increase was observed in conductivity values at 186 lux, as the number of days increased. At the 1st day, it reached the highest conductivity level (597.0 $\mu\text{S/cm}$). An increase was recorded in terms of cell numbers up to the 6th day, and then it started to fall and reached the smallest value (624700 pcs/mm³) at the end of the 15th day (Table 4). Similar results were reported by Solovchenko et al. [15] and Wahidin et al. [16].

As shown in Table 5, the pH value of *Chlorella protothecoides* species at 172 lux light intensity varied between 7.00 and 8.44, and while it reached the highest value on the 4th day, the smallest value was recorded on the 15th day. Salinity values generally increased with the increasing number of days and it reached the greatest value of 375.3 mg/L on the 11th day. While the highest conductivity was recorded on the 15th day as 675.7 $\mu\text{S/cm}$, the smallest value was seen on the 1st day as 608.0 $\mu\text{S/cm}$.

The number of cells tended to decrease with the increasing number of days, as opposed to other parameters examined, and the highest number of cells was counted on the first day with 1153000 pcs/mm³ and the least number was seen on the 15th day with 22930 pcs/mm³.

Statistical results according to different exposure times. Variance analysis results of pH, salinity, conductivity and cell number values obtained

under different light cycles of *Chlorella protothecoides* microalga species are given in Table 6.

In Table 7, while the highest pH value was obtained on the 15th day with 8.60 on 24 hours light cycle, the lowest value was measured on the first day with 8.12. As salinity values showed a similarity with pH values, the highest salinity value was on the 15th day with 406.3 mg/L and the lowest value was recorded on the first day with 342.7 mg/L. The values in terms of conductivity varied between 796.3 $\mu\text{S/cm}$ – 612.0 $\mu\text{S/cm}$, the highest and the lowest values were recorded on the 15th and 1st days respectively. The increase in the number of cells was directly proportional to the number of days, reaching the highest number (1629000 pcs/mm³) on the 15th day. Similar results were reported by Insel et al. [17].

In *Chlorella protothecoides* microalga species, the highest pH value was seen on the 6th day with 8.19 at 18 hours light / 6 hours dark cycle and the lowest value was determined on the 15th day with 6.82. The values regarding salinity varied between 333.7 mg/L and 403.7 mg/L, the highest value was reached on the 15th day. Regular increases were observed in the experiments made with respect to time under different light cycles. The best conductivity value was reached on the 15th day with the value of 693.3 $\mu\text{S/cm}$ and the lowest one was on the first day with 618.0 $\mu\text{S/cm}$. The number of cell values changed between 250700 pcs/mm³ and 1161000 pcs/mm³, while values show a decreasing trend with increasing number of days, the maximum number of cell value was recorded on the 2nd day by 1161000 pcs/mm³ (Table 8). This is in agreement with the reports of Wahidin et al. [16].

TABLE 7
The values determined under 24 hours light cycles

Days	pH	Salinity (mg/L)	Conductivity ($\mu\text{S/cm}$)	Cell number (pcs/mm ³)
1	8.125	342.7	612.0	1020000
2	8.144	349.3	619.0	1064000
3	8.186	356.3	625.3	1100000
4	8.226	363.3	633.7	1133000
5	8.265	366.3	642.3	1158000
6	8.312	368.3	648.7	1212000
7	8.338	371.7	655.0	1201000
8	8.384	376.3	659.0	1257000
9	8.425	379.7	668.7	1316000
10	8.464	382.0	684.7	1366000
11	8.505	386.7	715.0	1413000
12	8.527	391.3	736.3	1488000
13	8.543	396.7	774.7	1560000
14	8.566	400.3	786.0	1589000
15	8.600	406.3	796.3	1629000
Mean	8.374^a	375.8^a	683.8^a	1300000^a

TABLE 8
The values determined under 18 hours light / 6 hours dark light cycles

Days	ph	Salinity (mg/L)	Conductivity (µS/cm)	Cell number (pcs/mm ³)
1	8.175	333.7	618.0	1144000
2	8.132	336.7	623.0	1161000
3	8.090	342.7	627.3	1161000
4	8.010	346.7	630.7	1152000
5	7.926	352.0	635.7	1127000
6	8.192	359.0	637.7	1088000
7	7.782	358.3	622.3	1021000
8	7.689	370.3	633.7	960000
9	7.582	373.3	644.7	856000
10	7.507	377.3	651.7	677300
11	7.409	381.7	668.7	570700
12	7.320	388.0	677.3	434700
13	7.175	393.3	683.7	377300
14	6.983	399.3	689.7	310700
15	6.828	403.7	693.3	250700
Mean	7.653^c	367.7^b	649.2^b	819500^b

TABLE 9
The values determined under 12 hours light / 12 hours dark light cycles

Days	ph	Salinity (mg/L)	Conductivity (µS/cm)	Cell number (pcs/mm ³)
1	8.178	332.3	627.3	1136000
2	8.190	336.0	635.0	1168000
3	8.184	340.0	640.0	1105000
4	8.141	342.3	631.3	1075000
5	8.081	346.7	634.0	1045000
6	8.006	350.3	623.7	988000
7	7.941	355.7	615.3	953300
8	7.902	361.7	621.3	930700
9	7.853	368.3	636.0	862700
10	7.833	372.0	647.3	744000
11	7.760	377.3	652.7	629300
12	7.726	382.3	659.3	560700
13	7.700	388.7	665.3	465300
14	7.636	392.7	674.7	434700
15	7.617	397.3	688.3	377300
Mean	7.916^b	362.9^b	643.4^b	831600^b

TABLE 10
The values determined under 6 hours light / 18 hours dark light cycles

Days	ph	Salinity (mg/L)	Conductivity (µS/cm)	Cell number (pcs/mm ³)
1	8.142	324.7	631.7	1056000
2	8.076	319.7	621.0	1068000
3	8.009	314.3	610.0	984700
4	7.950	309.0	600.3	926700
5	7.901	303.0	590.7	821300
6	7.842	297.3	581.7	678700
7	7.761	293.0	571.3	581300
8	7.703	286.3	561.3	473300
9	7.640	279.7	554.7	401300
10	7.574	270.0	546.3	318700
11	7.500	260.7	539.3	250700
12	7.385	252.7	531.0	197300
13	7.290	243.7	521.3	112000
14	7.190	235.3	511.3	34670
15	7.092	226.0	503.7	12270
Mean	7.670^c	281.0^c	565.0^c	527800^c

In the experiments conducted under 12 hours light / 12 hours dark cycle, pH declined consistently, falling to 7.61 on the 15th day. In the same implementation, the highest salinity value was determined as 397.3 mg/L on the 15th day and the smallest value was recorded during the first day as 332.3 mg/L. The highest conductivity value was measured on the 15th day and the lowest value in the first day as 618.0 μ S/cm. While an increase was observed in the cell number measurement on the 2nd day, subsequent decreases were recorded and the minimum value was determined on the 15th day by 377300 pcs/mm³ (Table 9). Similar results were reported by Atta et al. [18].

In Table 10, Ph values recorded in algae within 6 hours light / 18 hours dark period changed between 7.092 and 8.142, the highest value was seen on the 1st day and the lowest value on the 15th day. As salinity values vary between 226.0 mg/L – 324.7 mg/L, it was determined that salinity values decrease with the number of days. Conductivity values were recorded least on the 15th day by 503.7 μ S/cm and highest on the first day by 631.7 μ S/cm. Number of cells decreased with increasing number of days, the lowest value was 12270 on the 15th day and the highest value was seen on the 2nd day by the number of 1068000 pcs/mm³. Similar results were also observed by Insel et al. [17].

CONCLUSION

When the effect of different light intensities on the pH, salinity and number of cells and recorded on different days was examined, it was understood that pH, salinity and the number of cell values increase is directly proportional to light intensity and conductivity decreases slightly with decreasing light intensity and then increases again. As the number of days observed increased, pH, salinity and conductivity values also increased, but it was recorded that the number of cell values increase between 5th and 8th days and then decrease on other days. In this study where different light cycles were evaluated in *Chlorella protothecoides* microalga species, the highest pH, salinity, conductivity and cell number values were observed in a 24 hour light cycle. Generally, the lowest pH, salinity, conductivity and number of cells were determined in 6 hours light and 18 hours dark cycle.

ACKNOWLEDGEMENTS

The research was supported by the University of Dicle, Scientific Research Projects Center (Project no: 12-ZF-72).

REFERENCES

- [1] Bedil, B. and Cetin, A.K. (2017) Toxicity of four fungicides to the growth and protein amount of *Chlorella vulgaris*. Fresen. Environ. Bull., 26(2a), 1778-1783.
- [2] Fukuda, H., Kondo, A. and Noda, H. (2001) Biodiesel fuel production by transesterification of oils. J Bioscience and Bioengineering, 92(5), 405–416.
- [3] Knothe, G., Dunn, R.O. and Bagby, M.O. (1997) Biodiesel: The use of vegetable oils and their derivatives as alternative diesel fuels. In: Fuels and Chemicals from Biomass, 1st edn. American Chemical Society, New York.
- [4] Romano, S.D., Gonzalez Suarez, E. and Laborde, M.A. (2006) Biodiesel In: Combustibles Alternativos, 2nd edn. Ediciones Cooperativas, Buenos Aires.
- [5] Agirman, N., Kendirlioglu, G. and Cetin, A.K. (2014) The effects of four pesticides on the growth of *Chlorella Vulgaris*. Fresen. Environ. Bull., 23(6), 1418-1422.
- [6] Freedman, B., Pryde, E.H. and Mounts, T.L. (1984) Variables affecting the yields of fatty esters from transesterified vegetable oils. J Am Oil Chem Soc, 61(19), 1638–1643.
- [7] Xu, H., Miao, X. and Wu, Q. (2006) High quality biodiesel production from a microalga *Chlorella protothecoides* by heterotrophic growth in fermenters. 126, 499-507.
- [8] Demirbas, A. (2007) Importance of biodiesel as transportation fuel. Energy Policy, 35, 4661-4670.
- [9] Demirbas, A. (2010) Use of algae as biofuel sources. Journal of Energy Conversion and Management. 51, 2738-2749.
- [10] Chisti Y. (2007) Biodiesel from microalgae, Biotechnology Advances, 25, 294-306.
- [11] Agra, I.B., Warnijati, S. and Wiratni, F. (1996) Two steps ethanolysis of castor oil using sulfuric acid as catalyst to producer motor oil. World Renewable Energy Congress Proceedings, 1025, June 15 – 21, Colorado.
- [12] Elicin, A.K., Kilickan, A. and Avcioglu, A.O. (2009) Biodiesel production from microalgae. 25th Agricultural Mechanization National Congress Proceedings, 273-278, Isparta. (In Turkish)
- [13] Huang, Y., Li, L. and Song, C. (2013) Effect of nitrogen and phosphorus levels on the lipid production of *Chlorella vulgaris* and evaluation of ultrasound-assisted lipid extraction. Fresen. Environ. Bull., 22(10), 2852-2858.
- [14] Kralova, K., Masarovicova, E. and Gyoryova, K. (2003) Inhibition of photosynthetic electron transport in spinach chloroplasts and *Chlorella vulgaris* and reduction of *Sinapis alba* L. growth by some Zn(II) compounds. Fresen. Environ. Bull., 12(8) 859-862.

- [15] Solovchenko, A.E., Khozin-Goldberg, I., Didi-Cohen, S., Cohen, Z. and Merzlyak, M.N. (2008) Effects of light intensity and nitrogen starvation on growth, total fatty acids and arachidonic acid in the green microalgae *Parietochloris insica*. *Journal of Applied Phycology*, 20, 245-251.
- [16] Wahidin, S., Idris, A. and Shaleh, S.R.M. (2013) The influence of light intensity and photoperiod on the growth and lipid content of microalgae *Nannochloropsis sp.* *Bioresource Technology*, 129, 7-11.
- [17] Insel, G., Gurel, M., Pehlivanoglu-Mantas, E., Okutman Tas, D., Ica, T., Ubay Cokgor, E., Gencsoy, E.B., Movahedpour, F., Gorgun, E. and Ozbasaran, M. (2017) Comparison of synthetic and domestic wastewater effluents for coupling nitrogen removal and chlorella vulgaris and *Scenedesmus dimorphus* production. *Fresen. Environ. Bull.*, 26(1) 433-488.
- [18] Atta, M., Idris, A., Bukhari, A. and Wahidin, S. (2013) Intensity of blue led light; A potential stimulus for biomass and lipid content in fresh

water *Chlorella vulgaris*. *Bioresource Technology*, 148, 373-378.

Received: 27.02.2016

Accepted: 27.05.2017

CORRESPONDING AUTHOR

Ahmet Konuralp Elicin
Agricultural Machinery and
Technology Engineering Department
Faculty of Agriculture
University of Dicle
Diyarbakir – TURKEY

E-mail: akelicin@gmail.com

IN VITRO SEED GERMINATION STUDY IN NARROW ENDEMIC PLANT *VERBASCUM ALYSSIFOLIUM* (SCROPHULARIACEAE)

Muhip Hilooglu*, Emel Sozen

Department of Biology, Faculty of Science, Anadolu University, 26470, Eskisehir, Turkey

ABSTRACT

Verbascum alyssifolium Boiss is an endemic species having considerable narrow distribution in Erzincan (Turkey) region. In this study, germination behavior of *Verbascum alyssifolium* under different concentrations of NaCl, HCl, KNO₃, GA₃ (100 and 200 μM), hot-cold stratification and mechanical scarification was examined. Treated seeds were exposed to a photoperiod of 8 h light/16 h dark with a 23/18 °C thermoperiod. Germination rates increased with GA₃-100 μM (56%), GA₃-200 μM (57%) and mechanical scarification (63%) treatments when compared to the control (42%). On the other hand, NaCl, HCl, KNO₃ treatments and hot-cold stratifications decreased germination. The highest speed of germination index was obtained at gibberellic acid (14.7). This study represents first report about germination characteristics of *V. alyssifolium* and will provide valuable data for *ex situ* conservation practices of this endemic plant.

KEYWORDS:

Verbascum alyssifolium, Scrophulariaceae, endemic, germination, *ex situ*

INTRODUCTION

Verbascum L. (Scrophulariaceae) is the second largest genus in Turkey, with 234 species and a high endemism level (80 %) [1, 2]. Endemic *Verbascum alyssifolium* Boiss is a rare plant species that shows narrow distribution around Erzincan (Turkey) region. The species was first collected by Sintenis from Iliç (Hasanova village and Kuruçay)/Erzincan district in 1899 [3]. At present, species is known only from three different localities exist in Erzincan. Many endemic plant species considered as a source of genetic diversity are faced with the risk of extinction due to various reasons in Turkey. According to the IUCN criteria, *V. alyssifolium* was evaluated as DD (Data-deficient) [4]. Currently, habitats of this species are under various pressures due to urbanisation and intensive human activities causing high risk of threats [5].

Seed germination is a feature of priority substance for the reproductive success of plants [6]. Information on the reproductive success of rare and endangered endemic species contributes to understanding of the rarity. It also helps to improve conservation strategies [7, 8]. Seed germination is a critical step for the abiding conservation of plant germplasm. In recent years, seed germination has become a universal concern among researchers to maintain the genetic diversity in threatened plants [9].

It is known that seed dormancy is a feature of plant species that delays germination until favourable conditions develops for seedling growth [10]. Some pre-treatments such as sanding, boiling or cold stratification, and chemical applications such as potassium nitrate, acid and gibberellic acid are used to break down seed dormancy under laboratory conditions [11]. To date only morphological [5] and molecular studies [12] have been conducted with *Verbascum alyssifolium*, but there is no information regarding seed germination characteristics and dormancy breaking in this plant. The purpose of this study was therefore to identify the effect of different chemical applications (NaCl, HCl, KNO₃, GA₃) and some pre-treatments techniques (hot/cold and mechanical) on seed germination of *Verbascum alyssifolium*. The results obtained from this study could provide basic information to develop effective *ex situ* conservation strategies for this rare and endemic plant species.

MATERIALS AND METHODS

Seed collection. Plant samples of *V. alyssifolium* were collected from Erzincan (37°45' E, 49°77' N, altitude 1015 m), Turkey (Fig. 1) between June and July 2014.

The collected plants were air dried for 7 days in room conditions. The mature capsules were carefully harvested. After counting the total number of seeds per fruit, fully developed and healthy seeds were considered as fertile seeds. The seed weight was determined according to Bonner [13].

Seed germination experiment. Seed germination experiments were performed on filter

paper in 9 mm diameter Petri dishes (sterilized) at constant 8 h light/16 h dark photoperiod with 23°C /18 °C thermoperiod. The Petri dishes containing seeds were subjected to different treatments namely:

a. Chemical applications; containing sodium chloride (NaCl), hydrochloric acid (HCl), potassium nitrate (KNO₃), gibberellic acid (GA₃) solution at 100 µM and 200 µM concentrations.

b. Mechanical scarification; sanding was gently made with sandpaper (grade 150) about 30 sec or 1 min.

c. Cold stratification; the petri dishes were wrapped with aluminum foil and placed at +4 °C and -20 °C for 7 days before transferring to growth chambers

d. Hot stratification; soaking in hot-boiling water for 30 sec, 1 min and 2 min.

e. Control treatment; distilled water was used to germinate seeds.

Each treatment was replicated 4 times with at least 100 seeds per replication. Germinated seeds were regularly noted every day, the radical emergence of 2-5 mm was accepted as a successful germination [14].



FIGURE 1

The general view of *Verbascum alyssifolium*

Data analysis. Germination percentage (GP) was calculated using the equation: “GP = number of germinated seeds /total number of seeds X 100”. Speed of germination (SG) was defined as the number of seeds germinated during a limited period according to the formula described by Yücel [15]. T50 (Time to 50% germination) was computed with the formula:

$$T50 = t_i (N/2 - n_i) (t_j - t_i) / n_j - n_i$$

(N: cumulative number of germinated seeds, n_j and n_i: total number of seeds germinated by adjoining counts at t_j times, t_i when n_i < N/2 < n_j) [16].

The data analysis was done using SPSS (V. 15.0, Chicago, IL) program and the results were classified with Duncan's new multiple range test (DMRT) (P<0.05).

RESULTS

Seed structure. The seeds of *V. alyssifolium* develop in capsules. Among 20 capsules randomly examined; two were empty and one contained undeveloped seed. The number of seeds in each capsule ranged from 4-22. About 57.4% of the total seeds were found to be healthy. Seed size is about 0.5 mm by 1 mm in dimension, ovoid in shape and its outer surface is indented (Fig. 2). Black-brown testa is very hard and seems impervious to water and gases. The weight of 1000 healthy seeds was found as 1220 mg.

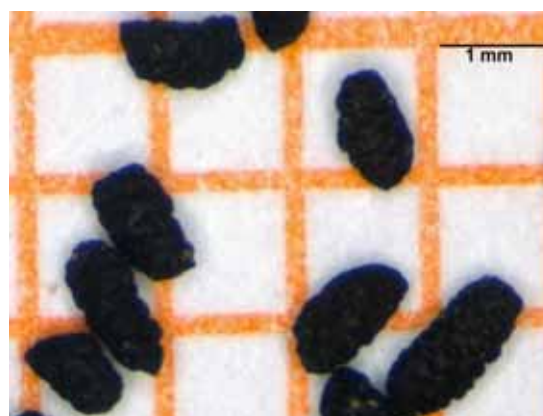


FIGURE 2

Seeds of *Verbascum alyssifolium*

Different applications and pre-treatments were utilized *in vitro* seed germination experiments for endemic *V. alyssifolium*. The effect of all treatments on breaking dormancy was showed in Table (1).

In vitro seed germination. Minimum and maximum values of time to 50% germination, germination percentage and speed of germination varied as 5.5 – 10.0, 0% - 63% and 8.5 – 14.7, respectively. The influence of treatments on germination showed that GA₃ (56-57%) and mechanical scarification with sandpaper (63%) have increased germination percentage in *V. alyssifolium* seeds, while the HCl-100 µM and cold stratification at -20°C treatments have no significant effect compared with the control (42%) according to Duncan test (P<0.05). On the other hand, significant decrease in germination percentage (P<0.05) were shown after treatments with KNO₃ (22% and 14%) and NaCl (27% and 18%) at 100µM-200µM and HCl (22%) at 200µM concentrations. The speed of germinations in the present study was low or insignificant in KNO₃ when compared to the control (P<0.05). The SGs were higher than that of the control in all treatments (P<0.05). The time to 50% germination (T50) of seeds in KNO₃ (100 µM) increased (T50= 10.0), when compared to control and also T50 was decreased in all other treatments, the lowest T50 was 5.5 in NaCl (100 µM) (Fig. 3).

TABLE 1
Mean values of GP, SG, T50 for *Verbascum alyssifolium* under different treatments

Treatment	Concentration (μM)	GP (%)	SG	T50 (Day)
Control	-	42 ^f (±2.3)	9.7 ^b (±0.51)	8.0 ^c (±1.2)
KNO ₃	100	22 ^{cd} (±1.5)	8.5 ^a (±0.52)	10.0 ^d (±1.8)
KNO ₃	200	14 ^b (±3.4)	10.5 ^b (±0.52)	7.5 ^c (±0.9)
GA-3	100	56 ^e (±9.5)	11.8 ^c (±0.67)	7.0 ^b (±1.1)
GA-3	200	57 ^e (±8.0)	14.7 ^f (±0.40)	6.2 ^a (±0.8)
NaCl	100	27 ^{de} (±2.0)	14.2 ^{cd} (±0.36)	5.5 ^a (±0.6)
NaCl	200	18 ^{bc} (±5.0)	13.7 ^{de} (±0.51)	6.5 ^b (±1.2)
HCl	100	40 ^f (±7.3)	13.4 ^{de} (±0.36)	7.3 ^c (±1.6)
HCl	200	22 ^{cd} (±2.3)	11.5 ^c (±0.52)	7.7 ^c (±0.9)
Sandpaper	-	63 ^h (±6.6)	12.8 ^d (±0.51)	7.2 ^b (±1.3)
Hot water (30sec)	-	8 ^a (±4.3)	-	-
Hot water (1 min)	-	4 ^a (±1.6)	-	-
Hot water (2 min)	-	-	-	-
Stratification (+4°C)	-	28 ^c (±3.0)	13.6 ^{de} (±0.62)	7.5 ^b (±1.0)
Stratification (-20°C)	-	40 ^f (±3.6)	11.6 ^c (±0.54)	7.8 ^c (±1.4)

In each column, means with different letter(s) differ significantly according to DMRT at $p < 0.05$. GP: Seed germination percentage, SG: Speed of germination, T50: Time to 50% germination (Standart deviation was given in brackets).

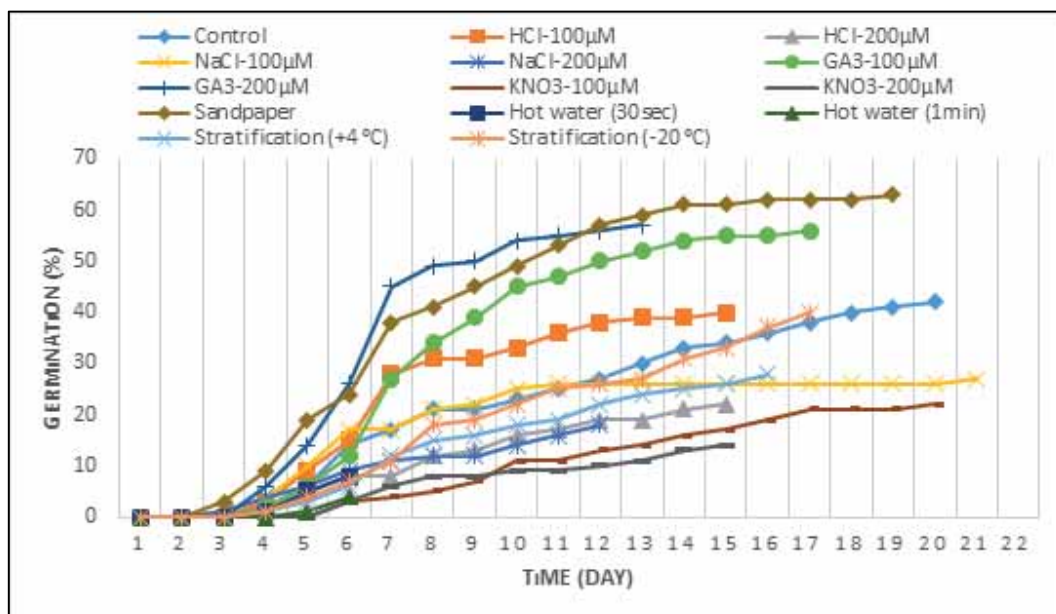


FIGURE 3

Diagram of germination percentage and time for *V. alyssifolium* seeds under different treatments

DISCUSSION

Information on seed germination behaviours of plants are very important to understand their reproductive biology and seedling reestablishment in a changing environment [17]. However, germination characteristics of many rare and/or endemic plant species have not been elucidated, because materials from these kind of species are more difficult to collect [18]. In this study, the seed germination characteristics of endemic plant *V. alyssifolium* were described. The highest germination percentage (63%) was obtained from seeds that were mechanically scarified with sandpaper and it was the best effective treatment. Yildiztugay and Kucukoduk [19] reported that sandpaper scarification of lignified palisade cell layer in seeds triggers germination due to water

penetration. Similarly, eliminating the lignified layer below the seed coat by mechanic scarification with sandpaper was reported to be the best method to defeat seed firmness of many plant species [20, 21]. Therefore, we can say that seeds of *V. alyssifolium* possess physical dormancy because of the hard seed coat layer that can be broken down with mechanical scarification to promote successful germination.

Endogenous GA₃ and other plant growth regulators are known as the basic important implementation to break the dormancy [22, 23]. Furthermore, it has been reported that endogenous GA₃ deficiency can be perfected by exogenous GA₃ application [24]. In this study, exogenous application of gibberellic acid (GA₃) at 100 and 200 μM concentrations increased germination percentage and germination speed of *V. alyssifolium* seeds. Exposure to 200 μM

GA₃ concentration caused an increase in germination speed and shortened time to 50% germination (P<0.05). Dormancy break by GA₃ is typical in seeds with non-deep physiological dormancy, but it was also reported for intermediate physiological dormancy [25]. GA₃ supplementation appears to be the second successful treatment for stimulating germination in *V. alyssifolium* and this may be related to intermediate physiological dormancy characteristics of its seeds.

On the other hand, germination levels decreased to 40%, 27%, 22% and 8-4% after 100 µM chemical applications of HCl, NaCl, KNO₃ and hot stratification treatments, respectively. There were no significant differences between HCl-100 µM, cold stratification (-20°C) and control groups in terms of germination percentage. Seed germination percentage and speed of germination decreased significantly with the increased concentrations of NaCl and HCl and soaking time in hot water treatments (Table 1). These results implied negative effect of salinity and acidity treatment on seed germination in *V. alyssifolium*. Similar results were shown by Teimouri and Mahallati [26]. They reported negative correlation between both salinity and acidity with germination in endemic *Hymenocrater platystegius*. In our study, germination percentage and T50 levels were not affected positively by cold stratifications (+4 °C and -20 °C), but speed of germination showed significant increase when compared with control treatments. Likewise, Leo [27] shown that cold stratification (in +5 °C) had no effect on dormancy breaking in some *Verbascum* species (*V. nigrum*, *V. speciosum* and *V. thapsus*). Also, similarly our hot stratification results, Luna *et al.* (2007) reported no germination in Mediterranean endemic *Verbascum rotundifolium* seeds after heat-shock treatments at 80°C, 100°C and 120°C.

In conclusion, the results of our experiments showed that the seed germination rates can be increased with mechanical scarification with sandpaper and application of giberellic acid in endemic *Verbascum alyssifolium*. As generally accepted, succesful seed germination is crucial step to develop effective ex situ conservation strategies for rare and endemic plants. Therefore, the data obtained from this study will provide basic information to establish rapid, efficient and affordable ex situ conservation strategies for *V. alyssifolium*.

ACKNOWLEDGEMENTS

We thank Prof. Dr. Ali Kandemir for his valuable help during collection and identification of the plant material. This study was supported by Anadolu University Scientific Research Found, Project No: 1409F389.

REFERENCES

- [1] Karaveliogulları, F.A., Celik, S. and Isık G. (2016). The Altitudinal, climatical and phenological classification of *Verbascum* L. species from different phytogeographical regions of Turkey. *App. Ecol. Env. Res.*, 14, 15–27.
- [2] Güteryüz, G., Kırmızı, S., Arslan, H. and Derya, S. (2016). The effects of heavy metals on the seed germination and seedling growth of two endemic *Verbascum* species. *Fresen Environ Bull.* 25, 1134–1142.
- [3] Davis, P.H. (1978). *Flora of Turkey and the East Aegean Islands*, Vol. 6, Edinburg, Scotland.
- [4] Ekim, T., Koyuncu, M., Vural, M., Duman, H., Aytaç Z. and Adıgüzel, N. (2000). *Türkiye Bitkileri Kırmızı Kitabı, Doğal Hayatı Koruma Derneği* (In Turkish), Ankara, Turkey.
- [5] Kandemir, A. and Makbul S. (2004). Erzincan yöresinde yayılış gösteren bazı nadir bitki türleri üzerine gözlemler. *Erzincan Eğitim Fakültesi Dergisi*, 6, 37–49 (In Turkish).
- [6] Bu, H., Du, G., Chen, X., Xu, X., Liu, K. and Wen, S. (2008). Community wide germination strategies in an alpine meadow on the eastern Qinghai-Tibet plateau: phylogenetic and life-history correlates. *Plant Ecol.* 195, 87–98.
- [7] Menges, E.S. (1986). Predicting the future of rare plant populations: demographic monitoring and modelling. *Nat. Area. J.* 6, 13–25.
- [8] Schemske, D.W., Husband, B.C., Ruckelshaus, C.G., Goodwillie, C., Parker, I.M. and Bishop, J.G. (1994). Evaluating approaches to the conservation of rare and endangered plants. *Ecology*, 75, 584–606.
- [9] Cousins, S.R., Witkowski, E.T.F. and Mycock, D.J. (2014). Seed storage and germination in *Kumara plicatilis*, a tree aloe endemic to mountain fynbos in the Boland, south-western Cape, South Africa. *S. Afr. J. Bot.* 94, 190–194.
- [10] Brusa, G., Ceriani, R. and Cerabolini, B. (2007). Seed germination in a narrow endemic species (*Telekia speciosissima*, Asteraceae): Implications for *ex situ* conservation, *Plant Biosystems* 141, 56–61.
- [11] Jones CD, Stevens MR, Jolley VD, Hopkins BG, Jensen SL, Turner D, Stettler JM (2016). Evaluation of thermal, chemical, and mechanical seed scarification methods for 4 Great Basin lupine species. *Native Plants Journal* 17:5-17.
- [12] Hilooğlu, M. and Sozen, E. (2017) Population Genetic Structure of Endemic *Verbascum alyssifolium* in Erzincan Region of Turkey. *Fresen. Environ. Bull.*, 26, 1756–1764.
- [13] Bonner, F.T. (1974). Seed testing in Seed of woody plants in the United States, *Agriculture handbook*, pp: 450-453. No. 450, For Service USDA Washington, USA.
- [14] Marquez-Garcia, B., Rodriguez, A.F.M. and

- Cordoba, F. (2009). Germination requirements of *Erica andevalensis*, an endemic species restricted to acid and metal/ metalloids-enriched soils of the Iberian Pyrite Belt (sw Iberian Peninsula). *Fresen Environ. Bull.* 18, 2259–2267.
- [15] Yücel, E. (2000). Effects of different salt (NaCl), potassium nitrate (KNO₃) and acid (H₂SO₄) concentrations on the germination of some *Salvia* species seeds. *Seed Sci. Technol.* 28, 853–860.
- [16] Farooq, M., Basra S.M.A., Hafeez K. and Ahmad, N. (2005). Thermal hardening: a new seed vigor enhancement tool in rice. *Acta Bot. Sin.* 47, 187–193.
- [17] Barpete, S., Oğuz, M.C., Özcan, S.F., Anayol, E., Ahmed, H.A., Khawar, K.M., Özcan, S. (2015). Effect of temperature on germination, seed vigor index and seedling growth of five Turkish cotton (*Gossypium hirsutum* L.) cultivars. *Fresen Environ. Bull.* 24, 2561–2566.
- [18] Cerabolini, B., Andreis, R.D., Ceriani, R.M., Pierce S. and Raimondi, B. (2004). Seed germination and conservation of endangered species from the Italian Alps: *Physoplexis comosa* and *Primula glaucescens*, *Biol. Cons.* 117, 351–356.
- [19] Yildiztugay, E. and Kucukoduk, M. (2012). Dormancy breaking and germination requirements for seeds of *Sphaerophysa kotschyana* Boiss. *J. Global Biosci.* 1, 20–27.
- [20] Sfairi, Y., Lahcen, O. Feddy, M.N.A. and Abbas, A. (2012). Dormancy-breaking and salinity/water stress effects on seed germination of Atlas Cypress, an endemic and threatened coniferous species in Morocco. *Afr. J. Biotechnol.* 11, 4385–4390.
- [21] Asaadi, A.M., Heshmati, G. and Dadkhah, A. (2015). Effects of Different Treatments to Stimulate Seed Germination of *Salsola arbusculiformis* Drob. *Ecopersia*, 3, 1077–1088.
- [22] Zheng, Y. and Sun, W. (2009). Seed Germination of Huagaimu, a Critically Endangered Plant Endemic to Southeastern Yunnan, China. *HortTechnology*, 1, 427–431.
- [23] Yücel, E. and Yılmaz, G. (2009). Effects of different alkaline metal salts (NaCl, KNO₃), acid concentrations (H₂SO₄) and growth regulator (GA₃) on the germination of *Salvia cyanescens* Boiss. & Bal. seeds. *G.U. J. of Sci.* 22, 123–127.
- [24] Hilhorst, H.W.M. and Karssen, C.M. (1992). Seed dormancy and germination: the role of abscisic acid and gibberellins and the importance of hormone mutants, *Plant Growth Regul.* 11, 225–238.
- [25] Schwienbacher, E., Navarro-Cano, J.A., Neuner, G. and Erschbamer, B. (2011). Seed dormancy in alpine species. *Flora*, 206, 845–856.
- [26] Teimouri, M.S. and Mahallati, M.N. (2013). Seed germination and breaking of seed dormancy techniques for endemic *Hymenocrater platystegius*. *Intl. J. Agri. Crop Sci.* 6, 885–889.
- [27] Leo, J., Salomon, B., Jeppson, S. and Ahman, I. (2013). The effect of cold stratification on germination in 28 cultural relict plant species, p. 58. Msc. Thesis. Swedish University of Agricultural Sciences, Ultuna, Sweden.

Received: 01.03.2017

Accepted: 05.06.2017

CORRESPONDING AUTHOR

Muhip Hilooglu

Anadolu University, Science Faculty, Biology Department, Yunus Emre Campus, 26470, Eskişehir, Turkey

e-mail: mhilooglu@anadolu.edu.tr

ACCUMULATION OF HEAVY METALS IN SURFACE SOILS OF BENGBU HIGHER EDUCATION MEGA CENTER, CHINA

Li Ma^{1,2,3,4}, Herong Gui^{2,4,*}

¹School of Material and Chemical Engineering, Bengbu University, Bengbu 233030, China

²National Engineering Research Center of Coal Mine Water Hazard Controlling, Suzhou 234000, China

³School of Earth and Space Science, University of Science and Technology of China, Hefei 230026, China

⁴School of Resources and Civil Engineering, Suzhou University, Suzhou 234000, China

ABSTRACT

Bengbu higher education mega center was selected as target area to study the accumulation of heavy metals based on the field investigation, sampling, indoor test and statistical analysis. The results indicated that the mean concentrations of heavy metals (Pb, Zn, Cr, Cu, Cd and Ni) in surface soils were 23.04, 60.69, 37.79, 24.06, 1.15 and 18.67 mg/kg respectively. Cd and Cu exceeded the soil background values of Anhui province by 11.86 and 1.18 times, whereas the others were within their background values. Compared with Grade II criterion of national environmental quality standards for soils in China, Cd concentrations in all samples were obviously more than the corresponding limits, suggesting that the accumulation of Cd observed was serious in the study area. Assessment on ecological risk revealed that Cd showed the potential ecological risk at high and very high level with the proportion of 29.4% and 70.6%, respectively. The strongest ecological risk occurred in Longhu Chuntian business street, which is a complex area with booming commerce, high population density and heavy traffic. Results of multivariate analyses indicated that Cr and Ni mainly originated from geological weathering, Pb, Zn and Cu came from vehicle traffic pollution, Cd was dominantly related to agricultural and industrial activities.

KEYWORDS:

Heavy metals, ecological risk, source, higher education mega center

INTRODUCTION

Urban soil is one of the important factors for the sustainable development of urban ecosystem, which has functions of storage, filtration, transformation and degradation. However, with the improvement of urbanization in the world, the problem of heavy metal pollution in urban soil is becoming more and more serious [1]. Heavy metals, especially the toxic ones (e.g. Cd, Pb, Cu et al.), have special characteristics (e.g. wide range of sources, serious toxicities and

difficulties of remediation) [2-3], they are easily accumulated in surface soils, and pose a threat to human health through dust ingestion, skin contact and food chain, so the soil heavy metal pollution has been the research focus in recent years [4-5].

Bengbu is the central city of northern Anhui province, with favourable geographic conditions, convenient transportation and solid industry foundation. The rapid economic development provided great development space and market for industry, and a large number of factories successively located there in the last decades (e.g. chemical factories, electroplating factories, pesticide factories et al.) [6]. The increasing industrial activity is accompanied by strengthened environmental pollution, especially the heavy metal pollution in surface soils. Meanwhile, as the important science and education bases of Anhui province, Bengbu has an independent higher education mega center, many students and teachers live there. Green space is an important place for the daily study and leisure of teachers and students. Therefore, accumulation of heavy metals in the green space may pose a potential threat to the health of the surrounding people. To the best of our knowledge, industrial city has been concerned for a long time, and a large number of studies have been processed on the analysis of the whole city, including pollution distribution, ecological risk and sources identification, etc [7-10]. However, similar work related to the particular area, especially the higher education mega center has not been processed. Therefore, in this paper, a total of 34 soil samples have been collected from the higher education mega center in Bengbu, Northern Anhui Province, China, and the concentrations, potential ecological risks, as well as source identification of heavy metals (Pb, Zn, Cr, Cu, Cd and Ni) have been reported. It will provide additional information for soil usage and management, as well as for developing effective measures to control the negative effect of heavy metals in future.

MATERIALS AND METHODS

Study area. There are five universities located in Bengbu higher education mega center (Fig. 1): Anhui university of finance & economics (VII), Anhui

science & technology university (II), Bengbu medical college (VIII), Bengbu university (I) and Anhui vocational college of electronics & information technology (IV). Longhu Chuntian business street (V) is located in the center of the area, which brings great convenience for the college students and surrounding residents, but also brings a great deal of problems with other various negative factors. The rests (III, VI and IX) are some businesses and villages along the high-speed railway station. Generally speaking, Bengbu higher education mega center lies to the east of Longzi lake (national AAAA-level scenic resort, China), west of the high-speed railway station, south of the Donghai avenue and north of the Huangshan avenue. It is worth mentioning that the well-known old eastern industry zone is in the northern of the area, and therefore, anthropogenic pollution can not be ruled out (e.g. discharge of wastes).

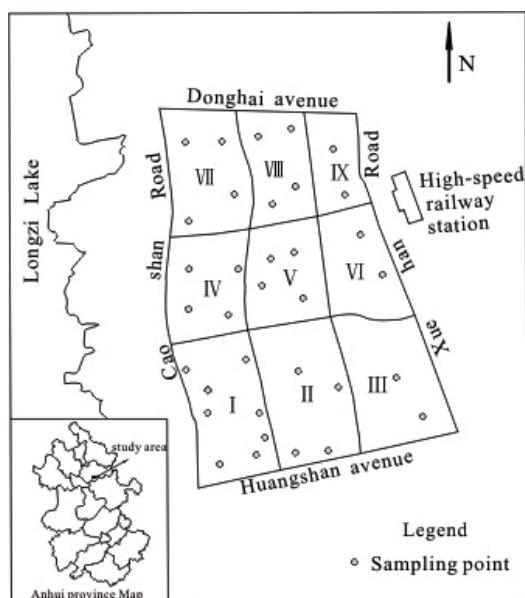


FIGURE 1

Location of the study area and sampling point

Soil sampling and chemical analysis. A total of 34 surface soil samples (0-15cm) were collected from Bengbu higher education mega center during November 2016 as showed in Figure 1. The exact location (longitudes and latitudes) of each sample point was taken by GPS. Surface soil samples were air-dried and homogenized using pestle and mortar. After the homogenization process, the surface soil samples were passed through 100-mesh sieve and stored in polyethylene bags for further analysis.

For sample digestion, About 0.10 g of milled soil from each sample was put in 100ml conical flask containing 6ml aqua regia solution (HNO_3 : HCl = 1:3, in volume) (HJ803-2016, China). The solution kept faint boiling for 2h on an electric heating thermostat. The above step of acid digestion were re-

peated until the mixture was evaporated to semi-dryness. All extracts were transferred to 50 mL volumetric flasks with slow filter paper. After filtration, a small amount of nitric acid solution was used to clean glass funnel, conical flask and filter residue at least three times to ensure that the residues were into the volumetric flasks. In the process, high purity acids were used in the analysis, glassware was cleaned and decontaminated in a 5% nitric acid solution for 24 h and then rinsed with distilled water.

Analytical processes were taken place in School of Material and Chemical Engineering, Bengbu University, China. Concentrations of six kinds of heavy metals (Pb, Zn, Cr, Cu, Cd and Ni) have been analyzed by Flame atomic absorption spectrometry (TAS, Beijing Purkinje General Instrument Co., China, TAS-990AFG). Quality control and assurance for elements in surface soils with the blank and duplicate samples, all the samples were analyzed in triplicate to guarantee the accuracy, and the analytical precision for all heavy metals was 10% relative standard deviation (RSD) or better.

Potential ecological risk index. The potential ecological risk index was used to evaluate the potential ecological risk of heavy metals in surface soils [11]. This method considers three factors: toxicity level, the sensitivity to heavy metal of research area and the difference of regional background value. It is a widely used method with the following formula:

$$C_f = C_i / C_n \quad E_r = T_r \cdot C_f \quad RI = \sum E_r \quad (1)$$

Where C_f is the pollution index of heavy metal, C_i is the content of heavy metal, C_n is the reference value of heavy metal, E_r is the potential ecological risk coefficient for a certain metal, T_r is the toxicity coefficient of a single pollutant. Based on previous research, the toxicity coefficient is defined as $\text{Pb}=5$, $\text{Zn}=1$, $\text{Cr}=2$, $\text{Cu}=5$, $\text{Cd}=30$, $\text{Ni}=5$ [12]. RI is the comprehensive potential ecological risk index. The criteria for ecological potential risk of heavy metals were presented in Table 1 [13].

TABLE 1
Criteria for ecological potential risk of heavy metals

Ranges of E_r	Grades	Ranges of RI	Grades
<40	Low	<110	Low
$40 \leq E_r < 80$	Moderate	$110 \leq RI < 220$	Moderate
$80 \leq E_r < 160$	Considerable	$220 \leq RI < 440$	High
$160 \leq E_r < 320$	High	≥ 440	Very high
≥ 320	Very high		

Statistical analysis. Descriptive statistics used in data analysis included minimum value, maximum value, median value, mean value, and coefficient of variation (CV). Multivariate statistical

TABLE 2
Descriptive statistics of metal concentrations (mg/kg)

	Pb	Zn	Cr	Cu	Cd	Ni
Minimum	16.71	36.20	24.11	16.49	0.78	11.40
Maximum	28.74	85.60	53.59	29.15	1.64	24.0
Median	23.06	59.01	38.23	24.15	1.14	18.78
Mean	23.04	60.69	37.79	24.06	1.15	18.67
Coefficient of Variation(%)	12.1	16.4	18.0	12.0	19.1	15.1
Background value of Anhui Province	26.6	62	66.5	20.4	0.097	29.8
Grade II criterion of soil quality standards	300	250	200	100	0.3	50
Percentage of exceeding background value (%)	17.65	41.18	0	88.24	100	0
Percentage of exceeding Grade II criterion (%)	0	0	0	0	100	0

TABLE 3
 E_r value of heavy metals in Bengbu higher education mega center

	Pb	Zn	Cr	Cu	Cd	Ni
E_r	3.14~5.40	0.58~1.38	0.73~1.61	4.04~7.04	240.46~507.99	1.91~4.03
Mean	4.33	0.98	1.14	5.90	354.49	3.13
Grades	Low	Low	Low	Low	High (29.4%) Very high (70.6%)	Low

TABLE 4
 RI value of Bengbu higher education mega center

Minimum	Maximum	Mean	Potential ecological risk			
			Low	Moderate	High	Very high
256.33	524.19	369.96	0	0	85.29%	14.71%

analyses, including correlation analysis (CA) and principal component analysis (PCA) were used for distinguishing the sources of heavy metal in surface soils. CA was performed to assess if there was significant relationship between pairs of variable, PCA was used to differentiate the association between Pb, Zn, Cr, Cu, Cd and Ni. Both the CA and PCA analysis were conducted by SPSS 19.0. ArcGIS 10.1 was applied for spatial distribution.

RESULTS AND DISCUSSION

Descriptive statistics. All of the analytical results are presented in Table 2. As can be seen from the Table 2, the concentrations of heavy metals (Pb, Zn, Cr, Cu, Cd and Ni) were in the ranges of 16.71-28.74, 36.20-85.60, 24.11-53.59, 16.49-29.15, 0.78-1.64, 11.40-24.0 mg/kg, and with the mean concentrations of 23.04, 60.69, 37.79, 24.06, 1.15 and 18.67mg/kg, respectively. Compared to the Grade II criterion of national environmental quality for soils in China [14], the contents of Pb, Zn, Cr, Cu and Ni were far lower than the corresponding limits. Whereas, Cd content greatly exceed the standard value, demonstrating Cd was the significant soil pollution in study area. Additionally, among the six elements, the contents of Cu, Zn and Pb in some samples were higher than their background value [15], with the proportion of 88.24%, 41.18% and 17.65%, respectively. Ni and Cr showed low contents because all the concentrations were within the background

values. The CV of the heavy metals were in the range of 0.120~0.191, which indicated moderate variation level in Bengbu higher education mega center.

Potential ecological risk assessment. The assessment calculates the potential ecological coefficient (E_r) and comprehensive potential ecological risk indice (RI) according to the formula (1). As can be seen from the Table 3, the mean E_r value of heavy metals followed the decreasing order of Cd > Cu > Pb > Ni > Cr > Zn. Among the six elements, Cd exhibited potential ecological risk at the high and very high level (29.4% and 70.6%, respectively), whereas the others had low ecological risk.

RI showed the comprehensive pollution level of the study area (Table 4). RI values of Bengbu higher education mega center ranged from 256.33 to 524.19, with the mean concentration of 369.96, and all the sample points presented potential ecological risk at the high and very high level (85.29% and 14.71%, respectively), dominated by the ecological risk of Cd. Therefore, Cd must be put in high attention and be of the prior contaminants considered to control.

In order to understand the pollution level of the soil heavy metals in Bengbu higher education mega center, Spatial distribution of E_r -Cd and RI in surface soils can be further obtained (Figure 2, Figure 3), and their high values were both mainly distributed in Anhui science & technology university, Longhu Chuntian business street, and Bengbu medical college, particularly in Longhu Chuntian

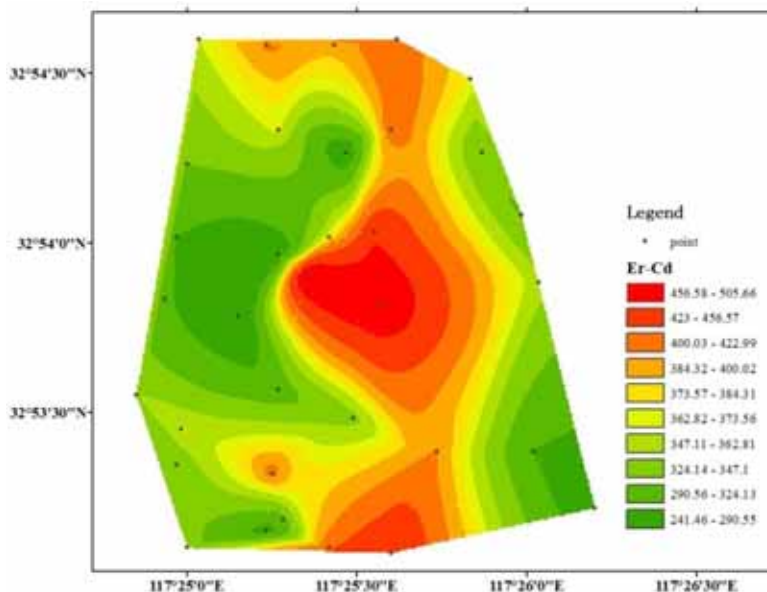


FIGURE 2
Spatial distribution of *Er-Cd*

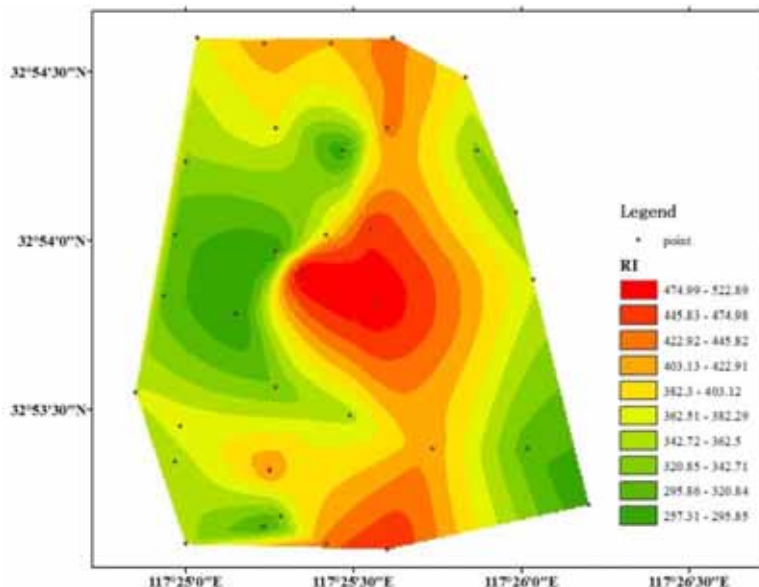


FIGURE 3
Spatial distribution of *RI*

business street, which is usually characterized by prosperous business, high levels of population, and heavy traffic. In addition, Anhui science & technology university and Bengbu medical college also need for attention.

Correlation matrix and principal component analysis. The Pearson correlation coefficients between the six heavy metals are listed in Table 5. Inter-element relationships can provide important information on element sources and pathways. Cu had significant correlation with Ni, Zn, Pb and Cr ($r=0.817, 0.639, 0.593$ and 0.533 , respectively) at 0.01 significant level. Ni also presented relatively strong correlation with Cr ($r=0.607$), Zn ($r=0.443$) at 0.01 significant level and Pb ($r=0.395$) at 0.05 significant

level, which could indicate the similar geochemical properties and behaviors in these heavy metals. Whereas, the heavy metal (Cd) showed no significant correlation with all the other metals, and in other words, a low correlations ($r=0.039, r=0.193, r=0.281$) and negative correlations ($r=-0.106, r=-0.152$) were evident for Cd-Cu, Cd-Cr, Cd-Ni, Cd-Pb and Cd-Zn pairs, suggesting that the sources of Cd may be different from the other five heavy metals. However, this method can not accurately identify the sources of heavy metals, but only provides a qualitative estimate.

To better understand the sources of the six heavy metals, PCA was adopted to transform an original set of variable into a minimum number of factors, which are able to account for the most of

TABLE 5
Correlation matrix between heavy metal concentrations

	Pb	Cu	Cd	Cr	Ni	Zn
Pb	1					
Cu	0.593**	1				
Cd	-0.106	0.039	1			
Cr	0.324	0.533**	0.193	1		
Ni	0.395*	0.817**	0.281	0.607**	1	
Zn	0.298	0.639**	-0.152	0.329	0.443**	1

* Correlation is significant at the 0.01 level

**Correlation is significant at the 0.05 level

TABLE 6
Component matrix of heavy metals from Bengbu higher education mega center

Elements	Principal components		Rotated principal components	
	PC1	PC2	PC1	PC2
Pb	0.645	-0.309	0.699	-0.150
Cu	0.935	-0.096	0.932	0.124
Cd	0.122	0.919	-0.096	0.922
Cr	0.723	0.275	0.639	0.436
Ni	0.873	0.264	0.788	0.459
Zn	0.680	-0.371	0.748	-0.202
Eigenvalue	3.053	1.231	2.954	1.330
Variance contribution rate (%)	50.833	20.520	49.240	22.164
Cumulative contribution rate (%)	50.833	71.404	49.240	71.404

Rotation method: varimax with kaiser normalization

the information of the original data [16]. In this study, PCA was conducted using SPSS 19.0 on the original data of the six heavy metals. As revealed in Table 6, two principle components were extracted (eigenvalues over 1.0). The first principal component (PC1) accounted for 50.833% of the total variance and showed the positive and high loading for Pb, Cu, Cr, Ni and Zn. The second principal component (PC2) was responsible for 20.520% of the total variance and was highly predominated by Cd. Two principle components explained about 71.404% of the total variance obtained.

The PC1 was considered to be the sources related to transportation and geological weathering. That's because the concentrations of Pb, Cu and Zn exceeded their background values, with the proportion of 17.65%, 88.24% and 41.18%, respectively. Whereas, Cr and Ni contents in all samples were within the background value (Table 2). As mentioned previously, Bengbu high speed rail station (North-South major transportation hub in China) and Longhu Chuntian business street are located there, with crowded people and heavy traffic in the vicinity. Additionally, construction of Anhui science & technology university is going on in Bengbu higher education mega center. Many muck trucks come and go in all directions, at the same time, it might have contributed to an increase in pollution levels. Previous research results also indicated that Pb was mainly contributed by fuel combustion and automobile exhaust [17-19], Zn originated from automobile tire wear [20-21], Cr and Ni were usually induced by natural activities such as geological weathering [22-23]. Therefore, PC1 can be explained to be

the sources related to vehicle traffic pollution and geological weathering. Pb, Cu and Zn has not brought significant harm to the environment, but the emission accumulation is worth regarding in the study area.

The PC2 includes Cd only. This component is defined as anthropogenic factor and related to agriculture activities, chiefly fertilization [24-25]. Cd contents of all the soil samples are above the Grade II criterion of the national environmental quality for soils in China. This provides evidence of Cd anthropogenic origin. Phosphate fertilizer was the main source of Cd in soils and the enrichment of Cd content was closely related to the time length of applying phosphate fertilizer [26]. According to the investigation, the study area were urban villages prior to the construction of Bengbu higher education mega center, and the soils were used for agriculture, the long history of farming along with the use of fertilizers resulted in extensive Cd accumulation in surface soils. Moreover, Bengbu higher education mega center is located in the south of old eastern industrial zone, atmospheric deposition of pollutant and sewage sludge also have contributions to the increased Cd content. Therefore, PC2 might originate from agricultural and industrial activities.

CONCLUSIONS

In this study, a total of 34 surface soil samples were collected from Bengbu higher education mega center and analyzed for the presence of heavy metals

(Pb, Zn, Cr, Cu, Cd and Ni). The results of the investigation provided integrated information about soil environment of this region. Potential ecological risk assessment indicated that Cd posed the highest ecological risk among the six heavy metals, and the higher ecological risk were observed in Anhui science & technology university, Longhu Chuntian business street, and Bengbu medical college, particularly in Longhu Chuntian business street influenced by human activities. The PCA together with CA indicated that Pb, Cu, and Zn in surface soils originated primarily from vehicle traffic pollution, Cd may come from agricultural and industrial activities. Whereas, Ni and Cr were mostly of nature origin.

ACKNOWLEDGEMENTS

This research project was supported by the National Natural Science Foundation of China (No. 41373095) and the Natural Science Foundation of Anhui Higher Education Institutions of China (No. KJ2016A459).

REFERENCES

- [1] Li, X., Poon, C.S., Liu, P.S. (2001) Heavy metal contamination of urban soils and street dusts in Hong Kong. *Applied Geochemistry*, 16(11-12), 1361-1368.
- [2] Nemati, K., Bakar, N.K.A., Abas, M.R., Sobhanzadeh, E. (2011) Speciation of heavy metals by modified BCR sequential extraction procedure in different depths of sediments from Sungai Buloh, Selangor, Malaysia. *Journal of Hazardous Materials*, 192(1), 402-410.
- [3] Sun, L., Liu X., Min N. (2016) Identifying the potential source of trace metals in water from subsidence area based on positive matrix factorization, *Water Practice & Technology*, 11(2), 279-287.
- [4] Mazur, Z, Radziemska, M, Maczuga, O, Makuch, A. (2013) Heavy metal concentrations in soil and moss (*Pleurozium schreberi*) near railroad lines in Olsztyn (Poland). *Fresen. Environ. Bull.*, 22(4), 955-961.
- [5] Diatta, J.B, Komisarek, J, Wiatrowska, K. (2012) Evaluation of heavy metals competitive sorption and potential mobility on the basis of Cu/Cd and Zn/Pb binary systems. *Fresen. Environ. Bull.*, 21(5), 1105-1109.
- [6] Yang, J., Zhao, Y. L., Zhen, Q., Zhang, J. (2014) Heavy metal pollution and health risk assessment of soil and vegetable in a sewage-irrigated area. *Journal of Ecology & Rural Environment*, 30(2), 234-238.
- [7] Diawara, M.M., Litt, J.S., Unis, D., Alfonso, N., Crock, J.G., Smith, D.B., Carsella, J. (2006) Arsenic, cadmium, lead, and mercury in surface soils, Pueblo, Colorado: implications for population health risk. *Environmental Geochemistry and Health*, 28(4), 297-315.
- [8] Zhang, X.Y., Lin, F.F., Wong, M.T., Feng, X.L., Wang, K. (2009) Identification of soil heavy metal sources from anthropogenic activities and pollution assessment of Fuyang County, China. *Environmental Monitoring & Assessment*, 154(1-4), 439-449.
- [9] Fang, T., Liu, G., Zhou, C., Yuan, Z, Lam, P.K. (2014) Distribution and assessment of Pb in the supergene environment of the Huainan Coal Mining Area, Anhui, China. *Environmental Monitoring & Assessment*, 186(8), 4753-4765.
- [10] Ma, L, Yang, Z, Li, L., Wang, L. (2016) Source identification and risk assessment of heavy metal contaminations in urban soils of Changsha, a mine-impacted city in Southern China. *Environmental Science and Pollution Research*, 23(17), 1-9.
- [11] Hakanson, L. (1980) An ecological risk index for aquatic pollution control: a sedimentological approach. *Water Research*, 14(8), 975-1001.
- [12] Xu, Z.Q., Ni, S.J., Xian-Guo, T., Zhang, C.J. (2008) Calculation of heavy metals' toxicity coefficient in the evaluation of potential ecological risk index. *Environmental Science & Technology*, 31(2), 112-115.
- [13] Liu, J.L., Li, Y.L., Bao, Z., Cao, J.L., Cao, Z.G., Domagalski, J. (2009) Ecological risk of heavy metals in sediments of Luan River source water. *Ecotoxicology*, 18(6), 748-758.
- [14] Chinese National Environmental Protection Agency (CEPA) (1995) Environmental quality standard for soils (GB15618-1995) (in Chinese).
- [15] Li, J., Zheng, C., Guo, X. (1989) Manual data of environmental background value. China Environment Science Press, Beijing (in Chinese).
- [16] Yuan, Z., Liu, G., Liu, R., Liu, H., Da, C. (2016) Characterization of the origin of polycyclic aromatic hydrocarbons in sediments from the Yellow River Estuary, China. *Analytical Letters*, 49(8), 1289-1303.
- [17] Bourliva, A., Christophoridis, C., Papadopoulou, L., Giouri, K., Papadopoulos, A, Mitsika, E., Fytianos, K. (2016) Characterization, heavy metal content and health risk assessment of urban road dusts from the historic center of the city of Thessaloniki, Greece. *Environmental Geochemistry & Health*, 1-24.
- [18] Dai, B., Lv, J.S., Zhan, J.C., Zhang, Z.L, Liu, Y., Zhou, R.J. (2015) Assessment of source, spatial distribution and ecological risk of heavy metals in soils in a typical industry-based city of Shandong province, Eastern China. *Environmental Science*, 36(2), 507-515 (in Chinese).
- [19] Keshavarzi, B., Tazarvi, Z, Rajabzadeh, M.A., Najmeddin, A. (2015) Chemical speciation, human health risk assessment and pollution level of selected heavy metals in urban street dust of

- shiaz, Iran. *Atmospheric Environment*, 119, 1-10.
- [20] Friedlander, S.K. (1973) Chemical element balances and identification of air pollution source. *Environmental Science & Technology*, 7(3), 235-240.
- [21] Karim, Z., Qureshi, B.A., Mumtaz, M., Qureshi, S. (2014). Heavy metal content in urban soils as an indicator of anthropogenic and natural influences on landscape of Karachi-A multivariate spatio-temporal analysis. *Ecological Indicators*, 42, 20-31.
- [22] Wang, Y., Yin, C., Zhang, J., Liu X., Kang W, Liu, L, Xiao, W. (2016) Risk assessment of heavy metals in farmland soils near mining areas in Daye city, Hubei province, China. *Fresen. Environ. Bull.*, 25(2), 490-499.
- [23] Xiong, S, Gui H., Lin M., Peng W. (2017) Contents and pollution characteristics of heavy metals in soil from coal mining area: a case study in Linhuan mining district, northern Anhui province. *Fresen. Environ. Bull.*, 26(3), 1989-1996.
- [24] Mendes, A. M.S, Duda, G.P, Silva, M.O. (2006) Bioavailability of cadmium and lead in a soil amended with phosphorus fertilizers. *Scientia Agricola*, 63(4), 328-332.
- [25] Naveedullah, Hashmi, M.Z., Yu, C., Shen, H., Duan, D., Shen, C., Lou, L., Chen, Y. (2013) Risk assessment of heavy metals pollution in agricultural soils of Siling reservoir watershed in Zhejiang Province, China. *BioMed Research International*, 3, 1-10.
- [26] Kelepertzis, E. (2014) Accumulation of heavy metals in agricultural soils of Mediterranean: insights from Argolida basin, Peloponnese, Greece. *Geoderma*, 221-222(27), 82-90.

Received: 08.03.2017
Accepted: 07.06.2017

CORRESPONDING AUTHOR

Herong Gui

School of Resources and Civil Engineering,
Suzhou University
Suzhou 234000 P.R.CHINA

e-mail: hrgui@163.com

TOXICOKINETIC OF CYPERMETHRIN IN BROILER CHICKENS

Gokhan Eraslan^{1,*}, Muhammet Yasin Tekeli¹, Mursel Karabacak²

¹Erciyes University, Faculty of Veterinary Medicine, Department of Pharmacology and Toxicology, Kayseri, Turkey

²Erciyes University, Safiye Çıkrıkçıoğlu Vocational Collage, Animal Health Department, Kayseri, Turkey

ABSTRACT

The toxicokinetics of single-dose intravenous and intracrop administration of cypermethrin has been described in broiler chickens. Twenty male broiler chickens were distributed in two groups of ten animals each. The animals in the groups mentioned were given cypermethrin in both routes at a single dose of 7.5 mg/kg b.w. Blood samples were collected by the wing vein of chickens at 0.083, 0.25, 0.50, 0.75, 1, 2, 4, 6, 8, 12, 18, 24 and 36 hours after administration of cypermethrin. Determination of serum cypermethrin levels was performed by the gas chromatography-electron capture detection. When the serum concentration-time graph of cypermethrin was evaluated, it was found that this pesticide showed a more convenient distribution tendency in the two-compartment open model. The values of $t_{1/2\beta}$, MRT and $AUC_{0\rightarrow\infty}$ were 7.35 ± 0.91 hours, 8.64 ± 1.59 hours and 8741.98 ± 1996.66 ng.h/ml, respectively, after intravenous administration of cypermethrin. On the other hand, C_{max} , t_{max} , $t_{1/2a}$, $t_{1/2\beta}$, MRT and $AUC_{0\rightarrow\infty}$ values calculated for intracrop applied cypermethrin were 422.75 ± 99.59 ng/ml, 0.80 ± 0.15 hours, 0.24 ± 0.05 hours, 10.97 ± 2.11 hours, 15.39 ± 2.56 hours and 4266.51 ± 967.65 ng.h/mL, respectively. The systemic bioavailability of cypermethrin administered intracrop was 48.80%. From the results obtained, bioavailability of cypermethrin and the MRT at the same time in the body are moderate. These results were considered to be an important indicator in the evaluation and treatment of cypermethrin poisoning in broiler chickens.

KEYWORDS:

Cypermethrin, toxicokinetic, broiler chickens, single-dose, kinetic disposition

INTRODUCTION

Cypermethrin is a synthetic pyrethroid insecticide and is classified as type II pyrethroid because of the cleavage of an alpha-cyano group [1]. Due to its lipophilic nature, it primarily tends to accumulate in the nervous system and fatty tissue [2-4]. The mechanism of action of this compound involves binding

to voltage-gated sodium channel alpha subunit located in nerve cells [5, 6]. Today, this pesticide is not only used for pest control, but also for lice infections [7-10]. Cypermethrin has been found to be more effective than other insecticides in control of the malaria and can be used in open areas [11, 12]. This compound is known to be effective against a wide range of agricultural pests [13, 14]. Furthermore, it can be used in residential buildings as much as commercial buildings [13]. Exposure to cypermethrin may occur via food/feed or water contaminated with pesticide residues or due to occupational exposure and household uses. Cypermethrin residues have also been found in milk of cows wearing cypermethrin impregnated ear tags against the horn fly [12-15].

As mentioned above, most pyrethroid insecticides are widely used for pest challenge in agriculture [11-14], veterinary medicine [16-18] and for disinfection of enclosed spaces [5, 19]. There are public health uses for the control of diseases where the pest acts as an intermediate host or vector. Cypermethrin is also applied to disinfect poultry pens and to control poultry mites [15-17, 19-21]. There are also previous studies on the toxic effects of cypermethrin in living animals [22-27]. Exposure to cypermethrin can be achieved either through direct intake of contaminants or disinfecting chicken pens, or by using acaricides in animals. While there is limited information on single-dose toxicokinetics of synthetic pyrethroids in poultry [28, 29], a detailed study of the toxicokinetics profile of cypermethrin in poultry is not available. For this reason, this study is considered to be novel.

MATERIAL AND METHODS

Animals and Experimental Design: In order to carry out this toxicokinetic study, twenty-30-day-old male Ross broilers weighing 1.5-2 kg were used as trial material. One-day-old chicks were fed and housed under the same conditions for 30 days. Animals were randomly allocated to two groups of ten animals in each. At the end of thirty days of age, the chickens in group 1 were given cypermethrin (Dr Ehrenstorfer GmbH) at a single dose of 7.5 mg/kg b.w.

via wing vein, intravenously. To group 2 was administered with a single same dose of cypermethrin (7.5 mg/kg b.w.) using the catheter directly into the crop. Cypermethrin was prepared in dimethyl sulfoxide/water (8:2, v/v). The administration dose was calculated taking into account the body weight of the animals. After the administration of cypermethrin, blood samples were taken from the wing vein of the animals at 0.083, 0.25, 0.50, 0.75, 1, 2, 4, 6, 8, 12, 18, 24 and 36 hours without anticoagulant tubes. All blood samples pooled in the tubes were centrifuged at $6000 \times g$ for 10 minutes at $+4^\circ\text{C}$. Harvested serum samples were frozen at -80°C and kept in deep freeze until analysis. Cypermethrin concentrations that can be determined in blood samples during the experiment for determination of a suitable dosage in chickens have been taken into account, survival of animals and previous studies [28-30]. Research protocol received the approval of Erciyes University experimental animals Ethical Board's.

Cypermethrin Analysis: 2.5 ml of a mixture of hexane and acetone (8: 2, v/v) into 0.5 ml of serum was added. The mixture was firstly shaken at a rate of about 1000 cycles/per min for 3 minutes and then centrifuged at $6000 \times g$ for 10 minutes at $+4^\circ\text{C}$. Subsequently, 1.5 ml of supernatant was transferred to another test tube and the extract was evaporated to dryness. One ml of n-hexane was added to the test tubes containing the cypermethrin residues. They were vortexed and the organic solution was then put into the fresh vials. Extraction of serum samples was performed with some modifications based on Yavuz et al.'s method [31]. In gas chromatography (GC), the serum cypermethrin concentration was analyzed according to the methods of Wang et al. [32] Mekebri et al. [33] and Hunter et al. [34] by making some modifications. All analyses were done using a GC instrument. For analysis, a μECD detector and capillary column (HP-5MS, 30 m x 0.25 mm x 0.25 μm film thickness, Agilent J & W) were used. The detector temperature was set at 325°C with makeup gas (N_2) flowing at 60 ml/min. Injection volume was 2 μl . The injection port temperature was worked at 260°C . The splitless injection mode was used. The carrier gas is helium and the substitute gas nitrogen. The helium gas flowing from the capillary column at 2.8 ml/min was used. The initial temperature is 70°C and it was held at 70°C for 2 minutes and then this was increased to by $25^\circ\text{C}/\text{min}$ to 150°C ; then a temperature of 200°C was reached with an increase of $3^\circ\text{C}/\text{min}$ and finally the temperature was increased by $8^\circ\text{C}/\text{min}$ to 280°C . Flumethrin (Dr Ehrenstorfer GmbH) was the internal standard for analytical measurements in gas chromatography.

While generating the calibration curve, certain amounts of cypermethrin (5-8000 ng/ml serum) were added to neat serum samples and then samples were extracted and analyzed. This obtained data was used for the calibration graph. In order to determine the

analytical recovery of the method, neat serum samples were also used with the addition of cypermethrin to certain levels to prepare the standard curve (5-8000 ng/ml serum) and these analyses were repeated three times. An estimate of the detection limit and the quantification limit for this chromatographic method was made using a method based on the ratio of signal to noise (S/N) [35]. The signal-to-noise ratio for the detection limit is calculated as 3:1, while the same ratio for the quantification limit is used as 10:1. To determine the sensitivity of a method following the extraction procedure, neat serum samples were supplemented with cypermethrin at three concentrations by adding 10 ng/ml, 100 ng/ml and 1000 ng/ml. Relative standard deviations were calculated for the inter-day and intra-day peak areas obtained for the indicated concentrations.

Toxicokinetic Analysis: Serum cypermethrin levels versus time values, 1, 2, and multi-compartmental models were evaluated visually and using PKCALC software. The most suitable model was chosen based on Akaike Information Criteria [36]. Maximum concentration in serum after intracrop administration (C_{max}) and time needed to reach C_{max} (t_{max}) values were calculated from the serum cypermethrin concentration versus time graph for each animal. Other kinetic variables [A_1 , A_2 , A_3 mathematical coefficients; k_a , first order rate constant related to absorption; α , first order rate constant related to distribution phases; β , first order rate constant related to elimination phase; $t_{1/2ab}$, absorption half-life; $t_{1/2\alpha}$, distribution half-life; $t_{1/2\beta}$, elimination half-life; MRT, mean residence time; V_{darea} , area volume of distribution; V_{dss} , steady-state volume of distribution; V_1 , volume of distribution of central compartment; V_2 , volume of distribution of peripheral compartment; Cl_T , total body clearance; k_{12} , first order rate constant of drug transfer from central to the peripheral compartment; k_{21} , first order rate constant of drug transfer from peripheral to the central compartment; k_{10} elimination rate constant; C_s^0 , serum drug concentration at time zero after bolus intravenous application] were calculated using PKCALC and GW-BASIC pharmacokinetic software according to the equations presented by Shumaker [37] and Wagner [38]. The $\text{AUC}_{0 \rightarrow t} / \text{AUC}_{0 \rightarrow \infty}$ parameters (area under the concentration-time curve from time zero to time t /area under the concentration-time curve from time zero to infinity) were used to determine systemic bioavailability (F).

STATISTICAL ANALYSIS

Analysis of all data was performed in SPSS for Windows (Version 13.0) statistical software. Results calculated were expressed as arithmetic means and standard deviations. Statistical differences between the groups were assessed by Student's t-test. $P < 0.05$

was accepted statistically significant differences.

RESULTS

Calibration graph showed linearity (r^2 : 0.9999) at 5 ng/ml sera from 8000 ng/ml sera concentrations. The average recovery rate with the addition of cypermethrin to neat serum samples at selected concentrations to prepare the standard curve was 94.40%. For the case of cypermethrin, the limit of detection was determined to be 3 ng/mL while the limit of quantification was determined to be 5 ng/mL. At different concentrations, the relative standard deviation for the inter-day applications was calculated as 4.80%. The average value for the intra-day applications was found to be 6.20%.

Measured serum cypermethrin levels were found to be 5937.15±2216.14 ng/ml, 1994.55±780.48 ng/ml, 968.69±259.33 ng/ml, 347.32±170.27 ng/ml, 188.19±74.73 ng/ml, 133.10±45.70 ng/ml, 93.76±16.30 ng/ml and 36.41±10.92 ng/ml, which corresponded to 0.083, 0.5, 1, 4, 8, 12, 18 and 36 hours after the intravenous administration. The levels of cypermethrin corresponding to 0.083, 0.5, 1, 4, 8, 12, 18 and 24 hours were 135.29±44.12 ng/ml, 295.72±60.58 ng/ml, 344.69±75.13 ng/ml, 217.38±41.84 ng/ml, 148.98±30.86 ng/ml, 119.05±24.36 ng/ml 93.66±21.58 ng/ml and 52.80±16.17 ng/ml after the intracrop administration. Significant changes are observed between intravenous and oral administration except for 6, 8, 12, 18, and 24 hours of the blood sampling period in serum cypermethrin levels (Table 1, Figure 1).

TABLE 1
Serum levels of cypermethrin in the blood collection periods after intravenous and intracrop administration in broiler chickens

Blood Sampling Periods (h)	Intravenous (ng/ml)	Intracrop (ng/ml)
0.083	5937.15±2216.14	135.29±44.12*
0.25	2532.32±956.15	214.04±53.61*
0.50	1994.55±780.48	295.72±60.58*
0.75	1427.34±391.19	396.92±119.96*
1	968.69±259.33	344.69±75.13*
2	472.45±201.31	262.16±50.78*
4	347.32±170.27	217.38±41.84*
6	244.58±96.91	182.15±36.69
8	188.19±74.73	148.98±30.86
12	133.10±45.70	119.05±24.36
18	93.76±16.30	93.66±21.58
24	64.72±14.66	52.80±16.17
36	36.41±10.92	-

*, $p < 0.05$

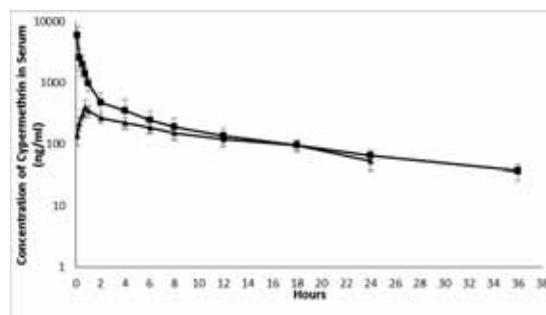


FIGURE 1
Semilogarithmic serum cypermethrin concentration versus time curve after intravenous and intracrop administration of cypermethrin in broiler chickens

TABLE 2
Some toxicokinetic parameters of cypermethrin after intravenous and intracrop administration in broiler chickens

Parameters ^a	Intravenous	Intracrop
A ₁ (ng/ml)	8383.40±4384.86	263.80±152.50*
A ₂ (ng/ml)	672.58±178.58	264.13±54.01*
A ₃ (ng/ml)	-	-490.53±191.62
k _a (h ⁻¹)	-	3.01±0.72
α (h ⁻¹)	5.47±2.73	0.99±0.60*
β (h ⁻¹)	0.09±0.01	0.06±0.01*
t _{1/2a} (h)	-	0.24±0.05
t _{1/2α} (h)	0.18±0.13	0.93±0.50*
t _{1/2β} (h)	7.35±0.91	10.97±2.11*
MRT (h)	8.64±1.59	15.39±2.66*
C _{max} (ng/ml)	-	422.75±99.59
t _{max} (h)	-	0.80±0.15
V _{darea} (ml/kg)	9694.64±3219.32	13582.21±2623.31*
V _{dss} (ml/kg)	7926.22±2940.89	64453.67±39065.13*
V ₁ (ml/kg)	1052.99±588.78	8694.05±1602.74*
V ₂ (ml/kg)	6873.23±2733.35	4258.10±2395.54*
Cl _T (ml/h/kg)	902.29±219.29	937.75±303.49
k ₁₂ (h ⁻¹)	4.01±2.27	0.32±0.26*
k ₂₁ (h ⁻¹)	0.49±0.16	0.62±0.36
k ₁₀ (h ⁻¹)	1.06±0.50	0.10±0.01*
C _s ⁰ (ng/ml)	9055.99±4403.78	-
AUC _{0→t} (ng.h/L)	8350.30±1971.18	3395.01±654.24*
AUC _{0→∞} (ng.h/L)	8741.98±1996.56	4266.51±967.65*
F (%)	-	48.80

^a. A₁, A₂, A₃ mathematical coefficients; k_a, first order rate constant related to absorption; α, first order rate constant related to distribution phases; β, first order rate constant related to elimination phase; t_{1/2ab}, absorption half-life; t_{1/2α}, distribution half-life; t_{1/2β}, elimination half-life; MRT, mean residence time; C_{max}, maximum concentration in serum after intracrop administration; t_{max}, time needed to reach C_{max}; V_{darea}, area volume of distribution; V_{dss}, steady-state volume of distribution; V₁, volume of distribution of central compartment; V₂, volume of distribution of peripheral compartment; Cl_T, total body clearance; k₁₂, first order rate constant of drug transfer from central to the peripheral compartment; k₂₁, first order rate constant of drug transfer from peripheral to the central compartment; k₁₀ elimination rate constant; C_s⁰, serum drug concentration at time zero after bolus intravenous application; AUC_{0→t}, area under the concentration-time curve from time zero to time t; AUC_{0→∞}, area under the concentration-time curve from time zero to infinity; F, systemic bioavailability. *, $p < 0.05$

An assessment of possible distribution models for the calculation of toxicokinetic variables revealed that cypermethrin exhibits a more consistent distribution pattern with the two-compartment open model. It has been shown that there are significant differences between the groups exposed to intravenous and intracrop cypermethrin application for some parameters in the calculations made according to the analyzed distribution model. Significant changes in the values of A_1 , A_2 , α , β , $t_{1/2\alpha}$, $t_{1/2\beta}$, MRT, $V_{d_{area}}$, $V_{d_{ss}}$, V_1 , V_2 , k_{12} , k_{10} , $AUC_{0 \rightarrow t}$ and $AUC_{0 \rightarrow \infty}$ were observed among the groups within toxicokinetic parameters. Compared with the intravenous administration group, it was found that there was a significant decrease in the values of A_1 , A_2 , α , β , V_2 , k_{12} , k_{10} , $AUC_{0 \rightarrow t}$ and $AUC_{0 \rightarrow \infty}$ in the intracrop administration group. On the other hand, $t_{1/2\alpha}$, $t_{1/2\beta}$, MRT, $V_{d_{area}}$, $V_{d_{ss}}$ and V_1 values were significantly increased in the intracrop group compared to the intravenous group. C_s^0 values were determined to be 9055.99 ± 4403.78 ng/ml for intravenous administration. The values of A_3 , k_a , $t_{1/2a}$, C_{max} , t_{max} and F values were -490.53 ± 191.62 ng/ml, 3.01 ± 0.72 h⁻¹, 0.24 ± 0.05 h⁻¹, 422.75 ± 99.59 ng/ml, 0.80 ± 0.15 h and 48.80% (Table 2).

All the animals that involved in the study lived until the end of the experiment. However, mild central nervous system findings (tremor, hypokinesia, hypersalivation) and fluffy feathers were seen within the first 4 hours after intravenous administration. The same symptoms were recorded 1-2 hours after intracrop application, but these symptoms were more pronounced in the group given intravenously with cypermethrin. These symptoms quickly and completely disappeared in the time periods that continued in both experimental groups.

DISCUSSION

Assessment revealed that the distribution of cypermethrin in broiler chickens was more consistent distribution tendency with the two-compartment open model. For this reason, compartmental calculations have been done according to this distribution model. Pharmacokinetic/toxicokinetic studies previously performed with pyrethroids in some laboratory animals [39, 40] and broilers [28, 29] showed that these pyrethroids tend to have a more favorable distribution pattern in the two-compartment open model. The shortness of $t_{1/2\alpha}$ of cypermethrin was faster when administered intravenously. This was confirmed by α value. On the other hand, the $t_{1/2\alpha}$ of cypermethrin is due to the high solubility of cypermethrin in fatty tissue [2, 6, 15]. Differences in $t_{1/2\alpha}$ in the event of intravenous and intracrop administration of cypermethrin play an important role in the route of administration and the amount of blood flowing at the location of application [41-43]. The $t_{1/2\beta}$ and the MRT of cypermethrin in the intracrop

route when compared to the intravenous route are associated with the likely continuation of the absorption of cypermethrin from the gastrointestinal tract during the period of drug excretion. The same conclusion is determined for the Cl_T . Compared to the results obtained in previous studies on pyrethroids in broilers [28, 29], $t_{1/2\beta}$ and MRT values were long in this study. This is thought to be due to the chemical and physical differences of the compounds. In the group given intracrop cypermethrin, the distribution volume of central compartment was lower than that of the group subjected to intravenous administration, suggesting that cypermethrin is not highly distributed in the central compartment in the case of intracrop administration. The differences observed between the two groups in terms of $V_{d_{ss}}$ and $V_{d_{area}}$ values confirm this finding. Because V_2 value is higher than V_1 value in group 1, it suggests that when cypermethrin is administered, it tends to stay in the peripheral area for a longer time. In terms of intravenous administration, the same situation exists in previous studies with permethrin [28] and deltamethrin [29] at the V_1 value in the broilers. However, the $V_{d_{ss}}$ and $V_{d_{area}}$ values in this study are quite high when compared to previous studies [28, 29]. The differences observed within and between groups in distribution volumes also support changes in the first-order rate constants associated with transfer of unbound cypermethrin between the central and peripheral compartments (on the basis of the k_{12} and k_{21} value).

From variables demonstrating the absorption and absorption rate of cypermethrin are the values of k_a and $t_{1/2a}$. AUC is a parameter affected both by the absorption and by the elimination processes. Hence the AUC is also a parameter indirectly associated with absorption. The high value of k_a and the shortness of $t_{1/2a}$ on the other side suggest that cypermethrin is quickly and extensively absorbed from the digestive system after intracrop administration. Another indicator of rapid absorption of cypermethrin is t_{max} , which is also expressed as the time required for cypermethrin reaching C_{max} . The calculated $AUC_{0 \rightarrow t} / AUC_{0 \rightarrow \infty}$ value indicates that the cypermethrin is absorbed moderately when given intracrop. Moderate bioavailability of cypermethrin (48.80%) can be explained not only by low absorption rate but also by partial disintegration at the site of cypermethrin absorption or by first pass effect at a high rate. In an earlier study conducted in broilers [28, 29] and rats [39], bioavailability was determined at a low level. In studies conducted in rats with lambda-cyhalothrin [40] and permethrin [44], and rabbit with flumethrin [30] the level of bioavailability was close to that in this research. In addition, $t_{1/2a}$ and k_a values were close to those obtain in the studies with some pyrethroids in broilers [28, 29].

The symptoms observed after the administration of cypermethrin were pertinent to the blood levels of cypermethrin. Furthermore, the fact that these

symptoms were monitored in a moderate in the group, which was given cypermethrin into the crop, was related to the moderate bioavailability of the pesticide. The evanescence of the intoxication symptoms observed at the beginning of the experiment in a little while in both application groups could be commented by the rapid metabolism and subsequent excretion of cypermethrin in broiler chickens. Hence, the toxicokinetic data of C_{max} , t_{max} , $t_{1/2\alpha}$, $t_{1/2\beta}$, MRT, Cl_T and F were closely related to the severity and the indication of cypermethrin poisoning. Similar results were obtained in previously conducted toxicokinetic studies on pyrethroid insecticides in chickens [28, 29].

CONCLUSIONS

In conclusion, when administered to broiler chickens by the intracrop route, although rapidly absorbed, the bioavailability of cypermethrin was found to be moderate. In the event of administration by both intracrop and intravenous route, the elimination half-life and mean residence time of the pesticide was not too short. When the toxicity of cypermethrin is considered, its effects are evaluated as disadvantageous. According to the authors' knowledge is the first detailed study of concerned with toxicokinetics of cypermethrin in poultry. The results of this work are considered to be significant in that they will constitute a document for further studies on the toxicokinetics, toxicology and safe use of this pesticide.

ACKNOWLEDGEMENTS

This research (project code: 11-3820) was supported by the Scientific Research Fund of Erciyes University.

The authors have declared no conflict of interest.

REFERENCES

- [1] Bradberry, S.M., Cage, S.A., Proudfoot, A.T., Vale, J.A. (2005) Poisoning due to pyrethroids. *Toxicol. Rev.* 24, 93-106.
- [2] Khanna, R.N., Gupta, G.S., Anand, M. (2002) Kinetics of distribution of cypermethrin in blood, brain, and spinal cord after a single administration to rabbits. *Bull. Environ. Contam. Toxicol.* 69, 749-755.
- [3] Laskowski, D.A. (2002) Physical and chemical properties of pyrethroids. *Rev. Environ. Contam. Toxicol.* 174, 49-170.
- [4] Starr, J.M., Scollon, E.J., Hughes, M.F., Ross, D.G., Graham, S.E., Crofton, K.M., Wolansky, M.J., Devito, M.J., Tornero-Velez, R. (2012) Environmentally relevant mixtures in cumulative assessments: an acute study of toxicokinetics and effects on motor activity in rats exposed to a mixture of pyrethroids. *Toxicol. Sci.* 130, 309-318.
- [5] Costa, L.G. (2008) Toxic effects of pesticides. In: Klasssen, C.D. (Ed) Casarett and Doull's Toxicology. The Basic Science of Poisons, Seventh Edition, McGraw Hill Medical, USA, pp. 883-930.
- [6] Anadón, A., Martínez-Larrañaga, M.R., Martínez, M.A. (2009) Use and abuse of pyrethrins and synthetic pyrethroids in veterinary medicine. *Vet. J.* 182, 7-20.
- [7] Titchener, R.N. (1985) The control of lice on domestic livestock. *Vet. Parasitol.* 8: 281-288.
- [8] Himonas, C.A., Liakos, V.D. (1989) Field trial of cypermethrin against lice infestations in goats. *Vet. Rec.* 125, 420-421.
- [9] James, P.J., Meade, R.J., Powell, D. (1989) Effect of insecticidal ear tags on populations of lice (*Damalinea ovis*) infesting sheep. *Aust. Vet. J.* 66, 134-137.
- [10] James, P.J., Erkerlenz, P., Meade, R.J. (1990) Evaluation of ear tags impregnated with cypermethrin for the control of sheep body lice (*Damalinea ovis*). *Aust. Vet. J.* 67, 128-131.
- [11] Bhatt, R.M., Sharma, S.N., Urabayala, S., Dash, A.P., Kamaraju, R. (2012) Effectiveness and durability of Interceptor® long-lasting insecticidal nets in a malaria endemic area of central India. *Malar. J.* 11: 189. doi: 10.1186/1475-2875-11-189.
- [12] Palmquist, K., Salatas, J., Fairbrother, A. (2012) Pyrethroid Insecticides: Use, environmental fate, and ecotoxicology, Insecticides-Advances in Integrated Pest Management, Perveen F (Ed.), InTech, China, pp. 251-278.
- [13] Thatheyus, A.J., Deborah Gnana Selvam, A. (2013) Synthetic pyrethroids: Toxicity and biodegradation. *Appl. Ecol. Environ. Sci.* 1, 33-36.
- [14] Banerjee, I., Tripathi, S.K., Roy, A.S., Sengupta, P. (2014) Pesticide use pattern among farmers in a rural district of West Bengal, India. *J. Nat. Sc. Biol. Med.* 5, 313-316.
- [15] Cox, C. (1996) Cypermethrin. *Journal of Pesticide Reform* 16, 15-20.
- [16] Masuh, H., De Licastro, S.A., Lopez, P.A., Vega, C., Zerba, E. (2003). Field evaluation of a smoke-generating formulation containing beta-cypermethrin against the dengue vector in Argentina. *J. Am. Mosq. Control. Assoc.* 19, 53-57.
- [17] Juan, L.W., Seccacini, E.A., Zerba, E.N., Canale, D., Alzogaray, R.A. (2013) Triatomid effect of new spot-on formulations applied to poultry in semi-field conditions. *Parasitol. Res.* 112, 155-161.
- [18] Amelotti, I., Catalá, S.S., Gorla, D.E. (2010) The effects of cypermethrin pour-on and piperonyl

- butoxide on *Triatoma infestans* under laboratory conditions. *J. Med. Entomol.* 47, 1135-1140.
- [19] Baynes, R.E. (2009) Ectoparasitocides. In: Riviere JE, Papich MG. (Eds). *Veterinary Pharmacology and Therapeutics*. 9th edn, Wiley-Blackwell, USA, pp 1181-1201.
- [20] Ong, S.Q., Ahmad, H., Jaal, Z., Rus, A.C. (2016) Comparative effectiveness of insecticides for use against the house fly (*Diptera: Muscidae*): Determination of resistance levels on a Malaysian poultry farm. *J. Econ. Entomol.* 109: 352-359.
- [21] Ong, S.Q., Ab Majid, A.H., Ahmad, H. (2016) Degradation of insecticides in poultry manure: Determining the insecticidal treatment interval for managing house fly (*Diptera: Muscidae*) populations in poultry farms. *J. Econ. Entomol.* 109, 952-957.
- [22] Lajmanovich, R., Lorenzatti, E., de la Sierra, P., Marino, F., Stringhini, G., Peltzer, P. (2003) Reduction in the mortality of tadpoles (*Physalasmus biligonigerus*; *Amphibia: Leptodactylidae*) exposed to cypermethrin in presence of aquatic ferns. *Fresen. Environ. Bull.* 12, 1558-1561.
- [23] Sakin, F., Ispir, U., Yonar, S.M., Yonar, M.E., Taysi, M.R. (2011) Effect of short-term cypermethrin exposure on oxidant-antioxidant balance in the whole body of rainbow trout fry (*Oncorhynchus mykiss*). *Fresen. Environ. Bull.* 20, 2806-2809.
- [24] Mugni H., Paracampo, A., Marrochi, N., Bonetto, C. (2012) Cypermethrin, chlorpyrifos and endosulfan toxicity to two non-target freshwater organisms. *Fresen. Environ. Bull.* 21, 2085-2089.
- [25] Yin, L.B., Li, X.H., Liu, Y. Zhang, D.Y.; Zhang, S.B., Luo, X.W. (2012) Biodegradation of cypermethrin by *Rhodospseudomonas palustris* GJ-22 isolated from activated sludge. *Fresen. Environ. Bull.* 21, 397-405.
- [26] Karadag, H., Uluca, H. (2015) Effect of deltamethrin and alpha cypermethrin pesticides on bovine liver catalase activity. *Fresen. Environ. Bull.* 24, 3562-3566.
- [27] Aydogdu, M., Gokalp, F.D., Guner, U. (2017) Toxic effects of pyrethrums lambda-cyhalothrin and alpha-cypermethrin on pest archips rosana (*Lepidoptera: tortricidae*) and its common parasitoid. *Fresen. Environ. Bull.* 26, 2436-2445.
- [28] Gögebakan, T., Eraslan, G. (2015) Single-dose toxicokinetics of permethrin in broiler chickens. *Br. Poult. Sci.* 56, 605-611.
- [29] Hüyük, R., Eraslan, G. (2017). Toxicokinetic of deltamethrin in broiler chickens. *Br. Poult. Sci.* 58: 95-99.
- [30] Başçi, Z., Eraslan, G. (2015) Toxicokinetic of flumethrin in rabbits. *Drug Chem. Toxicol.* 38, 92-97.
- [31] Yavuz, O., Aksoy, A., Das, Y.K., Atmaca, E. (2010) Evaluation of liquid-liquid and different solid phase extraction cartridges for determination of selected syntetic pyreroid insecticides in whole blood. *Asian J. Chem.* 22, 4026-4032.
- [32] Wang, D., Weston, D.P., Lydy, M.J. (2009) Method development for the analysis of organophosphate and pyrethroid insecticides at low parts per trillion levels in water. *Talanta.* 78, 1345-1351.
- [33] Mekebri, A., Crane, D.B., Blondina, G.J., Oros, D.R., Rocca, J.L. (2008) Extraction and analysis methods for the determination of pyrethroid insecticides in surface water, sediments and biological tissues at environmentally relevant concentrations. *Bull. Environ. Contam. Toxicol.* 80, 455-460.
- [34] Hunter, R.E., Riederer, A.M., Ryan, P.B. (2010) Method for the determination of organophosphorus and pyrethroid pesticides in food via gas chromatography with electron-capture detection. *J. Agric. Food Chem.* 58, 1396-1402.
- [35] Shrivastava, A., Gupta, V.B. (2011) Methods for the determination of limid of detection and limit of quantitation of the analytical methods. *Chron. Young Sci.* 2, 21-25.
- [36] Yamaoka, K., Nakagawa, T., Uno, T. (1978) Application of Akaike's information criterion (AIC) in the evaluation of linear pharmacokinetic equations. *J. Pharmacokinet. Biopharm.* 6, 165-175.
- [37] Shumaker, RC. (1986) PKCALC: a Basic interactive computer program for statistical and pharmacokinetic analysis of data. *Drug Metab. Rev.* 17, 331-348.
- [38] Wagner, J.G. (1975) Linear compartment models, in: Wager J.G. (Ed). *Fundamentals of clinical pharmacokinetics*, first edn., Hamilton Press, USA, pp. 57-128.
- [39] Anadón, A., Martínez-Larrañaga, M.R., Fernandez-Cruz, M.L., Diaz, M.J., Fernandez, M.C., Martinez, M.A. (1996) Toxicokinetics of deltamethrin and its 4'-HO-metabolite in the rat. *Toxicol. Appl. Pharmacol.* 141, 8-16.
- [40] Anadón, A., Martínez, M., Martínez, M.A., Díaz, M.J., Martínez-Larrañaga, M.R. (2006) Toxicokinetics of lambda-cyhalothrin in rats. *Toxicol. Lett.* 165, 47-56.
- [41] Baggot, J.D. (1992) Clinical pharmacokinetic in veterinary medicine. *Clin. Pharmacokinet.* 22, 254-273.
- [42] Riviere, J.E. (2009) Pharmacokinetic. In: Riviere JE, Papich, M.G. (Eds). *Veterinary Pharmacology and Therapeutics*. 9th edn. Wiley-Blackwell, USA, pp. 47-73.
- [43] Merwe, D.V.M., Gehring, R., Buur, J.L. (2012) Toxicokinetic. In: Gupta, R.C. (Ed) *Veterinary Toxicology, Basic and Clinical Principle*, 2nd eds, Academic Press, USA, pp. 37-47.
- [44] Anadón, A., Martínez-Larrañaga, M.R., Diaz, M.J., Bringas, P. (1991) Toxicokinetics of permethrin in the rat. *Toxicol. Appl. Pharmacol.*

110: 1-8.

Received: 10.03.2017

Accepted: 05.06.2017

CORRESPONDING AUTHOR

Gokhan Eraslan

Erciyes Üniversitesi, Veteriner Fakültesi,
Farmakoloji ve Toksikoloji Anabilim Dalı,
Kayseri/Turkey

e-mail: geraslan38@hotmail.com

LEVELS OF ORGANOCHLORINE PESTICIDES RESIDUES IN HUMAN BREAST MILK FROM THE NORTHERN DISTRICTS IN JORDAN IN 2014/2015

Tawfiq M AlAntary¹, Mahmoud A Alawi^{2,*}, Mohammad Abu Othman³, Nizar Haddad⁴

¹School of Agriculture, Department of Plant Protection University of Jordan, Amman-11942, Jordan

²School of Science, Department of Chemistry, University of Jordan, Amman-11942, Jordan

³Royal Scientific Society, Amman, 11942-Jordan

⁴Ministry of Environment, Amman 11942-Jordan

ABSTRACT

Organochlorine pesticides residues in mother milk samples from five districts in northern Jordan were analyzed in 2014 and 2015. Total number of samples was 100. The number of samples collected from each district was depending on population density. The results showed that 21% of all samples contained dieldrin, 10% *p,p'*-DDE and 8% *p,p'*-DDT. The highest concentration for dieldrin was 0.91 mg/kg milk fat in northern Shounah. The highest residue concentration and the highest percentage of positive samples were detected also in northern Shounah at 0.33 mg/kg milk fat and 40%, respectively. Aldrin, endrin, HCB, α -HCH, γ -HCH, heptachlor, α -endosulfan, β -endosulfan, *o,p'*-DDD, *o,p'*-DDT, *o,p'*-DDE and *p,p'*-DDD were not detected in any of the studied milk samples. In conclusion, Organochlorine residues in Jordan have been declined. Further regular studies on human breast milk pollution are needed.

KEYWORDS:

Pesticides, Organochlorines, Human milk, Jordan

INTRODUCTION

Organochlorine pesticides internationally are considered as important persistent organic pollutants (POPs). It has been widely used as insecticides between 1940 and 1970 to control agricultural pests and public health insects. Due to their adverse effects on human health, environmental impact and their high persistency in the surrounding environment and extremely lipophilic character, they have been prohibited in the developing countries such as north America and west Europe in the early of 1970 [1,2]. In Tunisia, most of organochlorine pesticides have been banned in the late 1980 [3].

In Jordan, all organochlorine pesticides have been banned in the early 1980 by Ministry of Agriculture to be used in controlling agricultural pests [4] and in middle 1990 against insects of public health [4,5]. These POPs are able to accumulate in the fat

tissues in the various biological systems through the food chain, reaching embryos and newborns through placenta and later across mother breast feeding causing several hazardous effects such as the delay in growth, nerve system development and thyroid gland [6, 7, 8, 9, 10].

It is the aim of this study to identify and to find the residues levels of DDTs, HCHs and cyclodiens and their metabolites or isomers in mother breast milk samples collected from the northern governorates and districts of Jordan in 2014 and 2015 as asked by the Ministry of Environment to establish data base to assist in taking the right regulations and decisions to protect human beings and the environment.

MATERIALS AND METHODS

Sampling. One hundred mother breast milk samples were collected from five governorates or districts in northern Jordan in September 2014 and April 2015 distributed as follows: 25 samples from Irbid, the largest city in the north, 20 samples from Jarash, 20 samples from Ajloun, 20 samples from Mafrq, and 15 samples from northern Shounah.

25-30 ml of mothers' milk were taken from each volunteer woman (Age range between 20 and 45 years) and placed in a 50-ml well-cleaned and dry glass bottle, transferred in cooling boxes to the laboratory, and stored at -20°C until analysis. Data concerning age, body weight, delivery number, last delivery date, fatty food intake, exposure to pesticides and sampling date for each lady were gathered in a prepared questionnaire. The human milk samples were collected in cooperation with the Ministry of Health. The number of samples which were gathered from the cities, towns and villages in the five ~~south-~~ northern Jordanian districts were proportional to the population density [9].

Chemicals, solvents and gases. The used solvents (acetone, dichloromethane, petroleum ether (40-60 $^{\circ}\text{C}$)) were all of the p.a. quality, whereas n-

hexane used was of GC-quality. Standards of the individual chlorinated pesticides were of purity between 99.5-99.9% and purchased from Dr. Ehrenstorfer GmbH (Augsburg/ Germany). Anhydrous sodium sulfate (p.a. quality) was heated at 550 °C for 2 h. Florisil (p.a. quality, 60-100 mesh) was heated overnight at 550 °C, mixed with distilled water to give 3% (w/w), mixed well and kept for 12 h in a closed container prior to use. Helium (99.99% purity) and make-up gas argon/methane (95+5%; 99.9% purity) were used. Elution mixture was petroleum ether + dichloromethane (80:20%, v/v) [9].

Methods and GC analysis. Extraction, cleanup and determination were carried out according to DFG-method [11], with the following details.

Glassware was dried at 110 °C after washing with water, soap, distilled water, acetone and n-hexane. The GC used was a PU-304 instrument, equipped with a ⁶³Ni-electron capture detector, a split injector and a SPB-608 capillary column (L = 30 m, I.D. = 0.25 mm, film thickness = 0.25 µm). The GC was used under the following operating conditions: injector (250 °C), detector (300 °C), column temperature program: 150 °C (5 min), 150-220 °C (10 °C/min), 220 °C (20 min), 220-290 °C (20 °C/min), and 290 °C (10 min). Carrier gas (He): 1.1 ml/min, make-up gas: 40 ml/min, and split ratio (1:50). For the confirmation of the results, a SPB-5 capillary column (L = 30m, I.D. = 0.25 mm, film thickness = 0.25 µm) was used [9].

Determination of fat content. The fat content (%) was determined according to [11, 12]. Ten g of each milk sample were weighed and mixed thoroughly in a separatory funnel with 2 ml of 25% ammonia, 25 ml diethyl ether and 25 ml petroleum ether (40-60 °C). The organic solvents layer was separated and the previous extraction steps were repeated twice. The pooled organic extracts were filtered through an anhydrous sodium sulfate layer into a weighed round bottom flask. The solvents were evaporated at 30 °C and 200 mbar. The round bottomed flask with the residues was placed overnight in a desiccator. The round bottom flask with residues was reweighed, and from the weight difference, the % milk fat content was calculated.

Pesticide extraction. Twenty five grams Florisil were added to chromatography column (50 x 2 cm with Teflon stopcock) containing 100 ml petroleum ether. Ten g milk sample were mixed with 25 g Florisil (3% water), added to the column, and the excess solvent was collected in a 500-ml round bottom flask. The column was eluted with 300 ml of the elution mixture. The eluates were evaporated nearly to dryness using the rotary evaporator at 35 °C and 12 mbar. The remaining solvent was evaporated using a stream of nitrogen gas. The residues were dissolved

in 2 ml n-hexane containing 0.3 µg/ml aldrin as internal standard (I.S.) and 2 µl of this final extract were injected onto the GC column [9].

Recovery test and detection limits. Extraction and clean-up methods were evaluated by spiking blank milk samples with known concentrations of each of the studied chlorinated pesticides to give the concentrations 0.05; 0.10 and 0.50 mg/kg milk fat. Each of these samples was extracted and cleaned-up according to the above-mentioned method. The experimentally found concentration was related to the theoretically added concentration, in order to calculate the % recovery. The detection limit for each compound was calculated as signal to noise (S/N) ≥ 3 from the chromatogram of the standard mixture of the sixteen studied pesticides after diluting several times. Each solution was injected twice. The results of recovery and detection limits are shown in Table 1.

TABLE 1
Average % recovery, and average detection limits for the monitored chlorinated pesticides

Pesticide	Average % Recovery	Average Detection Limits [ppm]
HCB	81.8	0.005
α-HCH	92.6	0.005
β-HCH	92.0	0.005
γ-HCH	94.0	0.005
Heptachlor	99.7	0.005
α-Endosulfan	93.9	0.005
β-Endosulfan	99.0	0.005
Aldrin	99.2	0.005
Dieldrin	88.8	0.005
Endrin	81.7	0.005
<i>p,p'</i> -DDT	90.1	0.005
<i>o,p'</i> -DDT	94.5	0.005
<i>p,p'</i> -DDD	90.9	0.005
<i>o,p'</i> -DDD	87.2	0.005
<i>p,p'</i> -DDE	98.0	0.005
<i>o,p'</i> -DDE	95.1	0.005

RESULTS

Table 2 shows average and range of residues concentrations of the chlorinated pesticides in breast milk samples collected from Irbid, Jarash, Ajloun, Mafrag and northern Shounah in 2014 and 2015. Dieldrin, *p,p'*-DDT and *p,p'*-DDE were detected in the collected samples. The average concentrations found in Irbid were 0.03, 0.08 and 0.08 mg/kg milk fat, respectively. The % of positive samples was 12, 16, and 8% of the total collected samples, respectively.

Table 2 shows the average concentrations of pesticides residues and % positive samples of breast milk collected from Jarash in 2014 and 2015. Dieldrin, *p,p'*-DDT and *p,p'*-DDE were detected in these samples. The average concentrations were 0.06, 0.19 and 0.02 mg/kg milk fat, respectively. The % of positive samples were 20, 45 and 10%, respectively.

TABLE 2
Number and % of positive samples; average and range of chlorinated pesticides residues in mother milk samples in mg/kg milk fat, collected from Irbid, Jarash, Ajloun, Mafrq and northern Shounah in 2014 and 2015

City	Total Analyzed Samples	Found Pesticide	N	N%	Average Concentration	Range	
						Min.	Max.
Irbid	25	Dieldrin	3	12	0.03	0.02	0.05
		<i>p,p'</i> -DDT	2	8	0.08	0.05	0.10
		<i>p,p'</i> -DDE	4	16	0.08	0.02	0.19
Jarash	20	Dieldrin	4	20	0.06	0.02	0.13
		<i>p,p'</i> -DDT	1	5	0.19	0.19	0.19
		<i>p,p'</i> -DDE	2	10	0.02	0.01	0.03
Ajloun	20	Dieldrin	4	20	0.07	0.03	0.09
Mafrq	20	Dieldrin	4	20	0.11	0.02	0.31
		<i>p,p'</i> -DDT	5	25	0.20	0.07	0.40
North Shounah	15	Dieldrin	6	40	0.33	0.03	0.91
		<i>p,p'</i> -DDE	4	27	0.13	0.03	0.29

Total number of analyzed samples: 20100 Average fat content for all samples: 3.0%

N = Number of positive samples

N% = Percentage of positive samples

TABLE 3
Average concentration of chlorinated pesticide residues (mg/kg milk fat) in mother milk from various countries and Jordan.

Compound	Indonesia, 2000 (n = 70) [21]	Turkey, 2003 (n = 37) [22]	Germany, 2001/2 (n = 39) [23]	Jordan, 2005 North districts (n = 80) [9]	Jordan, 2006 North districts (n = 80) [5]	Jordan, 2014/5 North districts (n = 100) [This study]
HCB	0.03	0.02	0.04	0.25	0.03	Nd*
<i>p,p'</i> -DDE	0.28	1.52	0.15	0.22	0.19	0.04
<i>p,p'</i> -DDT	0.06	0.07	0.005	0.10	0.03	0.09
<i>p,p'</i> -DDD	Nd	Nd	<0.005	Nd	Nd	Nd
DDTs Σ	0.34	1.60	0.15	0.32	0.22	0.13
ΣHCHs	0.10	0.15	0.02	0.19	0.02	Nd
Dieldrin	Nd	Nd	Nd	Nd	Nd	0.12

Nd = not detected

In the mother milk samples which were collected from Ajloun, only dieldrin was found at an average concentration of 0.07 mg/kg milk fat and the percentage of positive samples was 20%, as shown in Table 2.

Table 2 shows the average concentrations of pesticides residues and % positive samples of breast milk collected from Mafrq in 2014 and 2015. Dieldrin, and *p,p'*-DDT were detected in these samples. The average concentrations were 0.11 and 0.20 mg/kg milk fat, respectively. The % of positive samples was 20 and 25%, respectively.

Only dieldrin, and *p,p'*-DDT were detected in the breast milk samples collected from northern Shounah in 2014/2015 as shown in Table 2. The average concentrations were 0.33, and 0.13 mg/kg milk fat, respectively. The percentages of positive samples were 40 and 27%, respectively.

DISCUSSION

Organochlorine pesticides might be accumulated in the human body for long time as persistent and non polar organic pollutants [4]. These compounds are able to enter human bodies through food chains. DDT members and cyclodienes such as diel-

drin might reach maternal body fat. Body fat movement might be increased during lactation and fat soluble pollutants might also mobilized [13, 14]. Thus mother might be exposed to these toxic pollutants posing a risk of reaching breast milk where mothers cannot be able to avoid at the time of pregnancy and lactation [5, 13].

The present results showed that 21% of the samples contained dieldrin insecticide from the cyclodien organic pollutants, 10% contained *p,p'*-DDE and 8% contained *p,p'*-DDT. The highest concentration for dieldrin was 0.91 mg/kg milk fat in northern Shounah. The average concentration of dieldrin found in northern Shounah was 0.33 mg/kg milk fat. In addition, the highest % of positive samples was also in northern Shounah and was 40%. These results indicated that mothers in northern Shounah were exposed to pesticides application more than in other districts in north Jordan. This is true since northern Shounah is located in the Jordan Valley where extensive use of agriculture practices and pesticides spraying [4, 15]. In Tunisia, Ennaceur [3] reported in their study that *p,p'*-DDE and HCB residues occurred in mother breast milk. In Mexico, Waliszewski [16] detected *p,p'*-DDE in human milk samples. β-HCH isomer was the predominant pollutant in the breast milk samples from Bhopal, India [17], and β-HCH, γ-HCH, *p,p'*-DDD, *p,p'*-DDE, *p,p'*-DDT and endrin in

breast milk from Punjab, India [18], and *p,p'*-DDE and *p,p'*-DDT in breast milk from Thailand [19], and United Kingdom [20]. The present results indicated that the following compounds had not been detected in the breast milk samples from north Jordan. These compounds were: aldrin, endrin, HCB, α -HCH, γ -HCH, heptachlor, α -endosulfan, β -endosulfan, *o,p'*-DDD, *o,p'*-DDT, *o,p'*-DDE and *p,p'*-DDD. However, this study shows less concentrations and less number of detected compounds compared to previous studies conducted in Jordan as shown in Table 3, which allow the comparison with other countries [5, 9].

In conclusion, residue concentrations of organochlorine pesticides in Jordan have been declined. Further regular studies on breast milk contaminants are needed. Despite the presence of these pollutants in mother milk, natural breast feeding is highly recommended.

ACKNOWLEDGEMENTS

Thanks for University of Jordan for the help, Ministry of Environment for financing this work and the Royal Scientific Society for conducting sample analysis.

Disclosure of Interest. The authors report no conflicts of interest

Declaration of Interest. The authors declare that they have no conflict of interest. This study was financed by the Ministry of Environment of Jordan.

Compliance with Ethical Standards. Informed consent was obtained from all individual participants included in this study. The protocol of this research project has been approved by a constituted Ethics Committee of the institutions within which the samples were collected.

REFERENCES

- [1] Wong CK, Leung KM, Poon BH, Lan CY, and Wong MH. (2002) Organochlorine hydrocarbons in human breast milk collected in Hong and Guamgzhon. *Arch. Environ. Contam. Toxicol.* 43: 364 – 372.
- [2] Al Antary TM, Alawi M, Estityah H, and Al-Oqlah K. (2012) Comparison study of chlorinated pesticides in animal products within fourteen years in Jordan. *Fresen. Environ. Bull.* 21 (1a): 117 – 122.
- [3] Ennaceur N, Gandouira M, and Driss M. (2007) Organochlorine pesticides residues in human milk of mothers living in northern Tunisia. *Bulletin of Environmental Contamination and Toxicology* 78(5): 325 – 329.
- [4] Al Antary TM. (1996) Pesticides and Toxicology, Al-Quds Al-Maftouha University publications, Amman, Jordan. 643 pp.
- [5] Alawi M, Al Antary TM., Estityah H, Al-Aqqad S, and Haddad N. (2015) Chlorinated pesticides residues in human breast milk from southern Jordan: Comparative study between 2008 and 2012. *Fresen. Environ. Bull.* 24(12a): 4512 – 4518.
- [6] Siddiqui M, Strivastava S, Strivastava SP, Mehrotva K, Mathur N, and Tandon I. (2003) Persistent chlorinated pesticides and intra-uterine foetal growth retardation: a possible association. *Int. Arch. Occupational Environ. Health* 76: 75 – 80.
- [7] Nagayama J, Okamura K, Lida T, Hirakawa H, Matsueda T, Tsuji H, Hasegawa M, Sato K, Ma HY, Yanagawa T, Igarashi H, Fukushige J, and Watabane T. (1998) Postnatal exposure to chlorinated dioxins and related chemicals on thyroid hormone status in Japanese breast-feed infants. *Chemosphere* 37:1789 – 1793.
- [8] Al-Targi Z, Abou El-Ela R, and El-Dressi A. (2011) Organochlorine pesticides residues in human breast milk in El-Gabal Al-Akhdar, Libya. *International Proceedings of Chemical, Biological and Environmental Engineering (IP-CBEE)* 36: 146 – 149.
- [9] Alawi M, Al Antary TM, Estityah H, Al-Aqqad S, and Al-Oqlah K. (2013) Comparative study for chlorinated pesticides in mother milk from Jordan in four studies between 1993 and 2003. *Fresen. Environ. Bull.* 22(1a): 279 – 285.
- [10] Hajjar MJ, Al-Salam A. (2016) Organochlorine pesticides residues in human milk and estimated daily intake (EDI) for the infants from eastern Saudi Arabia. *Chemosphere* 164: 643 – 648.
- [11] Their HP. and Zeumer H. (1987) *Manual of Pesticides Residues Analysis*, DFG, VCH-Germany.
- [12] Alawi M, and Ababneh M. (1991) Residue analysis of chlorinated pesticides in Jordanian human adipose tissues. *Anal. Letters* 24(10): 1897 – 1911.
- [13] Heifetz R, and Taylor S. (1989) Mother's milk or mother's poison? Pesticides in breast milk. *Journal of Pesticides Reform* 9(3): 15 – 17.
- [14] Al Antary TM, Alawi M, Estityah H, and Al-Oqlah K. (2013) Comparative study for chlorinated pesticides in mother milk from Jordan in four studies between 2004 and 2008. *Fresen. Environ. Bull.* 22(5):1387 – 1393.
- [15] Al-Mommany A, and Al Antary TM. (2008) *Pests of Home and Garden*. Publication of the University of Jordan publications, Amman, Jordan. 518 pp.
- [16] Waliszewski S, Aquirre A, Infanzon R, Brenitez A, and Rivera A. (1999) Comparison of organochlorine pesticide levels in adipose tissue and

- human milk of mothers living in Varacruz, Mexico. *Bull. Environ. Contam. Toxicol.* 62:685 – 690.
- [17] Sanghi R, Pillia M, Jayalekshmi T, and Nair A. (2003) Organochlorine and Organophosphorus pesticide residues in breast milk from Bhopal, Madhya Pradesh, *Toxicology* 22: 73 – 76.
- [18] Bedi J, Gill J, Aulakh R, Kaur P, Sharma A, and Pooni P. (2013) Pesticides residues in human breast milk: risk assessment for infant from Punjab, India. *Sci. Total Environ.* Oct 1: 720 – 726.
- [19] Stuetz W, Prapamontol T, Erhardt J, and Clausen H. (2001) Organochlorine pesticide residues in human milk of a Hmong hill tribe living in northern Thailand. *Sci. Total Environ.* 273 (1-3): 53 – 60.
- [20] Kalantzi O, Martin F, Thomas G, Alcock R, Tang H, Drury S, Carichael P, Nicolson J, and Jones K. (2004) Different levels of polybrominated diphenyl ethers (PBDEs) and chlorinated compounds in breast milk from UK regions. *Environ Health Perspect* 112: 1085 – 1091.
- [21] Sudaryanto A, Kunisue T, Kajiwara N, Iwata, H., Adibroto T, Hartonoc P, Tanabe S. (2006) Specific accumulation of organochlorines in human breast milk from Indonesia: Levels, distribution, accumulation kinetics and infant health, risk. *Environ Pollu.* 139(1): 107 – 117.
- [22] Tanabe S, Kunisue T. (2007) Persistent organic pollutants in human breast milk from Asian countries. *Environ Pollu.* 146(2): 400-413
- [23] FAPAS (2012) Food Analysis Performances Assessment Scheme is a registered trademark of Central Science laboratories. Sixth Edition, York, UK.

Received: 13.03.2017
Accepted: 31.05.2017

CORRESPONDING AUTHOR

Mahmoud A. Alawi

School of Science, Department of Chemistry, University of Jordan, Amman-11942, Jordan

e-mail: alawima@ju.edu.jo

DETERMINATION OF ENERGY LOSS COEFFICIENT OF RAINWATER AND SEWER MANHOLES WITH CFD

Ismail Hakki Ozolcer*, Onur Dundar

Bulent Ecevit University, Civil Engineering Department, Zonguldak, Turkey

ABSTRACT

Overflowing and flooding in rainwater and sewer system manholes have become very common incidents in recent years. It is a well-known fact that floods spread out to large areas and cause loss of life and property. Consequently, using recent modelling approaches in the design of manholes has gained more importance than ever. The manhole geometry used today is given by national standards. Although the flood of a manhole is typically considered as a result of insufficient capacity of the system, the manhole geometry has distinctive role on the energy loss coefficients of manhole and water level in it. Nowadays, Computational Fluid Dynamic (CFD) programs and large computer capacity present opportunities in accurately modeling water flows in the manholes whose loss coefficients are calculated from the CFD modelling.

In this study, water flow is modelled with CFD in a typical half bench manhole given by the Turkish Standards TS EN1917/AC. Moreover, three alternative manholes geometries are generated and water flow in these manholes are modelled with CFD. The energy loss coefficients of all manhole models are calculated and compared.

KEYWORDS:

Rainwater and Sewer Manhole, Computational Fluid Dynamics, Energy Loss Coefficient.

INTRODUCTION

Manhole is one of the basic element in rainwater and sewer networks, and connects pieces of pipes to the rest of the networks and the transition of flows are generally observed around them. Understanding the hydraulics of sewers at junctions is important to model the system correctly [1, 2, 3, 4]. The perpendicular inlet and outlet manholes are located at the junctions and the direction changing points of the rainwater and sewer networks. The geometries of manholes are generally given by the national standards, and they are prefabricated.

Complex flow conditions are observed in manholes where perpendicular inlet and outlet flows are passing through [5]. The inlet and outlet flows with different directions make surface wavy, undulating,

and also vortex formation are observed in the some regions of the manhole. Moreover, generally transition between completely filled pipe and partially filled pipe can be observed at the manhole regions [1, 6, 4]. Sewer and rain water network pipes and manholes are designed for partially filled conditions. Surcharged flow conditions are frequently observed in the manholes, and it is allowed in the designing of the networks. However, if the water depth in the manhole exceeds the manhole depth, the overflow occurs. The overflow damages manholes and network pipes, spreads out to large areas, causes loss of life and property [5, 7]. Based on detailed hydraulic experimentation of Hager and Gossini [5], the main features of manhole flow in three manhole types were observed, including the through-flow, the bend and the junction manholes. Using systematic observations and a hydraulic approach, the large data sets allowed to present modified and generalized design criteria for such hydraulic structures. One of the primary solution of the high water flow depth in the manhole may be the increment of the diameter or the slopes of the pipes. But both of the solutions are limited with the flow velocity and the economic considerations. As a result, the manholes are the bottleneck of the sewer and rainwater collection systems.

Almost every city with incidents of overflowing of manholes should encounter heavy rains or storm events. Overflowed manholes could result in serious problems such as the blowout of manhole covers, occurrence of fountains, and flooding [8, 9]. In the City of Calgary, Alberta, a manhole cover on Edworthy Road was blown off, a fountain was formed during the storm, and large area is flooded. An experimental study on supercritical sewer flows at a junction chamber was conducted using a physical model suggested by Zhao et al. [1]. The model study has showed that a junction chamber with a small angle of two combining inflows helps to retain kinetic energy of the flow and reduces the water level in the surcharged chamber. A numerical modelling approach accounting for the energy losses in manholes is introduced by [7]. The resulting models are investigated numerically, highlighting the influence of the manhole on the network and displaying the total energy [7]. Yen and Akan [10] are discussed junctions as the most important auxiliary component in modeling the sewer and rain water networks. For sewers pipes of common size and length, the head loss for

the flow through a sewer is usually two to five times the velocity head. Thus, the head loss through a junction is comparable to the sewer pipe loss, and is not considered a minor loss.

The real capacity of the sewer and rainwater networks can be exactly estimated on the grounds that the friction loss of pipes and the local loss of the connection elements are correctly calculated [7]. For sewers of common size and length, the head loss for the flow through a sewer is usually two to five times the velocity head [10]. Thus, the head loss through a junction is comparable to the sewer pipe loss, and is not a minor loss. Correct representation of the junction hydraulics is important in realistic simulation and reliable computation of the flow in a sewer system [11]. The lateral and bend loss coefficients must be considered during the calculation of energy loss, and it is necessary to accurately calculate hydraulic grade line of the network [12]. There are number of studies in the literature on the pressurized network connections [13]. In early studies, the loss coefficients in T-junctions are used for manholes. Generally, free surface water flow studies comprise rectangular sectioned open channels [14].

Complex water flow conditions do not allow 1-D or 2-D numerical modeling of sewer or rainwater networks manholes. Physical representation of manhole CFD modelling might assure only 3 dimensional geometrical modelling of the junction region. The implementation in the computer hardware technology makes 3-D modelling of manhole possible with even standard desktop computers. The benefits of CFD modelling of urban drainage and sewer systems are discussed with Jarman et al. [15] in details. Overflowing manholes and distributions of pollutants are modeled with CFD by Chen et al. [16]. Moreover, specific structures that prevent separation of pollutants are designed by CFD solutions. Bennett, et al. [17] modelled the overflowing manholes pollution propagation and compared the computation results with the experimental ones. Lee [18] studied on improving hygienic conditions of home drainage systems with CFD approach. Mignot et al. [19] modelled 3-D open channel junction and analyzed the impact of the junction on the velocity distribution according to the distance from the junction, and thus evaluated the typical error derived from the computation of the flow rate close to the junction. Zhao et al. [2] established a CFD model to simulate fully surcharged flow at a 90° combining sewer junction. The model was carefully assessed by comparing its results with the measurements of detailed physical experiments. Good agreement was obtained between results of the computational model and the laboratory experiments. Motlagh et al. [4] numerically investigated the effects of different parameters on flow structure and energy loss coefficients in combining sewer junction consisting of manhole and lateral inflow. The main parameters investigated in

the study are the effects of dimension variations, main and lateral pipe slope, angle and the joint position of lateral pipe alongside the manhole, and geometry and outflow rate of manhole.

There are two different approaches proposed for the modeling the water surface in the manhole. The first one is the rigid lid or symmetry plane approach. In this approach, surface location and the shape are predefined, and the flow boundary conditions are directly assigned on relevant Computational grid points. On the other hand, in the second approach the surface location is a part of the solution. The free surface location is either calculated from the solution of the transport equation of volume fraction related to volume of fluid (VOF) method or obtained by the level set method. The VOF method is more common than the level set method since it requires less computational effort. However, on the second approach in the definition of the problem, it is a compulsory requirement that describes the second phase and its computational domain. Both methods suffer from the large iterative change of the surface and its computational cost to the solution. If it is not necessary to determine surface location and shape, the first approach might be enough to represent the surface effect on flow, and it gives much more inexpensive and rapid solution.

Bennet et al. [17] published the improved CFD simulation approaches for manhole mixing investigations. In their work, Bennet et al. [17] concluded that the k-ε realizable turbulence model and rigid lid approach appear to more accurately reproduce the mean flow field for different hydraulic regimes. Mignot et al. [19] performed a flow simulation at an open-channel junction. The free surface is defined as a rigid lid with free slip condition. The comparison of numerical and experimental results are in good agreement. However, one main limitation of the numerical approach arises from the greater flow rates where free surface oscillations could require the use of the VOF approach. Saiyudthong and Guymer [20] published the results from the simulation of CFD in terms of energy loss coefficient and visual mechanisms taking place in a circular surcharged manhole with changes in pipe direction. The free surface was specified as frictionless rigid lid. Saiyudthong and Guymer [20] conclude that the surface simulation technique has a small influence on energy loss coefficients when the manhole is highly surcharged. Zhao et al. [2] and Motlagh et al. [4] had performed numerical simulations for rectangular and circular shaped manholes at which they used VOF method to especially define the surface shape and location. Beside the surface properties, they also calculated the energy loss coefficients from the CFD results and compared them with the experimental results. The CFD results proved to be in good agreement with the experimental studies.

One of the most important design criteria for sewer and rain water collection networks is the occurrence of free surface water flow in pipes. The gravitational force is the only driving force for free surface flow, and application of pumping station is avoided. Saving the energy of the free surface flows as much as possible makes the system more efficient. The frictional losses on the pipes are the basic source for energy loss in the system. However, local energy loss in the manholes has a considerable effect on the total energy loss of the system [10].

In this study, four different bottom geometry surcharged circular cross section manholes are studied. All manholes have two inlets pipes and one outlet pipe, one of the inlet pipes is positioned perpendicular to the main flow direction. The first type bottom geometry is defined by TS EN 1917/AC standard, and it has a perpendicular half bench on the bottom. The second type has a full guided circular bench on the bottom. The third type has a flat bottom without any bench on the bottom. The last type is obtained with the modification of the third type. The circulation zones on the third type is filled with concrete, and an arrow shaped inner and bottom geometry is obtained. The flow conditions are simulated with the CFD. The energy loss coefficients are extracted from the CFD solution. The energy loss coefficients obtained from the CFD simulations are compared.

MATERIALS AND METHODS

Mathematical Model and Solution Equations. The CFD modelling is based on the solution by Reynolds Averaged Navier Stokes' equation. In Reynolds averaging, the solution variables in the instantaneous Navier-Stokes equations are decomposed into the mean and fluctuating components. For the velocity components: $u_i = \bar{u}_i + u_i'$ where \bar{u}_i and u_i' are the mean and fluctuating velocity components, respectively. Similarly, for pressure and other scalar quantities: $\varphi = \bar{\varphi} + \varphi'$ where $\bar{\varphi}$ denotes a scalar such as pressure, energy, or species concentration. Taking a time average to the instantaneous Navier-Stokes equations and dropping the over bar yield the ensemble-averaged equations. The continuity and momentum equations can be written in the Cartesian tensor form as:

$$\frac{\partial \rho}{\partial t} + \frac{\partial}{\partial x_i} (\rho u_i) = 0 \quad (1)$$

$$\frac{\partial \rho}{\partial t} (\rho u_i) + \frac{\partial}{\partial x_j} (\rho u_i u_j) = -\frac{\partial P}{\partial x_i} + \frac{\partial}{\partial x_j} \left[\mu \left(\frac{\partial u_i}{\partial x_j} + \frac{\partial u_j}{\partial x_i} \right) - \frac{2}{3} \delta_{ij} \frac{\partial u_k}{\partial x_k} \right] + \frac{\partial}{\partial x_j} (-\rho \overline{u_i' u_j'}) \quad (2)$$

In Equation 2, ρ is the density of the fluid and u_i is the i^{th} axis component of the velocity field. The last term in the equation is the turbulence shear stress, and must be modelled for high Reynolds number flows. The basic approach for the modelling of

turbulence shear stress based on the Boussinesq hypothesis given with Equation 3. The shear stresses are defined with the gradient of the average velocity field with the hypothesis.

$$(-\rho \overline{u_i' u_j'}) = \mu_t \left(\frac{\partial u_i}{\partial x_j} + \frac{\partial u_j}{\partial x_i} \right) - \frac{2}{3} \left(\rho k + \mu_t \frac{\partial u_k}{\partial x_k} \right) \delta_{ij} \quad (3)$$

The Boussinesq hypothesis is the basic approach for many different turbulence modelling structures such as one equation model Spalart Almaras, two equation models k- ϵ and k- ω . The term μ_t turbulence viscosity is a scalar quantity, and treated as isotropic in many turbulence models.

The governing equations are firstly transferred to generic transport equations. The construction of a numerical method for the solution of the transport equations requires the flow domain to be represented as a mesh of discrete points at which each term of the partial differential equations is evaluated. This results in a system of coupled algebraic equations that requires simultaneous solution by means of a suitable solution algorithm. The well-known commercial CFD package FLUENT is used for solutions. The discretization method used in the Fluent is the finite volume method Patankar [21] and Versteeg and Malalasekera [22]. The transport equations are integrated over each of control volumes by approximating the variation of the flow properties between mesh points with piecewise profiles. This integration ensures that the conservation laws used in the derivation of the transport equations are satisfied locally at each of the control volumes. The overall conservation of the flow properties is therefore automatically preserved. These piecewise approximations, also known as differencing schemes, are constructed to support physical flow behavior such as convection or diffusion.

Discretization of Equations. Conservation equation is integrated over the control volume to yield the following discrete equation

$$\sum_f^{N_{\text{face}}} J_f A_f = 0 \quad (4)$$

where J_f is the mass flux through face f , ρv_n and A_f are the area of faces. In order to proceed further, it is necessary to relate the face values of velocity, v_n , to the stored values of velocity at the cell centers. Linear interpolation of cell-centered velocities to the face results in unphysical checker-boarding of pressure. The Fluent uses a procedure similar to that outlined by Rhie and Chow [23] to prevent checker boarding.

The momentum equations are discretized like a scalar equation such as the discretization of x-momentum equation:

$$a_p u = \sum_{ab} a_{ab} u_{ab} + \sum p_f A \cdot i + S \quad (5)$$

If the pressure field and face mass fluxes are known, Equation 5 can be solved and a velocity field obtained. However, if pressure field and face mass

fluxes are not known a priori and must be obtained as a part of the solution. The Fluent uses a co-located scheme whereby pressure and velocity are both stored at cell centers. However, Equation 4 requires the value of the pressure at the face. Therefore, an interpolation scheme is required to compute the face values of pressure from the cell values. The default scheme Rhie and Chow [23] in the Fluent interpolates the pressure values at the faces using momentum equation coefficients

$$P_f = \frac{\frac{P_{c0}}{a_{p,c0}} + \frac{P_{c1}}{a_{p,c1}}}{\frac{1}{a_{p,c0}} + \frac{1}{a_{p,c1}}} \quad (6)$$

Pressure-Velocity Coupling. This procedure works well as long as the pressure variation between cell centers is smooth. When there are jumps or large gradients in the momentum source terms between control volumes, the pressure profile has a high gradient at the cell face, and cannot be interpolated using this scheme. The Fluent provides different segregated types of algorithms for pressure velocity coupling. The Pressure-Implicit with Splitting of Operators (PISO) algorithm with neighbor correction is highly recommended for all transient flow calculations which allow large time steps also. The PISO pressure-velocity coupling scheme, part of the SIMPLE family of algorithms, is based on the higher degree of the approximate relation between the corrections for pressure and velocity. One of the limitations of the SIMPLE and SIMPLEC algorithms is that new velocities and corresponding fluxes do not satisfy the momentum balance after the pressure-correction equation is solved. As a result, the calculation must be repeated until the balance is satisfied. To improve the efficiency of this calculation, the PISO algorithm performs two additional corrections: neighbor correction and skewness correction.

Turbulence Modelling. To close the previous equation sets for application, constitutive equations are required for turbulent Reynolds stress terms. In this study, the standard $k-\varepsilon$ two-equation model was used. To apply the $k-\varepsilon$ model, the Reynolds number of the flow needs to be high enough for an inertial subrange to exist. The model is proposed by Launder and Spalding [24] and it is popular in industrial flow simulations hence its robustness, economy, and reasonable accuracy for a wide range of turbulent flows. Two differential equations were solved to represent transport parameter kinetic energy, k and dissipation rate of the kinetic energy, ε .

$$\frac{\partial}{\partial t}(\rho k) + \frac{\partial}{\partial x_j}(\rho k u_j) = \frac{\partial}{\partial x_j} \left[\left(\mu + \frac{\mu_t}{\sigma_k} \right) \frac{\partial k}{\partial x_j} \right] + G_k + G_b - \rho \varepsilon - Y_M + S_k \quad (7)$$

$$\frac{\partial}{\partial t}(\rho \varepsilon) + \frac{\partial}{\partial x_j}(\rho \varepsilon u_j) = \frac{\partial}{\partial x_j} \left[\left(\mu + \frac{\mu_t}{\sigma_\varepsilon} \right) \frac{\partial \varepsilon}{\partial x_j} \right] + C_{1\varepsilon} \frac{\varepsilon}{k} (G_k + C_{3\varepsilon} G_b) - C_{2\varepsilon} \rho \frac{\varepsilon^2}{k} + S_\varepsilon \quad (8)$$

In these equations, G_k represents the generation of turbulence kinetic energy due to the mean velocity gradients, G_b is the generation of turbulence kinetic

energy due to buoyancy, Y_M represents the contribution of the fluctuating dilatation incompressible turbulence to the overall dissipation rate. $C_{1\varepsilon}$, $C_{2\varepsilon}$, and $C_{3\varepsilon}$ are constants. σ_k and σ_ε are the turbulent Prandtl numbers for k and ε , respectively. S_k and S_ε are user-defined source terms. The details of the calculation of the constants in the equations are given in Fluent [25].

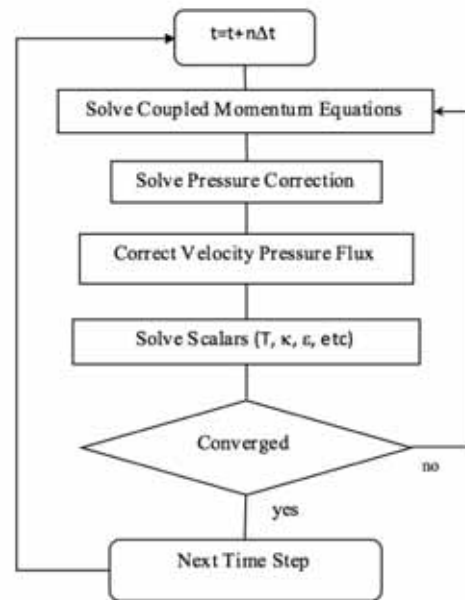


FIGURE 1
General flow chart of CFD

Numerical model. All equations are solved sequentially (the segregated option in the Fluent), coupled to a standard model with wall functions for turbulence closure. The continuity equation was enforced using a body force weighted PISO algorithm, resulting in a Poisson equation for the pressure (Figure 1).

Geometry, Boundary Conditions and Hydraulic Parameters. The present study has investigated fully surcharged flow at a junction that combines pipes connected as shown in Fig. 2, (for $\theta = 90^\circ$). The junction has three connecting pipes running full, and the lateral inlet pipe is laid out at q to the other two pipes. The straight inflow, lateral inflow and the outflow are denoted as Q_1 , Q_2 and Q_3 , respectively.

All connecting pipes have an identical diameter of $D=0.20$ m. The junction chamber is circular with a diameter of 1 m. The inlet and outlet pipes are located 0.1 m above the bottom for flat bottom manhole. The lengths of straight inflow, lateral inflow and outflow pipes are 3.0, 3.5 and 3.0 m, respectively. The energy loss coefficients at the combining sewer junctions are usually defined as [26, 27, 28]:

$$H_1 = \frac{P_1}{\rho g} + \frac{V_1^2}{2g}, H_2 = \frac{P_2}{\rho g} + \frac{V_2^2}{2g} \text{ ve } H_3 = \frac{P_3}{\rho g} + \frac{V_3^2}{2g}$$

(9)

$$K_{13} = \frac{H_1 - H_3}{V_3^2/2g}, K_{23} = \frac{H_2 - H_3}{V_3^2/2g}$$

(10)

$$K = \frac{Q_1}{Q_3} K_{13} + \frac{Q_2}{Q_3} K_{23}$$

(11)

where the average velocity in the outlet pipe is $V_3 = Q_3/A_3$. K_{13} and K_{23} denote energy changes in the straight and lateral streams, respectively. K is the head loss coefficient. As shown in Figure 2, the simulation domain has two inlets (Q_1 and Q_2) for which mass flowrate is assigned, assuming a turbulent intensity of 3.7% and an eddy length scale of $D/4$ [2]. In the outlet pipe, atmospheric pressure is assumed over the outlet boundary (Q_3). A symmetry boundary condition is applied to the top of the chamber which

does not allow flow across the surface but freely moves to tangential direction domain.

RESULTS AND DISCUSSIONS

In this study four different bottom geometry is modelled given with Figure 3. Type 1 is the standard bottom geometry which is defined with TS EN 1917/AC. The bottom of the manhole is shaped with half benched semicircular channel perpendicularly across. Type 2 manhole bottom is shaped with full bench U shaped guided channels. Type 3 manhole bottom is flat. The type 4 is designed with four redirecting attachments to obtain a guided manhole structure from the type 3.

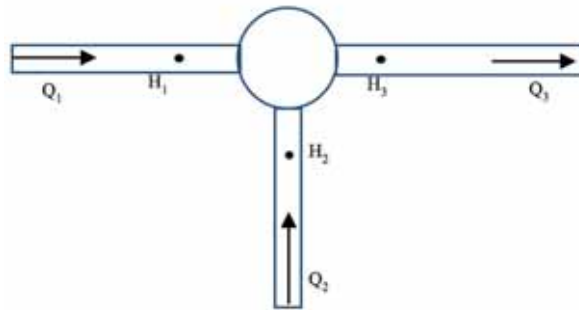
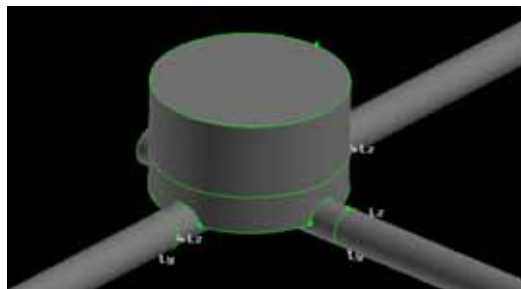
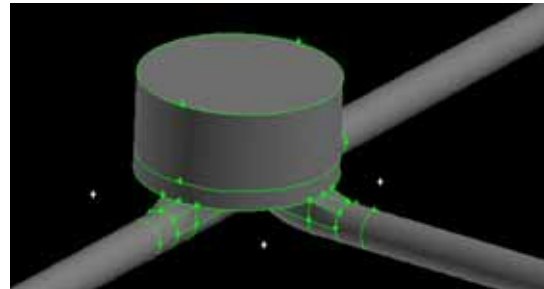


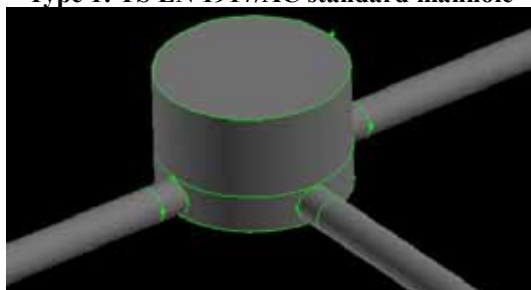
FIGURE 2
General hydraulic elements of manhole



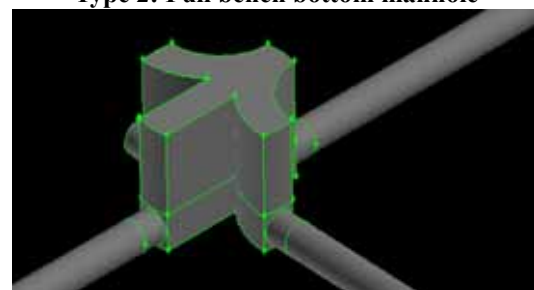
Type 1: TS EN 1917/AC standard manhole



Type 2: Full bench bottom manhole



Type 3: Flat bottom manhole



Type 4: Redesigned manhole

FIGURE 3
Manholes modelled in the presented study

TABLE 1
Inflow, outflow and total discharges

Q_2/Q_3	Q_2 (l/s)	Q_1 (l/s)	Q_3 (l/s)
0.2	16.152	64.608	80.76
0.4	32.304	48.456	80.76
0.5	40.38	40.38	80.76
0.6	48.456	32.304	80.76
0.8	64.608	16.152	80.76

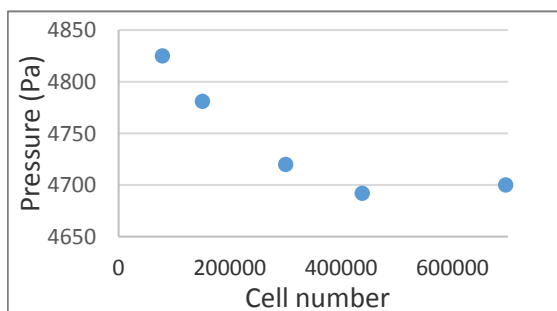
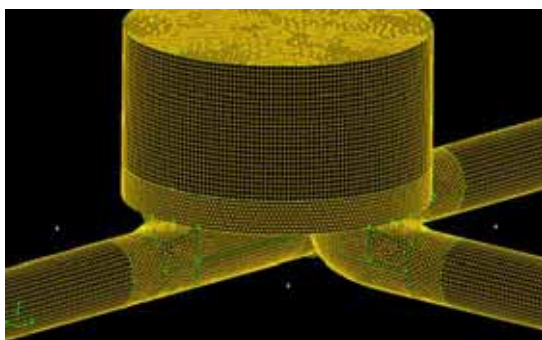


FIGURE 4

- a. Tetragonal and hexagonal elements mesh.**
b. Mesh sensitivity analysis

The applied mesh contains both structured hexagonal and unstructured tetragonal finite volume elements as shown in Figure 4a. The minimum mesh elements dimension is chosen as 10 % of the diameter of the pipes as a first approach [2, 4]. Then, a mesh sensitivity analysis is performed based on the pressure inside the manhole. The optimum mesh dimension is decided due to the convergence of the pressure value. As the minimum dimension of the pressure decreases, the pressure is converged with Figure 4b. The minimum finite element dimension is chosen as 7% of pipe diameter.

The main parameter affecting the energy loss coefficients is the ratio of lateral flow discharge to the total discharge. In the present research work, each bottom shapes were compared for flow ratios of $Q_2/Q_3=0.2, 0.4, 0.5, 0.6$ and 0.8 where $Q_3=80.76$ m³/s. The inflow discharges Q_1, Q_2 given in Table 1 are assigned to the fully flowed circular cross sections. The outflow discharge Q_3 is calculated from

the solution at the outflow cross-section and compared with the inflow and is used as convergence criteria.

Flow Structure in the Manhole. Flows in junction present complicated patterns of mixing, separation and turbulence. The flow field velocity vectors in the manhole is given Figure 5 for $Q_2/Q_3=0.5$. The inflow, outflow and total energy loss coefficients are calculated by the inner solution of manhole flow.

It can be observed that the existing flow structures for all cases are the same, meaning that, for all types of cross-sections, at small flow ratios (Q_2/Q_3), a weak and thin vortex forms in the upper part of the manhole, which at large flow ratios, turns into a strong circular vortex in the upper left corner of half bench and flat bottom manholes. The area and the magnitude of the vortex become smaller for full bench bottom manholes. In addition, at both small and large flow rate ratios, small and weak vortices are generated in the lower left and right corners. Without guidance the resultant vector field of lateral and horizontal flow heads toward to upper right side wall of the manhole. The flow ratio determines the angle of resultant vector field as it increases the angle of the vector field. The average velocity at outlet pipe is 2.6 m/s for all types and cases. However, the maximum velocity at that section increases up to 3.5 m/s for Type 1 and Type 3 in which manholes have either half bench or non. On the other hand, for full bench and Type 2 and the newly designed Type 4 manhole, the exit section the maximum velocity reaches 3 m/s only.

Energy Loss Coefficients. The pressure profile along the main flow direction is given in Figure 6. The center of the manhole is located at center of x axis, the entrance from the horizontal inlet pipe to the manhole is on the left ($x=-0.5$) and the exit to outlet pipe is on the right ($x=0.5$). The total head values H_1 is calculated at $x=-0.7$, and H_3 is calculated at $x=0.7$. The liner variation of pressure represents the head loss due to the pipe friction before and after that points. The head loss between these calculations points are considered as manhole energy loss. The pressure increase inside the manhole is apparently thought as a consequence of decrease in velocity. The atmospheric pressure is assigned at outlet pipe

exit as a boundary condition, however the pressure at the inlet sections in main and lateral direction are calculated from the inner solution. The maximum main pipe inlet section pressure is observed for Type 1 manhole which bottom geometry is described at TS EN 1917/AC. Type 3 manhole with flat bottom presents better performance than type 1 manhole. The best performance is observed at type 2 manhole

which has a U-shaped guided full bench on the bottom.

The total heads H_1 , H_2 and H_3 are calculated at 1, 2 and 3 sections from the area average values of CFD solution with equation 6. The head loss coefficients K_{13} and K_{23} and K values are calculated from equation 7 and 8. The variation of main direction energy loss coefficients K_{13} , K_{23} and K due to the flow ratio is given in figure 7, 8 and 9 respectively.

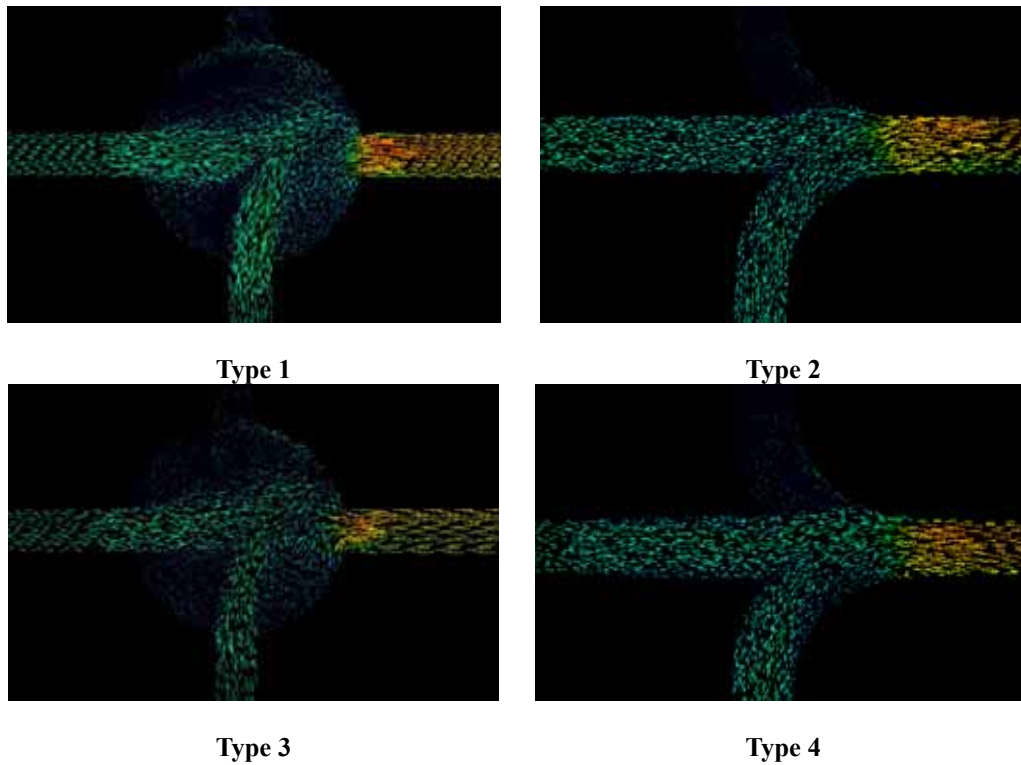


FIGURE 5
Velocity vector field

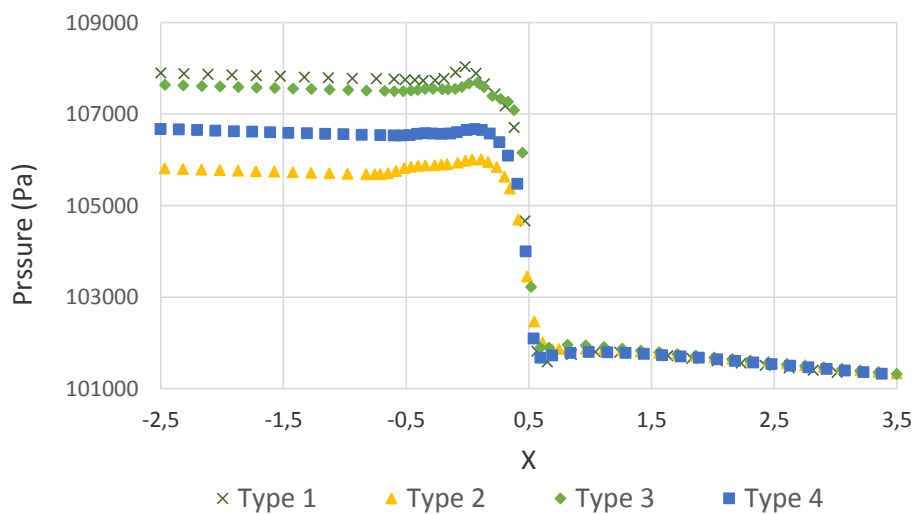


FIGURE 6
Pressure variation along the main axis

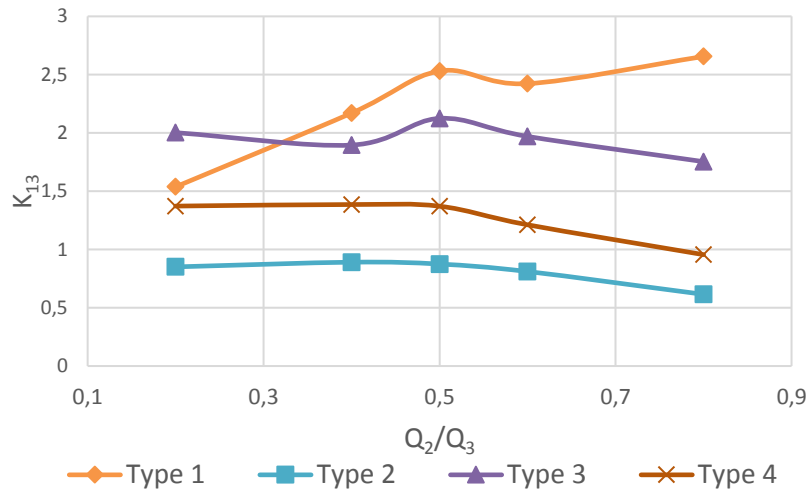


FIGURE 7
Main direction energy loss coefficient

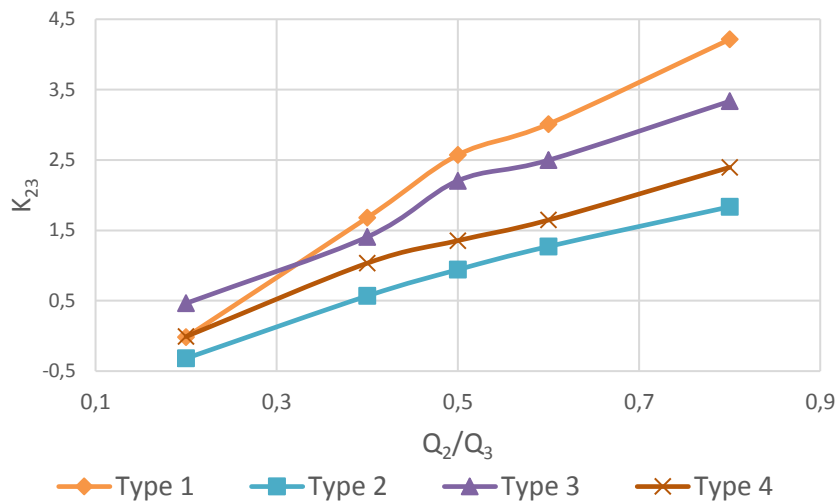


FIGURE 8
Lateral direction energy loss coefficient

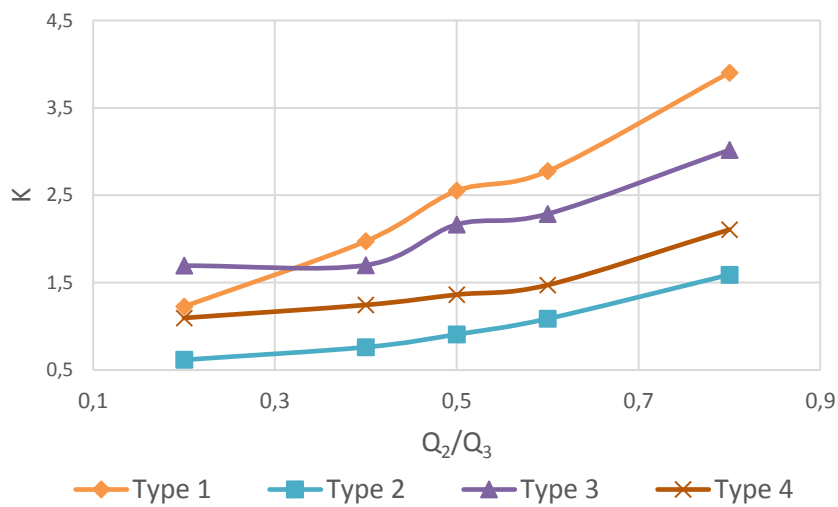


FIGURE 9
Manhole energy loss coefficient

CONCLUSIONS

The operation drainage systems under surcharge conditions allow maximum usage of the flow and detention capacities. Accurate and reliable description of loss coefficients at manholes is of great importance for the accuracy of hydrodynamic simulations. Although the energy losses at a single manhole relatively small, a total value of local losses is significant due to a huge number of such structures located every 50–60 meters on each conduit.

The type 1 manhole whose geometry is described by national standards has maximum energy loss coefficients in all flow ratios. On the other hand, Type 2 manhole with a U-shaped bench on the bottom has minimum energy loss coefficients for all flow ratios. The small loss coefficients make the sewer and rain water collection networks more efficient. Moreover, without knowing the exact manhole loss coefficients the behavior of the network cannot be understood.

When the vector field in the guided manholes (type 2 and type 4) are analyzed, it is clear that the dead eddy zones are either small or very weak. The detention time in the manholes is related with the extent and magnitude of the circulations of zones. Moreover, the better flow field decreases the sedimentation risk in manholes.

REFERENCES

- [1] Zhao, C., Zhu, D.Z and Rajaratnam, N. (2004) Supercritical sewer flow at a combining junction: a model study of Edworthy Trunk Junction, Calgary, Alberta, *Journal of Environmental Engineering and Science*, 3(5), 343-353.
- [2] Zhao, C., Ph, D., Zhu, D.Z. and Rajaratnam, N. (2008) Computational and Experimental Study of Surcharged Flow at a 90 ° Combining Sewer Junction. *Journal of Hydraulic Engineering*, 134(6), 688–700.
- [3] Hosseini, S.M. and Ghasemi, A. (2012) Hydraulic Performance Analysis of Sewer Systems with Uncertain Parameters, *Journal of Hydroinformatics*, 14(3), 682-696.
- [4] Motlagh, Y.Y., Nazemi, A.H., Sadraddini, A.A. and Abbaspour, A. (2013) Numerical Investigation of the Effects of Combining Sewer Junction Characteristics on the Hydraulic Parameters of Flow in Fully Surcharged Condition. *Water and Environment Journal*, 27, 301-316.
- [5] Hager, W.H. and Gisonni, C. (2005) Supercritical Flow in Sewer Manholes. *Journal of Hydraulic Research*, 43(6), 660–667.
- [6] Zhao, C. (2006) Experimental and Computational Investigation of Sewer Flow at Combining Junctions. University of Alberta, Canada.
- [7] Borsche, R. and Klar, A. (2014) Flooding in Urban Drainage Systems: Coupling Hyperbolic Conservation Laws for Sewer Systems and Surface Flow, *International Journal for Numerical Methods in Fluids*, 76, 789–810.
- [8] Goo, Q. and Song, C.S.S. (1991) Dropshaft Hydrodynamics under Transient Conditions, *Journal of Hydraulic Engineering*, 117(8), 1042-1055.
- [9] Zhou, F., Hicks, F.E. and Steffler, P.M. (2002) Transient Flow in a Rapidly Filling Horizontal Pipe Containing Trapped Air, *Journal of Hydraulic Engineering*, 128(6), 625-634.
- [10] Yen, B.C. and Akan, A.O. (2004) *Hydraulic Design Handbook*. McGraw-Hill.
- [11] Sevuk, A.S. and Yen, B.C. (1973) Comparison of four Approaches in Routing Flood Wave Trough Junction, *Proc. Int. Assoc. Hydr. Res. 15th Congress*, 5, 169-172, Istanbul.
- [12] AMEC Earth (2009) *Modeling Hydraulic and Energy Gradients in Storm Sewers: a Comparison of Computational Methods*. Denver, Colorado.
- [13] Abdulwahhab, M., Injeti, N.K. and Dakhil, S.F. (2012) CFD Simulations and Flow Analysis Through a T-Junction. *International Journal of Engineering Science and Technology (IJEST)*, 4(07), 3392-3407.
- [14] Al-Mussawi, W.H., Al-Shammari, M.H. and Alwan, H.H. (2009) Three-Dimensional Numerical Investigation of Flow at 90° Open Channel Junction, *Journal of Kerbala University*, 7(4), 265-272.
- [15] Jarman, D.S., Faram, M.G., Butler, D., Tabor, G., Stovin, V.R., Burt, D. and Throp, E. (2008) *Computational Fluid Dynamics as a Tool for Urban Drainage System Analysis : A Review of Applications and Best Practice*. 11th International Conference on Urban Drainage, Edinburgh, Scotland, UK, 1–10.
- [16] Chen, Z., Han, S., Zhou, F. and Wang, K. (2013) A CFD Modeling Approach for Municipal Sewer System Design Optimization to Minimize Emissions into Receiving Water Body. *Water Resour Management*, 27, 2053–2069.
- [17] Bennett, P., Stovin, V. and Guymer, I. (2011) Improved CFD Simulation Approaches for Manhole Mixing Investigations. 12th International Conference on Urban Drainage, Porto Alegre/Brazil, 1–8.
- [18] Lee, E.W. (2006) Preliminary Study on the Application of Computational Fluid Dynamics to Building Drainage System Design. *Surveying and Built Environment*, 17(1), 35–44.
- [19] Mignot, E., Bonakdari, H., Knothe, P., Kouyi, G. L., Besette, A. and Riviere, N. (2011) Experiments and 3D Simulations of Flow

- Structures in Junctions and of their Influence on Location of Flowmeters. 12th International Conference on Urban Drainage, Porto Alegre/Brazil, 1–8.
- [20] Saiyudthong, C. and Guymer, I. (2005) Simulation of Energy Loss Due to Changes in Pipe Direction Across a Manhole. 10th National Convention on Civil Engineering, Thailand, 5–9.
- [21] Patankar, S.V. (1980) Numerical Heat Transfer and Fluid Flow, Hemisphere Publishing Corporation, USA.
- [22] Versteeg, H.K. and Malalasekera, W. (1995) An Introduction to Computational Fluid Dynamics, The Finite Volume Method, Pearson Education Limited, England.
- [23] Rhie, C.M. and Chow, W.L. (1983) Numerical Study of the Turbulent Flow Past an Airfoil with Trailing Edge Separation, AIAA J. 21(11), 1525-1532.
- [24] Launder B.E. and Spalding D.B. (1974) The Numerical Computation of Turbulent Flows. Computer Methods in Applied Mechanics and Engineering, 3, 269-289.
- [25] Fluent. (2006) User's Guide to Safe computing. Computers & Security, Cavendish Court, Lebanon.
- [26] Marsalek, J. (1985) Head Losses at Selected Sewer Manholes, Special Report No.52, American Public Works Association, Chicago.
- [27] Wang, K.H., Cleveland, T.G., Towsley, C. and Umrigar, D. (1998) Head Loss at Manholes in Pressurized Sewer Systems, J. American Water Resources Association, 34(6), 1391-1400.
- [28] Zhao, C., Zhu, D.Z. and Rajaratnam, N. (2006) Experimental Study of Pressurized Flow at Combining Sewer Junctions, Journal of Hydraulic Engineering, 132(12), 1259-1271.

Received: 1603.2017

Accepted: 08.06.2017

CORRESPONDING AUTHOR

Ismail Hakki Ozolcer

Bulent Ecevit University
Engineering Faculty
Civil Engineering Department
Zonguldak – TURKEY

E-mail: ozolcer@hotmail.com

NEURITOGENIC ACTIVITY OF EPIGALLOCATECHIN GALLATE AND CURCUMIN COMBINATION ON RAT ADRENAL PHEOCHROMOCYTOMA CELLS

Miris Dikmen^{1,2,*}, Elif Kaya-Tilki¹, Selin Engur¹, Yusuf Ozturk¹

¹Anadolu University, Faculty of Pharmacy, Department of Pharmacology, Eskisehir, Turkey

²Anadolu University, Faculty of Pharmacy, Department of Clinical Pharmacy, Eskisehir, Turkey

ABSTRACT

Plant phytochemicals are important neuroprotective agents which mainly act as antioxidants by scavenging stress-induced free radicals in the brain. Phytochemicals from medicinal plants including epigallocatechin gallate and curcumin play a vital role in maintaining the brain's chemical balance by targeting neurotrophins. Many studies have shown that both curcumin, the yellow pigment in turmeric, and (-)-epigallocatechin gallate (EGCG) in green tea possess anti-inflammatory, anti-oxidative stress, tumor reduction, and neuroprotective properties against many neurodegenerative conditions. In this study, the neuritogenic potential of EGCG and curcumin combination treatment were evaluated on PC-12 Adh cells. The neuritogenic potential of EGCG and curcumin combined concentrations were evaluated by the cell differentiation analysis on xCELLigence real time cell analysis system (RTCA-DP) according to the changing in cell index (CI) values. Neurite outgrowth was observed with immunofluorescence staining and neurite lengths were measured. Nerve growth factor (NGF) was used as positive control. Also GAP-43 and β -tubulin mRNA expression levels, which are associated with neurite outgrowth promotion, were determined with RT-PCR method. According to our results, 100 nM EGCG and curcumin combination was significantly induced neurite outgrowth and also particularly up-regulated GAP-43 mRNA expression level on PC-12 Adh cells. The present study supports the notion that polyphenols such as EGCG and curcumin have potential to be effective as neuroprotective agents for the treatment of neurodegenerative diseases.

KEYWORDS:

neurodegeneration, neurite outgrowth, epigallocatechin gallate, curcumin, PC-12

INTRODUCTION

Although the precise mechanisms of oxidative stress are not completely characterized, there are growing interests in establishing therapeutic and dietary strategies to combat oxidative-stress induced damage to the central nervous system [1, 2]. There has been an increasing attention turning towards dietary antioxidants as having therapeutic or protective potential in neurodegenerative disorders, and many antioxidants have been examined, including flavonoids, for their neuroprotective properties. Antioxidant administration can protect neuronal cells from oxidative stress in several *in vitro* models of neurodegenerative diseases [1]. Many antioxidants derived from natural products could reduce toxic neuronal damages and act as neuroprotective agents. Many studies confirmed the efficacy of polyphenol antioxidants in fruits and vegetables such as EGCG from green tea and non-flavonoid polyphenols such as curcumin from turmeric to reduce neuronal death and to diminish oxidative stress [3].

Neurotrophins are important for the survival, maintenance, and regeneration of specific neuronal cells in the brain. Accumulating evidence indicates that dietary phytochemicals may prevent or reverse neurodegenerative disease by targeting neurotrophins that were identified as neuronal survival-promoting proteins in mammals include nerve growth factor (NGF). A decrease in neurotrophins has been associated with the pathology of several neurodegenerative diseases and their physiological symptoms [4]. Among the neurotrophins, NGF has been studied extensively as a drug target because of its strong association with neurodegenerative diseases [2]. Neurite outgrowth from the neurons is one of the critical steps in neuronal development whereas neurite loss is one of the fundamental features of neuronal damage. Promising potential of NGF against neurodegenerative disease by slowing down the progression of neuronal loss is well documented and supported by scientific studies previously [5], but

NGF is a large polypeptide molecule that do not penetrate into the blood brain barrier and also it is metabolized by peptidases when administered peripherally [6]. Therefore, using NGF as a neurotogenic agent is not possible currently. However, potentiating the actions of NGF with natural compounds can be an alternative therapeutic approach.

Curcumin is a polyphenol derived from the rhizome of *Curcuma longa* which has antioxidant, anti-inflammatory and anti-cancer effects and has been described as neuroprotective against neurological disorders such as Alzheimer's disease, multiple sclerosis, Parkinson's disease and epilepsy [7,8,9,10]. Curcumin is a highly lipophilic compound which can cross the blood brain barrier [11]. However, the common mechanisms through which curcumin elicits are not known. EGCG can also cross the blood brain barrier [12], and it is effective in neurodegenerative diseases such as Parkinson's disease through the improvement of progress in neural cell viability [8]. The neuroprotective effect of EGCG may also involve the regulation of antioxidant protective enzymes [13]. Confirmatory studies performed *in vitro* have established that EGCG protects neuronal cells against a wide spectrum of neurotoxic agents [14]. Also EGCG potentiates neurite outgrowth in PC-12 cells by maintaining the reactive oxygen species (ROS) at sublethal level [2].

Bioactive compounds from natural resources have been shown to act synergistically with neurotrophic factors to promote neuritogenesis in the cultured neurons [5]. Natural phytochemicals may not exert toxic side effects inherent to synthetic drugs [11]. Also, these compounds may have a greater potential than synthetic drugs with only one mechanism of action. In light of these data, neurotogenic potential of EGCG and curcumin combination on PC-12 Adh cells was evaluated. In particular, whether the combination of EGCG and curcumin synergistically promoted on neurite outgrowth was investigated.

MATERIALS AND METHODS

Cell culture and treatment. The PC-12 Adh (CRL-1721.1TM) cell line was obtained from ATCC and maintained undifferentiated in DMEM medium containing 10% horse serum, 5% fetal bovine serum and 1% penicillin/streptomycin at 37°C in a humidified incubator with 5% CO₂. To induce differentiation, 1% fetal bovine serum and 1% penicillin/streptomycin containing DMEM differentiation medium was used. NGF was used as positive control at 100 nM concentration. Curcumin and EGCG were dissolved in DMSO and diluted to working concentrations with fresh medium. Control

group was prepared with medium containing 0.1% DMSO.

PC-12 Adh Cell Differentiation Assay with Real-Time Cell Analysis System (RTCA DP). To investigate the differentiation of PC-12 Adh cells and determine the changing over time, a real-time cell analysis was performed with xCELLigence instrument (ACEA Biosciences, San Diego, CA) by using E-plates that contain micro-electrodes and measuring electrical impedance which indicated as cell index (CI) value, a dimensionless parameter which represents cell status [15,16]. NGF, EGCG and curcumin concentrations were used as 100 nM which showed non-cytotoxic effects according to our previous results [17].

Background of the E-plates (Roche Applied Sciences, Indianapolis, IN) were measured in 100 µl differentiation medium in the RTCA DP station. Afterwards, cells were seeded in a 2x10³ density per well onto 96-well E-plates in 100 µM differentiation medium. Cells were incubated up to 24 hours and the impedance of each well were monitored using the RTCA DP device at 1 hour intervals. After incubation the instrument was paused, 100 µl of the current medium was removed, twice of the substance concentrations were added into the wells and diluted to the final concentrations (100 nM) in differentiation medium. Assays were performed in octet and cell-free and concentration-free controls were run in parallel. Cells were monitored for up to 96 hours (4 days) at 1 hour intervals in order to determine the cell differentiation comparatively, according to the CI values of the instrument [17].

Neurite outgrowth analysis. PC-12 Adh cells were plated onto the collagen IV coated 96-well culture plate (BD BioCoatTM Collagen IV Cellware, San Diego, CA) at a density of 2x10³ cells per well in differentiation medium. 24 hours after plating, medium was replaced with 100 µl of 100 nM NGF, EGCG and curcumin alone or combined concentrations. On 4th day, morphometric analysis was performed on digitized images of live cells taken under a Leica DM 300 inverted microscope. Neurite outgrowth analysis was performed as described previously [15,16,17]. Briefly, neurite growth was determined by manually tracing the length of the longest neurite and branch (if present) on images by using Leica LAS Image Analysis programme in pixels then converted to µm by using ImageJ (NIH). Totally 50 neurites were measured for each concentration group. Total length was divided to 50 to find the average neurite length per group. Experiments were repeated at least three times independently.

Immunofluorescence staining. After neurite outgrowth analysis, cells were fixated with 80% methanol for 5 minutes and rinsed twice with 1xPBS

then permeabilized with 0.1% PBS-Tween 20 for 20 minutes. After two washes in PBS, the cells were incubated in 1%BSA/5% fetal bovine/5% horse serum/0.3M glycine in 0.1% PBS-Tween solution for 1 hour to permeabilise the cells and block non-specific protein-protein interactions. The anti-beta III tubulin antibody [2G10] (Abcam, Cat. No: ab78078, RRID: AB-2256751) was diluted 1:250 in the same solution and then the cells were incubated with 100 μ l of antibody overnight at +4°C. After the incubation period, cells were rinsed twice with PBS and secondary antibody goat anti-mouse IgG H&L (Alexa Fluor®488), (Abcam, Cat. No: ab150113, RRID:AB_2576208) at a 1:500 dilution was added to the wells and incubated for 1 hour in room temperature. Hoechst 33258 (10 μ g/ml) was used to stain the cell nuclei (blue) 10 minutes before the imaging with Cytation 3 Cell Imaging Multi-Mode Reader (Bio-Tek, USA).

Determination of Growth Associated Protein-43 (GAP-43) and Beta III-Tubulin (TUBB3) mRNA Expression Levels by Using RT-PCR Method. Growth Associated Protein-43(GAP-43) and Beta III-Tubulin (TUBB3) mRNA expression levels associated with neurite outgrowth pathway were determined with RT-PCR. PC-12 cells were seeded on 6-well plate 1×10^6 density per well and treated with 100 nM NGF, EGCG and curcumin alone or combined concentrations. After 4 days incubation period, cells were scratched and transferred into a tube containing MagNA Lyser Green Beads and the cell homogenization process started by using the MagNA Lyser Instrument. Subsequently, MagNA Pure Compact RNA Isolation Kit (Roche, Lot: 13243700) procedure was performed by using the MagNA Pure LC 2.0 system. The high quality of the RNA samples were confirmed by using the NanoDrop Instrument. From each RNA population, 500 ng total RNA was used

for cDNA synthesis with the Transcriptor High Fidelity cDNA Synthesis Kit (Roche, Lot: 14856520). The resulting total cDNA was then used in PCR to measure the GAP-43 and TUBB3 mRNA expression levels. The mRNA expression levels of β -actin were used as an internal positive control. Expressions of GAP-43 and TUBB3 genes were determined by using SYBR® Green based RT-PCR with PrimePCR™ primers, reagents (Bio-Rad) and LightCycler 480 (Roche). Samples were tested in triplicate runs, and specific mRNA levels quantified and compared with β -actin using Roche LC480 real-time PCR analysis software (version 1.5.0).

Statistical Analysis. Data were analyzed by one way ANOVA with Tukey's post-hoc, expressed as mean \pm standard error, $p > 0.05$ n.s., $p < 0.05^*$, $p < 0.01^{**}$, $p < 0.001^{***}$.

RESULTS

Determination of non-cytotoxic concentrations. In order to determine non-cytotoxic concentrations of EGCG, neuronal viability was determined by WST-1 method. In our previous study, 100 μ M curcumin was found non-cytotoxic on PC-12 cell viability (data not shown). As seen on Figure 1, EGCG significantly decreased PC-12 cell viability at 100, 200 and 400 μ M concentrations ($***p < 0.001$) for both 24 and 48 hours. Also, 1 and 10 μ M EGCG concentrations were reduced the cell viability non-significantly ($p > 0.05$). According to the WST-1 assay results, non-cytotoxic concentrations of EGCG concentrations were determined as 10 and 100 nM. For the further experiments in this study, 100 nM EGCG and curcumin concentrations were used (Figure 1).

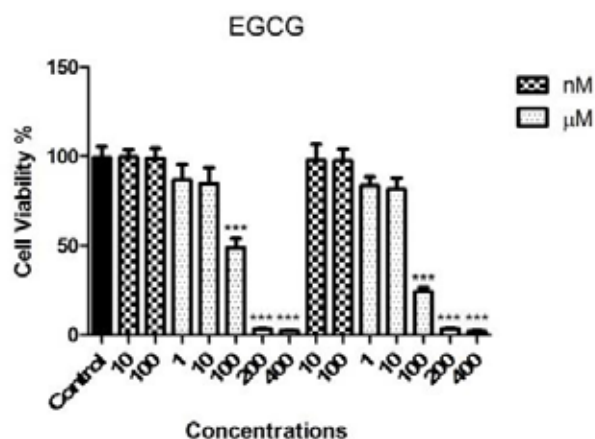


FIGURE 1

The effects of EGCC on PC-12 Adh cell viability. The results are the means of 3 independent experiments ($n=8$). The error bars represent the standard deviations ($p < 0.001^{***}$, significant compared to the control).

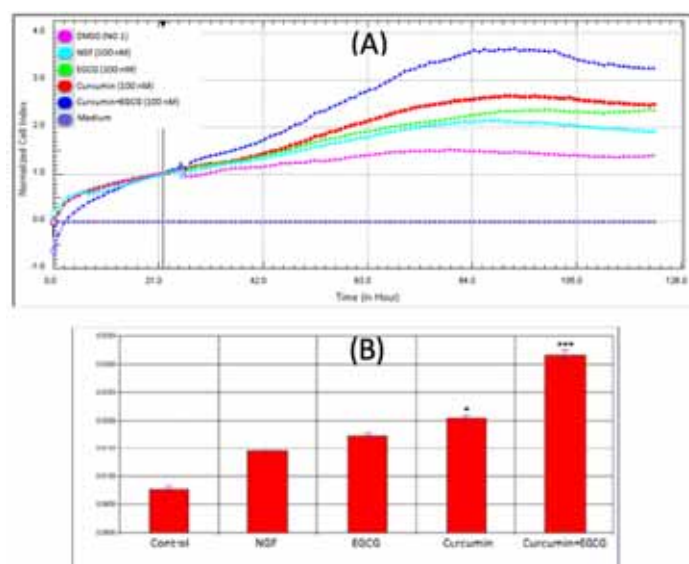


FIGURE 2

Real-time monitoring of control (0.1% DMSO), NGF (positive control), EGCG, curcumin, and EGCG+curcumin combination concentrations on PC-12 Adh cells according to the CI value changes during 4 days (96 hours) using RTCA-DP System (A), ($n=8$), all concentrations were 100nM. Slope graph was drawn according to the changing in the CI values (B), ($p>0.05$ n.s., $p<0.05^*$, $p<0.001^{***}$).

Effects of EGCG and Curcumin on PC-12 Adh Cell Differentiation. Neuronal differentiation % graph was drawn according to the CI values on 96th hour (Figure 2). According to the graphics, around 30th hour, differentiation has been started and the experiment was terminated around 96th hour. The rapid increase in the CI values were accepted as the initial stages of differentiation [18]. Because during the initiation, cell body becomes larger which cause an increase in the impedance, and then, the cell begins to extend neurites and cell body shrinks which cause a drop in the impedance. The CI values of the control group (untreated) obtained from RTCA DP instrument were like a plateau; however, the EGCG and curcumin alone or combination concentration groups showed rapid increase which were higher than the NGF positive control group (Figure 2A). Especially 100 nM EGCG and curcumin combination group showed the highest increase and neuronal differentiation levels of 100 nM alone EGCG and curcumin concentrations were almost same (Figure 2B).

Effects of Curcumin and EGCG on Neurite Outgrowth. PC-12 Adh cells were treated with 100 nM curcumin and EGCG for 4 days. At the end of the incubation, the wells were photographed and morphometric analysis was performed on 50 cells randomly for each group. Total neurite length was determined by manually tracing the length of the longest neurite and branch on images. As it is seen on Figure 3, the highest total neurite length was obtained with 100 nM curcumin and EGCG

combination concentration which has the highest neuritogenic effect on PC-12 Adh cells. Average neurite length of the cells treated with only 100 nM curcumin and 100 nM EGCG groups were also showed slightly higher neuritogenic effects than the cells treated with only 100 nM NGF group. This data support neuronal differentiation results. Immunofluorescence staining was performed with anti beta-III tubulin antibody related with neurite outgrowth. Cell nucleus was stained with Hoechst dye. In the images, neuronal differentiations and neurite outgrowth were stimulated by 100 nM curcumin and EGCG alone or combination concentrations according to solvent (0.1% DMSO) and NGF positive control groups (Figure 4).

Beta III-Tubulin (TUBB3) and Growth Associated Protein-43 (GAP43) mRNA Expression Levels. In this study, neurite outgrowth marker TUBB3 and GAP-43 mRNA expression levels of the cells were investigated. As it is shown in Figure 5, with all curcumin and EGCG groups, TUBB3 mRNA expression levels were increased according to the NGF positive control group. Especially, with alone curcumin and, curcumin and EGCG combination concentrations, mRNA expression levels were increased almost 2 fold.

As it is shown in Figure 5, GAP-43 mRNA expression levels were also increased with curcumin and EGCG concentrations compared to the NGF group. Especially 100 nM curcumin and EGCG combination increased GAP-43 mRNA expression levels almost 24 fold according to 100 nM NGF.

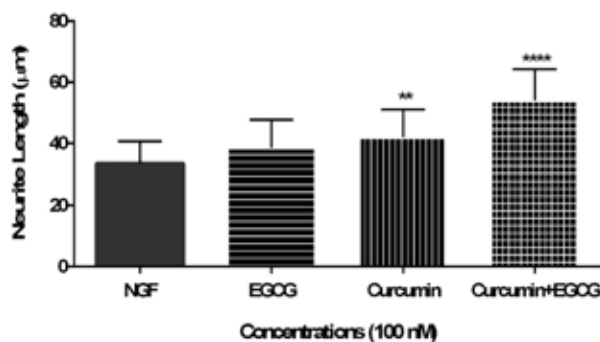


FIGURE 3

Neurite outgrowth analysis. Comparison of average neurite lengths on 4th day. Data are mean \pm SD values ($p < 0.01$ **, $p < 0.001$ ***; compared to NGF (positive control).

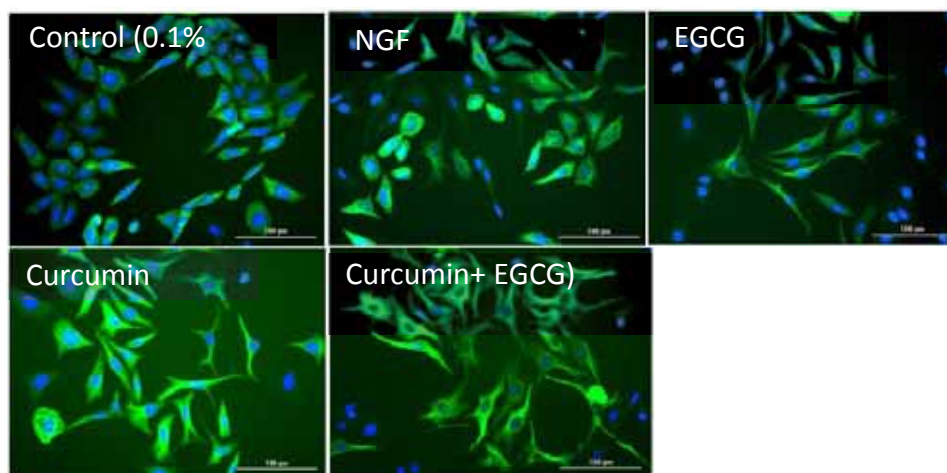


FIGURE 4

The images of PC-12 Adh cells were treated with 100 nM NGF, Curcumin, EGCG and Curcumin+EGCG on 4th day. Cell nuclei were stained with Hoechst 33258 (blue) and tubulins were stained with AlexaFluor@488 (green). Images were taken with Cytation 3 Cell Imaging Multi-Mode Reader with 20x objective.

DISCUSSION

Neuronal injury and degeneration are responsible for various neurodegenerative disorders that are associated with loss of brain cells and axons resulting in functional deficits. Due to limited regeneration capacity of damaged neurons, the regulation of neurite outgrowth is crucial in developing strategies to promote axon and dendrite regeneration after nerve injury and in degenerative diseases [19]. Many recent studies has focused on the specific components of the active herbs and the therapeutic effects of well-known active ingredients still need to be clarified with regard to their potential therapeutic effects, particularly their effects on neurodegenerative diseases [11]. Therefore, in this study the neuroprotective effects of the plant-derived well-known active compounds EGCG and curcumin combination on neuronal differentiation and neurite outgrowth. The effects of EGCG and curcumin

without NGF signaling were compared with combined concentrations.

PC-12 Adh cell line, a widely used neuron-like cell culture model derived from rat pheochromocytoma and it is a very popular model for studying cell differentiation and have capacity to grow neurite-like processes in response to NGF for neuronal differentiation and neurite outgrowth studies [20]. According to our results, the highest neuronal differentiation and neurite outgrowth were determined with 100 nM EGCG+curcumin combination according to 100 nM NGF after 4 days of treatment. Also, the effects of 100 nM curcumin alone on neuronal differentiation and neurite outgrowth were higher than 100 nM EGCG. These results were also supported with immunofluorescence cell imaging. In accordance with our results, it was evaluated that curcumin significantly increased the neurite lengths of the PC-12 Adh cells after 4 days of treatment [20]. It has

been reported that curcumin repaired the distorted neurites around the senile plaques in an Alzheimer mouse model, increased the number of neurites of pre-differentiated PC-12 Adh cells, and promoted neurite outgrowth without the presence of NGF [20, 21].

EGCG could be a potential therapeutic or modulating agent for neurodegenerative and other diseases influenced by oxidative damage [1], because of the active polyphenolic structure responsible for the potentiation of NGF induced neuritogenesis and activation of the ERK pathway [22]. In this respect, our results are similar with the previously published studies where EGCG alone or green tea extract induced neurite outgrowth [23, 24]. Mandel et al. (2003) reported that EGCG (0.1 and 1 μ M) significantly protects rat pheochromocytoma PC-12 cells from apoptosis induced by serum support withdrawal, suggesting that EGCG may play a role in the growth of PC-12 cells [25].

Neurite outgrowth depends on the coordinated work of actin and microtubules to establish cytoskeletal networks and neurite morphology. Previous reports also showed that curcumin affects the microtubule dynamics [20]. Neurotrophic factors, such as NGF, are a family of secreted proteins that play vital roles in promoting neural growth and survival during development, and are crucial for maintaining the integrity of neurons throughout an individual's entire lifetime. There is growing evidence about reduced neurotrophic

support is a significant factor in the pathogenesis of neurodegenerative diseases. Therefore, neurotrophic factors are attractive candidates for therapeutic agents in chronic neurodegenerative diseases and acute injuries including trauma and stroke. However, therapeutic application of neurotrophic factors is severely restricted by their poor penetration of the blood–brain barrier and undesirable apoptotic effect through interaction with the p75NTR receptor. Thus, there remains the need for identification of small molecules that are safe, nontoxic, and can mimic the neurotrophic action as an alternative therapy approach [17, 15, 26]. The extent of PC-12 Adh differentiation is therefore typically evaluated by counting the number of cells with expending neuritis or by measuring neurite length. To evaluate the neurotrophic effects of NGF and/or test compounds, the culture medium was shifted to low serum medium to induce transition from a proliferative phase to differentiation stage [15, 21]. The RTCA-DP system measures changes in impedance as cells attach with a readout given as cell index (CI) value and monitors cell behaviour in real time. An increase in the number of cells attaching, an increase in cell size or an increase in the strength of adhesion results in an increased CI value. Unexpectedly, the differentiated cells appear to adhere quicker to the surface than undifferentiated cells; however, the impedance falls off rapidly because they are not proliferating [18].

Sample Name	Target Name		Tgt Cp Mean	Ref. Cp Mean	Ratios	
	Targets	References			Tgt/Ref.	Norm
DMSO	GAP43	ACTB	38.65	19.93	2.31E-6	1.000
NGF	GAP43	ACTB	38.55	21.16	5.83E-6	2.527
Curcumin	GAP43	ACTB	34.82	20.90	6.44E-5	27.88
EGCG	GAP43	ACTB	37.39	21.04	1.20E-5	5.188
Curc EGCG	GAP43	ACTB	34.07	20.95	1.12E-4	48.65

Sample Name	Target Name		Tgt Cp Mean	Ref. Cp Mean	Ratios	
	Targets	References			Tgt/Ref.	Norm
DMSO	TUBB3	ACTB	36.58	19.93	9.67E-6	1.000
NGF	TUBB3	ACTB	36.33	21.16	2.72E-5	2.816
Curcumin	TUBB3	ACTB	35.01	20.90	5.64E-5	5.834
EGCG	TUBB3	ACTB	35.46	20.80	3.86E-5	3.993
Curc EGCG	TUBB3	ACTB	35.06	20.95	5.67E-5	5.859

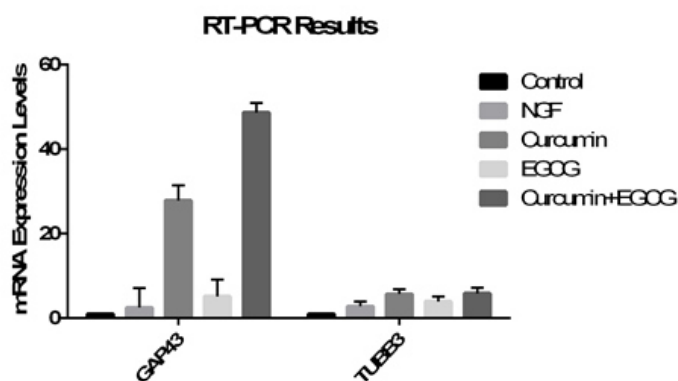


FIGURE 5
Neurite outgrowth marker GAP-43 and TUBB3 mRNA expression levels on 4th day.

GAP-43 contributes to neuronal growth and nerve terminal plasticity. The growth-associated protein (GAP-43) is associated with presynaptic neuronal outgrowth and neuronal plasticity in general [16, 21]. GAP-43 is a nervous system-specific phosphoprotein that is specifically enriched in the membrane skeleton of growth cones. In primary neuronal cultures and in NGF induced PC-12 Adh cells, GAP-43 expression correlates with the onset of neuronal differentiation as seen by the elongation of neurites and localization of the protein in the growth cones. Among the various tissue types and cell types that have been examined, GAP-43 mRNA is expressed only in neurons [27]. According to our results, EGCG and curcumin combination exerted neurotrophic action and promoted PC-12 Adh neurite outgrowth accompanied with the expression of neuronal differentiation marker GAP-43.

In conclusion, EGCG and curcumin combination acted synergistically on neuronal differentiation and neurite outgrowth. Natural phytochemical compounds also may be an important approach for the treatment of some neurodegenerative diseases.

REFERENCES

- [1] Koh, S.H., Kim, S.H., Kwon, H., Park, Y., Kim, K.S., Song, C.W., Kim, J., Kim, M.H., Yu, H.J., Henkel, J.S. and Jung, H.K. (2003) Epigallocatechin gallate protects nerve growth factor differentiated PC12 cells from oxidative-radical-stress-induced apoptosis through its effect on phosphoinositide 3-kinase/Akt and glycogen synthase kinase-3. *Mol Brain Res*, 118, 72-81.
- [2] Uguz, A.C., Oz, A. and Naziroglu, M. (2016) Curcumin inhibits apoptosis by regulating intracellular calcium release, reactive oxygen species and mitochondrial depolarization levels in SH-SY5Y neuronal cells. *J Recept Sig Transd*, 36, 395-401.
- [3] Ataie, A., Shadifar, M. and Ataee, R. (2016) Polyphenolic antioxidants and neuronal regeneration. *Basic and Clinical Neuroscience*, 7, 81-90.
- [4] Uguz, A.C., Naziroglu, M., Espino, J., Bejarano, I., Gonzalez, D., Rodriguez, A.B. and Pariente, J.A. (2009) Selenium modulates oxidative stress-induced cell apoptosis in human myeloid HL-60 cells through regulation of calcium release and caspase-3 and -9 activities. *J Membr Biol*, 232, 15-23.
- [5] Phan, C.W., Sabaratnam, V., Bovicelli, P., Righi, G. and Saso, L. (2016) Negletein as a neuroprotectant enhances the action of nerve growth factor and induces neurite outgrowth in PC12 cells. *BioFactors*, 42, 591-599.
- [6] Maruoka, H., Sasaya, H., Sugihara, K., Shimoke, K. and Ikeuchi, T. (2011) Low-molecular-weight compounds having neurotrophic activity in cultured PC12 cells and neurons. *J Biochem*, 150, 473-475.
- [7] Mendonca, L.M., da Silva Machado, C., Teixeira, C.C.C., de Freitas, L.A.P., Bianchi, M.D.L.P., Antunes, L.M.G. (2013) Curcumin reduces cisplatin-induced neurotoxicity in NGF-differentiated PC12 cells. *Neurotoxicology*, 34, 205-211.
- [8] Shahpiri, Z., Bahramsoltani, R., Hosein Farzaei, M., Farzaei, F. and Rahimi, R. (2016) Phytochemicals as future drugs for Parkinson's disease: a comprehensive review. *Rev Neuroscience*, 27, 651-668.
- [9] Subramaniam, D., Thombre, R., Dhar, A. and Anant, S. (2014) DNA Methyltransferases: A Novel Target for Prevention and Therapy. *Front Oncol*, 4, 80
- [10] Liu, Z., Xie, Z., Jones, W., Pavlovicz, R.E., Liu, S., Yu, J., Li, P.K., Lin, J., Fuchs, J.R., Marcucci, G., Li, C. and Chan, K.K. (2009) Curcumin is a potent DNA hypomethylation agent. *Bioorg Med Chem Lett*, 19, 706-9.
- [11] Venkatesan, R., Ji, E. and Kim, S.Y. (2015) Phytochemicals that regulate neurodegenerative disease by targeting neurotrophins: a comprehensive review. *Biomed Res Int*, 2015, 1-22.
- [12] Saganuma, M., Okabe, S., Oniyama, M., Tada, Y., Ito, H. and Fujiki, H. (1998) Wide distribution of [3H](-)-epigallocatechin gallate, a cancer preventive tea polyphenol, in mouse tissue. *Carcinogenesis*, 19, 1771-1776.
- [13] Mandel, S., Weinreb, O., Amit, T. and Youdim, M.B. (2004) Cell signaling pathways in the neuroprotective actions of the green tea polyphenol (-)- epigallocatechin -3- gallate: implications for neurodegenerative diseases. *J Neurochem*, 88, 1555-1569.
- [14] Mandel, S., Reznichenko, L., Amit, T. and Youdim, M.B. (2003) Green tea polyphenol (-)-epigallocatechin-3-gallate protects rat PC12 cells from apoptosis induced by serum withdrawal. *Neurotox Res*, 5, 419-424.
- [15] Mustafa, A.M., Maggi, F., Papa, F., Kaya, E., Dikmen, M. and Ozturk, Y. (2016) Isofuranodiene: A neuritogenic compound isolated from wild celery (*Smyrnum olusatrum* L., Apiaceae). *Food Chem*, 192, 782-787.
- [16] Mustafa, A.M., Caprioli, G., Dikmen, M., Kaya, E., Maggi, F., Sagratini, G., Vittori, S. and Ozturk, Y. (2015) Evaluation of neuritogenic activity of cultivated, wild and commercial roots of *Gentiana lutea* L. *J Funct Foods*, 19, 164-173.
- [17] Kaya-Tilki, E., Dikmen, M. and Ozturk, Y. (2016) Effects of DNMT and HDAC Inhibitors (RG108 and Trichostatin A) on NGF-induced Neurite Outgrowth and Cellular Migration. *Int J Pharmacol*, 12, 351-360.

- [18] Dwane, S., Durack, E. and Kiely, P.A. (2013) Optimising parameters for the differentiation of SH-SY5Y cells to study cell adhesion and cell migration. *BMC Res Notes*, 6, 366.
- [19] Wu, C.L., Chou, Y.H., Chang, Y.J., Teng, N.Y., Hsu, H.L. and Chen, L. (2012) Interplay between cell migration and neurite outgrowth determines SH2B1beta-enhanced neurite regeneration of differentiated PC12 cells. *PLoS one*, 7, e34999.
- [20] Bora-Tatar, G. and Erdem-Yurter, H. (2014) Investigations of Curcumin and Resveratrol on Neurite Outgrowth: Perspectives on Spinal Muscular Atrophy. *BioMed Res Int*, 2014, 8.
- [21] Liao, K.K., Wu, M.J., Chen, P.Y., Huang, S.W., Chiu, S.J., Ho, C.T. and Yen, J.H. (2012) Curcuminoids Promote Neurite Outgrowth in PC12 Cells through MAPK/ERK- and PKC-Dependent Pathways. *J Agr Food Chem*, 60, 433–443.
- [22] Lee, M.-J., Maliakal, P., Chen, L., Meng, X., Bondoc, F.Y., Prabhu, S., Lambert, G., Mohr, S. and Yang, C.S. (2002) Pharmacokinetics of tea catechins after ingestion of green tea and (–)-epigallocatechin-3-gallate by humans: formation of different metabolites and individual variability. *Cancer Epidemiol Biomarkers Prev*, 11, 1025–1032.
- [23] Reznichenko, L., Amit, T., Youdim, M.B.H. and Mandel, S. (2005) Green tea polyphenol (–)- epigallocatechin -3- gallate induces neurorescue of long-term serum-deprived PC12 cells and promotes neurite outgrowth. *J Neurochem*, 93, 1157–1167.
- [24] Shurygin, A.Y., Viktorov, I.V., Ignatova, E.A., Skorokhod, N.S., Abramova, N.O. and Malysheva, O.S. (2004) Stimulatory effect of green tea extract on the growth of neurites in the rat spinal ganglion culture. *Bull Exptl Biol Med*, 138, 262–263.
- [25] Mandel, S., Reznichenko, L., Amit, T. and Youdim, M.B. (2003) Green tea polyphenol (–)-epigallocatechin-3-gallate protects rat PC12 cells from apoptosis induced by serum withdrawal. *Neurotox Res*, 5, 419-424.
- [26] Hu, S.Q., Cui, W., Mak, S.H., Choi, C.L., Hu, Y.J., Li, G., Tsim, K.W., Pang, Y.P. and Han, Y.F. (2015) Robust Neuritogenesis-Promoting Activity by Bis(heptyl)-Cognitin Through the Activation of alpha 7-Nicotinic Acetylcholine Receptor/ERK Pathway, *CNS Neurosci Ther*, 21, 520-9.
- [27] Holahan, M.R. (2015) GAP-43 in synaptic plasticity: molecular perspectives. *Res Rep Biochem*, 5, 137-146.

Received: 20.03.2017

Accepted: 11.05.2017

CORRESPONDING AUTHOR

Miris Dikmen

Anadolu University
Faculty of Pharmacy
Department of Pharmacology
26470 Eskisehir – TURKEY

E-mail: mirisd@anadolu.edu.tr

COMPARING THE VOLUME METHODS THROUGH USING DIGITAL ELEVATION MODELS CREATED BY DIFFERENT INTERPOLATION METHODS

Nazan Yilmaz*

Karadeniz Technical University, Faculty of Engineering, Department of Geomatics, 61080 Trabzon, Turkey

ABSTRACT

The digital elevation model is a model which defines the surface of land three-dimensional and has been created through the elevation data of the land. The digital elevation model has been widely used in the fields of application such as, preparation of road projects, excavation-filling-related volume calculations, land arrangement studies, etc. The volume calculations which is the subject of this study and have been used in a variety of engineering services, have often been used in the reserve determination of mine sites, in the determination of splitting and filling soil removal works of the sites such as, road, airport, tunnels etc. Since the amount of the calculated volume burdened financially great expenses to employer, the calculations must be made in a precise manner. The aim of this study is to make and compare the volume calculations with different grid ranges and different interpolation methods. In this study, grid ranges were selected as 50 m, 100 m, 150 m and 200 m. The interpolation methods used are Inverse Distance to a Power ($k=1$ and $k=2$), Point Kriging, Minimum Curvature, Modified Shepard's Method, Natural Neighbor, Nearest Neighbor, Polynomial Regression (simple planar surface), Multi-quadratic Radial Basis Function, Triangulation with Linear Interpolation. The volume calculation methods used are Trapezoidal rule, Simpson's rule, Simpson's 3/8 rule. The digital elevation models were prepared in the "Surfer 8" program. The surface modeling of the land is made through the chosen different interpolation methods and the grid extended files of these resulting surfaces were created. Afterwards, the volumes of these surfaces with reference to the selected reference surface, $Z = 0$, were determined with different methods and were compared.

KEYWORDS:

Digital elevation model, Interpolation methods, Volume calculation, Surfer Software

INTRODUCTION

The volume calculations are important requirement of the construction and mining industry. The accurate volume estimation is important in many applications, for example road project, mining enterprise, geological works and building applications. The traditional methods such as the trapezoidal method (rectangular or triangular prisms), traditional cross sectioning (trapezoidal, Simpson, and average formula), and improved methods (Simpson-based, cubic spline, and cubic Hermite formula) have been used in volume computing. The main elements of these methods are to collect the points that appropriate distribution and density. These methods need more mathematical processes and take more time. The difficulties have been overcome by developments in computer technologies. The corrections of volume is direct proportional with the presentations of land surface in a best representation of land surface in best form is depend on the number of certain X, Y, Z coordinate points. The total station instrument has been used to determine the certain coordinate for land surface [1].

A digital elevation model (DEM) is a numerical representation of topography, usually made up of equal-sized grid cells, each with a value of elevation. Its simple data structure and widespread availability have made it a popular tool for land characterization. Because topography is a key parameter controlling the function of natural ecosystems, DEMs are highly useful to deal with ever-increasing environmental issues [2].

An elevation model can be represented as regular or irregular point clouds formed into a mathematical model. In order to represent the continuous Earth surface these point clouds should form into the shape of the surface. There are various methods for doing this and Triangulated Irregular Network (TIN) is one of the most popular models [3].

DEM quality is a function of (i) the quality of the individual data points within the surface, (ii) the density of data points used to represent the surface, and (iii) the distribution of data points within the surface. Both (ii) and (iii) are related to the field sampling strategy and to the hardware used to collect the data [4].

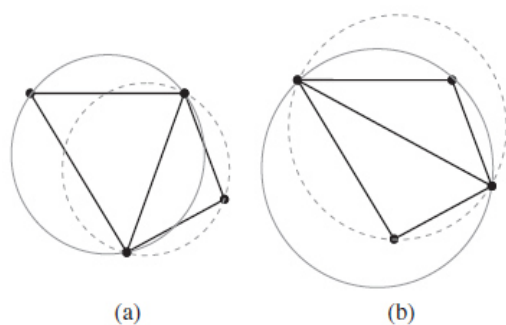


FIGURE 1
Circumcircle property of Delaunay triangulation. (a) A Delaunay triangulation. (b) Not a Delaunay triangulation because a circumcircle contains more than three points [9].

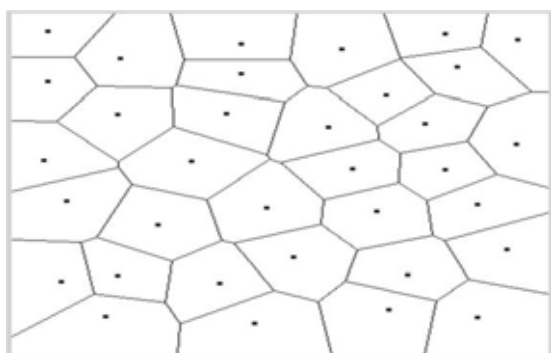


FIGURE 2
Voronoi diagram [10].

Surveys to collect data used to create DEMs can be airborne (e.g. photogrammetry, laser scanning and remote sensing, in particular space borne radar interferometry) or ground based (total station, global positioning system, including, most recently, terrestrial laser scanning) depending on the size of the reach and available technology [5, 6].

TRIANGULAR IRREGULAR NETWORK (TIN)

Triangular irregular network (TIN) and regular grid DEM are two commonly used terrain models. TIN can dynamically adjust storage terrain data according to terrain fluctuation and address the terrain characteristic curve appropriately to reproduce the actual terrain. The topological relation of GRID terrain data is simple and easy to store. However, data redundancy occurs because of the fixed and single topological relation of terrain data [7].

The irregularly spaced points of the TIN model can provide a more faithful representation of the terrain surface with more points in rugged terrain areas and fewer points in relatively flat areas. The TIN model suits visualization purposes because of the

continuous nature that the triangular facets of the model add to the digital representation. Furthermore, not much information can be derived from TIN models because unlike the case for DEM's, a comprehensive analysis framework for triangulated models does not yet exist. In a TIN model, the sample points are simply connected by lines to form triangles, which are represented by planes, which give a continuous representation of the terrain surface. Creating a TIN, despite its simplicity, requires decisions about how to pick the sample points from the original data set, and further how to triangulate them. When it comes to triangulating the sample points, a few triangulation methods are available for producing a TIN. Among the existing triangulation methods that are in use, the Delaunay Triangulation (DT) is very common and popular for its rigorous structure although it produces triangles that are not hierarchical [8].

DELAUNAY TRIANGULATION

Delaunay triangulation, a triangular mesh that connects a set of points in a plane, was proposed by Boris Delaunay in 1934. Delaunay triangulation maximizes the minimum angle of the triangles in the triangular mesh; therefore, the skinny triangles can be avoided to produce a better visual effect. Delaunay triangulation has many applications such as 3D object modeling and scatter interpolation.

Voronoi Diagram is a set of discrete points partitioning the plane into a set of polygon such that all points are nearest to any one site. Voronoi diagram is constructed by the lines of perpendicular bisectors which connect two neighbors. This diagram is approximate representation of nodes in the form of state in near distance or time.

Delaunay Triangulation is used to obtain the two nearest neighboring sites by taking shortest edge in triangulation. It is formed by partitioning a given site into triangles such that circumcircle of sites does not contain each other. Also, Delaunay Triangulation can be constructed by joining the nodes which share a common edge in the Voronoi diagram.

INTERPOLATION METHODS

Data were analysed, interpolated and visualized with Surfer 8.00 [11]. Interpolation methods are briefly described in [12, 2, 13, 14, 15, 16].

VOLUME CALCULATIONS

In surfer, three methods are used to determine volumes: Trapezoidal Rule, Simpson's Rule, and Simpson's 3/8 Rule. Mathematically, the volume under a function $f(x, y)$ is defined by a double integral

$$V = \int_{x_{min}}^{x_{max}} \int_{y_{min}}^{y_{max}} f(x, y) dx dy \quad (1)$$

In Surfer, this is computed by first integrating over X (the columns) to get the areas under the individual rows, and then integrating over Y (the rows) to get the final volume.

Surfer approximates the necessary one-dimensional integrals using three classical numerical integration algorithms: extended trapezoidal rule, extended Simpson's rule, and extended Simpson's 3/8 rule. In the following formula, Δx represents the grid column spacing, Δy represents the grid row spacing and H_{ij} represents the grid node value in row i and column j .

Extended Trapezoidal Rule;

$$A_i = \frac{\Delta x}{2} [H_{i,1} + 2H_{i,2} + 2H_{i,3} + \dots + 2H_{i,ncol-1} + H_{i,ncol}] \quad (2)$$

$$V \cong \frac{\Delta y}{2} [A_1 + 2A_2 + 2A_3 + \dots + 2A_{ncol-1} + A_{ncol}] \quad (3)$$

The pattern of the coefficients is $\{1, 2, 2, 2, \dots, 2, 2, 1\}$.

Extended Simpson's Rule;

$$A_i = \frac{\Delta x}{3} [H_{i,1} + 4H_{i,2} + 2H_{i,3} + 4H_{i,4} + \dots + 2H_{i,ncol-1} + H_{i,ncol}] \quad (4)$$

$$V \cong \frac{\Delta y}{3} [A_1 + 4A_2 + 2A_3 + 4A_4 + \dots + 2A_{ncol-1} + A_{ncol}] \quad (5)$$

The pattern of the coefficients is $\{1, 4, 2, 4, 2, 4, 2, \dots, 4, 2, 1\}$.

Extended Simpson's 3/8 Rule;

$$A_i = \frac{3\Delta x}{8} [H_{i,1} + 3H_{i,2} + 3H_{i,3} + 2H_{i,4} + \dots + 2H_{i,ncol-1} + H_{i,ncol}] \quad (6)$$

$$V \cong \frac{3\Delta y}{8} [A_1 + 3A_2 + 3A_3 + 2A_4 + \dots + 2A_{ncol-1} + A_{ncol}] \quad (7)$$

The pattern of the coefficients is $\{1, 3, 3, 2, 3, 3, 2, \dots, 3, 3, 2, 1\}$ [11, 17, 1].

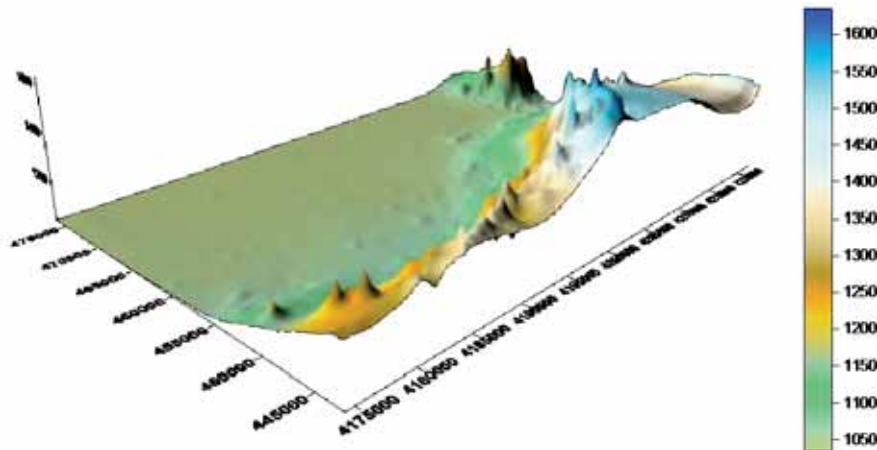


FIGURE 3
Three-dimensional surface view of the study area

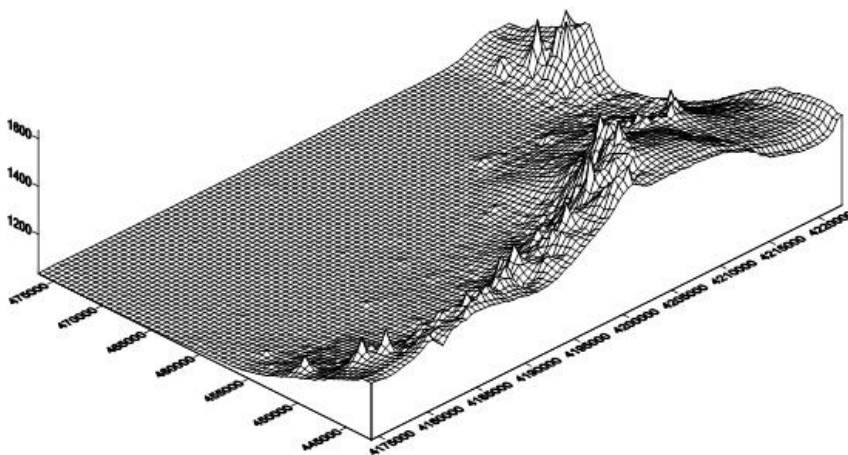


FIGURE 4
Three-dimensional view of the study area by the wireframe method

TABLE 1
The results of the volumes calculated with different volume calculation methods depending on the different interpolation methods and grid ranges

Interpolation methods	Grid ranges (m)	Volume calculation methods		
		Trapezoidal rule	Simpson's rule	Simpson's 3/8 rule
Inverse Distance to a Power (k=1)	50	1873063892573.60	1873053304065.40	1873064832869.50
	100	1873059712549.10	1873031819106.40	1873063854823.70
	150	1873047910977.70	1873044834373.50	1873038277428.80
	200	1873118855689.20	1873077533053.40	1873075626208.90
Inverse Distance to a Power (k=2)	50	1874988732022.50	1874983517357.80	1874989438476.00
	100	1874983336793.00	1874968392886.10	1874983630882.30
	150	1874979095000.20	1874975664864.80	1874975645025.50
	200	1875021088515.50	1875008182482.70	1875012230840.70
Kriging	50	1890669126848.40	1890664648539.00	1890669499593.70
	100	1890660938849.80	1890665785794.20	1890658667976.40
	150	1890663981903.90	1890651355131.90	1890660994133.80
	200	1890656510689.50	1890650019559.00	1890637786303.80
Minimum Curvature	50	1887255486394.60	1887252201199.40	1887252202665.40
	100	1883970464527.90	1883963925645.10	1883963896059.80
	150	1876261658283.20	1876254349189.40	1876255619304.20
	200	1880519658141.10	1880506202368.30	1880504208000.60
Modified Shepard's Method	50	1695389648358.00	1695414183124.80	1695397784210.80
	100	1695419879930.40	1695457080993.70	1695419061048.00
	150	1695394176404.30	1695271395651.00	1695503792596.10
	200	1695347759194.40	1695585380221.40	1695293885257.30
Natural Neighbor	50	1431232295188.70	1431264700544.10	1431270420902.90
	100	1426287826183.50	1426384070515.50	1426252849094.70
	150	1421137309559.90	1421355816146.20	1421183594979.40
	200	1416440820929.10	1416514253713.80	1416561413218.10
Nearest Neighbor	50	1882348910460.40	1882347606946.50	1882348121508.00
	100	1882364418326.70	1882348305723.30	1882389499454.90
	150	1882351613301.90	1882435927709.10	1882371998262.00
	200	1882398585456.00	1882361662497.80	1882364937768.50
Polynomial Regression	50	1848148187924.90	1848148187924.90	1848148187924.90
	100	1848148187924.90	1848148187924.90	1848148187924.90
	150	1848148187924.90	1848148187924.90	1848148187924.90
	200	1848148187924.90	1848148187924.90	1848148187924.90
Radial Basis Function	50	1895047179544.60	1895038765860.20	1895046695774.50
	100	1895051043047.00	1895058190116.80	1895046343354.30
	150	1895046555132.40	1895019253479.40	1895047703609.50
	200	1895036682491.70	1895031171674.10	1895007245275.10
Triangulation with Linear Interpolation	50	1436555123600.20	1436634127195.00	1436616258308.90
	100	1436336475464.00	1436560750795.30	1436491325418.90
	150	1436145696855.70	1436454584369.30	1436620300762.60
	200	1435565412824.90	1436354350787.70	1436015289880.00

MATERIALS AND METHODS

Study area. In practice, geodetic network with 1175 points, which was established in Konya, was used. x, y coordinates of these points were measured by GPS and the orthometric heights of which, were measured by levelling method. Minimum and maximum orthometric heights of these reference points were 1034.541 m and 1671.294 m, moreover, the topographical structure of the land was indicated in the form of three dimensional surfaces in Figure 3 and in the form of wireframe in Figure 4. The range in x and y directions of Gauss-Kruger projection system coordinates of these reference points were determined as $\Delta x=486.562$ m and $\Delta y=487.116$ m.

Volume Calculations. The real volume of the land was calculated through NETCAD5.0 software package program [18]. Following the triangulation process covering the land had been performed through AP program, regarding the volume calculation made by using Delaunay triangles, since the volume was calculated directly by using the coordinates of the reference points without applying interpolation, the result was accepted as the value of the actual volume. Real volume was determined as 1436639831721.4 m³.

- Then, without making any change in the standard settings of the Surfer program;
- The grid ranges were selected as 50 m, 100 m, 150 m and 200 m.

• Interpolation methods: The surface modeling was carried out within the limits we specified using the interpolation methods including Inverse Distance to a Power ($k=1$ and $k=2$), Point Kriging, Minimum Curvature, Modified Shepard's Method, Natural Neighbor, Nearest Neighbor, Polynomial Regression (simple planar surface), Multiquadratic Radial Basis Function, Triangulation with Linear Interpolation and .grid extended files of these resulting surfaces were created. The volume values of these surfaces, which were resulted by making surface modeling, with respect to specific reference surface, $Z=0$, were calculated according to the rules given below:

- Trapeze (Terminal areas method) Rule
- Simpson's Rule
- Simpson's 3/8 Rule

The results of the volumes calculated with different volume calculation methods depending on the

different interpolation methods and grid ranges applied are given in Table 1, and the differences of these results from the actual volume and the calculated relative errors with respect to these differences are given in Table 2.

Relative Error is given by (8)

$$E_{\text{relative}} = \frac{V_{\text{estimated}} - V_{\text{actual}}}{V_{\text{actual}}} \quad (8)$$

where E_{relative} is relative error; $V_{\text{estimated}}$ is estimated volume; V_{actual} is actual volume.

Relative errors regarding the differences between actual volume value and volume values obtained with different volume calculation methods according to the different interpolation methods and grid spacing are shown in Fig. 5, Fig. 6, Fig. 7 and Fig. 8 with bar graphs.

TABLE 2
Differences between actual volume and volumes calculated with different volume calculation methods depending on the different interpolation methods and grid ranges, and the calculated relative errors with respect to these differences

Interpolation methods	Grid ranges (m)	Trapezoidal rule		Simpson's rule		Simpson's 3/8 rule	
		Differences (m ³)	Relative error	Differences (m ³)	Relative error	Differences (m ³)	Relative error
Inverse Distance to a Power (k=1)	50	436424060852.20	0.304	436413472344.00	0.304	436425001148.10	0.304
	100	436419880827.70	0.304	436391987385.00	0.304	436424023102.30	0.304
	150	436408079256.30	0.304	436405002652.10	0.304	436398445707.40	0.304
	200	436479023967.80	0.304	436437701332.00	0.304	436435794487.50	0.304
Inverse Distance to a Power (k=2)	50	438348900301.10	0.305	438343685636.40	0.305	438349606754.60	0.305
	100	438343505071.60	0.305	438328561164.70	0.305	438343799160.90	0.305
	150	438339263278.80	0.305	438335833143.40	0.305	438335813304.10	0.305
	200	438381256794.10	0.305	438368350761.30	0.305	438372399119.30	0.305
Kriging	50	454029295127.00	0.316	454024816817.60	0.316	454029667872.30	0.316
	100	454021107128.40	0.316	454025954072.80	0.316	454018836255.00	0.316
	150	454024150182.50	0.316	454011523410.50	0.316	454021162412.40	0.316
	200	454016678968.10	0.316	454010187837.60	0.316	453997954582.40	0.316
Minimum Curvature	50	450615654673.20	0.314	450612369478.00	0.314	450612370944.00	0.314
	100	447330632806.50	0.311	447324093923.70	0.311	447324064338.40	0.311
	150	439621826561.80	0.306	439614517468.00	0.306	439615787582.80	0.306
	200	443879826419.70	0.309	443866370646.90	0.309	443864376279.20	0.309
Modified Shepard's Method	50	258749816636.60	0.180	258774351403.40	0.180	258759678786.60	0.180
	100	258780048209.00	0.180	258817249272.30	0.180	258779229326.60	0.180
	150	258754344682.90	0.180	258631563929.60	0.180	258863960874.70	0.180
	200	258707927473.00	0.180	258945548500.00	0.180	258654053535.90	0.180
Natural Neighbor	50	-5407536532.70	-0.004	-5375131177.30	-0.004	-5369410818.50	-0.004
	100	-10352005537.90	-0.007	-10255761205.90	-0.007	-10386982626.70	-0.007
	150	-15502522161.50	-0.011	-15284015575.20	-0.011	-15456236742.00	-0.011
	200	-20199010792.30	-0.014	-20125578007.60	-0.014	-20078418503.30	-0.014
Nearest Neighbor	50	445709078739.00	0.310	445707775225.10	0.310	445708289786.60	0.310
	100	445724586605.30	0.310	445708474001.90	0.310	445749667733.50	0.310
	150	445711781580.50	0.310	445796095987.70	0.310	445732166540.60	0.310
	200	445758753734.60	0.310	445721830776.40	0.310	445725106047.10	0.310
Polynomial Regression	50	411508356203.50	0.286	411508356203.50	0.286	411508356203.50	0.286
	100	411508356203.50	0.286	411508356203.50	0.286	411508356203.50	0.286
	150	411508356203.50	0.286	411508356203.50	0.286	411508356203.50	0.286
	200	411508356203.50	0.286	411508356203.50	0.286	411508356203.50	0.286
Radial Basis Function	50	458407347823.20	0.319	458398934138.80	0.319	458406864053.10	0.319
	100	458411211325.60	0.319	458418358395.40	0.319	458406511632.90	0.319
	150	458406723411.00	0.319	458379421758.00	0.319	458407871888.10	0.319
	200	458396850770.30	0.319	458391339952.70	0.319	458367413553.70	0.319
Triangulation with Linear Interpolation	50	-84708121.20	0.000	-5704526.40	0.000	-23573412.50	0.000
	100	-303356257.40	0.000	-79080926.10	0.000	-148506302.50	0.000
	150	-494134865.70	0.000	-185247352.10	0.000	-19530958.80	0.000
	200	-1074418896.50	-0.001	-285480933.70	0.000	-624541841.40	0.000

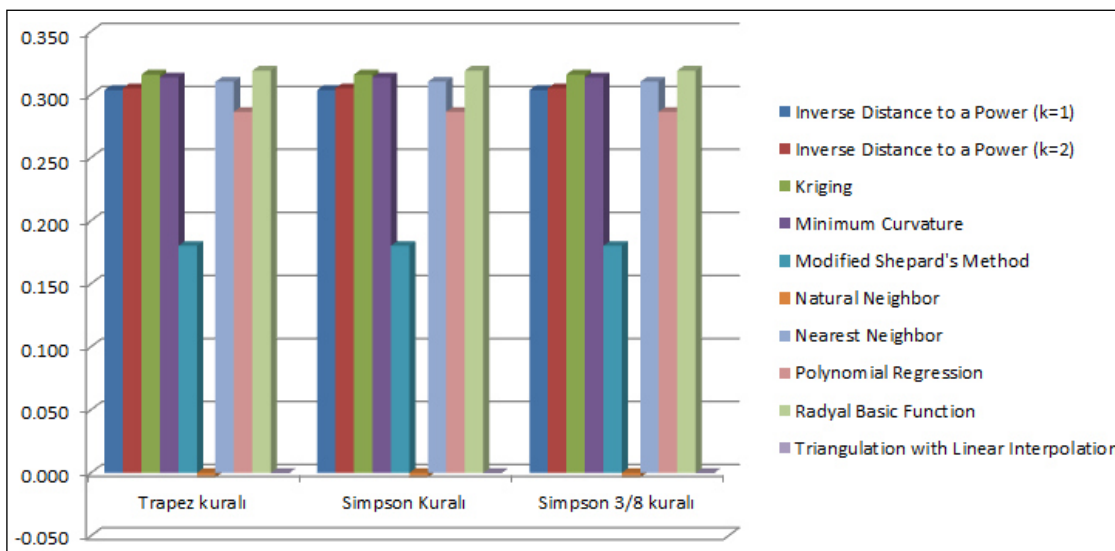


FIGURE 5
Variation of relative errors according to 50 m grid range

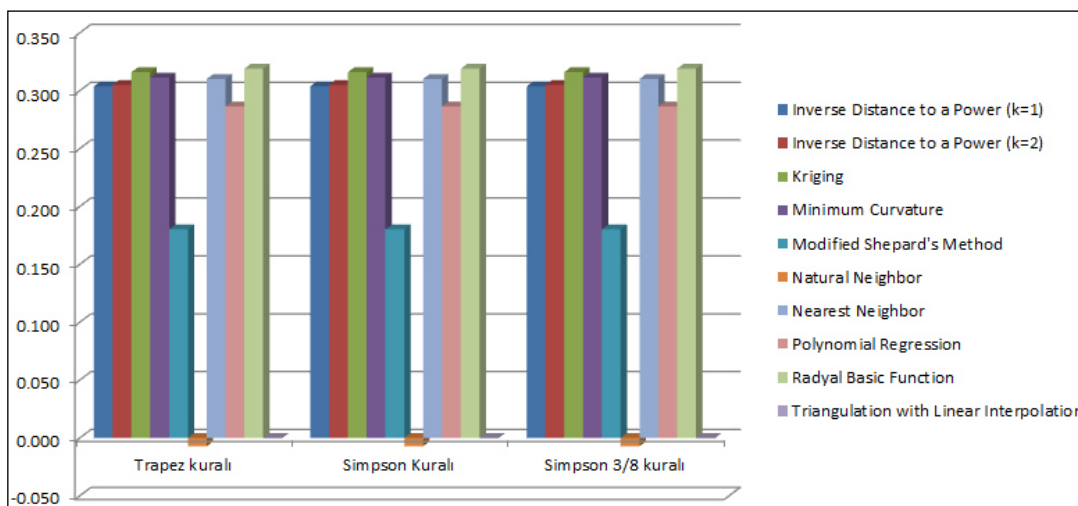


FIGURE 6
Variation of relative errors according to 100 m grid range

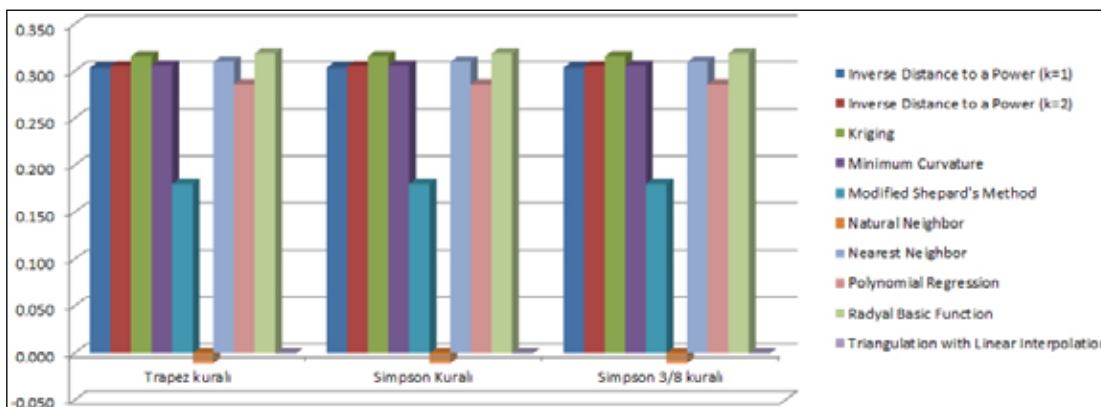


FIGURE 7
Variation of relative errors according to 150 m grid range

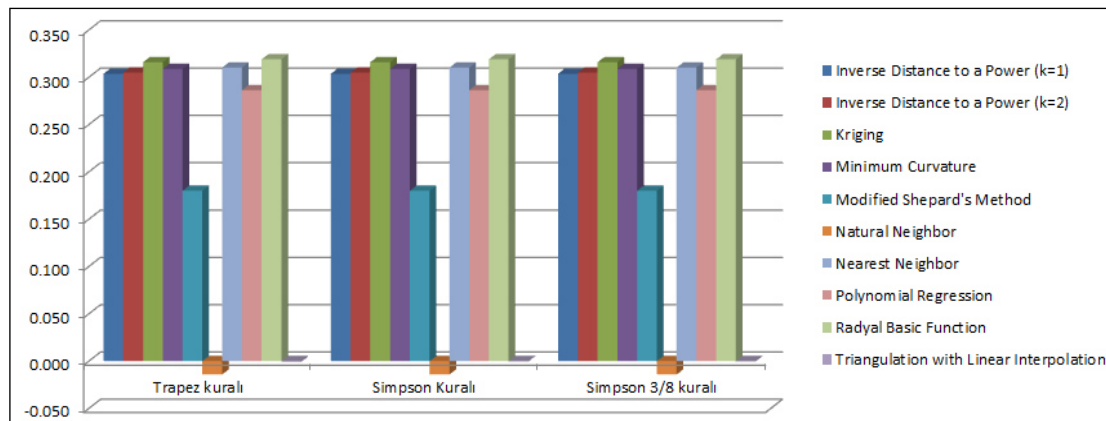


FIGURE 8
Variation of relative errors according to 200 m grid range

CONCLUSIONS

The volume calculations were made through Surfer8 program. The effects of the parameters such as, grid range, interpolation methods, volume calculation methods on the volume calculation was investigated in the study. Moreover, the discussions made taking into account the amount of relative errors are as follows:

- When the relative errors examined (see Table 2, Figure 5-6-7-8), it was seen that the most appropriate interpolation model was triangulation with linear. When the relative errors calculated with other interpolation methods examined, it was seen that the most appropriate interpolation models were respectively, from smaller to larger, Natural Neighbor, Modified Shepard's Method, Polynomial Regression, Inverse Distance to a Power ($k=1$), Inverse Distance to a Power ($k=2$), Nearest Neighbor, Kriging, Radial Basis Function.
- It was seen in the interpolation methods used including minimum curvature, natural neighbor that the relative errors changed depending on the different grid ranges. In other methods, the change in grid ranges didn't affect the relative error.
- Changing the volume calculation methods didn't affect the relative error. The amount of relative error wasn't changed with changing the method of volume calculation.

REFERENCES

- [1] Fawzy, H.E. (2015) The Accuracy of Determining the Volumes Using Close Range Photogrammetry. *IOSR Journal of Mechanical and Civil Engineering* 2015; 12, Issue 2 Ver. VII, PP 10-15.
- [2] Chaplot, V., Darboux, F., Bourennane, H., Leguedois, S., Silvera, N. and Phachomphon, K. (2006) Accuracy of Interpolation Techniques for the Derivation of Digital Elevation Models in Relation to Landform Types and Data Density. *Geomorphology*, 77, 126–141.
- [3] Bandara, K.R.M.U., Samarakoon, L., Shrestha, R.P. and Kamiya, Y. (2011) Automated Generation of Digital Terrain Model Using Point Clouds of Digital Surface Model in Forest Area. *Remote Sensing*, 3, 845-858.
- [4] Heritage, G.L., Milan, D.J., Large, A.R.G. and Fuller, I.C. (2009) Influence of Survey Strategy and Interpolation Model on DEM Quality. *Geomorphology*, 112, 334–344.
- [5] El-Ashmawy, K.L.A. (2015) A Comparison between Analytical Aerial Photogrammetry, Laser Scanning, Total Station and Global Positioning System Surveys for Generation of Digital Terrain Model. *Geocarto International*, 30, No. 2, 154–162.
- [6] Schwendel, A.C., Fuller, I.C. and Death, R.G. (2012) Assessing Dem Interpolation Methods for Effective Representation of Upland Stream Morphology for Rapid Appraisal of Bed Stability. *River Research and Applications*, 28, 567–584.
- [7] Zhang, T., Xu, X. and Xu, S. (2015) Method of Establishing an Underwater Digital Elevation Terrain Based on Kriging Interpolation. *Measurement*, 63, 287–298.
- [8] Ali, T. and Mehrabian, A. (2009) A Novel Computational Paradigm for Creating a Triangular Irregular Network (TIN) from LiDAR Data. *Nonlinear Analysis*, 71, 624-629.
- [9] Hong, W., Chen, T.S. and Chen, J. (2015) Reversible Data Hiding Using Delaunay Triangulation and Selective Embedment. *Information Sciences*, 308, 140–154.
- [10] Sangwan, A. and Singh, R.P. (2015) Survey on Coverage Problems in Wireless Sensor Networks. *Wireless Pers Commun*, 80, 1475–1500.
- [11] Surfer 8 software handbook, (2006).

- [12] Yanalak, M. (2003) Effect of Gridding Method on Digital Terrain Model Profile Data Based on Scattered Data. *Journal of Computing in Civil Engineering*, 17, No. 1.
- [13] Bogusz, J., Klos, A., Grzempowski, P. and Kontny, B. (2014) Modelling the Velocity Field in a Regular Grid in the Area of Poland on the Basis of the Velocities of European Permanent Stations. *Pure and Applied Geophysics*, 171, 809–833.
- [14] Yilmaz, H.M. (2007) The Effect of Interpolation Methods in Surface Definition: An Experimental Study. *Earth Surface Processes and Landforms*, 32, 1346–1361,
- [15] Yang, C.S., Kao, S.P., Lee, F.B. and Hung, P.S. (2004) Twelve Different Interpolation Methods: A Case Study of Surfer 8.0. *International Society for Photogrammetry and Remote Sensing (ISPRS)*, XXXV(Part B2), 778-785, Istanbul.
- [16] Vohat, P., Gupta, V., Bordoloi, T.K., Naswa, H., Singh, G. and Singh, M. (2013) Analysis of Different Interpolation Methods for Uphole Data Using Surfer Software. 10th Biennial International Conference & Exposition, Society of Petroleum Geophysicists, India.
- [17] Yakar, M. and Yilmaz, H.M. (2008) Using in Volume Computing of Digital Close Range Photogrammetry. *The International Archives of the Photogrammetry, Remote Sensing and Spatial Information Sciences*, XXXVII. Part B3b. Beijing 2008.
- [18] NETCAD5.0 Software, (1989) NETCAD YAZILIM A.S.: NETCAD 5.0 GIS for WINDOWS, <http://www.netcad.com>.

Received: 28.03.2017

Accepted: 31.05.2017

CORRESPONDING AUTHOR

Nazan Yilmaz

Karadeniz Technical University

Faculty of Engineering

Department of Geomatics

61080 Trabzon – TURKEY

E-mail: n_berber@ktu.edu.tr

IMPACTS OF CARBON TARIFFS ON CHINA'S ECONOMIC STRUCTURE AND CARBON INTENSITY: SIMULATION ANALYSIS USING A DYNAMIC CGE MODEL

Shi-Chun Xu*, Wen-Wen Zhang, Chang Gao, Ru-Yin Long, Hong Chen

Management School, China University of Mining and Technology, Xuzhou 221116, China

ABSTRACT

China is one of America's biggest trade partners, so its economy and society will be influenced by the carbon tariffs policy, which will be implemented by the USA in 2020. A multi-sectoral dynamic computable general equilibrium (CGE) model was employed to investigate the impacts of the carbon tariffs on the trade structure, output structure, energy structure, and carbon intensity in China. Simulations showed that the carbon tariffs will promote China's exports to other countries or regions instead of the USA, where the export ratio of low-carbon sectors will increase, whereas the export ratios will decline for some energy-intensive sectors and those that are highly dependent on exports to the USA. Carbon tariffs will have very slight inhibitory impacts on China's foreign trade scale and dependence. The output share of some sectors such as energy-intensive and upstream sectors will decrease, whereas the output share of some manufacturing sectors will increase. The proportion of coal consumption will decline dramatically, whereas the proportion of clean power consumption will increase, thereby improving China's energy consumption structure by reducing China's carbon intensity to some extent. Some policy implications that emerge from our study results are discussed.

KEYWORDS:

carbon tariffs; dynamic CGE model; carbon intensity; economic structure

INTRODUCTION

Climate change is a major focus in political and academic areas. China is the largest carbon emitter and the pressure due to international negotiations and emissions reduction targets is greater than ever. In order to solve this problem, on the eve of Copenhagen World Climate Conference in 2009, China officially announced that by 2020, the CO₂ per unit of GDP (carbon intensity) will decline by 40% to 45% compared with the level in 2005 [1]. At the APEC meeting, the Sino-US joint statement was issued and

the Chinese government promised that greenhouse gas emissions will peak around 2030 and that proportional non-fossil energy consumption will increase by around 20%. In addition, China officially announced a series of voluntary reduction targets in The National Plan on Climate Change (2014–2020) in September 2014, which stated that China will address the economic, energy structures and climate change actively by setting a suitable carbon tax policy for China's national conditions based on the reform of resource tax, environmental tax, consumption tax, import and export tax, and other taxes, as well as increasing the proportion of non-fossil energy in primary energy consumption to around 15% [2]. A carbon tax is considered to be an effective carbon reduction policy and it has been implemented in other countries. Carbon-based border tax adjustments (CBTAs) are considered to be an efficient approach for avoiding carbon leakage and promoting fair trade, which implies that CBTAs will be levied on imports according to the carbon content of their production process, so CBTAs are essentially carbon tariffs. The US House of Representatives passed a "border adjustment tax" on imported products on June 26, 2009, which is also called the American Clean Power and Security Act of 2009. This bill requires that the CBTAs policy will be implemented by the USA in 2020. China is one of America's biggest trade partners, so its economy, trade, and carbon emissions will be influenced by carbon tariffs. Thus, considered China's policies of structures adjustment and emissions reduction, it is necessary to study the effects of carbon tariffs on China's trade, output, and energy structures, and carbon intensity, in order to propose suitable strategies to allow China to deal with carbon tariffs in a scientific manner and avoid the negative impacts of carbon tariffs, as well as providing a theoretical basis and reference for policy.

The remainder of this paper is organized as follows. Section 2 reviews the current literature. Section 3 presents the methodology. Section 4 presents the data and parameter settings. In Section 5, we describe our simulation analysis. Section 6 discusses the main results, while Section 7 gives our conclusions and policy implications.

LITERATURE REVIEW

In recent years, studies related to CBTAs have focused mainly on their impacts on social welfare, the macro-economy, international competitiveness, and carbon leakage. Some previous studies investigated the effects of CBTAs on welfare from the global [3, 4, 5, 6], national [7, 8], and sectoral [9] perspectives. As for the impacts on macro-economy, previous studies examined impacts of carbon tariffs based on the carbon content of imports or the carbon content of domestic production, on the economy growth [10], sectoral carbon emissions [11], losses in heavy industry [12], and exports [13]. Some studies compared the impacts of CBTAs across large developing economies and compared the performance of different policy options to mitigate negative impacts [14]. These studies mainly explored the impacts of carbon tariffs on economic growth, foreign trade, and industrial sectors, but few studies examined the structural effects of carbon tariffs. From the perspective of the international competitiveness, previous studies focused mainly on the impacts of carbon tariffs on industrial competitiveness [15], such as the steel industry [16], import-competing industries [17], competitiveness of regions [18], and competitiveness of export products [19, 20]. In recent time, Keen and Kotsogiannis explored the effects of carbon tariffs on international competitiveness, as well as the coordinating climate and trade policies based on Pareto efficiency [21]. However, these studies ignored the impacts of carbon tariffs on national macro-economies and emissions reductions, such as economic structure, renewable or fossil energy use, and carbon intensity. From the perspective of carbon leakage, some previous studies examined the impacts of CBTAs on global [22, 23], sectoral [24], and regional carbon leakages [25]. In recent time, some topics related to anti-leakage policies and mitigating carbon leakage has been investigated. For example, Fischer and Fox explored various conditions to determine which anti-leakage policies might be more effective complements for domestic greenhouse gas emissions regulation [26]. Ghosh et al. used a CGE model to compare the efficiency and the distributional and emission leakage effects of carbon tariffs, and suggested that the carbon tariffs policies will have worse impacts on fossil fuel exporters and relatively better outcomes for oil importers [27]. Maria et al. summarized the channels through which carbon leakage can occur, and listed policies that have been suggested for mitigating carbon leakage [28]. Eichner and Pethig investigated the performance of a consumption-based carbon tax implemented as an instrument for unilateral climate damage mitigation in a two-period, two-country CGE model, and suggested that unilateral consumption-based carbon taxes will have a negative impact on carbon leakage [29]. Ploeg analyzed carbon leakage as well as globally altruistic and unilateral second-

best optimal carbon taxes in a three-country model of the global economy [30]. Sakai and Barrett examined how a number of issues involved in the implementation of carbon tariffs may affect their ability to cover emissions embodied in trade, thereby addressing the issue of carbon leakage [31].

Previous studies have examined the economic and environmental effects of carbon tariffs, but there are still some gaps in this research area. First, few studies have analyzed the impacts of carbon tariffs on industrial, trade, and energy consumption structures; thus, analyses of the structural effects of carbon tariffs are lacking at present. Second, static CGE models are mainly used to study carbon tariffs. Furthermore, the data in the input-output table were obtained before 2010, so they may be too old to accurately analyze the impacts of carbon tariffs on China's future economy and emissions reductions. To address the deficiencies of previous research, we considered dynamic factors such as technological progress, and capital accumulation, as well as 8 energy sectors and 13 non-energy sectors, and built a recursive multi-sectoral dynamic CGE model based on China's latest input-output table as the data source to analyze the impacts of the carbon tariffs to be implemented by the USA in 2020 on China's structures during the period 2020–2030, including the energy consumption, export commodity, export region, and industrial output structures. Thus, our study may provide novel insights into this issue.

METHODOLOGY

Based on Hosoe et al. [32], we constructed a recursive multi-sectoral dynamic CGE model, which comprises eight main parts: production activities (including 8 energy sectors and 13 non-energy sectors, as shown in Table 1), commodities (21 types), input factors (including labor and capital), household (including rural and urban residents), firms, government, investment and savings, and foreign trade (between China and the USA, Japan (JAP), EU (The EU includes the UK in this study because the data were obtained before 2016, so they do not affect the results.), and the rest of the world (ROW)). Thus, the dynamic CGE model mainly comprises six modules: production module, foreign trade module, income and expenditure module, model closure and market clearing module, carbon tariffs module, and dynamic module, as shown in Fig. 1.

Production module. The production module describes production activities. It is assumed that each sector produces only one distinct commodity, which follows a nested constant elasticity of substitute (CES) function. The inputs in each sector include labor, capital, energy, and combined intermediate input. The production process also follows the

principle of cost minimization. First, six types of fossil energy, thermal power, and clean power are synthesized to obtain the coal, oil, gas, and power composition bounds using the CES function, as depicted in Fig. 1. Second, the oil and natural gas composition bounds are synthesized to obtain the oil-gas composition bound. The oil-gas and coal composition bounds are synthesized to obtain the fossil energy composition bound. Third, the fossil energy and power composition bounds are synthesized to obtain the energy composition bound. Fourth, the energy composition bound and capital are synthesized to obtain the capital-energy composition bound. Fifth, the capital-energy composition bound and labor are synthesized to obtain the capital-energy-labor composition bound. Finally, the total output is obtained from

the capital-energy-labor composition bound and combined intermediate input using the CES function.

Foreign trade module. The foreign trade module describes the relationships between domestic goods, imports, and exports. China is a big country and it has a significant impact on international prices [32]. We assume that domestic goods are not completely substitutable for the corresponding imported goods, and that imported goods from different countries or regions cannot be completely substituted with each other; thus, there is a double Armington nested relationship [33], which can be described by a CES function.

TABLE 1
Codes for the 21 sectors in the dynamic CGE model

code	sub-sectors
sector 1	Agriculture, forestry, animal husbandry and fishery
sector 2	Mining industry
sector 3	Food manufacturing and tobacco processing industry
sector 4	Textile and products industry
sector 5	Wood-processing, paper, and printing industry
sector 6	Chemical industry
sector 7	Nonmetallic mineral production industry
sector 8	Metal smelting and production industry
sector 9	Machinery and equipment manufacturing
sector 10	Communications, instrumentation and other equipment manufacturing
sector 11	Construction
sector 12	Transportation, storage, and post
sector 13	Other services
sector 14*	Coal Mining and selection
sector 15*	Coking industry
sector 16*	Oil exploitation industry
sector 17*	Oil and nuclear fuel processing industry
sector 18*	Gas exploration industry
sector 19*	Gas production and supply
sector 20*	Thermal power
sector 21*	Clean energy

Note: the superscript * denotes energy sector

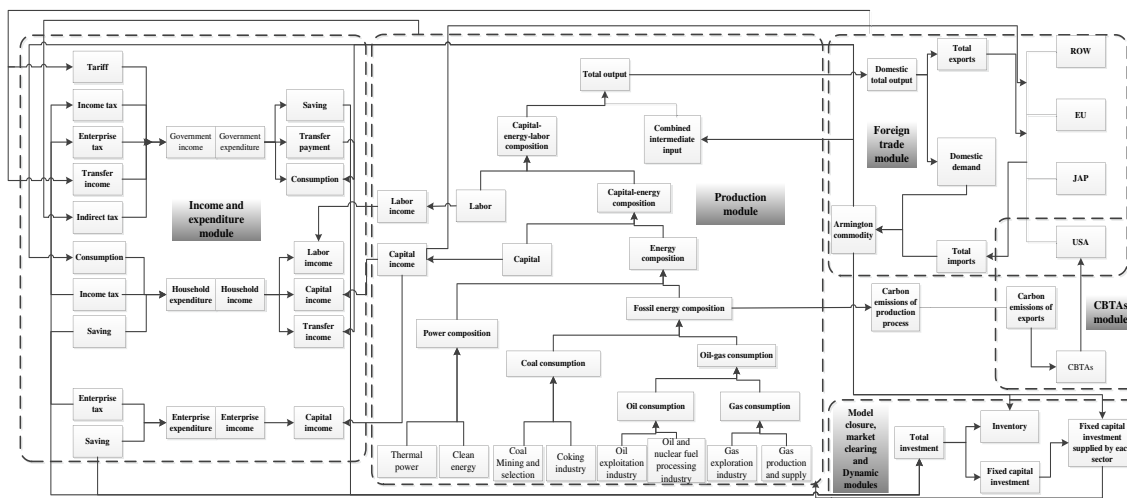


FIGURE 1
Basic framework of the dynamic CGE model

Income and expenditure module. The income and expenditure module describes the income and expenditure allocation behaviors of households, enterprises, and the government. It is assumed that the household income comes mainly from labor income, the returns on capital, and transfers by the government and overseas. After paying household income tax, households receive a disposable income, which can be consumed or saved. The enterprise income comes mainly from capital returns. After paying taxes, enterprises make savings and investments. The government revenue comes mainly from all types of taxes and transfer payments from foreign countries, and its expenditure includes consumption, transfers to households, and foreign aid.

Model closure and market clearing module.

It is assumed that commodity and factor markets are clearing, as well as the government budget, international payments, and the investment and savings balance. This model follows the principle of exogenous foreign savings and an endogenous exchange rate. The economic meaning is that exchange rate depreciation or appreciation can be adjusted to balance the trade. The government budget assumes that the government consumption is exogenous, while the government saving is endogenous. According to the "Neoclassical closure law" hypothesis, the total investment is determined by the total savings. In particular, there are two main purposes of investment: inventory changes and fixed capital investment. Part of the investment will be stored by various sectors in the form of inventory and another part will be assigned to each sector in the form of fixed capital investment.

Carbon tariffs module. The carbon tariffs module describes the price of commodities exported according to the carbon tariffs implemented by the USA. It is assumed that the carbon tariffs are only imposed by the USA to restrict the carbon contents of China's export commodities. According to the accounting rules of the Intergovernmental Panel on Climate Change (IPCC), we calculate the carbon content of the unit goods coefficient based on the carbon emission coefficient. We consider the fossil fuel inputs to avoid double-counting, as shown by Eqs. (1) – (3).

$$EMCO2_a = \sum_{fossil=1}^6 (QED_{fossil,a} \cdot a_{fossil} \cdot b_{fossil}) \quad (1)$$

$$Cem_c = \sum_a \left(\frac{EMCO2_a}{QA_a} \cdot sax_{a,c} \right) \quad (2)$$

$$pEs_{c,usa} + bct \cdot Cem_c \cdot EXR = pwe_c \cdot EXR \quad (3)$$

Eq. (1) represents the carbon emissions ($EMCO2_a$) by each sector, which are produced by the consumption of six types of fossil fuels during the production process, where $QED_{fossil,a}$ denotes the fossil fuel inputs for each sector, and a_{fossil} and

b_{fossil} are coefficients for converting different types of E into standard coal and the coefficient of carbon emissions, respectively. Eq. (2) represents the coefficient of carbon emissions per unit output of goods (Cem_c), where $sax_{a,c}$ denotes the fixed input to output ratio. Eq. (3) represents the changes in the price of commodities exported to the USA after levying carbon tariffs. As an extra tax, carbon tariffs can be treated as additional export costs by transforming the carbon tariff into prices of export commodities, where $pEs_{c,usa}$, bct , EXR , and pwe_c denote the price of the exported commodity, carbon tariffs tax rate, exchange rate, and international market price, respectively.

Dynamic module. In our recursive dynamic CGE model, the main driving factors for the model dynamics are technological progress, and capital accumulation. The capital-energy-labor composition bound comprises the capital-energy composition bound and labor based on the CES function, which is written as Eq. (7):

$$\min(PKE_a \cdot QKE_a + WL \cdot QLD_a), \quad (4)$$

$$s.t. QKEL_a = TFP_a \cdot \left[\delta_a^{KE} QKE_a^{\rho_a^{KEL}} + (1 - \delta_a^{KE}) QLD_a^{\rho_a^{KEL}} \right]^{\frac{1}{\rho_a^{KEL}}}$$

where TFP_a denotes the total factor productivity of sector a, and QKE_a , QLD_a , PKE_a and WL denote the capital-energy composition bound, labor demand, and their corresponding prices, respectively. δ_a^{KE} is the share parameter and $\sigma_a^{KEL} = 1/(1 - \rho_a^{KEL})$ is the elasticity of substitution between the capital-energy-labor composition bound and combined intermediate input. σ_a^{KEL} is the substitution elasticity parameter.

Eq. (5) reflects technological progress:

$$TFP_{a,t+1} = TFP_{a,t} \cdot (1 + tfp_t), \quad (5)$$

where tfp_t is the growth rate of TFP in period t.

DATA SOURCES AND PARAMETER SETTINGS

A social accounting matrix (SAM) must be constructed before the simulation analysis, where the basic data come mainly from the input-output table. The data for intermediate inputs, capital, output, imports, exports, asset depreciation, commodity consumption, investment, inventory, etc. came from China's input-output table (2012), which was taken from the China Statistical Yearbook (2015). The data regarding resident income, foreign investment income, government savings, transfer payments, etc. came from the China Statistical Yearbook (2013 and 2014). The data regarding import duties, household income tax, enterprise tax, etc. came from the China Finance Year Book (2013). The data about house-

hold savings came from the Almanac of China's Finance and Banking (2013). The data for the allocation proportions of commodities exported to and imported from different countries or regions, the proposed capital gains of different countries or regions, and the proposed foreign saving of different countries or regions came from the China Customs Statistics Yearbook (2013), UNCOMTRADE Database, and GTAP version 9 database statistics. Other data such as enterprise capital income, foreign savings, and government transfer to residents were obtained using the row-sum and column-sum equality rule.

There are many exogenous and endogenous parameters in the dynamic CGE model. The endogenous parameters were determined by the calibration method, including the share parameters for the production function, Armington function, and CET function, as well as the transformation parameters, miscellaneous tax rates, and propensities to consume. In the simulations, we entered the benchmark data derived from the SAM into the corresponding equations and we then solved the unknown parameters. Exogenous parameters such as miscellaneous substitution elasticities, carbon emission factors, total factor productivity, and the rate of population growth were obtained from previous studies [34, 35] and adjusted in our model. The dynamic exogenous parameters in our model, including the growth rates for GDP and total labor, were divided into two stages: the actual economic data from 2013 to 2015 (China Statistical Yearbook 2015), and the forecast data from 2016 to 2030 [35]. In addition, it was difficult to obtain some exogenous parameters such as the total factor productivity, so we used the historical simulation method [36]. For example, we changed the real GDP and total labor supply from endogenous to exogenous, and solved the total factor productivity as an endogenous parameter.

SIMULATION RESULTS

In this study, we used the following two simulation schemes: (1) no carbon tariffs implemented by the USA as a baseline scenario; and (2) Carbon tariffs implemented by the USA from 2020 on the carbon contents of goods imported from China. Based on comparisons with the baseline scenario, we analyzed the impacts of the carbon tariffs on China's trade structure, output structure, energy structure, and carbon intensity. According to the American Clean Power and Security Act of 2009, the international community predicts that the tax rate will be levied over a range from \$30 to \$80 dollars per ton of carbon emissions (\$/t CO₂). Previous studies [37, 38, 39] used the same tax rate schemes, so we set the tax rate for carbon tariffs imposed by the USA at

\$30/t CO₂ to \$80/t CO₂.

Impacts of carbon tariffs on the China's economic structure. (1) Impacts of carbon tariffs on the trade structure. (a) Regional export structure.

The regional export structure reflects changes in the proportions of exports to different countries among the total exports, as shown in Table 2 (Carbon tariffs imposed by US at any level of \$30/t CO₂, \$40/t CO₂, \$60/t CO₂, \$70/t CO₂, \$80/t CO₂, the simulation results have a similar tendency with minor changes.). It can be seen that most of the exports to the USA are clearly lower, whereas exports to other countries or regions increase. This means that carbon tariffs will lead to trade diversion, mainly because Chinese exports to the USA are hindered, thereby forcing China to search for other foreign markets. In addition, when the USA levies carbon tariffs, China will decrease the prices of exports as a large trading nation. Table 3 shows that most of the prices of China's exports will exhibit a downward trend when carbon tariffs are implemented by the USA. In particular, a decrease in prices will improve the attractiveness of Chinese exports so more goods can be exported if other conditions remain unchanged, which is referred to as the trade creation effect. Thus, this phenomenon will somewhat reduce the negative effect of carbon tariffs. Among the different exports, sector 17 (Oil and nuclear fuel processing industry) exports to the USA will decrease dramatically. For the exports to the USA, the total exports will decrease by about 35.7143% in 2020, i.e., from 2.38% before carbon tariffs to 1.53% after carbon tariffs, where the declining trend will decrease over the years reaching about 75.2101% in 2030. However, not all exports will be affected by trade diversion. For example, the proportions of exports in sector 3 (Food manufacturing and tobacco processing industry), sector 10 (Communications, instrumentation and other equipment manufacturing), sector 11 (Construction), and sector 18 (Gas exploration industry) to the USA will decline, whereas the proportions of these exports to JAP, EU, and ROW will remain unchanged because the demand elasticities for these commodities are relatively weak and not easy to change. Furthermore, some exports to JAP, EU, or ROW will increase to different extents. For example, the export ratios for sector 6 (Chemical industry), sector 8 (Metal smelting and production industry), sector 12 (Transportation, storage, and post), and sector 15 (Coking industry) to JAP will increase significantly, while the export ratios for sector 5 (Wood-processing, paper, and printing industry), sector 9 (Machinery and equipment manufacturing), and sector 13 (Other services) to EU will also increase. This is explained mainly by the regional export structure before carbon tariffs.

TABLE 2
Impacts of carbon tariffs on the regional export structure (%) at \$50/t CO₂ from 2020 to 2030

Sector	Region	2020	2022	2024	2026	2028	2030
sector 1	USA	-0.2577	-0.2577	-0.2577	-0.2577	-0.2577	-0.2577
	JAP	0.0000	0.0000	0.0000	0.0000	0.0000	0.0000
	EU	0.0000	0.0000	0.0000	0.0000	0.0000	0.0000
	Rest	0.0161	0.0161	0.0161	0.0161	0.0161	0.0161
sector 2	USA	-0.9314	-10.161	-11.008	-11.854	-12.701	-13.548
	JAP	0.1311	0.1311	0.1311	0.1311	0.1966	0.1966
	EU	0.1337	0.1337	0.1337	0.1337	0.1783	0.1783
	Rest	0.1386	0.1386	0.1584	0.1584	0.1782	0.1782
sector 3	USA	-0.0652	-0.0652	-0.0652	-0.0652	-0.0652	-0.0652
	JAP	0.0000	0.0000	0.0000	0.0000	0.0000	0.0000
	EU	0.0000	0.0000	0.0000	0.0000	0.0000	0.0000
	Rest	0.0000	0.0000	0.0000	0.0000	0.0000	0.0000
sector 4	USA	0.0000	0.0000	0.0000	0.0000	0.0000	0.0000
	JAP	0.0000	0.0000	0.0000	0.0000	0.0000	0.0000
	EU	0.0000	0.0000	0.0000	0.0000	0.0000	0.0000
	Rest	0.0209	0.0209	0.0209	0.0209	0.0209	0.0209
sector 5	USA	-0.0613	-0.0613	-0.0613	-0.0613	-0.0613	-0.0613
	JAP	0.0000	0.0000	0.0000	0.0000	0.0000	0.0000
	EU	0.0460	0.0460	0.0460	0.0460	0.0460	0.0460
	Rest	0.0268	0.0268	0.0268	0.0268	0.0268	0.0268
sector 6	USA	-11.765	-12.325	-12.885	-13.445	-14.006	-14.566
	JAP	0.3212	0.3212	0.3212	0.3212	0.3212	0.3212
	EU	0.2350	0.2350	0.2350	0.2350	0.2938	0.2938
	Rest	0.2509	0.2689	0.2868	0.2868	0.3047	0.3226
sector 7	USA	-0.9004	-0.9604	-10.204	-10.804	-11.405	-11.405
	JAP	0.1393	0.1393	0.1393	0.1393	0.1393	0.1393
	EU	0.1586	0.2114	0.2114	0.2114	0.2114	0.2114
	Rest	0.1922	0.1922	0.2096	0.2096	0.2271	0.2446
sector 8	USA	-0.5908	-0.5908	-0.5908	-0.5908	-0.5908	-0.5908
	JAP	0.1538	0.1538	0.1538	0.1538	0.1538	0.1538
	EU	0.0569	0.0569	0.0569	0.0569	0.1138	0.1138
	Rest	0.0962	0.0962	0.0962	0.0962	0.0962	0.0962
sector 9	USA	-0.0692	-0.0692	-0.0346	-0.0346	-0.0346	-0.0346
	JAP	0.0000	0.0000	0.0000	0.0000	0.0000	0.0000
	EU	0.0461	0.0461	0.0461	0.0461	0.0461	0.0461
	Rest	0.0240	0.0240	0.0240	0.0240	0.0240	0.0240
sector 10	USA	-0.0408	0.0000	0.0000	0.0000	0.0000	0.0000
	JAP	0.0000	0.0000	0.0000	0.0000	0.0000	0.0000
	EU	0.0000	0.0000	0.0000	0.0000	0.0000	0.0000
	Rest	0.0000	0.0000	0.0000	0.0000	0.0000	0.0000
sector 11	USA	-0.2252	-0.2252	-0.2252	-0.2252	-0.2252	-0.2252
	JAP	0.0000	0.0000	0.0000	0.0000	0.0000	0.0000
	EU	0.0000	0.0000	0.0000	0.0000	0.0000	0.0000
	Rest	0.0000	0.0000	0.0000	0.0000	0.0204	0.0204
sector 12	USA	-24.263	-25.130	-26.863	-27.730	-29.463	-30.329
	JAP	0.3295	0.3295	0.3295	0.4119	0.4119	0.4119
	EU	0.3230	0.3230	0.3523	0.3817	0.3817	0.4110
	Rest	0.3314	0.3550	0.3550	0.3787	0.4024	0.4260
sector 13	USA	-0.1092	-0.1092	-0.1092	-0.1092	-0.1092	-0.1092
	JAP	0.0000	0.0000	0.0000	0.0000	0.0000	0.0000
	EU	0.0353	0.0353	0.0353	0.0353	0.0353	0.0353
	Rest	0.0219	0.0219	0.0219	0.0219	0.0219	0.0219
sector 14	USA	0.0000	0.0000	0.0000	0.0000	0.0000	0.0000
	JAP	0.0000	0.0000	0.0000	0.0000	0.0000	0.0000
	EU	0.0000	0.0000	0.0000	0.0000	0.0000	0.0000
	Rest	0.0000	0.0000	0.0000	0.0000	0.0000	0.0000
sector 15	USA	-57.047	-60.403	-67.114	-73.826	-80.537	-87.248
	JAP	0.1969	0.1969	0.1969	0.1969	0.3937	0.3937
	EU	0.1235	0.1235	0.1235	0.1235	0.2469	0.2469
	Rest	0.1670	0.1908	0.2028	0.2266	0.2385	0.2624
sector 16	USA	-0.3356	-0.3356	-0.3356	-0.3356	-0.3356	-0.3356
	JAP	0.0000	0.0000	0.0000	0.0000	0.0000	0.0000
	EU	0.0000	0.0000	0.0000	0.0000	0.0000	0.0000
	Rest	0.0119	0.0119	0.0119	0.0119	0.0119	0.0119
sector 17	USA	-357.143	-424.370	-495.798	-579.832	-663.866	-752.101
	JAP	0.6993	0.6993	13.986	13.986	13.986	20.979
	EU	0.0000	0.0000	0.0000	0.0000	0.0000	0.0000
	Rest	0.8737	10.401	12.170	14.146	16.226	18.307

Sector	Region	2020	2022	2024	2026	2028	2030
sector 18	USA	-0.4170	-0.3890	-0.3643	-0.3421	-0.3217	-0.3030
	JAP	0.0000	0.0000	0.0000	0.0000	0.0000	0.0000
	EU	0.0000	0.0000	0.0000	0.0000	0.0000	0.0000
	Rest	0.0000	0.0000	0.0000	0.0000	0.0000	0.0000
sector 20	USA	-0.1587	0.0000	0.0000	0.0000	0.0000	0.0000
	JAP	0.0000	0.0000	0.0000	0.0000	0.0000	0.0000
	EU	0.0000	0.0000	0.0000	0.0000	0.0000	0.0000
	Rest	0.0133	0.0133	0.0133	0.0000	0.0000	0.0000
sector 21	USA	-0.1587	0.0000	0.0000	0.0000	0.0000	0.0000
	JAP	0.0000	0.0000	0.0000	0.0000	0.0000	0.0000
	EU	0.0000	0.0000	0.0000	0.0000	0.0000	0.0000
	Rest	0.0133	0.0133	0.0133	0.0000	0.0000	0.0000

Notes: Some values are “0” after four digits are retained, which indicates the influence is very small. Sector 19 is not displayed in the table because this sector has no foreign trade.

TABLE 3
Impacts of carbon tariffs on export prices (%) at \$50/t CO₂ from 2020 to 2030

Commodities	2020	2021	2022	2023	2024	2025	2026	2027	2028	2029	2030
sector 1	0.0564	0.0570	-0.0579	-0.2749	-0.6222	-1.1841	-1.9525	-3.0629	-4.5325	-6.3926	-8.6967
sector 2	0.1074	0.1351	-0.1248	-0.6055	-1.1631	-2.0435	-3.0682	-4.4739	-6.1575	-8.2197	-10.9084
sector 3	0.0597	0.0607	-0.0309	-0.2216	-0.5202	-1.0054	-1.6657	-2.6461	-3.9361	-5.6481	-7.8745
sector 4	0.0710	0.0617	0.0105	-0.1604	-0.3944	-0.8000	-1.3617	-2.2091	-3.3484	-4.8851	-6.9417
sector 5	0.0637	0.0758	-0.0222	-0.2049	-0.4693	-0.9220	-1.5247	-2.4442	-3.6511	-5.2601	-7.4337
sector 6	0.1842	0.1801	-0.0350	-0.4298	-0.9617	-1.7431	-2.6908	-4.0341	-5.6024	-7.6490	-10.2339
sector 7	0.1506	0.1436	-0.0770	-0.5167	-1.0454	-1.8452	-2.8224	-4.1772	-5.7927	-7.8255	-10.4532
sector 8	0.0996	0.1050	-0.0633	-0.4017	-0.8520	-1.5089	-2.3532	-3.5061	-4.9468	-6.8131	-9.2387
sector 9	0.0654	0.0670	-0.0115	-0.2124	-0.4879	-0.9359	-1.5411	-2.4515	-3.6340	-5.2350	-7.4243
sector 10	0.0657	0.0661	0.0381	-0.0580	-0.2162	-0.5318	-0.9778	-1.6757	-2.6593	-4.0321	-5.9608
sector 11	0.0444	0.0469	-0.1322	-0.5072	-0.9835	-1.6966	-2.6299	-3.8920	-5.4374	-7.3833	-9.9122
sector 12	0.2072	0.2040	0.0167	-0.3721	-0.8507	-1.5960	-2.5352	-3.7986	-5.3625	-7.3264	-9.9314
sector 13	0.0683	0.0696	-0.0102	-0.2087	-0.4952	-0.9815	-1.6729	-2.6751	-3.9954	-5.7554	-8.1281
sector 14	0.0324	0.0333	-0.0798	-0.3412	-0.6943	-1.2524	-1.9792	-3.0663	-4.4622	-6.2635	-8.6464
sector 15	0.1421	0.1586	-0.2061	-0.8525	-1.6088	-2.7721	-4.1002	-5.8584	-7.8330	-10.2382	-13.2364
sector 16	0.0523	0.0613	0.0529	0.0178	-0.0815	-0.2952	-0.6233	-1.1754	-1.9695	-3.1675	-4.9666
sector 17	0.5206	0.5735	0.0625	-0.9716	-2.0609	-3.8585	-5.7841	-8.3205	-10.9462	-14.3177	-18.3784
sector 18	0.0432	0.0433	0.0523	0.0088	-0.0714	-0.2817	-0.5950	-1.1465	-1.9257	-3.1208	-4.9061
sector 19	0	0	0	0	0	0	0	0	0	0	0
sector 20	0.0725	0.0787	0.3249	0.7295	1.1358	1.6436	2.0990	2.5630	2.8916	3.0505	2.9994
sector 21	0.0725	0.0787	0.3249	0.7295	1.1358	1.6436	2.0990	2.5630	2.8916	3.0505	2.9994

Note: The change in export commodity price of sector 19 is “0” because this sector has no foreign trade.

(b) Commodity export structure. The commodity export structure is the proportion of different commodity exports among the total exports. Fig. 2 shows the changes in the commodity export structure due to carbon tariffs being implemented by the USA at \$50/t CO₂ (If carbon tariffs are imposed by the USA at levels of \$30/t CO₂, \$40/t CO₂, \$60/t CO₂, \$70/t CO₂, or \$80/t CO₂, the export commodity structure will exhibit similar trends with minor differences.). Overall, excluding sector 10 (Communications, instrumentation and other equipment manufacturing), sector 16 (Oil exploitation industry), sector 18 (Gas exploration industry), sector 19 (Gas production and supply), sector 20 (Thermal power), and sector 21 (Clean energy), the exports ratios exhibit a downward trend where the export ratios of sector 17 (Oil and nuclear fuel processing industry), sector 15 (Coking industry), sector 2 (Mining industry), sector

11 (Construction), sector 6 (Chemical industry), sector 8 (Metal smelting and production industry), and sector 12 (Transportation, storage, and post) decrease by approximately 36.2535%, 22.3481%, 14.8936%, 14.2857%, 11.3636%, 9.4595%, and 9.3023%, respectively, from 2020 to 2030. These changes are mainly explained as follows. First, these sectors are energy-intensive with high carbon emissions during the production process, so they are inevitably affected greatly by carbon tariffs. Second, the exports ratios of these sectors to the USA are relatively high before carbon tariffs, so carbon tariffs have greater impacts on these sectors. Moreover, the export ratios of sector 10 (Communications, instrumentation and other equipment manufacturing), sector 16 (Oil exploitation industry), and sector 18 (Gas exploration industry) increase slightly (less than 7% in 2030). However, the export ratios of sector 20

(Thermal power) and sector 21 (Clean energy) increase dramatically by about 20.7692%, and 18.9189%, respectively, in 2030. This is because the exports in these sectors have price advantages compared with high carbon exports.

(c) Foreign trade dependence. The foreign trade dependence is the proportion of export and import values relative to the GDP, which comprises export and import dependencies. This metric can measure the economic dependence on foreign countries.

Fig. 3 and Fig. 4 indicate that China's foreign trade dependence and export dependence increase slightly compared with that pre-tax (\$0/tCO₂) in 2020 and 2021, whereas they exhibit a declining trend after 2021, where they decrease by approximately 21.5% and 10.73%, respectively, in 2030. In general, carbon tariffs implemented by the USA will

reduce China's foreign trade dependence and export dependence due to the following main reasons. First, China's export prices will decrease dramatically after 2021 (Table 3), which will somewhat inhibit China's exports. Second, the USA is one of China's largest trading partners, so carbon tariffs imposed by the USA on imports from China will reduce some of China's exports to US, thereby reducing China's foreign trade dependence and export dependence. However, due to an increase in tax rates, China's foreign trade dependence and export dependence will change little (Even if the elasticity is changed, China's foreign trade dependence and export dependence exhibit similar trends with minor differences), which means that carbon tariffs implemented by the USA will have only a limited negative impact on China's foreign trade dependence and export dependence.

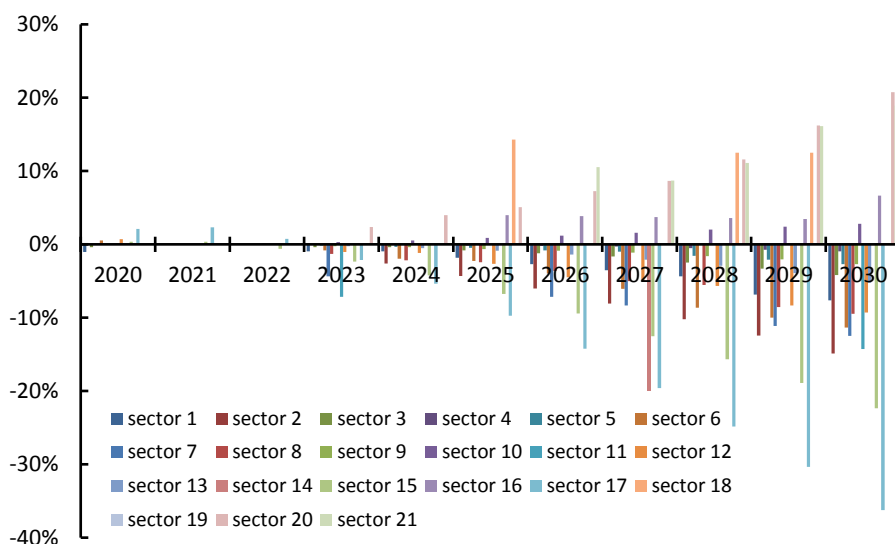


FIGURE 2
Impacts of carbon tariffs on the commodity export structure at \$50/t CO₂ from 2020 to 2030

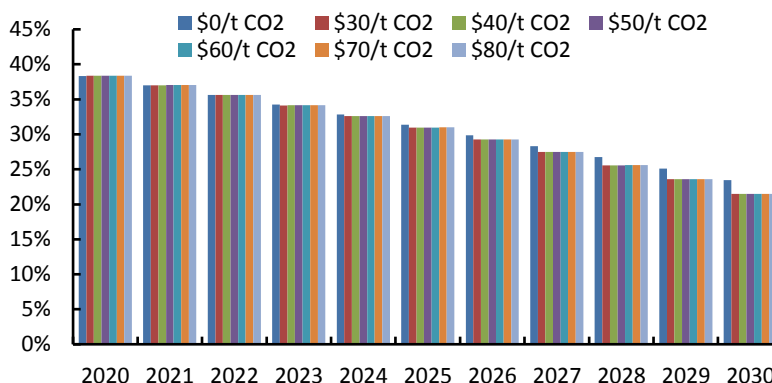


FIGURE 3
Impacts of carbon tariffs on China's foreign trade dependence under different scenarios

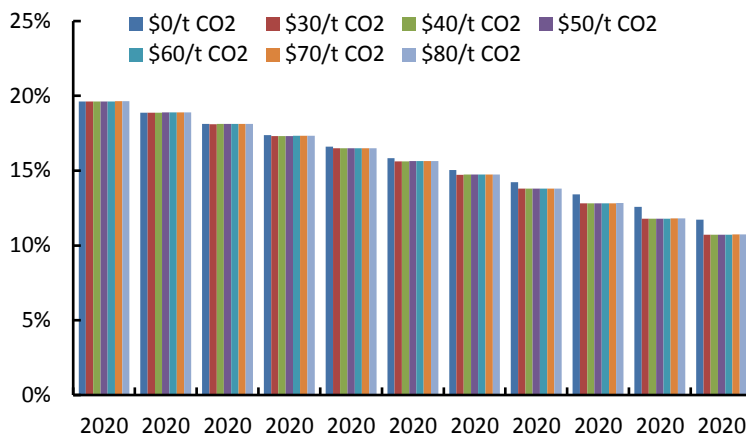


FIGURE 4
Impacts of carbon tariffs on China's export dependence under different scenarios

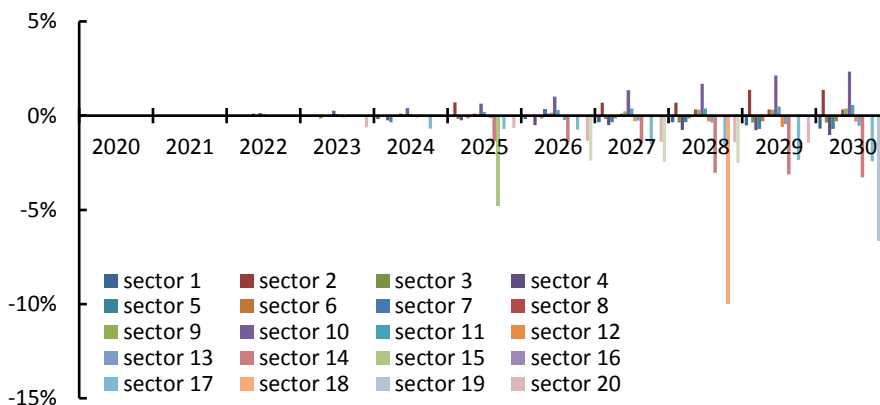


FIGURE 5
Impacts of carbon tariffs on China's output structure (%) at \$50/t CO₂ between 2020 and 2030

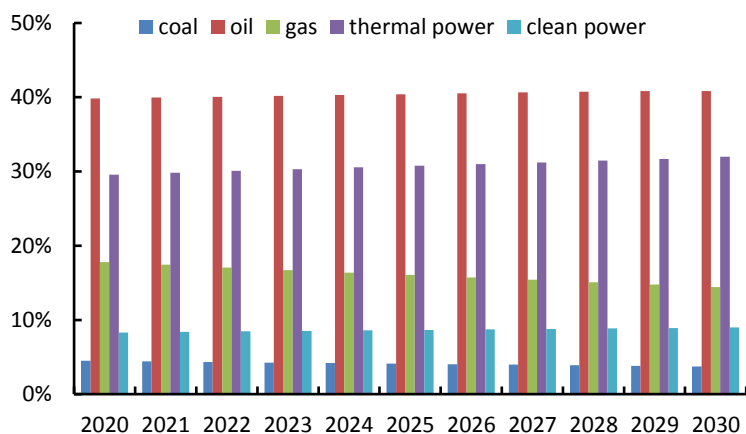


FIGURE 6
Energy consumption structure at \$50/t CO₂ between 2020 and 2030

(2) Impacts of carbon tariffs on the output structure. The output structure is the proportion of each sector's output relative to the GDP. Fig. 5 shows the changes in the output structure due to carbon tariffs being implemented by the USA at \$50/t

CO₂ from 2020 to 2030 (The output structure will exhibit similar trends with minor differences at levels of \$30/t CO₂, \$40/t CO₂, \$60/t CO₂, \$70/t CO₂, or \$80/t CO₂). The output structure will change little in 2020 and 2021, but it will change greatly from

2022 to 2030, where the output ratios of some sectors will decrease. For instance, the output shares of sector 14 (Coal Mining and selection), sector 21 (Clean energy), sector 17 (Oil and nuclear fuel processing industry), sector 20 (Thermal power), and sector 4 (Textile and products industry) will decline greatly by about 3.2787%, 2.56417%, 2.4194%, 1.4599%, and 1.0309%, respectively in 2030. The output shares of sector 1 (Agriculture, forestry, animal husbandry and fishery), sector 3 (Food manufacturing and tobacco processing industry), sector 5 (Wood-processing, paper, and printing industry), sector 6 (Chemical industry), sector 12 (Transportation, storage, and post), and sector 13 (Other services) will decline slightly in 2030 by about 0.6908%, 0.36166%, 0.7092%, 0.305343511%, 0.3077%, and 0.5418%, respectively. However, the output shares of sector 15 (Coking industry), sector 18 (Gas exploration industry), and sector 19 (Gas production and supply) will only change in specific years. The decreases in the output share of these sectors have two main characteristics: high export dependences and upstream sectors that provide raw materials or services for other commodities. Carbon tariffs can increase the output share for some sectors, but the size of the increase will only be slight. For example, the output shares of sector 2 (Mining industry), sector 8 (Metal smelting and production industry), sector 9 (Machinery and equipment manufacturing), sector 10 (Communications, instrumentation and other equipment manufacturing), and sector 11 (Construction) will only increase by 1.3605%, 0.3304%, 0.3808%, 2.331%, and 0.5676%, respectively, in 2030. In addition, the output share of sector 7 (Non-metallic mineral production industry) will only increase by 0.34965% in 2026, whereas sector 16 (Oil exploitation industry) will remain unchanged. This is mainly because most of these sectors produce energy-intensive goods, so their output share will be improved with lower prices for energy and input factors, and lower production costs.

(3) Impacts of carbon tariffs on the energy structure. Fig. 6 shows the different energy consumption shares at \$50/t CO₂ between 2020 and 2030 (other tax rates have similar trends). The coal and gas consumption shares will decline from 4.4975% and 17.7906% in 2020, respectively, to 3.7434% and 14.4377% in 2030, whereas the shares of oil, thermal power, and clean power consumption will increase from 39.8517%, 29.5501%, and 8.3101% in 2020 to 40.8407%, 31.9837%, and 8.9945% in 2030, respectively. Fig. 7 shows the impacts of carbon tariffs on changes in China's energy consumption structure at \$50/t CO₂ between 2020 and 2030, which demonstrates that there are minor changes in the energy consumption structure in 2020 and 2021, but the range and trend of the energy consumption structure are significantly different between 2022 and 2030. The changes in the coal and gas shares tend to increase where the trend is notable over the years, reaching 1.9506% and 1.7958%, respectively, in 2030. The changes in the thermal power and clean power shares clearly increase in a similar manner between 2021 and 2030. The oil consumption share increases gradually between 2020 and 2026 reaching a peak at 0.0813% in 2027, before declining. Clearly, the different changes in the energy consumption structure are affected greatly by carbon tariffs. In general, carbon tariffs can reduce coal consumption, which is helpful for improving the environment. Moreover, thermal power and clean power will obviously increase. These changes are attributable to the different impacts of carbon tariffs on energy prices, as shown in Fig. 8. The prices of coal, oil, gas, thermal power, and clean power will decline over the years due to carbon tariffs. In particular, the price of oil exhibits the greatest fall, followed by thermal power and clean power, but the prices of coal and gas decrease relatively slowly. Therefore, in order to optimize the allocation of resources, producers will prefer to use energy with a lower price such as oil, coal, and clean power.

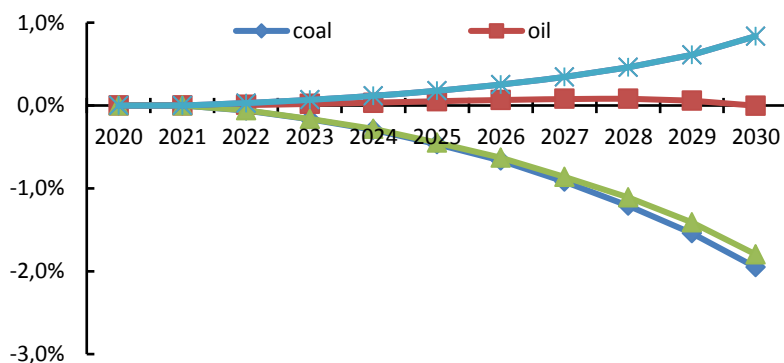


FIGURE 7
Impacts of carbon tariffs on changes in China's energy structure (%) at \$50/t CO₂ between 2020 and 2030

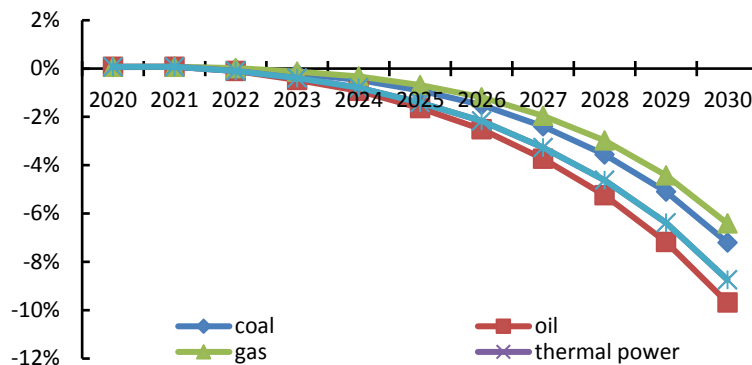


FIGURE 8
Impacts of carbon tariffs on China's energy prices at \$50/t CO₂ between 2020 and 2030

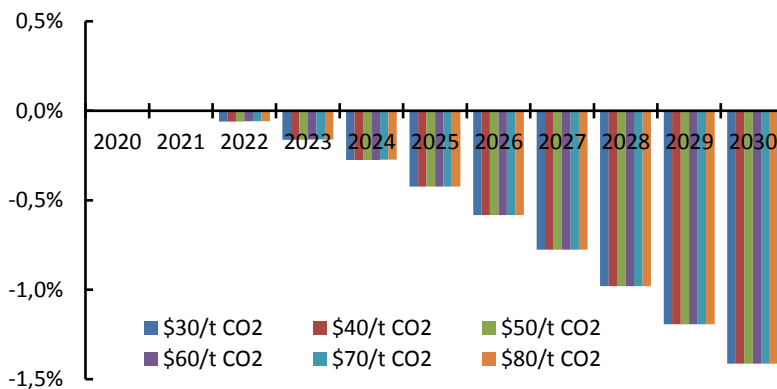


FIGURE 9
Effects of carbon tariffs on China's carbon intensity

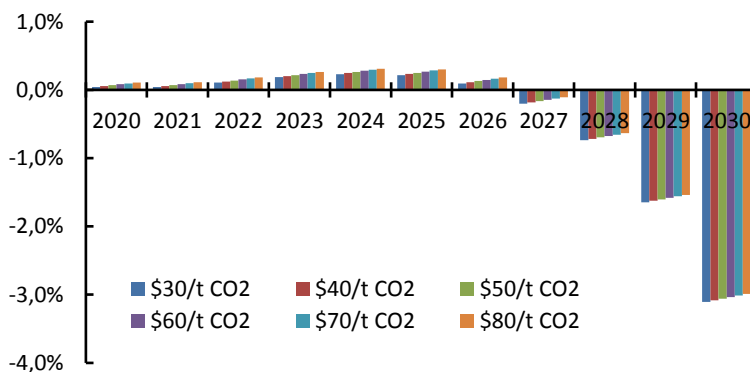


FIGURE 10
Impacts of carbon tariffs on China's exports

Impacts of carbon tariffs on the carbon intensity. The carbon intensity represents the carbon emissions per unit of GDP. Fig. 9 shows the impacts of carbon tariffs being implemented by the USA on China's carbon intensity. Clearly, carbon tariffs will lower China's carbon intensity between 2022 and 2030, except in 2020 and 2021. The decline will be enhanced slightly as the carbon tariffs rate increases. Therefore, carbon tariffs can contribute to low carbon development to some extent, but not obviously;

for example, the maximum inhibition rate of carbon tariffs only reaches about 1.413% in 2030. This is explained mainly by the changes in energy consumption structure during 2020–2030. In particular, the ratio of coal consumption decreases dramatically. By contrast, the ratio of clean power consumption increases gradually. China's carbon intensity will not decrease between 2020 and 2021 because carbon tariffs will have a time-delayed effect, e.g., producers

will require a period to adjust their production, energy structure, and energy-saving technology to cope with the challenges of carbon tariffs.

DISCUSSION

The empirical analysis results described above reveal several interesting phenomena.

(1) Carbon tariffs implemented by the USA will have great impacts on China's regional export structure and commodity export structure, but very slight impacts on China's foreign trade dependence. For the regional export structure, because the USA is one of China's largest trading partners, the implementation of carbon tariffs on imports from China will lead to a direct decrease in the ratio of exports to the USA, but increase the ratio of exports to other countries or regions. Overall, carbon tariffs will result in the transfer of China's exports to different countries or regions, which is known as the trade diversion effect. In addition, lower export prices will promote the demand from the international market and stimulate China's exports, i.e., a trade creation effect. For the commodity export structure, carbon tariffs will have a greater negative impact on exports in two types of sectors, in which there will be major declines in the ratio of energy-intensive and higher carbon exports to the USA. However, the export ratios of some sectors will tend to increase greatly, such as sector 20 (Thermal power) and sector 21 (Clean energy), because these sectors have a lower carbon content so they will be affected less. The implementation of carbon tariffs by the USA will help China to improve the commodity export structure to some extent, thereby reducing carbon-intensive production and even helping to improve China's environment. Carbon tariffs will slightly reduce China's foreign trade dependence. Thus, China's trade scale will remain largely unchanged. The impacts of carbon tariffs on China's exports are shown in Fig. 10. The changes in total exports are not obvious and the trends are divided into the following patterns: China's total exports will increase slightly between 2020 and 2026 due to the trade creation effect, whereas carbon tariffs will cut total exports between 2027 and 2030, but the largest decline is only 3.108%. Therefore, the implementation of carbon tariffs by the USA will have a limited impact on China's exports, which is consistent with the conclusions of [34, 35].

(2) Carbon tariffs implemented by USA from 2020 to 2030 will have different impacts on the output structure. The output structure remains almost unchanged during the early years of 2020 and 2021, which is attributable to the delayed effects of carbon tariffs policies, whereas the changes are different from 2022 to 2030. The output shares of some sectors that are high export dependences or located upstream will decrease, whereas the output shares of some manufacturing sectors will increase, such as

sector 8 (Metal smelting and production industry), sector 9 (Machinery and equipment manufacturing), sector 10 (Communications, instrumentation and other equipment manufacturing), and sector 11 (Construction), mainly because China is a very large manufacturing nation, and even if the USA implement carbon tariffs, the negative impacts on Chinese manufacturing will be very minor.

(3) Carbon tariffs will improve China's energy consumption structure and reduce China's carbon intensity to some extent. The changes in energy prices will be affected differently by carbon tariffs, thereby leading to changes in the energy consumption structure. The proportion of coal consumption will decline dramatically, whereas the proportion of clean power consumption increases. This is explained mainly by differences in energy prices because producers prefer to use lower cost energy, which is known as the energy substitution effect. These findings are consistent with [38, 40]. Therefore, carbon tariffs will help to improve China's energy consumption structure. In addition, carbon tariffs will reduce China's carbon intensity but not significantly; for example, the maximum inhibition rate will only reach about 1.413% in 2030, where this result agrees with the conclusions of [11, 13]. The carbon intensity will decline because carbon tariffs can help to improve China's energy consumption structure, especially by decreasing the ratio of coal consumption and increasing the ratio of clean power consumption. For many years, coal consumption in China will still account for the largest proportion of fossil energy consumption at approximately 70% [41, 42]. Coal has the largest carbon emission coefficient so it produces more carbon emissions compared with the equivalent of standard fossil energy consumption. Thus, reducing coal consumption will greatly decrease carbon emissions [43, 44, 45].

CONCLUSIONS AND POLICY IMPLICATIONS

By considering dynamic factors such as technological progress, and capital accumulation, as well as 8 energy sectors and 13 non-energy sectors, a multi-sectoral recursive dynamic CGE model was constructed in this study to investigate the impacts of the carbon tariffs to be implemented by the USA on the structures in China. The following conclusions were obtained based on the simulation analysis. (1) Carbon tariffs will have a great effect on China's regional export structure by promoting China's exports to other countries or regions instead of the USA. After the implementation of carbon tariffs, the export ratios of low-carbon sectors will increase, whereas the export ratios will decline for some energy-intensive sectors and those that are highly dependent on exports to the USA. Carbon tariffs will have very slight impacts on China's trade scale and foreign

trade dependence. (2) Carbon tariffs will have different influences on the output structure in China. The output share of some sectors will decrease, such as high carbon exports and upstream sectors, whereas the output shares of other manufacturing sectors will increase. (3) The proportion of coal consumption will decline dramatically, whereas the proportion of clean power consumption increases, thereby improving China's energy consumption structure and reducing China's carbon intensity to some extent.

Based on these conclusions, we propose the following policy implications. First, carbon tariffs will inhibit China's exports to countries that implement carbon tariffs, whereas it will increase trade with non-carbon tariffs regions. Therefore, to enhance exports, China should insist on multilateral trade, especially by continually boosting trade with other developing countries to avoid the impacts of carbon tariffs on China's trade. According to the principle of "avoiding double taxation," a domestic carbon tax could evade or partially offset carbon tariffs. Therefore, China should consider a domestic carbon tax to reduce carbon emissions, as well as serving as an effective method for resisting carbon tariffs. Second, the output proportions of sectors with high export dependencies or those provide raw materials or services to other sectors will decrease after the implementation of carbon tariffs, whereas the output proportions of some manufacturing sectors will increase. Thus, China should try to reduce the dependence of these sectors on the foreign economy by moderately reducing external demand and increasing domestic demand. In addition, China should enhance the core competitiveness of manufacturing and encourage manufacturers to develop a low-carbon and clean-energy industry. Third, carbon tariffs may help improve China's energy consumption structure and decrease carbon intensity. Thus, there is high potential for energy conservation and emissions reduction in China. The Chinese government should encourage enterprises to use clean power, such as increasing the share of clean power, which will improve the energy structure and output structure, especially the industrial output structure. In addition, China should favor low-carbon and sustainable developments, strongly promote scientific and technological innovation, vigorously develop new energy, and increase the support strength, as well as developing alternative energy and improving energy efficiency.

ACKNOWLEDGEMENTS

This study was financially supported by the Fundamental Research Funds for the Central Universities (grant No. 2017XKQY100).

REFERENCES

- [1] Xu, S.C. and Long, R.Y. (2014) Empirical research on the effects of carbon taxes on economy and carbon emissions in China. *Environmental Engineering and Management Journal*, 13,1071-1078.
- [2] Xu, S.C., He, Z.X., Long, R.Y., Chen, H., Han, H.M. and Zhang, W.W. (2016) Comparative analysis of the regional contributions to carbon emissions in China. *Journal of Cleaner Production* 127, 406–417.
- [3] Gros, D. (2009) Global welfare implications of carbon border taxes. CESIFO Working Paper, No. 2790.
- [4] Warwick, J. and Peter, J. (2008) The economic and environmental effects of border tax adjustments for climate policy. *Bookings Institution* 7, 1-37.
- [5] Dong, Y. and Whalley, J. (2009) How large are the impacts of carbon motivated border tax adjustments. NBER Working Paper, No. 15613.
- [6] Qu, R.X. and Wu, J. (2011) Study on welfare effects of carbon tariffs. *China Population, Resources and Environment* 21(4), 37-42 (in Chinese).
- [7] Hubler, M. (2009) Can carbon based import tariffs effectively reduce carbon emissions? *Kiel Institute for the World Economy* 55, 315–327.
- [8] Springmann, M. (2012) A look inwards: Carbon tariffs versus internal improvements in emissions-trading systems. *Energy Economics* 34(2), 228-239.
- [9] Wang, M.Z., Liu, J.L., Chan, H.L., Choi, T.M. and Yue, X.H. (2015) Effects of carbon tariffs trading policy on duopoly market entry decisions and price competition: Insights from textile firms of developing countries. *International Journal of Production Economics*,
- [10] Mattoo, A., Subramanian, A., Dominique, V.D.M. and He, J.W. (2009) Reconciling climate change and trade policy. *Social Science Electronic Publishing* 26(2), 296-319(24).
- [11] Bao, Q., Tang, L., Zhang, Z.X. and Wang, S.Y., (2013) Impacts of border carbon adjustments on China's sectoral emissions: Simulations with a dynamic computable general equilibrium model. *China Economic Review* 24(1), 77-94.
- [12] Branger, F. and Quirion, P. (2014) Would border carbon adjustments prevent carbon leakage and heavy industry competitiveness losses? Insights from a meta-analysis of recent economic studies. *Ecological Economics* 99, 29-39.
- [13] Dong, Y.L., Ishikawa, M. and Hagiwara, T. (2015) Economic and environmental impact analysis of carbon tariffs on Chinese exports. *Energy Economics* 50, 80-95.
- [14] Li, A.J., Zhang, A.Z., Cai, H.B., Li, X.F. and Peng, S.S. (2013) How large are the impacts of carbon-motivated border tax adjustments on

- China and how to mitigate them? *Energy Policy* 63(6), 927-934.
- [15] Weber, C.L. and Peters, G.P. (2009) Climate change policy and international trade: Policy considerations in the US. *Energy Policy* 37(2), 432-440.
- [16] Mathiesen, L. and Maestad, O. (2004) Climate policy and the steel industry: achieving global emission reductions by an incomplete climate agreement. *Energy Journal* 25(4), 91-114.
- [17] McKibbin W.J. and Wilcoxon, P.J. (2008) The economic and environmental effects of border tax adjustments for climate policy. *Brookings Working Paper* (7), 1-37.
- [18] Lin, B.Q. and Li, A. (2011) Impacts of carbon motivated border tax adjustments on competitiveness across regions in China. *Energy* 36(8), 5111-5118.
- [19] Pan, H. (2012) Influences of carbon tariffs on Chinese export and countermeasures. *China Population, Resources and Environment* 22(2), 41-46 (in Chinese).
- [20] Zhan, Z. (2015) Carbon tariff, export subsidy and the international competitiveness of developing countries' enterprises: a study based on Bertrand model. *International Economics and Trade Research* 31(3), 54-63 (in Chinese).
- [21] Keen, M. and Kotsogiannis, C. (2014) Coordinating climate and trade policies: Pareto efficiency and the role of border tax adjustments. *Journal of International Economics* 94, 119-128.
- [22] Majocchi, A. and Missaglia, M. (2002) Environmental taxes and border tax adjustment. *Societa Italiana Economia pubblica (SIEP) Working Paper* No. 127.
- [23] Reilly, J., Paltsev, S. and Winchester, N. (2010) Will border carbon adjustments work? MIT Joint Program on the Science & Policy of Global Change. Report No. 184.
- [24] Kuik, O. and Hofkes, M. (2010) Border adjustment for European emissions trading: Competitiveness and carbon leakage. *Energy Policy* 38(4), 1741-1748.
- [25] Li, A.J. and Zhang, A.Z. (2012) Will carbon motivated border tax adjustments function as a threat? *Energy Policy* 47(10), 81-90.
- [26] Fischer, C. and Fox, A.K. (2012) Comparing policies to combat emissions leakage: Border carbon adjustments versus rebates. *Journal of Environmental Economics and Management* 64(2), 199-216.
- [27] Ghosh, M., Luo, D., Siddiqui, M. S. and Zhu, Y.F. (2012) Border tax adjustments in the climate policy context: CO₂ versus broad-based GHG emission targeting. *Energy Economics* 34(2), 154-167.
- [28] Maria, C.D., Michielsen, T.O. and Werf, E.V.D. (2013) Carbon Leakage. *Encyclopedia of Energy Natural Resource & Environmental Economics*, 255-259.
- [29] Eichner, T. and Pethig, R. (2015) Unilateral consumption-based carbon taxes and negative leakage. *Resource and Energy Economics* 40, 127-142.
- [30] Ploeg, F.V.D. (2016) Second-best carbon taxation in the global economy: The Green Paradox and carbon leakage revisited. *Journal of Environmental Economics and Management* 78, 85-105.
- [31] Sakai, M. and Barrett, J. (2016) Border carbon adjustments: Addressing emissions embodied in trade. *Energy Policy* 92, 102-110.
- [32] Hosoe, N., Gasawa, K. and Hashimoto, H., (2011) Textbook of computable general equilibrium modeling: programming and simulations. Tokyo: University of Tokyo Press, 2nd Edition.
- [33] Armington, P.S. (1969) A theory of demand for products distinguished by place of production. *IMF Staff papers* 16, 159-176.
- [34] Wang, C. (2003) Climate change policy simulation and uncertainty analysis: a dynamic CGE model of China. Tsinghua University, Beijing (in Chinese).
- [35] Lou, F. (2015) The theory and application of Chinese economy-energy-environment-tax dynamic computable general equilibrium model. Beijing: China Social Sciences Press (in Chinese).
- [36] Dixon, P.B. and Rimmer, M.T. (2002) Dynamic general equilibrium modelling for forecasting and policy: a practical guide and documentation of Monash. Amsterdam: North-Holland Publishing Company.
- [37] Elliott, J., Foster, I., Kortum S., Munson T., Cervantes F. and Weisbach D. (2010) Trade and Carbon Taxes. *American Economic Review* 100(2), 465-69.
- [38] Bao, Q., Tang, L., Wang, S.Y. and Qiao, H. (2013) Impacts of USA's carbon motivated border tax adjustments on China's economy: An analysis based on dynamic computable general equilibrium model. *Systems Engineering Theory and Practice* 33(2), 345-353 (in Chinese).
- [39] Li, J. (2013) The impact of EU carbon tax to China's external trade and welfare. Nankai University (in Chinese).
- [40] He, Z.X., Shen, W.X., Xu, S.C. (2016) Corporate environmental behavior: from literature review to theoretical framework. *Fresen. Environ. Bull.*, 25, 910-932.
- [41] Xu, S.C., He, Z.X., Long, R.Y. and Chen, H. (2016) Factors that influence carbon emissions due to energy consumption based on different stages and sectors in China. *Journal of Cleaner Production* 115, 139-148.
- [42] Xu, S.C., He, Z.X. and Long, R.Y. (2014) Factors that influence carbon emissions due to energy consumption in China: Decomposition analysis using LMDI. *Applied Energy* 127, 182-193.

- [43] Xu, S.C., Han, H.M., Zhang, W.W., Zhang, Q.Q., Long, R.Y., Chen H. and He, Z.X. (2017) Analysis of regional contributions to the national carbon intensity in China in different Five-Year Plan periods. *Journal of Cleaner Production*, 145, 209-220.
- [44] Xu, S.C., Zhang, L., Liu, Y.T., Zhang, W.W., He, Z.X., Long, R.Y. and Chen H. (2017) Determination of the factors that influence increments in CO₂ emissions in Jiangsu, China using the SDA method. *Journal of Cleaner Production*, 142, 3061-3074.
- [45] Xu, S.C., He, Z.X., Long, R.Y., Chen, H., Han, H.M. and Zhang, W.W. (2016) Comparative analysis of the regional contributions to carbon emissions in China. *Journal of Cleaner Production*, 127, 406-417.

Received: 08.04.2017

Accepted: 06.06.2017

CORRESPONDING AUTHOR

Shi-Chun Xu

Management School

China University of Mining and Technology

221116 Xuzhou – CHINA

E-mail: xushichun78@163.com

DETERMINATION OF THERAPEUTIC POTENTIAL OF *MENTHA LONGIFOLIA* SSP. *LONGIFOLIA*

Mustafa Sevindik^{1,*}, Hasan Akgul¹, Mustafa Pehlivan², Zeliha Selamoglu³

¹Akdeniz University, Faculty of Science, Department of Biology, Antalya, Turkey

²Gaziantep University, Nurdagi Vocational School, Gaziantep, Turkey

³Omer Halisdemir University, Faculty of Arts and Science, Department of Biotechnology, Nigde, Turkey

ABSTRACT

The present study aimed to determine antioxidant, antimicrobial activities and oxidative stress properties of the ethanol extracts of *Mentha longifolia* L. Hudson subsp. *longifolia*. Antioxidant activity was determined with the DPPH method. Antimicrobial activity was tested on six different microorganisms (*Staphylococcus aureus*, *Enterococcus faecalis*, *Escherichia coli*, *Pseudomonas aeruginosa*, *Candida albicans*, *Candida tropicalis*) using modified agar dilution method. Total antioxidant status (TAS), total oxidant status (TOS) and oxidative stress index (OSI) were determined using Rel Assay kits. It was observed that DPPH and antimicrobial potentials of plant samples varied based on the locations they were collected. As a result, it was considered that plant samples could be used as natural antioxidant and antimicrobial resources, but suitable regions for OSI values should be selected.

KEYWORDS:

Mentha longifolia subsp. *longifolia*, antioxidant, antimicrobial, oxidant, oxidative stress.

INTRODUCTION

According to the World Health Organization (WHO) data, 80% of the population in developing countries fulfil their basic medical needs with traditional herbal medicines [1]. At least 25% of pharmacological drugs are of herbal origin [2]. Several medicinal and aromatic plants contain compounds with pharmacological activity [3, 4]. Recent studies determined that certain medicinal and aromatic plants have anti-septic, anti-carcinogenic, anti-viral, anti-allergic, anti-inflammatory, analgesic, estrogen and immune system stimulating effects [3, 5]. The Lamiaceae family that constitutes an important part of medical plants is represented by over 6000 species worldwide [6]. In Turkey, Lamiaceae is indigenous with 45 genera and 574 species [7]. Among these, *Mentha* L. species is an important aromatic plant

with economical benefits in food, medicine, cosmetics and hygiene industries as well as anti-septic, anti-carcinogenic, expectorant, calming, diuretic effects, and effects against common cold, indigestion, nausea, and sore throat [8-10]. Depending on the intended use of these plants, the determination of their potency and oxidative stress indices based on the areas that they were collected are important to use them for health purposes. Health problems such as heart diseases, neurological disorders, diabetes and leukemia could occur due to increased oxidative stress in living organisms [11]. Today, several plant species and their parts are used as antioxidant sources that are taken as human body supplements to reduce oxidative damage [12]. Furthermore, antimicrobial potential of several plant species against resistant microorganisms and emerging diseases that are serious threats against human health, are also being investigated [13].

The aim of the present study was to investigate the antioxidant and antimicrobial activities and oxidative stress status of *Mentha longifolia* (L.) Hudson subsp. *longifolia* specimens, collected from different habitats in Gaziantep Province (Sehitkamil and Sahinbey). It was considered that antioxidant and antimicrobial potentials of plant samples taken from habitats with different characteristics could provide better assessment.

MATERIALS AND METHODS

Collection of Plant Samples and Preparation of Extracts. Taking into consideration the flowering times of the plants, samples were collected from seven different localities in Sehitkamil and Sahinbey districts in Gaziantep province. Plant specimens were collected from vicinity of agricultural area (Localities 1), irrigation area near the highway (Localities 2), creek bed near the highway (Localities 3), mountain slope (Localities 4), areas close to settlements (Localities 5), agricultural land irrigation channel (Localities 6) and wetlands near the highway (Localities 7). Collected herbarium plant specimens were preserved in the Gaziantep University, Department of Biology Herbarium.

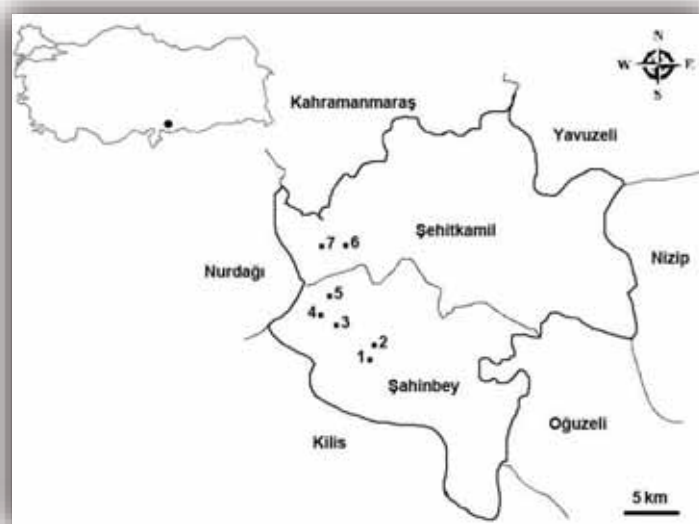


FIGURE 1
Localities of Collected of Plant Samples

The muddy parts of the plant samples were cleaned with distilled water before the drying procedure. After the samples were dried in the laboratory under adequate conditions and in the shade, over the ground sections of plant specimens (especially foliage and flowers) were pulverized by mechanical grinder. Then, the extraction process was conducted with 40 g plant material and ethanol in a soxhlet apparatus. Obtained extracts were then concentrated under pressure in a rotary evaporator and stored at +4 °C until the experiments were conducted.

Determination of Plant Antioxidant Activity. Plant free radical scavenging activities were determined with 1,1-diphenyl-2-picrylhydrazyl (DPPH) (Sigma, Aldrich) [14]. DPPH is a stable free radical with a maximum optical absorbance at 517 nm. The reaction between DPPH and the free radical scavenger decreases the absorbance level at 517 nm. Stock solutions containing 1 mg / mL compound were prepared in DMSO. 50µL solution was incubated for 30 minutes in the dark at room temperature by adding 160µL 0.039% DPPH. Then, absorbance was read at 517nm. Procedures for all concentrations and samples were repeated subsequently. Ascorbic acid was used as a reference antioxidant. Then DPPH free radical scavenging percentages were calculated using the formula below:

$$\text{Scavenging Activity (\%)} = \left[\frac{A_{\text{DPPH}} - A_{\text{Sample}}}{A_{\text{DPPH}}} \right] \times 100$$

Determination of Plant Sample TAS, TOS and OSI Values. Total antioxidant status (TAS) and total oxidant status (TOS) of plant samples were determined using Rel Assay kit (Rel Assay Kit Diagnostics, Turkey). Trolox, a water-soluble compound

of vitamin E, was used as a calibrator for TAS tests. The results are expressed as mmol Trolox equiv./L [15]. Hydrogen peroxide was used as calibrator for TOS tests. The results are expressed as µmol H₂O₂ equiv./L [16]. The following formula was used when calculating the OSI, the ratio of the TOS values to the TAS values [16].

$$\text{OSI} = \frac{\text{TOS, } \mu\text{mol H}_2\text{O}_2 \text{ equiv./L}}{\text{TAS, mmol Trolox equiv./L} \times 10}$$

Determination of Plant Sample Antimicrobial Activity. Antimicrobial activities of plant specimens were determined using the agar dilution method recommended by the Clinical and Laboratory Standards Institute (CLSI). Minimal inhibitor concentrations (MIC) for each compound were tested against standard bacterial and fungal strains. Utilized bacterial strains, *Staphylococcus aureus* ATCC 29213, *Enterococcus faecalis* ATCC 29212, *Escherichia coli* ATCC 25922, *Pseudomonas aeruginosa* ATCC 27853, and fungus strains, *Candida albicans* ATCC 10231, *Candida tropicalis* ATCC 13803 were procured from American Type Culture Collection (ATCC) Rockville, Md.

Bacterial strains were pre-cultured in Muller Hinton broth (Merck) medium, and fungal strains were pre-cultured in RPMI 1640 broth (Sigma-Aldrich Chemie GmbH, Taufkirchen, Germany) medium. Bacteria and fungi turbidity were prepared with Mcfarland no. 0.5 scale to obtain standard inoculum [17]. All solutions of the extracts were made using 50% dilution of DMSO. All extract dilutions were prepared with distilled water. Test compound concentrations were 800, 400, 200, 100, 50, 25, 12.5

and 6.25 µg / mL. For fluconazole fungi, Ampicillin and for bacteria, Ciprofloxacin were used as standard drugs. Standard inoculums of bacteria and fungi (10⁶ CFUs / mL) were planted on agar plates using sterile plastic ring nose loop (0.01 mL). All planted plates were stored at 35 °C for 16-20 hours for the bacteria and 48 hours for the fungi in the incubator. The minimum concentration that prevented bacteria and fungi reproduction was determined as minimal inhibitor concentration (MIC) [18, 19].

RESULTS AND DISCUSSION

DPPH Activity. The % inhibition values for different concentrations (µg / mL) of the ethanol extracts of plant samples collected from different regions are presented in Table 1.

Based on the findings presented in Table 1, the DPPH free radical scavenging activities of the samples varied depending on the sample concentrations and localities. Although all samples demonstrated low activity compared to the control, it was determined that the antioxidant levels were high. Furthermore, it was observed that antioxidant activities increased due to the increase in concentration. However, decreases were observed in the antioxidant activities of the plant samples collected from the 4th and 5th localities when compared to others. It was determined that the highest antioxidant activity was observed in samples collected from the creek near the highway and the lowest antioxidant activity was observed in samples collected from the close to settlements area.

In the present study, free radical scavenging activities of different concentrations of *Mentha longifolia* subsp. *longifolia* ethanol extracts were tested

with the DPPH method. Literature review demonstrated that the methanol extracts of *Mentha longifolia* subsp. *longifolia* also exhibited antioxidant activity [20]. Furthermore, DPPH free radical scavenging activity of methanol extracts of *Mentha longifolia* plant collected in Tunisia was investigated and it was determined as 53.29 % at 200 µg / mL concentration [21]. The plant sample scrutinized in the present study was *Mentha longifolia* subsp. *longifolia*. The findings obtained in the study demonstrated that the plant samples tested had higher DPPH scavenging activities compared to the results of other previous studies conducted by different researchers. The differences between the data obtained could have been due to the differences in the plant taxa, the solvents used and the locations where the samples were obtained.

Roadside plants are exposed to higher stress when compared to field crops [22]. It is known that the resistance mechanisms in plants increase the amount of secondary substance which can protect the plant against harsh conditions in case of exposure to stress. The synthesis and volume of phenolic compounds, which are an important group of secondary metabolites, would also increase due to the stimuli stemming from stress factors in plants. One of the most important known properties of phenolic substances is that they have antioxidant effects.

Current study findings demonstrated that the extracts of plants collected from the roadside had higher DPPH free radical scavenging activity when compared to plant samples collected from the vicinity of the fields, and this was considered to be due to the increased phenolic substance amount as a result of the exposed stress.

TABLE 1
DPPH Free Radical Sweeping Activity Percentages of Samples

Concentration (µg/mL)	Ascorbic Acid (%)	1(%)	2(%)	3(%)	4(%)	5(%)	6(%)	7(%)
25	64.38±0.69	53.58±1.50	56.14±1.21	56.36±1.88	49.15±1.55	48.46±1.32	54.22±2.33	52.65±1.94
50	92.52±0.95	70.36±1.78	73.26±1.50	74.91±2.26	62.76±2.18	61.63±1.29	71.17±1.14	70.01±0.89
100	95.42±0.71	87.52±0.39	90.68±1.46	92.94±1.83	79.64±1.95	76.67±2.61	89.36±2.26	80.94±2.27
200	96.91±1.00	85.13±1.27	87.74±1.30	89.16±1.12	79.40±1.57	74.54±1.67	86.35±0.76	80.14±1.13

Numbers from 1 to 7 indicate locations where plant samples are collected.

The results indicate % inhibition values.

Values are presented as mean ± SD; N = 3

TABLE 2
TAS, TOS and OSI Values of Samples

Samples	TAS (mmol/L)	TOS (µmol/L)	OSI (TOS/(TASx10))	Localities
Localities-1	3.628 ± 0.234	4.046 ± 0.615	0.112 ± 0.025	Vicinity of agricultural area
Localities-2	2.453 ± 0.322	13.698 ± 0.813	0.558 ± 0.115	Irrigation area near the highway
Localities-3	2.244 ± 0.279	11.545 ± 0.327	0.514 ± 0.052	Creek bed near the highway
Localities-4	1.856 ± 0.129	11.980 ± 0.652	0.645 ± 0.081	Mountain slope
Localities-5	1.809 ± 0.075	11.058 ± 0.610	0.611 ± 0.008	Areas close to settlements
Localities-6	1.862 ± 0.203	11.967 ± 0.690	0.643 ± 0.035	Agricultural land irrigation channel
Localities-7	2.215 ± 0.242	14.077 ± 0.634	0.635 ± 0.102	Wetlands near the highway

Values are presented as mean±S.D.; n=5

TABLE 3
Minimal Inhibitor Concentration (MIC) Values of Samples

Samples	<i>S. aureus</i> ($\mu\text{g/mL}$)	<i>E. faecalis</i> ($\mu\text{g/mL}$)	<i>E. coli</i> ($\mu\text{g/mL}$)	<i>P. aeruginosa</i> ($\mu\text{g/mL}$)	<i>C. albicans</i> ($\mu\text{g/mL}$)	<i>C. tropicalis</i> ($\mu\text{g/mL}$)
Localities -1	100	100	50	100	50	50
Localities -2	400	400	800	800	200	200
Localities -3	200	200	400	400	200	200
Localities -4	50	50	50	100	50	50
Localities -5	200	200	100	100	100	100
Localities -6	50	50	200	200	50	50
Localities -7	50	50	100	100	50	50
Flukonazole	-	-	-	-	1.56	3.12
Ampicillin	3.12	1.56	3.12	-	-	-
Ciprofloxacin	0.78	0.78	1.56	3.12	-	-

* 800, 400, 200, 100 and 50 ($\mu\text{g} / \text{mL}$) indicate extract concentrates affecting microorganisms.

TAS, TOS and OSI Values. TAS, TOS and OSI values for plant samples used in the study were determined by Rel Assay kits and the obtained findings are presented in Table 2.

Oxidative stress could occur in situations where antioxidant compounds that are effective in removing oxidative substances that form due to metabolic reactions and environmental factors are insufficient [23]. Oxidative stress causes lipid peroxidation and oxidative DNA damage, and it can also lead to dangerous phenomena such as physiological adaptation events and regulation of intracellular signal transduction [24]. As presented in Table 2, the TAS, TOS and OSI values of the plant ethanol extracts varied based on the location they were collected. It was observed that the sample collected vicinity of agricultural area had the highest TAS value with 3.628 (mmol / L). It was determined that the highest TOS value was 14.077 ($\mu\text{mol} / \text{L}$) in the sample collected from the wetlands near the highway. The samples collected from the mountain slopes had the highest OSI value. The lowest TAS value was found in samples collected near the settlement with 1.809 (mmol / L). The lowest TOS value was observed at 4.046 ($\mu\text{mol} / \text{L}$) in the samples collected in the vicinity of agricultural area. The lowest OSI value was determined in the samples obtained vicinity of agricultural area as well.

High levels of oxidative stress products in plants at the base of the food chain could be a threat and a factor that can cause oxidative damage to all living beings in the food chain that consume these plants [25]. In the present study, the oxidative stress status of *Mentha longifolia* subsp. *longifolia* was determined. Oxidative stress was observed in all plant samples obtained from each locality, and it was determined that the lowest OSI value was found in samples collected near the agricultural field. It was considered that this was due to the easier access of the organisms to nutrients and water in that area, and the more advantageous status of the plants in that area when compared to the other sites in terms of food competition. High OSI values were found due

to the high TOS values in all plant samples except the locality no. 1 (near the agricultural field). It could be argued that the collected plant samples were exposed to oxidative stress factors at all other locations except the agriculture field. The highest OSI values were determined in plant samples collected from mountain slopes, which are considered to be less exposed to environmental stressors.

Antimicrobial Activity. Sample ethanol extracts were studied with the CLSI-recommended agar dilution method and the obtained results are presented in Table 3.

The antimicrobial activities of *M. longifolia* subsp. *longifolia* essential oil and plant extracts were determined in several studies, and this activity was reported to be particularly related to the phenolic content of the plant [20, 26-28]. As a result of the antimicrobial activity tests conducted in the present study, it was found that the antimicrobial activities varied based on the localities where the plants were collected. As seen in Table 3, the highest antimicrobial activity was observed in the samples collected at the 4th location. The samples collected at the 4th location were effective against *P. aeruginosa* at 100 ($\mu\text{g} / \text{mL}$) extract concentration, while they exhibited antimicrobial activity against other microorganisms at an extract concentration of 50 ($\mu\text{g} / \text{mL}$). The lowest antimicrobial activity was determined in plant samples taken at 2nd and 3rd locations at different extract concentrations. Saeidi et al. found that *M. longifolia* subsp. *longifolia* essential oil content and amount varied based on geographical regions [29]. The findings obtained by Saeidi et al. are significant in explaining and supporting the differences in antimicrobial activity observed in different regions in the present study.

When the general antimicrobial activity data for all plant samples obtained in the present study are evaluated, it was found that the plant extracts used in the study were more effective against Gram positive bacteria and fungal strains when compared to Gram negative bacteria.

CONCLUSIONS

Free radicals are formed during vital activities in organisms (respiration, enzyme reactions, autoxidation reactions, etc.) and via external factors (cigarette smoke, air pollution, UV rays, ionizing radiation, xenobiotics, etc.). Oxidative lesions, tissue damage, mutations, and necrosis could also occur with the overproduction of reactive oxygen species (often free radicals). These effects of radicals could lead to various pathological conditions in the body. Agents known as antioxidants have a protective role against these harmful radicals. These agents could be taken either artificially or naturally from nutrients [30]. In recent years, the trend towards natural products that are considered as antioxidant, antimicrobial, anti-inflammatory and similar agents is rapidly increasing in prevention and treatment of diseases. Accordingly, various speculations on natural products could arise and lead to information pollution. It is our opinion that the present study, which aimed to determine in which ecological and phytogeographical area did plant samples collected from different regions have higher antioxidant and antimicrobial capacities, could serve as a scientific response to various speculations on the benefits of several natural products such as plants. The comparison of the abovementioned properties of natural biological material, especially the plants, and how to use these materials has been the center of increased attention recently. It was stated that the quality of natural products depended on the chemical components and floral origins as a result of plant polyphenol measurements. Phenolic content of these products are influenced by the environmental conditions, geographical and climatic characteristics of the regions where they were obtained. The quantity and identity of the polyphenols in plants are of interest due to these factors. Furthermore, the antioxidant capacity of these products is provided by flavonoids and phenolic acids. Phenolic acids are common metabolites found in plants [31]. In recent years, the focus was on phenolic acids that have a potent protective role against the damages caused by oxidative stress.

In the present study, conducted on herbal products that could be used as natural antioxidants; when the antimicrobial potentials of these products in conjunction with TAS, TOS and OSI values were analyzed, it was determined that the samples exhibited different properties based on the locations they were collected. It seems that this difference was due to the variations in chemical content of the samples and the environmental stress factors they were exposed to.

In the present study, *M. lonfigolia* subsp. *longifolia* specimens were extracted and TAS, TOS and OSI values and antimicrobial activities were determined using "Rel Assay" brand commercial kits. The present study is significant since it included *in vitro* analyses with highly reliable tests based on useful

and precise measurements. As a result, the data obtained in the present would contribute to the literature, as well as providing extremely important data about the comparison of bioactive properties of natural products and how they could be exploited.

Study results demonstrated that *M. lonfigolia* subsp. *longifolia* plant ethanol extracts exhibited variable activities. Especially the high antioxidant properties observed in the specimens with variable properties collected from the localities with high environmental stress factors such as roadsides suggested that the geographical conditions affect the antioxidant properties significantly. This deduction that resulted from antioxidant activity results was different for metabolites with antimicrobial activities. This could be due to the ability of the plant to develop different resistance mechanisms against various environmental factors such as environmental chemicals as antioxidant and antimicrobial activity mechanisms. In the present study, an assessment was made based on only biological activities. Phytochemical studies are planned to be conducted in the future.

REFERENCES

- [1] Deka, H., Deka, S. and Baruah, C.K. (2015) Plant Growth Promoting Rhizobacteria for Value Addition: Mechanism of Action. In: D. Egamberdieva et al. (eds.), Plant-Growth-Promoting Rhizobacteria (PGPR) and Medicinal Plants, Soil Biology 42. Springer International Publishing, Switzerland 305-321.
- [2] Berber, I., Avsar, C., Cine, N., Bozkurt, N. and Elmas, E. (2013) Sinop'da Yetisen Bazi Bitkilerin Metanolik Ekstraktlarının Antibakteriyel ve Antifungal Aktivitelerinin Belirlenmesi. *Karaelmas Science and Engineering Journal*, 3(1), 10-16.
- [3] Fatiha, B., Didier, H., Naima, G., Khodir, M., Martin, K., Leocadie, K., Caroline, S., Mohamed, C. and Pierre, D. (2015) Phenolic composition, *in vitro* antioxidant effects and tyrosinase inhibitory activity of three Algerian *Mentha* species: *M. spicata* (L.), *M. pulegium* (L.) and *M. rotundifolia* (L.) Huds. (Lamiaceae). *Ind. Crops Prod.*, 74, 722-730.
- [4] Benabdallah, A., Rahmoune, C., Boumendjel, M., Aissi, O. and Messaoud, C. (2016) Total phenolic content and antioxidant activity of six wild *Mentha* species (Lamiaceae) from northeast of Algeria. *Asian Pac J Trop Biomed*, 6(9), 760-766
- [5] Abdelli, M., Moghrani, H., Aboun, A. and Maachi, R. (2016) Algerian *Mentha pulegium* L. leaves essential oil: chemical composition, antimicrobial, insecticidal and antioxidant activities. *Ind. Crop. Prod.*, 94, 197-205.

- [6] Wagstaff, S.J., Hickerson, L., Spangler, R., Reeves, P.A. and Olmstead, R.G. (1998) Phylogeny in Labiatae s. l., inferred from cpDNA sequences. *Pl. Syst. Evol.*, 209,265-274.
- [7] Kahraman, A., Celep, F. and Dogan, M. (2009) Morphology, Anatomy and Palynology of *Salvia indica* L. (Labiatae). *World Applied Sciences Journal*, 6(2), 289-296.
- [8] Biswas, N.N., Saha, S. and Ali, M.K. (2014) Antioxidant, antimicrobial, cytotoxic and analgesic activities of ethanolic extract of *Mentha arvensis* L. *Asian Pacific Journal of Tropical Biomedicine*, 4(10), 792-797
- [9] Singh, R., Shushni, M.A.M. and Belkheir, A. (2015) Antibacterial and antioxidant activities of *Mentha piperita* L. *Arabian Journal of Chemistry*, 8, 322–328
- [10] Patel, A., Pandey, V. and Patra, D.D. (2016) Metal absorption properties of *Mentha spicata* grown under tannery sludge amended soil-its effect on antioxidant system and oil quality. *Chemosphere*, 147, 67-73.
- [11] Shameem, N., Kamili, N.A., Ahmad, M., Masoodi, F.A. and Parray, J.A. (2015) Radical scavenging potential and DNA damage protection of wild edible mushrooms of Kashmir Himalaya. *Journal of the Saudi Society of Agricultural Sciences*, <http://dx.doi.org/10.1016/j.jssas.2015.10.005>.
- [12] Mujic, I., Zekovic, Z., Lepojevic, Z., Vidovic, S. and Zivkovic, J. (2010) Antioxidant Properties of Selected Edible Mushroom Species. *Journal Central European Agriculture*, 11(4), 387-392.
- [13] Bakht, J., Shaheen, S. and Shafi, M. (2014) Antimicrobial potentials of *Mentha longifolia* by disc diffusion method. *Pak. J. Pharm. Sci.*, 27(4), 939-945.
- [14] Shimada, K., Fujikawa, K., Yahara, K. and Nakamura, T. (1992) Antioxidative properties of xanthan on the autoxidation of soybean oil in cyclodextrin emulsion. *Journal of Agricultural and Food Chemistry*, 40, 945–948.
- [15] Erel, O. (2004) A novel automated direct measurement method for total antioxidant capacity using a new generation, more stable ABTS radical cation. *Clin Biochem.*, 37, 277-285.
- [16] Erel, O. (2005) A new automated colorimetric method for measuring total oxidant status. *Clin Biochem.*, 38, 1103-1111.
- [17] Hindler, J., Hochstein, L. and Howell, A. (1992) Preparation of routine media and reagents used in antimicrobial susceptibility testing. Part 1. McFarland standards, p. 5.19.1-5.19.6. In H. D. Isenberg (ed.) *Clinical microbiology procedures handbook*, vol. 1. American Society for Microbiology, Washington, D.C.
- [18] CLSI (Clinical and Laboratory Standards Institute) (2003) *Methods for Dilution Antimicrobial Susceptibility Tests for Bacteria That Grow Aerobically*; Approved Standard-Seventh Edition, CLSI Document M7-A7, Pennsylvania USA.
- [19] CLSI (Clinical and Laboratory Standards Institute) (2002) *Reference Method for Broth Dilution Antifungal Susceptibility Testing of Yeasts*; Approved Standard-Second Edition. NCCLS document M27-A2 (ISBN 1-56238-469-4). NCCLS Pennsylvania USA.
- [20] Gulluce, M., Sahin, F., Sokmen, M., Ozer, H., Daferera, D., Sokmen, A., Polissiou, M., Adiguzel, A. and Ozkan, H. (2007) Antimicrobial and antioxidant properties of the essential oils and methanol extract from *Mentha longifolia* L. ssp. *longifolia*. *Food Chemistry*, 103, 1449–1456.
- [21] Hajlaoui, H., Trabelsi, N., Noumi, E., Snoussi, M., Fallah, H., Ksouri, R. and Bakhrouf, A. (2009) Biological activities of the essential oils and methanol extract of two cultivated mint species (*Mentha longifolia* and *Mentha pulegium*) used in the Tunisian folkloric medicine. *World J Microbiol Biotechnol.*, 25, 2227–2238.
- [22] Wagh, N.D., Shukla, P.V., Tambe, S.B. and Ingle, S.T. (2006) Biological monitoring of roadside plants exposed to vehicular pollution in Jalgaon city. *Journal of Environmental Biology*, 27(2), 419-421.
- [23] Rahman, T., Hosen, I., Islam, M.M.T. and Shekhar, H.U. (2012) Oxidative stress and human health. *Advances in Bioscience and Biotechnology*, 3, 997-1019.
- [24] Yoshikawa, T. and Naito, Y. (2002) What Is Oxidative Stress? *JMAJ*, 45(7), 271-276.
- [25] Stasinou, S., Nasopoulou, C., Tsirikla, C. and Zabetakis, I. (2014) The bioaccumulation and physiological effects of heavy metals in carrots, onions, and potatoes and dietary implications for Cr and Ni: a review. *J Food Sci.*, 79(5), 765-80.
- [26] Kitic, D., Jovanovic, T., Ristic, M., Palic, R. and Stojanovic, G. (2002) Chemical Composition and Antimicrobial Activity of the Essential Oil of *Calamintha nepeta* (L.) Savi ssp. *glandulosa* (Req.) P.W. Ball from Montenegro. *Journal of Essential Oil Research*, 14(2), 150-152.
- [27] Sahin, F., Karaman, I., Gulluce, M., Ogutcu, H., Sengul, M. and Adiguzel, A. (2003) Evaluation of antimicrobial activities of *Satureja hortensis* L. *J Ethnopharmacol.*, 87, 61–65.
- [28] Karaman, I., Sahin, F., Gulluce, M., Ogutcu, H., Sengul, M. and Adiguzel, A. (2003) Antimicrobial activity of aqueous and methanol extracts of *Juniperus oxycedrus* L. *J Ethnopharmacol.*, 85, 231–235.
- [29] Saeidi, Z., Babaahmadi, H., Saeidi, K.A., Salehi, A., Jouneghani, R.S., Amirshakari, H. and Taghipour, A. (2012) Essential oil content

and composition of *Mentha longifolia* (L.) Hudson grown wild in Iran. *Journal of Medicinal Plants Research*, 6(29), 4522-4525.

- [30] Selamoglu, Z., Akgul, H. and Dogan, H. (2016) Environmental Effects on Biologic Activities of Pollen Samples Obtained from Different Phyto-geographical Regions in Turkey. *Fresen. Environ. Bull.*, 25(7), 2484-2489.
- [31] Gomez-Caravaca, A.M., Gomez-Romero, M., Arraez-Roman, D., Segura-Carretero, A. and Fernandez-Gutierrez, A. (2006) Advances in the analysis of phenolic compounds in products derived from bees. *Journal of Pharmaceutical and Biomedical Analysis*, 41, 1220- 1234.

Received: 08.04.2017

Accepted: 27.05.2017

CORRESPONDING AUTHOR

Mustafa Sevindik

Department of Biology

Faculty of Science

Akdeniz University

Antalya, 07058 - TURKEY

E-mail: sevindik27@gmail.com

ALLEVIATION OF CARBOFURAN TOXICITY EFFECT BY PARSLEY ON LIPIDS PROFILE OF MALE ALBINO RATS

Yasmin Emam Abdel-Mobdy¹, Hossam Saad El-Beltagi^{2,*}, Ahmed Emam Abdel-Mobdy³

¹Entomology and Pesticide Dept, Faculty of Agriculture, Cairo University, Cairo- Egypt

²Biochemistry Dept, Faculty of Agriculture, Cairo University, P. Box 12613, Gamma St, Giza, Cairo- Egypt

³Dairy science Dept, Faculty of Agriculture, Cairo University, Cairo- Egypt

ABSTRACT

The influences of carbofuran on lipid profile in blood plasma as well as liver, kidneys and brain tissues which connected with the oxidative shunt of pentose phosphate pathway (glucose-6-phosphate dehydrogenase (G6PD) and 6-phosphogluconate dehydrogenase (6PGD)) enzymes were determined. Also the alleviation of carbofuran toxicity using parsley and its methanolic extract (ingestion and injection) was studied. Carbofuran was ingested orally at dose of 1/20 LD₅₀ for 3 months (one dose every 48 hours). Lipid profile such as total lipids, cholesterol, triglycerides, phospholipids and LDL-C contents of serum, liver, kidneys and brain were increased in carbofuran intoxicated rats relative to control, but the content of HDL-C was unchanged relative to control. The same trend was observed for G6PD and 6PGD activities of liver, kidneys and brain cytosols as well as serum of intoxicated animals which connected and associated with lipid anabolism. The carbofuran ingestion significantly augmented the both enzyme activities relative to control animals. It can be concluded that, the three parsley treatments as antioxidative agents ameliorated the desirable influences of the pesticide these may be due to the lipotropic factors of parsley. The values of lipid profile fractions were still higher in treated intoxicated rats than those of normal health control.

KEYWORDS:

Carbofuran, parsley, lipids Profile, pentose phosphate pathway, toxicity, rats

INTRODUCTION

Carbofuran is employed as a carbamate pesticide in the keeping and growing the agricultural crops. This pesticide has chemical name of 2, 3 dihydro-2, 2 dimethyl, 7-benzo furanyl methyl carbamate with registry no. (1563-66-2). Carbofuran similar to that of the organophosphates is cholinesterase inhibitor; it is systemic mode of action with predominantly contact and stomach action. It is using as control soil-dwelling and foliar-feeding

insects (including wire worms, white grubs, millipedes, symphylids, frit flies, been seed flies, root flies, flea beetles, weevils, semiarid flees, aphids trips, etc.) and nematodes in vegetable, ornamentals beet, maize, sorghum, sunflowers, oil seed rape, potato, alfalfa, peanuts, soya beans, sugar cane, rice, cotton, coffee, cucurbits, tobacco, lavender, citrus, vines, strawberries, bananas and other crops [1]. The contamination of food occurs from contact with pesticide-laden surfaces, thus increasing the potential for excess dietary exposure of children and adult [2]. To establish any toxicological data acute toxicity tests are considered to be the base line or preliminary studies for chronic toxicity tests. In this respect, carbofuran is one of the most widely used carbamate pesticides in Egyptian environment. Guidelines that limit pesticide residues on food are developed and enforced by public health agencies world wide. These guidelines incorporate data from many sources into the risk assessment process including high-dose animal toxicity studies [3]. Neelima et al. [4] reported that in rats, the body weight gain was significantly decreased according the type of carbamate. Abdel-Moneim et al. [5] observed markedly increased liver, kidneys and spleen relative weight by the effects of fenitrothion. Carbamate pesticides inhibit the activity of cholinesterase in rats [6-8].

Parsley is a member of the Umbelliferae family that has been employed in food, pharmaceutical, perfume and cosmetic industries [9]. Parsley is used as antioxidant in folk medicine and treats a wide variety of conditions [10]. Parsley contains two types of unusual components that provide unique health benefits such as volatile oil and flavonoids [11, 12]. Also, it is an excellent source of vitamin C, β -carotene and folic acid. β -carotene is important antioxidant, works in the fat-soluble areas in the body [13, 14].

Accordingly, interest has recently grown in the role and usage of natural antioxidant as strategy to prevent oxidative damage in various health disorders with oxidative stress [15]. Natural antioxidants from plants are reported to provide substantial protection that slows down the process of oxidative damage caused by ROS; they also find use as nutraceuticals due to their impact on the status of human health and disease prevention [16].

The objective of the present studies was to evaluate the biochemical perturbations induced by carbofuran in rat lipids profile as well as oxidative shunt enzymes of pentose phosphate pathway of serum as well as cytosolic fractions of liver, kidneys and brain tissues and to evaluate the alleviation and protective influences of parsley and its methanolic extract (ingestion and injection) against the oxidative stress and damage induced by carbofuran harmful.

MATERIALS AND METHODS

Materials. Carbofuran 75% wp technical (insecticide and nematicide), empirical formula: $C_{12}H_{15}NO_3$, molecular weight: 221.3 with colorless crystals. Solubility in water (351 mg/L, 25°C), dichloromethane (> 200 g/L, 10°C), isopropanol (20-50 g/L) and toluene (10-20) g/L). The technical carbofuran form was provided from Central Agricultural Pesticides Laboratory, ARC, Ministry of Agriculture, Dokki, Giza, Egypt which used of the present studies.

Samples of parsley (*Petroselinum crispum*) were purchased from the local markets. The leaves were identified by the Department of Agricultural Botany, Fac. Agric., Cairo Univ. The edible parts of the parsley were cut, dried at 50°C till to complete dryness and weighed to calculate the moisture content. The dried samples were ground to fine powder for the chemical analysis and biological experiment.

Chemical analysis. The determination of total phenols was performed according to the method described in AOAC [17] as Gallic acid equivalent.

The HPLC analysis of the plant for qualitative detection and qualitative determinates was done after the methanolic extraction [18]. The phenolic compounds of the methanolic extract determined by JASCO HPLC using hypersil C_{18} reversed phase column (250 × 4.6 mm) with 5 μ particle size.

Animals, diets and ethical statement. For the biological experiments 56 male albino rats (Sprague-Dawley) weighing 120±5 g were used in present study. The animals were obtained from Agriculture Research Center, Giza, Egypt. The animals were acclimated to laboratory condition in stainless cages for 2 weeks. Access of balanced diet and water were provided *ad libitum* during the 90 days experimental period [19]. All experimental protocols were approved by Cairo University Ethics Committee for the Care and Use of Experimental Animals in Education and Scientific Research (CU-IACUC).

Acute oral LD_{50} of carbofuran 75% wp as active ingredient was carried out according to Weil [21] as the following: 20 rats were divided into 4 groups, 5 rats of each. Serial concentration from the

carbofuran 75% wp were prepared, each group of rats were ingested orally with special dose of the pesticide. These groups of rats were kept under observation for 24 hours.

The other 36 rats (after the adaptation period) were divided into 6 groups, 6 rats of each. The first group (G1) as health normal control, rats fed on the normal balanced diet. Second group (G2), normal rats fed on the semi-modified diet (basal diet with 5% dried parsley). Third group (G3), as intoxicated control rats ingested by 1/20 of the carbofuran pesticide LD_{50} (every two days during 90 days of experimental period) and fed on the balanced diet. Fourth group (G4), the intoxicated animals fed on the semi-modified diet with 5% parsley. Fifth group (G5), the intoxicated rats ingested by 50 mg/kg body weight of the dried Parsley methanolic extract (every two days during the experimental period) and fed on the normal diet. Sixth group (G6), the intoxicated rats injected (i.p) by 50 mg/kg body weight of the dried Parsley methanolic extract in water every two days during the 90 day experimental period and fed on the normal diet.

At the end of the experimental period (90 days) rats were killed by decapitation and blood samples were collected and subjected to centrifugation to obtain serum. Liver, kidneys and brain of the all experimental rats were removed, their weight was recorded and chilled up for analysis. The cytoplasmic fractions (cytosol) of the three organs were done according to Astawrov [22] methods.

TABLE 1
Acute oral toxicity of carbofuran

Dose mg/kg b.w	No of treated rats	No of died rats	% of mortality	LD_{50} mg/kg Body weight
8.00	5	1	20	10.65
10.00	5	2	40	
12.00	5	3	60	
16.00	5	5	100	

TABLE 2
HPLC analysis of phenolics in methanolic extract of parsley with

No.	Compounds	D.W. (mg/100g)	%	F.W. ppm
1	Gallic acid	7	0.28	10.5
2	<i>P</i> -OH-benzoic	2	0.08	3
3	Catechin	171	6.95	256.5
4	Caffic acid	41	1.67	61.5
5	Phenol	102	4.14	153
6	Daidzin	10	0.41	15
7	<i>P</i> -Coumaric acid	94	3.82	141
8	Genistein	1917	77.90	2875.5
9	Furulic acid	35	1.42	52.2
19	Dadzein	35	1.42	52.2
11	Quercetin	41	1.67	61.5
12	Kaempferol	2	0.08	3
13	Chrysin	2.5	0.10	4
14	Galangin	1.5	0.06	2.3
	Total	2461	100	3691.8

TABLE 3
Organs weight ratio of the experimental male albino rats

Groups	Body weight	Liver		Kidneys		Brain	
		Weight (g)	Ratio %	Weight (g)	Ratio %	Weight (g)	Ratio %
G1	325.11±20.01	13.33±1.01	4.10±0.31 ^c	2.28±0.16	0.70±0.04 ^d	1.79±0.10	0.55±0.03 ^c
G2	310.00±17.23	12.65±0.97	4.08±0.30 ^c	2.20±0.12	0.71±0.03 ^d	1.74±0.11	0.56±0.04 ^c
G3	241.21±18.00	14.71±1.03	6.10±0.42 ^a	3.01±0.22	1.25±0.09 ^a	2.00±0.19	0.83±0.07 ^a
G4	284.20±20.02	13.21±1.00	4.65±0.40 ^b	2.41±0.16	0.85±0.05 ^c	1.89±0.17	0.67±0.07 ^b
G5	282.00±19.94	13.87±0.99	4.92±0.41 ^b	2.63±0.18	0.93±0.05 ^b	1.96±0.18	0.70±0.06 ^b
G6	290.21±18.84	13.74±1.11	4.73±0.43 ^b	2.54±0.20	0.88±0.06 ^{bc}	1.90±0.15	0.65±0.05 ^b

Values are expressed as means ± SD (n= 6). Values with different superscript letters within the same column are significantly different ($P < 0.05$). G1: Normal control, G2: Normal rats fed on semi-modified diet with 5% Parsley, G3: Intoxicated control, G4: Intoxicated rats fed on semi-modified diet with 5% Parsley, G5: Intoxicated rats ingested by Parsley methanolic extract (50 mg/kg b.w) and G6: Intoxicated rats injected by Parsley methanolic extract (50 mg/kg b.w).

TABLE 4
Serum lipid profile (mg/dl) of the experimental male albino rats

Groups	Total lipids	Triglycerides	Cholesterol	Phospholipids	HDL-C	LDL-C
G1	671.01±40.12 ^b	185.12±9.43 ^b	162.50±9.43 ^b	170.00±9.71 ^b	34.12±2.13 ^b	31.21±2.11 ^b
G2	627.51±39.21 ^b	174.33±9.81 ^b	153.17±7.99 ^b	158.96±8.16 ^b	36.66±1.99 ^{ab}	31.42±1.97 ^b
G3	780.11±41.21 ^a	218.61±11.23 ^a	185.24±8.88 ^a	197.16±10.11 ^a	33.99±2.22 ^b	37.01±2.34 ^a
G4	743.52±45.23 ^a	190.24±9.99 ^{ab}	178.11±9.81 ^a	189.26±9.99 ^a	38.11±2.41 ^a	33.10±2.01 ^b
G5	756.23±49.41 ^a	207.26±11.11 ^a	183.13±9.99 ^a	192.32±10.12 ^a	35.52±2.14 ^{ab}	33.99±2.00 ^{ab}
G6	736.11±39.91 ^{ab}	201.17±12.31 ^{ab}	177.32±8.97 ^{ab}	186.31±10.01 ^a	36.71±1.98 ^{ab}	32.11±2.11 ^b

Values are expressed as means ± SD (n= 6). Values with different superscript letters within the same column are significantly different ($P < 0.05$). G1: Normal control, G2: Normal rats fed on semi-modified diet with 5% Parsley, G3: Intoxicated control, G4: Intoxicated rats fed on semi-modified diet with 5% Parsley, G5: Intoxicated rats ingested by Parsley methanolic extract (50 mg/kg b.w) and G6: Intoxicated rats injected by Parsley methanolic extract (50 mg/kg b.w).

Biochemical analysis. The determination of glucose-6-phosphate dehydrogenase (G6PD) and 6-phosphogluconate dehydrogenase (6PGD) activities in cytosol of organs and serum were carried out by Glock and McLean [22]. Lipid profile as total lipids, cholesterol, triglycerides and phospholipids in serum and the three studied organs were determined [23-26]. Serum lipoprotein profile such as HDL-C and LDL-C contents were determined [27, 28]. Total soluble protein of serum and cytosol was determined by the method of Bradford [29].

Statistical analysis. The experimental results were expressed as mean standard deviation (SD) of triplicate measurements. The data were subjected to one way analysis of variance and the significance of differences between means were calculated by Duncan's multiple range test using SPSS for Windows, standard version 10, and the significance accepted at $P < 0.05$.

RESULTS AND DISCUSSION

It is common practice to utilize the LD₅₀ value to evaluate the toxicity of the pesticide. LD₅₀ of oral ingestion was estimated of single dose of carbofuran that can be expected to use death in 50% of rats (mg/kg b.w). The acute oral toxicity LD₅₀ value was 10.65 mg/kg body weight in male albino rats (Table 1). The results of carbofuran LD₅₀ are in agreement around those of pesticide Manual (1)

which showed values of 12-15 mg/kg b.w. Chemicals are considered highly toxic when the LD₅₀ is small (up to 650 mg/kg b.w) a practically non-toxic when the value is large (> 5000 mg/kg b.w). However, the LD₅₀ does not reflect any effects from long-term exposure such as cancer, birth defect or reproductive toxicity... etc., that may occur at levels below that level (3).

In case of parsley phenolic compounds (Table 2), HPLC analysis of its methanolic extract, showed 14 compounds (determined as mg/100g dry weight) which were gallic acid (7), *P*-OH-benzoic acid (2), catachin (171) caffeic acid (41), phenol (102), daidzein (10), *P*-coumaric acid (94), genistein (1917) furulic acid (35), dadzein (35), quercetin (41), Kaempferol (2), chrysin (2.5) and galangin (1.5). Genistein was the highest compound of phenols which amounted about 77.9% of the known phenolic compounds. The total phenols of dried parsley were 2461mg/100g. It can be observed that parsley was considered as a good source of phenolic compounds as antioxidant [30]. Phenolic compounds as antioxidant agents induced antioxidant activities against the xenobiotic harmful [31-33].

The results in Table (3) show that weight of the three organs (liver, kidneys and brain) was affected by carbofuran ingestion (1/20 LD₅₀). There were significant increases in the organs weigh at the end of the experimental period (90 days) either in organs weight or the ratio % relative to final body weight. Carbofuran caused lower effects on liver and brain than those of kidneys which had percent-

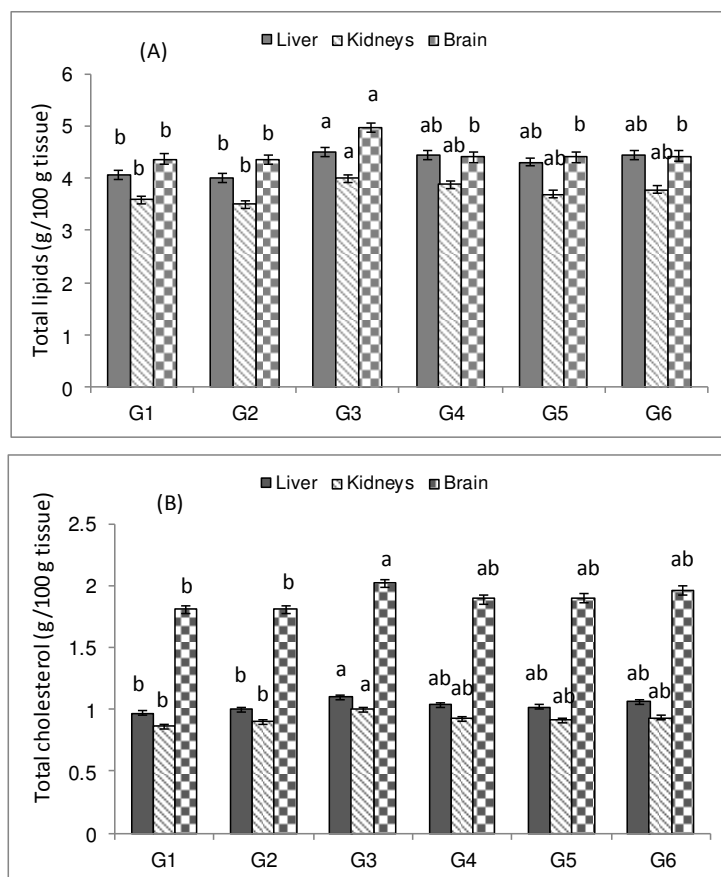


FIGURE 1

Total lipids and total cholesterol in the different organs tissue of the experimental male albino rats

Values are expressed as means \pm SD (n= 6). Values with different superscript letters within the same column are significantly different ($P < 0.05$). G1: Normal control, G2: Normal rats fed on semi-modified diet with 5% Parsley, G3: Intoxicated control, G4: Intoxicated rats fed on semi-modified diet with 5% Parsley, G5: Intoxicated rats ingested by Parsley methanolic extract (50 mg/kg b.w) and G6: Intoxicated rats injected by Parsley methanolic extract (50 mg/kg b.w).

ages of 149, 151 and 179% respectively relative to that of normal health control.

These abnormal values of the organs weight under the influences of 1/20 LD₅₀ of carbofuran ingestion were improved and the harmful was significant ameliorated by the treatments of parsley and its extract. But the values of parsley treated intoxicated animals were still higher than the normal health animals. Among parsley treatments, the semi-modified 5% parsley diet feeding was more effective than the both other treatments (methanolic extract ingestion or injection).

Data of the evaluation of parsley as an antioxidant agent against carbofuran harmful of lipid profiles in blood male albino rats were recorded in Table (4) of the six groups at the end of 90 days experimental period. The results showed increases in all parameters of lipids and lipoprotein fractions except HDL-C value which unchanged under the effects of the carbofuran toxicity.

The above increases were ranged between 114-119% relative to those of normal control for

cholesterol of (114%), total lipids and phospholipids (116%), triglycerides (118%) and LDL-C (119%). Findings also of Table (4) pointed out that the intoxicated rats fed on the semi-modified diet (G4) and that ingested (G5) or injected (G6) by parsley methanolic extract significantly reduced the toxic effects of the present pesticide ingestion and showed significant alleviation in the pesticide harmful, but the three treatments had about the same effects which observed insignificant variation between each other. The values of HDL-C were increased in all groups treated with parsley for intoxicated rats. Our results are in agreement with El-Kherbawy et al. [34] who found that adding parsley to diet of hypercholesterolemic rats lower the serum lipid profile compared to their corresponding values of the positive control but higher than those of negative control.

The results of Figure (1 A and B) showed that carbofuran orally ingestion significantly increased the total lipids and cholesterol in liver, kidneys and brain tissues in the intoxicated group (G3) relative

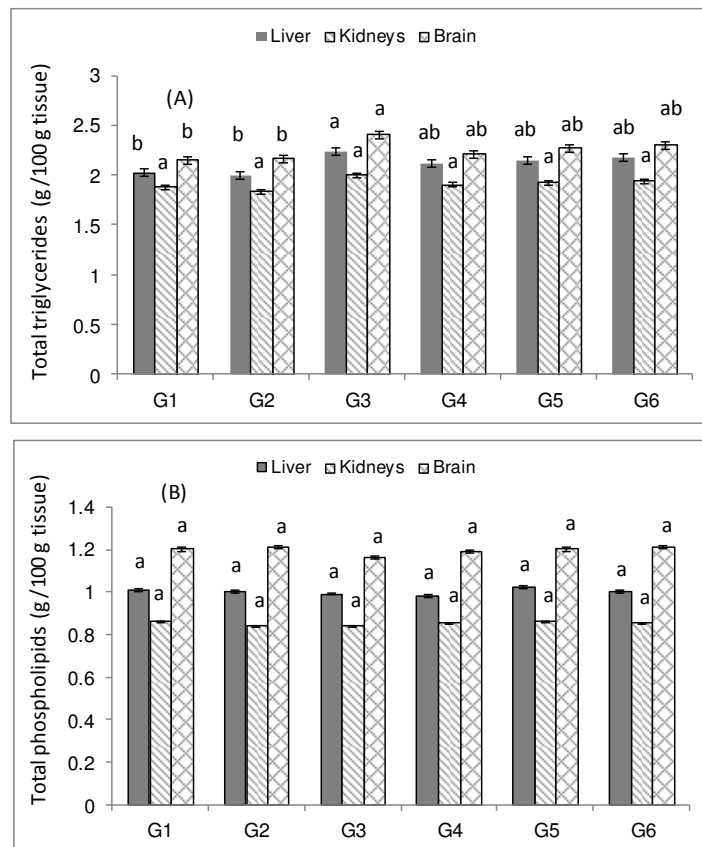


FIGURE 2

Total triglycerides and total phospholipids in the different organs tissue of the experimental male albino rats

Values are expressed as means \pm SD (n= 6). Values with different superscript letters within the same column are significantly different ($P < 0.05$). G1: Normal control, G2: Normal rats fed on semi-modified diet with 5% Parsley, G3: Intoxicated control, G4: Intoxicated rats fed on semi-modified diet with 5% Parsley, G5: Intoxicated rats ingested by Parsley methanolic extract (50 mg/kg b.w) and G6: Intoxicated rats injected by Parsley methanolic extract (50 mg/kg b.w).

to those of normal control. The increased values were ranged between 111 and 114% of the total lipid values and between 112 and 116% for total cholesterol in liver, kidneys and brain tissues when compared with the health control rats (G1). Among organs studied, the three tissues (liver, kidneys and brain) had about the same manners under the same condition. These harmful effects of carbofuran were improved by treatment with parsley either by feeding or ingestion and injection of intoxicated animals and the total lipid content was returned to around that of normal health control but the values were insignificantly more than control group. The same trend was observed in case of total cholesterol values of the same three organs tissue under the treatments with parsley in which the total cholesterol values of intoxicated rats were alleviated in the cytosol of liver, kidneys and brain tissues.

In connection Figure (2 A and B) showed significant increases in total triglycerides for liver (111%) and brain (112%) tissues, but insignificant for kidneys (106%) under the induction for carbofu-

ran (intoxicated rats) relative to those of normal health control rats. In case of the phospholipids contents of the three organs tissue the administration (ingestion) of this pesticide insignificantly changed phospholipids values where the percentage relative to control ranged from 98% and 101%. These increases values of total triglycerides of liver and brain was readjusted and improved by the treatments with parsley (feeding, ingestion and injection). This means that parsley either whole plant (feeding) or methanolic extract (ingestion and injection) as antioxidant agent, reduced the toxic effects of the present pesticide in the three organs tissue [34].

In addition, the effects of parsley feeding on the normal health rats showed safety effects in which all examined parameter were not effected by parsley administration and insignificantly changed the contents of total lipids, cholesterol, triglycerides and phospholipids of rat organs, also, insignificantly changed the lipid profile of health normal rats blood.

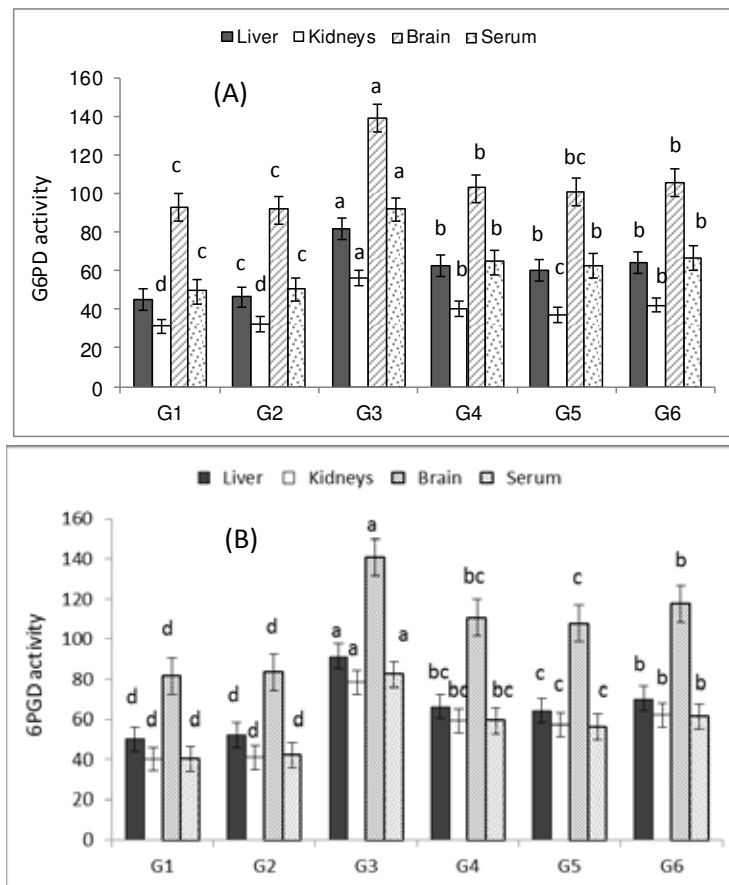


FIGURE 3

Glucose-6-phosphate dehydrogenase (G6PD) and 6-phosphogluconate dehydrogenase (6PGD) activity (pmol of NADPH.H⁺ /min/mg protein) of tissues cytosol and serum of the experimental male albino rats

Values are expressed as means \pm SD (n = 6). Values with different superscript letters within the same column are significantly different ($P < 0.05$). G1: Normal control, G2: Normal rats fed on semi-modified diet with 5% Parsley, G3: Intoxicated control, G4: Intoxicated rats fed on semi-modified diet with 5% Parsley, G5: Intoxicated rats ingested by Parsley methanolic extract (50 mg/kg b.w) and G6: Intoxicated rats injected by Parsley methanolic extract (50 mg/kg b.w).

In connection, the activity of the oxidative enzymes of pentose phosphate pathway (G6PD and 6PGD) was determined under the induction of carbofuran pesticide in male albino rats (feeding, ingestion and injection). G6PD and 6PGD reactions produce NADPH.H⁺ which is required for the reduction system during the fatty acid biosynthesis [35]. The data clearly demonstrate that the both activities of G6PD and 6PGD in the three cytosols of liver, kidneys and brain tissues as well as serum of the intoxicated rats were higher than those of the health control rats group in Figure (3 A and B). It is of interest to note that serum was characterized by higher increased G6PD and 6PGD activity than the other organs under the ingestion of the tested pesticide but brain had the lowest one relative to normal control. On the other hands, the treatments with parsley (feeding, ingestion or injection) ameliorated the effects of the pesticide ingestion as antioxidant agent. The results clearly show that carbofuran ingestion produced disturbed influences of the activi-

ty of oxidative pentose phosphate shunt (G6PD and 6PGD) in serum and cytosolic fractions of (liver, kidney and brain) of intoxicated animals, but the antioxidative agent (parsley) improved these disturbed effects of the pesticide toxicity.

Carbofuran ingestion produced hyperlipidemic condition in male albino rats. Parsley and its methanolic extract used as hypolipidemic lipotropic factor which significantly alleviated the drastic condition of hyperlipidemic induced by the tested carbofuran where 5% parsley semi-modified diet was the higher effective as lipotropic factor (antilipidemia).

The present results are confirmed each other, that the lipids profile of experimental animals blood is in agreement with the results of lipid fractions of liver, kidneys and brain tissues. Carbofuran ingestion produced hyperlipidemia and hypercholesterolemia, which increased total lipids, cholesterol, triglycerides and phospholipids in blood, liver, kidneys and brain. The same trend was observed for blood lipoprotein fractions (HDL-C and LDL-C) in

which the lipoprotein profile was elevated under the effects of the pesticide ingestion. The three treatments of parsley alleviated the carbofuran harmful induced. The treatment of semi-modified feeding was more effective than the other treatments. These may be due to the lipotropic factors of parsley. The values of the lipid profile fractions were still higher than the normal control. The tested treatments can be arranged in the following increasing order: 5% semi-modified diet, extract injection and extract ingestion respectively.

The present results are in agreement, with previous studies [36, 37], they observed marked increases in the weight of body organs such as brain as well as liver and kidneys under the effects of pesticides, these may be due to the tumefaction or enlargement influences on intoxicated animals [38, 39]. This also could be attributed to cells necrosis and apoptosis and the accumulation of lipids in the organs tissues [40].

Our results showed significant increases in total lipid, cholesterol and triglycerides in male albino rats in blood, liver, kidneys and brain by ingestion of carbofuran. But phospholipids content was not altered in normal control rats. Also, lipoprotein profile had the same trend in blood intoxicated animal under the same conditions. The present results are generally similar to previous studies, they mentioned that, lipid profile was changed significantly according to the type of pesticide and dosage used in tested animals [41-43]. Also, chlorpyrifos induction increased degeneration of lipid as a result of direct effect of the pesticide.

Recent results showed that harmful manifestation produced by pesticide associated with increased production of reactive oxygen species (ROS), which give an explanation of ROS is proposed to be caused by a mechanism in which the xenobiotic toxicant may produce oxidative stress with tissue damage. ROS may interact with cellular protein, lipid and DNA, causing alterations in the target cell fraction. Acute oxidative injury may produce selective cell death and compensatory increase in cell proliferation [44, 45]. The treatments with parsley, which contain antioxidant vitamins and other antioxidant protects several biomolecules (Lipids, protein and DNA) from oxidative harmful produced by oxygen-derived free radicals [46-48].

Carbamate ingestion induced abnormal lipoprotein profile in which LDL-C was increased, but HDL-C decreased, these produced risk and oxidative damage. Also, lipid profile had similar trend that accumulated lipid fractions in the body tissues. The treatments with parsley feeding and methanolic extract (ingestion or injection) improved the disturbed lipid profile. HDL-C is increase by the treatment paralleled with increasing Para Oxonase enzyme (PNO) that an enzyme with esterase activity which physically bound to HDL-C [49]. This enzyme has a key role in the action of HDL-C to-

ward protection of lipid fractions and biological membrane against oxidative damage, by virtue of its action on hydrolyzing lipid peroxides and preventing accumulation of lipid peroxides in oxidized LDL-C, elevation of catabolism by hydrolysis of lipid peroxides and protection against lipoprotein oxidation [50]. PON has antioxidant properties and hydrolyze aromatic and long-chain aliphatic lactones of pesticides [51, 52]. The hyperlipidemia produced by carbofuran ingestion is associated with several alterations in the lipid metabolism leading to changes in lipoprotein levels and compositions [53, 54]. Oxidative stress is increased with hyperlipidemic animals compared with healthy controls [55, 56] and lowered HDL-C and PON values and suggested that animals with lower PON activity are more exposed to oxidative damage [57]. The PON activity was correlated with low levels of HDL-C [58, 59]. Hyperlipidemia induced by carbofuran ingestion may be associated with 50-60% reduction in PON activity accompanied by fall in HDL-C and increase in LDL-C. These oxidative stress in intoxicated animals resulted decrease in HDL-PON activity. The lower paraoxonase activity and the compositional changes in HDL and LDL could contribute to greater risk associated with hypelipimia and hypercholesterolemia induced the xenobiotic ingestion [58].

In connection, the oxidative shunt of pentose phosphate pathway (G6PD and 6PGD) are the key enzymes of this direct oxidation shunt (P.P.P) which responsible for NADPH.H⁺ generation. The both enzymes play essential role in the regulation of oxidative stress by regulating NADPH.H⁺ values, the main intracellular reductant and fatty acid synthesis [35]. For that, G6PD and 6PGD are required for the antioxidant defense system and to protect and prevent the toxicity of xenobiotic [60]. The present results may suggest relation between the both enzyme activities and fatty acids then triglycerides and phospholipids also with the cholesterol biosynthesis from acetyl-CoA. Also, the increased lipids profile synthesis may use to store the pesticide in the lipid parts of tissue or in adipose tissue [61].

The primary physiological role of G6PD in mammalian cells is the defense against oxidative stress injury. The formation of GSH from GSSG is dependent on NADPH.H⁺ produced from the oxidation shunt of P.P.P. The activity of G6PD, 6PGD and glutathione peroxidase (GPx) are linked each other in their capacity to prevent tissue damage from the xenobiotic oxidant [46, 62].

The higher effectiveness of 5% semi-modified diet feeding than methanolic extract treatment in intoxicated animal may due to that parsley contains volatile oils and flavonoid compounds as antioxidant agents but its methanolic extract contains only phenolic and flavonoid constituents. Parsley edible portion has many of antioxidant agents. These in-

cluded ascorbic acid, vitamins (A and B₂) minerals (Na, K, Ca, Mg, Fe, Zn, Cu and P), also contains phenolics and flavonoids which act as good antioxidant agents [63].

CONCLUSION

It can be concluded that, these study showed that eating parsley semi-modified safety food could protect to a certain extent against the harmful of pesticide carbofuran, hyperlipidemia and hypercholesterolemia, which prevent the occurrence of atherosclerosis induced into animals.

ACKNOWLEDGEMENTS

Authors would like to thank the Faculty of Agriculture, Cairo University for ongoing collaboration to support research and that provided funds and facilities necessary to accomplish the desired goals of research.

REFERENCES

- [1] Pesticide Manual (2000) A world compendium the pesticide manual 20th ed. Tomlin CDS (ed). British Crop Protection Council. pp.137-139.
- [2] Rohrer, C.A, Hiaber, T.E, Melnyk, L.J. and Berry, M.R. (2003) Transfer efficiencies of pesticides from household flooring surfaces to food. *Journal of Exposure Analysis and Environmental Epidemiology* 13, 454-464.
- [3] USFPS (2000) Health and environmental effects profile for Dichlorvos U.S. environmental Protection Agency. 11-15.
- [4] Neelima, S., Neeta, A. and Saxena, D.K. (2001) Effect of endosulfan during fetal gonadal differentiation on spermatogenesis in rats. *Environmental Toxicology and Pharmacology* 10, 29-39.
- [5] Abdel Moneim, A.E. (2001) Effect of long term repeated administration of fenitrothin on male albino rats. *Journal of Union Arab Biology* 16, 89-106.
- [6] Usmani, K.A, Hodgson, E. and Rose, E.L. (2004) *In vitro* metabolism of carbofuran by human, mouse and rat cytochrome P450 and interaction with chlorpyrifos, testosterone and estradiol. *Chemico-Biological Interactions* 150, 221-232.
- [7] McDaniel, K.L., Padilla, S., Marshall, R.S., Phillips, P.M., Podhoriniak, L., Qian, Y.R. and Moser, V.C. (2007) Comparison of acute neurobehavioral and cholinesterase inhibitory effects of *N*-Methylcarbamates in rats. *Toxicological Sciences* 98, 552-560.
- [8] Afify, A.M.R. and El-Beltagi, H.S. (2011) Effect of the insecticide cyanophos on liver function in adult male rats. *Fresen. Environ. Bull.*, 20, 1084-1088.
- [9] Lopez, M.G., Sauchez-Mendoza, T.R. and Ochoa-Aljo, N. (1999) comparative study of volatile components and fatty acids of plants *in vitro* cultures of parsley (*Petroselinum crispum* (Mill) Nym. Ex Hill). *Agricultural and Food Chemistry* 47, 3292-3296.
- [10] Yanardag, R., Bolkent, S., Tabakogla-Oguz, A. and Ozsoy, O. (2003) Effect of *Petroselinum crispum* extract on pancreatic B cells and blood glucose of streptozotocin-induced diabetic rats. *Biological and Pharmaceutical Bulletin* 26, 1206-1210.
- [11] Fejes, S.Z., Blazovics, A., Lemberkovics, E., Petri, G., Szoke, E. and Kery, A. (2000) Free radical scavenging and membrane protective effect of methanol extracts of *Petroselinum crispum* (Mill.) Nym Ex. A.W. Hill. *Phytotherapy Research* 14, 362-365.
- [12] Darias V., Martin-Herrera, D., Abdala, S. and Fuente, D. (2001) Plants used in urinary pathologies in Canary Islands *Pharmaceutical Biology* 39, 170-175.
- [13] Sacan, O.O., Yanardag, R., Ork, H., Ozgen, Y., Yarat, A. and Tunali, T. (2005) Effect of parsley (*Petroselinum crispum*) extract versus glibornuride on the liver of rats *Journal of Ethnopharmacology* 104, 175-181.
- [14] Abdel-Rahim, E.A. and El-Beltagi, H.S. (2011) Alleviation of hyperlipidemia in hypercholesterolemic rats by lentil seeds and apple as well as parsley in semi-modified diets. *Advances in Food Sciences* 33, 2-7.
- [15] Coskum, O., Kanter, M., Korkmaz, A. and Oter, S. (2005) Quercetin, a flavonoid antioxidant, prevents and protects streptozotocin-induced oxidative stress and B-cell damage in rat pancreas. *Pharmacological Research* 51, 117-123.
- [16] Nagochi, C. and Nikki, E. (2000) Phenolic antioxidants, a rationale for design and elevation of novel antioxidant drugs for atherosclerosis. *Free Radical Biology and Medicine* 28, 1538-1546.
- [17] A.O.A.C (2000) Official methods of analysis of association of official analytical chemistry (17th ed.) Washington D.C. USA.
- [18] Duke, S.O., Rimando, A.M., Pace, P.F., Reddy, K.N. and Smeda, R.J. (2003) Isoflavone, glyphosate, and aminomethylphosphonic acid levels in seeds of glyphosate-treated, glyphosate-resistant soybean. *Journal of Agriculture and Food Chemistry* 51, 340-344.
- [19] Lane-Perter, W.A. and Pearson, A.E. (1971) Dietary requirements in, *The laboratory animal principles and practice*. Academic Press. London and New York. pp. 142.

- [20] Weil, C.S. (1952) Tables for convenient calculation of median effective dose (LD50 and LC50) and instruction in their use. *Biometrics* 8, 249-263.
- [21] Astawrov, B.L. (1974) *Methods in biological development Preparation of mitochondria and cytoplasm* Nauka, Moscow. pp. 336.
- [22] Glock, G.E. and McLean, P. (1953) Further studies on the properties and assay of glucose-6-phosphate dehydrogenase (G6PD) and 6-phogluconate dehydrogenase (6PGD) of rat liver. *Biochemistry Journal* 55, 440-443.
- [23] Joseph, R.K., Shauma, A. and Ames, M. (1971) Determination of total lipid in blood serum. *Powl. Clinical Chemistry* 18, 199-201.
- [24] Chaurchami, A.J., Miller, W. and Stein, J.D.B. (1959) Determination of total and free cholesterol. *Clinical Chemistry* 5, 609-611.
- [25] Young, A. and Pestaner, D.L. (1975) Determination of triglycerides in serum. *Clinical Chemistry* 21, 5-7.
- [26] Ketes, M. (1972) *Techniques of lipidology, Isolation, analysis and identification of lipids*. Amsterdam, North Holland and Publishing Co.
- [27] Warnick, G.R., Benderson, V. and Albers, N. (1983) Selected method of enzymatic analysis. *Lin. Chemistry* 10, 91-99.
- [28] Bergmenyer, H.U. (1974) *methods of enzymatic analysis, (2nd ed.)* English edition Academic press Inc. New York, San Francisco and London.
- [29] Bradford, M.M. (1976) A rapid sensitive method for the quantitation of microgram quantities of protein utilizing the principle of dye binding. *Analytical Biochemistry* 72, 248-254.
- [30] Abdel-Rahim E.A. and El-Beltagi H.S. (2010) Constituents of apple, parsley and lentil edible plants and their therapy treatments for blood picture as well as liver and kidney functions against epidemic disease. *EJEAFChe*, 9 (6), 1117-1127.
- [31] Pattison, D.J., Silman, A.J., Goodson, N.J., Lunt, M., Bunn, D., Luben, R., Welch, A., Bingham, S., Khaw, K.T., Day, N.S. and Symons, D.P. (2004) Parsley and the risk of developing inflammatory polyarthritis, prospective nested case-control study. *Annals of the Rheumatic Diseases* 63, 873-847.
- [32] Elshobeki, F.A., Abdel-Rahim, EA., El-Hawary, Z., Farrag, A.H. and Kassem, S. (2014) Protection from atherosclerosis by feeding on polyphenols rich vegetables and fruits or their extract. *International Journal of Academic Research* 6, 230-241.
- [33] El-Beltagi, H.S., Abdel-Mobdy, Y.E. and Abdel-Rahim, E. (2017) Toxicological influences of cyfluthrin attenuated by *Solenostemma argel* extracts on carbohydrate metabolism of male albino rats. *Fresen. Environ. Bull.*, 26, 1673-1681.
- [34] El-Kherbawy G.M., Ibrahem E.S. and Zaki S.A. (2011) Effects of Parsley and Coriander leaves on hypercholesterolemic rats. The 6th Arab and 3rd international annual scientific conference on development of higher specific education programs in Egypt and the arab world in the light of knowledge era requirements. Faculty of Specific Education Mansoura University – Egypt. April, 13-14, 2127-2143.
- [35] Murray, R.K., grennerm, D.K. and Rodwell, V.W. (2006) *Harper's illustrated biochemistry (24th ed.)* Mc-Graw Hill Comp. Inc. Boston, New York, Signopora.
- [36] Abdel-Rahim, G.A. (2008) reduction of the hazard influences of dimethoate by guava antioxidant on body growth rate and blood constituents of albino rats. *Journal of Biological Chemistry and Environmental Sciences* 3(4), 343-362.
- [37] Abdel-Rahim, G.A. and Mahmoud, G. (2011) Protective effects of a wheat germ rich diet against the toxic influence of profenofos on rat tissue lipids and oxidative pentose phosphate shunt enzymes. *Grasas Y Aceites* 62 (3), 344-352.
- [38] Gomes, J, Dawodu, A.H., Llyod, O, Revitt, DM and Anilal, S.V (1999), hepatic injury and disturbed amino acid metabolism in mice following prolonged exposure to organophosphorus insecticides. *Hum. Exp. Toxicol.* 18 (1), 33-37.
- [39] Bajnok, L., Seres, I., Varga, S., Peti, A., Karanyi, Z. Juhasz A., Csongradi E., Mezosi E., Nagy E.V. and Paragh G. (2008) Relationship of serum Resistin level to traits of Metabolic syndrome and serum paraoxonase 1 activity in population with a broad range of body mass index. *Experimental and Clinical Endocrinology & Diabetes* 116, 592-599.
- [40] Ibrahim, N.M., Eweis, E.A., El-Beltagi, H.S. and Abdel-Mobdy Y. (2011) The effect of lead acetate toxicity on Experimental male albino rats. *Biological Trace Element Research* 144, 1120-1132.
- [41] Goel, A, Dani, V. and Dhawan, D.K. (2005) Protective effects of zinc on lipid peroxidation antioxidant enzyme and hepatic histoarchitection in chlorpyrifos-induced toxicity. *Chemico-Biological Interactions* 156, 131-140.
- [42] Goel, A., Dani, V. and Dhawan, D.K. (2007) Zinc mediates normalization of hepatic drug metabolizing enzymes in chlorpyrifos-induced toxicity. *Toxicology Letters* 169, 25-33.
- [43] Kobeasy, M.I., Salem, S.M., Farid, M.M., Ahmed, S.H. and Abd Allah, A.A. (2009) Toxicity studies on the effect of carbofuran adjuvant on rats fertility. *Journal of Biological Chemistry and Environmental Scienc* 4, 501-515.
- [44] Klaunig, J.E., Xu, Y. and Isenherg, J.S. (1998) The role of oxidative stress in chemical carcin-

- ogenesis. *Environmental Health Perspectives* 1, 289-295.
- [45] El-Beltagi, H.S. and Mohamed, H.I. (2013) Reactive oxygen species, lipid peroxidation and antioxidative defense mechanism. *Notulae Botanicae Horti Agrobotanici Cluj-Napoca* 41, 44-57.
- [46] Karaoz, E., Gultekin, F., Akdogan, M., Oncu, M. and Gokciman A. (2002) Protective role of melatonin and a combination of vitamin C and Vitamin E on lung toxicity induced by chlorpyrifos-ethyl in rats. *Experimental and Toxicologic Pathology* 54, 97-108.
- [47] Varma, R.S., Mehta, A. and Sivastava, N. (2007) In vivo chlorpyrifos induced oxidative stress attenuation by antioxidant vitamins. *Pesticide Biochemistry and Physiology* 88, 191-196.
- [48] El-Beltagi, H.S. and Mahgoub M.A. (2016). Assessment the protective role of quercetin on acrylamide-induced oxidative stress in rats. *Journal of Food Biochemistry* 40, 715-723.
- [49] Ceron, J.J., Tecles, F. and Tvarijonaviciute, A. (2014) Serum paraoxonase I (PON1) measurement, An update. *BMC Veterinary Research* 10, 74.
- [50] Sabah, A.M., Reham, S., Abdul Baset, A.F., Eman, S. (2015) Role of paraoxonase activity and oxidative stress in renal vascular damage in type 2-diabetes Mellitus. *Clinical Medicine and Diagnostics* 5, 26-34.
- [51] Reddy, S.T., Wadleigh, D.J., Grijalva, V., Ng, C., Hama, S., Gangopadhyay A., Shih, D.M., Lusi, A.J., Navab, M., Fogelman, A.M. (2001) Human paraoxonase-3 is an HDL associated enzyme with biological activity similar to paraoxonase-1 protein but is not regulated by oxidized lipids. *Arteriosclerosis, Thrombosis, and Vascular Biology* 21, 542-547.
- [52] Kota, S.K., Meher, L.K., Kota, S.K., Jammula, S., Krishna, S.V.S and Modi, K.D. (2013) Implication of serum paraoxonase activity in obesity, diabetes mellitus and dystipidemia. *Indian Journal of Endocrinology and Metabolism* 17, 402-412.
- [53] Kota, S.K., Jammula, S., Kota, S.K., Krishna, S.V.S., Meher, L.K., Rao, E.S. and Modi, K.D. (2012) Nutraceuticals in pathogenic obesity, striking the right balance between energy imbalance and inflammation. *Journal of Medical Nutrition and Nutraceuticals* 1, 63-76.
- [54] Tarcin, O. (2001) Paraoxonase-1 and coronary heart diseases. *Marmara Medical Journal* 24, 59-63.
- [55] Mutlu-Turkoglu, U., Oztezcan, S., Telci, A., Aykac-Toker, G., Sivas, A. and Uysal, M. (2003) An increase in lipoprotein oxidation and endogenous lipid peroxides in serum of obese women. *Clinical and Experimental Medicine* 2, 171-174.
- [56] Rani, A. and Mythil, S. (2014) Paraoxonase I in type 2-diabetes Mellitus. *International Journal of Pharmaceutical Sciences Review and Research* 28, 175-179.
- [57] Martinelli, N., Consoli, L., Girelli, D., Grison, E., Corrocher, R. and Olivieri O. (2013) Paraoxonases: ancient substrate hunters and their evolving role in ischemic heart disease. *Advances in Clinical Chemistry* 59, 65-100.
- [58] Ferretti, G., Baccetti, T., Moroni, C., Savino, S., Liuzzi, A., Balzola, F., and Bicchiega, V. (2005). Paraoxonase activity in high-density lipoproteins, A comparison Between health and obese females. *Journal of Clinical Endocrinology & Metabolism* 90, 1728-1733.
- [59] Koncsos, P., Seres, I., Harangi, M., Illyes, I., Gonczi, F., Bajnok, L., and Paragh, G. (2010) Human paraoxanase-1 activity in childhood obesity and its Relation to leptin and adiponectin levels. *Pediatric Research* 67, 309-313.
- [60] Zhang, Z., Apse, K., Pang, J. and Stanton, R.C. (2004) High glucose inhibits glucose-6-phosphate dehydrogenase Via CAMP in aortic endothelial cell. *Journal of Biological Chemistry* 275, 40042-40050.
- [61] Abdollahi, M., Ranjbar, A., Shadnia, S., Nikfar, S. and Rezaiee, A. (2004) Pesticides and oxidative stress a review. *Medical Science Monitor* 106, 141-147.
- [62] Lukaszewicz-Hussain, A. and Monluszko-Jakoniuk, J. (2003) Organophosphate insecticide chlorfenvinphos effects enzymatic and nonenzymatic antioxidants in erythrocytes and serum of rats. *Polish Journal of Environmental Studies* 12, 417-423.
- [63] Nutrition Institute (2006) food composition tables for Egypt Nutrition Institute ARE (2nd ed.) Cairo Egypt. pp. 25.

Received: 17.04.2017

Accepted: 09.06.2017

CORRESPONDING AUTHOR

Hossam Saad El-Beltagi

Biochemistry Dept, Faculty of Agriculture, Cairo University, P. Box 12613, Gamma St, Giza, Cairo-Egypt

e-mail: lbtg@yahoo.com

OCCURRENCE OF EPILITHIC DIATOMS IN A STREAM WITH CLEAN WATER CONDITIONS: HARINGET STREAM, TURKEY

Feray Sonmez*

Firat University, Fisheries Faculty, Department of Basic Aquatic Sciences, 23119, Elazig, Turkey

ABSTRACT

In the study, species composition of diatoms and their seasonal variations in epilithic associations occurring in a clean water stream (Haringet) were determined between January and December 2014. Sampling was performed monthly at three stations chosen in upper, middle and lower parts of the stream. Water temperature, pH, electrical conductivity, total dissolved solid matter, dissolved oxygen, flow rate, total hardness, total alkalinity, organic matter, salinity, nitrate, ortho-phosphate, sulfate and silica values in water were measured and analysed monthly.

A total of 48 diatom taxa all belonging to pennales were identified throughout the study. Members of the genera *Cymbella*, *Diatoma*, *Epithemia*, *Gomphonema*, *Navicula*, *Nitzschia* and *Surirella* were common epilithic diatoms in the Stream. *Nitzschia* was the richest in species composition. *Cocconeis pediculus*, *Cymbella affinis*, *C. helvetica*, *Diatoma elongata*, *Fragilaria acus*, *Gomphonema intricatum*, *G. olivaceum*, *Navicula radiosa*, *Nitzschia sigmoidea* and *Ulnaria ulna* were noticeable diatoms with respect to frequency of occurrence and individual numbers in epilithon at all stations. Variations in occurrence of diatom species and their abundance were compared at stations and discussed in relation to physical and chemical properties of stream water. The physicochemical values yielded that Haringet Stream has Class I Water Quality according to the Inland Water Quality Criteria. This finding is somehow supported by the occurrence of certain clean water diatom species.

KEYWORDS:

Epilithon, Diatom, seasonal succession, Haringet Stream, Turkey.

INTRODUCTION

Algae are the major primary producers in many aquatic systems and are an important food source for other organisms. They include planktonic and benthic forms. Diatoms are common members of both

planktonic and benthic algal associations and they have been especially recognized as useful indicators for both ecological and water quality of lakes and rivers. In fact, the use of diatoms as water quality indicators has been reported in a number of articles [1-3]. In addition, phytoplankton and littoral epilithic diatoms are in high value in lakes for their relation to trophic status and acidification risk [4]. However, it may be important to analyse the different aquatic associations of diatoms separately due to their different ecology.

Studies on algae occurring in lotic systems [5-14] have received attention after 80's and since then, number of studies has rapidly increased in parallel to European Union the Water Framework Directive [15]. In fact, determination of water and ecological quality of surface waters has gained special importance through identification of diatoms (particularly planktonic and epilithic forms). Identification of the development of algal communities and the physical and chemical factors affecting them is of most importance in increasing the usefulness of rivers. There are many studies about epilithic diatoms of rivers in many countries [16-18].

Some of the organisms living in running waters can adopt to the changes that occur in the ecosystems due to several environmental factors whereas others not [19-23]. In fact, such adaptations related to presence or absence of algae are of great value to recognize the changes in both water and ecological quality of running waters particularly due to pollutants. It is also important to mention that water quality determination of running waters based on adaptation of algae particularly diatoms has been used for a long time [24-27]. In addition algae have extensively been used as indicator organisms to determine the environmental conditions [23, 28, 19-22, 29, 30, 25]. Particularly epilithic diatoms were reported to be good indicators in running waters [31-32].

The present study aimed to contribute to the relations between occurrence of epilithic diatom species and water quality in a clean water stream condition. For this purpose, the species composition and seasonal variations of epilithic diatoms in Haringet Stream were investigated together with physicochemical variables for a period of a year. The stream is one the main inflows of Keban Dam Lake that is

the second largest reservoir in Turkey. The study was also expected to contribute to the epilithic diatom list of Turkish freshwater ecosystems.

MATERIALS AND METHODS

The Haringet Stream is located in upper Euphrate Basin and three representative stations were selected in upper, middle and lower parts of the stream with the distance approximately 3 km away from each other. Stream bed in upper and middle parts consists mainly of rocks, stones and gravels whilst gravel and sands are dominant substrates in the lower part of the stream.

The water temperature, pH, total dissolved solid matter, dissolved oxygen and electrical conductivity of the stream were measured directly by means of a oxygenmeter (YSI 52) and a pH meter (YSI 63). Total hardness, total alkalinity, organic matter and salinity were determined through titration analysis whilst spectrophotometric method was employed for the analysis of nitrate, orto-phosphate, sulfate and silica [33]. Flow rate of Haringet Stream was

measured with flotation method and current value was calculated [34].

Water samples were collected using a water bottle. The epilithic diatoms were scrapped from stones/gravels into a plastic container. Olympus CX21FS1 microscope was employed for both identification of species and counting cells. The relative abundance method was applied for individual numbers of epilithic diatoms and results were expressed as “% organism” [35] since it was hard to identify the live cells during counting process through inverted microscope. At least 100-200 individuals based on the abundance of diatoms were observed and counted in per sample.

To prepare permanent diatom slides, subsamples were taken and acid solution was added to digest organic material. These samples were boiled on a hot plate for 15 minute to expedite the digestion process and were subsequently left the cool. Samples were neutralized by rinsing with distilled water and dried on coverslips that were mounted on glass slides with Entellan. Diatom species were identified according to Krammer & Lange-Bertalot [36-39]. Species named updated in accordance with Guiry and Guiry [40].

TABLE 1
Variations in degrees/concentrations of some physical and chemical parameters in Haringet Stream

	Water temperature (°C)	pH	Electrical conductivity (mV)	Total dissolved solid matter (mg/L)	Dissolved oxygen (mg O ₂ /L)	Flow rate (m ³ /sn)	Organic matter (mg O ₂ /L)	Salinity (%0)
January	7.5±1.00	6.62±0.08	458.67±63.13	418.67±53.38	13.0±0.20	0.07±0.03	5.00±1.00	2.00±0.50
February	9.5±2.65	7.19±0.22	439.67±78.68	408.67±54.92	12.9±0.20	0.52±0.44	4.00±1.00	1.33±0.29
March	13.2±2.89	8.11±0.48	347.67±96.57	403.33±42.44	11.57±0.87	0.77±0.68	2.00±1.00	2.67±0.58
April	13.2±2.52	8.10±0.57	311.33±64.63	322.67±46.23	10.83±1.11	0.06±0.04	7.00±1.00	3.00±0.50
May	17.2±2.75	7.78±0.10	283.33±28.10	274.00±11.14	9.90±0.46	0.05±0.04	10.33±2.08	2.00±0.50
June	16.3±3.33	7.77±0.13	273.33±27.54	233.33±8.33	8.67±0.57	0.02±0.02	17.33±4.16	2.00±0.00
September	16.2±2.08	7.38±0.45	279.67±27.75	234.67±7.02	9.57±0.40	0.03±0.02	3.67±2.52	2.00±0.00
October	14.2±2.08	7.21±0.39	278.33±52.04	236.67±22.48	10.13±0.47	0.04±0.03	3.67±3.79	2.33±0.29
November	11.2±3.06	6.99±0.48	316.67±94.51	280.67±65.43	10.73±0.42	0.04±0.03	1.67±0.58	1.83±0.29
December	7.5±1.00	6.79±0.34	440.00±82.61	391.33±57.83	12.57±0.59	0.09±0.09	1.33±0.58	1.50±0.00

TABLE 2
Variations in degrees/concentrations of some physical and chemical parameters in Haringet Stream

	Total hardness (mg CaCO ₃ /L)	Total alkalinity (mg CaCO ₃ /L)	Nitrate (mg NO ₃ -N/L)	Total phosphorus (mg P /L)	Sulfate (mg SO ₄ /L)	Silica (mg SiO ₂ /L)
January	145.00±20.00	206.67±11.55	0.33±0.40	0.02±0.01	30.33±6.66	18.41±2.12
February	146.67±20.82	176.67±15.28	0.33±0.25	0.03±0.01	28.00±2.00	16.24±2.78
March	138.33±5.77	160.00±20.00	0.50±0.00	0.05±0.00	27.33±18.01	12.98±1.65
April	148.33±12.58	196.67±20.82	0.50±0.00	0.15±0.15	29.00±24.02	11.43±0.92
May	156.67±25.17	170.00±10.00	0.47±0.12	1.85±2.66	14.00±5.30	21.29±1.48
June	186.67±5.77	193.33±23.09	0.37±0.21	0.02±0.01	21.67±6.81	21.51±4.08
September	186.67±30.55	273.33±11.55	0.57±0.55	0.07±0.09	40.67±15.37	6.45±0.97
October	166.67±37.86	186.67±23.09	0.23±0.15	0.02±0.01	50.33±37.81	8.42±0.74
November	175.00±40.93	140.00±10.00	0.30±0.20	0.01±0.01	49.00±40.36	11.29±1.10
December	163.33±25.17	136.67±15.28	0.27±0.12	0.01±0.01	43.00±34.40	19.50±2.69

RESULTS

Values of physical and chemical parameters measured and analysed in Haringet Stream were given at Table 1 and 2. Surface water temperature of the stream varied between 6.5 °C and 20 °C. Maximum temperature was recorded in May and June, minimum degree was in December and January. The highest pH values were noted in spring (8.1) whilst late autumn and winter coincided with lower values (6.62-6.99). Maximum (500 $\mu\text{S}/\text{cm}$) and minimum (210 $\mu\text{S}/\text{cm}$) electrical conductivity were observed in January and November respectively. The maximum amount of total solid matter (486 mg/L) was recorded in January whilst the minimum value (206 mg/L) was in November. Dissolved Oxygen concentration varied from 8.2 to 13.2 mg/L. The concentrations decreased in summer and increased in winter depending on the temperature. Flow rate of Haringet Stream were low and almost similar (0,01- m^3/sn) throughout the sampling period. The highest flow rate (1,37 m^3/sn) was recorded in February and March. Concentrations of organic matter varied seasonally. The lowest concentrations (1.3-1.6 mg O_2/L) were recorded in late autumn-early winter whilst the highest concentrations (10.3-17.3 mg O_2/L) occurred in late spring-early summer. Concentrations of salinity displayed slight variations through the seasons. The maximum (‰ 3.0) and minimum (‰ 1.3) values were measured in April and February, respectively. Total hardness at stations changed between 138 and 186 mg CaCO_3/L . Concentrations were almost similar between January and April. The highest concentrations were recorded in June and September. Total alkalinity was highest (273 mg CaCO_3/L) in September while the minimum (136 mg CaCO_3/L) was recorded in December.

Orto-phosphate concentrations changed between 0.01 and 1.85 mg $\text{PO}_4\text{-P}/\text{L}$ during the study (Table 2). The concentrations were generally low and similar (varied between 0.01 and 0.02 mg $\text{PO}_4\text{-P}/\text{L}$) at stations throughout the study. However, an exceptionally higher concentration was recorded in May. The nitrate concentrations were higher than those of phosphate ranging from 0.23 to 0.57 mg $\text{NO}_3\text{-N}/\text{L}$. Concentrations of sulfate were higher in autumn and early winter than those recorded in other seasons. The maximum concentration was recorded in October and the lowest in May. Variations in silica concentration occurred between 6.42 and 21.51 mg SiO_2/L . The maximum concentration of silica was observed in June whilst the minimum value was recorded in October. Silica concentrations were low in autumn and in the first two months of spring probably due the diatom use. However, it started to increase in May and reached to its maximum in June.

All the values of physical and chemical parameters yielded that the studied parts of Haringet Stream can be classified as Class I Water Quality (exclusive of the maximum concentration of ortho-

phosphate in may; appeared to be resulted through runoff coming from agricultural lands usually fertilized in spring) according to Surface Water Management Guide-Inland Water Resources Quality Criteria [41].

The total of 48 taxa belonging to 22 diatom genera were identified in the epilithon throughout the study. As seen from the Table 3 that the genus *Nitzschia* was the richest in species composition (6 taxa) followed by *Cymbella* (4 taxa), *Diatoma* (4 taxa), *Epithemia* (4 taxa), *Navicula* (4 taxa), *Gomphonema* (3 taxa), and *Surirella* (3 taxa). At species level, *Cocconeis pediculus*, *Cymbella affinis*, *C. helvetica*, *Diatoma elongata*, *Fragilaria acus*, *Gomphonema intricatum*, *G. olivaceum*, *Navicula radiosa*, *Nitzschia sigmoidea* and *Ulnaria ulna* were more noticeable diatoms with respect to frequency of occurrence and individual numbers in epilithon at all stations.

Fragilaria acus, *Navicula cryptonella*, *Rhicosphaneia abbreviata* and *Ulnaria ulna* were the most conspicuous species with their 100% frequency of occurrence at station I (Fig. 1). However, *F. acus* was also the most noticeable diatom with its higher relative abundance compare to other very frequently and generally occurring diatoms. The relative abundance of *F. acus* (50-72%) were higher in winter than those recored in other seasons. Oppositely its relative abundance was the lowest in summer. Although *N. cryptonella*, *R. abbreviata* and *U. ulna* also occurred with 100% frequency of occurrence, their relative abundances were much lower (generally remained under 10 %) than that of *F. acus*. This finding may show that although *N. cryptonella*, *R. abbreviata* and *U. ulna* were insistently present in the samples like *F. acus* but they failed to compete with it to increasae. This finding clearly showed that the high frequency of occurrence of species didnot coincide with high relative abundance in the present study. Other diatoms recorded at this station occurred with insignificant frequency of occurrence and relative abundance.

F. acus, *F. brevistriata*, *N. radiosa* and *U. ulna* were dominat species with their 100% frequency of occurrence at station II (Fig. 2) which were followed by *Cymbella affinis*, *Diatoma hyemalis*, *Nitzschia sigmoidea* and *Tabularia fasciculata* with their 60% frequency of occurrence. *C. pediculus*, *C. cistula*, *N. cryptocephala* and *R. abbreviata* were other noticeable diatoms with their occurrence in half of the samples. However, *Fragilaria acus*, *F. brevistriata* and *U. ulna* were also the most conspicuous diatoms with their higher relative abundance followed by *C. pediculus*. The relative abundance of these diatoms never exceeded % 35 throughout the study. The relative abundance of *F. acus* were higher in autumn and winter. The maximum of *F. acus* (15%) occurred in December whilst *F. brevistriata* reached its highest relative abundance in May. However, it is worth

to mention that higher relative abundance of the former diatom coincided with lower relative abundance of the latter. *U. ulna* was another noticeable diatom with high relative abundance particularly in winter.

C. pediculus, *C.affinis*, *G. intracatum* and *U. ulna*, were the most important diatoms with their 100% frequency of occurrence at station III (Fig. 1-3). *Diatoma tenuis* and *Epithemia argus* followed these species with their 70% frequency of occurrence. However *G. intracatum* and *C. affinis* drew attention with their much higher relative abundance than those of other very frequently and frequently occurring diatoms (Figs. 1-3). The relative abundance of *G. intracatum* was higher during winter and

spring whilst it decreased during summer and autumn. The relative abundance of *C. affinis* was higher in Spring and Autumn than those recorded in other seasons. *Ulnaria ulna* was also another noticeable diatoms with high relative abundance particularly in Autumn and early Winter. Oppositely, *C. pediculus* occurred with lower relative abundance compare to other very frequently occurring diatoms. However, it is worth to mention that the highest relative abundance of *C. Pediculus* in June coincided with low relative abundance of *C. affinis*, *G. intracatum* and *U. ulna*.

TABLE 3
The mean frequency of occurrence and mean relative abundance of epilithic diatoms of Haringet Stream

TAXA	Mean Relative Abundance (%)	Mean Frequency of Occurrence (%)
BACILLARIOPHYTA		
<i>Brachysira microcephala</i> (Grunow) Compère	0.30	3.33
<i>Ceratoneis arcus</i> (Ehrenberg) Kützing	0.15	1.00
<i>Cocconeis pediculus</i> Ehrenberg	7.90	70.00
<i>Cocconeis placentula</i> Ehrenberg	0.57	1.33
<i>Cymatopleura solea</i> (Brébisson) W.Smith	0.03	0.33
<i>Cymbella affinis</i> Kützing	7.46	70.00
<i>Cymbella cistula</i> (Ehrenberg) O.Kirchner	1.04	16.67
<i>Cymbella helvetica</i> Kützing	2.29	43.33
<i>Cymbella obtusiuscula</i> Kützing	0.04	0.33
<i>Diatoma elongata</i> (Lyngbye) C.Agardh	2.44	50.00
<i>Diatoma hyemalis</i> (Roth) Heiberg	1.23	20.00
<i>Diatoma tenuis</i> C.Agardh	0.66	23.33
<i>Diatoma vulgare</i> Bory	1.06	20.00
<i>Diploneis ovalis</i> (Hilse) Cleve	1.55	30.00
<i>Diploneis smithii</i> (Brébisson) Cleve	0.52	13.33
<i>Encyonema leibleinii</i> (C.Agardh) W.J.Silva, R.Jahn, T.A.Veiga Ludwig & M.Menezes	0.40	16.67
<i>Encyonema ventricosum</i> (C.Agardh) Grunow	0.67	13.33
<i>Epithemia adnata</i> var. <i>porcellus</i> (Kützing) R.Ross	0.31	10.00
<i>Epithemia argus</i> (Ehrenberg)Kützing	1.11	23.33
<i>Epithemia sorex</i> Kützing	1.59	20.00
<i>Epithemia turgida</i> (Ehrenberg)Kützing	0.67	20.00
<i>Fragilaria acus</i> (Kützing)Lange-Bertalot	14.55	86.67
<i>Fragilaria brevistriata</i> Grunow	7.37	53.33
<i>Gomphonema acuminatum</i> Ehrenberg	0.49	23.33
<i>Gomphonema intricatum</i> Kützing	7.48	70.00
<i>Gomphonema olivaceum</i> (Hornemann) Brébisson	2.89	43.33
<i>Halamphora veneta</i> (Kützing) Levkov	0.60	16.67
<i>Hantzschia amphioxys</i> (Ehrenberg) Grunow	0.15	10.00
<i>Navicula crytocephala</i> Kützing	0.57	16.67
<i>Navicula cryptonella</i> Lange-Bertalot	2.66	43.33
<i>Navicula radiosa</i> Kützing	4.52	76.67
<i>Navicula rhynchocephala</i> Kützing	2.98	23.33
<i>Nitzschia acicularis</i> (Kützing) W.Smith	0.99	20.00
<i>Nitzschia gracilis</i> Hantzsch	0.15	10.00
<i>Nitzschia linearis</i> W.Smith	0.38	20.00
<i>Nitzschia palea</i> (Kützing) W.Smith	0.63	13.33
<i>Nitzschia recta</i> Hantzsch ex Rabenhorst	0.31	10.00
<i>Nitzschia sigmoidea</i> (Nitzsch) W.Smith	1.60	53.33
<i>Pinnularia brebissonii</i> (Kützing) Rabenhorst	0.03	3.33
<i>Rhoicosphenia abbreviata</i> (C.Agardh) Lange-Bertalot	2.33	50.00
<i>Rhopalodia gibba</i> (Ehrenberg) Otto Müller	1.36	40.00
<i>Sellaphora bacilloides</i> (Hustedt) Z.Levkov, S.Krstic & T.Nakov	0.16	3.33
<i>Surirella ovalis</i> Brébisson	0.51	13.33
<i>Surirella ovata</i> var. <i>apiculata</i> W.Smith	0.34	13.33
<i>Surirella ovata</i> var. <i>salina</i> (W.Smith) Rabenhorst	0.04	3.33
<i>Tabularia fasciculata</i> (C.Agardh) D.M.Williams & Round	2.60	36.67
<i>Ulnaria amphirhynchus</i> (Ehrenberg) Compère & Bukhtiyarova	1.00	16.67
<i>Ulnaria ulna</i> (Nitzsch) P. Compère	11.31	100.00

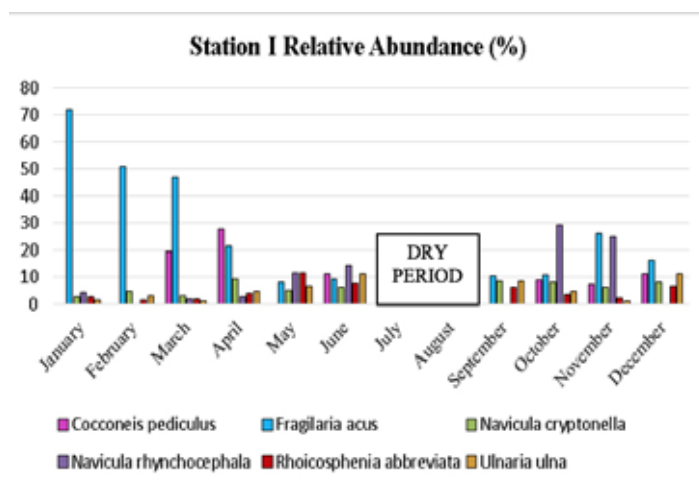


FIGURE 1
Seasonal variations in the relative density of *Cocconeis pediculus*, *Fragilaria acus*, *Navicula cryptonella*, *N. rhynchocephala*, *Rhoicosphenia abbreviata* and *Ulnaria ulna* species at station I.

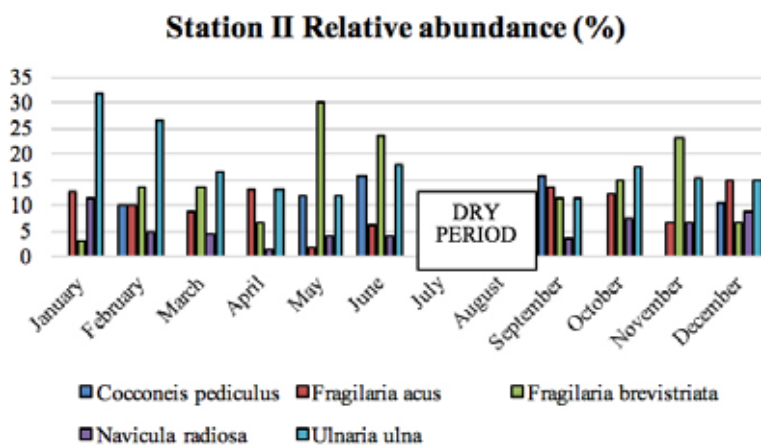


FIGURE 2
Seasonal variations in the relative density of *Cocconeis pediculus*, *Fragilaria acus*, *F. brevistriata*, *Navicula radiosa* and *Ulnaria ulna* species at station II.

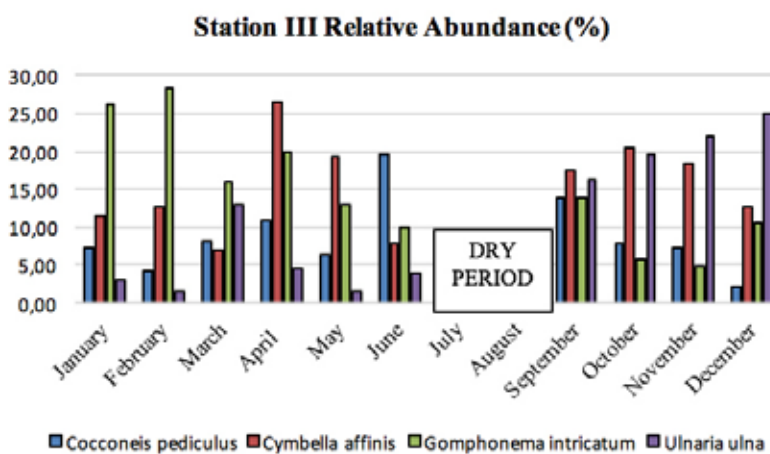


FIGURE 3
Seasonal variations in the relative density of *Cocconeis pediculus*, *Cymbella affinis*, *Gomphonema intricatum* and *Ulnaria ulna* species at station III.

Taxon diversity in epilithon was richer in spring (March, April) and autumn (September, October). Number of taxa recorded at stations were almost similar; 29, 23 and 24 taxa were recorded at stations I, II and III respectively. So as to seasonal growth of diatoms at species level at stations (Fig. 1-3), *F. acus* and *C. pediculus* at station I; *F. brevistriata* and *U. ulna* at station II; *C. affinis* and *G. intricatum* at station III grew better than other diatoms in spring. Growth of *C. pediculus* was conspicuous in summer both at stations I and III. The abundance of *Navicula radiosa* (station I) and *F. brevistriata* (station II) in summer was by far higher than all other months. *F. acus* was also drawn attention with its higher cell numbers in summer than other seasons at station III. *F. acus* and *N. rhynococephala* at station I; *F. brevistriata* and *U. ulna* at station II; *C. affinis* and *U. ulna* at station III were dominant autumn species. Growth of *F. acus* at station I; *U. ulna* at station II and *G. intricatum* at station III were really noticeable during winter period.

Of all, *Fragilaria acus* and *Ulnaria ulna* were most conspicuous diatoms with their frequency of occurrence than other diatoms in epilithon throughout the study. Thus, these diatoms are considered as permanent members of Haringet Stream. In addition, *Navicula cryptonella*, *Rhoicosphania abbreviata* (station I), *Fragilaria brevistriata*, *Navicula radiosa* (station II), *Cocconeis pediculus*, *Cymbella affinis* and *Gomphonema intricatum* (station III) were the most noticeable diatoms with their 100% frequency of occurrence (Figs. 1-3). This finding may show that these diatoms adopted to the clean water stream condition in Haringet Stream better than other diatoms.

The competition for increasing cell numbers between different members of genera and also the species belong to the same genus yielded interesting results in some cases. The genus *Fragilaria* represented by two species and *F. acus* was more noticeable with higher frequency of occurrence and relative abundance than *F. brevistriata* (Fig. 1-3). It is important to mention that higher relative abundance of the former usually coincided with lower relative abundance of the latter. Oppositely *F. brevistriata* occurred with higher cell numbers in the periods when *F. acus* was recorded with low individual numbers. This may be considered as a good example for ecological competition between species belong to the same genus. *U. ulna* station was another noticeable diatom in Haringet Stream and was present throughout the study at all stations (Fig. 1-3). The diatom was observed to be in a serious competition with *F. acus* at all stations. It is worth to mention that occurrence of *U. ulna* with low relative abundance (1-3%) was recorded during the periods in which *F. acus* occurred with high cell numbers. Oppositely, serious competition between *F. acus* and *U. ulna* was noticeable at station II and usually ended for favour of *U. ulna*. Competition between *Cymbella affinis* and *G. intricatum* with *U. ulna* was also remarkable

at station III. *Cocconeis pediculus* was also observed to participate in the competition in some periods. All these findings may be accepted as an evidence for ecological competition between different diatom species in Haringet Stream.

Occurrence and distribution of diatom species varied in different parts of the stream. *F. acus*, *F. brevistriata* and *U. ulna* were among the most noticeable diatoms in Haringet Stream and their occurrence constituted a good example to this. Both the frequency of occurrence and relative abundance of *F. acus* were much higher in the upper part of the stream than those recorded in middle and lower parts. Oppositely *U. ulna* was recorded with low occurrence and cell numbers in upper part although the diatom was quite noticeable in other parts of the stream. *F. brevistriata* was not observed in upper part whereas the diatom was one of the most noticeable species in middle part of the stream. These findings may be related to the adaptation ability and habitat preferences of the diatom species.

Although some diatoms (e.g. *N. cryptonella* and *R. abbreviata* at station I; *Cocconeis pediculus* at station III) were recorded with 100% frequency of occurrence, their relative abundance were extremely low compare to other continuously occurring diatoms. These findings may draw attention to that the high frequency of occurrence didnot always coincide with high relative abundance in the present study. This may be explained with the usual competition between diatom species for the same nutrients. Similarly, high relative abundance of *C. pediculus* in june (19.61 %) coinciding with low relative abundance of other continuously recording species such as *C. affinis* (7.84%), *G. intricatum* (9.80%) and *U. ulna* (3.92%) may also be explained with the same reason.

DISCUSSION

Chessman [42] stated that species of *Navicula* and *Nitzschia* are cosmopolitan. In fact, *Nitzschia* and *Navicula* are reported to be common diatoms in freshwater habitats and represented with more species than other diatom genera in many studies [1-3, 16-18]. In addition, these diatoms are also reported to grow well in organically polluted aquatic habitats with low dissolved oxygen concentrations [43]. Thus, the occurrence of *Nitzschia* and *Navicula* with many species in Haringet stream which has Class I water quality (very clean) may show that these diatoms grow well in polluted as well as in clean water conditions. *N. palea* is a common diatom in freshwater habitats and known to be highly tolerant to conditions from alpha mesosabrobic to polysabrobic. The diatom is also reported to occur in oligosabrobic zone of a polluted stream but couldnot increase in numbers [44]. In addition, *N. palea* are tolerant to toxic substances and comfortably occur in Class II and III quality waters [19]. These findings may show

that *N. palea* has a wide ecological tolerance to occur from clean to polluted waters but it grows better in polluted waters. The absence of *N. palea* in upper and the lower parts of the stream in Haringet Stream that has Class I Water Quality partly supported the findings of Cox [44].

Some species of *Cymbella* was also reported to be good indicators of clean waters with rich oxygen and poor organic nitrogen [43, 45]. This finding is in harmony with the occurrence of *Cymbella* spp. in Haringet Stream which is also rich in oxygen and poor in organic nitrogen. The present study also supports the finding of Mazhan and Mansor [46] who reported that *Cocconeis pediculus* and *C. placentula* are good indicators of clean water conditions and according to sabrobic index they are well known members of Class I water. *C. pediculus* was also an important representative of clean water of Haringet Stream. However good growth of *C. pediculus* in highly eutrophic waters is also emphasized [47]. *Gomphonema olivaceum* is known as one of the common species occurring in Class II and III Quality Water and regarded as good indicator for recovery zone of polluted waters [19]. In addition, *Gomphonema parvulum* and *C. accomada* are reported to be highly tolerant diatoms to pollution [44, 23]. However opposite to these findings, *G. olivaceum* is found to be present in all parts of Haringet Stream that has very clean water properties. It is worth to mention that another *Gomphonema* species (*G. intricatum*) is also the one of most conspicuous diatoms in clean water of Haringet Stream both with respect to frequency of occurrence and relative abundance. Thus, one may think that *Gomphonema* spp. may be considered as good indicators for both highly clean water as well as those of polluted water (Class II and III). In addition, *Gomphonema* spp. are also reported to be alkaliphilic [45]. This also hold true for the present study as Haringet Stream has also high alkalinity.

Although *Ulnaria ulna* and *Fragilaria acus* were among the most conspicuous diatoms with their occurrence and relative abundance in Haringet Stream, we came across with no studies reporting that these diatoms are good indicators of clean water. In opposite, *U. ulna* was reported to be one of the common diatoms in mesotrophic and eutrophic waters [44]. Thus, the present study is not in harmony with that of Cox [44].

Species composition and the seasonal variations of planktonic and benthic forms in freshwaters are dependent on interactions between physical and chemical factors. However which factors are more effective than others sometimes vary from one ecosystem to another due to their different ecological properties. However, water temperature and transparency among the most important physical factors affecting the species composition and numbers of individuals of diatoms in aquatic environments [48-

50]. None of the physical and chemical variables including water temperature seemed to have negative effects on the seasonal distribution of the epilithic diatoms in Haringet Stream. In addition, silica concentrations were always enough to support the diatom growth in all seasons. However low concentrations of nitrate and ortho-phosphate may be responsible for low biomass of diatoms in the stream.

Physicochemical analyses are widely accepted that they yield the water condition in a given time [51, 52]. Algae are also extensively used as indicator organisms to determine environmental conditions despite the fact that water quality evaluation with algae can show slight deviation [19]. Physicochemical values determined for Haringet Stream clearly yielded that the stream has I Class Water Quality along the stream (from upper part to the lower part). The occurrence of certain diatom species during the present study supported the clean water condition of Haringet Stream. Particularly the continuous presence of most noticeable diatoms *Cocconeis pediculus*, *Cymbella affinis*, *C. helvetica*, *Diatoma elongata*, *Fragilaria acus*, *Gomphonema intricatum*, *G. olivaceum*, *Navicula radiosa*, *Nitzschia sigmoidea* and *Ulnaria ulna* in Haringet Stream may be evaluated as a valuable finding that these diatom species can be monitored as indication of clean water stream condition.

ACKNOWLEDGEMENTS

This study was supported as an individual project with SUF.13.02 number by Firat University Scientific Research Projects (FUSRP). The author specially thanks to Prof. Dr. Bulent Sen for his valuable critics and advice.

REFERENCES

- [1] Lobo, E.A., Callegaro, V.L.M., Hermany, G., Bes, D., Wetzel, C.A. and Oliveira, M.A. (2004) Use of epilithic diatoms as bioindicators from lotic systems in southern Brazil, with special emphasis on eutrophication. *Acta Limnol. Bras.* 16(1): 25-40.
- [2] Winter, J.G. and Duthie, H.C. (2000) Epilithic diatoms as indicators of stream total N and total P concentration. *J. N. Benthol. Soc.* 19(1): 32-49.
- [3] Sherwood A.R., Rintoul T.L., Muller, K.M. and Sheath, R.G. (2000) Seasonality and distribution of epilithic diatoms, macroalgae and macrophytes in a spring-fed stream system in Ontario, Canada. *Hydrobiologia*, 435: 143-152.
- [4] Tolotti, M. (2001) Phytoplankton and littoral epilithic diatoms in high mountain lakes of the

- Adamello-Brenta Regional Park (Trentino, Italy) and their relation to trophic status and acidification risk. *J. Limnol.* 60 (2): 171-188.
- [5] Gurbuz, H. and Kivrak, E. (2002) Use of epilithic diatoms to evaluate water quality in the Karasu River of Turkey. *J Environ Biol.* 23(3): 239-246.
- [6] Sahin, B. (2003) Epipellic and epilithic algae of lower parts of Yanbolu River (Trabzon, Turkey) *J. Biol.* 27: 107-115.
- [7] Kalyoncu, H., Barlas, M., Ertan, O.O., Gulboy, H. (2004) The determination according to epilithic algae and physicochemical parameters of water quality of Aglasun Stream. Suleyman Demirel University. *Eğirdir Journal of Aquatic Products.* 2(12): 7-14.
- [8] Kalyoncu, H. (2006) The determination with epilithic diatoms and physicochemical parameters of water quality of Isparta Stream. Suleyman Demirel University. *Journal of Science.* 1(1-2): 14-25.
- [9] Akanil Bingol, N., Ozyurt, M.S., Dayioglu, H., Yamik, A. and Solak, C.N. (2007) Epilithic diatoms of Upper Porsuk Creek (Kutahya). *Journal of Ecology and Environment.* 15(62): 23-29.
- [10] Pala Toprak, G. ve Caglar, M. (2008) The monthly variations and epilithic diatoms of Peri Stream (Tunceli/Turkey). Firat University. *Journal of Science and Engineering.* 20(4): 557-562 (in Turkish).
- [11] Mumcu, F. Barlas, M. and Kalyoncu, H. (2009) Epilithic diatoms of Dipsiz-Çine Streams (Mugla-Aydin). Suleyman Demirel University. *Journal of Science.* 4(1): 23-34 (in Turkish).
- [12] Solak, C.N. (2011) The application of diatom indices in the upper Porsuk Creek Kutahya- Turkey, *Turkish Journal of Fisheries and Aquatic Science.* 11: 31-36.
- [13] Sonmez, F. and Asan, K. (2012) Occurrence and distribution of epipellic and epilithic diatoms of Batman Stream (Turkey). *Fresen. Environ. Bull.* 21(1): 31-35.
- [14] Cicek, N.L. and Ertan, O.O. (2015) Determination of water quality by epilithic diatoms in Koprucay River (Antalya). *Ege J Fish Aqua Sci.* 32(2): 65-78.
- [15] WFD (2000) EU Water Framework Directive (WFD) 2000/60/EC, 23.10.2000.
- [16] Euan, D.R. and John, P.S. (1998) Epilithic diatoms of the St. Lawrence River and their relationships to water quality. *Can. J. Bot.* 76(2): 251-257.
- [17] Dell'uomo, A., Pensieri, A. and Corradetti, D. (1999) Epilithic diatoms from the Esino River (Central Italy) and their use for the evaluation of the biological quality of the water. *Cryptogamie Algologie.* 20(3): 253-269.
- [18] Salomoni, S., Rocha, O., Callegaro, V. and Lobo, E. (2006) Epilithic diatoms as indicators of water quality in the Gravatai River, Rio Grande do Sul, Brazil *Hydrobiologia.* 559(1): 233-246.
- [19] Lange-Bertalot, H. (1978) Diatomeen-Differenzialorten anstelle von Leitformen: ein geeigneteres Kriterium der Gewässerbelastung. *Arch. Hydrobiol. Suppl.* 51. *Algological Studies* 21. Suttutgard, 393-427.
- [20] Lange-Bertalot, H. (1979a) Toleranzgrenzen und Populationsdynamik benthischer Diatomeen bei unterschiedlich starker Abwasserbelastung. *Arch. Hydrobiol. Suppl.* 56 *Algological Studies* 23, 184-219.
- [21] Lange-Bertalot, H. (1979b) Pollution Tolerance of Diatoms as a Criterion Water Quality Estimation. *Nova Hedwigia. Beiheft.* 64: 285-303.
- [22] Lange-Bertalot, H. (1980) Kieselalgen als Indikatoren der Gewässerqualität. Insbesondere bei hoher kommunaler und industrieller Belastung in Main und Rhein. *Cour. Forsch.-inst. Senckenberg,* 41: 97-110 pp. Frankfurt.
- [23] Steinberg, C. and Schiefele S. (1988) Biological Indication of Trophy and Pollution of Running Waters. 2. Wasser-Abwasser- Forschungsthemmen, 21, 227-234.
- [24] Kolkwitz, R. and Marsson, M. (1902) Grundsätze für die biologische Beurteilung des Wassers nach seiner Flora und Fauna. *Mitt. Prüfungsanst. Wasserversorgung. Abwasserreinigung.* 1, 33-72.
- [25] Sladeczek, V. (1973) System of Water Quality from the Biological point of View.-*Arch. Hydrobiol. Beih. Ergebn. Limnol.* 7, 1-218.
- [26] Elerante, P. and Andersson, K. (1998) Diatom indices in water quality monitoring of some South-Finnish rivers. *Verh. Internat. Verein. Limnol.* 26, 1213-1215.
- [27] Descy, J.P. and Coste, M. (1990) Utilisation des diatomees benthiques pour l'évaluation de la qualité des eaux courantes. *Contrat CEE B-71-23. Rapport final.* Cemagref.
- [28] Gomez, N. (1998) Use of epipellic diatoms for evaluation of water quality in Mantanza-Riachuelo (Argentina), a pampean plain river. *Water Res.* 32 (7), 2029-2034.
- [29] Round, F.E. (1993) A Review and Methods for The Use of Epilithic Diatoms for Detecting and Monitoring Changes in River Water Quality 1993. *Methods for the Examination of Waters and Associated Materials.* HMSO, London.
- [30] Dixit, S.S., Smol, J.P. and Kingston J.C. (1992) Diatoms: Powerful Indicators of Environmental Change. *Environment Science Technology,* 26, 23-32.
- [31] Katoh, K. (1991) A comparative study on some ecological methods of evaluation of water pollution. *Environ. Sci.* 5 (2): 91-98.
- [32] Biggs, B.J.F. (1996) Patterns in benthic algae of streams. In Stevenson, R.J., M.L. Bothwell and R.L. Lowe (eds.) *Algal ecology: Freshwater*

- benthic ecosystems. Academic Press Inc. San Diego: 31-56.
- [33] APHA (American Public Health Association) (1985) Standard methods for the examination of water and wastewater. 16th Edition. Washington. 1268 p.
- [34] Wetzel, R.G. and Likens, G.E. (2000) Limnological Analyses, 3rd ed. (Springer-Verlag.)
- [35] Round, F.E. (1953) An investigation of two benthic algal communities in Malham Tarn, Yorkshire, J. Ecol. 41: 97-174.
- [36] Krammer, K. and Lange-Bertalot, H. (1986) Bacillariophyceae. 1. Teil: Naviculaceae. In: Ettl H., Gerloff J., Heynig H. and Mollenhauer D. (eds.) Susswasser flora von Mitteleuropa, Band 2/1. Gustav Fischer Verlag: Stuttgart, New York, 1-876.
- [37] Krammer, K. and Lange-Bertalot, H. (1988) Bacillariophyceae. 2. Teil: Bacillariaceae, Epithemiaceae, Surirellaceae. In: Ettl H., Gerloff J., Heynig H. and Mollenhauer D. (eds.) Susswasserflora von Mitteleuropa, Band 2/2. VEB Gustav Fischer Verlag: Jena, 1-596.
- [38] Krammer, K. and Lange-Bertalot, H. (1991a) Bacillariophyceae. 3. Teil: Centrales, Fragilariaceae, Eunotiaceae. In: Ettl H., Gerloff J., Heynig H. and Mollenhauer D. (eds.) Susswasserflora von Mitteleuropa, Band 2/3. Gustav Fischer Verlag: Stuttgart, Jena, 1-576.
- [39] Krammer, K. and Lange-Bertalot, H. (1991b) Bacillariophyceae. 4. Teil: Achnantheaceae, Kritische Ergänzungen zu Navicula (Lineolatae) und Gomphonema, Gesamtliteraturverzeichnis Teil 1-4. In: Ettl H., Gerloff J., Heynig H. and Mollenhauer D. (eds.) Susswasserflora von Mitteleuropa, Band 2/4. Gustav Fischer Verlag: Stuttgart, Jena, 1-437.
- [40] Guiry, M.D. and Guiry, G.M. (2017) Algae-Base. World-wide electronic publication, National University of Ireland, Galway. <http://www.algaebase.org>
- [41] Anonymous (2012) Regulation on Management of Surface Water Quality 30 November 2012 history 28483 with number, Official newspaper, Ankara.
- [42] Chessman, B.C. (1986) Diatom flora of an Australian River System: Spatial patterns and environmental relationships. Freshwater Biology. 16: 805-819.
- [43] Van Dam, H., Mertens, A. and Sinkeldam, J. (1994) A coded checklist and ecological indicator values of freshwater diatoms from the Netherlands. Netherlands Journal of Aquatic Ecology, 28, 117-133.
- [44] Cox, E.J. (1996) Identification of Freshwater Diatoms from Live Material. Chapman & Hall. First edition. 158 p.
- [45] Potapova, M. and Charles, F.D. (2003) Distribution of benthic diatoms in U.S. rivers in relation to conductivity and ionic composition. Freshwater Biology, 48, 1311-1328.
- [46] Mazhan, W.O. and Mansor, M. (2002) Aquatic pollution assesment based on attached diatom communities in the Pinang river basin, Malaysia. Hydrobiologia, 487, 229-241.
- [47] Kwadrans, J., Elorante, P., Kwecka, B. and Wojtan, K. (1999) Use of bentic diatom communities to evaluate water quality in rivers of southern Poland. Journal of Applied Phycology, 10, 193-201.
- [48] Odum, E.P. (1971) Fundamentals of ecology. V.B. Sanders Comp., Philedelphia and London, 547 p.
- [49] Round, F.E. (1981) The ecology of algae, Cambridge University press. U.S.A. 653 p.
- [50] Lowe, R.L. and Pan, Y. (1996) Algal ecology. Benthic algal communities as biological monitors. Academic Pres. 705-739.
- [51] Fricke, G. and Steubing, L. (1984) Die Verbreitung von Makrophyten und Mikrophyten in Hartwasser - Zuflüssen des Ederstausees. Arch. Hydrobiol. 101, 3, 361-372.
- [52] Sonneman, J.A., Walsh, J.C., Sharpe, A.K. and Breen, F.P. (2001) Effects of Urbanization on Streams of The Melbourne Region, Victoria, Australia. II. Benthic Diatom Communities. Freshwater Biology 46, 553-565.

Received: 18.04.2017

Accepted: 09.06.2017

CORRESPONDING AUTHOR

Feray Sonmez

Firat University

Fisheries Faculty

Department of Basic Aquatic Sciences

23119, Elazig – TURKEY

Email: feraysonmez@gmail.com

EFFECT OF LIGHT PATH LENGTH OF TUBES ON GROWTH RATE OF *NANNOCHLOROPSIS OCULATA* USING INDUSTRIAL SCALE TUBULAR PHOTOBIOREACTOR IN THE MARINE HATCHERY

Yasar Durmaz*, Gokhun Cagatay Erbil

Ege University, Fisheries Faculty, Aquaculture Department, Bornova, Izmir, Turkey

ABSTRACT

Microalgal biotechnology have to solved for culture system for culturing of algae species. In this case, it should be optimised with key design parameters in an integrated way of photobioreactor used for cultivation of microalgae. The diameter of the tube was the predominant factor to determine the light gradient.

The experiments, which examined the effect of different light path length (LP) of tubes on the cell growth of *N. oculata* show that there was a relationship between light path length and growth rate. 50 mm LP PBR and nd 80 mm LP tubular PBR were inoculated with 61.0×10^6 cell/mL and 71.0×10^6 cell/mL, respectively. In the first 15 days, Cell numbers were increased in both systems without any fluctuotion, the maxiumum cell densities were also recorded as $590.67 \pm 8.60 \times 10^6$ (50 mm LP) cell/mL and $396.83 \pm 6.75 \times 10^6$ (80 mm LP) cell/mL.

Our results of biomass yield which was calculated as 2.8 g/L day for 50 mm LP PBR system.

KEYWORDS:

Nannochloropsis oculata, light path length, photobioreactor, tubular photobioreactor, semi-continuously, artificial light

INTRODUCTION

In last decades, microalgae have attracted great attention due to their many potential applications in different commercial sectors such as nutraceutical, pharmaceutical, cosmetic, food, and feed [1-3].

Composition of microalgae species can also change significantly depending on the culture conditions, including temperature and light [4-6], particularly their gross composition and content of fatty acids [7, 8].

Microalgae production for the aquaculture sector presents one of the main problems in the development of a number of processes due to the typically low productivity and poor quality of the resulting bi-

omass, along with contamination and high production costs [9,10]. For this reason, the utilization of closed tubular photobioreactors (PBRs) is advantageous due to the high control level of culture condition available with these systems, making enhanced biomass productivity possible although the production cost increases with respect to open systems [11, 12].

Light delivery to tubular photobioreactors is usually excellent because the maximum path length for light transfer is the diameter of the tubing. There are very few article on the quantitative effect of such different light path length of tubular diameter on the output rate of biomass in enclosed industrial reactors. Most of the physiological works on photoacclimation studied algal culture response to up and down shifts in the intensity of the light source. Yet, these parameters exert a most significant effect on the light regime to which the cells are exposed in photobioreactors [11, 13].

In this paper, we studied the indoor production of *N. oculata* using pilot-scale tubular PBRs in semi-continuous mode. Moreover, it was tried to find out whether 50 mm or 80 mm light path length (LP) of tubes would be better for the cultivation of *N. oculata*. The objective was to demonstrate the feasibility of this strain's indoor production at this scale and to determine the optimum LP for production. This research is a necessary step in the scale-up of any microalgae production process in order to prevent failures caused by inadequate strain performance at/under real scale/conditions or inadequate photobioreactor design or operation.

MATERIALS AND METHODS

Microalgae and culture medium. *Nannochloropsis oculata* (Droop) ([14].; CCAP 849/1) used in this study were obtained from The Culture Collection of Algae and Protozoa (CCAP), Scotland. The batch starter cultures were maintained axenically in F/2 medium [15] and pH was 7.5. The strain was inoculated in 1 L glass flasks at temperature $20 \pm 1^\circ\text{C}$, 24 hours' light as irradiance at bench height of 100 $\mu\text{mol photons}$ (Li-Core 195) obtained using 40-watt

gro-lux fluorescent lamps ((Sylvania, Germany). When the inoculum reached a concentration ranged between 10^6 and 10^7 cell/mL, it was transferred to larger glass balloons (5L), and the volume was completed to 200 L with F/2 medium for inoculation to tubular photobioreactor.

Culture medium for the tubular systems (F/2 medium, 1 mL/L [15]) was added daily, but vitamin solution was not added to medium. Cultures were maintained at 35g/L salinity and at $20 \pm 1^\circ\text{C}$.

In this experiment, the culture pH in both tubular systems were maintained at 7.50 ± 0.2 by adding pure CO_2 regulated through a pH-stat system.

At the beginning, light intensity was adjusted at lower level to prevent any photoinhibition phenomena on the low cell density inoculum. Light intensity was arranged as $96 \mu\text{mol}/\text{m}^2\text{s}$ at the surface of the tubing with activating half parts of fluorescent lamps until 8th day. After that day, the illumination was increased to $200 \mu\text{mol}/\text{m}^2\text{s}$ via activation of all lights after the cell density increased more than 2 times.

Experimental Photobioreactor. The experiments performed in this work took place in a tubular PBR which belongs to an aquaculture hatchery facility in Turkey (Akvatek Company), is shown in Figure 1 and 2. Both of the PBRs wound on a rigid vertical structure in such a 6 m length and 0.2 m width. The PBRs which have 80 mm and 50 mm light path length, divided into two main parts; illumination receiver and degasser and cooler tank. Illumination receivers of 50 mm LP is made of transparent plexiglass tubes and consisted of 240 m long (4.6 cm internal diameter, 0.2 cm wall thickness). The illumination receiver is divided into two lines as 120 meters of each. The other PBR which has 80 mm LP of

tube, divided into two main parts; illumination receiver and degasser and cooler tank. Illumination receiver is made of transparent plexiglass tubes and consisted of 96 m long (7.4 cm internal diameter, 0.3 cm wall thickness).



FIGURE 1
Tubular PBR real system. The upper side of PBR (50mm LP of tubes) and the bottom side of PBR (80mm LP of tubes).

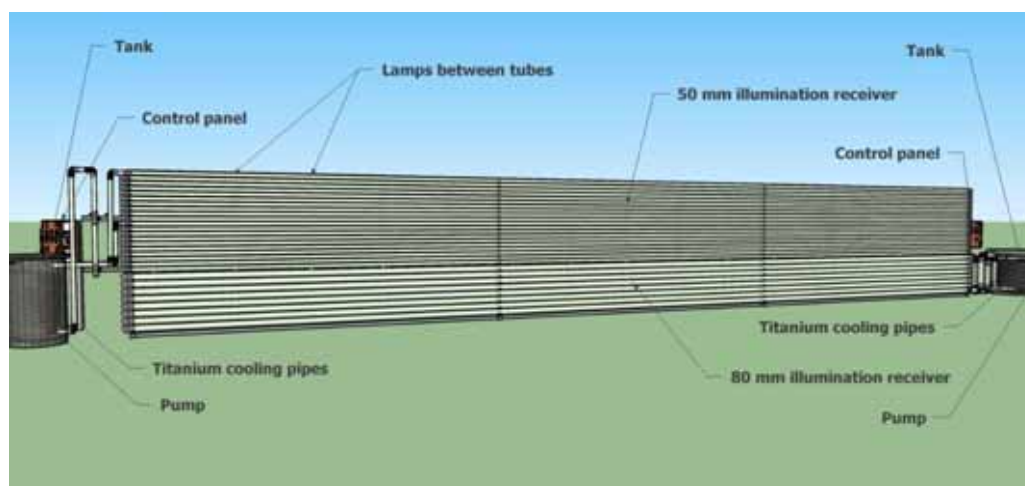


FIGURE 2
Tubular photobioreactorS (PBRs) system shema. The upper side of PBR (50mm LP of tubes) has degasser and cooler tank in the left. The bottom side of PBR (80mm LP of tubes) has degasser and cooler tank in the right.

The degasser and cooler tank which is made of double walled polyester fiber tank, is used for mixing, degassing and heat exchange culture. The culture temperature is controlled through an internal heat exchanger placed titanium tubes at the bubble column by passing cooling water at 100 L/h. Sea water was used as the cooling water, its temperature was generally 18°C that time. And room temperature was also kept at 20±1°C under continuously controlled air conditions. The culture was kept at 19±1°C. The microalgal culture was circulated as velocity of 0.6 m/s using a centrifugal pump located between the bubble column and the solar receiver. Depended on the specific growth rate of culture, the microalgae were grown photoautotrophically with continuous mode at a dilution rate of 10-20 % of total volume day. Moreover, the pH and temperature were being measured at several positions along the tube and degasser tank using Seko kontrol PR40 pH/redox and conductivity meter (Italy). Each measurement apparatus was in turn connected to a control computer through a data acquisition device. The pH of the culture was controlled by on-demand injection of pure industrial grade CO₂ gas at 5 L/min.

Cleaning of the tubular PBRs. Further perspective of mass culture of microalgae will have required closed system because the microalgae must be grown under conditions that are free from potential contaminants. It is not possible to completely sterilize the tubular PBRs, but in this study, the tubular PBRs was disinfected by using sodium hypochlorite overnight and neutralized for 2 h with sodium thiosulfate. While preparing the tubular PBRs for microalgae culture, marine water was sterilized by passing through 0.02 µm filtration system and also sterilized marine water was used for addition during the harvest period of the system.

Analytical methods. Samples were collected daily for analysis of dry weight and cell count. The

dry weight of the harvested cell mass was determined using 5–10 ml of the cultures, which was filtered through predried and preweighed Whatmann GF-52 glass- fiber filters (0.45 µm, Germany) and dried overnight in an oven at 105 °C [16]. Cell density was measured via Improved Neubauer hemocytometer at three times a day (08:00a.m., 12:00p.m. and 18:00 p.m) and at the same time, contamination was checked daily through visual observation. Growth rates (μ) were calculated with this equation (Eq.1):

$$\mu = \frac{\ln(N_t) - \ln(N_0)}{t - t_0} \quad (\text{Eq.1})$$

where N_t is biomass at time (t) and N_0 is the beginning biomass at time t_0 .

The volumetric productivity, P_v (g/L d), was calculated using this equation (Eq.2) depending on the change in biomass concentration, X (g/L), within a certain cultivation period (d):

$$P_v (\text{g/L d}) = \frac{X_2 - X_1}{t_2 - t_1} \quad (\text{Eq.2})$$

RESULTS

The variation of cell densities and harvest rates (% of total volume) at the both tubular PBRs of *N. oculata* culture under artificial illumination is shown in Figures 3 and 4. The experiments, which examined the effect of different LP on the cell growth of *N. oculata* show that there was a relationship between LP and growth rate. 50 mm LP of tubular PBR was inoculated with 61.0 x 10⁶ cell/mL and 80 mm LP of tubular PBR was inoculated with 71.0 x 10⁶ cell/mL. Cell numbers were increased in both PBR systems and maximum cell densities were recorded as 50 mm and 80 mm LP systems as 590.67±8.60 x 10⁶ cell/mL and 396.83±6.75 x 10⁶ cell/mL, respectively.

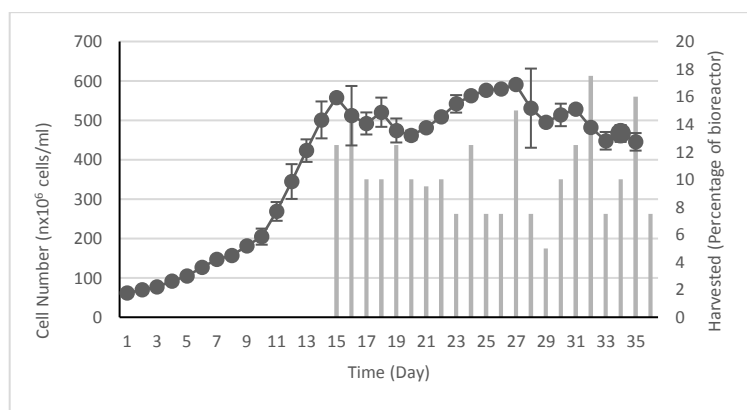


FIGURE 3

Growth curve and daily harvest rate of *N. oculata* for 50 mm light path length of tubular PBR. Data point represent mean (n=3), error bars indicate standart deviation.

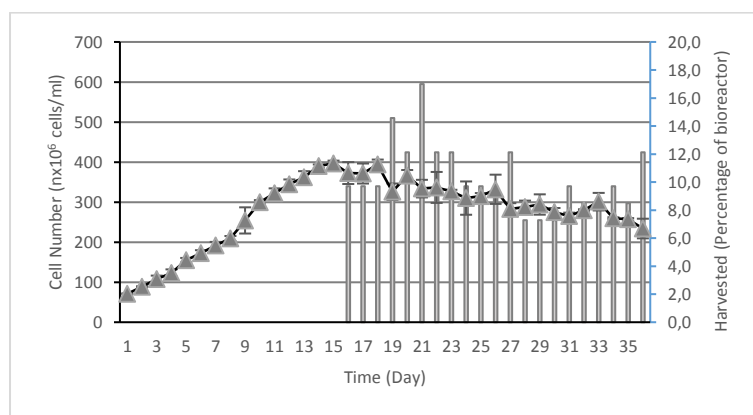


FIGURE 4

Growth curve and daily harvest rate of *N. oculata* for 80 mm light path length of tubular PBR. Data point represent mean (n=3), error bars indicate standart deviation.

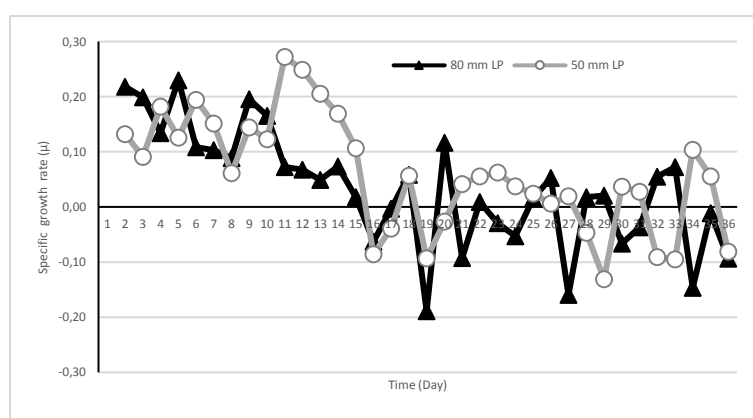


FIGURE 5

Specific growth rate (μ) of *N. oculata* culture for 50 mm and 80 mm LP of tubular PBRs.

Cell densities of *Nannochloropsis oculata* at 50 mm and 80 mm LP tubular PBR increased rapidly from 61.33×10^6 cell/mL and 71.0×10^6 cell/mL to $557.33 \pm 8.08 \times 10^6$ cell/mL and $396.83 \pm 6.75 \times 10^6$ cell/mL respectively in the first 15 days without any apparent log phase. Also, mean cell densities were calculated to be 386.99×10^6 cell/mL for 50 mm LP tubular PBR and 307.41×10^6 cell/mL for 80 mm LP tubular PBR. Most robust specific growth rates for *N. oculata* at 50 mm and 80 mm LP tubular PBRs were recorded as 0.27 day and 0.23 day, respectively (Figure 5). Due to starting of the harvest regime, gradual decreases were observed in both systems depending on the harvest rate.

Due to dry weights measurement of daily, mean volumetric productivity was calculated as 2.8 g/L day for 50 mm LP tubular PBR while which was calculated as 2 g/L day for 80 mm LP PBR. Also, highest volumetric productivities were calculated for 50 mm and 80 mm LP tubular PBRs as 3.25 g/L day and 2.2 g/L day, respectively.

The average harvest rate of 50 mm and 80 mm LP of tubular PBR were calculated as 10.0% and

10.3%, respectively. When daily harvest rate was exceeded by more than 10%, decrease in the cell number was determined. After cell numbers declined, harvest rates were reduced to less than 10% to allow increase of culture densities (Figure 3 and 4). The daily harvest rates have been altered for both persistence of the culture and protection of cells from degradation. So that, biomass concentrations were spanned through the entire experimental period.

DISCUSSIONS

Tubular PBRs are recommended as the most suitable system for the production of microalgae strains such as *N. oculata*. In these reactors, it is possible to provide better control of culture conditions. Results indicated that the cultures mainly perform as artificial light conditions, that *N. oculata* can be produced in pilot-scale tubular photobioreactors in continuous mode.

When the cell population density is too low, photodamage may cause the collapsing of culture,

even if the culture is exposed to low growth irradiance, or, it will be exposed to strong light often resulting in photodamage in several algal species [16, 17].

Biomass yields are comparable to typical biomass concentrations achieved in other photobioreactors. The total biomass yield was considerably higher than algae concentrations in open raceway ponds, which typically ranged between 0.1 and 0.5 g/L [18,19], but can reach up to 1.4 g/L [20,21]. Xu et al. [22] also reported as 1.10 and 1.20 g/L day productivity for fed batch culture at artificial light conditions. On the other hand, especially horizontal photobioreactor over the 165-day operation and *N. atomus* biomass were measured as the lowest at 2.07 g/L and the highest at 4.3 g/L [23]. Three different volumetric productivity calculations (based on different *N. oculata* cell dry weight references) were reported as 1.10-2.02 g/L day, 1.21-1.63 g/L day and 2.02-3.03 g/L day with continuous mode at 50 mm LP of helical tubular PBR (combined illumination solar and artificial) in summer [24]. Our results of biomass yield which was calculated as 2.8 g/L day for 50 mm LP PBR system was similar with the results of some finding reported. In fact, the result of 80 mm LP PBR system yield ratio (2 g/L day) was relatively lower than some reported results. Because of using of different algae, lower results might be obtained than those reported in tubular PBRs.

In a tubular photobioreactor with a short light path (2.6 cm) and operating at high biomass concentrations (up to 2 g/L), a maximal biomass productivity of 0.32 g/L day was reported by Molina-Grima et al. [25]. In terms of areal productivity, the maximum value reported here, of 20 g/m² day, is lower than that reported in raceway reactors, of 29 g/m² day [26]. Zou and Richmond [27] entertained cultures with cell concentrations above 10 g/L dry weight in flat plate bioreactor configurations, with narrow light-paths, under vigorous stirring and strong incident light: decreases in the light-path produced major improvements in photosynthetic productivity, up to optical paths of 1.0 cm. Results of those researches showed that if the low cm LP of PBRs were preferred, the yield of biomass increased although it causes the productivity to decrease. Therefore, there were not advantageous to use 1 cm LP in the PBRs.

In this study, 50 mm and 80 mm diameter tubes were used with continuous illumination both side of tubes. Light intensity bonded with culture depth and intensity. According to Zou and Richmond [28], the light regime prevailing in association with the narrower light-paths (less than 10cm) could not be effectively for the slow growing *Nannochloropsis* sp. cells. Uslu et al. [11] reported that flat plate glass PBR with 1, 3, 5, 7 and 10 cm LPs were used to grow in batch culture of *Phaeodactylum tricornutum*. They obtained best results with 7 cm LP as 1.280g/L dry weight. However, Richmond and Wu [29] obtained higher value of *Nannochloropsis* sp. biomass

with 1.3cm and 5.2cm light-paths (0.35g/L day dry weight). Having optimized the length of the light path, the population density, and the mode and the extent of stirring as well as adjusted the angle of inclination along the year, we report the records of high areal output rates of biomass, we have thereby elucidated a promising strategy for efficient utilization of solar energy for production of photoautotrophic microorganisms.

CONCLUSION

Our results indicate that this design offers the advantages of having a large surface to volume ratio, easy controlling of temperature and carbon dioxide transfer, while occupying in a small ground area. In addition, totally controlled lights ensure the persistence of production which is not possible for outdoor systems. The growth rate and biochemical composition of *N. oculata* are subjects for environmental conditions in each season. We have used this design to be able to grow algae throughout the year especially in hatchery production seasons at both LP of PBR system. The best productivity was obtained with 50 mm LP of tubular PBR system.

REFERENCES

- [1] Buono, S., Langellotti, A.L., Martello, A., Rinna, F. and Fogliano, V. (2014) Functional ingredients from microalgae. *Food Funct.*, 5, 1669-1685.
- [2] Dibenedetto, A. (2012) Production of aquatic biomass and extraction of oil. In: Aresta M, Dibenedetto A, Dumeignil, F. (eds) *Biorefinery: From biomass to chemicals and fuels*. Walter de Gruyter GmbH & Co KG, Berlin/Boston, 81-100.
- [3] Gouveia, L. (2011) *Microalgae as a Feedstock for Biofuels*- Springer-Verlag Berlin Heidelberg, 68.
- [4] Renaud, S.M., Zhou, H.C., Parry, D.L., Think, L.V., and Woo, K.C. (1995) Effect of temperature on the growth, total lipid content and fatty acid composition of recently isolated tropical microalgae *Isochrysis* sp., *Nitzschia closterium*, *Nitzschia paleacea*, and commercial species *Isochrysis* sp. (clone T. ISO). *Journal of Applied Phycology*, 7(6), 595-602.
- [5] Richmond, A. (2004) Principles for attaining maximal microalgal productivity in photobioreactors: an overview. *Hydrobiologia*, 512(1-3), 33-37.
- [6] Durmaz, Y., Donato, M., Monterio, M., Gouveia, L., Nunes, M.L., Gama P.T., Gokpinar, S., & Bandarra, N.M. (2008). Effect of Temperature on Growth and Biochemical Composition (Sterols, α -tocopherol, Carotenoids,

- Fatty Acid Profiles) of the Microalga, *Isochrysis galbana*. The Israeli Journal of Aquaculture - Bamidgeh, 60(3), 190-197.
- [7] Guckert, J.B., and Cooksey, K.E. (1990) Triglyceride accumulation and fatty acid profile changes in *Chlorella* (Chlorophyta) during high Ph-induced cell cycle Inhibition. Journal of Phycology, 26(1), 72-79.
- [8] Thompson, P.A., Guo, M.X. and Harrison, P.J. (1992) Effects of variation in temperature. I. On the biochemical composition of eight species of marine phytoplankton. Journal of Phycology, 28(4), 481-488.
- [9] Boeing, P. (2000) Larval feed alternatives. Global Aquac Advocate 3(1), 48-50
- [10] Muller-Feuga A. (2013) Microalgae for aquaculture: the current global situation and future trends. In: Richmond, A., Hu, Q. (Eds.), Handbook of microalgal culture: applied phycology and biotechnology. Wiley Blackwell, Chichester, 613-627
- [11] Uslu, L., Ak, B., Isik, O. and Durmaz, Y. (2014) Effect of light path length and nitrogen deficiency on the biochemical composition of *Phaeodactylum tricornutum*. Fresen. Environ. Bull. 23(6), 1309-1313.
- [12] Ippoliti, D., Gomez, C., Morales-Amaral, M.M., Pistocchi, R., Fernandez-Sevilla, J.M., Gabriel Acien, F. (2016) Modeling of photosynthesis and respiration rate for *Isochrysis galbana* (T-Iso) and its influence on the production of this strain. Bioresource Technology 203, 71-79
- [13] Richmond, A. (1986) Cell response to environmental factors In: Richmond, A. (ed.) Handbook of Microalgal Mass Culture, CRC Press, Boca Raton, Florida, 69-99.
- [14] Hibberd, D.J. (1981) Notes on the taxonomy and nomenclature of the algal classes Eustigmatophyceae and Tribophyceae (synonym Xanthophyceae). Botanical journal of the Linnean society, 82(2), 93-119.
- [15] Guillard, R.R., and Ryther, J.H. (1962) Studies of marine planktonic diatoms: I. *Cyclotella* Nana Hustedt, and *Detonula Confervacea* (CLEVE) Gran. Canadian journal of microbiology, 8(2), 229-239.
- [16] Hu, Q. and Richmond, A. (1994) Optimizing the population density in *Isochrysis galbana* grown outdoors in a glass column photobioreactor. Journal of Applied Phycology, 6(4), 391-396.
- [17] Vonshak, A. and Guy, R. 1988 Photoinhibition as a limiting factor in outdoor cultivation of *Spirulina platensis*. In Algal Biotechnology, T. Stadler J. Mollion, M.-C. Verdu, Y. Karamanos, H. Morvan, D. Christiaen (Eds), Elsevier Applied Science Publishers, London England, 1988, PP. 365-70.
- [18] Kumar, K.S., Dahms, H.U., Won, E.J., Lee, J.S. and Shin, K.H. (2015) Microalgae—A promising tool for heavy metal remediation. Ecotoxicology and environmental safety, 113, 329-352.
- [19] Zhu, L. (2015) Biorefinery as a promising approach to promote microalgae industry: An innovative framework. Renewable and sustainable energy reviews, 41, 1376-1384.
- [20] Ashokkumar, V., Agila, E., Sivakumar, P., Salam, Z., Rengasamy, R. and Ani, F.N. (2014) Optimization and characterization of biodiesel production from microalgae *Botryococcus* grown at semi-continuous system. Energy Conversion and Management, 88, 936-946.
- [21] Ketheesan, B., and Nirmalakhandan, N. (2012) Feasibility of microalgal cultivation in a pilot-scale airlift-driven raceway reactor. Bioresource technology, 108, 196-202.
- [22] Xu, F., Hu, H.H., Cong, W., Cai, Z.L. and Ouyang, F. (2004) Growth characteristics and eicosapentaenoic acid production by *Nannochloropsis* sp. in mixotrophic conditions. Biotechnology letters, 26(1), 51-53.
- [23] Dogaris, I., Welch, M., Meiser, A., Walmsley, L. and Philippidis, G. (2015) A novel horizontal photobioreactor for high-density cultivation of microalgae. Bioresource Technology, 198, 316-324.
- [24] Briassoulis, D., Panagakis, P., Chionidis, M., Tzenos, D., Lalos, A., Tsinos, C., Berberidis, K. and Jacobsen, A. (2010) An experimental helical-tubular photobioreactor for continuous production of *Nannochloropsis* sp., Bioresource Technology, 101(17), 6768-6777.
- [25] Molina-Grima, E., Sanchez Perez, J.A., Garcia Camacho, F., Garcia Sanchez, J.L., Acien Fernandez, F.G. and Lopez Alonso, D. (1994) Outdoor culture of *Isochrysis galbana* ALII-4 in a closed tubular photobioreactor. Journal of Biotechnology 37, 159-166.
- [26] Boussiba, S., Sandbank, E., Shelef, G., Cohen, Z., Vonshak, A. Ben-Amotz, A., Arad, S., Richmond, A. (1988) Outdoor cultivation of the marine microalga *Isochrysis galbana* in open reactors. Aquaculture, 72, 247-253.
- [27] Zou, N. and Richmond, A. (1999) Effect of light-path length in outdoor flat plate reactors on output rate of cell mass and of EPA in *Nannochloropsis* sp. Journal of Biotechnology, 70(1), 351-356.
- [28] Zou, N. and Richmond, A., (2000) Light-path length and population density in photoacclimation of *Nannochloropsis* sp. (Eustigmatophyceae), Journal of Applied Phycology, 12, 349-354.
- [29] Richmond, A. and Cheng-Wu, Z. (2001) Optimization of a flat plate glass reactor for mass production of *Nannochloropsis* sp. outdoors. Journal of biotechnology, 85(3), 259-269.

Received: 05.06.2017
Accepted: 09.06.2017

CORRESPONDING AUTHOR

Yasar Durmaz
Fisheries Faculty
Aquaculture Department
Ege University
35100 Bornova, Izmir – TURKEY

E-mail: yasar.durmaz@ege.edu.tr

ELECTRO-FILTER RECYCLE POWDER OF CEMENT INDUSTRY AS A LOW-COST ADSORBENT FOR REMOVAL OF TEXTILE DYE ASTRAZON BLUE FGRL

Ismail Nalbant¹, Halil Kumbur², Havva Duygu Bilgen², Gamze Koyuncu Turkey^{2,*}

¹Department of Bus Management, General Directorate of EGO, 06560 Ankara, Turkey

²Department of Environmental Engineering, Mersin University, 33343 Mersin, Turkey

ABSTRACT

The adsorption of Astrazon Blue FGRL onto cement industry electro-filter recycle powder was investigated in aqueous solutions in a batch system with respect to contact time, initial concentration, pH and temperature. The pseudo-first-order and pseudo-second-order kinetic models were used to describe the kinetic data and the rate constants were evaluated. The Langmuir and Freundlich adsorption models were applied to describe the equilibrium isotherms and the isotherm constants were also determined. The Langmuir model was the best-fit isotherm for the experimental data. The change of Standard free energy (ΔG°), enthalpy (ΔH°) and entropy (ΔS°) of adsorption were also evaluated for the adsorption of Astrazon Blue FGRL onto cement industry electro-filter powder. ΔH° and ΔS° changes for the adsorption process were 7.29 kJ mol^{-1} and $19.77 \text{ J mol}^{-1} \text{ K}^{-1}$. The adsorption of Astrazon Blue FGRL dye was increased with the increasing temperature, on the other hand, no change was observed within the range of pH 4.5-9.5. The maximum adsorption capacity of the adsorbent in the room temperature was found 73.53 mg g^{-1} . The results indicate that cement industry electro-filter recycle powder could be employed as low-cost material for the removal of textile dyes from aqueous solutions.

KEYWORDS:

adsorption, dye, electro-filter recycle powder, low-cost adsorbent, waste management

INTRODUCTION

Dyes usually have a synthetic origin and complex aromatic molecular structures which make them more stable and more difficult to biodegrade [1]. Today there are more than 10,000 dyes available commercially and they are widely use in textiles, paper, rubber, plastics, leather, cosmetics, pharmaceutical and food industries [2]. The extensive use of dyes often cause pollution problems in the form of colored wastewater

discharged into environmental water bodies. It not only affects aesthetic appearance but also prevents light penetration and reduces photosynthesis [3,4]. Furthermore, dyes can cause toxic, carcinogenic and mutagenic effects on to the aquatic organisms (i.e. fish) and human health such as liver, kidney, reproductive, brain and central nervous systems [5,6]. The conventional methods for treating dyes containing wastewaters are coagulation and flocculation, oxidation or ozonation, membrane separation and activated carbon adsorption [7]. Adsorption is generally considered to be an effective method for quickly lowering the concentration of dissolved dyes in an effluent, and activated carbon is the most widely used adsorbent for dye removal. However, activated carbon suffers from high-cost production and regeneration. Therefore, there have been attempts to utilize low-cost and naturally occurring adsorbents [8,9].

There are some studies on the use of low cost materials for removing dyes, such as various agricultural wastes [4,10,11,36], walnut shells [35], sawdust [12,13], fly ash [14,15], chitosan [16,17], perlite [18,19], bentonite [20,21], sepiolite [22,23], pyrophyllite [24,25] and zeolite [26,27].

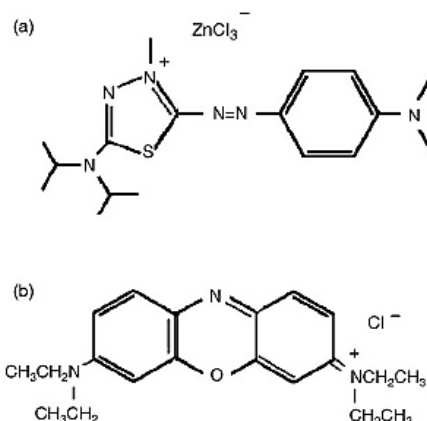


FIGURE 1
Chemical structures of (a) C.I. basic blue 159 and (b) C.I. basic blue 3.

In this study, cement industry electro-filter recycle powder was used as an adsorbent for removal of a cationic dye (Astrazon Blue FGRL).

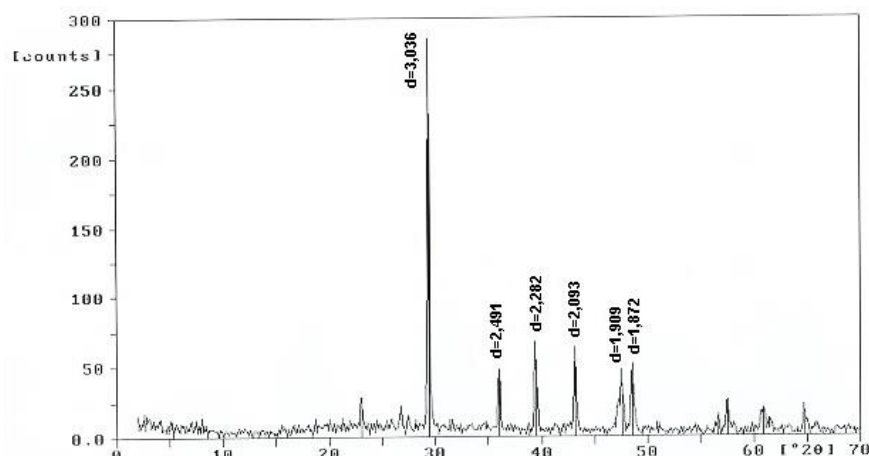


FIGURE 2
XRD diagram of adsorbent

The aim of this work is to study the adsorption of Astrazon Blue FGRL from aqueous solutions onto cement industry electro-filter recycle powder. The effects of contact time, initial concentration, pH values and temperature were examined. Also, thermodynamic and kinetic parameters were determined.

MATERIALS AND METHODS

Adsorbate. Astrazon Blue FGRL, a cationic dye, was supplied by Berdan Textile Co. Ltd. This commercial dye consists of two main components, which are C.I. basic blue 159 and C.I. basic blue 3. The ratio of the two components is approximately 5:1 by weight, respectively. The structures of these two dye components are shown in Fig. 1. The net charge of both C.I. basic blue 159 and C.I. basic blue 3 is equal to +1. Although Astrazon Blue FGRL is a mixture of two basic components, the following discussion will treat this as a single dye species [28].

The measurements of the dye concentrations were performed through light absorbance using a UV-VIS Shimadzu 160 spectrophotometer by measuring absorbance at λ_{max} of 602 nm for Astrazon Blue FGRL. The calibration curve was plotted from the dye solutions prepared in the concentration range of 5 to 30 mg L⁻¹.

Characterization and preparation of adsorbent. Cement industry electro-filter recycle powder which was used as adsorbent during the study, was taken from Cimsa Cement Industry Co. Ltd., Mersin Factory, Turkey. The surface area of the material was determined as 1.92 m² g⁻¹ and average particle size was 6.965 μ m by using “Quantachrome AUTOSORB-1” and “Mastersizer 2000” devices respectively in Tubitak Mam Laboratories, Turkey. XRD analysis of the adsorbent was built in General Directorate of Mineral Research and Exploration (MTA)

Laboratories, Turkey and was found that the calcite form the majority of the adsorbent (Fig. 2). The sample was analyzed by Cimsa Cement Industry Co.Ltd. for its chemical composition and found to contain 13.53% SiO₂, 3.71% Al₂O₃, 1.93% Fe₂O₃, 1.61% MgO, 42.73% CaO, 0.68% K₂O, 0.08% Na₂O, 0.23% SO₃, 35% loss on ignition and 0.5% unknown material.

Cement industry electro-filter recycle powder was dried in an oven at 103 °C for 24 hours and was brought to constant weight. Stock solution of adsorbent was prepared as 100 g L⁻¹ in distilled water and used in adsorption experiments.

Adsorption experiments. Adsorption tests were studied as a single-stage batch test using a Velp Model DLH mechanical stirrer. A suspension containing 0.5 g of adsorbent sample was mixed by stirring the mixture at 250 rpm with a 0.5 L aqueous solution of dye at a known initial concentration in a flask that was immersed in thermostated water in a bath keeping a constant temperature of 20°C. Aliquot of the solution were withdrawn at a predetermined time intervals and were centrifuged at 5600 rpm for 5 min to remove any adsorbent particles. The residual dye concentration in the filtrate was subsequently determined using a spectrophotometer at the wavelength corresponding to the maximum absorbance. The adsorption tests were run until the equilibrium concentration was reached. The experiments were carried out by varying the concentration of dye solution from 20 to 300 mg L⁻¹.

The data obtained from the adsorption tests were then used to calculate the adsorption capacity, q_e (mg g⁻¹), of the adsorbent by a mass–balance relationship, which represents the amount of adsorbed dye per the amount of dry adsorbent (Eqn. (1)),

$$q_e = \frac{(C_o - C_e)V}{W} \quad (1)$$

where C_o and C_e are the initial and equilibrium

concentrations of dye in solution (mg L^{-1}), respectively, V is the volume of the solution (L), and W is the weight of the dry adsorbent used (g). Finally, the adsorption capacity, q_e , was plotted against equilibrium concentration, C_e .

RESULTS AND DISCUSSIONS

Effect of initial concentration and contact time. To determine the equilibrium concentration and time, the adsorption of the cationic Astrazon Blue FGRL dye onto cement industry electro-filter recycle powder was studied as a function of contact time. Fig. 3. shows the effect of initial concentration of dyes on the adsorption capacity of cement industry electro-filter recycle powder with a solid/ liquid ratio of 1 g L^{-1} at pH 9.5 which is the natural pH of the mixture. At all initial dye concentrations studied, the adsorption takes place very fast initially: typically 90–95% of the ultimate adsorption occurs within the first 2 min of contact and gradually tails off thereafter. The independence of time required to achieve definite fraction of equilibrium adsorption on initial concentration may suggest that the adsorption process is second-order which will be discussed later. Then the amount of adsorption reaches a limiting value of around 71.85 mg g^{-1} for Astrazon Blue FGRL.

Effect of pH. The pH is one of the most important factors controlling the adsorption of the dye onto suspended particles. The suspension containing adsorbent used in the experiments has a pH value of 11.5, whereas the dye solution has a pH value of 5.5. When this two was mixed it was detected that the outcome solution has a pH of 9.5. This pH value was used in the experiments done to show the effect of contact time and initial concentration and temperature, e.i. the mixture pH was not changed by any external interference. However the pH range of 4.5- 9.5 (at 20°C) was used in the experiments done to show the effect of pH on the adsorption (Fig. 4). In this range of pH the removal of the dye, Astrazon Blue FGRL by Cement industry electro-filter recycle powder did not show a negligible change. It was detected that the surface charges of the compounds in the adsorbent were not changed in the pH range of 4.5-9.5. As a result of this cement industry electro-filter recycle powder can be used as an adsorbent in a wide range of pH.

Effect of temperature. The temperature has two major effects on the adsorption process. Increasing the temperature is known to increase the rate of diffusion of the adsorbate molecules across the external boundary layer and in the internal pores of the adsorbent particle, owing to the decrease in the viscosity of the solution. In addition, changing

to temperature will change the equilibrium capacity of the adsorbent for a particular adsorbate [29].

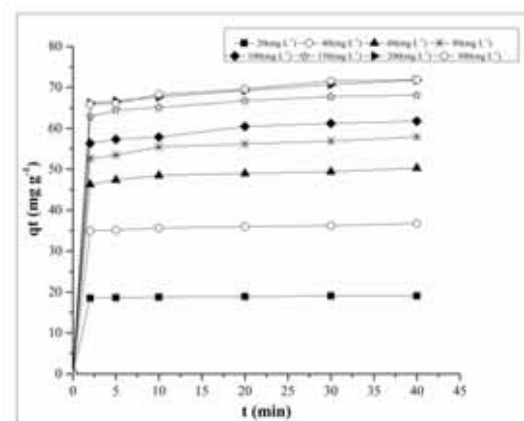


FIGURE 3

Effect of initial concentration on the adsorption of Astrazon Blue FGRL onto cement industry electro-filter recycle powder (Adsorbent concentration = 1 g L^{-1} , $T = 20^\circ\text{C}$, $\text{pH} = 9.5$)

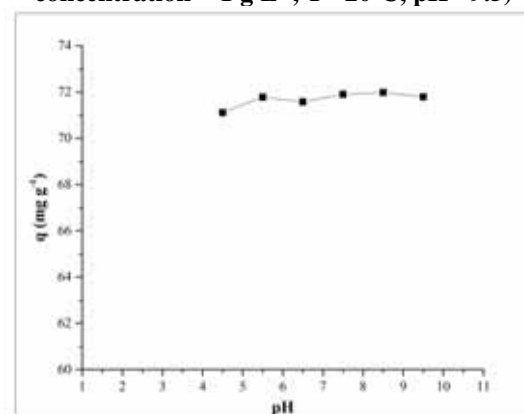


FIGURE 4

The effect of pH on adsorption capacity ($C_0 = 200 \text{ mg L}^{-1}$, $T = 20^\circ\text{C}$, $t = 40 \text{ min}$)

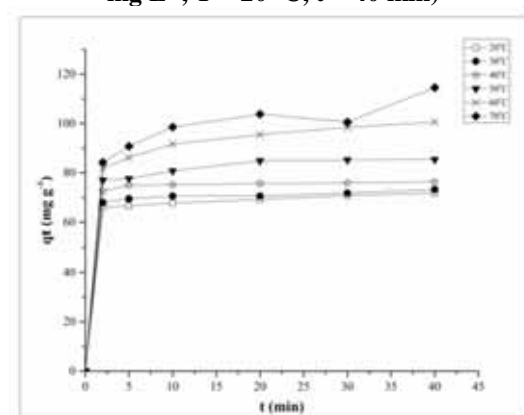


FIGURE 5

The effect of temperature on adsorption capacity ($C_0 = 200 \text{ mg L}^{-1}$, $\text{pH} = 9.5$, $t = 40 \text{ min}$)

Fig. 5 shows the results of contact time experiments carried out at different temperatures for Astrazon Blue FGRL adsorption on cement

industry electro-filter recycle powder. The removal of Astrazon Blue FGRL by adsorption on cement industry electro-filter recycle powder increases from 71.85 to 114.57 mg g⁻¹ by increasing the temperature of the solution from 20 to 70°C, indicating the process to be endothermic. This kind of temperature dependence of the amount of the dye adsorbed may reflect the increase in the case with which the dye penetrates into the perlite because of its larger diffusion coefficient.

Adsorption isotherms. Adsorption isotherms describe how adsorbates interact with adsorbents and are critical in optimizing the use of adsorbents. Therefore, the correlation of equilibrium data by either theoretical or empirical equations is essential to the practical design and operation of adsorption systems. The experimental data of equilibrium isotherms for Astrazon Blue FGRL dye was modeled using isotherms by Freundlich [30] and Langmuir [31].

The Langmuir isotherm has been widely used to describe single-solute systems. It is based on the assumption that intermolecular forces decrease rapidly with distance and consequently it predicts monolayer coverage of the adsorbate on the outer surface of the adsorbent. The isotherm equation further assumes that adsorption takes place at specific homogeneous sites within the adsorbent and there is no significant interaction among adsorbed species. Theoretically, the adsorbent has a finite capacity for the adsorbate. Once a dye molecule occupies a site, no further adsorption can take place at that site. The rate of sorption to the surface should be proportional to a driving force which times an area. The driving force is the concentration in the solution, and the area is the amount of bare surface [24].

The saturated or monolayer capacity can be represented by the expression (Eqn. (2)),

$$q_e = \frac{Q^0 b C_e}{1 + b C_e} \quad (2)$$

where q_e is solid-phase adsorbate concentration at equilibrium (mg g⁻¹), C_e is aqueous-phase adsorbate concentration at equilibrium (mg L⁻¹), Q^0 (mg g⁻¹) is the maximum amount of adsorbate per unit weight of adsorbent to form a complete monolayer on the surface, and b is the Langmuir isotherm constant (L mg⁻¹), related to the affinity of the adsorption sites.

A plot of C_e/q_e versus C_e gives a straight line of slope $1/Q^0$ and intercept $1/Q^0 b$, where Q^0 gives the theoretical monolayer saturation capacity. Therefore, a linear expression for the Langmuir Eqn.(3) is

$$\frac{C_e}{q_e} = \frac{1}{Q^0 b} + \frac{1}{Q^0} C_e \quad (3)$$

The adsorption data was analyzed first by using the Freundlich isotherm model (Fig. 6). However the experimental data did not fit to that model – R² values were dramatically low. So the linear form of the Langmuir isotherm was used and the data fitted with this model – R² values were close to 1 (Eq-3). The plots of specific sorption, C_e/q_e , against the equilibrium concentration, C_e , for Astrazon Blue FGRL was shown in Fig. 7. The isotherm constants, b , and equilibrium monolayer capacities, Q^0 , are presented in Table 1.

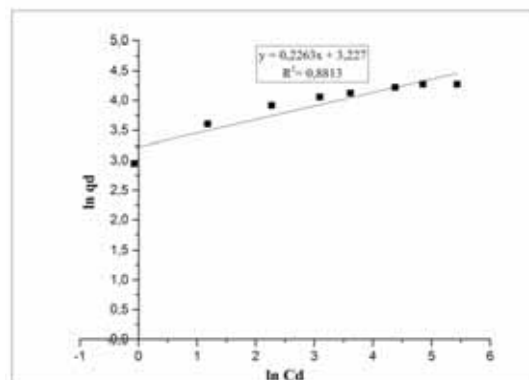


FIGURE 6
Freundlich isotherm of Astrazon Blue FGRL dye adsorbed on cement industry electro-filter recycle powder

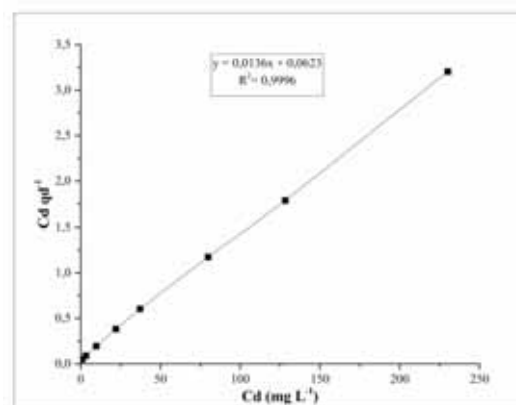


FIGURE 7
Langmuir isotherm of Astrazon Blue FGRL dye adsorbed on cement industry electro-filter recycle powder

The Langmuir monolayer capacity Q^0 of Astrazon Blue FGRL dye was 73.53 mg g⁻¹. The Langmuir model is applicable when there is a strong specific interaction between the surface and the adsorbate so that a single adsorbed layer forms.

The isotherms of the Astrazon Blue FGRL dye were found to be linear over the whole concentration range and the correlation coefficients, R^2 , were high (0.999 for Astrazon Blue FGRL), suggesting that the adsorption of Astrazon Blue FGRL dye onto cement industry electro-filter recycle powder closely follow a Langmuir isotherm.

TABLE 1
Langmuir adsorption isotherm constants for Astrazon Blue FGRL adsorption onto cement industry electro-filter recycle powder.

Langmuir isotherm			
Dye	Q^0 (mg g ⁻¹)	b (L mg ⁻¹)	R^2
Astrazon	73.53	0.218	0.999
Blue FGRL			

The effect of isotherm shape can be used to predict whether a sorption system is favorable or unfavorable in batch processes. The essential features of the Langmuir isotherm can be expressed in terms of a dimensionless constant separation factor or equilibrium parameter K_R , which is defined by the relationship (Eqn. (4)),

$$K_R = \frac{1}{1 + bC_0}, \quad (4)$$

where K_R is a dimensionless separation factor, C_0 is initial concentration (mg L⁻¹), and b is the Langmuir constant (L mg⁻¹). The parameter K_R indicates the shape of the isotherm accordingly: The value of K_R indicates the type of the isotherm to be either unfavorable ($K_R > 1$), linear ($K_R = 1$), favorable ($0 < K_R < 1$), or irreversible ($K_R = 0$) [32].

The K_R values calculated indicate that adsorption of Astrazon Blue FGRL dye on cement industry electro-filter recycle powder is favorable ($0 < K_R < 1$) for all initial dye ion concentrations.

Kinetics of adsorption. A study of adsorption kinetics is desirable as it provides information about the mechanism of adsorption, which is important for the efficiency of the process. Successful application of the adsorption demands innovation of cheap, easily available, and abundant adsorbents of known kinetic parameters and sorption characteristics. Adsorption kinetics can be modeled by some models as the pseudo-first-order Lagergren equation and pseudo-second-order rate equation Ho and McKay [33], Ho [34] given below as Eqn.(5) and Eqn.(6), respectively.

$$\log(q_e - q_t) = \log q_e - \frac{k_1}{2.303}t, \quad (5)$$

where q_e and q_t are the amount of adsorbed dye on the biosorbent at the equilibrium and at time t , respectively (mg g⁻¹), and k_1 is the rate constant of first-order sorption (L min⁻¹).

$$\frac{t}{q_t} = \frac{1}{k_2 q_e^2} + \frac{1}{q_e}t, \quad (6)$$

where k_2 is the pseudo second-order rate constant with a unit of g mg⁻¹ min⁻¹.

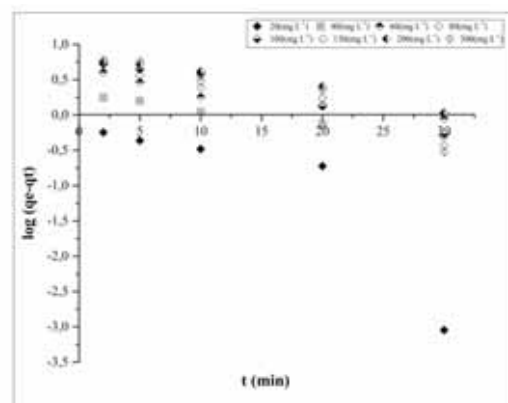


FIGURE 8
First-order sorption kinetics of Astrazon Blue FGRL at various initial dye concentrations

The first-order and the pseudo second-order kinetic models were applied to the experimental data. The plots of these two kinetic models at all initial concentrations are illustrated in Fig. 8 and 9, respectively. For the data to follow the first-order kinetics in Eqn. (4), the linear plot between $\log(q_e - q_t)$ and t should be observed. However, the results illustrate that this linear dependency could not be obtained indicating that the first-order Lagergren rate kinetics are not appropriate for the adsorption of basic dye. For the pseudo second-order kinetics, the parameters, q_e and k_2 , could be determined from the intercept and the slope of the plots in Fig. 9 and these are summarized in Table 2. Extremely good agreement between the results and the model was obtained as illustrated by the very high R^2 for the whole range of initial dye concentrations. Hence, it was concluded at this point that the adsorption here could be better represented by the pseudo second-order rate kinetics. The results also indicated that an increase in the initial dye concentration increased the equilibrium sorption capacity, q_e , while decreasing the rate constant, k_2 .

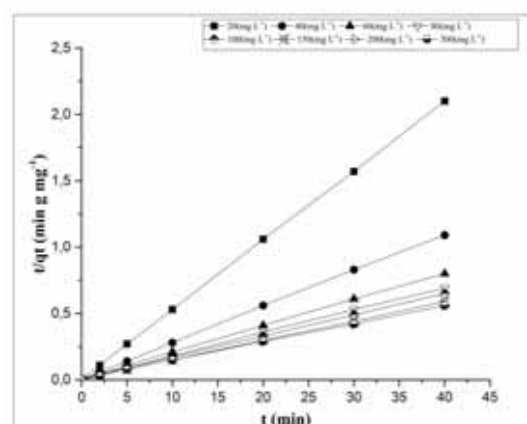


FIGURE 9
Pseudo second-order sorption kinetics of Astrazon Blue FGRL at various initial dye concentrations

TABLE 2
Comparison of the pseudo-first- and second-order and intraparticle diffusion adsorption constants at different initial concentrations of Astrazon Blue FGRL dye

Astrazon Blue FGRL (mg L ⁻¹)	$q_{e,exp}$ (mg g ⁻¹)	Pseudo-Second-Order		
		k_2 (g mg ⁻¹ min ⁻¹)	$q_{e,cal}$ (mg g ⁻¹)	R_2^2
20	19.07	0.514	19.16	0.9999
40	36.74	0.151	36.76	0.9998
60	50.29	0.083	50.25	0.9997
80	57.92	0.058	57.80	0.9997
100	61.76	0.030	62.50	0.9996
150	68.10	0.059	68.49	0.9998
200	71.79	0.043	71.94	0.9996
300	71.85	0.042	72.46	0.9997

Thermodynamic parameters. In any adsorption process, both energy and entropy considerations must be taken into account in order to determine what process will occur spontaneously. Values of thermodynamic parameters are the actual indicators for practical application of a process. The amount of dye adsorbed at equilibrium at different temperatures is 20, 40, 50 and 60 °C, have been examined to obtain thermodynamic parameters for the adsorption system.

The thermodynamic parameters, change in the Standard free energy (ΔG°), enthalpy (ΔH°), and entropy (ΔS°), were determined by using following Eqn.(7-9) Ozcan and Ozcan [22],

$$K_C = \frac{C_A}{C_S}, \quad (7)$$

$$\Delta G^\circ = -RT \ln K_C, \quad (8)$$

$$\ln K_C = \frac{\Delta S^\circ}{R} - \frac{\Delta H^\circ}{RT}, \quad (9)$$

where K_C is the equilibrium constant, C_A is the amount of dye adsorbed on the adsorbent of the solution at equilibrium (mg dm⁻³), C_S is the equilibrium concentration of the dye in the solution (mg dm⁻³). T is the solution temperature (K) and R is the gas constant. ΔH° and ΔS° were calculated the slope and intercept of Van't Hoff plots of $\ln K_C$ versus $1/T$ (Fig. 10). The results are given in Table 3.

The results obtained are +1.41 kJ mol⁻¹ at 20°C, +1.38 kJ mol⁻¹ at 30 °C, +1.21 kJ mol⁻¹ at 40 °C, +0.79 kJ mol⁻¹ at 50 °C indicated that the adsorption reaction was not a spontaneous one and that the system gained energy from an external source [33]. The change in enthalpy (ΔH°) was found to be positive.

The positive values confirm the endothermic nature of adsorption. The positive values of the entropy change show the increased randomness at the solid/solution interface with some structural changes in the adsorbate and adsorbent and an affinity of the adsorbent toward those basic dyes [22].

TABLE 3
Thermodynamic parameters

T (°C)	K_c	ΔG° (kJ mol ⁻¹)	ΔH° (kJ mol ⁻¹)	ΔS° (J mol ⁻¹ K ⁻¹)
20	0.560	1.41		
30	0.578	1.38	7.29	19.77
40	0.628	1.21		
50	0.745	0.79		

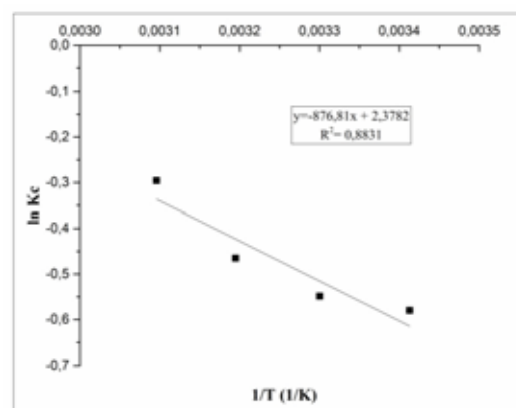


FIGURE 10
Plot of $\ln K_C$ vs. $1/T$ for estimation of thermodynamic parameters for the adsorption of Astrazon Blue FGRL onto cement industry electro-filter recycle powder

CONCLUSIONS

The study presented revealed that cement industry electro-filter recycle powder can be used as low-cost adsorbents for removing cationic dyes. The equilibrium adsorption data of the dye can be best modeled using a Langmuir approach with adsorption capacities of 73.53 mg g⁻¹ for Astrazon Blue FGRL. For the adsorption of Astrazon Blue FGRL dye, chemical reaction seems significant in the rate-controlling step and the pseudo-second-order chemical reaction kinetics provides the best correlation for the experimental data.

The enthalpy change (ΔH°) for the adsorption process was 7.29 kJ mol⁻¹, which indicates the chemical forces between the adsorbed dye molecules and cement industry electro-filter recycle

powder. The ΔG° values were positive therefore the adsorption was not spontaneous and the positive value of ΔS° suggests an increase in randomness at the solid/solution interface through the adsorption of Astrazon Blue FGRL onto cement industry electro-filter recycle powder.

ACKNOWLEDGEMENTS

This study was supported by the Research Fund of Mersin University in Turkey with Project Number: BAP -FBE ÇM (İN) 2005-1 YL.

REFERENCES

- [1] Tamez Uddin M.D., Akhtarul Islam M.D., Mahmud S, Rukanuzzaaman M.D., (2009). Adsorptive removal of methylene blue by tea waste, *J Hazard Mater.* 164 (1): 53–60.
- [2] Ubale M., Shelke R., Bharad J., Madje B., (2010). Adsorption of acid dyes from aqueous solution onto the surface of acid activated kammoni leaf powder: A case study. *J. Chem. Pharm. Res.* (4): 747-753.
- [3] Santos S.C.R., Boaventura R.A.R., (2015). Treatment of a simulated textile wastewater in a sequencing batch reactor (SBR) with addition of a low-cost adsorbent, *J Hazard Mater.* 291: 74-82.
- [4] Shakoor S., Nasar A.,(2016). Removal of methylene blue dye from artificially contaminated water using citrus limetta peel waste as a very low cost adsorbent, *J Taiwan Inst Chem Eng.* 66: 154–163.
- [5] Soni M., Sharma A.K., Srivastava J.K., Yadav JS., (2012). Adsorptive removal of methylene blue dye from an aqueous solution using water hyacinth root powder as a low cost adsorbent. *Int. J. Adv. Chem. Sci. Appl.* 3 (3): 338-345.
- [6] Yagub M.T., Sen T.K., Afroze S., Ang HM., (2014). Dye and its removal from aqueous solution by adsorption: A review, *Adv Colloid Interface Sci.* 209: 172–184.
- [7] Taha G.M., Mosaed M., (2010). Blast furnace slag of a ferrosilicon firm in aswan governorate, upper egypt, as an adsorbent for the removal of merocyanine dye from its aqueous solution. *Chem Biodivers.* 7: 878-886.
- [8] Chen H., Zhao J, Dai G., (2011) Silkworm exuviae- a new-non-conventional and low-cost adsorbent for removal of methylene blue from aqueous solutions. *J Hazard Mater.* 186: 1320-1327.
- [9] Alver E., Metin A.U., (2012). Anionic dye removal from aqueous solutions using modified zeolite: Adsorption kinetics and isotherm studies. *Chem. Eng. J.* 200-202: 59-67.
- [10] Ozsoy H.D., Kumbur H. Adsorption of Cu (II) ions on cotton boll, *J Hazard Mater.* 2006; B136: 911-916.
- [11] Subramaniam R., Ponnusamy SK., (2015). Novel adsorbent from agricultural waste (cashew NUT shell) for methylene blue dye removal: Optimization by response surface methodology, *Water Resour Res.* 11: 64–70.
- [12] Garg V.K., Amita M., Kumar R., Gupta R., (2004). Basic dye (methylene blue) removal from simulated wastewater by adsorption using Indian Rosewood sawdust: a timber industry waste, *Dyes Pigm.* 63: 243-250.
- [13] Agarwal S., Tyagi I., Gupta V.K., Ghasemi N., Shahivand M., Ghasemi M., (2016). Kinetics, equilibrium studies and thermodynamics of methylene blue adsorption on *Ephedra strobilacea* saw dust and modified using phosphoric acid and zinc chloride, *J. Mol. Liq.* 218: 208-218.
- [14] Sun D., Zhanga X. Wub Y., Liua X., (2010). Adsorption of anionic dyes from aqueous solution on fly ash, *J Hazard Mater.* 181: 335–342.
- [15] Mall I.D., Srivastava V.C., Agarwal N.K., Mishra I.M. (2005). Adsorptive removal of malachite green dye from aqueous solution by bagasse fly ash and activated carbon-kinetic study and equilibrium isotherm analyses, *Colloids Surf A Physicochem Eng Asp.* 264: 17–28.
- [16] Wu F., Tseng R., Juang R., (2001). Kinetic modeling of liquid-phase adsorption of reactive dyes and metal ions on chitosan, *Water Res.* 35 (3): 613–618.
- [17] Iqbal J., Wattoo FH., Wattoo MHS., Malik R., Tirmizi SA., Imran M., Ghangro AB., (2011). Adsorption of acid yellow dye on flakes of chitosan prepared from fishery wastes, *Arab J Chem.* 4: 389–395.
- [18] Dogan M., Alkan M., Turkyilmaz A., Ozdemir Y., (2004) Kinetics and mechanism of removal of methylene blue by adsorption onto perlite, *J Hazard Mater.* B109: 141-148.
- [19] Roulia M., Vassiliadis AA., (2008). Sorption characterization of a cationic dye retained by clays and perlite, *Micropor Mesopor Mat.* 116: 732–740.
- [20] Ozcan A.S., Erdem B., Ozcan A., (2005). Adsorption of Acid Blue 193 from aqueous solutions onto BTMA-bentonite. *Colloids Surf A Physicochem Eng Asp.* 266: 73-81.
- [21] Chinoune K., Bentaleb K., Bouberka Z., Nadim A., Maschke U., (2016). Adsorption of reactive dyes from aqueous solution by dirty bentonite, *Appl Clay Sci.* 123: 64–75.
- [22] Ozcan A., Ozcan A.S., (2005). Adsorption of Acid Red 57 from aqueous solutions onto surfactant-modified sepiolite, *J Hazard Mater.* B125: 252–259.

- [23] Santos S.C.R., Boaventura R.A.R., (2016). Adsorption of cationic and anionic azo dyes on sepiolite clay: Equilibrium and kinetic studies in batch mode, *J Environ Chem Eng.* 4: 1473–1483.
- [24] Gucek A., Sener S., Bilgen S., Mazmanci M.A., (2005). Adsorption and kinetic studies of cationic and anionic dyes on pyrophyllite from aqueous solutions, *J Colloid Interface Sci.* 286: 53-60.
- [25] Zhang J., Zhou Y., Jiang M., Li J., Sheng J.; (2015). Removal of methylene blue from aqueous solution by adsorption on pyrophyllite, *J Mol Liq.* 209: 267–271.
- [26] Benkli Y.E., Can M.F., Turan M., Celik M.S., (2005). Modification of organo-zeolite surface for the removal of reactive azo dyes in fixed-bed reactors, *Water Res.* 39: 487–493.
- [27] Jin X., Yu B., Chen Z., Arocena J.M., Thring R.W., (2014). Adsorption of Orange II dye in aqueous solution onto surfactant-coated zeolite: Characterization, kinetic and thermodynamic studies, *J Colloid Interface Sci.* 435: 15–20.
- [28] Apohan E., Yesilada O., (2005). Role of white rot fungus *Funalia trogii* in detoxification of textile dyes, *J Basic Microbiol.* 45 (2): 99–105.
- [29] Al-qodah Z., (2000). Adsorption of dyes using shale oil ash, *Water Res.* 34 (17): 4295-4303.
- [30] Freundlich H. (1926), *Colloid and Capillary Chemistry*, Methuen Co., London.
- [31] Langmuir I., (1918). Adsorption of gases on plain surfaces of glass mica platinum, *J Am Chem Soc.* 40 (9): 1316–1403.
- [32] Bhatnagar A., Jain A.K., (2005). A comparative adsorption study with different industrial wastes as adsorbents for the removal of cationic dyes from water, *J Colloid Interface Sci.* 281: 49-55.
- [33] Ho Y.S., McKay G., (1998). Sorption of dye from aqueous solution by peat, *Chem. Eng. J.* 70: 115-124.
- [34] Ho Y.S., (2004). Pseudo-isotherms using a second order kinetic expression constant, *Adsorption* 10: 151-158.
- [35] Lu X.U., Duan J.J., Yang L.Y., Huang L.Z., (2017). Static adsorption of Cr(VI) on the normal carbonized walnut shells. *Fresen. Environ. Bull.* 26 (1a):797-802.
- [36] Savcı S., (2017). Study of malachite green adsorption by waste ash using a batch method. *Fresen. Environ. Bull.*, 26 (1a):1026-1032.

Received: 28.04.2017

Accepted: 03.05.2017

CORRESPONDING AUTHOR

Gamze Koyuncu Turkey

Mersin University, Engineering Faculty,
Department of Environmental Engineering 33343,
Mersin, TURKEY

e-mail : gamzekoyuncu.33@gmail.com

EFFECTS OF EMISSION CONTROL AND METEOROLOGICAL PARAMETERS ON URBAN AIR QUALITY SHOWED BY THE 2014 YOUTH OLYMPIC GAMES IN CHINA

Xiao-San Luo^{1,*}, Zhen Zhao¹, Yan Chen¹, Xinlei Ge², Yu Huang³, Chen Suo¹, Xue Sun¹, Dan Zhang¹

¹International Center for Ecology, Meteorology, and Environment, School of Applied Meteorology, Nanjing University of Information Science & Technology, Nanjing 210044, China

²Jiangsu Key Laboratory of Atmospheric Environment Monitoring and Pollution Control, Nanjing University of Information Science & Technology, Nanjing 210044, China

³Key Lab of Aerosol Chemistry & Physics, Institute of Earth Environment, Chinese Academy of Sciences, Xi'an, 710075, China

ABSTRACT

Air pollution is a globally highlighted environmental issue, and deteriorated air quality is generally due to high pollutant emissions and stable weather conditions. Authoritative emission control actions are usually compelled to prevent the frequent air pollution episodes in megacities of China, thus the effects of pollution control measures and meteorological factors need differentiating. Strict control measures were implemented by local/regional authorities to reduce anthropogenic emissions for the 2014 Summer Youth Olympic Games (YOG) in Nanjing of eastern China, by restricting the coal-combustion, industrial activities, construction works, vehicles and barbecue. By comparing the air quality before, during, and after the YOG at 13 monitoring stations that scatter in urban, suburban and exurban areas, air pollution (represented by particulate matters and O₃) were reduced effectively by emission control measures, especially in urban areas. Moreover, precipitation eliminates air pollution directly. The daily Air Quality Index (AQI, considering PM_{2.5}, PM₁₀, SO₂, NO₂, CO, O₃) and local meteorological parameters (temperature, extreme wind speed, humidity, atmospheric pressure) show considerable correlations. Based on high-resolution data, these quantitative relationships could be adopted for air quality forecast and air pollution mitigation strategies.

KEYWORDS:

Air pollution; Emission control measures; Air quality index (AQI); Meteorological condition; Urbanization; Air quality forecast

INTRODUCTION

Air pollution is a worldwide environmental issue that has posed significant threats to human health

and ecological environments [1,2]. The public's concern with the serious impacts of air pollution has also aroused some authoritative control actions. In the developing China with rapid industrialization and urbanization [3-5], widespread haze and smog occurred with growing frequency [6-8]. Some efforts were made to achieve the clean air goal [4], such as the Air Pollution Prevention and Control Action Plan issued by State Council in 2013. For the positive outcomes, these actions still need empirical basis and theoretical analysis.

Due to the dramatically increased energy consumption and pollutant emissions, several regions in China were severely polluted [9], which are mostly located in the megalopolises, such as the northern Beijing-Tianjin-Hebei region (BTH), the eastern Yangtze River Delta (YRD), and the southern Pearl River Delta (PRD). Improvement of air quality in Beijing during the 2008 Olympics were reported in previous studies [10,11], which also raised a discussion about the contributions of emission control measures and weather conditions [12,13]. Based on former experiences, the authorities also implemented a series of air pollution mitigation strategies for the 2014 Youth Olympic Games (YOG) in Nanjing of YRD, which is another biggest international mega-event in China after the Beijing Olympics. Typically, both local and regional pollutant emissions from industry, traffic, construction, and biomass burning were restricted [14]. Therefore, the human efforts for improving air quality should be evaluated reasonably.

However, as a complex issue, air quality is also closely linked to meteorological conditions [15,16]. When pollutant emissions are relatively steady, various meteorological factors will dominate the dilution, diffusion, transportation, and transformation of air pollutants, and further affect their concentration and distribution. Meteorological elements such as humidity, pressure, wind, temperature, and rainfall might directly or indirectly contribute to the formation-elimination of air pollution [17,18]. Air pol-

lution episodes can occur during specific local meteorological conditions such as low wind and stable atmosphere [6]. Inhalable particulate matters ($PM_{2.5}$, PM_{10}), sulfur dioxide (SO_2), nitrogen dioxide (NO_2), carbon monoxide (CO), and ozone (O_3) are typical air pollutants, and the air quality index (AQI) is commonly used to represent levels of ambient air pollution in urban areas [16,19]. In 2012, China Ministry of Environmental Protection [20] approved the Technical Regulation on Ambient AQI (on trial), and some key cities began to publish local daily AQI (including $PM_{2.5}$, PM_{10} , SO_2 , NO_2 , CO, O_3) replacing the previous API (air pollution index; SO_2 , NO_2 , PM_{10}). Although there is increasing evidence of correlations between meteorological variables and some pollutant concentrations or API [21,22], their profound relationships and the influences of meteorological factors on AQI need investigating further.

Therefore, both the effects of meteorological factors and emission control measures on air quality need to be clarified. In this study, the variations of air quality (daily AQI for $PM_{2.5}$, PM_{10} , SO_2 , NO_2 , CO, and O_3) before, during and after the YOG period at 13 monitoring stations scattering across urban, suburban and exurban areas in Nanjing city were assessed together with local meteorological parameters. The main objectives are: (1) to evaluate the effects of authoritative strategies on air quality in different geographical areas; (2) and to explore the influences of meteorological factors on AQIs and its possible model prediction.

MATERIALS AND METHODS

Study Area. The YRD is one of the populous regions with the most dynamic economy and severe air pollution in China. It has been identified as a key region in the national plan for regional pollution control. Being the capital of Jiangsu province, Nanjing city located in western YRD is an important industry (steel smelting, petrochemical and automobile manufacturing) and transportation center. It covers an area of about 6600 km² and has a population of over 8.2 million. Nanjing has a north subtropical monsoon climate, and the prevailing wind is from southeast in summer while northeast in winter. Its average annual temperature is 16 °C and average annual precipitation is 1106 mm of 117 days. The main sources of air pollution in Nanjing include vehicular emissions (two million motor vehicles) and emissions from industry especially those with great energy consumption (coal), coupled with local construction dust and regional pollutant transportation from surrounding cities. Agricultural biomass burning is also an important pollution source in YRD during autumn [23].

Regular automatic monitoring of air quality is usually executed by recording crucial atmospheric constituents at monitoring stations. Administrated by

Nanjing Environmental Monitoring Center (NEMC; subordinate to Nanjing Municipal Environmental Protection Bureau, NMEPB), 13 stations are shown in Fig. 1, scattering across the Nanjing city. Nine sites are located in the main urban areas (U), two in surrounding suburban districts (SU) and two in remote exurban districts (EU).

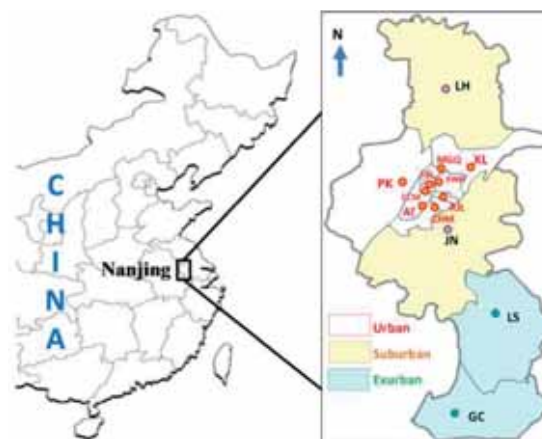


FIGURE 1

Location of study area and the 13 ground automatic monitoring stations in Nanjing city, China. Nine stations (Xuanwuhu-XWH, Ruijinlu-RJL, Zhonghuamen-ZHM, Caochangmen-CCM, Shanxilu-SXL, Maigaoqiao-MGQ, Xianlin-XL, Aoti-AT, Pukou-PK) are located in the main urban areas, two in suburban districts (Liuhe-LH and Jiangning-JN), and two in exurban districts (Lishui-LS and Gaochun-GC).

Authoritative Air Quality Program for the Nanjing Summer YOG. To guarantee the environmental quality of “green” YOG (16-28 August, 2014), a jointly authoritative network surrounding Nanjing in YRD for air quality monitoring and control was established by the CMEP, including 23 cities in Jiangsu, Anhui, and Zhejiang provinces and the Shanghai metropolitan area [14]. According to the regional Guarantee Scheme for Environment Quality (1-31 Aug) released by CMEP: 11 basic measures were implemented to control the major pollution sources from dust, vehicle exhaust and industrial emissions, and 5 stricter actions were prepared for the opening (15-16 Aug) and closing (27-28 Aug) ceremonies and the days while Nanjing AQI>100. Simultaneously, Interim Scheme for Nanjing Environmental Management and Control from 1 May to 31 Aug, and the Strengthening Scheme from 1 to 31 Aug, were also implemented by Nanjing to control local emissions. And in fact, the air pollution mitigation policies were extended one more week due to the 21st APEC SME Ministerial Meeting held in Nanjing (1-5 Sep). All regulation measures were in effect up to the end of YOG.

AQI and Data. The AQI is commonly used to report the levels of ambient air pollution [16]. It is a simple and generalized way to provide the public timely environmental information, and helps the public understand local air quality. The higher the AQI values, the more serious air pollution [19]. Here the AQI and health implications are drafted by CMEP [20], similar to the AIRNow system by US (<http://www.airnow.gov/index.cfm?action=aqibasic.s.aqi>). The individual AQI (IAQI) levels and corresponding pollutant concentration limits are also given [20]. The IAQI values are calculated by a linear interpolation of the reference scale values using Eq. (1), and then the AQI is calculated as a maximum IAQI of all air pollutants (PM_{2.5}, PM₁₀, SO₂, NO₂, CO, O₃) by Eq. (2). While AQI>50, the air pollutant with the highest IAQI is considered as the “leading pollutant”. The pollutant with IAQI>100 is recognized as “non-attainment pollutant”. For daily reports (00:00-24:00), seven pollutant factors are considered, including SO₂, NO₂, PM₁₀, PM_{2.5}, and CO based on 24 hour average concentration, the daily maximum O₃ 1-h based on 1 hour average, and the daily maximum O₃ 8-h based on 8 hour moving average values.

$$IAQI_P = \frac{IAQI_{High} - IAQI_{Low}}{BP_{High} - BP_{Low}} (C_P - BP_{Low}) +$$

IAQI_{Low} (Eq. 1)

$$AQI = \max \{IAQI_1, IAQI_2, IAQI_3, \dots, IAQI_n\}$$

(Eq. 2)

Where IAQI_P refers to the IAQI of pollutant *P*, *C_P* represents the concentration of pollutant *P*, *BP_{High}* stands for the break point that is greater than or equal to *C_P*, *BP_{Low}* represents the break point that is less than or equal to *C_P*, IAQI_{High} refers to the IAQI corresponding to *BP_{High}*, and IAQI_{Low} stands for the IAQI corresponding to *BP_{Low}* [20].

Since March 2013, the NMEPB publishes AQI instead of API for Nanjing city, routinely based on nine state-controlled monitoring stations. In this study, the daily AQI and IAQI data were obtained from their online Nanjing Air Quality Real-Time Publishing System (<http://222.190.111.117:8023/>). This air quality network includes data of total 13 ground automatic monitoring sites operated by NEMC, but among them, only the 9 state-controlled sites were used for assessing urban environment and averaged to derive the final daily AQI values representing Nanjing City, while other 4 province-controlled sites represent suburban/exurban areas (Fig. 1).

Meteorological Data. The meteorological data were provided by Nanjing Meteorology Bureau (NMB), and collected at the National Meteorological Station of Nanjing (ID 58238, 31°56' N, 118°54' E). Major daily surface meteorological elements used in this study include average values of air temperature (T), atmospheric pressure (AP), wind speed (WS), and WS_{extreme} represents the maximum value of

instantaneous wind speed), indicators of atmospheric moisture by relative humidity (RH) and the dew point depression (T-T_d, i.e., the difference between the air temperature and the dew point temperature), and precipitation (P), and their daily minimum (min) and maximum (max) values.

Data Analysis. In this study, meteorological parameters and synchronous AQI records of 57 days lasting from 25 Jul to 26 Sep 2014 in Nanjing were analyzed (data for 13-15 Aug and 4-7 Sep were missing). The data were temporally divided into periods of before (23 Jul-12 Aug), during (16 Aug-3 Sep), and after (8-26 Sep) YOG, and spatially classified to urban, suburban and exurban areas. They were also separated as rainy and non-rainy days. The statistical analysis was carried out using PASW Statistics 18 (IBM SPSS software). For relationships between various variables, besides correlation analysis (CA), the principal component analysis (PCA) was conducted using factor extraction with eigenvalues >1 after varimax rotation. To identify the key meteorological factors that best predict AQI or IAQI, multiple linear regression (MLR) models were performed by stepwise selection with a significance level of *p*<0.05 for variables to remain in the predictive equations.

RESULTS AND DISCUSSION

Temporal and Spatial Variations of AQI and the Principal IAQI. In order to sketch the air pollution pattern and its influencing factors, it is essential to understand the temporal and spatial variability of air quality. Daily AQI and typical IAQI-PM_{2.5} for different periods of the YOG in various geographical areas of Nanjing were showed in Fig. 2, together with the main meteorological parameters. Although summer is usually the best air quality season for Nanjing and there has been some pre-control measures, it still had pollution days (AQI>100, PM_{2.5} is the non-attainment pollutant) before and after YOG, and the PM_s (especially PM_{2.5}) or/and O₃ were the usual leading pollutants determining the AQI (Fig. 2). These phenomena indicate the generally disadvantageous air quality for Nanjing in PRD, and the urgent need of intervention measures. Accordingly, during 2014 YOG, the mean value of daily urban AQI is only 56 (PM_{2.5} or NO₂ is the leading pollutant) for Nanjing, with 32% excellent grade days. These AQIs are much lower than those of many other megacities in the same time, such as the average AQI of 115 and 72 for Beijing in northern and Guangzhou in southern China (O₃ or/and PM_{2.5} as leading pollutants), respectively. These AQIs are also lower than other time of Nanjing, such as the average

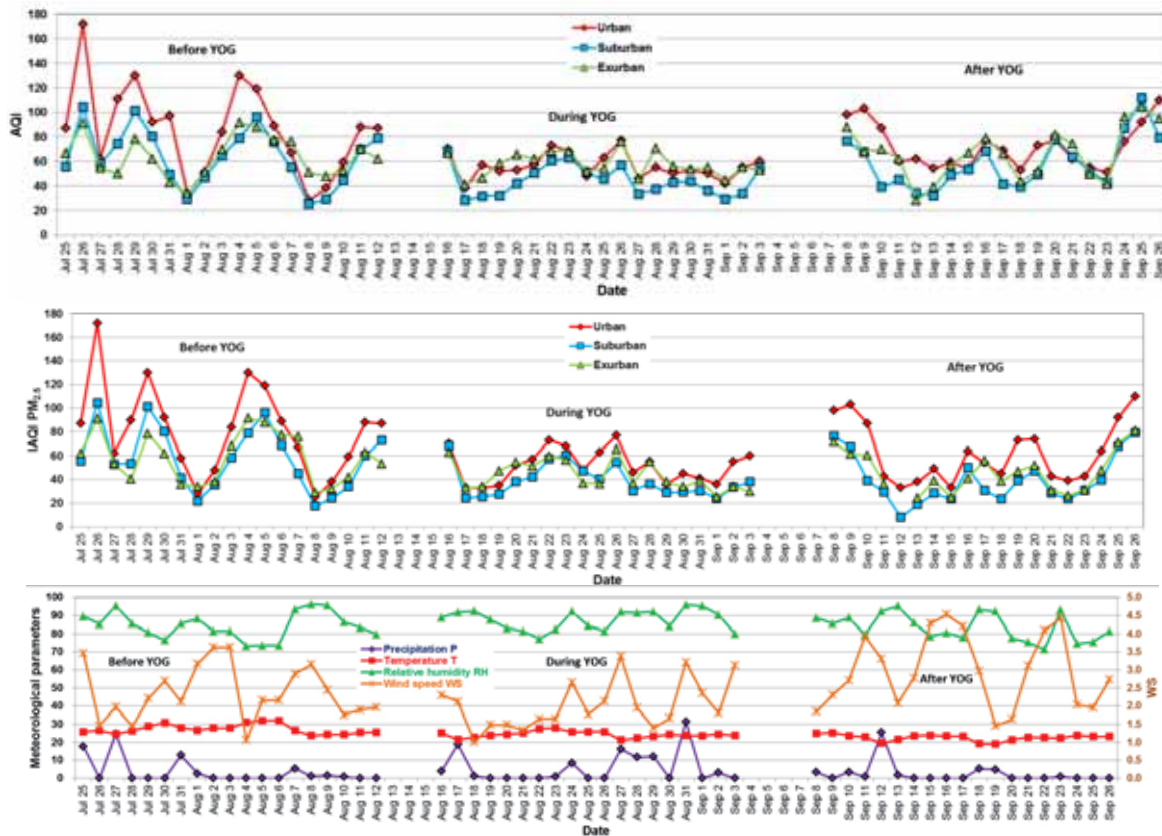


FIGURE 2

Variations of (a) daily overall AQI; and (b) PM_{2.5} IAQI for different periods of 2014 YOG in different functional areas of Nanjing; corresponding to (c) the main meteorological parameters (P - mm, T - °C, RH - %, WS - m s⁻¹).

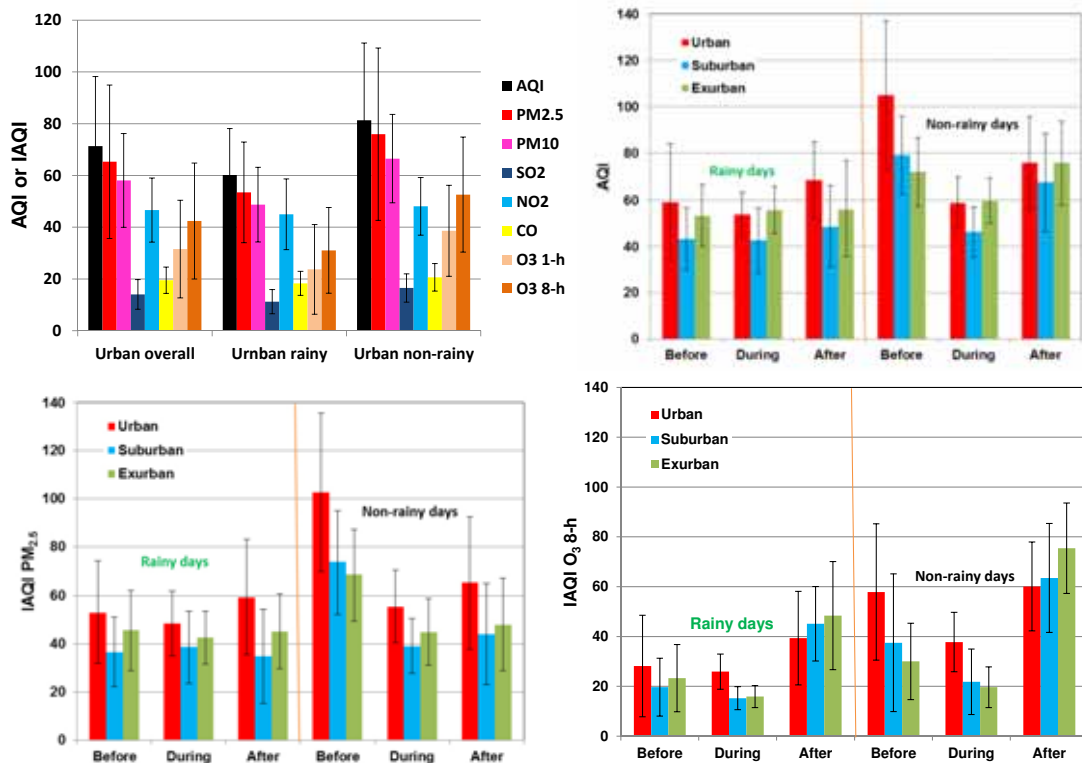


FIGURE 3

Mean values with standard deviation of daily overall AQI and each IAQI in rainy and non-rainy days for different periods of 2014 YOG in different functional areas of Nanjing.

urban AQI of 106 in the same period of 2015 with O_3 as the leading pollutant. These results indicate the relatively good air quality of Nanjing during the YOG period, and imply that the short-term emission control measures might have contributed to pollution reductions.

Average values were summarized in Fig. 3. Ignoring the weather effects, the order of average AQI is before (86 ± 37) > after (72 ± 18) > during (56 ± 10) YOG in urban area, and urban (71 ± 27) > exurban (63 ± 17) > suburban (56 ± 21) area. The order of the IAQI in urban for the overall periods (Fig. 3) is $PM_{2.5}$ (65 ± 30) > PM_{10} (58 ± 18) > NO_2 (47 ± 12) > O_3 8-h (42 ± 22) > O_3 1-h (32 ± 19) > CO (20 ± 5) > SO_2 (14 ± 6). In the total 30 non-rainy days (Fig. 3): the AQI order is before > after >> during YOG for various areas, and similar order is obvious for the urban IAQI of PMs, O_3 and SO_2 , while CO didn't vary much. However, in the total 27 rainy days, the differences were not so large, especially for IAQI of PMs. Furthermore, in the non-rainy days before YOG, typical order of urban >> suburban > exurban is showed for AQI and also for the IAQI of $PM_{2.5}$, O_3 and NO_2 ; but during YOG, the urban AQI was strongly decreased.

According to the national scale one-year AQI analysis during 2013-2014 for 31 provincial capital cities in China [9], $PM_{2.5}$ was the largest contributor to air pollution, followed by PM_{10} and O_3 , and strong correlation was found between different pollutants except O_3 . Based on the respective PCA results of the air pollutants' IAQIs in the whole investigated periods for various areas of Nanjing, the pollution pattern and main source of O_3 is different from those of PMs, SO_2 , CO and NO_2 in urban area, same to the national scale pattern [9]. Moreover, SO_2 is in another principal component group for suburban area, NO_2 and CO are also in a group for exurban area. It indicates that, in the urban area with poorer air quality, the concentrated anthropogenic sources contribute combined multi-pollutants. Chinese mega-cities under emission control policies showed similar air pollution pattern to Europe [16], where the air quality index refers more than 90% to the presence of high PM_{10} , O_3 and NO_2 concentrations, while SO_2 and CO play only a minor role.

Effects of Precipitation on the AQI and IAQIs. Besides the connection to the site characteristics of land use, topography and pollutant emissions, air quality is also closely linked to local meteorological conditions or the occurrence of weather regimes. Because precipitation is a discontinuous factor and there may be threshold values for the rainfall to eliminate pollution, it was not included in correlation analysis, and the AQIs were separately compared for rainy and non-rainy days to investigate the direct effects of rain events on air quality (Fig. 3). For the whole investigated

periods in urban area (Fig. 3), the order of the IAQI is $PM_{2.5}$ (76 ± 33) > PM_{10} (67 ± 17) > O_3 8-h (53 ± 22) > NO_2 (48 ± 11) > O_3 1-h (39 ± 18) > CO (21 ± 5) > SO_2 (17 ± 5) in non-rainy days, and $PM_{2.5}$ (53 ± 19) > PM_{10} (49 ± 14) > NO_2 (45 ± 14) > O_3 8-h (31 ± 17) > O_3 1-h (24 ± 17) > CO (18 ± 5) > SO_2 (11 ± 5) in rainy days. The average AQIs of rainy days were lower than those of non-rainy days, for various areas. Such phenomenon was typical for the IAQI of PMs and O_3 (Fig. 3), indicating the directly scavenging effects of rain on particles [22], and the driving effects of solar radiation on secondary gaseous pollutants by photochemical production [24]. According to respective PCA results of the urban IAQIs for rainy and non-rainy days, besides O_3 , the distribution patterns of NO_2 and SO_2 in rainy days were also different from those of PMs and CO. It implies that the aggregate emissions contribute integrated air pollution in non-rainy days.

Such effects were affirmed in other regions. In the northwest continental Europe [16], weather regimes with high daily precipitation generally lead to better air quality than dryer air masses, because of the lower contribution of PM_{10} to the daily air quality index (PM_{10} , SO_2 , NO_2 , CO, O_3). By comparing cool-wet years and hot-dry years in Oklahoma city, the heat decrease and precipitation increase in summertime also lead to substantial decreases in urban O_3 concentrations [21]. Considering nearly half days of our investigated periods are rainy, precipitation events exactly play positive role in summer air quality of Nanjing, both for aerosol and gaseous pollutants.

Relations Between AQI (or IAQI) and Meteorological Parameters.

Focus on the total 30 non-rainy days, the relationships between meteorological variables and urban AQI (or IAQI) were further investigated by correlation analysis (Table 1). As showed by the results, the variations of air pollutants were closely related to local meteorological conditions: T was positively related to AQI ($r = 0.502$), and to the IAQI of CO (0.599), $PM_{2.5}$ (0.562), SO_2 (0.417) and PM_{10} (0.391); AP was positively related to NO_2 (0.366) but negatively related to CO (-0.437) and $PM_{2.5}$ (-0.406); RH (all > 70%) was negatively related to SO_2 (-0.376), RH_{max} was negatively related to both SO_2 (-0.537) and PM_{10} (-0.378), RH_{min} was also negatively related to O_3 8-h (-0.525) and O_3 1-h (-0.411), and the T-Td was positively related to SO_2 (0.394) and O_3 8-h (0.361); WS was negatively related to CO (-0.542) and $PM_{2.5}$ (-0.385), and $WS_{extreme}$ was negatively related to CO (-0.650), NO_2 (-0.445) and $PM_{2.5}$ (-0.383).

Seen from Table 1, AQI and the IAQI of $PM_{2.5}$, PM_{10} , SO_2 and CO were all mostly positively related to temperature, while NO_2 and O_3 8-h was related to AP_{min} and T-Td, respectively. Negatively, $PM_{2.5}$ was most related to atmospheric pressure,

TABLE 1
Pearson correlation coefficients (*r*) between AQI (or IAQI) and the meteorological parameters over urban Nanjing for non-rainy days (*N*=30) of the overall investigated YOG periods.

	T	T _{min}	T _{max}	RH	RH _{min}	RH _{max}	T-Td	AP	AP _{min}	AP _{max}	WS	WS _{max}	WS _{extreme}
AQI	0.502**	0.486**	0.484**	-0.163	-0.231	-0.128	0.194	-0.332	-0.337	-0.336	-0.326	-0.286	-0.330
PM _{2.5}	0.562**	0.557**	0.535**	-0.149	-0.233	-0.150	0.184	-0.406*	-0.408*	-0.411*	-0.385*	-0.337	-0.383*
PM ₁₀	0.391*	0.404*	0.373*	-0.295	-0.312	-0.378*	0.302	-0.262	-0.251	-0.270	-0.135	-0.086	-0.178
SO ₂	0.417*	0.432*	0.389*	-0.376*	-0.266	-0.537**	0.394*	-0.209	-0.178	-0.214	0.069	-0.021	-0.166
NO ₂	-0.153	-0.219	-0.111	-0.087	-0.161	-0.036	0.065	0.366*	0.399*	0.342	-0.331	-0.364*	-0.445*
CO	0.599**	0.628**	0.568**	0.060	-0.133	-0.050	-0.007	-0.437*	-0.433*	-0.431*	-0.542**	-0.599**	-0.650**
O ₃ 1-h	0.166	0.051	0.248	-0.228	-0.411*	0.132	0.249	-0.044	-0.084	-0.021	-0.037	-0.086	-0.080
O ₃ 8-h	0.112	-0.029	0.219	-0.348	-0.525**	0.067	0.361*	0.024	-0.016	0.047	-0.006	-0.038	-0.028

* Significance level: $p < 0.05$.

** Significance level: $p < 0.01$.

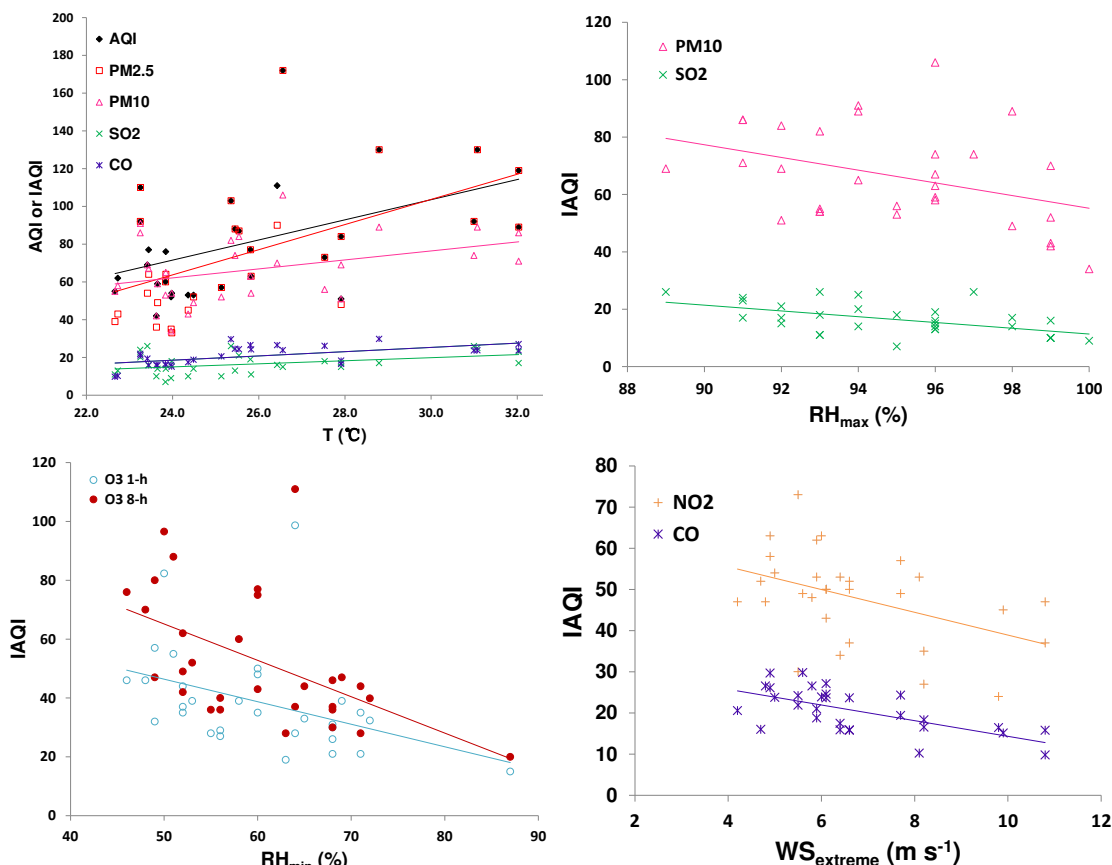


FIGURE 4

Typical linear correlations between AQI (or IAQI) and major related meteorological factors over urban Nanjing for non-rainy days (*N*=30) of the wholly investigated YOG periods.

while PM₁₀, SO₂, O₃ 1-h and O₃ 8-h were related to relative humidity, and NO₂ and CO were mostly related to wind speed. Typical correlations between AQI (or IAQI) and major related meteorological parameters were showed in Fig. 4. Because there were self-correlations between some of these meteorological factors, the most significant ones were than included in the multiple regression analysis. According to the linear regression equations (Table 2) of urban AQI or IAQI in non-rainy days against the key meteorological factors (T, RH_{min}, RH_{max}, T-Td, AP, WS_{extreme}), AQI and the IAQI of PM_s would be predicted by T; O₃ 1-h and O₃ 8-h might be predicted by RH_{min}, and SO₂ could be predicted by RH_{max} together

with WS_{extreme}; while NO₂ and CO could be predicted by WS_{extreme} with AP and with T, respectively.

Results indicated that, at the local-scale, meteorology was a relatively strong driver of air quality in Nanjing. Similarly, the positive relationships between API (SO₂, NO₂, PM₁₀) and T at short time-scales had been observed in PRD, China [22]. The changes in T_{max}, particularly when above 35 °C, also resulted in the strongest positive response for O₃, PM₁₀ and NO₂ concentrations in an Australian city (1999-2006), but the impacts of other important meteorological variables were less pronounced [25]. Furthermore, for the secondary pollutant O₃, although higher T was often used as a predictor for high

[O₃] [16,26], the RH was also negatively correlated with [O₃] [27], because RH is negatively correlated with T. These results indicate that, hotter and drier weather in summer could promote poorer air quality, which also suggest that climate change may worsen air quality [25]. Evidences are also available for other meteorological factors. The pollutants associated with traffic (CO, NO₂, SO₂, PM₁₀) were at the highest ambient concentration levels when WS was low in an Egypt city [27]. Trace gas concentrations (O₃, NO_x, SO₂ and CO) at a suburban site in the North China Plain also showed strong dependence on WS [24], and the PM₁₀ concentration in Europe decreased with the increasing WS [16]. They confirm the dilution and diffusion effects of wind on local air pollutants. Because wind speed and daily AQI are in anti-phase and change synchronously with no lag or lead time, the parameters WS_{max} and WS_{extreme} present coherences with AQI more and better than WS [22]. Such findings can help to explain the actual ambient air quality, and could assist in air quality forecasts.

TABLE 2

The stepwise linear regression equations of AQI (or IAQI) over urban Nanjing in non-rainy days (N = 30) of the wholly investigated YOG periods against basic meteorological parameters (T, RH_{min}, RH_{max}, T-Td, AP, WS_{extreme}). Variables with a significance level of $p < 0.05$ enter the predictive models.

Equations	R^2_{adj}
AQI = -57.7 + 5.38 T	0.226
PM _{2.5} = -97.6 + 6.72 T	0.291
PM ₁₀ = 4.47 + 2.40 T	0.123
SO ₂ = 112 - 1.01 RH _{max}	0.263
SO ₂ = 140 - 1.22 RH _{max} - 1.13 WS _{extreme}	0.368
NO ₂ = 66.6 - 2.76 WS _{extreme}	0.169
NO ₂ = -1026 - 3.27 WS _{extreme} + 1.09 AP	0.359
CO = 33.8 - 1.95 WS _{extreme}	0.403
CO = 9.25 - 1.53 WS _{extreme} + 0.84 T	0.563
O ₃ 1-h = 84.6 - 0.76 RH _{min}	0.139
O ₃ 8-h = 127 - 1.24 RH _{min}	0.249

Emission Control Actions & Meteorological Conditions. Deteriorated urban air quality is usually due to the intensive pollutant emissions, and the unfavorable terrain and meteorological conditions for pollutant diffusion and elimination. Local/regional authorities of China had accumulated some experiences for clean air by the provisionally stringent emission control measures, such as the 2008 Beijing Olympics [11-13], 2010 Shanghai Expo [23,28], and this 2014 Nanjing YOG, etc. Aimed at the leading air pollutants (PMs, O₃, NO₂) in summer Nanjing, the restricting of coal-combustion, industrial activities, construction works, vehicles and barbecue during YOG, decreased the emissions of PMs and O₃ obviously

and kept other air pollutants (SO₂, CO) at low level. The improvement of urban air quality was also enhanced notably by the precipitation events and winds (Fig. 3). However, the air quality deteriorated immediately after the relaxation of regulations, as can be seen in Sept. 8-10, although precipitation occurred during that time (Fig. 2). Therefore, the jointly regional control action took effect [14]. These efficient temporary measures might be extended for future long-term application, if the economy growth, human well-being, and environmental quality could be balanced properly. Challenges for the permanently clean air are the persistent efforts of curbing the highly anthropogenic emissions [28,29]. Changing the energy consumption to be resource-efficient and developing the environmentally friendly emission control devices might be the potential strategies.

Besides pollutant emissions, various meteorological factors also show aggregate effects on air quality trends. The pollution mitigation schemes and implementing degrees could be designed based on the weather forecasts. For instance, for those forthcoming unfavorable meteorological conditions, such as low winds and stable atmosphere that are responsible for air pollution episodes, early warning and strengthened emission control measures should be applied, and/or together with local weather modification.

Limitations. This short-term study was only based on the two-month comparison of daily AQI and meteorological parameters in a city. It presents the potential roles of authoritative emission control policy, but still has limitations. Detailed data of actual emissions and the site-specific wind directions would also be much useful for the result explanation. The equations for air quality prediction were restricted by both time scale and space scale. Of course, if open access available, the detailed hourly concentration data of all air pollutants in all monitoring stations, or even national-wide and historically documented concentration data, would be much better for the relationship analysis than the dimensionless AQI values. Similar difficulty also exists for accessing the meteorological data. But the future application of big data analytics should be expected. And then, using the high-resolution data, the quantified relationships between each air pollutant and meteorological factors for large scale would be well illuminated, and involved in the air quality forecasting model [30-32]. In fact, some simulating models begin to consider the meteorological [29,33] and to combine the geographical factors [34].

CONCLUSIONS

Deteriorated air quality is generally due to high pollutant emissions and stable weather conditions. Based on the 2014 summer Nanjing scenarios, some evidences of correlations between AQI and local meteorological factors were showed. However, to completely reveal their quantitative relationships, more abundant detailed data of wider space-scale and longer time-scale for the synchronous pollutant concentrations and meteorological parameters are needed. And then, they would be adopted for the environmental air quality forecast, and for designing the air pollution mitigation actions including the choice of weather modification. In particular, because the precipitation eliminates air pollution directly, future forecasting methods might be separately developed for rainy and non-rainy situations. By comparing the atmospheric characteristics in Nanjing before, during, and after the YOG period, air quality was improved by series of strict emission control measures. These experiences would be valuable for environmental managements, without ignoring the roles of meteorological conditions.

ACKNOWLEDGEMENTS

This work was supported by the Natural Science Foundation of China (NSFC 41471418 and 91543205), the Distinguished Talents of Six Domains in Jiangsu Province (2014-NY-016), and the Startup Foundation for Introducing Talent of NUIST. We are much grateful to China National Environmental Monitoring Centre and Nanjing Municipal Environmental Protection Bureau for making AQI available, and Nanjing Meteorological Observatory for sharing meteorological data.

REFERENCES

- [1] Silva, R.A., West, J.J., Zhang, Y., Anenberg, S.C., Lamarque, J.-F., Shindell, D. T., Collins, W. J., Dalsoren, S., Faluvegi, G., Folberth, G., Horowitz, L. W., Nagashima, T., Naik, V., Rumbold, S., Skeie, R., Sudo, K., Takemura, T., Bergmann, D., Cameron-Smith, P., Cionni, I., Doherty, R. M., Eyring, V., Josse, B., MacKenzie, I. A., Plummer, D., Righi, M., Stevenson, D. S., Strode, S., Szopa, S. and Zeng, G. (2013) Global premature mortality due to anthropogenic outdoor air pollution and the contribution of past climate change. *Environ. Res. Lett.*, 8, 034005.
- [2] Jin, L., Luo, X.S., Fu, P.Q. and Li, X.D. (2016) Airborne particulate matter pollution in urban China: A chemical mixture perspective from sources to impacts. *Natl. Sci. Rev.*, nww079.
- [3] Chen, Y., Ebenstein, A., Greenstone, M. and Li, H. (2013) Evidence on the impact of sustained exposure to air pollution on life expectancy from China's Huai river policy. *PNAS*, 110, 12936-12941.
- [4] Zhang, Q., He, K.B. and Huo, H. (2012) Cleaning china's air. *Nature*, 484, 161-162.
- [5] Luo, X.S., Ip, C.C.M., Li, W., Tao, S. and Li, X.D. (2014) Spatial-temporal variations, sources, and transport of airborne inhalable metals (PM10) in urban and rural areas of northern China. *Atmos. Chem. Phys. Discuss.*, 14, 13133-13165.
- [6] Wang, J.D., Wang, S.X., Jiang, J.K., Ding, A.J., Zheng, M., Zhao, B., Wong, D. C., Zhou, W., Zheng, G. J., Wang, L., Pleim, J. E. and Hao, J. M. (2014) Impact of aerosol-meteorology interactions on fine particle pollution during China's severe haze episode in January 2013. *Environ. Res. Lett.*, 9, 094002.
- [7] Wang, S.M., Yu, H., Song, L., Xie, Y.C. and Zhu, Q.H. (2015) Air quality in a mountainous city: a case study in Chongqing, China. *Fresen. Environ. Bull.*, 24, 2699-2706.
- [8] Luo, Z., Gao, M., Luo, X. and Yan, C. (2016) National pattern for heavy metal contamination of topsoil in remote farmland impacted by haze pollution in China. *Atmos. Res.*, 170, 34-40.
- [9] Wang, Y.G., Ying, Q., Hu, J.L. and Zhang, H.L. (2014) Spatial and temporal variations of six criteria air pollutants in 31 provincial capital cities in China during 2013-2014. *Environ. Int.*, 73, 413-422.
- [10] Streets, D.G., Fu, J.S., Jang, C.J., Hao, J.M., He, K.B., Tang, X. Y., Zhang, Y. H., Wang, Z. F., Li, Z. P., Zhang, Q., Wang, L. T., Wang, B. Y. and Yu, C. (2007) Air quality during the 2008 Beijing Olympic Games. *Atmos. Environ.*, 41, 480-492.
- [11] Wang, W.T., Primbs, T., Tao, S. and Simonich, S.L.M. (2009) Atmospheric particulate matter pollution during the 2008 Beijing Olympics. *Environ. Sci. Technol.*, 43, 5314-5320.
- [12] Wang, T., Nie, W., Gao, J., Xue, L.K., Gao, X.M., Wang, X. F., Qiu, J., Poon, C. N., Meinardi, S., Blake, D., Wang, S. L., Ding, A. J., Chai, F. H., Zhang, Q. Z. and Wang, W. X. (2010) Air quality during the 2008 Beijing Olympics: Secondary pollutants and regional impact. *Atmos. Chem. Phys.*, 10, 7603-7615.
- [13] Yang, Q., Wang, Y.H., Zhao, C., Liu, Z., Gustafson, W.I. and Shao, M. (2011) NOx emission reduction and its effects on ozone during the 2008 Olympic Games. *Environ. Sci. Technol.*, 45, 6404-6410.
- [14] Ding, J., van der A, R.J., Mijling, B., Levelt, P.F. and Hao, N. (2015) NOx emission estimates during the 2014 Youth Olympic Games in Nanjing. *Atmos. Chem. Phys.*, 15, 9399-9412.

- [15] Masoudi, M., Sakhaei, M., Behzadi, F. and Jokar, P. (2016) Status of PM₁₀ as an air pollutant and its prediction using meteorological parameters in Tehran, Iran. *Fresen. Environ. Bull.*, 25, 2008-2017.
- [16] Buchholz, S., Junk, J., Krein, A., Heinemann, G. and Hoffmann, L. (2010) Air pollution characteristics associated with mesoscale atmospheric patterns in northwest continental Europe. *Atmos. Environ.*, 44, 5183-5190.
- [17] Edwards, P.M., Brown, S.S., Roberts, J.M., Ahmadov, R., Banta, R.M., deGouw, J. A., Dube, W. P., Field, R. A., Flynn, J. H., Gilman, J. B., Graus, M., Helmig, D., Koss, A., Langford, A. O., Lefer, B. L., Lerner, B. M., Li, R., Li, S. M., McKeen, S. A., Murphy, S. M., Parrish, D. D., Senff, C. J., Soltis, J., Stutz, J., Sweeney, C., Thompson, C. R., Trainer, M. K., Tsai, C., Veres, P. R., Washenfelder, R. A., Warneke, C., Wild, R. J., Young, C. J., Yuan, B. and Zamora, R. (2014) High winter ozone pollution from carbonyl photolysis in an oil and gas basin. *Nature*, 514, 351-354.
- [18] Larissi, I.K., Antoniou, A., Nastos, P.T. and Patsos, A.G. (2010) The role of wind in the configuration of the ambient air quality in Athens, Greece. *Fresen. Environ. Bull.*, 19, 1989-1996.
- [19] Zheng, S., Cao, C.X. and Singh, R.P. (2014) Comparison of ground based indices (API and AQI) with satellite based aerosol products. *Sci. Total Environ.*, 488, 400-414.
- [20] CMEP. (2012) Technical regulation on ambient air quality index (on trial), HJ 633-2012, in Chinese, Ministry of Environmental Protection of the People's Republic of China.
- [21] Ramsey, N.R., Klein, P.M. and Moore, B. (2014) The impact of meteorological parameters on urban air quality. *Atmos. Environ.*, 86, 58-67.
- [22] Li, L., Qian, J., Ou, C.Q., Zhou, Y.X., Guo, C. and Guo, Y.M. (2014) Spatial and temporal analysis of air pollution index and its timescale-dependent relationship with meteorological factors in Guangzhou, China, 2001-2011. *Environ. Pollut.*, 190, 75-81.
- [23] Lin, Y.F., Huang, K., Zhuang, G.S., Fu, J.S., Xu, C., Shen, J. D., and Chen, S. Y. (2013) Air quality over the Yangtze river delta during the 2010 Shanghai Expo. *Aerosol Air Qual. Res.*, 13, 1655-1666.
- [24] Xu, W.Y., Zhao, C.S., Ran, L., Deng, Z.Z., Liu, P.F., Ma, N., Lin, W. L., Xu, X. B., Yan, P., He, X., Yu, J., Liang, W. D. and Chen, L. L. (2011) Characteristics of pollutants and their correlation to meteorological conditions at a suburban site in the north China plain. *Atmos. Chem. Phys.*, 11, 4353-4369.
- [25] Pearce, J.L., Beringer, J., Nicholls, N., Hyndman, R.J. and Tapper, N.J. (2011) Quantifying the influence of local meteorology on air quality using generalized additive models. *Atmos. Environ.*, 45, 1328-1336.
- [26] Steiner, A.L., Davis, A.J., Sillman, S., Owen, R.C., Michalak, A.M. and Fiore, A.M. (2010) Observed suppression of ozone formation at extremely high temperatures due to chemical and biophysical feedbacks. *PNAS*, 107, 19685-19690.
- [27] Elminir, H.K. (2005) Dependence of urban air pollutants on meteorology. *Sci. Total Environ.*, 350, 225-237.
- [28] Huang, K., Zhuang, G., Lin, Y., Wang, Q., Fu, J.S., Fu, Q., Liu, T. and Deng, C. (2013) How to improve the air quality over megacities in china: Pollution characterization and source analysis in Shanghai before, during, and after the 2010 world Expo. *Atmos. Chem. Phys.*, 13, 5927-5942.
- [29] Wang, L.T., Jang, C., Zhang, Y., Wang, K., Zhang, Q.A., Streets, D., Fu, J., Lei, Y., Schreifels, J., He, K. B., Hao, J. M., Lam, Y. F., Lin, J., Meskhidze, N., Voorhees, S., Evaris, D. and Phillips, S. (2010) Assessment of air quality benefits from national air pollution control policies in China. Part i: Background, emission scenarios and evaluation of meteorological predictions. *Atmos. Environ.*, 44, 3442-3448.
- [30] Al-Saadi, J., Szykman, J., Pierce, R.B., Kittaka, C., Neil, D., Chu, D. A., Remer, L., Gumley, L., Prins, E., Weinstock, L., MacDonald, C., Wayland, R., Dimmick, F. and Fishman, J. (2005) Improving national air quality forecasts with satellite aerosol observations. *Bull. Am. Meteorol. Soc.*, 86, 1249-1261.
- [31] Wang, T.J., Jiang, F., Deng, J.J., Shen, Y., Fu, Q.Y., Wang, Q., Fu, Y., Xu, J. H. and Zhang, D. N. (2012) Urban air quality and regional haze weather forecast for Yangtze river delta region. *Atmos. Environ.*, 58, 70-83.
- [32] Mu, Q., Liao, H. (2014) Simulation of the inter-annual variations of aerosols in china: Role of variations in meteorological parameters. *Atmos. Chem. Phys.*, 14, 9597-9612.
- [33] Hu, X., Waller, L.A., Lyapustin, A., Wang, Y. and Liu, Y. (2014) 10-year spatial and temporal trends of PM_{2.5} concentrations in the southeastern US estimated using high-resolution satellite data. *Atmos. Chem. Phys.*, 14, 6301-6314.
- [34] Adam-Poupart, A., Brand, A., Fournier, M., Jerratt, M. and Smargiassi, A. (2014) Spatiotemporal modeling of ozone levels in Quebec (Canada): A comparison of kriging, land-use regression (lur), and combined bayesian maximum entropy-lur approaches. *Environ. Health Perspect.*, 122, 970-976.

Received: 04.05.2017
Accepted: 11.06.2017

CORRESPONDING AUTHOR

Xiao-San Luo

International Center for Ecology, Meteorology, and Environment, School of Applied Meteorology, Nanjing University of Information Science & Technology, Nanjing 210044, China

e-mail: xsluo@nuist.edu.cn

AN IMPROVED EXPORT COEFFICIENT MODEL FOR PRIORITY AREA IDENTIFICATION AND LOAD ESTIMATION UNDER DIFFERENT HYDROLOGICAL YEAR IN MIYUN RESERVOIR WATERSHED, BEIJING, CHINA

Runzhe Geng^{1,2}, Xiaoyan Wang^{1*}

¹College of Resource Environment and Tourism, Capital Normal University, Beijing, China

²Policy Research Center for Environment and Economy, Ministry of Environmental Protection, P. R. China, Beijing, China

ABSTRACT

This study examined the potential effects of precipitation change on nutrient loads in the upper watershed of Miyun Reservoir. Using historical climate dataset, stream flow, and water quality data, the improved export coefficient model (IECM) was selected to simulate changes in TN and TP loads characteristics under different hydrological year. The results demonstrate that: 1) The major source of TN and TP was livestock, which accounted for 49.4% of the total, followed by rural living (26%), land use (24.6%), while for the TP ranked differently from those of TN with rural living first (71%), followed by livestock (26.15%) and land use (2.85%); 2) The impacts of precipitation amount change on pollution load are relatively greater when compared to the impacts of rural living, livestock and poultry breeding and land use pollution load increase; the effects from rainfall increment leads to approximately 24% and 27% increases of TN and TP pollution load, respectively; 3) The high-risk areas of TN and TP load were distributed accordance to the amount of precipitation in different hydrological years and the most of the CSAs were locates beside the main stream. Total nitrogen and total phosphorous load per unit area in Miyun, Chicheng and Fengning counties were higher than others. These data will be useful and valuable in evaluating potential NPS pollution load for the control of watershed pollution in the future and understanding its migration and transformation in a large-scale watershed where meteorological and hydrological data are mutative.

KEYWORDS:

Nonpoint source pollution; improved export coefficient model; different hydrological years; Miyun reservoir watershed

INTRODUCTION

Recent research suggests that the alteration of spatial and temporal patterns of precipitation could

modify stream discharge and chemical export characteristics [1, 2], and it will result in increased nutrient loads in wet year and decreased loads in dry year. Precipitation can potentially lead to changes in runoff and can significantly impact the regional hydrology and future availability of water resources, and it was believed to be the key factors affecting NPS pollution [3-10]. As has been well documented in many non-point source pollution studies, surface runoff and its associated nutrient load is highly correlated with rainfall variability [2, 11, 12]. Although it is widely recognized that precipitation change can affect non-point source pollution from the large scale watershed, there have been few research studies on that topic in upper watershed of Miyun Reservoir. In comparison to studies undertaken in other larger scale watershed, plot or field-scale studies are better able to capture local vulnerabilities to rapid and intense changes in precipitation. This study will have the vital significance to the implementation of the corresponding measures with different precipitation conditions.

In general, the distributed model could be better to study the impacts of precipitation on generation, development and transport processes, and spatial and temporal distribution of NPS pollution, as well as quantitative description of the generation, migration and output process of water, sand and non-point source pollutants in a basin caused by the different rainfall event. Many studies have been done to elucidate the effects of precipitation changes on total nitrogen and total phosphorus from agricultural watershed by integrated distribution models [2, 13-15]. However, the values of a large number of parameters could not be obtained from field data and must instead be determined through model calibration, then will hinder the application to some extent [16, 17]. The empirical models have the advantage of requiring less data and having fewer parameters. Reference to the related research results [13, 18-20], Precipitation and terrain are believed to be the primary factors that affect NPS pollution. Rainfall is the main driving force of NPS contamination, and terrain plays an important role in NPS pollutant transport [21]. Therefore, it is imperative to modify the ECM to

characterize the impact of rainfall and the heterogeneity of topography on NPS pollution simulation [21]. Therefore, in a large scale watershed with insufficient data, applying improved export coefficient model combined with GIS technology in the entire region for CSAs identification and load estimation from dry year to wet year is a practical way of delineating and evaluating the priority non-point source area identification, which will provide further support for BMPs selection.

The objective of this study is to: 1) Estimate the resource, loading and distribution of agricultural NPS pollution in the paper based on remote sensing and geographic information system by improved export coefficient model; 2) Assessment and analysis the impacts of different rainfall capacity (dry year 1997, normal year 2000 and wet year 2010) on the loss of non-point source nitrogen and phosphorus from a large-scale mountain catchment to its drainage system, aimed to provide references for water environmental protection and water resources management in the upper watershed of Miyun Reservoir.

METHODS AND MATERIALS

In this study, we are based on the relationship between annual rainfall and runoff developed by Sun et al(2007) and Li et al(2008) in which they were used the meteorological dataset in the four weather stations within the Miyun reservoir basin from 1961 to 2010, and based on the Matlab 7.0 platform to develop the relationship between annual runoff and runoff [22, 23], and then used frequency analysis method to predict the precipitation change trends and determined the climate scenarios from any scenario settings and a long series of historical data. The results indicated that 1997, 2000, 2010 were represented as dry year, normal year and wet year, respectively.

Study area. The Miyun Reservoir is the most important source of drinking water supply for Beijing. It is situated in Miyun County, covers a drainage area of 15788 km² (Fig.1). Recent two decades because of agricultural activities and increasing rural population, Agricultural NPS pollution has become the dominant factor affecting water quality of the Miyun Reservoir. In this area, nitrogen and phosphorus are the main limiting factors to eutrophication for water bodies [24], which can induce eutrophication in the receiving water and loss of biodiversity in the aquatic ecosystem. Therefore, to carry out forecasting NPS nitrogen and phosphorus pollution load is great significance for the protection of the water environment safety in this area, and for the promotion of the sustainable development of ecological environment in the reservoir area.

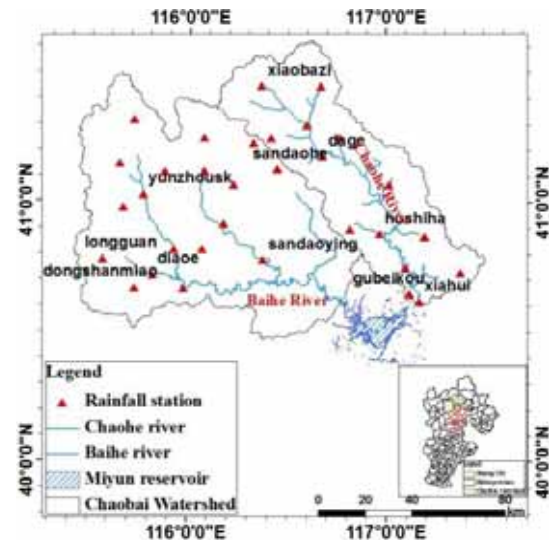


FIGURE 1
Map of study area

Improved Export Coefficient Model (IECM). Considering the effect of the nonuniformities of precipitation and terrain on NPS pollution, the improved ECM (IECM) was modified as equation (1) [21]. The results from the work by [25] indicated that the IECM had fairly good applicability in upper watershed of Miyun reservoir, the IECM was used to estimate the NPS loads from this area, and the model was calibrated and validated based on the daily discharge data from river gauging stations located at the outlet of watershed (Xiahui and Zhang Jiafen hydrological station):

$$L = \sum_{i=1}^n \alpha \beta E_i [A_i (I_i)] + p \quad (1)$$

where α is the precipitation impact factor, β is the terrain impact factor and α and β are correlated with the spatial unit (grid cell), which was set to be 100 m×100 m based on the digital elevation model (DEM) and land use map using ArcGIS 9.3 software [25], L is loss of nutrients (kg), E_i is export coefficient for nutrient source i (kg·ca⁻¹·a⁻¹ or kg·km⁻²·a⁻¹), A_i is area of the watershed occupied by land use type i (km²), or number of livestock type i , or of people, I_i is the input of nutrients to source i (kg), and p is the input of nutrients from precipitation (kg).

Source and Processing of data. As Table 1 shows, the study used data includes digital elevation model (DEM), land use map, weather data, hydrological data, social economic data of the study area and so on. The NPS of the study watershed was categorized into three type, rural living, livestock and land use [25]. The land uses were classified into five types; farmland, grassland, forest, residential land and unused land. The export coefficients of the land uses were calculated using hydrological and water quality data based on the mass balance of the non-

point source pollutants. The export coefficients of rural living and livestock were determined based on a literature review [4, 26, 27].

Satellite remote sensing images were interpreted to acquire the land use data, basin boundary, river map, watershed map were then obtained according to DEM map through ArcGIS, district bound atlas of the study area based on national district bound atlas and basin boundary of the study area was subsequently generated, and under the GIS platform, as well as loadings and spatio-temporal distributions of TN and TP in the study area were simulated, using importing basic data and export coefficients. All digital maps were projected in Albers conical equal-area. And the dual standard latitude were 25 and 47 degree respectively, the central longitude was 105°E, the coordinate origin latitude was zero degree, the spheroid

was Krassovsky one, and the unit was meter.

RESULTS

Calculation of Precipitation impact factor (α). The temporal unevenness and spatial unevenness were two aspects for determination the precipitation impact factor α . The calculated precipitation impact factor α_{TN} values ranged from 0.35 to 1.29 in dry year (1997), from 0.27 to 1.19 in normal year (2000), and from 1.28 to 4.83 in wet year (2010), while The α_{TP} values ranged from 0.23 to 0.86 in dry year (1997), from 0.24 to 1.07 in normal year (2000) and from 1.11 to 4.17 in wet year (2010) (Fig. 2).

TABLE 1
Source and description of basic data

Type	Scale	Resolution	Description	Source
Land use	1:50 000	30×30 m	Land use classifications	Institute of Geographical and Natural Resources Research, Chinese Academy of Sciences
DEM	1:100 000	30×30 m	Elevation, overland and channel slopes and lengths	National Geomatics Center of China
Administrative division	1:1 000 000	1000×1000 m	Towns and municipalities of study area	National Geomatics Center of China
Weather data	1961~2005	Daily step	Over 29 stations in the study area	China Meteorological Administration
Hydrological data	1990~2011	monthly step	Calibration and validation of IECM	China Meteorological Administration and field monitoring
Social economics	Each town	Township level	Population, livestock rearing, fertilizer application	Field investigation; Statistics year-book
The export coefficient	Different sources		Losses of various nutrient sources	Statistical data and field monitoring

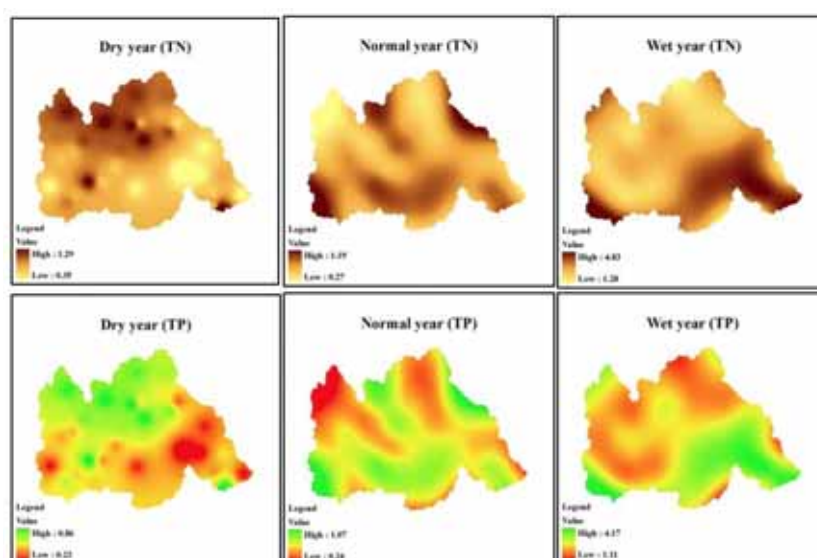


FIGURE 2
Precipitation impact factor values for TN and TP from dry year to wet year

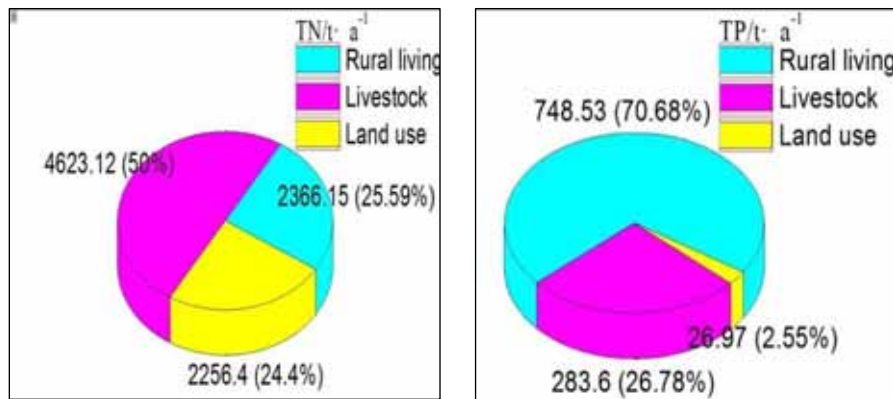


FIGURE 3
Percentage of TN and TP mean loads of different sources

Common features of pollution loads. The TN and TP loads from NPS for the research area from 1997 to 2010 were obtained using the export coefficient values, land use, population, domestic animal numbers, Precipitation factor (Fig. 2) and terrain impact factor in the upper watershed of Miyun reservoir[25]. The calculated TN and TP mean values in 1997~2010 were presented in Fig. 3. The results of simulation calculation indicated that TN load was much higher than the total TP load. It can be seen that the TN load was 9178.59 t, and then TP load was 1059.10 t. For different pollution sources, the pollution load of TN were 4623.12 t·a⁻¹, 2366.15 t·a⁻¹, 2256.4 t·a⁻¹ produced by livestock, rural living and land use, respectively. Among those four livestock types, poultry is the major contributor (1840.42 t·a⁻¹). For the economic yield improved from livestock, the amount of livestock may have increased and then lead to the environmental contamination raised. Furthermore, due to animal feed and livestock manure, which is not systematically managed, is an N-rich pollution source. Wheat was the most important crop in farm land, It is mainly because of the unreasonable fertilizers use rate and the conventional tillage for a long time, which may increase the nitrogen loss in this area, Among those five land use types, farmland is the major contributor for TN load (1222.97 t·a⁻¹). The major sources of TP ranked differently from those of TN: with rural living first (748.53 t·a⁻¹), followed by livestock (283.6 t·a⁻¹) and land use (26.97 t·a⁻¹). Poultry was still as the major contributor for livestock source. And the contribution of land use showed large difference between these two nutrients. It is mainly because of the domestic sewage treatment system are not perfect and the slather of Phosphorus-Containing detergent in this area, these two aspect will lead greatly loss of phosphorus. Although livestock accounted for a second portion in TP load, poultry was still identified as the dominant contributor among those four livestock types.

Pollution source analysis. The impact of changed precipitation on TN and TP loads in the Chaobai river watershed was obtained by applying the improved coefficient model at the GIS platform. Annual precipitation impact factor were simulated by ArcGIS 9.3 for the dry year, normal year and wet year was used as input. The differences in annual TN and TP losses are shown in Table 2. The NPS pollution load of TN and TP is closely related to changes of rainfall from dry year to wet year. From dry year to wet year (1997, 2000 and 2010), TN load were 7 351.39 t·a⁻¹, 7 505.28 t·a⁻¹ and 10 022.1 t·a⁻¹, respectively. TP load were 755.85 t·a⁻¹, 997.88 t·a⁻¹ and 755.85 t·a⁻¹, respectively. Livestock and rural living are still as the major sources of TN and TP under any rainfall condition, the pollution load of TN were 3865.51 t·a⁻¹, 3447.15 t·a⁻¹, 4646.8 t·a⁻¹, For TP, the pollution load were 508.8 t·a⁻¹, 748.7 t·a⁻¹, 753.1t·a⁻¹, respectively. With the increase of rainfall, TN and TP load produced by livestock were increases from 3 865.51 t·a⁻¹ to 4 646.8 t·a⁻¹ and 226.94 t·a⁻¹ to 289.9 t·a⁻¹, while the TN and TP load from land use source were increase from 1 868 t·a⁻¹ to 3 001.55 t·a⁻¹ and 20.11 t·a⁻¹ to 32.6 t·a⁻¹. While the contribution rate of TN and TP were declined 24% and 27% from wet year to dry year, respectively, As can be seen that the precipitation amount affect strongly to TN load than TP. The nutrient pollution from rural live failed to respond to precipitation, the increasing extent of TN and TP load in total pollution were also below 10%. The land use and livestock sources were also sensitive to precipitation change. Although source contribution rates of TN and TP load was different, the main sources of TN and TP load were both rural living (22.01% and 67.31%) and livestock (52.58% and 32.02%) in dry year, while land use (23.69% and 70.02%) and livestock (46.37% and 26.95) were mainly contributor in wet year (see Figure 4).

From the perspective of non-point sources causes in different hydrological years, the TN and TP loads of livestock, rural live, and farmland were produced by anthropogenic activities. From dry year to

wet year, the amount of population, Cattle, Pig, Goat and Poultry were increased by 0.37%, -54.34%, 11.19%, 1.53% and 5.55% respectively. While the TN and TP loads from anthropogenic activities were increases from 6 456.89 t to 8 709.49 t and 749.14 t to 1 065 t, the percentage increases of TN and TP were 34% and 42%, accounting for exceeded 85% and 90% of the total TN and TP respectively. Anthropogenic factor is the key of non-point source TN and TP in upper watershed of Miyun reservoir, natural causes should not be ignored as well.

Priority non-point source area identification.

The simulated spatial distribution of TN and TP loads in different hydrological years is shown in Fig. 5, respectively. The bar graphs (in Fig. 5) represent TN and TP loads from NPS from different township in research area. From the whole watershed, the high-risk areas are mainly concentrated in the

Chaohe river watershed and the most of the CSAs were locates beside the main stream. The differences of total nitrogen and total phosphorus loads were great among various districts/counties in this study area. Total nitrogen and total phosphorous load per unit area in Miyun, Chicheng and Fengning counties were higher than others. In addition, Dage is one of the important livestock and poultry breeding bases in Chicheng city, thus the frequent and intensive livestock and agricultural activities will led to increased NPS pollution in different hydrological year. And the high-risk areas were distributed according to the amount of precipitation from dry year to wet year. In dry year, the distribution of load intensity of TN and TP were varied between the western part and eastern part of Chaobai river watershed, in normal year and wet year, the distribution of load intensity of TN and TP were mainly located in Chaohe River watershed.

TABLE 2
NPS pollution load from various sources in different hydrological years

Source	Dry year (1997)		Normal year (2000)		Wet year (2010)		
	TN/t·a ⁻¹	TP/t·a ⁻¹	TN/t·a ⁻¹	TP/t·a ⁻¹	TN/t·a ⁻¹	TP/t·a ⁻¹	
Rural living	1617.88	508.8	2 359.7	748.7	2 373.74	753.1	
Livestock	Cattle	1439.47	60.63	1 428.8	60.18	885.52	37.3
	Pig	172.77	63.21	229.57	84	196.51	71.9
	Goat	985.6	31.68	991.72	31.9	831.28	26.7
	Poultry	1267.67	71.42	797.06	44.9	2 733.49	154
Land use	Farmland	973.5	13.4	1 006.47	17.51	1 688.95	22
	Forest	140.3	0.99	207.06	2.11	389.62	3.06
	Grassland	677.6	5.6	659.91	8.05	856.32	6.36
	unused land	45.3	0.07	12.46	0.41	43.27	0.66
	residential land	31.3	0.05	13.75	0.12	23.39	0.52
Total	7351.39	755.85	7 505.28	997.88	10 022.1	1 075.6	

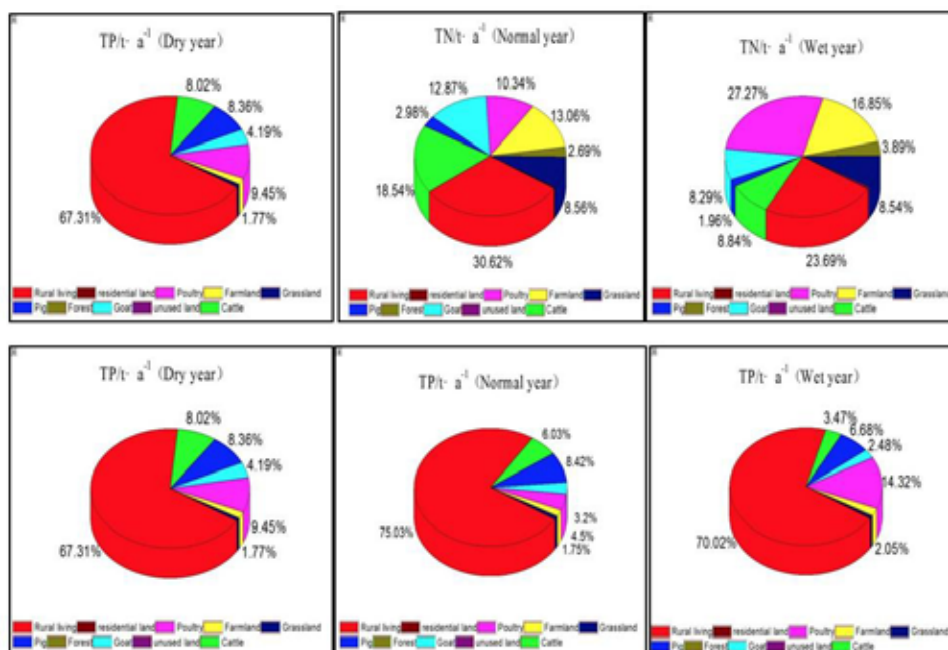


FIGURE 4
Percentage of TN and TP loads of different sources from dry year to wet year

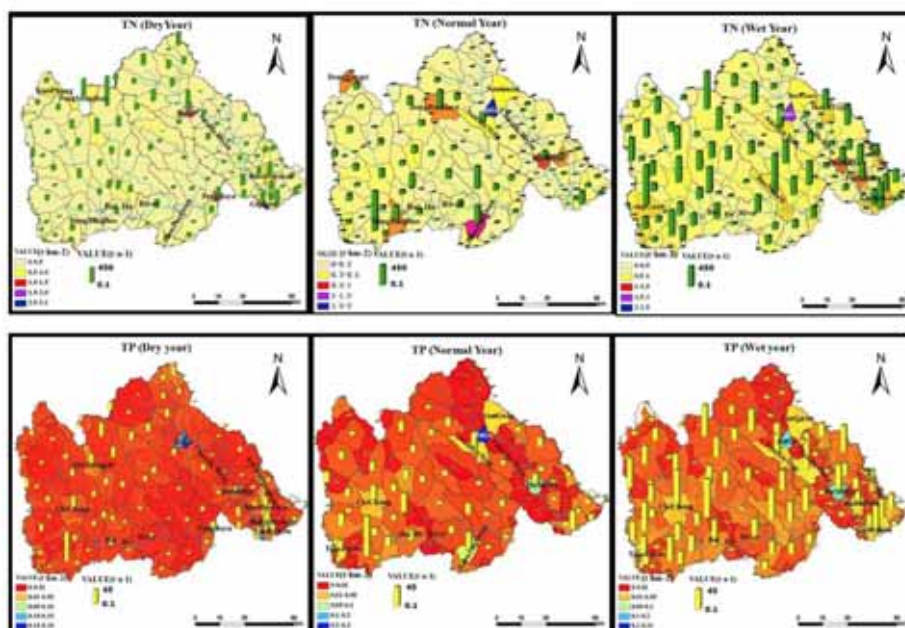


FIGURE 5
Simulated spatial distribution of TN and TP loads in different hydrological years

DISCUSSIONS

Rainfall change impact on pollution loads. In terms of the hydrological year scale, agricultural NPS pollution loads vary evidently in different year (see Figure 4). Pollution occurs under the condition of storm water runoff, which changes widely in different hydrologic year. Agricultural NPS pollution of the wet year is serious and in contrast, loading of dry year is small. The loss of agricultural NPS pollution is positive correlation with the rainfall, which indicates that agricultural NPS pollution accumulates in the dry season, and occurs in wet one with rainfall and soil erosion. Many study indicated that watersheds with greater precipitation and discharge will tend to have higher erosion rates, and this leads to higher fluxes of phosphorus from the landscape since most of the phosphorus in large rivers is particle bound [28, 29]. Nitrogen moves through the landscape primarily in dissolved forms, and nitrogen fluxes seem to be primarily controlled by the sources and sinks of nitrogen in the landscape [15].

With the development of agricultural production and rural economy in the Chaobai river watershed, the problem with excessive fertilizer use is increasingly acute. The declining moisture and fertility in the soil of Chaobai river watershed lead to correspondingly high levels of water pollution. In fact, the pollutants from farming activity mainly include the nutrient loss of farmland and the waste loss of livestock farming systems because of water and soil erosion, and it has been documented that conventional tillage is less effective for reducing nitrogen in surface water and sediments than no-till systems in the

vast mountainous area [30–32], but conventional tillage is just the primary tillage pattern in the upper watershed of Miyun reservoir. It will promote soil erosion and nutrient losses in response to every rainfall event during the growing season. Additionally, the topography of Chaobai river watershed is dominated by mountains and hills and the rain is plentiful in rainy season. As a result, NPS includes sand and silt, nutrient salts, pesticides and other contaminants from agricultural fields, in which N and P are transported to surface water and water bodies under the action of rainfall and irrigation, along with water and soil erosion, by means of surface runoff, subsurface flow, farm drainage, seepage and so on. The time distribution of potential TN and TP loads shows that the NPS pollution of the study areas has some relationships with human farming practice, resettlement and various development and construction activities. Therefore, further strengthening the development of ecological agriculture and the implementation of environmental conservation measures is urgently required and imperative for the control and management of NPS pollution in the upper watershed of Miyun reservoir.

Rainfall change impact on distribution of high risk area. The concept of nutrients loss risk assessment is based on the premise that most nutrients exported from a watershed originates from a small part of the landscape close to the stream channel, which can be activated by frequent storm events. These hydrologically active areas contributing surface runoff or erosion to stream flow (i.e., transport factors) can be large sources of nutrients when they

are coincident with areas of high soil nutrients or recent manure applications [33]. Fig. 5 shows location of the most top critical townships in Chaobai river watershed according to the improved coefficient model results. In dry year and normal year, the spatial distribution of high risk areas were aggregated, but in wet year it distributed as scattered form. The reasons for this phenomenon were concluded three point: 1) the common physiognomy of this study area is valley and the land is steep. Additionally, most of the rural population lives adjacent to water-courses and the rural livestock and poultry were raised in scattered communities. The animals' manure is not recycled to the land; 2) the spatial distribution of rainfall shows the increasing trend from the west to the east in the upper watershed of Miyun reservoir, and rainfall is just the main dynamic factor that causes soil loss and nutrients loss (Ou et al., 2008), then the CSAs more concentrate on the eastern part of this study in normal and wet years; 3) Owing to the higher altitude, the pollutants would inevitably accumulate in the eastern part, where the lower Dage, Dong Xingbao, Ba Keshiyang and LongGuan is located. In all regions that have relatively higher pollutant loads in this area (Fig. 5). Human activity and livestock is the mainstay of that area, and the livestock yield accounts for approximate 50% of fiscal revenue in their affiliated area (Chicheng, Fengning and Miyun city). Thus, the intensive human activity and livestock and poultry breeding raised the severe contamination.

Therefore, we need to further strengthen the implementation of “ecological environment measures” and “soil and water conservation”, the implementations of agricultural terracing land, contour farming, timely and reasonable fertilization and other scientific techniques are necessary to improve fertilizer use efficiency and to reduce soil loss; the manure from livestock and poultry breeding should be resource utilization and be used as methane fermentation or fertilizer returning to fields; and, the excreta and sewage from large-scale livestock and poultry breeding should be discharged after treatment through the establishment of wastewater treatment plants.

CONCLUSIONS

1) In this study, the ECM was modified through introduced two important impact factors to simulate the nutrient loads of the Chaobai River watershed. The results showed that the relative error between simulated value and the observed value was effectively reduced as compared to that obtained from the original model [25]. The results further demonstrated that the temporal–spatial heterogeneity of the precipitation and terrain are important impact factors of non-point source pollution that should be fully

considered during simulation, and while these adaptations will generation of a macroscopic temporal–spatial scale model for use in non-point source pollution research.

2) Results of this study show that precipitation plays a dominant role in changing basin hydrology and nutrients export in the Chaobai River basin of the Miyun reservoir. The analysis results of non-point source pollution characteristic shows that the major source of TN was livestock, followed by rural living and land use. The major sources of TP ranked differently from those of TN: with rural living first, followed by livestock and land use. From the perspective of non-point sources, 8212.24 t of TN loads and 1049.77 t of TP loads were caused by anthropogenic activities that include farmland, livestock and rural living, accounting for 89.4% and 99.15% of the total TN and TP respectively. Anthropogenic factor is the key of non-point source TN and TP of the upper watershed of Miyun reservoir, natural causes should not be ignored as well.

3) The results show a generally increasing trend in TN and TP loads from dry year to wet year. Annual changes in TN and TP loads may also be possible, with a significant increase occurring during dry year to wet year. Precipitation amount change and human activities are the two most important factors impacting pollution load in this paper and they interact with each other. An important implication of these findings is that it could be possible to mitigate undesired precipitation change effects on environment and water resources by planning land-use to achieve specific hydrological effects of land-cover in the basin.

4) The high-risk areas of TN and TP load were distributed according to the amount of precipitation in different hydrological years and the most of the CSAs were locates beside the main stream. In dry year, the distribution of TN and TP varied much between the western part and eastern part of the Chaobai river watershed, exhibiting a rough boundary; In wet year, the distribution of TN and TP were relatively concentrated in Chaohe River watershed along with the change of precipitation. While the focus of this study has been on the Chaobai River watershed in Miyun reservoir, results of the study can represent the situation in the upper watershed of Miyun reservoir as a whole. Thus, the results have applicability to this area for management of the land, vegetation, livestock and water resources in order to sustain the resources and environment as well as the region's economic growth.

ACKNOWLEDGEMENTS

This work was financially supported by the National Natural Science Foundation of China (No.40971258, 41271495) and Specialized Research Fund for the Doctoral Program of Higher Education (No. 20121108110006).

REFERENCES

- [1] Losleben, M., Caine, N. and Greenland, D. (1996) Changes in climate and hydrochemical responses in a high-elevation catchment in the Rocky Mountains, USA Mark W. Williams. *Limnol. Oceanogr*, 41(5), 939-946.
- [2] Wu, L., Long, T.Y, Liu, X and Guo, J.S. (2012) Impacts of climate and land-use changes on the migration of non-point source nitrogen and phosphorus during rainfall-runoff in the Jialing River Watershed, China. *Journal of Hydrology*, 475, 26-41.
- [3] Noto, L.V., Valeriy Y. Ivanov, Rafael L. Bras, and Enrique R. Vivoni. (2008) Effects of initialization on response of a fully-distributed hydrologic model. *Journal of Hydrology*, 352(1), 107-125.
- [4] Zheng, Y. T., Wang X. Y., and Yin, J. (2008) Feature of Rural Solid Waste from Various Types Villages in Sources Water Protection Area. *Journal of Agro-Environment Science*, 27(4), 1-5. (In chinese)
- [5] Beyene, T., Lettenmaier, D.P. and Kabat, P. (2010) Hydrologic impacts of climate change on the Nile River Basin: implications of the 2007 IPCC scenarios. *Climatic change*, 100(3-4), 433-461.
- [6] Bukovsky, M.S. and Karoly, D.J. (2011) A Regional Modeling Study of Climate Change Impacts on Warm-Season Precipitation in the Central United States. *Journal of Climate*, 24(7), 1985-2002.
- [7] Wang, E., Zhang, Y., Luo, J., Francis H. S. Chiew, and Wang, Q. (2011) Monthly and seasonal streamflow forecasts using rainfall-runoff modeling and historical weather data. *Water Resources Research*, 47(5), w05516
- [8] Vaze, J., Teng, J. and F. Chiew, F. (2011) Assessment of GCM simulations of annual and seasonal rainfall and daily rainfall distribution across south-east Australia. *Hydrological Processes*, 25(9), 1486-1497.
- [9] Liu, Q. and Cui, B. (2011) Impacts of climate change/variability on the streamflow in the Yellow River Basin, China. *Ecological Modelling*, 222(2), 268-274.
- [10] Clavero, M., Villero, D. and Brotons, L. (2011) Climate change or land use dynamics: do we know what climate change indicators indicate? *PLoS One*, 6(4), e18581.
- [11] Park, M.-H., Swamikannu, X. and Stenstrom, M.K. (2009) Accuracy and precision of the volume-concentration method for urban stormwater modeling. *Water research*, 43(11), 2773-2786.
- [12] Lee, E., Chounghyun Seong, Hakkwan Kim, Seungwoo Park, Moonseong Kang. (2010) Predicting the impacts of climate change on nonpoint source pollutant loads from agricultural small watershed using artificial neural network. *Journal of Environmental Sciences*, 22(6), 840-845.
- [13] Kovacs, A. and Clement, A. (2009) Impacts of the climate change on runoff and diffuse phosphorus load to Lake Balaton (Hungary). *Water Science & Technology*, 59(3), 417-423.
- [14] Andersen, H.E., et al. (2006) Climate-change impacts on hydrology and nutrients in a Danish lowland river basin. *Science of the Total Environment*, 365(1), 223-237.
- [15] Howarth, R., D.P. Swaney, E.W. Boyer, R. Marino, N. Jaworski And C. Goodale. (2006) The influence of climate on average nitrogen export from large watersheds in the Northeastern United States. *Biogeochemistry*, 79(1-2), 163-186.
- [16] Singh, J., H. Vernon Knapp, J.G. Arnold, and Misganaw Demissie.. (2005) Hydrological modeling of the iroquois river watershed using HSPF and SWAT1. *JAWRA Journal of the American Water Resources Association*, 41(2), 343-360.
- [17] Shen, Z., Liao, Q., Hong, Q., and Gong, Y. . (2012) An overview of research on agricultural non-point source pollution modelling in China. *Separation and Purification Technology*, 84, 104-111.
- [18] Alexander, R.B., Alexander H. Elliott, Ude Shankar, and Graham B. McBride. (2002) Estimating the sources and transport of nutrients in the Waikato River Basin, New Zealand. *Water Resources Research*, 38(12), 1268.
- [19] Cai, M., Li, H, and Zhuang, Y.. (2004) Application of modified export coefficient method in polluting load estimation of non-point source pollution. *Journal of Hydraulic Engineering*, 7, 40-45 (In chinese).
- [20] Dayyani, S., Shiv O. Prasher, Ali Madani, and Chandra A. Madramootoo. (2010) Development of DRAIN-WARMF model to simulate flow and nitrogen transport in a tile-drained agricultural watershed in Eastern Canada. *Agricultural Water Management*, 98(1), 55-68.
- [21] Ding, X., Shen, Z., Hong, Q., Yang, Z., Wu, X., and Liu, R.. (2010) Development and test of the export coefficient model in the upper reach of the Yangtze River. *Journal of Hydrology*, 383(3), 233-244.
- [22] Sun, N., Li, X., and Li, Z.. (2007) Simulation of impacts of changes in land use and cover on annual streamflow in the upper reach of Chaohe River Basin. *Journal of Beijing Forestry University*, 30(S2), 22-30 (In chinese).
- [23] Li, Z., Li, X. and Yu, X. (2008) Impacts of soil and water conservation measures on annual runoff in the upper Chaohe River Basin in northern China based on hydrological analysis method. *Journal of Beijing Forestry University*, 30(S2), 6-11 (In chinese).

- [24] Wang, X.Y., Wang, Z., and Wang, X.F., (2004) Loss of Non-point Source Pollutants from Shixia Small Watershed, Miyun Reservoir, Beijing. *Scientia Geographica Sinica*, 2, 227-231 (In chinese).
- [25] Geng, R., Wang, X., Jiao, S., Meng, F., and Duan, S. (2013) Application of improved export coefficient model in estimating non-point source nutrient load from Miyun reservoir watersheds. *Acta Scientiae Circumstantiae*, 33(5), 1484-1492 (In chinese).
- [26] Wang, X., Zhang, Y. and Ou, Y. (2009) Predicting effectiveness of best management practices for control of nonpoint source pollution---a case of Taishitun Town, Miyun County, Beijing. *Acta Scientiae Circumstantiae*, 29(11), 2440-2450 (In chinese).
- [27] Yin, J., Zheng, Y., and Wang X. . (2009) Discharge features of rural domestic wastewater from different types of villages in water source protection area in Miyun reservoir of Beijing. *Journal of Agro-Environment Science*, 28(6), 1200-1207 (In chinese).
- [28] Howarth, R., Jensen, H S, and Mario, R. (1995) Transport to and processing of P in near-shore and oceanic waters. *SCOPE*, 54, 323-345.
- [29] Howarth, R.W., Sharpley, A. and Walker, D. (2002) Sources of nutrient pollution to coastal waters in the United States: Implications for achieving coastal water quality goals. *Estuaries*, 25(4), 656-676.
- [30] Gitau, M., Gburek, W. and Jarrett, A. (2005) A tool for estimating best management practice effectiveness for phosphorus pollution control. *Journal of Soil and Water Conservation*, 60(1), 1-10.
- [31] Sovik, A.K. and Morkved, P.T. (2008) Use of stable nitrogen isotope fractionation to estimate denitrification in small constructed wetlands treating agricultural runoff. *Science of the Total Environment*, 392(1), 157-165.
- [32] Ma, Xiao, Ye Li, Meng Zhang, Fangzhao Zheng, and Shuang Du. (2011) Assessment and analysis of non-point source nitrogen and phosphorus loads in the Three Gorges Reservoir Area of Hubei Province, China. *Science of the Total Environment*, 412, 154-161.
- [33] Sharpley, A.N., Kleinman, Peter J. A, Heathwaite, and A. Louise. (2008) Integrating contributing areas and indexing phosphorus loss from agricultural watersheds. *Journal of environmental quality*, 37(4), 1488-1496.

Received: 30.06.2016

Accepted: 06.06.2017

CORRESPONDING AUTHOR

Xiaoyan Wang

College of Resource Environment and Tourism
Capital Normal University
Beijing – CHINA

E-mail: wangxy@cnu.edu.cn

DISSOLUTION OF $\text{Cu}(\text{OH})_2$ BY A NOVEL CHELATING SURFACTANT *N*-LAUROYL ETHYLENEDIAMINE TRIACETATE

Jingru Diao, Baowei Zhao*, Hongtao Qiao, Fengfeng Ma, Liping Huang

School of Environmental and Municipal Engineering, Lanzhou Jiaotong University, Lanzhou, 730070, P. R. China

ABSTRACT

The chelation performance of a novel chelating surfactant (i.e., sodium *N*-lauroyl ethylenediamine triacetate (*N*-LED3A)) was evaluated by dissolving $\text{Cu}(\text{OH})_2$ in this surfactant. The optimum dissolution equilibrium time was determined to be 120 minutes. The effects of the initial *N*-LED3A concentration, temperature, pH and coexisting ions (i.e., $\text{Ca}(\text{II})$ and $\text{Mg}(\text{II})$) on $\text{Cu}(\text{OH})_2$ dissolution by *N*-LED3A were investigated. The *N*-LED3A solution significantly enhanced the water solubility of $\text{Cu}(\text{OH})_2$ via a ligand-promoted hydroxide dissolution mechanism to form a water-soluble chelate complex (*N*-LED3A-Cu). The mechanism of interaction between $\text{Cu}(\text{II})$ and *N*-LED3A was further confirmed by Fourier transform infrared spectroscopy (FTIR). The dissolved $\text{Cu}(\text{II})$ concentration in the *N*-LED3A solution was promoted by increasing the temperature or *N*-LED3A concentration. The chelation capacity of *N*-LED3A micelles was stronger than that of monomers. The dissolved $\text{Cu}(\text{II})$ concentration was highly dependent on the initial pH of *N*-LED3A. Coexisting $\text{Ca}(\text{II})$ or $\text{Mg}(\text{II})$ weakened the dissolution of $\text{Cu}(\text{OH})_2$ due to competition for *N*-LED3A. These results indicate that *N*-LED3A has a strong ability to chelate with heavy metals and form stable water-soluble complexes. The results imply that *N*-LED3A was a potential washing agent for heavy metal contaminated soils.

KEYWORDS:

chelating surfactant; dissolution; $\text{Cu}(\text{OH})_2$; $\text{Cu}(\text{II})$; chelation

INTRODUCTION

The not-degradable and toxic heavy metals in soils have become a worldwide environmental problem [1]. Heavy metal contaminants are typically a result of various industrial activities, agricultural practices, vehicle emission discharge and inappropriate waste disposal methods [2-3]. Soil washing/flushing with chelators is considered to be one of

the most suitable in/ex situ techniques for the removal of heavy metals from the ecosystem [4-5]. The most common chelating agents, ethylenediaminetetraacetic acid and its salts (EDTA), can appreciably increase the dissolution and mobilization of heavy metals by forming stable and soluble complexes with heavy metals [6-9]. However, the low selectivity of EDTA causes increased consumption of this agent [10-11] and extensive dissolution of soil minerals due to complexation with macro-elements present in soil [12]. In addition, EDTA possesses a low degree of biodegradability and is absorbed on soil particles, which could render the treated soils unfit for future use for vegetation [13]. Therefore, other biodegradable chelating agents such as *S,S*-ethylenediaminedisuccinic acid (*S,S*-EDDS) and citric acid were employed in soil washing to extract heavy metals [14-16]. EDTA structure was ever modified to improve its selectivity in chelating target metals in some studies [12, 17-18].

In previous studies, EDTA also has been modified to synthesize chelating surfactants with improved stability in hard water [19]. The use of chelating surfactants could diminish environmental eutrophication problems resulting from the addition of sodium tripolyphosphate to anionic surfactants. The sodium *N*-lauroyl ethylenediamine triacetate (*N*-LED3A) surfactant is synthesized by substituting one of EDTA's acetic groups with lauroyl group [20]. *N*-LED3A consists of a hydrophilic polycarboxylic moiety and a hydrophobic lauroyl group. Compared with EDTA, *N*-LED3A exhibits metal-binding capability and surface activity (i.e., micellization) and is a biodegradable agent. The microbial degradation percentage for *N*-LED3A was 70.5% within 30 days [21]. Soil washing can be used for removing both metals and organic compounds contaminations if a suitable single reagent or combinational reagents can be identified [16, 22-24]. Therefore, *N*-LED3A is a promising washing agent for soils contaminated with heavy metals and organic compounds simultaneously because of its ability to form chelates with metals coupled with the capacity to enhance the aqueous solubility of hydrophobic organic compounds (HOCs). Our previous studies have shown that *N*-LED3A can effectively enhance the water solubility of phenanthrene [25]. The focus of this study

is to gain additional insight into the coordinating capacity of *N*-LED3A for heavy metals.

In this study, *N*-LED3A was used to dissolve $\text{Cu}(\text{OH})_2$ to evaluate its coordinating capacity as a chelating agent. Batch equilibrium experiments were conducted to determine its efficacy in dissolving $\text{Cu}(\text{OH})_2$ and to investigate the potential extraction mechanisms. The effects of several important parameters were investigated and discussed. The conclusions would further provide reference for simultaneously removing heavy metals and organics from contaminated soils by using *N*-LED3A.

MATERIALS AND METHODS

Chemicals. *N*-LED3A ($\text{C}_{20}\text{H}_{33}\text{N}_2\text{O}_7\text{Na}_3$, $482.46 \text{ g}\cdot\text{mol}^{-1}$) with a purity of 95% was purchased from Hangzhou Biotechnology Co., Ltd., China. Copper hydroxide ($\text{Cu}(\text{OH})_2$, $97.56 \text{ g}\cdot\text{mol}^{-1}$) with a purity of 97% was obtained from Shanghai Biological Technology Co., Ltd., China. The critical micelle concentration (CMC) was $707 \text{ mg}\cdot\text{L}^{-1}$ [25]. Calcium chloride, magnesium chloride, sodium hydroxide and hydrochloric acid were supplied by the Tianjin Chemical Reagent Factory, China. All of the reagents were of analytical grade and were used as received without further purification. Deionized water was used throughout the experimental process.

Procedure for studying the dissolution of $\text{Cu}(\text{OH})_2$. Batch equilibrium experiments were conducted to investigate the dissolution of $\text{Cu}(\text{OH})_2$ by the *N*-LED3A solution. $\text{Cu}(\text{OH})_2$ samples (0.0300 g) were weighed into 50 mL conical flasks with stoppers, and 25.0 mL 3000 or $6000 \text{ mg}\cdot\text{L}^{-1}$ *N*-LED3A solutions were added in them. Then, these samples were shaken on an SHZ-82A reciprocating shaker (Jiangsu Danyang Experimental Instrument Plant, China) at 150 rpm within the range of reaction time from 0 to 180 min at $25 \text{ }^\circ\text{C}$. At the end of the dissolution experiment, the samples were transferred into 10 mL centrifuge tubes and centrifuged for 30 min at $25 \text{ }^\circ\text{C}$ in a TD6 centrifuge (Changsha Instrument Co., Ltd., China) at 4000 rpm to separate the undissolved solute. Then, the supernatant was filtered through a $0.45 \text{ }\mu\text{m}$ membrane for heavy metal analysis. The $\text{Cu}(\text{II})$ concentration in the supernatant was determined using an atomic absorption spectrophotometer (Varian 220FS, USA) in accordance with the Standard Method. A series of experiments using this method were used to study the effects of used to study the effects of *N*-LED3A concentration (from 0 to $3000 \text{ mg}\cdot\text{L}^{-1}$), temperature ($15 \text{ }^\circ\text{C}$, $25 \text{ }^\circ\text{C}$ and $35 \text{ }^\circ\text{C}$), initial pH values (from 5 to 12) and coexisting inorganic cations ($\text{Ca}(\text{II})$ or $\text{Mg}(\text{II})$) on the dissolution of $\text{Cu}(\text{OH})_2$. The optimum reaction time was determined by kinetic experiments. All of the tests were performed in triplicate, and the results are reported as average values.

Test of *N*-LED3A-Cu chelate. FTIR was used to test chelation structure of *N*-LED3A-Cu. The supernatant from the samples after dissolution equilibrium of $\text{Cu}(\text{OH})_2$ using $3000 \text{ mg}\cdot\text{L}^{-1}$ *N*-LED3A was carefully withdrawn and added to a glass beaker. Then, the supernatant in the beaker was evaporated in a water bath at $50 \text{ }^\circ\text{C}$ for 24 h following by drying in a vacuum oven at $50 \text{ }^\circ\text{C}$ for 24 h. The characteristics of *N*-LED3A and $\text{Cu}(\text{II})$ chelate complex (*N*-LED3A-Cu) were analyzed using a Fourier transform infrared spectrometer (FTIR) (IFS 66V/S, Germany). 1 mg of dried *N*-LED3A-Cu or *N*-LED3A was mixed with 200 mg of potassium bromide. These materials were ground together in a mortar and pressed into a translucent disk. The recovered pellet was immediately analyzed in a range from 4000 to 400 cm^{-1} with a resolution of 1 cm^{-1} .

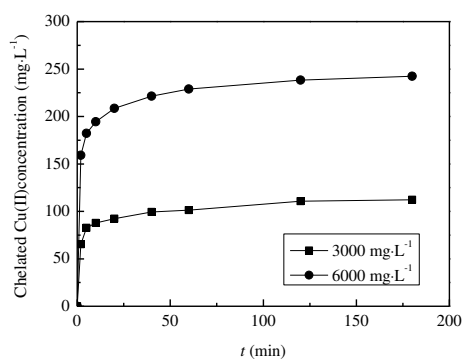


FIGURE 1
Dissolution kinetics of $\text{Cu}(\text{OH})_2$ by *N*-LED3A

RESULTS AND DISCUSSION

Dissolution kinetic. The dissolution kinetic experiments for $\text{Cu}(\text{OH})_2$ at $25 \pm 1 \text{ }^\circ\text{C}$ were conducted using *N*-LED3A solution with initial concentration of 3000 and $6000 \text{ mg}\cdot\text{L}^{-1}$ above its CMC. The results are shown in Fig. 1. The curves indicate that $\text{Cu}(\text{OH})_2$ can be quickly dissolved by *N*-LED3A, and the concentration of $\text{Cu}(\text{II})$ increased substantially within 20 min. Then, the dissolution rate decreased, and the $\text{Cu}(\text{II})$ concentration gradually became stable after 60 min. Therefore, 120 min was selected as the optimum dissolution equilibrium time for use in subsequent experiments. The equilibrium concentration of $\text{Cu}(\text{II})$ in the 3000 and $6000 \text{ mg}\cdot\text{L}^{-1}$ *N*-LED3A solution was 111 and $242 \text{ mg}\cdot\text{L}^{-1}$, respectively. The equilibrium $\text{Cu}(\text{II})$ concentration in $6000 \text{ mg}\cdot\text{L}^{-1}$ *N*-LED3A solution was approximately 2.16 times than that in the $3000 \text{ mg}\cdot\text{L}^{-1}$ *N*-LED3A solution. This result indicated that the dissolved strength of $\text{Cu}(\text{OH})_2$ increased as the *N*-LED3A micelles increased.

The complexation between *N*-LED3A and $\text{Cu}(\text{OH})_2$ was a pseudo-first-order reaction [26], ki-

netics data were fitted to the pseudo-first-order equation, with the obtained correlation coefficients and constants from the equations listed in Table 1. The kinetics rate equation could be expressed as Eq. (1).

$$\ln(1 - S_t / S_e) = -kt + a \quad (1)$$

Where, S_t ($\text{mg}\cdot\text{L}^{-1}$) is the chelated concentration of Cu(II) by *N*-LED3A at time t (min); S_e ($\text{mg}\cdot\text{L}^{-1}$) represents the equilibrium chelated concentration of Cu(II) by *N*-LED3A; t (min) was the contact time; k (min^{-1}) is rate constant; a is a constant.

Table 1 show the parameter k of $\text{Cu}(\text{OH})_2$ dissolved by 3000 and 6000 $\text{mg}\cdot\text{L}^{-1}$ *N*-LED3A were 0.0261 and 0.0248 min^{-1} , respectively. The result indicate that the value of k was a approximate constant, and was uncorrelated with *N*-LED3A concentration.

$\text{Cu}(\text{OH})_2$ is a poorly soluble metal hydroxide with a solubility product (K_{sp}) of 2.2×10^{-20} [27].

However, the water solubility of $\text{Cu}(\text{OH})_2$ can be significantly enhanced by *N*-LED3A due to the ability of *N*-LED3A to chelate with the metal ions. *N*-LED3A is a pentadentate aminoxatyl ligand. The *N*-LED3A molecule contains three carboxyl groups and one ethylenediamino group. The carboxyl oxygen and amino nitrogen atoms can coordinate with a metal atom and act as a bridge connecting the central metal ions and ligands. Cu is a transition metal ion with a coordinate number of 6 (sp^3d^2 hybridization) or 4 (dsp^2 hybridization) [27]. *N*-LED3A can form complexes with Cu(II), and the resulting shift in electron density toward the central ion weakens the link between Cu and the hydroxide ions, promoting detachment of Cu into solution [28]. Therefore, *N*-LED3A can attack $\text{Cu}(\text{OH})_2$ through a ligand-promoted hydroxide dissolution mechanism. The *N*-LED3A chelation for Cu(II) can take place through following reactions of (2) and (3).

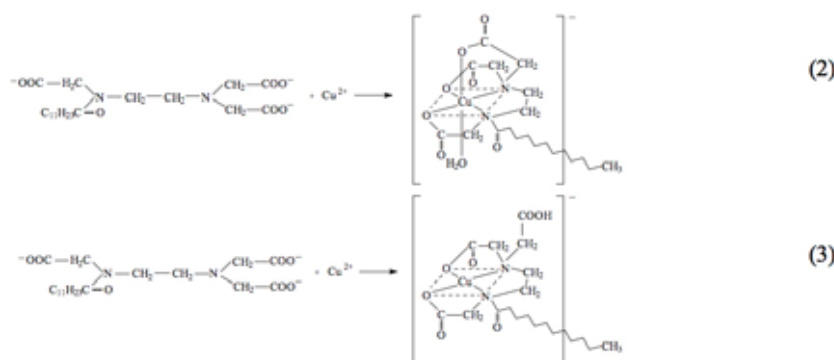


TABLE 1
Dissolution kinetics parameters calculated from pseudo-first order model

$c_0 = 3000 \text{ mg}\cdot\text{L}^{-1}$		$c_0 = 6000 \text{ mg}\cdot\text{L}^{-1}$	
k (min^{-1})	R^2	k (min^{-1})	R^2
0.0261	0.987	0.0248	0.9935

c_0 - initial concentration of *N*-LED3A solution

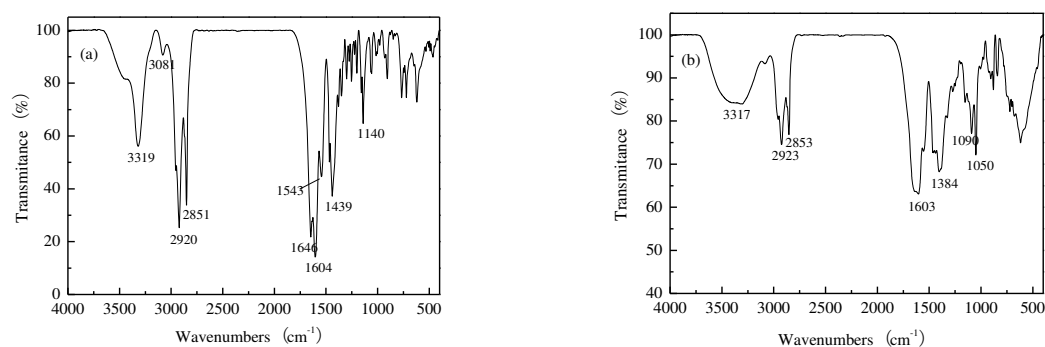


FIGURE 2
FTIR spectra of *N*-LED3A(a) and *N*-LED3A-Cu chelate (b)

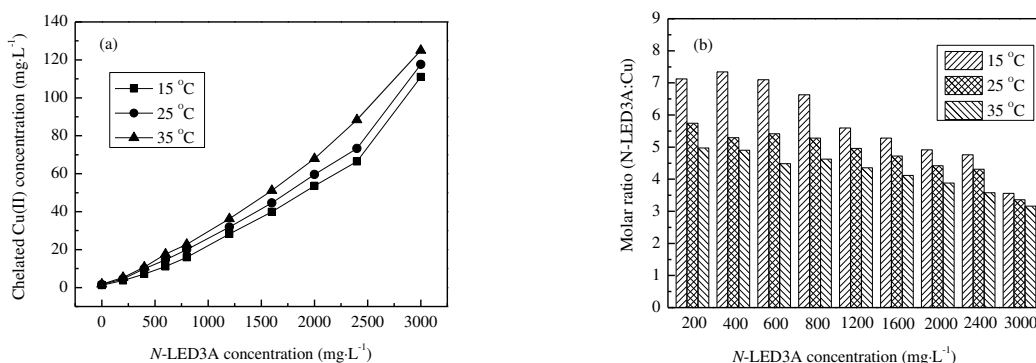


FIGURE 3
Effects of temperature on dissolution of $\text{Cu}(\text{OH})_2$ by *N*-LED3A

The *N*-LED3A-Cu complex was a 5-membered ring coordination complex or chelate. Chemical Eq. (2) indicates that the copper atom of *N*-LED3A-Cu complex is surrounded by six coordination atoms including two nitrogen atoms, three oxygen atoms in *N*-LED3A molecule and an oxygen atom in water molecule. *N*-LED3A-Cu has a “pentadentate tetracyclic single hydration” octahedron shape. Chemical Eq. (3) indicates that the copper atom is surrounded by four atoms, and the oxygen atom in remaining free carboxyl arm was not participate in the coordination with copper atom. The spatial structure of *N*-LED3A-Cu was “tetradentate tricyclic” planar square. According to the soft and hard acids and bases (HSAB) theory, Cu(II) corresponds to a junction acid, and *N*-LED3A corresponds to a junction base [29]. Therefore, *N*-LED3A-Cu which formed via coordination bonds between the multidentate organic ligand and the central metal ions should exhibit good stability with the stability constant K_r^\ominus of 6.9×10^{19} [26].

Due to its strong coordinating capacity, *N*-LED3A can seize metal ions from a metal hydroxide to form an aminoxatyl complex, which results in the precipitation-dissolution equilibrium of the metal hydroxide to shift toward dissolution. The *N*-LED3A dissolution of $\text{Cu}(\text{OH})_2$ is a dual-equilibrium system consisting of a precipitation-dissolution equilibrium and a chelation equilibrium. The concentration of soluble *N*-LED3A-Cu can continuously increase as Cu(II) is released until the chelation reaction reaches equilibrium.

***N*-LED3A-Cu characterization.** The FTIR spectra of *N*-LED3A and *N*-LED3A-Cu chelate are shown in Fig. 2.

The spectra exhibited some changes after *N*-LED3A chelation with Cu(II). The three major differences are as follows: (a) In the spectra of *N*-LED3A, the absorption bands located at 1646 cm^{-1} and 1604 cm^{-1} , which were associated with intense asymmetric stretching vibrations of the carboxylate groups, and 1439 cm^{-1} , which were associated with

symmetric stretching vibrations of carboxylate groups [30] were shifted to lower wavenumbers (i.e., 1603 and 1384 cm^{-1} , respectively) in the spectra of *N*-LED3A-Cu. In addition, the absorption bands located at 1603 cm^{-1} and 1384 cm^{-1} were significantly wider. These differences indicated that chelation occurred between Cu(II) and the hydrophilic groups of *N*-LED3A. (b) The absorption bands located at 2920 cm^{-1} and 2851 cm^{-1} , which correspond to asymmetric stretching vibrations and symmetric stretching vibrations of the $-\text{CH}_2-$ bond [31] in the ethyl bridge ($-\text{CH}_2-\text{CH}_2-$) were shifted to 2923 cm^{-1} and 2853 cm^{-1} , respectively, which indicated that the tertiary amine connected to the ethyl bridge participated in the chelation reaction. (c) The absorption peak at 3319 cm^{-1} , which was due to stretching vibration bands of the $-\text{OH}$ groups [30-31] shifted to 3317 cm^{-1} and became wider, which was due to the ion exchange between H^+ of the $-\text{COOH}$ groups and Cu(II) released from $\text{Cu}(\text{OH})_2$. The FTIR spectral analysis confirmed that the chelation reaction occurred between Cu(II) and the *N*-LED3A molecule. This result further demonstrated that *N*-LED3A can attack $\text{Cu}(\text{OH})_2$ via a ligand-promoted hydroxide dissolution mechanism to form a stable soluble *N*-LED3A-Cu complex.

Effect of temperature and concentration. The dissolution isotherms of $\text{Cu}(\text{OH})_2$ at different temperatures of 15, 25 and 35 °C are shown in Fig. 3(a). The relationship between chelate molar ratio (*N*-LED3A:Cu(II) (n:n)), which was calculated according to the data of Fig. 3(a), and the initial *N*-LED3A concentration is shown in Fig. 3(b). As shown in Fig. 3(a), an increase in the temperature or initial concentration of *N*-LED3A can improve the dissolution of $\text{Cu}(\text{OH})_2$. Fig. 3(b) indicated that the chelate molar ratio was not 1:1 between *N*-LED3A and $\text{Cu}(\text{OH})_2$ as expressed in Eq. (2) or (3). This experimental result may be attributed to the following reasons. (1) The purity of *N*-LED3A was not enough, some insoluble impurities was observed during the preparation of *N*-LED3A solution. (2) *N*-LED3A is

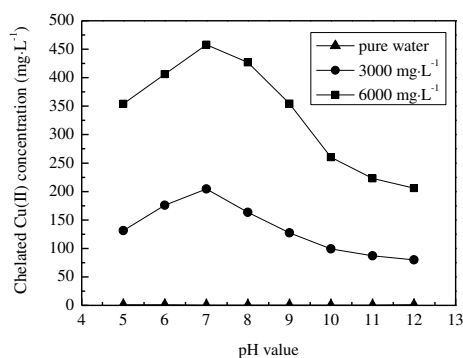


FIGURE 4
Effects of pH value on dissolution of $\text{Cu}(\text{OH})_2$ by *N*-LED3A

TABLE 3
Effects of inorganic cations on dissolution of $\text{Cu}(\text{OH})_2$ by *N*-LED3A

	Ca^{2+}						Mg^{2+}					
Cations ($\text{mmol}\cdot\text{L}^{-1}$)	0	0.1	0.2	0.3	0.5	1	0	0.1	0.2	0.3	0.5	1
S_e ($\text{mg}\cdot\text{L}^{-1}$)	204.2	150.4	123.9	119.4	113.2	100.5	209.7	94.6	104.9	110.7	98.4	111.1

S_e - equilibrium chelated concentration of $\text{Cu}(\text{II})$ by *N*-LED3A

The results shown in Fig. 4 indicate that the dissolution degree of $\text{Cu}(\text{OH})_2$ in the *N*-LED3A solution was affected by the pH value. The protonation degree of *N*-LED3A, which is related to the pH value, influenced the coordination ability, number of coordinating atoms and structure of the complex [12]. The different species of *N*-LED3A exhibit different coordination capacities for $\text{Cu}(\text{II})$. Therefore, the $\text{Cu}(\text{II})$ concentration captured from $\text{Cu}(\text{OH})_2$ by the chelating reaction varied accordingly. *N*-LED3A likely existed as H_2L^- species when the initial pH value was equal to 5. The protonation of *N*-LED3A would weaken the coordinating capacity of the ligands and dissolution efficiency of $\text{Cu}(\text{OH})_2$ due to competition between the protons and $\text{Cu}(\text{II})$ for the carboxylate of ligands.

The increase in the initial pH value of the *N*-LED3A solution would shift the equilibrium expressed in Eq. (4) to the right. When the initial pH of the *N*-LED3A solution increased from 6 to 9, *N*-LED3A exhibited better dissolution efficiency, and higher $\text{Cu}(\text{II})$ concentrations were detected in the dissolution equilibrium system. *N*-LED3A was present as HL^{2-} and L^{3-} under these pH conditions, and these two species exhibited a stronger coordinating capacity. The concentration of the *N*-LED3A- Cu complex improved significantly compared with that observed at pH 5. Because the proportion of HL^{2-} and L^{3-} in the system varied with the pH value, the dissolution degree of $\text{Cu}(\text{OH})_2$ varied. The optimum degree was observed at a pH of 7 for both the 3000 and 6000 $\text{mg}\cdot\text{L}^{-1}$ *N*-LED3A solutions, and the maximum $\text{Cu}(\text{II})$ concentration was 205 and 458 $\text{mg}\cdot\text{L}^{-1}$, respectively.

However, when the initial pH value was increased from 10 to 12, the concentration of chelated $\text{Cu}(\text{II})$ decreased gradually. The major form of *N*-LED3A under these strong alkaline conditions was L^{3-} . Although the increased negative charges could enhance the attraction between the ligands and the central ions, these charges could enhance the repulsion among ligands, which was adversely affect the formation of micelles. The comprehensive effect of the two factors resulted in a decrease in the coordination capacity, and therefore, the dissolution efficiency of $\text{Cu}(\text{OH})_2$ by *N*-LED3A was weakened. In addition, more alkaline conditions would inhibit the dissolution of $\text{Cu}(\text{OH})_2$ by *N*-LED3A. The gradually increasing hydroxyl concentration at these pH values could even replace L^{3-} from the *N*-LED3A- Cu complex to form $\text{Cu}(\text{OH})_2$ again [29].

Effects of inorganic cations. The effects of the coexisting divalent inorganic cations (i.e., $\text{Mg}(\text{II})$ or $\text{Ca}(\text{II})$) on the dissolution of $\text{Cu}(\text{OH})_2$ by 3000 $\text{mg}\cdot\text{L}^{-1}$ *N*-LED3A at pH of 7 were compared.

As shown in Table 3, coexisting $\text{Mg}(\text{II})$ or $\text{Ca}(\text{II})$ inhibited the dissolution of $\text{Cu}(\text{OH})_2$. It seems that the dissolution values of $\text{Cu}(\text{OH})_2$ decreased sharply at low concentration of $\text{Mg}(\text{II})$ or $\text{Ca}(\text{II})$. When free $\text{Mg}(\text{II})$ or $\text{Ca}(\text{II})$ were present in the *N*-LED3A solution, *N*-LED3A would prefer to chelated with them to form *N*-LED3A- Mg or *N*-LED3A- Ca complexes. Therefore, the capability of *N*-LED3A for chelating and seizing $\text{Cu}(\text{II})$ from $\text{Cu}(\text{OH})_2$ was reduced. The results in Table 3 also indicate that an increase in the $\text{Mg}(\text{II})$ or $\text{Ca}(\text{II})$ concentration from 0.2 to 1 $\text{mmol}\cdot\text{L}^{-1}$ produced a small variation in the dissolved $\text{Cu}(\text{II})$ concentration. Because $\text{Mg}(\text{II})$ or $\text{Ca}(\text{II})$ are

alkaline earth metals and hard acids, the stability of the *N*-LED3A-Ca or *N*-LED3A-Mg complex was lower than that of the *N*-LED3A-Cu complex. Mg(II) or Ca(II) can be partially replaced by Cu(II), which is released from Cu(OH)₂, to form the more stable *N*-LED3A-Cu complex. In comparison, the effect of Mg(II) on the dissolution of Cu(OH)₂ by *N*-LED3A was greater than that of Ca(II).

CONCLUSIONS

The results from this study indicated that the *N*-LED3A solution could significantly enhance the water solubility of Cu(OH)₂. *N*-LED3A could seize Cu(II) from Cu(OH)₂ via a ligand-promoted hydroxide dissolution mechanism to form a stable, water-soluble *N*-LED3A-Cu complex. The coordinating capacity of *N*-LED3A micelle is stronger than that of the *N*-LED3A monomer. FTIR spectral analysis confirmed that a chelating reaction occurs between Cu(II) and *N*-LED3A.

An increased in the temperature or *N*-LED3A concentration could promote the dissolution of Cu(OH)₂. The dissolved concentration of Cu(II) from Cu(OH)₂ was highly dependent on the pH. A significant dissolution capacity for Cu(OH)₂ was observed in a pH range from 6 to 9, with an optimum pH value of 7. Coexisting Ca(II) or Mg(II) can weaken the dissolution capacity of *N*-LED3A for Cu(OH)₂.

In combination with the results for chelating heavy metals and the previous results for solubilizing organic compounds, *N*-LED3A is potentially a practical washing agent for soils contaminated with heavy metals and organic compounds simultaneously.

ACKNOWLEDGEMENTS

The authors greatly appreciate the National Natural Science Foundation of China (41261077) and the Natural Science Foundation of Gansu Province (1010RJZA070).

REFERENCES

- [1] Lestan, D., Luo, C.L. and Li, X.D. (2008) The use of chelating agents in the remediation of metal-contaminated soils: a review. *Environ. Pollut.* 153, 3–13.
- [2] Hong, K.J., Tokunaga, S. and Kajiuchi, T. (2002) Evaluation of remediation process with plant-derived biosurfactant for recovery of heavy metals from contaminated soils. *Chemosphere*. 49, 379–387.
- [3] Martley, E., Gulson, B.L. and Pfeifer, H.-R. (2004) Metal concentrations in soils around the copper smelter and surrounding industrial complex of Port Kembla, NSW, Australia. *Sci. Total Environ.* 325, 113–127.
- [4] Tsang, D.C.W., Zhang, W.H. and Lo, I.M.C. (2007) Copper extraction effectiveness and soil dissolution issues of EDTA-flushing of artificially contaminated soils. *Chemosphere*. 68, 234–243.
- [5] Dermont, G., Bergeron, M., Mercier, G. and Richer-Lafleche, M. (2008) Soil washing for metal removal: a review of physical/chemical technologies and field applications. *J. Hazard. Mater.* 152, 1–31.
- [6] Zhang, W.H. and Lo, I.M.C. (2006) EDTA-enhanced washing for remediation of Pb- and/or Zn-contaminated soils. *J. Environ. Eng.* 132, 1282–1288.
- [7] Xia, W.B., Gao, H., Wang, X.H., Zhou, C.H., Liu, Y.G., Fan, T. and Wang X. (2008) Application of EDTA decontamination on soils affected by mining activities and impact of treatment on the geochemical partition of metal contaminants. *J. Hazard. Mater.* 164, 936–940.
- [8] Zhang, W.H., Tong, L.Z., Yuan, Y., Liu, Z.Y., Huang, H., Tan, F.F. and Qiu, R.L. (2010) Influence of soil washing with a chelators on subsequent chemical immobilization of heavy metals in a contaminated soil. *J. Hazard. Mater.* 178, 578–587.
- [9] Niesiobędzka, K. (2012) Transfer of copper, lead and zinc in soil-grass ecosystem in aspect of soils properties, in Poland. *B Environ. Contam. Tox.* 88, 627–633.
- [10] Kedziorek, M.A.M. and Bourg, A.C.M. (2000) Solubilization of lead and cadmium during the percolation of EDTA through a soil polluted by smelting activities. *J. Contam. Hydrol.* 40, 381–392.
- [11] Palma, L.D. and Ferrantelli, P. (2005) Copper leaching from a sandy soil: mechanism and parameters affecting EDTA extraction. *J. Hazard. Mater.* 122, 85–90.
- [12] Zhang, T., Liu, J.M., Huang, X.F., Xia, B., Su, C.Y., Luo, G.F., Xu, Y.W., Wu, Y.X., Mao, Z.W. and Qiu, R.L. (2013) Chelant extraction of heavy metals from contaminated soils using new selective EDTA derivatives. *J. Hazard. Mater.* 262, 464–471.
- [13] Wasay, S.A., Barrington, S. and Tokunaga, S. (2001) Organic acids for the in situ remediation of soils polluted by heavy metals: soil flushing in columns. *Water Air Soil Pollut.* 127, 301–314.
- [14] Schowanek, D., Feijtel, T.C.J., Perkins, C.M., Hartman, F.A., Federle, T.W. and Larson, R.J. (1997) Biodegradation of [S,S], [R,R] and mixed stereoisomers of ethylene diamine disuccinic acid (EDDS), a transition metal chelator. *Chemosphere*. 34, 2375–2391.
- [15] Palma, L.D. and Mecozzi, R. (2007) Heavy metals mobilization from harbour sediments using

- EDTA and citric acid as chelating agents. *J. Hazard. Mater.* 147, 768–775.
- [16] Wen, Y.X. and Marshall, W.D. (2011) Simultaneous mobilization of trace elements and polycyclic aromatic hydrocarbon (PHA) compounds from soil with a nonionic surfactant and [S,S]-EDDS in admixture: Metals. *J. Hazard. Mater.* 197, 361–368.
- [17] Namor, A.F.D. and Tanaka, D.A.P. (1998) Thermodynamics of protonation and complexation of EDTA derivatives and metal cations in water. *J. Chem. Soc. Faraday Trans.* 94, 3105–3110.
- [18] Amelia, S.M., Sofia, G., Lurdes, G. and Etelka, F. (2005) Bis (3-hydroxy-4-pyridinone)- EDTA derivative as a potential therapeutic Al-chelating agent. Synthesis, solution studies and biological assays. *J. Inorg. Biochem.* 99, 1845–1852.
- [19] Wang, X.X., Zhao, J.L., Yao, X.Z. and Chen, W.T. (2004) Synthesis and properties of N-hexadecyl ethylenediamine triacetic acid. *J. Colloid Interface Sci.* 279, 548–551.
- [20] Parker, B.A. and Crudden, J.J. (1996) The commercial synthesis and characterization of novel multifunctional surfactant chelates, 4th World surfactant conference, Barcelona. 187, 446–460.
- [21] Wang, J. (2009) Synthesis and application of functional surfactants. Chemical Industry Press, Beijing.
- [22] Yuan, S.H., Wu, X.F., Wan, J.Z., Long, H.Y., Lu, X.H., Wu, X.H. and Chen, J. (2010) Enhanced washing of HCB and Zn from aged sediments by TX-100 and EDTA mixed solutions. *Geoderma.* 156, 119–125.
- [23] Ullmann, A., Brauner, N., Vazana, S., Katz, Z., Goikhman, R., Seemann, B., Marom, H. and Gozin, M. (2013) New biodegradable organic-soluble chelating agents for simultaneous removal of heavy metals and organic pollutants from contaminated media. *J. Hazard. Mater.* 260, 676–688.
- [24] Meng, D., Wan, J., Zhang, S., Yao, H. and Lin, Y. (2014) Simultaneous removal of lindane and heavy metals from contaminated soils by rhamnolipids enhanced washing. *Acta Sci. Circumst.* 34, 229–237.
- [25] Diao, J.R., Zhao, B.W., Ma, F.F., Wang, X. and Wen J.D. (2016) Solubility enhancement of phenanthrene using novel chelating surfactant. *Chemical Papers.* 70, 375–383.
- [26] Diao, J.R., Zhao, B.W., Ma, F.F., Hong, T.Q. and Ding, W.J. (2015) Mechanism on Cu(OH)₂ dissolution in the presence of a novel chelating surfactant. *J. Lanzhou Jiaotong Univ.* 34, 1–5, 6.
- [27] Yang, H.X., Yan, X.R., Cui, J.Z., Wang, J.H., Wang, X.R. and Qin, X. (2010) Inorganic chemistry. Higher Education Press, Beijing.
- [28] Elliott, H.A. and Shastri, N.L. (1999) Extractive decontamination of metal polluted soils using oxalate. *Water Air Soil Pollut.* 110, 335–346.
- [29] Fang, J.L. (2008) Theory and application of coordination compounds in electroplating. Chemical Industry Press, Beijing.
- [30] Silverstein, R.M., Bassler, G.C. and Morrill, T.C. (1991) Spectrometric identification of organic compounds. Science Press, Beijing.
- [31] Xie, J.Y. (2001) Application of infrared spectra to organic chemistry and pharmaceutical chemistry. Science Press, Beijing.
- [32] Wasan, D. and Nikolov, A. (2004) Foaming-antiforming in boiling suspensions. *Ind. Eng. Chem. Res.* 43, 3812–3816.
- [33] Zhang, T., Wu, Y.X., Huang, X.F., Liu, J.M, Xia, B., Zhang, W.H. and Qiu, R.L. (2012) Simultaneous extraction of Cr(VI) and Cu(II) from humic acid with new synthesized EDTA derivatives. *Chemosphere.* 88, 730–735.
- [34] Mulligan, C.N., Yong, R.N. and Gibbs, B.F. (2001) Surfactant-enhanced remediation of contaminated soil: a review. *Eng. Geol.* 60, 371–380.
- [35] Pennell, K.D., Abriola, L.M. and Weber, W.J. (1993) Surfactant-enhanced solubilization of residual dodecane in soil columns experimental investigation. *Environ. Sci. Technol.* 27, 2332–2340.

Received: 24.09.2016

Accepted: 24.05.2017

CORRESPONDING AUTHOR

Baowei Zhao

School of Environmental and
Municipal Engineering
Lanzhou Jiaotong University
Lanzhou, 730070, P. R. CHINA

E-mail: baowei.zhao@yahoo.com

REMOVAL OF NITRATE AND PHOSPHATE BY IMMOBILIZED BIOCHARS PREPARED FROM REEDS AND HEMATITE

Bo Wang*, Deng-Yue Yang, Fa-Yun Li

Institute of Eco-Environmental Sciences, Liaoning Shihua University, Fushun 113001, China

ABSTRACT

The decomposition of aquatic plants in the autumn and winter results in secondary pollution in water bodies and biochars prepared from aquatic plants show the limited adsorption capacity of nitrate and phosphate. In the study, we prepared hematite-modified biochar (HMB) with reeds and hematite. Moreover, we studied the adsorption properties of nitrate and phosphate by HMB through batch adsorption experiments and explored adsorption mechanisms. In order to further enhance the application of HMB in natural waters and solve the problem that powdered biochar is easily removed with water, we explored the immobilization of HMB. The experimental results showed that the negative charge on the surface of HMB was reduced and the positive charge increased. Through electrostatic interaction and precipitation mechanism, HMB could effectively remove nitrate and phosphate in aqueous solution. Immobilized HMB microspheres could efficiently remove nitrate and phosphate from eutrophic water, and promote the utilization of aquatic plants.

KEYWORDS:

biochar; hematite; reed; nitrate; phosphate; immobilization

INTRODUCTION

With the rapid development of social economy, a large quantity of wastewater and agricultural runoff is discharged into natural water bodies, leading to the rising nitrate and phosphate content in water bodies as well as serious water eutrophication problems[1, 2]. Among many nitrate and phosphate removal methods, currently widely recognized more effective method is the aquatic plant restoration method[3, 4]. However, the decomposition of aquatic plants in the autumn and winter will result in secondary pollution in water bodies[5, 6]. The treatment and utilization of the decomposition litters of aquatic plants is one of the hotspots and difficulties in aquatic plant restoration

and litter disposal. The utilization of plant wastes for the preparation of biochars was studied[7, 8]. A biochar is one class of carbon-rich solid mixture obtained through the pyrolysis of biological residues at the high temperature under the conditions of limited oxygen[9]. It is a new inexpensive adsorbent material[10]. However, biochars were negatively charged groups and that cation exchange capacity was higher than anion exchange capacity[11, 12]. It was believed that biochars mainly adsorbed cations other than anions and that the adsorption capacity of nitrate and phosphate by biochars itself was very limited[12].

Several methods have thus been developed to modify biochar to enhance its adsorption of nitrate and phosphate [13]. For example, biochar composites prepared by pyrolyzing FeCl_3 greatly enhanced nitrate and phosphate adsorption ability of the biochars[7, 14].

However, the methods used to create these biochar are relatively complex and costly. Thus, additional investigations thus are needed to develop simple and cost-effective methods to modify biochars with iron, particularly with natural iron minerals.

Hematite is one of the most abundant natural iron oxide minerals and shows good phosphate adsorption ability[7, 15]. In addition, thermal treatment has also been used to 'activate' hematite to enhance its adsorption ability [7, 16].

The study aims to develop a new method to prepare iron-oxide biochar composites with aquatic plant and natural hematite, study its adsorption capability for nitrate and phosphate and establish dynamic adsorption model. Hematite-treated reed was used as the feedstock to produce the biochar through pyrolysis. Adsorption ability of hematite-modified biochar (HMB) to nitrate and phosphate was assessed through batch adsorption experiments in laboratory. Moreover, in order to further enhance the application of composite materials in natural waters, to solve the problem that powdered biochar is easily removed with water, we prepared immobilized HMB, which might be applied in nitrate and phosphate treatment in eutrophic water bodies and resource utilization of aquatic litters.

MATERIALS AND METHODS

Preparation and modification of biochars.

Stalks of reeds were acquired from Panshan County, Panjin City, Liaoning Province, China. Then stalks were washed with deionized water and dried. After crushing with plant crusher (FW177, Gongxing Corporation), the crushed stalks passed through a 100-mesh sieve and then collected.

Natural hematite was acquired from Anshan mine area, Liaoning Province, China. To determine the content of iron oxide is 90% by titration. Hematite was crushed with ground with a mortar and sieved to through a 100-mesh sieve and then collected

The method of preparing HMB was similar to that used by Wang. (2015)[7]. A hematite suspension was prepared by mixing 4 g of crushed mineral particles in 100 mL of deionized water. The suspension was stirred and sonicated for 1 h with an ultrasonicator (PS-20A, Jiehui Corporation) to form a stable suspension. About 40 g of the feedstock was well mixed with the suspension for 2 h and was then oven-dried at 80 °C.

The collected particles were put into a tubular resistance furnace. Nitrogen flow was purged into the furnace according to the flow rate of 400 mL/min in order to maintain the low oxygen content in the furnace. The temperature in the furnace was in-creased to 700 °C according to the program-control-led heating rate of 10 °C/min and then maintained for 20-min pyrolysis. After the pyrolysis process, biochars were naturally cooled to room temperature and then removed from the furnace. Then biochars were washed with deionized water to neutral pH and dried at 105 °C. Finally, modified biochar from reeds and hematite (HMB) was obtained.

Adsorption experiments and sample

analysis.(1) Adsorption kinetics of HMB. Firstly, 0.2 g of HMB was respectively weighed into a series of centrifuge tubes. Then, 10 mL of 20 mg·L⁻¹ KNO₃ solution was added into each centrifuge tube, which was put on the shaking table under the conditions of (20 ± 0.5) °C and 150 rpm. The tubes were taken out respectively after 5, 10, 20, 40, 80, 160, and 320 min. Then the solution in the tubes was filtered through the membrane with the pore size of 0.45 μm and the concentration of nitrate in the filtered solution from each tube was measured in 3 replicates. The measurement results were averaged.

Adsorption kinetics experiments of phosphate was designed as above. The difference was that K₃PO₄ solution was added into each centrifuge tube.

(2) Adsorption isotherms of HMB. Firstly,

0.2 g of HMB was respectively weighed into a series of centrifuge tubes. Then, 10 mL of 5, 10, 20, 40, 80, 160, and 320 mg·L⁻¹ KNO₃ solution was added into different centrifuge tubes. Three duplicates were arranged for each KNO₃ concentration. Centrifuge tubes were vibrated for 2 h on the shaking table under the conditions of (20 ± 0.5) °C and 150 rpm. The tubes were taken out and the solution in the tubes was filtered through the membrane with the pore size of 0.45 μm. The concentration of nitrate in the filtered solution from each tube was measured.

Adsorption isotherm experiments of phosphate was designed as above. The difference was that K₃PO₄ solution was added into different centrifuge tubes.

(3) Immobilized HMB microspheres. HMB was mixed with 20 mL of 2% sodium alginate solution. After thoroughly mixing, the mixture solution was extruded into 4% CaCl₂ solution to form microspheres. After standing for 1 h, microspheres were washed with distilled water. Then microspheres were immersed in CaCl₂ solution for 2 h crossing at 4 °C. According to subsection 1.2.2, nitrate and phosphate adsorption isotherms of immobilized HMB microspheres were experiment-tally studied.

(4) Removal efficiency of nitrate and phosphate from eutrophic water. Eutrophic water was acquired in October 2015 from Suzi river, Fushun City, Liaoning Province, China. Firstly, 0.2 g of immobilized HMB microspheres were respectively weighed into a series of centrifuge tubes. Then, 20 mL of eutrophic water (nitrate: 4.1 mg·L⁻¹, phosphate: 2.2 mg·L⁻¹, COD: 8.5 mg·L⁻¹, ammonia nitrogen: 4.6 mg·L⁻¹) was added into each centrifuge tube, which was put on the shaking table under the conditions of (20 ± 0.5) °C and 150 rpm. The tubes were taken out respectively after 5, 10, 20, 40, 80, 160, and 320 min. Then eutrophic water in the tubes was filtered through the membrane with the pore size of 0.45 μm, the concentration of nitrate and phosphate in the filtered solution from each tube was measured in 3 replicates. The measurement results were averaged.

(5) Analysis. The concentration of nitrate was determined with UV spectrophotometry. The concentration of phosphate was determined with molybdenum antimony spectrophotometry. Zeta potential analyzer (ZEN360, Brookhaven Corporation) was used to determine surface potentials of HMB. The surface morphology of HMB (JSM-6360LA, JEOL Corporation) was characterized by using microscope.

(6) Data processing. Experimental data were processed with SPSS 19.0 and Excel software and

the curves were plotted with Origin 8.0 software.

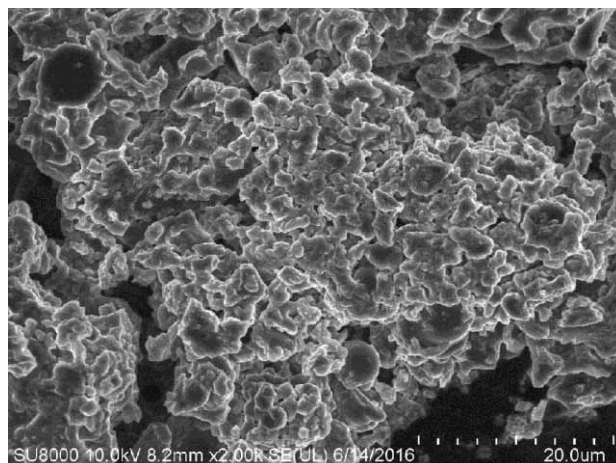


FIGURE 1
SEM of HMB

RESULTS AND DISCUSSION

Surface Zeta points. There were hydroxyl, phenolic hydroxyl group, cyclic lactone peroxide, and other oxygen-containing groups on the surface of modified biochars [17]. Due to the presence of these surface groups, biochars had different surface hydrophilicities and surface acidities, thus resulting in different surface charges (positive or negative) [18, 19]. It was determined that biochar of reeds was negatively charged with the Zeta potentials of -28.81 mV. HMB was positively charged with Zeta potentials of +2.55 mV. HMB reduced negative charges on biochar surface and increased positive charges. The modification of the biochars was conducive to the adsorption of negatively charged nitrate and phosphate. Moreover, immobilized HMB was positively charged with Zeta potentials of +2.18 mV.

Surface morphology. In the SEM images (Fig. 1), HMB show the surfaces containing many irregular cavities. Due to the decomposition of lots of cellulose during the pyrolysis at 700 °C, the surface sediments were decreased and micropores were formed on the surfaces of the biochars. High temperature and acid activation greatly increased the surface area of all biochars, which is more conducive to provide more adsorption sites for HMB.

Adsorption kinetics. As shown in Figs. 2 and 3, the adsorption effects of nitrate and phosphate by HMB is significant. The adsorption of nitrate by HMB was fast in the initial 10 min. After 80 min, the adsorption capacity was slowly increased and tended to be stable after adsorption. The adsorption of phosphate by HMB was fast in the initial 80 min.

After 160 min, the adsorption capacity was slowly increased and tended to be stable after adsorption. The high adsorption rate is of great significance to practical applications because rapid adsorption rate can ensure the high removal efficiency. The first phase could be ascribed to rapid occupation of easily accessible external surface adsorption sites such as outer sphere complexation [7, 20]. The slow phase could be related to the formation of inner layer complexes [7, 20].

The study of adsorption kinetics can enhance the understanding of the adsorption mechanism. Adsorption kinetics mainly involves the adsorption rate of solute by adsorbents from the solution [21, 22]. In order to study the control mechanism of the adsorption process, in the study, pseudo first-order equation, pseudo-second-order equation, and intra-particle diffusion equation were adopted to fit the experimental results.

Pseudo-first-order equation is

$$q_t = q_e(1 - e^{-k_1 t}); \quad (1)$$

Pseudo-second-order equation is

$$q_t = \frac{K_2 q_e^2 t}{1 + K_2 q_e t}; \quad (2)$$

Intra-diffusion equation is

$$q_t = q_i t^{1/2} + C; \quad (3)$$

Where q_t and q_e are respectively the nitrate and phosphate adsorption at the moment t and after reaching adsorption equilibrium, $\text{mg}\cdot\text{g}^{-1}$; t is adsorption time, min; k_1 , k_2 , and q_i are the rate constants of pseudo first-order equation, pseudo-second-order equation, and intra-particle diffusion equation and the units were respectively min^{-1} , $\text{g}\cdot\text{mg}^{-1}\cdot\text{min}^{-1}$, and $\text{mg}\cdot\text{g}^{-1}\cdot\text{min}^{-0.5}$.

The fitting results are shown in Table 1 and fitting curves of 3 equations are plotted in Figs. 1

and 2. In Table 1, Fig. 2 and Fig. 3, the fitting correlation coefficient for the nitrate and phosphate adsorption experimental results of HMB with pseudo-second-order equation was higher than that of pseudo-first-order equation. In addition, the theoretical values of adsorption of nitrate and phosphate onto HMB calculated with pseudo-second-order equation (q_e) was closer to the measured values, indicating that the pseudo-second kinetic model can better describe the adsorption process of nitrate and phosphate by HMB. The pseudo-second-order equation was used to describe

the process of chemical adsorption [23]. It showed that the adsorption process of nitrate and phosphate were mainly chemical process.

In intra-diffusion equation, if the fitted curve passed through the origin of coordinates, the intra-diffusion would be the control step of the adsorption rate [24]. However, the fitted curve for nitrate and phosphate adsorption experimental did not pass through the origin of coordinates in the experiment, indicating that the intra-diffusion was not the only control step in the adsorption process for nitrate and phosphate adsorption experimental.

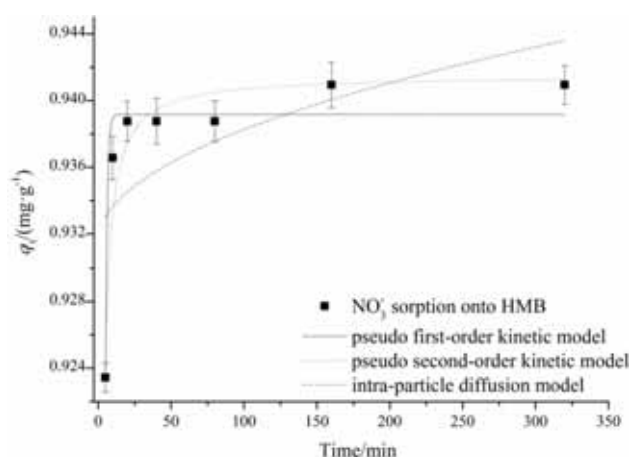


FIGURE 2
Kinetics of nitrate sorption onto HMB

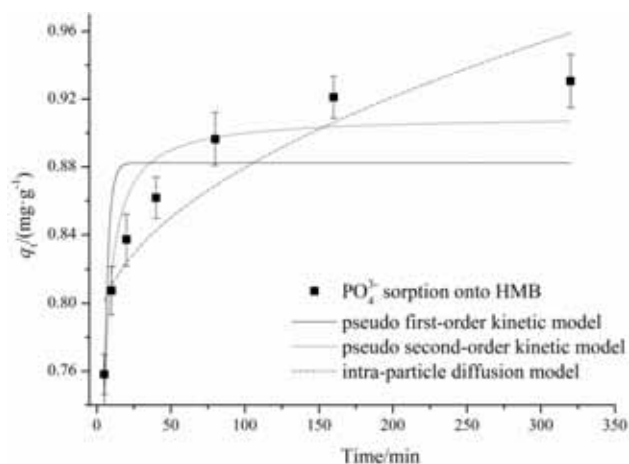


FIGURE 3
Kinetics of phosphate sorption onto HMB

TABLE 1
Kinetic parameters for nitrate and phosphate sorption onto HMB

Kinetic model	Parameter	NO ₃ ⁻	PO ₄ ³⁻
pseudo-first-order	k_1/min^{-1}	0.8092	0.8822
	$q_e/\text{mg}\cdot\text{L}^{-1}$	0.9391	0.3656
	R^2	0.8832	0.5193
pseudo-second-order	$k_2/\text{g}\cdot\text{mg}^{-1}\cdot\text{min}^{-1}$	11.7401	0.9636
	$q_e/\text{mg}\cdot\text{g}^{-1}$	0.9421	0.9101
	R^2	0.9491	0.8805

intra-particle diffusion model	$q/mg \cdot g^{-1} \cdot min^{-0.5}$	0.0007	0.0101
	R^2	0.2419	0.7892

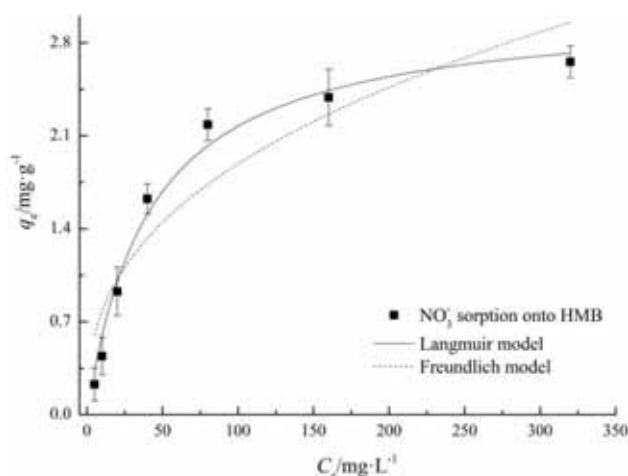


FIGURE 4
Sorption isotherm of nitrate onto HMB

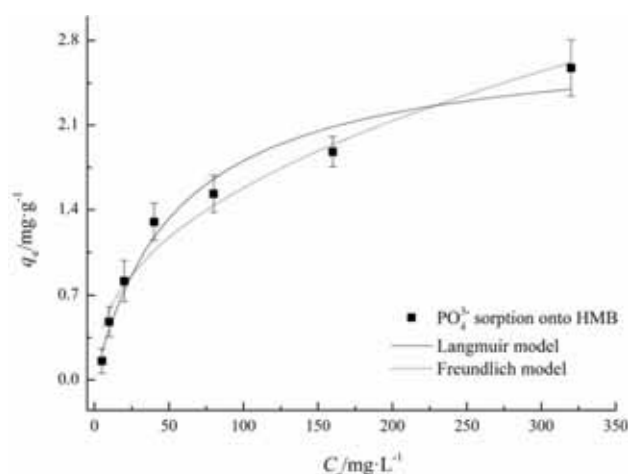


FIGURE 5
Sorption isotherm of phosphate onto HMB

Adsorption isotherms. The adsorption capacity of nitrate and phosphate by biochars itself was very limited [11, 12]. As shown in Figs. 4 and 5, with the increase in the initial concentration of nitrate and phosphate, the adsorption amounts of HMB also increase. Further suggesting the iron oxide particles serve as adsorption sites with higher capacity for nitrate and phosphate in aqueous solution [7].

The adsorption isotherms were fitted with Langmuir Equation and Freundlich Equation, which were often used to describe the adsorption process of ions onto the adsorbent as follows:

Langmuir Equation:

$$q_e = \frac{bQ_m c_e}{1 + bc_e}; \quad (4)$$

Freundlich Equation:

$$q_e = K_f c_e^{1/n}; \quad (5)$$

Where q_e is the equilibrium adsorption capacity, $mg \cdot g^{-1}$; c_e is the equilibrium concentration, $mg \cdot L^{-1}$; b is the Langmuir equilibrium constant, $L \cdot mg^{-1}$; Q_m is maximum theoretical adsorption capacity, $mg \cdot g^{-1}$; K_f is the Freundlich constant, $mg^{-1/n} \cdot g \cdot L^{-1/n}$; $1/n$ is the Freundlich exponent.

Data fitting results are provided in Table 2 and fitting curves of two models are plotted in Figs. 4 and 5. Freundlich Equation showed the better fitting results for nitrate and phosphate adsorption isotherms of HMB with the correlation coefficient (R^2) larger than 0.96.

Freundlich Equation belongs to the multilayer adsorption theory, which is more close to the practical experience [25]. It showed that the

adsorption of HMB on nitrate and phosphate was mainly based on multi molecular layer and heterogeneous adsorption model.

TABLE 2
Constants and correlation coefficient of Langmuir and Freundlich models for nitrate and phosphate sorption onto HMB

adsorbed ions	Langmuir model			Freundlich model		
	$Q_m/\text{mg}\cdot\text{g}^{-1}$	$b/\text{L}\cdot\text{mg}^{-1}$	R^2	$K/\text{mg}^{1-1/n}\cdot\text{g}^{-1}\cdot\text{L}^{-1/n}$	$1/n$	R^2
NO_3^-	3.0736	0.0241	0.8618	0.3223	0.3841	0.9819
PO_4^{3-}	2.8152	0.0178	0.9548	0.2146	0.4336	0.9659

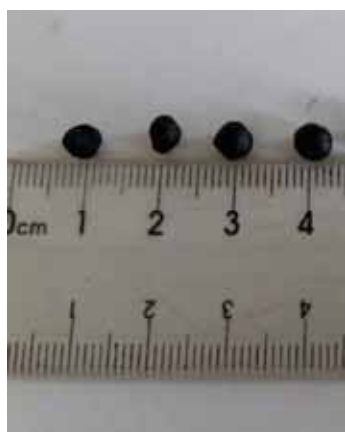


FIGURE 6a
Immobilized HMB microspheres



FIGURE 6b
Immobilized HMB microspheres

According to the Freundlich exponent of $1/n$, if $0.1 < 1/n < 1$, the adsorption process is easy; the smaller $1/n$ indicates the better adsorption effect [26]. HMB showed the better adsorption effects of nitrate and phosphate.

According to the maximum adsorption capacity of Q_m , nitrate and phosphate adsorption capacity of Q_m were $3.0736 \text{ mg}\cdot\text{g}^{-1}$ and $2.8152 \text{ mg}\cdot\text{g}^{-1}$.

The adsorption of nitrate and phosphate onto HMB could be controlled by multiple processes associated with both carbonaceous and iron oxide surfaces. Previous studies have suggested that biochar of iron loaded can encourage the formation of precipitates which can then remove phosphate from aqueous solutions [7, 27, 28].

The adsorption of nitrate and phosphate onto a solid surface is most likely controlled by the positive charge of the sorbent surface [29]. They were pre-dominantly positively charged under the experimental conditions. As a result, both the iron particles and surface functional groups of the HMB can serve as the adsorption site for nitrate and phosphate through electrostatic attractions and precipitates in aqueous solution.

Immobilized HMB microspheres. Biochar is powder and easily lost in water. In order to solve this problem, the modified biochar was immobilized. Natural sodium alginate has enough

mechanical, physical and chemical stability and does not interfere with the growth of microorganisms [30, 31]. More-over, sodium alginate is environmentally friendly and cheap [32, 33]. Therefore, this study utilized sodium alginate as embedding agent for HMB. After immobilization, we obtained the micro-spheres with the diameter of 2-3 mm as well as the complete spherical shape (Fig. 6a). HMB showed good settling characteristics (Fig. 6b).

The adsorption isotherms were fitted with Langmuir Equation and Freundlich Equation (Table 3). The maximum adsorption capacity of Q_m for nitrate and phosphate were $2.9667 \text{ mg}\cdot\text{g}^{-1}$ and $2.3301 \text{ mg}\cdot\text{g}^{-1}$. Immobilization did not significantly reduce the adsorption effect of HMB (nitrate and phosphate adsorption capacity of Q_m were $3.0736 \text{ mg}\cdot\text{g}^{-1}$ and $2.8152 \text{ mg}\cdot\text{g}^{-1}$). The immobilized HMB microspheres prepared with sodium alginate showed the high adsorption capacity, certain mechanical strength and good settling performance.

Removal efficiency of nitrate and phosphate from eutrophic water. In the eutrophic water, the nitrate and phosphate content decreased rapidly. After 5 min, the nitrate removal rate reached 65.03%. After 20 min, the removal efficiency was slowly increased and tended to be stable after sorption. After 320 min, the removal rate was the highest and reached 84.31%. After 5

min, the phosphate removal rate reached 61.81%. After 80 min, the removal efficiency was slowly increased and tended to be stable after sorption. After 320 min, the removal rate was the highest and

reached 82.06% (Fig. 7). Immobilized HMB microspheres could efficiently remove nitrate and phosphate from eutrophic water, and promote the utilization of aquatic plants.

TABLE 3
Constants and correlation coefficient of Langmuir and Freundlich models for nitrate and phosphate sorption onto immobilized HMB

adsorbed ions	Langmuir model			Freundlich model		
	$Q_m/\text{mg}\cdot\text{g}^{-1}$	$b/\text{L}\cdot\text{mg}^{-1}$	R^2	$K_f/\text{mg}^{1-1/n}\cdot\text{g}^{-1}\cdot\text{L}^{-1/n}$	$1/n$	R^2
NO_3^-	2.9667	0.0158	0.9648	0.3092	0.3864	0.9685
PO_4^{3-}	2.3301	0.0128	0.9456	0.1705	0.4239	0.9869

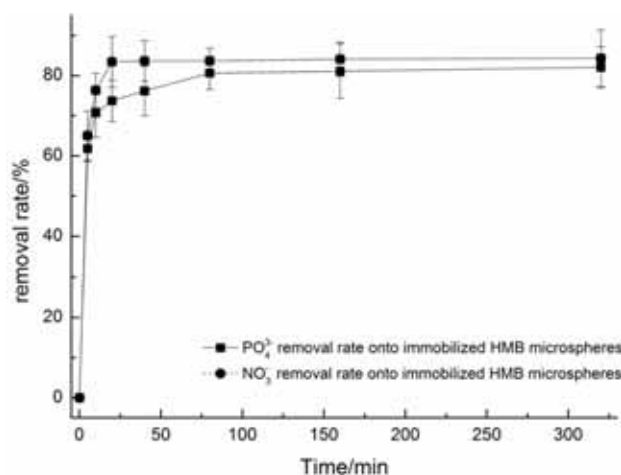


FIGURE 7
Removal efficiency of nitrate and phosphate from eutrophic water

CONCLUSIONS

Reeds and hematite are cheap and abundant natural materials. The composite material prepared with reeds and hematite through pyrolysis showed the decreased negative charge and the increased positive charge and could effectively adsorb nitrate and phosphate from aqueous solution. In order to further enhance the application of HMB in natural waters and solve the problem that powdered biochar is easily removed with water, we explored the immobilization of HMB. The adsorption capability of the immobilized HMB was not significantly decreased. Immobilized HMB microspheres could efficiently remove nitrate and phosphate from eutrophic water, and promote the utilization of aquatic plants.

ACKNOWLEDGEMENTS

This work was supported by the National Natural Science Foundation of China (No. 41401616).

REFERENCES

- [1] Wang, Z., Guo, H., Shen, F., Yang, G., Zhang, Y., Zeng, Y.. (2015) Biochar produced from oak sawdust by Lanthanum (La)-involved pyrolysis for adsorption of ammonium, nitrate, and phosphate. *Chemosphere*, 119, 646-653.
- [2] Ibelings, B.W., Portielje, R., Lammens, E.H., Noordhuis, R., van den Berg, M.S.. (2007) Resilience of alternative stable states during the recovery of shallow lakes from eutrophication: Lake Veluwe as a case study. *Ecosystems*, 10, 4-16.
- [3] Quilliam, R.S., van Niekerk, M.A., Chadwick, D.R., Cross, P., Hanley, N, David, M.. (2015) Can macrophyte harvesting from eutrophic water close the loop on nutrient loss from agricultural land? *Journal of environmental management*, 152, 210-217.
- [4] Valley, R.D., Johnson, M.B., Dustin, D.L., Jones, K.D., Lauenstein, M.R.. (2015) Combining hydroacoustic and point-intercept survey methods to assess aquatic plant species abundance patterns and community dominance. *Journal of Aquatic Plant Management*, 53, 121-129.
- [5] Krevs, A., Darginaviciene, J., Gylyte, B., Grigutyte, R., Jurkoniene, S., Karitonas, R.. (2013) Eco-toxicological effects evoked in

- hydrophytes by leachates of invasive *Acer negundo* and autochthonous *Alnus glutinosa* fallen off leaves during their microbial decomposition. *Environmental pollution*, 173, 75-84.
- [6] Zhang, W., Li, Q., Wang, X., Ding, Y. and Sun, J. (2009) Reducing organic substances from an-aerobic decomposition of hydrophytes. *Biogeo-chemistry*, 94, 1-11.
- [7] Wang, S., Gao, B., Zimmerman, A.R., Li, Y., Ma, L., Harris, W.. (2015) Removal of arsenic by magnetic biochar prepared from pinewood and natural hematite. *Bioresource technology*, 175, 391-395.
- [8] Zimmerman, A.R., Gao, B. and Ahn, M. (2011) Positive and negative carbon mineralization priming effects among a variety of biochar-amended soils. *Soil Biology and Biochemistry*, 43, 1169-1179.
- [9] Masek, O., Brownsort, P., Cross, A. and Sohi, S. (2013) Influence of production conditions on the yield and environmental stability of biochar. *Fuel*, 103, 151-155.
- [10] Al-Wabel, M.I., Al-Omran, A., El-Naggar, A.H., Nadeem, M. and Usman, A.R. (2013) Pyrolysis temperature induced changes in characteristics and chemical composition of biochar produced from *Conocarpus* wastes. *Bioresource technology*, 131, 374-379.
- [11] Mukherjee, A., Zimmerman, A.R. and Harris, W. (2011) Surface chemistry variations among a series of laboratory-produced biochars. *Geoderma*, 163, 247-255.
- [12] Yao, Y., Gao, B., Zhang, M., Inyang, M. and Zimmerman, A.R. (2012) Effect of biochar amendment on sorption and leaching of nitrate, ammonium, and phosphate in a sandy soil. *Chemosphere*, 89, 1467-1471.
- [13] Zhang, M. and Gao, B. (2013) Removal of arsenic, methylene blue, and phosphate by biochar/AlOOH nanocomposite. *Chemical engineering journal*, 226, 286-292.
- [14] Chen, B., Chen, Z. and Lv, S. (2011) A novel magnetic biochar efficiently sorbs organic pollutants and phosphate. *Bioresource technology*, 102, 716-723.
- [15] Breeuwsma, A. and Lyklema, J. (1973) Physical and chemical adsorption of ions in the electrical double layer on hematite (α -Fe₂O₃). *Journal of Colloid and Interface Science*, 43, 437-448.
- [16] Ramirez-Muniz, K., Jia, F. and Song, S. (2012) Adsorption of AsV in aqueous solutions on porous hematite prepared by thermal modification of a siderite-goethite concentrate. *Environmental Chemistry* 9: 512-520.
- [17] Dicke, C., Andert, J., Ammon, C., Kern, J., Meyer-Aurich, A., Kaupenjohann, M.. (2015) Effects of different biochars and digestate on N₂O fluxes under field conditions. *Science of The Total Environment*, 524–525, 310-318.
- [18] Hale, S.E., Alling, V., Martinsen, V., Mulder, J., Breedveld, G.D. Cornelissen, G.. (2013) The sorption and desorption of phosphate-P, ammonium-N and nitrate-N in cacao shell and corn cob biochars. *Chemosphere*, 91, 1612-1619.
- [19] Zhou, Y., Gao, B., Zimmerman, A.R., Fang, J., Sun, Y. Gao, X.. (2013) Sorption of heavy metals on chitosan-modified biochars and its biological effects. *Chemical Engineering Journal*, 231, 512-518.
- [20] Essington, M.E. (2004) *Soil and Water Chemistry: An Integrative Approach*: CRC Press. Boca Raton, London, New York, Washington, DC.
- [21] Piccin, J.S., Gomes, C.S., Feris, L.A. and Gutterres, M. (2012) Kinetics and isotherms of leather dye adsorption by tannery solid waste. *Chemical Engineering Journal*, 183, 30-38.
- [22] Toor, M. and Jin, B. (2012) Adsorption characteristics, isotherm, kinetics, and diffusion of modified natural bentonite for removing diazo dye. *Chemical Engineering Journal*, 187, 79-88.
- [23] Ho, Y. and McKay, G. (1999) Pseudo-second order model for sorption processes. *Process bio-chemistry*, 34, 451-465.
- [24] Ma, Z., Li, Q., Yue, Q., Gao, B., Li, W.. (2011) Adsorption removal of ammonium and phosphate from water by fertilizer controlled release agent prepared from wheat straw. *Chemical Engineering Journal* 171: 1209-1217.
- [25] Sposito, G. (1980) Derivation of the Freundlich equation for ion exchange reactions in soils. *Soil Science Society of America Journal*, 44, 652-654.
- [26] Raji, C. and Anirudhan, T.S. (1998) Batch Cr(VI) removal by polyacrylamide-grafted saw-dust: Kinetics and thermodynamics. *Water Research* 32: 3772-3780.
- [27] Yao, Y., Gao, B., Chen, J., Zhang, M., Inyang, M.. (2013) Engineered carbon (biochar) prepared by direct pyrolysis of Mg-accumulated tomato tissues: characterization and phosphate removal potential. *Bioresource technology*, 138, 8-13.
- [28] Yao, Y., Gao, B., Inyang, M., Zimmerman, A.R., Cao, X.. (2011) Removal of phosphate from aqueous solution by biochar derived from anaerobically digested sugar beet tailings. *Journal of hazardous materials*, 190, 501-507.
- [29] Chintala, R., Mollinedo, J., Schumacher, T.E., Papiernik, S.K., Malo, D.D., Kumar, S.. (2013) Nitrate sorption and desorption in biochars from fast pyrolysis. *Microporous and Mesoporous Materials*, 179, 250-257.
- [30] Yu, R., Liao, R., Cheng, L., Xie, Z., Wang, C. and Ma, X. (2015) Adsorption and surface precipitation of phosphate onto calcined calcite: effect of calcination temperature, pH and

- multi-variables interaction effects. *Fresen. Environ. Bull.*, 25, 3142-3149.
- [31] Motwani, S.K., Chopra, S., Talegaonkar, S., Kohli, K., Ahmad, F.J., Khar, R.. (2008) Chitosan–sodium alginate nanoparticles as submicro-scopic reservoirs for ocular delivery: formula-tion, optimisation and in vitro characterisation. *European Journal of Pharmaceutics and Bio-pharmaceutics*, 68, 513-525.
- [32] Ishikawa, K., Miyamoto, Y., Kon, M., Nagayama, M. and Asaoka, K. (1995) Non-decay type fast-setting calcium phosphate cement: composite with sodium alginate. *Bio-materials*, 16, 527-532.
- [33] L Huo, Q Yang, H Shang (2012) Kinetics and thermodynamic study of nitrate adsorption on granular ferric hydroxide. *Fresen. Environ. Bull.* 21, 789-796.

Received: 12.10.2016
Accepted: 10.02.2017

CORRESPONDING AUTHOR

Bo Wang

Institute of Eco-Environmental Sciences
Liaoning Shihua University
Fushun 113001 – CHINA

Email: 573184370@qq.com

FIRST ASSESSMENT OF MARINE LITTER IN SHALLOW SOUTH-EAST ADRIATIC SEA

Vesna Macic^{1,*}, Milica Mandic¹, Branka Pestoric¹, Zoran Gacic², Momir Paunovic³

¹Institute of Marine Biology, University of Montenegro, Kotor, Montenegro

²University of Belgrade Institute for multidisciplinary research, Belgrade, Serbia

³University of Belgrade, Institute for Biological Research "Sinisa Stankovic", Belgrade, Serbia

ABSTRACT

The typology and quantity of the marine litter was investigated in the shallow coastal area of south-east Adriatic Sea (Montenegro). Surveys were performed during the period 2012-2014 and 47 sites were analysed during underwater visual surveys by SCUBA diving. Litter items were classified in seven categories (plastic, metal, rubber, paper, clothing, glass and others) according to the nature of the material. Plastic litter was dominant (54%) followed by metal items (23%), and the density of marine litter was from 0 to 16.6/1000m² with an average of 2.49/1000m². As expected, a greater abundance of marine litter was found in the Boka Kotorska Bay and close to urbanised areas.

KEYWORDS:

litter, Adriatic Sea, shallow coastal area, pollution, SCUBA, seabed

INTRODUCTION

The marine environment faces a growing number of threats, of which four are currently considered to be the most important ones: pollution, habitat destruction, overfishing and invasive species [1]. As part of the pollution issue, various studies have dealt with marine litter (also called marine debris) over the last 50 years, but only in the last few decades serious attention has been paid to this topic [2-6]. Marine litter is any persistent, manufactured or processed solid material that is discarded, disposed of or abandoned in the marine and coastal environment [7]. Unfortunately, it is commonly observed everywhere in the oceans, drastically impacting the Mediterranean Sea, which is now one of the most affected areas [8] [9]. Harm caused by marine litter can be divided into three general categories: social (reduction in aesthetic value and public safety), economic (e.g. cost to tourism, damage to vessels, fishing gear and facilities, losses to fishery operations, cleaning costs) and ecological (mortality or sublethal effects on plants

and animals through entanglements, captures and entanglement from ghost nets, physical damage and ingestion including uptake of microparticles, mainly microplastics and the release of associated chemicals, facilitating the invasion of alien species, and altering the benthic community structure) [7].

Using figures from the North Sea and the waters around Australia, as well as from other locations, it has been estimated that up to 70% of the marine litter that enters the sea ends up on the seabed, whereas half of the remaining amount (i.e., 15%) is found on beaches and the remainder (another 15%) floats on the water surface [10]. Furthermore, it has been estimated that the weight of rubbish dumped into the world's oceans annually is 3 times the weight of caught fish [5]. From a situation that started as an aesthetic problem of littering (first of all on the beaches and floating), the number of potentially harmful implications of debris that have been identified has escalated and include the transport of persistent organic pollutants (POPs), the release of toxic compounds, the assistance of non-indigenous species transportation, the entanglement and mortality of many marine species, altering the structure of benthic communities, and socioeconomic impacts such as the threat of floating debris to navigation, reduction of the recreational value of beaches, the loss of income to the tourism industry and damage to fishing gear [5-7, 11].

Numerous international organisations, conventions, agreements and global activities have been set in place with the aim of evaluating the current state, gaps in the knowledge and priority measures. The importance of the marine litter issue is also recognised in the EU Marine Strategy Framework Directive (MSFD) [12] where, to define Good Environmental Status (GES), descriptor 10 is defined as follows: "Properties and quantities of marine litter do not cause harm to the coastal and marine environment" [13]. This is obligatory only for European countries, but as Montenegro is an EU candidate country, guidance on the monitoring of marine litter in European Seas [8] was consulted in this first assessment of the distribution, typology and quantity of the marine litter in shallow coastal areas in Montenegro (South-East Adriatic Sea).

TABLE 1
Surveyed locations and sampling period

Location	North	East	Year of Survey
iza Orahovca	42.489295°	18.752637°	2012
Inst. of marine biology	42.436545°	18.764025°	2012
iza Strpa	42.503114°	18.667054°	2012
Perast punta	42.484027°	18.705976°	2012
Perast parking	42.483694°	18.708496°	2012
Ljuta	42.483519°	18.764417°	2012
Risan	42.510139°	18.695790°	2012
Sv. Dorde	42.485295°	18.691213°	2012
Verige	42.477485°	18.690571°	2012
iza Perasta	42.494485°	18.691026°	2012
Morinj	42.488617°	18.651571°	2012
Prčanj	42.464945°	18.734818°	2012
Canj pecina	42.162484°	18.985576°	2012
Katič	42.194790°	18.9366365°	2012
Pristan (kod Kumbora)	42.426926°	18.597047°	2012
Miriste	42.394816°	18.578376°	2012
Mogren	42.274195°	18.830054°	2012
Jaz pecurke	42.277914°	18.820781°	2012
Ponta Veslo	42.365024°	18.612230°	2013
Trsteno	42.279534°	18.786392°	2013
cape Jaz	42.273355°	18.802062°	2013
cape Arza	42.390285°	18.571502°	2013
Nerin	42.306482°	18.732574°	2013
Plava spilja	42.373797°	18.596999°	2013
cape Macka	42.361599°	18.630454°	2013
cape Meret	42.018137°	19.142085°	2013
Kalafat	42.328011°	18.699792°	2013
cape Ceran	41.906307°	19.234770°	2013
Stari Ulcinj	41.991775°	19.139377°	2013
inlet Velika (Ulcinj)	41.926337°	19.196555°	2013
Velika Krekavica	42.290564°	18.750254°	2014
Zlatna vala	42.381013°	18.591764°	2014
Oblatno	42.378659°	18.653801°	2014
o. Sv. Nikola	42.269632°	18.850721°	2014
Galiola	42.269906°	18.855894°	2014
U Ploca (Dobrec)	42.411694°	18.556714°	2014
Platamuni	42.267017°	18.780903°	2014
Sv. Nedjelja	42.459214°	18.675039°	2014
Opatovo	42.461512°	18.682693°	2014
Lipci	42.494953°	18.654502°	2014
Kostanjica	42.482008°	18.679894°	2014
Sv. Nikola (Platamuni)	42.273540°	18.769822°	2014
Zli potok	42.313241°	18.719180°	2014
cape Zukovica	42.322461°	18.706758°	2014
inlet Zukovica	42.328115°	18.713633°	2014
Durdeva vala	42.309874°	18.724010°	2014
Mikovica pecina	42.072087°	18.088532°	2014

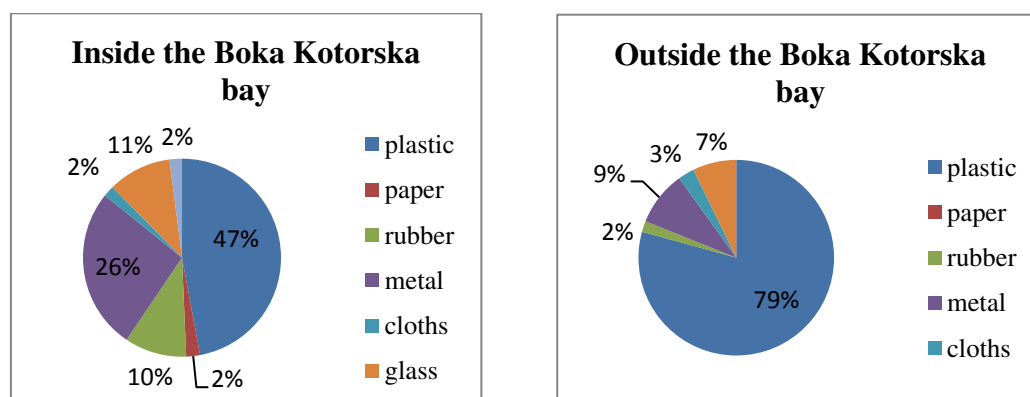


FIGURE 1
Percentage composition of the different marine litter materials inside and outside the Boka Kotorska Bay

MATERIALS AND METHODS

In the period from 2012-2014, the Institute of Marine Biology Kotor participated in different projects focused on habitat or protected species mapping and monitoring, but this was not particularly focused on marine litter monitoring. Because of the awareness of the importance of this topic, during underwater visual surveys by SCUBA diving we took the opportunity to also collect data about marine litter.

Benthic marine litter was recorded in 47 sites in Montenegro coastal waters, at depths between 0 and 40m. Names of locations, coordinates and sampling period is indicated in the Table 1. During each dive, two parallel, vertical transects 200m long and together 25m wide were checked by four divers, during a 1h dive. All found marine debris (bigger than 2.5 x 2.5cm) inside the checked area was photographed and classified into seven categories (plastic, metal, rubber, paper, clothing, glass and others) according to the nature of the material [8, 14]. Furthermore, all locations were mapped by Quantum GIS [15] and statistical Principal Component Analysis (PCA) was performed with PRIMER [16].

RESULTS

During the research period, a total of 585 items of marine litter were observed and the mean density of marine litter ranged from 0 to 16.6/1000m² with an average of 2.49/1000m². The large majority and practically more than half of the items of marine litter found (54%) were plastic materials. The second major class was belonging to metal items (23%), followed by glass (9%), rubber (8%) and cloth, paper and others (all by 2%). Comparing data for the locations inside the Boka Kotorska Bay and outside the bay (Figure 1) there is a significant difference in the percentage of the plastic, metal and rubber litter. Plastic litter was main component of the litter found outside of the bay (79%), while in the Boka Kotorska Bay it was almost half (47%). But, in the Boka Kotorska Bay percentage of metal (26%) and rubber litter (10%) was higher than on the open sea (9% and 2% consecutively).

The analysis of distribution for different categories of marine litter has shown characteristics as follows. Most of the plastic marine litter items were found in the Bay of Boka Kotorska (average 2.2 items/1000m²) and a maximum concentration of 11.6 items/1000m² was also registered in the same area. On the open sea, Budva town was also one of the hot spots (Figure 2A). In the most southern part of the coast, at two locations, we also registered a high quantity of marine litter items, some of which were in Albanian language.

Metal items were almost only registered inside the Boka Kotorska Bay (Figure 2B). The only location at the open part of the Montenegrin coast that had more than 5 items of metal debris was Kalafat. However, it is important to underline that at this location, metal debris appeared to originate from a few ship wrecks and one mine from the beginning of the 20th century. For all other locations, metal items were mostly aluminium beverage cans, followed by pots, cans, cars, anchors, domestic machines and other.

Again, the bay was the area with the highest amount of rubber items, more than 90% of which were car tires (Figure 2C). Glass items were concentrated in the inner part of the Bay and they were almost always in the form of different bottles (Figure 2D). In Figure 2E, the locations where paper items were found are shown (only inside the bay of Boka Kotorska). This type of marine litter was represented by newspapers and other small, light paper items. Cloth items, as expected, were found close to inhabited and tourist areas, mostly inside the bay, along with some other materials (Figure 2E).

According to the Principal Component Analysis (PCA), it can be seen that plastic and metal predominantly influence the position of sites in the resulting diagram (Figure 3).

Furthermore, the distribution of the marine litter items not on the basis of material category, but on the basis of fishery activity is shown in Figure 4. Here, locations with different types of nets and fishing lines (plastic), pots and anchors (metal) and ropes (other) are presented.

DISCUSSION

The highest quantity of marine litter in the area of research was in the form of plastic materials (54%). This is not only characteristic for the shallow coast of Montenegro, but is also reported for the Mediterranean Sea and other seas worldwide [17, 18]. Research carried out in the northern and central Adriatic Sea also indicates the dominance of plastic litter (34%) compared to the total amount of collected items [19]. Although plastics have only existed for just over a century, they have rapidly moved into all aspects of everyday life over the last few decades; however, unfortunately, the relevant literature leaves no doubt that plastics make up most of the marine debris worldwide. Furthermore, because of its floating properties, it is a principal component of floating marine debris or debris stranded on beaches, but not of marine debris on the sea bottom [5, 11, 17, 20]. Regardless, when plastic marine litter arrives at the sea bottom, because of its very long period of decomposition, it can persist there for decades and also accumulate in some locations, with unpredictable consequences on the marine ecosystem [5]. This is of special importance for those marine bays where,

because of low hydrodynamism, marine litter can accumulate and drastically increase quantities on the sea floor over time [14, 17]. Data from this research indicates the same situation on the coast of Montenegro. In the Bay of Boka Kotorska, we found several locations with significantly higher concentrations of marine litter than in the open sea. However, in bays, marine litter does not move far from the point of disposal, contrary to marine litter in the open sea. Close to the town of Ulcinj and the border with Albania, many, especially plastic, items of marine litter have been found with labels in Albanian language. We suppose that the transportation of marine litter by the River Bojana and also by wave action

and currents of the sea has contributed to this situation.

Close to locations where tourist facilities or settlements are located on the coast besides the "usual" plastic and metal debris (bottles, cans, food packages, etc.), a certain number of cloth items, newspapers, etc. were also found. Locations with no infrastructure on the coast were litter free in most cases, and when we found some marine debris it was from the fishery sector or composed of plastic materials.

Regarding marine litter related to fishery activities, the most diverse marine debris was found in the Boka Kotorska Bay (Fig 4). Because of the long tradition and higher intensity of fishery in this area, this result was expected.

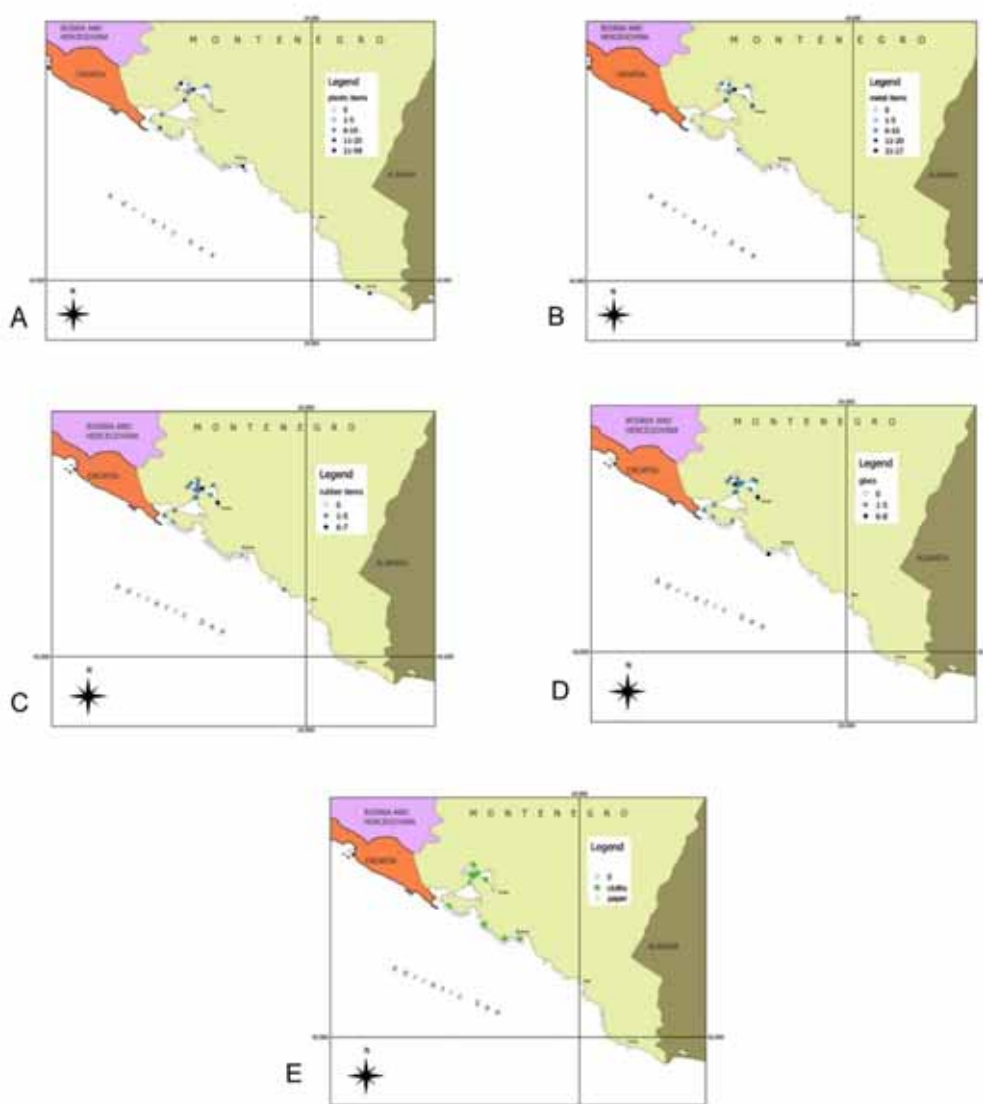


FIGURE 2

Spatial distribution of the A) plastic, B) metal, C) rubber, D) glass and E) cloths and paper litter

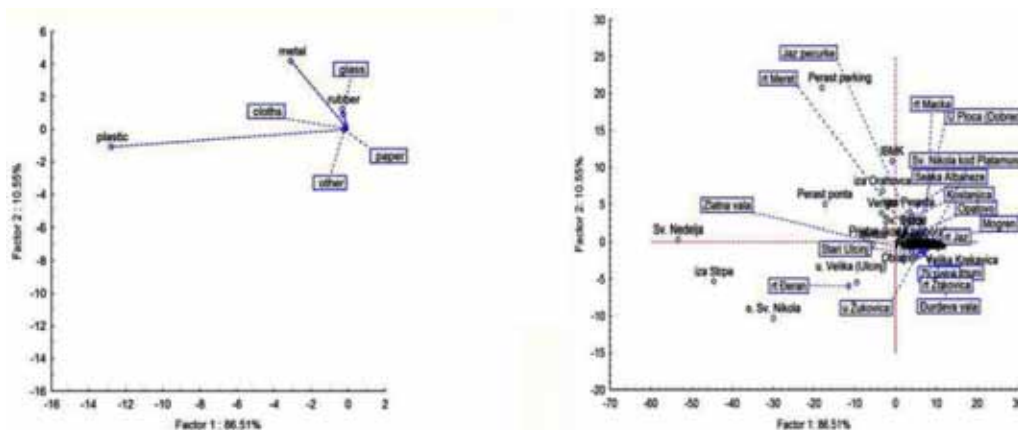


FIGURE 3
Principal Component Analysis (PCA) based on litter items category and stations

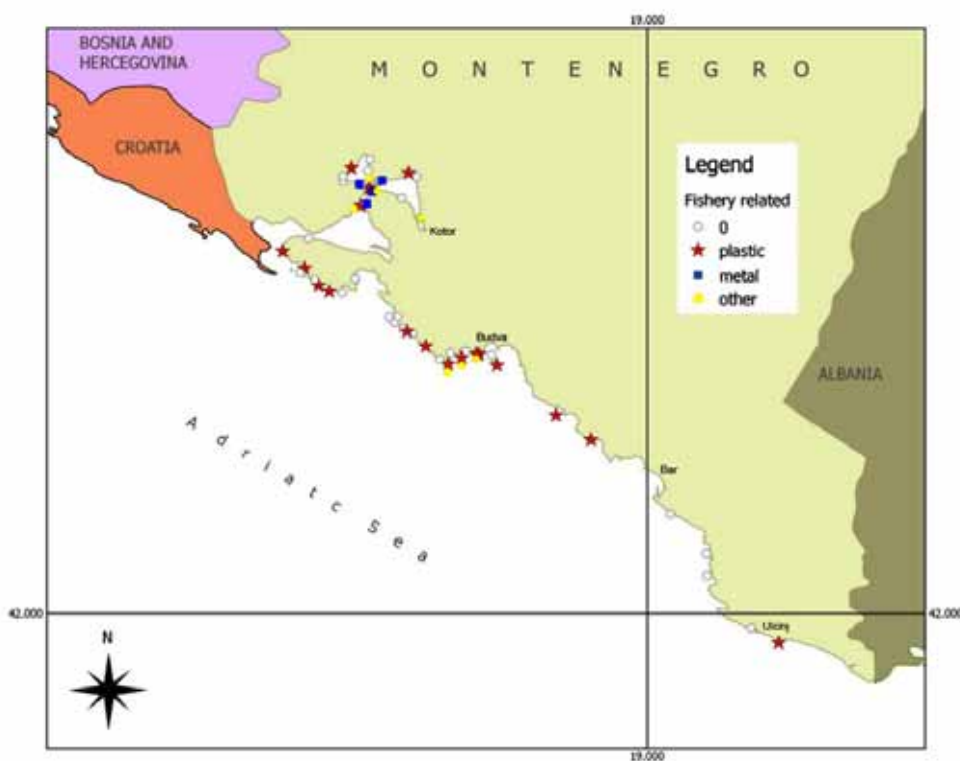


FIGURE 4
Distribution and type of marine litter items from fishery activity

Along with the expected results, such as the higher concentration of marine litter in the Boka Kotorska Bay and the dominance of plastic materials, an unexpected result was the high quantity of metal and rubber marine debris items in a few locations in the Boka Kotorska Bay. These locations are practically small underwater areas where different materials were previously dumped illegally on the coast, close to the road, and later on, because of irresponsible individuals they were dumped in the sea. The lack of appropriate measures for recycling and slow decomposition, together with a lack of awareness

and penalties, also contributed to the high quantities of glass (bottles) and rubber (tires) on the sea floor.

In general, the concentration of marine litter in the shallow coastal sea of Montenegro was lower than in some other locations of the Mediterranean and different regions of the world's oceans, but it was also higher than on the deep sea floor [5, 21]. Although scuba diving surveys were performed in different projects focused on habitat or protected species mapping and collecting of marine litter data was a secondary objective, presented information are valuable because of two main reasons. First of all these

results are first overview of the typology and quantity of the marine litter in South-East Adriatic Sea down to 40m depth. Furthermore, scuba dives were performed in all types of bottoms and on locations where bottom trawl net can not be used, while ROV, sonar and submersible are much more expensive. Another advantage of the scuba diving method is that marine litter is observed *in situ* without disturbing environment, but the limits are that only small areas can be surveyed at the time and use is restricted to shallow depths [22]. That is also the main reason why there are just a small number of such studies around the world and the most common method applied in the studies of benthic marine debris is bottom trawl net [5, 18, 21-23].

Taking into account the fact that quantities of marine litter continuously and exponentially increase the effect of marine litter on marine life and human economy, this is expected to become a more prominent issue in the future, and therefore deserves our attention and immediate action [5, 6, 17]. Many initiatives for the development of the criteria and international methodologies for the monitoring of marine litter (on the sea floor, floating, on the beaches, ingested or entanglements of animals) have been developed [6, 13, 24-26]. Furthermore, there are many other initiatives for cleaning beaches and coastal seas, testifying to the increased problems and consequently also about increased awareness. We think that additional initiatives for increasing awareness are necessary, together with the prevention of sea pollution and regional approaches, to deal with the problem of marine litter.

CONCLUSION

The present study represents the first step for the assessment of litter on the seafloor of the shallow south east Adriatic Sea. We found that in shallow coastal areas of Montenegro, the density of marine litter was from 0 to 16.6/1000m² with an average of 2.49/1000m². These values were lower than in some other areas of the Mediterranean and different regions of the world's oceans, but also higher than on the deep sea floor. Plastic litter was dominant (54%) followed by metal items (23%). As expected, a greater abundance of marine litter was found in the Boka Kotorska Bay. Furthermore, regarding marine litter related to fishery activities, the most diverse items were found also in the Boka Kotorska Bay, area where the tradition of fishery is the oldest.

Further initiatives to increase awareness are necessary, together with the prevention of pollution of the sea and regional approaches to the problem of marine litter.

ACKNOWLEDGEMENTS

This work was supported by the EU IPA project DeFishGear (grant number 1°str./00010). Furthermore, it is a secondary outcome from several projects focused on habitat or protected species mapping. These projects are: FP7 CoCoNet (grant number 287844); MedKEY habitats and MedMPAnet financially supported by UNEP RAC-SPA (Tunis) and National projects financially supported by Ministry of science of Montenegro no. 01-573/2012 and 01-574/2012.

REFERENCES

- [1] Galil, B.S. (2007) Loss or gain? Invasive aliens and biodiversity in the Mediterranean Sea. *Marine Pollution Bulletin* 55, 314-322.
- [2] Rees, G. and Pond, K. (1995) Marine litter monitoring programmes—A review of methods with special reference to national surveys. *Marine Pollution Bulletin* 30(2), 103-108.
- [3] Galgani, F., Souplet, A. and Cadiou, Y. (1996) Accumulation of debris on the deep sea floor off the French Mediterranean coast. *Mar. Ecol. Prog. Series* 142, 225-234.
- [4] Koutsodendris, A., Papatheodorou, G., Kougiourouki, O. and Georgiadis, M. (2008) Benthic marine litter in four Gulfs in Greece, Eastern Mediterranean; abundance, composition and source identification. *Estuarine, Coastal and Shelf Science* 77, 501-512.
- [5] Katsanevakis, S. (2008) Marine debris, a growing problem: sources, distribution, composition, and impacts. In: *Marine Pollution: New Research* (Hofer, T.N. Editor) Nova Science Publishers, Inc. Hauppauge NY, 53-100.
- [6] CIESM (2014) Marine litter in the Mediterranean and Black Seas. CIESM Workshop Monograph n° 46 [F. Briand, ed.], 180 p., CIESM Publisher, Monaco.
- [7] Galgani, F., Fleet, D., Van Franeker, J., Katsanevakis, S., Maes, T., Mouat, J., Oosterbaan, L., Poitou, I., Hanke, G., Thompson, R., Amato, E., Birkun, A. and Janssen, C. (2010) Marine Strategy Framework Directive Task Group 10 Report Marine litter (Zampoukas, N. Editor) European Union, IFREMER and ICES, Luxembourg, 1-57.
- [8] Galgani, F., Hanke, G., Werner, S., Oosterbaan, L., Nilsson, P., Fleet, D., Kinsey, S., Thompson, R., Franeker, J., Vlachogianni, T., Scoullou, M., Veiga J., Palatinus, A., Matiddi, M., Maes, T., Korpinen, S., Budziak, A., Leslie, H., Gago, J. and Liebezeit, G. (2013) Guidance on Monitoring of Marine Litter in European Seas. EUR 26113 EN – Joint Research Centre – Institute for

- Environment and Sustainability. EUR – Scientific and Technical Research series ISSN 1018-5593 (print) 128pp.
- [9] Suaria, G., Avio, C., Mineo, A., Lattin, G., Magaldi, M., Belmonte, G., Moore, C., Regoli, F. and Aliani, S. (2016) The Mediterranean plastic soup: synthetic polymers in Mediterranean surface waters. *Scientific Reports* 6, 37551; DOI: 10.1038/srep37551.
- [10] UNEP (2005) UNEP Regional Seas Programme, marine litter and abandoned fishing gear. Report to the Division of Ocean Affairs and the Law of the Sea, Office of Legal Affairs, UNHQ. Regional Seas Coordinating Office, UNEP, Nairobi. 30pp.
- [11] Sarafraz, J., Rajabizadeh, M. and Kamrani, E. (2016) The preliminary assessment of abundance and composition of marine beach debris in the northern Persian Gulf, Bandar Abbas City, Iran. *Journal of the Marine Biological Association of the United Kingdom*, 96(1), 131-135.
- [12] Directive 2008/56/EC (2008) EU Directive of the European Parliament and of the Council (2008) Establishing a framework for community action in the field of marine environmental policy (Marine Strategy Framework Directive) [online] <http://eur-lex.europa.eu/legal-content/EN/TXT/?uri=CELEX:32008L0056> (Accessed 15 July 2015).
- [13] EU decision 2010/477/EU (2010) EU decision on criteria and methodological standards on good environmental status of marine waters [online] <http://eur-lex.europa.eu/legal-content/EN/TXT/?uri=CELEX:32010D0477%2801%29> (Accessed 15 July 2015).
- [14] Katsanevakis, S. and Katsarou, A. (2004) Influences on the distribution of marine debris on the seafloor of shallow coastal areas in Greece (eastern Mediterranean). *Water, Air, and Soil Pollution*, 159(1), 325-337.
- [15] QGIS Software (2015) <http://www.qgis.org/en> (Accessed 10 July 2014).
- [16] Clarke, K.R. and Gorley, R.N. (2006) PRIMER v6: User Manual/Tutorial. PRIMER-E, Plymouth
- [17] Derraik, J. (2002) The pollution of the marine environment by plastic debris. *Marine Pollution Bulletin* 44, 842-852.
- [18] Pham, C., Ramirez-Llodra, E., Alt, C., Amaro, T., Bergmann, M., Canals, M., Company, J., Davies, J., Duineveld, J., Galgani, F., Howell, K., Huvenne, V., Isidro, E., Jones, D., Lastras, G., Morato, T., Nuno Gomes-Pereira, T., Purser, A., Stewart, H., Tojeira, I., Tubau, X., Van Rooij D. and Tyler, P. (2014) Marine litter distribution and density in European seas, from the shelves to deep basins. *Plos One* 9(4), e95839.
- [19] Strafella, P., Fabi, G., Spagnolo, A., Grati, F., Polidori, P., Punzo, E., Fortibuoni, T., Marceta, B., Raicevich, C., Cvitkovic, I., Despalatovic, M. and Scarcella, G. (2014) Spatial pattern and weight of seabed marine litter in the northern and central Adriatic Sea. *Marine Pollution Bulletin* 91(1), 120-127.
- [20] Laist, D.W. (1987) Overview of the biological effects of lost and discarded plastic debris in the marine environment. *Marine Pollution Bulletin* 18, 319-326.
- [21] Pasquini, G., Ronchi, F., Strafella, P., Scarcella, G. and Fortibuoni, T. (2016) Seabed litter composition, distribution and source in the Northern and Central Adriatic Sea (Mediterranean). *Waste Management* (in press)
- [22] Spenger, A. and Costa, M. (2008) methods applied in studies of benthic marine debris. *marine Pollution Bulletin* 56, 226-230.
- [23] Hanke, G., Galgani, F., Werner, S., Oosterbaan, L., Nilsson, P., Fleet, D., Kinsey, S., Thompson, R., Van Franeker, J.A., Vlachogianni, T. and Palatinus, A. (2013) Guidance on monitoring of marine litter in European seas. MSFD GES Technical Subgroup on Marine Litter (TSG-ML), Publications Office of the European Union, 124 pp.
- [24] OSPAR (2008) Background Document for the EcoQO on plastic particles in stomachs of seabirds. OSPAR Commission, Biodiversity Series. ISBN 978-1-905859-94-8 Publication Number: 355/2008. OSPAR, London, 13pp.
- [25] International Bottom Trawl Survey in the Mediterranean (Medits) (2007) Instruction manual, Version 5, April 2007.
- [26] Cheshire, A.C., Adler, E., Barbieri, J., Cohen, Y., Evans, S., Jarayabhand, S., Jeftic, L., Jung, R.T., Kinsey, S., Kusui, E.T., Lavine, I., Manjara, P., Oosterbaan, L., Pereira, M.A., Sheavly, S., Tkalin, A., Varadarajan, S., Wenneker, B. and Westphalen, G. (2009) UNEP/IOC, Guidelines on Survey and Monitoring of Marine Litter. UNEP Regional Seas Reports and Studies, No. 186; IOC, Technical Series No. 83: xii + 120 pp.

Received: 12.12.2016

Accepted: 23.06.2017

CORRESPONDING AUTHOR

Vesna Macic

Institute of Marine Biology

University of Montenegro

85330 Kotor – MONTENEGRO

E-mail: macic.v@ac.me

PREY SELECTION AND DIET COMPOSITION OF LARVAL PIKE, *ESOX LUCIUS* L., 1758, IN LAKE ISASZEG, HUNGARY

Sevil Demirci^{1,*}, Kaya Gokcek², Ahmet Bozkurt³, Tamas Szabo⁴, Bela Urbanyi⁴

¹Iskenderun Technical University, Marine Sciences and Technology Faculty, Department of Marine Technologies, Iskenderun Hatay, Turkey

²Mustafa Kemal University, Faculty of Agriculture, Department of Animal Science, Hatay, Turkey

³Iskenderun Technical University, Marine Sciences and Technology Faculty, Department of Marine Sciences, Iskenderun, Hatay, Turkey

⁴Szent Istvan University, Aquaculture Department, Godollo, Hungary

ABSTRACT

In this study, Northern Pike larvae's digestive tract contents were examined inhabiting in Isaszeg reservoir lake, Hungary. In totally 19 thousand varieties of nutrients were found out, 12 of them derived from zooplankton and 7 of them from phytoplankton. Northern Pike larvae's constitutive nutriment sources were zoological originated. Geometric Importance Index (GII) were highest for *Bosmina sp.* with 1097.49 in this specie's larval nutrition. This was followed by *Chydorus sp.* (503.836) and *Thermocyclops sp.* (493.299) respectively. Pike starts to exogenous feeding at 12 mm length. In contrast to GII, Selectivity index (SI) were revealed that *Thermocyclops sp.* were preferred by pike larvae as the main food organism.

KEYWORDS:

Larval Pike, *Esox lucius*, Diet Composition, Geometric Index of Importance (GII) Selectivity Index (SI)

INTRODUCTION

Pike (*Esox lucius* L., 1758) is an economically important fish species not only as food but also for angling. It is mostly found in freshwater lakes, rivers and estuarine regions in Northern hemisphere [1,2]. Recently, a significant decrease in its population has been observed in Europe. Over exploitation and diminishment of natural breeding sites are directly correlated to decreasing of the pike populations [3]. To protect natural stocks, recruitment should be supported in the future [4].

There is also inseparable correlation between sustainable freshwater fish populations and adequate natural foods in rivers and lakes. Especially, freshwater fish need to have a regular nourishment period in order to keep healthy ontogenic development in early stages. The availability of natural nutrients directly affects not only to the fish growing performance and health but also to population dynamics. Thus, digestive tract content and selectivity analyzes are very important to get information about ontogeny of species [5].

There are lots of studies on feeding habits on Pike [6-16], however, early larval feeding habits are still obscure [17, 18]. As well known, carnivorous fish species fed mainly on live preys after yolk sac absorptions. To make clear of feeding protocols of a candidate fish species for culture, prey selection should be revealed substantially. The main aim of this study is to present of prey preference of pike larvae in nature by geometric importance and selectivity index analyzes. By this means, growing performance and survival rates will be raised before artificial feeding under culture conditions.

MATERIALS AND METHODS

Source of pike larvae and plankton. Pike larvae were obtained from broodstock in Isaszeg, Hungary (Fig. 1). Standard production procedures were applied for production [19-21]. Fertilized eggs were hatched on 9th day and yolk sac was totally absorbed on DAH 10 at 10° C (Day after hatching, DAH). After incubation, larvae were transferred for study to the research unit of Szent Istvan University Aquaculture Department in oxygen supplied plastic bags. Plankton was harvested daily by vertically in a reservoir lake in Isaszeg, Hungary. Its mean depth is approximately 2 meters (Fig. 1).

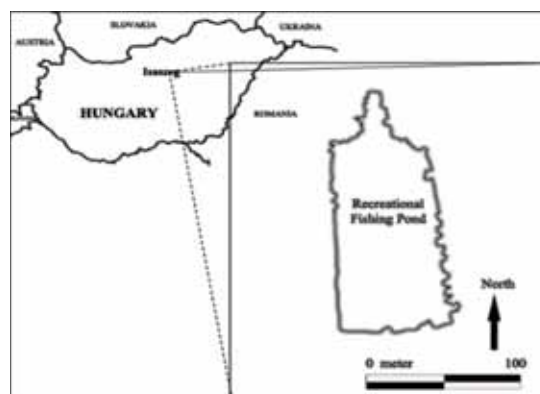


FIGURE 1
Study Area (Isaszeg, Hungary)

Experimental design and sampling. Larvae were stocked to 100 L aerated tank with 50 individuals/L. Larvae were fed 8 times a day and plankton were supplied to the tank in each feeding time. At least 12 larvae were sampled for ten days half an hour later after feeding activity once a day. Samples were collected into 3 ml Eppendorf tubes with 4% formaldehyde till the analyse day.

Geometric index of importance and selectivity index analyses. Totally 193 samples were examined and samples were classified according to length groups by using calliper gage. Larvae were dissected under stereo microscope and previous diagnostic keys were used to identification of organisms [22-26]. Then, semi or non-digested organisms were counted under inverted microscope by using Thoma slide.

Geometric Index of Importance (GII) and Selectivity index (SI) were performed to estimate the frequency of occurrence of food item and prey selection for this species [27, 28]. The formulas are below;

$$GII = (F+N+V) \cdot n^{-1}$$

Where; F: Percentage of frequency of occurrence for food items

N: Percentage of quantity

V: Percentage of volume

n: number of full of digestive tract

$$SI = (r - p) / (r + p)$$

Where; r: the share of eaten by predator preys (%)

p: the share of the left uneaten preys (%)

RESULTS AND DISCUSSION

Number of samples and the ratio of empty/full of digestive tracts, GII and Selectivity index results were given in Table 1, Fig. 2 and Fig. 3, respectively.

TABLE 1
Digestive tract's condition of samples according to size groups.

Total Length (mm)	N	Digestive system		Ratio (%)
		Empty	Filled	
11	44	42	2	95.45
12	85	55	30	64.71
13	41	19	22	46.34
14	23	4	19	17.39
Total	193	120	73	62.18

Samples were classified four length groups. The digestive tracts were almost empty in the smallest group (95.45%). By increasing of size classes, the full filled digestive tract rate of incidence was increased.

According to Fig.2, the main nutriments of pike were zooplankton and the phytoplankton were scarcely any in the diet of larvae. *Bosmina sp.* was the most preferred group (GII: 1097.49), and this was followed by *Chydorus sp.* (503.84), *Thermocyclops sp.* (493.30), *Filinia sp.* (440.66), *Keratella sp.* (438.93), *Brachionus sp.* (318.57), *Asplanchna sp.* (316.71). The other group's GII was dramatically decreased. Although *Bosmina sp.* and *Chydorus sp.* were the first two highest GII values, the SI values were determined as negative. In spite of that, *Thermocyclops sp.* were the most favored zooplankton group according to SII (+1). On the other hand, the phytoplankton were ranged as *Pediastrum sp.*, *Navicula sp.*, *Cymbella sp.*, *Fragilaria sp.*, *Synedra sp.*, *Coelastrum sp.* and *Chlorococcum sp.* according to GII values.

[18] reported that almost 60% of samples which were including 12.3-13.8 mm size group's digestive tract were empty. In this study, in contradistinction to previous study, the same empty digestive system ratio was obtained in the smallest length group (10.0-10.9 mm). Nevertheless, the percentage of full filled digestive tract samples were 46% in 12.0-12.9 mm length group.

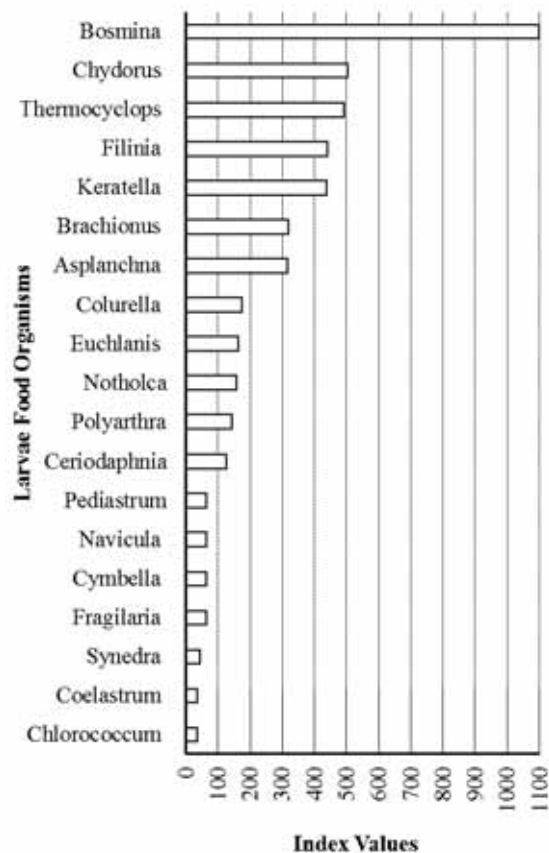


FIGURE 2
Geometric Index of Importance (GII) of Pike larvae.

According to Fig. 3, Pike larvae consumed *Bosmina sp.*, *Chydorus sp.* and *Thermocyclops sp.* as main nutriment plankton groups. The results were showed similarity with [18]. The authors were stated that pike particularly feed with *Ceriodaphnia sp.* and *Thermocyclops sp.* Furthermore, *Filinia sp.*, *Keratella sp.*, *Brachionus sp.*, *Asplanchna sp.*, *Colurella sp.* and *Euchlanis sp.* follow the formerly group as minor nutrients. On the other hand, phytoplankton were existed in biggest length group's digestive system, however the GII values were very low. This situation may be caused that phytoplankton were swallowed during feeding activity of main courses.

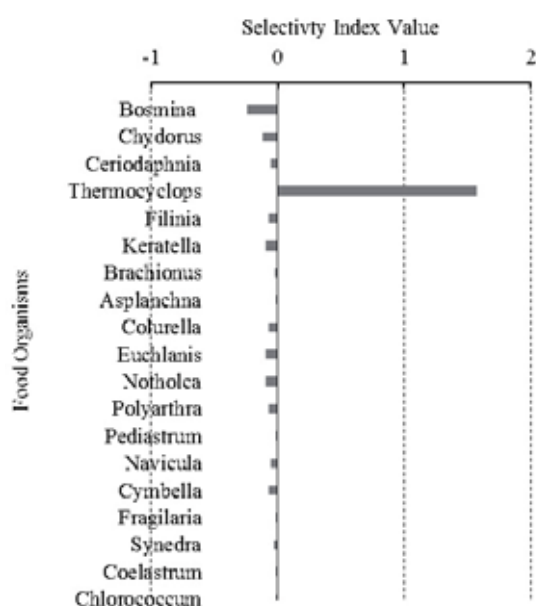


FIGURE 3
Selectivity index values of Pike larvae.

Pediastrum sp., *Navicula sp.* and *Cymbella sp.* were preferred by larvae with rate of 65.12, 64.54, and 64.21%, respectively. Even *Pediastrum sp.* were few in number in digestive tract samples, GII value were high due to its large mass. The same situation was observed for *Cymbella sp.* and *Navicula sp.* [29] reported the similar findings for *Capoeta barroisi*.

CONCLUSIONS

Plankton diversity and their morphologic and ecologic features are very important for fish larvae in nature. On the other hand, size of prey, prey visibility contrast and swim pattern have importance on feeding habits of carnivorous fish species [30]. The results showed that pike larvae were able to feed various plankton types, although they constitutively preferred zooplankton. In this study, *Bosmina sp.*

and *Chydorus sp.* were highly existed in digestive tract of pike larvae, in contrast to [18], pike preferred *Thermocyclops sp.*

REFERENCES

- [1] Zaachowski, W. (2000) Pike In: Freshwater Fishes of Poland (Ed.) Brylinska, M. Wyd. Pwn, Warszawa: 362, 368 (In Polish).
- [2] Bulut, S., Konuk, M., Uysal, K., Mert, R. and Cemek, M., (2011) Seasonal Variation in the Fatty Acid Composition and $\Omega 6/\Omega 3$ Ratio of the Pike (*Esox lucius*) Muscle Living in Karamik Lake, Turkey. Fresen. Environ. Bull., 19(10), 2227-2231.
- [3] Szabo, T., (2008) Use of Carbopol Resin for Carp Pituitary Administration Improves the Fertilization Percentage of Northern Pike (*Esox lucius* Linnaeus) Eggs in Commercial Hatcheries. Hydrobiologia, 601(1), 91-97.
- [4] Abdoli, A. and Naderi, M., (2008). Biodiversity of Fishes of the Southern Basin of the Caspian Sea. Abzeeyan Scientific Publications, Tehran, 238 pp.
- [5] Kocabatmaz, M.E. and Ekingen, G. (1978) Preliminary studies on some hematologic norms in five freshwater fish species. Journal of Firat University Faculty of Veterinary Medicine 4, 223-232.
- [6] Koz'min, A.K. (1980) The Biology of the Pike, *Esox Lucius*, From Lake Lacha. Journal of Ichthyology, 20(1) 44-48.
- [7] Karabatak, M., (1982) Aksehir Golu'ndeki Turna (*Esox Lucius* L.)'nin Buyume, Ureme ve Beslenme, Tubitak, Vhag Proje No: 392, Post-doctoral Dissertation, Ankara, 64 (In Turkish).
- [8] Giles, N., Wright, R.M. and Nord, M.E. (1986) Cannibalism in Pike Fry, *Esox Lucius* L.: Some Experiments with Fry Densities. Journal of Fish Biology, 29(1), 107-113.
- [9] Vollestad, L.A., Skurdal, J. and Qvenild, T., (1986) Habitat Use, Growth and Feeding of Pike (*Esox lucius* L.) In Four Norwegian Lakes. Archives of Hydrobiology, 108, 107-117.
- [10] Wright, R.M. and Giles, N. (1987) The Survival, Growth and Diet of Pike Fry, *Esox lucius* L., Stocked at Different Densities in Experimental Ponds. Journal of Fish Biology, 30(5), 617-629.
- [11] Aksun, F.Y. and Kuru, M. (1987) Karamik Golunde Yasayan Turna Balıklarının (*Esox lucius* L., 1758) Mide İçerikleri ve Beslenme Bilimi. Doga Türk Zooloji Dergisi, 11, 87-95 (In Turkish).
- [12] Shostak, A.W. and Dick, T.A. (1989) Helminth Position within The Intestine of Naturally Infected Pike (*Esox lucius*) Relative to Host Stomach Contents. The Journal of Parasitology, 75(6), 905-910.

- [13] Lucas, M.C. and Armstrong, J.D. (1991) Estimation of Meal Energy Intake from Heart Rate Records of Pike, *Esox lucius* L. *Journal of Fish Biology*, 38, 317-319.
- [14] Yalcin, S. (1995) Manyas (Kuş) Golu'nde Yasayan Turna Balıklarının (*Esox lucius* L. 1758) Mide İçerikleri ve Beslenme Biçimi. MSc thesis, Gazi Üniversitesi, Fen Bilimleri Enstitüsü Ankara. 62 pp (In Turkish).
- [15] Yilmaz, M. and Polat, N., (2005) Digestive System Contents of the Pike (*Esox lucius* L., 1758) Inhabiting Simenit Lake (Terme-Samsun). *Science and Engineering Journal of Firat University*, 17(3), 573-580.
- [16] Alp, A., Yegen, V., Apaydin Yagci, M., Uysal, R., Bicen, E. and Yagci, A. (2008) Diet composition and prey selection of the pike, *Esox lucius*, in Civril Lake, Turkey. *Journal of Applied Ichthyology*, 24(6), 670-677.
- [17] Morrow, J.R., James, V., Miller, G.L. and Killgore, K.J. (1997) Density, size, and foods of larval northern pike in natural and artificial wetlands. *North American Journal of Fisheries Management*, 17(1), 210-214.
- [18] Ziliukiene, V. and Ziliukas, V. (2006) Feeding of early larval pike *Esox lucius* L. reared in illuminated cages. *Aquaculture*, 258(1), 378-387.
- [19] Szabo, T. (2003) Ovulation induction in northern pike *Esox lucius* L. using different GnRH analogues, Ovaprim, Dagin and carp pituitary. *Aquaculture Research*, 34(6), 479-486.
- [20] Gokcek, K., Szabo, T., Szelei, Z. and Yilmaz, H. (2011) Extensive Culture of North Ern Pike (*Esox lucius*). *The Black Sea Journal of Science*, 2(5), 70-80.
- [21] Gokcek, K., Naz, M., Szabo, T. and Urbanyi, B. (2012) A preliminary study on protease activity of the Northern Pike (*Esox lucius* L. 1758) larvae. *Turkish Journal of Fisheries and Aquatic Sciences*, 12(4), 947-950.
- [22] Patrick, R. and Reimer, C.W. (1975) The Diatoms of Exclusive of Alaska and Hawaii. *The Academy of Naturel Sciences of Philadelphia Library of Congress Catalog Card, Philadelphia*. Volume 2, 325 pp.
- [23] Lind, E.M. and Brook, A.J. (1980) Desmids of the English Lake District. *Freshwater Biological Association Scientific Publication*, England. 320 pp.
- [24] Foged, N. (1981) Diatoms in Alaska, *J. Cramer Verlag Vaduz*, Germany. 317 pp
- [25] Korshikov, O.A. (1987) The Freshwater Algae of the Ukrainian SSR. Bishen Singh Mahendra Pal Singh and Koeltz Scientific Books, India. 624 pp.
- [26] Lund, H.C. and Lund, J.W.G. (1995) *Freshwater Algae*. Biopress Ltd, England, 526 pp.
- [27] Assis, C. (1996) Generalised Index for Stomach Contents Analysis in Fish. *Scientia Marina*, 60(2-3), 385-389.
- [28] Ivlev, V. S. (1961) *Experimental ecology of the feeding of fishes*. Yale University Press, New Haven, Connecticut, USA. 302 pp.
- [29] Demirci, S. and Yalcin Ozdilek, S. (2015). Feeding Habits of *Capoeta barroisi* (Cyprinidae) in the Asi Basin (Orontes) Turkey. *Journal of Fisheries Sciences*. 9(3), 55-62.
- [30] Buskey, E.J. (1993) Annual pattern of micro- and mesozooplankton abundance and biomass in a subtropical estuary. *Journal of Plankton Research*, 15(8), 907-924.

Received: 30.12.2016

Accepted: 06.06.2017

CORRESPONDING AUTHOR

Sevil Demirci

Iskenderun Technical University,
Marine Sciences and Technology Faculty,
Department of Marine Technologies,
31200, Iskenderun, Hatay – TURKEY

E-mail: sevil.demirci@gmail.com
sevil.demirci@iste.edu.tr

EVALUATION OF POLLUTION FROM RIVERS IN NORTHEASTERN MEDITERRANEAN REGION: HEAVY METALS

Meltem Dural Eken*, Besir Akman

Iskenderun Technical University Marine Sciences and Technology Faculty, 31200, Iskenderun, Hatay, Turkey

ABSTRACT

Samples of sediment were collected from 3 different discharge point (Ceyhan River, Payas Stream, Arsuz Brook) spilled into the Gulf of Iskenderun. The concentrations of heavy metals (Zn, Cd, Pb, Cu, Fe, Cr) were determined by using Microwave Plasma-Atomic Emission Spectrometry (MP-AES) AGILENT 4100 after applying the appropriate method based on heavy metals.

As a result of the analyses physicochemical Arsuz Brook, Payas Stream and Ceyhan River water temperature 12,15-26,00 °C, salinity ‰0,20-1,80 dissolved oxygen 5,40-10,75 mg^l⁻¹, electrical conductivity 316-742 μS/cm, pH 6,00-8,15 were fastened down. Heavy metal accumulation levels in the sediment were determined Fe>Cr>Zn>Cu>Pb>Cd in Arsuz brook, Fe>Zn>Pb>Cr>Cu>Cd in Payas stream and Fe>Cr>Zn>Cu>Pb>Cd Ceyhan river. The results of this study showed that high accumulation levels in sediment were determined Fe while low accumulation levels Cd.

KEYWORDS:

Heavy Metals, North Eastern Mediterranean, Iskenderun Bay, freshwater, sediment,

INTRODUCTION

Freshwater is fundamental to human life and monetary prosperity and social orders separate endless amounts of water from streams, lakes, wetlands, and underground aquifers to supply the necessities of urban areas, homesteads, and enterprises. Our requirement for freshwater has since quite a while ago made us disregard similarly key advantages of water that remaining parts the stream to maintain solid aquatic biological systems. Water is either polluted by humans or naturally. In recently recovered terrains, the rural and industrial activity may make diverse wellsprings of contamination. Expanding water contamination causes the decay of water quality as well as undermines human well-being and the adjust of aquatic ecosystems, financial improvement, and social thriving [1].

The sediment layer is a reservoir for pollutants. Persistent inorganic and organic contaminants can accumulate in the sediment, and for many years can be the result of accumulation, aquatic organisms and toxic effects for human health. The preservation of sediment quality, together with the protection of aquatic life, human life, and ecological balance, is important in the biological preservation and rehabilitation of water bodies on national borders. Sediment pollutants can either eliminate or reduce species that are recreational, general, or ecologically important, either directly or by affecting the food chains that sustainable populations need. Furthermore, some sediment pollutants can be bioaccumulated throughout the food chain as a consequence of physical, chemical and biological processes, or can migrate freely into the water layer on the sediment [2].

Urban streams having distinctive catchment territories and properties are examined to surmise their substantial metal commitment to the Iskenderun Bay. Particularly, there are numerous settlements through the Ceyhan River. Ceyhan is an essential town in the review territory and one of the critical mechanical communities for materials, maize drying, sustenance and refreshment, agrarian apparatus and oil preparing, and cotton-handling areas [3]. Baku-Ceyhan Unrefined petroleum Pipeline will likewise add to the key and industrial criticalness of the Ceyhan region. Though heavy metal contamination of the lower Ceyhan River catchment (Adana-Turkey) was studied [4], there is no knowledge about surface water pollution in the upper and middle basin of the Ceyhan River. These stations were detected, primarily the most polluting freshwater resources of the Gulf of Iskenderun which is Arsuz Brook, Payas Stream, and Ceyhan River.

The aim of this study was to describe the differences of Zn, Cd, Pb, Cu, Fe, Cr concentrations in the sediments of different discharge point (Ceyhan river, Payas stream, Arsuz brook) spilled into the Iskenderun Bay.



FIGURE 1
Sampling Stations
 (Station I: Arsuz Brook, Station II: Payas Stream and Station III: Ceyhan River)

MATERIALS AND METHODS

Sample Procedures. Iskenderun Bay as a result of rapid population growth and the booming industrial sector has been an area of considerable pollution problems in recent years. The development of the industry has increased ship traffic and unplanned urbanization in this area. With the opening of the Yumurtalik oil terminal for the export of Iraqi oil and the iron and steel industry in addition to this, the sewage discharged Adana to untreated Seyhan River affects the bay's water quality in a negative way [5]. These stations were detected, primarily the most polluting freshwater resources of the Gulf of Iskenderun is selected (Figure 1).

Experimental Procedures. Sampling February 2014 - is carried out between January 2015 has worked on a total of 24 sediment samples with seasonal 3-month intervals, including 2 from each station. Physicochemical parameters were measured at the stations with YSI brand devices. The sediment samples were taken from 0-10 cm layer of surface sediment at the stations. If necessary until the analysis is stored in a freezer at -18 °C. Then the collected samples were screened from the 63µm mesh plastic sieve. Samples are smaller than 63µm dried in an oven at 102 °C for 12 hours. After removal from the oven-dry samples were weighed 1 g of sample and Aqua-Regia (HCl: HNO₃ (3: 1)) was added and waited 24 hours in acids. The samples were then placed on the heater block was evaporated at 120°C until white smoke. The clarified samples after cooling filtered through a blue band paper filter completed to 50 ml with bidistilled water and made ready for measurement [6]. After dilution, metal contents

of sediment measured on an inductively coupled plasma atomic emission spectrometry (ICP-AES) (Varian model, Liberty Series II) and metal concentration in the tissue was presented as µg/g. For calibration ICP-AES was used as a High Purity Multi-Standard. All digested samples were analyzed three times for the each metal. In the study, Mustafa Kemal University Faculty of Marine Sciences and Technology Basic Sciences Laboratory and Margem is used. Data were analyzed statistically by a series of Duncan multiple range tests to identify any differences among seasons using SPSS statistical package program (a, b and c). Data shown in different letters are significant at the 0.05 level.

RESULTS AND DISCUSSION

In the study, some seasonal averages and annual averages of physicochemical parameters and heavy metals in sediment samples of some freshwater sources poured into Iskenderun Bay have been determined (Table 1, 4, 5, 6).

Water quality classes were determined according to the seasonal averages of the physicochemical parameters measured in the Arsuz Brook, Payas Stream, and Ceyhan River. Color codes are created according to water quality classes. The characteristics of the specified water quality classes have been determined (Table 2, 3).

According to the evaluation result in Table 3, Arsuz Brook, Payas Stream, and Ceyhan River have been determined as Class III- Contaminated water according to the temperature parameter in summer. Payas Stream has been determined to be Class III - Polluted water according to pH parameters during the summer season. Ceyhan River was found to be Class III- Contaminated water according to the dissolved oxygen parameter in the autumn season. Arsuz brook, Payas Stream, and Ceyhan river in other seasons, Class I-High quality water or Class II-Less contaminated water.

One of the most important elements in the river systems is sediments. Sediment is the field of harvesting, breeding, and nutrition for the survivors of the life in the aquatic system. Heavy metal contents accumulate in the sediment by sedimentation of micro-sized particles in the aquatic system. Sediments have direct and indirect effects on water quality and aquatic life. Therefore, sediment quality is an important determinant of biodiversity and water quality [8]. Sediment pollution is particularly affecting the continuity of aquatic life. The heavy metals accumulated in the sediment structure lead to changes in aquatic life and environmental conditions. With bioaccumulation, these pollution and changes extend to the upper rings of the ecological chain [9].

TABLE 1
Seasonal measurement of physicochemical parameters

Parameters	Spring			Summer			Autumn			Winter		
	A	P	C	A	P	C	A	P	C	A	P	C
T (°C)	23,75	20,25	23,15	26,00	25,50	25,75	23,00	19,55	24,60	17,10	12,15	13,75
D.O (mg ^l ⁻¹)	9,00	9,00	7,60	7,90	7,92	6,10	8,61	6,41	5,40	10,20	10,75	8,50
E.C (µS/cm)	573	316	531	588	348	535	721	494	742	637	383	689
pH	8,00	7,50	7,70	6,70	6,00	6,50	7,95	8,00	8,15	7,80	7,80	7,72

A: Arsuz Brook, P: Payas Stream ve C: Ceyhan River

T: Temperature, S: Salinity, D.O: Dissolved oxygen, E.C: conductivity

TABLE 2
Quality Criteria of Classes of Continuous Surface Water Resources [7]

Parameters	Water Quality Class			
	I	II	III	IV
Temperature(°C)	≤ 25	≤ 25	≤ 30	> 30
Dissolved Oxygen (mg ^l ⁻¹)	> 8	6-8	3-6	< 3
Conductivity (µS/cm)	< 400	400-1000	1001-3000	> 3000
pH	6,5-8,5	6,5-8,5	6,0-9,0	Outside 6,0-9,0

TABLE 3
Characteristics of Waters According to Quality Classes and Water Quality Class Color Codes ([7])

Water Quality	Characteristic	Color
Class I	High-quality water	Blue
ClassII	Less contaminated water	Green
Class III	Contaminated water	Yellow
Class IV	Highly contaminated water	Red

TABLE 4
Seasonal metal concentrations (µgg⁻¹wet weight) in sediments of Arsuz brook

Metals	Spring	Summer	Autumn	Winter	Average Annual
	$\bar{X} \pm S \bar{x}$	$\bar{X} \pm S \bar{x}$	$\bar{X} \pm S \bar{x}$	$\bar{X} \pm S \bar{x}$	$\bar{X} \pm S \bar{x}$
Fe	6366.1±4315.3 ^{ab}	9060.1±2256.2 ^{ab}	17215.2±3237.9 ^b	3079.8±1549.0 ^a	8930.3±2283.9
Zn	38.10±0.78 ^a	19.77±8.91 ^b	14.66±2.15 ^b	2.92±1.03 ^b	18.86±5.10
Cd	0.12±0.12	0.36±0.21	0.21±0.01	0.08±0.08	0.19±0.06
Cu	3.73±1.70 ^{ab}	11.43±3.69 ^a	6.65±1.53 ^{ab}	1.12±0.41 ^b	5.73±1.66
Pb	2.75±0.35 ^{ab}	3.90±1.60 ^{ab}	5.50±0.17 ^a	0.83±0.36 ^b	3.24±0.71
Cr	45.03±32.47	63.85±15.91	97.45±12.91	18.97±9.84	56.32±13.14

TABLE 5
Seasonal metal concentrations (µgg⁻¹wet weight) in sediments of Payas Stream

Metals	Spring	Summer	Autumn	Winter	Average Annual
	$\bar{X} \pm S \bar{x}$	$\bar{X} \pm S \bar{x}$	$\bar{X} \pm S \bar{x}$	$\bar{X} \pm S \bar{x}$	$\bar{X} \pm S \bar{x}$
Fe	13211.2±811.1 ^a	4899.5±1960.3 ^b	1657.9±938.9 ^b	24395.6±2259.8 ^c	11041.1±3376.9
Zn	805.19±61.19 ^a	27.77±15.53 ^b	6.43±1.07 ^b	1083.94±16.83 ^c	480.83±179.63
Cd	5.18±0.73 ^a	0.24±0.12 ^b	0.99±0.08 ^b	3.95±0.52 ^a	2.59±0.78
Cu	35.50±2.76 ^a	14.13±6.79 ^b	1.69±0.35 ^b	73.32±2.06 ^c	31.16±10.37
Pb	116.75±10.24 ^a	5.47±2.90 ^b	1.67±0.60 ^b	202.12±9.96 ^c	81.50±31.71
Cr	112.23±9.54 ^a	23.54±10.85 ^b	17.45±8.06 ^b	106.76±14.03 ^a	64.99±17.34

The present study shows that metal concentrations in the sediments tended to vary among seasons, and stations displayed particularly high levels. This

variation may be due to the differences in the sources of metal pollution and physical–chemical conditions favoring sediment contamination.

Seasonal averages and annual averages of heavy metals determined in the Arsuz brook, Payas stream, and Ceyhan river's sediment according to Duncan test results are given in Table 4, 5, 6 respectively.

According to the Duncan test results in Table 4, there is no statistical difference between Cd and Cr averages in the sediment samples taken from Arsuz Brook; Fe, Cu, and Pb were found in autumn and summer and Zn in summer and spring in higher amounts than the other seasons ($p < 0.05$). In the Arsuz Brook sediment, Fe is measured with the highest amount of $8930.3 \pm 2283.9 \mu\text{g g}^{-1}$ in the highest amount and the heavy metals are classified as $\text{Fe} > \text{Cr} > \text{Zn} > \text{Cu} > \text{Pb} > \text{Cd}$.

According to Duncan test results in Table 5, Fe, Zn, Cd, Cu, Pb, and Cr were found to be higher in winter and spring than the other seasons in sediment samples taken from Payas Stream ($p < 0.05$). It was determined that the highest amount of Fe in the Payas Stream sediment was measured with $11041.1 \pm 3376.9 \mu\text{g g}^{-1}$ and the heavy metals were classified as $\text{Fe} > \text{Zn} > \text{Pb} > \text{Cr} > \text{Cu} > \text{Cd}$.

According to the Duncan test results in Table 6, Fe, Cu and Cr were found in spring and autumn, Pb in spring and winter, and Zn in the spring and the other seasons, respectively, while there was no statistical difference between seasons in terms of Cd averages in sediment samples taken from Ceyhan River ($p < 0.05$). Ceyhan River sediment was measured with Fe at $10998.0 \pm 1581.6 \mu\text{g g}^{-1}$ at the highest annual average and it was determined that heavy metals were classified as $\text{Fe} > \text{Cr} > \text{Zn} > \text{Cu} > \text{Pb} > \text{Cd}$.

The determination of the environmental hazard dimension of the sediment layer and the establishment of standard or quality criteria for the sediment quality can be understood by comparison of the concentrations of pollutants by the toxicity and chemical analysis of the species in the sediment, the substances on these species [10].

The annual average of heavy metals in the Arsuz, Payas and Ceyhan River sediments was evaluated according to EPA (Environmental Protection Agency) Sediment quality directive. EPA (Environmental Protection Agency) Sediment quality directive is given in Table 7.

The evaluation was made on a dry weight basis. As a result of the evaluation, the accumulation of Fe, Zn, Cd, Cu, Pb in the Arsuz Brook sediment was found to be at the lowest effective concentration levels according to EPA (Environmental Protection Agency) Sediment quality directive and Cr was found above the lowest effective concentration levels. Fe accumulation in the Payas Stream sediment was above the lowest effective concentrations of Zn, Cd, Cu, Pb and Cr at low effective concentrations. The precipitation of Fe, Zn, Cd, Cu, Pb in the Ceyhan River sediment was found to be at the lowest effective concentration levels and Cr was above the lowest effective concentration levels.

Pollutants entering the stream and estuaries, particularly those in mechanical and populace focuses, has prompted to a critical increment in metal sullyng. Many reviews in various districts of the world have utilized the sediment of stream and estuaries as markers for heavy metals [12, 13, 14, 15, 16].

TABLE 6
Seasonal metal concentrations ($\mu\text{g g}^{-1}$ wet weight) in sediments of Ceyhan River

Metals	Spring	Summer	Autumn	Winter	Average Annual
	$\bar{X} \pm S_x$	$\bar{X} \pm S_x$	$\bar{X} \pm S_x$	$\bar{X} \pm S_x$	$\bar{X} \pm S_x$
Fe	13914.2 ± 539.9^a	10781.3 ± 2252.1^a	14652.7 ± 656.7^a	4643.7 ± 1401.6^b	10998.0 ± 1581.6
Zn	42.92 ± 3.04^a	23.96 ± 6.66^{ab}	19.69 ± 3.09^b	22.88 ± 5.63^b	27.36 ± 3.90
Cd	0.32 ± 0.14	0.12 ± 0.05	0.10 ± 0.02	0.08 ± 0.08	0.15 ± 0.04
Cu	12.11 ± 0.17^{ab}	10.11 ± 0.72^{ab}	15.10 ± 1.39^a	7.86 ± 2.31^b	11.29 ± 1.13
Pb	3.44 ± 0.61	1.65 ± 1.34	1.66 ± 0.59	3.47 ± 0.93	2.56 ± 0.48
Cr	44.54 ± 1.80^a	30.13 ± 6.65^{ab}	43.82 ± 3.01^a	18.19 ± 5.57^b	34.17 ± 4.47

TABLE 7
The sediment quality guidelines (mg/kg dryweight) [11]

Metals	Lowest Effective Concentration	High Effective Concentration
Fe	20000	40000
Zn	120	820
Cd	0,60	10
Cu	16	110
Pb	31	250
Cr	26	110

A number of studies on the metal distributions in river sediments and suspended particles, and on speciation of metals have been performed. Heavy metals entering the water body would be absorbed in sediments, and subsequently might migrate as a result of exchanges between water, sediment, and biota, through biological and chemical process. According to [17] concentrated the substantial metal fixations in suspended matter of a few streams in the USA, for example, the Mississippi, Susquehanna and Skunk waterways. Numerous heavy metals, for example, Cu and Pb, are involved with the sediment at Waihou Stream in Newzealand [18]. In a study on the Ceyhan river, suspended matters have high concentrations of Zn, Pb, and Cd heavy-metals, and have clues of anthropogenic pollution. Order of the heavy metals is suspended matter is Al>Mn>Ni>Cr>Pb>Zn>Co>Cu>Cd. Possible reasons for pollution are vehicle fuel remains and phosphate fertilizers. They examined water contamination by substantial metals in the Ceyhan Stream in Turkey and demonstrated the more noteworthy estimations of these metals found in the particulate stage and they expressed that waterway water could be delegated polluted with iron (Fe), aluminum (Al), and nickel (Ni), and unnecessarily sullied with lead (Pb), and cadmium (Cd) components [4]. In another review, [19] appeared there was no relationship between the increment of substantial metals and aggregate include of microbes a waterway.

In a study on agricultural land near Kosovo power plant, the heavy metal level in the agricultural soil was investigated. The results show that the content of some heavy metals (Pb, Zn, Cd, As, Cu) in the area close to the power plants is very high and often exceeds the target and even the intervention limits [20]. It has also been observed that the Payas Stream, which is close to the Demirçelik plant, has similarities with the yearly average. In another study in the same region, potato crops were examined this time. The results of this study show that the concentration of heavy metals in potato samples are from 0.78 to 32.25 mg kg⁻¹ for zinc, copper as of 2.34 to 7.55 mg kg⁻¹ and lead from 0.34 to 1.84 mg kg⁻¹. On the other hand, cadmium was below the minimal detectable value. As a result, agricultural areas near the power plant were found to be at risk for the health of local consumers [21].

Heavy metals content of river's catchment area relies on upon industrial and household waste contributions as well as on the geochemical structure of the region. High convergences of Cr is thought to have come about because of anthropogenic impacts, for all intents and purposes from industry and pesticides utilized as a part of horticulture, and are found to show a contamination hazard. Fe focuses in the Payas stream rely on upon the geochemical structure of the basin, which comprises of Fe-rich metamorphic rocks.

CONCLUSION

Iskenderun Bay is one of the settlement areas around the industrial establishments and areas under intense pollution due to the sea traffic that arises from it and also one of the regions where the terrestrial inputs are most concentrated in the northeastern Mediterranean. It is thought that the pollution load that will be formed in the freshwater sources pouring into Iskenderun Bay will cause pollution in the Gulf. Industrial Establishments should take the necessary precautions to comply with the Water Pollution Control Regulation and legal regulations. Otherwise, we think that it is inevitable to pollute water resources.

ACKNOWLEDGEMENTS

The authors gratefully acknowledge the financial support of Mustafa Kemal University (BAP 2015/11000).

REFERENCES

- [1] Milovanovic, M. (2007) Water quality assessment and determination of pollution sources along the Axios / Vardar River, Southeast Europe. *Desalination*, 213, 159-173.
- [2] USEPA (2001) Methods for Collection Storage and Manipulation of Sediments for Chemical and Toxicological Analyses: Technical Manual: EPA 823-B-01-002; US. Environmental Protection Agency, Office of Water, Washington, D.C.
- [3] Anonymous (2000) Aslantas Dam and related aspects of the Ceyhan River Basin, Turkey. A WCD case study prepared as an input to the World Commission on Dams. Agrin Co. Ltd. Cape Town. <http://www.dams.org>.
- [4] Yilmazer, D. and Yaman, S. (1999) Heavy Metal Pollution and Chemical Profile of Ceyhan River (Adana-Turkey), (in Turkish). *Turkish Journal of Engineering and Environmental Science*, 23, 59-61.
- [5] Anonymous (1997) Türkiye Kiyilarındaki Lagunlerin Yonetim ve Gelistirilme Stratejileri ve Islahi. 1. Cilt., Tarim ve Koyisleri Bakanligi Tarimsal Uretim ve Gelistirme Genel Mudurlugu, 578s.
- [6] UNEP (1984) Determination of total Cadmium, Zinc, Lead and Copper in Selected marine organisms by Flameless Atomic Absorption Spectrophotometry. Reference Methods for Marine Pollution Studies Number 11 Revision 1. http://www.iaea.org/inis/collection/NCLCollectionStore/_Public/23/062/23062642.pdf
- [7] YSKYY (2012) Yuzeysel Su Kalitesi Yonetimi Yonetmeligi. Orman ve Su Isleri Bakanligindan. Resmi Gazete, 30 November 2012, Volume: 28483. <http://www.resmigazete.gov.tr>

- //www.resmigazete.gov.tr/eskiler/2015/04/20150415-18.htm
- [8] Gale, R.J.B., Gale, S.J. and Winchester, H.P.M. (2006) Inorganic Pollution of the Sediments of The River Torrens, South Australia. *Environmental Geology*, 50, 62-75.
- [9] Kose, E. (2012) Porsuk Cayi Su, Sediment ve Bazi Balik Turlerinde Agir Metal Miktarlarinin Arastirilmesi (PhD Thesis). Dumlupinar Universitesi, Fen Bilimleri Enstitusu Biyoloji Anabilim Dalı, Kutahya, Turkiye.
- [10] Pedersen, F. and Bjornestad, E. (1988) Characterization of Sediments from Copenhagen Harbour by use of Biotests. *Water Science & Technology*, 37(6-7), 233-240. <http://wst.iwaponline.com/content/37/6-7/233>
- [11] EPA (2006) Environmental Protection Agency. Sediment kalite yonergesi. <http://www.ene.gov.on.ca/envision/gp/B1-3.pdf>.
- [12] El-Sammak, A.A. and El-Sabrouti, M.A. (1995) Assessment of metal pollution in the sediments of Lake Burullus, SE Mediterranean, Egypt. *Qatar University Science Journal*, 15: 451-455.
- [13] Binning, K. and Baird, D. (2001) Survey of heavy metals in the sediments of the Swartkops River Estuary, Port Elizabeth South Africa. *Water SA*. 27(4), 461. <http://www.wrc.org.za>
- [14] Forstner, U. and Thornton, I. (1983) Assessment of metal pollution in rivers and estuaries *Applied Environmental Geochemistry*, Academic Press, London, 395-423.
- [15] Tessier, A. and Campbell, P. (1988) Partitioning of trace metals in sediments, *Metal Speciation: Theory, Analysis and Application*, Lewis Publishers, Chelsea, MI, USA, 183-199.
- [16] Buckley, D. E., Smith, J. N. and Winters, G.V. (1995) Accumulation of Contaminant Metals in Marine Sediments of Halifax Harbour, Nova Scotia: Environmental Factors and Historical Trends. *Applied Geochemistry*. 10, 175-195.
- [17] Horowitz, A.J. (1986) Comparison of methods for the concentration of suspended sediment in river water for subsequent chemical analysis. *Environmental Science & Technology*, 20(2), 155.
- [18] Webster, J.G. (1995) Chemical processes affecting trace metal transport in the Waihou River and estuary, New Zealand. *Zealand Journal of Marine and Freshwater Research*, 29, 539.
- [19] Ezeronye, O.U. and Ubalua, A.O. (2005) Studies on the effect of abattior and industrial effluents on the heavy metals and microbial quality of Aba River in Nigeria. *African Journal of Biotechnology*. 4(3), 266-272.
- [20] Jusufi, K., Stafilov, T., Vasjari, M., Korça, B., Halili, J. and Berisha, A. (2016) Determination of Heavy Metals by ICP-AES in the Agricultural Soils Surrounding Kosovo's Power Plants. *Fresen. Environ. Bull.* 25(5) 1312-1320.
- [21] Jusufi, K., Stafilov, T., Vasjari, M., Korça, B., Halili, J. and Berisha, A. (2017) Measuring the Presence of Heavy Metals and Their Bioavailability in Potato Crops Around Kosovo's Power Plant. *Fresen. Environ. Bull.*, 26(2a), 1682-1686.

Received: 10.01.2017

Accepted: 22.06.2017

CORRESPONDING AUTHOR

Meltem Dural Eken

Iskenderun Technical University
Marine Sciences and Technology Faculty,
31200 Iskenderun, Hatay – TURKEY

E-mail: duralmeltem@yahoo.com

EFFECTS OF BRASSINOLIDE ON PHYSIOLOGICAL PARAMETERS OF *ROBINIA PSEUDOACACIA* SEEDLINGS IN CRUDE OIL CONTAMINATED SOIL

Gang Han^{1,*}, Yuanyuan Han², Kairong Li², Xiaoxi Zhang³

¹ College of Forestry, Northwest A&F University, Yangling 712100, Shaanxi, China

² College of Resources and Environment, Northwest A&F University, Yangling 712100, Shaanxi, China

³ Institute of Soil and Water Conservation, Northwest A&F University, Yangling 712100, Shaanxi, China

ABSTRACT

We conducted pot experiments to investigate the physiological effects of brassinolide on one-year-old *Robinia pseudoacacia* seedlings planted in crude oil contaminated soil. In the experiment, the oil concentration in soil of the pots was regulated to 10, 15 and 20 g/kg. The roots of seedlings were soaked in different concentrations of brassinolide (0, 0.1, 0.3 and 0.5 mg/L) before planting followed by a foliar application of brassinolide when the seedlings leafed out. After the seedlings were established, some physiological parameters were measured. The results showed that application of brassinolide significantly increased the contents of leaf osmotic regulation substances such as proline, soluble sugar and soluble protein of seedlings in different levels of crude oil contaminated soil during main growth period, simultaneously increased the activities of leaf enzymatic antioxidants including superoxide dismutase (SOD), catalase (CAT), ascorbate peroxidase (APX) and glutathione reductase (GR), as well as the contents of leaf non-enzymatic antioxidants as ascorbic acid (AsA) and glutathione (GSH), however decreased the content of leaf malondialdehyde (MDA). The best results were observed in 0.3 mg/L brassinolide treatment. The results indicate that brassinolide could alleviate the adverse effects of dehydration and toxicity of crude oil pollution on *R. pseudoacacia* seedlings by improving the osmotic regulation and antioxidant defense abilities of seedlings. Consequently, it enhances crude oil resistance of seedlings. In conclusion, treatment of seedlings with brassinolide may be a useful management tool for phytoremediation in oil contaminated areas.

KEYWORDS

Robinia pseudoacacia seedling; plant physiology; crude oil contaminated soil; brassinolide

INTRODUCTION

Brassinosteroids are natural substances which are essential for plant growth and development. It is well documented that brassinosteroids can induce a broad spectrum of responses among plants, including stem elongation, pollen tube growth, leaf growth and yield increase [1-4].

Many researchers have investigated the effects of brassinosteroids on stressed plants. Epibrassinolide treatment enhanced tolerance of tomato and brome grass to high temperature [5-6]. Application of brassinosteroids also increased in SOD and POD activities in tomato under high temperature conditions [7].

Brassinosteroids were shown to have positive effects on maize under chilling stress [8]. In rice, brassinosteroids increased seedling resistance to chilling injury [9] and increased the height, root length, root biomass, and total biomass of rice under low temperature conditions [10-11]. Wang and Zeng [9] also reported that treatment with 24-epibrassinolide reduced the MDA content, slowed the decrease in SOD activity, and increased the proline content of rice under chilling stress. The increase in chilling resistance was attributed to brassinolide-induced effects on membrane stability and osmoregulation.

Under saline conditions, 24-epibrassinolide prevented nucleus and chloroplast degradation in wheat by producing a protective effect on leaf cell ultrastructure [12]. Treatment of rice seeds with 24-epibrassinolide or 28-homobrassinolide promoted germination under salt stress. Moreover, the length, fresh and dry weights, and soluble protein content of the seedlings were enhanced. Sasse et al. [13] reported the ability of 24-epibrassinolide to activate the germination of *Eucalyptus camaldulensis* seeds under saline stress. Application of brassinosteroids increased the salinity tolerance in rice, tomato and chickpea [14-15].

Several studies have investigated the effect of brassinosteroids on water-stressed plants. Sairam [16] found that homobrassinolide significantly increased the relative water content, chlorophyll a con-

tent, photosynthetic rate, leaf area and biomass production of wheat under moisture stress. Brassinolide was also applied as plant regulator on maize to increase tolerance to drought stress [17].

Some other studies demonstrated that the brassinosteroids improved the shoot and root length, fresh and dry mass of *Brassica juncea* under copper stress [18-19]. Application of brassinosteroids reduced the impact of heavy metals stress on growth of *Chlorella vulgaris* cultures, prevented chlorophyll, sugar and protein loss [20-21]. Brassinosteroids also modified antioxidant enzyme activity in maize under heavy metals stress [22].

Many researches showed that oil pollution in soil impacted plant growth [23-26]. Xu [27] found that low concentration of oil promoted sorghum and maize growth, but high concentration of oil pollution inhibited the growth of the plant and decreased the plant biomass, especially the higher oil concentration cause irreversible damage to plants, and even lead to death of plants. In addition, the oil pollution in the soil also changes the physiological metabolism of plants. As the oil concentration increased, the soluble protein and starch content of alfalfa were decreased [28]. Soluble protein content and SOD activity of soybean were significantly decreased when the oil concentration reached 10 g/kg [29]. Song et al. [30] also found that wheat seedlings CAT activity was decreased with the increase of the concentration of active diesel pollution.

North Shaanxi is an important oil production area in China. The distribution of oil well is located at the top, slope and gully bottom of the hills in loess plateau. Crude oil contamination of soil is more serious. *Robinia pseudoacacia* is one of the species in the local area. It has developed roots and large biomass to repair oil-contaminated soil. The objective of this study was to investigate the effects of brassinolide on some important physiological parameters of *R. pseudoacacia* seedlings in crude oil contaminated soil. The results could provide an effective approach to strengthen the results of phytoremediation.

MATERIALS AND METHODS

Experimental field conditions. The experiment was conducted in the nursery of the Northwest A&F University in Shaanxi, China. The climate here is classified as continental monsoon climate of medium latitudes and the altitude is 454.5 m. The average annual sunshine hours are 2150. The average temperature is 12.9°C. The temperature over 10°C accumulates to 4185°C, frost-free period reaches 221 d and the average annual rainfall is 621.6 mm.

Plant materials and treatments. In the experiment, one-year-old *R. pseudoacacia* seedlings were from Huaziping town, Ansai County, China. The

crude oil is extracted from the same place. The soil was gathered from un-contaminated soil layer in waste grassland (0-20 cm), which contains 8.45 g/kg organic matter, 0.42 g/kg full N, 5.5 mg/kg available P, and 74.6 mg/kg available N. The concentration of petroleum in most of the contaminated soil was lower than 20 g/kg.

The experiment designs 3 levels of crude oil concentrations: 10, 15 and 20 g/kg. Add crude oil to the soil in a complete mixing way reach the designed concentrations. The soil and oil are evenly mixed with no organic solvent added, watering the mixture and let it stand [31].

In late March of 2013, seedling roots were soaked for five minutes in solutions containing 0, 0.1, 0.3 and 0.5 mg/l brassinolide and then the seedlings were planted in 31 cm×23 cm×27 cm pots where soil was treated by different crude oil concentrations as above. After planting, all pots were watered to keep the soil moisture at 75% of soil field capacity by weighing method so that the handled seedlings are all at optimum water condition. Each pot contained three seedlings. Each treatment has 9 replications. The pots were placed in a rain-out shelter.

The seedlings were sprayed with brassinolide solution when they leafed out in late April. The brassinolide concentration in the foliar spray was different for each treatment. Specifically, the brassinolide concentration in the spray was the same as the concentration that the roots had been dipped in at the beginning of the experiment.

At 9: 00 a.m. on the second day of each month from July to October respectively, the functional leaves from the middle part of the seedlings were collected and used for the determination of physiological parameters, including (1) the contents of proline, malondialdehyde, soluble sugar and soluble protein, (2) the activities of superoxide dismutase, catalase, ascorbate peroxidase and glutathione reductase and (3) the contents of ascorbic acid and glutathione. The specific methods for the determination were suggested by Li et al. [31].

Statistical analysis. Analysis of variance (GLM Univariate) was performed using SPSS software (17.0). Duncan's test was used to determine differences among treatment means at a significance level of $P < 0.05$. Origin 9.0 was used for drawing.

RESULTS AND DISCUSSION

Effects of brassinolide on osmotic regulation substances and MDA contents of seedlings. Under various crude oil contamination levels, the leaf proline, soluble sugar and protein contents of seedlings treated with brassinolide were significantly ($P < 0.05$) higher than the controls during growth period (Fig. 1). Their highest values were nearly observed in the 0.3 mg/l brassinolide treatment. However, the leaf

MDA contents of brassinolide treated seedlings were significantly ($P < 0.05$) lower compared to the controls and the lowest MDA content were almost all observed in 0.3 mg/l brassinolide treatment (Fig.1).

Petroleum can hinder water uptake of plants. This can be attributed to the hydrophobic properties of petroleum which has altered water infiltration and humidity of the soil [32]. The accumulation of osmotic regulation substances is an important mechanism of plants to survive in adversity. Several researchers have found that increased proline levels can protect plants from damage due to water stress. Lansac et al. [33] reported that proline, an osmoregulatory agent, rapidly accumulated in the leaves of water stressed plants. More importantly, proline seems to have a protective effect on plants under severe water stress [34]. Saradhi et al. [35] reported that proline protects protein structure and membranes from damage and reduces enzyme denaturation; this would minimize damage caused by dehydration [36]. A decrease in protein content in tomato plants grown under water stress was reported by Rahman et al. [37]. They postulated that water stress reduces the synthesis of protein, because of a possible suppression of the energy supply owing to reductions in photosynthesis and the overall adverse ef-

fects of the stress on the biochemical processes. Under crude oil pollution stress, brassinolide treatment increased the contents of proline, soluble sugar and protein to protect plants from damage due to oil pollution stress.

The observation that the MDA content in untreated plants increased as water stress increased agrees with the studies of bean by Zlatev et al. [38]. Temperature, drought, or salinity stress can result in oxidative damage to plant cell membranes. MDA is one of the end products of lipid peroxidation. MDA content is also a useful index to evaluate pollution levels and judge toxic effects of pollutants [39]. Increase in MDA content strengthened the idea of reactive oxygen species generation and subsequent oxidative stress by these pollutants [31]. Treatment with brassinolide resulted in a decrease in MDA of the seedling in oil contaminated soil. This suggests that brassinolide may reduce damage of plant cell membranes due to lipid peroxidation under oil contamination stress.

Bars represent \pm SE ($n = 5$). A, B and C represent 10, 15 and 20 g/kg crude oil concentration groups. Bars within the same oil concentration group followed by the different letters are significantly different at $P < 0.05$ according to Duncan's test.

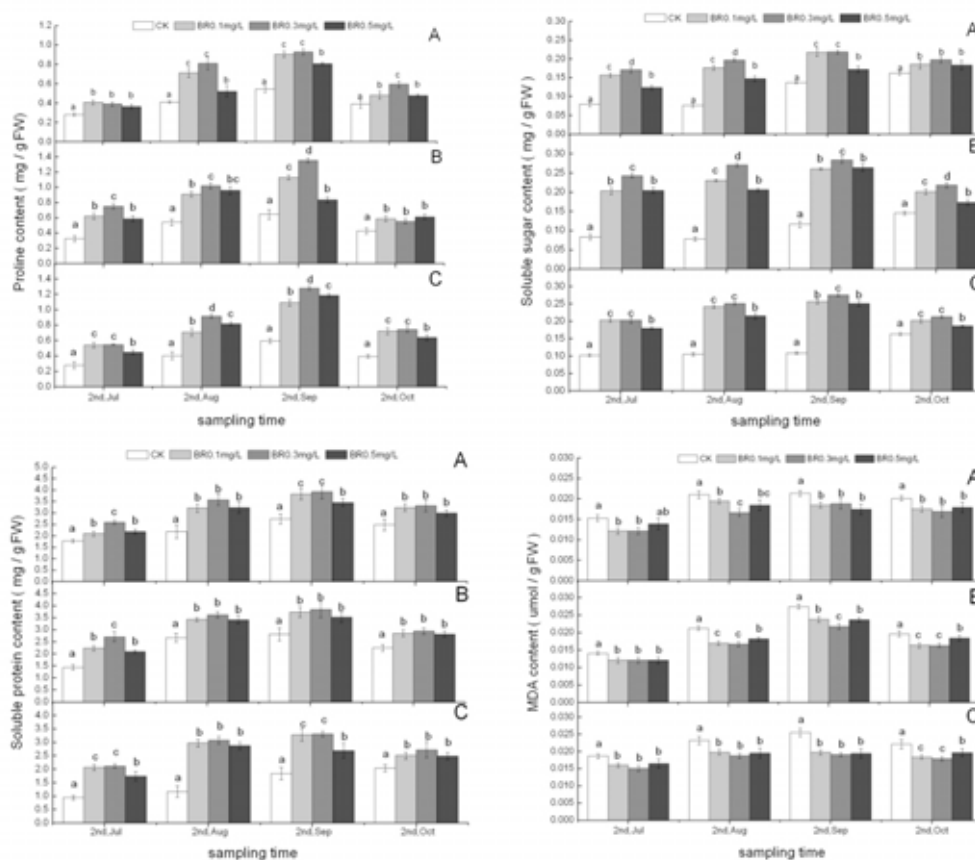


FIGURE 1

Effect of brassinolide (BL) on proline, soluble sugar and protein and MDA contents of *Robinia pseudoacacia* seedlings in crude oil contaminated soil.

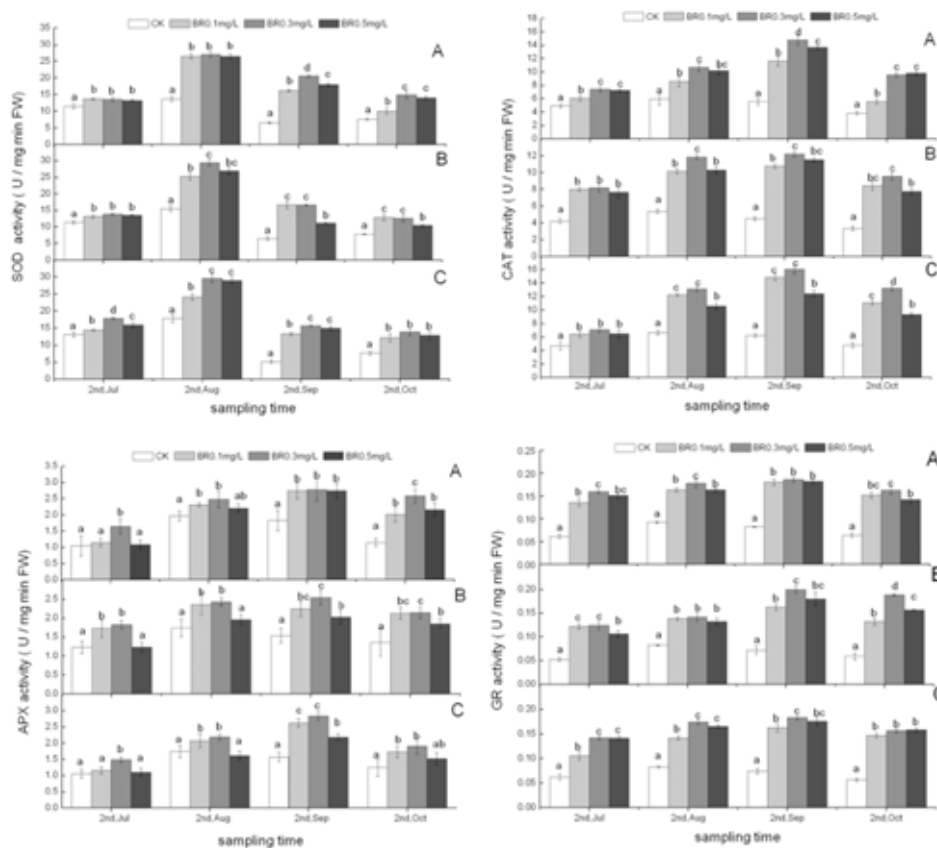


FIGURE 2

Effects of brassinolide (BL) on SOD, CAT, APX and GR activities of *Robinia pseudoacacia* seedlings in crude oil contaminated soil.

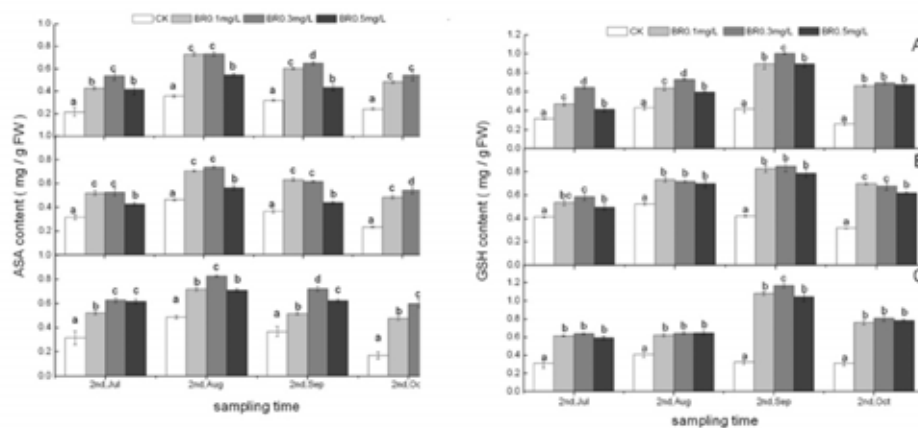


FIGURE 3

Effect of brassinolide (BL) on ASA and GSH contents of *Robinia pseudoacacia* seedlings in crude oil contaminated soil.

Effects of brassinolide on enzymatic antioxidants activities and non-enzymatic antioxidants contents of seedlings. Under various crude oil contamination levels, the leaf SOD, CAT, APX and GR activities of seedlings treated with brassinolide were significantly ($P < 0.05$) greater than the controls

(Fig.2). The highest SOD, CAT, APX and GR activities were also observed in 0.3 mg/l brassinolide treatment.

Bars represent \pm SE ($n = 5$). A, B and C represent 10, 15 and 20g/kg crude oil concentration groups. Bars within the same oil concentration group

followed by the different letters are significantly different at $P < 0.05$ according to Duncan's test.

The leaf AsA and GSH contents in brassinolide treatments under various crude oil contaminated levels were significantly greater compared to the controls (Fig.3). The AsA and GSH contents of seedlings in the 0.1 or 0.3 mg/l brassinolide treatments were significantly greater than that of 0.5 mg/l brassinolide treatments under crude oil pollution in soil.

Bars represent \pm SE ($n = 5$). A, B and C represent 10g/kg, 15g/kg and 20g/kg crude oil concentration groups. Bars within the same oil concentration group followed by the different letters are significantly different at $P < 0.05$ according to Duncan's test.

Plants have antioxidant enzymes to scavenge active oxygen species, these enzymes are postulated to be involved in the stress tolerance of plants. SOD, POD, CAT and APX are the major antioxidant enzymes associated with scavenging free oxygen radicals. SOD may be central in defending cells against toxic active oxygen species, however, SOD detoxifies superoxide anion free radicals by forming H_2O_2 , which is harmful to the chloroplast, nuclei acids and proteins [40]. Elstner and Osswald [41] reported that H_2O_2 can be eliminated by CAT and POD. Furthermore, the induction of SOD activity has been shown to coincide with an increase in POD and CAT activity [42]. Bowler et al. [44] and Scandalios [43] indicated that coordination between SOD, POD, and CAT played an important role in resisting environmental stress. APX is crucial for the removal of H_2O_2 in the cytosol and chloroplast. Inactivation of CAT and APX could result in an increase in levels of H_2O_2 inside leaf cells. Plant tissues also contain substantial amounts of carotenoids that serve as non-enzymatic oxygen radical scavengers. In addition, ascorbate can act directly as a free-radical scavenger [43]. Thus, changes in enzymatic and non-enzymatic antioxidative systems may be used to assess effects of stresses. Previous reports showed that application of brassinosteroids had a significant effect on antioxidant enzyme activity [17, 45]. Chen et al. [46] found that treatment with homobrassinolide increased SOD and POD activity in rice. Vardhini and Rao [47] reported that treatment with brassinosteroids increased CAT activity in sorghum seedlings and may have resulted in an increase in the oxidation of harmful substrates. Our research [29] found that treatment of brassinolide significantly increased POD, CAT and APX activities of *R. pseudoacacia* seedlings under mild water stress. Treatment with brassinolide significantly increased SOD, POD, CAT and APX activities in seedlings under severe water stress. The increase in SOD, POD, CAT and APX activities after treatment with brassinolide should significantly increase the tolerance of the seedlings to drought stress. In this study, Treatment with brassinolide sig-

nificantly increased SOD, CAT, APX and GR activity of *R. pseudoacacia* seedlings under oil pollution stress. ASA and GSH content were also significantly increased. The increases in these enzyme activity and antioxidant content show that brassinolide should significantly improve cell protection of the seedlings, maintain the balance of active oxygen in the plant, scavenge excessive production of active oxygen species in order to prevent possible cell damage, and significantly increase the tolerance of the seedlings to oil contaminated stress.

Our previous research discovered that under oil pollution stress, the soluble sugar content, soluble protein content, free proline content, ascorbic acid content and glutathione content as well as SOD, CAT, APX and GR activity were decreased, and MDA content was increased. The lower osmotic adjustment substances and antioxidant enzymes activity from the seedlings revealed that excessive reactive oxygen species cannot be eliminated, the normal growth of the plants were inhibited [48]. The study results showed that application of brassinolide caused a number of physiological changes in *R. pseudoacacia* seedlings. These changes included increases in soluble sugar content, soluble protein content, free proline content, ascorbic acid content and glutathione content as well as SOD, CAT, APX and GR activity, and decrease in MDA. It is suggested that brassinolide induced the tolerance by adjusting physiological process of the seedlings against crude oil pollution which was reflected by their increased growth and biomass production. The best result was obtained in the 0.3 mg/l brassinolide treatment. Overall, the results indicate that treatment with brassinolide can reduce the effects of crude oil pollution stress on *R. pseudoacacia* seedlings. Treatment of seedlings with brassinolide may be a useful management tool for phytoremediation in oil contaminated areas.

Effect of brassinolide on the growth of *Robinia pseudoacacia* seedlings. The growth of *R. pseudoacacia* seedlings are shown in Table 1. The height, root collar diameter and dry weight of the seedling grown in crude oil contaminated soil decreased with increased oil concentrations. Seedling growth in the 0.1-0.5mg/l brassinolide treatments was significantly different compared to the control under oil contamination. The height and root collar diameter of treated seedling grown in crude oil contaminated soil were significantly increased compared to the control. The dry weight of seedlings treated with brassinolide was significantly greater than untreated plants. A best effect was observed in 0.3 mg/l brassinolide treatment. The results indicated that brassinolide treatment improved the growth of *R. pseudoacacia* seedlings under oil pollution stress, which are in line with the positive effects of brassinolide on osmotic regulation and antioxidant defense abilities of seedlings.

TABLE 1

Effect of brassinolide (BL) on the growth of *Robinia pseudoacacia* seedlings in crude oil contaminated soil.

Crude oil concentration (g/kg)	BL concentration (mg/L)	Height (cm)	Root collar diameter (mm)	Dry weight (g/tree)
0	0	64.82±1.33c	9.48±0.74c	8.16±0.63d
	0	55.91±1.45a	8.06±0.44a	4.14±0.54a
	0.1	58.95±1.16b	8.92±0.40b	7.07±0.66b
	0.3	62.29±2.03c	9.02±0.62b	7.50±0.81b
	0.5	59.27±1.72b	8.76±0.38ab	6.77±0.72b
10	0	53.25±1.52a	8.04±0.38a	3.36±0.43a
	0.1	57.08±1.83b	9.50±0.40b	7.10±0.38b
	0.3	58.23±1.77b	9.58±0.42b	6.95±0.46b
	0.5	56.15±1.24b	9.26±0.48b	5.76±0.39c
15	0	53.39±1.77a	7.22±0.34a	3.41±0.45a
	0.1	56.39±1.35b	7.72±0.32ab	5.88±0.57b
	0.3	57.14±1.84b	7.86±0.28b	6.21±0.48b
	0.5	54.36±1.65ab	7.74±0.32ab	5.54±0.53b

Values in the table are mean ± SE (n = 27). Means in each column followed by different letters are significantly different at $P \leq 0.05$ according to Duncan's test.

Some research show that effect of lower concentration of oil pollution on plants is not significant. When oil pollution concentration reached 10g/kg, some wood plant growth was inhibited [49], the height, root collar diameter and biomass of *Caragana korshinskii* seedlings significantly decreased [50]. The inhibitory effect of high oil pollution on plant growth was observed in other researches [31, 51-52]. Brassinosteroids can participate in the whole process of regulating the growth and development of plants, and alleviate the damages caused by poor environmental stresses. Han et al. [53] reported that brassinolide could improve the growth of *Hippophae rhamnoides* seedlings, promote the aboveground and underground dry weight accumulation under drought conditions. In this research under oil pollution, brassinolide can promote the growth of *Robinia pseudoacacia* seedlings, and effectively alleviate the damage of oil pollution stress on the seedling.

CONCLUSIONS

Brassinolide could alleviate the adverse effects of dehydration and toxicity of crude oil pollution on *R. pseudoacacia* seedlings by improving the osmotic regulation and antioxidant defense abilities of seedlings, and improved the growth of the seedlings under oil pollution stress. In conclusion, treatment of seedlings with brassinolide may be a useful management tool for phytoremediation in oil contaminated areas.

ACKNOWLEDGEMENTS

The present research project is supported by the National Forestry Industry Research Special Funds

for Public Welfare Projects (201104002-4) and the Fundamental Research Funds for Northwest A&F University (QN2011162).

REFERENCES

- [1] Clouse, S.D. and Sasse, J.M. (1998) Brassinosteroids, essential regulators of plant growth and development. *Annu Rev Plant Physiol. Plant Mol. Biol.* 49, 427-451.
- [2] Kamuro, Y. and Takatsuto, S. (1999) Practical applications of brassinosteroids in agricultural fields. In: Sakuri, A., Yokota, T. and Clouse, S.D. (eds.), *Brassinosteroids – Steroidal Plant hormones*. Springer Tokyo, 223-241.
- [3] Khripach, V., Zhabinskii, V. and De Groot A. (2000) Twenty years of brassinosteroids, steroidal plant hormones warrant better crops for the 21st century. *Ann. Bot.* 86, 441-447.
- [4] Sasse, J.M. (1999) Physiological actions of brassinosteroids. In: Sakurai AT, Yakota SD, Clouse Eds. *Brassinosteroids, steroidal plant hormones*. Springer-Verlag Tokyo, 306-311.
- [5] Singh, I. and Shono, M. (2005) Physiological and Molecular effects of 24-epibrassinolide, a brassinosteroid on thermotolerance of tomato. *Plant Growth Reg.* 47, 111-119.
- [6] Wilen, R.W., Sacco, M., Lawrence, V.G. and Krishna, P. (1995) Effects of 24-epibrassinolide on greening and thermo tolerance of brome grass (*Bromus inermis*) cell cultures. *Physiol. Plant* 95, 195-202.
- [7] Mazonra, L.M., Nunez, M., Hechavarria, M., Coll, F. and Sanchezblanco, M.J. (2002) Influence of brassinosteroids on antioxidant enzymes activity in different temperatures. *Biol. Plant* 45, 593-596.

- [8] He, R.Y., Wang, G.J. and Wang, X.S. (1991) Effects of brassinolide on growth and chilling resistance of maize seedlings. In: Cultler, H.G., Yokota, T. and Adam, G. (eds.) *Brassinosteroids– Chemistry, Bioactivity and Application*. ACS Symp. Ser. American Chemical Society Washington DC, 220-230.
- [9] Wang, B. and Zeng, G. (1993) Effect of epibrassinolide on the resistance of rice seedlings to chilling injury. *J. Plant Physiol.* 19, 53-60.
- [10] Kim, K.S. and Sa, J.G. (1989) Effects of plant growth regulator, brassinolide, on seedling growth in rice (*Oryza sativa* L.). *Res. Rep. Rural. Devel. Administration Rice* 31, 49-53.
- [11] Hirai, K., Fujii, S. and Honjo, K. (1991) The effect of brassinolide on ripening of rice plants under low temperature condition. *Japanese J. Crop Sci.* 60, 29-35.
- [12] Kulaeva, O.N., Burkhanova, E.A. and Fedina, A.B. (1991) Effect of brassinosteroids on protein synthesis and plant-cell ultrastructure under stress conditions. In: Cultler, H.G., Yokota, T. and Adam, G. (eds.) *Brassinosteroids – Chemistry, Bioactivity and Application*. ACS Symp Ser American Chemical Society Washington DC, 141-157.
- [13] Sasse, J.M., Smith, R. and Hudson, I. (1995) Effect of 24-epibrassinolide on germination of seeds of *Eucalyptus camaldulensis* in saline conditions. *Proc. Plant Growth Regul. Soc. Amer.* 22, 136-141.
- [14] Prakash, M., Kannan, K., Kumar, J.S., Veeramani, B.B. and Ganeshan, J. (1999) Effect of brassinosteroids on germination and seedling behaviour of tomato. *Ann. Plant Physiol.* 13, 178-180.
- [15] Ali, B., Hayat, S. and Ahmad, A. (2007) 28-Homobrassinolide ameliorates the saline stress in chickpea (*Cicer arietinum* L.). *Environ. Exp. Bot.* 59, 217-223.
- [16] Sairam, R.K. (1994) Effect of homobrassinolide application on plant metabolism and grain yield under irrigated and moisture stress conditions of two wheat varieties. *Plant Growth Regul.* 14, 173-181.
- [17] Li, L. and Van Staden, J. (1998) Effects of plant growth regulators on the antioxidant system in callus of two maize cultivars subjected to crude oil pollution stress. *Plant Growth Regul.* 24, 55-66.
- [18] Sharma, P. and Bhardwaj, R. (2007) Effects of 24-epibrassinolide on growth and metal uptake in *Brassica juncea* L. under copper metal stress. *Acta Physiol. Plant* 29, 259-263.
- [19] Fariduddin, Q., Yusuf, M., Hayat, S. and Ahmad, A. (2009) Effect of 28-homobrassinolide on antioxidant capacity and photosynthesis in *Brassica juncea* plants exposed to different levels of copper. *Environ Exp. Bot.* 66, 418-424.
- [20] Bajguz, A. (2000) Blockade of heavy metals accumulation in *Chlorella vulgaris* cells by 24-epibrassinolide. *Plant Physiol. Biochem.* 38, 797-801.
- [21] Bajguz, A. (2002) Brassinosteroids and lead as stimulators of phytochelatin synthesis in *Chlorella vulgaris*. *J. Plant Physiol.* 159, 321-324.
- [22] Bhardwaj, R., Arora, N., Sharma, P. and Arora, H.K. (2007) Effects of 28-homobrassinolide on seedling growth, lipid peroxidation and antioxidative enzyme activities under nickel stress in seedlings of *Zea mays* L. *Asian J. Plant Sci.* 6, 765-772.
- [23] Ertekin, O., Erol, C., Ünlü, S., Yildizhan, Y., Pelitli, V., Yüksel, B. and Memon, A. (2011) Aliphatic hydrocarbon fingerprints in *Trifolium* spp. *Fresen. Environ. Bull.*, 20, 367-371.
- [24] Smreczak, B. and Maliszewska-Kordybach, B. (2003) Seeds germination and root growth of selected plants in PAH contaminated soil. *Fresen. Environ. Bull.*, 12, 946-949.
- [25] Onibon, V.O. and Fagbola, O. (2008) Effects of compost on remediation of crude oil polluted soil. *Fresen. Environ. Bull.*, 17, 1205-1209.
- [26] Ucak, A.B. and Bagdatli, M.C. (2017) Effects of deficit irrigation treatments on seed yield, oil ratio and water use efficiency of sunflower (*Helianthus annuus* L.). *Fresen. Environ. Bull.*, 26, 2983-2991.
- [27] Xu, D.P. and Wang, B. (2006) Effect of petroleum hydrocarbon in soil on growth of sorghum and corn. *Express Inform. Mining. Industry* 12, 28-30.
- [28] Yue, B.B., Li, X., Ren, F.F., Meng, F.J. and Sun, G.Y. (2011) Effects of petroleum contamination on some of physiological indexes of alfalfa. *Pratacultural. Sci* 28, 236-240.
- [29] Li, K.R., Wang, H.H., Han, G., Wang, Q.J. and Fan, J. (2008) Effects of brassinolide on the survival, growth and drought resistance of *Robinia pseudoacacia* seedlings under water-stress. *New For.* 35, 255-266.
- [30] Song, X.Y., Song, Y.F., Sun, T.H., Li, X.Q., Zhang, W. and Zhou, Q.X. (2006) Soil-based eco-toxicity of diesel oil contamination to seed germination and seedling growth of Wheat. *J. Agro-Environ Sci.* 25, 554-559.
- [31] Liu, H., Weisman, D., Ye, Y.B., Cui, B., Huang, Y.H., Colon-Carmona, A. and Wang, Z.H. (2009) An oxidative stress response to polycyclic aromatic hydrocarbon exposure is rapid and complex in *Arabidopsis thaliana*. *Plant Sci.* 176, 375-382.
- [32] Yavari, S., Malakahmad, A. and Sapari, N.B. (2015) A review on phytoremediation of crude oil spills. *Water Air Soil Pollu.* 226, 1-18.
- [33] Lansac, A.R., Zaballos, J.P. and Martin, A. (1994) Seasonal water potential change and proline accumulation in Mediterranean shrub species. *Vegetation* 113, 141-154.

- [34] AIn-Lhout, F., Zunzunegui, M., Diaz, M.C., Triado, R., Clavijo, A., Garcia, A. and Novo, F. (2001) Comparison of proline accumulation in two Mediterranean shrubs subjected to natural and experimental water deficit. *Plant Soil* 203, 175-183.
- [35] Saradhi, P.P., Alia, Arora, S. and Prasad, K.V.S.K. (1995) Proline accumulates in plants exposed to U V radiation and protects them against induced peroxidation. *Biophys. Res. Comm.* 290, 1-5.
- [36] Wang, H.L., Lee, P.D., Liu, L.F. and Su, J.C. (1999) Effect of sorbitol induced osmotic stress on the changes of carbohydrate and free amino acid pools in sweet potato cell suspension cultures. *Bot. Bull. Acad. Sin.* 40, 219-225.
- [37] Rahman, S.M.L., Mackay, W.A., Nawata, E., Sakuratani, T., Uddin, A.S.M.M. and Quebedeaux, B. (2004) Superoxide dismutase and stress tolerance of four tomato cultivars. *Hortscience* 39, 983-986.
- [38] Zlatev, Z.S., Lidon, F.C., Ramalho, J.C. and Yordanov, I.T. (2006) Comparison of resistance to drought of three bean cultivars. *Biologia. Plantarum* 50, 389-394.
- [39] Liao, B.H., Liu, H.Y., Zeng, Q.R., Yu, P.Z., Probst, A. and Probst, J.L. (2005) Complex toxic effects of Cd²⁺, Zn²⁺, and acid rain on growth of kidney bean (*Phaseolus vulgaris* L.). *Environ. Int.* 31, 891-895.
- [40] Fridovich, I. (1986) Biological effects of superoxide radical. *Arch. Biochem. Biophys.* 247, 1-11
- [41] Elstner, E.F. and Osswald, W. (1994) Mechanisms of oxygen activation during plant stress. *Proc. the Royal Soc. Edinburgh* 102, 131-154.
- [42] Liang, Y.C., Chen, Q. and Liu, Q. (2003) Exogenous silicon increases antioxidant enzyme activity and reduces lipid peroxidation in roots of salt-stressed barley (*Hordeum vulgare* L.). *J. Plant Physiol.* 160(10), 1157-1162.
- [43] Bowler, C., Van Montagu, M. and Inze, D. (1992) Superoxide dismutase and stress tolerance. *Annu. Rev. Plant Physiol. Plant Mol. Biol.* 43, 83-116.
- [44] Scandalios, J.G. (1990) Response of plant antioxidant defense genes to environment stress. *Adv. Genet.* 28, 1-14.
- [45] Li, L. and Van Staden, J. Effects of plant growth regulators on drought resistance of two maize cultivars. *South Afr. J. Bot.* 64, 116-120.
- [46] Chen, S.N., Li, J.N., You, H.L., Zhu, H.L., Qin, Z.B., Hong, G.M. and Shen, Y.G. (1997) The effect of a compound inducing cold resistance and homobrassinolide on chilling resistance of plateau rice. *Acta Bot. Yunnanica* 19, 184-190.
- [47] Vardhini, B.V. and Rao, S.S.R. (2003) Amelioration of osmotic stress by brassinosteroids on seed germination and seedling growth of three varieties of sorghum. *Plant Growth Regul.* 41, 25-31.
- [48] Wang, B., Li, K.R., Cui, B.X. and Han, G. (2014) Response of anti-oxidation protective system of *Robinia pseudoacacia* to petroleum contamination. *Res. Soil Water Conserv.* 21, 251-256.
- [49] Sun, W.H., Lo, J.B., Robert, F.M., Ray, C. and Tang, C.S. (2004) Phytoremediation of petroleum hydrocarbons in tropical coastal soils. I. selection of promising woody plants. *Environ. Sci. Pollu. Res. Int.* 11, 260-266.
- [50] Cui, B.X., Han, G., Li, K.R. and Wang, B. (2014) Response of growth and antioxidant protect system of *Caragana korshinskii* to oil-contaminated soil. *Pratacultural. Sci.* 31, 632-640.
- [51] Sun, Z.L., Xiao, X., Zhang, S., Wu, G.L. and Wang, Q. (2011) Tolerability of different plants for petroleum contaminated soil. *Environ. Sci. Manag.* 36, 130-132.
- [52] Li, X.L., Liu, G.B., Xue, S. and Xu, M.X. (2007) Effects of crude oil on growth of plant seedling and soil respiration in Loess Hilly Region of North Shaanxi. *J. Soil Water Conserv.* 21, 95-104.
- [53] Han, G., Han, E.X. and Li, K.R. (2007) Effects of brassinolide on several physiological indexes of *Hippophae rhamnoides* L. seedlings under water deficit. *J. Central South Univ. For. Tech.* 27, 5-9.

Received: 17.10.2016

Accepted: 16.06.2017

CORRESPONDING AUTHOR

Gang Han

College of Forestry
Northwest A&F University,
Yangling, Shaanxi – CHINA

E-mail: zxphg@nwsuaf.edu.cn.

WHEAT STRIPE RUST DISEASE: QUANTITATIVE PROFILING OF *YR10* GENE

Tulin Tascioglu¹, Yildiz Aydin², Kadir Akan³, Sandeep Kumar Verma¹,
Ozge Karakas Metin⁴, Ahu Altinkut Uncuoglu¹

¹Marmara University, Faculty of Engineering, Department of Bioengineering, 34722, Istanbul, Turkey

²Marmara University, Faculty of Arts and Sciences, Department of Biology, 34722, Istanbul, Turkey

³Central Research Institute for Field Crops, Sehit Cem Ersever Cd. No. 9-11, Yenimahalle, Ankara, Turkey

⁴TUBITAK, Marmara Research Center, Genetic Engineering and Biotechnology Institute, 41470 Kocaeli, Turkey

ABSTRACT

Yellow rust the destructive fungal disease of wheat (*Triticum aestivum* L.), caused by *Puccinia striiformis* f. sp. *tritici* (PST) results in high yield losses especially in the areas of epidemics frequently occurred in wheat all over the world. In this study, expression pattern of a yellow rust disease resistance gene (*Yr10*) in yellow rust resistant winter type bread wheat (*Triticum aestivum* L.) gene pool were investigated. *Yr10* gene real-time gene expression profile of *Yr10* gene was performed in Türkmen, Gerek79 and Avocet *Yr10* as a positive control at 7 different time points (0 hour - MOCK, 15 minutes, 12 hours, 24 hours, 48 hours, 72 hours, 96 hours) after inoculation. It was observed that the most dramatic down-regulation time point was 24 hpi for *Yr10* gene expression in all genotypes. After 24 hpi, expression pattern was followed by upregulation in all genotypes at 48 hpi. Avocet *Yr10* genotype had down-regulation pattern at 72 hpi while Türkmen and Gerek79 continue having the upregulation pattern till 96 hpi. In conclusion, expression of *Yr10* gene was fluctuated depends on short-range time scale among 3 genotypes. In the future, the increased time points for expression profiling are required for more effective evaluation of stripe rust resistance response in wheat. For better evaluations of the plant response to yellow rust attack can be done via connecting interactions among cellular responses at different molecular levels for all special crops. Our study is a good model to move forward the studies at RNA level for yellow rust resistance.

KEYWORDS:

Bread wheat, yellow rust, gene expression, real-time PCR, *Yr10* gene, inoculation.

INTRODUCTION

Wheat (*Triticum aestivum* L.) is the most important crop for Turkey, where Cafer Hoyuk, Cayonu, Can Hasan and Mersin regions were the main origins of wheat domestication [11].

A diverse group of pathogens including fungi, viruses, bacteria, and nematodes may attack wheat and cause significant yield losses. Among the fungal diseases of wheat, rusts are major disease-causing pathogens.

Turkey is the 10th largest wheat-producing country in the world with an average of 20 million tonnes per year and the economic damage caused by yellow rust as yield losses is quite serious. *Puccinia striiformis* f. sp. *tritici* is the fungal pathogen of wheat results in yellow rust disease. This pathogen also effects barley, rye and other types of cereals. Yellow rust is most frequently affecting rust disease rather than other rust diseases. In our country, inefficient seed production may cause yield loss up to 100%. Nevertheless, the yield loss caused by all types of rust diseases varying from 12-80%, while the yield loss caused by yellow rust reaches up to 100% in conditions where susceptible lines were cultivated. Fungicides are being used by most of the farmers to prevent from yield loss in wheat production. However, usage of fungicides is not an effective way to fight with the yellow rust disease because of the sharp changes at the virulence for yellow rust pathogen, also resulted in economic losses up to multimillion dollars, and it is dangerous to apply for users because of its toxic nature. The importance of the production of yellow rust resistant cultivars led scientists to determine the disease resistance genes. Currently, nearly 61 *Yr* genes were determined [17] and *Yr10* is the first race specific yellow rust resistance gene whose presence was determined in PI178383 bread wheat genotype [13]. The product of this gene is known as a protein which has a structure like *NBS-LRR* protein (R gene product). The *Yr10* gene is conserved *CC-NBS-LRR* coding gene [7]. The gain of durable disease resistance to plants should be the main objective of gene expression studies in pathogen-host interactions [9]. In a recent study, Dobon [1] was used RNA-seq technology to understand the gene expression profile of yellow rust in winter cultivar Vuka and an Avocet introgression line containing the resistance gene *Yr5*, were infected with *Puccinia striiformis* f. sp. *tritici* isolate 87/66.

TABLE 1
Primers used in this study to prove the presence of *Yr10* gene.

Primers	Sequence	T _m (°C)	T _a (°C)
Exon 1	F 5' CTT gCT ggC gAC CTg CTT A 3'	70	64,5
	R 5' TgT TTC gCT CCA CgC TgA CT 3'	70	
Exon 2	F 5' Tgg TAG TAG AgT AAT CgC AAC A 3'	68	62
	R 5' Tgg TAG TAG AgT AAT CgC AAC A 3'	66	

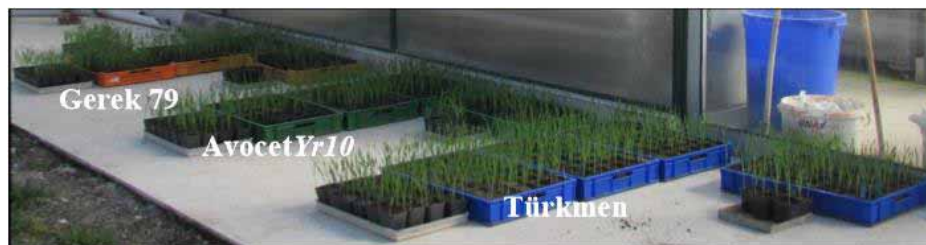


FIGURE 1
Plant material used for gene expression analysis of *Yr10*

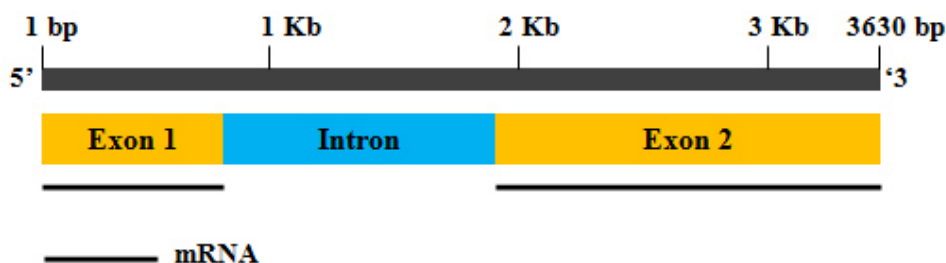


FIGURE 2
Schematic Illustration of *Yr10* Gene

For those kinds of RNA analyses, Real-time PCR technology is also a strong tool to quantify RNA levels of the specific gene or genes at the same time with a simple polymerase chain reaction. In this study, *Yr10* yellow rust resistance gene expression profile was analyzed in bread wheat cultivars (Türkmen, Gerek79 and Avocet *Yr10*) at seedling stage in seven different time points. This study is significant being the first study investigating *Yr10* gene expression profile in hours-post-inoculation at seedling stage of bread wheat.

MATERIALS AND METHODS

Selection of genotypes carrying *Yr10* gene.

Genotypes carrying *Yr10* gene (Türkmen, Gerek 79, and Avocet *Yr10*) obtained from Turkish Ministry of Food, Agriculture and Livestock, The Central Research Institute for Field Crops (CRIFC), Ankara (Fig. 1). To monitorize the expression pattern of seedling-stage yellow rust resistance gene *Yr10*, initially its presence in those genotypes was investigated by PCR analysis. The isolated DNAs were screened by specific *Yr10* gene's exon 1 and exon 2 primers (Fig. 2, Table 1) [12]. Exon 1 and exon 2 amplicons of *Yr10* gene were separated on 2% agarose gel for analysis of PCR products. GeneRulerTm 1 kb DNA ladder (Fermentas) was used to estimate the amplicon size. Electrophoresis was performed

for two hours at 200V. UViproMW Software (Version 11.02) belong to Uvitec Capturing System was used to visualize band pattern on agarose gel.

PST Supply. *Puccinia striiformis* f. sp. *tritici* was used as pathogen material for spray inoculation. Growing of plant material and spreading the inoculum of yellow rust pathogen (*Puccinia striiformis* f. sp. *tritici*) was performed at the greenhouse of the Central Research Institute for Field Crops (CRIFC), Republic of Turkey Ministry of Food, Agriculture and Livestock, Ankara.

PST Inoculation. Genotypes carrying *Yr10* gene (Türkmen and Gerek 79) confirmed by the analyses) were planted in soil and grown up till they became two weeks old. A yellow rust resistant genotype that carries *Yr10* yellow rust resistance gene, 'Avocet *Yr10*', was used as a positive control of the experiment and Little Cub genotype which is susceptible for yellow rust used as negative control to verify the success of the inoculations. Uredospores were grown on a winter wheat at its early life stage by covering with a nylon bag to avoid from any contamination of other isolates of rust fungus. The uredospores collected from the experimental research sites of CRIFC mixed with the simple oil used for spray inoculation (Fig. 3). As a negative control, mock samples were sprayed with only oil. Mock and pathogen inoculated samples were

TABLE 2
Resistance to susceptibility scale for pathogen infection

Infection type		Host response	Symptoms
Resistance	0	Immune	No visible uredia
	1	Very resistant	Necrotic flecks
	2	Resistant	Necrotic areas without sporulation
	3-4	Resistant	Necrotic and chlorotic areas with restricted sporulation
	5-6	Moderately resistant	Moderate sporulation with necrosis and chlorosis
Susceptibility	7-9	Moderately susceptible	Sporulation with chlorosis
	9	Susceptible	Abundant sporulation without chlorosis

collected at 7 different time points: 0 Hpi – mock, fifteen mpi, 12 hpi, 24 hpi, 48 hpi, 72 hpi, 96 hpi (mpi: minutes post inoculation; hpi: hours post inoculation). The first leaves of all tagged samples were collected and stored at -86°C freezer following treatment with liquid nitrogen (-196°C). Before beginning to total RNA isolations from samples, the success of inoculation was proved by phenotypic selection according to 0-9 scale given in Table 2 [10].



FIGURE 3

Inoculation of yellow rust uredospores and sampling. A: Plant material used for gene expression analysis of *Yr10*; B: Collected uredospores mixed with the simple oil used for spray inoculation; C, D: Negative control (Mock samples sprayed with only oil) and yellow rust inoculated plant material; E: All inoculated samples were kept at greenhouse; F, G: Primary leaf tissues from two leaf stage plants were taken to aluminum foils and kept at liquid nitrogen; H: All samples per each time point were kept at -86°C for further expressional studies.

RNA Isolation. The collected leaf samples were isolated following Roche's Protocol by using "Trizol Reagent". Total RNAs were separated on 1%

agarose gel stained by RedSafe (Intron Biotechnology, Catalog No: 21141) and visualized under UV light by MiniBIS Pro Visualizing System (DNr Bio-Imaging Systems). RNA samples were treated with DNase to avoid from DNA contamination. RNA dilutions were prepared for each sample in total volume of 15.5 µl for final 10 µg/µl RNA concentration. 1.5 µl of DNase (Promega) and 3 µl of DNase Reaction Buffer were dissolved in 10 µl dH₂O. Following, 10 µg/µl RNA samples were combined with DNase; then the mixture was incubated at 37°C for 10 minutes for DNase activation. RNA samples were used as template for 18S ribosomal DNA PCR to evaluate if there is any DNA contamination or not. With this aim; a PCR reaction was conducted at 25 µl volume in an Applied Biosystem GeneAmp® 9700 PCR System. 18S rDNA PCR products were loaded to 1.5% agarose gel and electrophoresis was run at 150V and a 100 bp marker (New England Biolabs) was used as marker. RNA samples (10µg/µl) were diluted (1/5) and RNA template (2 µg/µl) were used for first chain synthesis as complementary DNA. As biological control; three replicates of RNA samples per each genotype for each time point was pooled.

cDNA Synthesis. The RT-PCR (cDNA synthesis) was performed using 'High Capacity cDNA Reverse Transcription Kit, ABI' (Catalog No: 4368814). 10 µl of 2X master mix and 10 µl of diluted RNA were mixed to total volume at 20 µl at reverse transcriptase PCR. PCR reaction was performed at Applied Biosystem GeneAmp® 9700 PCR System.

Real Time PCR (Q-PCR). The RNAs which converted into cDNA by previous RT-PCR analyses were used as template for the *Yr10* gene expression analyses. The analyses were performed at StepOneTm Software (v2.2.2) at Real-Time PCR System, ABI (Catalog No: 4376600). Actin Beta and GAPDH (Glyceraldehyde-3-Phosphate Dehydrogenase) genes were used as multiple controls. Power Sybr® Green Master Mix, ABI (Catalog No: 4367659) was used for the detection of the amplification.

RESULTS

Presence of *Yr10* gene in wheat gene pool.

PCR analyses by *Yr10* gene-specific primers showed that there were exon 1 and exon 2 amplifications only in Türkmen and Gerek 79 genotypes from our gene pool as shown in Figure 4 and Figure 5. Türkmen, Gerek 79 and 'Avocet *Yr10*' genotypes were used as plant material both for validation and real-time PCR studies.

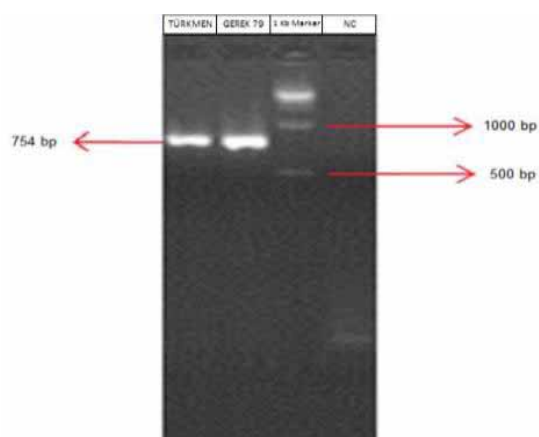


FIGURE 4

A single band at the band size of 754 (bp) obtained from PCR reaction by using exon 1 primer pair of *Yr10* gene at 2% agarose gel. Türkmen; Gerek 79; M: GeneRuler™ 1 Kb DNA Ladder (Fermentas); NC: Negative control.

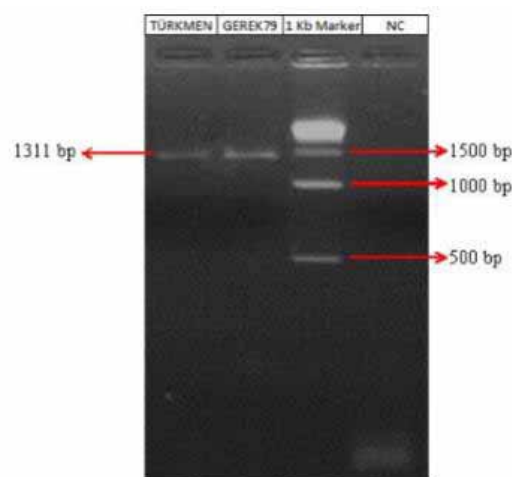


FIGURE 5

A single band obtained from PCR reaction by using exon 2 primer pairs of *Yr10* gene at 2% agarose gel. Türkmen; Gerek 79; M: GeneRuler™ 1 Kb DNA Ladder (Fermentas); NC: Negative control.

Validation of inoculation. After sampling, the accuracy of the infections were monitored and scored according to 0-9 scale given in Table 2. The scoring results were given in Table 3, 4, and 5. 'Little Cub' genotype were used a positive control of the infections because of its susceptible nature to yellow rust. The infected plant leaves were screened and shown in Figure 6.

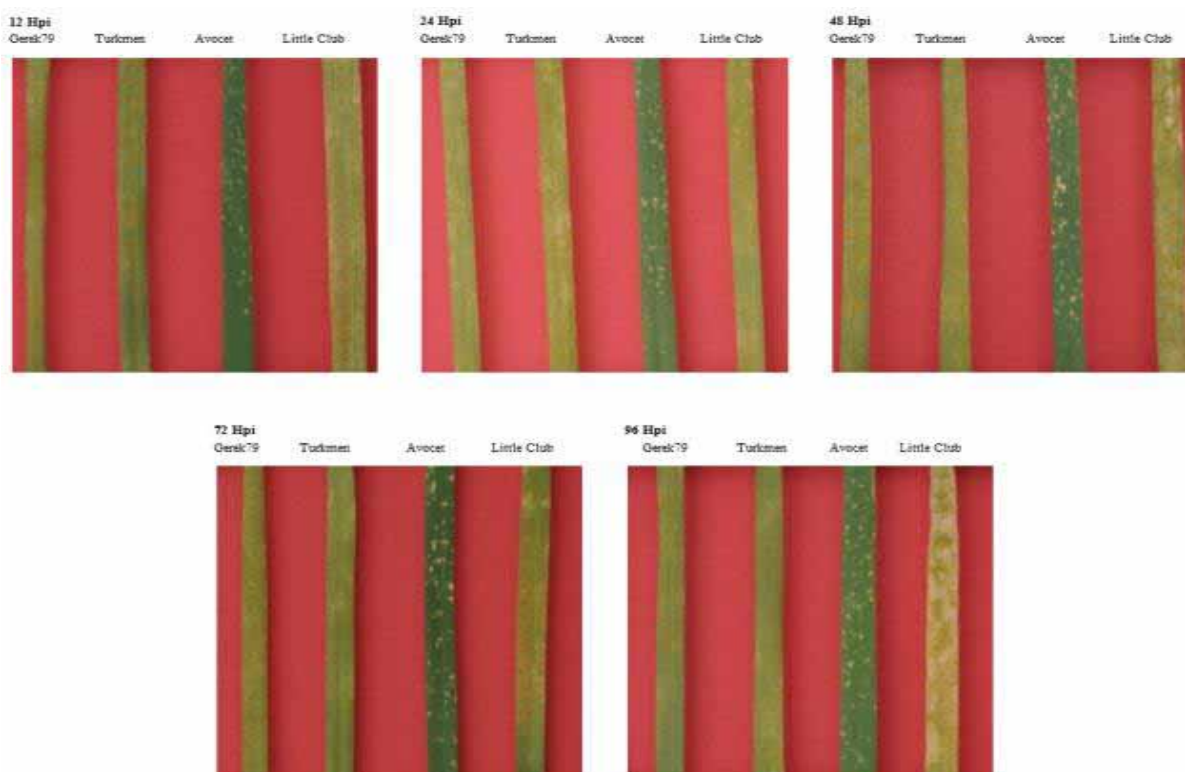


FIGURE 6

The inoculation results on infected leaves at 12, 24, 48, 72 and 96 hpi (Hypersensitive response was observed at Avocet *Yr10* genotype at all-time points)

TABLE 3

Inoculation scores of Türkmen genotype								
TÜRKMEN								
N	0 hpi	-	00:15	12	24	48	72	96
o	Mock	mpi	hpi	hpi	hpi	hpi	hpi	hpi
1	0		7	8	8	8	8	7
2	0		7	8	8	8	8	7
3	0		7	8	8	8	7	8

TABLE 4

Inoculation scores of Gerek 79 genotype								
GEREK 79								
N	0 hpi	-	00:15	12	24	48	72	96
o	Mock	mpi	hpi	hpi	hpi	hpi	hpi	hpi
1	0		8	8	7	8	7	7
2	0		8	8	7	7	8	7
3	0		8	7	8	7	7	7

TABLE 5

Inoculation scores of Avocet <i>Yr10</i> genotype								
AVOCET ' <i>Yr10</i> '								
N	0 hpi	-	00:15	12	24	48	72	96
o	Mock	mpi	hpi	hpi	hpi	hpi	hpi	hpi
1	0		1	1	1	1	1	1
2	0		0	1	1	1	1	1
3	0		1	1	1	1	1	1

Total RNA isolation. DNase-treated RNAs of samples were loaded on 1.5% DEPC-treated agarose gel (Fig. 7).

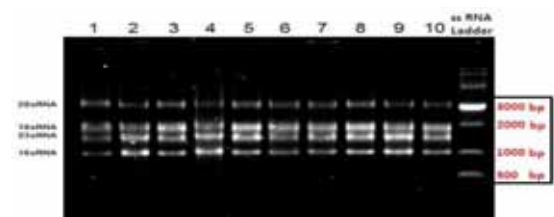


FIGURE 7

RNA samples after DNase treatment on 1.5% agarose gel. 1: Türkmen-0 hpi - mock, 2: Türkmen-15 mpi, 3: Türkmen-12 hpi, 4: Gerek 79-0 hpi mock, 5: Gerek 79-15 mpi, 6: Gerek 79-12 hpi, 7: Avocet *Yr10*-0 hpi - mock, 8: Avocet *Yr10*-15 mpi, 9: Avocet *Yr10*-12 hpi, 10: Türkmen-24 hpi.

Real-time PCR (Q-PCR) analysis. Gene expression analyses were conducted using *Yr10* gene-specific primers in Türkmen, Gerek 79 and Avocet *Yr10* genotypes at 7 different time points (0 hpi - mock, 15 mpi, 12 hpi, 24 hpi, 48 hpi, 72 hpi, 96 hpi). Three biological replicates of each genotype at each time point were pooled. These pooled 'cDNA's of each Türkmen, Gerek 79 and Avocet *Yr10* genotypes were used as template for cDNA synthesis for real-time PCR reaction. As a result of real-time PCR reactions, *Yr10* gene expression graphs of each genotype were obtained (Fig. 8 - 10). 'Mock' samples for Türkmen, Gerek 79 and Avocet *Yr10* genotypes were assumed as biological control of the reaction.

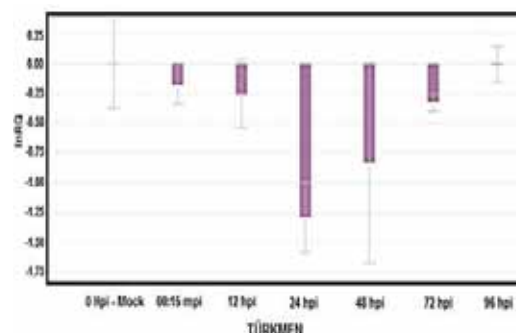


FIGURE 8

Yr10 gene expression in Türkmen genotype in seven time points: 0 hpi - mock, 00:15 mpi, 12 hpi, 24 hpi, 48 hpi, 72 hpi, 96 hpi. (lnRQ: logarithmic Relative Quantification)

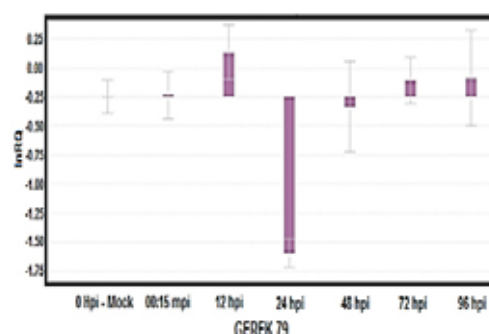


FIGURE 9

Yr10 gene expression in Gerek 79 genotype in seven time points: 0 hpi - mock, 00:15 mpi, 12 hpi, 24 hpi, 48 hpi, 72 hpi, 96 hpi. (lnRQ: logarithmic Relative Quantification)

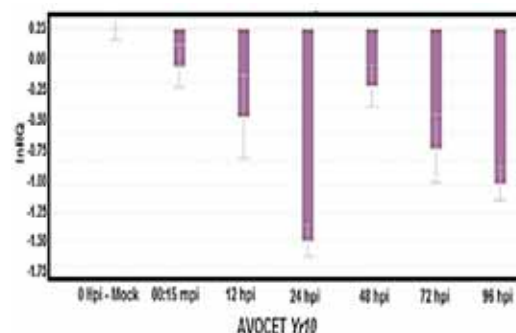


FIGURE 10

Yr10 gene expression in Avocet *Yr10* genotype in seven time points: 0 hpi - mock, 00:15 mpi, 12 hpi, 24 hpi, 48 hpi, 72 hpi, 96 hpi. (lnRQ: logarithmic Relative Quantification)

Amplifications obtained by ACBT and GAPDH primer pairs were used as multiplex endogenous control for the normalization of the *Yr10* gene expression for each reaction. The *Yr10* gene expression at Gerek 79 genotype was slightly up-regulated. Following this increase at gene expression, there was a significant increase at up-regulation of *Yr10* gene at 12 hpi. Conversely, there was a sharp down-regulation at 24 hpi. At 48 hpi, there was an increase at up-regulation of *Yr10* gene. The up-regulation was

continued to increase at 72 and 96 hpi. The *Yr10* gene expression of Avocet *Yr10* genotype was down-regulated at 15 mpi. Following, the down-regulation was increased at 12 hpi. Similar to other 24 hpi gene expression profiles of Türkmen and Gerek 79 genotypes; the down-regulation of *Yr10* gene at Avocet *Yr10* genotype was sharply increased at 24 hpi. But, the *Yr10* gene expression was up-regulated at 48 hpi. In contrast; there was an increase at the down-regulation of *Yr10* gene at 72 and 96 hpi.

DISCUSSION

Utilization of disease resistant varieties has proved to be the safest, most economical, and effective method to fight with yellow rust disease [3]. The danger caused by the use of limited resistance sources is becoming a great concern for breeders or pathologists [6]. The key problem is that there are breakdown of widely-used resistance genes occurs caused by the rapid improvement of PST pathogen isolates [3]. There are only three yellow rust disease resistance genes were cloned: *Yr10* [5], *Yr18* [4] and *Yr36* [2]. *Yr10* gene, responsible for yellow rust resistance at seedling-stage, was selected and used to investigate gene expression pattern by real-time PCR in this study. Expression profiling of *Yr10* in Türkmen and Gerek 79 genotypes after yellow rust attack at six different time points (15 min., 12 hours, 24 hours, 48 hours, 72 hours, 96 hours) at seedling stage was investigated by real time PCR which is one of the most widely-used techniques for gene expression profiling [8]. Real-time PCR results showed that *Yr10* gene was not expressed at basal level before PST infection (mock inoculated plants) in all genotypes. In contrast to our results Xingquan [14] reported the expression of eight candidate genes related with yellow rust resistance was observed at basal levels before infection of wheat plants. Expression profile of *Yr10* was down regulated at all six time points in Türkmen while Gerek 79 showed up-regulation at 15 mpi and 12 hpi in our study. The 24 hpi was critical for all genotypes because of the highest down regulation of *Yr10*. The lnRQ values for 24 hpi were ranged between (-1.30) – (-1.60). After 24 hpi, it was observed that lnRQ values were fluctuated and reached to almost basal level significantly in Türkmen and Gerek 79 suggesting that this gene may participate in plant defense response through different regulatory mechanisms. The fluctuations of expression levels of *Yr10* in Türkmen and Gerek 79 as well as positive control Avocet *Yr10* between different time points can be attributed short term effects of pathogen on plant after inoculation. It is also obvious that genes involved in stress response and signaling pathways are also down regulated in virulent infections. On the other hand, Yu [15] investigated the expression patterns of twelve genes involved in the

incompatible interaction between wheat and *Puccinia striiformis* f. sp. *tritici* at 12, 18, 24, 48, 72 and 120 hpi. According to their study, the most of defense-related genes were reached their maximum level at 24 hpi [15]. Similarly, Xingquan [13] were used wheat (*Triticum aestivum* L.) - *Secale cereale* alien disomic substitution NR1121 line as plant material and used CYR32 as pathogen for yellow rust disease inoculation at 0, 24, 48, 72, 96, 168, 240, and 336 hpi. As a result of their study, expression of six genes (AcsA, GST, LTP2, UPL2, CP450, and SPK-SNT7) transcripts were stimulated and up-regulated to their highest levels at 24 hpi, while that of two genes (SHMT and SAMDC) were significantly expressed at 48 hpi.

In our study, we investigated *Yr10* gene expression pattern assuming as responsible for seedling-stage yellow rust resistance as a major gene. Yet, to obtain more precise pattern of gene expression for yellow rust resistance at early stage of the infection, there should be additional study including various time points and different cultivars to elucidate this complex response. Furthermore, our results demonstrated that *Yr10* gene was induced after 24 hpi in Türkmen and Gerek 79, suggesting it is transcriptionally activated for the host defense response because the pathogen tries to mediate host cell expression by down regulating some genes so that plant can feed itself or suppress host defense mechanism thereby it can propagate.

Investigation of PST-wheat interaction at transcriptomic level is currently more environmentally friendly method to fight with yellow rust disease rather than using fungicides. Since we targeted *Yr10* gene which is already known as related to *NBS-LRR* family of plant defense genes. To examine the main role of this gene in yellow rust resistance pathway, it is important to represent the regulatory arrangements via exemplified RNA-based studies at transcriptome level in further investigation. Our study is a guide for studying yellow rust seedling-resistance at RNA-level. Wider-ranges of time points and additional studies (RNA-DNA interaction /or RNA-RNA interaction that targeted the *Yr10* gene) are necessity for a better understanding of *Yr10* gene's role in seedling resistance.

Zhang [16] indicated that there is a relation between *NBS-LRR* family defense genes and miRNAs. They investigated miRNAs across 70 land plant genomes and they pointed out a spectacular result. The Poaceae has the highest rate of heterogeneity among 70 plant species. They evidentially stated that there is a predominant effect of lncRNAs rather than miRNAs for *NBS-LRR* gene regulation in Poaceae too. They concluded that there is a higher rate of diversification by "local" rearrangements of *NBS-LRR* genes by wobble positioning in this family containing *T. aestivum*. The hexaploid structure of bread wheat may be the inducement of that much defense gene diversity. They stated that they concluded the

increased diversification of *NBS-LRR* families is raised by several kinds of different pathogen attack to different plant species. As a consequence, all the statements above can carry an explanation of our fluctuating real-time PCR results. In other words, the background behind sharp downregulations could be related to small RNAs (miRNA /or lncRNAs) - *Yr10* gene interactions. Recently, Dobon [1] showed global PST-wheat interaction at RNA level at 8 different time points. They stated that may pathogens suppress NLR expression to successfully penetrate and diffuse over the leaf tissues. They stated that this hypothesis require evidences supported by expanded-range of study of PST-wheat interactions. Our genotypes gave response to an admixed PST isolate while other studies are focused on one PST strain. This can also explain the fluctuated pattern of *Yr10* gene expression at seedling stage of bread wheat since several pathogen has various miRNAs and infection types. We recommend more studies on worldwide wheat gene pools with specific strain of PST in every step of the experiments since PST virulence and *NBS-LRR* families are in an ongoing change.

CONCLUSION

In this study expression pattern of a yellow rust disease resistance gene (*Yr10*) in three yellow rust resistant winter type bread wheat (*Triticum aestivum* L.) were investigated.

Identification of expression patterns of gene/s responsible for interested traits is another issue for plant breeding programs. In this study, we investigated the expression profile of yellow rust resistant gene, *Yr10* in wheat gene pool. It was observed that the most down-regulated time point was 24 hpi for *Yr10* gene expression in all genotypes and expression levels were fluctuated depends on the genotype and time points that we used. Expression of *Yr10* gene was down regulated until 24 hpi in Gerek79 while up regulation of *Yr10* was observed after 24 hpi in Türkmen. The increased time points for expression profiling is required for more effective evaluation of stripe rust resistance response in wheat. However better conclusions to understand the response of plant to yellow rust attack can be acquired as more genes identified in wheat and presented in future. In the frame of our results, Gerek 79 and Türkmen genotypes, carrying *Yr10* gene, can be used as material for wheat breeding programs focused on yellow rust resistance.

Further studies on genetic diversity and gene expression profiling can lead to develop novel breeding lines which are resistant or tolerant with higher genetic infrastructures as environmentally friendly and consuming the everlasting needs of human-being. For yellow rust epidemics, owing to the requirements for inoculation such as appropriate climatic

conditions or humidity; differ from region to region. With respect to these requirements, breeders should take the data obtained from geographical regions into account for wheat improvement studies against yellow rust. It is needed breeders to monitorize their fields consistently for yellow rust resistance due to the unstable yellow rust epidemics. The combination of recent RNA-based analyses in both wheat host and PST pathogen may lead breeders to estimate the further selection of cultivars to develop elite breeding lines resistant to fungal epidemics.

REFERENCES

- [1] Dobon, A., Bunting, D.C.E., Cabrera-Quio, L. E., Uauy, C., Saunders, D.G.O. (2016) The host-pathogen interaction between wheat and yellow rust induces temporally coordinated waves of gene expression. *BMC Genomics*
- [2] Fu, D.L., Uauy, C., Distelfeld, A., Blechl, A., Epstein, L., Chen, X., Sela, H., Fahima, T., Dubcovsky, J. (2009) A kinase START gene confers temperature dependent resistance to wheat stripe rust. *Science* 323, 1357–1360.
- [3] Jiang, Z., Ge, S., Zing, L., Han, D., Kang, Z., Zhang, G., Wang, X., Wang, X., Chen, P., Cao, A. (2013) *RLP1.1* a novel wheat receptor-like protein gene, is involved in the defense response against *Puccinia striiformis* f. sp. *tritici*. *Journal of Experimental Biology*.
- [4] Krattinger, S.G., Lagudah, E.S., Spielmeyer, W., Singh, R.P., Huerta-Espino J., McFadden, H., Bossolini, E., Selter, L.L., Keller, B. (2009) A putative ABC transporter confers durable resistance to multiple fungal pathogens in wheat. *Science* 323, 1360–1363.
- [5] Laroche, A., Frick, M.M., Huel, R., Nykiforuk, C., Conner, B., Kuzyk, A. (2000) Molecular identification of the wheat stripe rust resistance gene *Yr10*, the first full-length leucine zipper-nucleotide binding site-leucinerich-repeat resistance gene in cereals.
- [6] Li, Z. F., Xia, X. C., Zhou, X. C., Niu, Y. C., He, Z. H., Zhang, Y., Li, G. Q., Wan, A. M., Wang, D. S., Chen, X. M., Lu, Q. L., and Singh, R. P. (2006) Seedling and slow rusting resistance to stripe rust in Chinese common wheats. *Plant Disease*, 90:1302-1312.
- [7] Liu, W., Frick, M., Huel, R., Nykiforuk, C.L., Wang, X., Gaudet, D.A., Eudes, F., Conner, R.L., Kuzyk, A., Chen, Q., Kang, Z., Laroche, A. (2014) The Stripe Rust Resistance Gene *Yr10* Encodes an Evolutionary-Conserved and Unique CC-NBS-LRR Sequence in Wheat. *Molecular Plant* 7, 1740–1755.
- [8] Long, X-Y., Liu, Y-X., Rocheleau, H., Ouellet, T., Chen, G-Y. (2011) Identification and validation of internal control genes for gene expres-

- sion in wheat leaves infected by stripe rust. International Journal of Plant Breeding and Genetics, 5(3):255-267.
- [9] Lowe, I., Cantu, D., Dubcovsky, J. (2011) Durable resistance to the wheat rusts: integrating systems biology and traditional phenotype-based research methods to guide the deployment of resistance genes. *Euphytica*, 179:69-79.
- [10] McNeal, F.H., Konzak, C.F., Smith, E.P., Tate, W.S., Russell, T.S. (1971) A uniform system for recording and processing cereal research data. United States Department of Agriculture. Agricultural Research Service, 34: 121-43.
- [11] Salamini, F., Özkan, H., Brandolini, A., Schäfer-Preg, R., Martin, W. (2002) Genetics and geography of wild domestication in the near east. *Nature reviews-Genetics*, 3: 429-441.
- [12] Temel, A., Şentürk-Akfirat, F., Yumurtacı, A., Aydın, Y., Talaş-Oğraş, N., Gözükırmızı, N., Bolat, N., Yorgancılar, Ö., Belen, S., Yıldırım, M., Çakmak, M., Özdemir, E., Çetin, L., Mert, Z., Sipahi, H., Albustan, S., Akan, K., Düşünceli, F., Altinkut Uncuoğlu, A. (2008) *Yr10* gene polymorphism in bread wheat varieties. *African Journal of Biotechnology*, Vol. 7 (14), pp. 2328-2332.
- [13] Wang, L.F., MA, J.X., ZHOU, R.H., Wang, X.M., JIA, J.Z. (2002) Molecular tagging of the yellow rust resistance gene *Yr10* in common wheat, P.I. 178383 (*Triticum aestivum* L.). *Euphytica*, 124, 71-73.
- [14] Xingquan, Z., Changyou, W., Ali, M., Hong, Z., Xinlun, L., Weiyan, L., Wanquan, J.I. (2010) Profiling gene expression patterns of stripe rust (*Puccinia striiformis* f. sp. *tritici*) resistance gene in new wheat germplasm. *Pakistan Journal of Botany*, 42(6): 4253-4266.
- [15] Yu, X., Wang, X., Wang, C., Chen, X., Qu, Z., Yu, X., Han, Q., Zhao, J., Guo, J., Huang, L., Kang, Z. (2010) Wheat defense genes in fungal (*Puccinia striiformis*) infection. *Functional and Integrative Genomics*. 10:227-239.
- [16] Zhang, Y., Xia, R., Kuang, H., Meyers, B.C. (2016) The Diversification of Plant NBS-LRR Defense Genes Directs the Evolution of MicroRNAs That Target Them. *Mol. Biol. Evol.*
- [17] Zhou, X.L., Han, D.J., Chen, X.M., Gou, H.L., Guo, S.J., Rong, L., Wang, Q.L., Huang, L.L., Kang, Z.S. (2014) Characterization and molecular mapping of stripe rust resistance gene *Yr61* in winter wheat cultivar Pindong 34. *Theor Appl Genet*, 127: 935-945.

Received: 26.01.2017

Accepted: 23.06.2017

CORRESPONDING AUTHOR

Ahu Altinkut Uncuoğlu

Marmara University, Faculty of Engineering, Department of Bioengineering, 34722, Istanbul, Turkey.

Email: ahu.uncuoğlu@marmara.edu.tr

SELECTION OF OPTIMAL PARAMETERS FOR FUTURE RESEARCH MONITORING PROGRAMMES ON MSW LANDFILL IN NOVI SAD, SERBIA

Maja Djogo*, Jelena Radonic, Ivana Mihajlovic, Boris Obrovski, Dejan Ubavin,
Maja Turk Sekulic, Mirjana Vojinovic Miloradov

University of Novi Sad, Faculty of Technical Sciences, Department of Environmental Engineering, Novi Sad, Serbia

ABSTRACT

Leachate and groundwater samples were collected during quarterly sampling campaign, on unsanitary municipal solid waste (MSW) landfill in Novi Sad, Serbia, from April 2014. to February 2015. Determination of T, pH, EC, DO, BOD₅, COD, nitrite nitrogen (NO₂-N), nitrate nitrogen (NO₃-N), ammonia nitrogen (NH₄-N), total nitrogen (Tot N), total phosphorus (Tot P), boron (B), sulphate (SO₄²⁻), permanganate index (KMnO₄), and cations of metals (Ca, Mg, Na, K, B, Cr, Ni, Zn, Fe, Cd, Pb and Al), was performed. The comparison of the results obtained for leachate and groundwater samples and the limit values from laws and bylaws, literature, and the WHO guidelines, was performed. Principal component analysis (PCA) as a multivariate statistical method was later used for data filtering in order to classify the potential sources of pollution. Four principal components (PCs) were identified, explaining 93,802 % of the total variance. Cluster analysis (CA) was applied for grouping the sampling locations on MSW landfill in Novi Sad in accordance with the obtained values of physico-chemical parameters. Information obtained by CA has enabled the developing of future research monitoring programme, for each sampling location on the landfill in Novi Sad. The results obtained from this study could be very useful for planning of monitoring programmes on the landfills with similar structure and waste management practice.

KEYWORDS:

Landfill, Novi Sad, pollution, leachate, groundwater, PCA, CA

INTRODUCTION

The trend of population growth, high level of industrial activities and up-to-date technology continuously generate waste amounts. Sustainable municipal solid waste (MSW) management presents a significant social and environmental concern since the landfilling is the oldest and the most used disposing

method [1]. Separation of the mixed municipal waste containing different materials, at the source of production, is very significant [2]. In many countries including Serbia, it is not conducted properly. Waste management practice in Serbia could be described as undeveloped, consisting of only two operations, collection and land disposal [3]. The unlined landfills where potentially hazardous waste is disposed together with municipal waste, still exist in many parts of the world, particularly in the underdeveloped and developing countries [4], such as Serbia. These landfills can be harmful to the environment, in the terms of odor diffusion, methane emissions, leachate generation, contamination of groundwater nearby [5] and therefore, an appropriate monitoring programmes are needed.

Nowadays, a large number of landfills have established their monitoring programmes for leachate and groundwater. The parameters included in monitoring programmes of landfill sites vary not only between developed and undeveloped countries, but also within one country [6]. In most cases, these programmes propose the minimum number of physico-chemical parameters, including those suggested by the provincial and regional regulations. On the other hand, some programmes also comprise the observation of variables that are not of interest for specific landfill site. The composition of leachate and groundwater systems is mainly influenced by the composition and solubility of waste components, followed by annual precipitation, surface runoff, infiltration processes, average ambient temperature, depth of landfill [7] and external climate and hydrological characteristics. In most developing countries, the cost of laboratory analysis may affect the limitation of the number of physico-chemical parameters in the monitoring programmes. Therefore, it is necessary to determine the parameters of interest for individual sampling location on each landfill site, in order to optimize their number. It is possible to optimize the number of analysis included in large scale monitoring programmes using Multivariate Data Analysis (MVDA) [8].

In this study, one year monitoring programme was conducted on unsanitary municipal solid waste (MSW) landfill in Novi Sad, Serbia. The aims of the

study were: to assess the quality status of leachate and groundwater by analysing the large scale of physico-chemical parameters; to compare the results with the requirements of national laws and bylaws, as well as with the results reported in previous studies; to determine phase of the decomposition process of the landfill according to the concentration levels of selected parameters; and to define the optimal number of parameters which should be monitored in leachate and groundwater within the future research monitoring programmes.

MATERIALS AND METHODS

Landfill in Novi Sad. Unsanitary MSW landfill in Novi Sad was opened in 1963, but systematic landfilling has begun in 1980. The landfill is still in its operative status. Before the renovation in 2002, the landfill had the characteristics of wild dump such as inadequate disposing of waste, frequent fires, opened access of humans and animals, and poor control of leachate and groundwater quality. Fence and gate with a weight bridge were set up in order to prevent the entry of people and animals and to provide the weighting of disposed waste.

The landfill has a simple drainage system that collects leachate and storm water in the peripheral landfill canals. The canals are connected to a small stream that flows into the Danube-Tisa-Danube canal, and ultimately, into the river Danube.

The size of the landfill is 56 ha, the landfill body occupies 22 ha and is divided into 3 fields that are still in use. The city of Novi Sad generates about 2300 tonnes of waste per week with the higher rate during summer period. Organic waste (garden and biodegradable) is the dominant one (40-60%), plastic (10%), and paper, glass and cardboard are present in smaller amounts (2-10%) [9].

Sampling. Leachate samples were collected from the peripheral canals, SK1 and SK2, about 1 m

below the surface. Groundwater samples were collected from four piezometers (P2, P3, P4, P6) and well (B1), at a depth of 5-6 m, all located on the body of landfill, at a depth of 5-6 m (Fig. 1).

Four sampling campaigns were performed, quarterly, during the 2014. and 2015.: April 2014., September 2014., November 2014. and December 2015., according to the methods ISO 5667-11:2009 and ISO 5667-10:1992, for groundwater and leachate samples, respectively. Measurements of conductivity (EC), pH values and dissolved oxygen (DO) were performed *insitu*.

Laboratory analyses. The following parameters were determined in accredited Laboratory for monitoring of landfills, wastewater and air, University of Novi Sad, Faculty of Technical Sciences, Department of Environmental Engineering: biological oxygen demand (BOD₅), chemical oxygen demand (COD), nitrite nitrogen (NO₂-N), nitrate nitrogen (NO₃-N), ammonia nitrogen (NH₄-N), total nitrogen (Tot N), total phosphorus (Tot P), boron (B), sulphate (SO₄²⁻), permanganate index (KMnO₄), and cations of metals (Ca, Mg, Na, K, B, Cr, Ni, Zn, Fe, Cd, Pb and Al). BOD₅ was determined using the BOD Trak™ method, based on the manometric principle of operation. The COD, NO₂-N, NO₃-N, NH₄-N, and Tot P concentrations were measured with UV/VIS spectrophotometer (DR 5000, HACH, Germany). Precision and accuracy of the methods were verified with the certified reference materials Demand WP, Simple nutrients WP, Complex nutrients WP (RTC, UK). For the determination of metals cations, the wastewater samples were spiked with 5 ml of HNO₃ and digested using the microwave assisted digestion system MWS-3+ (Berghof, Germany). The analysis was done on Thermo flame atomic absorption spectrometer and the accuracy of the methods was tested using certified reference material LGC6175 (LGC, UK) and SPS-WW2 Batch 110 (SPS, Norway). The recoveries ranged from 89 % to 97 %.

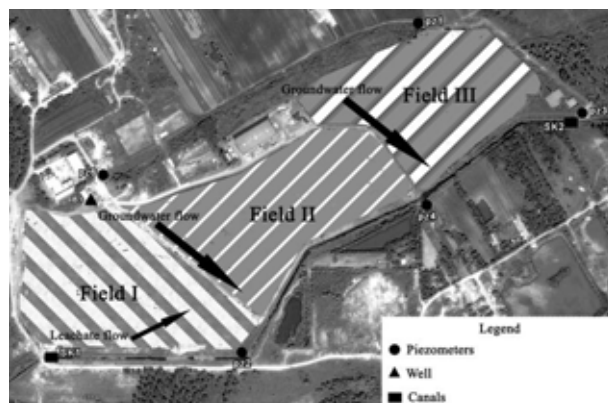


FIGURE 1
Sampling locations on MSW landfill in Novi Sad

TABLE 1
Physico-chemical composition of leachate from MSW landfill in Novi Sad (April 2014 – February 2015)

Parameter	Unit	SK1		SK2		Literature data [17-18]	Requirements for discharge of leachate [26]	Acid phase [27]	Methanogenic phase [27]
		Range	Average	Range	Average				
Tw	°C	8.4-19.4	14.12	3.9-21.7	14		30		
pH	-	7.6-7.7	7.65	7.6-7.8	7.72	4.5-9	6.5-9	4.5-7.5	7.5-9
EC	mS/cm	1.53-2.62	1.855	1.56-1.76	1.67				
DO	mg/L	0.3-2.7	1.8	1-4.8	2.3				
NO₂-N	mg/L	0.05-1.3	0.7625	0.2-1.6	0.75		2		
NO₃-N	mg/L	0.005-0.005	0.005	0.005-0.2	0.10125				
NH₄-N	mg/L	17.3-45.5	28.1	22.9-37	30.75				
Tot P	mg/L	0.1-3	1.625	0.1-6.3	2.925	0.1-23	3		
KMnO₄	mg/L	19.6-44.8	27.5	17.7-51.1	26.6				
COD	mg/L	77-316	163.75	62-383	189.75	140-152000	200	6000-60000	500-4500
BOD₅	mg/L	56-102	80.25	45-266	117.25	20-57000	20	4000-40000	20-550
SO₄²⁻	mg/L	21-102	45.75	86-96	90	8-7750		70-1750	10-420
Tot N	mg/L	5.7-47.6	23.6	1.2-33.9	19.375				
B	mg/L	0.2-0.5	0.35	0.2-0.4	0.325				
Ca	mg/L	70.5-147.8	117.175	76.1-138.9	113.225	10-7200		10-2500	20-600
Mg	mg/L	48.6-116.6	67.35	67-110.1	92.4	30-15000		50-1150	40-350
Na	mg/L	180.7-427.6	273.45	124.8-365.1	206.9	70-7700			
K	mg/L	31.8-52.3	45.725	26.7-75.3	42.45	50-3700			
Fe	mg/L	0.6-1.1	0.875	0.6-3	1.3	3-5500		20-2100	3-280
Zn	mg/L	0.025-0.6	0.1875	0.025-0.2	0.0875	0.03-1000	2		

Statistical methods. To evaluate the results of one year monitoring programme, principal component analysis (PCA) and cluster analysis (CA) were performed. PCA is a suitable statistical tool that explains the variance of the intercorrelated variables, transferring them into smaller groups of independent variables, principal components (PCs) [12-14]. In this study, PCA was proceeded on the physico-chemical parameters in order to extract significant PCs and to reduce the variables with low significance. CA is a suitable chemometric tool for compiling the objects according to their characteristics [15]. In this study, hierarchical clustering using Ward's method was performed on obtained dataset, in order to optimise the future research monitoring programme on each sampling spot.

RESULTS AND DISCUSSION

Leachate samples. The results obtained for leachate water samples collected during the four sampling campaigns (April 2014 – February 2015) on unsanitary MSW landfill in Novi Sad are presented in Table 1.

Different fields of the landfill might be in different phases of the transformation and decomposition processes at the same time, depending on the time and spatial coordinates of waste disposing in each area. Obtained results indicate that all 3 fields on landfill in Novi Sad are in low level of non-oxic sphere, i.e. in methanogenic phase, which is characterised by relatively slow dynamic biological degradation processes of organic substances and relatively low BOD₅ and COD values [16].

pH values in leachate samples showed nearly constant state varying from 7.6 to 7.7 and 7.6 to 7.8, for SK1 and SK2, respectively, during the whole

monitoring period, satisfying the limit values prescribed by Serbian regulation and ranges by previous studies [17-18].

The BOD₅ results, from the canals SK1 and SK2, were within the range that is characterized for mature landfill sites according to [19] and were greater than Serbian limit value of 20 mg/L, during whole sampling period. The COD values for leachate at SK1 and SK2 varied from 77-316 and 62-383 mg/L, respectively, and they exceeded the limit value (200 mg/L), issued in Serbian regulation, during April (SK1), September (SK2), and November (SK2). The values of BOD₅ and COD are lower by aging of landfill, due to dilution and catalytic process of methanogenesis [20]. Even though that results obtained for BOD₅ and COD are corresponding to the literature results [17-18], they indicate the need for leachate treatment.

The average BOD₅/N-NH₄ ratios were 3.04 and 3.78 for SK1 and SK2, respectively, which classifies leachate as young one (>1) [21]. This could be explained by continues occurrence of fresh leachate.

The average values of BOD₅/COD ratios were 0.57 and 0.63 for SK1 and SK2, respectively which are the characteristic values for landfills that are exploited less than five years [22]. Since the MSW landfill in Novi Sad operates more than five years these values could be explained by the continuous non-sanitary exploitation conditions and disposing of waste of different origin [16].

Concentration levels of SO₄²⁻ from SK1 and SK2 are consequent with the results obtained earlier [17-18] and are in the range of values which are characterised for mature landfills [19]. Sulphate anions are lower in the methanogenic phase due to redox conditions of SO₄²⁻ → S²⁻, by microbiological processes [17].

Cations of metals can be detected in leachates due to the metal based materials in waste streams, paints, pigment colours, polishing agent, electrical equipment and others [23]. The determined values for Mg, Ca Fe and Zn, were significantly lower than those from earlier literature [17-18] due to the higher pH value in methanogenic phase.

Groundwater samples. Groundwater physico-chemical characteristics from five sampling locations on MSW landfill in Novi Sad are shown in Table 2. Since the groundwater is a major source of drinking water, in general, the obtained results were compared to guideline values defined by World Health Organization (WHO). pH in groundwater samples showed nearly constant values varying from 7.3-7.5, 7.3-7.6, 7.3-7.7, 7.1-7.6 and 7.4-7.7, for P2, P3, P4, P6 and B1, respectively, during the whole monitoring period and were within guideline values according to the WHO. Average values for NO₃-N (B1) and total Fe and NH₄-N (P2, P3, P4, P6, B1) were higher than WHO standards for drinking water. The high concentration level of NO₃-N was obtained just in the case of well B1 during February 2015 (23.4 mg/L) which could suggest the potential impact of leachate on groundwater quality, in that period. Elevated values of total Fe and NH₄-N in all observed piezometers and well, during the whole monitoring programme, could be explained by the leaching of water containing toxic compounds and the aging of piezometers and well. Other observed parameters were within the limits prescribed in WHO guideline.

Concentration levels for Cr, Pb, Cd, Ni and Al in leachate and groundwater samples were under the limit of detection, <0.5, <1, <0.05, <0.3 and <1 mg/L, respectively.

PCA. In order to compare the compositional patterns between observed water systems (leachate

and groundwater) and to identify the intercorrelated factors, experimental data were processed using the PCA. Four principal components were revealed, explaining 93,802 % of the total variance. Principal component loadings of these variables with the variances are presented in Table 3.

PC1, which represents the higher percentage of variability, had high significant loadings for pH, conductivity, NH₄-N, Tot P, KMnO₄, COD, BOD, Na and K, accounting for 38,842% of the total variance. Strong loading of EC could be explained by soluble binary ionic salts (NaCl, NaHCO₃ and KCl), dominantly contained in food waste. According to [28], NH₄-N has significant positive correlation with phosphorus nutrients (Tot P) as the main components of the garden waste. The occurrence of these nutrients could be responsible for the higher values of BOD₅ and COD. Elevated values obtained for Na and K could be explained by the presence of food waste which contain significant amounts of highly soluble salts. Hence, PC1 could be defined as decomposition of biodegradable waste.

The second component, PC2, is dominated by Tot P, SO₄²⁻, Mg, K and Zn, accounting for 20.076% of the total variance. The dominance of SO₄²⁻ could be explained by the oxidation of sulphite minerals, industrial waste loaded by sulphur, or by decomposition of proteins. Sulphate anions are one of the major dissolved components of acid rain [29] and other atmospheric weathering precipitation. Although old landfills are anaerobic systems, oxygen input occur from heterogeneous mixture of new waste and rain-water [30]. Zn suggests the presence of toxic fractions of municipal solid waste coming, with high probability, from battery cells, used cans and aerosol cans, fluorescent tubes and other materials [31]. Therefore, PC2 could be defined as precipitation processes and degradation of waste containing toxic materials.

TABLE 2
Physico-chemical quality of groundwater from MSW landfill in Novi Sad (April 2014 – February 2015)

		P2		P3		P4		P6		B1		WHO
		Range	Average	Range	Average	Range	Average	Range	Average	Range	Average	
Tw	°C	11.7-19.1	15.525	9.6-17.6	14.225	9.9-18.8	14.875	13.2-16.1	15.15	4.5-17.6	13.025	/
pH	-	7.3-7.5	7.425	7.3-7.6	7.5	7.3-7.7	7.525	7.1-7.6	7.375	7.4-7.7	7.525	6.5-8.5 ^a
EC	mS/cm	1.52-2.02	1.65	1.06-1.16	1.1125	1.36-1.78	1.5375	0.83-1.38	1.16	0.86-1.55	1.1175	/
DO	mg/L	1-2.7	2.1	2.1-3.5	2.9	2.6-3.3	3	0.2-3.4	2.025	1.1-3.8	2.95	/
NO ₂ -N	mg/L	0.05-2	0.9375	0.5-1.4	0.85	0.05-1.9	0.7875	0.3-1.1	0.7	0.05-23.4	6.3625	3 ^a
NO ₃ -N	mg/L	0.005-0.1	0.02875	0.005-0.5	0.1525	0.005-0.5	0.12625	0.005-0.1	0.07625	0.005-0.1	0.07625	10 ^a
NH ₄ -N	mg/L	9.7-14.8	12.45	1.25-2.1	1.7625	4.1-5.9	4.95	1-19.1	7.2625	0.3-1.9	1.1125	1.5 ^b
Tot P	mg/L	0.1-0.3	0.175	0.1-0.2	0.125	0.2-0.4	0.3	0.1-1.6	0.8	0.1-0.3	0.2	/
KMnO ₄	mg/L	3.2-18.3	10.65	6.2-9.8	7.875	14.3-21.4	17.025	3.9-15.2	9.075	3.8-12.2	8.975	/
COD	mg/L	81-147	114.3	20-41.8	28.7	61-80	71.475	13-131.9	62.225	16-61	40.725	/
BOD ₅	mg/L	52-105	68.25	8-38	23	2-64	33.75	3-48	21.75	1-24	11.75	/
SO ₄ ²⁻	mg/L	1-1	1	1-1	1	1-3	1.5	96-97	96.5	1-101	38	200 ^b
Tot N	mg/L	6.4-68.9	38.475	6.2-67.5	35.5	8.9-26.9	20.225	7.1-43.9	23.475	4.9-20.7	8.975	/
B	mg/L	0.2-3.4	1.3	0.05-0.4	0.2625	0.05-0.5	0.3375	0.1-1	0.4	0.1-0.7	0.35	2.4 ^a
Ca	mg/L	50.3-229.6	167.4	80.9-128.5	107.475	78.5-126.2	99.95	96.3-207.7	175.725	69.7-213.6	123.875	/
Mg	mg/L	34.1-70.4	54.6	28.7-48.6	37.1	44.2-85.7	59.425	55.4-94.4	72.45	39.7-68.2	51.2	/
Na	mg/L	28.5-259.2	168.95	47-359.9	168.125	156.4-254.4	193.275	55.4-217.3	98.175	9.5-259.2	133.1	200 ^a
K	mg/L	5.9-18.9	13.75	5.8-36.2	14.35	19.7-32.2	24.85	5.9-37.4	22.55	1.1-33.8	15.175	/
Fe	mg/L	1.4-5	3.6	2.4-6.4	4.825	2.7-9.2	4.975	0.15-3.6	2.3375	0.15-1.4	0.6125	0.3 ^a
Zn	mg/L	0.3-2.1	1.4	0.1-0.9	0.5	0.1-0.5	0.2	0.025-0.1	0.04375	0.025-0.3	0.18125	3 ^a

^aWHO (2011), ^bWHO (2003)

TABLE 3
PCA loadings of significant principal component variables

Parameters	Rotated Component Matrix			
	PC1	PC2	PC3	PC4
Temperature	-0.099	-0.016	.380	.879
pH	.850	.119	-.340	-.344
EC	.901	-.056	.292	.161
DO	-.404	-.465	-.680	-.239
NO ₂ -N	-.380	-.159	.046	-.898
NO ₃ -N	-.344	-.083	-.838	.213
NH ₄ -N	.896	.376	.206	.024
Tot P	.736	.617	-.067	-.062
KMnO ₄	.940	.275	-.100	-.074
COD	.902	.300	.270	.045
BOD ₅	.892	.201	.204	.135
SO ₄ ²⁻	.083	.957	.115	-.237
Tot N	.015	-.397	.291	.773
B	-.017	-.390	.821	.302
Ca	-.434	.318	.802	.258
Mg	.522	.772	.090	.028
Na	.924	-.217	-.100	-.016
K	.748	.600	-.180	.139
Fe	-.280	-.510	-.333	.730
Zn	-.036	-.658	.613	.350
Eigen value	7.768	4.015	3.634	3.342
% of variance	38.842	20.076	18.171	16.712
Cumulative %	38.842	58.919	77.090	93.802

PCA loadings which are higher than 0.6 are marked

Component 3, PC3, explaining 18.171% of the total variance, has strong positive loading on DO, NO₃-N, B, Ca and Zn. Cinders, slag, and plastic were reported as waste with positive correlation with boron levels in the water streams from landfills [32]. Consequently, PC3 could be defined as decomposition of plastic and mineral waste.

The fourth component, PC4, explains 16.712% of the total variance by positive loading for temperature, NO₂-N, Tot N and Fe. The appearance of iron in water streams of landfills can be explained by the presence of waste containing iron based materials such as construction waste, paints, pigments, polishing agents, electrical appliances and others [33]. The main source of Tot N in landfill water streams is waste containing proteins. The kinetics of large proteins (high molecular mass) hydrolysis is slow which may be the reason for elevated values of ammonia in mature water from landfill sites [34]. Therefore, PC4 could be defined as the influence of destruction processes of construction waste, paints, chemical agents and electrical appliances, as well as the decomposition of waste containing proteins.

CA. Hierarchical clustering using Ward's method was applied on obtained dataset and dendrograms are presented in Figure 2.

The first dendrogram (Fig. 2a) suggests three clusters which have similar characteristic features. Cluster 1 consists of sampling locations P3, B1, and P6, cluster 2 comprises locations P2 and P4 while cluster 3 covers locations SK1 and SK2. Both, clusters 1 and 2, are characterised by similar trends of variation of all parameters from PC1, except for

NH₄-N which exceeded the guideline value defined by WHO, in all piezometers and well. This could be explained by the percolation of water through the significant amounts of biodegradable waste which is disposed on daily basis at all three fields of landfill site. The higher concentration levels of all parameters from PC1, in piezometers P2 and P4 could be explained by the groundwater flow direction caused by position and slope of terrain (Fig.1). Canals SK1 and SK2, partially surrounding landfill body, were the most polluted during whole sampling campaign. The average values of NH₄-N in both canals were much higher than the values obtained in piezometers and well from clusters 1 and 2, and one of the main reasons for these results could be the large amount of biodegradable waste with the highest volume at the edges of the landfill site (Fig. 1). On the other hand, the vicinity of a highway and arable land, as well as precipitation, could contribute to the significant pollution of leachate from these canals.

The second dendrogram which is compared to the second factor, PC2 is presented in Figure 2b. Four clusters have been allocated whereby fourth cluster contains just one location, SK2, and was the most loaded one. Since the PC2 is defined as precipitation processes and degradation of waste containing toxic materials, it can be concluded that leachate water from this canal is highly influenced by the percolation of water through the heterogenic mixture of disposed waste and precipitation. Additionally, SK2 is located downstream from canal 1 (Fig. 1) and could suffer the pollution from this site. It should be noted that piezometer P2, from the second cluster, is the most loaded by Zn (Field I). As the field I is the

oldest one, it could be assumed that groundwater from P2 is contaminated by migration and percolation of water through the old deposits of waste containing toxic materials.

The third dendrogram which is compared to the PC3 has been defined as decomposition of plastic and mineral waste (Fig. 2c). Four clusters have been separated, cluster 1 containing P3 and P4, cluster 2 containing B1 and SK2, cluster 3 including P6 and SK1 and cluster 4 which includes just one location, P2. At location P2, the dominant occurrence of B and Zn was observed, which could be explained by the flow stream of contaminated liquids from landfill site. The vehicular emissions and agricultural activities in the vicinity of P2 could also contribute to the pollution of groundwater.

The fourth dendrogram was obtained by comparison with the PC4 (Fig. 2d). Dendrogram separates

cluster 1 (SK1, SK2), cluster 2 (P4, P6), cluster 3 (P2, P3) and cluster 4 (B1). B1 is the most loaded by the NO₂-N, which is in correspondence with the NO₃-N concentration levels determined in groundwater sample, in the last campaign. It could be assumed that the percolation of leachate had the negative impact on the quality of groundwater from the well, in winter period. Average concentration levels of Tot N and Fe in cluster 3 (P2 and P3) should be highlighted, as they were much higher compared to the other sampling points. This could be explained by the migration of water contaminated by the food waste, construction waste, paints, chemical agents and electrical appliances. Since the examined piezometers are old, they could contribute to the occurrence of elevated levels of Fe, as well.

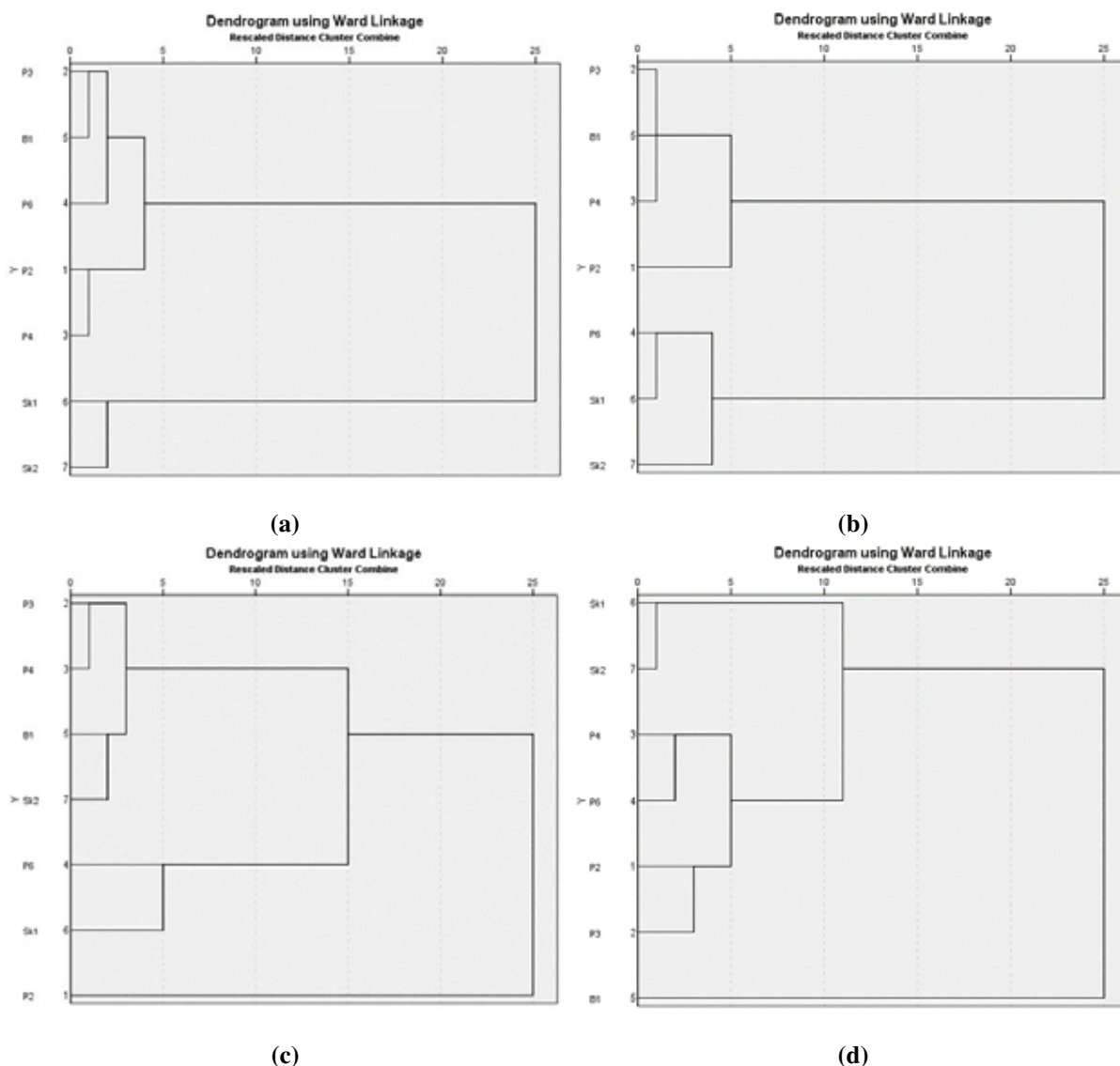


FIGURE 2
 The CA dendrograms of sampling locations compared to principal components
 a) PC1, b) PC2, c) PC3 and d) PC4

TABLE 4
Selection of parameters that should be included in future research monitoring programmes on the MSW landfill in Novi Sad

	Tw	pH	EC	DO	NO ₂ -N	NO ₃ -N	NH ₄ -N	Tot P	KMnO ₄	COD
P2	x	x	x	/	x	x	x	x	/	x
P3	x	x	x	/	x	x	x	x	/	x
P4	x	x	x	/	x	x	x	x	/	x
P6	x	x	x	/	x	x	x	x	/	x
B1	x	x	x	/	x	x	x	x	/	x
SK1	x	x	x	/	x	x	x	x	/	x
SK2	x	x	x	/	x	x	x	x	/	x
	BOD ₅	SO ₄ ²⁻	Tot N	B	Ca	Mg	Na	K	Fe	Zn
P2	x	x	x	x	/	/	x	/	x	x
P3	x	x	x	/	/	/	x	/	x	/
P4	x	x	/	/	/	/	x	/	x	/
P6	x	x	/	x	/	/	x	/	x	/
B1	x	x	/	/	/	/	x	/	x	/
SK1	x	/	x	/	/	/	/	/	/	x
SK2	x	/	x	/	/	/	/	/	x	/

Serbian bylaws prescribe the limit values of physico chemical parameters that should be monitored in leachate water samples on the place of discharge, 4 times a year. Some of the parameters were not examined (total suspended solids, hydrocarbon index, toxicity to fish) since the study was conducted before the Regulation on emission limit values of waster pollutants and deadlines for their achievement (Off. Gazette of Republic of Serbia, no. 1/16) was adopted. In order to create the comprehensive research monitoring programmes, some additional inorganic parameters were analyzed (KMnO₄, SO₄²⁻, B, Ca, Mg, Na, K, Fe, Zn, Pb, Cd, Ni, Al and Cr). The selection of the physico chemical parameters that should be included in the future research monitoring programmes was conducted according to the data obtained using PCA and CA (Table 4).

CONCLUSION

This type of research monitoring programme is scars and has been realized for the first time in Novi Sad, Serbia. Leachate and groundwater samples were collected during one year sampling campaign, on MSW landfill in Novi Sad. The study was focused on determination of the following parameters: T, pH, EC, DO, BOD₅, COD, (NO₂-N), NO₃-N, NH₄-N, Tot N, Tot P, B, SO₄²⁻, KMnO₄, Ca, Mg, Na, K, B, Cr, Ni, Zn, Fe, Cd, Pb and Al. Results indicate that all 3 fields on MSW landfill in Novi Sad are in methanogenic phase of decomposition with continuous generation of fresh leachate. The results obtained for leachate samples are consequent with the results from earlier literature and they indicate the need for leachate treatment. The presence of particular con-

taminants above the WHO guideline values in samples from piezometers and well, indicate the potential threat of leachate on the quality of groundwater.

Application of PCA and CA appeared to be the good statistical approaches for interpretation of physico-chemical results of leachate and groundwater samples and significant tools for selection of the optimal parameters for future research monitoring programmes. Obtained results could be very useful for developing of monitoring programme plans, for the landfills with similar structure and waste management practice and could contribute in strengthening the capacity of national legislation.

Landfill environment is high loaded heterogeneous system and, there is a need for extension of the number of parameters by persistent organic pollutants and emerging substances in order to obtain more comprehensive research monitoring programmes and more realistic feature on the environment of MSW landfill sites.

ACKNOWLEDGEMENTS

This environmental study has been financially supported by Ministry of Education, Science and Technological Development, Republic of Serbia (Project III46009 and Project TR34014).

Many thanks to Dr. Bojan Batinic, MSc. Nikola Maodus, MSc. Maja Brboric and MSc. Sabolc Pap for participation in this environmental study, during its realisation, and to their valuable comments and suggestions.

REFERENCES

- [1] Çaliskan, Y., Bektas, N. and Tekbas, M. (2016) Anaerobic composting of organic fraction of municipal solid waste. *Fresen. Environ. Bull.*, 25(4), 1097-1104.
- [2] Abbasi, F., Samaei, M.R., Khodadadi, H., Karimi, A. and Hoshang, M. (2016) Effects of materials recovery facility construction on the release of fungal bioaerosols: A case study in Southern of Iran. *Fresen. Environ. Bull.*, 25(4), 1097-1103.
- [3] Stanisavljevic, N., Ubavin, D., Batinic, B., Fellner, J. and Vujic, G. (2012). Methane emissions from landfills in Serbia and potential mitigation strategies: A case study. *Waste Management & Research*, 30(10), 1095-1103.
- [4] Kumar, D. and Alappat, B. (2005) Evaluating leachate potential of landfill sites using leachate pollution index. *Clean Technologies and Environmental Policy*, 7, 190-197.
- [5] Ma, Q., Shen, F., Yuan, H., Zou, D., Liu, Y., Zhu, B. and Li, X. (2015) Investigation on anaerobic digestion of the organic fraction of municipal solid waste (OFMSW) after pretreatment of fast aerobic fermentation. *Fresen. Environ. Bull.*, 24(3b), 1039-1046.
- [6] Hjelmar, O., Johannessen, L. M., Knox, K., Ehrig, H.-J., Flyvbjerg, J., Winther, P. and Christensen, T. H. (1994). Management and composition of leachate from landfills, Final Report, DGXI A.4 Waste 92. Commission of the European Communities, Water Quality Institute, Hørsholm, Denmark, 12-14 and 117-124.
- [7] Chen, P.H. (1996) Assessment of leachates from sanitary landfills: Impact of age, rainfall, and treatment. *Environmental International*, 22, 225-237.
- [8] Kylefors, K. (2003) Evaluation of leachate composition by multivariate data analysis (MVDA). *Journal of Environmental Management*, 68, 367-376.
- [9] Vujic, G., Jovcic, N., Redzic, N., Jovcic, G., Batinic, B., Stanisavljevic, N. and Altabt, A.O. (2010) A fast method for the analysis of municipal solid waste in developing countries – Case study of Serbia. *Environmental Engineering and Management*, 9(8), 1021-1029.
- [10] ISO 5667-10:1992. (1992) Water quality -- Sampling -- Part 10: Guidance on sampling of waste waters.
- [11] ISO 5667-11:2009. (2009) Water quality -- Sampling -- Part 11: Guidance on sampling of groundwaters.
- [12] Kiurski, J., Oros, I., Ralevic, N., Kovacevic, I., Adamovic, S., Krstic, J. and Comic, L. (2013) Cluster and principal component analysis in the assessment of fountain solution quality. *Carpathian Journal of earth and Environmental Sciences*, 7(1), 19-28.
- [13] Loska, K. and Wiechuya, D. (2003) Application of principle component analysis for the estimation of source of heavy metal contamination in surface sediments from the Rybnik reservoir. *Chemosphere*, 51(8), 723-733.
- [14] Crrito, A., Carlon, C. and Marcomini, A. (2003) Characterisation of contaminated soil and groundwater surrounding an illegal landfill (S. Guliano, Venice, Italy) by principal component analysis and kriging. *Environmental Pollution*, 122, 235-244.
- [15] McKenna, Jr. J.E. (2003) An enhanced cluster analysis program with bootstrap significance testing for ecological community analysis. *Environmental modelling and software*, 18(3), 205-220.
- [16] Slomczyńska, B. and Slomczyński, T. (2004) Physio-chemical and toxicological characteristics of leachate from MSW landfills. *Polish Journal of Environmental Studies*, 13(6), 627-637.
- [17] Kjeldesn, P., Barlaz, M.A., Rooker, A.P., Baun, A., Ledin, A. and Christensen, T.H. (2002) Present and long-term composition of MSW landfill leachate: A review. *Critical Reviews in Environmental Science and technology*, 32, 297-336.
- [18] Kjeldesn, P. and Christophersen, M. (2001) Composition of leachates from old landfills in Denmark. *Waste Management & Research*, 19, 249-256.
- [19] Tchobanoglous, G., Theisen, H. and Vigil, S.A. (1993) Integrated solid waste management engineering principles and management issues (1st edition). New York, NY: McGraw-Hill.
- [20] Adhikari, B. and Nath Khanal, S. (2015) Qualitative study of landfill leachate from different ages of landfill sites of various countries including Nepal. *IOSR Journal of Environmental Science, Toxicology and Food Technology*, 9(1), 23-36.
- [21] Mc Bean, E.A. and Rovers, F.A. (1995) Solid waste landfill engineering and design. Englewood Cliffs. New Jersey.
- [22] Kulikovska, D. and Klimiuk, E. (2008) The effect of landfill age on municipal leachate composition. *Bioresource Technology*, 99, 5981-5985.
- [23] Aziz, H., Yusoff, M.S., Adlan, M.N., Adnan, N.H. and Alias, S. (2004) Physico-chemical removal of iron from semi-aerobic landfill leachate by limestone filter. *Waste Management*, 24, 353-358.
- [24] WHO (2003) Guideline for drinking-water quality, Geneva (WHO/SDE/WSH 03.04).
- [25] WHO (2011) Guidelines for drinking-water quality. 4th Edition. World Health Organisation, Geneva.
- [26] Regulation on emission limit values of waster pollutants and deadlines for their achievement

- (Off. Gazette of Republic of Serbia, no. 1/16).
- [27] Ehrig, H.J. (1983) Quality and quantity of sanitary landfill leachate. *Waste Management & Research*, 1, 53-68.
- [28] Wani, K.A., Mamta and Rao, R.J. (2013) Bio-conversion of garden waste, kitchen waste and cow dung into value-added products using earthworm *Eisenia fetida*. *Saudi Journal of Biological Sciences*, 20, 149-154.
- [29] Raman, N. and Narayanan, D.S. (2008) Impact of solid waste effect on ground water and soil quality nearer to pallavaram solid waste landfill site in Chennai. *Rasayan journal of Chemistry*, 1(4), 828-836.
- [30] Abd El-Salam, M.M. and Abu-Zuid, G.I. (2015) Impact of landfill leachate on groundwater quality: A case study in Egypt. *Journal of Advanced research*, 6, 579-586.
- [31] Akinbile, C.O. (2012) Environmental of landfill on groundwater quality and agricultural soils in Nigeria. *Soil and Water Research*, 7(1), 18-26.
- [32] Yoshinaga, J., Kida, A. and Nakasugi, O.J. (2001) Statistical approach for the source identification of boron in leachates from industrial landfills. *Journal of Material Cycles and Waste Management*, 3(1), 60-65.
- [33] Zainol, N. A., Aziz, H. A. and Yusoff, M. S. (2012). Characterization of Leachate from Kuala Sepetang and Kulim Landfills: A Comparative Study. *Energy and Environment Research*, 2(2), 45-52.
- [34] Kulikowska, D. and Klimiuk, E. (2004) Removal of organics and nitrogen from municipal landfill leachate in two-stage SBR reactors. *Polish Journal of Environmental Studies*, 4(13), 389-396.

Received: 16.02.2017

Accepted: 09.06.2017

CORRESPONDING AUTHOR

Maja Djogo

University of Novi Sad
Faculty of Technical Sciences
Department of Environmental Engineering
Novi Sad – SERBIA

E-mail: majadjogo@uns.ac.rs

INFLUENCES OF *PHYSALIS PERUVIANA* L. AND *LUPINUS ALBUS* L. EXTRACTS ON THE LEVELS OF SOME BIOCHEMICAL PARAMETERS IN ERYTHROCYTES AND SERUM OF STREPTOZOTOCIN INDUCED DIABETIC RATS

Fazilet Erman¹, Tubay Kaya², Okkes Yilmaz², Orhan Erman², Ayse Dilek Ozsahin^{3,*}

¹Firat University, Faculty of Health Sciences, 23169, Elazig, Turkey

²Firat University, Faculty of Science, Biology Department, 23169, Elazig, Turkey

³Bitlis Eren University, Faculty of Science, Biology Department, 13000, Bitlis, Turkey

ABSTRACT

In this study, the effects of goldenberry and lupin on some biochemical parameters in erythrocytes and serum of streptozotocin-induced diabetic rats were investigated. Type II diabetes was produced in rats by the streptozotocin injection.

Rats were divided into four groups, each one containing 10 rats: non-diabetic control group, STZ-Diabetes type II group, STZ-Diabetes type II+goldenberry group, and STZ-Diabetes type II+lupin group. After one week from the injection, goldenberry and lupin were administered to rats for 2 months. Malondialdehyde, glutathione and fatty acid levels, which are signs of lipid peroxidation, were measured in erythrocytes and serum.

At the beginning and end of the study, postprandial blood glucose levels of the rats were measured. In type II diabetes, malondialdehyde level was increased when compared to control group. Glutathione level was decreased in the erythrocytes and all of the STZ-induced diabetic groups. It has been determined that the treatment with similar doses of goldenberry and lupin significantly reduced postprandial hyperglycemia, oxidative stress and augmented antioxidant system. The results of the present study showed that the plant extracts exerted anti-hyperglycemic effects and consequently may alleviate tissue damage caused by streptozotocin-induced diabetes.

KEYWORDS:

Diabetes, Erythrocytes, Goldenberry, Lipid peroxidation, Lupin, Serum

INTRODUCTION

Chronic non-communicable diseases such as diabetes are increasing public health problems worldwide [1]. Diabetes mellitus is characterized by chronic high glucose levels in the blood due to irregularities in insulin levels; further, patients have an

altered cellular homeostasis that produces diffuse vascular damage and multi-organ dysfunction. Diabetes is a metabolic disorder of multiple etiologies characterized by chronic hyperglycemia with disturbance of carbohydrate, fat and protein metabolism resulting from defects in insulin secretion, insulin action or both [2]. There are two types of diabetes mellitus: Type 1, insulin dependent diabetes mellitus, is hereditary and is treated by insulin, and type 2, non-insulin dependent diabetes mellitus is age-associated which occurs in elderly people and is treated by controlling the diet and oral hypoglycemic drugs [3]. Many oral antihyperglycemic agents, such as sulfonylurea and biguanides are available along with insulin for the treatment of diabetes, but these agents have significant side effects and some of them could be ineffective in chronic diabetic patients [4]. Thus, there is an increasing need for new, natural and more effective anti-hyperglycemic products especially nutraceuticals with less side effects, safe and high anti-hyperglycemic potential. There are known plants and secondary metabolites that are effective in management and control of diabetes.

Recently, *Physalis peruviana* and *Lupinus albus* are very much appreciated by researchers worldwide for their effect as hypoglycemic agents. Medically, *Physalis peruviana* and *Lupinus albus* have been used as a medicinal herb against to cancer, leukemia, asthma, hepatitis and diabetes[5-8]. The present study was conducted to determine the anti-diabetic effects and biochemical activities of *Physalis peruviana* and *Lupinus albus* fruit extracts in erythrocytes and serum of diabetic rats.

MATERIALS AND METHODS

Animals. Animals, experimental design, and experimental protocols were approved by the Committee on the Ethics of Laboratory Animal Experiments of Firat University (Elazig, Turkey). Animal care and experimental protocols were compatible with the NIH Guide for the Care and Use of Laboratory Animals (NIH publication no.

30.06.2011/2011/7/101). Thirty-seven healthy adult male Wistar albino rats, aged 8–10 weeks were obtained from Firat University Experimental Research Centre. The animals were housed in the polycarbonate cages in a room with a 12-h day-night cycle, temperature of $24 \pm 3^\circ\text{C}$, and humidity of 45% to 65%. During the whole experimental period, the animals were fed with a balanced commercial diet (Elazig Food Company, Elazig, Turkey) *ad libitum*.

Experimental Design. The first group was used as the control group (n=7) and the others were as follows: second group, Diabetes (n=10); third group, Diabetes+ *Physalis peruviana* group (D+PP) (n=10); fourth group, Diabetes+ *Lupinus albus* group (D+LA) (n=10). Groups were made diabetic by a single intraperitoneal injection of 40mg/kg streptozotocin (STZ) solved in citrate buffer (pH 4.5). Control group rats were injected intraperitoneally with buffer alone. One week after administration of STZ, the tail vein blood glucose levels of all the animals were measured. Blood glucose levels of 140-200 mg/dl were considered as diabetic. The rats in D+PP group were injected intraperitoneally with 1 mL/kg *P. peruviana* fruit extract. Also the addition of 2 gr *P. peruviana* extract added to 500 mL drinking water was administered to the rats two times per week. The rats in D+LA group were injected intraperitoneally with 1 mL/kg *L. albus* fruit extract. Also the addition of 2 gr *L. albus* extract added to 500 mL drinking water was administered to the rats two times per week. These treatments continued for 8 weeks and after this period, each experimental rat was anesthetized with ether. Blood from rats was taken into EDTA vacutainer tubes. Erythrocyte pellets were separated from plasma by centrifugation in 4,000 rpm. Then, erythrocyte pellets were washed three times with cold (4°C) phosphate-buffered saline (pH 7.4). Blood samples were dissected and stored at -85°C prior to biochemical analysis.

Homogenate Preparation. Blood samples were homogenized in Tris-HCl buffer (pH 7.5) and

centrifuged at 9000 rpm for 20 min at 4°C . Supernatants were collected, aliquoted, and stored at -70°C until use. The supernatant obtained from the TBARS, reduced glutathione and total protein analysis, fatty acid analysis of the pellets were performed.

Chemical Analyses. Lipid peroxides (TBARS) in blood samples homogenate were estimated using thiobarbituric acid reactive substances by the method of Ohkawa et al. [9] the resulting nmol/g tissue was calculated. The glutathione (GSH) contents of the erythrocytes and serum were measured at 412 nm by the method of Ellman [10]. Extraction of lipids from the tissue specimens was performed according to the method of Hara and Radin [11]. Preparation of fatty acid methyl esters was analyzed according to the method of Christie [12]. The fatty acid methyl esters were analyzed in a gas chromatograph with a Macherey-Nagel capillary column. During the analysis, column heat was maintained at $120\text{--}220^\circ\text{C}$, injection heat was maintained at 240°C , and detector heat was maintained at 280°C . The column heat program was regulated to 220°C from 120°C ; the heat increase was set to $5^\circ\text{C}/\text{min}$ until reaching 200°C and to $4^\circ\text{C}/\text{min}$ from 200 to 220°C , and it was then held at 220°C for 8 min. Nitrogen was the carrier gas and the detector was a flame-ionization detector. Total protein contents in erythrocytes and serum were determined as Lowry's method described. The procedure for measuring protein was followed according to Lowry et al. [13] using BSA (Bovine serum albumin) as standard.

Statistical Analysis. One-way analysis of variance (ANOVA) and Post Hoc Tukey-HSD test were used to determine differences between groups. Results are presented as mean \pm S.E.M. Values were considered statistically significant if $p < 0.05$. The SPSS/PC program (Version 15.0; SPSS, Chicago, IL) was used for the statistical analysis.

TABLE 1
The blood glucose concentration changes in all groups

Blood Glucose Levels	C	D	D+PP	D+LA
	61.83 \pm 3.86	138.17 \pm 29.46	162.55 \pm 27.15	153.80 \pm 29.96
2 Weeks	66.83 \pm 2.61	141.42 \pm 13.63	138.91 \pm 8.51	150.00 \pm 15.13
3 Weeks	67.00 \pm 8.11	144.17 \pm 19.24	132.73 \pm 7.21	149.40 \pm 9.12
4 Weeks	96.50 \pm 12.34	152.75 \pm 19.38	129.27 \pm 9.45	144.90 \pm 7.41
5 Weeks	106.50 \pm 15.17	155.00 \pm 23.94	124.82 \pm 9.54	136.20 \pm 3.40
6 Weeks	108.00 \pm 10.34	211.75 \pm 43.33	121.00 \pm 15.53	135.80 \pm 7.06
End Applications	109.33 \pm 2.58	249.00 \pm 28.31	113.73 \pm 17.65	124.20 \pm 5.61

RESULTS AND DISCUSSION

Changes in Blood Glucose Levels. Even though fasting blood glucose levels measured at the 1st, 4th, and 7th (at the end of study) weeks were within normal limits in the control group during the study, a continuous increase was observed in the diabetic group (Table 1). A decrease was determined in time in D+PP and D+LA groups (Table 1).

In the last few years, the use of traditional medicine has increased. Epidemiological studies and in vitro and in vivo tests in animals and humans show that diets based on the consumption of vegetables may have a hypoglycemic effect and reduce the risk of chronic diseases [14-16]. In the present study, we showed that *P. peruviana* and *L. albus* could prevent development of STZ-induced type-2 diabetes in the rat erythrocytes and serum. The pancreas plays an important role in glucose homeostasis [17]. The role of oxidative stress is implicated in the decline of pancreatic function in diabetes mellitus. The diabetic effect of STZ is due to an excess in the production of reactive oxygen species (ROS). This excess leads to toxicity in pancreatic cells, which, in turn, reduces the synthesis and release of insulin while concurrently affecting other organs [18]. In the present study, blood glucose levels were observed to be increased in diabetic groups, however, blood glucose levels were observed to be reduced again with goldenberry and lupin extracts administration. In the study conducted with goldenberry, it was shown that it controlled glucose level by absorbing carbohydrates owing to its fibrous structure [19, 20]. Blood glucose level was also observed to decrease after lupin was given to diabetic rats [20]. The polyphenols content of the fresh *Physalis* is juice 70mg/100mL [21, 22]. *Physalis* polyphenols may, therefore, prevent the damage and death of pancreatic-cells and/or stimulate the regeneration of this type of cells in diabetic rats. The obtained results of *Physalis* were agreed with Estakhr and Javdan [23] who recorded that oral administration of ethanolic extract of *Physalis* normalized the levels of blood glucose. The presence of potent anti-diabetic active principles as physalin, citric acid and vitamin C in the extract inhibits glycogen phosphorylase enzyme that catalyzes the process of glycogenolysis thereby inhibiting glucagon on feedback inhibition in the production of insulin.

Values of Erythrocytes and Serum in Type-2 Diabetes. The levels of MDA, GSH and total protein in the erythrocytes of control and diabetic rats are presented in the Table 2. Compared to control group, a significant increase was observed in MDA level in the diabetic group ($p<0.001$). A significant increase was observed in the D+PP group ($p<0.01$) and partial decreases were observed in D+LA group as compared to the control group. As diabetic group was compared with D+PP and D+LA groups, a

significant decreasing difference was determined between both groups ($p<0.001$).

GSH level in the diabetic group was significantly decreased as compared to control group ($p<0.001$) (Table 2). GSH amount were observed to partially decrease in plant extract groups when compared with the control group ($p<0.05$). Significant differences in increasing tendency between diabetic group and D+PP and D+LA groups were observed ($p<0.001$) (Table 2).

Protein levels were significantly decreased in the all groups as compared to control group ($p<0.01$, $p<0.001$). When diabetic group was compared to D+PP and D+LA groups, a partial decrease was determined between both groups ($p<0.01$) (Table 2).

TABLE 2
The MDA, GSH and protein levels of erythrocytes in all groups

Groups	MDA (nmol/g)	GSH ($\mu\text{g/g}$)	Protein ($\mu\text{g/g}$)
C	2.62 \pm 0.14	446.96 \pm 18.25	11.17 \pm 0.29
D	4.55 \pm 0.11 ^d	249.01 \pm 2.25 ^d	5.91 \pm 0.18 ^c
D+PP	3.25 \pm 0.17 ^c	359.56 \pm 1.05 ^b	5.19 \pm 0.18 ^d
D+LA	1.92 \pm 0.09 ^d	349.88 \pm 1.91 ^b	5.28 \pm 0.13 ^d

b: $p<0.05$, c: $p<0.01$, d: $p<0.001$

Table 3 shows fatty acid levels in erythrocytes of type-2 diabetic rats. Compared to control group, there were a significant decrease in 16:0 (Palmitic acid), 20:4 n-6 (Arachidonic acid) and 22:6 n-6 (Docosahexaenoic acid) levels ($p<0.001$). Furthermore, 18:0 (Stearic acid), 18:1 n-9 (Oleic acid) and 18:2 n-6 (Linoleic acid) levels ($p<0.05$) were decreased relatively in the diabetic group. In D+PP group, an evident decrease in 16:0, 18:1 n-9 and 22:6 levels was observed ($p<0.001$); whereas a significant difference was determined in 18:2 n-6 and 20:4 n-6 levels ($p<0.01$). A partial decrease was found in 18:0 level ($p<0.05$). Compared to diabetic group, a significant difference in 16:0, 20:4 n-6 and 22:6 n-6 levels ($p<0,01$) and an evident difference in 18:0, 18:1 n-9 and 18:2 n-6 levels ($p<0,001$) were observed in D+PP group. In D+LA group, 16:0, 20:4 n-6 and 22:6 n-3 levels increased significantly ($p<0,01$); whereas, significant decreases were determined in 18:0, 18:1 n-9 and 18:2 n-6 levels ($p<0.001$).

The levels of MDA and total protein in the serum of control and diabetic rats are presented in the Table 4. Compared to control group, a significant increase was observed in MDA level in the diabetic group ($p<0.01$). While a partial decrease was found in D+PP group ($p<0.01$), any difference wasn't observed in D+LA group ($p>0.05$). As diabetic group was compared with D+PP and D+LA groups, a significant decreasing difference was determined between both groups ($p<0.001$).

TABLE 3
The fatty acids levels of erythrocytes in all groups (mg/g)

Fatty Acids	C	D	D+PP	D+LA
16:0	172.14±31.90	49.19±0.35 ^d	76.06±1.64 ^c	67.25±1.33 ^b
18:0	74.22±12.55	46.23±24.41 ^b	41.85±14.07 ^c	32.09±12.46 ^d
∑SFA	246.36±44.45	95.42±24.76	117.91±15.71	99.34±13.79
18:1, n-9	53.80±1.88	31.53±1.22 ^b	21.51±5.41 ^d	24.13±7.69 ^c
∑MUFA	53.80±1.88	31.53±1.22	21.51±5.41	24.13±7.69
18:2, n-6	71.35±14.79	48.07±24.58 ^b	34.86±0.66 ^c	27.92±0.62 ^d
20:4, n-6	154.34±14.35	63.20±1.17 ^d	93.52±0.60 ^b	78.06±0.62 ^c
22:6, n-3	82.98±2.35	26.42±0.71 ^d	34.92±10.31 ^b	31.211±7.61 ^c
∑PUFA	308.67±31.49	137.69±26.46	163.30±11.57	137.19±8.85

b: p<0.05, c: p<0.01, d: p<0.001

TABLE 4
The MDA and protein levels of serum in all groups

Groups	MDA (nmol/g)	Protein (µg/g)
C	2.67±0.69	2.67±0.69
D	4.76±0.13 ^d	4.76±0.13 ^d
D+PP	3.54±0.21 ^c	3.54±0.21 ^c
D+LA	2.59±0.10 ^a	2.59±0.10 ^a

a: p>0.05, c: p<0.01, d: p<0.001

TABLE 5
The fatty acids levels of serum in all groups (mg/g)

Fatty Acids	C	D	D+PP	D+LA
16:0	244.58±13.92	214.55±16.54 ^c	220.74±15.89 ^b	156.67±12.35 ^d
18:0	67.93±1.50	109.48±3.92 ^d	107.25±7.88 ^d	69.93±0.24 ^a
∑SFA	312.51±15.42	324.03±20.46	327.99±23.77	226.6±12.59
16:1, n-7	49.00±0.27	49.09±0.27 ^a	33.85±1.22 ^c	36.87±1.73 ^b
18:1, n-9	246.89±13.03	188.11±18.32 ^b	167.31±15.84 ^d	174.72±20.66 ^c
∑MUFA	295.89±13.30	237.2±18.59	201.16±17.06	211.59±22.39
18:2, n-6	243.12±13.37	203.41±9.97 ^b	195.21±15.34 ^c	175.93±15.40 ^d
20:4, n-6	164.38±15.95	180.38±12.48 ^d	179.32±16.64 ^d	151.07±6.54 ^b
22:6, n-3	42.95±0.24	48.75±9.89 ^c	48.19±0.95 ^c	60.81±0.79 ^d
∑PUFA	450.45±29.56	432.54±32.34	422.72±32.93	387.81±22.73

a: p>0.05, b: p<0.05, c: p<0.01, d: p<0.001

It was found that protein levels significantly increased in the diabetic and D+LA groups compared to control group (p<0.001, p<0.01, respectively). When compared to control group, no significant difference was seen in total protein level in D+PP group (p>0.05). When diabetic group was compared to D+PP and D+LA groups, a distinct decrease was determined between both groups (p<0.001) (Table 4).

Table 5 shows fatty acid levels in serum of type-2 diabetic rats. Compared to control group, there were an evident increase in 18:0 (Stearic acid), 20:4 n-6 (Arachidonic acid) and 22:6 n-6 (Docosahexaenoic acid) levels (p<0.001) and 16:0 (Palmitic acid), (p<0.01), 18:1 n-9 (Oleic acid) and 18:2 n-6 (Linoleic acid) levels (p<0.01, p<0.05, respectively), while relative decrease in the diabetic

group. In D+PP group, an evident increase in 18:0 level was observed (p<0.001); whereas, a significant decrease was determined in 16:1 n-7, 18:1 n-9, 18:2 n-6, 20:4 n-6 levels (p<0.001). A partial decrease was found in 16:0 level (p<0.05). 22:6 n-6 level was determined to get close to C group (p>0.05). While 16:0, 16:1 n-7, 18:1 n-9, 18:2 n-6, 20:4 n-6 levels significantly decreased in D+LA group (p<0.001), 18:0 level got close to C group (p>0.05). Compared to diabetic group, a partial differences in 16:0, 18:0 and 20:4 n-6 levels (p<0.05) and evident differences in 16:1 n-7, 18:1 n-9, and 18:2 n-6 levels (p<0.001) were observed in D+PP group. In D+LA group, 22:6 n-6 level increased significantly (p<0.01); whereas, an evident decrease was found in 16:0, 16:1 n-7, 18:0, 18:1 n-9, 18:2 n-6, 20:3 n-6 and 20:4 n-6 levels (p<0.001, p<0.01, respectively).

The erythrocyte was an early model of oxidative stress studies [24]. It should be prone to oxidative reactions, because of relatively high oxygen tensions, presence of hemoglobin, and a plasma membrane rich in PUFAs. The present study revealed that while a distinct increase in MDA was determined in diabetic groups as compared to control group, it generally decreased in blood samples. Additionally, it was observed that MDA levels in D+PP and D+LA groups had a value close to control group and a decrease compared to diabetic group after the administration. We suggest that the induction of antioxidant enzymatic and non-enzymatic defense systems and suppression of MDA by *Physalis* could be effective in preventing apoptosis activation which might be supported by previous findings [25, 26]. In a study conducted on goldenberry, malondialdehyde (MDA) levels of diabetics were examined and positive outcomes were obtained as a result of administration. The effect of *Physalis* was shown upon effect of anti-free radicals in pancreatic beta cells [6].

In erythrocyte, GSH antioxidant systems is very important and plays a fundamental role in cellular defense against reactive free radicals and other oxidant species [27]. GSH is the most prevalent low molecular weight antioxidant within cells and protects cellular constituents from oxidative damage by reacting directly with oxidants or acting as the substrate for glutathione peroxidase to scavenge peroxides [28]. When the GSH molecule neutralizes the free radicals, the GSH molecule is converted to oxidized form (GSSG). The GSSG is again converted to GSH use to NADPH by the GSH reductase enzyme. The conservation and formation of NADPH in the cells are realized by the activity of pentose-phosphate pathway and malic enzyme [29]. With an insufficient insulin level, the activities of glucose-6-phosphate dehydrogenase in pentose phosphate shunt decreased and glutathione reductase led to impairment of GSH regeneration and increased the level of GSSG. Declined GSH level in the diabetic group may be associated with the lack of insulin. The results of the present study revealed that the level of GSH in diabetic group was lower than the control group. However, GSH level was higher in the plant extract groups. The progression of variable measurements in STZ-diabetic rats after plant extracts treatment might offer a protective influence of *Physalis* and *Lupinus* against STZ action that could be induced through suppression of oxygen free radicals mediated by STZ.

Lipid profile abnormalities form 40% of cases of diabetes and diabetic complications are one of the most common. Fatty acid is required for both the structure and function of every cell in the body and forms an important component of cell membranes [30]. Fatty acid composition is changed in humans [31] and animals with diabetes [32]. In the FA composition of blood samples, palmitic acid level in

diabetic and D+LA groups were lower than the control group. In mammalian cells, palmitic acid is the major products of *de novo* synthesis by the activity of cytoplasmic FA synthase [33]. The present study showed that the level of 18:1 n-9 in fatty acid composition of erythrocyte and serum was low in the diabetic group. Desaturases are key enzymes in the biosynthesis of the monounsaturated and polyunsaturated fatty acids and thereby contribute to the control of the fatty acid-dependent structure and disorder of the membrane. A relationship has been observed between the 16:0/16:1 and 18:0/18:1 ratios usually used as an index of *in vivo* Δ 9-desaturase activity. Brenner et al. [34] have stressed that the activities of fatty acid desaturases, such as Δ 9, Δ 6 and Δ 5 were depressed in STZ induced diabetic rats. Changes in the fatty acid composition of rat liver, heart, kidney, testis, spleen, and brain phospholipids were examined at various stages of STZ-induced diabetes. Brenner [35] reported that STZ-induced diabetes depressed Δ -9, Δ -6 and Δ -5 fatty acid desaturases, decreased arachidonic and increased linoleic acid levels. Desaturase activities in Δ -6 pathway may be increased by insulin and diet restriction [36].

CONCLUSION

Consequently, the possible effects of diabetes on various tissues and protective and therapeutic properties of goldenberry and lupin in these tissues were investigated in this study. It can be asserted that goldenberry and lupin decreased blood glucose and lipid peroxidation levels and increased glutathione level. However, it was observed that they were not sufficiently effective on especially enzyme activities at molecular level. As a result of the obtained results, it is concluded that these plants can be used for diabetic patient follow-up and recovery process. This will be important as an indication of the potentially medicinal and economical utility of *P. peruviana* and *L. albus* as new sources of bioactive phytochemicals and functional foods.

ACKNOWLEDGEMENTS

This study was supported by the project FF.11.40 FUBAP, Firat University.

REFERENCES

- [1] Cuevas, A., Alvarez, V. and Carrasco, F. (2011) Epidemic of metabolic syndrome in Latin America. *Current Opinion in Endocrinology, Diabetes and Obesity*, 18, 134-138.
- [2] Nayak, B.S. and Roberts L. (2006) Relationship between inflammatory markers, metabolic and

- anthropometric variables in the Caribbean type 2 diabetic patients with and without microvascular complications. *Journal of Inflammation*, 3, 17.
- [3] Warjeet, S.L. (2011) Traditional medicinal plants of Manipur as antidiabetics. *Journal of Medicinal Plant Research*, 5, 677-687.
- [4] Pari, L. and Suman, S. (2010) Antihyperglycemic and antilipidperoxidative effects of flavanoid naringin in streptozotocin-nicotinamide induced diabetic rats. *International Journal of Biological and Medical Research*, 1(4), 206-210.
- [5] Kasali, F.M., Kadima, J.N., Mpiana, P.T., Ngbolua, K. and Tshibangu, D.S. (2013) Assessment of antidiabetic activity and acute toxicity of leaf extracts from *Physalis peruviana* L. in guinea-pig. *Asian Pacific Journal of Tropical Biomedicine*, 3(11), 841-846.
- [6] Hassan, A.I., and Ghoneim, M.A.M. (2013) A possible inhibitory effect of *Physalis* (*Physalis pubescens* L.) on diabetes in male rats. *World Appl Sci J*, 21(5), 681-688.
- [7] Garcia Lopez, P.M., De La Mora, P.G., Wysocka, W., Maiztegui, B., Alzugaray, M.E., Del Zotto, H. and Borelli, M.I. (2004) Quinolizidine alkaloids isolated from *Lupinus* species enhance insulin secretion. *European Journal of Pharmacology*, 504, 139-142.
- [8] Eskander, E.F. and Won Jun, H. (1995) Hypoglycemic and hyperinsulinemic effects of some egyptian herbs used for the treatment of diabetes mellitus in rats. *Egyptian Journal of Pharmacology Science*, 36(1-6), 331-342.
- [9] Ohkawa, H., Ohishi, N. and Yagi, K. (1979) Assay for lipid peroxides in animal tissues by thiobarbituric acid reaction. *Analytical Biochemistry*, 95, 351-358.
- [10] Elman, G.I. (1958) Tissue sulfhydryl groups. *Archives of Biochemistry and Biophysics*, 82, 70-77.
- [11] Hara, A. and Radin, N.S. (1978) Lipid extraction of tissues with a lowtoxicity solvent. *Analytical Biochemistry*, 90, 420-426.
- [12] Christie, W.W. (1999) *Gas chromatography and lipids: A Practical Guide*. The Oily Press, Ayr, Scotland.
- [13] Lowry, O.H., Rosebrough, N.J., Farr, A.L. and Randall, R.J. (1951) Protein measurement with the folin phenol reagent. *The Journal of Biological Chemistry*, 193(1), 265-275.
- [14] Emordi, J.E., Agbaje, E.O., Oreagba, I.A. and Iribhogbe, O.I. (2016) Antidiabetic and hypolipidemic activities of hydroethanolic root extract of *Uvaria chamae* in streptozotocin induced diabetic albino rats. *BMC Complementary and Alternative Medicine*, 16, 1-8.
- [15] Zhang, Y., Feng, F., Chen, T., Li, Z. and Shen, Q.W. (2016) Antidiabetic and antihyperlipidemic activities of *Forsythia suspensa* (Thunb.) valh (fruit) in streptozotocin induced diabetes mice. *Journal of Ethnopharmacology*, 192, 256-263.
- [16] Poodineh, J. and Nakhaee, A. (2016) Hypoglycemic and hypolipidemic effects of *Caralluma tuberculata* and its safety on liver and kidneys of diabetic rats. *Turkish Journal of Biochemistry*, 41, 136-143.
- [17] Klip, A. and Vranic, M. (2006) Muscle, liver and pancreas: three musketeers fighting to control glycemia. *American Journal of Physiology: Endocrinology and Metabolism*, 291, 1141-1143.
- [18] Richmond, N. (1973) Colorimetric method of determination of total cholesterol and high density lipoprotein cholesterol. *Clinical Chemistry*, 19, 1350-1356.
- [19] Bornet, F.R.J., Billaux, M.S. and Messing, B. (1997) Glycemic index concept and metabolic diseases. *International Journal of Biological Macromolecules*, 21, 207-219.
- [20] Garzon-de la Mora, P., Moreno-Sandoval, L.E., Villafan-Bernal, J.R., Avalos-Alcantara, G., Gurrola-Diaz, C. and Garcia-Lopez, P.M. (2008) *Lupinus albus* seed globulins induce hypoglycaemia and hypotriglyceridemia in wistar rats. *Lupins for Health and Wealth Proceedings of the 12th International Lupin Conference Canterbury*, 469-472.
- [21] Dahech, I., Belghith, K.S., Hamden, K., Feki, A., Belghith, H. and Mejdoub, H. (2011) Antidiabetic activity of levan polysaccharide in alloxan-induced diabetic rats. *International Journal of Biological Macromolecules*, 49(4), 742-746.
- [22] El-Sheikha, A.F., Riberye, F., Larroque, M. and Reynes, M. (2010) Quality of *Physalis* juice packaged in glass bottles and flexible laminated packs during storage at 5 °C. *Fruit*, 6, 1388-1405.
- [23] Estakhr, J. and Javdan, N. (2011) The Effects of Hydroalcoholic Extract of *Physalis alkekegi* in Alloxan Induced Diabetic Rats. *Pharmacology&Therapeutics*, 2, 874-878.
- [24] Yilmaz O, Ozkan Y, Yildirim M, Ozturk, A.I. and Ersan, Y. (2002) Effects of alpha lipoic acid, ascorbic acid-6-palmitata and fish oil on the glutathione, malonaldehyde and fatty acids levels in erythrocytes of streptozotocin induced diabetic male rats. *Journal of Cell Biochemistry*, 86, 530-539.
- [25] Pari, L. and Murugan, P. (2005) Effect of tetrahydrocurcumin on blood glucose, plasma insulin and hepatic key enzymes in streptozotocin induced diabetic rats. *Journal of Basic Clinical Physiology and Pharmacology*, 16, 257-274.
- [26] El-Mahdy, M.A., Zhu, Q., Wang, Q.E., Wani, G., Patnaik, S., Zhao, Q., Arafa, E.L., Barakat, B., Mir, S.N. and Wani, A.A. (2008) Naringenin protects hacat human keratinocytes against uvb-

- induced apoptosis and enhances the removal of cyclobutane pyrimidine dimers from the genome. *Photochemistry and Photobiology*, 84, 307-316.
- [27] Giron, M.D., Salto, R., Gonzales, Y., Giron J.A., Suarez, D. and Hortelano, P. (1999) Modulation of hepatic and intestinal glutathione S transferases and other antioxidant enzymes by dietary lipids in streptozotocin induced diabetic rats. *Chemosphere*, 38(13), 3003-3013.
- [28] Beutler, E. (1989) Nutritional and metabolic aspects of glutathione. *Annual Review Nutrition*, 9, 287-302.
- [29] Sies, H. (1990) Glutathione and its role in cellular functions. *Free Radical Biology Medicine*, 27, 916-921.
- [30] Kirecci, O.A., Ozsahin, A.D., Yilmaz, O., Erdem, F. and Sarigul H. (2017) Heavy metals (Chromium, copper, lead, and aluminum) on some biochemical parameters in *Saccharomyces cerevisiae* culture medium. *Fresen. Environ. Bull.*, 26(3), 2177-2187.
- [31] Ruiz-Gutierrez, V., Stiefel, P., Villar, J., Garcia-Donas, M.A., Acosta, D. and Carneado, J. (1993) Cell membrane fatty acid composition in type 1 (insulin dependent) diabetic patients: Relationship with sodium transport abnormalities and metabolic control. *Diabetol*, 6, 850-856.
- [32] Holman, R.T., Johnson, S.B., Gerrard, J.M., Mauer, S.M., Kupcho-Sandberg, S. and Brown, D.M. (1983) Arachidonic acid deficiency in streptozotocin-induced diabetes. *Proceedings of National Academy of Sciences of The United States of America*, 80, 2375-2379.
- [33] Leonardo, A.E., Pereiraa, S.L., Sprecherb, H., Huangam, Y.S. (2004) Elongation of long-chain fatty acids. *Progress in Lipid Research*, 43, 36-54.
- [34] Brenner, R.R., Bernasconi, A.M. and Garda, H.A. (2000) Effect of experimental diabetes on the fatty acid composition, molecular species of phosphatidyl-choline and physical properties of hepatic microsomal membranes. *Prostaglandins, Leukotrienes & Essential Fatty Acid*, 63(3), 167-176.
- [35] Brenner, R.R. (2003) Hormonal modulation of D6 and D5 desaturases: case of diabetes. *Prostaglandins, Leukotrienes & Essential Fatty Acid*, 68 (2), 151-162.
- [36] Frenkel, A.L., Canetti, L. and Halpern, Z. (2004) Effects of nutritional lipids on diabetic manifestations and D6 desaturase mRNA level in streptozotocin treated mice. *Nutrition Research*, 24, 303-312.

Received: 18.04.2017

Accepted: 09.06.2017

CORRESPONDING AUTHOR

Ayşe Dilek Ozsahin

Bitlis Eren University,

Faculty of Science Biology Department

13000, Bitlis – TURKEY

E-mail: molekuler@gmail.com

BIOCHEMICAL AND HISTOPATHOLOGICAL CHANGES OF BABESIOSIS IN NATURALLY INFECTED SHEEP IN GAZIANTEP REGION

Haci Ahmet Deveci¹, Gokhan Nur^{1,*}, Abdulsamed Kukurt²

¹Gaziantep University, Vocational School of Higher Education in Islahiye, Gaziantep, Turkey.

²Kafkas University, Faculty of Veterinary Medicine, Department of Biochemistry, Kars, Turkey.

ABSTRACT

The aim of this study is to determine the changes occurring in serum paraoxonase (PON) activity, high density lipoprotein (HDL), total antioxidant / oxidant status (TAS/TOS), nitric oxide (NO), and whole blood glutathione (GSH) levels in sheep with Babesiosis (pre-treatment and post-treatment) compared to healthy sheep. 24 adult awassi sheep with Babesiosis (pre-treatment and post-treatment) that had a weight of 25-35 kg, were 3-5 years old, and were clinically suspicious (body temperature of 39–42°C, icterus, anemia, hematuria) as well as 20 healthy adult awassi sheep were used in the study. PON activity, HDL, TAS/TOS, NO, and whole blood GSH levels were measured in complete blood and serum samples obtained from blood samples taken from animals. Compared to healthy sheep, PON activity, TAS, HDL, and whole blood GSH levels of sheep naturally infected with *Babesia ovis* decreased, their TOS and NO levels increased. After the treatment, biochemical parameters of sheep with Babesiosis were determined to become closer to values of healthy sheep. Cholangiohepatitis, hyperemia in central and portal vein, lymphohistiocytic, areas of focal necrosis, and leukocyte cell infiltration in perivascular/parenchymal areas were observed in histopathological examination of liver cross sections from animals with Babesiosis. Consequently, it was determined that in sheep with Babesiosis parasites caused a shift in oxidant/antioxidant balance of host organism in favor of oxidants and this caused negative conditions to occur in development of animal by creating oxidative stress.

KEYWORDS:

Babesia ovis, glutathion, liver histopatology, oxidant/antioksidant status, paraoxonase activity

INTRODUCTION

Even though geography in which Turkey is located is quite convenient in terms of sheep breeding, its location in subtropical climate zone

causes numerous diseases to be seen. Tick-borne diseases are more common in sheep and goats, and show their effect in tropical and subtropical zones further. Babesiosis is among the most important ones of these diseases and frequently seen in summer months when ticks are active in Turkey [1-3]. Sheep babesiosis is the most critical tick-borne hemoparasitic disease of small ruminants caused by *Babesia ovis*, *Babesia motasi*, and *Babesia crassa*. Sheep Babesiosis caused by *Babesia ovis*, is an important seasonal disease observed in sheep and goats in all geographical regions of Turkey. *Babesia ovis*, which is extremely pathogenic particularly in sheep, causes an infection associated with symptoms such as fever, hemoglobinuria, icterus, and anemia [4-7].

In Babesiosis, membrane permeability and phagocytosis of erythrocytes is increased by activated macrophages and erythrocytes break down [8]. As a result of invasion of erythrocytes by species of *Babesia*, important changes occur in their antioxidant potential. These parasites settling in erythrocyte lead to cellular degradation and eventually lipid peroxidation by causing anemia [9-11]. Increased reactive oxygen species (ROS) and reactive nitrogen species (NOS) cause oxidative stress. As is in several diseases, oxidative stress has a crucial role in pathogenesis of parasitic infections. These reactive species are produced to attack invasive microorganisms in the organism in the first place via nitration and oxidation reactions. Nitric oxide mediates host defense mechanism against numerous intracellular parasites. In addition, excessive amount of ROS and RNS may lead to host cell injury and tissue damage [12-14]. In Babesiosis, oxidative stress and lipid peroxidation have an important role in pathogenesis of anemia. Antioxidant system of the organism weakens and oxidative stress occurs as a result of excessive accumulation of many reactive oxygen species (ROS) such as superoxide, hydrogen peroxide, and hydroxyl radical [15-17].

Paraoxonase enzyme (PON1) is a 43-45 kDa glycoprotein esterase of 354 amino acids. This enzyme, which catalyzes hydrolysis of organophosphates, is associated with HDL in liver, kidney, intestine, and serum [18, 19]. Even though

there are numerous medical studies on paraoxonase enzyme, there is very limited number of studies in veterinary medicine. Limited number of studies [20, 21]. on Paraoxonase activity in Babesiosis, which is an important disease in livestock industry, was found in literature reviews. Therefore, the aim of this study was to determine paraoxonase activity and oxidant/antioxidant balance in sheep naturally infected with *Babesia ovis* in Gaziantep region.

MATERIALS AND METHODS

Experimental Design. 29 adult awassi sheep with Babesiosis (pre-treatment and post-treatment) that were raised in a farm located in Islahiye district of Gaziantep, had a weight of 25-35 kg, were 3-5 years old, and were clinically suspicious (body temperature of 39–42°C, icterus, anemia, hematuria) as well as 20 healthy adult awassi sheep were used in the study. Blood smear staining was performed with 5% Giemsa stain by taking blood samples from Vena jugularis of the animals. Piroplasma forms were found in erythrocytes of 24 sheep out of 29 clinically suspicious sheep in microscopic examination performed under immersion objective (X100). 20 healthy sheep and 24 sheep with Babesiosis which were definitively diagnosed with disease were included in the study. After separating some of blood samples, which were taken from Vena jugularis of sheep with Babesiosis for biochemical measurements before the treatment, as complete blood into tubes containing anticoagulant (EDTA), serums of blood samples were obtained by centrifuging them in tubes without anticoagulant at 3000 rpm for 15 minutes. While whole blood GSH level was measured in the same day, serums were kept at -20 °C until the analysis. 3 doses (0.5 ml/50 kg b.w., 1.2 mg/kg b.w.) of the drug Imicarp (imidokarp dipropiyonat), which is used for treatment, were administered to sheep with Babesiosis. Also, Beforvel vitamin complex was administered for 3 days in addition to the treatment. PON activity, HDL, TAS/TOS, NO, and GSH levels were measured in complete blood and serum samples taken from sheep, which showed recovery in clinical symptoms of disease 1 week after the treatment, by using the same method.

Histopathological Analysis. Liver tissue taken from animals was dissected in appropriate sizes and fixed in formol solution containing 10% buffer. Tissues taken after routine tissue processing (grade alcohols, methyl benzoate, and benzol processing) following the fixation were embedded into paraffine, 5-µm serial cross-sections were taken via microtome

onto microscope slides that were previously coated with chrome alum gelatin (CAG) from blocks. Histopathological changes were examined at the light microscopic level by applying hematoxylin-eosin staining, one of histological staining methods, to the cross-sections [22].

Biochemical Analysis. Measurement of Paraoxonase (PON1) activity: PON1 activity was measured according to methods of Eckerson et al., [23]. and Gülcü and Gürsu [24]. PON1 activity was determined by measuring spectrophotometrically absorbance of colorful product by 4-nitrophenol, resulting from enzymatic hydrolysis of paraoxon (Sigma Co, Lon-don, UK), used as substrate, at 25°C and by using 412 nanometer. The unit for paraoxonase activity was described as enzyme activity of enzyme in 1 ml serum converting 1 nmol paraoxon into 4-nitrophenol within 1 minute and the results were given in U/L.

Measurement of total oxidant status (TOS): TOS was measured by using automated measuring method [25]. Oxidants in the sample had tasks of transferring ferrous ion complex into ferric ion. Ferric ion (Fe^{+3}) forming by oxidation of iron (Fe^{+2}) into more stable form (Fe_2O_3) formed color reaction with xylenol orange in the acidic media. Density of the spectrophotometrically measured color was associated with total amount of oxidant molecules found in the sample. The measurement was calibrated with hydrogen peroxide (H_2O_2) and the results were given in micromolar H_2O_2 equivalent ($\mu mol H_2O_2 equiv./L$) per liter.

Measurement of total antioxidant status (TAS): TAS was measured by using the automated measuring method based on bleaching of the characteristic color of 2,2'-azino-bis (3-ethylbenzothiazoline-6-sulfonic acid) (ABTS) radical by antioxidants of sample added in the medium [26]. The results were given in mmol Trolox equivalent/L.

Measurement of Nitric Oxide: Serum NO levels were measured in spectrophotometer according to method reported by Miranda et al., [27]. In this method, nitrate was transformed into nitrite via Vanadium (III) chloride. Complex diazonium compound formed as a result of the reaction of nitrite and sulphanilamide with N-(1-Naphthyl) ethylenediamine dihydrochloride in acidic medium. This resultant colorful complex was measured at 540 nm. Levels of nitrate and nitrite were determined separately and then sum of these two indicated the amount of NO.

Measurement of whole blood Glutathion (GSH): Whole blood GSH level was analyzed according to the method reported by [28]. In hemolysis of EDTA containing blood prepared with

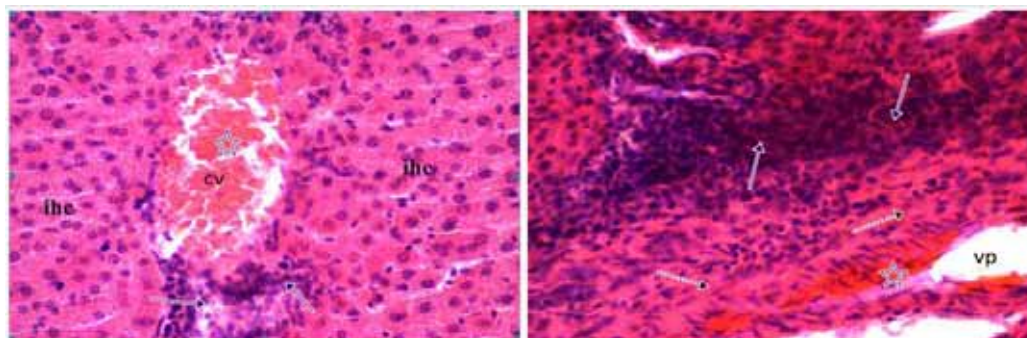


FIGURE 1

Images of liver cross-sections of animals with Babesiosis: sinusoidal, central and portal veins congestion (asterisks), cell infiltrations (arrows), areas of focal necrosis (split arrows), ihc: irregularity hepatic cords, cv: central veins, vp: portal veins.

TABLE 1
PON activity, HDL, TAS, TOS, NO, and GSH levels of all three groups.

PARAMETERS	GROUPS			p
	CONTROL (n:20) (Mean± SD)	BABESIOSIS (n:24) (Pre-treatment) (Mean± SD)	BABESIOSIS (n:24) (Post-treatment) (Mean± SD)	
PON1 (U/L)	205,85±20,47 ^a	159,64±19,13 ^b	181,99±20,30 ^c	*
TAS (mmol Trolox eq/L)	1,42±0,13 ^a	1,06±0,16 ^b	1,21±0,18 ^c	**
TOS (µmol H ₂ O ₂ eq/L)	6,96±0,50 ^a	9,09±0,76 ^b	7,97±0,80 ^c	**
HDL (mg/dl)	64,29±6,44 ^a	53,75±6,18 ^b	58,05±6,68 ^c	**
NO (µmol/L)	13,34±1,04 ^a	17,38±1,67 ^b	15,12±1,45 ^c	**
GSH (mg/dl)	19,32±1,53 ^a	10,45±1,49 ^b	15,07±1,58 ^c	*

* p<0.001: Statistically significant difference. ** p<0.01: Statistically significant difference. ^{a, b, c}: Values with different letter indicate significant differences. SD: Standard deviation.

distilled water, all proteins not carrying sulfhydryl (-SH) groups were precipitated. GSH levels are obtained by spectrophotometric measurement of yellow complexes, formed by -SH groups with DTNB (5,5'-2-ditiobis nitrobenzoic acid) in clear liquid, at 412 nm wave length.

Measurement of high density lipoprotein (HDL): HDL level was examined in the autoanalyzer using a commercial kit and given in mg/dl.

Statistical Analysis. The data obtained from the study were statistically analyzed by using IBM SPSS statistical 22 program. One way analysis of variance (ANOVA) was used to determine whether or not there was a difference between means of experimental group and if there was a difference between means of experimental groups, 'Anova-Duncan' test was applied on mean scores of groups to determine which group or groups caused this difference and the value of p<0.05 was accepted to be statistically significant. The results were given in mean ± standard deviation (X±SD).

RESULTS

Histopathological findings. In examinations of liver tissues obtained from animals with Babesiosis under light microscope; cholangiohepatitis, irregularity in hepatic cords, congestion in central and interlobular vein, lymphohistiocytic, areas of focal necrosis, and leukocyte cell infiltration in perivascular/parenchymal area were observed. There was an indicator for strong inflammation in liver (Figure 1).

Biochemical findings. Table 1 shows PON activity, HDL, TAS, TOS, NO, and GSH levels based on the data obtained from this study conducted to determine paraoxonase activity and oxidant/antioxidant balance in sheep with Babesiosis, one of the tick-borne diseases causing major economic losses for animal husbandry in Turkey.

Accordingly, when control group and the groups with Babesiosis (pre-treatment and post-treatment) were compared in terms of PON1 activity and GSH level, the difference between all

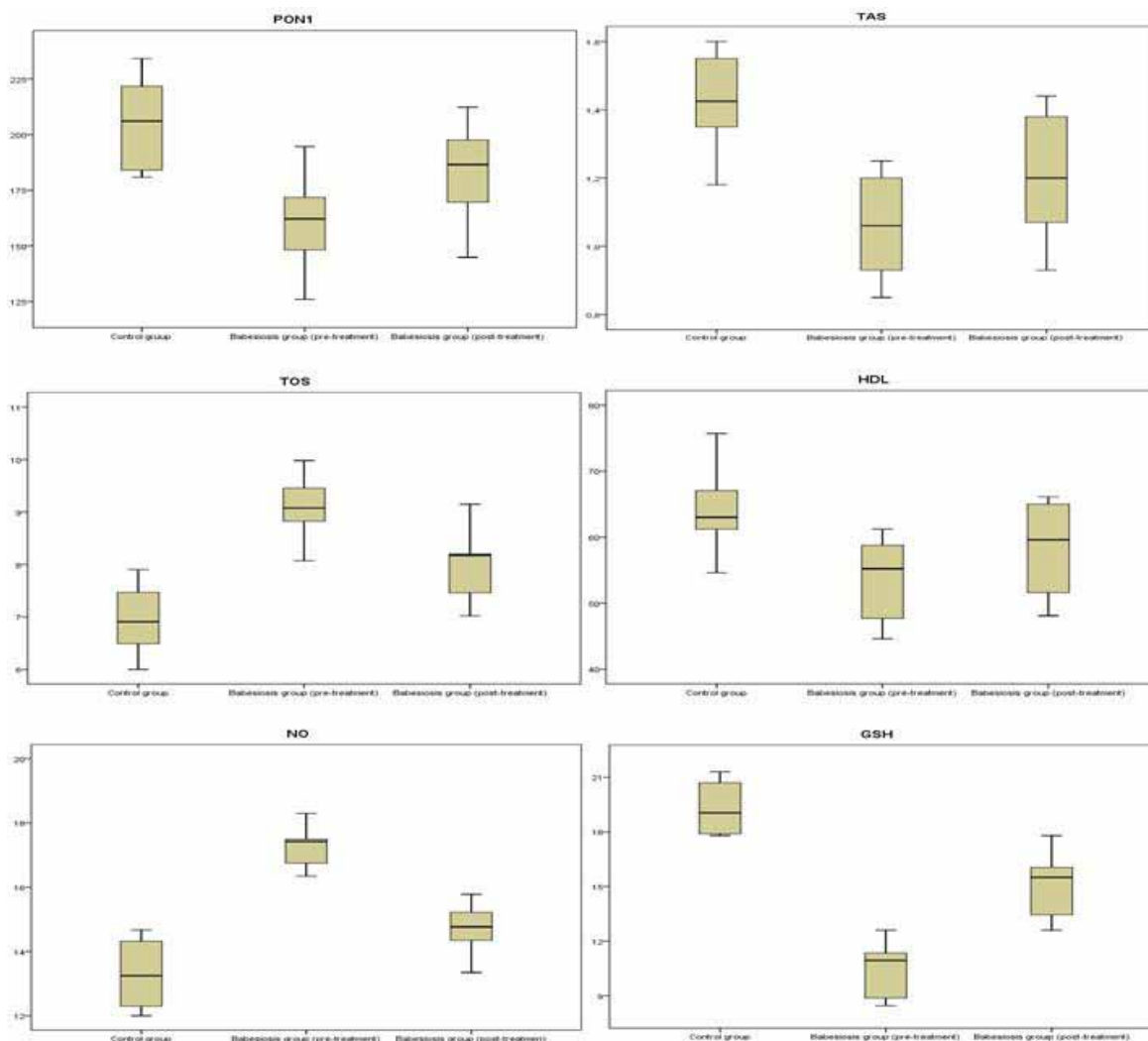


FIGURE 2

Statistical box plot display of biochemical parameters in control and babesiosis groups (pre-treatment and post-treatment).

three groups was found to be statistically significant ($p < 0.001$). Compared to control group, PON1 activity and GSH levels decreased significantly in group with Babesiosis (pre-treatment); whereas, values were observed to increase in the post-treatment group. Similarly, when control group and the groups with Babesiosis (pre-treatment and post-treatment) were compared in terms of TAS/TOS, HDL, and NO levels ($p < 0.01$), the statistically difference between all groups was found to be significant ($p < 0.01$). When groups with Babesiosis were compared with control group, it was determined that while TAS and HDL levels significantly decreased in pre-treatment group with Babesiosis, TOS and NO levels increased significantly. Additionally, TAS/TOS, HDL, and NO levels in the post-treatment group became closer to values of control group.

DISCUSSION AND CONCLUSION

Tick-borne diseases are prevalent in Turkey due to the convenience of climate conditions. Babesiosis, among these diseases, is frequently seen particularly in sheep, causes great losses in terms of animal-based economy in Turkey. Factors causing Babesiosis lead to major changes in biochemical parameters of its host [20, 29, 30]. *Babesia* species cause both anemia by hemolyzing erythrocytes and damage in erythrocytes. Thus, lipid peroxidation occurs as a result of oxidative stress developing based on damage in erythrocytes and antioxidant system which is responsible for protecting cells declines [3, 20, 30].

Under normal physiological conditions, free radicals and antioxidant mechanisms in the organism are in a balance. It is vital for these substances to be in balance for an effective immune system and prevention of tissue damage in living organism. Increased reactive oxygen species in the cells cause oxidative damage in protein, lipid, and DNA. This

results in inhibition of antioxidant enzyme activity and protein synthesis, DNA damage, and cell death [16, 31, 42]. Because oxidant and antioxidant agents will have antagonistic and synergistic effect with each other in the blood, it has been reported to be more beneficial to measure TOS and TAS instead of measuring oxidants and antioxidants individually in order to determine total oxidant/antioxidant balance [25, 26]. It was determined in the present study that TAS values decreased but TOS values increased in sheep with Babesiosis compared to control group. Post-treatment TAS and TOS values in sheep with Babesiosis became closer to those in control group. It was thought that TAS values were low and TOS values were high in sheep with Babesiosis because parasites settling in erythrocyte cause lipid peroxidation and accordingly they may create oxidative stress in animals by weakening antioxidant defense system.

Glutathione (GSH) is a strong antioxidant taking part in elimination of oxidants, which form as a result of increased free radical and lipid peroxidation, from the medium by easily reacting with these substances that are harmful for metabolism [33]. Babesia species leads GSH levels to decrease in erythrocytes and other cells in which they settled. Therefore, the decrease in GSH content indicates that excessive amount of reactive oxygen species forms in these cells [34]. In studies on various species of Babesia, it was reported that GSH levels decreased and lipid peroxidation elevated in Babesiosis [3, 35]. In the present study, compared to control group, whole blood GSH levels decreased significantly in the group with Babesiosis (pre-treatment); whereas, GSH levels of post-treatment group became closer to control group. Low GSH level in sheep with Babesiosis was associated with the fact that Babesia ovis parasites developing in erythrocytes and causing erythrocyte degradation could cause a decrease in GSH levels, which has an important task in antioxidant defense system, by causing oxidative damage in erythrocytes.

Nitric oxide (NO) is a molecule synthesized from L-arginin by means of nitric oxide synthase enzyme and has a role in many physiological and pathophysiological processes [36]. In addition to its inflammatory characteristic, nitric oxide is transformed into peroxynitrite which is considerably harmful for many pathogens merous organs and tissues. Nitric oxide transforming into peroxynitrite inhibits enzyme of many pathogens such as bacteria, virus, and parasite and takes part in defense of organism against bacteria, virus, and parasite [37-40]. Several studies [41-44] reported that NO level increased in Babesiosis. It was determined in the present study that NO levels increased significantly in sheep with Babesiosis and became closer to values of health sheep after the treatment. The reason behind why NO levels increased in sheep with Babesiosis could be that Babesia ovis stimulates NO

production in sheep macrophages and increases release of NO.

Paraoxonase enzyme is an antioxidant enzyme found in various tissues particularly liver, kidney, intestine, and serum. PON1, which is associated with HDL in plasma, acts as target for lipid peroxides. Due to the ability of hydrolyzing lipid peroxides, PON also has an important role for elimination of potential oxidants. A decrease in serum PON1 activity is accepted as an inflammatory response and also as an indicator of increased oxidative damage [18, 45-48]. In limited number of studies [20, 21] on animals with Babesiosis, PON activity was reported to decrease and the decreased PON activity could cause HDL levels to decrease as well. In another study, Mrljak et al. [49] determined that HDL levels decreased in dogs infected with babesiosis and HDL levels increased again after the treatment. In the present study, PON activity and HDL levels were detected to decrease significantly in sheep with Babesiosis compared to healthy sheep and became closer to values of healthy sheep after the treatment. The decreased PON activity in sheep with Babesiosis made us think that this could be associated with increased free radical and lipid peroxidation caused by Babesia parasites; on the other hand, decreased HDL level might be associated with the decreased in PON activity as well as LDL oxidation.

Consequently, decreased whole blood GSH, serum PON activity, TAS and HDL levels and increased TOS and NO levels in sheep naturally infected with Babesia ovis is an indicator for a shift in favor of oxidants in oxidant/antioxidant balance of host organism of parasites in tick-borne diseases. In addition, the fact that the same parameters became closer to values of healthy sheep in the post-treatment period reveals consideration of oxidative stress in fighting against animal diseases and importance of the use of vitamin complexes along with anti-parasitic medication.

REFERENCES

- [1] Hacılarlıoğlu, S., and Karagenc, T. (2015) Koyun babesiosis; Animal Health. Production and Hygiene 4(1), 373-379.
- [2] Razmi, G.R., Naghibi, A., Aslani, M.R., Fathivand, M., and Dastjerdi, K. (2003) An epidemiological study on babesia infection in small ruminants in mashhad suburb, khorasan province. Iran. Small Ruminant Research 50, 39-44.
- [3] Şanlı, Ü., and Değer, Y. (2008) Babesiosisli koyunlarda hemoglobin tipleri ve glutatyon düzeyleri. Y.Y.Ü. Veteriner Fakültesi Dergisi 2, 21-24.
- [4] Almeria, S., Castella, J., Ferrer, D., Ortuno, A., Estrada-Pena, A., and Gutierrez, J.F. (2001) Bovine piroplasm in minorca (Balaric Island

- Spain): a comparison of PCR-based and light microscopy detection. *Vet. Parasitol* 99, 249-259.
- [5] Homer, M.J., Aguilar-Delfin, I., Telford, S.R., Krause, P.J., and Persing, D.H. (2000) Babesiosis. *Clin. Microbiol. Rev* 13(3), 451-469.
- [6] Rahbari, S., Nabian, S., Khaki, Z., Alidadi, N., and Ashrafihelan, J. (2008) Clinical, haematologic and pathologic aspects of experimental ovine babesiosis in Iran. *Iran J. Vet. Res* 9, 59-64.
- [7] Sayın, F., Dinçer, S., Karaer, Z., Cakmak, A., Yukarı, B.A., Eren, H., Değer, S., and Nalbantoğlu, S. (1997) Status of tick-borne diseases in sheep and goats in Turkey. *Parasitologia* 39, 153-156.
- [8] Saleh, M.A. (2009) Erythrocytic oxidative damage in crossbred cattle naturally infected with babesia bigemina. *Res Vet Sci* 86, 43-48.
- [9] Annetta, Zintl., Grace, Mulcahy., Helen, E., Skerret, Stuart, M., Taylor and Jeremy, S. (2003) Gray Babesia divergens, a bovine blood parasite of veterinary and zoonotic importance. *Clinical. Microbiology Reviews*, Oct, p 622-636.
- [10] Değer, Y., Dede, S., Kahraman, T., Deger, S., Ormanci, N., and Biçek, K. (2001) Babesiosisli koyunlarda lipid peroksidasyonu, nitric oksit oksidasyon ürünleri ve antioksidan durumunun saptanması. *Türkiye Parazit Derg* 25(1), 25-27.
- [11] Ginsburg, H., and Atamina, H. (1994) The redox status of malaria infected erythrocytes: an overview with an emphasis on unresolved problems. *Parasite* 18, 5-13.
- [12] Bildik, A., Kargin, F., Seyrek, K., Pasa, S., and Özensoy, S. (2004) Oxidative stress and non-enzymatic antioxidative status in dogs with visceral leishmaniasis. *Res Vet Sci* 77, 63-6.
- [13] Koçyigit, A., Keleş, H., Selek, S., Güzel, S., Çelik, H., and Erel, Ö. (2005) Increased DNA damage and oxidative stress in patients with cutaneous leishmaniasis. *Mutat Res* 585, 71-8.
- [14] Oliveira, F.J.A., and Cechini, R. (2002) Oxidative stress of liver in hamsters infected with leishmania (L.) chagasi. *J Parasitol* 86, 1067-72.
- [15] Brunet, L.R. (2001) Nitric oxide in parasitic infections. *International immunopharmacology* 1, 1457-1467.
- [16] Deveci, H.A., Karapehlivan, M., Kaya, İ., Kükürt, A., and Alpay, M. (2015) Protective role of caffeic acid phenethyl ester against chlorpyrifos-ethyl acute poisoning. *Ankara Üniv. Vet. Fak.Derg* 62(4), 255-260.
- [17] Zaidi, S.M., AL-Qirim, T.M., and Bani, N. (2005) Effect of antioxidant vitamins on glutathione depletion and lipid peroxidation induced by restrained stress in the rat liver. *Drug R.D* 157-165.
- [18] Deveci, H.A., Kükürt, A., Uzlu, E., Sözdutmaz, İ., Merhan, O., Aktaş, S., Alpay, M., Kaya, İ., and Karapehlivan, M. (2017) Evaluation of paraoxonase activity, total sialic acid and oxidative stress in sheep with ecthyma contagiosa. *Kafkas Univ Vet Fak Derg* 23 (3), 453-457.
- [19] Watson, A.D., Berliner, J.A., Rama, S.Y., La Du, B.N., Faul, K.F., Fogelman, A.M., and Navab, M. (1995) Protective effect of high density lipoprotein associated paraoxonase. Inhibition of the biological activity of minimally oxidized low density lipoprotein. *J. Clin. Invest* 96, 2882.
- [20] Azimzadeh, K., Nouri, K., Farooqi, H., Rasouli, S., and Zamani, N. (2013) Plasma malondialdehyde, thyroid hormones and some blood profiles in ovine babesiosis. *Kafkas Univ. Vet. Fak. Derg* 19 (3), 489-493.
- [21] Rossi, G., Kuleš, J., Baric´ Rafaj, R., Mrljak, V., Lauzi, S., Giordano, A., and Paltrinieri, S. (2014) Relationship between paraoxonase 1 activity and high density lipoprotein concentration during naturally occurring babesiosis in dogs. *Research in Veterinary Science* 97(2), 318-324.
- [22] Luna, L.G. (1968) Manual of histologic staining methods of armed forces institute of pathology. Third Ed. MC. Graw. Hill Book Comp. London.
- [23] Eckerson, H.W., Romson, J., Wyte, C.M., and La Du, B.N. (1983) The human serum paraoxonase polymorphism: Identification of phenotypes by their response to salts. *Am. J. Hum. Genet* 35, 214-227.
- [24] Gülcü, F., and Gürsu, M.F. (2003) Paraoksonaz ve aril esteraz aktivite ölçümlerinin standardizasyonu. *Turk J. Biochem* 28, 45-49.
- [25] Erel, Ö. (2005) A new automated colorimetric method for measuring total oxidant status. *Clin. Biochem* 38, 1103-1111.
- [26] Erel, Ö. (2004) A novel automated direct measurement method for total antioxidant capacity using a new generation, more stable abts radical cation. *Clin. Biochem* 37, 277-285.
- [27] Miranda, K.M., Espey, M.G., Wink, D.A. (2001) A rapid, simple spectrophotometric method for simultaneous detection of nitrate and nitrite. *Nitric Oxide* 5(1), 62-71.
- [28] Beutler, E., Duran, O., and Kelley, B.M., (1963) Improved method for determination of blood glutathione. *J. Lab. Clin. Med* 61, 882-888.
- [29] Akış, M.E., and Dede, S. (2009) Babesiosisli koyunlarda çinko ve bakır konsantrasyonları ve karbonik anhidraz enzim aktivitesinin saptanması. *YYU Veteriner Fakültesi Dergisi* 20(2), 33-37.
- [30] Esmaeilnejada, B., Tavassolia, M., Asri-Rezaeib, S., and Dalir-Naghadeh, B. (2012) Evaluation of antioxidant status and oxidative stress in sheep naturally infected with babesia ovis. *Veterinary Parasitology* 185, 124-130.
- [31] Özcan, A., and Ogun, M. (2015) Biochemistry of reactive oxygen and nitrogen species. In Gowder SJT (Ed): *Basic Principles and Clinical*

- Significance of Oxidative Stress. InTech, DOI 10, 5772-61193.
- [32] Salman, K.A., and Ashraf, S. (2013) Review: Reactive oxygen species: A link between chronic inflammation and cancer. *As Pac J Mol Biol Biotechnol* 21, 42-49.
- [33] Anderson, M.E. (1998) Glutathione an overview of biosynthesis and modulation *Chem. Biol. Interact* 1-4, 111-112.
- [34] Guha, M., Kumar, S., Choubey, V., Maity, P., and Bandyopadhyay, U. (2006) Apoptosis in liver during malaria: role of oxidative stress biomed research international 7 and implication of mitochondrial pathway. *The FASEB Journal*, vol. 20, no. 8, pp 1224–1226.
- [35] Biçek, K., Değer, Y., and Değer, S. (2005) Some biochemical and haematological parameters of sheep infected with babesia species. *YYÜ Vet Fak Derg* 16 (1), 33-35.
- [36] Marletta, M.A. (1988) Mammalian synthesis of nitrite, nitrate, nitric oxide, and N-nitrosating agents. *Chem Res Toxicol* 1, 249-257.
- [37] Akaike, T., Suga, M., and Maeda, H. (1998) Free radicals in viral pathogenesis. Molecular mechanisms involving superoxide and nitric oxide. *Proc. Soc. Biol. Med* 217, 64-73.
- [38] Kreil, T.R., and Eibl, M.M. (1996) Nitric oxide and viral infection. No antiviral activity against a flavivirus in vitro, and evidence for contribution to pathogenesis in experimental infection in vivo. *Virology* 219, 304-306.
- [39] Petermann, H., Vogl, S., Schulze, E., and Dargel, R. (1999) Chronic liver injury alters basal and stimulated nitric oxide production and 3H-thymidine incorporation in cultured sinusoidal endothelial liver cells from rats. *J Hepatol* 31, 284- 292.
- [40] Vespa, G.N., Cunha, F.Q., and Silva, J.D. (1994) Nitric oxide is involved in control of *Trypanosoma cruzi*-induced parasitemia and directly kills the parasite in vitro. *Infection and Immunity* 62, 5177-5182.
- [41] Hanafusa, Y., Cho, K.O., Kanemaru, T., Wada, R., Sugimoto, C., and Onuma, M. (1998) Pathogenesis of babesia caballi infection in experimental horses. *J. Vet. Med. Sci* 60, 1127–1132.
- [42] Kontaş, T., and Salmanoğlu, B. (2006) Tumour necrosis factor- α , adenosine deaminase and nitric oxide levels in cattle babesiosis before and after treatment. *Bull Vet Inst Pulawy* 50, 485-487.
- [43] Mert, H., Yörük, I., Değer, Y., Mert, N., Dede, S., and Yur, F. (2009) Concentration of products of nitric oxide oxidation and some vitamins in sheep with naturally acquired babesiosis *Turk. J. Vet. Anim. Sci* 33(2), 131-135.
- [44] Stich, W.R., Shoda, L.K.M., Dreeuwess, M., Adler, B., Thomas, W. (1998) Stimulation of nitric oxide production in macrophages by babesia bovis. *Infect Immun* 66 (9), 4130-4136.
- [45] Korkmaz, I., Aydın, H., Eren, Ş.H., Güven, F.M.K., Yıldırım, B., Beydilli, İ., and Eren, M. (2013) The relationship between oxidative stress, paraoxanase and injury severity in blunt trauma patients. *Journal of Clinical and Analytical Medicine* 4, 196-199.
- [46] Marsillach, J., Camps, J., Beltran-Debón, R., Rull, A., Aragones, G., Maestre-Martínez, C., Sabench, F., Hernández, M., Castillo, D.D., Joven, J., Mackness, M., and Mackness, B. (2011) Immunohistochemical analysis of paraoxonases 1 and 3 in human atheromatous plaques. *Eur J Clin Invest* 41, 308-314.
- [47] Deveci, H.A., Kaya, İ., Yılmaz, M., Karapehlivan, M. (2015) Effect of zinc sulphate on the levels of plasma paraoxonase activity, total oxidant and high density lipoprotein of transcaucasian barb (*Capoeta capoeta* [Guldenstaedt, 1773]). *Fresen. Environ. Bull.*, 24 (9), 2732-2735.
- [48] Deveci, H.A., Ünal S., Karapehlivan, M., Ayata, M.K., Gaffaroğlu, M., Kaya, İ., Yılmaz, M., Effects of glyphosate (herbicide) on serum paraoxonase activity, high density lipoprotein, total antioxidant and oxidant levels in Kars Creek Transcaucasian Barbs (*Capoeta capoeta* [Guldenstaedt, 1773]). *Fresen. Environ. Bull.*, 26 (5), 3514-3518, 2017.
- [49] Mrljak, V., Kučer, N., Kuleš, J., Tvari-jonaviciute, A., Brkljačić, M., Crnogaj, M., Zivičnjak, T., Smit, I., Ceron, J.J., and Rafaj, R.B. (2014) Serum concentrations of eicosanoids and lipids in dogs naturally infected with *Babesia canis*. *Veterinary Parasitology* 201, 24–30.

Received: 27.04.2017

Accepted: 12.06.2017

CORRESPONDING AUTHOR

Gokhan Nur

Gaziantep University, Vocational School of Higher Education in Islahiye, Gaziantep, Turkey

e-mail: gokhannur@gantep.edu.tr

ASSESSMENT THE NOISE LEVEL IN LIBRARIES AND DORMITORIES OF KERMANSHAH UNIVERSITY OF MEDICAL SCIENCES IN 2016 (KERMANSHAH, IRAN)

Amir Hossein Nafez^{1,2}, Soheila Lotfi³, Reza Rostami^{2,*}, Reza Saeedi⁴, Shahla Lotfi⁵

¹Department of Environmental Health Engineering, Kermanshah University of Medical Sciences, Kermanshah, Iran

²Student research committee, Kermanshah University of Medical sciences, Kermanshah, Iran

³Student Research Committee, Kurdistan University of Medical Sciences, Sanandaj, Iran

⁴Department of Environmental Health, Faculty of Health, Safety and Environment, Shahid Beheshti University of Medical Sciences, Tehran, Iran

⁵M.S Knowledge and information Science of AL Zahra University, Tehran, Iran

ABSTRACT

The stress driving from noise is one of the important reasons that endanger health. The extra noise causes hearing damage, sleep disorders, and release of the stress hormone (Cortisol) that can influence the immune system and body metabolism. This study aimed to assess the noise level in libraries and dormitories of Kermanshah University of Medical Sciences (KUMS) in Iran, 2016.

This study is a descriptive-analytic, cross sectional study that assessed the noise level in different part of libraries of five faculties including: pharmacy, dentistry, medical, paramedical, and health schools in KUMS and two dormitories of this university. For this aim we used 5969 Casella phonometer and finally the obtained data were compared with the Iranian and USA federal standards.

According to the results, all of the assessed dormitories and libraries had a noise level higher than the Iranian standards and 46% of dormitories and 41% of libraries had a noise level higher than the USA standard.

This condition causes physical and psychological harms to students and it reduces the students' attention and effectiveness; so reduction of these distractive noises is essential for raising the libraries and dormitories qualification.

KEYWORDS:

noise pollution, library, dormitory, Kermanshah

INTRODUCTION

Sound shows a sine variation of air pressure with a defined frequency that is being transferred through the air with variable velocity. The noise composed of a combination of several sounds. These sounds can damage the hearing [1]. The sound waves circulate in a wide limitation but only in 20-20000 Hz can stimulate the human ear for hearing [2]. Noise exposure in addition to hearing drop creates

many problems such as; distractions, bothering, tiredness, decrease of efficiency, sleep disturbance, and also irritation and stress [3, 4]. The important point beside the physical problems is the psychological problems [5].

The dormitory as a place for students reside, can play a significant role during a students' educational period. All the different circumferential aspects have effects on popularity living condition in dormitories [6]. One of these aspects is the problem of noise in dormitories that can be mentioned as an important factor influencing sleep, study, and psychological situation in students. In addition to this important part, libraries are also one of the important places that noise controls in them needed an especial attention [7]. That is due to noise pollution and insecurity of the desire situation of noises in these places, can be excluded as one of the physical risk factors [8, 9].

The maximum acceptable level of noise is established by the federal or local rules. This maximum level according to the federal rules in libraries is 40-45 dB and for dormitories is 45 dB [10]. Also the permitted limitations acoustic pressure balance in libraries and bedroom according to national residential rules of Iran is between 35-40 dB and 30-35 dB respectively [11]. Considering that existence of a calm and quiet element in libraries' spaces can affect study efficiency significantly [12]. This study aimed to measuring this physically parameter in reading rooms (study hall) and dormitories of KUMS in comparison with standard scales.

MATERIAL AND METHODS

This study is a descriptive-analytical, cross sectional study which is done in 2016 spring, in libraries of faculties and boys dormitories of KUMS and overall five book reservoir, five IT lounges, five study halls, two study halls in dormitories and also 13 halls of dormitories including: student's rooms, hall ways and kitchens. For measuring sounds and noises, we used the 5969Casella-BS phonometer

TABLE 1
The noise level in libraries of KUMS

No.	Location	Min.(dB)	Max.(dB)	Mean (dB)	Standard deviation
1	Book reservoir of medical school	30.12	44.20	39.40	2.64
2	IT lounge of medical school	35.60	46.00	42.25	1.82
3	Study hall of dentistry school	39.00	49.50	45.00	2.34
4	Study hall of Boostan dormitory	31.70	41.20	39.55	2.32
5	Study hall of Mofatteh dormitory	44.00	54.00	47.13	2.02
6	Book reservoir of dentistry school	38.00	46.50	43.36	1.12
7	Study hall of paramedical school	42.30	54.90	49.83	1.75
8	Study hall of pharmacy school	33.60	38.00	35.03	1.05
9	Book reservoir of pharmacy school	37.50	44.00	42.50	1.56
10	IT lounge of pharmacy school	43.00	48.60	47.14	1.25
11	Book reservoir of health school	34.80	42.50	37.66	2.25
12	IT lounge of health school	47.00	54.90	52.74	1.75
13	Book reservoir of paramedical school	45.60	55.00	47.97	1.25
14	Study hall of health school	48.00	51.00	50.13	0.28
15	Study hall of medical school	32.00	37.80	36.98	1.71
16	IT lounge of paramedical school	38.80	51.00	48.58	1.25
17	IT lounge of dentistry school	36.00	43.70	40.70	1.04

TABLE 2
Noise level in dormitories of KUMS

No.	Location	Min.(dB)	Max.(dB)	Mean (dB)	Standard deviation
1	Boostan dormitory block 1, 1st floor	35	49	40.05	2.35
2	Boostan dormitory block 1, 2nd floor	37.7	50	46.13	3.25
3	Boostan dormitory block 1, 3rd floor	37.8	47	43.78	2.75
4	Boostan dormitory block 2, floor 1	35	45	39.28	1.85
5	Boostan dormitory block 2, floor 2	40	56.9	44.2	2.25
6	Boostan dormitory block 2, floor 3	43.7	59	47.49	1.56
7	Boostan dormitory block 3, floor 1	30.1	43.3	38.5	2.24
8	Boostan dormitory block 3, floor 2	37.2	52.3	41.67	1.25
9	Boostan dormitory block 3, floor 3	35.8	48.5	39.85	1.63
10	Mofatteh dormitory floor 1	39	51.9	48.8	2.56
11	Mofatteh dormitory floor 2	36.8	50	46.2	2.56
12	Mofatteh dormitory floor 3	42.5	49	48	1.36
13	Mofatteh dormitory floor 4	40	50	47.5	1.45

made in England. To ensure the accuracy of measurements by the phonometer we had to calibrate it with a standard sound generator. This device produces certain frequencies equal to 94 to 114 dB and the calibration was done in the laboratory by this device. The measurements were done at the height of one and half meters above the ground. During all measurements the device range was on A-Lo (30-100 dB) and the measure speed was on fast and there was a sponge protector on the device's microphone to reduce the effects of air current to the minimum level. To determine stations, the surface was divided into 3×3 squares. In this way the measurement stations were determined. All measurements in centers of determined stations, in decibels, were read from the device and recorded in special forms. All samplings were done without attracting the attention of people at the library and the mean level of measured noise was reported.

Research findings. A summary result of measured noise in investigated libraries and dormitories is listed in Tables 1 and 2 and figures 1 and 2.

According to the results those are given in table 1 100% of the assessed libraries had the noise level

higher than the national residential standards of Iran (35-40dB). However, the resulting data are more than the USA standards (40-45dB) in 41% of cases and in 35% cases were in the standard range and in 24% cases were less than standards.

According to the results from table 2 all of the assessed dormitories had a noise level higher than the national residential standards of Iran (30-35 dB). However the resulting data compared to the USA standards (45 dB) were less than standards, in 54% of cases.

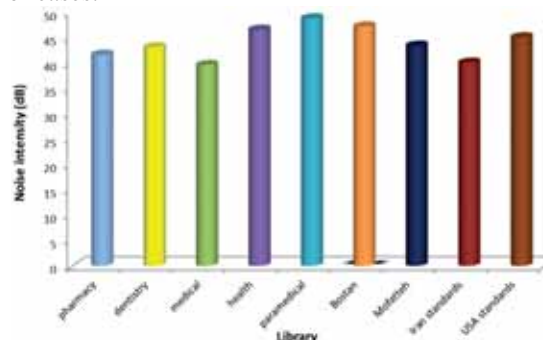


FIGURE 1
Comparison of the measured noise intensity in libraries

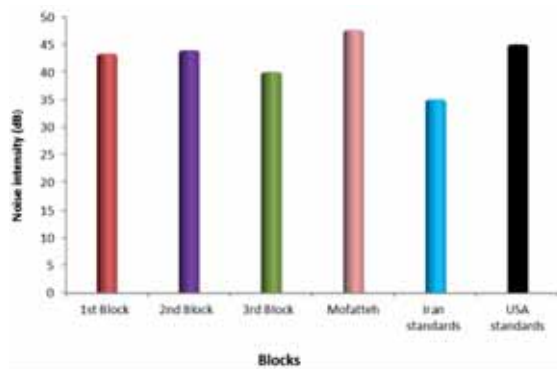


FIGURE 2

Comparison of the measured noise intensity in dormitories (dB)

DISCUSSION

According to the results from the Fig 1 among assessed libraries, the paramedical study hall with the mean of 48.79 dB had the highest level and the medical library with the mean of 39.54 dB had the lowest level. Among boys dormitories which were assessed in this study according to the Fig 2 the Mofatteh dormitory with the mean of 47.62 dB had the highest level and the Boostan dormitory block 3 (3rd block) with the mean of 40.00 dB had the lowest level.

In another classification of the resulting data from libraries, it was estimated that, the highest level with the mean of 52.74 dB for the IT lounge of the health school and the lowest level was for the study hall of pharmacy school with the mean of 35.03 dB. Also among the data resulting from boys dormitories the highest level was for the first floor in Mofatteh dormitory with the mean level of 48.80 dB and the lowest level was for the first floor of Boostan dormitory block 3 (3rd Block) with the mean of 38.50 dB.

In the research of Tajic et al. in 2008, in a metal industry in Arak city of Iran revealed that in some working units of this factory noise pollution and hearing loss have a high prevalence [13]. Asgharnia et al. (2012) in Babol city, Iran, stated that in their assessed hospitals the balance of noise intensity, on ordinary days and holidays in all three time interval; morning, afternoon and visiting hours, has been more than the specified level by WHO guidelines [14]. In Muasheri et al. research in 2010 in Birjand, Iran the mean balance noise of the morning and night in all the stations of crowded places were significantly more than the allowable limit [15]. The results of Juang et al. (2010) showed that in every day as an average the level of noise in hospital during day had been between 52.6 - 64.6 dB, and the high level of noise in this hospital has a direct effect on physical and psychological health of personnel and patients [16]. Among the levels of noise in libraries and student dormitories can be mentioned to the adjacent

spaces sounds, voice of vehicle traffic, student commuter, ventilation systems, the sound of moving chairs and other furniture.

CONCLUSION

Generally based on the results and assessments, the balance of noise pressure in libraries and dormitories, is more than the standard level of Iran and USA. This causes physical and psychological harm in students and decreases attention and efficiency. So, reduction of the disturbing noises is essential for promotion the qualification of libraries and dormitories. Corrective action, including double glazed windows, using rubber at the end of the seats, using carpet as a floor covering and also keeping and on time repair of all electronic equipment is recommended.

REFERENCES

- [1] Webster, D.B. (1977) Neonatal sound deprivation affects brain stem auditory nuclei. *Archives of Otolaryngology*; 103(7):392-6
- [2] Rabiyan, M, Gharib, M. (2003) Noise pollution in operating rooms and intensive care units. *Medicine and cultivation*; 12(4):50-56[Persian].
- [3] Basner, M, Babisch, W, Davis, A, Brink, M, Clark, C, Janssen, S, Stansfeld, S. (2014) Auditory and non-auditory effects of noise on health. *The Lancet*; 383(9925):1325-1332.
- [4] Farhang Dehghan, S, Monazzam, M.R., Nassiri, P, Haghghi, Kafash, Z, Jahangiri, M. (2013) The Assessment of Noise Exposure and Noise Annoyance at a Petrochemical Company. *Journal of Health and Safety at Work*; 3(3):11-24[Persian].
- [5] Zonouzi, F, Ranjbarian, M, Afjeie, S.A. (2006) Evaluation of noises in neonatal intensive care unit in Mofid Children's Hospital. *Medical Sciences*; 16(3):129-134[Persian].
- [6] Khozaei, F, Hassan, A.S, Al Kodmany, K, Aarab, Y. (2014) Examination of student housing preferences, their similarities and differences. *Facilities*; 32(11/12):709-722.
- [7] Huisman, E.R, Morales, E, Van Hoof, J, Kort, H.S. (2012) Healing environment: A review of the impact of physical environmental factors on users. *Building and Environment*; 58:70-80.
- [8] Farajpahlou, A.H, Danesh, F. (2009) Job description requirements for systems librarians in Iranian university libraries. *The Electronic Library*; 27(1):58-73.
- [9] Ilali, E.S, Taraghi, Z, Siamian, H, Mahdian, P, Rad A.A, Mohammadpour, R.A, Mazaheri, K. (2010) Assessment of academic libraries in Mazandran, Goleston and Babul Medical Universities. *Journal of Mazandaran University of Medical Sciences*; 20(74):84-90[Persian].

- [10] Stansfeld, S.A, Matheson, M.P. (2003) Noise pollution: non-auditory effects on health. *British medical bulletin*; 68(1):243-257.
- [11] Environmental Protection Organization (1998): *Environmental Protection Organization Standard and regulations*, Tehran, Iran.
- [12] Nafez, A.H, Azizi, S.A, Lotfi, S, Rostami, R. (2016) Assessment of interior general and local lighting and UV radiation in the libraries of the faculties in the Kermanshah University of Medical Sciences (2016). *International Journal of Pharmacy and Technology*; 8(3):18934-18940.
- [13] Tajic, R, Ghadami, A, Ghamari, F (2008) The Effects of Noise Pollution and Hearing of Metal Workers in Arak. *Zahedan Journal of Research in Medical Sciences*; 10(4):291-299 [Persian].
- [14] Asgharnia, H.A, Tirgar, A, Amouei, A, Fallah, S.H, Khafri, S, Mohammadi, A.A, Peykarporsan, F, Rahimi, D, Beykaei S.B, Shirkhani, Z. (2014) Noise Pollution in the Teaching Hospitals of Babol (Iran) in 2012. *Journal of Babol University of Medical Sciences*; 16(4):64-69 [Persian].
- [15] Moasheri, B.N, Abolhasannejad, V, Vahdatparast, Z, Sharifi, S, Hojatpanah, R, Taghizadeh, A.A. (2015) Assessment of Day Average Sound Level Index in Overcrowded Areas of Birjand City in 2011. *Journal of Health*; 6(1):115-124 [Persian].
- [16] Juang, D.F, Lee, C.H, Yang, T, Chang, M.C. (2010) Noise pollution and its effects on medical care workers and patients in hospitals. *International Journal of Environmental Science & Technology*; 7(4):705-716.

Received: 03.05.2017
Accepted: 11.05.2017

CORRESPONDING AUTHOR

Reza Rostami

Student research committee, Kermanshah University of Medical Sciences, Kermanshah, Iran

E-mail: rezarostami745@gmail.com

AUTHOR INDEX

A

Aasim, M.	4671	AlAntary, T. M. A.	4711
Ahmad, K.	4332	Alawi, M. A.	4711
Ahmad, K.	4345	Ali, A.	4602
Ahmad, M. S.	4345	Ali, H. M.	4645
Akan, K.	4859	Alkan, S.	4416
Akbar, K. F.	4602	Al-Khaishany, M. Y. Y.	4645
Akdemir, F. N. E.	4375	Almasri, M.	4504
Akgul, H.	4470	Alp, F. M.	4568
Akgul, H.	4757	Al-Qutami, M. A.	4645
Akkol, E. K.	4420	Amjad, N.	4345
Akman, B.	4845	Asicioglu, F.	4650
Akyol, H.	4677	Aubrey, D.	4504
Alakeel, K. A.	4645	Ayan, S.	4606
Alamri, S. A.	4645	Aydin, Y.	4859

B

Bai, C.	4325	Beltagi, H. S. E.	4764
Bashir, H.	4332, 4345, 4602	Beyhan, O.	4456
Batool, A. I.	4345	Bilgen, H. D.	4790
Batool, F.	4345	Bozkurt, A.	4841
Beev, G.	4367		

C

Cai, J.	4325	Chen, Y.	4798
Cai, M.	4574	Cheng, S.	4350
Cai, S.	4549	Chun Xu, S.	4742
Cankaya, M.	4375	Coban, A.	4375
Chao, J.	4325	Cui, M.	4409
Chen, H.	4742		

D

Dai, J.	4325	Diao, J.	4817
Dai, Y.	4522	Diao, Y.	4536
Day, S.	4671	Dikmen, M.	4726
Demiral, H.	4484	Ding, S.-I.	4588
Demiral, I.	4484	Djogo, M.	4867
Demirci, S.	4841	Dogan, M.	4470
Deng, R.	4517	Du, X.	4522
Dermendzhieva, D.	4367	Dundar, O.	4716
Deveci, H. A.	4883	Durmaz, Y.	4783

E

Ejaz, A.	4345	Eraslan, G.	4704
Eken, M. D.	4845	Erbey, G.	4420
Elicin, A. K.	4684	Erbil, G. C.	4783
Enez, B.	4446	Erken, O.	4383
Engindeniz, S.	4555	Erman, F.	4876
Engur, S.	4726	Erman, O.	4876

F

Fincan, S. A.	4446		
---------------	------	--	--

G

Gacic, Z.	4834	Ghafoor, A.	4602
Gan, J.	4549	Gokcek, K.	4841



Gao, C.	4742	Gong, Y.	4325
Gao, G.	4325	Gui, H.	4697
Gao, J.	4390	Gul, A.	4602
Ge, X.	4798	Gul, M.	4375
Gebologlu, M. D.	4568	Gumus, S.	4656
Geng, R.	4808	Gursul, C.	4375
H			
Haddad, N.	4711	Hou, B.	4517
Hamid, S.	4345	Hu, C.	4400, 4542
Han, G.	4851	Hu, Y.	4325
Han, J.	4574	Huang, L.	4817
Han, Y.	4851	Huang, Y.	4798
Hatay, T. Y.	4656	Huanhuan, D.	4528
Hayat, Z.	4345	Hussain, R.	4602
Hilooglu, M.	4692		
I			
Ige, J. O.	4623	Iqbal, S.	4345
Ijaz, A.	4602	Iyiola, O. A.	4623
Inan, O. G.	4470		
J			
Jamil, M.	4602		
K			
Kara, U.	4650	Keskin, S.	4357
Karabacak, M.	4704	Khan, Z. I.	4332, 4345
Karademir, C.	4477	Khodavandi, A.	4561
Karademir, E.	4477	Kilicgun, H.	4375
Karaman, A. D.	4637	Kostadinova, G.	4367
Kaya, S.	4383	Kukurt, A.	4883
Kaya, T.	4876	Kumbur, H.	4790
Kaya-Tilki, E.	4726	Kuranc, A.	4663
Kazi, A. M.	4602	Kurtca, M.	4420
Keles, H.	4420	Kuzu, M.	4677
L			
Lan, W.	4528	Lian, Z.	4536
Lawal, I. A.	4623	Liang, W.-J.	4495
Li, G.	4574	Libo, C.	4528
Li, J.	4350	Liu, B.	4549
Li, J.-L.	4462	Liu, H.	4400
Li, K.	4851	Liu, K.	4582
Li, Y.	4429, 4542	Liyun, G.	4528
Li, Y.-L.	4495	Lotfi, S.	4890
Li, Z.	4517	Lu, N.	4574
M			
Ma, F.	4817	Mian, S.	4504
Ma, J.	4595	Mihajlovic, I.	4867
Ma, L.	4697	Miloradov, M. V.	4867
Macic, V.	4834	Mobdy, A. E. A.	4764
Mandic, M.	4834	Mobdy, Y. E. A.	4764
Masakorala, K.	4400	Muneeb, A.	4345, 4602
Mehmood, N.	4332, 4345	Muqaddas, H.	4345
Metin, O. K.	4859	Muradoglu, F.	4456

**N**

Nafez, A. H.	4890	Negahdary, M.	4561
Nalbant, I.	4790	Ngila, C. J.	4623
Napar, A. A.	4602	Noorka, I. R.	4345
Naveed, N. H.	4602	Nur, G.	4883

O

Obrovski, B.	4867	Ozen, S. A.	4338
Okoro, H. K.	4623	Ozolcer, I. H.	4716
Ortakaya, V.	4446	Ozsahin, A. D.	4876
Othman, M. A.	4711	Ozturk, Y.	4726

P

Pandey, S.	4623	Peker, K.	4375
Parveen, R.	4332	Pestoric, B.	4834
Paunovic, M.	4834	Petkov, G.	4367
Pavlov, D.	4367	Pranovich, A.	4420
Pehlivan, M.	4470, 4757		

Q

Qiao, H.	4817		3148
----------	------	--	------

R

Radonic, J.	4867	Ren, B.	4517
Rahimi, G.	4561	Reunanen, M.	4420
Ramadanoglu, S. S.	4650	Rostami, R.	4890
Rasheed, M.	4504		

S

Sadri, F.	4561	Shi, W.	4582
Saeedi, R.	4890	Shi, X.-J.	4495
Samdan, C. A.	4484	Shi, Y.	4409
San Luo, X.	4798	Siddiqui, M. H.	4645
Saner, G.	4555	Slowik, T.	4663
Sayar, I.	4375	Sohail, M.	4345
Sekulic, M. T.	4867	Song, C.	4595
Selamoglu, Z.	4757	Song, N.	4409
Sener, S.	4616	Sonmez, F.	4456, 4774
Sevilmis, U.	4477	Sozen, E.	4692
Sevindik, M.	4757	Su, S.-J.	4588
Shamsazar, A.	4561	Sun, W.-Y.	4588
Shao, K.	4325	Sun, X.	4798
Sheikh, Z.	4345	Suntar, I.	4420
Shen, H.	4582	Suo, C.	4798
Sher, M.	4345	Szabo, T.	4841
Shi, R.	4495	Szyszlak-Barglowicz, J.	4663

T

Taj, F. N.	4345	Turemis, N. F.	4616
Tang, X.	4325	Turfan, N.	4606
Tascioglu, T.	4859	Turgut, U.	4416
Tekeli, M. Y.	4704	Turkay, G. K.	4790
Tumen, I.	4420		

U

Ubavin, D.	4867	Uncuoglu, A. A.	4859
Ucar, K.	4555	Urbanyi, B.	4841

**V**

Valkova, E.	4367	Verma, S. K.	4859
-------------	------	--------------	------

W

Wan, Z.	4400	Wang, X.	4542, 4808
Wang, B.	4825	Wang, Y.	4325
Wang, B.-Z.	4588	Wang, Z.	4390
Wang, J.	4536, 4549	Wasilewski, J.	4663
Wang, K.	4409	Wei, Y.	4574
Wang, L.	4542, 4595	Wen Zhang, W.	4742
Wang, S.	4595	Wenxiu, Z.	4528

X

Xie, C.	4390	Xie, X.	4390
Xie, L.	4429		

Y

Yaman, M.	4338	Yildirim, E. M.	4637
Yan, B.	4574	Yilmaz, N.	4734
Yan, H.	4522	Yilmaz, O.	4876
Yang, G.	4350	Yin Long, R.	4742
Yang, R.	4536	Yu, H.	4350
Yao, J.	4400	Yu, J.-N.	4462
Yasin, N. A.	4602	Yue Yang, D.	4825
Yer, E. N.	4606	Yukseloglu, E. H.	4650
Yerlikaya, H.	4637	Yun Li, F.	4825

Z

Zajac, G.	4663	Zhao, Y.	4536
Zhang, D.	4798	Zhao, Z.	4798
Zhang, F.	4595	Zhou, B.	4400
Zhang, H.	4390	Zhu, D.	4574
Zhang, L.	4350	Zhu, J.	4390
Zhang, X.	4429, 4851	Zhu, Y.	4429
Zhang, Y.-H.	4462	Zhu, Z.	4429
Zhao, B.	4817	Zubair, F.	4345
Zhao, C.-C.	4462	Zvinowanda, C.	4623
Zhao, X.	4542		

SUBJECT INDEX

A

abiotic stress	4606	Alkalinity	4588
accumulation	4409	α -amylase	4446
actinomycete	4400	Anti-inflammatory	4420
activated carbon	4484	antimicrobial	4757
Adriatic Sea	4834	Antimony (III)	4429
adsorption	4416, 4484, 4790	antioxidant	4606, 4616, 4757
Adsorption kinetics	4390	Apple	4456
Adsorption thermodynamics	4390	Apricot	4555
Advanced treatment	4517	artificial light	4783
Air pollution	4798	ascorbic	4616
Air quality forecast	4798	assessment	4367
Air quality index (AQI)	4798		

B

Babesia ovis	4883	biodiesel	4684
Bacillus simplex	4446	biomass	4663
Backwashing	4517	Biomorph-genetic magnetic composite	4429
BAP	4671	brassinolide	4851
Bioavailability	4542	Bread wheat	4859
Biochar	4390, 4825	broiler chickens	4704
Biodegradable	4462		

C

CA	4867	Coal chemical industry wastewater	4517
Cable Extraction	4656	combustion	4663
Calcium oxide	4495	community diversity	4400
Carbofuran	4764	Compressive strength	4588
Carbon	4429	Computational Fluid Dynamics	4716
carbon intensity	4742	Configuration	4656
carbon tariffs	4742	Contamination factor	4357
characterization	4446	coriander	4345, 4568
chelating surfactant	4817	Cost-effectiveness	4656
chelation	4817	Cotton	4477
chemical activation	4484	Cruciferous	4383
Chishui River	4549	crude oil contaminated soil	4851
Chloramphenicol	4390	Cu (II)	4817
Chlorella protothecoides	4684	Cu(OH) ₂	4817
clone library analysis	4400	curcumin	4726
CO	4663	Cypermethrin	4704
CO ₂	4663	Cyprinus carpio	4549

D

DDTs	4623	dissolution	4817
degradation	4595	Distribution	4522
Diabetes	4876	DNA analysis	4650
Diatom	4774	dormitory	4890
Diet Composition	4841	dye	4790
different hydrological years	4808	dynamic CGE model	4742
Digital elevation model	4734		

E

EC	4671	Enrichment factor	4357
ecological risk	4697	Enrofloxacin	4528
Ecological risk index	4357	enzymatic saccharification	4462
Economic analysis	4555	epigallocatechin gallate	4726
economic structure	4742	Epilithon	4774
EIA	4504	Erythrocytes	4876

electro-filter recycle powder	4790	Esox lucius	4841
Emission control measures	4798	Essential oil	4420
endemic	4692	Eucalyptus wood microstructure	4429
Endocrine Disruptive Chemicals	4623	ex situ	4692
Endocrine disruptor	4623	Expansive flow biological aerated filter	4517
Energy Loss Coefficient	4716	Extraction	4383
F			
Feasibility	4656	Fly ash	4542, 4574
fiber technological properties	4477	food facility	4637
Fishing Port	4504	Food safety	4637
Fixed-bed column sorption	4429	Forensic Genetics	4650
Flavonoids	4383	freshwater	4845
G			
gene expression	4859	glutathion	4883
genetic diversity	4477, 4568	Goldenberry	4876
Geometric Index of Importance (GII)	4841	groundwater	4867
germination	4692	growth	4470
H			
Haringet Stream	4774	hematite	4825
Health impact	4623	Hepatic ischemia–reperfusion injury	4375
health risk	4345	Hg ⁰	4536
health risk index	4332	higher education mega center	4697
Heat Susceptibility Index (H S I)	4602	Human milk	4711
heavy metal	4456, 4542, 4677	Hydraulic characteristic	4574
Heavy metals	4332, 4345, 4367, 4697, 4845		
I			
ICP-OES	4338	Interpolation methods	4734
immobilization	4416, 4825	ion-exchange	4582
improved export coefficient model	4808	IPBS-retrotransposon	4568
In vitro	4671	Iron oxide	4429
Inhibition	4677	Iskenderun Bay	4845
inoculation	4859	isolation	4446
J			
Jordan	4711		
K			
Kaolinite	4416	kinetic	4416
KCl	4671	kinetic disposition	4704
Kermanshah	4890	Kinetics	4522, 4528
L			
Landfill	4867	ligninase	4462
Landslide	4350	lipase enzyme	4416
Langmuir and Freundlich isotherm	4522	Lipid peroxidation	4876
Larval Pike	4841	lipids Profile	4764
Leach	4542	litter	4834
leachate	4867	liver	4375
Lead	4470	liver histopatology	4883
lead(II) removal	4484	loess	4574
library	4890	low-cost adsorbent	4790
light path length	4783	Lupin	4876
lignin	4462		
M			
Magnetic silver-loaded polytetrafluoroethylene	4536	microalgae	4684

Magnetism	4582	Microbial Fuel Cell	4561
Marine Water	4504	microbiological parameters	4367
Maritsa River	4367	migration	4409
Market analysis	4555	mineral nutrients	4470
MC-LR	4595	Mirabilis jalapa	4470
Melen river	4357	Miyun reservoir watershed	4808
Melia azedarach	4645	Momordica charantia	4332
Mentha longifolia subsp longifolia	4757	mulch	4616
Metal	4549	Myrtaceae	4420
Metal mobility	4338	Myrtus communis	4420
Meteorological condition	4798	Mystus macropterus	4549
N			
NaCl	4671	nitrate	4825
Nannochloropsis oculata	4783	NO	4663
Nano-biological Modification	4561	noise pollution	4890
naringin	4375	Nonpoint source pollution	4808
neurite outgrowth	4726	North Eastern Mediterranean	4845
neurodegeneration	4726	Novi Sad	4867
Neutral red	4522	NO _x	4663
New Generation Sequencing (NGS)	4650	nutrients content	4645
NiFe ₂ O ₄	4582		
O			
oil contamination	4400	oxidant	4757
organic agriculture	4616	oxidant/antioksidant status	4883
Organic farming	4555	oxidative balance	4606
Organochlorines	4711	oxidative stress	4757
Oriental beech	4606	ozone	4375
origin	4477		
P			
Parameters optimization	4495	physicochemical parameters	4367
paraoxonase activity	4883	π - π electro-donor-acceptor	4390
parsley	4764	plant growth	4645
partial purification	4446	plant physiology	4851
pathways	4528	plastic films	4409
PC-12	4726	Plough layer	4574
PCA	4867	Plow pan	4574
PCBs	4623	pollen viability	4456
peanut	4409	polluted water	4325
pellets	4663	Pollution	4338, 4834, 4867
pentose phosphate pathway	4764	pollution load index	4332
pest management	4637	preconditioning	4671
Pesticides	4711	precursor	4595
Phenolics	4383, 4616	pretreatment	4462
phosphate	4825	production	4446
photobioreactor	4783	Productivity	4656
photocatalytic	4582	Profitability analysis	4555
photodegradation	4528	Pumpkin seed shell	4484
phthalate esters (PAEs)	4409	Purification	4677
R			
Radical scavenging	4383	Removal efficiency	4536
Rainwater and Sewer Manhole	4716	Renewable energy	4684
rats	4764	Residue of manganese dioxide ore	4588
real-time PCR	4859	Response surface methodology	4495
reed	4825	Robinia pseudoacacia seedling	4851
Regeneration	4536		

S			
salinity	4671	Single Nucleotide Polymorphism (SNP)	4650
Scrophulariaceae	4692	single-dose	4704
SCUBA	4834	Skyline Yarder	4656
seabed	4834	Sludge dewatering	4495
seasonal succession	4774	SO ₂ emission	4663
sediment	4845	Soil water properties	4350
sediment bacterial community	4325	source	4697
Sediment quality	4357	Speciation	4338
Selectivity Index (SI)	4841	SSR	4568
semi-continuously	4783	strawberry	4616
Serum	4876	Sulphoaluminate cement	4588
shallow coastal area	4834	Surfer Software	4734
Shanmei reservoir	4325	Sustainable agriculture	4555
silver NPs	4561		
T			
Temperate forests	4350	toxicokinetic	4704
tetrazolium	4456	Tree mortality	4350
Thioredoxin Reductase	4677	tubular photobioreactor	4783
Toxic metals	4338	Turkey	4637, 4774
toxicity	4764		
U			
Ultrasonic	4495	Urbanization	4798
V			
Verbascum alyssifolium	4692	Volume calculation	4734
visible light	4595		
W			
waste management	4790	Wheat	4602
Wastewater	4645	white-rot fungi	4462
water qua-lity	4367	Wound Healing	4420
Wenchuan	4350		
Y			
Yellow River Beach	4574	Yield Reduction	4602
yellow rust	4859	Yr10 gene	4859
yield	4477		
1,.....,9			
454 pyrosequencing	4325		



FEB – GUIDE FOR AUTHORS

General

FEB accepts original papers, review articles, short communications, research abstracts from the entire sphere of environmental-chemistry,-biology,-microbiology,- technology, -biotechnology and-management, furthermore, about residue analysis/ and ecotoxicology of contaminants.

Acceptance or no acceptance of a contribution will be decided, as in the case of other scientific journals, by a board of reviewers. Papers are processed with the understanding that they have not been published before (except in form of an abstract or as a part of a published lecture, review or thesis); that they are not under consideration for publication elsewhere; that their publication has been approved by all co-authors, if any, as well as tacitly or explicitly- by the responsible authorities at the institute where the work has been carried out and that, if accepted, it will not be published elsewhere in the same form, in either the same or another language, without the consent of the copyright holders.

Language

Papers must be written in English. Spelling may either follow American (Webster) or British (Oxford) usage but must be consistent. Authors who are less familiar with the English language should seek assistance from proficient colleagues in order to produce manuscripts that are grammatically and linguistically correct.

Size of manuscript

Review articles should not exceed 30 typewritten pages. In addition up to 5 figures may be included. Original papers must not exceed 14 typewritten pages. In addition up to 5 figures may be included. Short-Communications should be limited to 4 typewritten pages plus not more than 1 illustration. Short descriptions of the authors, presentation of their groups and their research activities (with photo) should together not exceed 1 typewritten page. Short research abstracts should report in a

few brief sentences (one-fourth to one page) particularly significant findings. Short articles by relative newcomers to the chemical innovation arena highlight the key elements of their Master and PhD-works in about 1 page.

Book Reviews are normally written in-house, but suggestions for books to review are welcome.

Preparation of manuscript

Dear authors,

FEB is available both as printed journal and as online journal on the web. You can now e-mail your manuscripts with an attached file. Save both time and money. To avoid any problems handling your text please follow the instructions given below:

When preparing your manuscripts have the formula K/SS (Keep It Simple and Stupid) in mind. Most word processing programs such as MS-Word offer a lot of features. Some of them can do serious harm to our layout. So please do not insert hyperlinks and/or automatic cross-references, tables of contents, references, footnotes, etc.

1. Please use the standard format features of your word processor (such as standard.dot for MS Word).
2. Please do not insert automatisms or secret link-ups between your text and your figures or tables. These features will drive our graphic department sometimes mad.
3. Please only use two fonts for text or tables "Times New Roman" and for graphical presentations "Arial".
4. Stylesheets, text, tables and graphics in shade of grey
5. Turn on the automatic language detection in English (American or British)
6. Please - check your files for viruses before you send them to us!!

**Manuscripts should send to: parlar@wzw.tum.de
or: parlar@prt-parlar.de**

Thank you very much!

STRUCTURE OF THE MANUSCRIPT

Title page: The first page of the manuscript should contain the following items in the sequence given: A concise title of the paper (no abbreviations). The names of all authors with at least one first name spelled out for every author. The names of Universities with Faculty, City and Country of all authors.

Abstracts: The second page of the manuscript should start with an abstract that summarizes briefly the contents of the paper (except short communications). Its length should not exceed 150-200 words. The abstract should be as informative as possible. An extended repetition of the paper's title is not considered to be an abstract.

Keywords: Below the Summary up to 6 key words have to be provided which will assist indexers in cross-indexing your article.

Introduction: This should define the problem and, if possible, the frame of existing knowledge. Please ensure that people not working in that particular field will be able to understand the intention. The word length of the introduction should be 150 to 300 words.

Materials and methods:

Please be as precise as possible to enable other scientists to repeat the work.

Results: Only material pertinent to the subject must be included. Data must not be repeated in figures and tables.

Acknowledgements: Acknowledgements of financial support, advice or other kind of assistance should be given at the end of the text under the heading "Acknowledgements". The names of funding organisations should be written in full.

References: Responsibility for the accuracy of references rests with the authors. References are to be limited in number to those absolutely necessary. References should appear in numerical order in brackets and in order of their citation in the text. They should be grouped at the end of the paper in numerical order of appearance. Abbreviated titles of periodicals are to be used according to Chemical or Biological Abstracts, but names of lesser known journals should be typed in full. References should be styled and punctuated according to the following examples:

ORIGINAL PAPERS:

1. Author, N.N. and Author, N.N. (Year) Full title of the article. Journal and Volume, first and last page.

BOOK OR PROCEEDING:

2. Author, N.N. and Author, N.N. (Year) Title of the contribution.

In: Title of the book or proceeding. Volume (Edition of klitor-s, ed-s) Publisher, City, first and last page

DOCTORAL THESIS:

3. Author, N.N. (Year) Title of the thesis, University and Faculty, City

UNPUBLISHED WORK:

Papers that are unpublished but have been submitted to a journal may be cited with the journal's name followed by "in press". However, this practice is acceptable only if the author has at least received galley proofs of his paper. In all other cases reference must be made to "unpublished work" or "personal communication".

Discussion and Conclusion: This part should interpret the results in reference to the problem outlined in the introduction and of related observations by the author/s or others. Implications for further studies or application may be discussed. A conclusion should be added if results and discussion are combined.

Corresponding author: The name of the corresponding author with complete postal address

Precondition for publishing:

A minimum number of 25 reprints must be ordered and prepaid.

1 - 4 pp.: 200,- EURO + postage/handling

5 - 8 pp.: 250,- EURO + postage/ handling

More than 8pp: 1.50 EURO/page x number of reprints +postage/ handling.

The prices are based upon the number of pages in our journal layout (not on the page numbers of the submitted manuscript).

Postage/ Handling: The current freight rate is Germany 10 €, Europe 18,00 €, International 30 €.

VAT: In certain circumstances (if no VAT registration number exists) we may be obliged to charge 7% VAT on sales to other EU member countries. MESAEP and SECOTOX members get a further discount of 20% (postage/ handling full).